

METABOLOMICS AND ETHNOPHARMACOLOGY IN THE DEVELOPMENT OF HERBAL AND TRADITIONAL MEDICINE

EDITED BY: Sayeed Ahmad, Chandra Kant Katiyar, Pulok Kumar Mukherjee and
Gudrun S. Ulrich-Merzenich
PUBLISHED IN: Frontiers in Pharmacology





frontiers

Frontiers eBook Copyright Statement

The copyright in the text of individual articles in this eBook is the property of their respective authors or their respective institutions or funders. The copyright in graphics and images within each article may be subject to copyright of other parties. In both cases this is subject to a license granted to Frontiers.

The compilation of articles constituting this eBook is the property of Frontiers.

Each article within this eBook, and the eBook itself, are published under the most recent version of the Creative Commons CC-BY licence.

The version current at the date of publication of this eBook is CC-BY 4.0. If the CC-BY licence is updated, the licence granted by Frontiers is automatically updated to the new version.

When exercising any right under the CC-BY licence, Frontiers must be attributed as the original publisher of the article or eBook, as applicable.

Authors have the responsibility of ensuring that any graphics or other materials which are the property of others may be included in the CC-BY licence, but this should be checked before relying on the CC-BY licence to reproduce those materials. Any copyright notices relating to those materials must be complied with.

Copyright and source acknowledgement notices may not be removed and must be displayed in any copy, derivative work or partial copy which includes the elements in question.

All copyright, and all rights therein, are protected by national and international copyright laws. The above represents a summary only. For further information please read Frontiers' Conditions for Website Use and Copyright Statement, and the applicable CC-BY licence.

ISSN 1664-8714

ISBN 978-2-88974-985-0

DOI 10.3389/978-2-88974-985-0

About Frontiers

Frontiers is more than just an open-access publisher of scholarly articles: it is a pioneering approach to the world of academia, radically improving the way scholarly research is managed. The grand vision of Frontiers is a world where all people have an equal opportunity to seek, share and generate knowledge. Frontiers provides immediate and permanent online open access to all its publications, but this alone is not enough to realize our grand goals.

Frontiers Journal Series

The Frontiers Journal Series is a multi-tier and interdisciplinary set of open-access, online journals, promising a paradigm shift from the current review, selection and dissemination processes in academic publishing. All Frontiers journals are driven by researchers for researchers; therefore, they constitute a service to the scholarly community. At the same time, the Frontiers Journal Series operates on a revolutionary invention, the tiered publishing system, initially addressing specific communities of scholars, and gradually climbing up to broader public understanding, thus serving the interests of the lay society, too.

Dedication to Quality

Each Frontiers article is a landmark of the highest quality, thanks to genuinely collaborative interactions between authors and review editors, who include some of the world's best academicians. Research must be certified by peers before entering a stream of knowledge that may eventually reach the public - and shape society; therefore, Frontiers only applies the most rigorous and unbiased reviews.

Frontiers revolutionizes research publishing by freely delivering the most outstanding research, evaluated with no bias from both the academic and social point of view. By applying the most advanced information technologies, Frontiers is catapulting scholarly publishing into a new generation.

What are Frontiers Research Topics?

Frontiers Research Topics are very popular trademarks of the Frontiers Journals Series: they are collections of at least ten articles, all centered on a particular subject. With their unique mix of varied contributions from Original Research to Review Articles, Frontiers Research Topics unify the most influential researchers, the latest key findings and historical advances in a hot research area! Find out more on how to host your own Frontiers Research Topic or contribute to one as an author by contacting the Frontiers Editorial Office: frontiersin.org/about/contact

METABOLOMICS AND ETHNOPHARMACOLOGY IN THE DEVELOPMENT OF HERBAL AND TRADITIONAL MEDICINE

Topic Editors:

Sayeed Ahmad, Jamia Hamdard University, India

Chandra Kant Katiyar, Emami (India), India

Pulok Kumar Mukherjee, Institute of Bio-Resources and Sustainable Development (IBSD), India

Gudrun S. Ulrich-Merzenich, University Hospital Bonn, Germany

Citation: Ahmad, S., Katiyar, C. K., Mukherjee, P. K., Ulrich-Merzenich, G. S., eds. (2022). Metabolomics and Ethnopharmacology in the Development of Herbal and Traditional Medicine. Lausanne: Frontiers Media SA.
doi: 10.3389/978-2-88974-985-0

Table of Contents

- 07 Editorial: Metabolomics and Ethnopharmacology in the Development of Herbal and Traditional Medicine**
Sayeed Ahmad, Chandra Kant Katiyar, Gudrun S. Ulrich-Merzenich and Pulok Kumar Mukherjee
- 11 Tetrahydrocannabinol-Rich Extracts From Cannabis Sativa L. Improve Glucose Consumption and Modulate Metabolic Complications Linked to Neurodegenerative Diseases in Isolated Rat Brains**
Ochuko L. Erukainure, Mottalepula G. Matsabisa, Veronica F. Salau and Md. Shahidul Islam
- 21 Phytochemistry, Pharmacology and Medicinal Uses of Plants of the Genus Salix: An Updated Review**
Nora Tawfeek, Mona F. Mahmoud, Dalia I Hamdan, Mansour Sobeh, Nawaal Farrag, Michael Wink and Assem M. El-Shazly
- 51 Downregulation of Candidate Gene Expression and Neuroprotection by Piperine in Streptozotocin-Induced Hyperglycemia and Memory Impairment in Rats**
Suresh Kumar, Suman Chowdhury, Ajay Razdan, Deepa Kumari, Ram Singh Purty, Heera Ram, Pramod Kumar, Prasunpriya Nayak and Sunil Dutt Shukla
- 69 Studies on the Changes of Pharmacokinetics Behaviors of Phytochemicals and the Influence on Endogenous Metabolites After the Combination of Radix Bupleuri and Radix Paeoniae Alba Based on Multi-Component Pharmacokinetics and Metabolomics**
Congcong Chen, Qicai Yin, Junshen Tian, Xiaoxia Gao, Xuemei Qin, Guanhua Du and Yuzhi Zhou
- 86 Mahuang Decoction Antagonizes Acute Liver Failure via Modulating Tricarboxylic Acid Cycle and Amino Acids Metabolism**
Wenting Liao, Qiwen Jin, Junning Liu, Yiling Ruan, Xinran Li, Yueyue Shen, Zhicheng Zhang, Yong Wang, Shengming Wu, Junying Zhang, Lifeng Kang and Chunyong Wu
- 99 Anti-Inflammatory and Anti-Arthritic Potential of Standardized Extract of Clerodendrum serratum (L.) Moon**
Raj Kumar Tiwari, Silpi Chanda, Udayabanu M, Manisha Singh and Shriya Agarwal
- 110 Pharmacological Evaluation of Safoof-e-Pathar Phori- A Polyherbal Unani Formulation for Urolithiasis**
Wasim Ahmad, Mohammad Ahmed Khan, Kamran Ashraf, Ayaz Ahmad, Mohammad Daud Ali, Mohd Nazam Ansari, YT Kamal, Shadma Wahab, SM Arif Zaidi, Mohd. Mujeeb and Sayeed Ahmad
- 121 Ramulus Mori (Sangzhi) Alkaloids (SZ-A) Ameliorate Glucose Metabolism Accompanied by the Modulation of Gut Microbiota and Ileal Inflammatory Damage in Type 2 Diabetic KKAY Mice**
Quan Liu, Shuainan Liu, Hui Cao, Wenming Ji, Caina Li, Yi Huan, Lei Lei, Yaxin Fu, Xuefeng Gao, Yuling Liu and Zhufang Shen

- 134 ***Methanolic Extract of Lysimachia Candida Lindl. Prevents High-Fat High-Fructose-Induced Fatty Liver in Rats: Understanding the Molecular Mechanism Through Untargeted Metabolomics Study***
Parul Kamboj, Soumalya Sarkar, Sonu Kumar Gupta, Neema Bisht, Deepika Kumari, Md. Jahangir Alam, Sagar Barge, Bhaswati Kashyap, Barsha Deka, Simanta Bharadwaj, Seydur Rahman, Partha Pratim Dutta, Jagat C. Borah, Narayan Chandra Talukdar, Sanjay K. Banerjee and Yashwant Kumar
- 146 ***Transcriptomic and Metabolomic Profiling Reveals the Protective Effect of Acanthopanax senticosus (Rupr. & Maxim.) Harms Combined With Gastrodia elata Blume on Cerebral Ischemia-Reperfusion Injury***
Bingfeng Lin, Renhao Chen, Qi Wang, Zhifeng Li, ShiLin Yang and YuLin Feng
- 159 ***Identification, Biological Activities and Biosynthetic Pathway of Dendrobium Alkaloids***
Zongmin Mou, Yi Zhao, Fei Ye, Yana Shi, Edward J. Kennelly, Suiyun Chen and Dake Zhao
- 173 ***Andrographolide Against Lung Cancer-New Pharmacological Insights Based on High-Throughput Metabolomics Analysis Combined With Network Pharmacology***
Wen Luo, Li Jia, Jia-Wen Zhang, Dong-Jie Wang, Qiu Ren and Wei Zhang
- 189 ***Huanglong Antitussive Granule Relieves Acute Asthma Through Regulating Pulmonary Lipid Homeostasis***
Hua Yan, Guiying Qian, Rui Yang, Zichen Luo, Xianzheng Wang, Tong Xie, Xia Zhao and Jinjun Shan
- 203 ***Pharmacokinetic Profile and Oral Bioavailability of Diosgenin, Charantin, and Hydroxychalcone From a Polyherbal Formulation***
Ruchira Salunkhe, Chhaya Gadgoli, Archana Naik and Nikita Patil
- 217 ***Anti-Myocardial Ischemia Reperfusion Injury Mechanism of Dried Ginger-Aconite Decoction Based on Network Pharmacology***
Feng Xie, Yuan-Yuan Wu, Guang-Jing Duan, Bin Wang, Feng Gao, Pei-Feng Wei, Lin Chen, A-Ping Liu and Min Li
- 232 ***Estimation of Andrographolides and Gradation of Andrographis paniculata Leaves Using Near Infrared Spectroscopy Together With Support Vector Machine***
Dilip Sing, Subhadip Banerjee, Shibu Narayan Jana, Ranajoy Mallik, Sudarshana Ghosh Dastidar, Kalyan Majumdar, Amitabha Bandyopadhyay, Rajib Bandyopadhyay and Pulok K. Mukherjee
- 240 ***In-Vitro α -amylase, α -glucosidase Inhibitory Activities and In-Vivo Anti-Hyperglycemic Potential of Different Dosage Forms of Guduchi (Tinospora Cordifolia [Willd.] Miers) Prepared With Ayurvedic Bhavana Process***
Rohit Sharma, Rajesh Bolleddu, Jayanta K. Maji, Galib Ruknuddin and Pradeep K. Prajapati
- 254 ***Metabolite Profiling of the Indian Food Spice Lichen, Pseudevernia furfuracea Combined With Optimised Extraction Methodology to Obtain Bioactive Phenolic Compounds***
Rishu Kalra, Xavier A. Conlan, Carlos Areche, Rahul Dilawari and Mayurika Goel

- 270 Polyphenolic-Rich Compounds From *Dillenia pentagyna* (Roxb.) Attenuates the Doxorubicin-Induced Cardiotoxicity: A High-Frequency Ultrasonography Assisted Approach**
Kalyani Tene, M. Kalyan Kumar, G. Basveshwar, P. Eswara Rao, G. Jagadeesh Kumar, Pramod kumar, Deepak B. Pemmaraju, U. S. N. Murty, Ranadeep Gogoi and V. G. M. Naidu
- 285 *Turbina oblongata* Protects Against Oxidative Cardiotoxicity by Suppressing Lipid Dysmetabolism and Modulating Cardiometabolic Activities Linked to Cardiac Dysfunctions**
Ochuko L. Erukainure, Chika I. Chukwuma, Motlalepula G. Matsabisa, Miranda T. Javu, Veronica F. Salau, Neil A. Koorbanally and Md. Shahidul Islam
- 298 A Critical Review and Scientific Prospective on Contraceptive Therapeutics From Ayurveda and Allied Ancient Knowledge**
Narendra Bhatt and Manasi Deshpande
- 330 Yeast-Host Interactions: *Anadenanthera colubrina* Modulates Virulence Factors of *C. albicans* and Inflammatory Response In Vitro**
Carolina Medeiros de Almeida Maia, Silvana Pasetto, Cassiano Francisco Weege Nonaka, Edja Maria Melo de Brito Costa and Ramiro Mendonça Murata
- 343 *Dendrobium Officinale* Polysaccharide Attenuates Insulin Resistance and Abnormal Lipid Metabolism in Obese Mice**
Jian Qu, Shengyu Tan, Xinyan Xie, Wenqiang Wu, Haihong Zhu, Hang Li, Xiaobo Liao, Jiaojiao Wang, Zhi-Ang Zhou, Song Huang and Qiong Lu
- 354 Variable Secondary Metabolite Profiles Across Cultivars of *Curcuma longa* L. and *C. aromatica* Salisb.**
Poonam Kulyal, Satyabrata Acharya, Aditya B. Ankari, Praveen K. Kokkiripati, Sarada D. Tetali and Agepati S. Raghavendra
- 378 Multielemental Analysis and In Vitro Evaluation of Free Radical Scavenging Activity of Natural Phytopigments by ICP-OES and HPTLC**
S. M. Nandanwadkar, P. J. Hurkadale, C. M. Bidikar and M. M. Godbole
- 385 The Effects of Erchen Decoction on Gut Microbiota and Lipid Metabolism Disorders in Zucker Diabetic Fatty Rats**
Tian Zhao, Libin Zhan, Wen Zhou, Wanxin Chen, Jintong Luo, Lijing Zhang, Zebin Weng, Chunyan Zhao and Shenlin Liu
- 404 Metabolomics Reveals the Mechanisms for the Pulmonary Toxicity of *Siegesbeckia orientalis* L. and the Toxicity-Reducing Effect of Processing**
Ting Jiang, Linsheng Liu, Mi Zhang, Zhiping Qiao, Tingxiu Zhao, Junfang Su, Gang Cao and Tao Su
- 414 Ethnopharmacological, Phytochemical, Pharmacological, and Toxicological Review on *Senna auriculata* (L.) Roxb.: A Special Insight to Antidiabetic Property**
Guruprasad C. Nille, Shardendu Kumar Mishra, Anand Kumar Chaudhary and K. R. C. Reddy
- 437 Supercritical Carbon Dioxide Extracts of *Cordyceps sinensis*: Chromatography-based Metabolite Profiling and Protective Efficacy Against Hypobaric Hypoxia**
Jigni Mishra, Washim Khan, Sayeed Ahmad and Kshipra Misra

- 457 Dose-Effect/Toxicity of Bupleuri Radix on Chronic Unpredictable Mild Stress and Normal Rats Based on Liver Metabolomics**
Peng Wang, Xiaoxia Gao, Meili Liang, Yuan Fang, Jinping Jia, Junsheng Tian, Zhenyu Li and Xuemei Qin
- 480 The Novel Chinese Medicine JY5 Formula Alleviates Hepatic Fibrosis by Inhibiting the Notch Signaling Pathway**
Yadong Fu, Zhun Xiao, Xiaoting Tian, Wei Liu, Zhou Xu, Tao Yang, Yonghong Hu, Xiaoxi Zhou, Jing Fang, Siqi Gao, Dingqi Zhang, Yongping Mu, Hua Zhang, Yiyang Hu, Chenggang Huang, Jiamei Chen and Ping Liu
- 495 Standardization of Berberis aristata DC and Nigella sativa L. Using HPTLC and GCMS and Their Antineoplasia Activity in 7,12-Dimethylbenz[a]anthracene-Induced Mouse Models**
Mohd Mazhar and S S Agrawal
- 508 Metabolomic Profiling and Immunomodulatory Activity of a Polyherbal Combination in Cyclophosphamide-Induced Immunosuppressed Mice**
Sultan Zahiruddin, Abida Parveen, Washim Khan, Mohammad Ibrahim, Muzamil Y. Want, Rabea Parveen and Sayeed Ahmad



Editorial: Metabolomics and Ethnopharmacology in the Development of Herbal and Traditional Medicine

Sayeed Ahmad^{1*}, Chandra Kant Katiyar², Gudrun S. Ulrich-Merzenich³ and Pulok Kumar Mukherjee^{3,4}

¹Bioactive Natural Product Laboratory, Department of Pharmacognosy and Phytochemistry, School of Pharmaceutical Education and Research, Jamia Hamdard University, New Delhi, India, ²Emami Ltd., Kolkata, India, ³Medical Clinic III, AG Synergy Research and Experimental Medicine, University Hospital Bonn, Bonn, Germany, ⁴School of Natural Product Studies, Jadavpur University, Kolkata, India, ⁵Institute of Bio-Resources and Sustainable Development (IBSD), Imphal, India

Keywords: ethnopharmacology, medicinal plants, AYUSH DRUGS, metabolomics, traditional medicine, herbal medicine

Editorial on the Research Topic

Metabolomics and Ethnopharmacology in the Development of Herbal and Traditional Medicine

Herbal and traditional medicines are again gaining popularity around the world for the management of a variety of health problems. As the use of herbal/traditional medicines and other botanical products grows and more new products are introduced to the market, new and efficient methods to assess safety and efficacy become a major concern for researchers in drug development. It is important to understand the composition, safety, effectiveness, drug–drug or drug–food interactions, and also the possible side effects of traditionally used herbal medicines. The safety and efficacy data for herbal and traditional medicines are presently insufficient to meet the requirements for their worldwide use.

Traditional medicines are derived from local and empirical knowledge often transmitted orally and have been developed over generations. The traditional healers of Indian AYUSH (Ayurveda, Yoga, Naturopathy, Unani, Siddha, Sowa-Rigpa, and Homeopathy), traditional Chinese medicine (TCM), and other traditional systems of medicine mainly emphasize on holistic approaches with a focus on therapeutic practice and outcomes.

Metabolomics and the metabolomic profiling of herbal medicines and medicinal plants have provided new avenues of research in drug development. Metabolomic approaches allow the simultaneous identification of thousands of metabolites present in medicinal plants or herbal medicines. Furthermore, these support the mechanistic understanding of the concept of multicomponent multitarget effects and polypharmacology as well as the holistic approaches of treatments as per the AYUSH and other traditional systems of medicine. Synergistic effects are often claimed in experimental and clinical studies using multicomponent herbal preparations. Incorporating omics technologies into the assessment of the mode of action of herbal and traditional medicine will help in rationalizing the biological effects by unfolding the possible mechanism of synergistic actions. Such tools will allow us to explore the possibilities of standardization of multi-component extracts and formulations, for dereplication, and prediction of toxicity and safety of herbal preparations. Such a system biology approach should include network pharmacology assessments as well.

Metabolomics is one of the techniques used to identify targeted and untargeted metabolites for scientific validation and the development of herbal and traditional medicine, especially by using

OPEN ACCESS

Edited and reviewed by:

Michael Heinrich,
University College London,
United Kingdom

*Correspondence:

Sayeed Ahmad
sahmad_jh@yahoo.co.in

Specialty section:

This article was submitted to
Ethnopharmacology,
a section of the journal
Frontiers in Pharmacology

Received: 08 January 2022

Accepted: 11 February 2022

Published: 31 March 2022

Citation:

Ahmad S, Katiyar CK,
Ulrich-Merzenich GS and
Mukherjee PK (2022) Editorial:
Metabolomics and
Ethnopharmacology in the
Development of Herbal and
Traditional Medicine.
Front. Pharmacol. 13:851023.
doi: 10.3389/fphar.2022.851023

high-throughput screening methods. The probability of repetition or working on numerous samples with similar active metabolites is one of the challenges of natural product-based drug development. To overcome these challenges, various “dereplication” methods have been developed. A metabolomic technique combined with a suitable biostatistical method has the ability to facilitate the fast analysis of composite data generated by high-throughput screening.

The scope of this special issue on ethnopharmacology and metabolomics is to focus on the quality, safety, and efficacy of traditional, specially AYUSH, and herbal medicines with more emphasis on metabolomic studies using hyphenated techniques. This issue contains four review articles and 29 research articles by different research groups around the globe on related topics.

Fu et al. studied the active constituents and mechanism of action of the Fuzheng Huayu formula (FZHY), which is a traditional Chinese medicine used for liver fibrosis. The main active components of FZHY are salvianolic acid B, schisantherin A, and amygdalin, which significantly improve the condition of CCl₄- and BDL-induced fibrotic liver in rats and mice. In addition to this, the formulation inhibits the activation of hepatic stellate cells by inactivating notch signaling. The authors conclude that the results provide promising scientific evidence for further investigations with the ultimate goal to bring the formula into clinical research as a potential candidate for liver fibrosis.

Dendrobium officinale Kimura & Migo (Orchidaceae) polysaccharide is used in Chinese medicine for liver protection and hypoglycemic action. Qu et al. studied the *in vitro* and *in vivo* effects of *D. officinale* polysaccharides in insulin resistance and abnormal lipid metabolism. The results of the study proved that this traditional medicine may serve as a potential therapeutic agent for obesity-related insulin resistance and lipid metabolism.

Kulyal and group studied the variability in secondary metabolites across five cultivars of *Curcuma longa* L. and two cultivars of *C. aromatica* Salisb. The analysis was carried out on rhizomes and essential oils using gas chromatography–mass spectrometry (GC–MS) and liquid chromatography–mass spectrometry (LC–MS) methods. Among many compounds detected by the authors, 28 compounds were common in all seven cultivars and 39 new metabolites were detected from all seven species.

The work of Yan et al. includes the effect of Huanglong granule (HL Granule) in acute asthma and the possible underlying mechanism of action on mice. Changes in lipid composition were identified using UHPLC–Q-exactive Orbitrap MS with a focus on pulmonary lipid homeostasis. In positive and negative ion modes, a total of 304 and 167 lipids, respectively, were identified in lung tissues, with 162 and 109 lipids significantly elevated in the model group. The authors observed that the HL Granules reversed 104 and 73 lipids, respectively, with a statistical difference (false discovery rate <0.05). It was concluded that lipid homeostasis plays an important role in asthma, and HL Granule might be further investigated and developed as an adjuvant therapy for acute asthma.

The effect of *Lysimachia candida* Lindl. on fatty liver disease in rats was investigated by Kamboj et al. The majority of the

metabolites found in both control and treatment groups were related to lipid metabolism. Treatment with *L. candida* extract improved the control of lipid metabolism and reversed the metabolic syndrome phenotype in rats.

Zhao et al. investigated the mechanism of a traditional Chinese medicine, Erchen decoction. The composition and function of gut microbiota in obesity and its relation with lipid metabolism disorders were investigated. The underlying mechanism of obesity due to changes in the composition of gut microbiota was also studied by the authors. The Erchen decoction reduced body weight, improved insulin resistance and lipid metabolism, and reduced the concentration of free fatty acids released from white adipose tissue due to excessive lipolysis in rats. This study supports the hypothesis that the basis for treatment of obesity lies in changes in gut microbiota.

According to Liu et al., the traditional Chinese medicine *Ramulus mori* (Sangzhi) alkaloid (SZ-A) tablets improved the overall metabolic profile in mice, including glucose metabolism with enhanced insulin response, and also improved lipid metabolism, which was collectively linked to the modulation of gut microbiota.

Sharma et al. worked on three different dosage forms of Guduchi stem, i.e., *Tinospora cardifolia* (Willd.) Miers, by adopting the Ayurvedic pharmaceutical process of Bhavana (levigation). The findings of this study indicated the effectiveness of Svarasa Bhavita Guduchi Churna and Kwatha Bhavita Guduchi Churna in the treatment of diabetes mellitus. This study provides scientific support to Ayurvedic claims that the Bhavana process has pharmaceutico-therapeutic significance in Ayurvedic drug development.

Zahiruddin et al. used response surface methodology to optimize the ratio of aqueous extracts of *Phyllanthus emblica* L., *Piper nigrum* L., *Withania somnifera* (L.) Dunal, and *T. cordifolia* (Willd.) Miers for the development of a combination formulation. The developed polyherbal formulation showed significant immunomodulatory activity on cyclophosphamide-induced immunosuppressed mice. The metabolomic study showed more than 180 metabolites, identified through LC–MS in the optimized combination. Polyherbal combination treatment significantly ($p < 0.01$) enhanced the subsets of immune cells such as NK cells, B cells, CD4 cells, and CD8 cells.

Berberis aristata DC. and *Nigella sativa* L. are plants traditionally used for several diseases. Mazhar et al. describe a method of standardization of *B. aristata* and *N. sativa* and investigated their anticancer activity in a 7,12-dimethylbenz [a]anthracene (DMBA)-induced mouse model. Molecular docking was carried out for the marker compounds of both plants with metabolomic studies of essential oils using GC–MS. The study showed that the extracts of *N. sativa* and *B. aristata*, as well as their marker compounds, showed an antitumor activity and had no harmful effects on female mice. Furthermore, they protected against DMBA-induced tumor in a mouse model.

Sigesbeckia orientalis L. (syn.: *Siegesbeckia orientalis* L.) (SO) is a remedy in TCM used to reduce the symptoms of joint disorders. It is a toxic herb, but it is hypothesized that by processing, according to TCM theory, its toxicity can be lowered. Jiang

and co-authors demonstrated using metabolomics that the raw SO causes pulmonary toxicity and that by processing with rice wine its toxicity is reduced. This supports the classical SO processing theory with scientific evidence.

Anadenanthera colubrina (Vell.) Brenan, a plant with antifungal and anti-inflammatory properties, was studied by Maia et al. for its antifungal activity against *Candida albicans*, *C. glabrata*, *C. tropicalis*, and *C. dubliniensis* using the broth microdilution method. Antifungal activity was assessed in terms of antibiofilm effects, proteolytic enzyme activities, viability assays, gene expression, and cytokine expressions. The extract showed a significant antifungal activity against different *Candida* strains with low toxic effects to the host cells.

Salunkhe et al. formulated two formulations of spray-dried alcoholic extracts from three different herbs, namely, *Trigonella foenum-graecum* L, *Momordica charantia* L, and *Cinnamomum verum* J. Presl. The oral bioavailability and pharmacokinetic profile of the formulations were evaluated in terms of their markers diosgenin, charantin, and hydroxychalcone in male Wistar rats. Maximum oral bioavailability was found for charantin, followed by diosgenin and then hydroxychalcone. A significant increase in bioavailability of all the markers was observed after the addition of piperine.

Supercritical fluid extraction is one of the extraction methods with the advantages of short extraction time and high purity of extracts. Mishra et al. described the metabolite profile of supercritical CO₂ extracts of the Indian variety of *Ophiocordyceps sinensis*, earlier known as *Cordyceps sinensis*, using high-performance thin-layer chromatography and GC-MS, followed by chemometric analysis. The extract was found effective against *Escherichia coli* and *Salmonella typhi* by the generation of reactive oxygen species and can be utilized in mycotherapeutics for multiple bioeffects.

Wang et al. explored the dose-effect/toxicity relationships between the high and low doses of the lower polar fraction of *Bupleuri Radix* (root of *Bupleurum chinense* DC) and its mechanism using liver metabolomics in chronic unpredictable mild stress (CUMS) rats. The median toxicity dose and effective safe dose of *Bupleuri Radix* which caused liver injury at a high dose and psychiatric diseases at a low dose were calculated.

Tene et al. investigated the cardioprotective effect of *Dillenia pentagyna* Roxb. (DP) against doxorubicin (Dox)-induced cardiotoxicity *in vitro* as well as *in vivo*. The finding suggested that the phenol-rich extract/fractions of DP helped in alleviating Dox-induced cardiotoxicity. The LC-quadrupole time-of-flight electrospray ionization MS analysis of bioactive extract/fractions indicated that polyphenols like gallic acid, syringic acid, and sinapic acid could be responsible for the potent cardioprotective effect due to their antioxidant properties.

Erukainure et al. investigated the cardioprotective mechanisms of a traditional medicinal plant of South Africa, *Turbina oblongata* (E. Mey. ex Choisy) A. Meeuse. The results indicated that such plant has the potential to mitigate lipotoxicity and control dysregulated cardio-metabolic activities due to its antioxidant potential and suppressive effects on angiotensin-converting enzyme, lipase, and acetyl cholinesterase enzymes.

Mahuang decoction (MHD) is a well-known traditional Chinese medicine; its protective effect against lipopolysaccharide and D-galactosamine (LPS/D-GalN)-induced acute liver failure (ALF) in a mouse model was reported by Liao and his co-workers. The MHD showed a protective effect by regulating the tricarboxylic acid cycle and amino acid metabolism. Ultra-performance liquid chromatography (UPLC)-MS was undertaken for metabolomic studies, and it revealed that, in serum samples, 36 metabolites were identified as contributing to LPS/D-GalN-induced ALF, whereas 27 among them were ameliorated on the administration of MHD.

Erukainure et al. worked on the tetrahydrocannabinol-rich extract of *Cannabis sativa* L. in the context of neurodegenerative disorders. The extract was found to improve glucose intake and to suppress oxidative stress and cholinergic dysfunction as well as to modulate purinergic and gluconeogenic activity in the brain tissues of rats. The *in silico* analysis revealed that the constituents of the extract can pass through the blood-brain barrier, whereas the GC-MS analysis confirmed the presence of tetrahydrocannabinol in the plant extract.

Safoof-e-Pathar phori (SPP) is a poly-herbomineral formulation, which has been used traditionally for urolithiasis as per the Unani Pharmacopoeia of India. Ahmad et al. investigated the traditional claim pre-clinically. The study involved the oral administration of SPP at low and high doses. They significantly ($p < 0.001$) reduced urinary calcium, serum creatinine, blood urea, and lipid peroxidation in urolithiatic Wistar rats. The long-term oral toxicity study showed that SPP was safe in Wistar rats for up to 3 months. The study provides scientific evidence in support of traditional claims for SPP as an anti-urolithiatic formulation.

Luo et al. used high-throughput metabolomic analysis to identify the biomarkers and pathways that would reveal the therapeutic action and mechanism of andrographolide against lung cancer using UPLC-time-of-flight MS. The findings suggest that 11 metabolism pathways are regulated by andrographolides in cancer. The network pharmacology revealed the involvement of 570 proteins. Amino acid metabolism and arachidonic acid metabolism pathways are the potential target pathways for andrographolide in this model of lung cancer.

Kumar et al. investigated the neuroprotective effect of piperine on streptozotocin-induced hyperglycemia and also observed the gene expression in diabetic rats. Piperine leads not only to a significant improvement in memory but also to a significant reduction in the expression of specific Alzheimer's disease-related genes, like BACE1, PSEN1, APOA1, CASPASE3, and CATALASE.

Radix Bupleuri (RB) and *Radix paeoniae Alba* (RPA) are components of a well-known herb combination used clinically to treat depression. Chen et al. developed a novel and efficient technique for analyzing the impact of the combination of RB and RPA in *in vivo* behaviors by combining multi-component pharmacokinetics with metabolomics. The finding of the study suggested that the combination can increase the bioavailability of 6 components in RPA and 5 in RB and also boost neuroprotective and anti-inflammatory effects.

Tiwari et al. used chromatographically standardized extracts of *Clerodendrum serratum* (L.) Moon (Verbenaceae) for assessing its anti-inflammatory and anti-arthritic activities. Scientific evidence for the ethnomedicinal use of the plant in arthritis is thereby provided.

Nandanwadkar et al. used the inductive coupled plasma-optical emission spectroscopy technique to carry out multi-elemental assessments of phyto-pigments. They also used a chromatographic technique to evaluate their biotherapeutic potential. The screening for heavy metals and micro- and macro-minerals was undertaken using routine quality control and the safety profile of food additives and contaminants.

Lin et al. focused on two traditional Chinese medicine [*Acanthopanax senticosus* (Rupr. and Maxim.) Harms and *Gastrodia elata* Blume] for the treatment of stroke and cerebrovascular diseases. Using transcriptomic and metabolomic studies together, the authors hypothesized that both drugs can be used for the treatment of cerebrovascular diseases. Six metabolites and six genes were found to be significantly altered. The therapeutic effect of the extracts in cerebrovascular diseases was found to be related to the regulation of the phenylalanine and pyrimidine metabolic pathways.

Pseudevernia furfuracea (L.) is an epiphytic lichen used in Indian spice mixtures, curries, and food preparations as a preservative. Goel et al. attempted to find the optimal extraction method for polyphenol- and flavonoid-enriched extracts of *P. furfuracea*. Scanning electron microscopy and high-performance liquid chromatography were used to analyze and compare the effect of pre-processing conditions on the extraction method. Ultra-high-performance liquid chromatography–diode array detector MS was used to study the metabolomic profile of the lichen extracts. After mixing and grinding the raw material by using Soxhlet, it was found that 70% methanol extract was the most effective for extracting a combination of polyphenolic and flavonoidal-rich metabolites. The work also suggested *P. furfuracea* as a potent antioxidant.

Sing et al. suggested a system for grading *Andrographis paniculata* (Burm. F) raw ground samples using near-infrared reflectance (NIR) spectroscopy and support vector machine (SVM) classifier based on the content of the marker, andrographolide. The estimation accuracy based on extracts was marginally higher than that based on powder leaf samples. However, it had no effect on the samples' grading pattern. The finding of the study suggested that combining the NIR-based estimate of powdered leaf samples with an SVM classifier can be a low-cost solution for grading the samples rapidly.

Mou et al. summarized the structural types, pharmacological activities, and mechanisms of *Dendrobium* alkaloids as well as the suggested biogenetic pathways of dendrobine, which is an important sesquiterpene alkaloid.

Tawfeek et al. provided a comprehensive overview of the phytochemistry, traditional use, and pharmacology of plant

extracts and constituents from the genus *Salix* (willows). They also demonstrated its ability to reduce inflammatory pathways and hypothesized that they could be useful in cancer prevention and therapy as well as other chronic diseases.

Bhatt et al. explored the Indian system of medicines for possible male and female contraceptives. The review concluded that the Indian system of medicine offers highly promising opportunities with potential analytical, biological, technological, and clinical advances collectively integrated with therapeutic rationale based on Ayurvedic principles.

Nille et al. provided information on a traditional plant, Avartaki [*Senna auriculata* (L.) Roxb.], and its wide usefulness in the Ayurveda and Siddha systems of medicine for the treatment of numerous diseases. The ethnomedicinal, phytochemical, pharmacological, and toxicological features of the plant were discussed in this review article, with more focus on therapeutic significance in diabetes.

Overall, this special issue provides an insight into the role of metabolomics and ethnopharmacology in the development of herbal and traditional medicine. It provides the readers with a plethora of generally up-to-date information to support their understanding of these rapidly evolving areas of metabolomics. There is still an enormous scope to work on the metabolomics and network pharmacology of traditional medicine for a better understanding of the molecular mechanism of pharmacological actions by identifying metabolites through dereplication and to provide data for scientific validation of traditional claims.

AUTHOR CONTRIBUTIONS

SA, CK, PM, and GU prepared the manuscript.

Conflict of Interest: Author CK was employed by company Emami Ltd.

The remaining authors declare that the research was conducted in the absence of any commercial or financial relationships that could be construed as a potential conflict of interest.

Publisher's Note: All claims expressed in this article are solely those of the authors and do not necessarily represent those of their affiliated organizations or those of the publisher, the editors, and the reviewers. Any product that may be evaluated in this article or claim that may be made by its manufacturer is not guaranteed or endorsed by the publisher.

Copyright © 2022 Ahmad, Katiyar, Ulrich-Merzenich and Mukherjee. This is an open-access article distributed under the terms of the Creative Commons Attribution License (CC BY). The use, distribution or reproduction in other forums is permitted, provided the original author(s) and the copyright owner(s) are credited and that the original publication in this journal is cited, in accordance with accepted academic practice. No use, distribution or reproduction is permitted which does not comply with these terms.



Tetrahydrocannabinol-Rich Extracts From *Cannabis Sativa* L. Improve Glucose Consumption and Modulate Metabolic Complications Linked to Neurodegenerative Diseases in Isolated Rat Brains

Ochuko L. Erukainure¹, Motlalepula G. Matsabisa^{1*}, Veronica F. Salau² and Md. Shahidul Islam²

¹Department of Pharmacology, School of Clinical Medicine, Faculty of Health Sciences, University of the Free State, Bloemfontein, South Africa, ²Department of Biochemistry, School of Life Sciences, University of KwaZulu-Natal, Durban, South Africa

OPEN ACCESS

Edited by:

Gudrun S. Ulrich-Merzenich,
University Hospital Bonn, Germany

Reviewed by:

Ramesh Bhonde,
Dr. D. Y. Patil Vidyapeeth, India
Ahmed Esmat Abdel Moneim,
Helwan University, Egypt

*Correspondence:

Motlalepula G. Matsabisa
matsabisamg@ufs.ac.za

Specialty section:

This article was submitted to
Ethnopharmacology,
a section of the journal
Frontiers in Pharmacology

Received: 08 August 2020

Accepted: 14 October 2020

Published: 24 November 2020

Citation:

Erukainure OL, Matsabisa MG, Salau VF and Islam MS (2020) Tetrahydrocannabinol-Rich Extracts From *Cannabis Sativa* L. Improve Glucose Consumption and Modulate Metabolic Complications Linked to Neurodegenerative Diseases in Isolated Rat Brains. *Front. Pharmacol.* 11:592981. doi: 10.3389/fphar.2020.592981

Reduced brain glucose consumption arising from impaired glucose uptake and utilization has been linked to the pathogenesis and complications of neurodegenerative diseases. The ability of *Cannabis sativa* L. tetrahydrocannabinol (THC)-rich extracts to stimulate brain glucose uptake and utilization as well as its modulatory effect on gluconeogenesis, antioxidative, purinergic and cholinergic activities were investigated in isolated rats' brains. *C. sativa* leaves were sequentially extracted to yield the hexane and dichloromethane extracts. The extracts were incubated at 37°C with freshly harvested brains in the presence of glucose for 2 h. The control consisted of incubation without the extracts, while brains without the extracts and glucose served as the normal control. Metformin was used as the standard drug. *C. sativa* extracts caused a significant ($p < 0.05$) increase in brain glucose uptake, with concomitant elevation of glutathione level, superoxide dismutase, catalase, and ecto-nucleoside triphosphate diphosphohydrolase activities compared to the controls. Incubation with *C. sativa* extracts also led to depletion in malondialdehyde and nitric oxide levels, acetylcholinesterase, butyrylcholinesterase, glucose 6-phosphatase and fructose-1,6-biphosphatase activities. GC-MS analysis of the extracts revealed the presence of THC. *In silico* analysis predicted THC to be permeable across the blood-brain-barrier. THC was also predicted to have an oral LD₅₀ and toxicity class values of 482 mg/kg and 4 respectively. These results indicate that *C. sativa* improves glucose consumption with concomitant suppression of oxidative stress and cholinergic dysfunction, and modulation of purinergic and gluconeogenic activities in brain tissues

Keywords: brain glucose consumption, *Cannabis sativa*, neurodegenerative diseases, tetrahydrocannabinol 3, carbohydrate metabolism

INTRODUCTION

The brain's dependence on glucose for energy generation is well documented. Brain glucose homeostasis has also been reported to be important for neuronal generation and maintenance, regulation of neurotransmitter, cognitive function and synaptic plasticity (Neumann et al., 2008). Glucose transporters aid in transporting glucose across the blood brain barrier (BBB) from the blood stream to the brain. Altered glucose homeostasis in the central nervous system (CNS) has been reported in most neurodegenerative diseases such as Alzheimer's and Parkinson diseases (An et al., 2018). This has been attributed to abnormalities in insulin signaling pathways in the brain as well as alteration of the glucose transporters at the BBB (Gejl et al., 2017; An et al., 2018). These abnormalities and alterations often cause decreased brain glucose consumption which can lead to a hypometabolic brain state characterized by glucose dysmetabolism (Zilberter and Zilberter, 2017). Thus, making the brain susceptible to degenerative diseases. This is evident in studies which correlated the risk of Alzheimer's disease with reduced brain glucose metabolism (Duran-Aniotz and Hetz, 2016).

Increased oxidative stress has been linked with decreased brain glucose uptake (Erukainure et al., 2019c). Increased glucose uptake has been shown to improve proteostasis which causes an upregulation of the unfolded protein response that protects against endoplasmic reticulum stress (Scheper and Hoozemans, 2015; Duran-Aniotz and Hetz, 2016). Oxidative stress has been implicated in the etiology and pathogenesis of neurodegenerative diseases (Erukainure et al., 2019b; Salau et al., 2020b). This is evident in the use of antioxidants in treating and managing most neurodegenerative diseases such as Alzheimer's and Parkinson's diseases (Gilgun-Sherki et al., 2001; Kim et al., 2015). Antioxidants have been reported for their ability to scavenge free radicals as well as improve the activities of the endogenous antioxidant enzymes (Salau et al., 2020). Oxidative stress has also been implicated in the disturbances of cholinergic and purinergic enzymes activities of the CNS (Erukainure et al., 2019a; Salau et al., 2020). These enzymes have been reported for their respective neurotransmission and bioenergetic roles which are critical for normal functioning of the brain (Ademiluyi et al., 2016; Pepeu and Giovannini, 2017).

Cannabis sativa L. is among the medicinal plants used in the treatment and management of neurological diseases. It is an annual herbaceous plant that belongs to the *Cannabis* genus and Cannabaceae family. It is globally distributed, with Africa accounting for 25% of its global production (UNODC, 2012). Its common names include weed, Indian hemp and marijuana. *C. sativa* is utilized for food, therapeutic, recreational and religious purposes (Bonini et al., 2018). Phytocannabinoids make up the major phytochemical constituents of *C. sativa*, with tetrahydrocannabinol (THC), cannabinol, and cannabidiol among the most common (Andre et al., 2016). The therapeutic role of *C. sativa* against neurodegenerative diseases and other psychopathic ailments have been reported (Lafuente et al., 2011; Campos et al., 2017; Lim et al., 2017). The aqueous and ethanol extracts of the leaves have been reported to confer

protective effects on α -motor neurons via antioxidative and anti-apoptotic activities (Moosavi et al., 2013). Cannabidiol has been reported for its ability to activate metabotropic receptors for serotonin and/or adenosine as well as nuclear receptors of the PPAR family (Fernández-Ruiz et al., 2013). The leaves improved tremor, bradykinesia and rigidity in Parkinsonian patients (Lotan et al., 2014). The neuroprotective effects of *C. sativa* have been demonstrated on basal ganglia disorders (Sagredo et al., 2007). Other reported medicinal properties of *C. sativa* include anti-diabetes (Ren et al., 2016), anticancer (Guzman, 2003), pain suppression (Whiting et al., 2015), anti-epilepsy (Fusar-Poli et al., 2009), and sleep management (Ramar et al., 2018).

Despite the reported neuroprotective effect of *C. sativa* and its phytoconstituents, there are still dearth in its ability to promote brain glucose uptake and/or utilization. Thus, this present study was aimed at investigating the ability of the leaves to stimulate glucose uptake and utilization, as well as its modulatory effect on antioxidative, purinergic and cholinergic activities, and gluconeogenesis in isolated brains. The cytotoxic effect of the leaves was also investigated in glioblastoma multiforme (U87 MG) cells.

MATERIALS AND METHODS

Plant Permit Approval

This research has been undertaken under the permit approval (Permit No. POS 248/2019/2020) from the South African Health Products Regulatory Authority to conduct, collect, possess, transport and store cannabis plant, plant parts and products for research purposes. The study was also conducted to collect cannabis plants in Lesotho under the permit (Permit #: 01/LS/2019/10/02-01).

Plant Material

Cannabis sativa leaves were obtained from Mohale's Hoek District, Lesotho (GPS coordinates: $-30.333776^{\circ}\text{S}$ and $27.651201^{\circ}\text{E}$). They were authenticated by the Geo Potts Herbarium at the University of the Free State, Bloemfontein 9300, South Africa and assigned the voucher number, BLFU MGM 0018. The leaves were pulverized to dry powder, after air drying to a constant weight.

The powdered samples were thereafter sequentially extracted with solvents of increasing polarity vis-à-vis hexane and dichloromethane (DCM) for 48 h with mild agitation of 100 rpm at room temperature. The solvents were respectively decanted and concentrated *in vacuo* using an R-215 rotary evaporator (Buchi, Switzerland). The extracts were collected in glass vials and stored in the dark at ambient room temperature for further *ex vivo* studies.

Animals

A day to the experiment, sixteen male albino rats (Sprague Dawley strain) weighing 180 – 200 g were obtained from the Biomedical Research Unit, University of KwaZulu-Natal, Durban, South Africa and housed in plastic cages. They were fasted for 8 h before humanely sacrificed by euthanizing with

Isofor. Their brains were harvested and rinsed in normal saline to remove blood stains. Each brain was divided into its hemispheres and used immediately for *ex vivo* study.

Glucose Uptake in Isolated Rat Brain

Each hemisphere of the freshly harvested rat brains was incubated in 8 ml of Krebs buffer containing 11.1 mM glucose and the different concentrations of *C. sativa* extracts (hexane and DCM) for 2 h under a 5% CO₂, 95% oxygen and 37°C conditions as described in previously published methods (Erukainure et al., 2019c; Salau et al., 2020a). The untreated control consisted of incubation without the extracts, while brains incubated without the extracts and glucose served as the normal control. Metformin was used as the standard drug. Each treatment group consisted of 3 brain hemispheres.

After incubation, the brain tissues were collected and homogenized in 50 mM phosphate buffer (pH 7.5) with 1% triton X-100, and thereafter centrifuged at 15,000 rpm at 4°C for 10 min (Erukainure et al., 2019c). The supernatants were collected and stored at –20°C until further analysis.

The study was carried out under the approved guidelines of the animal ethics committee of the University of KwaZulu-Natal, Durban, South Africa (protocol approval number: AREC/020/017D).

Determination of Glucose Utilization

Aliquots from the incubating buffer was collected prior and after the incubation for determination of glucose utilization. This was carried out by measuring the glucose concentrations using an automated chemistry analyzer (Labmax Plenno, Labtest Inc., Lagoa Santa, Brazil). Glucose utilization was thereafter calculated with the formula:

$$\text{Glucose uptake} = \frac{\text{GC1} - \text{GC2}}{\text{Weight of brain tissue (g)}}$$

Where GC1 and GC2 are glucose concentrations (mg/dL) before and after incubation, respectively.

Determination of Antioxidative Activity Reduced glutathione level

The Ellman's method (Ellman, 1959) was used in determining the GSH level of the brain tissue. Briefly, the resulting supernatant was deproteinized with an equal volume of 10% Trichloroacetic acid (TCA) and centrifuged for 5 min at 3,500 rpm. 200 µl aliquot was collected from the deproteinized sample into a 96 well plate. 50 µl of Ellman reagent was thereafter added and the reaction mixture was allowed to stand for 5 min. Absorbance was read at 415 nm. The GSH concentration was extrapolated from a standard curve.

Superoxide dismutase Activity

The superoxide dismutase (SOD) activity of the brain tissues was determined using a method based on the principle that 6-hydroxydopamine (6-HD) is oxidized by H₂O₂ from SOD catalyzed dismutation of O₂^{•–}, which produces a colored product (Gee and Davison, 1989). Briefly, 15 µl of the tissue

supernatants were dissolved in 170 µl of 0.1 mM diethylenetriaminepentaacetic acid (DETAPAC) in a 96 well plate. Thereafter, 15 µl of 1.6 mM 6-HD was added. Absorbance was measured at 492 nm for 5 min at 1 min interval.

Catalase Activity

The catalase activity of the brain tissue was determined using a previously established protocol (Aebi, 1984). Briefly, 10 µL of the tissue supernatants was mixed with 340 µL of 50 mM sodium phosphate buffer (pH 7.0). Thereafter, 150 µL of 2 M H₂O₂ was added to the reaction mixture. Absorbance was read at 240 nm at 1 min interval for 3 mins.

Lipid Peroxidation Level

The lipid peroxidation level of the brain tissues was determined by measuring the thiobarbituric acid reactive substances (TBARS) in the tissues and expressed as malondialdehyde (MDA) equivalent (Chowdhury and Soulsby, 2002). Briefly, a reaction mixture consisting of 100 µl of the supernatants, 100 µl of 8.1% SDS solution, 375 µl of 20% acetic acid, 1 ml of 0.25% thiobarbituric acid (TBA), and 425 µL of distilled water was heated at 95°C for 1 h in a water bath. A 200 µl aliquot was thereafter collected from the reaction mixture into a 96 well plate, and absorbance read at 532 nm.

Nitric Oxide Level

The brain tissues were assayed for nitric oxide level using the Griess method as previously described (Tsikas, 2005; Erukainure et al., 2019c). Briefly, 100 µl of the tissue samples and/or distilled water (blank) were incubated with an equal volume of Griess reagent for 30 min at 25°C in the dark. Absorbance was read at 548 nm.

Cholinergic Enzymes Activities

The brain tissues were assayed for cholinergic activities by analyzing the activities of acetylcholinesterase (Ellman et al., 1961) and butyrylcholinesterase (Adefegha et al., 2017) respectively in the tissue supernatants. Briefly, 20 µl of the tissue supernatants was incubated with 10 µl of 3.3 mM Ellman's reagent (pH 7.0) and 50 µl of 0.1 M phosphate buffer (pH 8) for 20 min at 25°C. For acetylcholinesterase activity, the reaction was stopped by adding 10 µl of 0.05 M acetylcholine iodide to the reaction mixture. While 10 µl of 0.05 M butyrylcholine iodide was used to stop the reaction for butyrylcholinesterase activity. Absorbances were read at 412 nm at 3 min intervals.

Purinergic Enzymes Activities

Th brain tissues were assayed for purinergic activities by analyzing for the activity of ecto-nucleoside triphosphate diphosphohydrolase (E-NTPDase) (Akomolafe et al., 2017) in the tissue supernatants. Briefly, 20 µl of the tissue supernatants was incubated with 200 µl of the reaction buffer (1.5 mM CaCl₂, 5 mM KCl, 0.1 mM EDTA, 10 mM glucose, 225 mM sucrose and 45 mM Tris-HCl) at 37°C for 10 min 20 µl of 50 mM ATP was added to the reaction mixture and further incubated at 37°C for 20 min in a shaker. The reaction was stopped with 200 µl of 10%

TCA and incubated on ice for 10 min. Absorbance was read 600 nm.

Determination of Gluconeogenic Enzymes Activities

The gluconeogenic enzymes activities of the brain tissues were determined by analyzing the supernatants for glucose 6 phosphatase (Mahato et al., 2011; Erukainure et al., 2017), and fructose-1,6-bisphosphatase (Gancedo and Gancedo, 1971; Balogun and Ashafa, 2017) activities with slight modifications.

To determine glucose 6 phosphatase activity, 200 μ l of the tissue supernatants was incubated with 100 μ l of 0.25 M glucose, 200 μ l of 5 mM KCl, 1300 μ l of 0.1 M Tris-HCl buffer, and 40 μ l of 50 mM ATP at 37°C in a shaker for 30 min. The reaction was stopped with 1 ml of distilled water and 1.25% ammonium molybdate. 1 ml of freshly prepared 9% ascorbic acid was then added to the reaction mixture and allowed to stand for 30 min. Absorbance was read at 660 nm. ATPase activity was calculated as the amount of inorganic phosphate (Pi) released/min/mg protein.

For fructose-1,6-bisphosphatase activity, 100 μ l of the tissue supernatant was incubated with 1,200 μ l of Tris-HCl buffer (0.1 M, pH 7.0), 100 μ l of fructose (0.05 M), 250 μ l 0.1 M $MgCl_2$, 100 μ l 0.1 M KCl, and 250 μ l 1 mM EDTA at 37°C for 15 min. The reaction was stopped with 1 ml of 10% TCA and incubated on ice for 10 min. Absorbance was read at 680 nm and the activity calculated as the amount of inorganic phosphate (Pi) released/min/mg protein.

3-(4,5-Dimethylthiazol-2-yl)-2,5-Diphenyltetrazolium Bromide Assay

Cell Lines and Cell Culturing

The human U87 MG glioblastoma cancer (ATCC® HTB-14™) cell line was obtained from the American Type Culture Collection (ATCC, Virginia, United States). Dulbecco's Minimum Essential Media (DMEM), Eagle's Minimum Essential Media (EMEM), Fetal bovine serum (FBS) and Phosphate Buffer Saline (PBS) were purchased from Life technologies (Pty) Ltd. (Fairlands, Johannesburg, RSA). The 3-(4,5-Dimethylthiazol-2-yl)-2,5-Diphenyltetrazolium Bromide (MTT), Dimethyl Sulfoxide (DMSO), Trypsin, and all other chemicals and reagents were of analytical grade and acquired from Merck (Pty) Ltd. (Modderfontein, Johannesburg, RSA). The U87 cell line was maintained in DMEM:EMEM (1:1), supplemented with 10% heat-inactivated FBS and grown at 37°C in a humidified incubator set at 5% CO₂. Cells were sub-cultured with 0.25% (w/v) trypsin 0.53 mM ethylenediaminetetraacetic acid (EDTA) for a maximum of 15 min every 2 and 3 days after they had formed an 80% confluent monolayer.

Cell Proliferation Assay

To analyze the effect of the samples on the cell viability, the MTT method was utilized. Cells were seeded in 100 μ l medium in 96-well microtiter plates at a concentration of 1×10^5 . Stock

solutions of 4 mg/ml of the samples were prepared in 20% ethanol. The positive control, doxorubicin was dissolved in 50% DMSO to obtain a stock concentration of 10 mg/mL. Serial dilutions were made to achieve target concentrations of the samples and doxorubicin in a range 30, 60, 120, 240 μ g/ml and 12.5–100 μ g/ml, respectively. Subsequently, cells were exposed to the samples, doxorubicin and the controls, which included vehicle-treated cells exposed to 1.2% ethanol or 0.5% DMSO and cells propagated in growth medium. After the 48 h treatment period, the cells were subjected to the MTT reagent (0.5 mg/mL). The colorimetric reaction was measured by means of a plate reader (Multiskan Go, Thermofischer Scientific) at 570 nm wavelength. Color control blanks were included and utilized to normalize the results and the vehicle control treated cells were regarded as 100% cell viability. The samples were evaluated in at least three independent experimental repeats and each sample was evaluated in triplicate for each experimental repeat. The results given are representative of the average percentage inhibition of all the experimental repeats.

GC-MS analysis of *Cannabis sativa* Extracts Apparatus

An Agilent technologies 6890N GC-MS machine coupled with a 5973-network mass selective detector was used for the analysis. An Agilent technologies 7683 Series injector and screw neck glass vials (separations) were used for sample injection.

GC-MS Conditions

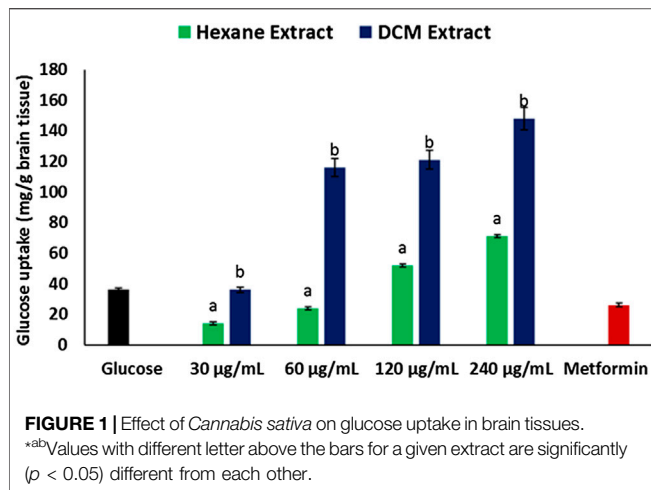
The extracts were analyzed using a HP-5ms capillary column phase. The injection volume was set to 2 μ l at 80°C. the flow rate of the helium gas was 1 ml/min at a constant flow. The oven program was set at 80°C for 2 min and increased to 300°C at 20°C/min for 3 min. A mass selective detector was used for the detection of the volatile compounds present in the standards and tests samples. The NIST mass spectral library database software was used to analyze the data. The mass spectrometer data system has a reporting software module that combines the data results with the NIST library and ADMIS software search for target compounds into a single report.

In Silico Prediction of Blood Brain Barrier Permeability and Oral Lethal Dose Toxicity

The ability of the GC-MS identified compound to cross the BBB was predicted *in silico* using the SwissADME online server (<http://www.swissadme.ch/index.php>) (Daina et al., 2017). Its oral lethal dose toxicity (LD₅₀) and toxicity class were predicted using the PROTOX II online server (http://tox.charite.de/protox_II/) (Banerjee et al., 2018). These were done by obtaining the Canonical SMILES of the GC-MS identified compound from PubChem (<https://pubchem.ncbi.nlm.nih.gov/>), and computed into the respective servers for the predictions.

Statistical Analysis

Data were subjected to one-way ANOVA and presented as mean \pm SD. Significant differences between means at $p < 0.05$ were obtained using the Tukey's HSD-multiple range post-hoc



test. Statistical analyses were done using IBM Statistical Package for the Social Sciences (SPSS) for Windows, version 23.0 (IBM Corp., Armonk, NY, United States).

RESULTS

Incubation of brain tissues with glucose in the presence of hexane and DCM extracts of *C. sativa* leaves led to significant ($p < 0.05$)

increase in glucose utilization, with the DCM extract having a higher activity as depicted in **Figure 1**. The activity was dose-dependent, with the highest concentration having the highest activity. Incubation with metformin had no significant effect on brain glucose utilization.

Incubation of brain tissues with glucose led to significant ($p < 0.05$) depletion in the levels of GSH, SOD and catalase activities, while significantly elevating MDA level as shown in **Figures 2A–D**. Incubation with the extracts significantly ($p < 0.05$) reversed these levels and activities dose-dependently to near normal.

As shown in **Figure 3**, incubation with glucose led to significant ($p < 0.05$) elevation of NO level in brain tissues. This level was significantly ($p < 0.05$) depleted on incubation with *C. sativa* extracts.

There was a significant ($p < 0.05$) elevation in acetylcholinesterase and butyrylcholinesterase activities in brain tissues incubated with glucose as depicted in **Figures 4A,B**. The acetylcholinesterase activity was significantly ($p < 0.05$) reversed dose-dependently on incubation with DCM extract (**Figure 4A**). However, the hexane extract significantly ($p < 0.05$) elevated acetylcholinesterase activity dose-dependently (**Figure 4A**). Both extracts significantly ($p < 0.05$) depleted butyrylcholinesterase activity in a dose-dependent manner (**Figure 4B**).

As shown in **Figure 5**, there was a significant ($p < 0.05$) depletion in E-NTPDase activity in brain tissues incubation with

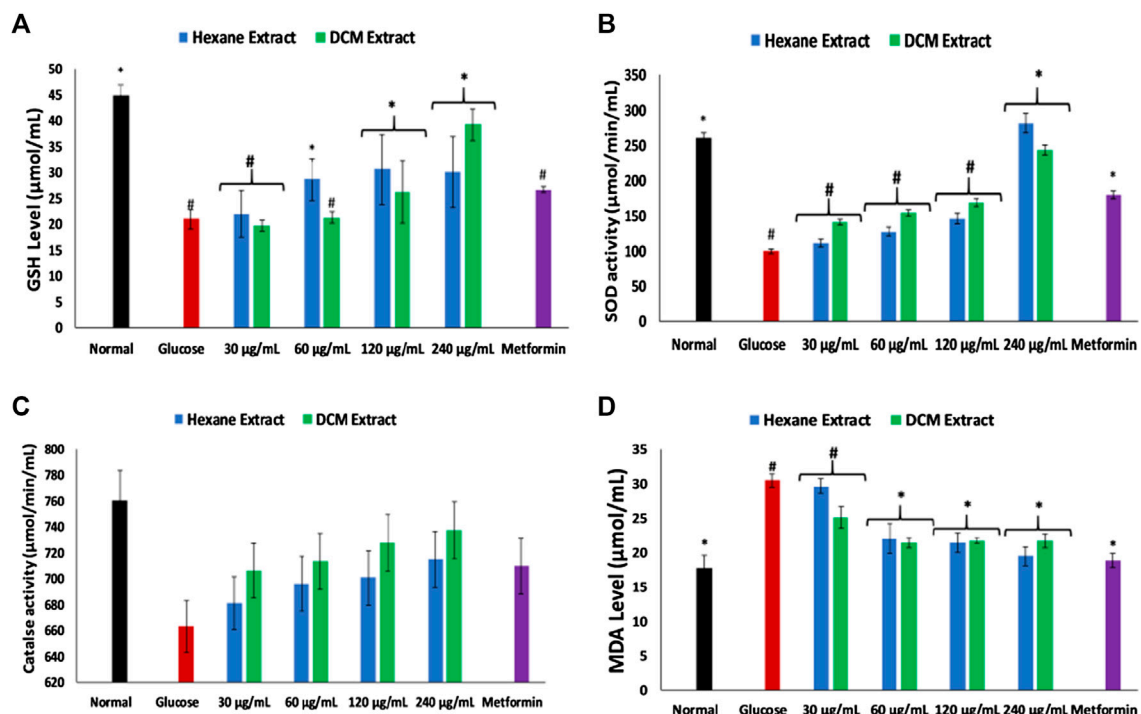


FIGURE 2 | Effect of *Cannabis sativa* on (A) glutathione (GSH) level, (B) superoxide dismutase (SOD) activity, (C) catalase activity, and (D) malondialdehyde (MDA) level in brain glucose uptake. Value = mean \pm SD; $n = 3$. *Statistically significant ($p < 0.05$) compared to glucose-treated tissue; #statistically significant ($p < 0.05$) compared to normal tissue. Normal, No glucose/*C. sativa*.

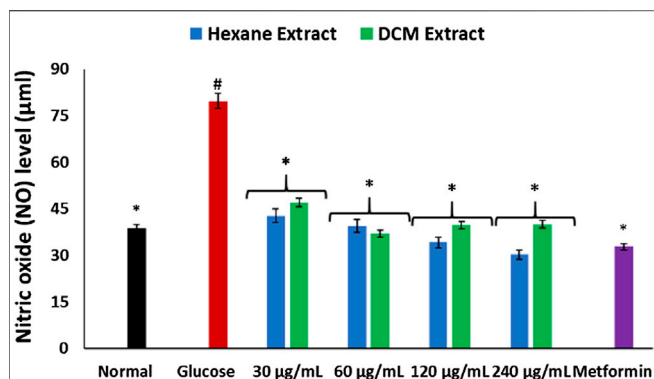


FIGURE 3 | Effect of *Cannabis sativa* on NO level in brain glucose uptake. Values = mean \pm SD; n = 3. *Statistically significant ($p < 0.05$) compared to glucose-treated tissue; #statistically significant ($p < 0.05$) compared to normal tissue. Normal, No glucose/*C. sativa*.

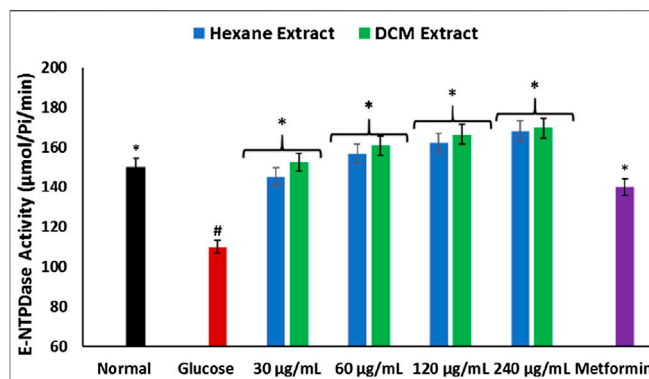


FIGURE 5 | Effect of *Cannabis sativa* on ecto-nucleoside triphosphate diphosphohydrolase activity in brain glucose uptake. Values = mean \pm SD; n = 3. *Statistically significant ($p < 0.05$) compared to glucose-treated tissue; #statistically significant ($p < 0.05$) compared to normal tissue. Normal, No glucose/*C. sativa*.

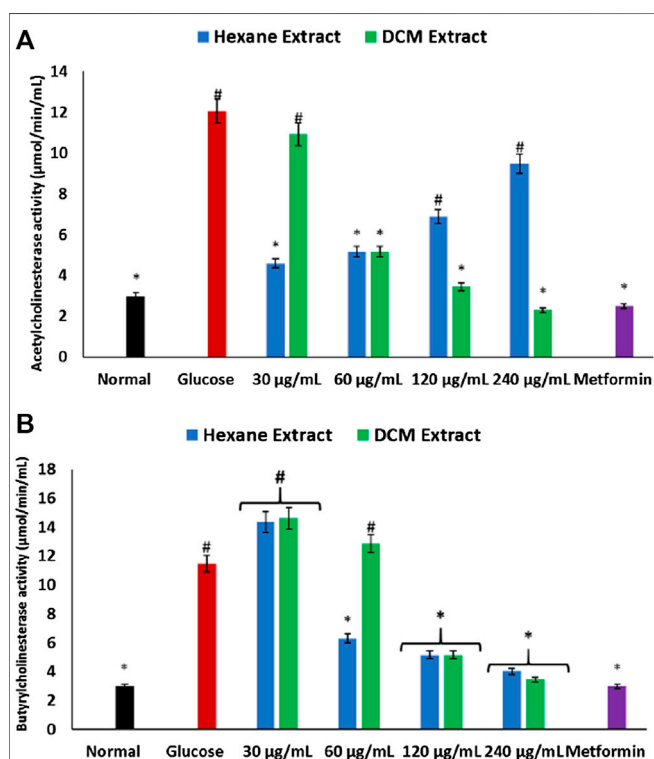


FIGURE 4 | Effect of *Cannabis sativa* on (A) acetylcholinesterase and (B) butyrylcholinesterase activities in brain glucose uptake. Values = mean \pm SD; n = 3. *Statistically significant ($p < 0.05$) compared to glucose-treated tissue; #statistically significant ($p < 0.05$) compared to normal tissue. Normal, No glucose/*C. sativa*.

glucose only. Incubation with *C. sativa* extracts led to significant ($p < 0.05$) reversion of the activity to levels indistinguishable from the normal tissues.

As depicted in **Figures 6A,B**, there was a significant ($p < 0.05$) elevation in the activities of glucose 6-phosphatase and fructose-1,6-biphosphate in brain tissues incubated with glucose only. These activities were significantly ($p < 0.05$) reversed in tissues incubated with *C. sativa* extracts to levels indistinguishable from the normal tissues.

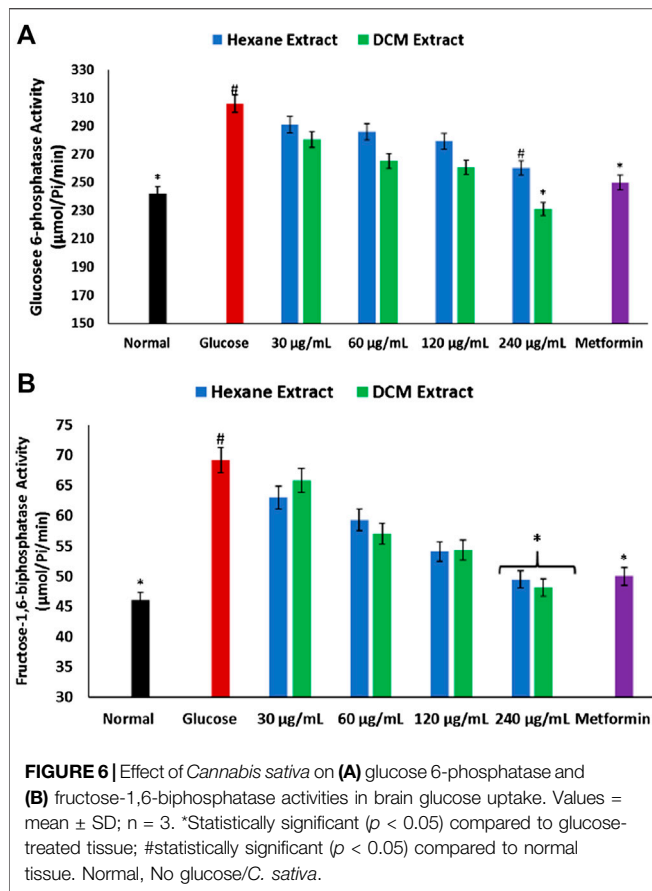
MTT assay revealed *C. sativa* extracts had little or no cytotoxic effect on U87 MG cells, while doxorubicin significantly ($p < 0.05$) inhibited the proliferation of the cells as depicted in **Figure 7**.

GC-MS analysis of the extracts revealed the presence of THC in both extracts as shown in **Figure 8; Supplementary Figure S1**.

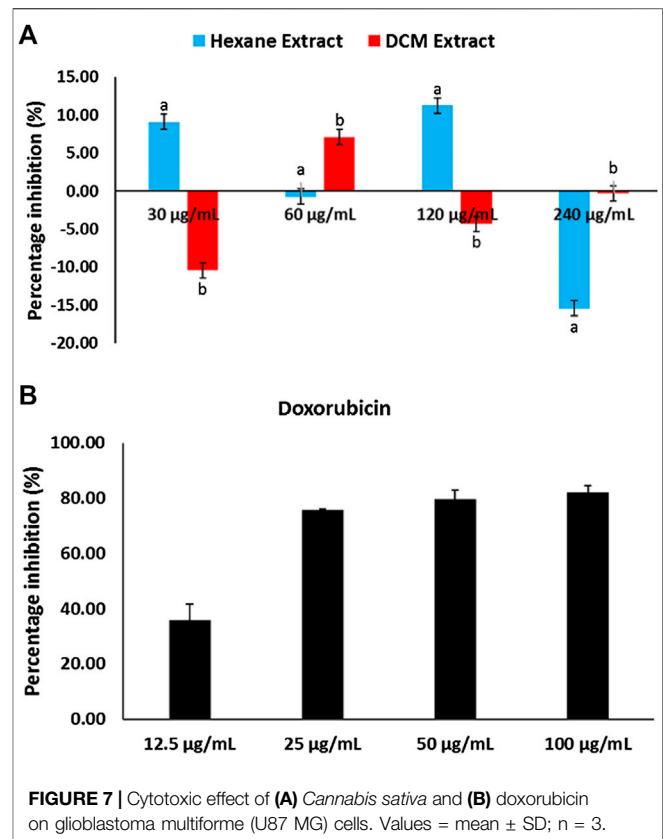
In silico BBB permeability prediction revealed THC to be permeable across the BBB as shown in **Table 1**. THC was further predicted *in silico* to be in the toxic class of 4, with a LD₅₀ value of 482 mg/kg.

DISCUSSION

Impaired brain glucose uptake leading to diminished neuronal glucose consumption has been linked to the pathogenesis and progression of neurodegenerative diseases such as Alzheimer's and Parkinson's diseases (Zilberter and Zilberter, 2017; An et al., 2018). In the present study, the increased glucose uptake in brain tissues incubated with *C. sativa* extracts (**Figure 1**) indicates an increased glucose utilization which insinuates an increased neuronal glucose consumption. This activity portrays a facilitative uptake potential of *C. sativa* leaves which corresponds with previous studies on the use of medicinal plant leaves in facilitating brain glucose uptake (Erukainure et al., 2019c). This activity can be attributed to the GC-MS identified compound in the extracts, THC (**Figs. 8 and S1**) which can bind and activate the cannabinoid receptors of the endocannabinoid anandamide transporters at the BBB (Maccarrone et al., 2006). Thus, facilitating transportation across the BBB.



Oxidative stress and proinflammation have been implicated in the pathogenesis of neurological diseases, and have been reported among the major mechanisms in the etiology of the diseases (Wajner et al., 2004; Mahadik et al., 2006). The depleted GSH level, SOD and catalase activities on incubation of brain tissues with glucose (Figures 2A–C) insinuates an oxidative state. This is further revealed by the exacerbated MDA level (Figure 2D) which indicates an occurrence of lipid peroxidation. This is in agreement with previous studies on exacerbated oxidative activities in brain tissues incubated with glucose (Erukainure et al., 2019c). The brain has been reported for its high susceptibility to oxidative stress owing to its polyunsaturated fatty acids contents, redox-active metal load, low endogenous antioxidant system, and auto-oxidizable neurotransmitters dependence (Butterfield et al., 2001; Huang et al., 2004; Patel, 2016; Erukainure et al., 2019c). The increased brain NO level (Figure 3) with concomitant low SOD activity on incubation with glucose may insinuate a proinflammatory effect. In the presence of depleted SOD activity, peroxynitrite (ONOO[−]) is generated from the reaction of NO and superoxide (O₂[−]) (Erukainure et al., 2020; Salau et al., 2020). Peroxynitrite has been reported for its potent proinflammatory roles in several diseases including neuropathy as it has been implicated in the pathogenesis of Alzheimer's and Parkinson's diseases, and multiple sclerosis (Smith et al., 1997; Pacher et al., 2007). Antioxidants have been reported for their therapeutic roles in the treatment and



management of neurodegenerative diseases (Gilgun-Sherki et al., 2001; Kim et al., 2015). The elevated GSH level, SOD and catalase activities, with concomitant depleted levels of MDA and NO on incubation with *C. sativa* extracts indicate an antioxidative and anti-proinflammatory effect. THC has been reported for its potent antioxidant and anti-proinflammatory activities in the treatment and management of neurological diseases (Hampson et al., 1998; Costa, 2007; Borges et al., 2013). Thus, may be responsible for the antioxidative effect of the extracts.

Cholinergic dysfunction has been recognized as one of the major defects of neurodegenerative diseases such as Alzheimer's, Parkinson's diseases and multiple sclerosis (Greig et al., 2002). It is characterized by increased activities of acetylcholinesterase and butyrylcholinesterase which catalyze the hydrolysis of the neurotransmitter acetylcholine (Reid et al., 2013). Thus, implying that the elevated activities of these enzymes on incubation of brain tissues with glucose (Figures 4A,B) indicates a cholinergic dysfunction and may insinuate a neurodegenerative symptom. Several therapies have targeted the inhibition of these enzymes in the treatment and management of neurodegenerative diseases (Erukainure et al., 2019a; Salau et al., 2020b). Thus, the inhibitory effect of the extracts on these enzymes portrays a neuroprotective activity of *C. sativa*. This corroborates previous reports on the inhibitory effect of *C. sativa* and its major phytochemical constituents on acetylcholinesterase and butyrylcholinesterase activities (Eubanks et al., 2006; Abdel-Salam et al., 2018). However, the increasing acetylcholinesterase activity with increasing

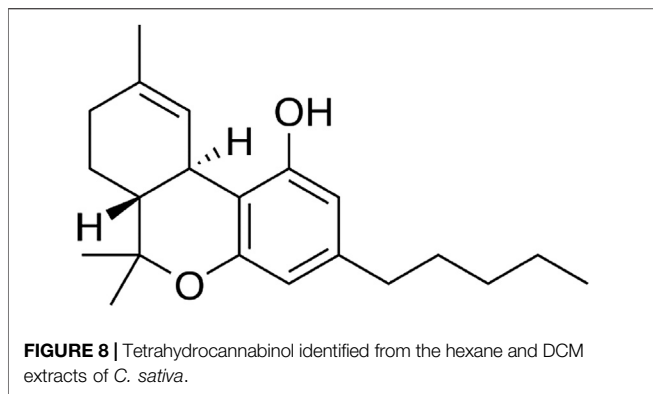


TABLE 1 | In silico prediction of BBB permeability and toxicity of tetrahydrocannabinol.

In Silico activity	Predictions
LD ₅₀	482 mg/kg
Toxicity class	4
BBB permeability	Yes

BBB, blood brain barrier; LD₅₀, ethal dose.

concentration of the hexane extract (**Figure 4A**) may insinuate the inhibitory effect of the extract on the enzyme diminishes with increasing concentrations.

The depleted E-NTPDase activity in brain tissues incubated with glucose (**Figure 5**) indicates a depleted adenosine level which portrays a decreased purinergic activity. Impaired purinergic activity has been implicated in the pathogenesis of neurodegenerative diseases (Akomolafe et al., 2017; Salau et al., 2020). It is characterized by decreased production of adenosines which are involved in energy transfer reactions and facilitative transportation (Akomolafe et al., 2017). The increased E-NTPDase activity in brain tissues incubated with *C. sativa* extracts insinuates the ability of *C. sativa* to improve neuronal purinergic activity.

Diminished brain glucose consumption is often characterized by increased glycogenolysis and impaired glycolytic flux to compensate for the low glucose level (Hoyer, 1996; Atlante et al., 2017). This has been implicated in the pathogenesis of Alzheimer and other neurodegenerative diseases (Atlante et al., 2017). In the present study, the depleted brain glucose consumption (**Figure 1**) corroborates with the exacerbated glucose 6-phosphatase and fructose-1,6-biphosphatase activities in brain tissues incubated in glucose (**Figures. 6A,B**). Both enzymes are involved in gluconeogenesis, with glucose 6-phosphatase and fructose-1,6-biphosphatase catalyzing the hydrolysis of glucose 6-phosphate to glucose in the glycogenolytic pathway and fructose-1,6-biphosphate to fructose 6-phosphate in the gluconeogenic pathway respectively. The continuous activation of these enzymes will lead to glucose accumulation which can serve as metabolite precursors for the hexosamine, polyol, protein kinase C, and AGE pathways which have been linked to the pathogenesis of neurodegenerative diseases (Li et al., 2012; Xu et al., 2016).

Glucose has also been reported as an intermediate for the generation of free radicals, as it is oxidized in its enediol form into reactive ketoaldehydes and superoxide anion radicals (Maritim et al., 2003). Thus, the dose-dependent inhibited activity of these enzymes in brain tissues incubated with *C. sativa* extracts further indicates the neuroprotective effect of *C. sativa*.

Glioblastoma multiforme (GBM) is a malignant primary brain tumor common in young kids (Erukainure et al., 2018). Studies have reported therapeutic failures in patients owing to difficulty in treatment (Puli et al., 2006). Although medicinal plants have reported to arrest the proliferation of GBM (Erukainure et al., 2018), *C. sativa* extracts showed no cytotoxic effect on the cells (**Figure 7**). Thus, insinuating that the plant may not be beneficial in the treatment of GBM.

The predicted ability of THC to permeate the BBB (**Table 1**) further connotes the neuroprotective effect of *C. sativa* and corroborates previous reports on the ability of cannabinoids to modulate the cannabinoid receptors of anandamide transport across the BBB (Maccarrone et al., 2006). The predicted oral LD₅₀ and toxicity class values of THC (**Table 1**) indicates that the compound is relatively safe when orally consumed.

CONCLUSION

As portrayed by these results, *C. sativa* improves glucose consumption with concomitant suppression of oxidative stress and cholinergic dysfunction, and modulation of purinergic and gluconeogenic activities in brain tissues. Further studies are recommended to decipher the molecular mechanisms that may be involved in these neuroprotective activities in *in vivo* studies.

DATA AVAILABILITY STATEMENT

The original contributions presented in the study are included in the article/**Supplementary Material**, further inquiries can be directed to the corresponding author.

ETHICS STATEMENT

The animal study was reviewed and approved by The animal ethics committee of the University of KwaZulu-Natal, Durban, South Africa (protocol approval number: AREC/020/017D).

AUTHOR CONTRIBUTIONS

MM and OE conceptualized and designed the research project; OE, VS and MI carried out the experiments; MM and OE wrote the original manuscript; all authors revised and approved the final manuscript draft; MM supervised the project.

FUNDING

Authors are thankful to IKS Based Technology Innovation Unit of DSI South Africa, for financial support (Grant contracts: DST/CON 0162/201 and DST/CON 0206/2019/2020) and University of the Free State for technical support and postdoctoral support for OE.

ACKNOWLEDGMENTS

The authors are also thankful for the assistance and support from the Free State Provincial Police and the Police at Port St Johns and Lusikisiki in the Eastern Cape. The authors are further thankful to

Mirrada Javu, senior community liaison officer, Department of Pharmacology UFS for community engagement and negotiations on the cannabis collections. Similar appreciation goes to LR Mafura and SE Molomo both from the Ministry of Forestry, Range, Soil & Water Conservation, Mafeteng, Lesotho for the assistance with the cannabis project and cannabis plants wild collections.

SUPPLEMENTARY MATERIAL

The Supplementary Material for this article can be found online at: <https://www.frontiersin.org/articles/10.3389/fphar.2020.592981/full#supplementary-material>

REFERENCES

- Abdel-Salam, O. E., Sleem, A., Youness, E., and Morsy, F. (2018). Preventive effects of cannabis on neurotoxic and hepatotoxic activities of malathion in rat. *Asian Pac. J. Trop. Med.* 11, 272–279. doi:10.4103/1995-7645.231467
- Adefegha, S. A., Oboh, G., Oyeleye, S. I., Dada, F. A., Ejakpovi, I., and Boligon, A. A. (2017). Cognitive enhancing and antioxidative potentials of velvet beans (*Mucuna pruriens*) and horseradish (*Moringa oleifera*) seeds extracts: a comparative study. *J. Food Biochem.* 41, e12292. doi:10.1111/jfbc.12292
- Ademiluyi, A. O., Ogunsuyi, O. B., and Oboh, G. (2016). Alkaloid extracts from Jimson weed (*Datura stramonium* L.) modulate purinergic enzymes in rat brain. *Neurotoxicology* 56, 107–117. doi:10.1016/j.neuro.2016.06.012
- Aebi, H. (1984). [13] Catalase *in vitro*. *Methods Enzymol.* 105, 121–126. doi:10.1016/s0076-6879(84)05016-3
- Akomolafe, S. F., Akinyemi, A. J., Ogunsuyi, O. B., Oyeleye, S. I., Oboh, G., Adeoyo, O. O., et al. (2017). Effect of caffeine, caffeic acid and their various combinations on enzymes of cholinergic, monoaminergic and purinergic systems critical to neurodegeneration in rat brain *in vitro*. *Neuro. Toxicol.* 62, 6–13. doi:10.1016/j.neuro.2017.04.008
- An, Y., Varma, V. R., Varma, S., Casanova, R., Dammer, E., Pletnikova, O., et al. (2018). Evidence for brain glucose dysregulation in Alzheimer's disease. *Alzheimer's Dementia*. 14, 318–329. doi:10.1016/j.jalz.2017.09.011
- Andre, C. M., Hausman, J.-F., and Guerriero, G. (2016). *Cannabis sativa*: the plant of the thousand and one molecules. *Front. Plant Sci.* 7, 19. doi:10.3389/fpls.2016.00019
- Atlante, A., De Bari, L., Bobba, A., and Amadoro, G. (2017). A disease with a sweet tooth: exploring the Warburg effect in Alzheimer's disease. *Biogerontology* 18, 301–319. doi:10.1007/s10522-017-9692-x
- Balogun, F. O., and Ashafa, A. O. T. (2017). Aqueous root extracts of *Dicoma anomala* (Sond.) extenuates postprandial hyperglycaemia *in vitro* and its modulation on the activities of carbohydrate-metabolizing enzymes in streptozotocin-induced diabetic Wistar rats. *South Afr. J. Bot.* 112, 102–111. doi:10.1016/j.sajb.2017.05.014
- Banerjee, P., Eckert, A. O., Schrey, A. K., and Preissner, R. (2018). ProTox-II: a webserver for the prediction of toxicity of chemicals. *Nucleic Acids Res.* 46, W257–W263. doi:10.1093/nar/gky318
- Bonini, S. A., Premoli, M., Tambaro, S., Kumar, A., Maccarinelli, G., Memo, M., et al. (2018). *Cannabis sativa*: a comprehensive ethnopharmacological review of a medicinal plant with a long history. *J. Ethnopharmacol.* 227, 300–315. doi:10.1016/j.jep.2018.09.004
- Borges, R., Batista, J., Viana, R., Baetas, A., Orestes, E., Andrade, M., et al. (2013). Understanding the molecular aspects of tetrahydrocannabinol and cannabidiol as antioxidants. *Molecules* 18, 12663–12674. doi:10.3390/molecules181012663
- Butterfield, D. A., Drake, J., Pocernich, C., and Castegna, A. (2001). Evidence of oxidative damage in Alzheimer's disease brain: central role for amyloid β -peptide. *Trends Mol. Med.* 7, 548–554. doi:10.1016/s1471-4914(01)02173-6
- Campos, A. C., Fogaça, M. V., Scarante, F. F., Joca, S. R., Sales, A. J., Gomes, F. V., et al. (2017). Plastic and neuroprotective mechanisms involved in the therapeutic effects of cannabidiol in psychiatric disorders. *Front. Pharmacol.* 8, 269. doi:10.3389/fphar.2017.00269
- Chowdhury, P., and Soulsby, M. (2002). Lipid peroxidation in rat brain is increased by simulated weightlessness and decreased by a soy-protein diet. *Ann. Clin. Lab. Sci.* 32, 188–192.
- Costa, B. (2007). On the pharmacological properties of d9-tetrahydrocannabinol (THC). *Curr. Biol.* 4, 1664–1677. doi:10.1002/cbdv.200790146
- Daina, A., Michielin, O., and Zoete, V. (2017). SwissADME: a free web tool to evaluate pharmacokinetics, drug-likeness and medicinal chemistry friendliness of small molecules. *Sci. Rep.* 7, 42717. doi:10.1038/srep42717
- Duran-Aniotz, C., and Hetz, C. (2016). Glucose metabolism: a sweet relief of Alzheimer's disease. *Curr. Biol.* 26, R806–R809. doi:10.1016/j.cub.2016.07.060
- Ellman, G. L. (1959). Tissue sulfhydryl groups. *Arch. Biochem. Biophys.* 82, 70–77. doi:10.1016/0003-9861(59)90090-6
- Ellman, G. L., Courtney, K. D., Andres, V., Jr, and Featherstone, R. M. (1961). A new and rapid colorimetric determination of acetylcholinesterase activity. *Biochem. Pharmacol.* 7, 88–95. doi:10.1016/0006-2952(61)90145-9
- Erukainure, O. L., Ashraf, N., Naqvi, A. S., Zaruwa, M. Z., Muhammad, A., Odusote, A. D., et al. (2018). Fatty acids rich extract from *clerodendrum volubile* suppresses cell migration; abates oxidative stress; and regulates cell cycle progression in glioblastoma multiforme (U87 MG) cells. *Front. Pharmacol.* 9, 251. doi:10.3389/fphar.2018.00251
- Erukainure, O. L., Chukwuma, C. I., Matsabisa, M. G., Salau, V. F., Koorbanally, N. A., and Islam, M. S. (2020). *Buddleja saligna* Willd (Loganiaceae) inhibits angiotensin-converting enzyme activity in oxidative cardiopathy with concomitant modulation of nucleotide hydrolyzing enzymatic activities and dysregulated lipid metabolic pathways. *J. Ethnopharmacol.* 248, 112358. doi:10.1016/j.jep.2019.112358
- Erukainure, O. L., Ijomone, O. M., Oyeboode, O. A., Chukwuma, C. I., Aschner, M., and Islam, M. S. (2019a). Hyperglycemia-induced oxidative brain injury: therapeutic effects of *Cola nitida* infusion against redox imbalance, cerebellar neuronal insults, and upregulated Nrf2 expression in type 2 diabetic rats. *Food Chem. Toxicol.* 127, 206–217. doi:10.1016/j.fct.2019.03.044
- Erukainure, O. L., Ijomone, O. M., Sanni, O., Aschner, M., and Islam, M. S. (2019b). Type 2 diabetes induced oxidative brain injury involves altered cerebellar neuronal integrity and elemental distribution, and exacerbated Nrf2 expression: therapeutic potential of raffia palm (*Raphia hookeri*) wine. *Metab. Brain. Dis.* 34, 1385–1399. doi:10.1007/s11011-019-00444-x
- Erukainure, O. L., Mopuri, R., Oyeboode, O. A., Koorbanally, N. A., and Islam, M. S. (2017). *Dacryodes edulis* enhances antioxidant activities, suppresses DNA fragmentation in oxidative pancreatic and hepatic injuries; and inhibits carbohydrate digestive enzymes linked to type 2 diabetes. *Biomed. Pharmacother.* 96, 37–47. doi:10.1016/j.biopha.2017.09.106
- Erukainure, O. L., Oyeboode, O. A., Ibeji, C. U., Koorbanally, N. A., and Islam, M. S. (2019c). *Vernonia amygdalina* Del. stimulated glucose uptake in brain tissues enhances antioxidative activities; and modulates functional chemistry and dysregulated metabolic pathways. *Metab. Brain. Dis.* 34, 721–732. doi:10.1007/s11011-018-0363-7
- Eubanks, L. M., Rogers, C. J., Beuscher, A. E., Koob, G. F., Olson, A. J., Dickerson, T. J., et al. (2006). A molecular link between the active component of marijuana and Alzheimer's disease pathology. *Mol. Pharm.* 3, 773–777. doi:10.1021/mp060066m
- Fernández-Ruiz, J., Sagredo, O., Pazos, M. R., García, C., Pertwee, R., Mechoulam, R., et al. (2013). Cannabidiol for neurodegenerative disorders: important new clinical applications for this phytocannabinoid? *Br. J. Clin. Pharmacol.* 75, 323–333. doi:10.1111/j.1365-2125.2012.04341.x
- Fusar-Poli, P., Crippa, J. A., Bhattacharyya, S., Borgwardt, S. J., Allen, P., Martin-Santos, R., et al. (2009). Distinct effects of d9-tetrahydrocannabinol and

- cannabidiol on neural activation during emotional processing. *Arch. Gen. Psychiatr.* 66, 95–105. doi:10.1001/archgenpsychiatry.2008.519
- Gancedo, J. M., and Gancedo, C. (1971). Fructose-1,6-diphosphatase, phosphofructokinase and glucose-6-phosphate dehydrogenase from fermenting and non fermenting yeasts. *Arch. Mikrobiol.* 76, 132–138. doi:10.1007/bf00411787
- Gee, D. J., and Davison, A. J. (1989). Book review: pathology of neck injury. *Med. Sci. Law* 29, 271. doi:10.1016/0891-5849(89)90054-3
- Gejl, M., Brock, B., Egefjord, L., Vang, K., Rungby, J., and Gjedde, A. (2017). Blood-brain glucose transfer in Alzheimer's disease: effect of GLP-1 Analog treatment. *Sci. Rep.* 7, 17490. doi:10.1038/s41598-017-17718-y
- Gilgun-Sherki, Y., Melamed, E., and Offen, D. (2001). Oxidative stress induced-neurodegenerative diseases: the need for antioxidants that penetrate the blood brain barrier. *Neuropharmacology* 40, 959–975. doi:10.1016/s0028-3908(01)00019-3
- Greig, N. H., Lahiri, D. K., and Sambamurti, K. (2002). Butyrylcholinesterase: an important new target in Alzheimer's disease therapy. *Int. Psychogeriatr.* 14, 77–91. doi:10.1017/s1041610203008676
- Guzmán, M. (2003). Cannabinoids: potential anticancer agents. *Nat. Rev. Cancer* 3, 745. doi:10.1038/nrc1188
- Hampson, A. J., Grimaldi, M., Axelrod, J., and Wink, D. (1998). Cannabidiol and (-)-9-tetrahydrocannabinol are neuroprotective antioxidants. *Proc. Natl. Acad. Sci. U.S.A.* 95, 8268–8273. doi:10.1073/pnas.95.14.8268
- Hoyer, S. (1996). Oxidative metabolism deficiencies in brains of patients with Alzheimer's disease. *Acta Neurol. Scand.* 94, 18–24. doi:10.1111/j.1600-0404.1996.tb05868.x
- Huang, X., Moir, R. D., Tanzi, R. E., Bush, A. I., and Rogers, J. T. (2004). Redox-Active metals, oxidative stress, and Alzheimer's disease pathology. *Ann. N. Y. Acad. Sci.* 1012, 153–163. doi:10.1196/annals.1306.012
- Kim, G. H., Kim, J. E., Rhie, S. J., and Yoon, S. (2015). The role of oxidative stress in neurodegenerative diseases. *Exp. Neurobiol.* 24, 325–340. doi:10.5607/en.2015.24.4.325
- Lafuente, H., Alvarez, F. J., Pazos, M. R., Alvarez, A., Rey-Santano, M. C., Mielgo, V., et al. (2011). Cannabidiol reduces brain damage and improves functional recovery after acute hypoxia-ischemia in newborn pigs. *Pediatr. Res.* 70, 272–277. doi:10.1203/pdr.0b013e3182276b11
- Li, X.-H., Lv, B.-L., Xie, J.-Z., Liu, J., Zhou, X.-W., and Wang, J.-Z. (2012). AGEs induce Alzheimer-like tau pathology and memory deficit via RAGE-mediated GSK-3 activation. *Neurobiol. Aging* 33, 1400–1410. doi:10.1016/j.neurobiolaging.2011.02.003
- Lim, K., See, Y. M., and Lee, J. (2017). A systematic review of the effectiveness of medical cannabis for psychiatric, movement and neurodegenerative disorders. *Clin. Psychopharmacol. Neurosci.* 15, 301. doi:10.9758/cpn.2017.15.4.301
- Lotan, I., Treves, T. A., Roditi, Y., and Djaldetti, R. (2014). Cannabis (medical marijuana) treatment for motor and non-motor symptoms of Parkinson disease. *Clin. Neuropharmacol.* 37, 41–44. doi:10.1097/wnf.000000000000016
- Maccarrone, M., Fiori, A., Bari, M., Granata, F., Gasperi, V., De Stefano, M. E., et al. (2006). Regulation by cannabinoid receptors of anandamide transport across the blood-brain barrier and through other endothelial cells. *Thromb. Haemostasis* 95, 117–127. doi:10.1160/TH05-06-0413
- Mahadik, S. P., Pillai, A., Joshi, S., and Foster, A. (2006). Prevention of oxidative stress-mediated neuropathology and improved clinical outcome by adjunctive use of a combination of antioxidants and omega-3 fatty acids in schizophrenia. *Int. Rev. Psychiatr.* 18, 119–131. doi:10.1080/09540260600581993
- Mahato, A. K., Bhattacharya, S., and Shanthi, N. (2011). Design, synthesis and glucose-6-phosphatase inhibitory activity of diaminoguanidine analogues of 3-guanidinopropionic acid and amino substituted (Pyridin-2-Yl) thiourea derivatives. *J. Pharmaceut. Sci. Res.* 3, 896–902.
- Maritim, A. C., Sanders, R. A., and Watkins, J. B., III (2003). Diabetes, oxidative stress, and antioxidants: a review. *J. Biochem. Mol. Toxicol.* 17, 24–38. doi:10.1002/jbt.10058
- Moosavi, B. Z. J., Tehranipour, M., Mollashahi, M., and Mahmoodzadeh, H. (2013). Neuroprotective effects of *Cannabis sativa* leaves extracts on α -motoneurons density after sciatic nerve injury in rats. *Life. Sci. J.* 10, 644–648.
- Neumann, K., Rojo, L., Navarrete, L., Farias, G., Reyes, P., and Maccioni, R. (2008). Insulin resistance and alzheimer's disease: molecular links & clinical implications. *Curr. Alzheimer Res.* 5, 438–447. doi:10.2174/156720508785908919
- Pacher, P., Beckman, J. S., and Liaudet, L. (2007). Nitric oxide and peroxynitrite in health and disease. *Physiol. Rev.* 87, 315–424. doi:10.1152/physrev.00029.2006
- Patel, M. (2016). Targeting oxidative stress in central nervous system disorders. *Trends Pharmacol. Sci.* 37, 768–778. doi:10.1016/j.tips.2016.06.007
- Pepeu, G., and Grazia Giovannini, M. (2017). The fate of the brain cholinergic neurons in neurodegenerative diseases. *Brain Res.* 1670, 173–184. doi:10.1016/j.brainres.2017.06.023
- Puli, S., Lai, J. C. K., and Bhushan, A. (2006). Inhibition of matrix degrading enzymes and invasion in human glioblastoma (U87MG) cells by isoflavones. *J. Neuro. Oncol.* 79, 135–142. doi:10.1007/s11060-006-9126-0
- Ramar, K., Rosen, I. M., Kirsch, D. B., Chervin, R. D., Carden, K. A., Aurora, R. N., et al. (2018). Medical cannabis and the treatment of obstructive sleep apnea: an American academy of sleep medicine position statement. *J. Clin. Sleep Med.* 14, 679–681. doi:10.5664/jcsm.7070
- Reid, G. A., Chilukuri, N., and Darvesh, S. (2013). Butyrylcholinesterase and the cholinergic system. *Neuroscience* 234, 53–68. doi:10.1016/j.neuroscience.2012.12.054
- Ren, Y., Liang, K., Jin, Y., Zhang, M., Chen, Y., Wu, H., et al. (2016). Identification and characterization of two novel α -glucosidase inhibitory oligopeptides from hemp (*Cannabis sativa* L.) seed protein. *J. Funct. Foods* 26, 439–450. doi:10.1016/j.jff.2016.07.024
- Sagredo, O., García-Arencibia, M., De Lago, E., Finetti, S., Decio, A., and Fernández-Ruiz, J. (2007). Cannabinoids and neuroprotection in basal ganglia disorders. *Mol. Neurobiol.* 36, 82–91. doi:10.1007/s12035-007-0004-3
- Salau, V. F., Erukainure, O. L., Bharuth, V., Ibeji, C. U., Olasehinde, T. A., and Islam, M. S. (2020a). Kolaviron stimulates glucose uptake with concomitant modulation of metabolic activities implicated in neurodegeneration in isolated rat brain, without perturbation of tissue ultrastructural morphology. *Neurosci. Res.* doi:10.1016/j.neures.2020.06.008
- Salau, V. F., Erukainure, O. L., Ibeji, C. U., Olasehinde, T. A., Koorbanally, N. A., and Islam, M. S. (2020). Ferulic acid modulates dysfunctional metabolic pathways and purinergic activities, while stalling redox imbalance and cholinergic activities in oxidative brain injury. *Neurotox. Res.* 37, 944–955. doi:10.1007/s12640-019-00099-7
- Salau, V. F., Erukainure, O. L., Ibeji, C. U., Olasehinde, T. A., Koorbanally, N. A., and Islam, M. S. (2020b). Vanillin and vanillic acid modulate antioxidant defense system via amelioration of metabolic complications linked to Fe²⁺-induced brain tissues damage. *Metab. Brain. Dis.* 35, 727–738. doi:10.1007/s11011-020-00545-y
- Scheper, W., and Hoozemans, J. J. M. (2015). The unfolded protein response in neurodegenerative diseases: a neuropathological perspective. *Acta Neuropathol.* 130, 315–331. doi:10.1007/s00401-015-1462-8
- Smith, M. A., Richey Harris, P. L., Sayre, L. M., Beckman, J. S., and Perry, G. (1997). Widespread peroxynitrite-mediated damage in Alzheimer's disease. *J. Neurosci.* 17, 2653–2657. doi:10.1523/jneurosci.17-08-02653.1997
- Tsikis, D. (2005). Review methods of quantitative analysis of the nitric oxide metabolites nitrite and nitrate in human biological fluids. *Free Radic. Res.* 39, 797–815. doi:10.1080/10715760500053651
- UNODC (2012). Cannabis: a short review. Available at: https://www.unodc.org/documents/drug-prevention-and-treatment/cannabis_review.pdf (Accessed November 12 2019).
- Wajner, M., Latini, A., Wyse, A. T. S., and Dutra-Filho, C. S. (2004). The role of oxidative damage in the neuropathology of organic acidurias: insights from animal studies. *J. Inher. Metab. Dis.* 27, 427–448. doi:10.1023/b:boli.0000037353.13085.e2
- Whiting, P. F., Wolff, R. F., Deshpande, S., Di Nisio, M., Duffy, S., Hernandez, A. V., et al. (2015). Cannabinoids for medical use. *JAMA* 313, 2456–2473. doi:10.1001/jama.2015.6358
- Xu, J., Begley, P., Church, S. J., Patassini, S., Mcharg, S., Kureishy, N., et al. (2016). Elevation of brain glucose and polyol-pathway intermediates with accompanying brain-copper deficiency in patients with Alzheimer's disease: metabolic basis for dementia. *Sci. Rep.* 6, 1–12. doi:10.1038/srep27524
- Zilberter, Y., and Zilberter, M. (2017). The vicious circle of hypometabolism in neurodegenerative diseases: ways and mechanisms of metabolic correction. *J. Neurosci. Res.* 95, 2217–2235. doi:10.1002/jnr.24064

Conflict of Interest: The authors declare that the research was conducted in the absence of any commercial or financial relationships that could be construed as a potential conflict of interest.

Copyright © 2020 Erukainure, Matsabisa, Salau and Islam. This is an open-access article distributed under the terms of the Creative Commons Attribution License (CC BY). The use, distribution or reproduction in other forums is permitted, provided the original author(s) and the copyright owner(s) are credited and that the original publication in this journal is cited, in accordance with accepted academic practice. No use, distribution or reproduction is permitted which does not comply with these terms.



Phytochemistry, Pharmacology and Medicinal Uses of Plants of the Genus *Salix*: An Updated Review

Nora Tawfeek^{1,2}, Mona F. Mahmoud³, Dalia I Hamdan⁴, Mansour Sobeh^{1,5}, Nawaal Farrag², Michael Wink^{1*} and Assem M. El-Shazly^{2*}

¹Institute of Pharmacy and Molecular Biotechnology, Heidelberg University, Heidelberg, Germany, ²Department of Pharmacognosy, Faculty of Pharmacy, Zagazig University, Zagazig, Egypt, ³Department of Pharmacology and Toxicology, Faculty of Pharmacy, Zagazig University, Zagazig, Egypt, ⁴Department of Pharmacognosy, Faculty of Pharmacy, Menoufia University, Shibin Elkom, Egypt, ⁵AgroBioSciences Research Division, Mohammed VI Polytechnic University, Ben-Guerir, Morocco

OPEN ACCESS

Edited by:

Javier Echeverria,
University of Santiago, Chile

Reviewed by:

Souaibou Yaouba,
Université de Lorraine, France
Young-Ji Shiao,
National Research Institute of Chinese
Medicine, Taiwan

*Correspondence:

Michael Wink
wink@uni-heidelberg.de
Assem M. El-Shazly
assem2002@yahoo.co.uk

Specialty section:

This article was submitted to
Ethnopharmacology,
a section of the journal
Frontiers in Pharmacology

Received: 11 August 2020

Accepted: 07 January 2021

Published: 12 February 2021

Citation:

Tawfeek N, Mahmoud MF,
Hamdan DI, Sobeh M, Farrag N,
Wink M and El-Shazly AM (2021)
Phytochemistry, Pharmacology and
Medicinal Uses of Plants of the Genus
Salix: An Updated Review.
Front. Pharmacol. 12:593856.
doi: 10.3389/fphar.2021.593856

The Willows (genus *Salix*), with more than 330–500 species and 200 hybrids, are trees, shrubs or prostrate plants that are widely distributed in Africa, North America, Europe, and Asia. The genus is traditionally used in folk medicine and represents a valuable source of biologically active compounds among them salicin, a prodrug for salicylic acid. Altogether, 322 secondary metabolites were characterized in the genus including flavonoids 94) (flavonols, flavones, flavanones, isoflavones, flavan-3-ols (catechins and procyanidins), chalcones, dihydrochalcone, anthocyanins, dihydroflavonols), phenolic glycosides (76), organic acids (28), and non-phenolic glycosides (17), sterols and terpenes (17), simple phenolics 13) and lignans 7) in addition to volatiles and fatty acids (69). Furthermore, willows exert analgesic, anti-inflammatory, antioxidant, anticancer, cytotoxic, antidiabetic, antimicrobial, antiobesity, neuroprotective and hepatoprotective activities. The current review provides an updated summary of the importance of willows, their chemical composition and pharmacological activities.

Keywords: salix, phytochemistry, pharmacology, medicinal and traditional uses, inflammation

INTRODUCTION

Salicaceae (the Willow and Poplar family) traditionally includes the genera *Populus* (poplar) and *Salix* (willow), which are common in Northern temperate regions, and are amentiferous (bearing catkins) (Isebrands and Richardson, 2014). Presently, the Salicaceae have been enlarged to contain most tropical members of Flacourtiaceae, which do not produce catkin (Thadeo et al., 2014). Thus, the family Salicaceae now comprises about 56 genera and 1,220 species (Christenhusz and Byng, 2016).

The members of Salicaceae are fast growing trees or shrubs (Isebrands and Richardson, 2014). They are used for many economic purposes as production of timber, paper, fences, shelter, snowshoes, arrow shafts, fish traps, whistles, nets, rope, as a biomass fuel (a source of renewable energy), for ornamental, architectural and horticulture uses. Also, they are used for environmental enhancement through soil erosion control (Kuzovkina and Vietto, 2014). Willow twigs are elastic and were used to interweave baskets, for caning, and to manufacture woven fences and other lattices (Isebrands and Richardson, 2014).

The genus *Salix* (the willow) includes 330–500 species and more than 200 hybrids (Isebrands and Richardson, 2014), which are most widely distributed in the Northern hemisphere with a limited

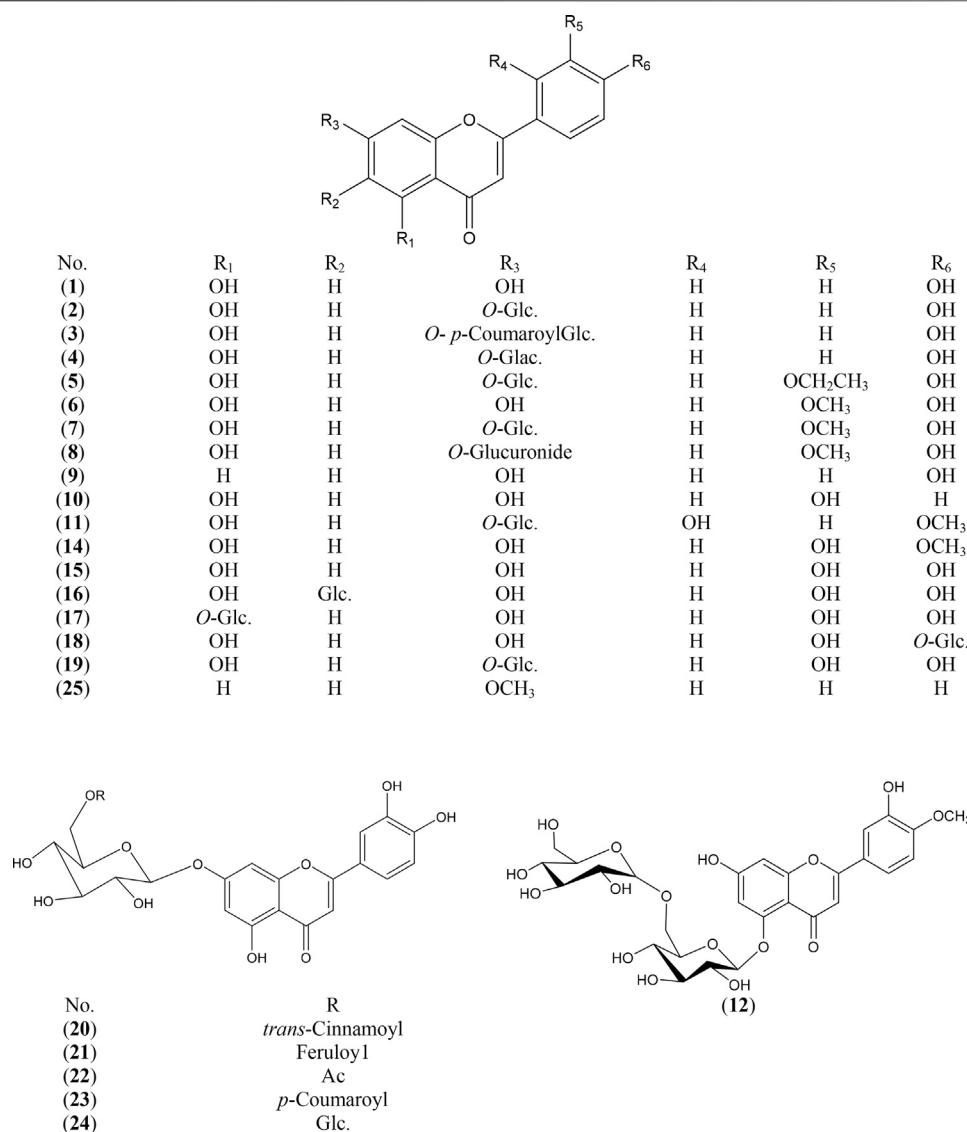


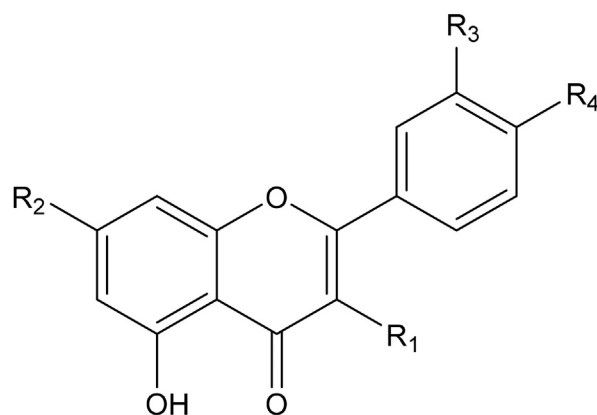
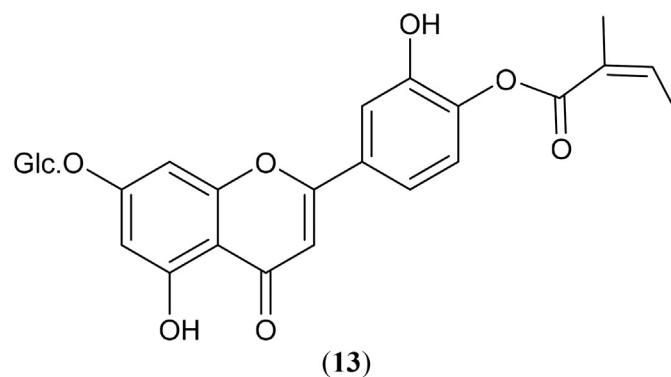
FIGURE 1 | Structures of reported flavonoids from the genus *Salix*.

number of species occur in the Southern hemisphere (Zhen-Fu, 1987). *Salix* species are widely distributed in Africa, North America, Europe, and Asia (Argus, 2007). *Salix* species are fast growing trees, shrubs or prostrate plants; they can withstand a wide range of different weathers more than *Populus* species, as they grow in temperate, subtropic and tropic regions (Isebrands and Richardson, 2014).

Taxonomy

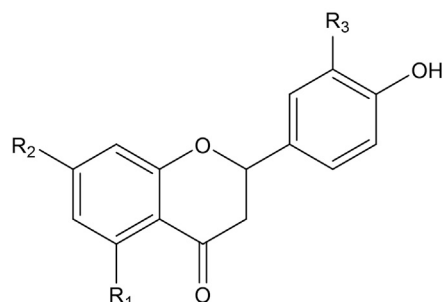
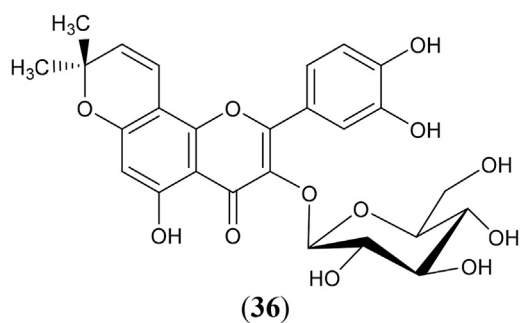
General morphological characters of genus *Salix* were reported (Argus, 2006; Lauron-Moreau, et al., 2015). Willows are 6–10 m high trees or shrubs with spirally arranged, sometimes silvery, oblong leaves. The latter is commonly hairy on the underside and often turn black when drying. Leaves are simple, petiolate showing different shapes of lamina (oblong, linear, ovate, obovate or round), stipulate with linear to rounded stipules

and with entire, serrate or dentate margin. Their arrangement is mostly alternate or rarely opposite (Lauron-Moreau, et al., 2015). The flowers are catkins, dioecious, with nectaries (glands) instead of perianth and they have bracts, which are pale or black, pubescent or glabrate, constant in male flowers and deciduous in female ones. The flowers blossom in spring, generally prior the leaves (Mabberley 2008). The male catkins have mostly two stamens, more prominent yellow, with few species having 3–12 stamens while the female catkins are greenish, have single pistil with single ovary, style, two-lobed stigma and 2 to 42 ovules per each ovary (Mabberley 2008). The nectar of flowering Willow is the first food source for bees in spring. The seeds are small, with limited longevity, fine hairy coat enabling their spread by wind and they germinate after few days of exposure to moistured surfaces (Mabberley 2008). Recently, the taxonomy of neotropical Salicaceae (formerly

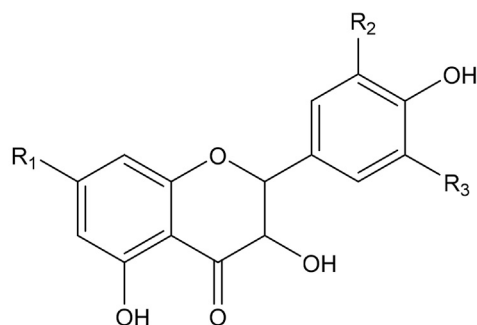


No.	R ₁	R ₂	R ₃	R ₄
(26)	<i>O</i> -Glc.	OH	OCH ₃	OH
(27)	<i>O</i> -Rut.	OH	OCH ₃	OH
(28)	<i>O</i> -Pent.-Rut.	OH	OCH ₃	OH
(29)	<i>O</i> -Rh.	OH	OCH ₃	OH
(30)	<i>O</i> -Pent.-Hex.	OH	OCH ₃	OH
(31)	<i>O</i> -Hex.	OH	H	OCH ₃
(32)	OH	OH	H	OH
(33)	OH	OCH ₃	H	OCH ₃
(34)	OH	<i>O</i> -Glc.	H	OH
(37)	OH	OH	OH	OH
(38)	<i>O</i> -Glc.	OH	OH	OH
(39)	<i>O</i> -Rh.	OH	OH	OH
(40)	<i>O</i> -Glc.	OH	OH	OH
(41)	<i>O</i> -Rut.	OH	OH	OH
(42)	<i>O</i> -Glac.	OH	OH	OH
(43)	<i>O</i> -Gluc.	OH	OH	OH
(44)	<i>O</i> -Hex.-Hex.	OH	OH	OH
(45)	<i>O</i> -Pent.-Rut.	OH	OH	OH
(46)	<i>O</i> -Pent.-Hex.	OH	OH	OH
(47)	OH	OCH ₃	OH	OH

FIGURE 1 | (Continued).



No.	R ₁	R ₂	R ₃
(48)	OH	OH	OH
(49)	OSO ₃ H	OH	OH
(50)	OH	<i>O</i> -Glc.	OH
(51)	OH	OH	H
(52)	OSO ₃ H	OH	H
(53)	<i>O</i> -Glc.	OH	H
(54)	OH	<i>O</i> -Glc.	H
(55)	<i>O</i> -(6''- <i>trans</i> - <i>p</i> -Coumaroyl) glucosyl	OH	H



No.	R ₁	R ₂	R ₃
(56)	OH	OH	OH
(57)	OH	H	H
(58)	OSO ₃ H	H	H
(59)	OH	OH	H
(60)	OSO ₃ H	OH	H
(61)	OCH ₃	OH	H
(62)	OCH ₃	<i>O</i> -Glc.	H

FIGURE 1 | (Continued).

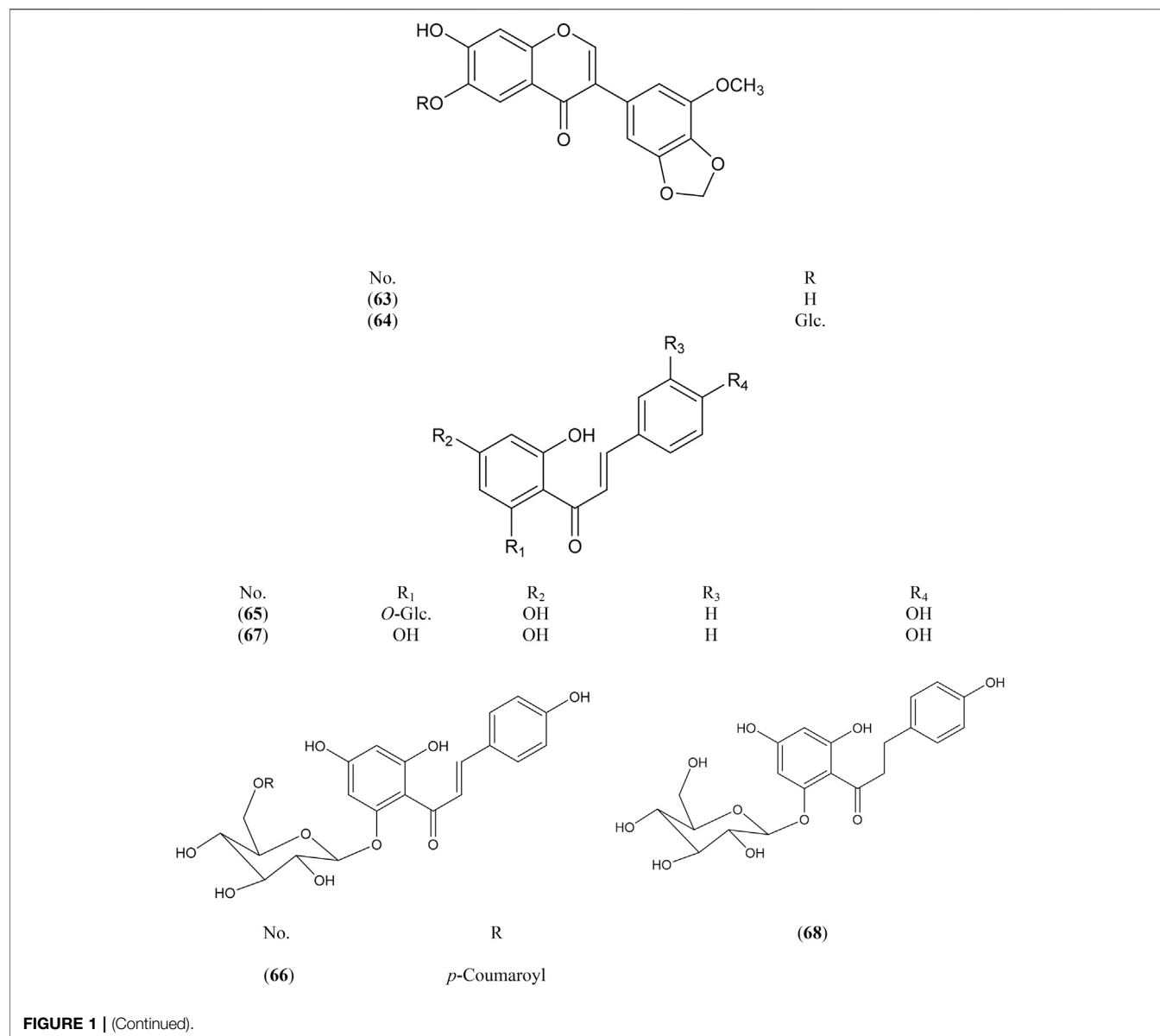


FIGURE 1 | (Continued).

Flacourtiaceae) is difficult, as they show very different morphology and exhibit numerous characteristics in common with several other families. The neotropical Salicaceae and Salicaceae displayed similar characters such as the presence of salicoid leaf teeth, collateral and arch-shaped vascular system at the midrib, abundance of crystals, brachyparacytic stomata, secondary growth of the petiole and sclerenchyma accompanying the bundles (Thadeo et al., 2014).

Phytochemistry

Different phytoconstituents or secondary metabolites of the genus *Salix* as flavonoids, glycosides (phenolic and non-phenolic glycosides), procyanidins, organic acids and their derivatives, simple phenolics, sterols and terpenes, lignans, volatiles and fatty acids were reported (Supplementary Tables S1–S7, included in Supplementary materials). *Salix* leaves mainly

contain flavonoids, phenolic acids, their derivatives, and phenolic glycosides, while stem bark mainly contains procyanidins.

Flavonoids

Salix contains a wide variety of flavonoids, which are distinctive for each species, as flavones, flavonols, flavanones, dihydroflavonols, isoflavones, chalcones, dihydrochalcones, flavan-3-ols and anthocyanins (Nasudari et al., 1972; Pobłocka-Olech and Krauze-Shao et al., 1989; Du et al., 2004; Zeid, 2006; Jürgenliemk et al., 2007; Baranowska, 2008; Freischmidt et al., 2010; Li et al., 2013). Data are summarized in **Supplementary Table S1** and the structures are presented in **Figure 1**.

The highest numbers of different classes of flavonoids (A–E) were detected in leaves and rarely in roots. The flavones as apigenin and its glycosides (1, 2, 4, 5) are major constituents of *S. acutifolia* Willd. leaves (Shelyuto and Bondarenko, 1985), *S.*

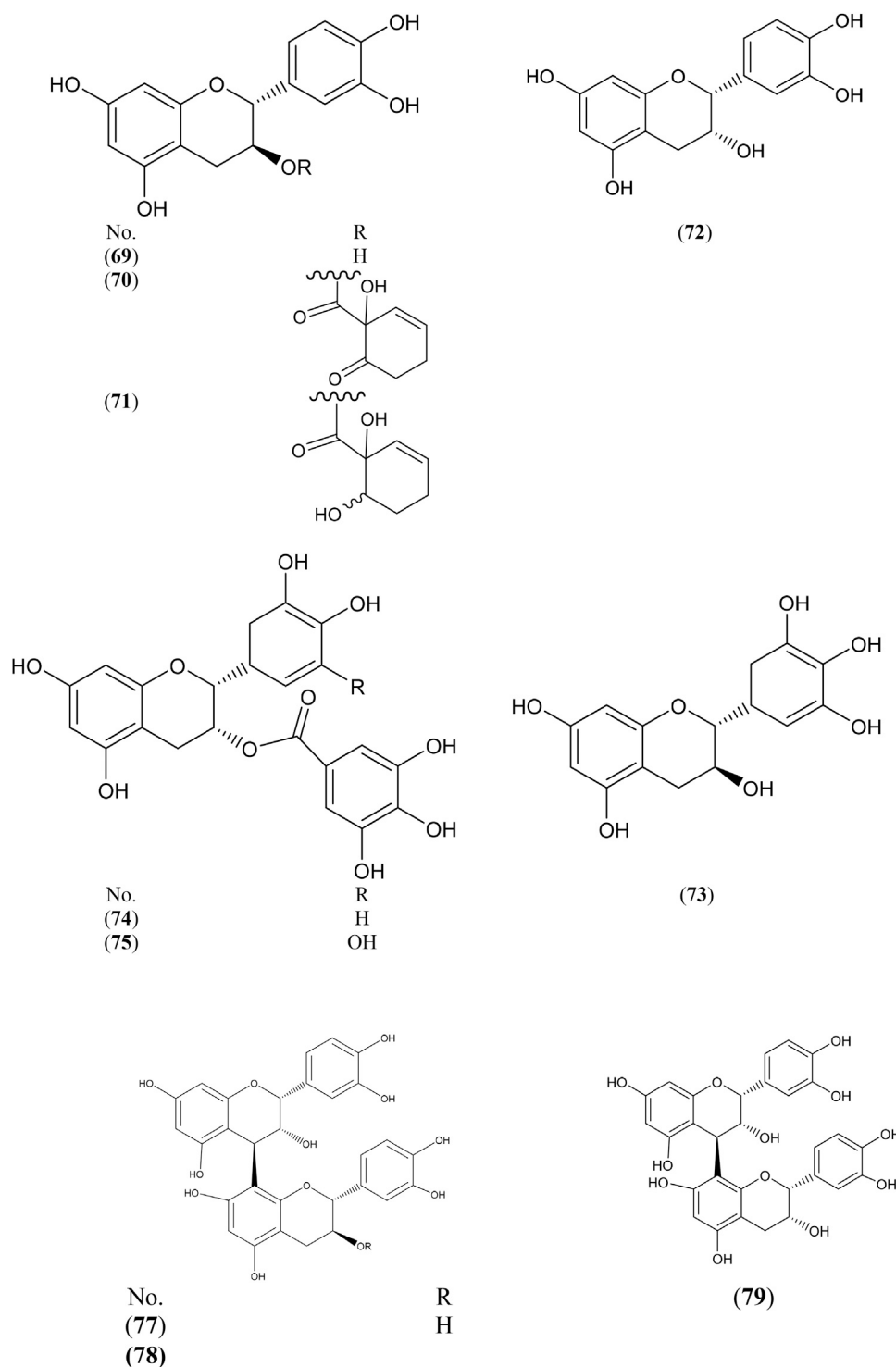


FIGURE 1 | (Continued).

matsudana Koidz. leaves (Han et al., 2003a) and *S. babylonica* L. leaves and roots (Khatoun et al., 1988; Singh et al., 2017). Whereas, chrysoeriol (6), its 7-O-D-glucoside (7) and 7-O-glucuronide (8) are major constituents of *S. babylonica* L. (Liu et al., 2008), *S. matsudana* Koidz. leaves (Han et al., 2003b) and *S.*

suberrata Willd. leaves (Tawfeek et al., 2019), respectively. Compounds (12, 14) were reported in *S. denticulate* leaves (Rawat et al., 2009; Semwal et al., 2011). *S. gilgiana* Seemen. leaves were characterized by the accumulation of acylated luteolin glucosides (19–23) (Mizuno et al., 1987). Compounds (25, 35) are

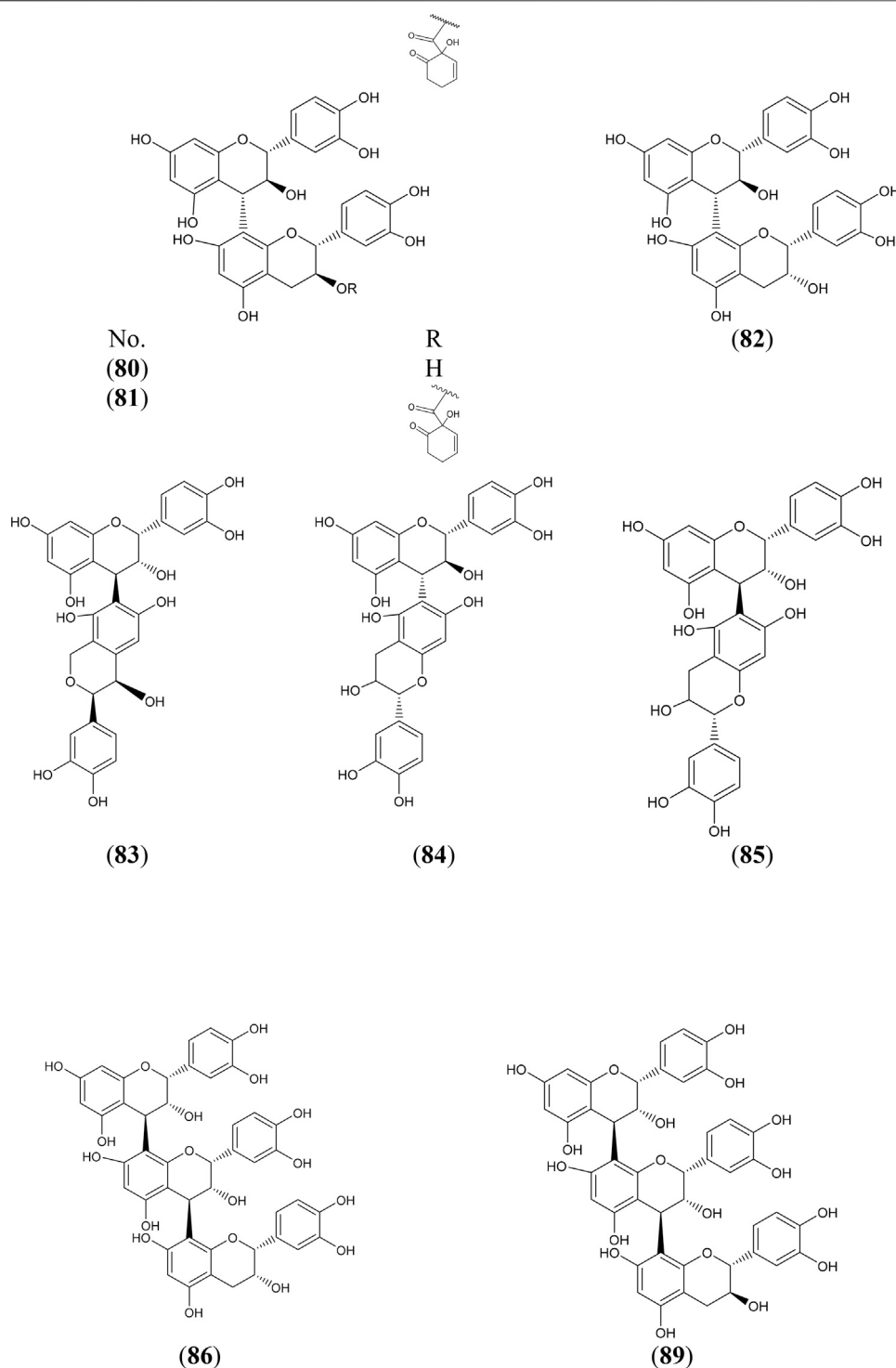


FIGURE 1 | (Continued).

chemical markers for *S. matsudana* Koidz. leaves (Li et al., 2008). Kaempferol 32) and its 7,4'-dimethyl derivative 33) were found to be most prominent constituents in *S. bordensis* Turcz. (Zhao et al., 2014). Also, kaempferol-7-O-glucoside 34) is a major

compound in *S. babylonica* L. leaves and roots (Khatoon et al., 1988; Singh et al., 2017).

Angeloxylflavone 13) and isoflavones (63, 64) are chemical markers for *S. cheilophila* C. K. Schneid. twigs (Shen et al., 2008).

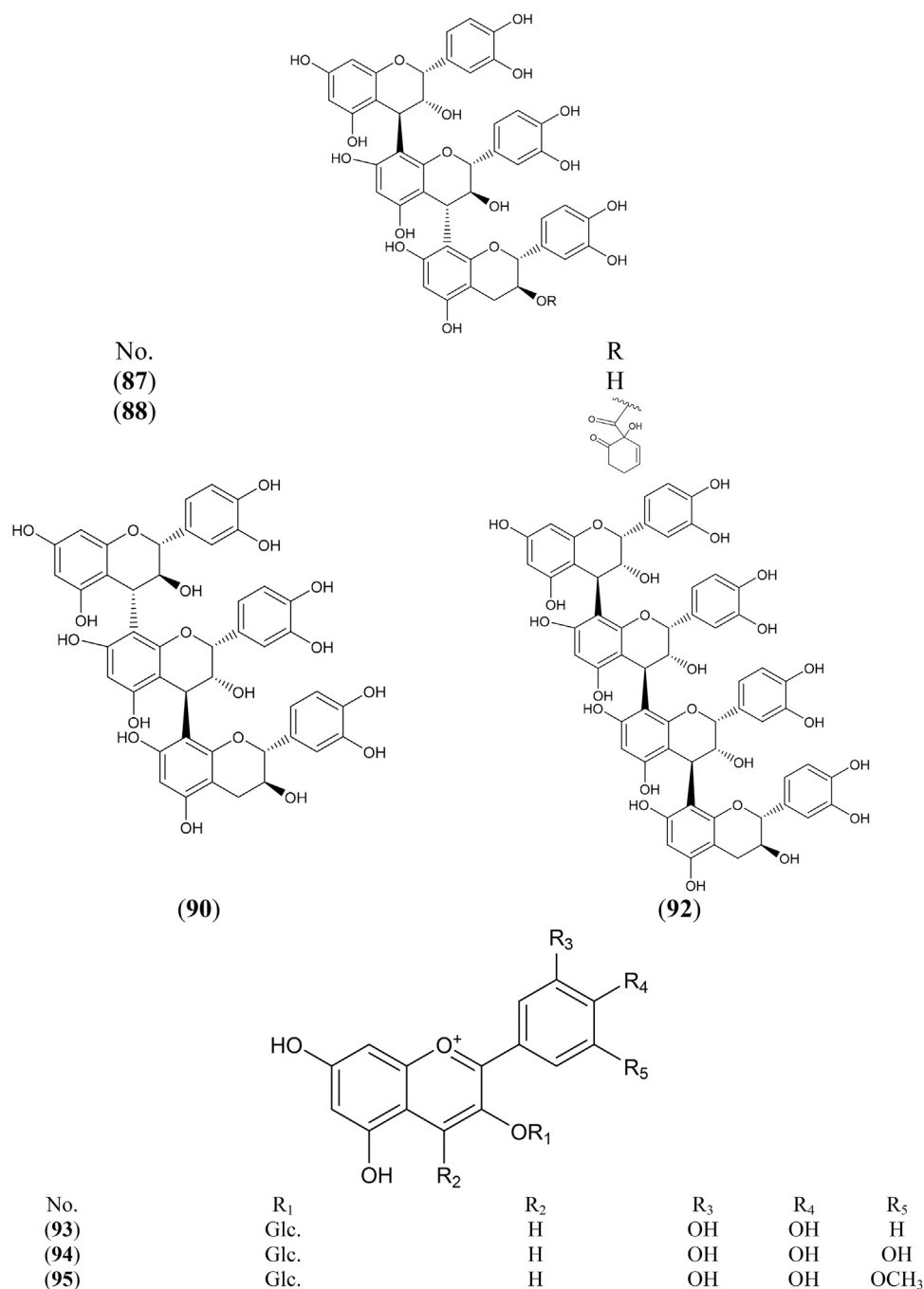


FIGURE 1 | (Continued).

S. integra \times *S. suchowensis* young stem was characterized by the accumulation of sulfated flavanones and dihydroflavonol as compounds (49, 52, 58, 60). Compound 11) was reported in the erial parts of *S. denticulate* Andersson.

The highest number of chalcones, catechins, procyanidins and anthocyanins were detected in the bark of willows. The bark of *S. daphnoides* Vill., *S. elbursensis* Boiss., *S. acutifolia* Willd. and *S. rubra* Huds. were characterized by the accumulation of chalcones

(65–67) (Kompantsev, 1969; Kompantsev and Shinkarenko, 1975; Vinokurov, 1979; Zapesochaya et al., 2002; Krauze-Baranowska et al., 2013). Catechin 69) and its derivatives (70, 71), epicatechin (72), procyanidin B1 77) and its derivative (78), procyanidin B3 (80) and its derivative (81), procyanidins B6 (84), B7 85) and trimeric procyanidins (87–89) were found to be major constituents of *S. sieboldiana* Blume bark (Hsu et al., 1985). Also, procyanidins (77, 79, 80, 82, 83, 85, 86, 89, 90, 92) are major

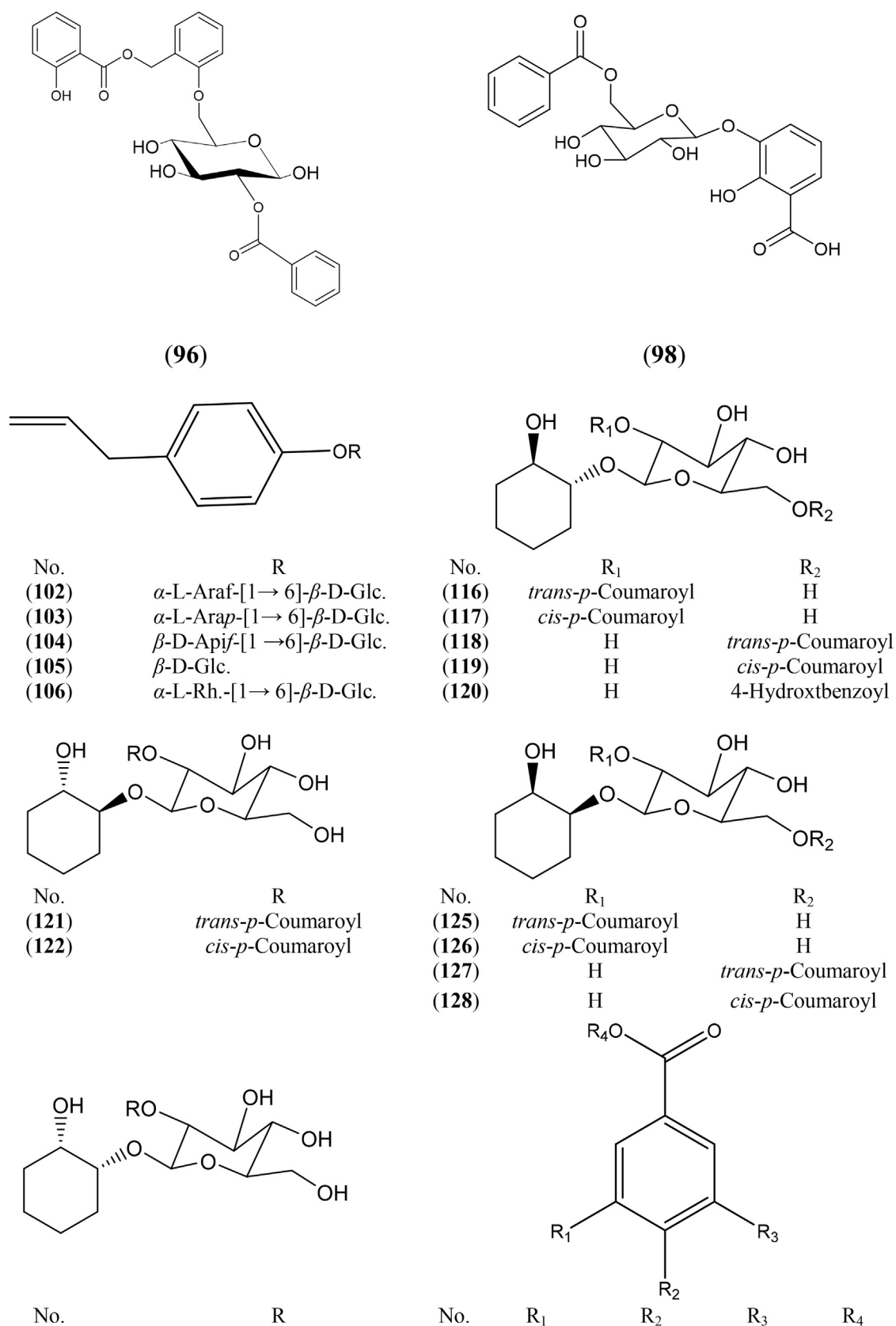
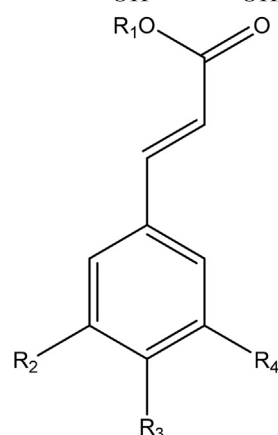
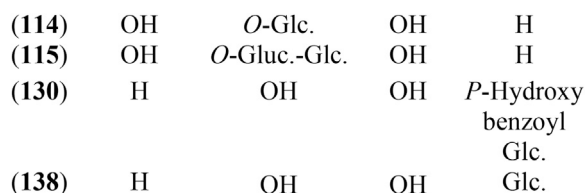
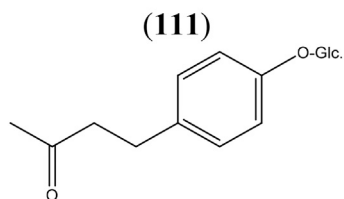
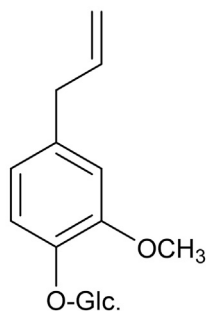
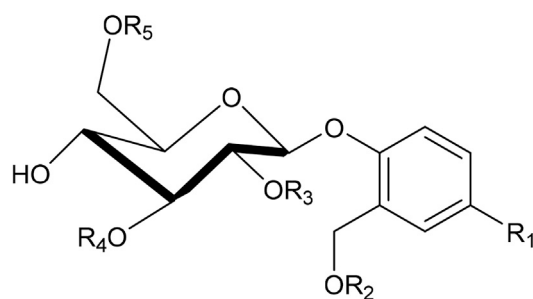


FIGURE 2 | Structures of reported phenolic glycosides from genus *Salix*.



No.	R ₁	R ₂	R ₃	R ₄
(108)	Galloyl-Glc.	H	OH	H

(109)	Galloyl- pent.	H	OH	H
(110)	Glc.	H	OH	H
(112)	Glc.	H	OH	OCH ₃
(162)	Glc.	OCH ₃	OH	OCH ₃



No.	R ₁	R ₂	R ₃	R ₄	R ₅
(97)	H	Salicyloyl	H	H	Ac
(100)	OH	Benzoyl	H	Benzoyl	H
(101)	H	H	H	Benzoyl	H
(107)	H	HCH	H	Benzoyl	H
(113)	H	H	H	H	Ac
(133)	H	HCH	Ac	H	HCH
(136)	H	H	H	H	Benzoyl
(137)	H	<i>p</i> -Coumaroyl	H	H	H
(141)	H	H	H	H	H

FIGURE 2 | (Continued).

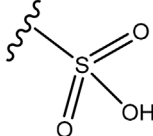
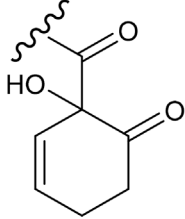
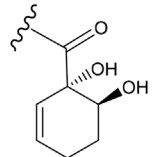
(142)	H	H	Ac	H	H
(143)	H	H	H	Ac	H
(144)	H	H	-(E)- <i>p</i> -Coumaroyl	H	H
(145)	H	H	-(Z)- <i>p</i> -Coumaroyl	H	H
(146)	H	H	H	H	-(E)- <i>p</i> -Coumaroyl
(147)	H	H	H	H	-(Z)- <i>p</i> -Coumaroyl
(148)	H	H	<i>p</i> -Coumaroyl	H	Dihydrobenzoyl
(149)	H	H	Cinnamoyl	H	H
(150)	H	H	Dihydrocinnamoyl	H	H
(151)	H	Malate	H	H	H
(152)	H		H	H	H
(153)	H	Salicyloyl (<i>o</i> -Hydroxybenzoyl)	H	H	H
(154)	H	HCH (1-hydroxy-6-oxo-2-cyclohexen-1-carboxylate) = 	H	H	H
(155)	H	HCH	Ac	H	H
(156)	H	HCH	H	Ac	H
(157)	H	HCH	H	H	Ac
(158)	H	HCH	Ac	H	Ac
(159)	H	HCH	(E)-Cinnamoyl	H	H
(161)	H		Ac	H	H
(164)	H	H	Benzoyl	H	H
(165)	H	Salicyloyl	Benzoyl	H	H
(166)	H	HCH	Benzoyl	H	H
(167)	H	H	H	H	<i>p</i> -Coumaroyl

FIGURE 2 | (Continued).

constituents of *S. daphnoides* Vill. bark (Wiesneth, 2019). Anthocyanins (93–95) were detected in the bark of *S. purpurea* L., *S. daphnoides* Vill., *S. alba* L., *S. phylicifolia* L., *S. nigricans* Sm., *S. calodendron* Wimm. and *S. viminalis* L., *S. triandra* L. and *S. amygdalina* L. (Bridle et al., 1970; Bridle et al., 1973).

Phenolic Glycosides

Glycosides are major secondary metabolites in Salicaceae (Binns et al., 1968; Kompantsev and Shinkarenko, 1973; Kompantsev et al., 1974; Nichols-Orians et al., 1992; Fernandes et al., 2009). Phenolic glycosides represent up to 30% of dry plant mass.

They are classified into two main classes: Salicin derived glycosides (salicinoids) and other phenolic glycosides as glycosylated phenylpropanoids, phenylethanoids and benzenoids and glycosylated salicylic acid derivatives. Salicinoids, which are considered as taxonomic markers for genus *Salix*, are derivatives of salicin, produced by esterification of one or more hydroxyl groups of salicyl alcohol or glucose moieties, mainly 2' and/or 6' of glucose, with organic acids as acetic, benzoic and 1-hydroxy-6-oxocyclohex-2-en-1-carboxylic (HCH) acids. The phenolic glycosides isolated and/or identified from genus *Salix* are presented in **Supplementary Table S2** and **Figure 2**.

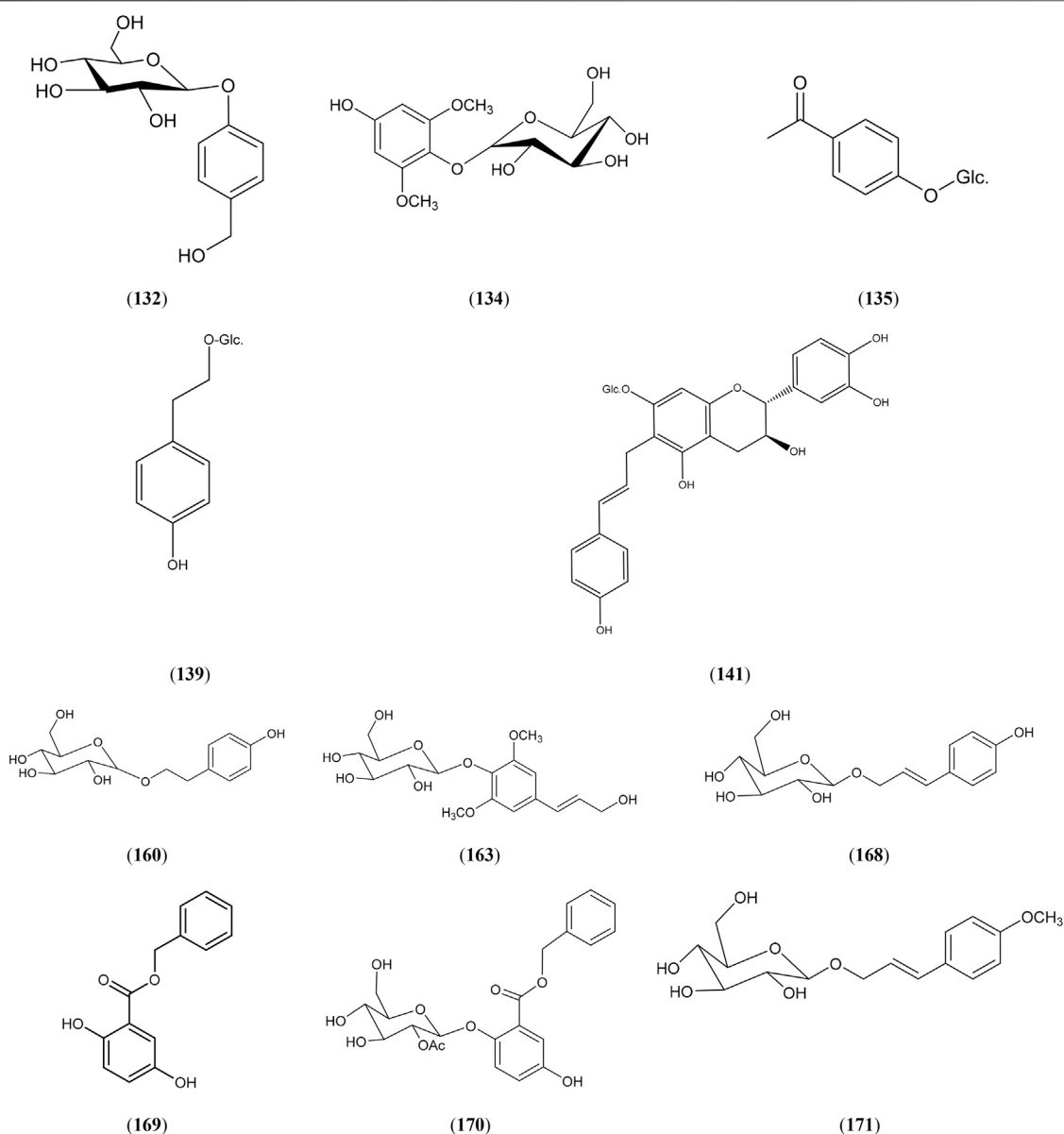


FIGURE 2 | (Continued).

The highest number of phenolic glycosides were reported in *Salix* leaves, followed by twigs, stems and bark. Salicin (141), tremuloidin (164), tremulacin 166) were found to be the major constituents in *S. Acutifolia* Willd. juvenile stem and bark (Zapsochnaya et al., 2002; Wu et al., 2016), *S. chaenomeloides* Kimura leaves (Mizuno et al., 1991), *S. glandulosa* Seemen. twigs (Kim et al., 2015) and *S. tetrasperma* Roxb. leaves (El-Shazly et al., 2012).

Some phenolic glycosides were identified as taxonomic markers for different *Salix* species. Acrophyllin A 96) and acrophyllin B 97) identified as taxonomic marker for *S. acmophylla* Boiss. leaves (Shah et al., 2016). Chaenomeloidin (101), cochinchiside A (107), lasiandrin (133), leonuriside A (134), salicin-7-sulfate 152) identified

as taxonomic markers for *S. chaenomeloides* Kimura leaves (Mizuno et al., 1991), *S. glandulosa* Seemen. twigs (Kim et al., 2015), *S. lasiandra* leaves and twigs (Reichardt et al., 1992), *S. matsudana* Koidz. leaves (Li et al., 2008) and *S. koriyanagi* Kimura. Stems (Noleto-Dias et al., 2018), respectively. Sachaliside 1 139) and sachaliside 2 (140) were identified as taxonomic markers for *S. sachalinensis* F. Schmidt (Mizuno et al., 1990).

Some *Salix* species were characterized by accumulation of 1,2-cyclohexanediol glycosides. Compounds (116–128) were detected in *S. glandulosa* Seemen. twigs (Kim et al., 2014). Also, acutifoliside, a benzoic acid derivative 98) was a chemical marker for *S. acutifolia* Willd. juvenile stem (Wu et al., 2016).

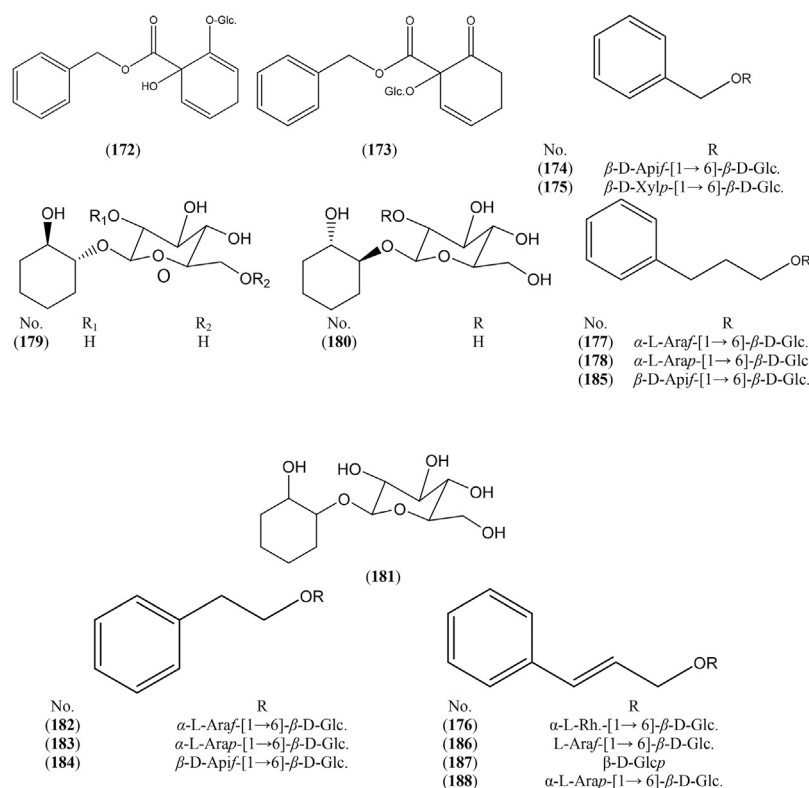


FIGURE 3 | Structures of reported non-phenolic glycosides from genus *Salix*.

Non-Phenolic Glycosides

Non-phenolic glycosides (172, 173, 174, 175, 176, 182–188) were found to be the major constituents in *S. triandra* L. *x* *dasyclados* Wimmer Wood (Noletto-Dias et al., 2019). Also, compounds (170, 171) are the major constituents in *S. arbusculoides* Andersson twigs (Evans et al., 1995). Some *Salix* species were characterized by accumulation of 1,2-cyclohexanediol glycosides. Compounds (177, 180) were detected in *S. glandulosa* Seemen. twigs (Kim et al., 2014) and grandidentin (181) was reported in *S. purpurea* L. bark (Pearl and Darling, 1970) (**Supplementary Table S3** and **Figure 3**).

Organic Acids

Salix species are rich sources for phenolic acids, either in free or esterified form, as benzyl, cinnamyl or phenyl ethyl esters. The aromatic acids are either benzoic or cinnamic acid derivatives: benzoic acid derivatives as *p*-hydroxybenzoic, *p*-anisic, gallic, salicylic, gentisic, vanillic, 2-amino-3-methoxy benzoic and protocatechuic acids, while hydroxycinnamic acid derivatives as *p*-coumaric, caffeic, isoferulic, and ferulic acids, (**Supplementary Table S4** and **Figure 4**).

The highest number of organic acids were detected in *S. purpurea* L., *S. alba* L. bark (Agnolet et al., 2012) which contain compounds (192–194, 198–200, 214), *S. tetrasperma* Roxb. flowers and bark (Sobeh et al., 2019; Mostafa et al., 2020) which contain compounds (197, 202, 203, 204, 205–206, 208, 209, 215).

Simple Phenolics

Genus *Salix* comprises a vast variety of simple phenolic compounds (Phenolic acids and their derivatives) (Tuberoso et al., 2011). *S. capensis* Thunb. bark (Masika et al., 2005), *S. acutifolia* Willd. bark (Zapesochayna et al., 2002), *S. subserata* Willd. bark (Hussain et al., 2011), *S. caprea* L. inflorescence (Ahmed et al., 2017) were characterized by the accumulation of salicyl alcohol (228) which is the basic nucleus for salicinoids. Also, *S. caprea* L. wood was characterized by the accumulation of different simple phenolics as aucuparin (218), methoxyaucuparin (219), coniferyl alcohol (221), *p*-coumaryl alcohol (222), 4,2'-dihydroxy-3,5-dimethoxybiphenyl (223) and sinapylaldehyde (229) (Malterud and Dugstad, 1985; Pohjamo et al., 2003), as illustrated in **Supplementary Table S5** and **Figure 5**.

Sterols and Terpenes

The highest number of sterols and triterpenes was detected in *S. cheilophila* C. K. Schneid. twigs (Shen et al., 2008), *S. tetrasperma* Roxb. bark, leaves and flowers (El-Shazly et al., 2012; Sobeh et al., 2019), *S. subserata* Willd. leaves (Balbaa et al., 1979), *S. denticulate* erial parts (Rawat et al., 2009), *S. babylonica* L. roots (Singh et al., 2017), *S. subserata* Willd. bark and leaves (Hussain et al., 2011). Whereas phytane and pimarane diterpene were found to be the major constituents in *S. cheilophila* C. K. Schneid. twigs (Shen et al., 2008), as illustrated in **Supplementary Table S6** and **Figure 6**.

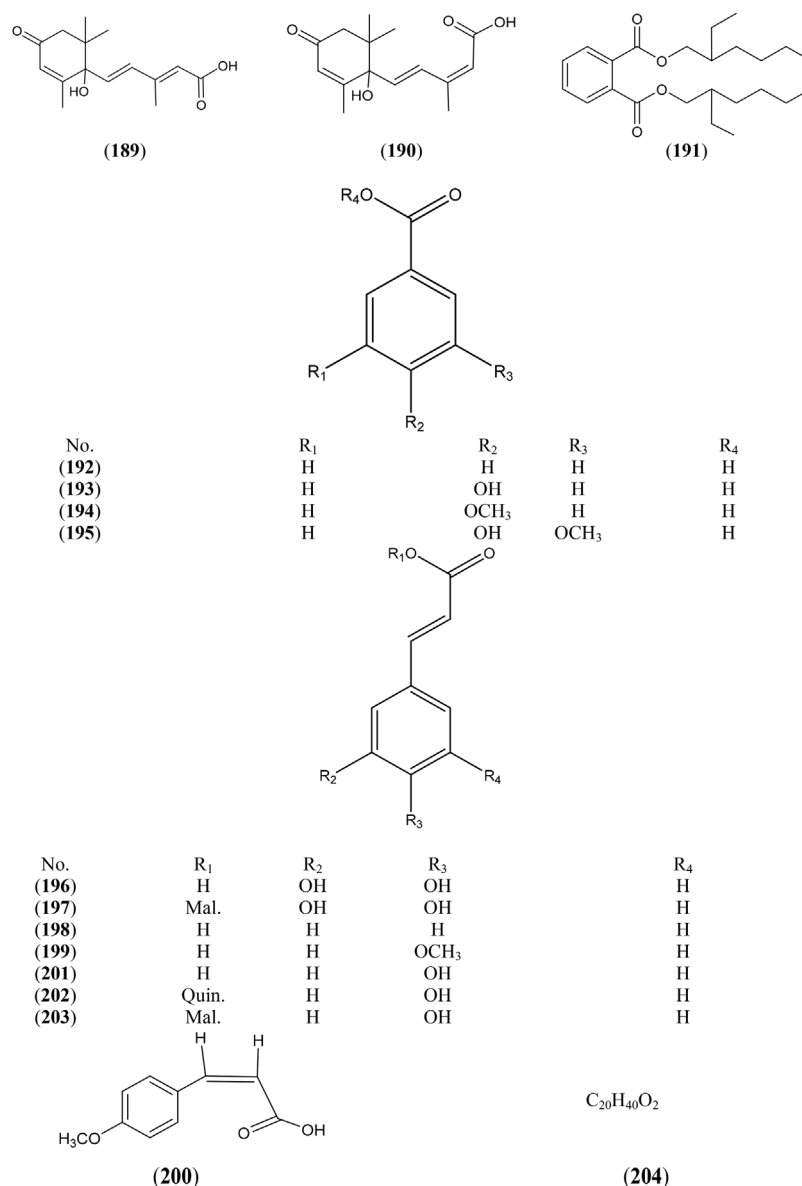


FIGURE 4 | Structures of reported organic acids from genus *Salix*.

Lignans

Sisymbriofolin a lignan derivative (247) had been isolated from the bark of *S. alba* L. (Du et al., 2007). Recently, pinoresinol (248), lariciresinol (249), secoisolariciresinol (250), 7-hydroxymatairesinol (251), medioresinol (252), and lariciresinol-sesquilignan (253) were detected in the biomass of five willow sp. cultivated in Quebec, Canada (Brereton et al., 2017) as illustrated in **Figure 7**.

Volatiles

Terpenes (hemi-, mono- and sesqui-terpenes) and non-terpene (aliphatic, aromatic acids, their esters, carbonyl compounds and hydrocarbons) volatiles were identified in the genus *Salix*. The highest percent of volatiles and fatty acids was reported in *S. caprea* L. inflorescence (Ahmed et al., 2017), and the leaves of *S. egyptiaca*

L. (Karimi et al., 2011), *S. babylonica* L. (Salem et al., 2011), and *S. alba* L. (Zarger et al., 2014) (**Supplementary Table S7** and **Figure 8**).

Traditional Uses

Salix plants have been used medicinally since antiquity and have been linked to the discovery of acetylsalicylic acid and aspirin. These plants had been traditionally used to treat painful musculoskeletal joint pain conditions, inflammation, and fever. Salicin is a major pharmacologically active metabolite in *Salix* and hydrolyzes in the gastrointestinal tract to confer salicyl alcohol and D-glucose. The latter is oxidized, upon absorption, into salicylic acid, the active drug which inhibits cyclooxygenases (COX I, II) (Mahdi, 2010).

S. egyptiaca L (Musk Willow) was important in the Middle East, especially in Iran, as it has been traditionally used to treat anemia and

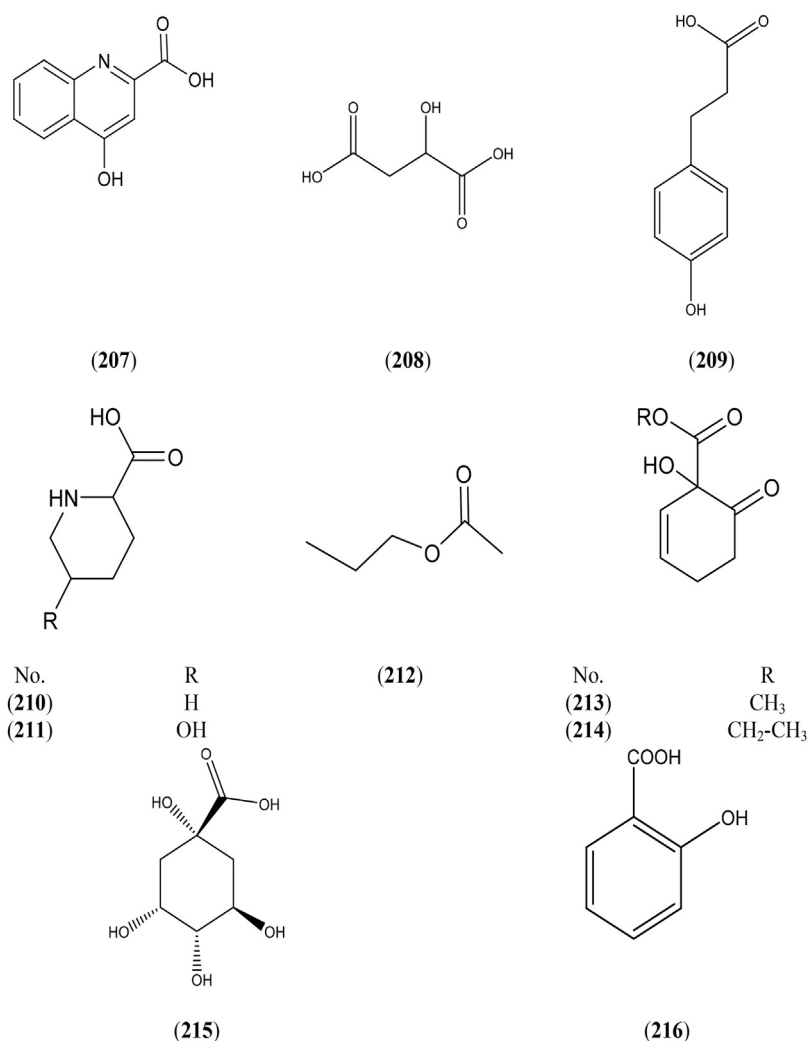


FIGURE 4 | (Continued).

vertigo, as a cardiotonic agent, and also in the preparation of local candies as a fragrance additive (Asgarpanah, 2012). *S. alba* L (white willow), had used in folk medicine to treat fever, chronic and acute inflammation, pain and infection (Zengion and Yarnell, 2011; Maistro et al., 2019). *S. tetrasperma* Roxb. had been used to treat diseases such as epilepsy, diabetes, fever, rheumatism, piles, swellings, stones in bladder, dysentery, wound, ear pain, cough and cold (Prashith Kekuda et al., 2017). *S. alba* L. bark is traditionally used for treatment of flu, rheumatism, fever and headache (Van Wyk and Wink, 2018).

Pharmacological Activity

Different *Salix* species and the isolated compounds as salicylic acid and salicin have been utilized in folk medicine to treat rheumatic diseases, back pain, toothache, headache, and menstrual cramps (Highfield and Kemper, 1999). They exert analgesic, anti-inflammatory, antioxidant, anticancer, cytotoxic,

antidiabetic, antimicrobial, anti-obesity, neuroprotective and hepatoprotective activities. The main targets of salicylic acid are cyclooxygenases (COX I, II) which are key enzymes of pathway to prostaglandins which control inflammation and pain. The available scientifically based reports on biological activities of genus *Salix* are summarized in Tables 1–8.

Antimicrobial Effects of Salix

Multidrug-resistant bacteria are widely spread, and natural resources have been used as a means of discovering novel antibacterial compounds as they offer limitless opportunities for the discovery of new agents, particularly against multidrug resistant bacteria.

The main methods used to evaluate the antimicrobial activity of *Salix* extracts are disc diffusion assays, agar well diffusion, broth microdilution methods and the assessment of antibiofilm function (Masika et al., 2005; Fayaz and Sivakumaar, 2014;

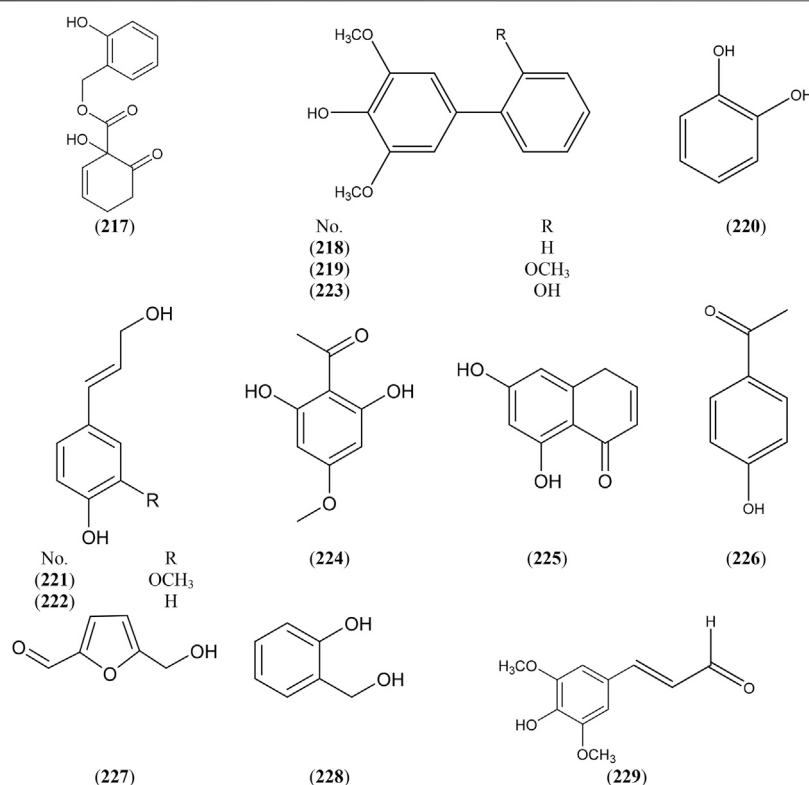


FIGURE 5 | Structures of reported simple phenolics from genus *Salix*.

Popova and Kaleva, 2015; Mostafa et al., 2020). As detailed in **Table 1**, microbial growth inhibition zones and percentages along with minimum inhibitory concentrations (MICs) displayed the potential of *Salix* species as substantial antimicrobials and predict their efficacy as functional foods (Mostafa et al., 2020).

Antibacterial Activity

Many previous studies evaluated the antibacterial activity of *Salix* plants and active constituents of their extracts against different types of bacteria such as *Pseudomonas eruginosa*, *Escherichia coli*, *Staphylococcus aureus* and *Bacillus subtilis*, dental biofilm forming bacteria (*Streptococcus mutans* and *Lactobacillus*), and *Salmonella enterica* (**Table 1**). Catechol and 2-hydroxybenzyl alcohol derived from the bark of *S. capensis* Thunb. were previously tested for their antibacterial activity. Both compounds exhibited similar antibacterial activity against *P. eruginosa* (Masika et al., 2005). Moreover, *Salix alba* L. bark extract demonstrated antimicrobial activity against the dental biofilm forming bacteria with MIC of 125 µg/ml. Furthermore, it also exhibited a moderate potential against the *Staphylococcus aureus* but the least activity was observed against *E. coli* (Fayaz and Sivakumaar, 2014). Previous studies also showed that the twigs aqueous extract with leaves of *S. babylonica* L. exhibited potent antimicrobial properties against Gram-negative bacteria (*E. coli*, *Salmonella enterica*, MIC₅₀ is 70.4 ± 17.41 mg/ml) with a comparable activities to thiamphenicol (The broad spectrum antibiotic). Its effects cover Gram-positive bacteria such as *S. aureus* (Popova and Kaleva,

2015). A recent study performed in our laboratories tested the extracts of both stem bark and flowers of *S. tetrasperma* Roxb. for anti-quorum sensing activity against *Pseudomonas eruginosa*. Both extracts inhibited *P. eruginosa* bacterial growth at 40 mg/ml; however, the bacterial viability was not affected by 1/4 and 1/8 MIC concentrations. When the extracts were tested as anti-quorum sensing agents, they impaired virulence of *P. eruginosa* by declining its swimming and swarming motilities and reducing its hemolytic and proteolytic properties (Mostafa et al., 2020).

Antifungal Activity

Poisoned food technique, broth microdilution method, filter disc assay and growth curve study methods were used to determine the antifungal properties of *Salix* extracts (**Table 2**). The antifungal activity was evaluated against *Candida guilliermondii*, *C. glabrata*, *C. parapsilosis* and *Fusarium oxysporum*.

Anthelmintic Activity

The anthelmintic potential of *Salix* species to inhibit gastrointestinal and pulmonary parasites in animals was studied. The anthelmintic activity was evaluated against *Ostertagia*, *Moniezia*, *Dictyocaulus*, *Eimeria*, *Chabertia*, *Cooperia*, and *Hemonchus contortus* (**Table 2**). It was reported *Salix babylonica* L. (at dose of 20 ml, weekly) was effective against the main parasite species detected in sheep (*Eimeriaspp.*, *Dictyocaulus spp.*, and *Chabertia spp.*) more than the most

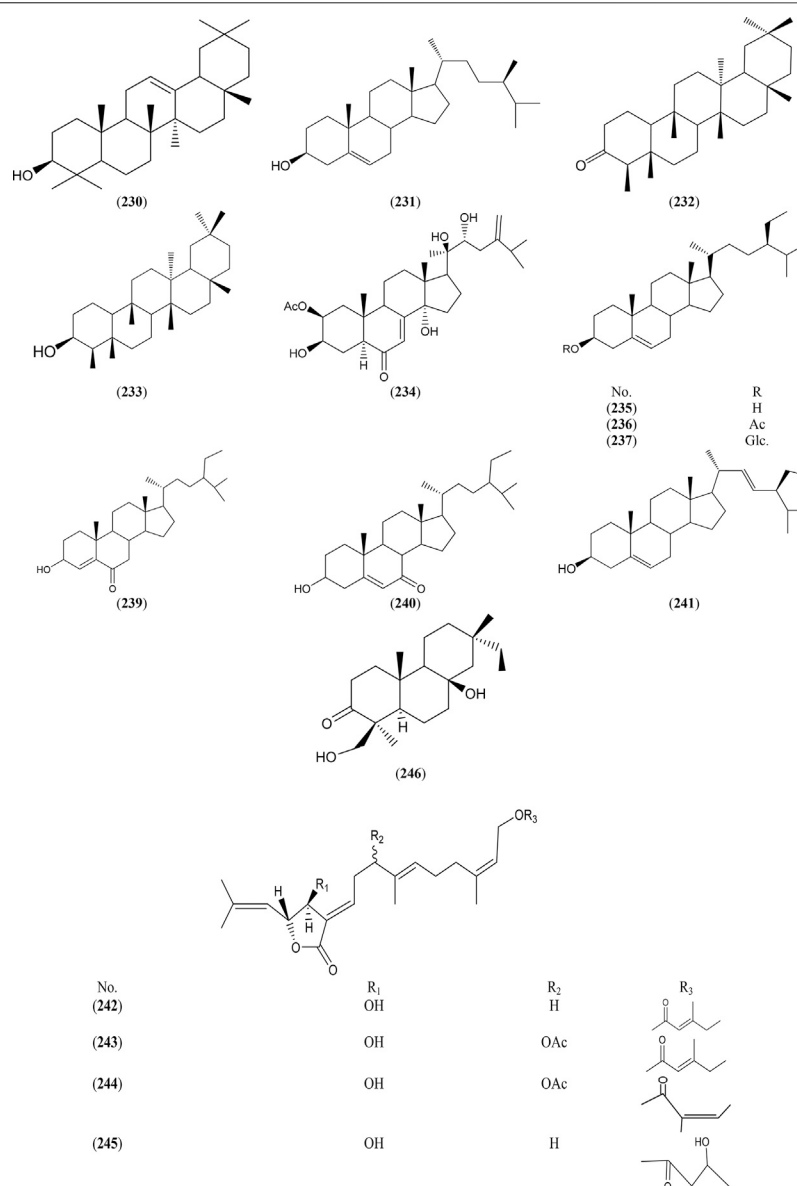


FIGURE 6 | Structures of reported sterols and terpenes from genus *Salix*.

common parasites in goats in southern Mexico farms (*Dictyocaulus* spp. and *Chabertia* spp.) (Salem et al., 2017).

Anti -HIV Activity

Human immunodeficiency virus (HIV) infection that causes acquired immunodeficiency syndrome (AIDS) represents a major health problem worldwide. Chemical anti-retroviral agents are usually used to treat AIDS patients. However, they possess many adverse effects and resistance emerged for many of them. Recently, novel anti-retroviral agents isolated from medicinal plants, played an essential role to replace synthetic drugs. One study investigated the anti-retroviral effects of *S. egyptiaca* L. extract. Results of this study and bioinformatics

analyses suggested that the plant had anti-HIV properties and might be a substantial candidate for AIDS patients (Table 2) (Eftekhari et al., 2014).

Antioxidant Activity

Reactive oxygen species (ROS) are associated with several human diseases, such as inflammation, diabetes, ulcers, autoimmune and cardiovascular diseases, viral infections and cancer (Howlett, 2008; Rubió et al., 2013; Salem et al., 2020). Most of the activities of *Salix* species were attributed to the presence of several polyphenolic with robust antioxidant activities (Table 3). The antioxidant effects of *Salix* extracts and their flavonoids were mainly assessed by DPPH, ABTS, FRAP, total

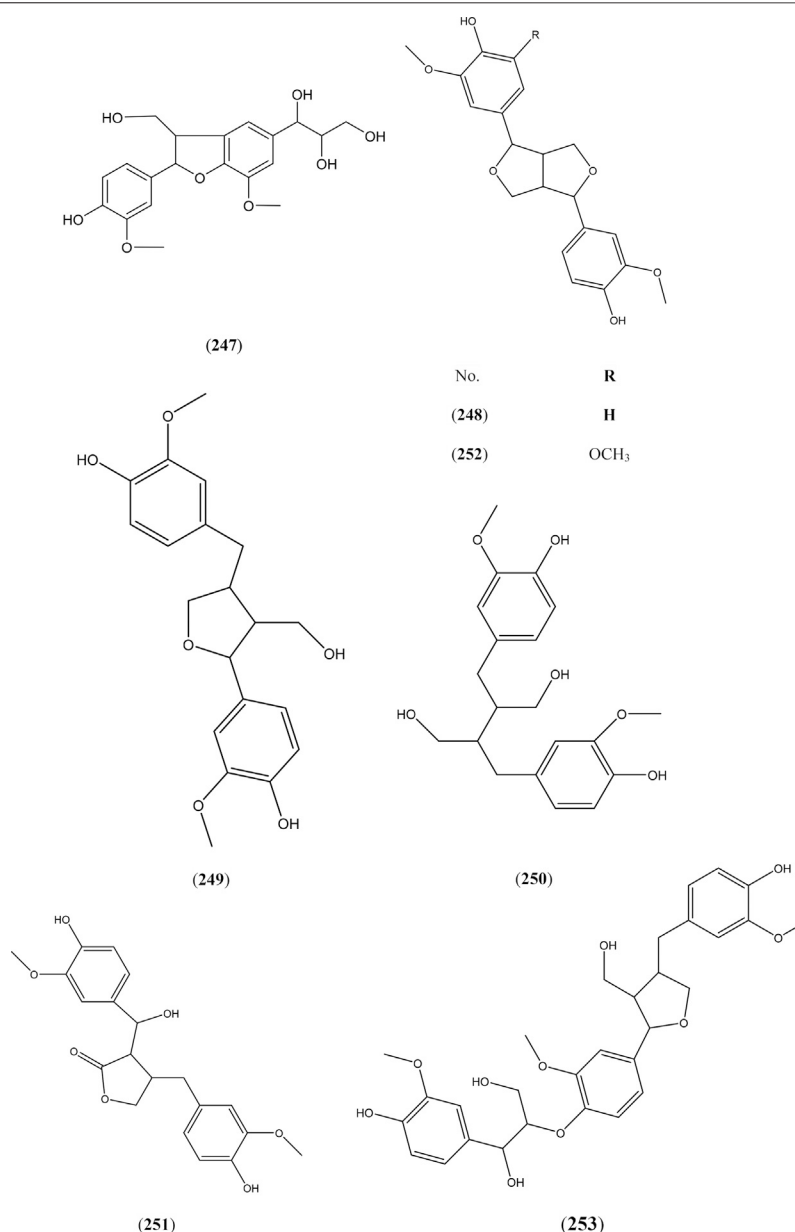


FIGURE 7 | Structures of reported lignans from genus *Salix*.

antioxidant capacity (TAC) assays, Folin-Ciocalteu method, β -carotene bleaching, lipid peroxidation capacity, inhibition of linoleic acid oxidation, superoxide anion radical scavenging, and alkyl radical scavenging assays (Ceyhan, 2014; Gawlik-Dziki et al., 2014; Tavakoli et al., 2016; Zaiter et al., 2016; Nauman et al., 2018; Zabihi et al., 2018; Gligoric' et al., 2019). A recent study from our lab investigated the possible effect of *S. tetrasperma* Roxb. extract on neuropathic pain and its mechanism of action showed a potent *in vitro* and *in vivo* antioxidant effects (Sobeh et al., 2019). Furthermore, *S. atrocinerea* Brot., *S. fragilis* L. and *S. viminalis* L. showed antioxidant effects mediated by their polyphenolic contents (Ramos et al., 2019). Another study from our laboratory showed that *S. suberrata* Willd. leaf extracts contained

isorhamnetin-3-*O*- β -D-rutinoside, triandrin, gallicocatechin, tremuloidin, aromadendrin, salicin, and chrysoeriol-7-*O*-glucuronid and exerted antioxidant effects against oxidative stress in *Caenorhabditis elegans* (Tawfeek et al., 2019).

Anti-Inflammatory Activity

Inflammation is a frequent condition because of exposure to different stimuli including microbial infection and wounding. It decreases the spread of infection, followed by resolution and the restoration of normal structural and functional of affected tissues (Nathan and Ding, 2010). However, non-resolving inflammation contributes significantly to the pathogenesis of many diseases such as atherosclerosis, obesity, cancer, and inflammatory bowel

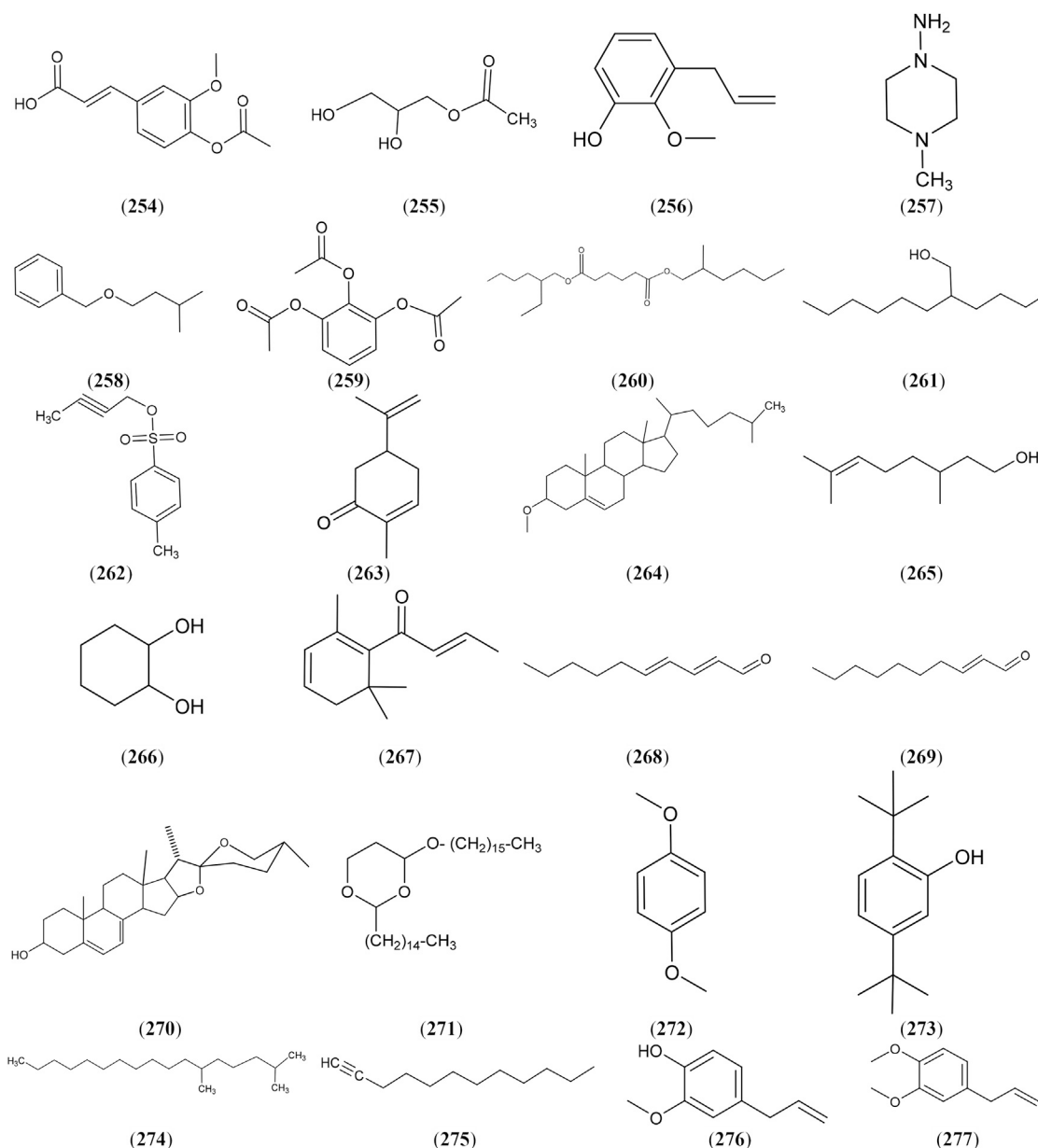


FIGURE 8 | Structures of reported volatiles and fatty acids from genus *Salix*.

disease. *Salix* extracts exert potent anti-inflammatory effects that are responsible for many biological effects. The hydroalcoholic extract of *S. tetrasperma* Roxb. in two dose levels (100 and 200 mg/kg) demonstrated anti-inflammatory effects in carrageenan induced rat paw edema model (Kishore et al., 2014). We showed previously that the flower extract of *S. tetrasperma* Roxb. has analgesic, antipyretic, and anti-inflammatory effects against carrageenan induced vascular permeability and carrageenan induced hind paw edema. It inhibited COX-1, COX-2 and LOX and suppressed elevated levels of TNF- α and NF- κ B in chronic neuropathic pain model (Sobeh et al., 2019). Oral administration of *S. canariensis* extract

significantly decreased writhing, moderately reduced formalin-induced pain and showed a promising dose-dependent anti-inflammatory activities. These effects were attributed to the presence of pentacyclic triterpenes and polyphenolics (Gutiérrez et al., 2017). An early study showed that *S. caprea* L. is a potent cyclooxygenase inhibitor (Tunon et al., 1995). Another study showed that *S. subserrata* Willd. and *S. tetrasperma* Roxb. showed anti-inflammatory effects against carrageenan induced hind paw edema due to the presence of phenolic glycosides mainly salicin as well as the flavonoids luteolin, quercetin and rutin (Karawya et al., 2010). *S. matsudana* Koidz. leaves methanol extract also showed

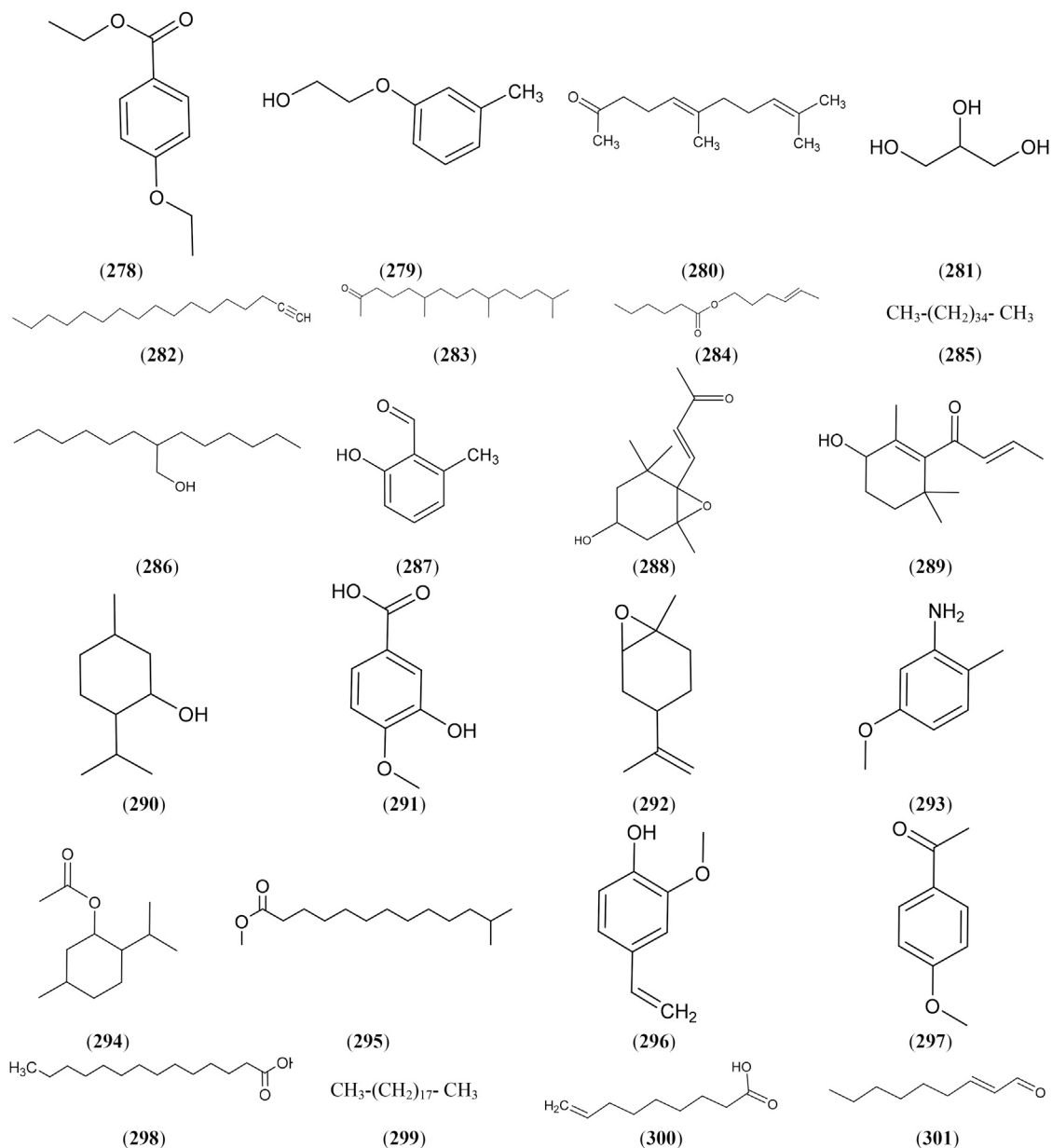


FIGURE 8 | (Continued).

significant inhibitory activities against cyclooxygenases (COX-1 and COX-2) due to the presence of matsudone, luteolin 7-O-glucoside and 4',7-dihydroxyflavone (Li et al., 2008).

Anticancer Activity

There are several risk factors that can increase the development of cancer that have a basis of low-grade inflammation and oxidative stress. Therefore, targeting inflammatory pathways and suppressing oxidative stress may contribute to inhibition of initiation, proliferation and even cancer metastasis and subside resistance to chemotherapy and radiation. *Salix* extracts, by possessing both anti-inflammatory and potent antioxidant potential, are promising natural

sources in fighting cancer. The antiproliferative activities of *Salix* extracts were determined by cell viability percentages and IC₅₀ values using several *in vitro* assays. The most commonly utilized cancer cell lines were human acute lymphoblastic leukemia (ALL cells), human acute myeloid leukemia cells (AML cells), PC3 cells (Prostate cancer cells), Hep G2 cells (Liver cancer cells), HCT116 (Colorectal cancer cells), MCF7 (Breast cancer cells), HT-29 and HCT 116 (human colon COX-2 positive and negative cells respectively), A549, SW2 cells, and human lung cancer cell line (H1299).

It was observed that a fraction of *Salix* extracted by non-polar solvents such as (petroleum ether, ether, and chloroform) has the minimum killing potential against AML cells while fraction

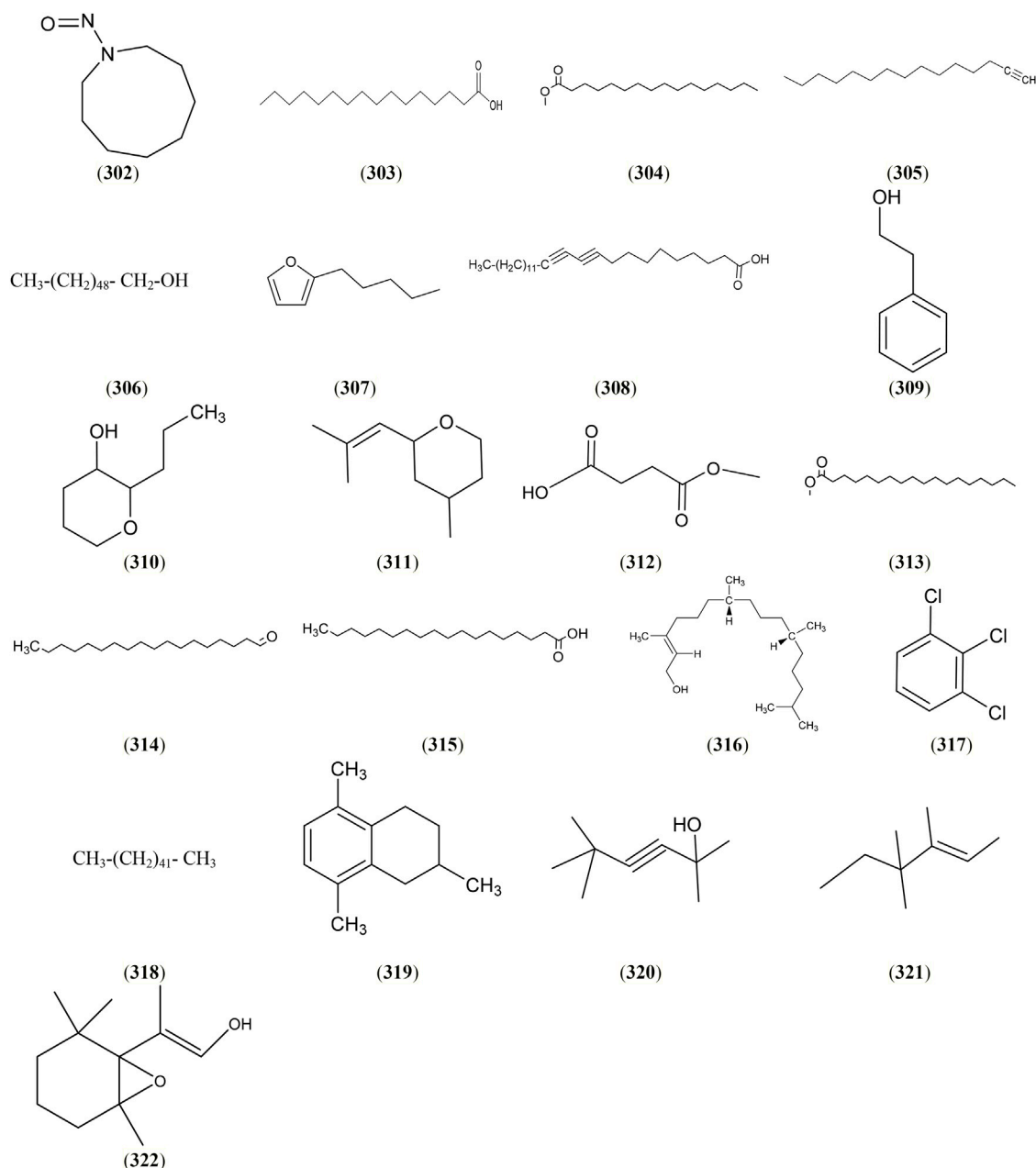


FIGURE 8 | (Continued).

extracted by polar solvents such as 70% ethanol and water has major destructive effect on AML cells (El-Shemy et al., 2003). Thus, *Salix* cytotoxic activity could be attributed to the polyphenolics, tannins, and glycosides, that are commonly dissolved in water or ethanol solutions including salicin and saligenin. When salicin is tested against leukemic cells it caused destruction of myeloblasts by 70–75%. Eight compounds isolated from *S. hulteni* Flod (1-*p*-coumaroyl- β -D-glucoside, aromadendrin, catechin, 4-hydroxyacetophenone, picein, sachalide 1, naringenin and dihydromyricetin) were tested

for their cytotoxic potential against brine shrimp and a human lung cancer cell line (H1299). Naringenin, aromadendrin, catechin, and 1-*p*-coumaroyl- β -D-glucoside showed mild cytotoxic activity, with dihydromyricetin showing the strongest cytotoxic effects. 4-Hydroxyacetophenone, picein, and sachalide one did not show a significant cytotoxic activity indicating that flavonoid compounds are responsible for the cytotoxic effects of *S. hulteni* Flod. (Jeon et al., 2008). Brine shrimp lethality test is commonly used to test cytotoxic effects of natural products. The methanol extract of *S. nigra* exerted

TABLE 1 | Anti-bacterial activity of *Salix* species.

Bacteria	Extract/Compound	Used method	Effects	References
<i>B. subtilis</i> <i>S. aureus</i> <i>E. coli</i> <i>P. eruginosa</i>	<i>S. capensis</i> thunb. Bark catechol 2-hydroxybenzyl alcohol	Bioautographic assay on TLC plate, microplate dilution method broth culture	MIC = 62.5–250 µg/ml	Masika et al. (2005)
<i>S. mutans</i> <i>S. aureus</i> <i>Lactobacillus</i> sp	<i>S. alba</i> L. bark methanol extract	Disc diffusion method	MIC = 125 µg/ml 250 µg/ml for <i>Lactobacillus</i>	Fayaz and Sivakumaar (2014)
<i>E. coli</i> <i>Salmonella enterica</i> <i>E. coli</i> , <i>S. aureus</i> <i>Listeria monocytogenes</i>	Aqueous extracts of <i>S. babylonica</i> L. leaves Hydroalcoholic extract, fractions, and subfractions of <i>S. babylonica</i> L.	Agar-gel diffusion method and twofold serial dilutions on mueller-hinton s agar Broth microdilution method	Inhibition zones with an average diameter of 13.38 ± 2.22 mm MIC ₅₀ = 70.4 ± 17.41 mg/ml MIC = 0.78 mg/ml for <i>Listeria monocytogenes</i> , MIC = 0.39 mg/ml for <i>S. aureus</i>	Popova and Kaleva (2015) González-Alamilla et al. (2019)
<i>P. eruginosa</i>	Methanol extracts of <i>S. tetrasperma</i> roxb. Stem bark and flower	Broth microdilution method, skim milk agar method	Inhibition of swimming and swarming motilities, and proteolytic and hemolytic activities	Mostafa et al. (2020)

TABLE 2 | Antifungal, anthelmintic and anti-retroviral activity of *Salix* species.

Micro-organism	Extract/compounds	Used method	Effects	References
Fungi				
<i>Fusarium oxysporum</i>	Ethanol extract of <i>S. babylonica</i> L. root	Poisoned food technique	Good fungicidal activity at 20% concentration	Sati et al. (2013)
<i>Candida guilliermondii</i> , <i>C. glabrata</i> and <i>C. parapsilosis</i>	Methanol extract of <i>S. alba</i> L. leaves	Broth microdilution method, filter disc assay and growth curve study	MIC = 800 µg/ml, 800 µg/ml and 1,600 µg/ml respectively. Inhibition i.e. 12 mm for <i>C. glabrata</i> followed by 11 mm measured in <i>C. parapsilosis</i> . <i>C. guilliermondii</i> inhibition was 10 mm	Zarger et al. (2014)
Parasites				
<i>Hemonchus contortus</i> , <i>Eimeria</i> <i>Cooperia</i> , <i>Chabertia</i> , <i>Dictyocaulus</i> , <i>Moniezia</i> , and <i>Ostertagia</i> <i>Bonostomum</i> sp., <i>Strongiloides papillosus</i> , and <i>Nematodirus pathiger</i> <i>Nematodirus battus</i>	Leaves of <i>S. babylonica</i> L. extract Leaves extract of <i>S. babylonica</i> L.	Oocyst and egg count technique in goat and sheep Salt floatation technique and McMaster method	20 ml oral doses decrease oocyst and egg count in both species The extract caused egg and worm count reductions in lamb feces by 47% vs. the control lambs	Salem et al. (2017) Hernandez et al. (2014)
Virus				
HIV-1	<i>S. egyptiaca</i> L. PI extract	XTT method. Inhibition of p24 Ag production level assay	The IC ₅₀ in HeLa infected cells was 45 µg/ml 100 µg/ml extract inhibited the production of HIV-1 p24 Ag by more than 80%	Eftekhari et al. (2014)

concentration dependent cytotoxic effects against brine shrimp indicating promising cytotoxic effects (Ahmed et al., 2016). Willow bark extract (A pharmaceutically used extract BNO 1455) and its fractions (flavonoids, proanthocyanidins, salicyl alcohol derivatives) showed dose dependent cytotoxic effects against human colon and lung cancer irrespective of their COX-2 selectivity (Hostanska et al., 2007). *S. caprea* L. exerted a protective effect against phorbol ester induced skin tumor promotion when applied to the skin of mice prior to the application of phorbol ester. Anti-tumor activity of *S. caprea* L. may be attributed to potent antioxidants constituents of *S.*

caprea L. such as luteolin, dihydrokaempferol and quercetin (Sultana and Saleem, 2004).

Neuroprotective Effect

Only few studies investigated the effect of *Salix* species on central and peripheral nervous system. Virupaksha et al. (2016) investigated the effects of *S. tetrasperma* Roxb. leaf extract on locomotor activity and muscle relaxant activity. They demonstrated that the extract decreased locomotor activity indicating central nervous system (CNS) depressant activity and induced a decrease in fall off time due to loss of muscle grip implying skeletal relaxation (Virupaksha

TABLE 3 | *In vitro* antioxidant activity of *Salix* species.

Plant part	Extract/compound	Method	Effects	References
Stem and leaves	Four sulfated flavonoids (taxifolin-7-sulfate, dihydrokaempferol-7-sulfate, eridictyol-7-sulfate and naringenin-7-sulfate) isolated from hybrid species of <i>Salix×alberti</i> L.	DPPH	7-Sulfation of taxifolin and eridictyol attenuated but does not remove antioxidant activity	Noletto-Dias et al. (2020)
Leaves	Methanol extracts of <i>S. purpurea</i> L., <i>S. cinerea</i> L., <i>Salix×smithiana</i> Willd., <i>S. alba</i> L., <i>S. eriocephala</i> Michx., <i>Salix×rubra</i> Huds.	DPPH	The scavenging effect ranged between 33.6 (<i>S. purpurea</i> L.) and 45.7% (<i>S. cinerea</i> L.), 50.7 (<i>S. purpurea</i> L.) to 56.3% (<i>Salix×rubra</i> Huds.)	Gąsecka et al. (2017)
Leaves	Ethyl acetate extract of <i>S. tetrasperma</i> Roxb.	DPPH assay	IC ₅₀ = 65.89 µg/ml	Januarta et al. (2019)
Leaves	Methanol extract of <i>S. mucronata</i> Andersson	DPPH, ABTS and TAC assays	DPPH (EC ₅₀ = 98.76 ± 0.46 (µg/ml), ABTS = 45.83 ± 0.32 mm, trolox eq./100 gm extract and TAC = 199.18 ± 2.19 mg equivalent of ascorbic acid/g extract). EtOAc fraction derived from MeOH (85%) extract demonstrated the highest antioxidant potential; DPPH EC ₅₀ = 50.19 ± 0.24 (µg/ml), ABTS = 76.22 ± 1.61 (mm trolox eq./100 gm extract) and TAC = 249.86 ± 3.74 (mg equivalent of ascorbic acid/g extract)	El-Sayed et al. (2015)
Male inflorescence	Methanol extract of <i>S. egyptiaca</i> L.	DPPH and the folin–Ciocalteu method	Butanol fraction showed the highest antioxidant potential with an IC ₅₀ value of 27.7 µg/ml	Sonboli et al. (2010)
Flowers	Ethanol extract of <i>S. caprea</i> L.	DPPH, superoxide hydrogen peroxide and nitric oxide scavenging assay	At a concentration of 250 µg/ml, 85.04% of DPPH radicals and at µg/mL 45.97%, 17.97% and 56.53% of O ₂ · ⁻ , H ₂ O ₂ and NO, respectively, were scavenged by the <i>S. caprea</i> L. flower extract	Alam et al. (2006)
Leaves, bark, catkins	Cyclohexane, butanol, ethanol and water extract of <i>S. egyptica</i> L.	DPPH assay	Ethanol extract of the bark (highest activities, IC ₅₀ = 19 µg/ml)	Enayat and Banerjee (2009)
Bark	Hot ethanol extract of <i>S. alba</i> L.	DPPH and folin–Ciocalteu method	Free radical scavenging activity values ranged between 12.50, 37.50 and 80.00% of 10, 50 and 100 µg/ml, respectively	Sulaiman et al. (2013)
Bark	<i>S. alba</i> L., <i>S. daphnoides</i> Vill., <i>S. purpurea</i> L., and <i>S. daphnoides</i> Vill. × <i>purpurea</i> L. hybrid willow clones	ABTS	<i>S. daphnoides</i> Vill. × <i>purpurea</i> L. extracts were the most active ones.	Gawlik-Dziki et al. (2014)
Leaves and young stems	Hydroethanolic extract of <i>S. alba</i> L.	DPPH	IC ₅₀ = 19.1 µg/ml.	Zabihi et al. (2018)
Leaves and male inflorescence catkin	<i>S. matsudana</i> Koidz. <i>S. aegyptiaca</i> L. <i>S. babylonica</i> L. <i>S. excelsa</i> S. G. Gmel. <i>S. acmophylla</i> Boiss.	DPPH, superoxide, nitric oxide and hydrogen peroxide radical scavenging activity	DPPH results ranged from 40.08% (<i>S. excelsa</i>) to 91.94% (<i>S. aegyptiaca</i> L.) and <i>S. excelsa</i> S. G. Gmel. displayed the potent superoxide (99.00%) and nitric oxide (71.73%) scavenging potential. Similar activities were found for hydrogen peroxide radical scavenging (50%) for <i>S. matsudana</i> Koidz., <i>S. acmophylla</i> Boiss. and <i>S. babylonica</i> L.. Male inflorescence catkin extracts, <i>S. excelsa</i> S. G. Gmel (70.63%), <i>S. acmophylla</i> Boiss. (60.25%) and <i>S. matsudana</i> Koidz. (62.37%) presented the most activities in DPPH, nitric oxide and hydrogen peroxide, respectively. The <i>S. excelsa</i> S. G. Gmel, <i>S. aegyptiaca</i> L. and <i>S. babylonica</i> L. showed 99% superoxide radical inhibition.	Tavakoli et al. (2016)
Bark	Gallic acid, quercetin, rutin, vanillin and acetylsalicylic acid obtained from <i>S. aegyptiaca</i> L.	DPPH	gallic acid > quercetin > rutin > vanillin > acetylsalicylic acid.	Nauman et al. (2018)
Bark	Ethanol extract of <i>S. aegyptiaca</i> L.	DPPH	Ethyl acetate fraction showed the highest activity (11 ± 1 µg/ml).	Ceyhan (2014)

(Continued on following page)

TABLE 3 | (Continued) *In vitro* antioxidant activity of *Salix* species.

Plant part	Extract/compound	Method	Effects	References
Bark	<i>S. alba</i> L.	DPPH	All granulometric classes revealed a high antioxidant activity. The best results were obtained for the 50–100 μ m granulometric class.	Zaiter et al. (2016)
Flowers	Methanol extract of <i>S. tetrasperma</i> Roxb	TAC	30.97 \pm 2.6, 26.8 \pm 2.1 U/L for the extract and ascorbic acid, respectively.	Sobeh et al. (2019)
Bark	<i>S. atrocinerea</i> Brot., <i>S. fragilis</i> L., and <i>S. viminalis</i> L. bark polar extracts	DPPH and ABTS.	Strong free radical scavenging activity (5.58–23.62 μ g mL ⁻¹ IC ₅₀ range.	Ramos et al. (2019)
Leaves and bark	n- Hexane, dichloromethane, ethyl acetate and n- butanol extracts of <i>S. subserrata</i> Willd.	DPPH and FRAP assays.	IC ₅₀ μ g/mL = 9.30 - 206.67 for DPPH assay and 2.90-26.89 mM FeSO ₄ /mg extract for FRAP assay.	Tawfeek et al. (2019)
bark and leaves	<i>S. alba</i> L., <i>S. amplexicaulis</i> Bory & Chaub., <i>S. babylonica</i> L., <i>S. eleagnos</i> Scop., <i>S. fragilis</i> L., <i>S. purpurea</i> L. and <i>S. triandra</i> L.	DPPH and OH radical scavenging assay.	IC ₅₀ of DPPH ranged from 1.83–7.79 μ g/mL in bark and 1.95–8.07 μ g/mL in leaves extracts of different species of the genus <i>Salix</i>	Gligorić et al. (2019)

TABLE 4 | *In vitro* antiproliferative effects of *Salix* species.

Extract/compound	Cell line	Methods	Results	Mechanism of action	References
Aqueous extract from <i>S. safsaf</i> forsk	AML	Trypan blue exclusion test	Killed most of the blasts of acute myeloid leukemia (AML, 73.8%)	Cells are killed through denaturation of some enzymes and proteins that are induced by salicin and saligenin	El-Shemy et al. (2003)
Aqueous extract of leaves extract of <i>S. safsaf</i> forsk. Salicin and saligenin	ALL and AML	Trypan blue exclusion test	A remarkable destruction of lymphoblasts (75%) was observed after 24 h incubation of the mononuclear ALL cells with extract. Similar trends were observed for mononuclear AML cells. The mean viability of willow extract treated cells was 26.2%	Unknown receptors on the surface of leukemic cells may be binding with <i>Salix</i> extract compounds and leading to DNA destruction	El-Shemy et al. (2007)
Salicylalcohol derivatives, flavonoids, proanthocyanidins, and salicin isolated from willow bark extract BNO 1455	Human colon cyclooxygenase-2 (COX-2)-positive HT 29 and (COX-2)-negative HCT 116 or lung COX-2 proficient a 549 and low COX-2 expressing SW2 cells	WST-1 assay and propidium iodide uptake by flow cytometry, annexin V adhesion using flow cytometry for apoptosis	GI ₅₀ 33.3–103.3 μ g/ml for flavonoids and proanthocyanidins fractions and 50.0–243.0 μ g/ml for salicyl alcohol derivatives and extract	ND	Hostanska et al. (2007)

et al., 2016). The CNS depressant activity of the extract was attributed to binding of flavonoids to gamma-aminobutyric acid (GABA) receptors in the CNS (Hossain et al., 2009). Another study from our laboratory investigated the possible protective effect of *S. tetrasperma* Roxb. on neuropathic pain model, chronic constriction injury of sciatic nerve model. In this work, we explored the effects of the extract on central and peripheral nervous system in this model. We showed that the extract improved hyperalgesia and allodynia, the major signs of neuropathic pain through inhibition of oxidative stress and inflammation in sciatic nerve and brain stem (Sobeh et al., 2019).

Hepatoprotective Effects

S. subserrata Willd. flower extract showed marked hepatoprotective effects mostly through lowering the elevated

liver enzymes and decreasing the protein levels of two inflammatory biomarkers (NF- κ B and TNF- α) in carbon tetrachloride (CCl₄)-induced liver damage model (Wahid et al., 2016). It also presented a remarkable ability to reduce lipid peroxidation and had antioxidant effects related to several active ingredients that include flavonoids such as quercetrin, luteolin-7-glucoside, rutin, and quercetin and phenolic compounds such as salignin and catechins.

Anti-Obesity and Anti-lipidemic Effects

As shown in Table 8, remarkable anti-obesity and anti-lipidemic effects have been attributed to *Salix* extracts. The reduction of parametrial adipose tissue weight and body weight gain, the reduction of liver total cholesterol contents and inhibition of the elevated blood triacylglycerol are among the most

TABLE 5 | *In vivo* anticancer effects of *Salix* species.

Extract/compound	Doses	Route of administration	Methods	Effects	Mode of action	References
Aqueous extract from the young developing leaves of willow (<i>S. safsaf</i> forsk.)	0.2 and 0.6 ml of extract (10% w/v)	Oral	EACC were injected into the intraperitoneal cavity of mice	The willow extract reduced the tumor growth and delayed the death was delayed	Promote apoptosis, cause DNA damage, and affect cell membranes and/or denature proteins	El-Shemy et al. (2007)
Acetone soluble fraction of <i>S. caprea</i> L. flowers	0.5, 1.0 and 1.5 mg/kg	Topical application on the skin	7,12-Dimethyl benz [a] anthracene DMBA-initiated croton oil (phorbol ester)mice	Reduction in tumor incidence and number of tumors per mouse ranging from 20 to 50% and 50–63%	Intercept the free radicals and protect cellular macromolecules from oxidant damage. Effectiveness in inhibiting the ornithine decarboxylase activity and maintaining the activity of phase II enzymes after toxicant exposure	(Sultana and Saleem (2004)

TABLE 6 | *In vivo* neuroprotective effects of *Salix* species and their major constituents.

Extract/Compound	Doses	Route	Model	Effect	References
Ethanol and aqueous extracts of <i>S. tetrasperma</i> roxb. Leaves	200 and 400 mg/kg	Oral	Mice	Decrease locomotor activity indicating CNS depressant activity in mice and has muscle relaxant activity	Virupaksha et al. (2016)
Methanol extract of <i>S. tetrasperma</i> roxb. Flowers	200 and 400 mg/kg	Oral	CCI rat model	Relieve hyperalgesia and allodynia responses	Sobeh et al. (2019)

TABLE 7 | *In vivo* hepatoprotective effects of *Salix* species and their major constituents.

Extract/Compound	Doses	Route	Model	Effect	References
Ethanol extract of <i>S. subserata</i> willd. Flowers	150 mg/kg	Oral	CCl ₄ -induced chronic hepatotoxicity in rats	The elevated serum levels of intracellular liver enzymes and the expression levels of TNF- α and NF κ B proteins were reduced	Wahid et al. (2016)
<i>S. caprea</i> L. flowers	50, 100, 150 mg/kg	Oral	Mice injected with ferric nitrilotriacetate (FeNTA)	Decreased hepatic lipid peroxidation, increased hepatic glutathione (GSH) content and the activities of antioxidant enzymes (catalase (CAT), glutathione reductase (GR) and glutathione peroxidase)	Alam et al. (2006)

TABLE 8 | *In vivo* anti-obesity and anti-lipidemic effects of *Salix* species and their major constituents.

Extract/compound	Doses	Route of administration	Model	Effects	References
Ethanol extracts prepared from <i>S. babylonica</i> L. leaves	2.5 or 10 g (extract)/kg food	Supplemented in diet	HFD mice	Decreased body weight and parametrial adipose tissue weight	Liu (2012)
Ethanol extracts prepared from <i>S. babylonica</i> L. leaves	10%	Supplemented in diet	Rats orally administered 1 ml of a lipid emulsion composed	The extracts inhibited the elevation of blood triacylglycerol	Liu (2012)
Polyphenol fractions of <i>S. matsudana</i> koidz. Leaves	5%	Supplemented in diet	HFD mice	Decreased body weight and reduced the hepatic total cholesterol content	Han et al. (2003a)

prominent, directly attributed to its ability to inhibition of intestinal absorption of dietary fat (Liu, 2012). These effects have been mostly attributed to polyphenol fractions (apigenin-7-*O*-D-glucoside, luteolin-*O*-D-glucoside and chrysoeriol-7-*O*-D-glucoside) which inhibited palmitic acid incorporation into small intestinal brush border membrane vesicles (Han et al., 2003). It was reported that

methanol extract of *S. pseudo-lasiogyne* H. Lévl. twigs and salicortin derivatives reduced lipid accumulation in a concentration-dependent manner. They inhibited the differentiation of adipocytes in 3T3-L1 cells. The 2',6'-*O*-acetylsalicortin exhibited the most potent inhibitory activity with IC₅₀ = 11.6 μ M. It remarkably downregulated the expressions of sterol regulatory element binding protein

1 (SREBP1c) and CCAAT/enhancer binding protein α (C/EBP α). Thus, salicortin derivatives possessed anti-adipogenic effects via down-regulation of SREBP1c and C/EBP α dependent pathways (Lee et al., 2013).

CONCLUSION AND FUTURE PERSPECTIVES

The current review outlined the complete research progress in the phytochemistry, traditional use and pharmacology of genus *Salix* plant extracts and constituents. *Salix* extracts and some of its components exerted potent antioxidant, anti-inflammatory, antiproliferative, and antimicrobial properties confirming the traditional use of willow extracts in folk medicine. They also demonstrated substantial abilities in suppressing inflammatory pathways, both in cancer prevention and treatment, and in other chronic diseases. Thus, as a potential perspective, *Salix* extracts alone or their isolated active components should be examined more thoroughly, and its anti-HIV, hepatoprotective and neuroprotective therapeutic approach should also be discussed.

REFERENCES

- Agnolet, S., Wiese, S., Verpoorte, R., and Staerk, D. (2012). Comprehensive analysis of commercial willow bark extracts by new technology platform: combined use of metabolomics, high-performance liquid chromatography–solid-phase extraction–nuclear magnetic resonance spectroscopy and high-resolution radical scavenging assay. *J. Chromatogr. A* 1262, 130–137. doi:10.1016/j.chroma.2012.09.013
- Ahmed, A., Akbar, S., and Shah, W. A. (2017). Chemical composition and pharmacological potential of aromatic water from *Salix caprea* inflorescence. *Chin. J. Integr. Med.* 1–5. doi:10.1007/s11655-017-2781-5
- Ahmed, W., Ahmad, M., Khan, R. A., and Mustaq, N. (2016). Promising inhibition of krait snake's venom acetylcholinesterase by *Salix nigra* and its role as anticancer, antioxidant agent. *Indian J. Anim. Res.* 50, 317–323. doi:10.18805/ijar.10711
- Alam, M. S., Kaur, G., Jabbar, Z., Javed, K., and Athar, M. (2006). Evaluation of antioxidant activity of *Salix caprea* flowers. *Phytother. Res.* 20, 479–483. doi:10.1002/ptr.1882
- Argus, G. W. (2006). *Guide to the identification of salix (willow) in Illinois, Indiana, Ohio, and Pennsylvania*. Ottawa, Ontario: Canadian Museum of Nature, 47.
- Argus, G. W. (2007). *Salix* (Salicaceae) distribution maps and a synopsis of their classification in North America, North of Mexico. *Harv. Pap. Bot.* 12, 335–368. doi:10.3100/1043-4534(2007)12[335:ssdmaa]2.0.co;2
- Asgarpanah, J. (2012). Phytopharmacology and medicinal properties of *Salix aegyptiaca* L. *Afr. J. Biotechnol.* 11, 7145–7150. doi:10.5897/AJB12.418
- Balbas, S., Khafagy, S., Haggag, M., and Sahsah, N. (1979). Phytochemical study of certain *Salix* species cultivated in Egypt. *J. Pharmacol. Sci.* 20, 153–164.
- Binns, W. W., Blunden, G., and Woods, D. L. (1968). Distribution of leucoanthocyanidins, phenolic glycosides and imino-acids in leaves of *Salix* species. *Phytochemistry* 7, 1577–1581. doi:10.1016/s0031-9422(00)88609-4
- Brereton, N. J. B., Berthod, N., Lafleur, B., Pedneault, K., Pitre, F. E., and Labrecque, M. (2017). Extractable phenolic yield variation in five cultivars of mature short rotation coppice willow from four plantations in Quebec. *Ind. Crop. Prod.* 97, 525–535. doi:10.1016/j.indcrop.2016.12.049
- Bridle, P., Stott, K. G., and Timberlake, C. F. (1970). Anthocyanins in *salix* species. *Phytochemistry* 9, 1097–1098. doi:10.1016/s0031-9422(00)85231-0

AUTHOR CONTRIBUTION

NT retrieved the relevant literature and drafted the manuscript. AME and MW originated the work, led the discussions, provided helpful comments, and revised the manuscript. MF wrote the biological activity part. DH, MS and NF provided helpful comments and revised the manuscript. All authors read and approved the final version of the manuscript.

ACKNOWLEDGMENTS

The authors would like to thank the Egyptian Government for the Ph.D. scholarship of N.T.

SUPPLEMENTARY MATERIAL

The Supplementary Material for this article can be found online at: <https://www.frontiersin.org/articles/10.3389/fphar.2021.593856/full#supplementary-material>.

- Bridle, P., Stott, K. G., and Timberlake, C. F. (1973). Anthocyanins in *Salix* species: a new anthocyanin in *Salix purpurea* bark. *Phytochemistry* 12, 1103–1106. doi:10.1016/0031-9422(73)85023-x
- Ceyhan, M. S. (2014). Investigation of antioxidant properties and anticarcinogenic effects of ethanolic extract from bark of *Salix aegyptiaca* and its fractions. *MS thesis*. Ankara, Turkey: Middle East Technical University.
- Christenhusz, M. J. M., and Byng, J. W. (2016). The number of known plants species in the world and its annual increase. *Phytotaxa* 261, 201–217. doi:10.11646/phytotaxa.261.3.1
- Du, Q., Jerz, G., Shen, L., Xiu, L., and Winterhalter, P. (2007). Isolation and structure determination of a lignan from the bark of *Salix alba*. *Nat. Prod. Res.* 21, 451–454. doi:10.1080/14786410601083845
- Du, Q., Jerz, G., and Winterhalter, P. (2004). Preparation of three flavonoids from the bark of *Salix alba* by high-speed countercurrent chromatographic separation. *J. Liq. Chromatogr. Relat. Technol.* 27, 3257–3264. doi:10.1081/jlc-200034917
- Eftekhari, Y., Rustaiyan, A., Monajjemi, M., and Khavari-nejad, R. A. (2014). Study of anti-retroviral effects of *salix aegyptiaca* L. herbal extract on HIV-1 *in-vitro*. *Int. J. Mol. Clin. Microbiol.* 1, 398–405.
- El-Sayed, M. M., El-Hashash, M. M., Mohamed, H. R., and Abdel-Lateef, E. E.-S. (2015). Phytochemical Investigation and *in vitro* antioxidant activity of different leaf extracts of *Salix mucronata* Thunb. *J. Appl. Pharmaceut. Sci.* 5, 080–085. doi:10.7324/japs.2015.501213
- El-Shazly, A., El-Sayed, A., and Fikrey, E. (2012). Bioactive secondary metabolites from *Salix tetrasperma* Roxb. *Z. Naturforsch. C Biosci.* 67, 353–359. doi:10.5560/znc.2012.67c0353
- El-Shemy, H. A., Aboul-Enein, A. M., Aboul-Enein, K. M., and Fujita, K. (2007). Willow leaves' extracts contain anti-tumor agents effective against three cell types. *PloS One* 2, e178. doi:10.1371/journal.pone.0000178
- El-Shemy, H. A., Aboul-Enein, A. M., Aboul-Enein, M. I., Issa, S. I., and Fujita, K. (2003). The effect of willow leaf extracts on human leukemic cells *in vitro*. *J. Biochem. Mol. Biol.* 36, 387–389. doi:10.5483/bmbrep.2003.36.4.387
- Enayat, S., and Banerjee, S. (2009). Comparative antioxidant activity of extracts from leaves, bark and catkins of *Salix aegyptiaca* sp. *Food Chem.* 116, 23–28. doi:10.1016/j.foodchem.2009.01.092
- Evans, T. P., Clausen, T. P., Reichardt, P. B., and Chang, S. (1995). Structurally intriguing glucosides from Alaskan littletree willow (*Salix arbusculoides*). *J. Nat. Prod.* 58, 1897–1900. doi:10.1021/np50126a015

- Fayaz, M., and Sivakumaar, P. K. (2014). Phytochemical Analysis and antimicrobial activity of *Salix alba* against dental biofilm forming bacteria. *Int. J. Pharm. Biol. Arch.* 5, 137–140. doi:10.22377/IJPBA.V5I2.1273
- Fernandes, C. C., de Carvalho Cursino, L. M., Novaes, J. d. A. P., Demetrio, C. A., Júnior, O. L. P., Nunez, C. V., et al. (2009). Salicylates isolated from leaves and stems of *Salix martiana* Leyb. (Salicaceae). *Quím. Nova.* 32, 983–986. doi:10.1590/s0100-40422009000400029
- Freischmidt, A., Jürgenliemk, G., Kraus, B., Okpanyi, S., Müller, J., Kelber, O., et al. (2010). Phenolic compounds in the ethyl acetate fraction of a standardized willow bark extract. *Planta. Med.* 76, P283. doi:10.1055/s-0030-1264581
- Gawlik-Dziki, U., Sugier, D., Dziki, D., and Sugier, P. (2014). Bioaccessibility *in vitro* of nutraceuticals from bark of selected *Salix* species. *Sci. World J.* 2014, 782763. doi:10.1155/2014/782763
- Glgorić, E., Igić, R., Suvađžić, L., and Grujić-Letić, N. (2019). Species of the genus *Salix* L.: biochemical screening and molecular docking approach to potential acetylcholinesterase inhibitors. *Appl. Sci.* 9, 1842. doi:10.3390/app9091842
- González-Alamilla, E. N., Gonzalez-Cortazar, M., Valladares-Carranza, B., Rivas-Jacobo, M. A., Herrera-Corredor, C. A., Ojeda-Ramírez, D., et al. (2019). Chemical constituents of *Salix babylonica* L. and their antibacterial activity against gram-positive and gram-negative animal bacteria. *Molecules* 24, 2992. doi:10.3390/molecules24162992
- Gutiérrez, S. D., Kuri, S. A., and Martín-Herrera, D. (2017). The bioguided fractionation and pharmacological activity of an endemic *Salix canariensis* species. *Acta Pharm.* 67, 265–273. doi:10.1515/acph-2017-0012
- Gąsecka, M., Młeczek, M., Jutrzenka, A., Goliński, P., and Stuper-Szablewska, K. (2017). Phenolic compounds in leaves of *Salix* species and hybrids growing under different soil conditions. *Chem. Ecol.* 33, 196–212. doi:10.1080/02757540.2017.1289186
- Han, L. K., Sumiyoshi, M., Zhang, J., Liu, M. X., Zhang, X. F., Zheng, Y. N., et al. (2003a). Anti-obesity action of *Salix matsudana* leaves (Part 1). Anti-obesity action by polyphenols of *Salix matsudana* in high fat-diet treated rodent animals. *Phytother. Res.* 17, 1188–1194. doi:10.1002/ptr.1404
- Han, L. K., Sumiyoshi, M., Zheng, Y. N., Okuda, H., and Kimura, Y. (2003b). Anti-obesity action of *Salix matsudana* leaves (Part 2). Isolation of anti-obesity effectors from polyphenol fractions of *Salix matsudana*. *Phytother. Res.* 17, 1195–1198. doi:10.1002/ptr.1405
- Hernandez, P. M., Salem, A. Z., Elghandour, M. M., Cipriano-Salazar, M., Cruz-Lagunas, B., and Camacho, L. M. (2014). Anthelmintic effects of *Salix babylonica* L. and *Leucaena leucocephala* Lam. extracts in growing lambs. *Trop. Anim. Health Prod.* 46, 173–178. doi:10.1007/s11250-013-0471-7
- Highfield, E. S., and Kemper, K. J. (1999). Long wood herbal task force white willow bark (*Salix alba*). Available at: www.mcp.edu/herbal/default.htm (Accessed July 13, 1999).
- Hossain, M. M., Biva, I. J., Jahangir, R., and Vhuiyan, M. M. I. (2009). Central nervous system depressant and analgesic activity of *Aphanamixis polystachya* (Wall.) parker leaf extract in mice. *Afr. J. Pharm. Pharmacol.* 3, 282–286. doi:10.5897/AJPP.9000073
- Hostanska, K., Jürgenliemk, G., Abel, G., Nahrstedt, A., and Saller, R. (2007). Willow bark extract (BNO1455) and its fractions suppress growth and induce apoptosis in human colon and lung cancer cells. *Canc. Detect. Prev.* 31, 129–139. doi:10.1016/j.cdp.2007.03.001
- Howlett, J. (2008). *Functional foods: from science to health and claims*. Brussels, Belgium: ILSI Europe, 3772–3781.
- Hsu, F.-L., Nonaka, G.-I., and Nishioka, I. (1985). Acylated flavanols and procyanidins from *Salix sieboldiana*. *Phytochemistry* 24, 2089–2092. doi:10.1016/s0031-9422(00)83128-3
- Hussain, H., Badawy, A., Elshazly, A., Elsayed, A., Krohn, K., Riaz, M., et al. (2011). Chemical constituents and antimicrobial activity of *Salix suberrata*. *Record Nat. Prod.* 5, 133–137.
- Isebrands, J. G., and Richardson, J. (2014). *Poplars and willows: trees for society and the environment*. Boston, USA: The Food and Agriculture Organization of the United Nations and CABI, 634.
- Januarti, R., Santoni, A., and Efdi, M. (2019). Isolation of flavonoid compound and antioxidant activity of *Salix tetrasperma* Roxb. leaves. *Indones. J. Fundamental Appl. Chem.* 4, 42–46. doi:10.24845/ijfac.v4.i2.42
- Jeon, S. H., Chun, W., Choi, Y. J., and Kwon, Y. S. (2008). Cytotoxic constituents from the bark of *Salix hulteni*. *Arch. Pharm. Res.* 31, 978–982. doi:10.1007/s12272-001-1255-9
- Jürgenliemk, G., Petereit, F., and Nahrstedt, A. (2007). Flavan-3-ols and procyanidins from the bark of *Salix purpurea* L. *Pharmazie.* 62, 231–234. doi:10.1691/ph.2007.3.6577
- Karawya, M. S., Ammar, N. M., and Hifnawy, M. S. (2010). Phytochemical study and evaluation of the anti-inflammatory activity of some medicinal plants growing in Egypt. *Med. J. Islamic World Acad. Sci.* 109, 1–12.
- Karimi, I., Hayatgheybi, H., Kamalak, A., Pooyanmehr, M., and Marandi, Y. (2011). Chemical composition and effect of an essential oil of *Salix aegyptiaca* L., Salicaceae, (musk willow) in hypercholesterolemic rabbit model. *Rev. Bras. Farmacogn.* 21, 407–414. doi:10.1590/s0102-695x2011005000030
- Khatoon, F., Khabiruddin, M., and Ansari, W. (1988). Phenolic glycosides from *Salix babylonica*. *Phytochemistry* 27, 3010–3011. doi:10.1016/0031-9422(88)80716-7
- Kim, C. S., Kwon, O. W., Kim, S. Y., Choi, S. U., Kim, J. Y., Han, J. Y., et al. (2014). Phenolic glycosides from the twigs of *Salix glandulosa*. *J. Nat. Prod.* 77, 1955–1961. doi:10.1021/np500488v
- Kim, C. S., Subedi, L., Park, K. J., Kim, S. Y., Choi, S. U., Kim, K. H., et al. (2015). Salicin derivatives from *Salix glandulosa* and their biological activities. *Fitoterapia.* 106, 147–152. doi:10.1016/j.fitote.2015.08.013
- Kishore, R. N., Mangilal, T., Anjaneyulu, N., Abhinayani, G., and Sravya, N. (2014). Investigation of anti-inflammatory and invitro antioxidant activities of hydroalcoholic extract of bark of *Salix tetrasperma* Roxb. *Int. J. Pharm. Drug Anal.* 2, 506–509.
- Kompantsev, V. A., and Shinkarenko, A. L. (1975). (–)-Salipurposide from the bark of *Salix elbursensis*. *Chem. Nat. Compd.* 11, 682. doi:10.1007/bf00567714
- Kompantsev, V. (1969). Flavonoids of the bark of *Salix elbursensis*. *Chem. Nat. Compd.* 5, 274. doi:10.1007/bf00683860
- Kompantsev, V., Gaidash, P., and Dauksha, A. (1974). Phenolic compounds of the bark of *Salix alba* × *babylonica*. *Chem. Nat. Compd.* 10, 839. doi:10.1007/bf00564031
- Kompantsev, V., and Shinkarenko, A. (1973). Phenolic glycosides of the roots of *Salix pentandroides*. *Chem. Nat. Compd.* 9, 127. doi:10.1007/bf00580924
- Krauze-Baranowska, M., Pobłocka-Olech, L., Glód, D., Wiwart, M., Zieliński, J., and Migas, P. (2013). HPLC of flavanones and chalcones in different species and clones of *Salix*. *Acta Pol. Pharm.* 70, 27–34.
- Kuzovkina, Y. A., and Vietto, L. (2014). An update on the cultivar registration of *Populus* and *Salix* (Salicaceae). *Skvortsovia* 1, 133–148.
- Lauron-Moreau, A., Pitre, F. E., Argus, G. W., Labrecque, M., and Brouillet, L. (2015). Phylogenetic relationships of american willows (*salix* L., Salicaceae). *PLoS One* 10, e0121965. doi:10.1371/journal.pone.0121965
- Lee, M., Lee, S. H., Kang, J., Yang, H., Jeong, E. J., Kim, H. P., et al. (2013). Salicortin-derivatives from *Salix pseudo-lasiogyne* twigs inhibit adipogenesis in 3T3-L1 cells via modulation of C/EBPα and SREBP1c dependent pathway. *Molecules* 18, 10484–10496. doi:10.3390/molecules180910484
- Li, W., Shi, L. L., Han, L. Q., and Zhang, J. (2013). Development and validation of a RP-HPLC method for simultaneous determination of salicin and eight flavonoids in leaves of *Salix Matsudana* Koidz. *Acta Chromatograph.* 25, 735–743. doi:10.1556/achrom.25.2013.4.11
- Li, X., Liu, Z., Zhang, X.-f., Wang, L.-j., Zheng, Y.-n., Yuan, C.-c., et al. (2008). Isolation and characterization of phenolic compounds from the leaves of *Salix matsudana*. *Molecules.* 13, 1530–1537. doi:10.3390/molecules13081530
- Liu, K.-Y., Liu, H.-J., Zhou, B., and Han, L.-k. (2008). Studies on chemical constituents from *Salix babylonica* L. and their stimulating lipolysis activity. *J. Fudan Uni.* 4, 022.
- Liu, K. Y. (2012). Stimulatory effects of extracts prepared from *Salix babylonica* L. on fat catabolism in mice fed high-fat diet. *Adv. Mater. Res.* 518–523, 498–501. doi:10.4028/www.scientific.net/amr.518-523.498
- Mabberley, D. J. (2008). *Mabberley's plant-book: a portable dictionary of plants, their classifications and uses*. Cambridge: Cambridge University Press, 972.
- Mahdi, J. G. (2010). Medicinal potential of willow: a chemical perspective of aspirin discovery. *J. Saudi Chem. Soc.* 14, 317–322. doi:10.1016/j.jscs.2010.04.010
- Maistro, E. L., Terrazzas, P. M., Perazzo, F. F., Gaivão, I. O. N. D. M., Sawaya, A. C. H. F., and Rosa, P. C. P. (2019). *Salix alba* (white willow) medicinal plant presents genotoxic effects in human cultured leukocytes. *J. Toxicol. Environ. Part A.* 82, 1223–1234. doi:10.1080/15287394.2019.1711476
- Malterud, K. E., and Dugstad, E. K. S. (1985). 4, 2'-dihydroxy-3, 5-dimethoxybiphenyl, a new phenol from the wood of *Salix caprea* L. *Z. Naturforsch. B Chem. Sci.* 40, 853–854. doi:10.1515/znB-1985-0629

- Masika, P., Sultana, N., Afolayan, A., and Houghton, P. (2005). Isolation of two antibacterial compounds from the bark of *Salix capensis*. *South Afr. J. Bot.* 71, 441–443. doi:10.1016/s0254-6299(15)30117-4
- Mizuno, M., Kato, M., Hosoi, N., Iinuma, M., Tanaka, T., Kimura, A., et al. (1990). Phenolic compounds from *Salix sachalinensis*. *Heterocycles* 31, 1409–1412. doi:10.3987/com-90-5425
- Mizuno, M., Kato, M., Iinuma, M., Tanaka, T., Kimura, A., Ohashi, H., et al. (1987). Acylated luteolin glucosides from *Salix gilgiana*. *Phytochemistry* 26, 2418–2420. doi:10.1016/s0031-9422(00)84739-1
- Mizuno, M., Kato, M., Misu, C., Iinuma, M., and Tanaka, T. (1991). Chaenomeloidin: a phenolic glucoside from leaves of *Salix chaenomeloides*. *J. Nat. Prod.* 54, 1447–1450. doi:10.1021/np50077a042
- Mostafa, I., Abbas, H. A., Ashour, M. L., Yasri, A., El-Shazly, A. M., Wink, M., et al. (2020). Polyphenols from *Salix tetrasperma* impair virulence and inhibit quorum sensing of *Pseudomonas aeruginosa*. *Molecules* 25, 1341. doi:10.3390/molecules25061341
- Nasaduri, A. A., Kompantsev, V. A., Oganessian, É. T., and Shinkarenko, A. L. (1972). Luteolin 7-glucoside from the leaves of *Salix caprea*. *Chem. Nat. Compd.* 8, 388. doi:10.1007/bf00563763
- Nathan, C., and Ding, A. (2010). Nonresolving inflammation. *Cell* 140, 871–882. doi:10.1016/j.cell.2010.02.029
- Nauman, M., Kale, R., and Singh, R. P. (2018). Polyphenols of *Salix aegyptiaca* modulate the activities of drug metabolizing and antioxidant enzymes, and level of lipid peroxidation. *BMC Compl. Alter. Med.* 18, 81. doi:10.1186/s12906-018-2143-7
- Nichols-Orians, C. M., Clausen, T. P., Fritz, R. S., Reichardt, P. B., and Wu, J. (1992). 2'-Cinnamoylsalicylic acid, a phenolic glycoside from *Salix sericea*. *Phytochemistry* 31, 2180–2181. doi:10.1016/0031-9422(92)80397-w
- Noletto-Dias, C., Harflett, C., Beale, M. H., and Ward, J. L. (2020). Sulfated flavanones and dihydroflavonols from willow. *Phytochem. Lett.* 35, 88–93. doi:10.1016/j.phytol.2019.11.008
- Noletto-Dias, C., Ward, J. L., Bellisai, A., Lomax, C., and Beale, M. H. (2018). Salicin-7-sulfate: a new salicinoid from willow and implications for herbal medicine. *Fitoterapia* 127, 166–172. doi:10.1016/j.fitote.2018.02.009
- Noletto-Dias, C., Wu, Y., Bellisai, A., Macalpine, W., Beale, M., and Ward, J. (2019). Phenylalkanoic glycosides (Non-Salicycinoids) from wood chips of *Salix triandra* *dasyclados* hybrid willow. *Molecules* 24, 1152. doi:10.3390/molecules24061152
- Pearl, I. A., and Darling, S. F. (1970). Purpurein, a new glucoside from the bark of *Salix purpurea*. *Phytochemistry* 9, 853–856. doi:10.1016/s0031-9422(00)85192-4
- Poblocka-Olech, L., and Krauze-Baranowska, M. (2008). SPE-HPTLC of procyanidins from the barks of different species and clones of *Salix*. *J. Pharmaceut. Biomed. Anal.* 48, 965–968. doi:10.1016/j.jpba.2008.05.039
- Pohjamo, S. P., Hemming, J. E., Willför, S. M., Reunanen, M. H., and Holmbom, B. R. (2003). Phenolic extractives in *Salix caprea* wood and knots. *Phytochemistry* 63, 165–169. doi:10.1016/s0031-9422(03)00050-5
- Popova, T. P., and Kaleva, M. D. (2015). Antimicrobial effect *in vitro* of aqueous extracts of leaves and branches of willow (*Salix babylonica* L.). *Int. J. Curr. Microbiol. Appl. Sci.* 4, 146–152.
- Prashith Kekuda, T., Vinayaka, K., and Raghavendra, H. (2017). Ethnobotanical uses, phytochemistry and biological activities of *Salix tetrasperma* roxb. (Salicaceae)-A review. *J. Med. Plants* 5, 201–206.
- Ramos, P. A. B., Moreirinha, C., Silva, S., Costa, E. M., Veiga, M., Coscueta, E., et al. (2019). The health-promoting potential of *Salix* spp. bark polar extracts: key insights on phenolic composition and *in vitro* bioactivity and biocompatibility. *Antioxidants* 8, 609. doi:10.3390/antiox8120609
- Rawat, U., Semwal, S., Semwal, D., Badoni, R., and Bamola, A. (2009). A new flavonoid glycoside from *salix denticulata* aerial parts. *Molbank*. 2009, M622. doi:10.3390/M622
- Reichardt, P. B., Merken, H. M., Clausen, T. P., and Wu, J. (1992). Phenolic glycosides from *Salix lasiandra*. *J. Nat. Prod.* 55, 970–973. doi:10.1021/np50085a022
- Rubió, L., Motilva, M.-J., and Romero, M.-P. (2013). Recent advances in biologically active compounds in herbs and spices: a review of the most effective antioxidant and anti-inflammatory active principles. *Crit. Rev. Food Sci. Nutr.* 53, 943–953. doi:10.1080/10408398.2011.574802
- Salem, A.-F. Z., Salem, M. Z., Gonzalez-Ronquillo, M., Camacho, L., and Cipriano, M. (2011). Major chemical constituents of *Leucaena leucocephala* and *Salix babylonica* leaf extracts. *J. Trop. Agric.* 49, 95–98.
- Salem, A. Z., Elghandour, M. M., Kholif, A. E., López, S., Pliego, A. B., Cipriano-Salazar, M., et al. (2017). Tree leaves of *Salix babylonica* extract as a natural anthelmintic for small-ruminant farms in a semiarid region in Mexico. *Agrofor. Syst.* 91, 111–122. doi:10.1007/s10457-016-9909-z
- Salem, M. A., Hamdan, D. I., Mostafa, I., Adel, R., Elissawy, A., and El-Shazly, A. M. (2020). “Natural products, the new intervention regime of metabolic disorders,” in *Natural products in clinical trials, attar-ur-rahman, shazia anjum and hesham R. El-seedi*. Singapore: Bentham Book Imprint, Chapter 2, Vol. 2, 32–122.
- Sati, S., Singh, H., Badoni, P., and Sati, M. (2013). Screening of fungicidal activity of *salix* and *triumfetta* species of garhwal himalaya. *AJPCT* 1, 486–489.
- Semwal, S., Rawat, U., and Sharma, R. K. (2011). Isolation and characterization of a new flavone diglucoside from *Salix denticulata*. *Chem. Nat. Compd.* 47, 366. doi:10.1007/s10600-011-9935-z
- Shah, Z. A., Hameed, A., Ahmed, A., Simjee, S. U., Jabeen, A., Ullah, A., et al. (2016). Cytotoxic and anti-inflammatory salicin glycosides from leaves of *Salix acmophylla*. *Phytochem. Lett.* 17, 107–113. doi:10.1016/j.phytol.2016.07.013
- Shao, Y., Lahloub, M., Meier, B., and Sticher, O. (1989). Isolation of phenolic compounds from the bark of *Salix pentandra*. *Planta Med.* 55, 617–618. doi:10.1055/s-2006-962172
- Shelyuto, V. L., and Bondarenko, V. G. (1985). Flavonoids of *Salix acutifolia*. *Chem. Nat. Compd.* 21, 534. doi:10.1007/bf00579161
- Shen, T., Tian, Y.-Q., Liu, W.-X., and Zheng, S.-Z. (2008). Acyclic diterpene- γ -lactones and flavonoid from *Salix cheilophila* Omitted. *J. Chin. Chem. Soc.* 55, 401–405. doi:10.1002/jccs.200800059
- Singh, H., Raturi, R., and Badoni, P. (2017). Isolation of secondary metabolites from the roots of *salix babylonica*. *Mater. Sci. Eng.* 225, 012094. doi:10.1088/1757-899x/225/1/012094
- Sobeh, M., Mahmoud, M. F., Rezaq, S., Alsemeh, A. E., Sabry, O. M., Mostafa, I., et al. (2019). *Salix tetrasperma* roxb. Extract alleviates neuropathic pain in rats via modulation of the NF- κ B/TNF- α /NOX/iNOS pathway. *Antioxidants* 8, 482. doi:10.3390/antiox8100482
- Sonboli, A., Mojarad, M., Ebrahimi, S. N., and Enayat, S. (2010). Free radical scavenging activity and total phenolic content of methanolic extracts from male inflorescence of *Salix aegyptiaca* grown in Iran. *Iran. J. Pharm. Res. (IJPR)*. 9, 293–296.
- Sulaiman, G. M., Hussien, N. N., Marzoog, T. R., and Awad, H. A. (2013). Phenolic content, antioxidant, antimicrobial and cytotoxic activities of ethanolic extract of *Salix alba*. *Am. J. Biochem. Biotechnol.* 9, 41–46. doi:10.3844/ajbbsp.2013.41.46
- Sultana, S., and Saleem, M. (2004). *Salix caprea* inhibits skin carcinogenesis in murine skin: inhibition of oxidative stress, ornithine decarboxylase activity and DNA synthesis. *J. Ethnopharmacol.* 91, 267–276. doi:10.1016/j.jep.2003.12.028
- Tavakoli, F., Rahmani, F., and Heidari, R. (2016). Radical scavenging activity and total phenolic content in methanolic extracts of leaves and male inflorescence catkin of willow. *Curr. Nutr. Food Sci.* 12, 241–248. doi:10.2174/1573401312666160901123434
- Tawfeek, N., Sobeh, M., Hamdan, D. I., Farrag, N., Roxo, M., El-Shazly, A. M., et al. (2019). Phenolic compounds from *Populus alba* L. and *Salix subserata* Willd. (Salicaceae) counteract oxidative stress in *Caenorhabditis elegans*. *Molecules* 24, 1999. doi:10.3390/molecules24101999
- Thadeo, M., Azevedo, A. A., and Meira, R. M. S. A. (2014). Foliar anatomy of neotropical Salicaceae: potentially useful characters for taxonomy. *Plant Systemat. Evol.* 300, 2073–2089. doi:10.1007/s00606-014-1037-5
- Tuberoso, C. I., Jerković, I., Bifulco, E., and Marijanović, Z. (2011). Biodiversity of *Salix* spp. honeydew and nectar honeys determined by RP-HPLC and evaluation of their antioxidant capacity. *Chem. Biodivers.* 8, 872–879. doi:10.1002/cbdv.201000359
- Tunon, H., Olavsdotter, C., and Bohlin, L. (1995). Evaluation of anti-inflammatory activity of some Swedish medicinal plants. Inhibition of prostaglandin biosynthesis and PAF-induced exocytosis. *J. Ethnopharmacol.* 48, 61–76. doi:10.1016/0378-8741(95)01285-1
- Van Wyk, B.-E., and Wink, M. (2018). *Medicinal plants of the world*. Pretoria, South Africa: CABI, 648.
- Vinokurov, I. I. (1979). Flavonoid glycosides of *Salix rubra*. *Chem. Nat. Compd.* 15, 355–356. doi:10.1007/bf00566096
- Virupaksha, J. H., Nadendla, R. R., Kumar, M. S., and Kavya, S. (2016). Effect of *Salix tetrasperma* Roxburgh leaf extracts on central nervous system activities. *Res. J. Pharmaceut. Biol. Chem. Sci.* 7, 2060–2064.

- Wahid, A., Hamed, A. N., Eltahir, H. M., and Abouzied, M. M. (2016). Hepatoprotective activity of ethanolic extract of *Salix subserata* against CCl₄-induced chronic hepatotoxicity in rats. *BMC Compl. Alternative Med.* 16, 263. doi:10.1186/s12906-016-1238-2
- Wiesneth, S. C. (2019). Phytochemische Untersuchung des phenolischen Inhaltsstoffspektrums in *Salix* Spezies unter besonderer Berücksichtigung der Flavan-3-ole. Ph.D. dissertation. Germany: Universität Regensburg.
- Wu, Y., Dobermann, D., Beale, M. H., and Ward, J. L. (2016). Acutifoliside, a novel benzoic acid glycoside from *Salix acutifolia*. *Nat. Prod. Res.* 30, 1731–1739. doi:10.1080/14786419.2015.1137571
- Zabihi, N. A., Mahmoudabady, M., Soukhtanloo, M., Hayatdavoudi, P., Beheshti, F., and Niazmand, S. (2018). *Salix alba* attenuated oxidative stress in the heart and kidney of hypercholesterolemic rabbits. *Avicenna J. Phytomed.* 8, 63.
- Zaiter, A., Becker, L., Petit, J., Zimmer, D., Karam, M.-C., Baudelaire, É., et al. (2016). Antioxidant and antiacetylcholinesterase activities of different granulometric classes of *Salix alba* (L.) bark powders. *Powder Technol.* 301, 649–656. doi:10.1016/j.powtec.2016.07.014
- Zapesochnaya, G. G., Kurkin, V. A., Braslavskii, V. B., and Filatova, N. V. (2002). Phenolic compounds of *Salix acutifolia* bark. *Chem. Nat. Compd.* 38, 314–318. doi:10.1023/a:1021661621628
- Zarger, M. S. S., Khatoon, F., and Akhtar, N. (2014). Phytochemical investigation and growth inhibiting effects of *Salix alba* leaves against some pathogenic fungal isolates. *World J. Pharm. Pharmacol.* 3, 1320–1330.
- Zeid, A., Hifnawy, M., Saleh, M., Sleem, A., and Mohamed, R. (2006). Phenolics, volatiles and biological activities of *Salix babylonica* L. leaves and stem bark. *Planta Med.* 72, 335. doi:10.1055/s-2006-950135
- Zengion, A. H., and Yarnell, E. (2011). “Herbal and nutritional supplements for painful conditions,” in *Pain procedures in clinical practice*. Editors T. A. Lennard, S. A. Walkowski, K. A. Singla, and D. Vivian (Philadelphia, PA: Elsevier Saunders), 3, 187–204.
- Zhao, L., Liu, L., and Li, J. (2014). Qualitative and quantitative analysis of five bioactive flavonoids in *Salix bordensis* Turcz. by HPLC-DAD and HPLC-ESI-MS. *Am. J. Anal. Chem.* 5, 851. doi:10.4236/ajac.2014.513094
- Zhen-Fu, F. (1987). On the distribution and origin of *Salix* in the world. *J. Systemat. Evol.* 25, 307–313.

Conflict of Interest: The authors declare that the research was conducted in the absence of any commercial or financial relationships that could be construed as a potential conflict of interest.

Copyright © 2021 Tawfeek, Mahmoud, Hamdan, Sobeh, Farrag, Wink and El-Shazly. This is an open-access article distributed under the terms of the Creative Commons Attribution License (CC BY). The use, distribution or reproduction in other forums is permitted, provided the original author(s) and the copyright owner(s) are credited and that the original publication in this journal is cited, in accordance with accepted academic practice. No use, distribution or reproduction is permitted which does not comply with these terms.

GLOSSARY

ABTS 2,2'-azinobis-(3- ethylbenzothiazoline-6-sulfonic acid)

AIDs Acquired immunodeficiency syndrome

Apif Apiofuranosyl

Araf Arabinofuranosyl

Arap Arabinopyranosyl

CCl₄ Carbon tetrachloride

C/EBP α CCAAT/enhancer binding protein α

DPPH 2,2-Diphenyl, one- Picryl Hydrazyl

EACC Ehrlich ascites carcinoma cells

EtOAc Ethyl acetate

FRAP Ferric reducing antioxidant power

Glac Galactosyl

Glc Glucosyl

Gluc Glucuronoyl

Hex Hexosyl

HFD High-fat diet

HIV Human immunodeficiency virus

IC₅₀ Half maximal inhibitory concentration

MeOH Methanol

MIC Minimal inhibitory concentration

NF- κ B Nuclear factor kappa-B

ORAC Oxygen radical absorbance capacity

Pent Pentosyl

Ph Phenyl

Rh Rhamanosyl

Rut Rutinosyl

SREBP1c Sterol regulatory element binding protein 1

TAC Total antioxidant capacity

TFC Total flavonoid content

TLC Thin layer chromatography

TNF- α Tumor necrosis factor-alpha

TPC Total phenolic content

XTT 2,3-bis-(2-methoxy-4-nitro-5-sulfophenyl)-2H- tetrazolium-5-carboxanilide

Xylp Xylopyranosyl.



Downregulation of Candidate Gene Expression and Neuroprotection by Piperine in Streptozotocin-Induced Hyperglycemia and Memory Impairment in Rats

Suresh Kumar^{1*}, Suman Chowdhury¹, Ajay Razdan¹, Deepa Kumari¹, Ram Singh Purty¹, Heera Ram², Pramod Kumar², Prasunpriya Nayak³ and Sunil Dutt Shukla⁴

¹University School of Biotechnology, GGS Indraprastha University, New Delhi, India, ²Department of Zoology, Jai Narain Vyas University, Jodhpur, India, ³Department of Physiology, All India Institute of Medical Sciences, Jodhpur, India, ⁴Government Meera Girls College, Mohanlal Sukhadia University, Udaipur, India

OPEN ACCESS

Edited by:

Sayed Ahmad,
Jamia Hamdard University, India

Reviewed by:

Islam Husain,
University of Mississippi,
United States
Kumar Vaibhav,
Augusta University,
United States

*Correspondence:

Suresh Kumar
sureshkumar@ipu.ac.in

Specialty section:

This article was submitted to
Ethnopharmacology,
a section of the journal
Frontiers in Pharmacology

Received: 16 August 2020

Accepted: 21 December 2020

Published: 02 March 2021

Citation:

Kumar S, Chowdhury S, Razdan A,
Kumari D, Purty RS, Ram H, Kumar P,
Nayak P and Shukla SD (2021)
Downregulation of Candidate Gene
Expression and Neuroprotection by
Piperine in Streptozotocin-Induced
Hyperglycemia and Memory
Impairment in Rats.
Front. Pharmacol. 11:595471.
doi: 10.3389/fphar.2020.595471

There is accumulating evidence showing that hyperglycemia conditions like diabetes possess a greater risk of impairment to the neuronal system because high glucose levels exacerbate oxidative stress, accumulation of amyloid-beta peptides, and mitochondrial dysfunction, and impair cognitive functions and cause neurodegeneration conditions like Alzheimer's diseases. Due to the extensive focus on pharmacological intervention to prevent neuronal cells' impairment induced by hyperglycemia, the underlying molecular mechanism that links between Diabetes and Alzheimer's is still lacking. Given this, the present study aimed to evaluate the protective effect of piperine on streptozotocin (STZ) induced hyperglycemia and candidate gene expression. In the present study, rats were divided into four groups: control (Vehicle only), diabetic control (STZ only), piperine treated (20 mg/kg day, i.p), and sitagliptin (Positive control) treated. The memory function was assessed by Morris water maze and probe test. After treatment, biochemical parameters such as HOMA index and lipid profile were estimated in the serum, whereas histopathology was evaluated in pancreatic and brain tissue samples. Gene expression studies were done by real-time PCR technique. Present data indicated that piperine caused significant memory improvement as compared to diabetic (STZ) control. The assessment of HOMA indices in serum samples showed that piperine and sitagliptin (positive control, PC) caused significant alterations of insulin resistance, β cell function, and insulin sensitivity. Assessment of brain and pancreas histopathology shows significant improvement in tissue architecture in piperine and sitagliptin treated groups compared to diabetic control. The gene expression profile in brain tissue shows significantly reduced BACE1, PSEN1, APOA1, CASPASE3, and CATALASE genes in the piperine and sitagliptin (PC) treated groups compared to Diabetic (STZ) control. The present study demonstrated that piperine not only improves memory in diabetic rats but also reduces the expression of specific AD-related genes that can help design a novel strategy for therapeutic intervention at the molecular level.

Keywords: neuroprotection, gene expression, hyperglycemia, piperine, Alzheimer's

INTRODUCTION

There is growing evidence showing a link between Diabetes mellitus (DM) and Alzheimer's disease (AD). However, the mechanism is not known yet at the molecular level (Butterfield et al., 2014). The intricate link between these two diseases might be due to the dysregulation of blood sugar levels in the body that affects many cells, including brain cells in the central nervous system (CNS) (Malone, 2016). Blood glucose homeostasis is a well-coordinated physiological process controlled by hormone insulin and glucagon released by the pancreas (Roder et al., 2016). Alteration in blood sugar levels in conditions like hyperglycemia deteriorates brain cells and its functions, leading to the development of mild cognitive impairment, which is the early stage of AD (Duarte, 2015). A higher level of glucose not only increases amyloid-beta production in the brain but affects tau phosphorylation in the brain (Mullins et al., 2017). There is accumulating evidence showing that hyperglycemia conditions like diabetes possess a greater risk of impairment to the neuronal system (González-Reyes et al., 2016; Pruzin et al., 2018; Rojas-carranza et al., 2018) because high glucose levels exacerbate oxidative stress, accumulation of amyloid-beta peptides, and mitochondrial dysfunction, and impair cognitive functions, and cause neurodegeneration conditions like Alzheimer's diseases (Macauley et al., 2015; Gaspar et al., 2016; Kim et al., 2016; Rom et al., 2018; Silzer and Phillips, 2018). It is well established that administration of dexamethasone and streptozotocin (STZ) induced hyperglycemia in rodents (rats), resulting in increased levels of amyloid aggregation, tau phosphorylation, synapses loss, impairment of memory performance, and cognition deficit. STZ is commonly used to induce diabetes in rats. STZ uptake by pancreatic β cells is detrimental for β cells as STZ causes the generation of reactive oxygen species (ROS) (Vessal et al., 2003). It also results in cognitive impairment, glucose metabolism dysfunction, oxidative stress, and phosphorylation of tau protein resulting in neuronal cell death, a hallmark feature of AD (Salkovic-Petrisic et al., 2013; Moreira-Silva et al., 2018).

Oxidative stress is also responsible for many metabolic and neurologic disorders such as Alzheimer's disease, Parkinson's disease, cardiovascular disease, diabetes, and cancer (Kumar et al., 2015). In AD, oxidative stress is triggered by the accumulation of free radicals in the brain that leads to neuronal cell damage. Some of the genes that play a crucial role in amyloid processing, apoptosis, and oxidative stress are BACE1, PSEN1, APAF1, CASPASE3, and CATALASE. Hence, decreasing the expression levels of specific genes involved in apoptosis and oxidative stress pathways by particular therapeutic intervention will be an attractive strategy to counter neurodegeneration in a disease like AD. Several foods, nutrients, and phytochemicals such as resveratrol and curcumin have been investigated for preventive and intervention approaches that might help to prevent diabetes-related cognitive impairment (Mazzanti and Di Giacomo, 2016). Because of these, the present study demonstrated the neuroprotective effects of piperine on a high rich sucrose diet with Dexamethasone and STZ induced hyperglycemia and memory impairment in rats and relevant gene expression profile to address the molecular mechanism underlying the pathway.

MATERIAL AND METHODS

Materials

Roswell Park Memorial Institute (culture medium) (RPMI1640), Fetal bovine serum, penicillin (100 U/ml), and streptomycin (100 μ g/ml) were purchased from Himedia, India. The general chemicals were also purchased from Sigma or Merck, India. The rat pheochromocytoma (PC12) cells line used in the present study were obtained from the National Center for Cell Science, Pune, India.

GC-MS Analysis for Authentication of Piperine

The commercially procured piperine sample was identified using GC-MS for its authentication and purity check. GC-MS analysis was achieved using GC-MS-QP2010 Plus, with 230°C and 270°C selected for ion source and an interface temperature, respectively. An Rtx 5 MS capillary column (Restek Company, Bellefonte, United States) with 30 m (length) \times 0.25 mm (diameter) \times 0.25 μ m (film thickness) was used with a solvent cut time of 3.50 min, a threshold of 1,000 eV, and a mass range of 40–650 m/z settings input, as described previously (Chowdhury and Kumar, 2020). In brief, a 260°C injector temperature was programmed from 50°C for 2 min and further increased for up to 250°C with a rate of 4°C/min (3 min hold), followed by an increase of 280°C with a rate of 10°C/min (7 min hold). The peak obtained was compared with the spectrum of the known compounds available in the National Institute of Standards and Technology, U.S. Department of Commerce, and Wiley (John Wiley & Sons Ltd.) libraries.

Animals and Treatments

Development of Type -2 Diabetic Animal Model and Experimental Design

The healthy colony bred albino rats were used to develop a type 2 diabetic animal model with a weight of 150 gm to 200 gm. The rats were fed with a high sucrose diet, and dexamethasone intraperitoneal injections were administered (1.0 mg/kg/day i.e., for 20 days). A single dose of STZ (40 mg/kg) was given on the 21st day to properly develop the diabetic status (Chao et al., 2018). After the development of imbalance in glucose homeostasis through the sucrose feeding with dexamethasone, the mild dose of STZ (40 mg/kg) aggravated the induction of type 2 diabetes and started the treatments of piperine and sitagliptin from the next day as following the modified method of Ghasemi et al. (2014). The diabetic status was confirmed by monitoring glucose levels and insulin production by calculating glucose homeostasis (HOMA). The animals were kept under controlled environmental conditions as per CPCSEA norms. All the experimental protocols were approved by IAEC (Institutional Animal Ethical Committee) registered under the CPCSEA, India (Reg. No.1646/GO/a/12/CPCSEA valid up to 27.03.23).

The experimental design [1s(b)] was categorized into two comparative sets of control groups and treatment groups (**Supplementary Material**). The control groups consisting of two groups i.e., vehicle control and diabetic control, whereas

treatment groups were divided into two groups i.e., piperine treatment groups and sitagliptin treated groups (Positive control). Each group consisted of seven animals ($n = 7$). The contributing animal groups were categorized as follows.

- Group A: Vehicle control (VC)
- Group B: Diabetic control (STZ)
- Group C: Piperine treatment (STZ/PIP)
- Group D: Sitagliptin group (STZ/SITA)

Both piperine (20 mg/kg/day) and Sitagliptin (25 mg/kg/day) were administered daily for 4 weeks during the course of the experiment. The dose of 20 mg/kg/day of piperine is considered the standard dose, also mentioned in the literature (Ren et al., 2018; Guo et al., 2020).

Morris Water Maze

To evaluate the neurocognitive damage in these animal groups, a spatial memory task was used. Morris water maze (MWM) was employed to compare the spatial task performances of diabetic rats with that of control animals. The procedure for the training and assessment of behavioral task was carried out as described elsewhere (Dasari et al., 2016).

Animals were allowed to swim in a circular tank filled with water and a hidden (1 cm below the water level) platform in an isolated area. On the first day, animals were dropped on the opposite quadrant (in relation to the hidden platform), and the time required for finding the platform was noted as escape latency. If any animal could not find the platform within 3 min of exposure, they were guided to the platform, and the escape latency was noted as 180 s. Once the animal has reached the platform, it was allowed to rest there for 1 min. On the first day, three training trials were given with a gap of 30 min between tests. However, escape latency (Day 0) was recorded from the first trial only. On the 2nd day, escape latencies (Day 1) of animals were recorded with a single trial releasing the animals from the opposite quadrant. On the third day, escape latencies (Day 2) were noted with releases from the opposite quadrant, left quadrant, and right quadrant with respect to the quadrant where the platform was hidden. The hidden platform was removed on the fourth day (probe test), and the times the animal spent in all the quadrants were noted during a swimming session of 3 min.

Serum Biochemistry of Insulin, Glucose and Glucose Homeostasis (HOMA)

The HOMA was calculated for insulin and glucose by following the standard formula of Matthews et al. (1985).

HOMA – IR

$$= \frac{\text{Fasting Insulin (U/L)} \times \text{Fasting Glucose (mmol/L)}}{22.5}$$

$$\text{Insulinsensitivity (IS)} = \frac{1}{[(\text{Insulin (U/L)} \times \text{Log}(\text{glucose (mmol/L)})]}$$

$$\text{HOMA} - \beta = \frac{20 \times \text{fasting Insulin (U/L)}}{\text{fasting Glucose (mmol/L)}} - 3.5$$

Lipid Profile

The lipid profile parameters, total cholesterol, triglyceride, HDL-cholesterol, VLDL-cholesterol, LDL-cholesterol, and atherogenic indices of plasma were calculated by following standard methods using the Fieldward formula (Dobiášová and Frohlich, 2001; Ram et al., 2020).

$$\text{LDL} - \text{C (mg/dL)} = \text{TC (mg/dL)} - \text{HDL} - \text{C (mg/dL)} - \text{TG (mg/dL)}/5.$$

Histopathology of Pancreases and Brain

The animals were sacrificed after four weeks of experimentation (28 days) by cervical dislocation as per standard norms and further proceeded for histological preparations.

Pancreas Histology. The pancreatic histology was evaluated by following the paraffin sectioning following ascending and descending dehydration with hematoxylin-eosin (H&E) staining (Saravanan et al., 2017). The microphotography of stained slides of the pancreatic islets of the Langerhans performed by the Radical microscope (Model No. RXLr-5), India attached with supported software of ProgRes® SpeedXT core 5 by Jenoptiric, Germany.

Histopathology of Brain Tissues. Paraffin sections were stained with Cresyl violet to study the neurodegenerative and cytoarchitectural changes. 10 µm thick coronal sections were cut using a rotary microtome. Sections passing through the hippocampus (bregma –1.8 mm to –5.8 mm) were stained with cresyl violet.

Morphological Variables

To measure the effects of various treatments on hippocampal neurons, neuronal cells were subjected to morphological parameters somatic perimeter (µm), somatic area (µm²), somatic aspect ratio, somatic compactness, somatic form factor, and somatic roundness. Both area and perimeter can be used to mark the size, and the rest can be assigned to the shape of a neuron. The following table depicts the methods and formulas for calculating the morphological variables (McGarry et al., 2010).

S. No	Morphological variable name	Abbreviation	Formula
1	Somatic perimeter (µm)	SP	The perimeter of the Soma
2	Somatic area (µm ²)	SA	Area of Soma
3	Somatic aspect ratio	SAR	Max diameter of soma/min diameter of soma
4	Somatic compactness	SCom	$[(4/\pi) \times \text{Area}]^{1/2} / \text{max diameter}$
5	Somatic form factor	SFF	$(4\pi \times \text{Area}) / (\text{Perimeter}^2)$
6	Somatic roundness	SRO	$(4 \times \text{Area}) / (\pi \times \text{max diameter}^2)$

Cell Counting

Brain areas were identified using the brain atlas, and slides were examined under an Olympus Ch20i microscope. Images were captured, and cell count was performed using ImageJ. Only neurons with clear somatic nuclei and nucleolus were counted. To obtain an unbiased estimate of cell numbers, Abercrombie's correction factor was applied to total cell count, which compensates for the over counting of sectioned profiles, using the equation:

$$P = A * \left[\frac{M}{M + L} \right]$$

P is the corrected value, A is the raw density measure, M is the thickness of the section (in micrometers), and L is the average diameter of cell bodies along the axis perpendicular to the section's plane (Abercrombie, 1946).

To Determine the Cytoprotective Activity of Piperine Against H₂O₂ Induced Oxidative Stress and A β ₁₋₄₂ Induced Toxicity in PC12 Cells

RPMI-1640 media enriched with 10% heat-inactivated fetal bovine serum and 1% penicillin (100 U/ml), streptomycin (100 U/ml) was used to maintain PC12 cells in a carbon dioxide (CO₂) incubator at 37°C in a T-25 flask. The protective effect of piperine against H₂O₂ induced oxidative stress in PC12 cells was determined by supplementing the cells with different piperine concentrations and performing an MTT assay described previously (Chowdhury and Kumar, 2020). In brief, cells were pre-treated with piperine at concentrations ranging from 1 μ M to 0.25 μ M for 2 h before exposure to a half-maximal (IC₅₀) concentration of H₂O₂ (100 μ M final concentration). In another experiment, piperine's protective effect was determined against A β ₁₋₄₂ (40 μ M final concentration) induced toxicity. In this experiment, A β ₁₋₄₂ pre-formed fibrils were used to induce toxicity to PC12 cells. MTT assay was carried out, and absorption was read at 570 nm using a UV spectrophotometer (Molecular Device Spectramax M3, equipped with Softmax Pro V 5.4.1 software).

Gene Expression Studies

RNA Isolation

Total RNA was extracted from each mice group's cerebral cortex brain tissue using the standard Trizol method (Chomczynski 1993). The RNA quantity and purity were estimated by analyzing their A260/A280 ratio using the NanoDrop spectrophotometer (Thermo scientific). For further confirmation, the isolated RNA was analyzed by 1.2% agarose gel electrophoresis and visualized using the AlphaImager Gel documentation system (Alpha Innotech Corporation, CA, United States).

cDNA Preparation

Total RNA isolated from four different treatment groups i.e., untreated group (Vehicle control), Streptozotocin (STZ) treated group (Diabetes control), piperine plus STZ treated

group, and sitagliptin plus STZ treated group (Positive control), were used as a template for the cDNA synthesis. Around 4 μ g total RNA was used for first-strand cDNA synthesis by following the manufacturer's protocol.

Quantitative Real-time PCR was performed with the SYBR green PCR master mix kit with the following thermocycling conditions: Gene-specific primers for all the genes were designed manually using the exon-exon junction region amplify, and their specificity was examined through Primer Blast software of NCBI. OligoAnalyzer tool was used to calculate the T_m of the primers. The forward and reverse primers sequences for the following genes were as follows: forward 5'-CTCTTCCCAGGA CACTCC-3' and reverse 5'-TGAGTGGCCTGACTTTTGAC-3' for Apaf1, forward 5'-GGAGCTTGGAACGCGAAGA-3' and reverse 5'-CATCGGTACCATTTGCCGAGC-3' for Caspase3, forward 5'-CAAGAGCTGCTGTCCAGGA-3' and reverse 5'-GTAAGGCACAGGCCGATCA-3' for Presenilin-1, 5'-ACC AACCTTCGTTTGCCCAA-3' and 5'-CACCAATCAGTCCTT CCGC-3' for BACE-1, 5'-CTTCTGGAGTCTTTGTCCAG-3' and 5'-CCTGGTCAGTCTTGTAATGG-3' for Catalase, forward 5'-AGATCAAGATCATTGCTCCTC-3' and reverse 5'-CGCAGC TCAGTAACAGTCC-3' for β -actin. β -actin was used as an internal control. The melting curve obtained was analyzed, and the relative expression of transcripts was quantified by 2^{- $\Delta\Delta$ ct} value method (Livak and Schmittgen 2001).

Molecular Docking

Docking studies were carried out using the SwissDock server (Grosdidier et al., 2011). The X-ray crystallographic structure of APAF1(PDB code: 1Z6T), BACE1(PDB code: 4D8C), PSEN1(PDB code: 6IDF), Catalase (PDB code: 1TGU) and Caspase 3(PDB code: 3DEK) were retrieved from Protein Data Bank. The missing hydrogen atoms and charges were added by DockPrep application within UCSF Chimera, followed by energy minimization using Gasteiger charges (Pettersen et al., 2004). The structure of piperine was downloaded from PubChem in sdf format and converted to. mol format. Docking of piperine with proteins was carried out using the default parameter of the SwissDock server.

Statistical Analysis

All the data represent the means \pm standard deviation of triplicate determinations. The student t-test was performed for statistical analysis using online software, GraphPad. The significance value of $p < 0.05$ was considered significant, and $p < 0.01$ was considered very significant, and $p < 0.001$ was extremely significant.

RESULTS

Characterization of Piperine

For piperine's characterization, the GC-MS of commercially procured piperine was compared with the fragmentation pattern of piperine structure present in the NSIT library (Figure 1A). The chromatogram shows the presence of three

very minor peaks of 3-cyclohexene-1-methanol, alpha, alpha,4-trimethyl-, acetate; piperidine, and pyrrolidine, 1-[5-(1,3-benzodioxol-5-yl)-1-oxo-2,4-pentadienyl]- (E,E) with area percentage of 0.97, 0.40, and 1.12, respectively. Though the sample showed a strong peak of piperine with an area of 97.51%.

Effect of Piperine on the Viability of PC12 Cell Against H₂O₂ Induced Oxidative Stress

The PC12 cells were pre-treated with piperine, followed by H₂O₂ induction to determine the protective effect of piperine against H₂O₂ induced oxidative stress. At 1 μ M final concentration of piperine, 99.39 \pm 4.70% percentage of viability was observed as compared to the negative control (H₂O₂ only) (**Figure 2A**), showing that piperine significantly protected PC12 cells against H₂O₂ induced oxidative stress ($p < 0.01$).

Effect of Piperine on the Viability of PC12 Cells Against A β ₁₋₄₂ Induced Toxicity

To study the protective effect, PC12 cells were pre-treated with varying concentrations of piperine (0.25–1 μ M). The pre-treatment of piperine prior to induction of A β ₁₋₄₂ fibrils (40 μ M), showed concentration-dependent attenuation of A β ₁₋₄₂ induced toxicity, with maximum cell viability of 78.28 \pm 13.90% as compared to the negative control at 1 μ M concentration of piperine (**Figure 2B**).

Effect on Glucose Homeostasis (HOMA) and Lipid Profile of Serum

Effect of Treatments in Glucose Homeostasis (HOMA)

The significant ($p < 0.001$) increased insulin resistance (IR), β -cell function ($\beta\%$), and insulin sensitivity (S%) were seen in the diabetic group in comparison to the vehicle control group. Accordingly, the insulin and glucose levels were represented its levels in the diabetic group. Although the piperine and sitagliptin, treatments caused significant alterations in HOMA indices of IR, $\beta\%$, and S%. Accordingly, reductions were observed in levels of insulin and glucose (**Figure 3**).

Effects of Treatments in Lipid Profile and AI

In the diabetic group, lipid profile (total cholesterol, LDL-cholesterol, VLDL-cholesterol, and triglyceride (Tg)), as well as the atherogenic index (AI = log(Tg/HDL)), were elevated significantly in comparison to the vehicle control group. The piperine and sitagliptin treatments made significant reductions in lipid profile and AI (**Figure 4**).

Effects of Piperine on Learning and Memory in STZ-Treated Rats

The cognitive-behavioral task was evaluated through MWM. The water escape task evaluates spatial learning and memory. On day 1, when the animals were exposed to a circular water tank

for the first time, diabetic group B took the maximum time to find the hidden platform. In contrast, the sitagliptin-treated group D took the lowest time, which was even better than the control group of rats A (**Figure 5A**). The piperine-treated group C demonstrated escape latency that was lesser (38%) than the Diabetic control B but higher (21%) than the group D. Interestingly, the swimming speeds of A, D, and C were in the comparable range (<5% differences), while that of group B was relatively less (~17%) compared to other groups. Similarly, group B showed the most unsatisfactory performance in terms of path length and cumulative path distance. Contrary to these observations, swim path efficiency was better in group B and group C.

Exposure to the same task after 24 h evaluated the memory function of the animals. The animals of group B took the longest time to escape with the longest path and slowest swimming speed (**Figure 5B**). Though group B animals' path efficiencies were very close to that old vehicle control animals, their slow swimming speed increased the nominal high path length (15%) into a considerably higher cumulative distance (100%). On the other hand, PR and SR animals showed very good escape latency, path length, cumulative distance, and swimming path efficiency. Their values were comparable for these parameters, even in the presence of significant differences in swimming speed. The swimming speed in SR was lesser than group C and was comparable to group B.

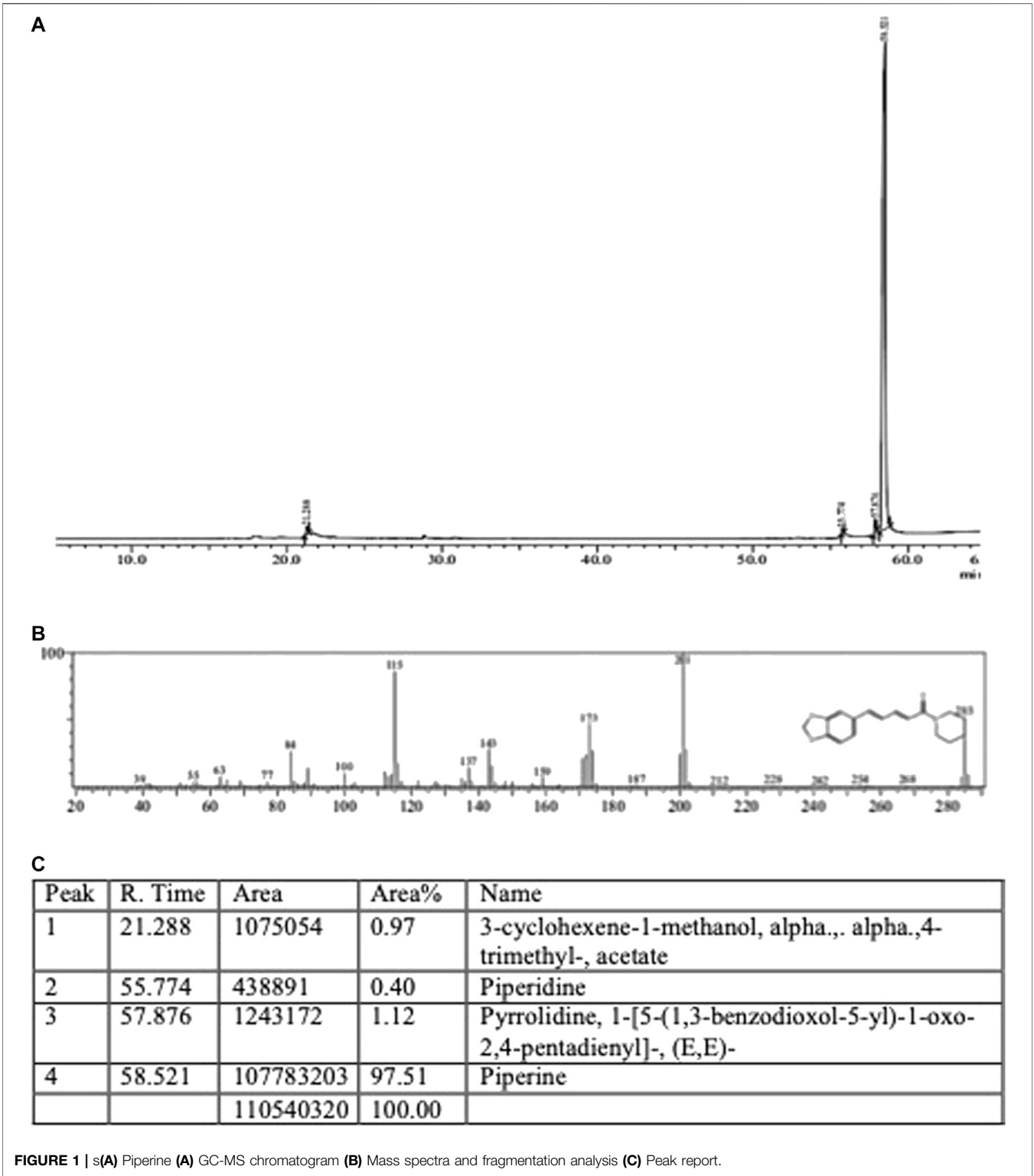
There were increases in escape latencies, path length, cumulative distance, and decreases in swim path efficiencies for groups A, D, and C on day 3 compared to that2 for the same task performances (**Figure 5C**). Nevertheless, cumulative distance, path length, and escape latency of group B were high with lower swim path efficiency, in comparison to group D and group C. The speed of swimming in B was in between that of D and C.

When the starting point for the task changed by +90° or –90°, DR animals performed very poorly in swim path efficiency. However, variations in performances of D and C were also noted. Even group A animals also deteriorated in their performances in some cases. A probe test on day 4 was carried out to evaluate the cognitive functions in the absence of the hidden platform. Of all the animal groups, the B group animals spent the minimum time in the target quadrant and maximum time in the opposite quadrant.

Histopathology

Effect of Piperine on Pancreatic Histoarchitecture of the Islet of Langerhans

The high sucrose diet and a mild dose of STZ caused significant alterations in histoarchitecture of the pancreas by promoted degenerative changes in the islet of the Langerhans as well as different degrees of necrosis in the nucleus in comparison to the vehicle control group (**Figures 6A,B**). The degenerative changes also were seen in vascular tissues and connective tissues. Whereas the treatments of piperine and sitagliptin promoted the restoration of histoarchitectures by increasing cellular mass and subsiding the necrosis of nucleus of islet cells with rearrangements of vascular tissues and connective tissues (**Figures 6C,D**).



Effect of Piperine on Brain Tissue Histopathology
Significant differences were observed in CA3 (*Cornu Ammonis* areas) and dentate gyrus (Dg) neurons

morphology between the experimental groups. Other regions of hippocampus CA1, CA2, and CA4 have not exhibited any marked changes. The present study shows

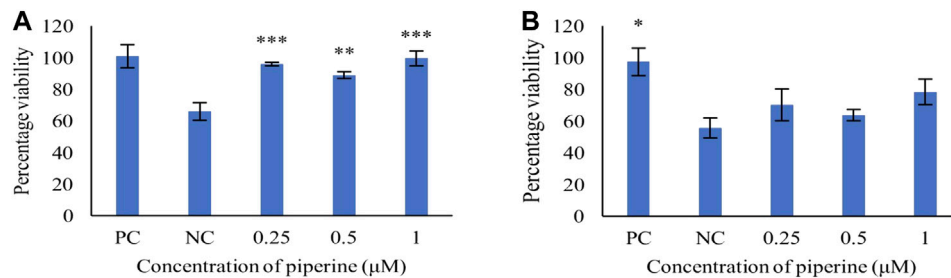


FIGURE 2 | Concentration-dependent protective effect of piperine against (A) H₂O₂ induced oxidative stress and (B) Aβ₁₋₄₂ fibrils induced cytotoxicity in PC12 cells. NC: Negative control (Aβ₁₋₄₂ only), PC: Positive control (No Aβ₁₋₄₂). Data are presented as mean ± SD of three separate experiments performed in triplicate. **p* < 0.05, ***p* < 0.01 with the negative control (NC).

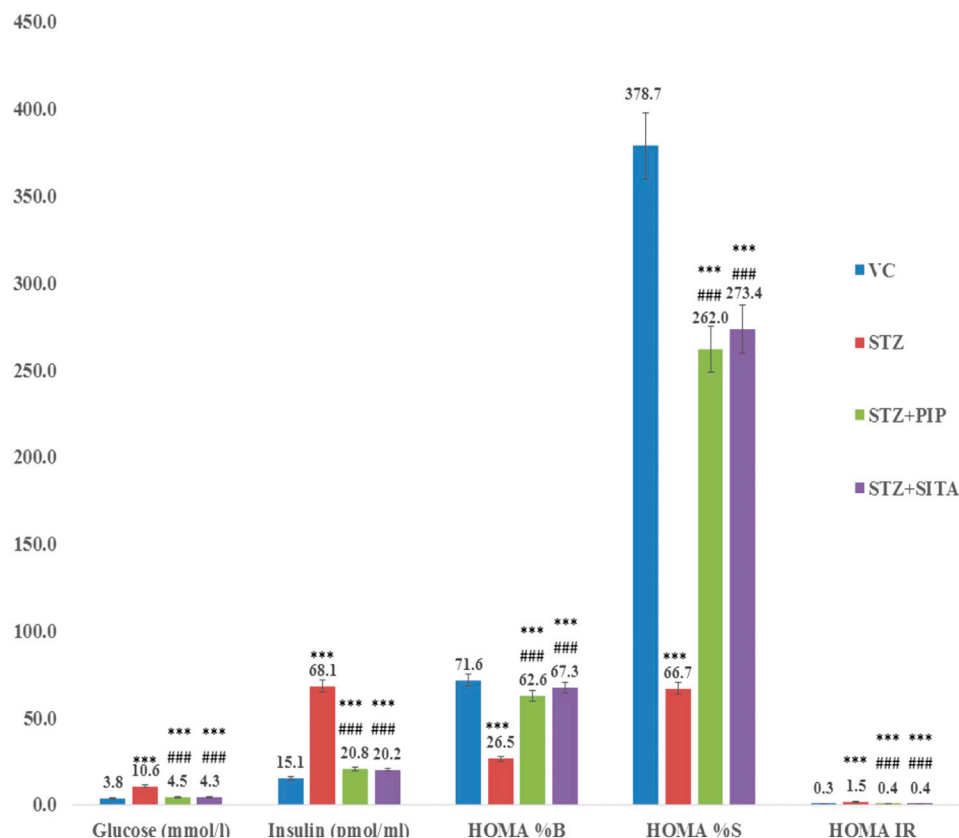


FIGURE 3 | Effect of the piperine on glucose homeostasis (HOMA) (A, B, C, and D were experimental group) (See the experimental design in material and methods section) (Data are means ± S.E.M. (n = 7); *, *p* ≤ 0.05 and c, *** ≤ 0.001 as compared to the respective control values and g, ### ≤ 0.001 and d = nonsignificant as compared to the respective values of the diabetic control group). Blue-Vehicle Control (VC); Red-Diabetic control (STZ); Green-Piperine treatment (STZ + PIP); Purple-Sitagliptin treatment (STZ + SITA).

more significant effects on neuronal soma size as compared to neuronal shape factors.

Treatment with dexamethasone reduced the size probably because of the degenerative process. In contrast, treatment with piperine and sitagliptin exhibited recovery, and larger soma could be interpreted as protective effects (Figures 7i,ii). Larger soma may have better metabolic and cellular systems

required to have better synaptic connections and neuronal activities, which corresponds to enhanced learning ability and memory. SA of CA3 neurons in the Diabetics group was $266.40 \pm 10.72 \mu\text{m}^2$, whereas it was $306.73 \pm 13.96 \mu\text{m}^2$ for the control group. Treatment with piperine and sitagliptin increased the SA and found to be 279.15 ± 16.71 and $289.15 \pm 15.60 \mu\text{m}^2$, respectively. More significant changes were observed in Dg Neurons after dexamethasone

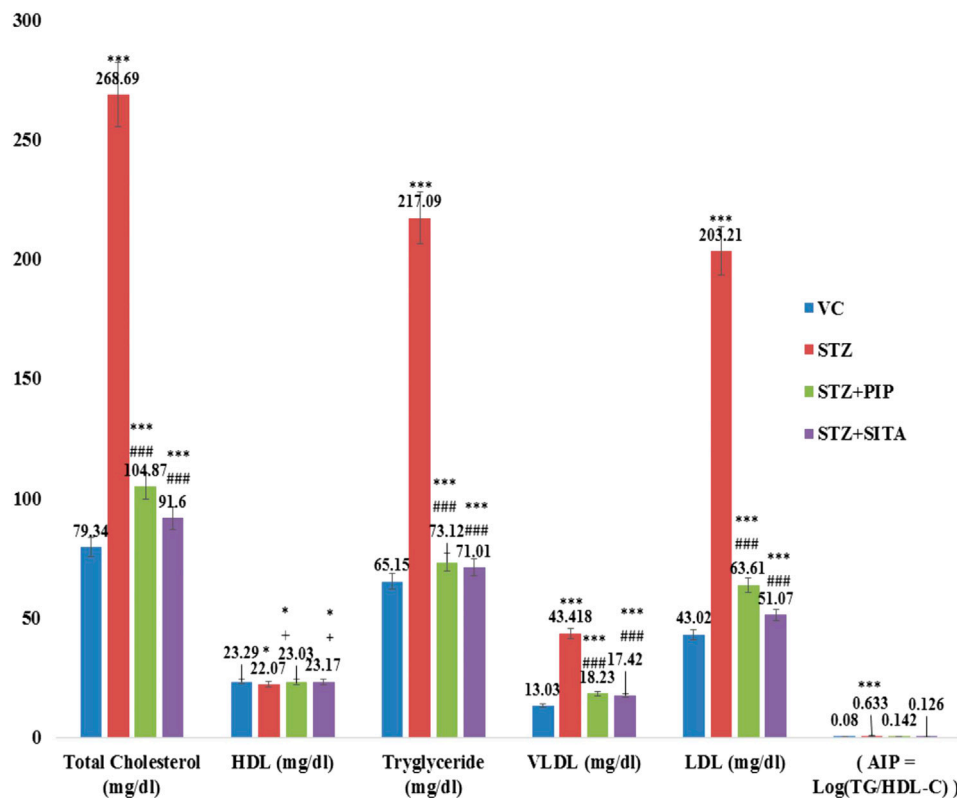


FIGURE 4 | Effect of the piperine on lipid profile and AI (Atherogenic Index) (Data are means \pm S.E.M. ($n = 7$); *, $p \leq 0.05$ and c, *** ≤ 0.001 as compared to the respective control values and g, ### ≤ 0.001 and d = non-significant as compared to the respective values of the diabetic control group). Blue-Vehicle Control (VC); Red-Diabetic control (STZ); Green-Piperine treatment (STZ + PIP); Purple-Sitagliptin treatment (STZ + SITA).

treatment SA was decreased by 18.36 percent, and piperine and sitagliptin treatment exhibited SA values matching with control animals (249.15 ± 13.76 and 251.95 ± 12.98), respectively.

A 23 percent decrease in SP was observed for CA3 neurons in dexamethasone-treated animals. This was found to approximately close to control animals in piperine and sitagliptin treated animals; a change of 10.57 and 3.39 percent was observed, respectively. Similar observations were evident for Dg also SP for control neurons was measured $61.63 \pm 3.67 \mu\text{m}$ and reduced to $51.26 \pm 1.16 \mu\text{m}$ in dexamethasone-treated animals, here no doubt to state that sitagliptin performed better ($59.61 \pm 3.99 \mu\text{m}$) as compared to piperine ($56.46 \pm 1.35 \mu\text{m}$) (Figures 8i,ii).

Morphometry

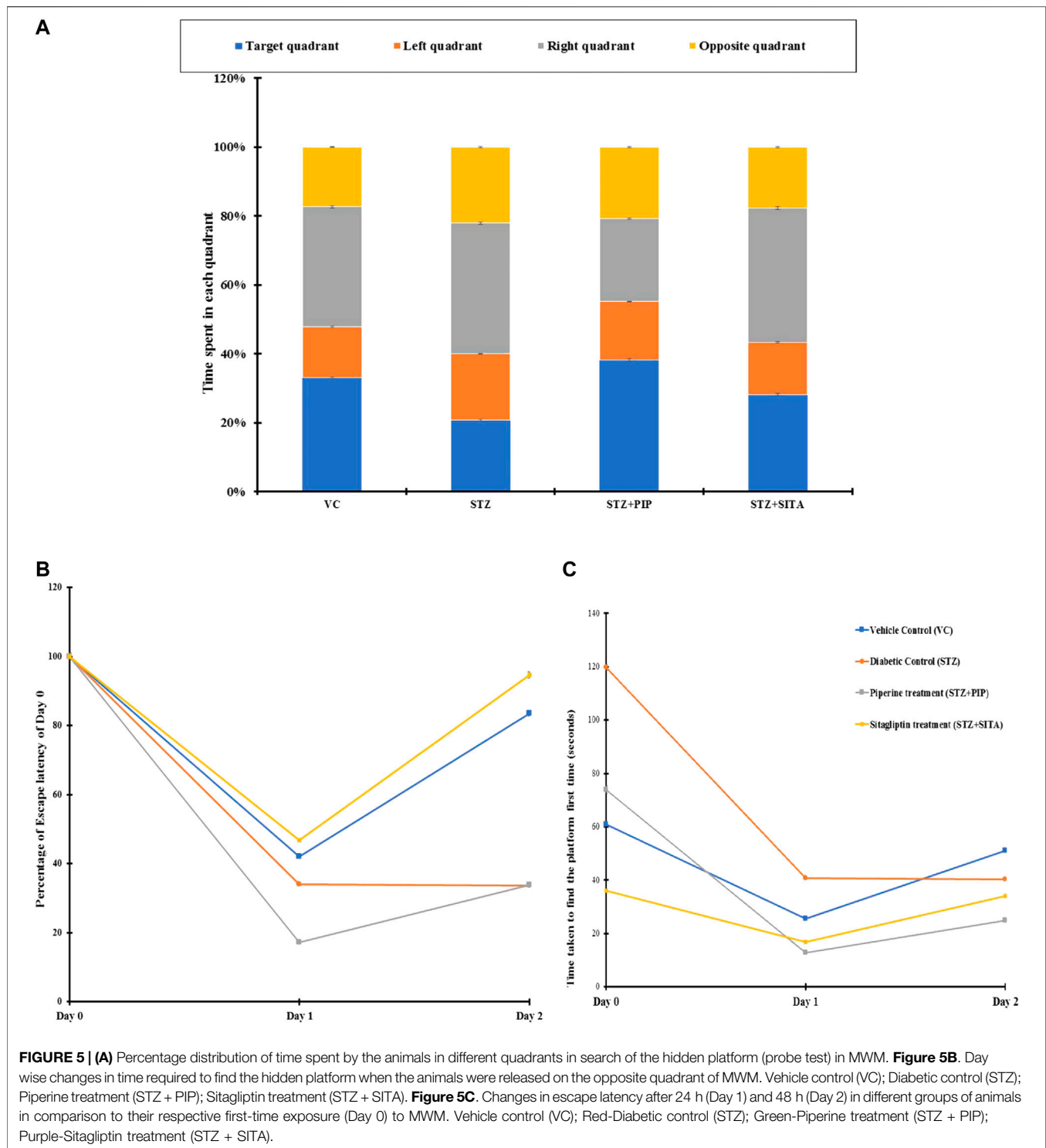
Cell count shows a decrease in number after dexamethasone treatment in CA3 and Dg area; this was further restored with the treatment of piperine and sitagliptin. A significant decrease was observed both in CA3 and Dg neurons after treatment with dexamethasone. A close analysis of data exhibited that both the areas were affected equally with a reduction of 29 and 28 percent, respectively. The total number of neuronal cells in the CA3 and Dg sub-region of the hippocampus of piperine and sitagliptin was approximately closer to control animals, and values for the CA3 sub-region were 22.43 ± 0.40 and 23.03 ± 0.55 (Table 1). For the Dg sub-region, the total number of cells in piperine and

sitagliptin treated animals was 38.76 ± 1.05 and 38.96 ± 1.19 , respectively (Table 2). The decrease in cell number indicates cell death, and protective effects are indicated by the restored number of cells compared to control animals.

The morphological shape of cell bodies was analyzed based on the somatic aspect ratio (SAR), somatic circularity index (SCI), and somatic roundness (SRO). SAR exhibits the symmetry of cellular shape. SAR value close to 1 is indicative of circular or spherical shape. CA3 neurons exhibited higher SAR values, and this was further increased in dexamethasone-treated animals (1.40 ± 0.05), indicative of a disruption of pyramidal shape. Animals treated with piperine and sitagliptin exhibited SAR values close to control animals, reflecting the pyramidal shape's retention. As expected, Dg neurons exhibited SAR values close to 1.0, and no significant difference was observed between various experimental groups. We found no significant changes in the SCom, SFF, SRO, suggesting that the soma size changes were uniform rather than shrinkage or expansion along a particular axis.

Gene Expression Analysis in the Cerebral Cortex Brain Tissue of Rat

For gene expression analysis, total RNA was isolated from the cerebral cortex, and its quality was analyzed by assessing the RNA



purity and integrity. The absorbance ratio A260/280 ratios were greater than 1.9 of all the RNA samples. The sharp bands for 28S and 18S ribosomal RNA were observed when separated in 1.2% agarose gel electrophoresis, indicating the good quality RNA. Using the manufacturer instructions, cDNA was prepared and

used as a template for gene expression analysis. Using the Real quantitative Time-PCR, the expression of selected genes, including *BACE1*, *PSEN1*, *APAF1*, *CASPASE3*, and *CATALASE*, in rat's cerebral cortex brain tissue was analyzed in four different treatment groups. In STZ treated group

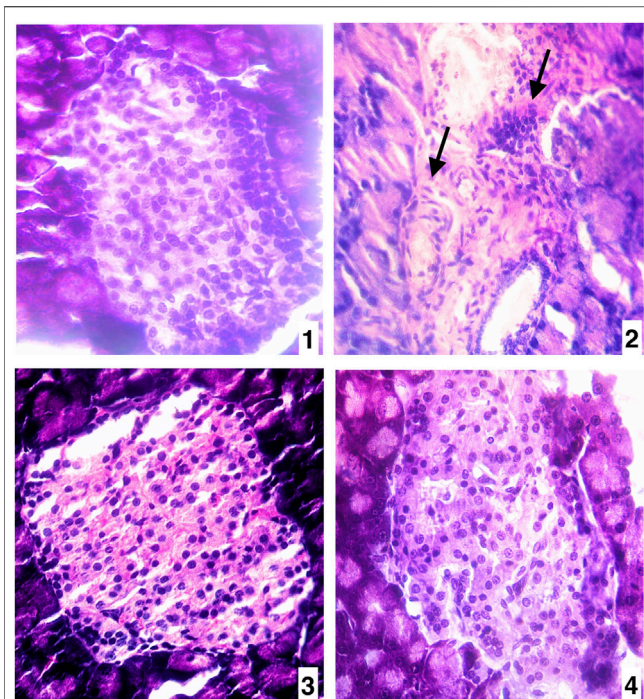


FIGURE 6 | (A) Pancreas of vehicle control (VC) (400X H&E) **(B)** Pancreas of diabetic control (STZ)(400X H&E) **(C)** Pancreas of the piperine treatment (STZ + PIP)(400X H&E) **(D)** Pancreas of sitagliptin treatment (STZ + SITA)(400X H&E).

(Diabetes control), the expression of *BACE1*, *PSEN1*, *APAF1*, *CASPASE3*, and *CATALASE* genes were upregulated in the cerebral cortex of the rat brain as compared to the untreated group (Vehicle control) (Table 3). The fold change increase in these genes' expression levels varied, and it ranged between 1.5 and 2.8-fold increases (Figure 9). However, their expression decreased drastically when treated with sitagliptin (Positive control). Reduction percentage in the expression of these genes ranged between 59 and 96% decreases in sitagliptin treated (Positive group) in comparison to the STZ treated group (Diabetes control). Upon treatment with piperine, the expressions of these genes were significantly decreased ($p \leq 0.05$). When these genes' expression was compared between the piperine treated group and the Diabetes control group, statistically significant changes ($p \leq 0.05$) were observed.

Molecular Docking Analysis

In the present study, the interaction between piperine and some proteins involved in amyloid processing, apoptosis, and oxidative stress such as *BACE1*, *PSEN1*, *APAF1*, *CASPASE3*, and *CATALASE* were studied to explore the binding mode, using SwissDock server. The binding affinity of the proteins with piperine was measured by FullFitness score and deltaG (kcal/mol). The FullFitness score was highest for *APAF1* with -8.02 kcal/mol deltaG followed by *CATALASE* (-7.51 kcal/mol), *PSEN1* (-7.35 kcal/mol), *BACE1* (-7.20 kcal/mol), and the least score was found *CASPASE3* (-6.55 kcal/mol) as shown

in Table 4 and Figure 10. Besides, hydrogen bond formation was seen in all four proteins except *CATALASE* when docked with piperine. The molecular docking study predicted a binding interaction between each protein and piperine ligand, validated by hydrogen bonding between the proteins and piperine. Molecular docking of piperine with *APAF1* revealed H-bonding with Val127 of α/β fold of protein (Figure 10A). Docking analysis of *BACE1* revealed that Thr221 residue participates in forming H-bond with piperine. Thr221 was also found to interact with the ligand of the X-ray crystal structure of *BACE1* (PDB code: 4D8C); therefore, this interaction plays an important role (Figure 10B). In *CATALASE* protein, no single H-bond interaction was found to be formed with the catalytic residues (Figure 10C). The binding interaction of *PSEN1* (PDB code: 6IDF) revealed that Gly384 residues are involved in H-bond formation with piperine (Figure 10D). *CASPASE 3* was found to interact with amino residue Arg 164, to form H-bond interaction with piperine (Figure 10E).

DISCUSSION

AD and DM are two independent metabolic syndromes but recently reported increasing evidence shows a link between AD and DM (Akter et al., 2011). The complications associated with DM leads to a hyperglycemic condition. The increase in blood sugar level affects neuronal cells. The higher blood sugar levels lead to faster cognitive decline and neuronal cell death. The increased blood glucose levels also result in higher glycation end-products (AGEs) that damage the neuronal cells by inducing oxidative stress, promoting inflammation, and causing direct neurotoxicity to brain cells. The other pathway involved in neuronal cell death is apoptosis (Singh et al., 2014). The administration of dexamethasone and STZ increases oxidative stress in the rat brain. This oxidative stress causes ROS accumulation in the brain that further damage cellular components such as proteins and neuronal cells' membranes (Uttara et al., 2009). STZ treatment produces free radical's generation causing oxidative stress, mitochondrial abnormalities which further trigger caspase mediated apoptotic cell death, neuroinflammation which are collectively detrimental to neuronal function which further implicate in the AD pathology (Rai et al., 2013). STZ produces brain insulin resistance or impaired insulin receptor in the brain which leads to A β accumulation forming senile plaques and increased tau-phosphorylation forming neurofibrillary tangles by increasing the activity of GSK-3 β that results in neuronal and synaptic dysfunction, memory impairment which further leads to AD like pathology (Shingo et al., 2012; Stöhr et al., 2013). STZ exacerbates the pathological changes associated with AD such as amyloidogenic processing of APP, glucose metabolism, insulin signaling, synaptic function (Chen et al., 2014; Zhang et al., 2015).

This study evaluated the neuroprotective effects of piperine and expression of five candidate genes (*BACE1*, *PSEN1*, *APAF1*, *CASPASE3*, and *CATALASE*) in rat's cerebral cortex induced hyperglycemia with STZ rat model. Our results showed that all

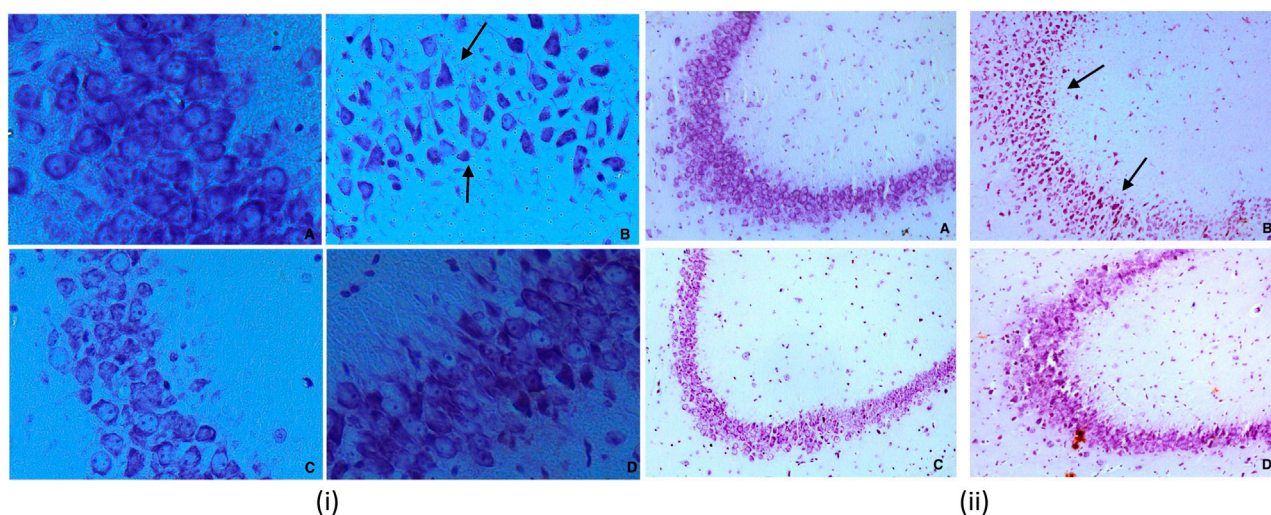


FIGURE 7 | (i) Nissl staining for CA3 sub region of hippocampus for various groups at 40X (A) Vehicle control (VC) (B) Diabetic control (STZ) (C) Piperine treatment (STZ + PIP) (D) Sitagliptin group (STZ + SITA). 7 (ii) Nissl staining for CA3 sub region of hippocampus for various groups at 10X (A) Vehicle control (VC) (B) Diabetic control (STZ) (C) Piperine treatment (STZ + PIP) (D) Sitagliptin group (STZ + SITA).

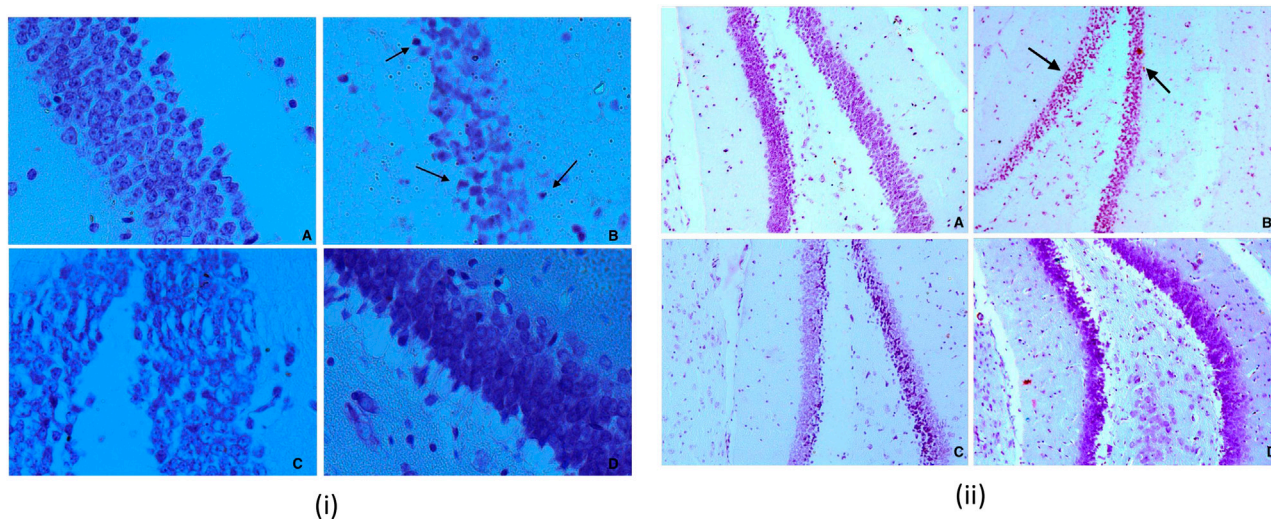


FIGURE 8 | (i) Nissl staining for Dg sub region of hippocampus for various groups at 40X (A) Vehicle control (VC) (B) Diabetic control (STZ) (C) Piperine treatment (STZ + PIP) (D) Sitagliptin group (STZ + SITA). 8 (ii) Nissl staining for Dg sub region of hippocampus for various groups at 10X (A) Vehicle control (VC) (B) Diabetic control (STZ) (C) Piperine treatment (STZ + PIP) (D) Sitagliptin group (STZ + SITA).

TABLE 1 | Measurements of the morphological size and shape of CA₃ neurons.

CA3	Control	Diabetic	Piperine	Sitagliptin
Area	306.73 ± 13.96	266.40 ± 10.72*	279.15 ± 16.71	289.15 ± 15.60
Perimeter	115.44 ± 7.90	95.13 ± 7.58	103.23 ± 9.73	111.52 ± 7.20
Cell count	24.99 ± 0.21	17.66 ± 0.26**	22.43 ± 0.40**	23.03 ± 0.55**
Somatic aspect ratio	1.27 ± 0.042	1.40 ± 0.05	1.32 ± 0.04	1.29 ± 0.05
Somatic compactness	1.02 ± 0.03	1.09 ± 0.04	1.01 ± 0.06	1.00 ± 0.04
Somatic form factor	0.47 ± 0.08	0.79 ± 0.3	1.60 ± 0.98	0.48 ± 0.09
Area	1.08 ± 0.07	1.25 ± 0.10	1.14 ± 0.17	1.06 ± 0.09

Significance level *p value < 0.05, **p value < 0.01.

TABLE 2 | Measurements of the morphological size and shape of Dg neurons.

Dg	Control	Diabetic	Piperine	Sitagliptin
Area	272.94 ± 12.06	222.75 ± 9.71**	249.15 ± 13.76	251.95 ± 12.98
Perimeter	61.63 ± 3.67	51.26 ± 1.16**	56.46 ± 1.35	59.61 ± 3.99
Cell count	43.33 ± 0.80	31.00 ± 0.67**	38.76 ± 1.05**	38.96 ± 1.19**
Somatic aspect ratio	1.03 ± 0.03	1.01 ± 0.05	1.01 ± 0.03	1.02 ± 0.02
Somatic compactness	1.08 ± 0.02	1.20 ± 0.09	1.24 ± 0.05*	1.15 ± 0.03
Somatic form factor	1.13 ± 0.14	1.11 ± 0.07	1.03 ± 0.07	2.78 ± 1.56
Somatic roundness	1.20 ± 0.06	1.68 ± 0.30	1.64 ± 0.15**	1.36 ± 0.08

Significance level *p value < 0.05, **p value < 0.01.

TABLE 3 | Gene expression profile.

Groups	Genes				
	Caspase 2	PSEN1	BACE1	Apaf 1	Catalase
Control (NORMAL GP)	↓	↓	↓	↓	↓
Diabetic control (STZ)	↑	↑	↑	↑	↑
Positive control (SITA/STZ)	↓	↓	↓	↓	↓
Piperine (PIPERINE/STZ)	↓	↓	↓	↓	↓

five genes *BACE1*, *PSEN1*, *APAF1*, *CASPASE3*, and *CATALASE* were significantly down-regulated in the piperine treated group compared to the Diabetic rats (STZ induced) group. It has been reported that piperine has the ability to enhance the bioavailability of compounds by several different mechanisms such as modulation of cell signal transduction, DNA receptor binding, inhibition of drug efflux pump and increasing the absorption of drugs (Bajad et al., 2001). Moreover, study suggested that piperine strongly inhibits human P-glycoprotein and cytochrome P4503A4 (Bhardwaj et al., 2002). A previous study reported the protective role of Piperine in cerebral ischemia induced inflammation rat model by downregulating the expression of Cox-2, NOS-2 and NFkB (Vaibhav et al., 2012). The neuroprotective effect of Piperine in 6-OHDA induced Parkinson's rat model by its anti-apoptotic and anti-inflammatory activity (Shrivastava et al., 2013). Piperine attenuated Trauma brain injury (TBI) by downregulating the expression of TNF-α, IL-1β and BDNF in TBI mice (Song et al., 2020). A more recent study showed that Piperine treatment enhances memory performance and improves myelin repair in LPC induced demyelination rat model. (Roshanbakhsh et al., 2020). The present study substantiates the claim that piperine can binds to the molecular targets as mentioned in the previous studies mentioned above and can have effect of CNS related neuroprotective effects.

AD is characterized by neuritic plaques, the main pathological hallmarks of AD, primarily consist of amyloid β (Aβ) peptides. Aβ peptides are generated by the non-amyloidogenic pathway when amyloid precursor protein (APP) was cleaved by an enzyme called β-site APP cleaving enzyme 1 (BACE1). BACE1 plays an important role in APP processing (Resende et al., 2008; Da Costa Dias et al., 2011). Expression of the β-secretase gene is implicated in late-onset

Alzheimer's Disease (LOAD) because of its function in initiating Aβ production of PSEN1 (Presenilin 1) component of γ secretase enzyme. *BACE1* gene expression is upregulated in oxidative stress, ischemia, and hypoxia (Guglielmotto et al., 2009). *BACE1* cleavage is also affected by a mutation in gene PSEN1 and PSEN2, resulting in the overproduction of Aβ isoforms. Aβ induced toxicity ultimately leads to neuron cell death by activating caspases 3, 6, and 7 (Elmore, 2007). Piperine downregulated both *BACE1* and *PSEN1* gene expression as compared to STZ treated group. Another, pro-apoptotic genes such as *APAF1* and *CASPASE* are involved in the apoptotic pathway. Gene expression study showed increased expression of pro-apoptotic genes such as *CASPASE* and *APAF1* involved in neuronal cell death via an apoptotic pathway in the AD brain (Papaliagkas et al., 2007). *APAF1* is the gene responsible for encoding a multiprotein complex that plays a crucial role in cell death's mitochondrial pathway. The role of *APAF1* is not very clear in neurodegeneration, although evidence has shown a correlation between *APAF1* and *CASPASE*. The activated Apaf1 is required for the downstream executioner caspase family of genes (Shakeri et al., 2017). Caspase-3 is a cysteine protease family of genes. Many caspases are involved in initiating the signaling and execution of the apoptosis pathway. Caspase-3 is an executioner caspase an important component of the apoptosis pathway (Shi, 2004). It has been found that the activation of caspase-3 is an early event in the pathogenesis of AD. Activation of caspase-3 results in morphological changes leading to neuronal cell death. *In vitro* and *in-vivo* studies suggested that Caspase-3 has a significant role in the neuronal cell death associated with a high level of expression and activation of caspase-3 seen in AD models (Gorman et al., 1998). Gene expression study showed increased expression of pro-apoptotic genes such as caspases and apaf1 are involved in neuronal cell death via an apoptotic pathway in the AD brain (Fortin et al., 2001; Papaliagkas et al., 2007). Both Apaf1 and caspase gene expression were significantly downregulated in the piperine treated group compared to the diabetic control group (STZ treated). The biological system has an antioxidant defense system consists of an enzyme such as catalase widely distributed in the human body (Chen et al., 2012). Catalase breaks down two hydrogen peroxide into oxygen and water using iron or manganese as a cofactor and thus protects cells (Nandi et al., 2019). The catalase gene expression was

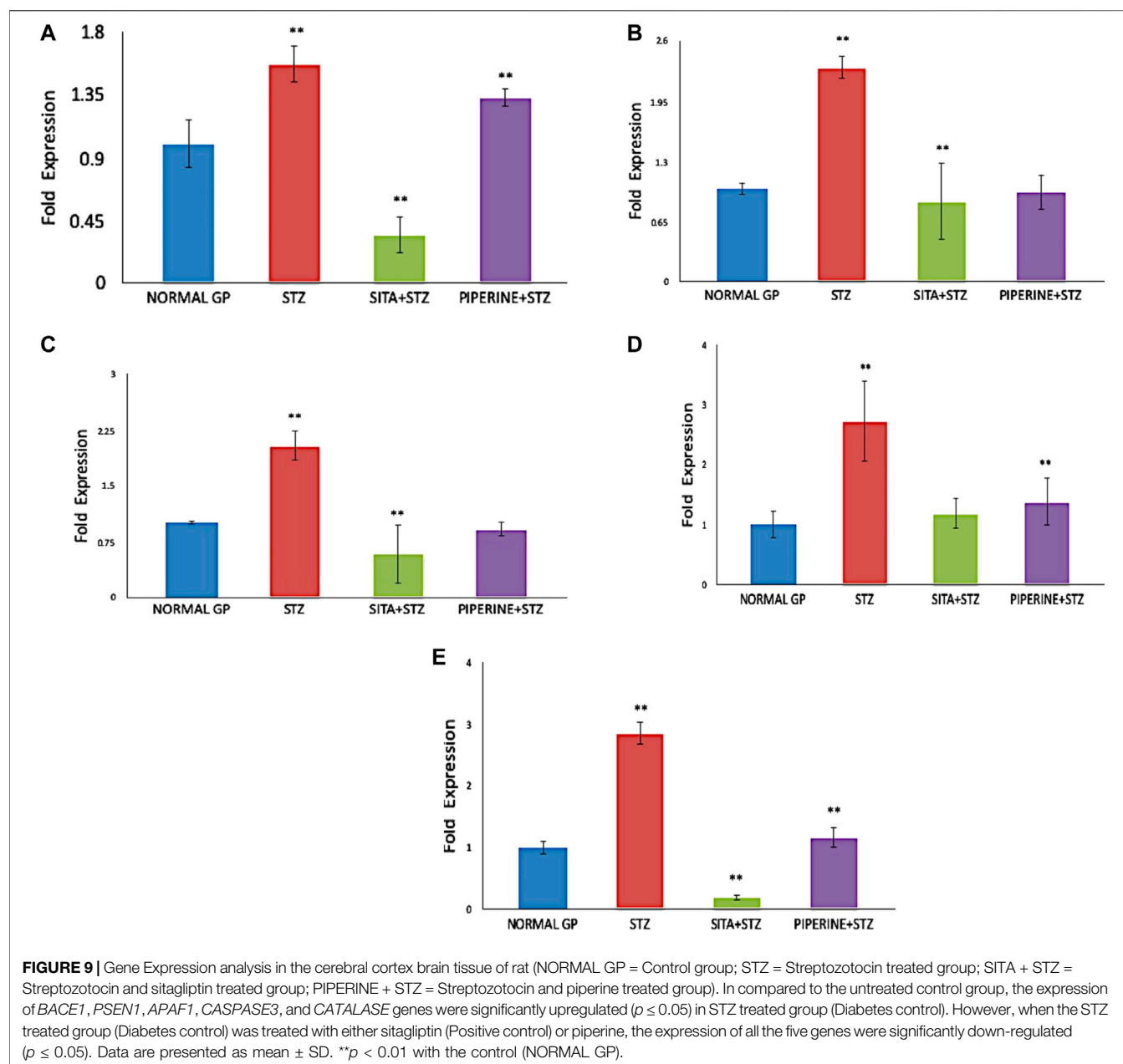


TABLE 4 | Molecular docking result of piperine in terms of full fitness and estimated ΔG values predicted by SwissDock.

Protein	deltaG (Kcal/mol)	FullFitness	Interacting residues	Bond length (Å)
Apaf1	-8.02	-3452.89	Val 127	2.275
Catalase	-7.51	-2139.90	—	—
Psen1	-7.35	-1129.81	Gly384	2.049
Bace1	-7.20	-1529.14	Thr 221	2.216
Casapase3	-6.55	-1380.32	Arg164	2.685

significantly increased in the group treated with STZ alone (Diabetic control), whereas it was significantly down-regulated in the piperine treated group.

In vivo experiments in the diabetic rat model demonstrated improvement of memory functions in the piperine treatment group was observed in neurocognitive function assays. The

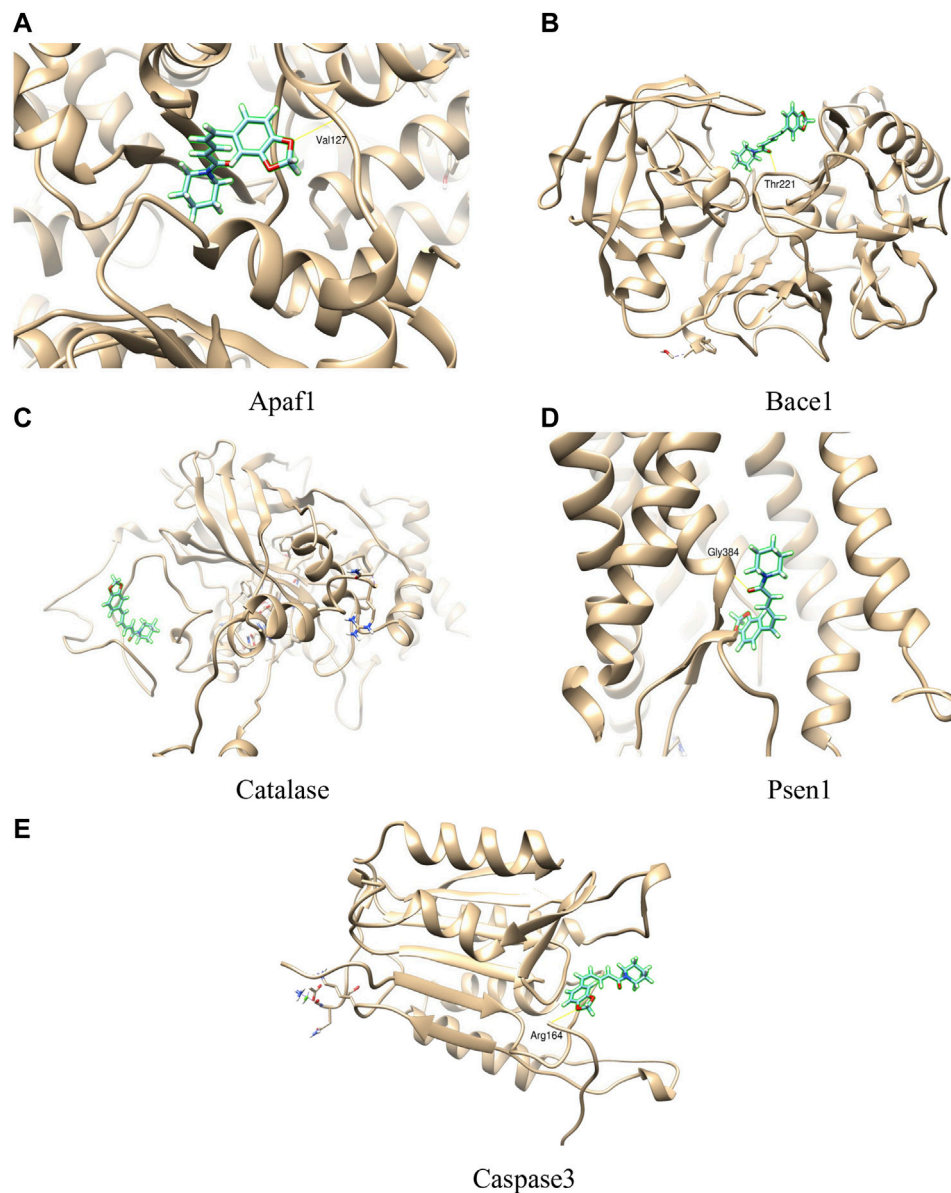


FIGURE 10 | Molecular interactions of piperine with different proteins (A = APAF1, B= BACE1, C= CATALASE, D = PSEN1, E = CASPASE3).

piperine group showed a relatively shorter time to find the hidden platform in the Morris Water Maze test. However, the escape latency for this group was not better than the diabetic group of animals. Similarly, the memory function of the piperine treated group of animals was also found to be improved compared to that of the diabetic group. This has been further confirmed by the probe test, where similar effects of piperine treatment were reflected.

The increased glucose and insulin levels with abnormal HOMA indices seen in a diabetic animal model may be following the decreased uptake of glucose and insulin resistance, which is further seen in degenerative cellular changes in pancreatic tissues.

Several studies reported that increased insulin resistance caused reductions in glucose uptake, which also resulted in apoptosis in several tissues, as seen in pancreatic tissues of the diabetic animal model (Borona, 2008; Khan et al., 2016). The treatments of piperine and sitagliptin caused significant alterations in HOMA indices of IR, $\beta\%$, and S%, which indicate the interferences of piperine in the metabolism of glucose as well as insulin action. Accordingly, it is a well-established illustration that dietary or orally administered supplement stimulates insulin secretion by increasing GLP-1 activity through gut action (Girard, 2008; Mudaliar and Henry, 2012; Brandt et al., 2018). Supportively, the glucose transporter isoform GLUT4 might be a critical target to treat insulin resistance.

Meanwhile, GLUT4 is an insulin-dependent isoform that is accountable for furthestmost insulin-encouraged glucose uptake (Abdel Aziz et al., 2020). Consequently, the treatments caused significant reductions in lipid profile and the atherogenic index, which may follow the subside of the gluconeogenesis and inhibition of lipid biosynthesis (Bano, 2013; Petersen and Shulman, 2018). Accordingly, the pancreatic tissues gained restorations in histoarchitecture, which indicates the interference of stimulation may produce by the piperine to increase islet cell mass, which is also seen in reduced insulin resistance and related HOMA indices. It is reported that postprandial dietary stimuli promote the secretion of GLP-1 and GIP by gut cells, which further stimulate insulin secretion and restoration or regeneration of islet β -cells (Wu et al., 2015; Prassannaraja et al., 2020).

There were significant differences in hippocampal CA3 and Dg neuronal morphology between the experimental groups (Tables 1, 2; Figures 7, 8). Here we have used a chronic dose of dexamethasone and a single mild streptozotocin dose to induce Hyperglycemia and Insulin resistance. Diabetics' control animals exhibited changes both in neuronal morphology and number. Histology revealed cell death both in CA3 and Dg sub-regions of the hippocampus. Dexamethasone treatment is comparable to adrenalectomy and leads to corticosteroid depletion and cell death in the hippocampus's Dg (Hassan et al., 1996; Hornsby et al., 1996), a phenomenon that is well documented after adrenalectomy (Sloviter et al., 1993). Streptozotocin can also induce cell death in the hippocampus, especially in CA3 neurons, by altering the brain antioxidant status and energy impairment (Salkovic-Petrisic et al., 2013). Neuronal damage in the hippocampus contributes to cognitive brain dysfunctions (Agrawal et al., 2009; Saxena et al., 2010).

Nazem et al. (2015) suggested that neuroinflammation leads to the accumulation of $A\beta$ and tau and ultimately leading to Alzheimer's. Streptozotocin treated animals exhibit an insulin-resistant brain state, which promotes the accumulation of tau and $A\beta$ (Salkovic-Petrisic et al., 2013). Our *in vivo* results also confirm this streptozotocin up-regulated *BACE1*, *PSEN1*, *APAF1*, *CASPASE3*, and *CATALASE* genes in the animal model. Molecular interaction between piperine and protein of these genes was also studied using molecular docking. Antioxidants are considered to be good neuroprotectants and can ameliorate cognitive impairments. Quercetin, a flavonoid, is useful in the amelioration of STZ-induced cognitive impairment (Liu et al., 2012). Piperine also possesses antioxidant properties and can cross the blood-brain barrier (Srinivasan, 2007; Elnaggar et al., 2015). The beneficial effects of piperine on neurons' morphology and cognitive functions can be attributed to inherent antioxidant capabilities. The down-regulation of *BACE1*, *PSEN1*, *APAF1*, *CASPASE3*, and *CATALASE* genes in the animal model and binding of piperine with protein in the *silico* model, shows that the neuroprotective activity of piperine may be closely related.

In cells, $A\beta_{1-42}$ toxicity causes deterioration of chaperoning and proteasomal processing involved in clearance of deposited peptides (Mena et al., 2009). To overcome this failure, cytoprotective property elucidation of a molecule is necessary. This cytoprotective effect of piperine was demonstrated in PC12 cells, which is the standard *in vitro* model used to study neuroprotective compounds. Piperine showed significant protection of PC12 cells against both H_2O_2 and $A\beta_{1-42}$ induced toxicity under *in vitro* conditions. Understanding molecular interaction with protein targets and genes regulated by the piperine can provide information regarding its mechanisms of action. Additionally, drug targets do not always affect gene expression changes; they work via signaling cascades. Hence, drugs act on their drug targets and modulate the signaling mechanism (Xie et al., 2016; Makhouri and Ghasemi, 2018). Therefore, we performed *in silico* molecular docking of piperine with a protein involved in amyloid processing, apoptosis, and oxidative stress, and suggested interaction of piperine with important amino acid residues. In the present study, *in silico* studies used was molecular docking approach. Molecular docking is powerful computation tool to understand the structural and chemical basis of ligand-target specificities. The molecular docking results showed the interaction between piperine and specific proteins involved in amyloid processing, apoptosis, and oxidative stress such as *BACE1*, *PSEN1*, *APAF1*, *CASPASE3*, and *CATALASE*. The binding affinity of the proteins with piperine was measured by FullFitness score and deltaG (kcal/mol). As these proteins are encoded by specific genes, which express these proteins *BACE1*, *PSEN1*, *APAF1*, *CASPASE3*, and *CATALASE*, the gene specific primers were designed and gene expression studies using RT-PCR showed alteration of the gene expression profile in the piperine treated group of the abovementioned genes as compared to control. As the genes control most of the biological function through specific proteins, the molecule which can either bind to protein or alter gene expression can be used for therapeutic intervention in amelioration complex conditions line hyperglycemia induced neurodegeneration process. The gene expression profile in response to the piperine support the docking results and propose a credible viewpoint on the pathways associated with protein responses to piperine binding in AD-related drug targets.

CONCLUSION

In conclusion, piperine demonstrated to possess neuroprotective properties in STZ induced diabetic rodent model as it can be used as an interventional strategy to protect neuronal cells in hyperglycemic conditions. The improvement of HOMA indices, histo-architectures, and downregulation to genes involved in apoptosis and oxidative stress are scientific evidence underlying the protective mechanism.

DATA AVAILABILITY STATEMENT

The authors confirm that the data supporting the findings of this study are available within the article and its supplementary materials.

ETHICS STATEMENT

The animal study was reviewed and approved by IAEC, Department of Zoology, JNVU, Jodhpur, India.

AUTHOR CONTRIBUTIONS

SK designed and conceived the idea of this research work. SK wrote the original manuscript. SC performed all the cell culture and docking experiments, RP, AR, and DK performed all gene expression studies, HR, PK, and PN completed all *in vivo* experiments, SS performed histopathology related experiments. All the authors contributed to writing the manuscript.

REFERENCES

- Abdel Aziz, S. M., Ahmed, O. M., Abd El-Twab, S. M., Al-Muzafar, H. M., Amin, K. A., and Abdel-Gabbar, M. (2020). Antihyperglycemic effects and mode of actions of musa paradisiaca leaf and fruit peel hydroethanolic extracts in nicotinamide/streptozotocin-induced diabetic rats. *J. Evid. Based. Complementary. Altern. Med.* 2020, 9276343. doi:10.1155/2020/9276343
- Abercrombie, M. (1946). Estimation of nuclear population from microtome sections. *Anat. Rec.* 94, 239–247. doi:10.1002/ar.1090940210
- Agrawal, R., Tyagi, E., Shukla, R., and Nath, C. (2009). A study of brain insulin receptors, AChE activity and oxidative stress in rat model of ICV STZ induced dementia. *Neuropharmacology*. 56, 779–787. doi:10.1016/j.neuropharm.2009.01.005
- Akter, K., Lanza, E. A., Martin, S. A., Myronyuk, N., Rua, M., and Raffa, R. B. (2011). Diabetes mellitus and Alzheimer's disease: shared pathology and treatment?. *Br. J. Clin. Pharmacol.* 71, 365–376. doi:10.1111/j.1365-2125.2010.03830.x
- Bajad, S., Bedi, K. L., Singla, A. K., and Johri, R. K. (2001). Piperine inhibits gastric emptying and gastrointestinal transit in rats and mice. *Planta Med.* 67, 176–179. doi:10.1055/s-2001-11505
- Bano, G. (2013). Glucose homeostasis, obesity and diabetes. *Best Pract. Res. Clin. Obstet. Gynaecol.* 27, 715–726. doi:10.1016/j.bpobgyn.2013.02.007
- Bhardwaj, R. K., Glaeser, H., Becquemont, L., Klotz, U., Gupta, S. K., and Fromm, M. F. (2002). Piperine, a major constituent of black pepper, inhibits human P-glycoprotein and CYP3A4. *J. Pharmacol. Exp. Therapeut.* 302, 645–650. doi:10.1124/jpet.102.034728
- Bonora, E. (2008). Protection of pancreatic beta-cells: is it feasible?. *Nutr. Metabol. Cardiovasc. Dis.* 18, 74–83. doi:10.1016/j.numecd.2007.05.004
- Brandt, S. J., Götz, A., Tschöp, M. H., and Müller, T. D. (2018). Gut hormone polyagonists for the treatment of type 2 diabetes. *Peptides*. 100, 190–201. doi:10.1016/j.peptides.2017.12.021
- Butterfield, D. A., Di Domenico, F., and Barone, E. (2014). Elevated risk of type 2 diabetes for development of Alzheimer disease: a key role for oxidative stress in brain. *Biochim. Biophys. Acta*. 1842, 1693–1706. doi:10.1016/j.bbdis.2014.06.010
- Chao, P. C., Li, Y., Chang, C. H., Shieh, J. P., Cheng, J. T., and Cheng, K. C. (2018). Investigation of insulin resistance in the popularly used four rat models of type-2 diabetes. *Biomed. Pharmacother.* 101, 155–161. doi:10.1016/j.biopha.2018.02.084
- Chen, S., An, F. M., Yin, L., Liu, A. R., Yin, D. K., Yao, W. B., et al. (2014). Glucagon-like peptide-1 protects hippocampal neurons against advanced glycation end product-induced tau hyperphosphorylation. *Neuroscience*. 256, 137–146. doi:10.1016/j.neuroscience.2013.10.038
- Chen, X., Guo, C., and Kong, J. (2012). Oxidative stress in neurodegenerative diseases. *Neural. Regen. Res.* 7 (5), 376–385. doi:10.3969/j.issn.1673-5374.2012.05.009
- Chomczynski, P. (1993). A reagent for the single-step simultaneous isolation of RNA, DNA and proteins from cell and tissue samples. *Biotechniques*. 15, 532–537.
- Chowdhury, S., and Kumar, S. (2020). Alpha-terpinyl acetate: a natural monoterpene from *Elettaria cardamomum* as multi-target directed ligand in Alzheimer's disease. *J. Funct. Foods*. 68, 103892. doi:10.1016/j.jff.2020.103892
- Da Costa Dias, B., Jovanovic, K., Gonsalves, D., and Weiss, S. F. (2011). Structural and mechanistic commonalities of amyloid- β and the prion protein. *Prion*. 5, 126–137. doi:10.4161/pri.5.3.17025
- Dasari, P., Anandamurali, R., and Nayak, P. (2016). Tocotrienol opposes the effect of light to moderate ethanol exposures in elevated plus maze performance of rats. *Asian J. Pharmaceut. Clin. Res.* 9, 122–127.
- Dobiášová, M., and Frohlich, J. (2001). The plasma parameter log (TG/HDL-C) as an atherogenic index: correlation with lipoprotein particle size & esterification rate in apoB-lipoprotein-depleted plasma (FER_{HDL}). *Clin. Biochem.* 34, 583–588. doi:10.1016/S0009-9120(01)00263-6
- Duarte, J. M. (2015). Metabolic alterations associated to brain dysfunction in diabetes. *Aging. Dis.* 6, 304–321. doi:10.14336/AD.2014.1104
- Elmore, S. (2007). Apoptosis: a review of programmed cell death. *Toxicol. Pathol.* 35, 495–516. doi:10.1080/01926230701320337
- Elnaggar, Y. S., Etmann, S. M., Abdelmonsif, D. A., and Abdallah, O. Y. (2015). Novel piperine-loaded Tween-integrated monoolein cubosomes as brain-targeted oral nanomedicine in Alzheimer's disease: pharmaceutical, biological, and toxicological studies. *Int. J. Nanomed.* 10, 5459–5473. doi:10.2147/IJN.S87336
- Fortin, A., Cregan, S. P., MacLaurin, J. G., Kushwaha, N., Hickman, E. S., Thompson, C. S., et al. (2001). APAF1 is a key transcriptional target for p53 in the regulation of neuronal cell death. *J. Cell. Biol.* 155, 207–216. doi:10.1083/jcb.200105137
- Gaspar, J. M., Baptista, F. I., Macedo, M. P., and Ambrósio, A. F. (2016). Inside the diabetic brain: role of different players involved in cognitive decline. *ACS Chem. Neurosci.* 7, 131–142. doi:10.1021/acschemneuro.5b00240
- Ghasemi, A., Khalifi, S., and Jedi, S. (2014). Streptozotocin-nicotinamide-induced rat model of type 2 diabetes (review). *Acta Physiol. Hung.* 101, 408–420. doi:10.1556/APhysiol.101.2014.4.2

FUNDING

The consumables are managed from the FRGS grant number 2020-21 by Guru Gobind Singh Indraprastha University. Indian Council of Medical Research (ICMR), New Delhi, provided Senior Research Fellowship (SRF) to SC.

ACKNOWLEDGMENTS

We would like to acknowledge the help and support of Prof. Meenu Kapoor and Nikita (USBT, GGSIP University) for assistance in conducting RT-PCR experiments.

SUPPLEMENTARY MATERIAL

The Supplementary Material for this article can be found online at: <https://www.frontiersin.org/articles/10.3389/fphar.2020.595471/full#supplementary-material>.

- Girard, J. (2008). The incretins: from the concept to their use in the treatment of type 2 diabetes. Part A: incretins: concept and physiological functions. *Diabetes Metab.* 34, 550–559. doi:10.1016/j.diabet.2008.09.001
- González-Reyes, R. E., Aliev, G., Ávila-Rodríguez, M., and Barreto, G. E. (2016). Alterations in glucose metabolism on cognition: a possible link between diabetes and dementia. *Curr. Pharmaceut. Des.* 22, 812–818. doi:10.2174/1381612822666151209152013
- Gorman, A. M., Orrenius, S., and Ceccatelli, S. (1998). Apoptosis in neuronal cells: role of caspases. *Neuroreport.* 9, R49–R55. doi:10.1097/00001756-199807130-00001
- Grosdidier, A., Zoete, V., and Michielin, O. (2011). SwissDock, a protein-small molecule docking web service based on EADock DSS. *Nucleic. Acids. Res.* 39 (Web Server issue), 270–277. doi:10.1093/nar/gkr366
- Guglielmo, M., Aragno, M., Autelli, R., Giliberto, L., Novo, E., Colombatto, S., et al. (2009). The up-regulation of BACE1 mediated by hypoxia and ischemic injury: role of oxidative stress and HIF1 α . *J. Neurochem.* 108, 1045–1056. doi:10.1111/j.1471-4159.2008.05858.x
- Guo, G., Shi, F., Zhu, J., Shao, Y., Gong, W., Zhou, G., et al. (2020). Piperine, A functional food alkaloid Exhibits inhibitory potential against TNBS-induced colitis via the inhibition of I κ B- α /NF- κ B and induces tight junction protein (claudin-1, occluding, and ZO-1) signalling pathway in Experimental mice. *Hum. Exp. Toxicol.* 39, 4. doi:10.1177/0960327119892042
- Hassan, A. H., Von Rosenstiel, P., Patchev, V. K., Holsboer, F., and Almeida, O. F. (1996). Exacerbation of apoptosis in the dentate gyrus of the aged rat by dexamethasone and the protective role of corticosterone. *Exp. Neurol.* 140, 43–52. doi:10.1006/exnr.1996.0113
- Hornsby, C. D., Grootendorst, J., and de Kloet, E. R. (1996). Dexamethasone does not prevent seven-day ADX-induced apoptosis in the dentate gyrus of the rat hippocampus. *Stress.* 1, 51–64. doi:10.3109/10253899609001095
- Khan, H. J., Ahmad, M. K., Khan, A. R., Rastogi, N., Mahdi, A. A., Ansari, J. A., et al. (2016). Identification of Anticancer and Antioxidant phytoconstituents from chloroform fraction of *Solanum nigrum* L. berries using GC-MS/MS analysis. *Indian J. Exp. Biol.* 54, 774–782. doi:10.3109/13880209.2016.1172320
- Kim, D. J., Yu, J. H., Shin, M. S., Shin, Y. W., and Kim, M. S. (2016). Hyperglycemia reduces efficiency of brain networks in subjects with type 2 diabetes. *PLoS One.* 11, e0157268. doi:10.1371/journal.pone.0157268
- Kumar, V., Khan, A. A., Tripathi, A., Dixit, P. K., and Bajaj, U. K. (2015). Role of oxidative stress in various diseases: relevance of dietary antioxidants. *J. Pharmacol. Exp. Therapeut.* 4, 126–132.
- Liu, S. H., Chang, C. D., Chen, P. H., Su, J. R., Chen, C. C., and Chaung, H. C. (2012). Docosahexaenoic acid and phosphatidylserine supplementations improve antioxidant activities and cognitive functions of the developing brain on pentylentetrazol-induced seizure model. *Brain Res.* 1451, 19–26. doi:10.1016/j.brainres.2012.02.060
- Livak, K. J., and Schmittgen, T. D. (2001). Analysis of relative gene expression data using real-time quantitative PCR and the 2⁻(Delta Delta C(T)) Method. *Methods.* 25, 402–408. doi:10.1006/meth.2001.1262
- Macauley, S. L., Stanley, M., Caesar, E. E., Yamada, S. A., Raichle, M. E., Perez, R., et al. (2015). Hyperglycemia modulates extracellular amyloid- β concentrations and neuronal activity *in vivo*. *J. Clin. Invest.* 125, 2463–2467. doi:10.1172/JCI79742
- Makhouri, F. R., and Ghasemi, J. B. (2018). *In Silico* studies in drug research against neurodegenerative diseases. *Curr. Neuropharmacol.* 16, 664–725. doi:10.2174/1570159X15666170823095628
- Malone, J. I. (2016). Diabetic central neuropathy: CNS damage related to hyperglycemia. *Diabetes.* 65, 355–357. doi:10.2337/dbi15-0034
- Matthews, D. R., Hosker, J. P., Rudenski, A. S., Naylor, B. A., Treacher, D. F., and Turner, R. C. (1985). Homeostasis model assessment: insulin resistance and beta-cell function from fasting plasma glucose and insulin concentrations in man. *Diabetologia.* 28, 412–419. doi:10.1007/BF00280883
- Mazzanti, G., and Di Giacomo, S. (2016). Curcumin and resveratrol in the management of cognitive disorders: what is the clinical evidence?. *Molecules.* 21, 1243. doi:10.3390/molecules21091243
- McGarry, L. M., Packer, A. M., Fino, E., Nikolenko, V., Sippy, T., and Yuste, R. (2010). Quantitative classification of somatostatin-positive neocortical interneurons identifies three interneuron subtypes. *Front. Neural Circ.* 4, 12. doi:10.3389/fncir.2010.00012
- Mena, M. A., Rodríguez-Navarro, J. A., and de Yébenes, J. G. (2009). The multiple mechanisms of amyloid deposition: the role of parkin. *Prion.* 3, 5–11. doi:10.4161/pri.3.1.8122
- Moreira-Silva, D., Carrettiro, D. C., Oliveira, A. S. A., Rodrigues, S., dos Santos-Lopes, J., Canas, P. M., et al. (2018). Anandamide effects in a streptozotocin-induced Alzheimer's disease-like sporadic dementia in rats. *Front. Neurosci.* 12, 653. doi:10.3389/fnins.2018.00653
- Mudaliar, S., and Henry, R. R. (2012). The incretin hormones: from scientific discovery to practical therapeutics. *Diabetologia.* 55, 1865–1868. doi:10.1007/s00125-012-2561-x
- Mullins, R. J., Diehl, T. C., Chia, C. W., and Kapogiannis, D. (2017). Insulin resistance as a link between amyloid-beta and tau pathologies in Alzheimer's disease. *Front. Aging Neurosci.* 9, 118. doi:10.3389/fnagi.2017.00118
- Nandi, A., Yan, L. J., Jana, C. K., and Das, N. (2019). Role of catalase in oxidative stress- and age-associated degenerative diseases. *Oxid. Med. Cell. Longev.* 2019, 9613090. doi:10.1155/2019/9613090
- Nazem, A., Sankowski, R., Bacher, M., and Al-Abed, Y. (2015). Rodent models of neuroinflammation for Alzheimer's disease. *J. Neuroinflammation.* 12, 74. doi:10.1186/s12974-015-0291-y
- Papaliagkas, V., Anogianaki, A., Anogianakis, G., and Ilonidis, G. (2007). The proteins and the mechanisms of apoptosis: a mini-review of the fundamentals. *Hippokratia.* 11, 108–113.
- Petersen, M. C., and Shulman, G. I. (2018). Mechanisms of insulin action and insulin resistance. *Physiol. Rev.* 98, 2133–2223. doi:10.1152/physrev.00063.2017
- Petersen, E. F., Goddard, T. D., Huang, C. C., Couch, G. S., Greenblatt, D. M., Meng, E. C., et al. (2004). UCSF Chimera—a visualization system for exploratory research and analysis. *J. Comput. Chem.* 25, 1605–1612. doi:10.1002/jcc.20084
- Prasannaraja, C., Kamalanathan, A. S., Vijayalakshmi, M. A., and Venkataraman, K. (2020). A dipyrrole derivative from Aloe vera inhibits an anti-diabetic drug target Dipeptidyl Peptidase (DPP)-IV *in vitro*. *Prep. Biochem. Biotechnol.* 50, 511–520. doi:10.1080/10826068.2019.1710712
- Pruzin, J. J., Nelson, P. T., Abner, E. L., and Arvanitakis, Z. (2018). Review: relationship of type 2 diabetes to human brain pathology. *Neuropathol. Appl. Neurobiol.* 44, 347–362. doi:10.1111/nan.12476
- Rai, S., Kamat, P. K., Nath, C., and Shukla, R. (2013). A study on neuroinflammation and NMDA receptor function in STZ (ICV) induced memory impaired rats. *J. Neuroimmunol.* 254, 1–9. doi:10.1016/j.jneuroim.2012.08.008
- Ram, H., Jaipal, N., Charan, J., Kashyap, P., Kumar, S., Tripathi, R., et al. (2020). Phytoconstituents of an ethanolic pod extract of *Prosopis cineraria* triggers the inhibition of HMG-CoA reductase and the regression of atherosclerotic plaque in hypercholesterolemic rabbits. *Lipids Health Dis.* 19, 6. doi:10.1186/s12944-020-1188-z
- Ren, T., Wang, Q., Li, C., Yang, M., and Zuo, Z. (2018). Efficient Brain uptake of piperine and its pharmacokinetics characterization after oral administration. *Xenobiotica.* 48, 1249–1257. doi:10.1080/00498254.2017.1405293
- Resende, R., Ferreira, E., Pereira, C., and Resende de Oliveira, C. (2008). Neurotoxic effect of oligomeric and fibrillar species of amyloid-beta peptide 1–42: involvement of endoplasmic reticulum calcium release in oligomer-induced cell death. *Neuroscience.* 155, 725–737. doi:10.1016/j.neuroscience.2008.06.036
- Röder, P. V., Wu, B., Liu, Y., and Han, W. (2016). Pancreatic regulation of glucose homeostasis. *Exp. Mol. Med.* 48, e219. doi:10.1038/emmm.2016.6
- Rojas-Carranza, C. A., Bustos-Cruz, R. H., Pino-Pinzon, C. J., Ariza-Marquez, Y. V., Gomez-Bello, R. M., and Canadas-Garre, M. (2018). Diabetes-related neurological implications and pharmacogenomics. *Curr. Pharmaceut. Des.* 24, 1695. doi:10.2174/1381612823666170317165350
- Rom, S., Zuluaga-Ramirez, V., Gajghate, S., Seliga, A., Winfield, M., Heldt, N. A., et al. (2019). Hyperglycemia-driven neuroinflammation compromises BBB leading to memory loss in both diabetes mellitus (DM) type 1 and type 2 mouse models. *Mol. Neurobiol.* 56, 1883–1896. doi:10.1007/s12035-018-1195-5
- Roshanbakhsh, H., Elahdadi Salmani, M., Dehghan, S., Nazari, A., Javan, M., and Pourabdolhossein, F. (2020). Piperine ameliorated memory impairment and myelin damage in lysolecithin induced hippocampal demyelination. *Life Sci.* 253, 117671. doi:10.1016/j.lfs.2020.117671
- Salkovic-Petrisic, M., Knezovic, A., Hoyer, S., and Riederer, P. (2013). What have we learned from the streptozotocin-induced animal model of sporadic

- Alzheimer's disease, about the therapeutic strategies in Alzheimer's research. *J. Neural. Transm.* 120, 233–252. doi:10.1007/s00702-012-0877-9
- Saravanan, N., Patil, M. A., Kumar, P. U., Suryanarayana, P., and Reddy, G. B. (2017). Dietary ginger improves glucose dysregulation in a long-term high-fat high-fructose fed prediabetic rat model. *Indian J. Exp. Biol.* 55, 142–150.
- Saxena, G., Bharti, S., Kamat, P. K., Sharma, S., and Nath, C. (2010). Melatonin alleviates memory deficits and neuronal degeneration induced by intracerebroventricular administration of streptozotocin in rats. *Pharmacol. Biochem. Behav.* 94, 397–403. doi:10.1016/j.pbb.2009.09.022
- Shakeri, R., Kheirollahi, A., and Davoodi, J. (2017). Apaf-1: regulation and function in cell death. *Biochimie.* 135, 111–125. doi:10.1016/j.biochi.2017.02.001
- Shi, Y. (2004). Caspase activation, inhibition, and reactivation: a mechanistic view. *Protein Sci.* 13, 1979–1987. doi:10.1110/ps.04789804
- Shingo, A. S., Kanabayashi, T., Kito, S., and Murase, T. (2012). Intracerebroventricular administration of an insulin analogue recovers STZ-induced cognitive decline in rats. *Behav. Brain Res.* 241, 105–111. doi:10.1016/j.bbr.2012.12.005
- Shrivastava, P., Vaibhav, K., Tabassum, R., Khan, A., Ishrat, T., Khan, M. M., et al. (2013). Anti-apoptotic and anti-inflammatory effect of piperine on 6-OHDA induced Parkinson's rat model. *J. Nutr. Biochem.* 24, 680–687. doi:10.1016/j.jnutbio.2012.03.018
- Silzer, T. K., and Phillips, N. R. (2018). Etiology of type 2 diabetes and Alzheimer's disease: exploring the mitochondria. *Mitochondrion.* 43, 16–24. doi:10.1016/j.mito.2018.04.004
- Singh, V. P., Bali, A., Singh, N., and Jaggi, A. S. (2014). Advanced glycation end products and diabetic complications. *Korean J. Physiol. Pharmacol.* 18, 1–14. doi:10.4196/kjpp.2014.18.1.1
- Sloviter, R. S., Dean, E., and Neubort, S. (1993). Electron microscopic analysis of adrenalectomy-induced hippocampal granule cell degeneration in the rat: apoptosis in the adult central nervous system. *J. Comp. Neurol.* 330, 337–351. doi:10.1002/cne.903300305
- Song, Y., Cao, C., Xu, Q., Gu, S., Wang, F., Huang, X., et al. (2020). Piperine attenuates TBI-induced seizures via inhibiting cytokine-activated reactive astrogliosis. *Front. Neurol.* 11, 431. doi:10.3389/fneur.2020.00431
- Srinivasan, K. (2007). Black pepper and its pungent principle-piperine: a review of diverse physiological effects. *Crit. Rev. Food Sci. Nutr.* 47, 735–748. doi:10.1080/10408390601062054
- Stöhr, O., Schilbach, K., Moll, L., Hettich, M. M., Freude, S., Wunderlich, F. T., et al. (2013). Insulin receptor signaling mediates APP processing and β -amyloid accumulation without altering survival in a transgenic mouse model of Alzheimer's disease. *Age.* 35, 83–101. doi:10.1007/s11357-011-9333-2
- Uttara, B., Singh, A. V., Zamboni, P., and Mahajan, R. T. (2009). Oxidative stress and neurodegenerative diseases: a review of upstream and downstream antioxidant therapeutic options. *Curr. Neuropharmacol.* 7, 65–74. doi:10.2174/157015909787602823
- Vaibhav, K., Shrivastava, P., Javed, H., Khan, A., Ahmed, M. E., Tabassum, R., et al. (2012). Piperine suppresses cerebral ischemia-reperfusion-induced inflammation through the repression of COX-2, NOS-2, and NF- κ B in middle cerebral artery occlusion rat model. *Mol. Cell. Biochem.* 367, 73–84. doi:10.1007/s11010-012-1321-z
- Vessal, M., Hemmati, M., and Vasei, M. (2003). Antidiabetic effects of quercetin in streptozotocin-induced diabetic rats. *Comp. Biochem. Physiol. C Toxicol. Pharmacol.* 135C, 357–364. doi:10.1016/s1532-0456(03)00140-6
- Wu, Y. J., Guo, X., Li, C. J., Li, D. Q., Zhang, J., Yang, Y., et al. (2015). Dipeptidyl peptidase-4 inhibitor, vildagliptin, inhibits pancreatic beta cell apoptosis in association with its effects suppressing endoplasmic reticulum stress in db/db mice. *Metab. Clin. Exp.* 64, 226–235. doi:10.1016/j.metabol.2014.08.006
- Xie, H., Wen, H., Qin, M., Xia, J., Zhang, D., Liu, L., et al. (2016). *In silico* drug repositioning for the treatment of Alzheimer's disease using molecular docking and gene expression data. *RSC Adv.* 6, 98080–98090. doi:10.1039/c6ra21941a
- Zhang, Y., Yin, F., Liu, J., Liu, Z., Guo, L., Xia, Z., et al. (2015). Geniposide attenuates insulin-deficiency-induced acceleration of β -amyloidosis in an APP/PS1 transgenic model of Alzheimer's disease. *Neurochem. Int.* 89, 7–16. doi:10.1016/j.neuint.2015.04.002

Conflict of Interest: The authors declare that the research was conducted in the absence of any commercial or financial relationships that could be construed as a potential conflict of interest.

Copyright © 2021 Kumar, Chowdhury, Razdan, Kumari, Purty, Ram, Kumar, Nayak and Shukla. This is an open-access article distributed under the terms of the Creative Commons Attribution License (CC BY). The use, distribution or reproduction in other forums is permitted, provided the original author(s) and the copyright owner(s) are credited and that the original publication in this journal is cited, in accordance with accepted academic practice. No use, distribution or reproduction is permitted which does not comply with these terms.



Studies on the Changes of Pharmacokinetics Behaviors of Phytochemicals and the Influence on Endogenous Metabolites After the Combination of Radix Bupleuri and Radix Paeoniae Alba Based on Multi-Component Pharmacokinetics and Metabolomics

Congcong Chen^{1,2}, Qicai Yin^{1,2}, Junshen Tian¹, Xiaoxia Gao¹, Xuemei Qin¹, Guanhua Du^{1,3} and Yuzhi Zhou^{1*}

OPEN ACCESS

Edited by:

Gudrun S. Ulrich-Merzenich,
University Hospital Bonn, Germany

Reviewed by:

Chee Wun How,
Monash University Malaysia, Malaysia

Yun Zhang,
Biology Institute of Shandong
Academy of Sciences, China

*Correspondence:

Yuzhi Zhou
zhouyuzhi@sxu.edu.cn

Specialty section:

This article was submitted to
Ethnopharmacology,
a section of the journal
Frontiers in Pharmacology

Received: 18 November 2020

Accepted: 25 January 2021

Published: 08 March 2021

Citation:

Chen C, Yin Q, Tian J, Gao X, Qin X, Du G and Zhou Y (2021) Studies on the Changes of Pharmacokinetics Behaviors of Phytochemicals and the Influence on Endogenous Metabolites After the Combination of Radix Bupleuri and Radix Paeoniae Alba Based on Multi-Component Pharmacokinetics and Metabolomics. *Front. Pharmacol.* 12:630970. doi: 10.3389/fphar.2021.630970

¹Modern Research Center for Traditional Chinese Medicine of Shanxi University, Taiyuan, China, ²College of Chemistry and Chemical Engineering, Shanxi University, Taiyuan, China, ³Institute of Materia Medica, Chinese Academy of Medical Sciences and Peking Union Medical College, Beijing, China

Radix Bupleuri-Radix Paeoniae Alba (RB-RPA) is a classic herb pair, which is commonly used to treat depression by soothing “liver qi stagnation” in the clinic. However, little is yet known concerning the combination mechanism of Radix Bupleuri (RB) and Radix Paeoniae Alba (RPA), their bioactive forms *in vivo* and the regulatory effects on the organism. The present study aimed to elucidate the changes in multi-component pharmacokinetics (PK) behavior after the combination of RB and RPA by a high-resolution full-scan mode of UPLC-HRMS method (a total of 38 components PK profiles were obtained, of which 23 components come from RB and 15 components come from RPA). Moreover, the metabolomics approach was used to analyze the dynamic response of endogenous metabolites intervened by RB-RPA, and the correlation between concentration-time curves of 38 components from RB-RPA and the dynamic response profiles of endogenous metabolites was characterized by Pearson correlation analysis. The results demonstrated that the combination of RB and RPA could significantly improve the bioavailability of five components in RB, and six components in RPA. Besides, metabolomics results indicated that a total of 21 endogenous metabolites exhibited time-dependent changes in response to the RB-RPA administration, of which 12 endogenous metabolites were significantly increased, and nine endogenous metabolites were significantly decreased. Furthermore, correlation analysis results indicated that the components with significantly improved bioavailability after combination such as saikogenin F, saikogenin G, albiflorin, methyl gallate, paeonimetabolin II were significantly positively correlated with picolinic acid, a metabolite with neuroprotective effect; saikogenin F, saikogenin G were significantly

positively correlated with itaconic acid, a endogenous metabolite with anti-inflammatory activity; and albiflorin, paeonimetabolin II were significantly positively correlated with α -linolenic acid, a metabolite with strong protective actions on brain functions. These results indicated that the combination of RB and RPA can enhance each other's neuroprotective and anti-inflammatory activities. In this study, A novel and efficient strategy has been developed to analyze the influence of the combination of RB and RPA *in vivo* behaviors by combining multi-component pharmacokinetics with metabolomics, which was contributed to clarifying the scientific connotation of herb-herb compatibility.

Keywords: Radix Bupleuri-Radix Paeoniae Alba herb pair, multi-component pharmacokinetics, metabolomics, correlation analysis, herb-herb compatibility

INTRODUCTION

RB is the dried root of the umbelliferous plant *Bupleurum chinense* DC. It has been widely used in Asia for thousands of years due to its pharmaceutical effects on antipyretic, analgesic, anti-inflammatory and anti-depressant (Ashour and Wink, 2011). The saponins such as saikosaponin A, saikosaponin D were the main active components of antidepressant effect (Tian et al., 2016). RPA is derived from the dried roots of *Paeonia lactiflora* Pall. In “Shennong’s Classic of Material Medical,” the efficacy of RPA was described in detail. Modern pharmacological studies have found that RPA has a variety of biological activities, such as analgesia, anti-inflammatory, immune-enhancing and

anti-depression effects (Xu et al., 2008). Paeoniflorin and albiflorin were the main active ingredients in the antidepressant effect of RPA (Qiu et al., 2013). RB-RPA was a common herb pair, which was regarded as the core drug pair in Xiaoyaosan, Sinisan and Chaihu-Shugan San which all were classic prescriptions for treating depression, and exerted antidepressant effect by relieving “liver qi stagnation.” Herb-herb compatibility is a common form of TCM, it can achieve an optimal effect by obtaining synergy or reducing possible adverse reactions (Zhao et al., 2010). Modern pharmacological studies have shown that the analgesic, anti-inflammatory, and antidepressant effect was significantly improved after the combination of RB and RPA (Wang et al.,

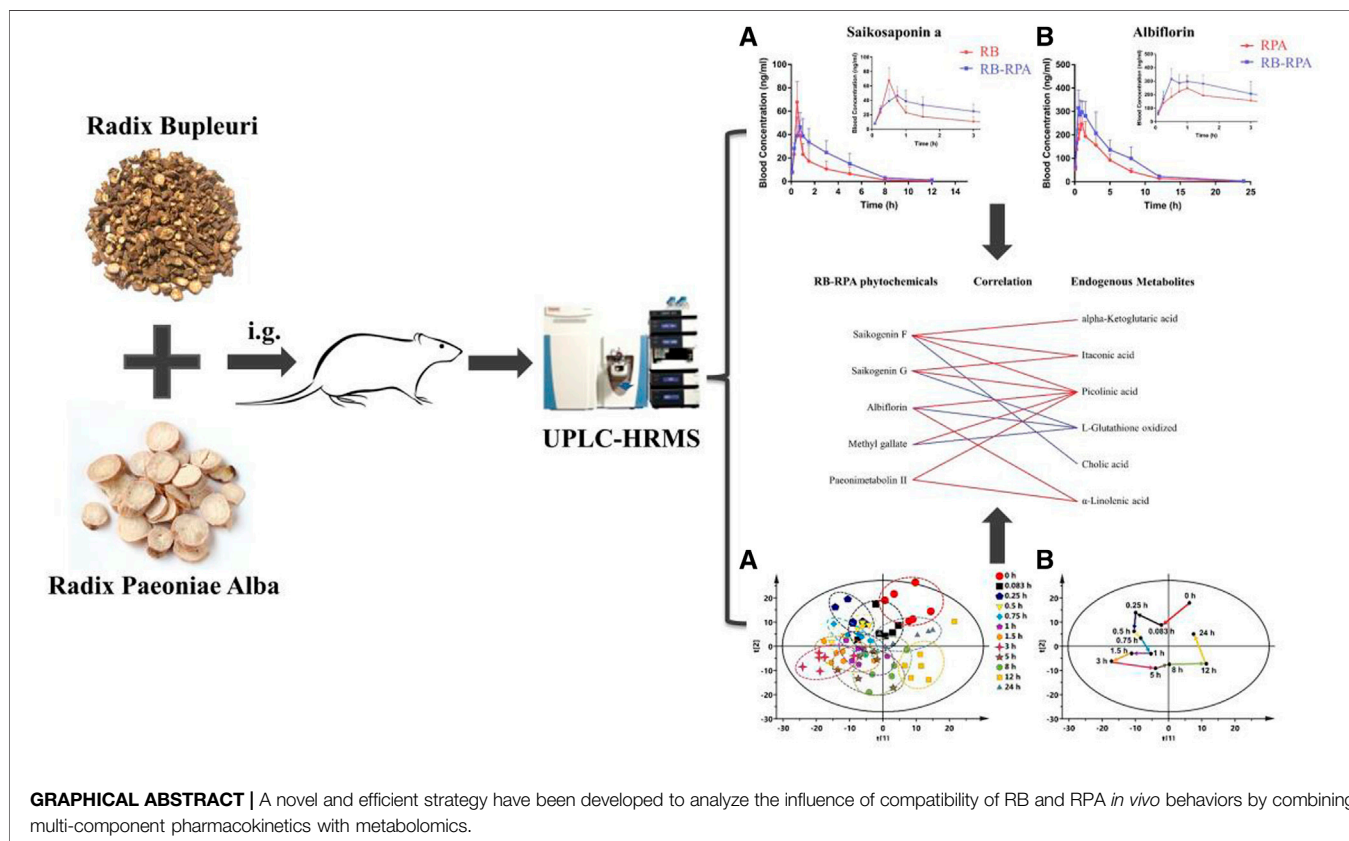


TABLE 1 | The prototype components and their metabolites characterized by UPLC/MS/MS after oral administration of RB-RPA herb pair in rat plasma, and the extracted ion ranges of 38 components.

No.	Name	t _R /min	Formula	Ion mode	m/z	Source or parent	Extracted ion ranges
P1	Desbenzoylpaeoniflorin	0.972	C ₁₆ H ₂₄ O ₁₀	[M + HCOO] ⁻	421.13408	RPA	421.13405–421.13410
P2	Methyl gallate	3.473	C ₉ H ₈ O ₅	[M-H] ⁻	183.02991	RPA	183.02988–183.02993
P3	Oxypaeoniflorin	4.695	C ₂₃ H ₂₈ O ₁₂	[M-H] ⁻	495.15087	RPA	495.15084–495.15090
P4	Albiflorin	6.658	C ₂₃ H ₂₈ O ₁₁	[M + HCOO] ⁻	525.16021	RPA	525.16019–525.16024
P5	Paeoniflorin	7.693	C ₂₃ H ₂₈ O ₁₁	[M + HCOO] ⁻	525.16029	RPA	525.16026–525.16032
P6	Saikosaponin C	13.856	C ₄₈ H ₇₈ O ₁₇	[M + HCOO] ⁻	971.52109	RB	971.52107–971.52112
P7	Saikosaponin A	15.069	C ₄₂ H ₆₈ O ₁₃	[M + HCOO] ⁻	825.45521	RB	825.45518–825.45523
P8	Saikosaponin B ₂	15.516	C ₄₂ H ₆₈ O ₁₃	[M + HCOO] ⁻	825.45520	RB	825.45518–825.45523
P9	Acetyl-saikosaponin A	16.183	C ₄₄ H ₇₀ O ₁₄	[M + HCOO] ⁻	867.47362	RB	867.47360–867.47370
P10	Saikosaponin D	16.525	C ₄₂ H ₆₈ O ₁₃	[M + HCOO] ⁻	825.45521	RB	825.45518–825.45523
P11	Acetyl-saikosaponin B ₂	16.615	C ₄₄ H ₇₀ O ₁₄	[M + HCOO] ⁻	867.47364	RB	867.47360–867.47370
P12	Acetyl-saikosaponin D	17.583	C ₄₄ H ₇₀ O ₁₄	[M + HCOO] ⁻	867.47368	RB	867.47360–867.47370
M1	Paeonimetabolin I	9.674	C ₁₀ H ₁₄ O ₄	[M-H] ⁻	197.08117	Paeoniflorin	197.08115–197.08123
M2	Paeonimetabolin II	11.311	C ₁₀ H ₁₆ O ₄	[M-H] ⁻	199.09755	Paeoniflorin	199.09753–199.09758
M3	Paeonimetabolin I glucuronide isomer	6.033	C ₁₆ H ₂₂ O ₁₀	[M-H] ⁻	373.11411	Paeoniflorin	373.11408–373.11414
M4	Methylgallic acid glucuronide	6.957	C ₁₄ H ₁₆ O ₁₁	[M-H] ⁻	359.06197	Methyl gallate	359.06195–359.06199
M5	Methylgallic acid sulfate	2.968	C ₉ H ₈ O ₈ S	[M-H] ⁻	262.98679	Methyl gallate	262.98675–262.98682
M6	3,4-di-O-methyl gallic acid sulfate	10.353	C ₉ H ₁₀ O ₈ S	[M-H] ⁻	277.00231	Methyl gallate	277.00228–277.00233
M7	Pyrogallol glucuronide	1.284	C ₁₂ H ₁₄ O ₉	[M-H] ⁻	301.05658	Methyl gallate	301.05656–301.05662
M8	Pyrogallol sulfate	6.745	C ₈ H ₆ O ₆ S	[M-H] ⁻	204.98135	Methyl gallate	204.98133–204.98138
M9	Methylpyrogallol sulfate	2.082	C ₇ H ₈ O ₆ S	[M-H] ⁻	218.99695	Methyl gallate	218.99692–218.99698
M10	Methylpyrogallol glucuronide	1.049	C ₁₃ H ₁₆ O ₉	[M-H] ⁻	315.07209	Methyl gallate	315.07206–315.07213
M11	Prosaikogenin F	14.972	C ₃₆ H ₅₇ O ₈	[M + HCOO] ⁻	662.40253	Saikosaponin A	662.40247–662.40257
M12	Saikogenin F	13.123	C ₃₀ H ₄₉ O ₄	[M-H ₂ O + H] ⁺	455.35191	Saikosaponin A	455.35188–455.35198
M13	Hydroxy-saikogenin F	13.905	C ₃₀ H ₄₉ O ₅	[M-H ₂ O + H] ⁺	471.34678	Saikosaponin A	471.34674–471.34692
M14	Dihydroxyl-dehydrogenation-saikogenin F	13.021	C ₃₀ H ₄₆ O ₆	[M-H ₂ O + H] ⁺	485.32603	Saikosaponin A	485.32600–485.32606
M15	Hydroxyl-dehydrogenation-saikogenin F	16.142	C ₃₀ H ₄₆ O ₅	[M-H ₂ O + H] ⁺	469.33111	Saikosaponin A	469.33108–469.33118
M16	Dihydroxyl-saikogenin F	13.648	C ₃₀ H ₄₈ O ₆	[M-H ₂ O + H] ⁺	487.34168	Saikosaponin A	487.34164–487.34172
M17	Trihydroxyl-dehydrogenation-saikogenin F	13.336	C ₃₀ H ₄₆ O ₇	[M-H ₂ O + H] ⁺	501.32095	Saikosaponin A	501.32090–501.32099
M18	Saikogenin E	16.086	C ₃₀ H ₄₈ O ₃	[M-H ₂ O + H] ⁺	439.35692	Saikosaponin C	439.35686–439.35696
M19	Hydroxy-saikogenin E	17.372	C ₃₀ H ₄₈ O ₄	[M-H ₂ O + H] ⁺	455.35182	Saikosaponin C	455.35178–455.35186
M20	Dihydroxyl-dehydrogenation-saikogenin E	16.321	C ₃₀ H ₄₆ O ₅	[M-H ₂ O + H] ⁺	469.33115	Saikosaponin C	469.33108–469.33118
M21	Hydroxyl-dehydrogenation-saikogenin E	16.894	C ₃₀ H ₄₆ O ₄	[M-H ₂ O + H] ⁺	453.33621	Saikosaponin C	453.33618–453.33625
M22	Dihydroxyl-saikogenin E	14.757	C ₃₀ H ₄₈ O ₅	[M-H ₂ O + H] ⁺	471.34669	Saikosaponin C	471.34666–471.34676
M23	Prosaikogenin G	17.669	C ₃₆ H ₅₇ O ₈	[M + HCOO] ⁻	662.40251	Saikosaponin D	662.40247–662.40257
M24	Saikogenin G	16.516	C ₃₀ H ₄₉ O ₄	[M-H ₂ O + H] ⁺	455.35196	Saikosaponin D	455.35188–455.35198
M25	Prosaikogenin D	15.947	C ₃₆ H ₅₇ O ₈	[M + HCOO] ⁻	662.40249	Saikosaponin B ₂	662.40247–662.40257
M26	Saikogenin D	14.544	C ₃₀ H ₄₈ O ₄	[M-H ₂ O + H] ⁺	455.35193	Saikosaponin B ₂	455.35188–455.35198

P: prototype components absorbed into the plasma; M: metabolites of prototype components; RB: *Radix Bupleuri*; RPA: *Radix Paeoniae Alba*.

2016; Li et al., 2021). However, the scientific connotation of RB and RPA combination and the potential theoretical basis of increasing therapeutic effect after combination were unclear. Currently, pharmacokinetic research has become a reliable way to elucidate the synergistic mechanism of herb-herb compatibility, as it can reflect the dynamic changes of the pharmacodynamic substances before and after compatibility (Wang et al., 2012; Zhou et al., 2017).

Recently, we have also analyzed the chemical components in rat plasma after oral administration of RB-RPA herb pair, a total of 55 components were detected in rat plasma, of which 16 were prototype components and 39 were metabolites of prototype components (Yin et al., 2019). The analysis of the chemical profile of RB-RPA in rat plasma makes it possible to conduct a comprehensive PK study. In this work, we employed the Thermo-Fisher Dionex UltiMate 3000 UHPLC-Q Exactive Orbitrap-MS system, with a high-resolution and high-throughput platform to conduct the PK study of 38 marker

compounds (due to the low concentration of the other 17 components, the time points that could be detected were less than six, their PK curves were not available), and the mass spectrum information and extracted ion ranges of the 38 components were listed in **Table 1**. The method was based on a high-resolution full-scan mode, to acquire a comprehensive profile of all ionized components in rat plasma, and previous studies have confirmed the reliability of this analytical method in PK studies (Wang et al., 2019). So, based on the above research, the impact on pharmacokinetic parameters before and after the combination of RB and RPA was analyzed by multi-component pharmacokinetics research method.

Distinct from chemical drugs, the large number and wide concentration range of compounds were present in TCM. Besides, the vast number of compounds were ingested would have a series of regulatory effects in the body (including endogenous metabolites that were significantly regulated in response to the intake of herbal medicines compounds), multi-

compounds interact with multi-targets to achieve a maximal therapeutic effect and could exert a holistic treatment to multi-targets diseases such as depression (Xue and Roy, 2003). Therefore, establishing the evidence-based pharmacokinetics (PK) and pharmacodynamics (PD) research methods for multicomponent TCM was still a difficult issue. It was worth noting that many of today's major diseases (such as diabetes, hyperuricemia, and depression) have a strong metabolic foundation or a definite metabolic cause (Wishart, 2016). Besides, the nutraceutical intervention of multicomponent herbal medicines was regarded as a process in which the plant metabolome interacts with the body metabolome (Xie et al., 2018). Therefore, endogenous metabolites as an indicator of PD become a reliable method to solve this difficult problem (Zhang et al., 2019). At the same time, revealing the dynamic response and interactions between herbal phytochemistry and endogenous metabolites was provided a new opportunity to clarify the holistic and synergistic mechanisms of TCM (Xie et al., 2012). In this study, metabolomics technology was applied to analyze the dynamic response of endogenous metabolites after oral RB-RPA. At the same time, PK-PD correlation analysis was used to comprehensively analyze the effect of "plant metabolome" on "body metabolome" by integrating pharmacokinetics and metabonomics technology.

MATERIALS AND METHODS

Chemicals and Reagents

HPLC grade acetonitrile, methanol, and LC-MS grade formic acid were obtained from Thermo-Fisher Scientific Inc. (United States). Purification of deionized water using the Milli-Q system (Millipore, Billerica, MA, United States). The Chinese Herbal Slices of Radix Bupleuri and Radix Paeoniae Alba were purchased from Anguo Qiao Chinese herbal sliced medicine Co., Ltd. and the batch number were 1710436111 and 1708255131 respectively. Moreover, Traditional Chinese medicines Radix Bupleuri and Radix Paeoniae Alba were authenticated by Prof. Xue-Mei Qin of Shanxi University, which confirmed that Radix Bupleuri is the dried root of the umbelliferous plant *Bupleurum chinense* DC and Radix Paeoniae Alba is derived from the dried roots of *Paeonia lactiflora* Pall. Voucher specimens of Radix Bupleuri and Radix Paeoniae Alba were deposited in the Modern Research Center for Traditional Chinese Medicine of Shanxi University, labeled as YZ-2018-0403001 (Radix Paeoniae Alba) and YZ-2018-0403002 (Radix Bupleuri), respectively. Saikosaponin A (batch number BWB50206), saikosaponin D (batch number BWB50210), saikosaponin C (batch number BWB50209), saikosaponin B₂ (batch number BWB50208) and methyl gallate (batch number BWB50638) were purchased from Chengdu Ruiensi Biological Technology Co., Ltd. (Sichuan, China). Paeoniflorin (batch number Y0001856), albiflorin (batch number ASB-00001513-005), oxypaeoniflorin (batch number BWB50094) and glycyrrhizin (IS; batch number 14110717) were purchased from the Chinese National Institute of Pharmaceutical and Biological Products (Beijing, China). The purities of all standards were at least 98%, and all other organic reagents were of analytical grade.

Preparation of Herb Extracts

As described in previous reports (Chen et al., 2020; Li et al., 2021), Radix Bupleuri (3 kg) or Radix Paeoniae Alba (3 kg) were soaked in 70% ethanol (2.4 L) for 1.5 h before extraction. Then Radix Bupleuri or Radix Paeoniae Alba were extracted twice with 70% ethanol under reflux, each time for 1.5 h. The extracts were filtrated and concentrated in vacuo and lyophilized into powders (15.15% yield for Radix Bupleuri, and 11.78% yield for Radix Paeoniae Alba), and then stored at 4°C until use and UPLC-MS analysis.

Besides, to assure the quality of Radix Bupleuri and Radix Paeoniae Alba, the chemical fingerprinting was analyzed by HPLC. For Radix Bupleuri, the saikosaponin A, saikosaponin D, saikosaponin B₂, and saikosaponin C were identified as chemical markers for quality monitoring; For Radix Paeoniae Alba, the albiflorin, paeoniflorin, oxypaeoniflorin, and methyl gallate were identified as chemical markers for quality monitoring. The representative HPLC was shown in **Supplementary Figure S1** and the content of the eight constituents in herb extracts was shown in **Supplementary Table S1**.

Preparation of Standards, Calibration Standards, and QC Samples

Individual stock solutions (1.00 mg mL⁻¹) of saikosaponin A, saikosaponin D, saikosaponin C, saikosaponin B₂, paeoniflorin, albiflorin, oxypaeoniflorin and methyl gallate were prepared by accurately weighing the required amounts into volumetric flasks and dissolving in methanol. The individual stock solutions were serially diluted with methanol and then mixed to provide working standard solutions of the desired concentrations. The Internal standard (IS) stock solutions of glycyrrhizin (1.00 µg mL⁻¹) were also prepared in methanol, and then diluted with methanol to the desired concentrations of 300 ng mL⁻¹.

Calibration standard solutions were prepared by spiking 50 µL of a mixed standard solution with 150 µL blank rat plasma to give a desired concentrations: saikosaponin D, saikosaponin C, saikosaponin B₂, and oxypaeoniflorin at 0.1, 0.2, 0.5, 1.0, 5.0, 10.0, 20.0, 50.0, 250.0 ng mL⁻¹; saikosaponin A and methyl gallate at 0.2, 0.4, 1.0, 2.0, 10.0, 20.0, 40.0, 100.0, 500.0 ng mL⁻¹; albiflorin at 0.5, 1.0, 2.5, 5.0, 25.0, 50.0, 100.0, 250.0, 1250.0 ng mL⁻¹; paeoniflorin at 2.0, 4.0, 10.0, 20.0, 100.0, 200.0, 400.0, 1000.0, 5000.0 ng mL⁻¹.

For method validation, QC samples were prepared using three concentration levels of the standard solution in the same manner, with the desired concentrations of saikosaponin D, saikosaponin C, saikosaponin B₂, and oxypaeoniflorin at 0.2, 5.0, 50.0 ng mL⁻¹; saikosaponin A and methyl gallate at 0.4, 10.0, 100.0 ng mL⁻¹; albiflorin at 1.0, 25.0, 250.0 ng mL⁻¹; paeoniflorin at 4.0, 100.0, 1000.0 ng mL⁻¹.

Plasma Sample Pretreatment

150 µL of plasma was mixed with 50 µL of IS solution and 300 µL methanol-water (1:1, v/v). The above mixtures were vortexed for 2 min, ultrasonicated for 5 min, and then centrifuged at 4°C/13,000 rpm for 15 min. The supernatant was separated and evaporated to dryness with a SCIENTZ-50F vacuum centrifugal concentrator (Scientz Biotechnology Co., Ltd., Ningbo, China). The dry extracts were reconstituted in 150 µL

methanol-water (1:5, v/v), vortexed for 2 min, and centrifuged at 4°C/13,000 rpm for 10 min. Finally, transferred 100 µL to autosampler vials for UPLC-MS analysis.

Animal Handling and Sampling

Male Sprague-Dawley rats, weighing 220 ± 20 g (aged 8 weeks), were provided by the Beijing Vital Laboratory Animal Co., Ltd. (Beijing, China, No. SCXK2018-0011). All of the rats were adapted to the novel experimental environment for 7 days (room temperature $22 \pm 2^\circ\text{C}$, $55 \pm 5\%$ relative humidity and 12 h light-dark cycle); All rats were free to access the water and food until 12 h before the experiment. The animal study was reviewed and approved by the Experimental Animal Ethical Committee of Modern Research Center for Traditional Chinese Medicine, Shanxi University (animal ethic approval number: SXULL2018018), and all experimental procedures were carried out in accordance with the NIH Guide for the Care and Use of Laboratory Animals. After one week of adaptation, twenty-one rats were divided into three groups randomly, with seven rats in each group: 1) RPA group, were oral administration of Radix Paeoniae Alba extract (45 g-herb/kg); 2) RB group, were oral administration of Radix Bupleuri extract (45 g-herb/kg); 3) RB-RPA group, were oral administration of powder mixture of Radix Bupleuri and Radix Paeoniae Alba extracts (containing 45 g-herb/kg Radix Bupleuri and 45 g-herb/kg Radix Paeoniae Alba). The medicinal powders of all groups were dissolved in distilled water at concentrations of 0.53 g/ml for RPA, 0.68 g/ml for RB and 1.21 g/ml for RB-RPA. Each group received intragastric administration with a volume of 10 ml/kg (rat body weight). The dosage of Radix Bupleuri and Radix Paeoniae Alba is equivalent to a 3-fold clinical dosage of component herbs in Xiaoyao San (Chen et al., 2020). The blood samples (0.3 ml) were collected from the ophthalmic venous plexus into heparinized tubes before oral administration and subsequently at 0.083, 0.25, 0.5, 0.75, 1, 1.5, 3, 5, 8, 12, and 24 h after dosing. All rats were free to access the water during the experiment. The blood samples at each time point were collected from seven rats. The blood samples were centrifuged at 4,000 rpm for 10 min and frozen at -80°C until analysis.

UPLC-HRMS Analysis for Herb Extracts and Plasma Sample

Using a Thermo-Fisher Dionex UltiMate 3000 UHPLC system coupled with a Q Exactive Orbitrap-MS (Thermo-Fisher, United States) and Xcalibur workstation (Thermo-Fisher Scientific Inc., Waltham, MA, United States) to acquire UPLC-HRMS raw data. Chromatographic separation of herb extracts and plasma samples was performed on an Acquity UPLC HSS T3 column (2.1 mm \times 100 mm, 1.8 µm) maintained at 37°C. The flow rate was 0.2 ml/min and the injection volume was 5 µL. The mobile phase consisted of (solvent A) 0.1% formic acid in water (v/v) and (solvent B) 0.1% formic acid in acetonitrile (v/v), the gradient elution conditions for herb extracts and plasma samples were operated under the following program: 0~5.5 min, 5% B; 5.5~9.5 min, 5~15% B; 9.5~13 min, 15~35% B; 13~17 min, 35~60% B; 17~20 min, 60~90% B; 20~22 min, 90% B; 22~23 min, 90~5%B; 23~25 min, 5% B. Mass spectrometry

detection conditions were set as follows: the MS data were acquired under positive and negative ionization modes via heated electrospray ionization (HESI) source. The scan mode was Full Scan and the scan range was set 50–1000 m/z; heater temperature, 300°C; capillary temperature, 330°C; spray voltage, 3.5 kV (positive mode) and 2.6 kV (negative mode); sheath gas velocity, 35 arb; auxiliary gas flow, 10 arb. The Q Exactive Orbitrap-MS has a fast positive and negative ion switching function, which could switch between positive-negative ion modes during the analysis of the same sample. So, we applied the method of switching ion modes in the detection process to quantify all analytes better. Glycyrrhizin was selected as the internal standard because it could be detected in both positive and negative ion modes.

Pharmacokinetics Analysis

UPLC/MS/MS calibration and quantitation data were processed with Xcalibur workstation (Thermo-Fisher Scientific Inc., Waltham, MA, United States). For the eight components with standard reference, calculating their concentrations from the standard curves. For the other 30 components without standard reference, their concentrations were analyzed following the regression equations of homologous compounds (Qiao et al., 2012): paeoniflorin for P1 and M1 to M3; methylgallate for M4 to M10; saikosaponin A for P9 and M11 to M17; saikosaponin C for M18 to M22; saikosaponin D for P12 and M23 to M24; saikosaponin B₂ for P11 and M25 to M26. For the PK studies, the maximum concentration (C_{\max}), time of maximum plasma concentration (t_{\max}), terminal elimination half-life ($t_{1/2}$), areas under the concentration-time curve (AUC_{0-t} and $\text{AUC}_{0-\infty}$) of each compound were analyzed by a non-compartmental analysis using Drug And Statistics Version 3.0 (DAS 3.0) software (Mathematical Pharmacology Committee, Chinese Pharmacological Society, China).

Analysis of Radix Bupleuri-Radix Paeoniae Alba Herb Pair-Induced Endogenous Metabolites Variations

The UPLC-HRMS raw data were imported to Compound Discoverer 3.0 (Thermo Fisher, United States) for matching and aligning peak data. The parameters were set as follows: mass tolerance, 5 ppm; RT tolerance, 0.05 min; S/N threshold, 10; intensity tolerance, 30%; assignment threshold, 60; mass range, 50–1000 Da. The peak area data of all metabolites obtained from Compound Discoverer 3.0 was normalized by IS (glycyrrhizin) in Microsoft Excel 2013.

To analyze the RB-RPA herb pair-induced endogenous metabolites variations, the acquired data at each time point from Compound Discoverer 3.0 (removal of 55 RB-RPA herb pair metabolites previously identified in rats plasma (Yin et al., 2019)) were imported into SIMCA-P software (version 16.0, Umetrics, Sweden) for multivariate statistical analysis, such as the principal components analysis (PCA), partial least-squares discriminant analysis (PLS-DA) and orthogonal partial least-squares discriminant analysis (OPLS-DA). The altered endogenous metabolites were screened according to the VIP-

value of S-plot ($VIP > 1$) and T-test ($p < 0.05$). The selected metabolites of LC-MS analysis were identified based on the molecular formula, accurate m/z values, MS/MS fragments, and online databases including KEGG (<http://www.kegg.jp>), m/z cloud (<https://www.mzcloud.org/>), PubChem (<https://pubchem.ncbi.nlm.nih.gov/>), HMDB (<http://www.hmdb.ca>), Lipid Maps (<http://www.lipidmaps.org>), and Massbank (<http://www.massbank.jp>). Meanwhile, based on the investigation of metabolomics and the semi-quantification, the mean value of each altered endogenous metabolite at each time point, representing the average response, was calculated to analyze the relationship of the dynamic response for endogenous metabolites along with the time course.

Correlation analysis of 38 Radix Bupleuri-Radix Paeoniae Alba Herb Pair Phytochemicals in Rat Plasma and Altered Endogenous Metabolites

Pearson correlation analysis was further applied to find the high linear relationship of phytochemicals and altered endogenous metabolites. To analyze the relationship of the dynamic response for endogenous metabolites along with the time course, the mean value of each endogenous metabolite was calculated at each time point (0 h \rightarrow 0.083 h \rightarrow 0.25 h \rightarrow 0.5 h \rightarrow 0.75 h \rightarrow 1 h \rightarrow 1.5 h \rightarrow 3 h \rightarrow 5 h \rightarrow 8 h \rightarrow 12 h \rightarrow 24 h). A new metabolite vector with 12 mean values calculated at 12 different time points, representing the average response was constructed. Pearson correlation analysis to study the correlation between two new metabolite vectors (representing RB-RPA herb pair phytochemicals and altered endogenous metabolites, respectively). The $|r| \geq 0.8$ and $p < 0.05$ represented that there was a high correlation between RB-RPA herb pair phytochemicals and altered endogenous metabolites.

Statistical Analyses

All data were expressed as the mean \pm standard deviation (SD). Data were statistically analyzed by SPSS 18.0 software (SPSS Inc., United States) and SIMCA-P 16.0 software (Umetrics, Sweden). PCA and PLS-DA were used to explore altered endogenous metabolites. Statistical analyses from two groups were analyzed using a two-tailed unpaired t-test, and statistical analyses from more groups were analyzed using one-way ANOVA. The $p < 0.05$ were considered statistically significant.

RESULT AND DISCUSSION

Comparison of the Content of Eight Compounds Between Single Extracts and a Mixture of Radix Bupleuri and Radix Paeoniae Alba Extracts

The content of eight compounds in single (RB or RPA) extracts and mixture of RB and RPA extracts were analyzed by UPLC-HRMS. The base peak chromatograms of herb extracts and mixed standards (saikosaponin A, saikosaponin D, saikosaponin C,

saikosaponin B₂, paeoniflorin, albiflorin, oxypaeoniflorin, methyl gallate, and the internal standard) were shown in **Supplementary Figure S1**. The content of the eight constituents in herb extracts was shown in **Supplementary Table S1**. The statistical results showed that the content of eight compounds had no statistical difference between single (RB or RPA) extracts and mixture extracts. These results suggested that mixing process of RB and RPA extracts didn't affect the content changed of each component in RB or RPA extracts. Previous studies have shown that co-decoction of RB and RPA *in vitro* can significantly increase the content of paeoniflorin and galloylpaeoniflorin in the RPA extract, and significantly reduce the content of saikosaponin A in the RB extract (He et al., 2018). Therefore, in order to avoid the content changes of prototype compounds caused by co-decocting *in vitro*, we used mixture of RB and RPA extracts to analyze the impact on pharmacokinetic parameters before and after the combination of RB and RPA.

Validation of the UPLC-MS/MS *in vivo* Analysis Method Specificity

The specificity was investigated by comparing extracted-ion chromatograms (XICs) of the blank plasma sample, spiked plasma sample, and a plasma sample after oral administration of RB, RPA, and RB-RPA. As shown in **Supplementary Figure S2**, there were no significant endogenous substances interference peak was observed.

Calibration Curve and LLOQ

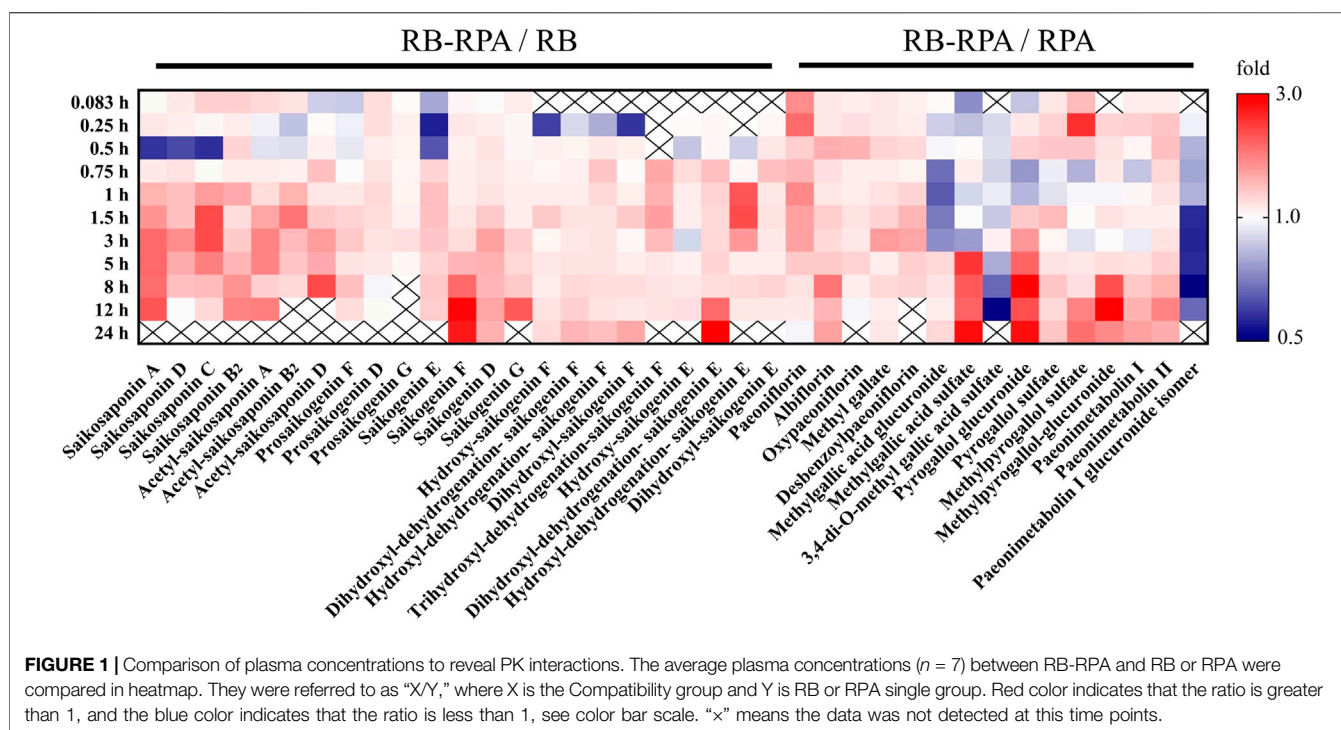
The calibration curves, linear ranges, correlation coefficients (r), and LLOQ of the eight analytes were represented in **Supplementary Table S2**. The coefficient of correlation (r^2) values greater than 0.995 and the LLOQs varied from 0.1–2.0 ng/ml for all analytes. This suggested that the calibration curves of these analytes showed good linearity within a certain concentration range in rat plasmas.

Matrix Effect and Extraction Recovery

The results of the matrix effect and extraction recoveries of the eight analytes were listed in **Supplementary Table S3**. The extraction recoveries of the eight analytes in rat plasmas at three different concentrations were in range of 81.32–106.83%, and the matrix effects of the analytes were in range of 79.61–111.53%, indicating that there was no significant ion suppression/enhancement in this bioanalytical method.

Precision and Accuracy

Precision and accuracy were evaluated by analyzing QC samples at three different concentrations (low, medium, and high) in six replicates on the same day (intra-day) and on three consecutive days (inter-day), respectively. As shown in **Supplementary Table S4**, the intra- and inter-day precisions values (RSD) ranged from 1.82 to 9.11% and from 2.21 to 11.48%, respectively, and the accuracy values (RE) ranged from –8.11 to 8.12%. The results suggest that this method is feasible.



Stability

The stability of the eight analytes during the sample processing and storage procedures was assessed by analyzing five replicates for QC samples at three different concentrations. The results were summarized in **Supplementary Table S5**, which showed that the eight analytes in plasma were all stable at room temperature for 24 h, at autosampler (4°C) for 24 h, three freeze-thaw cycles and 30 days storage at -20°C with values of RE (%) in the range -8.92 to 6.35%.

Pharmacokinetics

Determination of Plasma Concentration of 38 Compounds from “Plant Metabolome”

The validated UPLC-HRMS method was applied to simultaneously determine the plasma concentrations of 38 compounds after oral administration of RB-RPA herb pair in rats, including 12 prototype compounds and 26 metabolized products (**Table 1**). The peak areas of the 38 compounds were extracted from the extracted-ion chromatograms using a mass extraction window centered on the theoretical m/z , which was attributed to the high-resolution and high-throughput acquisition of HRMS. By comparing the plasma concentrations to reveal PK parameters of the 38 compounds before and after combination, we found that the combination of RB and RPA significantly changed the plasma concentrations of 38 compounds compared with the single herbal group (**Figure 1**).

Comparison of Pharmacokinetics of 23 Compounds from RB Before and After Compatibility

The time-concentration curves of 23 compounds from RB before and after combination were shown in **Figure 2**. Furthermore, to clearly observe differences among the 23 compounds from RB before and after combination, the main PK parameters were

calculated using a non-compartment model in DAS 3.0 software, and the results were listed in **Supplementary Table S6**. By comparing the PK parameters (C_{\max} , t_{\max} , $t_{1/2}$, and $AUC_{0-\infty}$) of 23 compounds between the RB-RPA group and the RB groups, the results showed that the combination of RB and RPA could impact the pharmacokinetic behaviors of 23 compounds from RB (**Figure 3**). For saikosaponin A and saikosaponin D, the PK profile of administration of RB alone was similar to a previous report (Xu et al., 2012). When saikosaponin A and saikosaponin D were administered in RB-RPA herbs, the C_{\max} of saikosaponin A and saikosaponin D were decreased remarkably: from 68.37 ± 16.95 to 46.47 ± 12.41 , and from 42.84 ± 11.53 to 26.57 ± 6.99 ng mL^{-1} , respectively (**Figure 3C**, **Supplementary Table S6**). In contrast, the $t_{1/2}$ of saikosaponin A and saikosaponin D were longer in the RB-RPA group than the single herbal group, which indicated that combination can extend the residence time of saikosaponin A and saikosaponin D in system circulation (**Figure 3B**). As a result, the $AUC_{0-\infty}$ of saikosaponin A was significantly improved from 103.55 ± 38.59 to 175.55 ± 45.92 $\text{ng mL}^{-1} \text{h}$ after combination (in RB-RBA group), and the $AUC_{0-\infty}$ of saikosaponin D was improved from 69.92 ± 17.38 to 103.56 ± 33.67 $\text{ng mL}^{-1} \text{h}$ (**Figure 3D**). Besides, as for acetyl-saikosaponin D, prosaikogenin F, prosaikogenin G, and dihydroxyl-dehydrogenation-saikogenin E, the $t_{1/2}$ of these compounds were significantly increased after combination, which indicated that combination can extend the residence time of these compounds in system circulation (**Figure 3B**). As a result, the $AUC_{0-\infty}$ of prosaikogenin F, prosaikogenin G, and dihydroxyl-dehydrogenation-saikogenin E were significantly increased after combination (**Figure 3D**). As for saikosaponin b₂, when saikosaponin b₂ were administered in RB-RPA herbs, the C_{\max} increased remarkably: 22.33 ± 2.99 to 28.19 ± 5.50 ng mL^{-1} ,

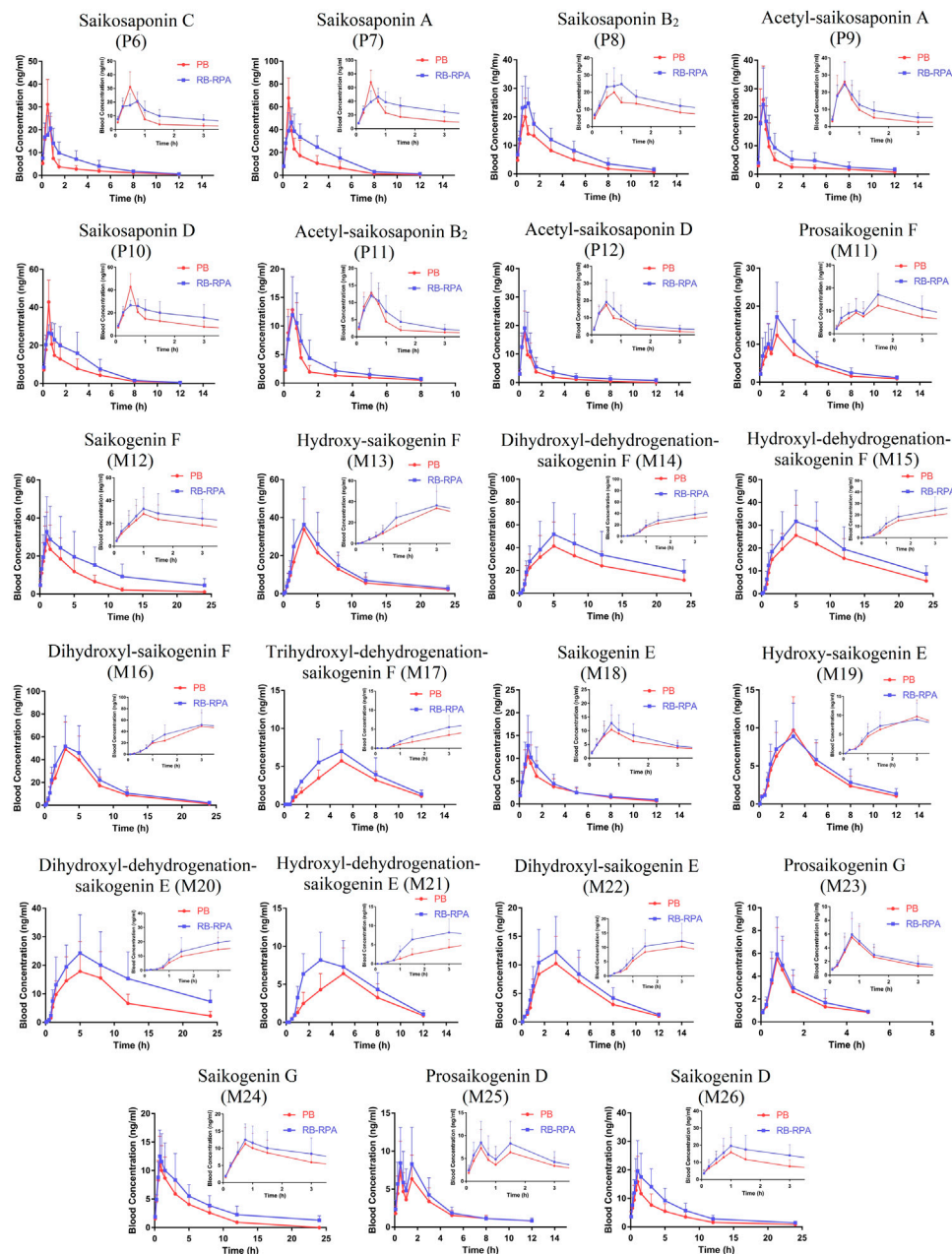
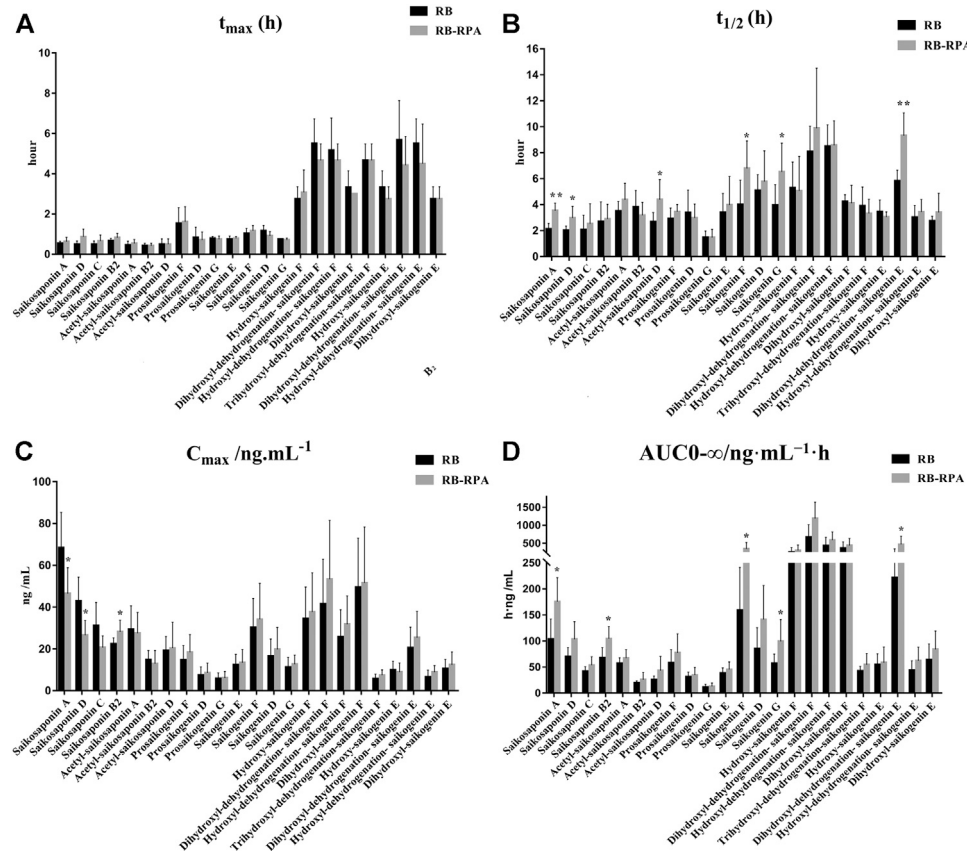


FIGURE 2 | Plasma concentration-time profiles (mean \pm SD, $n = 7$) of 23 compounds from RB after oral administration of the RB (single extract) and RB-RPA (RB and RPA compatibility). The compounds represented by the numbers in the figure are consistent with the compounds represented by the numbers in **Table 1**.

which indicated that combination can promote the absorption of saikosaponin b_2 . As a result, the $AUC_{0-\infty}$ of saikosaponin b_2 was significantly increased after the combination. However, there was no significant effect on the t_{max} of 23 compounds from RB before and after combination (**Figure 3A**). These results indicated that the combination of RB and RPA played a critical role in improving the bioavailability of five components (saikosaponin A, saikosaponin B_2 , prosaikogenin F, prosaikogenin G, dihydroxyl-dehydrogenation-saikogenin E) in RB.

Comparison of Pharmacokinetics of 15 Compounds from RPA Before and After Combination

The time-concentration curves of 15 compounds from RPA before and after combination were shown in **Figure 4**, and the main PK parameters (C_{max} , t_{max} , $t_{1/2}$, and $AUC_{0-\infty}$) were listed in **Supplementary Table S7**. It was clearly observed that the PK parameters of the combination group were remarkably different from those in RPA group (**Figure 5**). Specifically, the PK profile of administration of RPA alone was similar to the previous report



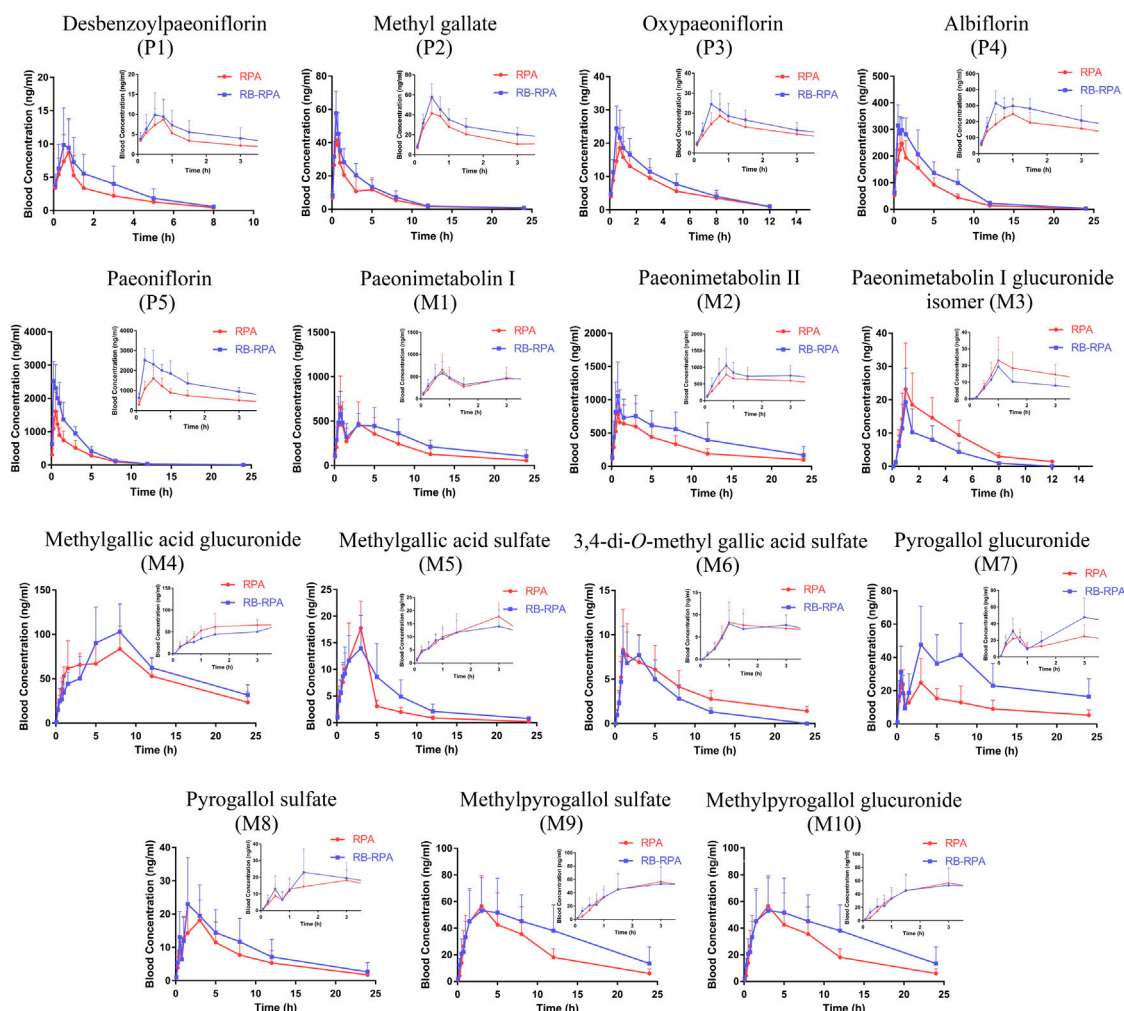


FIGURE 4 | Plasma concentration-time profiles (mean \pm SD, $n = 7$) of 15 compounds from RPA after oral administration of the RPA (single extract) and RB-RPA (RB and RPA compatibility). The compounds represented by the numbers in the figure are consistent with the compounds represented by the numbers in **Table 1**.

are shown in **Supplementary Figure S3**. The metabolomics data acquired from Compound Discoverer 3.0 was imported into SIMCA-P V16.0 for multivariate statistical analysis. The principal component analysis (PCA) was conducted to investigate the trends of endogenous metabolite profiles at different time points after RB-RPA administration. The dynamic response profiles of endogenous metabolites intervened by RB-RPA based on PCA score plots were shown in **Figure 6A**, and a time-dependent trajectory of endogenous metabolite profiles was shown in **Figure 6B**. In **Figure 6A**, each spot represents a plasma sample, and each assembly of samples indicated a specific metabolic profile at different time points. From **Figure 6B**, endogenous metabolite profiles at different time points after administration were clearly separated from those at the time-point 0 before the RB-RPA intake. The time-dependent trajectory showed that endogenous metabolic profiles underwent a significant change from 0 to 24 h, which may be related to changes in plasma concentrations of RB-RPA components. Furthermore, the endogenous metabolite profiles

at 24 h were closed to the pre-dose metabolite profiles, indicating that the metabolic profiles of the subjects showed a recovery trend. Simultaneously, the relative distance calculation between post-dose all time points metabolite profiles and pre-dose metabolite profile from PCA score plot with the average value (x-axis and y-axis) of all samples, to quantify all time points contributions after administration, according to the method described in the literature (Duan et al., 2016), and the results were listed in **Supplementary Table S8**. As shown in **Supplementary Table S8**, different relative distance calculation at different time points after administration, indicating that the ability to regulate endogenous metabolic profiles was different, and above all, 3 h after RB-RPA administration displayed the greatest ability to regulate endogenous metabolites as it showed the longest distance calculation. Accordingly, the altered endogenous metabolites associated with RB-RPA were selected by comparing VIP values (VIP > 1) and T-test ($p < 0.05$) between the metabolites at time-point 3 h after the RB-RPA intake (3 h group) and the

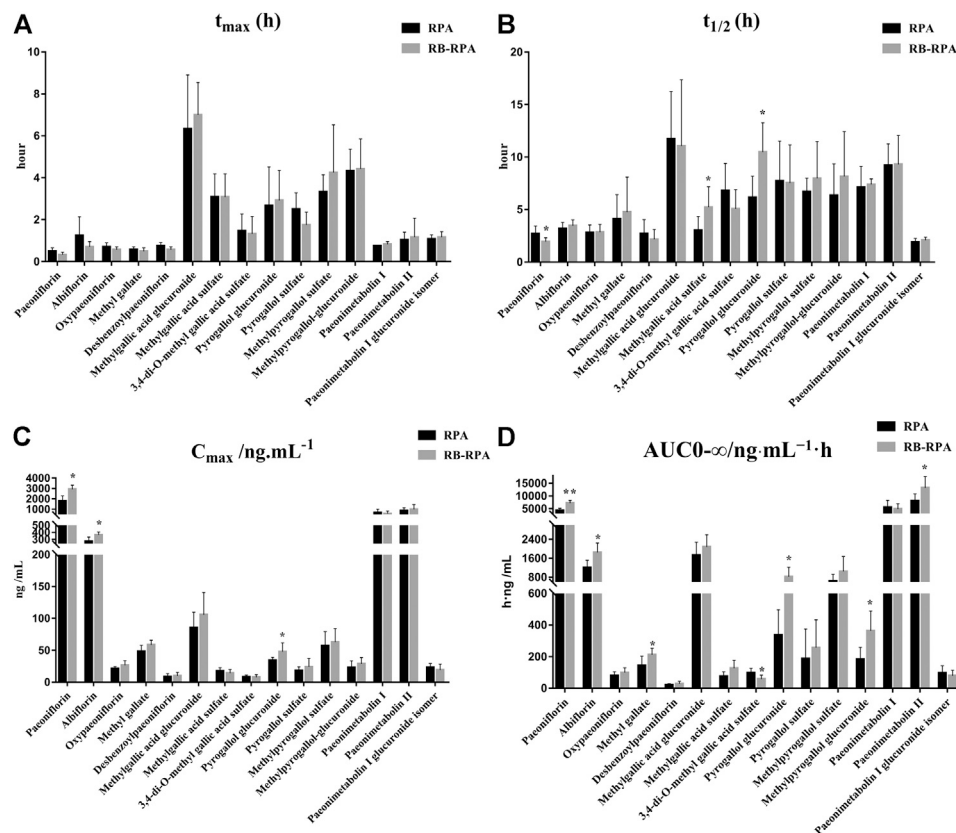


FIGURE 5 | Main pharmacokinetic parameters of 15 compounds from RPA in rat plasma after oral administration of the single extract group (RPA) and the compatibility group (RB-RPA). (A) t_{\max} (h); (B) $t_{1/2}$ (h); (C) C_{\max} (ng mL⁻¹); (D) $AUC_{0-\infty}$ (ng mL⁻¹ h). All data were expressed as mean \pm SD, ($n = 7$). * $p < 0.05$, ** $p < 0.01$ compared with RPA group.

metabolites at time-point 0 h before the RB-RPA intake (0 h group) based on multivariate statistical analysis.

Screening and Identification of Endogenous Differential Metabolites Regulated by Radix Bupleuri-Radix Paeoniae Alba

As mentioned above, the endogenous differential metabolites regulated by RB-RPA were selected by comparing the different variables between the 3 h group and the 0 h group based on multivariate statistical analyses. As shown in **Figures 6C–F**, The PCA score plots indicated that the 3 h group could be obviously separated from the 0 h group (**Figure 6C**). This finding indicated that 3 h after the RB-RPA intake significantly altered the metabolic fingerprints of plasma compared with the 0 h group. Using the permutation plot test of the PLS-DA model to check the predictive ability and overfitting of the multivariate statistical analysis model (**Figure 6D**). The permutation test parameters of R^2X , R^2Y , and Q^2 were 0.436, 0.948, and 0.911, respectively. These results showed that the multivariate statistical analysis model had excellent predictive power and had not overfitted. To further enhance the ability of differential metabolite discovery between the 3 h group and 0 h group, the OPLS-DA model was used. The OPLS-DA score plots showed that obvious separation has occurred between the 3 h

group and the 0 h group (**Figure 6E**). The differential metabolites between the 3 h group and the 0 h group were screened by S-plots and VIP values in the OPLS-DA model (**Figure 6F**), and VIP >1.0 with $p < 0.05$ were considered. Besides, the selected differential metabolites were identified based on the molecular formula, accurate m/z values, MS/MS fragments, and online databases. At last, a total of 21 endogenous differential metabolites were screened and identified (**Table 2**). Compared with the 0 h, 12 endogenous differential metabolites (DL-ornithine, DL-histidine, choline, gamma-aminobutyric acid, L-glutamic acid, valine, alpha-ketoglutaric acid, L(-)-asparagine, itaconic acid, picolinic acid, N-acetyl-L-leucine, α -linolenic acid) were significantly increased, and 9 [DL-glutamine, citric acid, L-tyrosine, DL-tryptophan, L-glutathione oxidized, thymidine 5'-monophosphate, taurochenodeoxycholic acid, lysoPC (18:3), cholic acid] were significantly decreased in 3 h group.

Based on the investigation of metabolomics and the semi-quantification, the relative peak areas of endogenous differential metabolites were calculated at various time points before and after administration. The detailed data was listed in **Supplementary Table S9**. Furthermore, Metabonomic response profiles response to RB-RPA intervention at various time points after administration were depicted as a heat map

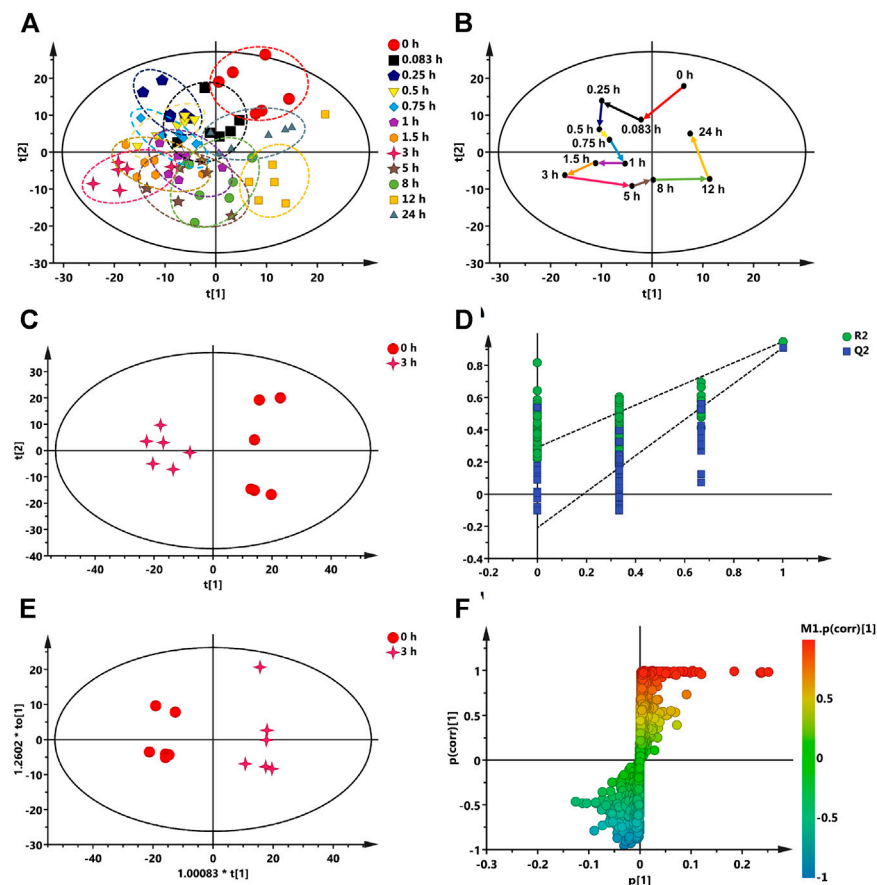


FIGURE 6 | Multivariate data analysis from UPLC-MS/MS. **(A)** The dynamic response profiles of endogenous metabolites intervened by RB-RPA based on PCA score plots. **(B)** A time-dependent trajectory of endogenous metabolite profiles at different time points after RB-RPA intake. **(C)** PCA score plots from 3 h group and 0 h group. **(D)** PLS-DA model validation diagram. **(E)** OPLS-DA score plots from 3 h group and 0 h group. **(F)** S-plot of OPLS-DA.

(Figure 7). In heat map, each cell represents the fold change between the two time points for a particular endogenous differential metabolite. These results indicated that 21 endogenous differential metabolites exhibited varying degrees of dynamic changes after RB-RPA administration.

The Potential Link Between Radix Bupleuri-Radix Paeoniae Alba Phytochemicals and the Altered Endogenous Metabolites

The correlation between the RB-RPA concentration-time curves of 38 components and the dynamic response profile of altered 21 endogenous metabolites was presented in Figure 8, with positive (red color) and negative (blue color) ($p < 0.05$, $|r| > 0.8$) values. Correlation analysis demonstrated that RB-RPA herb pair phytochemicals had an impact on endogenous metabolites. In general, the change of the plasma concentration of endogenous metabolites in response to the alteration of the bioavailability of RB-RPA phytochemicals. As shown in Figure 8, most of RB-RPA phytochemicals were positively correlated with DL-ornithine, gamma-aminobutyric acid, valine, alpha-ketoglutaric acid,

itaconic acid, picolinic acid, α -linolenic acid, and were negatively correlated with L-glutathione oxidized and cholic acid.

Besides, to investigate the effects of the combination of RB and RPA on endogenous metabolites, the correlation between the phytochemicals improved bioavailability after combination and endogenous metabolites was summarized. As shown in Figure 9, the components for bioavailability significantly improved after combination such as saikogenin F, saikogenin G, albiflorin, methyl gallate, paeonimetalbin II were significantly positively correlated with picolinic acid; saikogenin F, saikogenin G were significantly positively correlated with itaconic acid; albiflorin, paeonimetalbin II were significantly positively correlated with α -linolenic acid; saikogenin G, albiflorin, methyl gallate were significantly negatively correlated with L-glutathione oxidized; saikogenin F was significantly positively correlated with alpha-ketoglutaric acid and was significantly negatively correlated with cholic acid. It was worth noting that picolinic acid and α -linolenic acid were endogenous metabolites with a strong neuroprotective effect, and itaconic acid was endogenous metabolites with anti-inflammatory activity. These results indicated that the combination of RB and RPA can enhance each other's neuroprotective and anti-inflammatory activities.

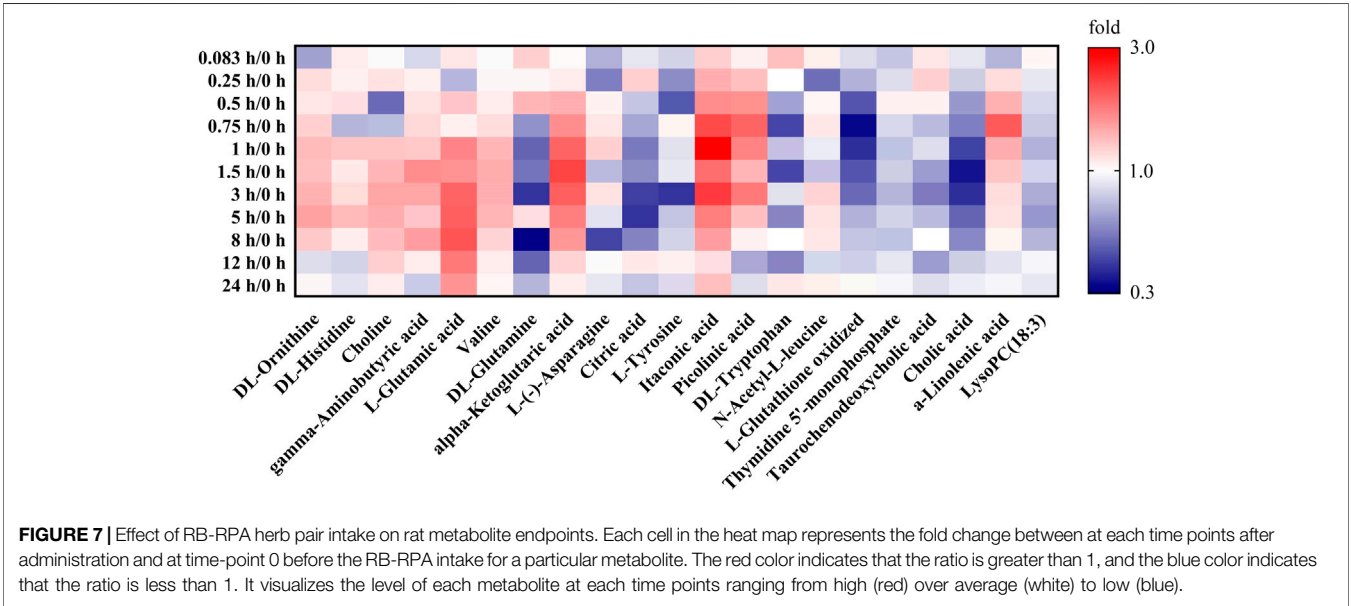
TABLE 2 | Altered endogenous metabolites were detected by UPLC-MS/MS.

No.	Metabolites	T _R (min)	m/z	Formula	VIP	HMDB ID	3 h/0 h	Ion mode
1	DL-Ornithine	0.706	133.09723	C ₅ H ₁₂ N ₂ O ₂	1.32	32455	↑*	[M + H] ⁺
2	DL-Histidine	0.736	156.07683	C ₆ H ₉ N ₃ O ₂	1.04	00177	↑*	[M + H] ⁺
3	Choline	0.820	104.10671	C ₅ H ₁₃ NO	1.74	00097	↑**	[M + H] ⁺
4	Gamma-Aminobutyric acid	0.856	104.07063	C ₄ H ₉ NO ₂	1.63	00112	↑***	[M + H] ⁺
5	L-Glutamic acid ^a	0.860	146.04568	C ₅ H ₉ NO ₄	2.13	00148	↑***	[M-H] ⁻
6	Valine	0.899	118.08636	C ₅ H ₁₁ NO ₂	1.62	00883	↑**	[M + H] ⁺
7	DL-Glutamine	0.908	145.06167	C ₅ H ₁₀ N ₂ O ₃	2.48	00641	↓***	[M-H] ⁻
8	Alpha-ketoglutaric acid	0.931	145.01433	C ₅ H ₆ O ₅	2.32	00208	↑***	[M-H] ⁻
9	L-(-)-Asparagine	0.941	115.05036	C ₄ H ₈ N ₂ O ₃	1.03	00168	↑*	[M-H ₂ O + H] ⁺
10	Citric acid	0.983	191.01963	C ₆ H ₈ O ₇	2.07	00094	↓***	[M-H] ⁻
11	L-Tyrosine ^a	1.032	182.08116	C ₉ H ₉ NO ₃	2.18	00158	↓***	[M + H] ⁺
12	Itaconic acid	1.062	259.04666	C ₅ H ₆ O ₄	2.52	02092	↑***	[2M-H] ⁻
13	Picolinic acid ^a	1.902	124.03942	C ₆ H ₅ NO ₂	1.96	02243	↑**	[M + H] ⁺
14	DL-Tryptophan	3.412	205.09694	C ₁₁ H ₁₂ N ₂ O ₂	1.51	13609	↓*	[M + H] ⁺
15	N-Acetyl-L-leucine	7.195	172.09740	C ₈ H ₁₅ NO ₃	1.72	11756	↑**	[M-H] ⁻
16	L-Glutathione oxidized	7.830	613.15913	C ₂₀ H ₃₂ N ₆ O ₁₂ S ₂	1.76	03337	↓**	[M + H] ⁺
17	Thymidine 5'-monophosphate	11.572	321.04513	C ₁₅ H ₁₆ O ₄ P ₂	1.05	01227	↓*	[M-H] ⁻
18	Taurochenodeoxycholic acid	12.272	498.28967	C ₂₆ H ₄₅ NO ₆ S	1.33	00951	↓*	[M-H] ⁻
19	Cholic acid	14.329	407.28021	C ₂₄ H ₄₀ O ₅	2.43	00619	↓***	[M-H] ⁻
20	α-Linolenic acid	15.936	279.23164	C ₁₈ H ₃₀ O ₂	1.11	01388	↑*	[M + H] ⁺
21	LysoPC (18:3)	17.149	518.32404	C ₂₆ H ₄₈ NO ₇ P	1.04	10387	↓*	[M + H] ⁺

“↓” or “↑” means the metabolite significantly decreased or increased in 3 h group compared with 0 h group.

*p < 0.05, **p < 0.01, ***p < 0.001 compared with 0 h group.

^aValidated with standard.



Picolinic Acid

Picolinic acid is an end-product of the kynurenine pathway with a strong neuroprotective effect (Lovelace et al., 2017). Recent research has indicated that picolinic acid showed antidepressant effects by decreasing the immobile time of forced swim test and reversing the significant rise in plasma corticosterone level in CUMS-induced depression rats (Dubey et al., 2015). Furthermore, as well as clinically, decreased plasma picolinic acid levels have been demonstrated in depressed patients (Ryan

et al., 2020), and picolinic acid has also been shown to produce significant antidepressant effects in a typical depression (Davidson et al., 2003). Our study demonstrated that the five phytochemicals with improved bioavailability after combination (saikogenin F, saikogenin G, albiflorin, methyl gallate, paeonimetabolin II) were significantly positively correlated with picolinic acid, a metabolite that was significantly downregulated in depressed patients (Colle et al., 2020). Besides, chronic stress can cause imbalances in the kynurenine metabolic pathway and excessively produce the

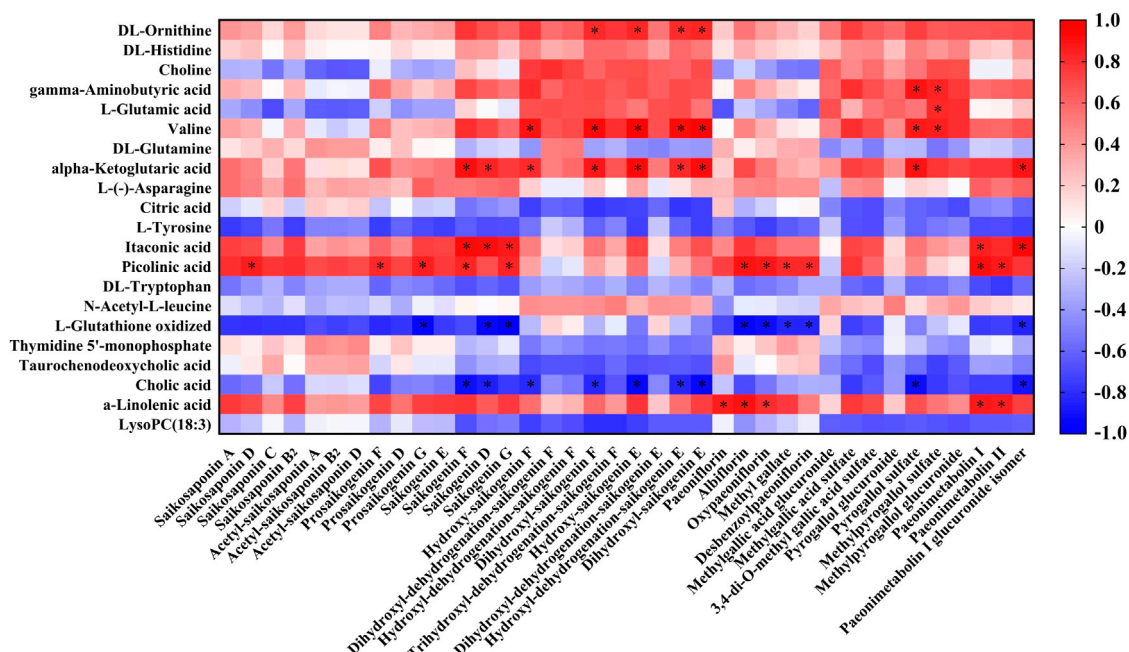


FIGURE 8 | Correlation analysis between the 38 RB-RPA herb pair phytochemicals and the altered 21 endogenous metabolites according to Pearson correlation coefficient. Red color indicated that $|r|$ was a positive value and blue indicated that $|r|$ was a negative value. The darker the color, the larger the $|r|$ value. * represents $p < 0.05$ and $|r| > 0.8$.

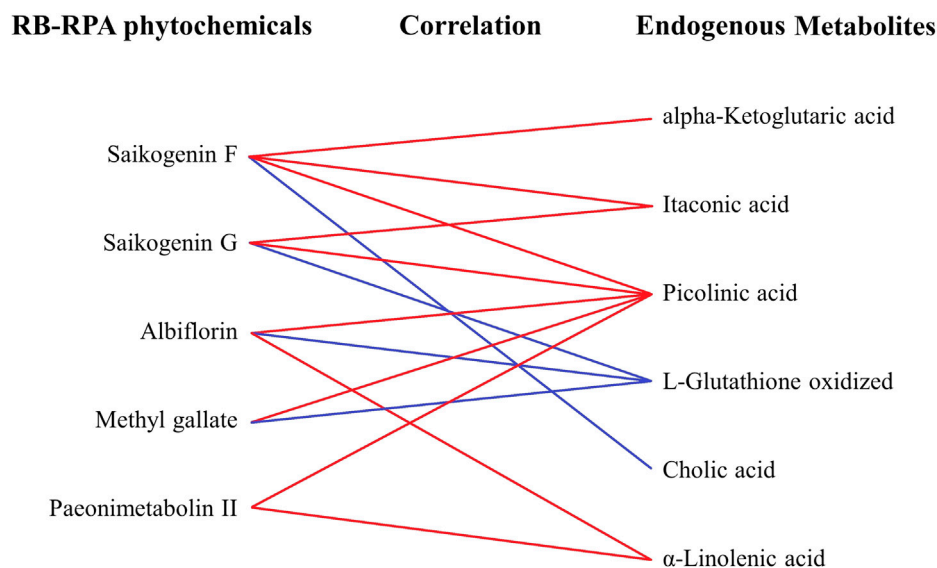


FIGURE 9 | The correlation between the phytochemicals improved bioavailability after compatibility and the altered endogenous metabolites. The relationships among the phytochemicals and endogenous metabolites were visualized in the form of correlation maps, which are displayed by red (positive) or blue (negative) lines.

neurotoxic product quinolinic acid, thereby promoting the occurrence of depressive behavior (Won and Kim., 2016). It was worth noting that as a neuroprotective product, picolinic acid has also been shown to antagonize the adverse effects of quinolinic acid on the nervous system to prevent depression and anxiety symptoms (Grant et al., 2009). These results indicated that these five phytochemicals can inhibit the neurotoxic effects of quinolinic

acid and maintain the balance of the kynurenine metabolic pathway by acting with picolinic acid, thereby avoiding the occurrence of depressive behavior. Besides, several studies have shown that RB, RPA, and their main active ingredients (such as saikosaponins, albiflorin, methyl gallate, etc.) have significant neuroprotective and antidepressant activity (Wang et al., 2016; Li et al., 2017; Li et al., 2018). Therefore, we speculated that the

combination of RB and RPA by increasing the bioavailability of these five phytochemicals, the impact on picolinic acid was strengthened to enhance each other's neuroprotective.

Itaconic Acid

Itaconic acid is a crucial anti-inflammatory endogenous metabolite, which was produced by the decarboxylation of *cis*-aconitate, a tricarboxylic acid cycle intermediate (Michelucci et al., 2013), previous studies have found that itaconate exerts anti-inflammatory effects by inhibiting succinate dehydrogenase (Bordon, 2018). Additionally, recent studies have confirmed that itaconic acid was required for the activation of the anti-inflammatory transcription factor Nrf2 by lipopolysaccharide in macrophages, enabling Nrf2 to increase the expression of downstream genes with anti-oxidant and anti-inflammatory capacities (Mills et al., 2018). Further, RB has also been proven to exert anti-inflammatory effects by regulating the Nrf2 signaling pathway (Jia et al., 2019). Our study suggests that the two phytochemicals with improved bioavailability after RB and RPA combination (saikogenin F, saikogenin G) were significantly positively correlated with itaconic acid. The saikogenin F, saikogenin G were deglycosylated metabolites of saikosaponin A and saikosaponin D transformed by intestinal bacteria in the gastrointestinal tract (Shimizu et al., 1985). In addition, related studies speculated that saikosaponins, the main component of RB, was transformed into saikogenins by human intestinal flora, and then exerts pharmacological activity (Liu et al., 2019). These research results indicated that compared to saikosaponin A and saikosaponin D, the pharmacological activity of saikogenin F and saikogenin G in the body may be more significant. And the saikogenin F and saikogenin G maybe activate the Nrf2 signaling pathway by acting on itaconic acid, thereby exerting an anti-inflammatory effect. Meanwhile, saikogenins have also been reported to have anti-inflammatory pharmacological activity (Cheng and Tsai, 1986; Toriniwa et al., 2006), which is in accordance with our research. we speculated that the combination of RB and RRA can enhance the anti-inflammatory effect of saikogenin F and saikogenin G.

α -linolenic Acid

The α -linolenic acid is a polyunsaturated omega-3 fatty acid whose metabolism in the body has been well characterized. When α -linolenic acid was ingested, the body converts it to long-chain polyunsaturated fatty acids: eicosapentaenoic acid and docosahexaenoic acid, both of which were considered to exert strong actions on brain functions (Connor, 1999). BDNF is a neurotrophin, it's known for its effects on promoting neurogenesis and neuronal survival, which is significantly associated with depression (Oh et al., 2019). Studies have found that oral consumption of α -linolenic acid increases serum BDNF levels in healthy adults, which may be due to the neuroprotective impact of eicosapentaenoic acid and docosahexaenoic acid on the nervous system (Hadjighassem et al., 2015). Besides, chronic dietary α -linolenic acid deficiency alters dopaminergic and serotonergic neurotransmission (Delion et al., 1994), which finally accelerates the development of depression. The albiflorin and

paeonimetabolin II were the prototype components and metabolites in RPA, respectively. Our study suggests that the two phytochemicals with improved bioavailability after RB and RPA combination (albiflorin, paeonimetabolin II) were significantly positively correlated with α -linolenic acid. It has been reported that albiflorin, the main active component of RPA, can be used as inhibitors of D-amino acid oxidase in the brain, improved brain function and exerted antidepressant activity (Zhao et al., 2018). In addition, this experiment also found that the combination of RB and RPA can enhance the regulation of α -linolenic acid to enhance the antidepressant activity of RPA. However, it was not clear how RPA and albiflorin can improve brain function and exert antidepressant activity by regulating α -linolenic acid.

CONCLUSION

In conclusion, RB and RPA compatibility could significantly improve the bioavailability of five components in RB, and improve the bioavailability of six components in RPA, which could be summarized into two aspects: improvement in the plasma concentration (C_{max}) and prolongation in system circulation ($t_{1/2}$). Furthermore, "plant metabolome" and "body metabolome" correlation analysis results indicated that compatibility of RB and RPA can enhance each other's neuroprotective and anti-inflammatory activities, which provided a research basis for further research on the synergistic pharmacological mechanism of the compatibility of RB and RPA.

DATA AVAILABILITY STATEMENT

The original contributions presented in the study are included in the article/**Supplementary Material**, further inquiries can be directed to the corresponding author.

ETHICS STATEMENT

The animal study was reviewed and approved by the Experimental Animal Ethical Committee of Modern Research Center for Traditional Chinese Medicine, Shanxi University.

AUTHOR CONTRIBUTIONS

YZ, XQ, and GD conceived and designed the experiments; CC and QY performed the experiments; CC drafted the manuscript; JT, XG, and XQ reviewed the paper.

FUNDING

This study is funded by the National Nature Science Foundation of China (No. 81673572, 82074323). The major science and

technology project for “Significant New Drugs Creation” (No. 2017ZX09301047). Research Project Supported by Shanxi Scholarship Council of China (No. 2020019). Fund Program for the Scientific Activities of Selected Returned Overseas Professionals in Shanxi Province (No. 201991).

REFERENCES

- Ashour, M. L., and Wink, M. (2011). Genus *Bupleurum*: a review of its phytochemistry, pharmacology and modes of action. *J. Pharm. Pharmacol.* 63, 305–321. doi:10.1111/j.2042-7158.2010.01170.x
- Bordon, Y. (2018). Itaconate charges down inflammation. *Nat. Rev. Immunol.* 18, 360–361. doi:10.1038/s41577-018-0016-4
- Chen, C. C., Yin, Q. C., Tian, J. S., Gao, X. X., Qin, X. M., Du, G. H., et al. (2020). Studies on the potential link between antidepressant effect of Xiaoyao San and its pharmacological activity of hepatoprotection based on multi-platform metabolomics. *J. Ethnopharmacol.* 249, 112432. doi:10.1016/j.jep.2019.112432
- Chen, Y., Wang, J. Y., Yuan, L., Zhou, L., Jia, X. B., and Tan, X. B. (2011). Interaction of the main components from the traditional Chinese drug pair Chaihu-Shaoyao based on rat intestinal absorption. *Molecules* 16, 9600–9610. doi:10.3390/molecules16119600
- Cheng, J. T., and Tsai, C. L. (1986). Anti-inflammatory effect of saikogenin A. *Biochem. Pharmacol.* 35, 2483–2487. doi:10.1016/0006-2952(86)90043-2
- Colle, R., Masson, P., Verstuyft, C., Fève, B., Werner, E., Boursier-Neyret, C., et al. (2020). Peripheral tryptophan, serotonin, kynurenine, and their metabolites in major depression: a case-control study. *Psychiatry Clin. Neurosci.* 74, 112–117. doi:10.1111/pcn.12944
- Connor, W. E. (1999). Alpha-linolenic acid in health and disease. *Am. J. Clin. Nutr.* 69, 827–828. doi:10.1093/ajcn/69.5.827
- Davidson, J. R., Abraham, K., Connor, K. M., and McLeod, M. N. (2003). Effectiveness of chromium in atypical depression: a placebo-controlled trial. *Biol. Psychiatry* 53, 261–264. doi:10.1016/s0006-3223(02)01500-7
- Delion, S., Chalou, S., Héroult, J., Guilloteau, D., Besnard, J. C., and Durand, G. (1994). Chronic dietary alpha-linolenic acid deficiency alters dopaminergic and serotonergic neurotransmission in rats. *J. Nutr.* 124, 2466–2476. doi:10.1093/jn/124.12.466
- Duan, Y., Pei, K., Cai, H., Tu, S. C., Cheng, X. W., Zhang, Z. W., et al. (2016). Strategy of integrated evaluation on treatment of traditional Chinese medicine as “interaction of system to system” and establishment of novel fuzzy target contribution recognition with herb-pairs, a case study on Astragali Radix-Fructus Corni. *Mol. Cel Endocrinol* 434, 219–237. doi:10.1016/j.mce.2016.07.006
- Dubey, V. K., Ansari, F., Vohora, D., and Khanam, R. (2015). Possible involvement of corticosterone and serotonin in antidepressant and anti-anxiety effects of chromium picolinate in chronic unpredictable mild stress induced depression and anxiety in rats. *J. Trace Elem. Med. Biol.* 29, 222–226. doi:10.1016/j.jtemb.2014.06.014
- Gong, C., Yang, H., Wei, H., Qi, C., and Wang, C. H. (2015). Pharmacokinetic comparisons by UPLC-MS/MS of isomer paeoniflorin and albizflorin after oral administration decoctions of single-herb Radix Paeoniae Alba and Zengmian Yiliu prescription to rats. *Biomed. Chromatogr.* 29, 416–424. doi:10.1002/bmc.3292
- Grant, R. S., Coggan, S. E., and Smythe, G. A. (2009). The physiological action of picolinic acid in the human brain. *Int. J. Tryptophan Res.* 2, 71–79. doi:10.4137/ijtr.s2469
- Hadjighassem, M., Kamalidehghan, B., Shekarriz, N., Baseerat, A., Molavi, N., Mehrpour, M., et al. (2015). Oral consumption of α -linolenic acid increases serum BDNF levels in healthy adult humans. *Nutr. J.* 14, 20. doi:10.1186/s12937-015-0012-5
- He, J., Gao, X. X., Tian, J. S., Qin, X. M., Du, G. H., and Zhou, Y. Z. (2018). Changes of chemical composition of *Bupleuri Radix*-*Paeoniae Radix Alba* herb pair before and after compatibility by UPLC-MS background subtraction and metabolomics. *Chin. Tradit Herb Drugs* 49, 1779–1788. doi:10.7501/j.issn.0253-2670.2018.08.007
- Jia, R., Gu, Z. Y., He, Q., Du, J. L., Cao, L. P., Jeney, G., et al. (2019). Anti-oxidative, anti-inflammatory and hepatoprotective effects of Radix Bupleuri extract against oxidative damage in tilapia (*Oreochromis niloticus*) via Nrf2 and TLRs signaling pathway. *Fish. Shellfish Immunol.* 93, 395–405. doi:10.1016/j.fsi.2019.07.080
- Li, H. Y., Zhao, Y. H., Zeng, M. J., Fang, F., Li, M., Qin, T. T., et al. (2017). Saikosaponin D relieves unpredictable chronic mild stress induced depressive-like behavior in rats: involvement of HPA axis and hippocampal neurogenesis. *Psychopharmacology* 234, 3385–3394. doi:10.1007/s00213-017-4720-8
- Li, S. J., Chu, Y. J., Zhang, R. W., Sun, L. J., and Chen, X. H. (2018). Prophylactic neuroprotection of total glucosides of *Paeoniae Radix Alba* against semen strychni-induced neurotoxicity in rats: suppressing oxidative stress and reducing the absorption of toxic components. *Nutrients* 10, 514. doi:10.3390/nu10040514
- Li, X., Qin, X. M., Tian, J. S., Gao, X. X., Du, G. H., and Zhou, Y. Z. (2021). Integrated network pharmacology and metabolomics to dissect the combination mechanisms of *Bupleurum chinense* DC-*Paeonia lactiflora* Pall herb pair for treating depression. *J. Ethnopharmacol.* 264, 113281. doi:10.1016/j.jep.2020.113281
- Liu, J. J., Xue, Y. W., Sun, J. B., Fu, R. J., Ren, S. Q., Zhang, Z. J., et al. (2019). Pharmacokinetics and oral bioavailability studies of three saikogenins in rats using a validated UFLC-MS/MS method. *J. Chromatogr. B Analyt. Technol. Biomed. Life Sci.* 1124, 265–272. doi:10.1016/j.jchromb.2019.06.020
- Lovelace, M. D., Varney, B., Sundaram, G., Lennon, M. J., Lim, C. K., Jacobs, K., et al. (2017). Recent evidence for an expanded role of the kynurenine pathway of tryptophan metabolism in neurological diseases. *Neuropharmacology* 112, 373–388. doi:10.1016/j.neuropharm.2016.03.024
- Michelucci, A., Cordes, T., Ghelfi, J., Pailot, A., Reiling, N., Goldmann, O., et al. (2013). Immune-responsive gene 1 protein links metabolism to immunity by catalyzing itaconic acid production. *Proc. Natl. Acad. Sci. U S A.* 110, 7820–7825. doi:10.1073/pnas.1218599110
- Mills, E. L., Ryan, D. G., Prag, H. A., Dikovskaya, D., Menon, D., Zaslon, Z., et al. (2018). Itaconate is an anti-inflammatory metabolite that activates Nrf2 via alkylation of KEAP1. *Nature* 556, 113–117. doi:10.1038/nature25986
- Oh, H., Piantadosi, S. C., Rocco, B. R., Lewis, D. A., Watkins, S. C., and Sibille, E. (2019). The role of dendritic brain-derived neurotrophic factor transcripts on altered inhibitory circuitry in depression. *Biol. Psychiatry* 85, 517–526. doi:10.1016/j.biopsych.2018.09.026
- Qiao, X., Ye, M., Xiang, C., Wang, Q., Liu, C. F., Miao, W. J., et al. (2012). Analytical strategy to reveal the *in vivo* process of multi-component herbal medicine: a pharmacokinetic study of licorice using liquid chromatography coupled with triple quadrupole mass spectrometry. *J. Chromatogr. A.* 1258, 84–93. doi:10.1016/j.chroma.2012.08.041
- Qiu, F. M., Zhong, X. M., Mao, Q. Q., and Zhen, H. (2013). Antidepressant-like effects of paeoniflorin on the behavioural, biochemical, and neurochemical patterns of rats exposed to chronic unpredictable stress. *Neurosci. Lett.* 541, 209–213. doi:10.1016/j.neulet.2013.02.029
- Ryan, K. M., Allers, K. A., McLoughlin, D. M., and Harkin, A. (2020). Tryptophan metabolite concentrations in depressed patients before and after electroconvulsive therapy. *Brain Behav. Immun.* 83, 153–162. doi:10.1016/j.bbi.2019.10.005
- Shimizu, K., Amagaya, S., and Ogihara, Y. (1985). Structural transformation of saikosaponins by gastric juice and intestinal flora. *J. Pharmacobiodyn.* 8, 718–725. doi:10.1248/bpb1978.8.718
- Tian, W., Zhen, Y. Q., Cao, W. L., Zhen, Z. N., and Niu, L. Y. (2016). Simultaneous determination of saikosaponin a, b₁, b₂ and c in radix Bupleuri formula granules by HPLC-MS/MS. *Chin. Pharm. J.* 51, 2068–2071. doi:10.11669/cpj.2016.23.019
- Toriniwa, Y., Lv, X., Kodama, Y., Ohizumi, Y., Yoshida, M., and Nakahata, N. (2006). Participation of epoxigenase activation in saikogenin D-induced inhibition of prostaglandin E(2) synthesis. *J. Pharm. Pharmacol.* 58, 859–866. doi:10.1211/jpp.58.6.0017
- Wang, P., Zhang, T. L., Yu, G. H., Li, M. J., SuZhang, J. J. Q., et al. (2019). Poly-pharmacokinetic strategy-delineated metabolic fate of bioactive compounds in

SUPPLEMENTARY MATERIAL

The **Supplementary Material** for this article can be found online at: <https://www.frontiersin.org/articles/10.3389/fphar.2021.630970/full#supplementary-material>.

- a traditional Chinese medicine formula, Yuanhu Zhitong tablets, using parallel reaction monitoring mode. *Phytomedicine* 53, 53–61. doi:10.1016/j.phymed.2018.09.026
- Wang, S. P., Hu, Y. Y., Tan, W., Wu, X., Chen, R., Cao, J., et al. (2012). Compatibility art of traditional Chinese medicine: from the perspective of herb pairs. *J. Ethnopharmacol* 143, 12–23. doi:10.1016/j.jep.2012.07.033
- Wang, Y., Gao, S. M., Li, R., Zhang, M., Gao, S., and Yu, C. Q. (2016). Antidepressant-like effects of the Radix Bupleuri and Radix Paeoniae Alba drug pair. *Neurosci. Lett.* 633, 14–20. doi:10.1016/j.neulet.2016.09.001
- Wishart, D. S. (2016). Emerging applications of metabolomics in drug discovery and precision medicine. *Nat. Rev. Drug Discov.* 15, 473–484. doi:10.1038/nrd.2016.32
- Won, E., and Kim, Y. K. (2016). Stress, the autonomic nervous system, and the immune-kynurenine pathway in the etiology of depression. *Curr. Neuropharmacol* 14, 665–673. doi:10.2174/1570159x14666151208113006
- Xie, G. X., Wang, S. L., Zhang, H., Zhao, A. H., Liu, J. J., Ma, Y. M., et al. (2018). Poly-pharmacokinetic study of a multicomponent herbal medicine in healthy Chinese volunteers. *Clin. Pharmacol. Ther.* 103, 692–702. doi:10.1002/cpt.784
- Xie, G. X., Zhao, A. H., Zhao, L. J., Chen, T. L., Chen, H. Y., Qi, X., et al. (2012). Metabolic fate of tea polyphenols in humans. *J. Proteome Res.* 11, 3449–3457. doi:10.1021/pr300318m
- Xu, L., Song, R., Tian, J. X., Tian, Y., Liu, G. Q., and Zhang, Z. J. (2012). Analysis of saikosaponins in rat plasma by anionic adducts-based liquid chromatography tandem mass spectrometry method. *Biomed. Chromatogr.* 26, 808–815. doi:10.1002/bmc.1734
- Xu, S. J., Yang, L., Lin, Q. L., Liu, Z. J., Feng, Q. R., Ma, L., et al. (2008). Simultaneous determination of paeoniflorin, albiflorin and benzoylpaeoniflorin in Radix Paeoniae Alba by TLC. *Chromatographia* 68, 459–462.
- Xue, T. H., and Roy, R. (2003). Studying traditional Chinese medicine. *Science* 300, 740–741. doi:10.1126/science.300.5620.740
- Yin, Q. C., Chen, C. C., Tian, J. S., Gao, X. X., Qin, D., X. M. G. H., et al. (2019). Analysis of serum pharmacokinetics from Radix Bupleuri-Radix Paeoniae Alba herb using UPLC-QE-Orbitrap-MS technology. *Acta Pharm. Sin.* 54, 2296–2302. doi:10.16438/j.0513-4870.2019-0435
- Zhang, Y. W., Lv, X. Y., Liu, R., Zhang, M. Y., Liu, H. P., Gao, H., et al. (2019). An integrated strategy for ascertaining quality marker of *Schisandra chinensis* (Turcz.) Baill based on correlation analysis between depression-related monoaminergic metabolites and chemical components profiling. *J. Chromatogr. A.* 1598, 122–131. doi:10.1016/j.chroma.2019.03.056
- Zhao, J., Jiang, P., and Zhang, W. D. (2010). Molecular networks for the study of TCM pharmacology. *Brief Bioinform.* 11, 417–430. doi:10.1093/bib/bbp063
- Zhao, Z. X., Fu, J., Ma, S. R., Peng, R., Yu, J. B., Cong, L., et al. (2018). Gut-brain axis metabolic pathway regulates antidepressant efficacy of albiflorin. *Theranostics* 8, 5945–5959. doi:10.7150/thno.28068
- Zhou, M. M., Hong, Y. L., Lin, X., Shen, L., and Feng, Y. (2017). Recent pharmaceutical evidence on the compatibility rationality of traditional Chinese medicine. *J. Ethnopharmacol.* 206, 363–375. doi:10.1016/j.jep.2017.06.007

Conflict of Interest: The authors declare that the research was conducted in the absence of any commercial or financial relationships that could be construed as a potential conflict of interest.

Copyright © 2021 Chen, Yin, Tian, Gao, Qin, Du and Zhou. This is an open-access article distributed under the terms of the Creative Commons Attribution License (CC BY). The use, distribution or reproduction in other forums is permitted, provided the original author(s) and the copyright owner(s) are credited and that the original publication in this journal is cited, in accordance with accepted academic practice. No use, distribution or reproduction is permitted which does not comply with these terms.



Mahuang Decoction Antagonizes Acute Liver Failure via Modulating Tricarboxylic Acid Cycle and Amino Acids Metabolism

Wenting Liao^{1†}, Qiwen Jin^{1†}, Junning Liu², Yiling Ruan¹, Xinran Li¹, Yueyue Shen¹, Zhicheng Zhang², Yong Wang², Shengming Wu³, Junying Zhang⁴, Lifeng Kang⁵ and Chunyong Wu^{1*}

OPEN ACCESS

Edited by:

Chandra Kant Katiyar,
Emami (India), India

Reviewed by:

Lixin Duan,
Guangzhou University of Chinese
Medicine, China
Wei Zhang,
Macau University of Science and
Technology, Macau

*Correspondence:

Chunyong Wu
cywu@cpu.edu.cn

[†]These authors have contributed
equally to this work

Specialty section:

This article was submitted to
Ethnopharmacology,
a section of the journal
Frontiers in Pharmacology

Received: 26 August 2020

Accepted: 04 February 2021

Published: 29 March 2021

Citation:

Liao W, Jin Q, Liu J, Ruan Y, Li X,
Shen Y, Zhang Z, Wang Y, Wu S,
Zhang J, Kang L and Wu C (2021)
Mahuang Decoction Antagonizes
Acute Liver Failure via Modulating
Tricarboxylic Acid Cycle and Amino
Acids Metabolism.
Front. Pharmacol. 12:599180.
doi: 10.3389/fphar.2021.599180

¹Department of Pharmaceutical Analysis, China Pharmaceutical University, Nanjing, China, ²Institute of Forensic Science, Nanjing Municipal Public Security Bureau, Nanjing, China, ³Nanjing Liuhe District Hospital of Traditional Chinese Medicine, Nanjing, China, ⁴Department of TCMs Pharmaceuticals, School of Traditional Chinese Pharmacy, China Pharmaceutical University, Nanjing, China, ⁵Faculty of Medicine and Health, School of Pharmacy, University of Sydney, Sydney, NSW, Australia

Acute liver failure (ALF) is a serious clinical disorder with high fatality rates. Mahuang decoction (MHD), a well-known traditional Chinese medicine, has multiple pharmacological effects, such as anti-inflammation, anti-allergy, anti-asthma, and anti-hyperglycemia. In this study, we investigated the protective effect of MHD against ALF. In the lipopolysaccharide and D-galactosamine (LPS/D-GalN)-induced ALF mouse model, the elevated activities of the serum alanine and aspartate transaminases as well as the liver pathological damage were markedly alleviated by MHD. Subsequently, a metabolomics study based on the ultrahigh performance liquid chromatograph coupled with Q Exactive Orbitrap mass spectrometry was carried to clarify the therapeutic mechanisms of MHD against ALF. A total of 36 metabolites contributing to LPS/D-GalN-induced ALF were identified in the serum samples, among which the abnormalities of 27 metabolites were ameliorated by MHD. The analysis of metabolic pathways revealed that the therapeutic effects of MHD are likely due to the modulation of the metabolic disorders of tricarboxylic acid (TCA) cycle, retinol metabolism, tryptophan metabolism, arginine and proline metabolism, nicotinate and nicotinamide metabolism, phenylalanine metabolism, phenylalanine, tyrosine and tryptophan synthesis, as well as cysteine and methionine metabolism. This study demonstrated for the first time that MHD exerted an obvious protective effect against ALF mainly through the regulation of TCA cycle and amino acid metabolism, highlighting the importance of metabolomics to investigate the drug-targeted metabolic pathways.

Keywords: mahuang decoction, acute liver failure, metabolomics, UPLC-Q-exactive-MS, tricarboxylic acid cycle, amino acids metabolism

INTRODUCTION

Acute liver failure (ALF) is a serious clinical disorder that arises from the development of hepatocellular dysfunction, which is predominantly caused by the viral infections (hepatitis A, B and E) in developing world and drug-induced liver injury in developed countries (Bernal and Wendon, 2013; Jiang et al., 2016). To date fatality rates associated with ALF is still as high as 60–80% depending on the disease etiology and patient's access to care (Patterson et al., 2020). Although the liver transplantation is the best choice for the treatment of ALF, it is clinically limited by many factors, such as lack of available liver organs and immune rejection (Nie et al., 2020). Therefore, it is imperative to seek novel effective medicines for ALF disease.

Mahuang decoction (MHD), a famous prescription in *Treatise on Febrile Disease* (Shang Han Lun in Chinese), consists of *Ephedrae Herba* (Ephedra), *Cinnamomi Ramulus* (Cassia twig), *Armeniacae Semen Amarum* (Bitter apricot kernel) and *Glycyrrhizae Radix* (Prepared licorice), and has been extensively used in treating asthma, cough and cold for thousands of years (He et al., 2018; Huang et al., 2020). Modern research demonstrated that MHD has multiple pharmacological effects, such as anti-inflammation, anti-allergy, anti-asthma, and anti-hyperglycemia (Zheng et al., 2015). It is reported that *Ephedra sinica* Stapf, as well as its two main components pseudoephedrine and ephedrine could prevent lethal liver injury by suppressing hepatocyte apoptosis (Yamada et al., 2008; Wu et al., 2014). As Ephedra is the monarch medicine in MHD and is considered to play a leading role in treating the main syndrome of diseases (He et al., 2018), we hypothesized that MHD is an effective therapeutic strategy for ameliorating ALF.

Evaluating the mechanism of pharmacological action of traditional Chinese medicine (TCM) is difficult because of the unclear active components and their possible synergistic actions (Yang et al., 2015). Metabolomics can comprehensively profile the metabolites in the entire organism that alter in responses to the pathophysiological or drug stimuli, identify their related metabolic pathways, and systematically clarify the mechanism of drug actions (Newgard, 2017; Fu et al., 2019). Thus metabolomics may be a powerful approach to unveil the underlying mechanism of MHD. Recently, ultrahigh performance liquid chromatography (UPLC) coupled with a high resolution mass spectrometer (MS) such as Q-Exactive Orbitrap MS are drawing great attention in metabolomics because of the superior peak resolution, selectivity, sensitivity, reproducibility and analysis speed (Fu et al., 2019; Zhong et al., 2019).

In this study, lipopolysaccharide and D-galactosamine (LPS/D-GalN)-induced ALF mice were used to explore the therapeutic benefits of MHD. The underlying mechanism was clarified by the untargeted metabolomics based on UPLC-Q Exactive Orbitrap MS. Our research uncovered for the first time that MHD could ameliorate ALF mainly through the regulation of TCA cycle and amino acids metabolism, providing new understanding of pathological changes and alternative therapeutic strategies for ALF.

MATERIALS AND METHODS

Chemicals and Reagents

Herbs of Ephedra (*Ephedra sinica* Stapf), Cassia twig (*Cinnamomum cassia* Presl), Bitter apricot kernel (*Prunus armeniaca* L.) and Prepared licorice (*Glycyrrhiza uralensis* Fisch.) were provided by Nanjing Liuhe District Hospital of Traditional Chinese Medicine (Nanjing, China) and were identified by Associate Prof. Junying Zhang from the School of Traditional Chinese Pharmacy of China Pharmaceutical University. Lipopolysaccharide (LPS, from *Escherichia coli*, serotype O55:B5), D-galactosamine (D-GalN), L-2-chlorophenylalanine, amygdalin and trans-cinnamaldehyde were purchased from Aladdin (Shanghai, China). Citric acid, cis-aconitic acid, phenylalanine, tyrosine, tryptophan, valine, arginine, proline, glutamine, pyroglutamic acid, methionine, phenylpyruvic acid, lysine and carnitine were purchased from Shanghai Jingchun Reagent Co., LTD. Lysophosphatidylcholine (LysoPC, 16:0), LysoPC (18:0), and LysoPC (18:2) were obtained from Sigma-Aldrich (St. Louis, MO). Ephedrine hydrochloride, pseudoephedrine hydrochloride and methylephedrine hydrochloride were obtained from National Institutes for Food and Drug Control (Beijing, China). Cinnamic acid was purchased from Nanjing Spring and Autumn Biological Engineering Co., Ltd (Nanjing, China). Glycyrrhizic acid was purchased from Bide Pharmatech Ltd (Shanghai, China). Methanol, acetonitrile, and other reagents were LC/MS grade and obtained from the commercial sources. Water was purified with a Millipore Milli Q-Plus system (Millipore, MA, United States).

Preparation of MHD

The mixture of Ephedra 3 g, Cassia twig 2 g, Bitter apricot kernel 2 g, and Prepared licorice 1 g was immersed in water for 30 min and extracted twice with 120 ml boiling water for 2 h each time. The extract was filtered and the two filtrates were combined and subsequently concentrated to 40 ml to prepare MHD. HPLC analysis of MHD was performed with Shimadzu LC-20AT system (Shimadzu, Kyoto, Japan) on a Welch Ultimate XB-Phenyl column (4.6 × 250 mm, 5 μm). The column temperature and flow rate was set at 30°C and 1.0 ml/min, respectively. The mobile phase consisted of 0.05% formic acid-0.05% triethylamine aqueous solution (A) and acetonitrile (B) with the gradient elution program as follows: 0–15 min, 8–10% B; 15–20 min, 10% B; 20–50 min, 10–27% B; 50–55 min, 27–38% B; 55–60 min, 38% B; 60–65 min, 38–8% B; 65–75 min, 8% B. The detection wavelengths were 210, 252, 278 and 291 nm (He et al., 2014). The injection volume was 10 μl. The chromatogram of MHD was presented in **Supplementary Figure S1**. Ephedrine, pseudoephedrine, methylephedrine, amygdalin, cinnamic acid, cinnamaldehyde and glycyrrhizic acid were found in MHD and identified with each standard sample.

Animals and Treatment

Male ICR mice (25–28 g) were purchased from Comparative Medicine Center of Yangzhou University (Yangzhou, China). All animals were housed in a controlled environment with a 12 h

light/dark cycle with *ad libitum* access to food and water. The study was conducted following the protocols approved by the Animal Ethics Committee of China Pharmaceutical University. All animals were randomly divided into three groups including the control group ($n = 8$), model group ($n = 15$) and MHD group ($n = 8$). Mice in the model group were given LPS (10 $\mu\text{g/kg}$) and D-GalN (700 mg/kg) intraperitoneally to establish an acute liver failure model (Xia et al., 2014). The MHD group was orally administered with MHD (100 mg/kg, calculated as Ephedra) at 12 h and 30 min before exposed to LPS/D-GalN. The control group was treated with equal amounts of saline. Four mice of the model group and one mouse of the MHD group were excluded because of death. At 8 h after treatment of LPS/D-GalN, blood samples were collected from the retro-orbital plexus, clot at room temperature for 1 h, and then centrifuged at 3000 g for 10 min (4°C). The serum was prepared and stored at -80°C immediately until analysis.

Biochemical Assay

The alanine aminotransferase (ALT) and the aspartate aminotransferase (AST) are important indicators of the liver function (Farooq et al., 2019). ALT and AST in serum were determined using the assay kits purchased from Jiancheng Bioengineering Institute (Nanjing, China) according to the instructions attached to the kits.

Histopathology

After the mice were sacrificed, the livers were collected and fixed in 4% paraformaldehyde. Then the samples were sent to Pathology and PDX Efficacy Evaluation Center of China Pharmaceutical University for haematoxylin and eosin (H&E) staining.

Pretreatment of Serum Sample

Prior to analysis, serum samples were thawed on ice and mixed for 5 s at room temperature. An aliquot of 40 μl serum were added to 160 μl pre-cold methanol containing L-2-chlorophenylalanine (2.5 $\mu\text{g/ml}$) as the internal standard, followed by vortex-mixing for 3 min and then was placed on ice for 20 min. After the mixture was centrifuged at 14000 g for 15 min at 4°C , the supernatant was diluted with 0.1% formic acid at the ratio of 1:1 (v/v) followed by UPLC-Q-Exactive-MS analysis. To verify the repeatability of the LC-MS system, Quality control (QC) samples were prepared by mixing equal aliquots of each sample and were randomly distributed in the real sample sequence (Sangster et al., 2006). In order to avoid the possible signal drift of the mass spectrometer over time, the samples were injected into UPLC-Q-Exactive-MS in a random order.

UPLC-Q Exactive-MS Analysis

The LC-MS analysis was performed with Q-Exactive Orbitrap coupled to a Ultimate™ 3000 UPLC system (Thermo Fisher Scientific, United States). Analytes were separated on ACQUITY UPLC HSS T3 C18 column (1.8 μm , 2.1×100 mm; Waters, Ireland) at 40°C . The mobile phase consisted of 0.1% formic acid solution (A) and acetonitrile containing 0.1% formic acid (B). The gradient program was as following: 5% B at

0–2.5 min, 5–95% B at 2.5–18 min, 95% B at 18–21.5 min, 95–5% B at 21.5–22 min, and 5% B at 22–27 min. The flow rate was 0.4 ml/min. The injection volume was 5 μl . Q Exactive-MS was operated with heated electrospray ionization (HESI)-II. Samples were analyzed under positive mode with full-scan and dd MS². The resolution was 70000; mass-to-charge range was from 60 to 900 m/z; sheath gas, aux gas and sweep gas flow rate were set at 40, 10 and 1, respectively; capillary temperature and aux gas heater temperature were set at 320°C and 350°C , respectively; spray voltage was 3.5 kV; S-lens RF level was 50; maximum IT was 200 ms and AGC target was 3×10^6 at full MS. For dd MS², the resolution was 17500; maximum IT was 50 ms; AGC target was 1×10^5 ; normalized collision energy (NCE) was set at 10, 25, and 40; other parameters were same as full-scan mode.

Data Pre-processing

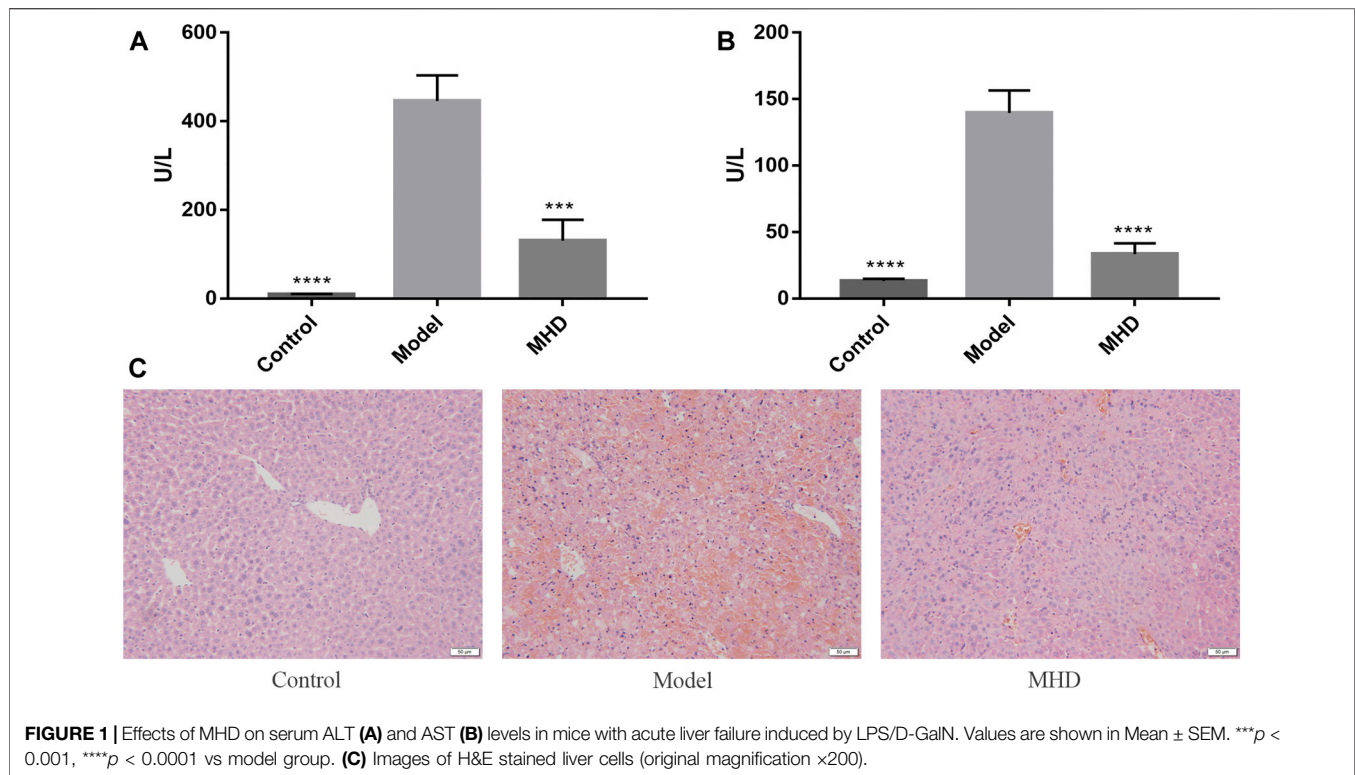
All the LC-MS raw data were converted to CDF format by Xcalibur 4.2. Data pre-processing, such as peak discrimination, alignment, and matching, were carried out by XCMS package-based R software (Smith et al., 2006). The CentWave algorithm was adopted and algorithm parameters were default settings except for the following: *snthresh* = 6, *peakwidth* = *c*(5, 25), *ppm* = 30, *bw* = 5, *mzwd* = 0.025. The output data matrix contained missing values, which could have a downstream effect on the analysis of the data (Mais et al., 2018). To solve such problem, the variables present in more than 80% of each group were retained (Bijlsma et al., 2006) and the remaining missing values were replaced by a small value that is half of the minimum value in the original data (Mais et al., 2018). After the above steps, the data matrix was normalized by the internal standard.

Multivariate Analysis

The pre-processed data was imported into SIMCA-P 14.1 (Umetrics, Sweden), followed by multivariate data analysis, such as principle component analysis (PCA), partial least squares discrimination analysis (PLS-DA) and orthogonal partial least squares discrimination analysis (OPLS-DA). The outliers and the general clustering trends were analyzed by PCA. The differences among the control group, model group, and MHD group were observed by PLS-DA. OPLS-DA was utilized to examine the metabolic differences between two groups. Besides, all PLS-DA and OPLS-DA models were subjected to the permutation test.

Metabolites Identification and Metabolic Pathway Analysis

Metabolite identification was performed according to our previous report (Tan et al., 2018). Briefly, the quasi-molecular ions were judged according to the positive scanning in MS. The molecular information was obtained from a freely accessible database of HMDB (Wishart et al., 2018), METLIN (Guijas et al., 2018) and KEGG (Kanehisa et al., 2014) within a mass accuracy of 10 ppm. To narrow the scope of target metabolites, the quasi-molecular ions were then subjected to MS/MS analysis. The affected metabolic pathways were analyzed and visualized via MetaboAnalyst (<https://www.metaboanalyst.ca/>) with identified



differential metabolites (Chong et al., 2018, 2019). Finally, 17 available standards were adopted to confirm the identified metabolites.

Statistical Analysis

The normality and homogeneity of variance of all samples were tested by IBM SPSS Statistics 26. One-way ANOVA or Kruskal-Wallis was used to test the statistical differences of the samples according to whether they obey normal distribution and homogeneity of variance. The resultant p values were corrected by Bonferroni correction to α/n , where $\alpha = 0.05$ and n is the number of comparisons in statistical analysis (Berben et al., 2012; Araújo et al., 2018). Adjusted $p < 0.05$ was considered statistically significant.

RESULTS

Biochemical Assay and Pathological Changes

The serum ALT and AST levels of each group are shown in Figures 1A,B, where ALT reflects the degree of liver cell damage and AST reflects the degree of hepatocyte necrosis. The levels of ALT together with AST in the model group were significantly higher than those in the control group, and were similar to the levels reported previously (Wu et al., 2014). Meanwhile, the notably decreased levels of ALT and AST were observed in MHD groups. Consistent with this result, large areas of hepatocytes necrosis were visible in model group by H&E staining, which was remarkably improved by the treatment of

MHD (Figure 1C), demonstrating that MHD has a hepatoprotective effect.

Metabolic Profiling and Multivariate Analysis

The typical total ion current (TIC) chromatogram of UPLC-Q-Exactive MS is shown in Supplementary Figure S2. The relative standard deviation (RSD) for the peak intensity of the internal standard was less than 3.0% in QC samples. After peak alignment, filtering and normalization, the RSD of intensity of all peaks in QC samples was calculated. The RSD of 30% covered 88.0% features, indicating that the analytical method had good repeatability. With the RSD less than 30% in QC samples, 7770 molecular features were obtained for further multivariate data analysis.

To analyze the protective effect of MHD, PCA and PLS-DA models were established. An unsupervised PCA model was carried out to observe the tendency of MHD group separated from model group and control group. As shown in Figure 2A, a separated trend of the inter-group was observed on the scores plot. The main parameter of PCA, namely R^2X value, was greater than 0.4, indicating that the models were well-fitted. As one of the supervised analysis, PLS-DA could ignore intra-group errors as well as random errors, and focus on the analysis of differences between groups. PLS-DA scores plot showed good discrimination power among control, model and MHD groups (Figure 2B). The predictive capability of the model was assessed by the internal validation ($R^2Y = 0.937$, $Q^2 = 0.824$), suggesting the goodness of fit and predictive capability of the model. A random permutation

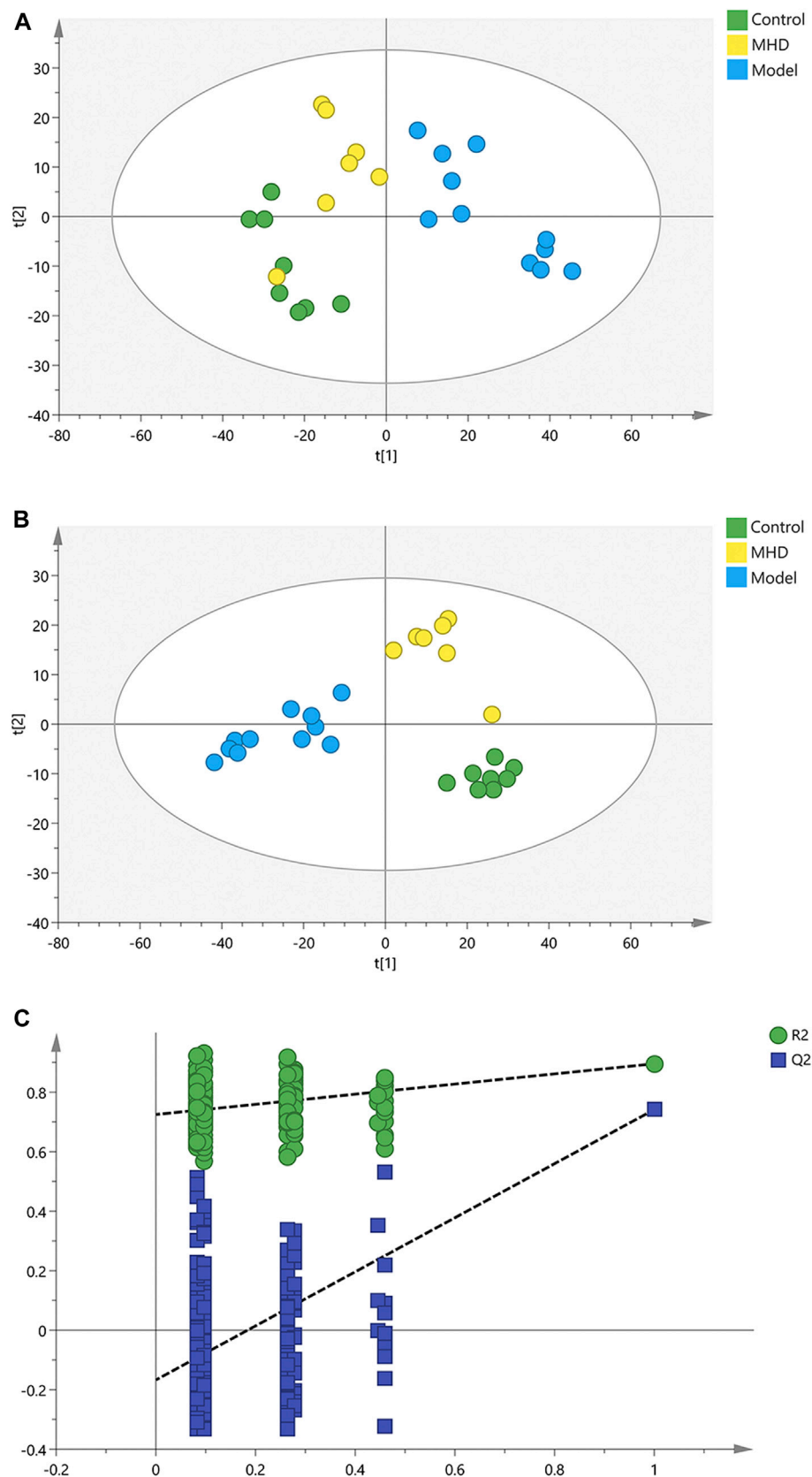


FIGURE 2 | PCA, PLS-DA and permutation test of serum samples. **(A)** PCA score scatter plots. **(B)** PLS-DA score scatter plots. **(C)** Permutation tests of PLS-DA.

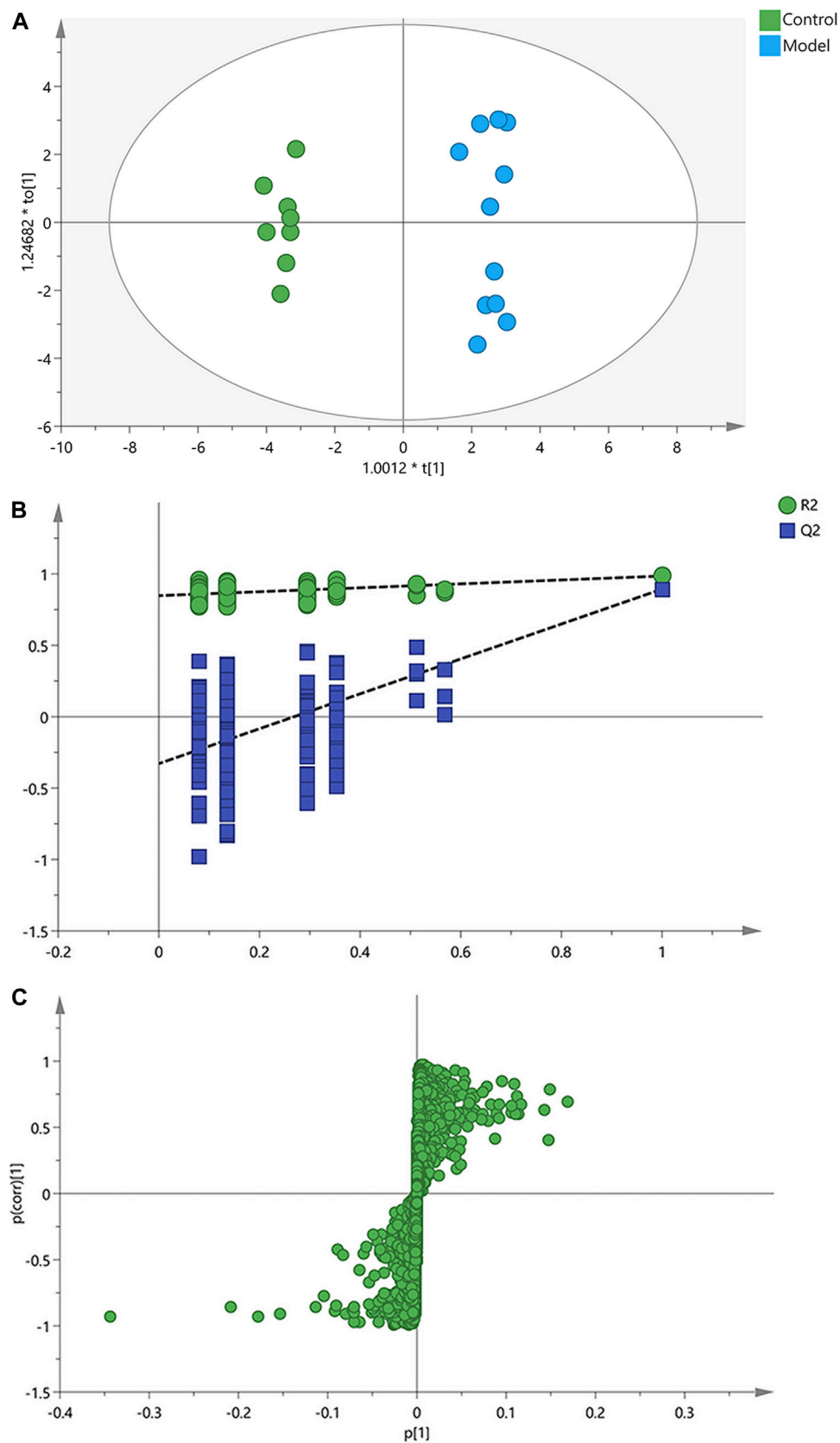


FIGURE 3 | OPLS-DA score plots, permutation test and S-plots of serum samples. **(A)** OPLS-DA score plots. **(B)** Permutation tests of OPLS-DA. **(C)** S-plots obtained from OPLS-DA model.

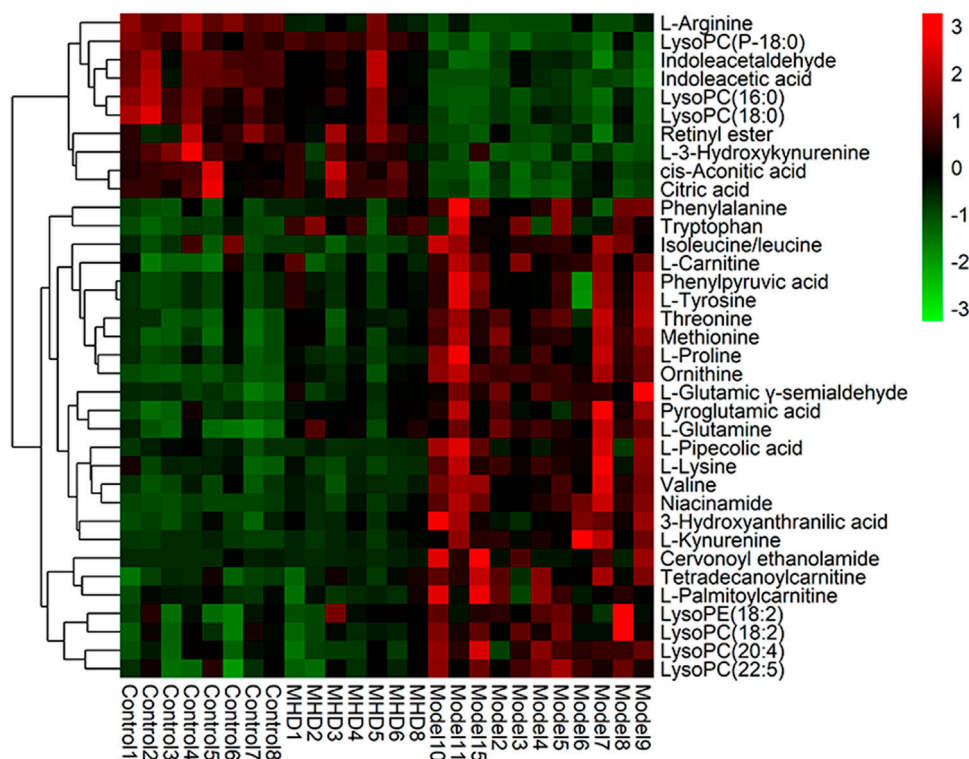


FIGURE 4 | Heatmap of the protective activity of MHD for ALF. The degree of change is marked with different colors. Red and green indicate up-regulation and down-regulation respectively. Each row represents a metabolite. Each column represents an individual sample.

test (200 times) was further used to validate the reliability of the PLS-DA model. As R^2_{cum} and Q^2_{cum} values were lower than the original values of the validation plot (**Figure 2C**), the results were non-overfitting and reliable.

Identification of Differential Metabolites

Afterwards, OPLS-DA was applied to search the differential metabolites between the control and model groups, and a good discrimination between groups was observed (**Figure 3A**). The predictive capability of the model was assessed by the internal validation ($R^2Y = 0.985$, $Q^2 = 0.893$), suggesting a satisfactory fit with high predictive power. In the random permutation test (200 times), R^2_{cum} and Q^2_{cum} values in permuted classes were lower than those in original classes, revealing that the OPLS-DA models were not over-fitting (**Figure 3B**). The S-plot generated from OPLS-DA model was used to find potential biomarkers, since the variables distributed at both ends of the S-plot markedly contribute to the clustering and discrimination (**Figure 3C**).

Differential metabolites between the model and control groups were identified by using a threshold of variable importance in the projection (VIP) values ($VIP > 1.0$) produced from the OPLS-DA model (Fan et al., 2016). After restricting with univariate statistical analysis ($p < 0.05$), 36 significantly changed metabolites were designated as biomarkers of ALF (**Table 1**). The MS/MS spectra of these biomarkers together with their proposed fragmentation

pathways are presented in **Supplementary Figure S3**. The relative levels of these biomarkers in each mouse were visualized in **Figure 4**. Compared to the model group, the relative intensity of most biomarkers were reverted by MHD, among which 27 metabolites were significantly regulated (**Figure 5**).

Metabolic Pathways Analysis

To figure out the potential LPS/D-GalN-induced and MHD-modulated metabolic pathways, 36 significantly altered metabolites in ALF model group (vs. control group) and 27 significantly reverted metabolites in MHD group (vs. model group) were imported into MetaboAnalyst 4.0. By using a threshold of the impact-value (≥ 0.10), 11 metabolic pathways were identified to be the potential targets of ALF, including phenylalanine, tyrosine and tryptophan biosynthesis, phenylalanine metabolism, tryptophan metabolism, arginine and proline metabolism, nicotinate and nicotinamide metabolism, retinol metabolism, arginine biosynthesis, tricarboxylic acid (TCA) cycle (citric acid cycle), tyrosine metabolism, alanine, aspartate and glutamate metabolism, as well as cysteine and methionine metabolism (**Figure 6A** and **Supplementary Table S1**). MHD-regulated metabolic pathways were identified to be TCA cycle, retinol metabolism, tryptophan metabolism, arginine and proline metabolism, nicotinate and nicotinamide metabolism, phenylalanine metabolism, phenylalanine, tyrosine and tryptophan synthesis, as well as

Table 1 | Changes of metabolites in mice with acute liver failure.

Metabolites	Experimental [M + H] ⁺ (m/z)	Retention times (min)	Adduction	Theoretical [M + H] ⁺ (m/z)	MS fragments	Delta (ppm)	Trend	Fold Change	
								CON/M	MHD/M
L-Proline ^a	116.0707	0.673	M + H	116.0706	70.07	1	↓	0.6**	0.6*
Valine ^a	118.0863	0.684	M + H	118.0863	72.08, 55.06	0	↓	0.6**	0.7**
Threonine ^b	120.0655	0.653	M + H	120.0655	102.06, 74.06, 60.99	0	↓	0.6****	0.8**
Niacinamide ^b	123.0553	1.000	M + H	123.0553	106.03, 79.02	0	↓	0.3****	0.5***
Pyroglutamic acid ^a	130.0498	0.652	M + H	130.0499	84.04, 70.07, 56.06	1	↓	0.7**	0.8
L-Pipecolic acid ^b	130.0862	0.633	M + H	130.0863	112.04, 84.04	1	↓	0.4*	0.4*
L-Glutamic ?-semialdehyde ^b	132.0656	0.653	M + H	132.0655	114.07, 86.06	1	↓	0.6***	0.8*
Isoleucine/leucine ^b	132.1018	0.765	M + H	132.1019	86.06, 56.97	1	↓	0.8**	0.7*
Ornithine ^b	133.0970	0.553	M + H	133.0972	116.07, 70.07	1	↓	0.2****	0.5*
L-Glutamine ^a	147.0762	0.648	M + H	147.0764	130.05, 102.06, 84.04	1	↓	0.6**	0.9
L-Lysine ^a	147.1126	0.558	M + H	147.1128	130.09, 84.08, 56.05	1	↓	0.6**	0.6**
Methionine ^a	150.0581	0.710	M + H	150.0583	133.03, 104.05	1	↓	0.5***	0.7*
3-Hydroxyanthranilic acid ^b	154.0496	1.262	M + H	154.0499	136.04, 109.96, 67.05	2	↓	0.5**	0.7
Indoleacetaldehyde ^b	160.0755	1.576	M + H	160.0757	141.92, 131.97	1	↑	2.7***	2.0*
L-Carnitine ^a	162.1122	0.647	M + H	162.1125	103.04, 85.03, 60.08	2	↓	0.7***	0.8**
Phenylpyruvic acid ^a	165.0544	1.070	M + H	165.0546	147.04, 119.05	1	↓	0.6**	0.7
Phenylalanine ^a	166.0860	2.057	M + H	166.0863	149.06, 131.05, 120.08	2	↓	0.7**	0.8*
cis-Aconitic acid ^a	175.0234	0.996	M + H	175.0237	157.11, 61.53	2	↑	1.7**	1.7**
L-Arginine ^a	175.1187	0.595	M + H	175.1190	158.00, 70.07, 60.06	2	↑	10.7****	3.7
Indoleacetic acid ^a	176.0704	1.577	M + H	176.0706	158.00, 106.99	1	↑	2.6***	2.0*
L-Tyrosine ^a	182.0809	1.070	M + H	182.0812	165.05, 136.08	2	↓	0.6**	0.7
Citric acid ^a	193.0344	0.996	M + H	193.0343	175.03, 133.01, 61.04	1	↑	1.7****	1.6****
Tryptophan ^a	205.0968	4.374	M + H	205.0972	188.07, 170.06	2	↓	0.8*	1.0
L-Kynurenine ^b	209.0917	1.972	M + H	209.0921	192.07, 120.04, 94.07	2	↓	0.2***	0.4*
L-3-Hydroxykynurenine ^b	225.0865	1.049	M + H	225.0870	207.02, 179.02, 161.01	2	↑	5.1**	3.1**
Retinyl ester ^b	303.2311	15.346	M + H	303.2319	285.22, 267.21, 256.88	3	↑	2.8***	2.7***
Tetradecanoylcarnitine ^b	372.3099	13.325	M + H	372.3108	313.24, 85.03, 60.08	2	↓	0.5**	0.7*
Cervonoyl ethanolamide ^b	373.2728	11.073	M + H	373.2737	355.26, 241.19, 161.13, 81.07	2	↓	0.1**	0.1**
L-Palmitoylcarnitine ^b	400.3412	14.522	M + H	400.3421	341.26, 144.10, 85.03	2	↓	0.5*	0.6
LysoPE(18:2) ^b	478.2918	14.002	M + H	478.2928	460.28, 337.27	2	↓	0.7*	0.8
LysoPC(16:0) ^a	496.3387	14.260	M + H	496.3398	258.11, 184.07	2	↑	2.1****	1.7*
LysoPC(P-18:0) ^b	508.3751	15.304	M + H	508.3762	184.07, 125.00, 104.11, 86.10	2	↑	2.5****	2.3****
LysoPC(18:2) ^a	520.3387	14.063	M + H	520.3398	184.07, 104.11	2	↓	0.8**	0.8**
LysoPC(18:0) ^a	524.3699	15.761	M + H	524.3711	506.36, 184.07, 86.10	2	↑	2.2**	1.6*
LysoPC(20:4) ^b	544.3386	14.115	M + H	544.3398	184.07, 104.11, 86.10, 60.08	2	↓	0.7**	0.7**
LysoPC(22:5) ^b	570.3540	14.459	M + H	570.3554	387.29, 184.07, 104.11	2	↓	0.7*	0.8*

Delta = (abs (experimental m/z – theoretical m/z) / theoretical m/z) × 1000000. Trend: change trend of contents of metabolites in each group compared to the model group. Fold change: relative amount of each group compared to the model group. *adjusted p < 0.05, **adjusted p < 0.01, ***adjusted p < 0.001, ****adjusted p < 0.0001, adjusted p: p values corrected by Bonferroni.

^aMetabolites validated with standard sample.

^bMetabolites putatively annotated. Abbreviations: LysoPE, lysophosphatidyl ethanolamine; LysoPC, Lysophosphatidylcholine.

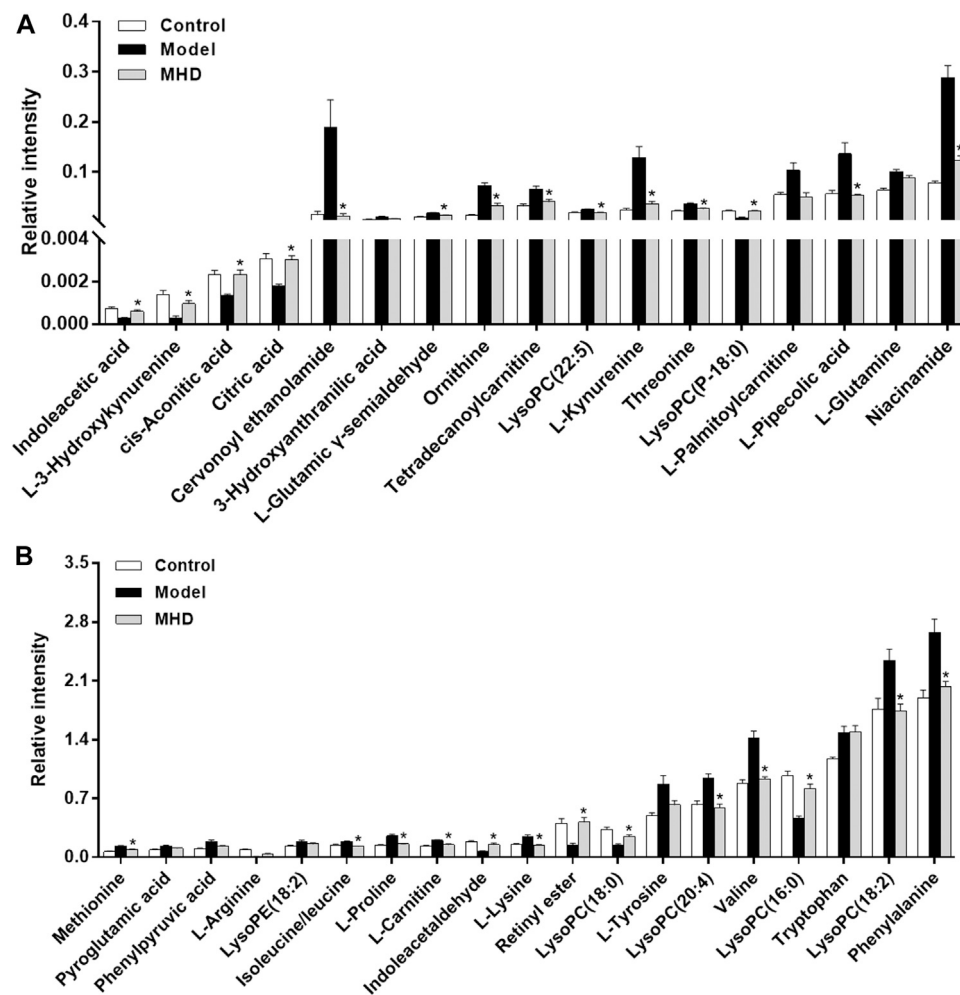


FIGURE 5 | Changes in the relative intensity of target metabolites. Statistical significance was performed using univariate statistical analysis. 27 metabolites were significantly reversed by MHD. Values are shown in Mean \pm SEM. * $p < 0.05$ vs. model group.

cysteine and methionine metabolism (Figure 6B and Supplementary Table S2). A schematic metabolic network of LPS/D-GalN-induced ALF and MHD modulation were analyzed with the KEGG database (Kanehisa et al., 2014) by relating the major metabolic pathways (Figure 7).

DISCUSSION

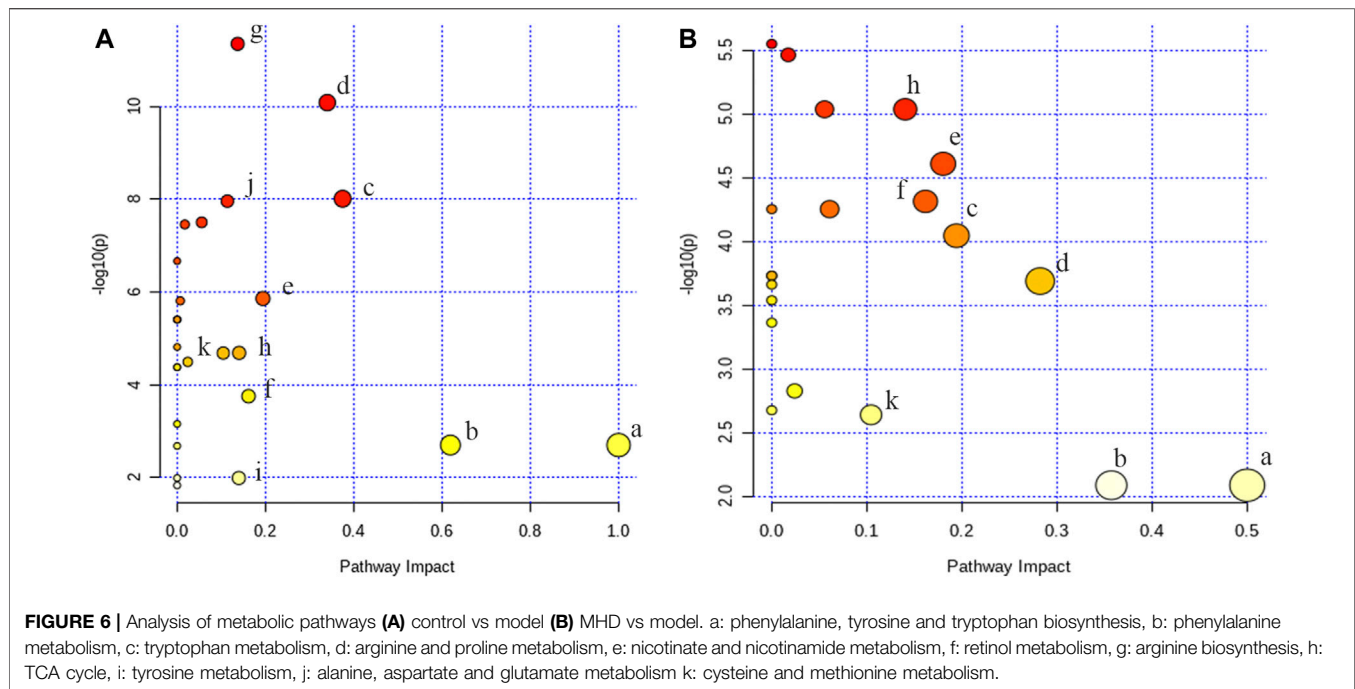
Mahuang decoction (MHD) has been widely utilized to treat asthma, cough, and exogenous wind-cold (He et al., 2018; Huang et al., 2020). The monarch medicine of MHD, *Ephedra sinica* Stapf, and its two main components pseudoephedrine and ephedrine have been reported to prevent lethal liver injury (Yamada et al., 2008; Wu et al., 2014). Therefore, we hypothesized that MHD has protective effect against ALF.

To verify our hypothesis, the serum transaminase test and histopathology together with a UPLC-Q-Exactive-MS-based metabolomics study were performed to explore the potential

efficacy and mechanisms of MHD against ALF. The serum ALT and AST levels in LPS/D-GalN-induced ALF mice were markedly reduced with the treatment of MHD, providing strong evidences for the protective effect of MHD on ALF. Furthermore, a total of 36 metabolites were identified to be ALF relevant biomarkers, among which 27 metabolites were significantly reverted by the treatment of MHD. By constructing the relevant metabolic pathways of these reverted biomarkers, eight metabolic pathways were filtered out to be the most important pathways for the anti-ALF efficacy of MHD, including TCA cycle, retinol metabolism, tryptophan metabolism, arginine and proline metabolism, nicotinate and nicotinamide metabolism, phenylalanine metabolism, phenylalanine, tyrosine and tryptophan synthesis, as well as cysteine and methionine metabolism.

TCA Cycle and Energy Metabolism

The TCA cycle is essential for the aerobic metabolism, which could facilitate the adequate throughput of the substrates derived



from carbohydrates, fatty acids and certain amino acids. The two pivotal intermediates, namely citric acid and cis-aconitic acid, were altered following LPS/D-GalN inducement, suggesting that ALF could perturb TCA cycle. This result is supported by the previous studies (Carvalho et al., 2002; Dabos et al., 2011; Pathania et al., 2020). An unbalanced TCA cycle was indicative of the decreased oxidative metabolism. After treating with MHD, the levels of citric acid and cis-aconitic acid were higher than that in ALF mice, demonstrating that TCA metabolism tended to be normal.

As the principal precursors of β -oxidation substrates and acylcarnitines in serum, the long-chain acylcarnitines (LCAC) mainly come from the liver (Sandor et al., 1990; Jones et al., 2010). The levels of LCAC including tetradecanoylcarnitine and palmitoylcarnitine were significantly increased in ALF group compared to the control group, implying that ALF condition could inhibit the fatty acid oxidation. This finding is supported by the previous studies in which acylcarnitines were elevated under ALF condition (Bi et al., 2013; McGill et al., 2014). The high levels of LCAC in ALF mice may be related to the downregulation of carnitine palmitoyltransferase I (Cpt1) and acyl-CoA thioesterase 1 (Acot1) genes that are involved in the fatty acid β -oxidation pathway (Bi et al., 2013). After the treatment of MHD, the level of tetradecanoylcarnitine was significantly reverted, demonstrating that the modulation of herapeutic fatty acid β -oxidation is involved in the pharmacological process of MHD.

Branched chain amino acids (BCAAs) are important energy substrates, including valine, leucine, and isoleucine, and they enter the TCA cycle through deamination, decarboxylation, and β -oxidation processes. The serum levels of BCAAs were up-regulated in ALF mice, while down-regulated towards normal when treated with MHD. A possible mechanism is that the TCA

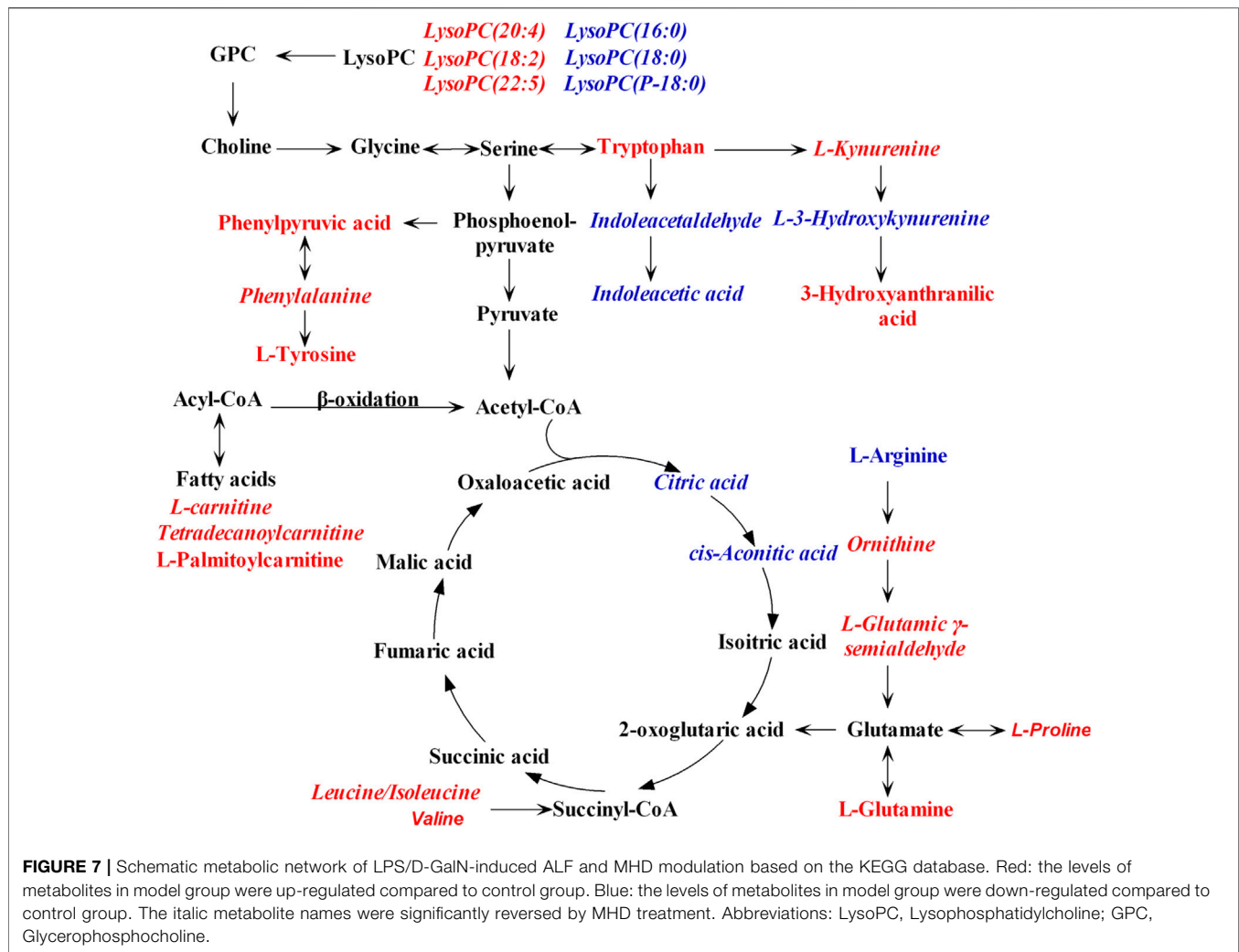
cycle in mice is inhibited under the condition of ALF, leading to a reduction of ATP production. Energy compensation may be achieved by consuming BCAAs and accelerating β -oxidation of fatty acids since the level of citric acid and cis-aconitic acid in TCA cycle were elevated but the level of BCAAs and LCAC were reduced after MHD treatment.

Together, these results suggest that the hepatoprotective activities of MHD against ALF are highly likely due to the modulation of the energy metabolism in liver.

Amino Acids Metabolism

The serum levels of aromatic amino acids (AAA) including phenylalanine, tyrosine and tryptophan were elevated in ALF mice. A previous study has implied that the levels of AAA, especially phenylalanine and tryptophan, are good biomarkers of ALF severity, which is probably caused by the inefficient degradation or gluconeogenesis-based conversion of AAA in the damaged liver (Cao et al., 2012). Beside, elevated AAA is closely related with hepatic encephalopathy associated with ALF (Dejong et al., 2007; Wijdsicks, 2016). After the treatment of MHD, the serum level of phenylalanine was significantly reverted, suggesting that MHD can promote the recovery of liver function and thus reduce the risk of hepatic encephalopathy.

Consistent with previous reports (Clària et al., 2019; Sekine and Fukuwatari, 2019), the present study observed that tryptophan metabolism is one of the significantly disturbed pathways in ALF mice. This abnormality was regulated by MHD treatment, and similar activity was observed in other TCM such as Yin-Chen-Hao Tang (Liu et al., 2019). Tryptophan and its metabolites play critical roles in many physiological processes, such as inflammation, immune



response, and neurotransmission (Cervenka et al., 2017). Free tryptophan is mainly converted to kynurenine with the involvement of microglial indoleamine-2,3-dioxygenase 1, and the process could be stimulated by inflammation (Platten et al., 2019). The substrates of kynurenine pathways increased by kynurenine metabolism will transfer to the central nervous system (CNS) and be degraded locally, which eventually damage the CNS (Müller and Schwarz, 2007). Compared with the control group, the serum level of kynurenine is up-regulated in model group but reverted by MHD, which indicates that MHD may have anti-inflammatory effect.

Moreover, arginine and proline metabolism was disturbed in ALF mice while reverted by MHD. A similar activity was observed in Yin-Chen-Hao Tang (Liu et al., 2019). L-Arginine is an essential amino acid. Catabolic diseases such as cancer and injury will increase the utilization of arginine, leading to arginine consumption. In ALF mice, arginine levels were significantly decreased (>10-fold change, adjusted $p < 0.001$) and the levels of intermediates of arginine metabolism such as ornithine and L-glutamic- γ -semialdehyde were increased, suggesting that ALF

caused excessive consumption of arginine. With the treatment of MHD, the level of ornithine and L-glutamic- γ -semialdehyde were down-regulated, indicating the disturbance of arginine metabolism was alleviated to a certain extent.

CONCLUSION

In this study, the hepatoprotective activity of MHD against ALF was confirmed by the serum transaminase test and histopathology, and the underlying mechanisms was studied by the UPLC-Q Exactive-MS-based metabolomics. We have identified 36 biomarkers of ALF, among which the abnormalities of 27 metabolites were regulated by the treatment of MHD. Metabolic pathway analysis revealed that the anti-ALF mechanisms of MHD may be mainly attributed to the modulation of metabolic disorders of TCA cycle and amino acids metabolism. To obtain a more complete understanding of MHD, future studies is necessary to find the key factors of the identified metabolic pathways and determine their relationship with the chemical components of MHD.

DATA AVAILABILITY STATEMENT

The raw data supporting the conclusions of this article will be made available by the authors, without undue reservation, to any qualified researcher.

AUTHOR CONTRIBUTIONS

CW and WL conceived and designed the experiments. QJ, YR, XL, YS and JZ performed the experiment. JL, ZZ and YW assisted the UPLC-Q-Exactive-MS experiments. SW provided the crude herbs. WL and QJ wrote the first draft of the manuscript. CW and LK edited the final manuscript. All authors have read and approved the manuscript.

REFERENCES

- Araújo, A. M., Bastos, M. L., Fernandes, E., Carvalho, F., Carvalho, M., and Guedes de Pinho, P. (2018). GC-MS metabolomics reveals disturbed metabolic pathways in primary mouse hepatocytes exposed to subtoxic levels of 3,4-methylenedioxymethamphetamine (MDMA). *Arch. Toxicol.* 92, 3307–3323. doi:10.1007/s00204-018-2314-9
- Berben, L., Sereika, S. M., and Engberg, S. (2012). Effect size estimation: methods and examples. *Int. J. Nurs. Stud.* 49, 1039–1047. doi:10.1016/j.ijnurstu.2012.01.015
- Bernal, W., and Wendon, J. (2013). Acute liver failure. *N. Engl. J. Med.* 369, 2525–2534. doi:10.1056/NEJMra1208937
- Bi, H., Li, F., Krausz, K. W., Qu, A., Johnson, C. H., and Gonzalez, F. J. (2013). Targeted metabolomics of serum acylcarnitines evaluates hepatoprotective effect of wuzhi tablet (schisandra sphenanthera extract) against acute acetaminophen toxicity. *Evid. Based Complement. Alternat Med.* 2013, 985257. doi:10.1155/2013/985257
- Bijlsma, S., Bobeldijk, I., Verheij, E. R., Ramaker, R., Kochhar, S., Macdonald, I. A., et al. (2006). Large-scale human metabolomics studies: a strategy for data (pre-) processing and validation. *Anal. Chem.* 78, 567–574. doi:10.1021/ac051495j
- Cao, H., Yang, J., Yu, J., Pan, Q., Li, J., Zhou, P., et al. (2012). Therapeutic potential of transplanted placental mesenchymal stem cells in treating Chinese miniature pigs with acute liver failure. *BMC Med.* 10, 56. doi:10.1186/1741-7015-10-56
- Carvalho, R. A., Jones, J. G., McGuirk, C., Sherry, A. D., and Malloy, C. R. (2002). Hepatic gluconeogenesis and Krebs cycle fluxes in a CCl4 model of acute liver failure. *NMR Biomed.* 15, 45–51. doi:10.1002/nbm.745
- Cervenka, I., Agudelo, L. Z., and Ruas, J. L. (2017). Kynurenines: tryptophan's metabolites in exercise, inflammation, and mental health. *Science* 357, eaaf9794. doi:10.1126/science.aaf9794
- Chong, J., Soufan, O., Li, C., Caraus, I., Li, S., Bourque, G., et al. (2018). MetaboAnalyst 4.0: towards more transparent and integrative metabolomics analysis. *Nucleic Acids Res.* 46, W486–W494. doi:10.1093/nar/gky310
- Chong, J., Wishart, D. S., and Xia, J. (2019). Using MetaboAnalyst 4.0 for comprehensive and integrative metabolomics data analysis. *Curr. Protoc. Bioinformatics.* 68, e86. doi:10.1002/cpbi.86
- Clària, J., Moreau, R., Fenaille, F., Amorós, A., Junot, C., Gronbaek, H., et al. (2019). Orchestration of tryptophan-kynurenine pathway, acute decompensation, and acute-on-chronic liver failure in cirrhosis. *Hepatology* 69, 1686–1701. doi:10.1002/hep.30363
- Dabos, K. J., Whalen, H. R., Newsome, P. N., Parkinson, J. A., Henderson, N. C., and Sadler, I. H., et al. (2011). Impaired gluconeogenesis in a porcine model of paracetamol induced acute liver failure. *World J. Gastroenterol.* 17, 1457–1461. doi:10.3748/wjg.v17.i11.1457
- Dejong, C. H., van de Poll, M. C., Soeters, P. B., Jalan, R., and Olde Damink, S. W. (2007). Aromatic amino acid metabolism during liver failure. *J. Nutr.* 137, 1579S–1598S. doi:10.1093/jn/137.6.1579S

FUNDING

This research was supported by the National Natural Science Foundation of China (Nos. 82074128, 81473357, 81673681), the Priority Academic Program Development of Jiangsu Higher Education Institutions, and the Fundamental Research Funds for the Central Universities (No.2632020ZD06).

SUPPLEMENTARY MATERIAL

The Supplementary Material for this article can be found online at: <https://www.frontiersin.org/articles/10.3389/fphar.2021.599180/full#supplementary-material>.

- Fan, Y., Li, Y., Chen, Y., Zhao, Y. J., Liu, L. W., and Li, J., et al. (2016). Comprehensive metabolomic characterization of coronary artery diseases. *J. Am. Coll. Cardiol.* 68, 1281–1293. doi:10.1016/j.jacc.2016.06.044
- Farooq, M., Filliol, A., Simoes Eugénio, M., Piquet-Pellorce, C., Dion, S., Raguene-Nicol, C., et al. (2019). Depletion of RIPK1 in hepatocytes exacerbates liver damage in fulminant viral hepatitis. *Cell Death Dis.* 10, 12. doi:10.1038/s41419-018-1277-3
- Fu, C., Wu, Q., Zhang, Z., Xia, Z., Ji, H., Lu, H., et al. (2019). UPLC-ESI-IT-TOF-MS metabolomic study of the therapeutic effect of Xuefu Zhuyu decoction on rats with traumatic brain injury. *J. Ethnopharmacol.* 245, 112149. doi:10.1016/j.jep.2019.112149
- Guijas, C., Montenegro-Burke, J. R., Domingo-Almenara, X., Palermo, A., Warth, B., Hermann, G., et al. (2018). METLIN: a Technology platform for identifying knowns and unknowns. *Anal. Chem.* 90, 3156–3164. doi:10.1021/acs.analchem.7b04424
- He, Y., Lou, X., Jin, Z., Yu, L., Deng, L., and Wan, H. (2018). Mahuang decoction mitigates airway inflammation and regulates IL-21/STAT3 signaling pathway in rat asthma model. *J. Ethnopharmacol.* 224, 373–380. doi:10.1016/j.jep.2018.06.011
- He, Y., Zhu, Y., Zhang, R., Ge, L., and Wan, H. (2014). Simultaneous quantification of nine major active components in traditional Chinese prescription Mahuang decoction and the influence of herbal compatibility on their contents. *Pharmacogn. Mag.* 10, S72–S79. doi:10.4103/0973-1296.127346
- Huang, P., Tang, Y., Li, C., Zhou, H., Yu, L., Wan, H., et al. (2020). Correlation study between the pharmacokinetics of seven main active ingredients of Mahuang decoction and its pharmacodynamics in asthmatic rats. *J. Pharm. Biomed. Anal.* 183, 113144. doi:10.1016/j.jpba.2020.113144
- Jiang, X., Li, Z., Jiang, S., Tong, X., Zou, X., Wang, W., et al. (2016). Lipoxin A4 exerts protective effects against experimental acute liver failure by inhibiting the NF-κB pathway. *Int. J. Mol. Med.* 37, 773–780. doi:10.3892/ijmm.2016.2483
- Jones, L. L., McDonald, D. A., and Borum, P. R. (2010). Acylcarnitines: role in brain. *Prog. Lipid Res.* 49, 61–75. doi:10.1016/j.plipres.2009.08.004
- Kanehisa, M., Goto, S., Sato, Y., Kawashima, M., Furumichi, M., and Tanabe, M. (2014). Data, information, knowledge and principle: back to metabolism in KEGG. *Nucleic Acids Res.* 42, D199–D205. doi:10.1093/nar/gkt1076
- Liu, F., Sun, Z., Hu, P., Tian, Q., Xu, Z., Li, Z., et al. (2019). Determining the protective effects of Yin-Chen-Hao Tang against acute liver injury induced by carbon tetrachloride using 16S rRNA gene sequencing and LC/MS-based metabolomics. *J. Pharm. Biomed. Anal.* 174, 567–577. doi:10.1016/j.jpba.2019.06.028
- Mais, E., Alolga, R. N., Wang, S. L., Linus, L. O., Yin, X., and Qi, L. W. (2018). A comparative UPLC-Q/TOF-MS-based metabolomics approach for distinguishing Zingiber officinale Roscoe of two geographical origins. *Food Chem.* 240, 239–244. doi:10.1016/j.foodchem.2017.07.106
- McGill, M. R., Li, F., Sharpe, M. R., Williams, C. D., Curry, S. C., Ma, X., et al. (2014). Circulating acylcarnitines as biomarkers of mitochondrial dysfunction after acetaminophen overdose in mice and humans. *Arch. Toxicol.* 88, 391–401. doi:10.1007/s00204-013-1118-1

- Müller, N., and Schwarz, M. J. (2007). The immune-mediated alteration of serotonin and glutamate: towards an integrated view of depression. *Mol. Psychiatry*. 12, 988–1000. doi:10.1038/sj.mp.4002006
- Newgard, C. B. (2017). Metabolomics and metabolic diseases: where do we stand?. *Cell Metab.* 25, 43–56. doi:10.1016/j.cmet.2016.09.018
- Nie, H., An, F., Mei, J., Yang, C., Zhan, Q., and Zhang, Q. (2020). IL-1 β pretreatment improves the efficacy of mesenchymal stem cells on acute liver failure by enhancing CXCR4 expression. *Stem Cells Int.* 2020, 1498315. doi:10.1155/2020/1498315
- Pathania, A., Rawat, A., Dahiya, S. S., Dhanda, S., Barnwal, R. P., Baishya, B., et al. (2020). 1H NMR-based metabolic signatures in the liver and brain in a rat model of hepatic encephalopathy. *J. Proteome Res.* 19, 3668–3679. doi:10.1021/acs.jproteome.0c00165
- Patterson, J., Hussey, H. S., Silal, S., Goddard, L., Setshedi, M., Spearman, W., et al. (2020). Systematic review of the global epidemiology of viral-induced acute liver failure. *BMJ Open* 10, e037473. doi:10.1136/bmjopen-2020-037473
- Platten, M., Nollen, E. A. A., Röhrig, U. F., Fallarino, F., and Opitz, C. A. (2019). Tryptophan metabolism as a common therapeutic target in cancer, neurodegeneration and beyond. *Nat. Rev. Drug Discov.* 18, 379–401. doi:10.1038/s41573-019-0016-5
- Sandor, A., Cseko, J., Kispal, G., and Alkonyi, I. (1990). Surplus acylcarnitines in the plasma of starved rats derive from the liver. *J. Biol. Chem.* 265, 22313–22316. doi:10.1016/s0021-9258(18)45706-7
- Sangster, T., Major, H., Plumb, R., Wilson, A. J., and Wilson, I. D. (2006). A pragmatic and readily implemented quality control strategy for HPLC-MS and GC-MS-based metabolomic analysis. *Analyst*. 131, 1075–1078. doi:10.1039/b604498k
- Sekine, A., and Fukuwatari, T. (2019). Acute liver failure increases kynurenic acid production in rat brain via changes in tryptophan metabolism in the periphery. *Neurosci. Lett.* 701, 14–19. doi:10.1016/j.neulet.2019.02.004
- Smith, C. A., Want, E. J., O'Maille, G., Abagyan, R., and Siuzdak, G. (2006). XCMS: processing mass spectrometry data for metabolite profiling using nonlinear peak alignment, matching, and identification. *Anal. Chem.* 78, 779–787. doi:10.1021/ac051437y
- Tan, G., Zhou, Q., Liu, K., Dong, X., Li, L., Liao, W., et al. (2018). Cross-platform metabolic profiling deciphering the potential targets of Shenfu injection against acute viral myocarditis in mice. *J. Pharm. Biomed. Anal.* 160, 1–11. doi:10.1016/j.jpba.2018.07.042
- Wijdsicks, E. F. (2016). Hepatic encephalopathy. *N. Engl. J. Med.* 375, 1660–1670. doi:10.1056/NEJMra1600561
- Wishart, D. S., Feunang, Y. D., Marcu, A., Guo, A. C., Liang, K., Vázquez-Fresno, R., et al. (2018). HMDB 4.0: the human metabolome database for 2018. *Nucleic Acids Res.* 46, D608–D617. doi:10.1093/nar/gkx1089
- Wu, Z., Kong, X., Zhang, T., Ye, J., Fang, Z., and Yang, X. (2014). Pseudoephedrine/ephedrine shows potent anti-inflammatory activity against TNF- α -mediated acute liver failure induced by lipopolysaccharide/D-galactosamine. *Eur. J. Pharmacol.* 724, 112–121. doi:10.1016/j.ejphar.2013.11.032
- Xia, X., Su, C., Fu, J., Zhang, P., Jiang, X., Xu, D., et al. (2014). Role of α -lipoic acid in LPS/d-GalN induced fulminant hepatic failure in mice: studies on oxidative stress, inflammation and apoptosis. *Int. Immunopharmacol.* 22, 293–302. doi:10.1016/j.intimp.2014.07.008
- Yamada, I., Goto, T., Takeuchi, S., Ohshima, S., Yoneyama, K., and Shibuya, T., et al. (2008). Mao (Ephedra sinica Stapf) protects against D-galactosamine and lipopolysaccharide-induced hepatic failure. *Cytokine*. 41, 293–301. doi:10.1016/j.cyto.2007.12.003
- Yang, D., Wang, X., Wu, Y., Lu, B., Yuan, A., Leon, C., et al. (2015). Urinary metabolomic profiling reveals the effect of shenfu decoction on chronic heart failure in rats. *Molecules* 20, 11915–11929. doi:10.3390/molecules200711915
- Zheng, M., Zhou, H., Wan, H., Chen, Y. L., and He, Y. (2015). Effects of herbal drugs in Mahuang decoction and their main components on intestinal transport characteristics of Ephedra alkaloids evaluated by a Caco-2 cell monolayer model. *J. Ethnopharmacol.* 164, 22–29. doi:10.1016/j.jep.2015.01.043
- Zhong, Z., Mao, S., Lin, H., Li, H., Lin, J., and Lin, J. M. (2019). Alteration of intracellular metabolome in osteosarcoma stem cells revealed by liquid chromatography-tandem mass spectrometry. *Talanta*. 204, 6–12. doi:10.1016/j.talanta.2019.05.088

Conflict of Interest: The authors declare that the research was conducted in the absence of any commercial or financial relationships that could be construed as a potential conflict of interest.

Copyright © 2021 Liao, Jin, Liu, Ruan, Li, Shen, Zhang, Wang, Wu, Zhang, Kang and Wu. This is an open-access article distributed under the terms of the Creative Commons Attribution License (CC BY). The use, distribution or reproduction in other forums is permitted, provided the original author(s) and the copyright owner(s) are credited and that the original publication in this journal is cited, in accordance with accepted academic practice. No use, distribution or reproduction is permitted which does not comply with these terms.



Anti-Inflammatory and Anti-Arthritic Potential of Standardized Extract of *Clerodendrum serratum* (L.) Moon

Raj Kumar Tiwari^{1*}, Silpi Chanda², Udayabanu M³, Manisha Singh⁴ and Shriya Agarwal⁴

¹Pharmacognosy and Phytochemistry, School of Health Sciences, Pharmaceutical Sciences, UPES, Dehradun, India,

²Pharmacognosy and Phytochemistry, IEC School of Pharmacy, IEC University, Solan, India, ³Pharmacology, Department of Biotechnology and Bioinformatics, Jaypee University of Information Technology, Solan, India, ⁴Department of Biotechnology, Centre for Emerging Disease, Jaypee Institute of Information Technology, Noida, India

Aims: Scientific biological evaluation of standardized extracts is becoming one of the central needs for the globalization of customary medication in current times. And to validate the presence of active constituents in crude medicinal extracts, analytical techniques like HPLC and HPTLC are the most suitable authentication systems. In the current study we aimed to standardize and evaluate *Clerodendrum serratum* (L.) Moon (Verbenaceae). For its unique anti-inflammatory and anti-arthritic properties. Evaluation and analysis of the plant, therefore, offers a new platform for the development of the herbal drug and could prove to be a safe and cost effective treatment for arthritis management.

Methods: The aqueous extract of *C. serratum*, a common plant in the Southeastern Asian region, was used for phytochemical investigation and standardization by HPTLC and HPLC. The standardized HPLC method was further validated by using ICH guidelines. The standardized extract was investigated for anti-inflammatory and anti-arthritic activity. Complete Freund's adjuvant (CFA) model was performed to evaluate the activity. Paw diameter, joint diameter, arthritic score, and body weight was accepted as a parameter for the evaluation of biological activity.

Results: HPTLC method revealed the presence of ursolic acid with an R_f value of 0.38 and the amount quantified was 0.03% w/w. The presence of the bioactive phytochemical was further analyzed and confirmed by HPLC for which the validation was done successfully in accordance with ICH guidelines. The assay content for ursolic acid was found to be 0.059% with relative standard deviation (RSD) <2.5% for specificity and precision with spike recovery between 95–110%. The anti-arthritic activity of aqueous extract exhibited COX-2 and TNF- α inhibition as observed in various parameters like paw edema, arthritic index, and joint diameter. Plant extract showed reclamation of arthritis in regard to body weight, arthritic score, paw edema, and joint diameter. The extract showed significant results for TNF- α and COX-2 ($p < 0.0001$). The plant extract also exhibited *in-vitro* anti-inflammatory activity.

Conclusion: The current study established the scientific basis of ethnomedicinal use of the plant for anti-inflammatory purposes and the management of arthritis and can also be used for quality control purposes.

OPEN ACCESS

Edited by:

Sayed Ahmad,
Jamia Hamdard University, India

Reviewed by:

Armando Caceres,
Universidad de San Carlos de
Guatemala, Guatemala

*Correspondence:

Raj Kumar Tiwari
raj_t365@yahoo.com

Specialty section:

This article was submitted to
Ethnopharmacology,
a section of the journal
Frontiers in Pharmacology

Received: 15 November 2020

Accepted: 17 February 2021

Published: 12 April 2021

Citation:

Tiwari RK, Chanda S, M U, Singh M
and Agarwal S (2021) Anti-
Inflammatory and Anti-Arthritic
Potential of Standardized Extract of
Clerodendrum serratum (L.) Moon.
Front. Pharmacol. 12:629607.
doi: 10.3389/fphar.2021.629607

Keywords: anti-inflammatory, ursolic acid, standardization, HPTLC, arthritic, *Clerodendrum serratum*

INTRODUCTION

Arthritis and its associated musculoskeletal imbalances is one of the common afflictions, affecting millions of people and greatly restricting their activities of daily living (Baranwal et al., 2012b). It is a common term used by medical practitioners to describe the progressive inflammatory responses to one or more joint structures due to various causes ranging from traumatic, rheumatic, to degenerative concerns resulting in muscular stiffness and restricted physical movements. Further, arthritis commonly affects persons from all age groups, race, sex, and global regions with more than 100 different types, such as juvenile arthritis, rheumatoid arthritis, ankylosing spondylitis, gout, psoriatic arthritis, and osteoarthritis, the last of which is degenerative. Its clinical features in suffering patients may vary from person to person and range from mild pain and swelling to intense forms like complete/partial joint immobility, muscular atrophy, and contractures (Rho et al., 2009). Subsequently, the drug regime includes administration of non-steroidal anti-inflammatory drugs (NSAIDs) to patients as a first line of treatment but its long term usage has led to certain potential adverse reactions, such as gastroduodenal diseases and renal insufficiency (Harirforoosh and Jamil, 2009), that are probably induced by the inhibition of cyclo-oxygenase for reduction in prostaglandin content. Although various types of treatments are available today, like NSAIDs, corticosteroids, and DMARDs, they are mainly used to treat the symptomatic concerns and do not target the pathological origin like membrane stabilizing, protein denaturation, etc. Moreover, treatment by the above available modes can cause serious hepatic damage, gastric bleeding (Craig and Cappelli, 2019), Hospitalization, and death (Rostom et al., 2005).

Therefore, to surpass all these issues and find a more harmless and equally efficacious therapeutic option, researchers are considering plants as a source of medicine. Initially, these plant-based medicinal systems have formed the foundation of folk or ethno medicines, practiced in India and some other parts of the world like China, Africa, and South America. Later a considerable part of this indigenous knowledge was formulated, documented, and eventually passed into organized systems of medicine such as Ayurveda, Unani Siddha, etc. Traditionally plants were used for various therapeutic claims by tribal communities throughout India (Jain and Singh, 2010; Balasankar et al., 2013; Nayak and Dhal, 2013). In our study we have selected the plant *Clerodendrum serratum* (L.) Moon belonging to the family *Verbenaceae*. This is a deciduous shrub widely distributed in the Western Ghats (Manjunatha, 2004) of India. In Ayurveda, the plant is popularly known as Bharangi (Sanskrit) and customarily called Blue Glory (English). As per the traditional claims, the roots of this plant are a potential source of medicine for ailments such as

allergic disease, body soreness, respiratory illness, infectious disease, dropsy, eye diseases, fever, inflammation, malaria, ophthalmia, rheumatism, snakebite, tuberculosis, ulcers, and wounds (Keshavamurthy, 1994). Studies reported various chemical constituents from the plant, like stigmaterol, bis(2-ethylhexyl) phthalate, hispulidin, serratumin A, acteoside, martynoside, serratumoside-A, myricoside, ursolic acid, spinasterol, spinasteryl- β -D-glucopyranoside etc., in various parts of plant including the stem, root, and aerial part (Singh et al., 2012; Kumar and Nishteswar, 2013; Padal et al., 2013). The current study was focused on its *in-vitro* anti-inflammatory activity and *in-vivo* arthritis activity by using Complete Freund's adjuvant (CFA) induced arthritis model.

MATERIALS AND METHODS

All the chemicals used in the current study were procured from Sigma Aldrich Co., St. Louis, United States. All other chemicals/solvent adopted were of analytical grade.

Collection and Preparation of Extract

Roots of *C. serratum* L. were collected from Faizabad, Uttar Pradesh, India and taxonomical identification was done at the Department of Agronomy, Acharya Narendra Dev Agriculture Technical University, Dist. Faizabad, Uttar Pradesh. The prepared brown colored powdered root (100 g) was extracted (decoction) with water (500 ml) at a temperature not exceeding 110°C for 2 h. The extract was strained and lyophilized. The yield of obtained dried extract was 10% w/w.

Standardization of an Extract

Qualitative Estimation by High-Performance Thin Layer Chromatography

The presence of ursolic acid was identified by performing High-performance thin layer chromatography (HPTLC). The solvent system used for the analysis was toluene: ethyl acetate (8:2 v/v) as a binary mobile phase system. For spot detection, anisaldehyde sulfuric acid was used as the spraying reagent. Standard analytical grade of ursolic acid was used as a reference by dissolving in HPLC grade methanol. The obtained concentration was 1,070 μ g/ml, which was further used for preparing the subsequent working standards. Camag Linomat V HPTLC system (Switzerland) equipped with 100 μ l Camag syringe and scanner III was used for the current qualitative estimation. Sample and standard as narrow bands of a width of 3 mm were applied to precoated silica gel aluminum plate 60F-254.

Quantitative Estimation by High-Performance Thin Layer Chromatography

An isocratic HPLC method was developed and validated for the identification of ursolic acid. A prepacked column, C18

(25 cm × 4.6 mm) 5 µm, with UV detector (210 nm) was used for the current study. The injection volume was 20 µl and its flow rate was maintained at 0.6 ml/min. Run time for standard and sample were 45 min and the data acquisition was done. For HPLC analytical development studies, methanol and acetonitrile (30:70, v/v) were selected as the binary mobile phase system. Before using, it was filtered and degassed. Thereafter, the standard solution was prepared by adding 10 mg of ursolic acid in methanol (10 ml) and subjected for sonication. The solution was settled to room temperature and diluted further with the help of diluent up to the mark.

Then the sample solution was prepared by taking 1.5 g of the test sample in iodine flask and adding 25 ml of water followed by 20 min of sonication. Reflux was done for about 30 min in reflux assembly and filtered. The process was repeated twice and the filtrate was evaporated to dryness. The obtained residue was dissolved in methanol and the volume was made up of 10 ml methanol. A further 0.5 ml of this solution was taken into a 10 ml volumetric flask and diluted with methanol. Injection of equal volumes of the standard solution was done and chromatograms were recorded along with measurement of peak area. The percentage of ursolic acid was calculated by using the formula:

$$\% \text{ of Assay} = \frac{At \times C_s \times P}{As \times C_u}$$

At= Peak area of a test sample, As = Peak area of reference standard, Cs = Concentration of reference standard, Cu = Concentration of test sample, P = Potency of ursolic acid working standard

The developed method was validated according to ICH guidelines (Baranwal et al., 2012a). The parameters adopted for its validation are Linearity, Specificity, Accuracy, Range, Precision, Repeatability, Intermediate precision, Robustness, Limit of Detection, and Limit of Quantification (Manukumar and Umesha, 2015).

Evaluation of Anti-inflammatory Hypotonic Solution-Induced Haemolysis or Membrane-Stabilizing Activity

The evaluation test was performed as per the method reported by Manukumar and Umesha (2015). The extracted sample contains 0.03 ml stock erythrocytes suspension infused with 5 ml hypotonic solution prepared with 154 mM NaCl in 10 mM Sodium Phosphate Buffer at pH 7.4, along with the test sample ranging from 100–500 µg/ml. The blank (without the test samples) and the standard (acetylsalicylic drug) was also treated accordingly. This mixture was incubated at room temperature for 10 min, followed by centrifugation for 10 min at 3,000 rpm. The absorbance of the supernatant was observed spectrophotometrically at 540 nm. The experiment was performed in triplicate. The percentage inhibition of haemolysis was computed by the following formula:

$$\% \text{ inhibition of haemolysis} = 100 \cdot [(A1 - A2/A1)]$$

where: A1 = absorbance of blank; A2 = Absorbance of test and standard sample

Effect of Protein Denaturation

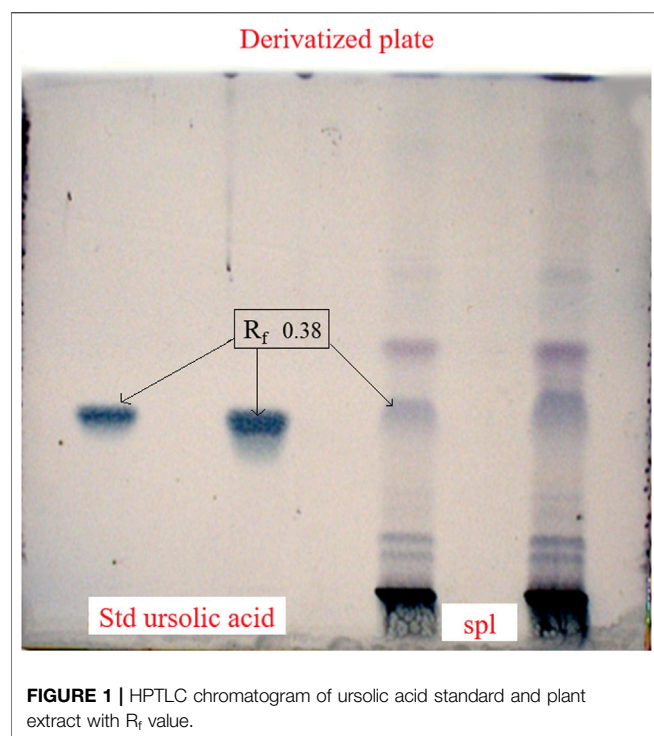
The effect of protein denaturation was performed as per the procedure mentioned below. The concentrations ranging from 100–500 µg/ml for both test sample and standard acetylsalicylic sample with 1 ml of 1 mM egg albumin solution were incubated at 27°C for 15 min. The mixture was further denatured at 70°C in a water bath for 10 min. The samples were allowed to cool down and observed spectrophotometrically at 660 nm. This experiment was performed in triplicate. Percentage inhibition of denaturation was calculated from the control without sample and standard (Badii and Howell, 2002; Chung et al., 2012). The percentage inhibition of denaturation was done by the below-mentioned formula:

$$\% \text{ Inhibition of haemolysis} = 100X[(A1 - A2/A1)]$$

Evaluation of *In-Vivo* Anti-Arthritic Study Complete Freund's Adjuvant Induced Arthritis

For the *in-vivo* anti-arthritic activity, the Complete Freund's Adjuvant (CFA) model was adopted. For this model, Albino Wistar male rats weighing 200 ± 25 g were considered. The oral route of administration was given to rats placed in different cage groups under a controlled temperature of 22 ± 2°C conditions with administration of golden feed diet and water to all the animals regularly. The dose adopted was 100 and 200 mg/kg body weight (b.w.). Paw diameter, joint diameter, arthritic score, and body weight were used as parameters for the activity. The histopathological estimation of TNF-α and COX-2 were also performed as confirmative studies. Institutional Animal Ethics Committee (IAEC) approval (Reg No. 1824/PO/ERe/S/15/CPCSEA) as well as Protocol Approval (Reference No. IAEC/PN-16045) were taken before performing the experiments.

In the current study, animals (6 nos.) were divided into five different groups. Group 1 received vehicle normal saline (10 ml/kg) orally before the 30 min waiting period. To group 2, 0.1 ml of CFA (0.05% *Mycobacterium butyricum* in mineral oil; 10 ml/kg b.w.) and vehicle (10 ml/kg) was injected into the left hind paw (subplantar surface) with the help of a 26 gauge needle. Group 3 received CFA and indomethacin (3 mg/kg b.w.) whereas group 4 and 5 administered samples at a dose of 100 mg/kg b.w. and 200 mg/kg b.w. respectively. For the arthritic evaluations, the paw diameter, joint diameter, arthritic score, and body weight measurements were carried out on the third, seventh, 14th, and 21st days. After completion of the protocol on the 21st day, the blood (terminal) samples were collected and the inflammatory mediators, like TNF-α and COX-2 levels, were estimated from the collected serum using ELISA kit assay for all the assigned groups. The ankle joint tissues were fixed with formalin and preserved for further histopathological studies.



All obtained results were compared and evaluated with the standard (Pincus et al., 2003; Kamal and Baldi, 2015; Ghosh et al., 2016). The statistical analysis was subjected to mean \pm Standard Error Mean (SEM). Differences were considered significant at $p < 0.001$, or $p < 0.01$, or $p < 0.05$ when compared test group vs. control (–ve) group. For numerical results, a one-way analysis of variance (ANOVA) (compare all vs. control) was performed using Graph Pad InStat Version 3 (GraphPad Software).

RESULTS

Qualitative

Estimation by High-Performance Thin Layer Chromatography

The presence of ursolic acid was confirmed by performing the HPTLC from the aqueous extract of *C. serratum* L. using standard ursolic acid. The stabilized HPTLC system produced a compact spot of standard ursolic acid with an R_f value of 0.38. HPTLC chromatogram of ursolic acid standard and plant extract are shown in **Figure 1**. UV scanning for sample (A) and standard (B,C) were graphically presented in **Figures 2A–C**.

Quantitative Estimation by HPLC and Method Validation as per ICH Guidelines

The statistical analysis was performed by plotting the standard ursolic acid concentration and the peak

responded with a straight line of correlation coefficient 0.998. The observed results showed good recovery within 95–110% when spiked with the standard sample at four different concentrations levels. The developed HPLC method was found to provide repeatable results at various concentrations; thus, the developed protocol was found to be reliable. The sample peak purity was confirmed by comparing with the standards of retention time and peak area. The LOD and LOQ were quantified at 33 $\mu\text{g/ml}$ and 0.059% respectively for the ursolic acid of the test sample (extract). The performed analytical development and validation was assured as per the ICH guidelines and graphically presented in **Figure 3** for sample (A) and standard (B).

Evaluation of Anti-inflammatory and Anti-Arthritic

Hypotonic Solution-Induced Haemolysis or Membrane-Stabilizing Activity

Membrane stabilizing activity (8%) at a concentration level of 100 $\mu\text{g/ml}$ was shown in **Figure 4**.

Effect of Protein Denaturation

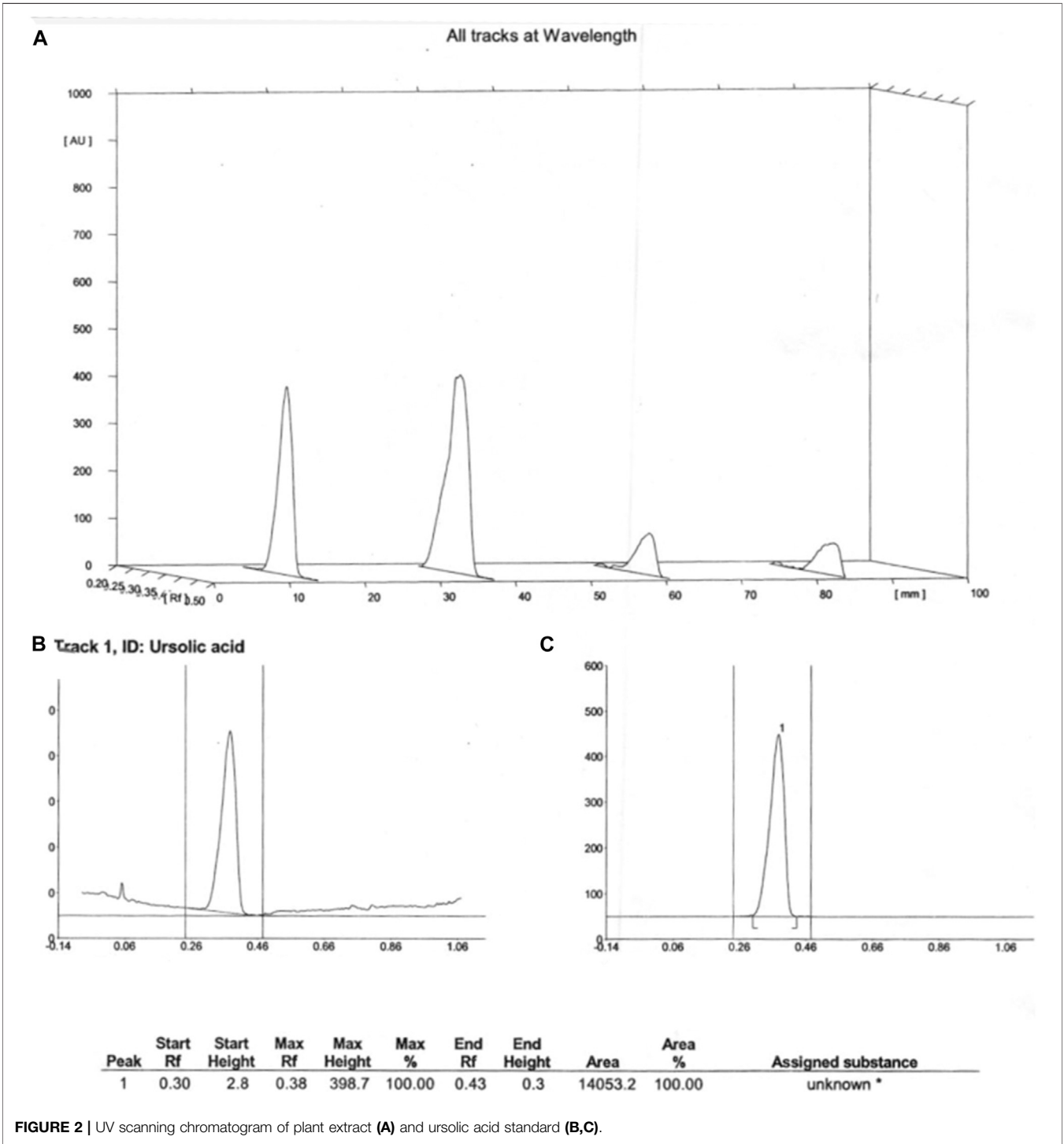
Around 40% of protein denaturation with 100 $\mu\text{g/ml}$ concentration was shown in **Figure 5**.

Evaluation of *In-Vivo* Anti-Arthritic Study

The measured arthritic parameters like paw diameter, joint diameter, arthritic score, and body weight were presented in **Figures 6–9**. Assessment of the blood sample was collected from the terminal parts of the animals. The level of TNF- α and COX-2 was estimated by using ELISA assay (**Figure 10**). The histopathological analysis of ankle joints after 21 days at a dose of 200 mg/kg was shown in **Figure 11**.

DISCUSSION

Arthritis is a persistent disease that equally affects adults and the elderly. Although the prevalence rate ranges between 0.3 and 1% (World Health Organization, 2020), women are mostly affected. As per Sharon et al., (2017), the high arthritis prevalence rate in low to middle-income countries leads to an inability to meet the daily personal as well as social needs. Fundamental endeavors toward prevention and management of arthritis should be prioritized. The majority of the manufactured medicines, like NSAIDs (Ghosh et al., 2016), Glucocorticoids (Joseph et al., 2016), DMARDs (Pincus et al., 2003; Donahue et al., 2008; Luo et al., 2013; Kapoor et al., 2014) and certain biologicals (Banse et al., 2015; Brady et al., 2015; Zengin et al., 2017), target the symptoms but not the etiology of the disease with extreme adverse drug effects, whereas the surgical treatments (Krause and Matteson, 2014) can lead to post-operative complexities with mental unacceptance.



The natural product has a significant impact with fewer side effects and co-morbidities. Natural cures could be used to combat the constraints related with current accessible synthetic treatments. The plant Bharangi is a popular folk medicine used for inflammation, rheumatism, and pain. Specialists are considering utilizing the Bharangu plant to improve the symptoms of arthritis.

The identification of metabolites with proper integration of modern scientific techniques in herbal research is an essential step for the global market and also for reproducible results. Thus, both HPLC and HPTLC analytical methods were used in the current study as the most applicable tools for identification and standardization.

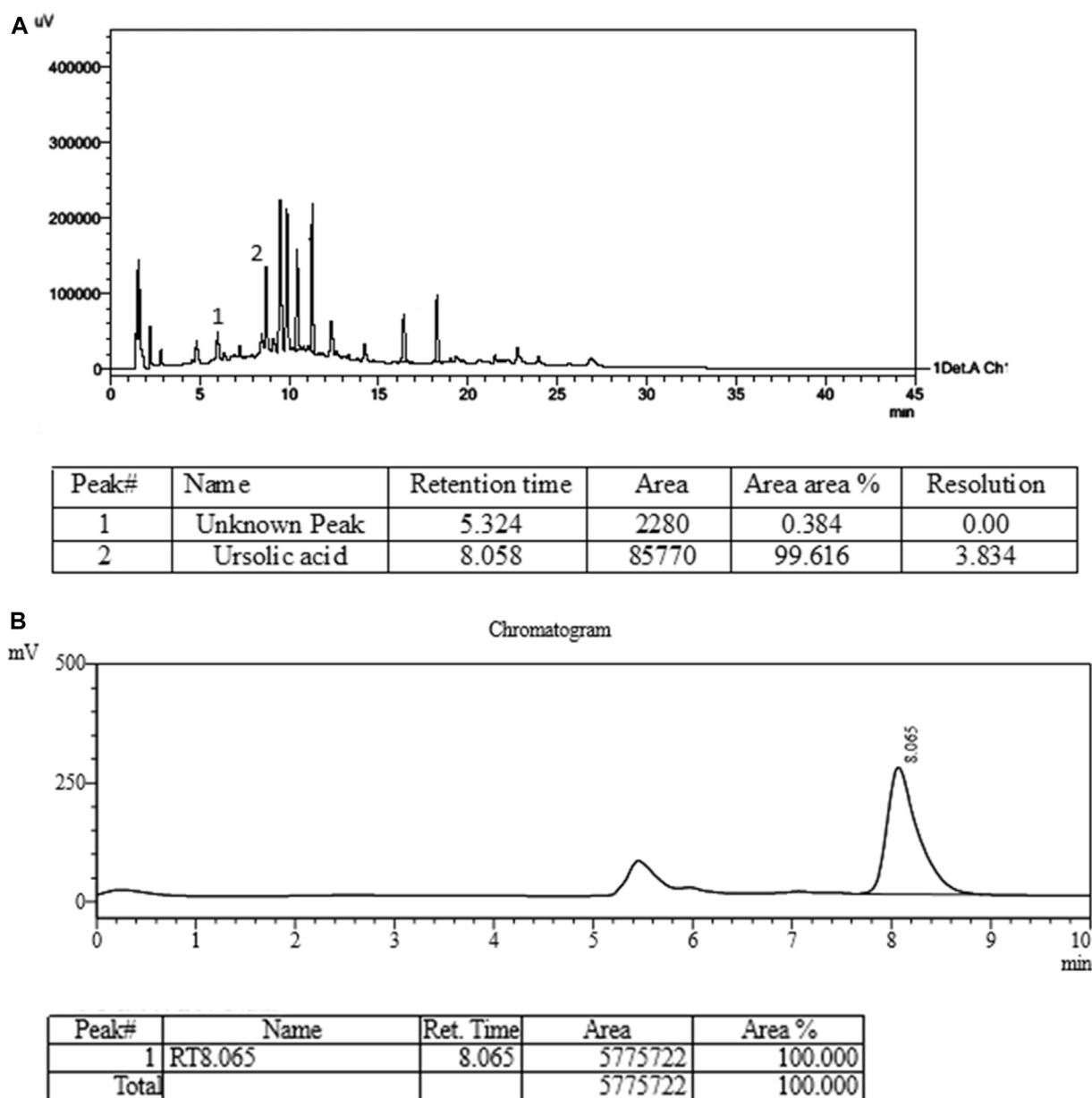


FIGURE 3 | HPLC chromatogram of plant extract (A) and ursolic acid standard (B).

In the current study, we focused on the root as a biological source in Ayurvedic Pharmacopoeia of India. Ursolic acid was identified and quantified by HPTLC and HPLC in the aqueous extract of the root. The developed HPLC method was also validated as per ICH guidelines. Shanmuga et al. (2017) likewise quantified the metabolites apigenin and luteolin by reverse phase high-performance liquid chromatography (RP-HPLC) from its leaf extract (Shanmuga et al., 2017). Followed by its analytical analysis, our study focused on its anti-inflammatory and anti-arthritic activity. In our study, it has been found that the presence of secondary metabolites enhances the stability of the biological membranes when

stressed under lysis conditions, considered to be the preliminary investigation involved during the screening of anti-inflammatory activity. The RBC membrane structurally resembles the lysosomal membrane. The protein denaturation of the anti-arthritic property was successfully evaluated using *in-vitro* assessments. Literature (Krause and Matteson, 2014) also supported the use of ursolic acid in inhibition of the release of proinflammatory cytokines TNF- α , IL-2, and IFN- γ . Studies also revealed the presence of β -sitosterol as an anti-arthritic potential in ethanolic extract of the leaf of the plant. The methanolic extract demonstrated dual inhibitory effects on arachidonic acid metabolism which is responsible for the

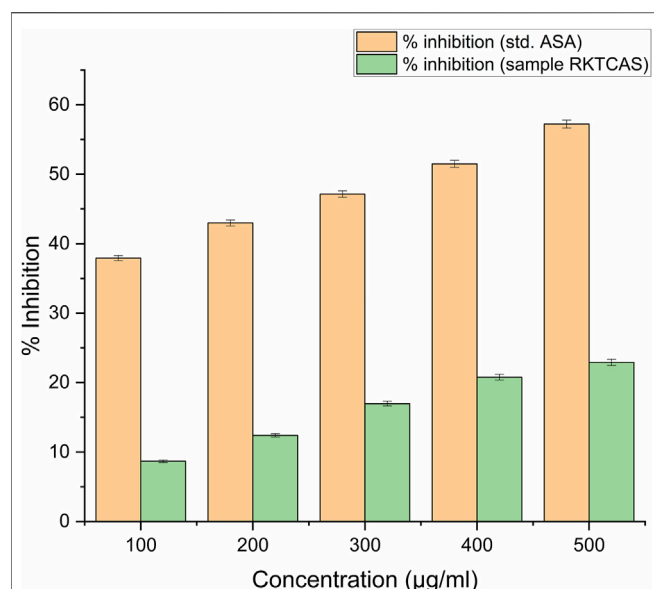


FIGURE 4 | *In-vitro* membrane stabilizing activity showing the possible mechanism of action for the anti-inflammatory activity of aqueous extract of *Clerodendrum serratum* L.

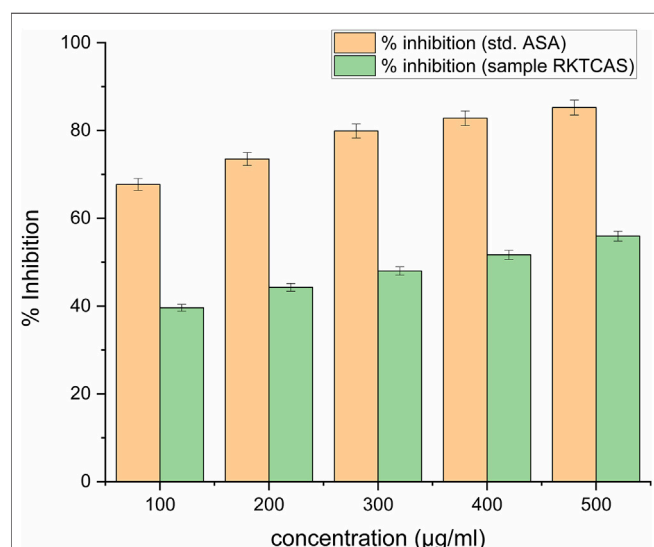


FIGURE 5 | *In-vitro* protein denaturation activity of aqueous extract of *Clerodendrum serratum* L. against protein denaturation using egg albumin.

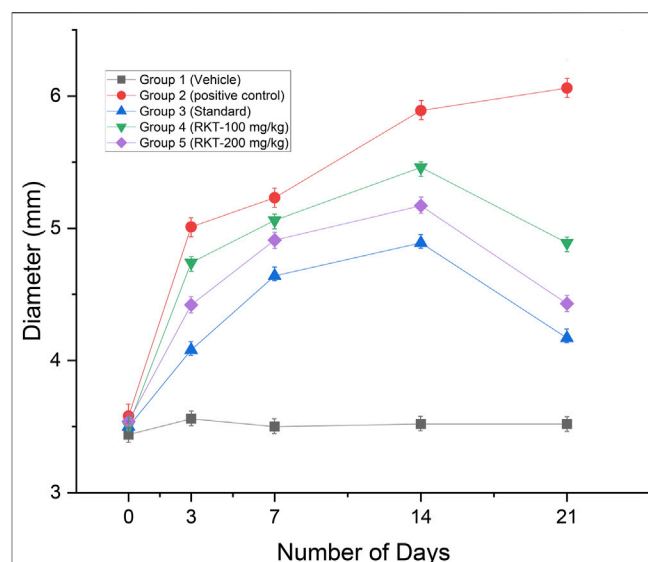


FIGURE 6 | *In-vivo* anti-arthritis activity (Paw diameter in mm) $n = 6$; Data = Mean \pm SEM; ** $p < 0.01$ (G2 Vs G4); *** $p < 0.001$ (G2 vs. G3, G4 and G5).

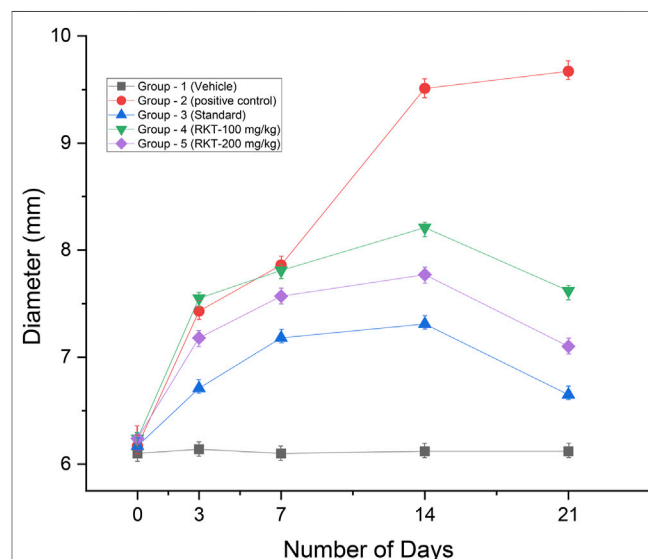


FIGURE 7 | *In-vivo* anti-arthritis activity (joint diameter in mm). All the values are expressed as Mean \pm SEM ($n = 6$) ** $p < 0.01$ (G2 vs. G4); *** $p < 0.001$ (G2 vs. G3, G4 and G5).

inhibition of the synthesis of inflammatory mediators released through cyclooxygenase and lipoxygenase pathways (Cargnin and Gnoatto, 2017). Patel et al. (2014) revealed the presence of Apigenin-7-glucoside which further confirmed its anti-inflammatory effects and also claimed pain relief to knee osteoarthritis patients in a randomized controlled clinical trial study (Shoara et al., 2015). Thus the presence of phytochemicals like ursolic acid, flavonoid, apigenin, and β -sitosterol strongly

support the traditional use and potentiality of *C. Serratum* as an anti-inflammatory and anti-arthritis.

CONCLUSION

The current study showed that the extract possesses both anti-inflammatory and anti-arthritis activities. The possible mode of action of the anti-arthritis activity of the aqueous extract of *C.*

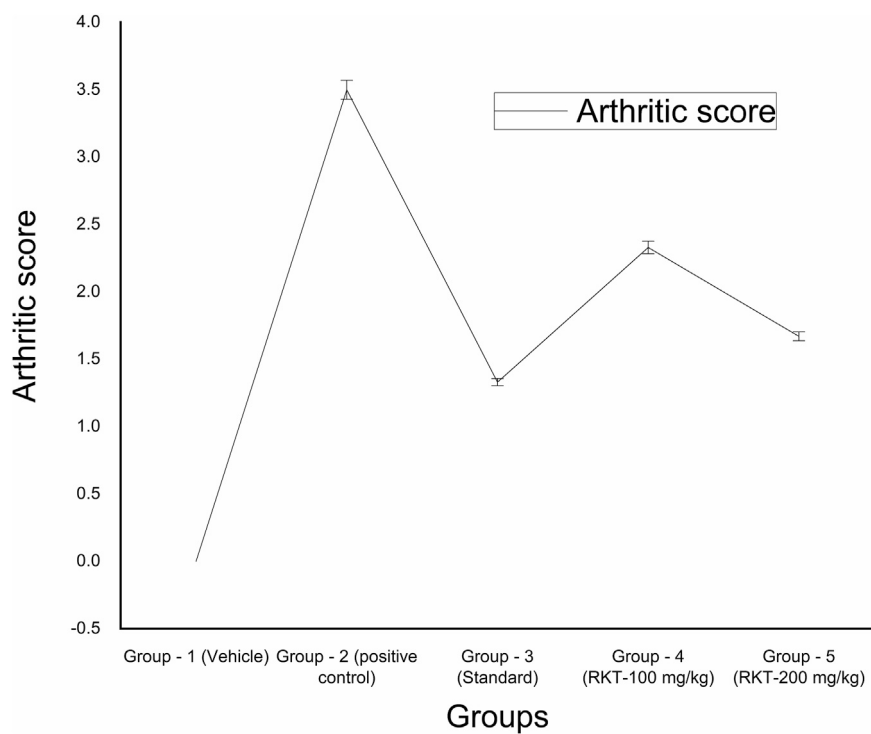


FIGURE 8 | *In-vivo* anti-arthritic activity (arthritic score). All the values are expressed as Mean ± SEM ($n = 6$) * $p < 0.05$ (G2 vs. G4); *** $p < 0.001$ (G2 vs. G3 and G5).

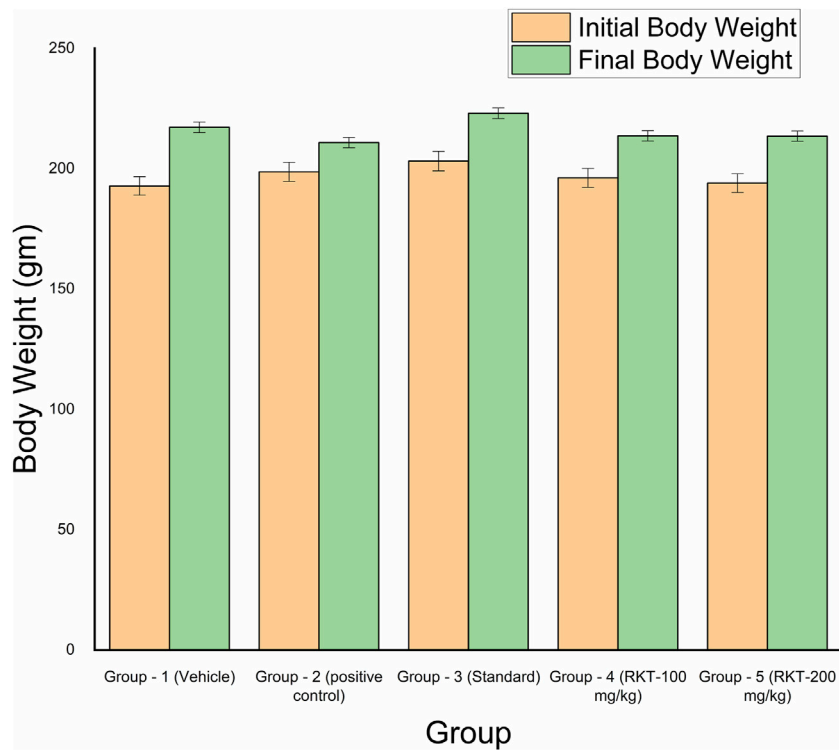


FIGURE 9 | *In-vivo* anti-arthritic activity (bodyweight in gm).

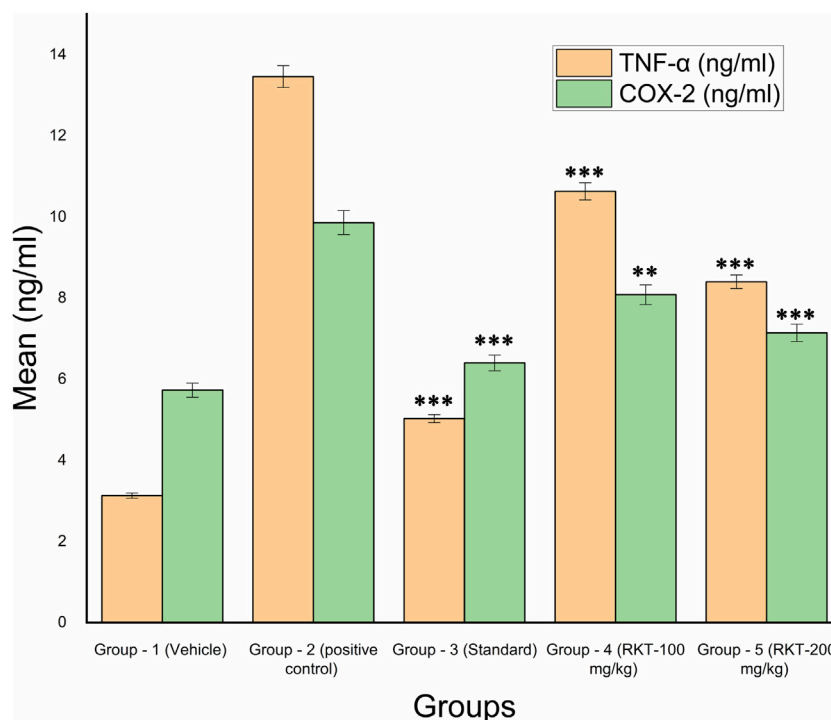


FIGURE 10 | *In-vivo* TNF- α and COX-2 Estimation. All the values are expressed as Mean \pm SEM ($n = 6$) *** $p < 0.001$ (G2 vs. G3, G4 and G5) For COX 2: ** $p < 0.01$ (G2 vs. G4); *** $p < 0.001$ (G2 Vs G3 and G5).

HISTOLOGY (Joint Tissue)

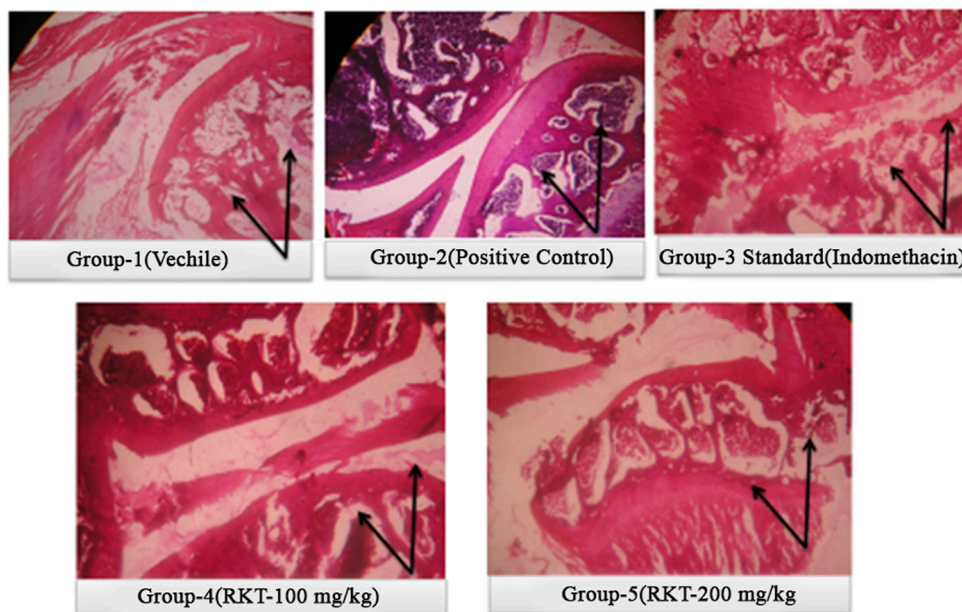


FIGURE 11 | Histopathological study of ankle joint at 21 days of treatment after Complete Freund's adjuvant (CFA) injection.

serratum may be mediated by the inhibition of COX-2 and TNF- α . Based on the results, anti-arthritic activity may be due to shielding of a synovial membrane, obstruction of cartilage destruction, and inhibition of vascular permeability. Through our intensive efforts and thorough research, the results confirmed to show favorable arthritis restoration using arthritis parameters and histopathological observations from the selected plant *C. serratum*. The developed HPTLC and HPLC method could be used as an analytical tool for its quality control purpose.

DATA AVAILABILITY STATEMENT

The original contributions presented in the study are included in the article/Supplementary Material, further inquiries can be directed to the corresponding author.

REFERENCES

- Badii, F., and Howell, N. K. (2002). Effect of antioxidants, citrate, and cryoprotectants on protein denaturation and texture of frozen cod (*Gadus morhua*). *J. Agric. Food Chem.* 50 (7), 2053–2061. doi:10.1021/jf010824f
- Balasankar, D., Vanilarasu, K., Preetha, P. S., Umadevi, S. R. M., and Bhowmik, D. (2013). Journal of medicinal plants studies. *J. Med. Plants* 1 (3), 191–200.
- Banase, C., Benhamou, Y., Lequerré, T., Le Cam-Duchez, V., Lévesque, H., and Vittecoq, O. (2015). Acquired hemophilia possibly induced by etanercept in a patient with rheumatoid arthritis. *Joint Bone Spine* 82 (3), 200–202. doi:10.1016/j.jbspin.2014.12.003
- Baranwal, V. K., Irchhaiya, R., and Alok, S. (2012a). Anti-arthritic activity of some indigenous plants: a review. *Int. J. Pharm. Sci. Res.* 3 (4), 981. doi:10.13040/IJPSR.0975-8232.3(4).981-86
- Baranwal, V. K., Irchhaiya, R., and Alok, S. (2012b). Antiarthritic activity of some indigenous plants. *Res. J. Pharmacogn. Phytochem.* 4 (3), 152–157.
- Brady, B. L., Tkacz, J. P., Lofland, J., Meyer, R., and Bolge, S. C. (2015). Prescribing patterns of intravenous golimumab for rheumatoid arthritis. *Clin. Ther.* 37 (9), 2028–2036. doi:10.1016/j.clinthera.2015.06.017
- Cargnin, S. T., and Gnoatto, S. B. (2017). Ursolic acid from apple pomace and traditional plants: a valuable triterpenoid with functional properties. *Food Chem.* 220, 477–489. doi:10.1016/j.foodchem.2016.10.029
- Chung, J.-I., Barua, S., Choi, B. H., Min, B.-H., Han, H. C., and Baik, E. J. (2012). Anti-inflammatory effect of low intensity ultrasound (LIUS) on complete Freund's adjuvant-induced arthritis synovium. *Osteoarthritis Cartil.* 20 (4), 314–322. doi:10.1016/j.joca.2012.01.005
- Craig, E., and Cappelli, L. C. (2019). Gastrointestinal and hepatic disease in rheumatoid arthritis. *Rheum. Dis. Clin. North. Am.* 44, 89–111. doi:10.1016/j.rdc.2017.09.005
- Donahue, K. E., Gartlehner, G., Jonas, D. E., Lux, L. J., Thieda, P., Jonas, B. L., et al. (2008). Systematic review: comparative effectiveness and harms of disease-modifying medications for rheumatoid arthritis. *Ann. Intern. Med.* 148 (2), 124–134. doi:10.7326/0003-4819-148-2-200801150-00192
- Ghosh, R., Hwang, S. M., Cui, Z., Gilda, J. E., and Gomes, A. V. (2016). Different effects of the nonsteroidal anti-inflammatory drugs meclofenamate sodium and naproxen sodium on proteasome activity in cardiac cells. *J. Mol. Cell. Cardiol.* 94, 131–144. doi:10.1016/j.yjmcc.2016.03.016
- Harirforoosh, S., and Jamali, F. (2009). Renal adverse effects of nonsteroidal anti-inflammatory drugs. *Expert Opin. Drug Saf.* 8 (6), 669–681. doi:10.1517/14740330903311023
- Jain, S., and Singh, J. (2010). Traditional medicinal practices among the tribal people of Raigarh (Chhatisgarh), India. *Indian J. Nat. Prod. Resour.* 1 (1), 109–115.
- Joseph, R. M., Hunter, A. L., Ray, D. W., and Dixon, W. G. (2016). Systemic glucocorticoid therapy and adrenal insufficiency in adults: a systematic review. *Semin. Arthritis Rheum.* 46, 133–141. doi:10.1016/j.semarthrit.2016.03.001

ETHICS STATEMENT

The animal study was reviewed and approved by the Institutional Animal Ethics Committee (IAEC) (Reg No. 1824/PO/ERE/S/15/CPCSEA; Protocol Approval Reference No. IAEC/PN-16045).

AUTHOR CONTRIBUTIONS

Conceived and design the experiment : RT and UM Conduct experiment : RT, SC, MS and SA Writing of Manuscript : RT, SC, UM and MS Analysis the statistical data and interpretation : RT, SC, UM Manuscript Approval : All authors approved the manuscript.

- Kamal, J., and Baldi, A. (2015). Approaches to overcome NSAID induced ulceration in arthritic pain management: perspectives and prospects. *J. Drug Deliv. Ther.* 5 (2), 9–16. doi:10.22270/jddt.v5i2.1069
- Kapoor, B., Singh, S. K., Gulati, M., Gupta, R., and Vaidya, Y. (2014). Application of liposomes in treatment of rheumatoid arthritis: quo vadis. *Sci. World J.* 2014, 1–17. doi:10.1155/2014/978351
- Keshavamurthy, K. (1994). *Medicinal plants of Karnataka*. Bangalore, India: Karnataka Forest Department, 223–224.
- Krause, M. L., and Matteson, E. L. (2014). Perioperative management of the patient with rheumatoid arthritis. *WJO* 5 (3), 283. doi:10.5312/wjo.v5.i3.283
- Kumar, P., and Nishteswar, K. (2013). Phytochemical and pharmacological profiles of *Clerodendrum serratum* linn. (bharngi): a review. *Int. J. Res. Ayurveda Pharm.* 4 (2), 276–278. doi:10.7897/2277-4343.04239
- Luo, Q., Sun, Y., Liu, W., Qian, C., Jin, B., Tao, F., et al. (2013). A novel disease-modifying antirheumatic drug, iguratimod, ameliorates murine arthritis by blocking IL-17 signaling, distinct from methotrexate and leflunomide. *J. Immunol.* 191 (10), 4969–4978. doi:10.4049/jimmunol.1300832
- Manjunatha, B. K. (2004). *Flora of davanagere district*. Karnataka, India: Daya Books.
- Manukumar, H. M. G., and Umesha, S. (2015). Assessment of membrane stabilizing activity from honey. an *in-vitro* approach. *Acta Sci. Pol. Technol. Aliment.* 14 (1), 85–90. doi:10.17306/j.ajs.2015.1.10
- Nayak, C. S. R., and Dhal, N. (2013). 2. Ethnomedicine and magico-religious beliefs of the kondh tribe in boudh district of Odisha India by CR Sahu, RK Nayak and NK Dhal. *Life Sci. leaflets* 45, 10–22.
- Padal, S., Raju, J. B., and Chandrasekhar, P. (2013). Traditional knowledge of konda dora tribes, visakhapatnam district, Andhra Pradesh, India. *IOSR J. Pharm.* 3 (4), 22–28. doi:10.9790/3013-034202228
- Patel, J. J., Acharya, S. R., and Acharya, N. S. (2014). *Clerodendrum serratum* (L.) Moon.—a review on traditional uses, phytochemistry and pharmacological activities. *J. ethnopharmacol.* 154 (2), 268–285. doi:10.1016/j.jep.2014.03.071
- Pincus, T., Yazici, Y., Sokka, T., Aletaha, D., and Smolen, J. S. (2003). Methotrexate as the “anchor drug” for the treatment of early rheumatoid arthritis. *Clin. Exp. Rheumatol.* 21 (5), S179–S185.
- Rho, Y. H., Oeser, A., Chung, C. P., Milne, G. L., and Stein, C. M. (2009). Drugs used in the treatment of rheumatoid arthritis: relationship between current use and cardiovascular risk factors. *Arch. Drug Inf.* 2 (2), 34–40. doi:10.1111/j.1753-5174.2009.00019.x
- Rostom, A., Goldkind, L., and Laine, L. (2005). Nonsteroidal anti-inflammatory drugs and hepatic toxicity: a systematic review of randomized controlled trials in arthritis patients. *Clin. Gastroenterol. Hepatol.* 3 (5), 489–498. doi:10.1016/s1542-3565(04)00777-3
- Shanmuga, S. R., Babitha, K. V., Varghese, Li., and Mahadevan, N. (2017). Development and validation of RP-HPLC method for simultaneous determination of apigenin and luteolin in ethanol extract of *Clerodendrum serratum* (Linn.) leaves. *Asian J. Appl. Sci.* 5, 1–5. doi:10.1155/2015/503139
- Sharon, S. L., Cook, S., Leech, M. T., Bowe, S. J., Kowal, P., Naidoo, N., et al. (2017). Prevalence of arthritis according to age, sex and socioeconomic status in six low

- and middle income countries: analysis of data from the World Health Organization study on global AGEing and adult health (SAGE) wave 1. *BMC Musculoskelet. Disord.* 18, 271. doi:10.1186/s12891-017-1624-z
- Shoara, R., Hashempur, M. H., Ashraf, A., Salehi, A., Dehshahri, S., and Habibagahi, Z. (2015). Efficacy and safety of topical *Matricaria chamomilla* L. (chamomile) oil for knee osteoarthritis: a randomized controlled clinical trial. *Complement. Ther. Clin. Pract.* 21 (3), 181–187. doi:10.1016/j.ctcp.2015.06.003
- Singh, M. K., Khare, G., Iyer, S. K., Sharwan, G., and Tripathi, D. (2012). *Clerodendrum serratum*: a clinical approach. *J. Appl. Pharm. Sci.* 2 (2), 11–15. doi:10.7324/japs.2012.2513
- World Health Organization (2020). Chronic disease and health promotion. Available at: <https://www.who.int/chp/topics/rheumatic/en/#:~:text=Worldwide%20estimates%20are%20that%209.6,major%20daily%20activities%20of%20life> (Accessed November 15, 2020).
- Zengin, O., Onder, M. E., Alkan, S., Kimyon, G., Hüseyinova, N., Demir, Z. H., et al. (2017). Three cases of anti-TNF induced myositis and literature review. *Rev. Bras. Reumatol. Engl. Ed.* 57 (6), 590–595. doi:10.1016/j.rbre.2016.05.003

Conflict of Interest: The authors declare that the research was conducted in the absence of any commercial or financial relationships that could be construed as a potential conflict of interest.

Copyright © 2021 Tiwari, Chanda, M, Singh and Agarwal. This is an open-access article distributed under the terms of the Creative Commons Attribution License (CC BY). The use, distribution or reproduction in other forums is permitted, provided the original author(s) and the copyright owner(s) are credited and that the original publication in this journal is cited, in accordance with accepted academic practice. No use, distribution or reproduction is permitted which does not comply with these terms.



Pharmacological Evaluation of Safoof-e-Pathar Phori- A Polyherbal Unani Formulation for Urolithiasis

Wasim Ahmad^{1,2*}, Mohammad Ahmed Khan³, Kamran Ashraf⁴, Ayaz Ahmad¹, Mohammad Daud Ali¹, Mohd Nazam Ansari⁵, YT Kamal⁶, Shadma Wahab⁶, SM Arif Zaidi⁷, Mohd. Mujeeb² and Sayeed Ahmad²

¹Department of Pharmacy, Mohammed Al-Mana College for Medical Sciences, Dammam-34222, Saudi Arabia, ²Bioactive Natural Product Laboratory, Department of Pharmacognosy and Phytochemistry, School of Pharmaceutical Education and Research, Jamia Hamdard, India, ³Department of Pharmacology, School of Pharmaceutical Education and Research, Jamia Hamdard, India, ⁴Faculty of Pharmacy, Universiti Teknologi MARA (UiTM), Cawangan Selangor, Kampus Puncak Alam, Selangor Darul Ehsan, Malaysia, ⁵Department of Pharmacology and Toxicology, College of Pharmacy, Prince Sattam Bin Abdulaziz University, Alkharj, Saudi Arabia, ⁶Department of Pharmacognosy, College of Pharmacy, King Khalid University, Abha, Saudi Arabia, ⁷Department of Surgery, School of Unani Medical Education and Research, Jamia Hamdard, India

OPEN ACCESS

Edited by:

Ismail Laher,
University of British Columbia, Canada

Reviewed by:

Showkat Ganie,
University of Kashmir, India
Aslam Khan,
King Saud bin Abdulaziz University for
Health Sciences, Saudi Arabia

*Correspondence:

Wasim Ahmad
wasimahmadansari@yahoo.com

Specialty section:

This article was submitted to
Ethnopharmacology,
a section of the journal
Frontiers in Pharmacology

Received: 23 August 2020

Accepted: 24 February 2021

Published: 14 April 2021

Citation:

Ahmad W, Khan MA, Ashraf K, Ahmad A, Daud Ali M, Ansari MN, Kamal YT, Wahab S, Zaidi SMA, Mujeeb M and Ahmad S (2021) Pharmacological Evaluation of Safoof-e-Pathar Phori- A Polyherbal Unani Formulation for Urolithiasis. *Front. Pharmacol.* 12:597990. doi: 10.3389/fphar.2021.597990

Safoof-e-Pathar phori (SPP) is an Unani poly-herbomineral formulation, which has for a long time been used as a medicine due to its antiurolithiatic activity, as per the Unani Pharmacopoeia. This powder formulation is prepared using six different plant/mineral constituents. In this study, we explored the antiurolithiatic and antioxidant potentials of SPP (at 700 and 1,000 mg/kg) in albino Wistar rats with urolithiasis induced by 0.75% ethylene glycol (EG) and 1% ammonium chloride (AC). Long-term oral toxicity studies were performed according to the Organization for Economic Co-operation and Development (OECD) guidelines for 90 days at an oral dose of 700 mg/kg of SPP. The EG urolithiatic toxicant group had significantly higher levels of urinary calcium, serum creatinine, blood urea, and tissue lipid peroxidation and significantly ($p < 0.001$ vs control) lower levels of urinary sodium and potassium than the normal control group. Histopathological examination revealed the presence of refractile crystals in the tubular epithelial cell and damage to proximal tubular epithelium in the toxicant group but not in the SPP treatment groups. Treatment of SPP at 700 and 1,000 mg/kg significantly ($p < 0.001$ vs toxicant) lowered urinary calcium, serum creatinine, blood urea, and lipid peroxidation in urolithiatic rats, 21 days after induction of urolithiasis compared to the toxicant group. A long-term oral toxicity study revealed the normal growth of animals without any significant change in hematological, hepatic, and renal parameters; there was no evidence of abnormal histology of the heart, kidney, liver, spleen, or stomach tissues. These results suggest the usefulness of SPP as an antiurolithiatic and an antioxidant agent, and long-term daily oral consumption of SPP was found to be safe in albino Wistar rats for up to 3 months. Thus, SPP may be safe for clinical use as an antiurolithiatic formulation.

Keywords: Urolithiasis, antioxidant, ethylene glycol, ammonium chloride, safoof-e-pathar phori, long term oral toxicity

INTRODUCTION

Urolithiasis is the formation of a stone in the kidney, and it is the most common medical problem in humans. Kidney stones have been reported even before 4000 BC in Egyptian mummies and in remains of old North American Indians dating back to 1,500–1000 BC (Patankar et al., 2008). Kidney stones affect up to 5% of the population, with a lifetime risk of passing a kidney stone in approximately 8–10% of the population (Asplin et al., 1996). Presumably, nearly 12% of the global population is affected by kidney stones, with a higher recurrence rate in males than in females (70–80% vs 47–60%) (Soundararajan et al., 2006).

Urolithiasis is a complex process because stones can originate in any part of the urinary tract and kidney, leading to a deficiency of various vitamins and hormones in the body. The frequency of stones in men is twice as high compared to women, and the prevalence is highest among men aged between 30 and 35 years and among women aged between 35 and 55 years (Sutherland et al., 1985; Srinivas et al., 2012). Kidney stone formation or urolithiasis is a complex process that arises due to differences among promoters and inhibitors in the kidneys (Sathish et al., 2010). Factors affecting stone formation are urinary output (hence, the concentration), concentration of a particular component, urinary pH, and infection or injury within the urinary tract (Michell et al., 1989).

Stones are made up of various components. The first step in the formation of any stone is the supersaturation of urine (Chandhoke, 2002). Calcium oxalate (CaOx) is the principal constituent of most stones, accounting for more than 80% of stones (Moe, 2006), and the remaining 20% of the stone comprises struvite, cystine, uric acid, and other stones (Park and Pearle, 2007). As mentioned, calcium stone formation is caused by supersaturation of the urine with calcium salts forming a stone. Metabolic irregularities such as hypercalciuria, hypocitraturia, hyperoxaluria, hyperuricosuria, and gouty diathesis can change the composition or saturation of urine, increasing the risk of stone formation. Urolithiasis requires preventive and curative therapies because of its high recurrence rate.

Presently, no suitable drugs are available in modern medicine for the prevention and management of kidney stones. Thiazide diuretics and alkali citrate, the most effective hypocalciuric agents, are used to prevent kidney stone formation; however, no allopathic medicine is available for the dissolution or expulsion of the kidney stone (Ikshait et al., 2017). Treatment and management of renal stones relies on surgical techniques, such as extracorporeal shock wave lithotripsy, percutaneous lithotripsy, and transureteral lithotripsy (Mandavia et al., 2013; Mina et al., 2018). These surgeries are complex and expensive and do not affect the recurrence of stones. However, they cause adverse effects including tubular necrosis (Ikshait et al., 2017), hypertension, hemorrhage, and subsequent fibrosis of the kidney (Hardik et al., 2016), which cause cell injury and reappearance of the renal stone (Kaur et al., 2009).

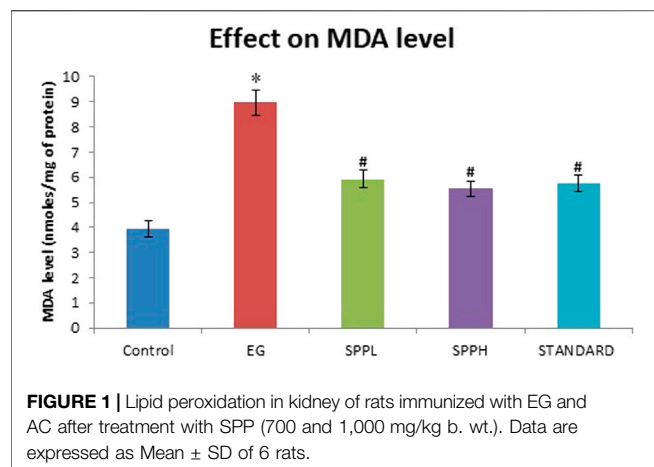
Medicine obtained from herbal sources is a substitute and last resort drug for the prevention and treatment of kidney stones. Several medicinal plants have been used because of their curative

and preventive properties against urinary calculi, for example, *Didymocarpus pedicellatus* R. Br (leaf) (Ahmad et al., 2014; Khaling et al., 2014), *Tribulus terrestris* L (fruit and leaves), *Solanum virginianum* L (fruit) (Kumar and Pandey, 2014), and Gokhsuradi churan (an ayurvedic formulation) are commonly and frequently used in traditional medicine in India (Srinivasa et al., 2013).

Traditional medicine provides several alternatives for modern invasive operational treatments in allopathy, for instance, the use of Safoof-e-Pathar phori (SPP) in the treatment of urolithiasis (Anonymous, 1986; Ahmad et al., 2016). SPP, for the treatment of urolithiasis, has been used for a long time in the Unani system of medicine and has been found to be a clinically sound medicine.

In the Unani system of medicine, powdered drugs are termed ‘Safoof’. Safoof is an important class of Unani medicinal preparations, which are obtained by powdering and mixing herbs, metals, minerals, and animal products (Dubey et al., 2008). SPP is an Unani poly-herbomineral formulation, and has been used as a medicine for a long time because of its antiurolithiatic activity, as per Unani Pharmacopoeia (Anonymous, 1986). This powder formulation is prepared using plant and mineral constituents such as *Didymocarpus pedicellatus* R. Br (Gesneriaceae) (Anonymous, 2006; Ahmad et al., 2014; Ahmad et al., 2017), *Macrotyloma biflorum* var. *biflorum* (Leguminosae) (Anonymous, 2007a), *Rheum webbianum* Royle (Polygonaceae) (Anonymous, 2007b; Ahmad W. et al., 2014), *Raphanus raphanistrum* subsp. *sativus* (L.) Domin (Brassicaceae), *Hordeum vulgare* Linn (Poaceae), and potassium nitrate (Ahmad et al., 2013; Ahmad W. et al., 2014; Zaidi and Ahmed, 2016).

Ahmad et al. (2016) reported extensive quality control analysis of SPP for the first time, which comprised phytochemical and physicochemical analyses, high-performance thin-layer chromatography (HPTLC), high-performance liquid chromatography (HPLC), and gas-chromatography coupled to mass spectrometry (GC-MS) fingerprinting profiles, to check the authenticity and to determine the adulterants in this traditional formulation. Quantitative estimation of marker compounds such as emodin (C₁₅H₁₀O₅; 98% purity), chrysophanic acid (C₁₅H₁₀O₄; 98% purity), and alpha-humulene (96% purity) in SPP has been performed using various analytical techniques such as HPTLC, HPLC photodiode array detector, ultra-performance liquid chromatography coupled with quadrupole time-of-flight mass spectrometry, and GC-MS (Ahmad W. et al., 2014; Ahmad et al., 2015; Ahmad et al., 2016; Ahmad et al., 2019). Additionally, a quality control analysis of individual constituents of SPP (*Didymocarpus pedicellatus* R. Br, *Macrotyloma biflorum* var. *biflorum*, and *Rheum webbianum* Royle) has been reported (Ahmad et al., 2010; Ahmad et al., 2013; Ahmad W. et al., 2014; Ahmad et al., 2017). Ahmad et al. (2020) reported a comprehensive quality assessment method consisting of HPTLC, HPLC, and GC-MS comparative fingerprinting profiles for SPP and its constituents, using extracts in petroleum ether, chloroform, methanol, and hexane to provide further chemical information. This method can be used for the identification of crude drugs present in other herbal formulations. HPTLC fingerprint profiles of petroleum ether, chloroform, and



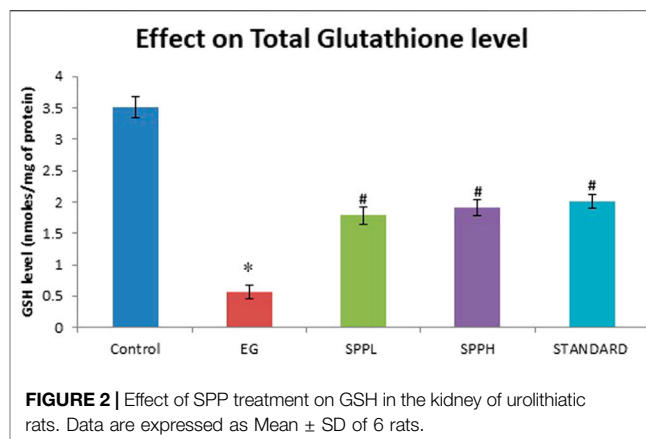
methanol extracts displayed different bands at different wavelengths for SPP and its constituents. Various solvent systems, chemical compositions, and chromatograms are reported by Ahmad et al. (2020). The HPLC finger print profile data showed the presence of 23, 14, 10, and 13 compounds was detected in methanolic extracts of SPP, *Didymocarpous pedicellatus* R. Br., *Macrotyloma biflorum* var. *biflorum*, and *Rheum webbianum* Royle, respectively, whereas the GC-MS fingerprint profile demonstrated the presence of 22, 51, 28, and 16 metabolites in hexane extracts of SPP, *Didymocarpous pedicellatus* R. Br., *Macrotyloma biflorum* var. *biflorum*, and *Rheum webbianum* Royle, respectively, which were identified by reviewing NIST and Wiley libraries on the basis of m/z (Ahmad et al., 2020). The formulation and composition used in this study are similar to those described by Ahmad et al. (2020).

To the best of our knowledge, no published scientific evidence is available to prove the effectiveness of SPP in urolithiasis. Hence, this study aimed to investigate phytochemical-based lithotriptic activity of SPP. In addition to investigating the therapeutic effects, obtaining comprehensive toxicological information on SPP is essential to ensure safety upon use, mainly for long-term use. Therefore, this study was conducted to evaluate the effect of SPP [same formulation as used by Ahmad et al. (2014), Ahmad W. et al. (2014), Ahmad et al. (2015), Ahmad et al. (2016), Ahmad et al. (2019), Ahmad et al. (2020)] on urolithiasis induced by ethylene glycol (EG) and ammonium chloride (AC) in albino Wistar rats and its long-term oral toxicity.

MATERIAL AND METHODS

Plant Material

Crude drugs such as *R. webbianum* Royle, *D. pedicellatus* R. Br. and *M. biflorum* var. *biflorum* were collected from the local drug market in Khari Baoli, New Delhi, and taxonomic authentication was performed by Dr. H. B. Singh, Ref. NISCAIR/RHMD/1327/129, New Delhi.



Method of Safoof-e-Pathar Phori Preparation

SPP was prepared as per the process described in Qarabadeen Majeedi. For the 100 g unit formula for SPP preparation, finely powdered plant drugs: *Didymocarpous pedicellatus* R. Br. 50 g, *Macrotyloma biflorum* var. *biflorum* 12.5 g, *Rheum webbianum* Royle 12.5 g, salts: *Hordeum vulgare* Linn. 12.5g, *Raphanus raphanistrum subsp. sativus* (L.), Domin 6.25 g, and potassium nitrate 6.25 g were mixed properly and passed through mesh # 60 to obtain a uniform powder (Table 1). This formulation was prepared in the bioactive natural product laboratory, Jamia Hamdard, New Delhi, and a voucher specimen was submitted to the lab BNPL/SPP/02/2010. The same formulation and composition were used by Ahmad et al. (2014), Ahmad W. et al. (2014), Ahmed et al. (2015), Ahmed et al. (2019), Ahmed et al. (2020).

Chemicals and Apparatus

Biochemical kits for the estimation of calcium, sodium, and potassium were purchased from Span Diagnostics Ltd, Surat, India. All the chemicals were purchased from Sigma Chemicals Co., St Louis, United States, and Hi-media, Mumbai. Apparatus including metabolic cages (INCO, Ambala, India), refrigerated research centrifuge (Remi centrifuge instrument, Mumbai), and UV-spectrometer (model UV 1800; Shimadzu, Japan) were used in the study.

Experimental Animals

Male albino Wistar rats (body weight range 180–220 g) were used for the pharmacological (antiurolithiatic and antioxidant activities) studies, and healthy young adult male and female albino Wistar rats (weighing 125–160 g) were used for the long-term oral toxicity studies. Females were nulliparous and non-pregnant. Animals were procured from the central animal house facility of Jamia Hamdard. The study protocol was approved by the Institutional Animal Ethics Committee (Registration Number 173/CPCSEA and Approval Number 691) following guidelines of the Committee for the Purpose of Control and Supervision of Experiments on Animals (CPCSEA), Government of India.

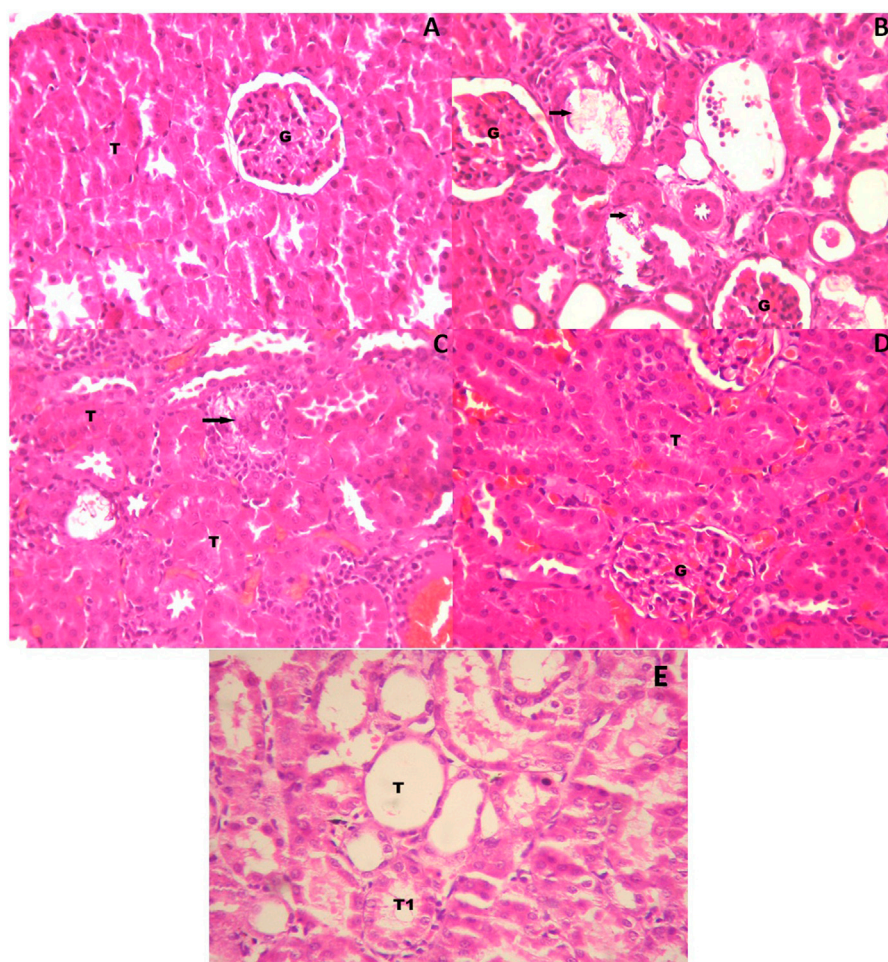


FIGURE 3 | High power photomicrograph of section of kidney **(A)** control group showing a normal glomerulus and tubules **(B)** urolithiatic group showing damaged proximal tubules (arrow) with deposits of refractile crystals and loss of tubular epithelium. The distal tubules (DT) are not affected, glomerulus shows no damage **(C)** urolithiatic group treated with SPP 700 mg/kg/day showing a single damaged proximal tubule (Arrow) with loss of tubular epithelium with several undamaged tubules (T) around it **(D)** Urolithiatic group treated with SPP 1000 mg/kg/day showing a normal glomerulus and tubules. No evidence of tubular damage was seen in this sample. G = Glomerulus, T = Tubule. **(E)** But the Neeri standard group's rat kidneys showing a few dilated tubules along with a number of undamaged tubules (HE \times 40).

All animals were fed a standard laboratory diet and maintained under standard laboratory conditions (temperature, 22–24°C; relative humidity, 60–70%), standard light and dark cycle, and water *ad libitum*. All the healthy albino Wistar rats were allowed to acclimatize for 1 week prior to the experiment.

Ethylene Glycol- and Ammonium chloride-Induced Urolithiasis

Animals were divided into the following five groups (six animals in each group): control, toxicant, Safoof-e-Pathar phori lower dose (SPPL) treatment group, Safoof-e-Pathar phori higher dose (SPPH) treatment group, and neeri syrup standard group (Table 1). To induce CaOx crystal formation, animals were exposed to 0.75% EG with 1.0% AC in their drinking water for 21 days (Bashir and Gilani, 2009). The experimental groups are summarized as follows:

Group I: Normal rats; received vehicle along with simple drinking water for 21 days.

Group II: Toxicant; received 0.75% EG with 1.0% AC in drinking water for 5 days and 0.75% EG for the next 16 days.

Group III: Standard; received 0.75% EG with 1.0% AC in drinking water for 5 days and 0.75% EG for the next 16 days along with the standard drug neeri 2.65 ml/kg/day for all 21 days.

Group IV: SPPL; received 0.75% EG with 1.0% AC in drinking water for 5 days and 0.75% EG for the next 16 days along with SPP at 700 mg/kg/day for all 21 days.

Group 5: SPPH; received 0.75% EG with 1.0% AC in drinking water for 5 days and 0.75% EG for the next 16 days along with SPP at 1,000 mg/kg/day for all 21 days.

For the antiurolithiatic study, fresh suspensions of SPP (700 and 1,000 mg/kg; using 0.25% CMC) were administered once daily by oral gavage to the corresponding group of animals for 21 days.

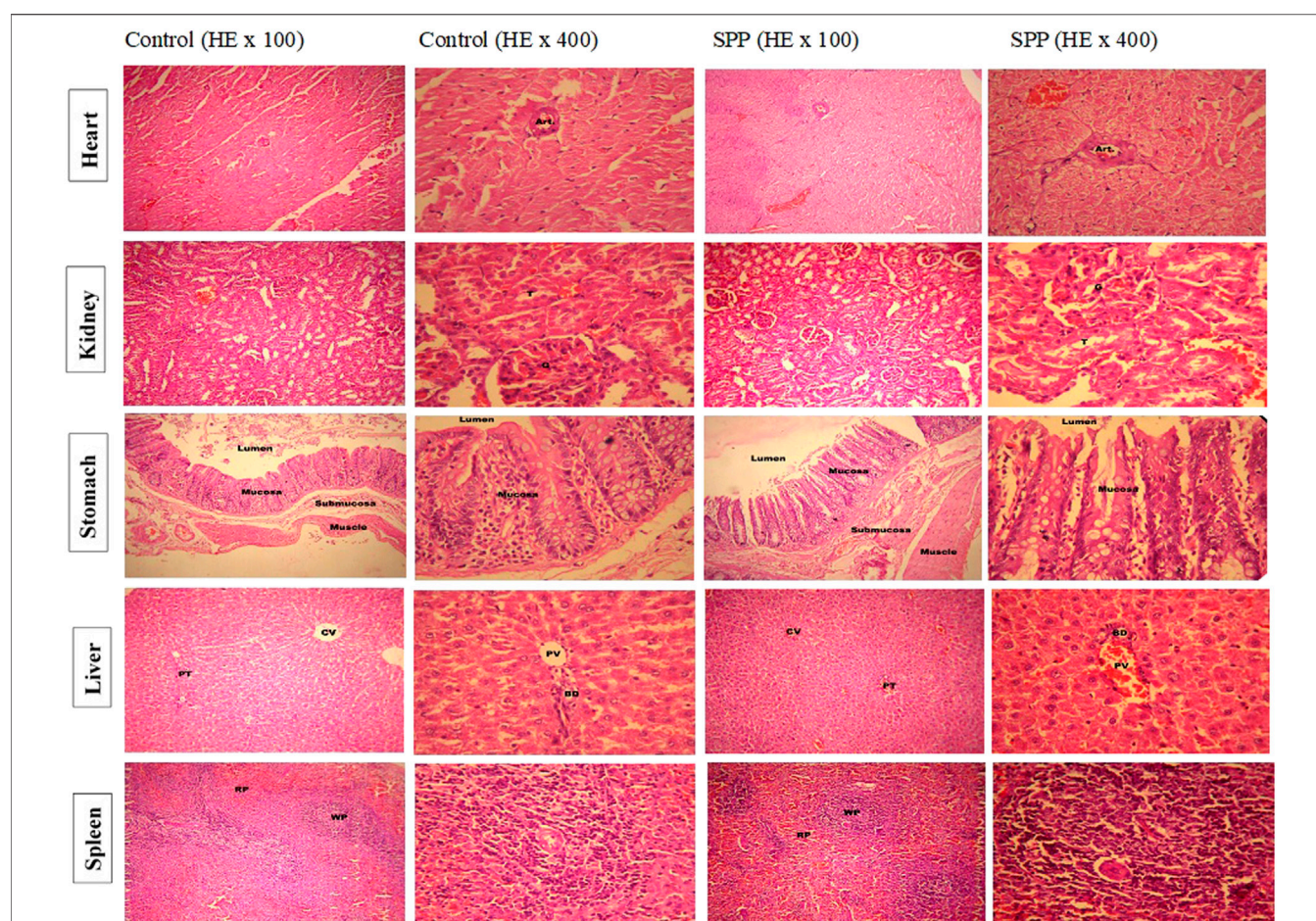


FIGURE 4 | Low and high-power photomicrograph of SPP treated rats showed the normal histological appearance without any significant change in heart, kidney, liver, spleen and stomach compare to normal control rats. Histopathological examination of heart tissue showed normal appearance of cardiac muscle fibers and no evidence of necrosis or myocardial damage is seen. Cardiac muscle fibers with striated cytoplasm and central oval nuclei. A coronary vessel (Art.) cut in cross section is also seen. Histopathological examination of kidney tissues showed normal histopathological appearance of renal parenchyma, glomerular tubule in all treatment groups including control. The histopathological examination of stomach tissues showed normal histological appearance of different layers of stomach walls and mucosa of the stomach showing gastric glands in photomicrographs of all treatment groups including control. Histopathological examination of liver tissues showed normal histological appearance of portal triad (PT), central vein (CV) (100×), bile duct (BD) and portal vein (PV) (400×) in all treatment group including control. The histopathological examination of spleen tissues showed normal histological appearance of white pulp (WP), red pulp (RP) (100×), areas in the splenic parenchyma. Splenic arteriole (SA) and lymphocytes in photomicrographs of all treatment groups including control.

TABLE 1 | Composition of Safoof-e-Pathar phori (Anonymous, 1986).

S. No	Ingredients common name	Ingredients botanical name	Family (part used)	Category	Unit formula per 100 g
	Pathar phori	<i>Didymocarpus pedicellatus</i> R.Br	Gesneriaceae (leaves)	Active ingredient	50 g
	Jawakhar desi	<i>Hordeum vulgare</i> L	Poaceae (whole plant)	Active ingredient	12.5 g
	Revand chini	<i>Rheum webbianum</i> Royle	Polygonaceae (Rhizome)	Active ingredient	12.5 g
	Namak turb	<i>Raphanus raphanistrum subsp. sativus</i> (L.) domin	Brassicaceae (Whole plant)	Active ingredient	6.25 g
	Kulthi	<i>Macrotyloma biflorum</i> var. <i>biflorum</i>	Leguminosae (Seed)	Active ingredient	12.5 g
	Shora qalmi	Potassium Nitrate		Active ingredient	6.25 g
				Total	100

Long-Term Oral Toxicity Study

Young adult male and female albino Wistar rats were divided into the following four groups (five rats in each group):

Group I: Normal control (NC); consisting of males receiving vehicle 0.4ml/animal daily for 90days.

Group II: NC; consisting of females receiving vehicle 0.4 ml/animal daily for 90 days.

Group III: SPP (700 mg/kg/day for 90 days); consisting of males.

Group IV: SPP (700 mg/kg/day for 90 days); consisting of females.

For the long-term oral toxicity study, a freshly prepared suspension of SPP (700 mg/kg) was administered daily in the rats for 90 days. The animals were dosed at approximately the same time each day. All animals were observed daily for body weight and mortality throughout the study. Histopathological and biochemical changes in the animals were analyzed at the end of the study period following sacrificing of the animals.

Collection and Analysis of Urine

On the 21st day, animals were kept in a urine collection cage, and urine from the first 3 h of the morning was collected for investigation of crystalluria. All the animals were kept individually in the metabolic cages, and the urine sample at 24 h was collected. The urine samples were acidified by adding a few drops of concentrated HCl and stored at 4°C until further use. Urine was also analyzed for calcium, sodium, and potassium as per the manufacturer's protocol (Span Diagnostics Ltd, Surat, India) (Ikshita et al., 2017)

Hematological and Serum Biochemical Analysis

Blood samples were collected 24 h after the last dose of treatment by puncturing the retro-orbital sinus under a mild anesthetic condition, and the animals were sacrificed by cervical decapitation. In the pharmacological study, hematological parameters such as hemoglobin (Hb), total red blood cells (RBCs), and white blood cells (WBCs) were analyzed in the whole blood. The serum was separated by centrifugation at 1,500 rpm for 15 min in refrigerated research centrifuge and used for the estimation of serum creatinine and blood urea nitrogen (BUN) using commercially available kits (Span Diagnostics Ltd, Surat, India) and the Star-21 plus semi-auto analyzer. In long-term oral toxicity studies, hematological parameters such as Hb, erythrocyte count, total leukocytes and biochemical parameters in the blood serum including serum glutamic oxaloacetic transaminase, serum glutamic pyruvic transaminase, alkaline phosphatase, urea, albumin, bilirubin, total protein, creatinine, uric acid, sodium, and potassium were analyzed using commercially available kits (Span Diagnostics Ltd, Surat, India) as per the manufacturer's protocol.

Histopathological Study of the Kidney, Heart, Liver, Stomach, and Spleen

For investigating the antiuro lithiatic activity, the sacrificed animals were dissected after blood sample collection, and only the kidneys were removed and immediately washed with ice-cold saline. After washing with saline, kidneys were preserved for biochemical estimation and fixed in 10% formalin for histopathological studies. For the long-term oral toxicity study, the kidney, heart, liver, stomach, and spleen of animals were dissected. Isolated organs were fixed in 10% neutral buffered formalin, processed in a series of graded alcohol and xylene, and finally embedded in paraffin wax. Histological sections (approximately 5m thickness) were prepared by microtomy and stained with hematoxylin and eosin dye for histological examination. Histological slides were examined under a light microscope at low (10×) and high (40×) magnifications. Statistical Analysis

Results are expressed as mean \pm standard deviation. A two-way analysis of variance followed by a Tukey's test was used for statistical analysis. A *p* value of <0.05 was considered statistically significant.

RESULTS

Antiuro lithiatic Effect of Safoof-e-Pathar Phori on Ethylene Glycol Induced Urolithiasis

The concentrations of urinary calcium, potassium, and sodium in groups I–V are given in **Table 2**. In this study, 0.75% EG (v/v) with 1% AC induced urolithiasis in male rats and resulted in hypercalciuria and hyperoxaluria. The level of urinary calcium was significantly elevated compared with the Normal control (NC) (**Table 2**). However, rats treated with SPPL (700 mg/kg; Group IV) and SPPH (1,000 mg/kg; Group V) demonstrated significantly lower calcium levels and increased potassium and sodium excretion in urine than those in NC (*p* < 0.01). A decrease in calcium and an increase in potassium and sodium in SPPL and SPPH treated rats were similar to those in Neeri-treated rats (Group III).

Urolithiasis induced by EG and AC caused impairment of renal functions in untreated rats as marked by the increased levels of serum creatinine, uric acid, and urea. Renal function was evaluated by determining the serum creatinine and BUN in EG- and AC-induced urolithiasis and treated rats (**Table 2**). Levels of serum creatinine and BUN were significantly increased in the toxicant group when compared with the NC, indicating impairment of renal functions. However, SPPL (700 mg/kg) and SPPH (1,000 mg/kg) significantly (*p* < 0.001) decreased the levels of serum creatinine and BUN excreted by kidneys compared with the toxicant group. Moreover, treatment with SPPL (700 mg/kg) and SPPH (1,000 mg/kg) significantly lowered the elevated serum creatinine level, SPPH showed dose-dependent activity due to maximum decrease in serum creatinine and BUN levels. These results suggested that SPP treatment ameliorates the renal functions compared with urolithiatic control rats. The results of SPP were found to be similar to those of the standard drug neeri.

TABLE 2 | Results of ions estimations in urine of control and urolithiatic group and group treated with Neeri, SPP 700 and 1000 mg/kg oral dose.

Parameter	Group I	Group II	Group III	Group IV	Group V
	Control	Toxicant	Neeri	SPP 700 mg/kg	SPP 1000 mg/kg
Calcium (mg/dl)	4.27 ± 0.12	8.90 ± 0.06 ^a	5.20 ± 0.13 ^b	5.95 ± 0.11 ^b	5.28 ± 0.12 ^b
Potassium (mg/dl)	7.10 ± 0.11	4.40 ± 0.03 ^a	7.20 ± 0.07 ^b	6.80 ± 0.10 ^b	7.41 ± 0.06 ^b
Sodium (mg/dl)	28.2 ± 0.52	10.13 ± 0.85 ^a	28.1 ± 0.41 ^b	25.92 ± 0.47 ^b	29.92 ± 0.62 ^b
Oxalate crystals	Nil	+++	Nil ^b	Nil ^b	Nil ^b
BUN (mg/dl)	19.3 ± 4.5	134.7 ± 14.86 ^a	27.11 ± 6.2 ^b	43.26 ± 3.20 ^b	23.74 ± 2.34 ^b
Creatinine (mg/dl)	0.23 ± 0.02	0.69 ± 0.04 ^a	0.21 ± 0.01 ^b	0.27 ± 0.01 ^b	0.20 ± 0.01 ^b
TBARS (nmoles/mg)	3.95 ± 0.33	8.97 ± 0.51 ^a	5.14 ± 0.14 ^b	5.10 ± 0.37 ^b	5.54 ± 0.29 ^b
GSH (nmoles/mg)	3.51 ± 0.17	0.57 ± 0.11 ^a	3.20 ± 0.09 ^b	2.53 ± 0.04 ^b	2.82 ± 0.08 ^b
RBC (×10 ⁶ /mm ³)	5.88 ± 0.2	6.18 ± 0.3	6.33 ± 0.16	6.23 ± 0.2	6.41 ± 0.3
WBC (×10 ³ /mm ³)	9.7 ± 0.3	10.3 ± 0.2	9.7 ± 0.22	10.1 ± 0.4	10.9 ± 0.2
Hb Content (g/dl)	10.4 ± 0.3	11.7 ± 0.4	11.1 ± 0.31	11.8 ± 0.4	11.3 ± 0.3

^ap < 0.001 vs. Control.^bP<0.001 vs. Toxicant a denotes that data were compared with normal control and b denotes that data were with toxicant group <0.001.

The antioxidant parameters were assessed by measuring the malondialdehyde (measured as TBARS) and glutathione (GSH) level. Treatment with EG and AC significantly increased ($p < 0.001$) the TBARS level and decreased the GSH level in urolithiasis-induced rats compared with NC (Table 2). Treatment with SPPL (700 mg/kg) and SPPH (1,000 mg/kg) decreased the TBARS level significantly (Figure 1) and improved the GSH concentration (Figure 2) compared with the toxicant group.

The crystalluria study revealed the absence of crystals (oxalate crystals) in the rat group treated with standard neeri syrup (2.65 ml/kg), SPPL (700 mg/kg), and SPPH (1,000 mg/kg), which supported the preventive effect of low and high doses of SPP on the induction of urolithiasis. Hematological analysis of various groups of rats showed normal RBC, WBC, and Hb levels and absence of hemolysis in all the groups (Table 2).

Figure 3 shows the histopathological examination of the rat kidneys. The histopathological section of the kidneys of rats in the control group exhibited no abnormalities; glomerulus and proximal tubules were normal (Figure 3A). The kidneys of rats in the toxicant group exhibited damaged proximal tubules, with deposits of refractile crystals and loss of tubular epithelium. The distal tubules were not affected, and glomerulus did not show any damage. It exhibited the characteristic signs of stone development on continuous ingestion of 0.75% EG with 1.0% AC (Figure 3B). The kidneys of rats in the urolithiatic group treated with SPPL (700 mg/kg/day) exhibited a single damaged proximal tubule with loss of tubular epithelium with several undamaged tubules around it (Figure 3C), whereas those treated with SPPH 1000 mg/kg/day exhibited a normal glomerulus and tubules. No evidence of tubular damage was observed in this sample (Figure 3D). However, the kidneys of rats in the neeri standard group exhibited a few dilated tubules along with numerous undamaged tubules (Figure 3E).

Long Term Oral Toxicity Study of Safoof-e-Pathar Phori 700 mg/Kg

The long-term oral toxicity study of SPP was performed as per the OECD guideline (OECD, 2020) for 90 days. For determining the

long-term oral toxicity of the animals, observations were noted based on the following aspects: cage side observation of all animals, mortality record, body weight record, hematological observation, and liver and renal function test with histopathological observations of the heart, kidney, liver, spleen, and stomach.

The cage side observation of animals subjected to toxicity was performed based on several parameters on each day up to 90 days, but no abnormality was observed during the complete course of the study. Of the 20 rats, none showed mortality up to 90 days (Table 3). The body weight record of the rats (Table 4) did not exhibit any irregularity in all the treatment groups. Similarly, 13-weeks treatment of the rats with 700 mg/kg SPP did not exhibit any significant difference in hematological parameters (Table 5) as well as in liver and kidney function tests (Table 5). There was insignificant variation in the wet weight of vital organs in the SPP (700 mg/kg/day)-treated group compared with the control group, and these results were observed in both male and female rats (Table 5). Histopathological analysis of the heart, kidney, liver, spleen, and stomach in the SPP-treated rats revealed the normal histological appearance of all the organs without any significant change compared with NC rats (Figure 4). Thus, SPP was found to be safe after its oral administration at 700 mg/kg for up to 3 months (90 days).

DISCUSSION

The most commonly used medical therapies in the management of urolithiasis include calcium channel blockers, steroids, and α_1 adrenergic blockers (Shekar and Patki, 2011), which exhibit some adverse effects. Some herbal remedies have been used in the management of urinary calculi; however, their efficacy has not been scientifically proven. With the understanding of various pathophysiological functions underlying renal stones and the mechanism of herbal remedies that can play a role in preventing the formation and management of urinary calculi, phytotherapy might be a better alternative in the preventive and curative management of urinary calculi. Oral citrate is the most commonly used medicinal agent in the prevention of urinary

TABLE 3 | Mortality record of animals in control and treatment group.

Days	Control male	Control female	SPP 700 mg/kg male	SPP 700 mg/kg female
Week 1	-	-	-	-
Week 2	-	-	-	-
Week 3	-	-	-	-
Week 4	-	-	-	-
Week 5	-	-	-	-
Week 6	-	-	-	-
Week 7	-	-	-	-
Week 8	-	-	-	-
Week 9	-	-	-	-
Week 10	-	-	-	-
Week 11	-	-	-	-
Week 12	-	-	-	-
Week 13	-	-	-	-
Mortality	0/5	0/5	0/5	0/5

SPP-Safoof-e-Pathar phori.

TABLE 4 | Body weight records of animals in male and female rats orally treated with SPP 700 mg/kg and control group.

Dose	Male (g)		Female (g)	
	Control	SPP 700	Control	SPP 700
0 Week (18/07/2010)	148 ± 13.26	142 ± 11.66	133.43 ± 38.36	128.22 ± 36.55
Week 1 (25/07/2010)	149 ± 14.96	147 ± 11.66	136.16 ± 38.60	131.97 ± 37.66
Week 2 (01/08/2010)	158 ± 14.35	157 ± 11.66	142.69 ± 40.84	141.13 ± 40.33
Week 3 (8/08/2010)	163 ± 14.35	164 ± 11.13	147.69 ± 42.45	147.92 ± 42.20
Week 4 (15/08/2010)	169 ± 13.56	175 ± 8.94	152.29 ± 43.86	157.41 ± 45.49
Week 5 (22/08/2010)	173 ± 14.35	183 ± 6.63	156.02 ± 44.83	163.05 ± 47.41
Week 6 (29/08/2010)	180 ± 12.64	189 ± 6.63	161.88 ± 47.14	169.63 ± 49.74
Week 7 (5/09/2010)	184 ± 12	195 ± 7.07	166.33 ± 48.60	175.58 ± 51.33
Week 8 (12/09/2010)	189 ± 10.19	201 ± 8	171.59 ± 50.05	182.41 ± 53.03
Week 9 (19/09/2010)	196 ± 11.57	209 ± 8	177.71 ± 51.42	189.75 ± 55.29
Week 10 (26/09/2010)	202 ± 12.08	214 ± 3.74	183.67 ± 53.28	193.97 ± 57.71
Week 11 (3/10/2010)	208 ± 12.88	221 ± 3.74	190.07 ± 54.88	199.97 ± 59.50
Week 12 (10/10/2010)	214 ± 13.92	228 ± 4	196.49 ± 56.62	206 ± 61.18
Week 13 (17/10/2010)	225 ± 12.24	236 ± 3.74	206.85 ± 59.57	214.14 ± 63.64

calculi (Gurocak et al., 2006). Because of the adverse effects of these agents, alternative management modalities comprising herbal remedies have been significant agents in the treatment (Gurocak et al., 2006). The use of medicinal plants to treat diseases is as old as civilization itself. Plants provide crude drugs, which are used without any modification, and numerous chemical constituents can be used for the synthesis of new drugs with better pharmacological effects (Potterat and Hostettman, 1995; Zaidi and Ahmad, 2016). Additionally, the World Health Organization (WHO) has highlighted the development and application of herbal and traditional medicines considering their beneficial effects, such as cost-effectiveness and the avoidance of side effects of synthetic medicines. The WHO has estimated that approximately 80% of the population living in the developing countries rely on traditional medicines for their healthcare needs (WHO, 2002).

The present study was performed to evaluate the antirolithiatic effects of SPP on EG-induced urolithiasis in male Wistar rats used by several investigators. (Bashir and Gilani, 2009; Pareta et al., 2011; Aggarwal et al., 2012; Lin et al., 2012; Nanu et al., 2012; Saeidi et al., 2012; Khan et al., 2016).

EG is a metabolic precursor of oxalate. EG is oxidized to glycolic acid and further to oxalic acid. Administration of EG causes hypercalciuria, leading to urolithiasis. Administration of EG causes hypercalciuria and hyperoxaluria to induce urolithiasis (Verma et al., 2009). AC ingestion, which induces metabolic acidosis, has been used in conjunction with EG to promote the deposition of CaOx crystals in the rat kidneys. Various doses of AC in combination with EG resulted in CaOx depositions in the rat kidneys within 7 days (Khan et al., 2016). After 21 days, crystalluria analysis of rats in the EG-induced urolithiasis group revealed that untreated rats exhibited bigger crystals than treated rats (Bashir and Gilani, 2009). Studies have consistently reported that calculi induced by hyperoxaluria causes an increase in oxalate and a decrease in calcium excretions in the toxicant group (Fan et al., 1999; Park et al., 2007); SPP treatment produced reversible effects in a dose-dependent manner.

Results of the urinary calcium level showed a significant ($p < 0.001$ vs control) elevation in the toxicant group, whereas sodium and potassium level significantly ($p < 0.001$ vs control) reduced compared

TABLE 5 | Results of hematological, liver, renal and organ weight assessment of control and SPP 700 mg/kg group.

Test	Male		Female	
	Control	SPP 700	Control	SPP 700
Erythrocyte count (mill/C.mm)	5.81 ± 0.01	7.30 ± 0.06	5.31 ± 1.59	6.61 ± 1.97
Hemoglobin (g/dl)	9.84 ± 0.16	13.22 ± 0.08	9.52 ± 2.88	11.70 ± 3.53
Total leukocytes	11.84 ± 0.10	11.18 ± 0.06	10.49 ± 3.16	10.14 ± 3.04
Bilirubin (mg/dl)	00.93 ± 0.02	0.88 ± 0.01	00.85 ± 0.25	00.79 ± 0.23
SGPT (U/L)	30.92 ± 0.66	69.68 ± 0.93	27.69 ± 8.21	63.55 ± 18.89
SGOT (U/L)	35.26 ± 0.34	67.4 ± 0.61	32.24 ± 9.63	60.95 ± 18.22
ALP (U/L)	75.11 ± 0.28	25.34 ± 0.53	67.90 ± 20.42	14.73 ± 10.67
Total Protein(g/dL)	00.13 ± 0.01	04.70 ± 0.08	05.71 ± 1.69	04.26 ± 1.26
Albumin (g/dl)	03.12 ± 0.14	1.30 ± 0.02	02.77 ± 0.80	01.18 ± 0.35
Blood Urea (mg/dl)	34.6 ± 1.01	49.22 ± 0.16	31.30 ± 9.19	81.90 ± 124.3
Creatinin (mg%)	00.73 ± 0.02	00.44 ± 0.01	00.66 ± 0.19	00.40 ± 0.11
Serum Uric acid(mg/100 ml)	07.06 ± 0.10	08.02 ± 0.11	06.40 ± 1.90	07.27 ± 2.16
Sodium (meq/L)	143.8 ± 2.31	140 ± 1.41	130.42 ± 38.70	127.03 ± 37.95
Potassium (meq/L)	04.16 ± 0.13	07.24 ± 0.13	03.69 ± 1.09	06.48 ± 1.93
Kidney	0.68 ± 0.01	0.69 ± 0.007	0.61 ± 0.18	0.63 ± 0.18
Spleen	0.31 ± 0.01	0.31 ± 0.01	0.28 ± 0.08	0.29 ± 0.08
Heart	0.40 ± 0.01	0.41 ± 0.006	0.37 ± 0.11	0.37 ± 0.11
Liver	2.01 ± 0.08	1.94 ± 0.10	1.87 ± 0.54	1.80 ± 0.51
Stomach	0.38 ± 0.02	0.37 ± 0.007	0.35 ± 0.10	0.34 ± 0.10

to the control group. Sodium and potassium levels significantly ($p < 0.001$ vs toxicant) increased, and calcium levels were decreased in the urine of the rats treated with SPP compared with the toxicant group. Comparison of the SPP and Neeri group showed an insignificant difference. This suggests an increased urinary loss of electrolytes (Hess and Kok, 1996). In urolithiasis, creatinine and BUN accumulate in blood. In this study, we observed that serum creatinine and BUN levels were significantly ($p < 0.001$ vs control) elevated in the serum of rats with EG- and AC-induced urolithiasis (toxicant group). It is suggested that EG and AC cause renal tubular damage and lower glomerular filtration rate. SPP-treated rats significantly ($p < 0.001$ vs. toxicant) reduced the BUN and serum creatinine levels compared with the control group at the dose of 700 and 1,000 mg/kg, and these results were similar to those of the standard drug Neeri.

The toxicant group showed a significantly ($p < 0.001$ vs control) elevated level of TBARS compared to the control group. Lipid peroxidation was measured as a Nano-gram of TBARS per mg of protein level in kidney tissue. Lipid peroxidation is another critical cause of injury that occurs during urolithiasis. Increased TBARS levels due to increased oxidative stress, decreased antioxidant enzymes and GSH levels in kidneys, and impaired kidney functions. Oxalate has been reported as the major stone forming component causing peroxidative injury to the renal epithelial cells (Kato et al., 2007). The SPP treatment protected against various injuries associated with oxidative stress. The biochemical alterations were supported by histopathological interpretations of the kidney (Muthukumar and Selvam, 1998). The urolithiasis toxicant group exhibited the presence of refractile crystals in the tubular epithelial cell and damage to the proximal tubular epithelium, whereas groups treated with SPP along with EG and AC exhibited protection, as evident from the reduction in tubular cell damage and normal kidney histology. Our results suggest that SPP has both protective and preventive effects in rats with EG- and AC-induced urolithiasis, which is consistent with previous studies (Saha

and Verma, 2011). Zaidi and Ahmad (2016) reported that SPP is an effective and safe non-invasive polyherbal remedy for patients with urolithiatic, with no adverse reactions.

Medicinal plants and herbal medicines are progressively required by patients as a source of prescription drugs, in the form of active constituents, in developed and developing countries. They have been shown to possess undeniable and tangible therapeutic benefits with limited toxicity because of their long-term use as traditional medicines. The WHO claims that safety is a critical parameter of herbal medicines in the quality control of healthcare products (Tatke et al., 2012). Toxicity studies are considered to be important during new drug development, keeping in mind that herbal medicines are frequently used indiscriminately without considering their potential side effects, which can vary from mild-severe to life-threatening (World Health Organization, 1987; World Health Organization, 2000). Various herbal preparations have been shown to be beneficial in treating kidney disease; however, the toxicity and safety data for many of these herbal treatments are not available (Tatke et al., 2012).

In this study, the long-term oral toxicity of SPP was evaluated in albino Wistar rats using biochemical, hematological, and histopathological parameters. Weight gain and behavioral activity was similar to the control animals in all single-dosed males and females during the study period. There were no marked abnormal changes observed throughout the study period. Hematology in rats at a single dose of SPP exhibited insignificant differences compared to the control group. Additionally, the functioning of major organs (heart, kidney, liver, spleen, and stomach) was found to be similar to that in the control group. Histopathological examination of the heart, kidney, liver, spleen, and stomach did not exhibit any changes. Oral SPP ingested at 700 mg/kg for up to 3 months resulted in normal growth with no changes in hematological, hepatic, or renal functioning parameters. There was no evidence of abnormal histology. Thus, long-term daily oral consumption of SPP

was found to be safe in Wistar rats, and it may be safe for clinical use as an antirolithiatic formulation.

CONCLUSION

The results indicated that the administration of the traditional Unani poly-herbomineral formulation SPP reduced and prevented the growth of urinary stones in rats with EG- and AC-induced urolithiasis. The toxicity study indicated no serious signs and significant changes in the physical, hematological, biochemical, and histopathological parameters after 90-days administration of SPP (700 mg/kg). SPP was found to be safe for oral administration at 700 mg/kg for up to 3 months. Hence, SPP was observed to be a curative and safe poly-herbomineral formulation, useful in the prevention and management of urolithiasis. Further studies at lower dose levels and using extracts of the formulation to reduce the dose are necessary to make it more pharmacologically relevant and to elucidate the mechanism underlying the pharmacological effect of SPP.

DATA AVAILABILITY STATEMENT

The original contributions presented in the study are included in the article, further inquiries can be directed to the corresponding author.

REFERENCES

- Aggarwal, A., Singla, SK, Gandhi, M., and Tandon, C. (2012). Preventive and curative effects of *Achyranthes aspera* Linn. extract in experimentally induced nephrolithiasis. *Indian J. Exp. Biol.* 50, 201–8.
- Ahmad, W., Ali, A., Ali, M., Mir, S. R., Zaidi, S. M. A., and Ahmad, S. (2017). New fatty acid and aromatic monoterpenic esters from the leaves of *Didymocarpus pedicellata* R. Br. *Indian Drugs*. 54 (11), 28–32.
- Ahmad, W., Khan, W., Khan, M. S., Mujeeb, M., Zaidi, S. M. A., and Ahmad, S. (2016). Quality control analysis of Safoof-e-Pathar phori: antirolithiatic formulation. *Drug Dev. Ther.* 7 (1), 20–25. doi:10.4103/2394-6555.180163
- Ahmad, W., Mujeeb, M., Zaidi, S. M. A., and Ahmad, S. (2013). Current strategy for research on quality identification of *Rheum emodi* Wall. rhizome. *Int. J. Drug Dev. Res.* 5, 1–10.
- Ahmad, W., Mujeeb, M., and Zaidi, S. M. A. (2010). Quality control analysis of seed of *Dolichous biflorus* Linn. *Int. J. Drug Dev. Res.* 2, 669–674.
- Ahmad, W., Parveen, R., Mujeeb, M., and Zaidi, S. M. A. (2020). Comparative fingerprint profiling of Unani polyherbomineral (Safoof-e-Pathar phori) formulation by HPTLC, HPLC, and GC-MS. *J. AOAC Int.* 103, 659–668. doi:10.5740/jaoacint.19-0286
- Ahmad, W., T. Tamboli, E., Ali, A., Amir, M., Zaidi, S. M. A., and Ahmad, S. (2019). *Didymocarpus pedicellatus* R. Br.: qualitative and quantitative GCMS approach for quality control in traditional poly-herbal formulation with in vitro antioxidant and antimicrobial activity. *Orient. J. Chem* 35, 648–657. doi:10.13005/ojc/350220
- Ahmad, W., Zaidi, S. M. A., and Ahmad, S. (2014). Quality control analysis of *Didymocarpus pedicellata* R. Br. *Indian J. Traditional Knowledge*. 13, 175–180.
- Ahmad, W., Zaidi, S. M. A., Mujeeb, M., Ansari, S. H., and Ahmad, S. (2014). HPLC and HPTLC methods by design for quantitative characterization and in vitro anti-oxidant activity of polyherbal formulation containing *Rheum*

ETHICS STATEMENT

The animal study was reviewed and approved by Jamia Hamdard, Institutional Animal Ethics Committee (Registration Number 173/CPCSEA and Approval Number 691) following guidelines of the Committee for the Purpose of Control and Supervision of Experiments on Animals (CPCSEA).

AUTHOR CONTRIBUTIONS

WA: Experimental studies and manuscript preparation MK: Experimental studies and statistical analysis KA: Manuscript editing AA: Review and manuscript editing MD: Review and manuscript editing MA: Critical evaluation of manuscript KY: Literature review SW: Literature review SZ: Formulation preparation SA and MM: Conceived idea of research and data analysis.

ACKNOWLEDGMENTS

The authors would like to thank CCRUM for providing financial assistance and the Bioactive Natural Product Laboratory, Department of Pharmacognosy and Phytochemistry, School of Pharmaceutical Education and Research, Jamia Hamdard, New Delhi, India, for conceptualizing the project and providing the lab facility and technical assistance for conducting this study.

emodi. *Journal of Chromatographic Science* 52, 911–918. doi:10.1093/chromsci/bmt123

- Ahmad, W., Zaidi, S. M. A., and Ahmad, S. (2015). Validated UPLC-Q-TOF-MS method for quantitative determination of emodin in rhizome of *Rheum emodi* Wall. ex Meissn. and its traditional polyherbal formulation using three different extraction techniques. *Ann. Phytomedicine* 4, 68–73.
- Anonymous (2006). *The wealth of India second supplement series raw material*. 58.
- Anonymous (2007a). *The Unani Pharmacopoeia of India*. 58–59.
- Anonymous (2007b). *The Unani Pharmacopoeia of India*. 91–92.
- Anonymous (1986). *Qarabadeen majeedi all India Unani tibbi conference*. Delhi.
- Asplin, J. R., Favus, M. J., and Coe, F. L. (1996). “Nephrolithiasis,” in *Brenner and Rector's the kidney*. Editor B. M. Brenner. 5th ed. (Philadelphia: Saunders). 1893–1935.
- Bashir, S., and Gilani, A. H. (2009). Antirolithic effect of *Bergenia ligulata* rhizome: an explanation of the underlying mechanisms. *Journal of Ethnopharmacology* 122, 106–116. doi:10.1016/j.jep.2008.12.004
- Chandhoke, P. S. (2002). When is Medical Prophylaxis Cost-effective for Recurrent Calcium Stones?. *The Journal of Urology* 168, 937–940. doi:10.1097/00005392-200209000-00009
- Dubey, N., Mehta, R. S., Saluja, A. K., and Jain, D. K. (2008). Quality assessment of Khusta-e-Gaodanti: a traditional Unani medicine. *Asian J. Res. Chem.* 1, 46–50.
- Fan, J., Glass, M. A., and Chandhoke, P. S. (1999). Impact of ammonium chloride administration on rat ethylene glycol urolithiasis model. *Scanning Microsc.* 13, 299–306.
- Gürocak, S., and Küpeli, B. (2006). Consumption of historical and current phytotherapeutic agents for urolithiasis: a critical review. *Journal of Urology* 176, 450–455. doi:10.1016/j.juro.2006.03.034
- Hardik, G., Maunick, C., and Pinakin, J. (2016). Diuretic and antirolithiatic activities of an ethanolic extract of *Acorus calamus* L. rhizome in experimental animal models. *J. Tradit Complement. Med.* 6(4), 431–436. doi:10.1016/j.jtcme.2015.12.004

- Hess, B., and Kok, D. J. (1996). Nucleation growth and aggregation of crystals. In: *Kidney stones, medical and surgical management*. Editors: Coe, F. L., Favus, M. J., Pak, C. Y., and Parks, J. H. Philadelphia, PA, USA: Lippincott-Raven. 3–32.
- Ikshit, S., Washim, K., Rabea, P., Md, J. A., Iftekhar, A., Mohd, H. R. A., et al. (2017). Antiuro lithiasis activity of bioactivity guided fraction of *Bergenia ligulata* against ethylene glycol induced renal calculi in rat. *Biomed. Res. Int.* 1969525. doi:10.1155/2017/1969525
- Kato, J., Ruram, A. A., Singh, S. S., Devi, S. B., Devi, T. L., and Singh, W. G. (2007). Lipid peroxidation and antioxidant vitamins in urolithiasis. *Indian J. Clin. Biochem.* 22, 128–130. doi:10.1007/bf02912895
- Kaur, T., Bijarnia, R. K., Singla, S. K., and Tandon, C. (2009). *In vivo* efficacy of *Trachyspermum ammi* anticalcifying protein in urolithiatic rat model. *Journal of Ethnopharmacology* 126, 459–462. doi:10.1016/j.jep.2009.09.015
- Khaling, M., Suresh, K., and Vandana, R. (2014). Current scenario of urolithiasis and the use of medicinal plants as antiuro lithiatic agents in Manipur (North East India): a review. *Int. J. Herb. Med.* 2, 1–12.
- Khan, M. A., Kumar, S., Gupta, A., and Ahmad, S. (2016). Screening of two new herbal formulations in rodent model of urolithiasis. *Drug Dev. Ther.* 7, 34–38. doi:10.4103/2394-6555.180160
- Kumar, S., and Pandey, A. K. (2014). Medicinal attributes of *Solanum xanthocarpum* fruit consumed by several tribal communities as food in *in vitro* antioxidant, anticancer and anti HIV perspective. *BMC Complement. Altern. Med.* 14, 112. doi:10.1186/1472-6882-14-112
- Lin, W.-C., Lai, M.-T., Chen, H.-Y., Ho, C.-Y., Man, K.-M., Shen, J.-L., et al. (2012). Protective effect of *Flos carthami* extract against ethylene glycol-induced urolithiasis in rats. *Urol. Res.* 40, 655–661. doi:10.1007/s00240-012-0472-4
- Mandavia, DR, Patel, MK, Patel, JC, Anovadiya, AP, Baxi, SN, and Tripathi, CR (2013). Anti-urolithiatic effect of ethanolic extract of *Pedaliu murex* linn. fruits on ethylene glycol-induced renal calculi. *Urol. J.* 10, 946–52.
- Michell, R., and Med, J. R. Soc. (1989). Urolithiasis-historical, comparative and pathophysiological aspects: a review. *J. Mol. Sci.* 82, 669–672. doi:10.1177/014107688908201112
- Mina, C. N., Marziyeh, H., Roja, R., Mohammad, H. F., Stéphane, Z., Seyed, M. N., et al. (2018). Dietary plants for the prevention and management of kidney stones: preclinical and clinical evidence and molecular mechanisms. *Int. J. Mol. Sci.* 19(3) 765. doi:10.3390/ijms19030765
- Moe, O. W. (2006). Kidney stones: pathophysiology and medical management. *The Lancet* 367, 333–344. doi:10.1016/s0140-6736(06)68071-9
- Muthukumar, A., and Selvam, R. (1998). Role of glutathione on renal mitochondrial status in hyperoxaluria. *Mol. Cel Biochem* 185, 77–84. doi:10.1023/a:1006817319876
- Nanu, R. R., Dipak, B., Havagiray, R. C., Sanjeev, R., Muchandi, I. S., and Ramesh, C. (2012). Anti-urolithiatic effects of *Punica granatum* in male rats. *J. Ethnopharmacol.* 140, 234–238. doi:10.1016/j.jep.2012.01.003
- OECD (2020). *OECD guidelines for the testing of chemical. Repeated dose 90 days oral toxicity study in rodents*. Available at: <https://www.oecd-ilibrary.org/docserver/9789264070707-n.pdf?expires=1616865109&id=id&accname=guest&checksum=2EECD0312717F23C7B804C6EA616492B> (Accessed July 15, 2020).
- Pareta, SK, Patra, KC, Mazumder, PM, and Sasmal, D (2011). Aqueous extract of *Boerhaavia diffusa* root ameliorates ethylene glycol-induced hyperoxaluric oxidative stress and renal injury in rat kidney. *Pharm. Biol.* 49, 1224. doi:10.3109/13880209.2011.581671[Epub ahead of print]
- Park, HK, Jeong, BC, Sung, MK, Park, MY, Choi, EY, Kim, BS, et al. (2007). Reduction of oxidative stress in cultured renal tubular cells and preventive effects on renal stone formation by the bioflavonoid quercetin. *J. Urol.* 179, 1620–6. doi:10.1016/j.juro.2007.11.039
- Park, S., and Pearle, M. S. (2007). Pathophysiology and management of calcium stones. *Urologic Clinics of North America* 34, 323–334. doi:10.1016/j.ucl.2007.04.009
- Patankar, S., Dobhada, S., Bhansali, M., Khaladkar, S., and Modi, J. (2008). A prospective, randomized, controlled study to evaluate the efficacy and tolerability of Ayurvedic formulation “varuna and banana stem” in the management of urinary stones. *J. Altern. Complement. Med.* 14, 1287–1290. doi:10.1089/acm.2008.0189
- Potterat, O., and Hostettman, K. (1995). “Plant source of natural drugs and compounds”. *Encyclopedia of environmental biology*. Editor W. A. Nierenberg (London: Academic Press), 13, 139–153.
- Saeidi, J., Bozorgi, H., Zende del, A., and Mehrzad, J (2012). Therapeutic effects of aqueous extracts of *Petroselinum sativum* on ethylene glycol-induced kidney calculi in rats. *Urol J* 9, 361–6.
- Saha, S, and Verma, RJ (2011). *Bergenia ciliata* extract prevents ethylene glycol induced histopathological changes in the kidney. *Acta Pol. Pharm.* 68, 711–5.
- Sathish, R., Natarajan, K., and Nikhad, M. M. (2010). Effect of *Hygrophila spinosa* tanders on ethylene glycol induced urolithiasis in rats. *Asian J. Pharma. Clin. Res.* 3, 61–63. doi:10.4103/0253-7613.100402
- Shekar, K. M. G., and Patki, P. S. (2011). Evaluation of an Ayurvedic formulation (Cystone), in urolithiasis: a double blind, placebo-controlled study. *Eur. J. Integr. Med.* 3, 23–28. doi:10.1016/j.eujim.2011.02.003
- Srinivas, S., Venkanna, B., Mohan, E. M., and Mohan, C. K. (2012). Urolithiasis: overview. *Int. J. Pharma RBA.* 1, 20–31.
- Srinivasa, A. K. B., Kuruba, L., and Saran, G. S. (2013). Antiuro lithiatic activity of Gokhsuradichuran, an Ayurvedic formulation by *in-vitro* method. *Adv. Pharm. Bull.* 3, 477–479. doi:10.5681/apb.2013.080
- Soundararajan, P., Kahesh, R., Ramesh, T., and Hazeena, V. (2006). Effect of *Aervalanta* on calcium oxalate urolithiasis in rats. *Indian J. Exp. Biol.* 44, 981–986. doi:10.2514/1.17320
- Sutherland, JW, Parks, JH, and Coe, FL (1985). Recurrence after a single renal stone in a community practice. *Miner Electrolyte Metab.* 11, 267–9.
- Tatke, P., Deshpande, S., and Nidhiya, I. S. R. (2012). Safety profile of a polyherbal formulation (gynocare capsules) in female rats by subchronic oral toxicity study. *Toxicol. Int.* 19, 106–1110. doi:10.4103/0971-6580.97196
- Verma, N. K., Patel, S. S., Saleem, T. S. M., Christina, A. J. M., and Chidambaranathan, N. (2009). Modulatory effect of NONI-Herbal formulation against ethylene glycol-induced nephrolithiasis in albino rats. *J. Pharm. Sci. Res.* 1, 83–89.
- World Health Organization (2000). *General guidelines for methodologies on research and evaluation of traditional medicine*. Geneva: World Health Organization.
- World Health Organization (1987). Principles for the safety assessment of food additives and contaminants in food. In *IPCS environmental Health criteria* 70. Geneva: World Health Organization.
- World Health Organization (2002). *World Health organization monographs on selected medicinal plants*. Geneva: World Health Organization. 159. doi:10.1111/j.2042-7166.2000.tb02454.x
- Zaidi, S. M. A., and Ahmad, W. (2016). Randomized single-blind clinical evaluation of Safoof-e-Pathar phori in urolithiasis patients. *Drug Dev. Ther.* 7 (2), 92–95. doi:10.4103/2394-6555.191151

Conflict of Interest: The authors declare that the research was conducted in the absence of any commercial or financial relationships that could be construed as a potential conflict of interest.

Copyright © 2021 Ahmad, Khan, Ashraf, Ahmad, Daud Ali, Ansari, Kamal, Wahab, Zaidi, Mujeeb and Ahmad. This is an open-access article distributed under the terms of the Creative Commons Attribution License (CC BY). The use, distribution or reproduction in other forums is permitted, provided the original author(s) and the copyright owner(s) are credited and that the original publication in this journal is cited, in accordance with accepted academic practice. No use, distribution or reproduction is permitted which does not comply with these terms.



Ramulus Mori (Sangzhi) Alkaloids (SZ-A) Ameliorate Glucose Metabolism Accompanied by the Modulation of Gut Microbiota and Ileal Inflammatory Damage in Type 2 Diabetic KKAY Mice

Quan Liu^{1,2,3†}, Shuainan Liu^{1,2,3*†}, Hui Cao^{1,2,3}, Wenming Ji^{1,2}, Caina Li^{1,2,3}, Yi Huan^{1,2,3}, Lei Lei^{1,2,3}, Yaxin Fu^{1,2}, Xuefeng Gao^{1,2}, Yuling Liu^{1,2,4} and Zhufang Shen^{1,2,3}

¹Institute of Materia Medica, Chinese Academy of Medical Sciences and Peking Union Medical College, Beijing, China, ²State Key Laboratory of Bioactive Substances and Functions of Natural Medicines, Key Laboratory of Polymorphic Drugs of Beijing, Institute of Materia Medica, Chinese Academy of Medical Sciences and Peking Union Medical College, Beijing, China, ³Diabetes Research Center of Chinese Academy of Medical Sciences and Peking Union Medical College, Beijing, China, ⁴Drug Delivery Technology and Novel Formulation, Institute of Materia Medica, Chinese Academy of Medical Sciences and Peking Union Medical College, Beijing, China

OPEN ACCESS

Edited by:

Prof Pulok Kumar Mukherjee,
Institute of Bio-Resources and
Sustainable Development (IBSD), India

Reviewed by:

Yun K. Tam,
Sinoveda Canada Inc., Canada
Johanna Mahwahwate Bapela,
University of Pretoria, South Africa

*Correspondence:

Shuainan Liu
liusn@imm.ac.cn

[†]These authors share first authorship

Specialty section:

This article was submitted to
Ethnopharmacology,
a section of the journal
Frontiers in Pharmacology

Received: 16 December 2020

Accepted: 10 March 2021

Published: 15 April 2021

Citation:

Liu Q, Liu S, Cao H, Ji W, Li C, Huan Y,
Lei L, Fu Y, Gao X, Liu Y and Shen Z
(2021) Ramulus Mori (Sangzhi)
Alkaloids (SZ-A) Ameliorate Glucose
Metabolism Accompanied by the
Modulation of Gut Microbiota and Ileal
Inflammatory Damage in Type 2
Diabetic KKAY Mice.
Front. Pharmacol. 12:642400.
doi: 10.3389/fphar.2021.642400

The novel Traditional Chinese Medicine Ramulus Mori (Sangzhi) alkaloid tablets (SZ-A) are approved by The China National Medical Products Administration for the treatment of type 2 diabetes mellitus (T2DM). However, the extensive pharmacological characteristics and the underlying mechanism are unknown. This study investigated the mechanisms by which SZ-A ameliorates glucose metabolism in KKAY mice, an animal model of T2DM. Diabetic KKAY mice were treated intragastrically with SZ-A once daily for 8 weeks, after which glucose levels, lipid metabolism, gut microbiome, systemic inflammatory factors, luminal concentrations of short-chain fatty acids (fecal samples), and ileal proteomic changes were evaluated. The ileum tissues were collected, and the effects of SZ-A on pathological inflammatory damage were evaluated by hematoxylin and eosin staining, immunofluorescence, and immunohistochemistry. The mRNA and protein expression levels of various inflammatory markers, including monocyte chemoattractant protein-1 and phosphorylated nuclear factor kappa B p65, were detected in the ileum tissues. SZ-A improved glucose metabolism with enhanced insulin response and elevated glucagon-like peptide 1 (GLP-1) nearly 2.7-fold during the glucose tolerance test in diabetic KKAY mice. Gut microbiota analysis demonstrated that SZ-A administration elevated the abundance of *Bacteroidaceae* and *Verrucomicrobia*, reduced the levels of *Rikenellaceae* and *Desulfovibrionaceae*; and increased the concentrations of fecal acetic and propionic acids

Abbreviations: Ccl11, Chemokine C-C-Motif Ligand 1; Ccl4, Chemokine C-C-Motif Ligand 4; Ccl5, Chemokine C-C-Motif Ligand 5; CXCL1, CXC chemokine ligand 1; CD36, cluster of differentiation 36; 1-DNJ, 1-deoxynojirimycin; DAB, 1,4-dideoxy-1, 4-iminod-D-arabinitol; FAG, fagomine; F4/80, adhesion G protein-coupled receptor E1; GLP-1, glucagon-like peptide 1; HbA1c, glycated hemoglobin; IL-1 β , Interleukin 1 β ; IL-5, Interleukin 5; IL-10, Interleukin 10; IL-13, Interleukin 13; IL-1a, Interleukin 1a; IL-6, Interleukin 6; IL-12b, Interleukin 12b; LPS, lipopolysaccharides; MCT1, monocarboxylate transporter-1; MHC II, major histocompatibility complex class II; MCP1, monocyte chemotactic protein 1; NF- κ B, Nuclear factor kappa B; SCFAs, short-chain fatty acids; SLC5A8, sodium-coupled monocarboxylate transporter 1; T2DM, type 2 diabetes mellitus; TCM, Traditiona l Chinese Medicine; TNF α , tumor necrosis factor α ; ZO-1, Zonula Occludens-1.

compared to the diabetic model group. Additionally, SZ-A markedly improved ileal inflammatory injury and pro-inflammatory macrophage infiltration and improved intestinal mucosal barrier function in diabetic KKAY mice. SZ-A also attenuated the levels of circulating endotoxin, pro-inflammatory cytokines, and chemokines in the mice sera. Collectively, SZ-A ameliorated the overall metabolic profile including glucose and lipid metabolism in KKAY mice, which may be associated with an improvement in GLP-1 and insulin secretion, at least in part by modulating the gut microbiome and relieving the degree of ileal and systemic inflammation.

Keywords: *ramulus mori* (sangzhi) alkaloids, type 2 diabetes, gut microbiome, ileal damage, inflammation

INTRODUCTION

The gut microbiome plays important roles in the regulation of glucose and energy homeostasis. It also plays a critical role in obesity, glycemic control, and type 2 diabetes mellitus (T2DM) (Harris et al., 2012), which is a chronic and multifactorial disease in which diverse physiopathologic mechanisms lead to a persistent state of hyperglycemia. T2DM is fundamentally the result of beta cell and alpha cell dysfunction, and insulin resistance in different tissues of the body (Kahn et al., 2014). T2DM may also be due to the activation of pro-inflammatory mechanisms that involve several factors. Gut microbiota-mediated low-grade inflammation is also involved in the onset and progression of T2DM. Studies in mice and humans have shown that there is dysregulation in the gut microenvironment accompanied by immunological and metabolic dysfunctions in individuals who have T2DM (Ge et al., 2018).

Metabolites derived from the gut microbiota, such as short-chain fatty acids (SCFAs) and lipopolysaccharides (LPS), may act as potent immune modulators (Blaak et al., 2020). During eubiosis, the production of SCFAs is essential for maintaining the integrity of the intestinal barrier as well as for immunogenic tolerance. In addition, the effects of SCFAs are not limited to immunomodulatory functions (Salazar et al., 2020), as they can also stimulate the secretion of intestinal peptides that participate in the regulation of appetite and insulin secretion such as glucagon-like peptide 1 (GLP-1) (Grasset et al., 2017). Conversely, in the presence of gut dysbiosis during the progression of T2DM, diet-driven unfavorable microbiota composition can lead to the increased production of pro-inflammatory LPS, which are associated with alterations in gut permeability (Fuke et al., 2019). Subsequently, these inflammatory states might exacerbate the disruption of the mucus layer barrier and increase the epithelial permeability of the small intestine, resulting in elevated LPS levels in the bloodstream, metabolic endotoxemia (Kuti et al., 2020), increased levels of systemic inflammatory mediators, adiposity, obesity, insulin resistance, and hyperglycemia.

Thus, restoration of gut dysbiosis could potentially treat metabolic disorder. Modulation of the intestinal microbiota by interventions has led to a major impact on both the immunological and metabolic functions of the host. In recent years, there has been increasing interest in investigating the use of prebiotics (non-digestible carbohydrates), probiotics (live bacteria), and anti-diabetic drugs for the modulation of gut dysbiosis (Bauer et al., 2018; Hamada et al., 2020). Traditional Chinese Medicine (TCM) has been used to manage T2DM. A large number of studies have shown that the effects of TCM may be, at least

in part, *via* modulation of gut microbiota (Shao et al., 2020; Xiao et al., 2020; Zheng et al., 2020).

The novel TCM *Ramulus mori* (Sangzhi) alkaloid (SZ-A) tablets, also known as Sangzhi Zong Shengwujian, is approved by The China National Medical Products Administration (NMPA, formerly known as the China Food and Drug Administration) for the treatment of patients with T2DM (Approve Number Z20200002). The main components of SZ-A powder (materials for SZ-A tablets) include alkaloids, flavonoids, polysaccharides, coumarin, quercetin, resveratrol, amino acids, and organic acids. SZ-A is a group of effective polyhydroxy alkaloids (50% or more by weight) that potently inhibit α -glucosidase, including 1-deoxynojirimycin (1-DNJ), fagomine (FAG), 1,4-dideoxy-1, 4-iminod-D-arabinitol (DAB), and other soluble polyhydroxy alkaloids or glycosides with a similar structure (Liu et al., 2019a). In preclinical pharmacological studies, chronic treatment of SZ-A was shown to lower fasting and postprandial blood glucose levels in alloxan-induced diabetic mice and rats. SZ-A has also been shown to reduce the peak of postprandial blood glucose in sucrose/starch loading tests in both healthy and diabetic mice after a single dose through the inhibition of intestinal disaccharidases. Moreover, available evidence from our previous study suggests that SZ-A improves dyslipidemia and glucose-stimulated insulin secretion in high-fat diet-induced obese C57 mice after long-term intragastric administration (Liu et al., 2019b). These data suggest that the beneficial role of SZ-A may involve multiple mechanisms in addition to α -glucosidase inhibition. Previous studies have systematically investigated the tissue distribution of the three major active alkaloids, and they found that 1-DNJ, FAG, and DAB are mainly found in the gastrointestinal tract, liver, and kidney, respectively (Yang et al., 2017). Therefore, we hypothesized that the anti-diabetic effects of SZ-A may be *via* regulation of gut microbiota and intestinal metabolites.

In this study, we evaluated the anti-diabetic effects and underlying mechanisms of SZ-A, especially on modulation of gut microbiota, intestinal metabolites, and gut barrier integrity in type 2 diabetic KKAY mice.

MATERIALS AND METHODS

Reagents

SZ-A powder (lot number: 201707008, The total polyhydroxy alkaloid content in SZ-A powder is about 63% by weight, which

was mainly composed of 39% of DNJ, 10.5% of FAG, and 7% of DAB), was kindly provided by the Department of Research & Development of Beijing Wehand-bio Pharmaceutical Co Ltd.

Animal Experimental Design

Animal experiments were performed following the “3R” principles and guidelines for laboratory animals (GB14925-2001 and MOST 2006a) established by the People’s Republic of China. The animal protocol used was approved by the Institutional Animal Care and Use Committee of Institute of Materia Medica (Chinese Academy of Medical Sciences and Peking Union Medical College, Beijing, China). 14-week-old male KKAY mice (30 g) were purchased from Beijing Huafukang Bioscience Co., Ltd (Beijing, China). Animals were maintained at $22 \pm 2^\circ\text{C}$ with a 12 h light-dark cycle with free access to food and water. The 14-week-old male KKAY mice were fed with high-fat diets (45% of energy from fat; D12451; Research Diets, United States). And after 4 weeks of high-fat diets feeding, twenty-four KKAY mice were selected and randomly divided into three groups ($n = 8$) according to the levels of blood glucose, triglyceride, total cholesterol, body weight, and percentage of blood glucose increase at 30 min after oral glucose loading: diabetic model group (DM), SZ-A-low dose-treated group (SZ-A 100, 100 mg/kg), SZ-A-high dose-treated group (SZ-A 200, 200 mg/kg). All mice were treated intragastrically with SZ-A solution or an equivalent volume of water once daily for 8 weeks. After 56 days of treatments, all of the mice were fasted overnight and weighted, then were sacrificed *via* cervical dislocation. Subsequently, the ileum tissues were isolated, fixed in paraformaldehyde solution.

Blood Glucose, Lipid, and Glycated Hemoglobin Measurements

After 4 weeks of treatment, blood samples (10 μl from each mouse) were collected from tail tips at the baseline and 4 h after fasting. Fasting blood glucose (FBG) and postprandial blood glucose (PBG) levels were measured using the glucose oxidase method (Biosino Bio-Technology and Science Inc., Beijing, China). After 42 days of treatment, all of the mice were fasted for 4 hours with free access to water. Blood samples (20 μl from each mouse) were collected from tail tips. Blood triglycerides, total cholesterol levels, and glycated hemoglobin (HbA1c) levels were assessed using commercial kits (A5911; Homa Biological, Beijing, China).

Oral Glucose-Stimulated Insulin and Glucagon-like Peptide 1 (GLP-1) Secretion Test

To evaluate the response of insulin and GLP-1 secretion after the oral glucose stimulation, oral glucose-stimulated insulin and GLP-1 secretion test were performed after 5 weeks of treatment. All of the 24 mice were fasted overnight and given D-glucose (2 g/kg) intragastrically, and the orbital blood samples were collected at 0 and 15 min after glucose administration. The levels of insulin and active GLP-1 in blood were monitored using

ELISA kits (80-INSMSU-E10; 43-GP1HU-E01; ALPCO, United States).

Gut Microbiota Profiling and Fecal Short-Chain Fatty Acids Analysis

All of the 24 mice were sacrificed and the luminal contents were collected from the ileum (as the fecal samples) and snap-frozen in liquid nitrogen after 40 days at the end of treatment, followed by storage at -80°C . The gut microbiome in feces was assayed and the abundance and diversity of gut microbiota were analyzed using Illumina MiSeq sequencing (Major Bio-Pharm Technology, Shanghai, China) according to the standard protocol as previously described (Li et al., 2020). The sequence data were processed and analyzed on the free online Majorbio I-Sanger Cloud Platform (www.i-sanger.com). SCFAs in these fecal samples were detected based on our previous report (Cao et al., 2020). Briefly, the SCFAs in each sample were assayed by gas chromatography coupled to a mass spectrometer detector (GC-MS) (Agilent Technologies Inc. CA, United States) and quantified using Masshunter quantitative software. Correlation analysis of SCFAs and gut microbiota was performed on the platform of Majorbio I-Sanger Cloud (www.i-sanger.com). R and p values were obtained using Spearman’s rank correlation.

Histopathological Evaluation, Immunofluorescence, and Immunohistochemistry Assay of the Ileum

About 4 cm of ileum was fixed in 4% paraformaldehyde to prepare 5 μm paraffin slides. The ileum sections from the 24 mice at the end of experiment were stained with hematoxylin and eosin (H&E) for the analysis of inflammatory changes ($n = 8$). Histopathological assessment of inflammatory and crypt damages was assessed as previously stated by a light microscope (Dieleman et al., 1998). Six randomly selected fields from each slide were analyzed. The ileum sections were also stained with the first antibodies against F4/80 (ARG22476) and CD11c ($n = 5$) (ARG59698; Arigo Biolaboratories Corp, Taiwan). For immunohistochemistry analysis, we used Anti-NF- κB p65 (phospho S536) (ab86299, Abcam, Cambridge, United Kingdom) ($n = 5$). Images were captured with a Mirax scanner (3DHISTECH, Hungary), and the area of positive points was calculated with Image Pro (MediaCybernetics, Rockville, MD).

Cytokines and Chemokines Assay in Serum

Blood was collected when the mice were sacrificed after 40 days at the end of treatment. Serum was prepared followed by centrifuged at 4000 rpm and stored at -80°C . The concentration of Endotoxin was determined by ELISA kit, and the concentrations of Interleukin 1 β (IL-1 β), Interleukin 5 (IL-5), Interleukin 10 (IL-10), Interleukin 13 (IL-13), Interleukin 1a (IL-1a), Interleukin 6 (IL-6), Interleukin 12b (IL-12b), Chemokine C-C-Motif Ligand 1 (Ccl11), Chemokine C-C-Motif Ligand 4 (Ccl4), Chemokine C-C-Motif Ligand 5 (Ccl5) and CXCL

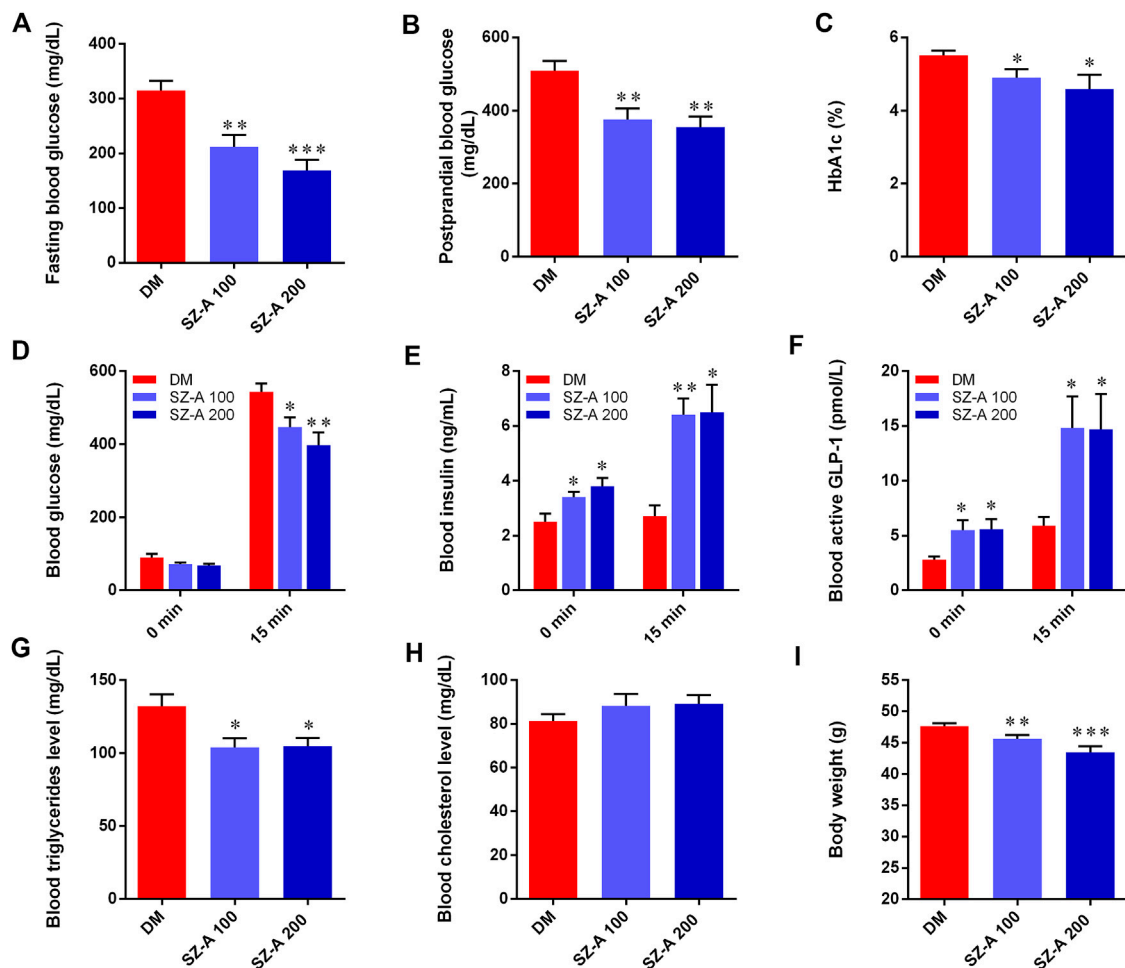


FIGURE 1 | SZ-A ameliorates glucose and lipid metabolism in KKAY mice. **(A)** Fasting blood glucose. **(B)** Postprandial blood glucose. **(C)** Hemoglobin A1c (HbA1c) levels. **(D)** Blood glucose, **(E)** Blood insulin and **(F)** active glucagon-like peptide 1 (GLP-1) levels at 0 and 30 min in oral glucose-stimulated insulin and GLP-1 secretion test. **(G)** Blood triglyceride levels. **(H)** Blood total cholesterol levels. **(I)** Body weight of mice. Data are expressed as mean ± standard error of the mean (SEM), $n = 8$. * $p < 0.05$, ** $p < 0.01$, *** $p < 0.001$ vs. DM. DM, diabetic model group, SZ-A 100, SZ-A low-dose-treated group, SZ-A 200, SZ-A-high-dose-treated group.

chemokine ligand 1 (CXCL1) in serum were determined by Luminex liquid suspension chip detection, which was performed by Wayen Biotechnologies (Shanghai, China). The mouse 23-plex Multi-Analyte kit (Bio-Plex suspension Array System; Bio-rad, Hercules, CA, United States) was used following the manufacturer's instructions. The exact protocol was administered according to what had been reported before (Wei et al., 2015).

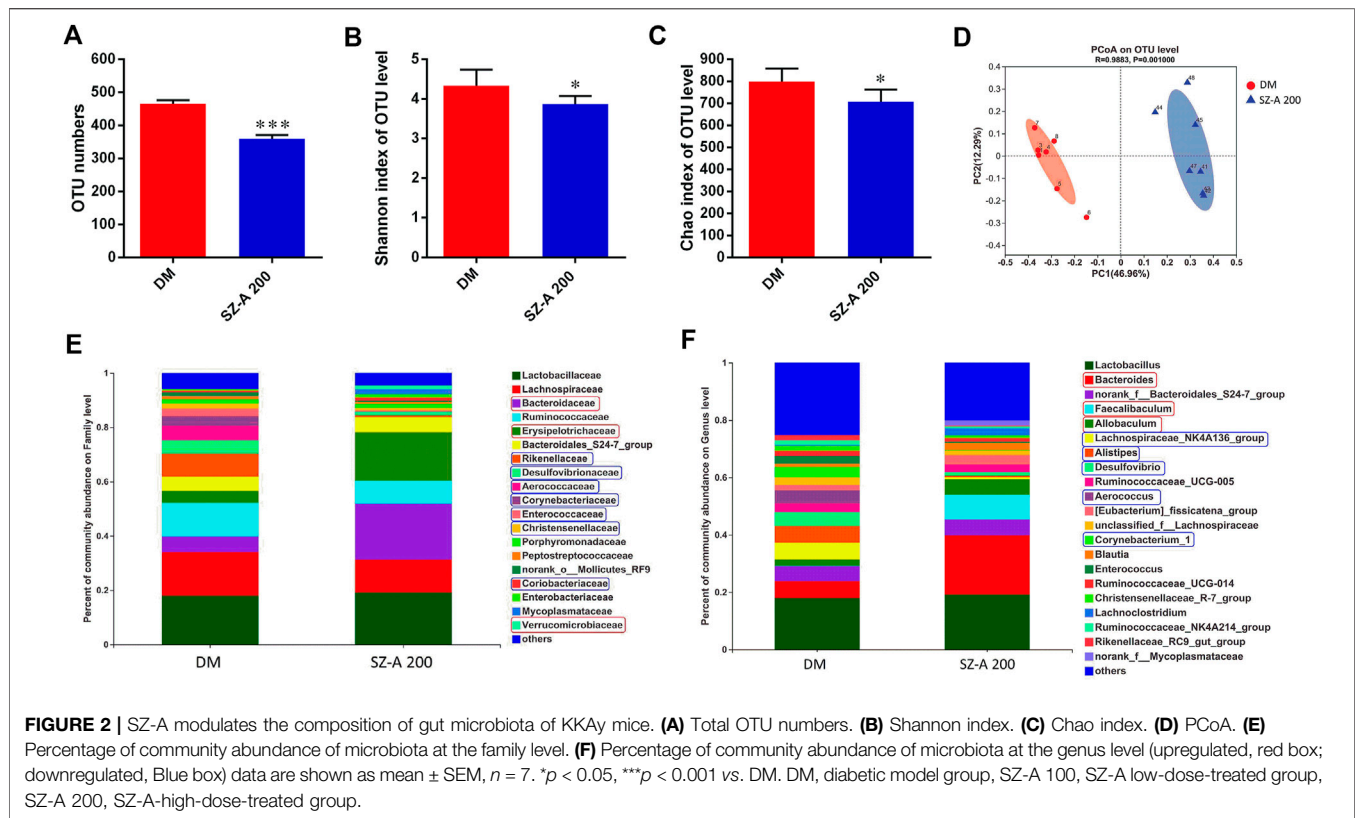
Western Blotting and Quantitative Real-Time Polymerase Chain Reaction

Ileum tissues were homogenized and lyzed in radio-immunoprecipitation assay buffer, and protein concentrations were determined using a BCA protein quantitation kit. Information of the antibodies are as follow, anti-CD11c (97,585, CST, United States), anti-MHC-II (68,258, CST, United States), anti-MCP1 (ARG56590, Arigo Biolaboratories

Corp, Taiwan), anti-SLC5A8 (21433-1-AP), anti-MCT1 (20139-1-AP), and anti-CD36 (18836-1-AP) were from Proteintech Group Inc. Zonula Occludens-1 (ZO-1, 61-7300, Invitrogen, United States), β -Actin antibody (C1313) and secondary antibodies were from (Applygen Technologies Inc., China). Protein levels were normalized to those of β -actin. Quantitative real-time PCR was conducted as previously described. The detailed procedure is presented in the Supplementary Methods. The primer sequences used in this study are shown in Supplementary Table S1.

Tandem Mass Tagging Proteomics Analysis

The primary experimental procedures for TMT proteomics analysis include protein preparation, trypsin digestion, TMT labeling, HPLC fractionation, LC-MS/MS analysis, and data analysis. The detailed procedure is presented in the Supplementary Material. The TMT proteomics analysis in our research is supported by Jingjie PTM BioLabs.



Statistical Analysis

The data are presented as the mean \pm SEM. Statistical analysis was performed using GraphPad Prism 7.0. Differences in FBG, PBG, insulin, GLP-1, lipid levels, and body weight were assessed using a two-way analysis of variance (ANOVA) with Tukey's test. Data sets involved in two groups or multiple groups were analyzed using unpaired two-tailed Student's *t*-test or one-way ANOVA depending on the experiments. Differences with $p < 0.05$ were considered statistically significant.

RESULTS

SZ-A Ameliorates Glucose Metabolism, Enhances the Insulin Response, and Elevates Active GLP-1 Levels During Oral Glucose Tolerance Tests in Diabetic KKAY Mice

After a 4-week treatment, the levels of fasting blood glucose ($p < 0.01$, $p < 0.001$) and postprandial blood glucose ($p < 0.01$, $p < 0.01$) in both SZ-A-treated groups were significantly decreased compared to the DM group (Figures 1A,B). Hemoglobin A1c (HbA1c) levels in SZ-A-treated groups were lower than those in the DM group after a 6-weeks treatment ($p < 0.05$, $p < 0.05$; Figure 1C), indicating that SZ-A exhibited good glycemic control in the KKAY mice during chronic treatment. As shown in Figure 1D, compared to the DM group, both doses of SZ-A significantly reduced blood glucose levels at 15 min after oral glucose loading ($p < 0.05$, $p < 0.01$). We further detected the blood

insulin content and active GLP-1 levels as an indication of insulin and GLP-1 secretory function, respectively. As shown in Figures 1E,F, there was no notable increase in blood insulin content and active GLP-1 level in the DM group after oral glucose loading; however, SZ-A-treated groups had increased both insulin content and active GLP-1 levels at both baseline and 15 min after glucose stimulation. SZ-A 100 and SZ-A 200 significantly enhanced insulin secretion nearly 1.73-fold and 1.88-fold from baseline at 15 min after glucose stimulation, respectively ($p < 0.01$, $p < 0.05$), compared to the DM group (1.11-fold). In addition, both doses of SZ-A elevated active GLP-1 levels nearly 2.7-fold and 2.6-fold at 15 min after glucose stimulation from baseline ($p < 0.01$, $p < 0.05$), respectively, compared to the DM group (2.1-fold). Moreover, both doses of SZ-A resulted in decreased blood triglyceride levels after 6 weeks ($p < 0.05$, $p < 0.05$), and induced significant weight loss compared to the DM group at the end of treatment ($p < 0.01$, $p < 0.001$).

SZ-A Modulates Gut Microbiota Profiling and SCFA Concentration in Feces

The effects of high-dose SZ-A (SZ-A 200, 200 mg/kg) on intestinal microbiota composition were examined by Illumina sequencing-based analysis of bacterial 16S ribosomal RNA in fecal samples collected at the end of 8 weeks treatment. Compared to the DM group, the operational taxonomic unit (OTU) numbers were reduced in the SZ-A 200 group (Figure 2A; $p < 0.001$). The Shannon and Chao indices reflect the diversity and richness of

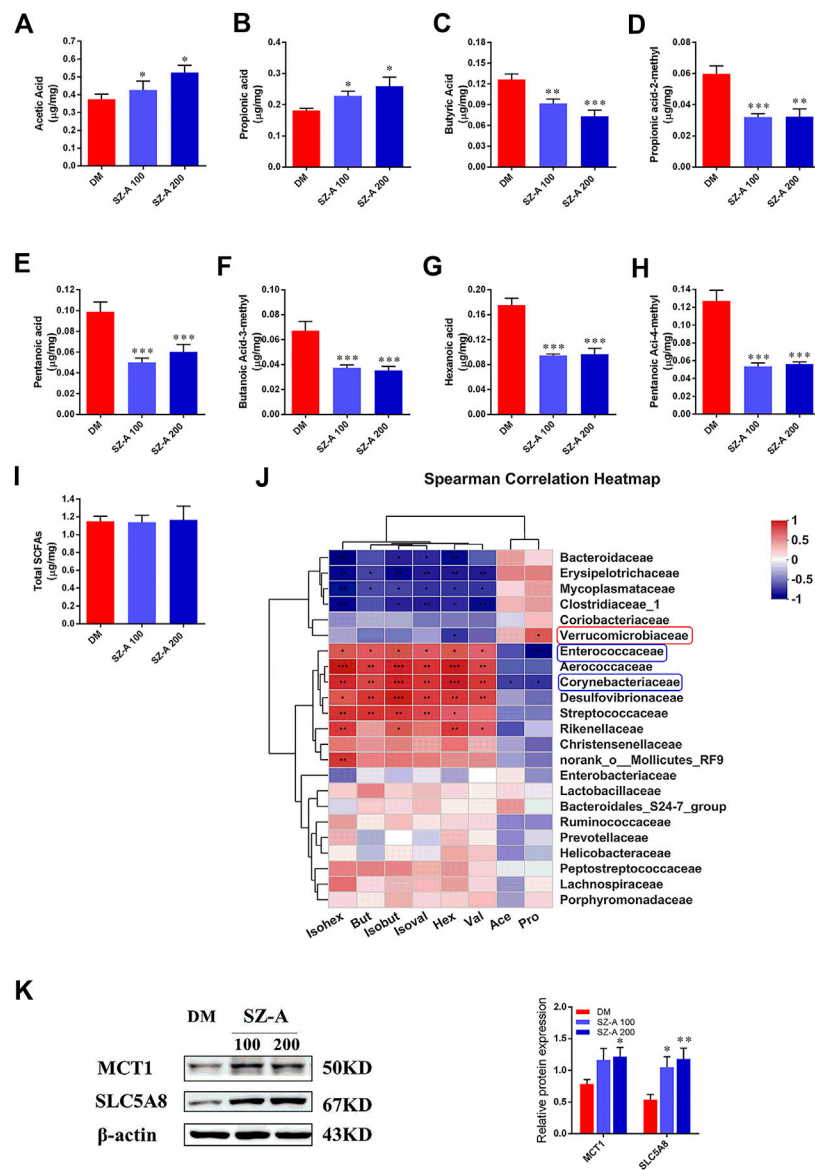


FIGURE 3 | SZ-A alters SCFA composition of fecal samples in KKAY mice. Fecal SCFA concentration, including (A) acetic acid, (B) propionic acid, (C) butyric acid, (D) propionic acid-2-methyl, (E) pentanoic acid, (F) butanoic acid-3-methyl, (G) hexanoic acid, (H) pentanoic acid-4-methyl and (I) total SCFAs. (J) Correlation analysis of SCFAs and specific microbiota at the family level. The p values are shown in different colors in the diagram. The blue represents negative correlation, and red represents positive correlation. $n = 7-8$. (K) MCT1 and SLC5A8 protein abundance in the ileum tissue. The blots shown are representative images. $n = 6$. Data are mean \pm SEM, * $p < 0.05$, ** $p < 0.01$, *** $p < 0.001$ vs. DM. DM, diabetic model group, SZ-A 100, SZ-A low-dose-treated group, SZ-A 200, SZ-A-high-dose-treated group.

gut microbiota, respectively. As shown in Figures 2B,C, SZ-A diminished the indices of Shannon and Chao ($p < 0.05$, $p < 0.05$). Unweighted Unifrac principal coordinate analysis (PCoA) based on OTU levels revealed distinct clustering of microbiota composition in each group (Figure 2D). Multivariate analysis of variance of PCoA matrix scores revealed that the microbiota community of mice in the SZ-A 200 group differed from that of the DM group ($p < 0.001$). Additionally, the bacterial community of SZ-A 200-treated mice differed from that of the DM group. Taxonomic profiling at the family level revealed that SZ-A treatments elevated the abundance of *Bacteroidaceae*,

Erysipelotrichaceae, and *Verrucomicrobia* and reduced that of *Rikenellaceae*, *Desulfovibrionaceae*, and *Aerococcaceae* compared with DM mice (Figure 2E). Similar results were also observed at the genus level. SZ-A 200 decreased the abundance of *Alistipes*, *Desulfovibrio*, and *Aerococcus*, and increased the abundance of *Bacteroides*, *Faecalibaculum*, and *Allobaculum* compared with the DM group (Figure 2F). Collectively, these findings indicate that SZ-A 200 modulates the composition of gut microbiota.

Short-chain fatty acids (SCFAs) are generated in the gut by bacterial fermentation of dietary fiber. Fecal SCFA concentrations were quantified to assess the impact of SZ-A on bacterial metabolic

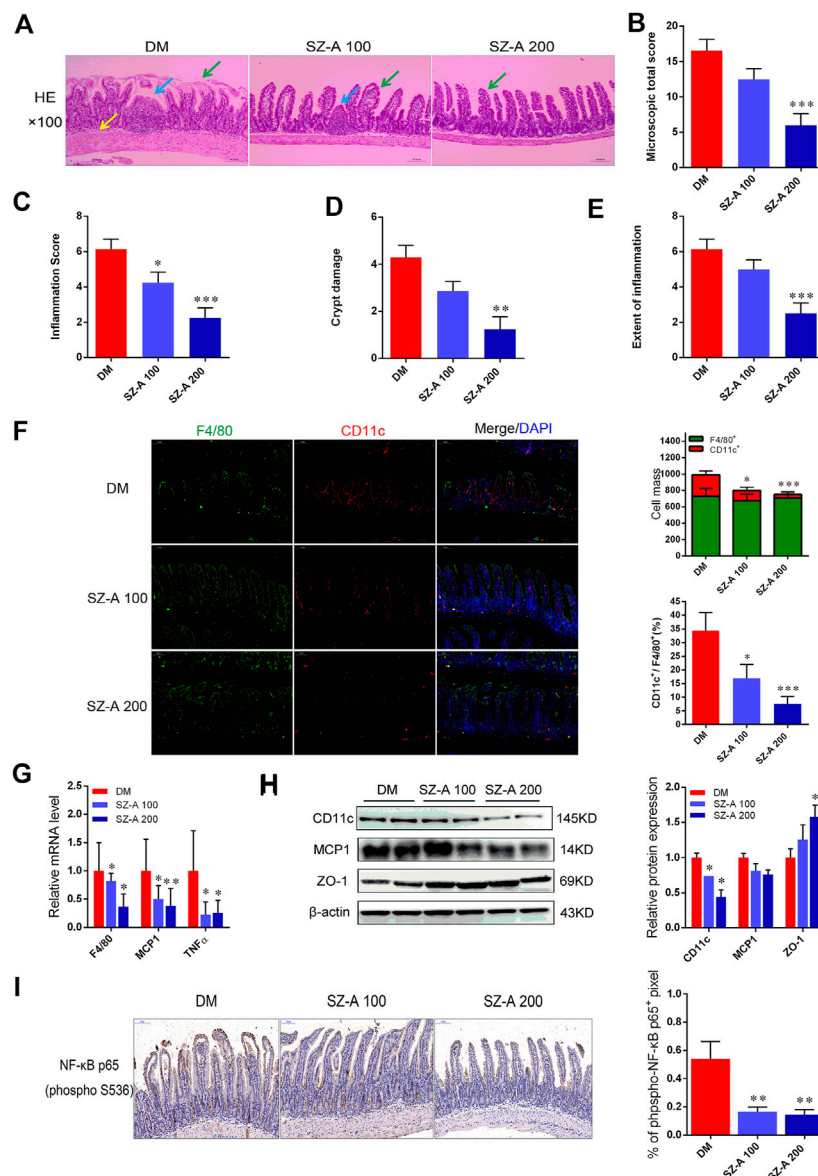


FIGURE 4 | SZ-A alleviates ileal inflammatory injury and pro-inflammatory macrophage infiltration in KKAY mice. **(A)** Representative H&E staining of the ileal section (scale bar, 200 μm). **(B)** Histopathological assessment of total score. **(C)** Inflammation score. **(D)** Crypt damages score. **(E)** Extent of inflammation score of ileal sections. **(F)** Representative F4/80 (green), CD11c (red) and DAPI (blue) immunofluorescence staining of ileum tissues (Scale bar, 100 μm). The histograms indicate quantification of F4/80 (F4/80⁺) or CD11c (CD11c⁺) positive cells per field and percentages of CD11c positive cells in macrophages (F4/80⁺) ($n = 5$ per group). **(G)** Real-time PCR analysis of F4/80, MCP1 and TNF-α levels in ileal homogenates ($n = 5$ per group). **(H)** CD11c, MCP1 and ZO-1 protein abundant levels. The blots shown were representative images. **(I)** Sections of the ileum were stained with anti-NF-κB p65 (p-S536), the histograms indicate quantification of p-NF-κB p65 positive area per field ($n = 5$ per group). Data were mean ± SEM, * $p < 0.05$, ** $p < 0.01$, *** $p < 0.001$ vs. DM. DM, diabetic model group, SZ-A 100, SZ-A low-dose-treated group, SZ-A 200, SZ-A-high-dose-treated group.

activity in KKAY mice. The concentrations of acetic ($p < 0.05$, $p < 0.05$) and propionic acids ($p < 0.05$, $p < 0.05$) were elevated in both SZ-A-treated groups (Figures 3A,B), whereas butyric, isobutyric (propionic acid-2-methyl), pentanoic, isopentanoic (butanoic acid-3-methyl), hexanoic, and isohexanoic (pentanoic acid-4-methyl) acids decreased in the SZ-A-treated groups compared to the DM group (Figures 3C–H). No significant changes were observed in total SCFA concentration between the SZ-A-treated and DM groups

(Figure 3I). Subsequently, the relationship between fecal SCFAs and intestinal bacterial at the family level was analyzed (Figure 3J). The results showed that *Enterococcaceae* and *Corynebacteriaceae*, *Aerococcaceae*, *Desulfovibrionaceae*, and *Rikenellaceae* were positively correlated with the decreased SCFAs, including butyric, isobutyric, hexanoic, isohexanoic, pentanoic, and isopentanoic acids (Figure 3J). *Enterococcaceae* and *Corynebacteriaceae* abundance was negatively correlated with propionic acid, *Corynebacteriaceae*

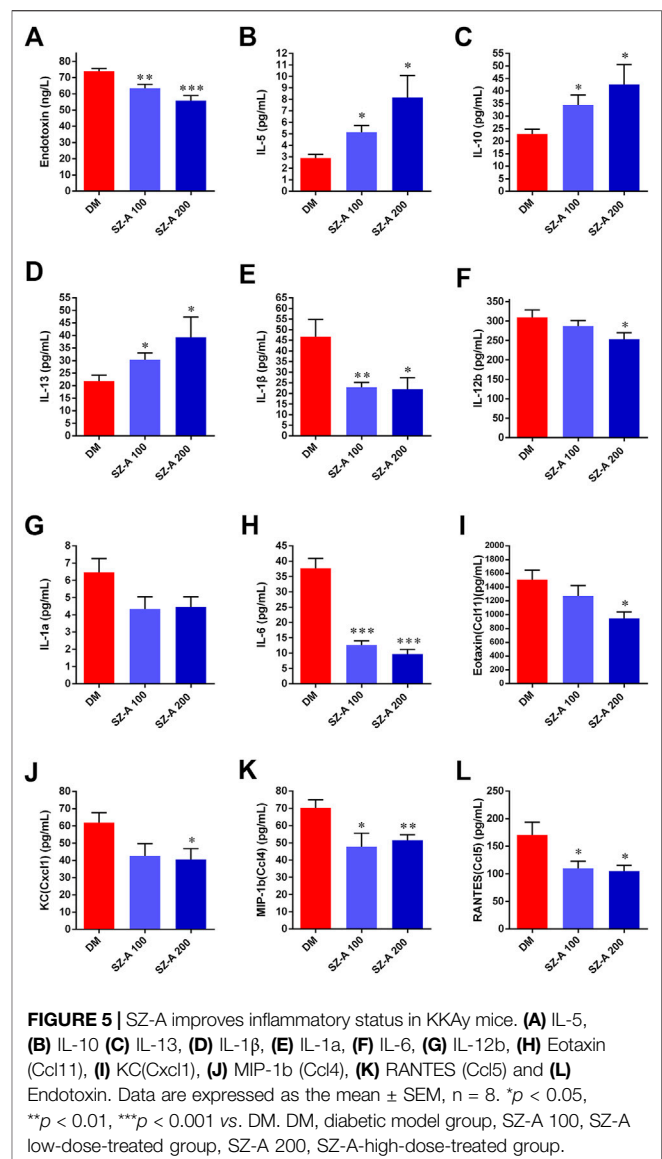
showed no correlation with acetic acid, and *Verrucomicrobiaceae* was positively correlated and propionic acid was observed (Figure 3J). Several transport systems play a role in the cellular uptake of SCFAs in the gut, including monocarboxylate transporter-1 (MCT1) and sodium-coupled monocarboxylate transporter 1 (SMCT1) (SLC5A8). As the transporters responsible for the entry and transcellular transfer of these bacterial products in epithelium are critical determinants of gut function, we detected MCT1 and SLC5A8 protein expression levels in the ileum tissue after SZ-A treatment in KKAY mice. The results showed that MCT1 and SLC5A8 protein levels in ileum from SZ-A-treated mice were significantly increased compared with the DM group.

SZ-A Alleviates Ileal Inflammatory Injury and Pro-Inflammatory Macrophage Infiltration in KKAY Mice

Considering microbial SCFAs production (especially acetate, propionate, and butyrate) is essential for gut integrity by regulating the mucus production, providing fuel for epithelial cells and effects on mucosal immune function, the histological alteration of ileum tissue were evaluated by hematoxylin and eosin (H&E) staining. As shown in Figure 4A, in the DM group, a dense inflammatory cellular infiltrate was present in the mucosa and submucosa and crypts showed typical shortening. Focal crypts were lost and the surface epithelium was damaged (Figure 4A). Microscopic total score and scores for the three features (inflammation, extent of inflammation, and crypt damage) were given for each group (Figures 4B–E). Inflammation scores were significantly reduced by both doses of SZ-A ($p < 0.05$, $p < 0.001$). Moreover, microscopic total score, crypt damage score, and inflammation score were significantly reduced in the SZ-A 200 group ($p < 0.001$, $p < 0.01$, and $p < 0.001$). Collectively, long-term SZ-A treatment prevented the development of inflammation and restored ileal barrier integrity in diabetic KKAY mice.

The KKAY mice were fed a high-fat diet (HFD) to induce diabetic syndrome. Given the critical role of M1 macrophages in HFD-induced intestinal inflammation, in parallel to those histological changes, macrophage-specific F4/80 and CD11c expression was measured to verify whether SZ-A treatment was able to modulate macrophage infiltration in the ileum tissue. As shown in Figure 4F, compared to the DM group, fewer pro-inflammatory CD11c-positive macrophages were observed in both doses of SZ-A-treated groups ($p < 0.05$, $p < 0.001$). This indicates a reduced inflammatory state after SZ-A treatment, and fully consistent with this result, we found downregulated mRNA expression of F4/80 ($p < 0.05$, $p < 0.05$) and multiple pro-inflammatory factors, including MCP1 ($p < 0.05$, $p < 0.01$) and TNF- α ($p < 0.05$, $p < 0.05$; Figure 4G), and also reduced CD11c protein expression in the ileum of SZ-A-treated groups ($p < 0.05$, $p < 0.05$; Figure 4H), compared to the DM group. Given that inflammation damages gut permeability and integrity, we also detected the protein expression levels of zonula occludens-1 (ZO-1), an intestinal tight junction component. SZ-A 200 markedly elevated ZO-1 protein levels ($p < 0.05$) compared to the DM group.

Nuclear factor kappa B (NF- κ B) is critically associated with the progression of inflammation and cell proliferation in the



intestinal mucosa. Therefore, the effects of SZ-A on NF- κ B activity on the ileal mucosa were investigated. The indices of the phosphorylated (p-NF- κ B) p65-positive area were markedly reduced with SZ-A treatment ($p < 0.01$, $p < 0.01$; Figure 4I). These findings indicate that SZ-A significantly alleviated ileal inflammatory injury and attenuated the inflammatory state induced by pro-inflammatory macrophage infiltration of the ileum tissue in diabetic KKAY mice.

SZ-A Attenuates Endotoxin Content, Pro-Inflammatory Cytokine, and Chemokine Levels in Serum of Diabetic KKAY Mice

Gut dysbiosis not only leads to increased intestinal permeability, but it also results in the translocation of

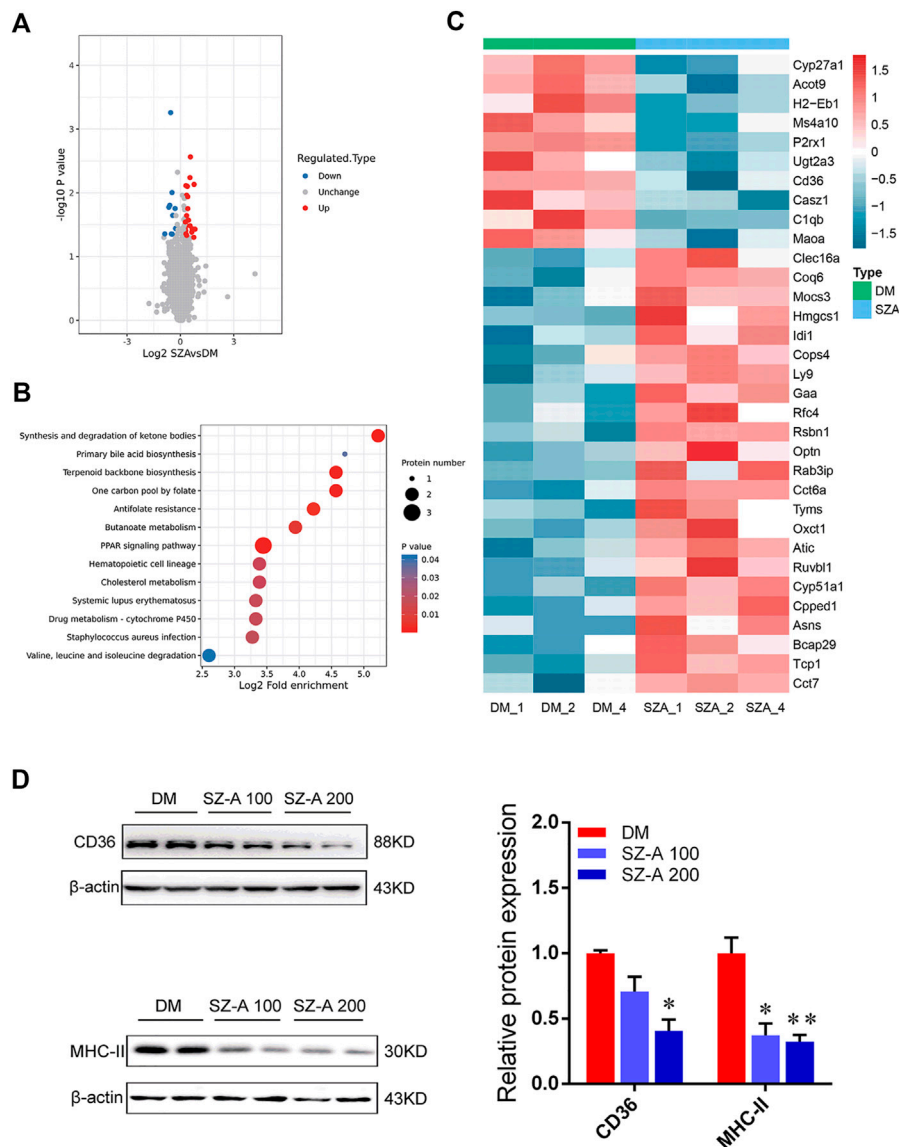


FIGURE 6 | Functional enrichment analysis of differentially abundant proteins in the ileum tissues of KKAY mice after long-term SZ-A treatment. **(A)** Volcano plot shows the differentially abundant proteins in the ileum of SZ-A-treated group (FDR < 0.01). Significantly differentially abundant proteins were color-coded: red indicates upregulated proteins, blue shows downregulated proteins. Two clusters consisting of 24 upregulated and 10 downregulated proteins. **(B)** Bubble diagram of enrichment of differentially abundant proteins in KEGG. The results of the first 20 classifications with the most significant enrichment were given in the bubble diagram ($p < 0.05$). **(C)** The heat map from three independent proteomic analyses of testes from the DM and SZA group. **(D)** Validated the downregulated proteins in ileum of DM and SZ-A-treated groups by Western blotting. CD36 and MHC-II protein abundant levels. The blots shown were representative images. Data are mean \pm SEM, $n = 6$. * $p < 0.05$, ** $p < 0.01$ vs. DM. DM, diabetic model group, SZA, SZ-A-high-dose-treated group.

bacterial products into circulation, inducing a state of chronic low-grade inflammation, such as LPS in HFD-induced diabetes. Considering the effects of SZ-A on modulating gut microbiota profiling and alleviating ileal inflammatory injury, serum endotoxin content, and levels of cytokines and chemokines were determined after SZ-A treatment of diabetic KKAY mice.

Compared with the DM group, both doses of SZ-A markedly diminished serum levels of the endotoxin content ($p < 0.01$, $p < 0.001$; **Figure 5A**), inflammatory cytokines and

also chemokines, such as interleukin 1β (IL- 1β , $p < 0.01$, $p < 0.05$; **Figure 5E**), IL-6 ($p < 0.001$, $p < 0.001$; **Figure 5H**), chemokine ligand 4 (CCL4) ($p < 0.05$, $p < 0.01$; **Figure 5K**), and CCL5 ($p < 0.05$, $p < 0.05$; **Figure 5L**). Additionally, serum levels of IL-12 β ($p < 0.05$; **Figure 5F**), CCL11 ($p < 0.05$; **Figure 5I**), and CXCL1 ($p < 0.05$; **Figure 5J**) were also significantly reduced in the SZ-A 200-treated group. However, serum levels of anti-inflammatory cytokines IL-10 ($p < 0.05$, $p < 0.05$; **Figure 5C**) and IL-13 ($p < 0.05$, $p < 0.05$; **Figure 5D**) serum were markedly elevated.

Functional Enrichment Analysis of Differentially Abundant Proteins in the Ileum after SZ-A Treatment

Proteomics were used to determine the molecular characteristics of the ileum in the high-dose SZ-A-treated group (SZ-A) and DM group in KKAY mice. Refer to the supplementary data **Supplementary Figure S1**, liquid chromatography tandem mass spectrometry identified 208,219 secondary spectra. A total of 42,677 matching effective spectra were obtained. Using a false discovery rate (FDR) < 1% at the peptide and protein levels, 25,060 of the 25,816 peptides were identified as specific, and 4352 of the 5043 proteins were quantifiable (**Supplementary Figure S1A**). A total of 34 proteins were differentially expressed (fold change >1.2, $p < 0.05$; **Figure 6A**) between the DM group and SZ-A group, of which 24 proteins were upregulated and 10 were downregulated. To determine the characteristics of the differentially expressed proteins, we annotated the subcellular localization, Clusters of Orthologous Group, and Gene Ontology (GO) of the 34 proteins. Annotation of the subcellular localization showed that 44.12% of all identified differentially expressed proteins were localized in the cytoplasm, 14.71% in the plasma membrane, 14.71% in the mitochondria, 11.76% in the nucleus, 8.82% in the extracellular space, and 5.88% in the endoplasmic reticulum (**Supplementary Figure S1B**). Most differentially abundant proteins participated in and regulated the cellular and metabolic processes (**Supplementary Figure S1C**). COG functional classification revealed that most of these differentially abundant proteins played a role in posttranslational modification, protein turnover, and chaperones (**Supplementary Figure S1D**).

Bioinformatics analysis was performed to identify the main biological pathways and functional categories of the differentially abundant proteins (fold change >1.2; $p < 0.05$). Kyoto Encyclopedia of Genes and Genomes (KEGG) analysis showed that the most significantly altered pathways were involved in primary bile acid biosynthesis, peroxisome proliferator-activated receptor (PPAR) signaling pathway, synthesis and degradation of ketone bodies, and terpenoid backbone biosynthesis (**Figure 6B**). We identified 34 abundant proteins that were mainly involved in the above-mentioned pathways (**Figure 6C**). These proteins included downregulation of cluster of differentiation 36 (CD36), a protein related to the PPAR pathway; CYP27A1, the representative differentially abundant protein related to primary bile acid biosynthesis; and histocompatibility 2 class II antigen E beta, which is critical in the antigen processing and presentation pathway and is also described as major histocompatibility complex class II (MHC II). The expression level of these key regulators identified *via* proteomics was also confirmed by Western blotting. The results showed the level of CD36 (SZ-A 200 group; $p < 0.05$) and MHC II ($p < 0.05$, $p < 0.01$) were significantly reduced in SZ-A-treated groups compared to the DM group (**Figure 6D**), which is consistent with proteomics analysis.

DISCUSSION

In this study, we evaluated the therapeutic efficacy of SZ-A in glucose and lipid metabolism *in vivo* in the diabetic KKAY mice.

We found that SZ-A ameliorated glucose metabolism and enhanced the insulin response to oral glucose tolerance tests and elevated active GLP-1 levels in diabetic KKAY mice. We suspect that the increased glucose-stimulated insulin secretion might be primarily linked to the improved β -cell function after SZ-A treatment, or related to the elevated blood levels of active GLP-1 in KKAY mice. However, the fact that oral (current study) but not intraperitoneal injection of glucose was associated with improved glucose tolerance in KKAY mice after SZ-A treatment indicated the potential involvement of incretin hormones.

GLP-1, an incretin hormone released in response to the ingestion of nutrients, acts as a hypoglycemic hormone to improve postprandial glucose homeostasis by enhancing meal-induced insulin secretion. GLP-1 activity is mediated by the GLP-1 receptor (GLP-1R). GLP-1Rs are highly expressed in pancreatic β -cells and other tissues including neurons in specific central brain regions, the kidney, and the gut tract (Gray et al., 2020). Findings from the clinical trials have also revealed that the administration of GLP-1R agonists (GLP-1RAs) induces weight loss in addition to glucose improvement (Salehi and Purnell, 2019). In our study, we also found that both doses of SZ-A induced significant weight loss at the end of long-term treatment, whereas the glycemic-lowering effects of GLP-1RAs were mainly attributed to endocrine actions at the level of pancreatic islets. Thus, we evaluated changes in α - and β -cell mass or distribution to analyze the functional state of islets after SZ-A treatment. In **Supplementary Figure S2**, immunofluorescence staining showed that the glucagon-positive area was significantly scattered around the islets in the DM group, suggesting the imbalanced distribution of α -cells. SZ-A decreased the ratio of glucagon-positive area and improved the distribution of α -cells.

GLP-1 is predominantly secreted by neuroendocrine L-cells in the gut. L cells, which produce both GLP-1 and peptide YY, are predominantly expressed in the distal ileum. In humans, prebiotic treatment increases microbiome diversity, which in turn may modulate levels of GLP-1 (Grasset et al., 2017). Moreover, with ileal transposition surgery, L cells located in the transposed ileum are rapidly stimulated by ingested nutrients to produce GLP-1 (Oh et al., 2016). Given the close anatomical proximity, gut microbiota could potentially alter the nutrient-sensing capacity of enteroendocrine cells and subsequent gut peptide release. Additionally, the major components of SZ-A (DNJ, FAG, and DAB) were mainly distributed in the gastrointestinal tract. Therefore, we hypothesized that SZ-A caused the altered active GLP-1 levels, possibly by regulating gut microbiota composition. No study has investigated the effect of SZ-A on the distal ileum microbiota, a site that is crucial for intestinal sensing and absorption of nutrients. Therefore, in this study, we evaluated the interaction between SZ-A and ileal microbiota. Then the effects of SZ-A on the gut microbiota were investigated.

We first characterized the microbiota composition from DM and the high dose-SZ-A treated group (SZ-A 200). Mice were sacrificed and the luminal contents were collected from the ileum (nearly 12 cm distal to the pyloric sphincter). SZ-A increased the abundance of *Bacteroidaceae*, *Erysipelotrichaceae*, and *Verrucomicrobia*. SZ-A also markedly decreased the abundance

of *Rikenellaceae*, *Desulfovibrionaceae*, and *Aerococcaceae* at the family level compared with DM mice (**Figure 2E**). Similar results were observed at the genus level. SZ-A reduced the abundance of *Alistipes*, *Desulfovibrio*, and *Aerococcus*, and increased the abundance of *Bacteroides*, *Faecalibaculum*, and *Allobaculum*. *Bacteroidetes* and *Verrucomicrobia* play crucial roles in producing SCFAs (Harris et al., 2012). We also detected measurable fecal SCFA concentrations in the DM and SZ-A-treated groups, which is consistent with previous studies characterizing the ileal microbiota composition of diabetic KKAY mice. We observed elevated propionate and acetate in the SZ-A-treated groups (**Figures 3A,B**). Propionate and acetate are two of the main SCFAs that are produced by bacteria as a result of resistant starch fermentation. SZ-A-induced microbiota changes facilitated propionate and acetate production in the ileum, which might explain the elevated basal and glucose-stimulated blood active GLP-1 levels in diabetic KKAY mice after SZ-A treatment.

The microbiota-derived metabolites in the luminal contents also represent a potential link to expression changes of nutrient sensors, ligand-receptors, or transporters. **Figure 3** shows that with the exception of propionate and acetate, other SCFA concentrations in ileal luminal contents were decreased after SZ-A treatment. Several transport proteins are involved in the uptake of SCFAs in the gut, including MCT1 and SMCT1 (SLC5A8). These transporters are critical determinants of the entry and transcellular transfer of SCFAs into intestinal epithelium under physiological conditions and in disease states (Bauer et al., 2018). We detected the protein expression levels of these two transporters. There was significant upregulation in the expression of MCT1 and SMCT1 (SLC5A8) in the ileum of SZ-A-treated groups (**Figure 3K**), which is consistent with the decreased level of SCFAs following SZ-A treatment. Collectively, we determined a connection between SZ-A action and changes in ileal microbiota to regulate SCFA production, which in turn, affect glucose homeostasis through the regulation of GLP-1 secretion.

LPS is a major component of the cell wall of gram-negative bacteria and is considered an endotoxin when present in the blood. Increased LPS levels can induce a large number of proinflammatory responses and inflammatory cytokine release (Fuks et al., 2019). Of note, among the changes in the gut microbiota of KKAY mice after SZ-A treatment, the decreased abundance of LPS-containing *Desulfovibrionaceae* was observed. *Desulfovibrionaceae* is an endotoxin producer and has been linked to gut permeability (Clemente-Postigo et al., 2012). There is increasing evidence of the role of gut microbiota in various inflammatory diseases, especially those affecting gastrointestinal tract inflammation. Additionally, butyrate, propionate and acetate are SCFAs that are produced by bacteria as a result of resistant starch fermentation, and have anti-inflammatory properties (Blaak et al., 2020). Due to these effects of SZ-A on the composition of the gut microbiota, it is speculated that SZ-A treatment might repair the inflammatory damage of intestine by modulating the abundance of LPS and SCFA-producing gut microbiota.

Subsequently, H&E staining was performed on the ileum of KKAY mice after SZ-A treatment. Three different sections were studied for each animal. Histological inflammation was scored by two blinded investigators using a modified scoring system

(Dieleman et al., 1998). Considering the degree of inflammation, the transmural vertical extent of inflammation, and the crypt damage score, related to the percentage of involvement of mucosal surface in each slide. As shown in **Figures 4A–E**, this finding supported the occurrence of damage of the ileal mucosal barrier in diabetic KKAY mice (DM group) and repaired ileal inflammatory damage after treatment with both doses of SZ-A. LPS production is also responsible for inducing monocyte- and macrophage-mediated inflammation in the intestine (Wang et al., 2020). Gut macrophages, which reside in the connective tissue underlying the gut epithelium, the lamina propria, are considered key players for the maintenance of intestinal homeostasis and inflammation (Yang et al., 2020). We observed that in ileal tissues, the percentage of macrophages (CD11c⁺/F4/80⁺) and the cell mass of CD11c-positive monocytes were significantly decreased with both doses of SZ-A compared with the control (**Figure 4F**). The degree of expression of F4/80, MCP-1, and TNF α mRNA in both SZ-A-treated groups was significantly decreased compared to the DM group. Similarly, the protein levels of CD11c and MCP1 in the ileum were also reduced by SZ-A treatment (**Figures 4G,H**). The NF- κ B signaling pathway was also detected in the ileum. The phosphorylation of p65 and its nuclear translocation were significantly decreased by SZ-A treatment. These results suggest that SZ-A treatment ameliorate ileal inflammatory damage in KKAY mice with down-regulated inflammatory signaling pathways partly *via* reducing the monocyte recruitment in the ileum.

Over time, major inflammatory signals (e.g., NF- κ B-dependent) become activated in diabetic KKAY mice, thereby stimulating pro-inflammatory cytokine secretion in the small intestine. This inflammatory state might subsequently exacerbate the disruption of the mucus layer barrier and increase epithelial permeability of the small intestine. We observed increased protein levels of the tight junction protein ZO-1 in the SZ-A-treated group, which can reflect the intestinal mucosal barrier function. Our results also confirmed the results that the intestinal mucosal barrier function was improved after treatment of KKAY mice with SZ-A. The persistent inflammatory state not only increases intestinal permeability but also the destruction of tight junction proteins attached to epithelial cells, increasing portal vein and systemic plasma LPS concentrations, and eventually promoting the development of systemic inflammation (Clemente-Postigo et al., 2012). Therefore, we subsequently determined the concentrations of endotoxin and inflammatory cytokines in the serum of KKAY mice. The serum endotoxin levels significantly decreased after both doses of SZ-A treatment, compared to the DM group. The serum levels of inflammatory factors (e.g., IL-1 β , IL-6, CCL4, and CCL5) indicated that low-grade inflammation in diabetic KKAY mice decreased after SZ-A treatment, which corresponded to the endotoxin level. Thus, ileal inflammatory damage in the diabetic KKAY mice was positively associated with low-grade inflammation, which was effectively alleviated by SZ-A treatment.

The production of pro-inflammatory cytokines is related to the LPS-induced activation and polarization of macrophage. We observed there was significantly suppressed polarization of macrophages in the ileum after SZ-A treatment in diabetic KKAY mice. The molecular characteristics of the ileal tissues in the high-dose SZ-A and DM groups in diabetic KKAY mice

were investigated through proteomics. Proteomics analysis revealed that monocyte differentiation into intestinal macrophages involves phenotypic changes with MHCII expression was downregulated by SZ-A treatment, which may be responsible for the improvement of ileal inflammatory damage after SZ-A treatment. Beyond that, the representative differentially downregulated abundant proteins related to PPAR pathway and fat digestion and absorption, ileal CD36 expression level was significantly decreased in SZ-A-treated groups (**Figure 6D**), which might be related to improved blood triglyceride levels.

CONCLUSION

Here, we reported that long-term treatment of SZ-A (8 weeks) is sufficient to alter the microbiota composition in the ileum of diabetic KKAY mice. Our data, together with enriched literature, provide novel mechanistic insights into the role of SZ-A in mediating gut microbial community in ileal inflammatory damage and glucose metabolism.

DATA AVAILABILITY STATEMENT

The datasets presented in this study can be found in online repositories. The names of the repository/repositories and accession number(s) can be found below: NCBI SRA; BioProject ID PRJNA701784. The mass spectrometry proteomics data have been deposited to the ProteomeXchange Consortium via the PRIDE [1] partner repository with the dataset identifier PXD024241.

ETHICS STATEMENT

The animal study was reviewed and approved by the Institutional Animal Care and Use Committee of the Institute of Materia

Medica (Chinese Academy of Medical Sciences and Peking Union Medical College, Beijing, China).

AUTHOR CONTRIBUTIONS

QL, SL: Conceptualization, Methodology, Software. QL, SL: Data curation, Writing- Original draft preparation. HC, CL, and WJ: Visualization, Investigation. YH, LL, YF, and XG: Software, Validation. ZS and YL: Writing-Reviewing and Editing. SL, ZS: Supervision.

FUNDING

The work was supported by the Natural Science Foundation of Beijing Municipality (No. 7202137), National Natural Science Foundation of China (No. 81973379), the Drug Innovation Major Project (No. 2018ZX09711001-003-011 and 2018ZX09711001-009-014), and the CAMS Initiative for Innovative Medicine (CAMSIM) (No. 2020-I2M-1-003).

ACKNOWLEDGMENTS

The authors thank Jingjie PTM BioLab Co. Ltd. (Hangzhou, China) for the mass spectrometry analysis. We would also like to thank Ming Liu (Jingjie PTM Biolabs, Inc.) for technical assistance during this work. We thank LetPub (www.letpub.com) for its linguistic assistance during the preparation of this manuscript.

SUPPLEMENTARY MATERIAL

The Supplementary Material for this article can be found online at: <https://www.frontiersin.org/articles/10.3389/fphar.2021.642400/full#supplementary-material>.

REFERENCES

- Bauer, P. V., Duca, F. A., Waise, T. M. Z., Rasmussen, B. A., Abraham, M. A., Dranse, H. J., et al. (2018). Metformin alters upper small intestinal microbiota that impact a glucose-SGLT1-sensing glucoregulatory pathway. *Cel Metab.* 27 (1), 101–117. doi:10.1016/j.cmet.2017.09.019
- Blaak, E. E., Canfora, E. E., Theis, S., Frost, G., Groen, A. K., Mithieux, G., et al. (2020). Short chain fatty acids in human gut and metabolic health. *Beneficial Micro.* 11 (5), 411–455. doi:10.3920/bm2020.0057
- Cao, H., Li, C., Lei, L., Wang, X., Liu, S., Liu, Q., et al. (2020). Stachyose improves the effects of berberine on glucose metabolism by regulating intestinal microbiota and short-chain fatty acids in spontaneous type 2 diabetic KKAY mice. *Front. Pharmacol.* 11, 578943. doi:10.3389/fphar.2020.578943
- Clemente-Postigo, M., Queipo-Ortuño, M. I., Murri, M., Boto-Ordoñez, M., Perez-Martinez, P., Andres-Lacueva, C., et al. (2012). Endotoxin increase after fat overload is related to postprandial hypertriglyceridemia in morbidly obese patients. *J. Lipid Res.* 53 (5), 973–978. doi:10.1194/jlr.P020909
- Dieleman, L. A., Palmen, M. J., Akol, H., Bloemena, E., Peña, A. S., Meuwissen, S. G., et al. (1998). Chronic experimental colitis induced by dextran sulphate sodium (DSS) is characterized by Th₁ and Th₂ cytokines. *Clin. Exp. Immunol.* 114 (3), 385–391. doi:10.1046/j.1365-2249.1998.00728.x
- Fuke, N., Nagata, N., Suganuma, H., and Ota, T. (2019). Regulation of gut microbiota and metabolic endotoxemia with dietary factors. *Nutrients* 11 (10), 2277. doi:10.3390/nu11102277
- Ge, X., Pan, J., Liu, Y., Wang, H., Zhou, W., and Wang, X. (2018). Intestinal crosstalk between microbiota and serotonin and its impact on gut motility. *Curr Pharm Biotechnol.* 19 (3), 190–195. doi:10.2174/1389201019666180528094202
- Grasset, E., Puel, A., Charpentier, J., Collet, X., Christensen, J. E., Tercé, F., et al. (2017). A specific gut microbiota dysbiosis of type 2 diabetic mice induces GLP-1 resistance through an enteric NO-dependent and gut-brain *Axis* mechanism. *Cel Metab.* 25 (5), 1075–1090. doi:10.1016/j.cmet.2017.04.013
- Gray, S. M., Xin, Y., Ross, E. C., Chazotte, B. M., Capozzi, M. E., El, K., et al. (2020). Discordance between GLP-1R gene and protein expression in mouse pancreatic islet cells. *J. Biol. Chem.* 295 (33), 11529–11541. doi:10.1074/jbc.RA120.014368
- Hamada, Y., Goto, M., Nishimura, G., Nagasaki, H., Seino, Y., Kamiya, H., et al. (2020). The alpha-glucosidase inhibitor miglitol increases hepatic CYP7A1 activity in association with altered short-chain fatty acid production in the gut of obese diabetic mice. *Metab. Open* 5, 100024. doi:10.1016/j.metop.2020.100024
- Harris, K., Kassis, A., Major, G., and Chou, C. J. (2012). Is the gut microbiota a new factor contributing to obesity and its metabolic disorders? *J. Obes.* 2012, 1. doi:10.1155/2012/879151

- Kahn, S. E., Cooper, M. E., and Del Prato, S. (2014). Pathophysiology and treatment of type 2 diabetes: perspectives on the past, present, and future. *Lancet* 383 (9922), 1068–1083. doi:10.1016/S0140-6736(13)62154-6
- Kuti, D., Winkler, Z., Horváth, K., Juhász, B., Páholcsék, M., Stágel, A., et al. (2020). Gastrointestinal (non-systemic) antibiotic rifaximin differentially affects chronic stress-induced changes in colon microbiome and gut permeability without effect on behavior. *Brain Behav. Immun.* 84, 218–228. doi:10.1016/j.bbi.2019.12.004
- Li, C. N., Wang, X., Lei, L., Liu, M. Z., Li, R. C., Sun, S. J., et al. (2020). Berberine combined with stachyose induces better glycometabolism than berberine alone through modulating gut microbiota and fecal metabolomics in diabetic mice. *Phytotherapy Res.* 34 (5), 1166–1174. doi:10.1002/ptr.6588
- Liu, S. N., Liu, Q., Sun, S. J., Li, C., Huan, Y., and Shen, Z. F. (2019a). Anti-diabetic effects of the fraction of alkaloids from *Ramulus Mori*, an innovative Sangzhi alkaloids as an α -glucosidase inhibitor. *Yao Xue Xue Bao* 54 (7), 1233.
- Liu, Z., Yang, Y., Dong, W., Liu, Q., Wang, R., Pang, J., et al. (2019b). Investigation on the enzymatic profile of mulberry alkaloids by enzymatic study and molecular docking. *Molecules* 24 (9), 1776. doi:10.3390/molecules24091776
- Oh, T. J., Ahn, C. H., and Cho, Y. M. (2016). Contribution of the distal small intestine to metabolic improvement after bariatric/metabolic surgery: lessons from ileal transposition surgery. *J. Diabetes Investig.* 7 (Suppl. 1), 94–101. doi:10.1111/jdi.12444
- Salazar, J., Angarita, L., Morillo, V., Navarro, C., Martínez, M. S., Chacín, M., et al. (2020). Microbiota and diabetes mellitus: role of lipid mediators. *Nutrients* 12 (10), 3039. doi:10.3390/nu12103039
- Salehi, M., and Purnell, J. Q. (2019). The role of glucagon-like peptide-1 in energy homeostasis. *Metab. Syndr. Relat. Disord.* 17 (4), 183–191. doi:10.1089/met.2018.0088
- Shao, J., Liu, Y., Wang, H., Luo, Y., and Chen, L. (2020). An integrated fecal microbiome and metabolomics in T2DM rats reveal antidiabetes effects from host-microbial metabolic Axis of EtOAc extract from *Sophora flavescens*. *Oxi. Med. Cell Longev.* 2020, 1805418. doi:10.1155/2020/1805418
- Wang, L., Gong, Z., Zhang, X., Zhu, F., Liu, Y., Jin, C., et al. (2020). Gut microbial bile acid metabolite skews macrophage polarization and contributes to high-fat diet-induced colonic inflammation. *Gut Microbes* 12 (1), 1819155–1819220. doi:10.1080/19490976.2020.1819155
- Wei, Y., Liu, B., Sun, J., Lv, Y., Luo, Q., Liu, F., et al. (2015). Regulation of Th17/Treg function contributes to the attenuation of chronic airway inflammation by icariin in ovalbumin-induced murine asthma model. *Immunobiology* 220 (6), 789–797. doi:10.1016/j.imbio.2014.12.015
- Xiao, S., Liu, C., Chen, M., Zou, J., Zhang, Z., Cui, X., et al. (2020). *Scutellariae radix* and *coptidis rhizoma* ameliorate glycolipid metabolism of type 2 diabetic rats by modulating gut microbiota and its metabolites. *Appl. Microbiol. Biotechnol.* 104 (1), 303–317. doi:10.1007/s00253-019-10174-w
- Yang, S., Mi, J., Liu, Z., Wang, B., Xia, X., Wang, R., et al. (2017). Pharmacokinetics, tissue distribution, and elimination of three active alkaloids in rats after oral administration of the effective fraction of alkaloids from *Ramulus Mori*, an innovative hypoglycemic agent. *Molecules* 22 (10), 1616. doi:10.3390/molecules22101616
- Yang, Y., Li, L., Xu, C., Wang, Y., Wang, Z., Chen, M., et al. (2020). Cross-talk between the gut microbiota and monocyte-like macrophages mediates an inflammatory response to promote colitis-associated tumorigenesis. *Gut* 2020, 320777. doi:10.1136/gutjnl-2020-320777
- Zheng, Y., Ding, Q., Zhang, L., Gou, X., Wei, Y., Li, M., et al. (2020). The effect of traditional Chinese medicine on gut microbiota in adults with type 2 diabetes. *Medicine* 99 (38), e22233. doi:10.1097/md.00000000000022233

Conflict of Interest: The authors declare that the research was conducted in the absence of any commercial or financial relationships that could be construed as a potential conflict of interest.

Copyright © 2021 Liu, Liu, Cao, Ji, Li, Huan, Lei, Fu, Gao, Liu and Shen. This is an open-access article distributed under the terms of the Creative Commons Attribution License (CC BY). The use, distribution or reproduction in other forums is permitted, provided the original author(s) and the copyright owner(s) are credited and that the original publication in this journal is cited, in accordance with accepted academic practice. No use, distribution or reproduction is permitted which does not comply with these terms.



Methanolic Extract of *Lysimachia Candida* Lindl. Prevents High-Fat High-Fructose-Induced Fatty Liver in Rats: Understanding the Molecular Mechanism Through Untargeted Metabolomics Study

OPEN ACCESS

Edited by:

Sayeed Ahmad,
Jamia Hamdard University, India

Reviewed by:

Washim Khan,
University of Mississippi, United States
Md Tanwir Athar,
Prince Sultan Military Medical City,
Saudi Arabia

*Correspondence:

Yashwant Kumar
y.kumar@thsti.res.in
Sanjay K. Banerjee
sanjayk.banerjee@
niperguwahati.res.in
Narayan Chandra Talukdar
nctalukdar@yahoo.com

Specialty section:

This article was submitted to
Ethnopharmacology,
a section of the journal
Frontiers in Pharmacology

Received: 15 January 2021

Accepted: 10 March 2021

Published: 15 April 2021

Citation:

Kamboj P, Sarkar S, Gupta SK, Bisht N, Kumari D, Alam MJ, Barge S, Kashyap B, Deka B, Bharadwaj S, Rahman S, Dutta PP, Borah JC, Talukdar NC, Banerjee SK and Kumar Y (2021) Methanolic Extract of *Lysimachia Candida* Lindl. Prevents High-Fat High-Fructose-Induced Fatty Liver in Rats: Understanding the Molecular Mechanism Through Untargeted Metabolomics Study. *Front. Pharmacol.* 12:653872. doi: 10.3389/fphar.2021.653872

Parul Kamboj¹, Soumalya Sarkar¹, Sonu Kumar Gupta¹, Neema Bisht¹, Deepika Kumari¹, Md. Jahangir Alam², Sagar Barge³, Bhaswati Kashyap³, Barsha Deka³, Simanta Bharadwaj³, Seydur Rahman³, Partha Pratim Dutta^{3,4}, Jagat C. Borah³, Narayan Chandra Talukdar^{3,4*}, Sanjay K. Banerjee^{1,2*} and Yashwant Kumar^{1*}

¹Non-communicable Disease Group, Translational Health Science and Technology Institute (THSTI), Faridabad, India,

²Department of Biotechnology, National Institute of Pharmaceutical Education and Research (NIPER), Guwahati, India, ³Institute of Advanced Study in Science and Technology (IASST), Guwahati, India, ⁴Assam Down Town University, Guwahati, India

Fatty liver is one of the most common metabolic syndrome affecting the global population. Presently, limited treatment modalities with symptomatic approach are available for alleviating fatty liver. Traditional and herbal treatment modalities have shown evidence to improve the disease pathology. In the present research work, evaluation of a selected medicinal plant *Lysimachia candida* Lindl. was carried out to investigate its beneficial effects on fatty liver disease in rats. Male Sprague Dawley (SD) rats were fed with high-fat high-fructose diet to induce fatty liver phenotypes. After induction for 15 weeks, methanolic extract of *Lysimachia candida* Lindl. (250 mg/kg b. w. p. o.) was administered to the rats daily for the next 17 weeks. Blood samples were collected at different time points to analyze fasting blood glucose levels and relevant biochemical parameters important for the assessment of metabolic disease phenotypes. Liquid chromatography-mass spectrometry (LC-MS) based metabolomics was done to study the dynamics of metabolic changes in the serum during disease progression and how the medicinally important plant extract treatment reversed the metabolic diseases. Multivariate data analysis approaches have been employed to understand the metabolome changes and disease pathology. This study has identified the interplay of some metabolic pathways that alter the disease progression and their reversal after administration of the plant extract. Different group of metabolites mainly bile acids, fatty acids, carnitines, and their derivatives were found to be altered in the diseased rats. However, all the metabolites identified between control and disease groups are mainly related to lipid metabolism. The results depict that the treatment with the above-mentioned plant extract improves the regulation of aberrant lipid metabolism, and reverses the metabolic syndrome phenotype. Therefore, the present study reveals the potential mechanism of the herbal extract to prevent metabolic syndrome in rats.

Keywords: animal model, herbal extract, LC-MS/MS, bile acids, fatty acids, PPAR α

INTRODUCTION

The condition in which surplus lipids accumulate in the hepatocytes is known as fatty liver or hepatic steatosis (Allison, 2004). Accumulation of more than 5% lipids in hepatocytes is known as hepatic steatosis as the human liver does not have much capacity to store lipids (Li et al., 2018). Alcohol, chronic hepatitis C, Wilson's disease, abetalipoproteinemia, and porphyria cutanea tarda are mostly found to be associated with hepatic steatosis. Medications like steroids, tamoxifen, and amiodarone are found to precipitate hepatic steatosis (Allison, 2004). Fatty liver disease can be categorized into two main types: non-alcoholic fatty liver disease (NAFLD) and alcoholic fatty liver disease (AFLD) (Singh et al., 2017). NAFLD is a chronic and progressive disease starting from non-alcoholic fatty liver (NAFL) to hepatic cirrhosis and ultimately leading to hepatocellular carcinoma (Sarkar et al., 2020). As per recent prevalence status, 20–46% of the world population has been stated to suffer from NAFLD (Li et al., 2018) with 15–40% patients in the western countries and 9–40% in Asian countries (Amarapurkar et al., 2007). There are no particular clinical symptoms of NAFLD other than discomfort in the right upper quadrant and fatigue. Some other signs include hepatomegaly, splenomegaly, spider naevi, and palmar erythema, although in most cases, the disease is asymptomatic with no signs of clinical manifestation (Allison, 2004).

NAFL is initiated by the deposition of small lipid droplets in hepatocytes, and overtime accumulation of these lipid droplets triggers lipotoxicity. The circulating cytokines together with elevated hepatic reactive oxygen species induce lobular inflammation, which results in the typical characteristic feature of non-alcoholic steatohepatitis (NASH) called hepatocellular ballooning. At advanced stages, the replacement of hepatic tissue with collagen results in the development of fibrotic scar tissues and leads to hepatic cirrhosis and ultimately hepatocellular carcinoma (Rinella, 2015; Carr et al., 2016; Foulds et al., 2017). The histopathological features of NAFLD are similar to alcoholic hepatic damage. Despite extensive research in understanding the pathophysiology of fatty liver diseases, there are still no targeted treatments available till date. The current treatment modalities for AFLD are identical to what it was 50 years ago i.e., abstinence, nutritional support, and corticosteroids (or pentoxifylline unless steroids are contraindicated). Whereas those for NAFLD include weight loss and co-morbidity management (Singh et al., 2017).

There are several evidences where traditional or herbal remedies are found to be useful in ameliorating several pathological features of fatty liver (Xiao et al., 2013). Based on the evidence to practice in North-east part of India by local people, we have selected a plant known as *Lysimachia candida* Lindl. belonging to the family *Primulaceae* (Yang et al., 2012). The plant is native to the north-east region of India and mainly found in Assam and Manipur states. It is commonly known as

loosestrife or kengoi in Manipuri. It is reported to have some pharmacological activity such as ailment of fever, swelling, fracture of bone, dermatitis, and antifungal activity (Xia et al., 2013). This plant has not been explored for its pharmacological effects on fatty liver disease. We have chosen this plant to explore its beneficial effect on fatty liver and validate this plant in the context of its therapeutic effects.

We have demonstrated that feeding high-fat high-fructose (HFHF) diet to Sprague Dawley (SD) rats over a period of 32 weeks not only induces fatty liver phenotypes such as biochemical and histopathological changes but also differentially regulates the level of several metabolites such as bile acids, unsaturated fatty acids and other metabolites involved in inflammation and homeostasis. Therefore, using the untargeted metabolomics approach, the metabolomic profile of rat serum from all three groups were used to identify the different metabolites involved in disease development and how the reversal of disease happens after the intervention of treatment. We identified various metabolites with the help of liquid chromatography-mass spectrometry (LC-MS) and both the enrichment and the pathway analyses demonstrated that peroxisome proliferator-activated receptor alpha is a central pathway through which *Lysimachia candida* Lindl. extract may show a beneficial effect on fatty liver.

MATERIALS AND METHODS

Plant Collection and Identification of Bioactive Compounds

The whole plant *Lysimachia candida* Lindl. were collected from Moirang Kampu, Manipur (Latitude: 25°5'31.995"N to 24°39'45.25"N; Longitude: 94°8'49.324"E to 93°53'47.559"E) in June and July 2017. The Botanical Survey of India, Eastern Regional Centre, Shillong, Meghalaya authenticated the plant (Accession No. 95588). The *Lysimachia candida* Lindl. plant was air-dried for 2–3 weeks and then pulverized to a fine powder by the electric grinder. Exhaustive extraction was performed in a Soxhlet apparatus for 11 h using methanol (Merck) as a solvent. After which, the extract was concentrated under reduced vacuum pressure at 40°C in a rotary vacuum evaporator. The concentrated extracts were further lyophilized using Eyela Freeze Dryer (FDU-506, United States). 1 kg of fresh plant material yielded 100 g of dry powder losing 90% of moisture content and from extraction 1 kg plant material using methanol as solvent yielded 80 gm of dry extract. The final yield of methanolic extract was 8% w/w. Finally, the lyophilized extract was tested for residual methanol present using GC-MS and stored in a sterile container and placed at –20°C until further use. The stored lyophilized extract did not show the presence of any methanol. The extract was reconstituted in 100% methanol to identify bioactive compounds in LC-MS and LC-MS/MS. The Orbitrap Fusion Mass Spectrometer was used to acquire data that is fitted with heated electrospray ionization (HESI) source. Both the negative and positive ions were scanned

at 120,000 resolution in the MS1 mode and 30,000 resolution in the data-dependent MS2 scan mode. The spray voltage of 4,000 and 35,000 V were set for positive and negative modes, respectively. Auxiliary gas and Sheath gas were used and set to 11 and 42, respectively. The Mass scan analyzer was set to scan in the range of 50–1,000 m/z. For MS we have used an automatic gain control target of 200,000 ions with maximum injection time at 80 ms and 20,000 ions were used as an automatic gain control target at a maximum injection time of 60 ms for MSMS analysis. The methanolic extract was separated using HSS T3 column (100 × 2:1 mm i. d. 1.7 µm, Waters) in “UPLC Ultimate 3,000” and the temperature was maintained at 40°C. Mobile phase A containing water with 0.1% formic acid and acetonitrile with 0.1% formic acid was used in mobile phase B. The elution conditions were followed as 0 min, 1% B; 1 min, 15% B; 4 min, 35% B; 7 min, 95% B; 9 min, 95% B; 10 min, 1% B; and 14 min, 1% B with flow rate of 0.3 ml/min and 5 µl sample was injected. The data has been processed using Progenesis QI software with an untargeted approach. We have used different libraries of natural products i. e., spectral data matching with mzCloud and MassBank, Global Natural Products Social Molecular Networking (GNPS) for metabolite identification and in-house developed library of compounds based on purchase authentic metabolites standards and predicting the retention time of metabolites not available with us. Metabolites were confirmed through accurate mass, MS/MS fragmentation and retention time matching.

Animals

To evaluate the potential effect of *Lysimachia candida* Lindl. on fatty liver, male Sprague Dawley (SD) rats were fed with high-fat high-fructose (HFHF) diet for 32 weeks. The animal protocols were approved by the Institutional Animal Ethics Committee (IAEC) of Translational Health Science and Technology Institute (THSTI), Faridabad, India (Protocol No. BIO-IAEC-3357). The study was performed in AAALAC accredited facility in Bionees Pvt. Ltd. Male SD rats aged between 8–12 weeks (200–250 g) was maintained at uniform laboratory conditions in standard steel cages and provided with food and water *ad libitum* during the study period. Rats were housed under standard laboratory conditions environmentally monitored, air-conditioned room with fresh air supply (12–15 air changes per hour), room temperature 22 ± 3°C and relative humidity 30–70%, with 12 h light and 12 h dark cycle. The temperature and relative humidity were recorded once daily.

Study Design and Sample Collection

The plant extract was evaluated in rats using a curative model. Animals were randomly divided into three groups viz., control group, high-fat high-fructose (HFHF) group, and treatment group. All studies were carried out using six rats ($n = 6$) in each group. In the control group, the rats were fed with a normal chow diet for 32 weeks. At starting rats from the other two groups were fed with a high-fat high-fructose diet (Catalog no. D16030909, Research Diet, Inc. United States) for 15 weeks. After 15 weeks, the animals were selected and randomized into two groups viz., vehicle control (HFHF) and test group (Treatment), based on their fasting blood glucose level. The

dose was selected based on efficacy study, LD50 was measured and it is found that dose is safe until 2.5 gm/kg oral dose. We chose one tenth of the dose as efficacy dose. 0.3% CMC vehicle and the plant extract (250 mg/kg/day) in the same vehicle were administered via oral gavage to the HFHF group and treatment group respectively, for 17 weeks along with HFHF diet. At the end of the study, the blood samples were collected in 2 ml ependroff tubes from the retro-orbital sinus for serum isolation. The animals were sacrificed and the liver was collected at the end of the study. All the serum samples and liver were stored at –80°C immediately for further use.

Bodyweight and Food Intake

Changes in body weight and food intake patterns of rats in all groups were noted throughout the experimental period. The weight of each rat was recorded on day 0 and at weekly intervals throughout the study. The quantity of food consumed by each group was recorded weekly.

Blood Glucose Level

Fasting blood glucose level was measured at day 0 (basal), before test item administration and thereafter once in 2 weeks throughout the experimental period. Animals were fasted overnight (approximately 12–16 h) before the experiment. Blood glucose level was measured using a Code-free glucometer through the tail prick method.

Intraperitoneal Glucose Tolerance Test

Overnight fasted (12 h) rats from all groups were subjected to IPGTT at the end of study period. Freshly prepared glucose load of 2 g/kg of body weight was injected intraperitoneally (i.p.) just before 0 min of the experimental timepoint and a drop of blood was withdrawn from the tail vein by small puncture using a needle. Using a commercially available glucometer, blood glucose level was analyzed at 0, 15, 30, 60, and 120 min after injecting the glucose load.

Biochemical Analysis

Serum and tissue triglycerides (TG) assay (Cayman Chemical, Triglyceride Colorimetric Assay Kit), free fatty acids (FFA) assay (FFA Kit, Biovision), and insulin assay (Insulin Kit, Cayman Chemical) were performed according to the instructions provided by the manufacture. For the hepatic TG, liver tissues of each rat were homogenized in NP-40 lysis buffer and centrifuged at 12,000 g for 30 min at 4°C.

Histopathology

At the end of the experimental period, each animal was sacrificed and tissues were collected and washed by buffered normal saline. Tissues were fixed into 10% formalin solution and then dehydrated through graded alcohol series (70–100%), cleared in xylene, and embedded in paraffin. 5–6 µm thick paraffin sections were cut and stained with hematoxylin-eosin (H&E) and Masson's trichrome (MT). Cryopreserved samples were used for Oil-O-Red (OOR) staining. These slides were investigated and analyzed under a light microscope at 40X and 60X magnification.

Metabolomics Analysis

Metabolomics Sample Preparation

Prior to experimentation, the serum samples were thawed at 4°C and kept for 30 min(s). Then, metabolite extraction was carried out by adding 150 µl of ice-cold 100% methanol (LCMS-grade, Merck) in 50 µl serum. The samples were briefly vortexed ~30 s and left on ice for 20 min(s) protein precipitation. Then, samples were centrifuged at 10,000 rpm for 10 min at 4°C. Approximately 150 µl of the supernatant was collected and divided into two microcentrifuge tubes and evaporated to dryness in a vacuum dryer. The samples were stored at –80°C until data acquisition. For reverse-phase chromatography, samples were resuspended in 100 µl of water: methanol (15:85, V/V) and for polar phase chromatography samples were resuspended in 100 µl of water: acetonitrile (50:50, V/V). After brief vortexing, the mixture was centrifuged at 10,000 rpm for 10 min at 4°C. All the supernatants were collected in fresh vials. A Quality Control (QC) sample was prepared by pooling 10 µl from each vial in a microcentrifuge tube (Naz et al., 2017).

Metabolite Measurement

Sample acquisition was done on Dionex Ultimate 3000 RS LC (Thermo Scientific) coupled with Orbitrap fusion MS (Thermo Scientific). Electrospray ionization was used for the better coverage and identification of polar and nonpolar metabolites. Metabolites were separated on reverse phase (C18) and hydrophilic interaction chromatography (HILIC column) in separate runs. The data was acquired in positive and negative ionization modes. The reverse phase column was HSS T3 and the HILIC column was XBridge BEH Amide (Waters Corporation). For, polar compound separation, solvent A was 20 mM ammonium acetate in the water of PH 9.0, and mobile phase B was 100% acetonitrile. The elution gradient starts from 85% B to 10% B over 14 min with a flow rate of 0.35 ml/min. For the reverse-phase, Solvent A was water and B was methanol with 0.1% formic acids added in both. The elution gradient starts with 1% B to 95% B over 10 min with a flow rate of 0.3 ml/min (Yuan et al., 2012; Kumar et al., 2020).

For each sample, injection volume was 5 µl and column temperature was kept at 40°C. The MS1 mass scan range was set to 65–1,000 da. The resolution for MS was 120,000 and for MSMS was 30,000. The MSMS analysis was acquired in ddMS2 mode. The flow rate for Auxiliary and Sheath gas was set at 42 arbs and 11 arbs, respectively. The spray voltage was 3.5 kV for positive mode and 3.0 kV for negative mode. The temperature of the vaporizer was 310°C and the capillary temperature was 300°C. Pool quality control (QC) sample was run after every five samples to monitor signal variation and drift in mass error.

Data Analysis

Metabolomic data analysis was done using compound discoverer (Thermo Scientific) 3.0. Retention time alignment, peak picking, and database search were done in compound discoverer 3.0 with default settings. Metabolite identification was done using the in-house library with retention time, accurate mass, and fragmentation pattern. Additionally, we

used spectral library downloaded from different online databases. All features whose fragmentation score > 30% and retention time were within ± 0.5 min of the in-house library and a CV score of < 30% in the QC samples were selected for further statistical analysis. The statistical analysis and pathway enrichment analysis were done on freely available online metabolomics data analysis tool, MetaboAnalyst (<https://www.metaboanalyst.ca/>). One-way analysis of variance (ANOVA) and Bonferroni's test was applied to compare values between control and treated groups using Graph Pad Prism. Results were expressed as mean ± standard deviation (SD). The values depicting $p < 0.05$ were considered as statistically significant.

RESULTS

Characterization of Methanolic Extract of *Lysimachia Candida* Lindl. by Liquid Chromatography-Mass Spectrometry

The methanolic extract of *Lysimachia candida* Lindl. was characterised by LC-ESI-MS/MS. The LC-MS/MS chromatographic profile (both negative mode and positive mode) showed the presence of several metabolites which include *trans*-3-indoleacetic acid, L-phenylalanine, N-methylalanine, dehydrophyto sphingosine, 3-phenyllactic acid, azelate, 3,5 dimethoxycinnamic acid and cinnamic acid (Supplementary Figures S1, S2). All these compounds were identified by MS/MS fragmentation pattern (Supplementary Figure S3A–I).

Effect of Methanolic Extract of *Lysimachia Candida* Lindl. on Body Weight of High-Fat High-Fructose Diet-Fed Rats

During the experimental period, increase in body weight was observed in all the groups. A substantial increase ($p < 0.001$) in body weight was observed in HFHF diet-fed animals (Figures 1A,B) when compared to normal chow diet animals (Control). Significant ($p < 0.001$) reduction of body weight gain was observed in HFHF diet-fed animals treated with a dose of 250 mg/kg p. o. methanolic extract of *Lysimachia candida* Lindl. over a period of 17 weeks (Figures 1A,B).

Effect of Methanolic Extract of *Lysimachia Candida* Lindl. on Fasting Blood Glucose Level and Insulin Resistance in the High-Fat High-Fructose Diet-Fed Rats

The study showed that there was an increase in fasting blood glucose levels after 15 weeks of HFHF diet. Fasting blood glucose levels were further increased after 17 weeks of HFHF diet (Figure 1C). Oral administration of methanolic extract of *Lysimachia candida* Lindl. to the HFHF-fed animals for 17 weeks showed alleviation in the fasting blood glucose levels (Figure 1C).

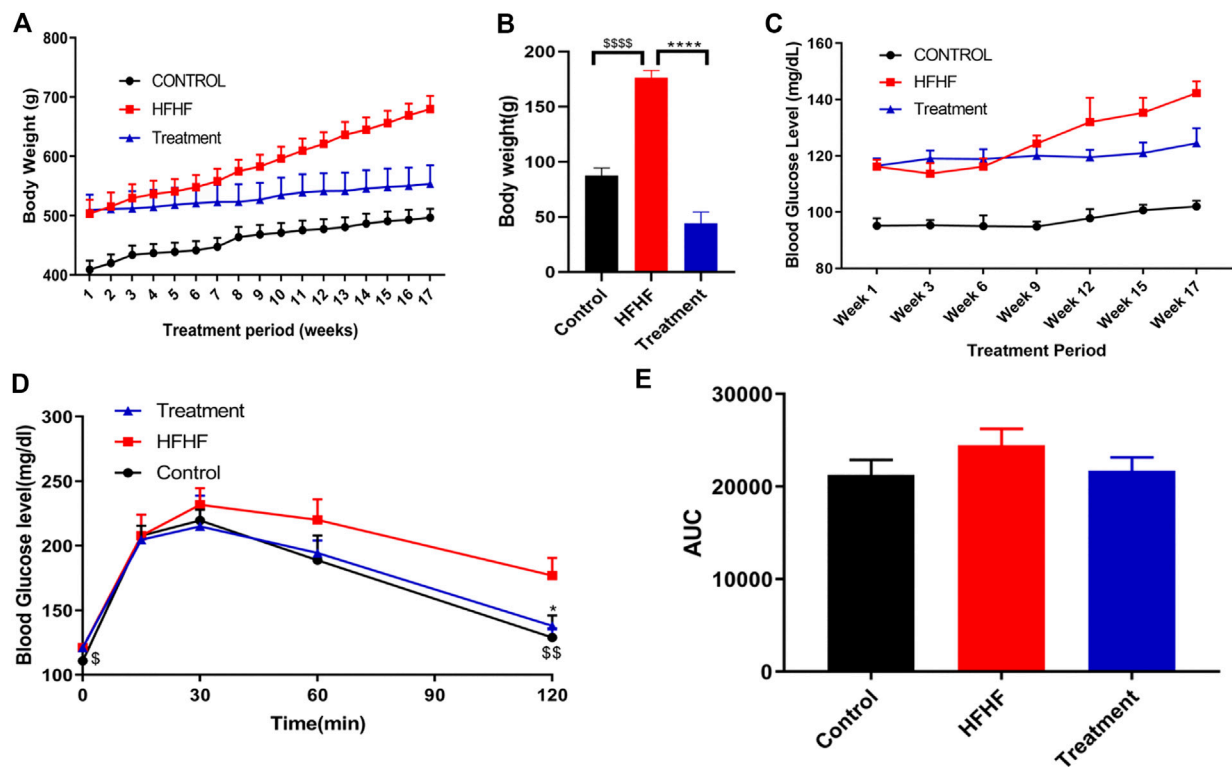


FIGURE 1 | Effect of *Lysimachia candida* Lindl. extract administration on the physical parameters of rats (A) Body weight, (B) Body weight change, (C) Fasting blood glucose, (D) IPGTT, (E) AUC of glucose level. Data are expressed as mean \pm SD ($n = 6$) each group, $p < 0.0001$ **** signifies the statistical difference between HFHF and Treatment, $p < 0.05$ * signifies the statistical difference between HFHF and Treatment, $p < 0.0001$ \$\$\$\$ signifies the statistical difference between HFHF and Control, $p < 0.005$ \$\$\$ signifies the statistical difference between HFHF and Control, $p < 0.05$ \$ signifies the statistical difference between HFHF and Control.

Intraperitoneal glucose tolerance test (IPGTT) was carried out to check insulin resistance of the different experimental groups. As compared to the HFHF group, administration of methanolic extract of *Lysimachia candida* Lindl. prevented the rise in serum glucose levels after 17 weeks of treatment (Figure 1D). Similarly, the area under the curve (AUC) of glucose level in the IPGTT also reveals that HFHF groups have a higher area than control whereas treatment with the extract reduced the AUC to that of the Control group (Figure 1E).

Effect of Methanolic Extract of *Lysimachia Candida* Lindl. on Biochemical Parameters of the High-Fat High-Fructose Diet-Fed Rats

To further explore the effectiveness of the *Lysimachia candida* Lindl. extract, biochemical parameters in the HFHF diet-fed rats were monitored. As shown in Figure 2A, serum insulin level was markedly increased in the HFHF group compared to the Control and treatment groups at the end of the study. Similarly, the HOMA IR data confirmed that there was remarkable insulin resistance in the HFHF group when compared to the other two groups. The increased levels of serum insulin and HOMA IR were decreased in the treatment group when compared to the HFHF group (Figures 2A,B). The increased level of serum and hepatic

triglycerides (TG) in the HFHF group was decreased to the baseline in the treatment group (Figures 2C,D). However, there was no change in the serum of FFA levels among the three groups (Figure 2E). Similar to the change in TG level, increased hepatic FFA was observed in the HFHF group and it decreased after treatment (Figure 2F). Taken together, these data showed that the biochemical parameters were remarkably recovered to baseline in the treatment group although data were not statistically significant.

Effect of Methanolic Extract of *Lysimachia Candida* Lindl. on Histological Changes in High-Fat High-Fructose Diet-Fed Rats

To examine the histological changes in all the groups, the slides were stained with H&E, Masson's Trichrome stain and Oil-O-Red. H&E-stained liver sections of the control group revealed the normal hepatic structure and no hepatocellular ballooning and degeneration characterized by cell swelling with empty intracellular content, indicating cell necrosis and inflammation. By contrast, the liver histology of the HFHF group showed discernible changes such as increased fat accumulation, as well as ballooning and degeneration of hepatocytes. Interestingly, the liver sections of the treatment group showed no to mild ballooning and degeneration of

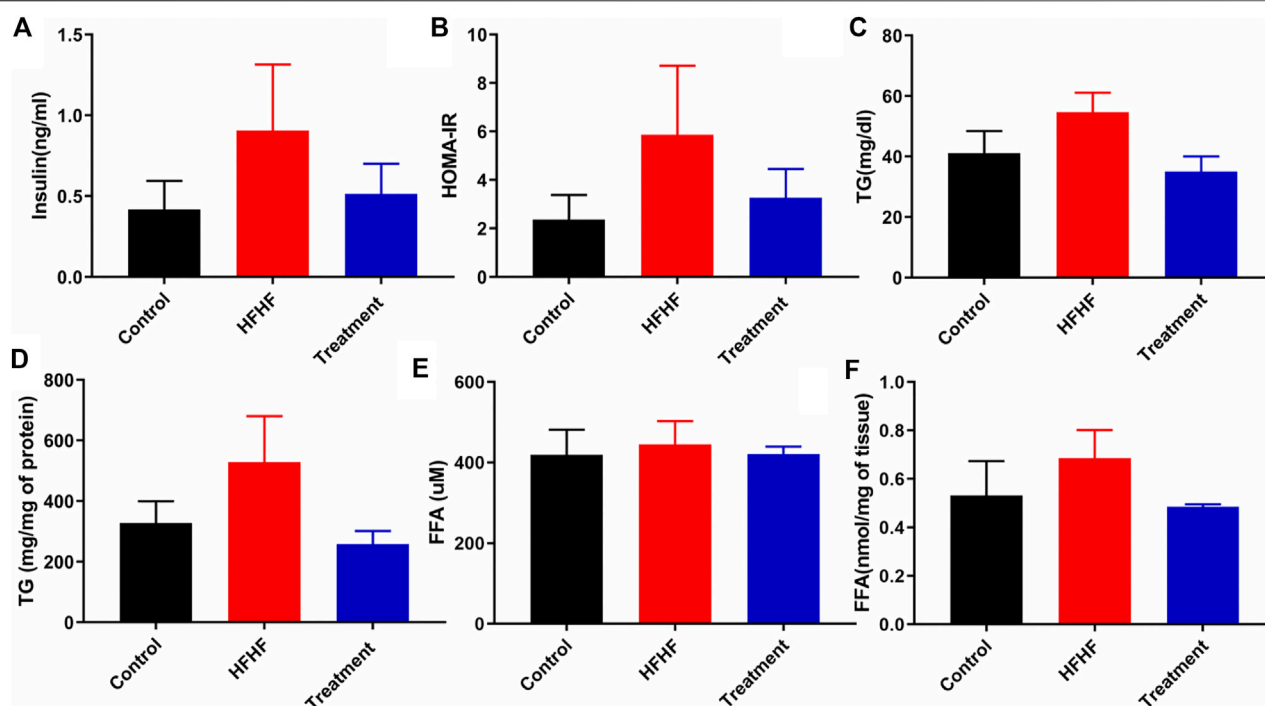


FIGURE 2 | Effect of *Lysimachia candida* Lindl. extract administration on the serum and liver levels of biochemical parameters of rats (A) Serum insulin, (B) HOMA IR, (C) Serum triglycerides, (D) Liver triglycerides, (E) Serum free fatty acid, (F) Liver free fatty acid. Data are expressed as mean \pm SD ($n = 6$) each group, compared with HFHF group.

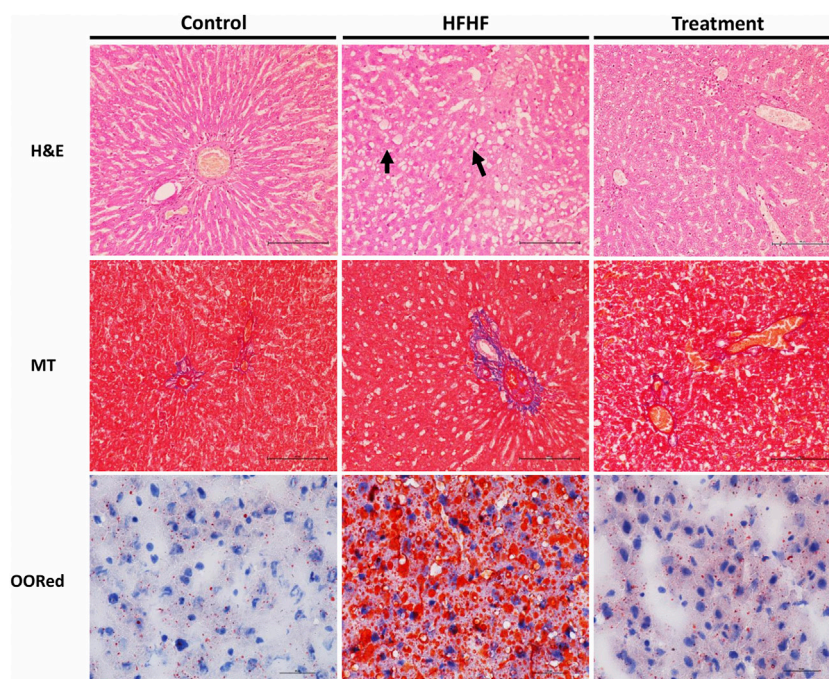
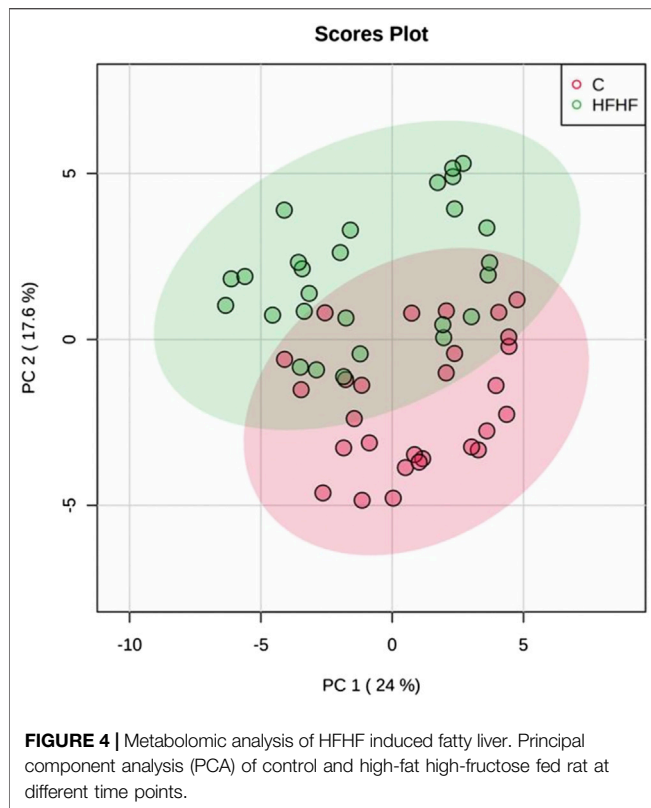


FIGURE 3 | Representative sections of rat liver showing histological alteration in the liver by H&E stain (40X) arrows indicating fat globules, MT stain (40X) indicating fibrosis, and Oil-O-Red stain (60X) indicating the fat accumulation.



hepatocytes. It seems to be in the recovery stage as the central vein was found to be slightly dilated but cells were healthy (Figure 3). Masson's Trichrome stained sections did not show much changes in collagen fiber pattern except a little thinning of connective tissue around the portal tracts of HFHF diet-fed animals (HFHF) as compared to control. Interestingly, treatment group animals did not show any such thinning effect (Figure 3). Oil-O-Red staining unveiled huge macrovascular lipid accumulation in all areas of the lobe indicating steatohepatitis in the HFHF group when compared to the Control and Treatment groups. However, *Lysimachia candida* Lindl. extract treatment reduced the lipid droplets to the levels observed in the control group (Figure 3).

Effect of Methanolic Extract of *Lysimachia Candida* Lindl. on Metabolite Profiling of High-Fat High-Fructose Diet-Fed Rat Serum

To understand the mechanism by which methanolic extract of *Lysimachia candida* Lindl. treatment reverses the disease pathophysiology in high-fat high-fructose (HFHF)-fed rats, we conducted untargeted metabolic profiling using orbitrap fusion mass spectrometry (MS) coupled with ultra-performance liquid chromatography (UPLC). To maximize the coverage of different classes of metabolites and to identify the different classes of metabolites, we have run the rat serum on reverse phase and hydrophilic column. We have identified a total of 155 metabolites in serum samples after combining data from the positive and negative modes (Supplementary Table

S1). Principal component analysis (PCA) has clearly indicated a good separation between the control and HFHF rat serum metabolome. As shown in Figure 4, principal component 1 explains 24% of data and principal component 2 explains 17.6% of the data. The third component explains another 10.9% of the data, then fourth and fifth components explain 7.2 and 4.6% of data respectively. Total variation explained by all the five components is 64.3%. Further, we did a clustering analysis of data to visualize the different metabolites in more detail. Comparison among control, HFHF, and treatment have been done by ANOVA and significantly altered metabolites have been shown in the heatmap (Figure 5). Comparison between control and HFHF rat serum metabolites using clustering indicated the change in bile acids, biosynthesis of unsaturated fatty acid, carnitines, and other metabolites involved in the peroxisome proliferator-activated receptors (PPAR) pathways (Figure 5). Interestingly, the expression of these metabolites has been found to be reversed in the Treatment group. The expression of metabolites such as (+/-) 8-hydroxy eicosapentaenoic acid ((+/-)8-HEPE), pentadecanoic acid, and heptadecanoate was decreased in HFHF group and reversed after the treatment with the plant extract. Similarly, different bile acid levels such as muricholic acid, deoxycholic acid, glycocholic acid, glycochenodeoxycholic acid, and glycodeoxycholic acid were decreased in the serum of HFHF group rats and were found to be normalized after plant extract treatment in early time points (Figure 5). We have also observed that unsaturated fatty acids like linoleic acid and α -eleostearic were decreased in the HFHF group and reversed after treatment (Figure 5). Pathway analysis using metaboanalyst using different metabolites showed that important pathway intervene were linoleic acid metabolism, biosynthesis of unsaturated fatty acids, glycerophospholipid metabolism, and primary bile acid biosynthesis pathway (Figure 6).

DISCUSSION

Non-alcoholic fatty liver disease (NAFLD) is increasingly recognized as a major health problem in developed and developing countries. It includes a spectrum of liver disease ranging from simple steatosis to non-alcoholic steatohepatitis (NASH), advanced fibrosis, and rarely, progression to cirrhosis. NAFLD is associated with several diseases like obesity, insulin resistance, type 2 diabetes mellitus, hyperlipidemia, hypertension, and metabolic syndrome (Bedogni et al., 2005). It has been shown that NAFLD is strongly associated with the features of metabolic syndrome. Insulin resistance is a key pathogenic factor in both NAFLD and metabolic syndrome. Data from experimental and clinical studies indicate that NAFLD may be the hepatic manifestation of metabolic syndrome (Marchesini et al., 2001). There are no drugs i.e., small molecules approved by the FDA to treat NAFLD or NASH. However, few pharmacological modalities have been practiced to ease the associated co-morbidities. Considering the presence of several active biomolecules in herbs and their well-

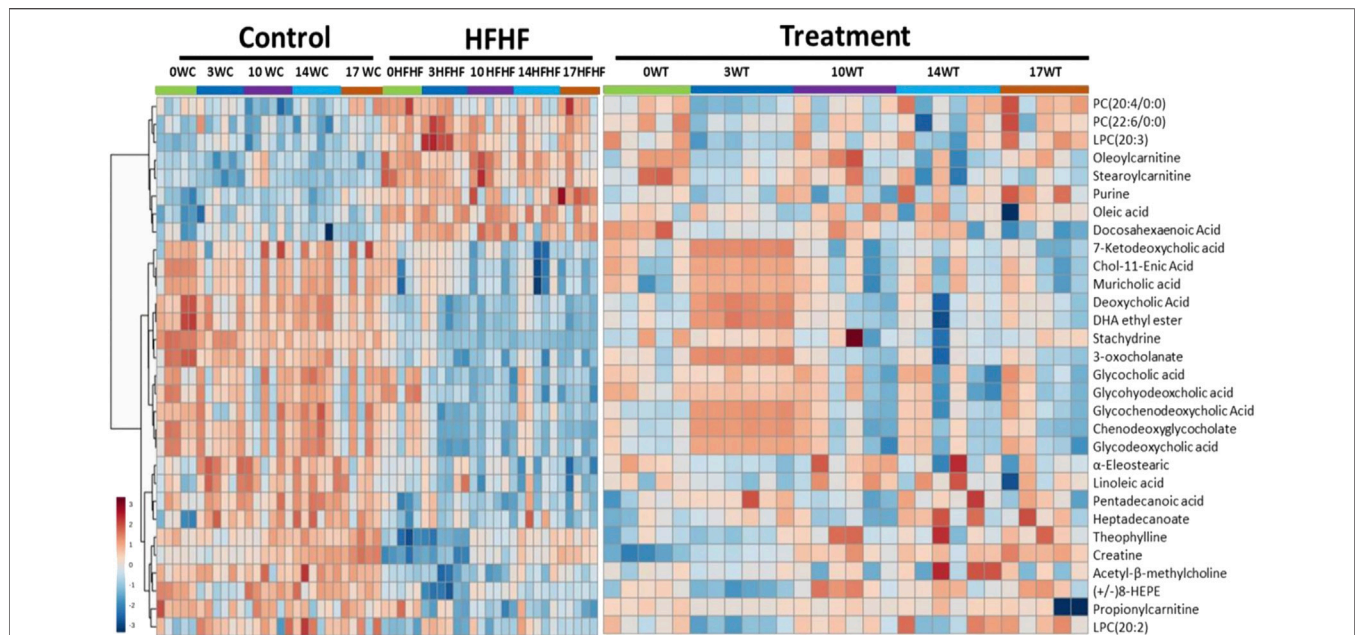


FIGURE 5 | Metabolomic analysis of HFHF-induced fatty liver and the effect of the treatment (*Lysimachia candida* Lindl.). Heat map analysis of different metabolites depicting the effect of treatment on the altered metabolites. Hot (red) colour indicates high expression and cool (blue) colour represents low expression.

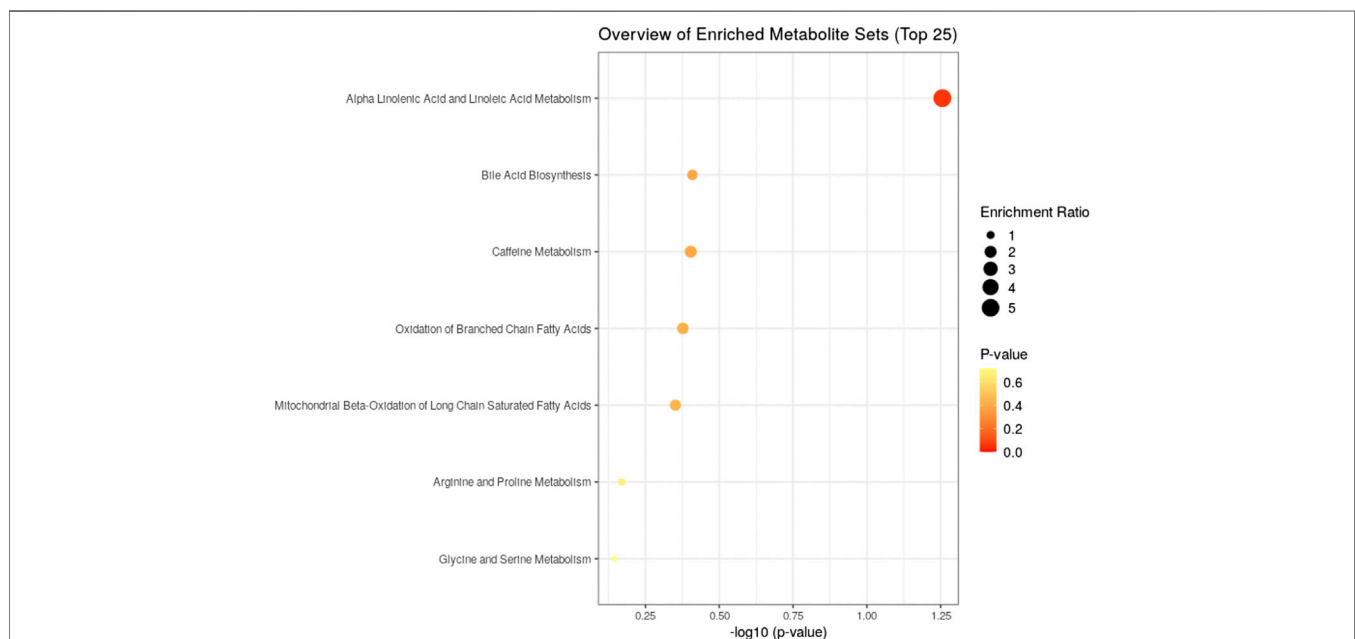


FIGURE 6 | Identified pathway and the metabolites which have the most impact on the pathway using MetaboAnalyst from enriched metabolites.

proven role in health and disease, further research is necessary to confirm the therapeutic role of herbs in patient with NAFLD. Few herbal preparations have already found to be beneficial in ameliorating several pathological features of fatty liver (Hong et al., 2006; Park et al., 2006; Bose et al., 2008; Chidambaram et al., 2010). Here, in the present study, we have selected the

plant *Lysimachia candida* Lindl. widely used by the native population of the northeastern region to cure different metabolic disease, to explore its potential role in preventing HFHF-induced fatty liver in SD rats.

Previously, we and others showed that chronic feeding of high-fat high-fructose diet causes increase in body weight, insulin

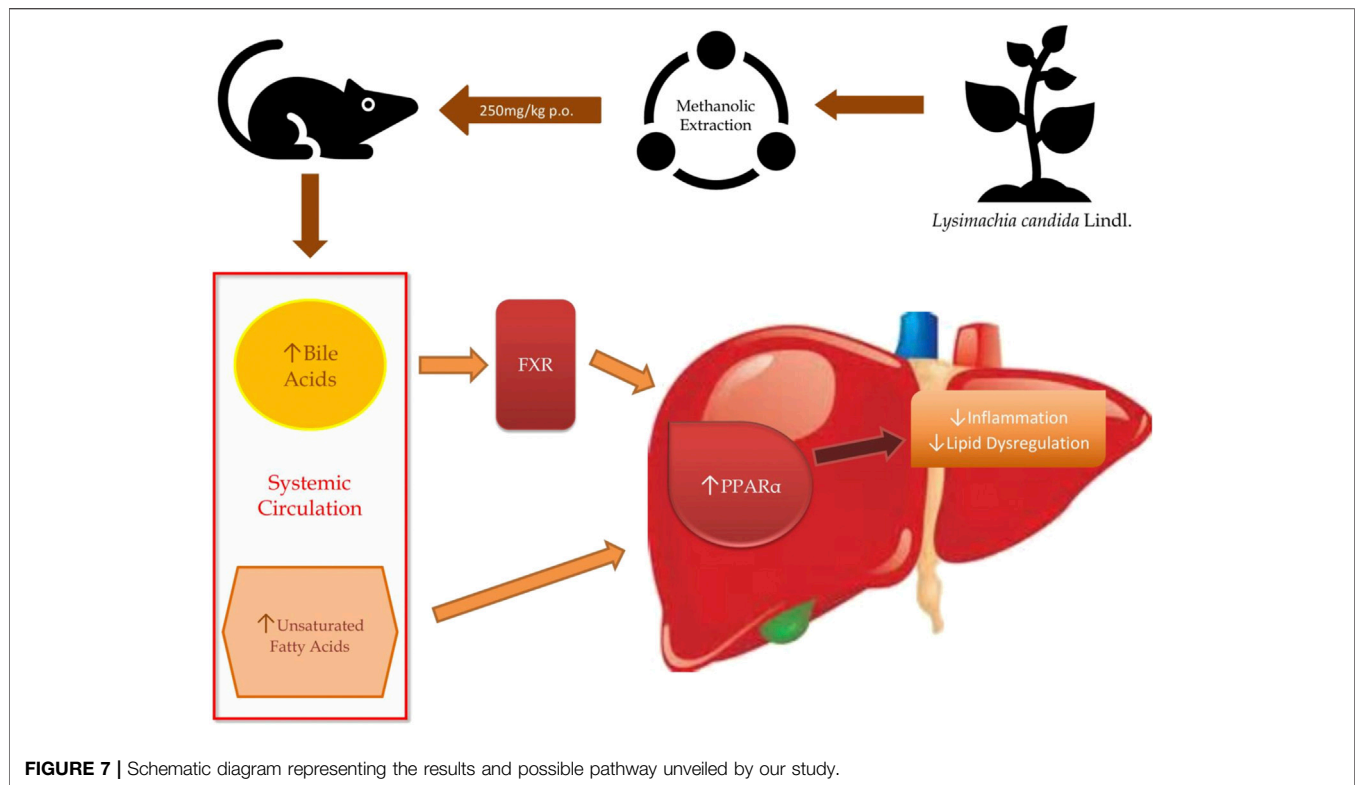


FIGURE 7 | Schematic diagram representing the results and possible pathway unveiled by our study.

resistance, and hyperglycemia (Nizami et al., 2019). In the present study, we have observed a remarkable increase in body weight in the HFHF group indicating obesity in rats. However, reduction in body weight was observed in high-fat high-fructose diet-fed rats after treatment with methanolic extract of *Lysimachia candida*, with not much change in its timeline. Similarly, fasting blood glucose (FBG) level was found to be decreased in the treatment group. The data clearly demonstrate that the methanolic extract of *Lysimachia candida* Lindl. was able to control the FBG levels in the treatment group. The IPGTT curve and its area under the curve reveals that there is an increase in insulin resistance in HFHF group. High levels of insulin were also observed in the HFHF group contrary to the Control group. Insulin resistance in the HFHF was confirmed by the increase in the HOMA IR whereas the treatment with methanolic extract of *Lysimachia candida* Lindl. alleviated the HOMA IR near to the Control, suggesting its potential activity to combat insulin resistance. To check the lipid levels, we measured the TG and FFAs in both serum and hepatic tissue. We found that the serum and hepatic triglyceride levels were increased in the HFHF group while TG levels decreased in the Treatment group when compared with Control. Hence, again the methanolic extract of *Lysimachia candida* Lindl. was successfully able to normalize the TG levels in both serum and liver. Similarly, high levels of hepatic FFAs were observed in the HFHF group, which was decreased after treatment. Therefore, the methanolic extract of *Lysimachia candida* Lindl. is capable of reversing and managing body weight changes, FBG, insulin resistance, TG, and FFA levels.

Histology analysis confirmed the development of fatty liver with early fibrosis. Since Oil-O-Red specifically stains triglycerides together with cholesterol ester, this stain represents the real representation of lipid accumulation (Sarkar et al., 2020). We have observed a high level of lipid deposition in the HFHF group. However, the methanolic extract of *Lysimachia candida* Lindl. administration reduced the fat accumulation similar to the control group. Liver samples from the HFHF group exhibited prominent steatosis, ballooning, and lobular inflammation with mild fibrosis, while the Treatment group unveiled reduced levels of steatohepatitis with no fibrosis. Overall, the histopathology study confirmed the presence of hepatic steatosis, ballooning, lobular inflammation, and perisinusoidal fibrosis in the disease group, which was alleviated in the treatment group.

After confirming the fatty liver phenotype, we wanted to correlate the phenotypic changes in HFHF rats with serum metabolic profiles. The untargeted metabolomic analysis with multivariate data analysis (Principal component analysis) and clustering revealed a clear separation of rat serum metabolome between Control and HFHF groups. Principal component analysis clearly indicates the difference in metabolome in HFHF as compared to control at different time points. Clustering analysis also indicates change in levels of different metabolites in the control and HFHF group. Pathway enrichment analysis of different metabolites suggests a change in linoleic acid metabolism, biosynthesis of unsaturated fatty acids, glycerophospholipid metabolism, and primary bile acid

biosynthesis pathway. Hence, we could infer from our result that high-fat high-fructose diet has altered various metabolites from the normal physiological level. Changes in bile acids, unsaturated fatty acids, carnitines, and other metabolites involved in the peroxisome proliferator-activated receptors (PPAR) pathways were found in HFHF animals. Interestingly, the altered levels of these metabolites have been found to be reversed in the treatment group. PPAR alpha and PPAR gamma are highly expressed in the liver and play a significant role in the synthesis of bile acid and fatty acid uptake (Lee et al., 1995; Mandard et al., 2004). Oxidation of fatty acid and expression of fatty acid transport protein shares a close relationship with nuclear receptor PPAR α and PPAR γ in liver steatosis (Pyper et al., 2010).

The serum metabolites such as (+/-)-8-hydroxyeicosapentaenoic acid ((+/-)-8-HEPE), pentadecanoic acid, heptadecanoate were downregulated in the HFHF group and interestingly, plant extract treatment has reversed their expression. (+/-) 8-hydroxyeicosapentaenoic acid acts as a ligand of PPAR (Forman et al., 1997; Yamada et al., 2014). For the first time, Yamada et al. demonstrated that orally administered 8-HEPE can activate PPAR α , resulting in the decrease of plasma and hepatic TG levels (Yamada et al., 2016). As stated, 8-HEPE is a stimulator of PPAR α , hence decrease levels of 8-HEPE can reduce the activation of PPAR α and increase the serum and hepatic TG levels as we observed in the HFHF group. However, the methanolic extract of *Lysimachia candida* Lindl. administration increased the serum 8-HEPE levels similar to the control group. Two fatty acids, pentadecanoic acid (C15) and heptadecanoic acid (C17) were reduced in HFHF group. Epidemiological researches have revealed that plasma concentrations of odd chain saturated fatty acids like pentadecanoic acid and heptadecanoic acid are related to reduced risks for metabolic disorders like type II diabetes and coronary heart disease (Jenkins et al., 2015). Interestingly, the treatment with methanolic extract of *Lysimachia candida* Lindl. was able to upregulate these odd chain saturated fatty acids levels similar to Control.

Bile acids play a crucial role in maintaining the level of both free and conjugated forms of bile acids in the peripheral circulation. In hepatic disease, levels of bile acids are aberrated especially in synthesis, excretion, and reabsorption of bile acids, which raises the level of total bile acids. Some studies have demonstrated the effect of liver injury on bile acid metabolism (Wang et al., 2012; Beyoğlu and Idle, 2013). A previous study reported that the levels of bile acid were found to be low in carbon tetrachloride (CCl₄) induced fatty liver rats (Zhang et al., 2019). When there is a disruption in the bile acid metabolism, it leads to a decrease in the activation of nuclear receptors such as FXR (farnesoid X receptor) and dysregulation in these receptors leads to NAFLD (Parséus et al., 2017; Chen et al., 2019; Liu et al., 2020). Chenodeoxycholic acid, muricholic acid and other cholic acids are primary bile acids produced in the liver as derivatives of cholesterol and secreted in the intestine as taurine and glycine conjugates. These bile acids interact with FXR and regulate glycemia and other metabolic functions (Grabherr et al., 2019). In the present

study, we have found that different bile acids such as Muricholic acid, Deoxycholic Acid, Glycocholic acid, Glychenodeoxycholic Acid, and Glycodeoxycholic acid were lowered in the serum of HFHF rats. However, their serum levels were normalized after the treatment of the methanolic extract of *Lysimachia candida* Lindl. especially after 3 weeks. Lower serum levels of bile acids in the HFHF group may reduce the activation of FXR and enhance the fat accumulation in the rat liver which is similar to NAFLD pathologies. Our findings might be working through similar pathway as evidenced in the study by Sun (Sun et al., 2018). Bile acids activate mRNA expression of PPAR α via binding of FXR in the PPAR promoter (Pineda Torra et al., 2003). Therefore, it seems that the FXR-PPAR α pathway might be involved for the attenuation of fatty liver after the treatment of methanolic extract of *Lysimachia candida* Lindl. (Figure 7).

Unsaturated fatty acids like Linoleic acid and α -Eleostearic acid were lowered in HFHF rats and increased after treatment of the plant extract. Our finding was similar to previous study where it was shown that Linoleic acid, an essential polyunsaturated fatty acid, was declined in non-alcoholic steatohepatitis (NASH) (Puri et al., 2009). α -Eleostearic acid, a PPAR α activator, is lowered in HFHF rats. α -Eleostearic acid also upregulates peroxisomal acyl-CoA oxidase activity and cytochrome P450 4A1 genes in rats, which in turn activates PPAR α (Chao et al., 2001). Hence, lower levels of α -Eleostearic acid in HFHF group may cause inactivation of PPAR α pathways, and therefore fatty liver pathologies. The methanolic extract of *Lysimachia candida* Lindl. was able to nullify these pathological features by upregulating α -Eleostearic acid expression and activating PPAR α pathways (Figure 7).

Pathway analysis, using metaboanalyst by the exploration of different metabolites confirms that important disrupted pathway are linoleic acid metabolism, biosynthesis of unsaturated fatty acids, glycerophospholipid metabolism, and primary bile acid biosynthesis pathway (Figure 6). The summarized pathway of our study is revealed in (Figure 7).

Although we have established the link between altered serum metabolites levels and fatty liver phenotypes, there are some limitations of the study. First, there are many different components in the methanolic extract of *Lysimachia candida* Lindl. and we have not looked which particular component(s) or compound(s) is activating PPAR α . Secondly, the molecular signaling pathway of PPAR α activation has not been deciphered after the treatment with plant extract.

CONCLUSION

Our study concludes that the methanolic extract of *Lysimachia candida* Lindl. reduces insulin resistance along with fatty liver phenotypes in rats. After analyzing various metabolites and pathways associated with fatty liver, we found that activation of PPAR α by methanolic extract of *Lysimachia candida* Lindl. might be responsible to prevent the high-fat high-fructose induced fatty liver in rats.

DATA AVAILABILITY STATEMENT

The authors acknowledge that the data presented in this study must be deposited and made publicly available in an acceptable repository, prior to publication. Frontiers cannot accept a article that does not adhere to our open data policies.

ETHICS STATEMENT

The animal study was reviewed and approved by Translational Health Science and Technology Institute (THSTI), Faridabad, India (Protocol No. BIO-IAEC-3357).

AUTHOR CONTRIBUTIONS

JB, BD, and SB did the collection of plants and extraction of the methanolic extract; PK, DK, SB, and BK did animal experimentation; PK, SS, DK, SR, and PD conducted biochemical assays, data analysis, and data interpretation; YK, JA, SG, and NB did metabolomics experiments, metabolomic data analysis, and interpretation; PK, SS, and JA wrote the original manuscript; YK, NT, and SB designed the study,

interpreted results, reviewed and edited the manuscript. All authors have read and accepted the manuscript.

FUNDING

The authors are thankful to the Department of Biotechnology (DBT) for providing funds (Grant number DBT-NER/Health/42/2013.) for the study, Translational Health Science and Technology Institute (THSTI), Faridabad for providing all-around facility and support for the study.

ACKNOWLEDGMENTS

We would also like to thank the AAALAC accredited facility of the Bioneds Pvt. Ltd. for conducting the animal experimentation.

SUPPLEMENTARY MATERIAL

The Supplementary Material for this article can be found online at: <https://www.frontiersin.org/articles/10.3389/fphar.2021.653872/full#supplementary-material>.

REFERENCES

- Allison, M. E. (2004). Fatty liver. *Hosp. Med.* 65 (10), 609–612. doi:10.12968/hosp.2004.65.10.16611
- Amarapurkar, D., Kamani, P., Patel, N., Gupta, P., Kumar, P., Agal, S., et al. (2007). Prevalence of non-alcoholic fatty liver disease: population based study. *Ann. Hepatol.* 6 (3), 161–163. doi:10.1016/s1665-2681(19)31922-2
- Bedogni, G., Miglioli, L., Masutti, F., Tiribelli, C., Marchesini, G., and Bellentani, S. (2005). Prevalence of and risk factors for nonalcoholic fatty liver disease: the Dionysos nutrition and liver study. *Hepatology* 42 (1), 44–52. doi:10.1002/hep.20734
- Beyoğlu, D., and Idle, J. R. (2013). The metabolomic window into hepatobiliary disease. *J. Hepatol.* 59 (4), 842–858. doi:10.1016/j.jhep.2013.05.030
- Bose, M., Lambert, J. D., Ju, J., Reuhl, K. R., Shapses, S. A., and Yang, C. S. (2008). The major green tea polyphenol, (-)-Epigallocatechin-3-Gallate, inhibits obesity, metabolic syndrome, and fatty liver disease in high-fat-fed mice. *J. Nutr.* 138 (9), 1677–1683. doi:10.1093/jn/138.9.1677
- Carr, R. M., Oranu, A., and Khungar, V. (2016). Nonalcoholic fatty liver disease. *Gastroenterol. Clin. North America* 45 (4), 639–652. doi:10.1016/j.gtc.2016.07.003
- Chao, P.-M., Chao, C.-Y., Lin, F.-J., and Huang, C. (2001). Oxidized frying Oil up-regulates hepatic acyl-CoA oxidase and cytochrome P450 4 A1 genes in rats and activates PPARα. *J. Nutr.* 131 (12), 3166–3174. doi:10.1093/jn/131.12.3166
- Chen, J., Thomsen, M., and Vitetta, L. (2019). Interaction of gut microbiota with dysregulation of bile acids in the pathogenesis of nonalcoholic fatty liver disease and potential therapeutic implications of probiotics. *J. Cel. Biochem.* 120 (3), 2713–2720. doi:10.1002/jcb.27635
- Chidambaram, J., Venkatraman, A. C. J. F., and Toxicology, C. (2010). Cissus quadrangularis stem alleviates insulin resistance, oxidative injury and fatty liver disease in rats fed high fat plus fructose diet. *Food Chem. Toxicol.* 48 (8–9), 2021–2029. doi:10.1016/j.fct.2010.04.044
- Forman, B. M., Chen, J., and Evans, R. M. (1997). Hypolipidemic drugs, polyunsaturated fatty acids, and eicosanoids are ligands for peroxisome proliferator-activated receptors and. *Proc. Natl. Acad. Sci.* 94 (9), 4312–4317. doi:10.1073/pnas.94.9.4312
- Foulds, C. E., Treviño, L. S., York, B., and Walker, C. L. (2017). Endocrine-disrupting chemicals and fatty liver disease. *Nat. Rev. Endocrinol.* 13 (8), 445–457. doi:10.1038/nrendo.2017.42
- Grabherr, F., Grander, C., Effenberger, M., Adolph, T. E., and Tilg, H. (2019). Gut dysfunction and non-alcoholic fatty liver disease. *Front. Endocrinol.* 10 (611). doi:10.3389/fendo.2019.00611
- Hong, X., Tang, H., Wu, L., and Li, L. (2006). Protective effects of the *Alisma orientalis* extract on the experimental nonalcoholic fatty liver disease. *J. Pharm. Pharmacol.* 58 (10), 1391–1398. doi:10.1211/jpp.57.10.0013
- Jenkins, B., West, J., and Koulman, A. (2015). A review of odd-chain fatty acid metabolism and the role of pentadecanoic Acid (c15:0) and heptadecanoic Acid (c17:0) in health and disease. *Molecules* 20 (2), 2425–2444. doi:10.3390/molecules20022425
- Kumar, A., Kumar, Y., Sevak, J. K., Kumar, S., Kumar, N., and Gopinath, S. D. (2020). Metabolomic analysis of primary human skeletal muscle cells during myogenic progression. *Sci. Rep.* 10 (1), 11824. doi:10.1038/s41598-020-68796-4
- Lee, S. S., Pineau, T., Drago, J., Lee, E. J., Owens, J. W., Kroetz, D. L., et al. (1995). Targeted disruption of the alpha isoform of the peroxisome proliferator-activated receptor gene in mice results in abolishment of the pleiotropic effects of peroxisome proliferators. *Mol. Cel. Biol.* 15 (6), 3012–3022. doi:10.1128/mcb.15.6.3012
- Li, Q., Dhyani, M., Grajo, J. R., Sirlin, C., and Samir, A. E. (2018). Current status of imaging in nonalcoholic fatty liver disease. *World J. Hepatol.* 10 (8), 530–542. doi:10.4254/wjh.v10.i8.530
- Liu, L., Liu, Z., Li, H., Cao, Z., Li, W., Song, Z., et al. (2020). Naturally occurring TPE-CA maintains gut microbiota and bile acids homeostasis via FXR signaling modulation of the liver-gut Axis. *Front. Pharmacol.* 11, 12. doi:10.3389/fphar.2020.00012
- Mandart, S., Müller, M., and Kersten, S. (2004). Peroxisome proliferator-activated receptor a target genes. *Cell Mol. Life Sci.* 61 (4), 393–416. doi:10.1007/s00018-003-3216-3
- Marchesini, G., Brizi, M., Bianchi, G., Tomassetti, S., Bugianesi, E., Lenzi, M., et al. (2001). Nonalcoholic fatty liver disease: a feature of the metabolic syndrome. *Diabetes* 50 (8), 1844–1850. doi:10.2337/diabetes.50.8.1844
- Naz, S., Gallart-Ayala, H., Reinke, S. N., Mathon, C., Blankley, R., Chaleckis, R., et al. (2017). Development of a liquid chromatography-high resolution mass spectrometry metabolomics method with high specificity for metabolite identification using all ion fragmentation acquisition. *Anal. Chem.* 89 (15), 7933–7942. doi:10.1021/acs.analchem.7b00925

- Nizami, H. L., Katare, P., Prabhakar, P., Kumar, Y., Arava, S. K., Chakraborty, P., et al. (2019). Vitamin D deficiency in rats causes cardiac dysfunction by inducing myocardial insulin resistance. *Mol. Nutr. Food Res.* 63 (17), e1900109. doi:10.1002/mnfr.201900109
- Park, S. H., Lee, S. G., Kang, S. K., and Chung, S. H. (2006). Acanthopanax senticosus reverses fatty liver disease and hyperglycemia in ob/ob mice. *Arch. Pharm. Res.* 29 (9), 768. doi:10.1007/bf02974078
- Parséus, A., Sommer, N., Sommer, F., Caesar, R., Molinaro, A., Ståhlman, M., et al. (2017). Microbiota-induced obesity requires farnesoid X receptor. *Gut* 66 (3), 429–437. doi:10.1136/gutjnl-2015-310283
- Pineda Torra, I., Claudel, T., Duval, C., Kosykh, V., Fruchart, J.-C., and Staels, B. (2003). Bile acids induce the expression of the human peroxisome proliferator-activated receptor α gene via activation of the farnesoid X receptor. *Mol. Endocrinol.* 17 (2), 259–272. doi:10.1210/me.2002-0120
- Puri, P., Wiest, M. M., Cheung, O., Mirshahi, F., Sargeant, C., Min, H.-K., et al. (2009). The plasma lipidomic signature of nonalcoholic steatohepatitis. *Hepatology* 50 (6), 1827–1838. doi:10.1002/hep.23229
- Pyper, S. R., Viswakarma, N., Yu, S., and Reddy, J. K. (2010). PPAR α : energy combustion, hypolipidemia, inflammation and cancer. *Nucl. Recept Signal.* 8 (1), 08002. doi:10.1621/nrs.08002
- Rinella, M. E. (2015). Nonalcoholic fatty liver disease. *JAMA* 313 (22), 2263–2273. doi:10.1001/jama.2015.5370
- Sarkar, S., Bhattacharya, S., Alam, M. J., Yadav, R., and Banerjee, S. K. (2020). Hypoxia aggravates non-alcoholic fatty liver disease in presence of high fat choline deficient diet: a pilot study. *Life Sci.* 260, 118404. doi:10.1016/j.lfs.2020.118404
- Singh, S., Osna, N. A., and Kharbanda, K. K. (2017). Treatment options for alcoholic and non-alcoholic fatty liver disease: A review. *World J. Gastroenterol.* 23 (36), 6549–6570. doi:10.3748/wjg.v23.i36.6549
- Sun, L., Xie, C., Wang, G., Wu, Y., Wu, Q., Wang, X., et al. (2018). Gut microbiota and intestinal FXR mediate the clinical benefits of metformin. *Nat. Med.* 24 (12), 1919–1929. doi:10.1038/s41591-018-0222-4
- Wang, R., Xiong, A.-Z., Teng, Z.-Q., Yang, Q.-W., Shi, Y.-H., and Yang, L. J. I. j. o. m. s. (2012). Radix paeoniae rubra and radix paeoniae alba attenuate CCl₄-induced acute liver injury: an ultra-performance liquid chromatography-mass spectrometry (UPLC-MS) based metabolomic approach for the pharmacodynamic study of traditional Chinese medicines (TCMs). *Int. J. Mol. Sci.* 13 (11), 14634–14647. doi:10.3390/ijms131114634
- Xia, X., Wei, X., and Lin, L. (2013). Triterpenoid saponins from *Lysimachia candida* Lindl. *Pharmacognosy J.* 5 (3), 119–122. doi:10.1016/j.phcgj.2013.05.001
- Xiao, J., So, K. F., Liong, E. C., and Tipoe, G. L. (2013). Recent advances in the herbal treatment of non-alcoholic Fatty liver disease. *J. Traditional Complement. Med.* 3 (2), 88–94. doi:10.4103/2225-4110.110411
- Yamada, H., Kikuchi, S., Hakoziaki, M., Motodate, K., Nagahora, N., and Hirose, M. (2016). 8-Hydroxyeicosapentaenoic acid decreases plasma and hepatic triglycerides via activation of peroxisome proliferator-activated receptor α in high-fat diet-induced obese mice. *J. Lipids* 2016, 1. doi:10.1155/2016/7498508
- Yamada, H., Oshiro, E., Kikuchi, S., Hakoziaki, M., Takahashi, H., and Kimura, K.-I. (2014). Hydroxyeicosapentaenoic acids from the Pacific krill show high ligand activities for PPARs. *J. lipid Res.* 55 (5), 895–904. doi:10.1194/jlr.M047514
- Yang, T. A., Grabovskaya, A., Illarionova, I., and Chen, C.-H. J. T. (2012). *Lysimachia candida* Lindl. (Primulaceae), extinct Species also a New Rec. Species Taiwan. *Taiwania* 57 (4), 434–442. doi:10.6165/tai.2012.57.434
- Yuan, M., Breitkopf, S. B., Yang, X., and Asara, J. M. (2012). A positive/negative ion-switching, targeted mass spectrometry-based metabolomics platform for bodily fluids, cells, and fresh and fixed tissue. *Nat. Protoc.* 7 (5), 872–881. doi:10.1038/nprot.2012.024
- Zhang, K., Zhang, Y., Li, N., Xing, F., Zhao, J., Yang, T., et al. (2019). An herbal-compound-based combination therapy that relieves cirrhotic ascites by affecting the L-arginine/nitric oxide pathway: A metabolomics-based systematic study. *J. Ethnopharmacol.* 241, 112034. doi:10.1016/j.jep.2019.112034

Conflict of Interest: The authors declare that the research was conducted in the absence of any commercial or financial relationships that could be construed as a potential conflict of interest.

Copyright © 2021 Kamboj, Sarkar, Gupta, Bisht, Kumari, Alam, Barge, Kashyap, Deka, Bharadwaj, Rahman, Dutta, Borah, Talukdar, Banerjee and Kumar. This is an open-access article distributed under the terms of the Creative Commons Attribution License (CC BY). The use, distribution or reproduction in other forums is permitted, provided the original author(s) and the copyright owner(s) are credited and that the original publication in this journal is cited, in accordance with accepted academic practice. No use, distribution or reproduction is permitted which does not comply with these terms.



Transcriptomic and Metabolomic Profiling Reveals the Protective Effect of *Acanthopanax senticosus* (Rupr. & Maxim.) Harms Combined With *Gastrodia elata* Blume on Cerebral Ischemia-Reperfusion Injury

Bingfeng Lin¹, Renhao Chen¹, Qi Wang², Zhifeng Li^{1,3*}, ShiLin Yang² and YuLin Feng^{2*}

¹Jiangxi University of Traditional Chinese Medicine, Nanchang, China, ²State Key Laboratory of Innovative Drug and Efficient Energy-Saving Pharmaceutical Equipment, Nanchang, China, ³Nanchang Key Laboratory of Active Ingredients of Traditional Chinese Medicine and Natural Medicine, Nanchang, China

OPEN ACCESS

Edited by:

Gudrun S. Ulrich-Merzenich,
University Hospital Bonn, Germany

Reviewed by:

Wentzel Christoffel Gelderblom,
Cape Peninsula University of
Technology, South Africa
Rufeng Wang,
Beijing University of Chinese Medicine,
China

*Correspondence:

Zhifeng Li
20101040@jxutcm.edu.cn
YuLin Feng
fengyulin2003@126.com

Specialty section:

This article was submitted to
Ethnopharmacology,
a section of the journal
Frontiers in Pharmacology

Received: 19 October 2020

Accepted: 25 March 2021

Published: 16 April 2021

Citation:

Lin B, Chen R, Wang Q, Li Z, Yang S
and Feng Y (2021) Transcriptomic and
Metabolomic Profiling Reveals the
Protective Effect of *Acanthopanax*
senticosus (Rupr. & Maxim.) Harms
Combined With *Gastrodia elata* Blume
on Cerebral Ischemia-
Reperfusion Injury.
Front. Pharmacol. 12:619076.
doi: 10.3389/fphar.2021.619076

The effects of current treatment strategies used in ischemic stroke are weakened by cerebral ischemia-reperfusion (CIR) injury. Suitable treatment regimens targeting CIR injury are still lacking. Two herbs, namely, *Acanthopanax senticosus* (Rupr. & Maxim.) Harms (ASE) and *Gastrodia elata* Blume (GEB), have been used as traditional Chinese medicine and are indicated in the treatment of stroke and cerebrovascular diseases. However, there are no studies that report the effects of ASE combined with GEB in the treatment of CIR injury. In this study, we used the Zea Longa method to induce CIR injury in male Wistar rats. Results of the pharmacodynamic studies revealed that co-administration of ASE and GEB may improve neuronal injury and prevent neuronal apoptosis by reducing oxidative stress and inflammation, and also help prevent CIR injury. On the basis of our hypothesis, we combined the results from transcriptomic and metabolomic analyses and found that ASE and GEB could prevent CIR injury by targeting phenylalanine, pyrimidine, methionine, and sphingolipid metabolism. Therefore, our study provides the basis for the compatibility and efficacy of ASE and GEB.

Keywords: cerebral ischemia-reperfusion injury, *Acanthopanax senticosus* harms, *Gastrodia elata* blume, transcriptomic, metabolomic

INTRODUCTION

Stroke is a common clinical neurological condition that seriously endangers human health and life. It is the fifth most common cause of death in America (Mozaffarian et al., 2016). The incidence of stroke is high; approximately 7,950,000 individuals, 87% of whom are ischemic, suffer from stroke each year in the United States alone (Lloyd-Jones et al., 2009). Ischemic stroke, the most common variant, affects the nervous system at the morphological and molecular levels. Brain tissue is sensitive to ischemia and hypoxia, and early recovery of blood reperfusion is the primary focus in the clinical management of ischemic strokes (Soares et al., 2009). However, when blood is perfused into the ischemic brain tissue, inflammatory reactions and neuronal death may be intensified owing to the generation of free radicals, calcium overload, and other factors (Bai and Lyden, 2015). Alleviation of

the pathophysiological process of cerebral ischemia-reperfusion (CIR) injury has become a research hotspot worldwide; however, the progress is not satisfactory. The treatment windows of the thrombolytic drugs and neuroprotective agents that are currently used for therapy are narrow and pose challenges during the therapy of stroke (Green, 2008; Boese et al., 2020).

Traditional Chinese medicine (TCM) has a long history in the treatment of stroke. Based on the pathogenesis theory of TCM and the so-called “Syndrome Differentiation and Pattern Diagnosis,” most patients who have suffered an ischemic stroke can be grouped as being deficient in Qi and wind movement (Jhong et al., 2013). Therefore, herbs with Qi-replenishing, wind-dispelling, and blood-activating effects are frequently used to reverse the damage caused by ischemic stroke (Zhang and Zhao, 2014; Lu et al., 2018). *Acanthopanax senticosus* (Rupr. & Maxim.) Harms [ASE, *Eleutherococcus senticosus* (Rupr. & Maxim.) Maxim.] is widely used as a potent Qi supplement to strengthen the spleen as a means to treat cardiovascular diseases (Xie et al., 2015). *Gastrodia elata* Blume (GEB) is a typical herbal medicine in TCM, which suppresses the hyperactive liver and reduces endogenous wind (Huang et al., 2019). ASE and GEB are herbal medicines that have been widely used for the treatment of ischemic stroke. Using data mining and the Delphi expert questionnaire, Rongrong Zhou was found that ASE-GEB may be a pair of drugs suitable for the treatment of stroke (Zhou et al., 2020). Previous studies have revealed the primary active constituents of ASE to be eleutheroside E (Bai et al., 2011), isofraxidin (Bai et al., 2011), hyperoside (Liu et al., 2012), eleutheroside B (Tohda et al., 2008), and quercetin (Pei et al., 2016), which can inhibit ischemic brain injury and protect against neuritic atrophy and cell death. The main active constituents of GEB include 4-hydroxybenzyl alcohol, gastrodin, and parishin. 4-Hydroxybenzyl alcohol ameliorates ischemic injury by inhibiting the activation of caspase-3 and increasing the expression of Bcl-2 (Yu et al., 2010). Gastrodin ameliorates oxidative stress and inflammation by activating the Akt/Nrf2 pathway (Peng et al., 2015). In addition, parishin is mainly degraded to gastrodin *in vivo* (Tang et al., 2014). ASE and GEB have been abundantly reported in the treatment of CIR injury and nerve protection; however, the combined effect and mechanism of the two drugs are not clear. In this study, we explored the efficacy of ASE combined with GEB for the treatment of CIR injury and attempted to explore the mechanism of action underlying this combination. However, as the multi-component and multi-targeting characteristics of TCM play an important role in the efficacy of this combination, the potential mechanism of the combination of ASE and GEB is not clear.

In recent decades, emerging “omics” technologies, including transcriptomics and metabonomics, have immensely improved the ability to study the biochemical changes caused by TCM interventions in biological systems. Metabolomics techniques provide insight into the mechanisms of various physiological conditions and abnormal processes at the systems level of metabolites (Johnson et al., 2016). Transcriptomics studies can be used to perform rapid qualitative and quantitative analysis of mRNA transcripts of up-stream genes (Wang et al., 2009).

Therefore, the integration of transcriptomics and metabonomics is of great significance for comprehensive research to determine the efficacies of and mechanisms of the formulations used as TCM (Du et al., 2018; Wu et al., 2019).

In this study, through the combination of transcriptomic analysis and metabonomics, we revealed the mechanism of the combination of GEB-ASE in alleviating CIR injury in rats.

EXPERIMENTAL APPROACHES

Extraction Methods

Medicinal materials were collected from Heilongjiang Province and identified as the dried roots and rhizomes or stems of *Acanthopanax senticosus* (Rupr. & Maxim.) Harms (ASE, *Eleutherococcus senticosus* (Rupr. & Maxim.) Maxim.), and *Gastrodia elata* Blume (GEB) by Professor Guoyue Zhong of the Jiangxi University of Traditional Chinese Medicine. Voucher specimens (accession number JZ-2017GYZ-CWJ-A2 and JZ-2017GYZ-TM-A3) were deposited in the Center of National Medicine Resource, Jiangxi University of Traditional Chinese Medicine, China.

The plant materials were washed, dried, sliced, and ground to a powder. To prepare the AEGE extract, 500 g of ASE and 500 g of GEB were mixed with 5,000 ml of 70% ethanol, refluxed and extracted for 2 h. The residue was subjected to re-extraction three times using 5,000 ml of ethanol for each subsequent extraction. All fractions were mixed, filtered, concentrated at 60°C using a rotary evaporator and freeze-dried. Lastly, AEGE extract at a concentration of 200 mg/kg was prepared by adding an appropriate volume of 0.5% carboxymethyl cellulose sodium (CMCNa; Xilong Science and Technology Co., Ltd, Shantou, China) solution to the dried extract.

Ethanol extracts of AEGE were analyzed using a Shimadzu UHPLC (ESI) system (Shimadzu, Kyoto, Japan) and an AB SCIEX quadrupole time-of-flight mass spectrometer (TripleTOF® 5,600, AB SCIEX, Framingham, MA, USA). The extract was dissolved in methanol and then filtered through a 0.22-μm membrane filter. Samples were analyzed using an ACQUITY UPLC C18 column (100 mm × 2.1 mm, 1.7 μm, Waters) at 40°C. The mobile phase comprised water containing 0.1% formic acid (A) and acetonitrile (B), and the proportion of mobile phase B was as follows: 2–10%, 0–8 min; 10–20%, 8–16 min; 20–30%, 16–24 min; 30–90%, 24–29 min; 90%, 29–34 min. The injection volume was 1 μl and the flow rate was 0.3 ml/min. TOF-MS and TOF-MS/MS were performed synchronously. Mass spectra were acquired in the negative ion mode. The parameters were set as follows: turbo spray temperature, 550°C; ion spray voltage floating, -4,500 V; collision gas, -35 eV. The mass range was set at 50–1,250 Da. The obtained data were analyzed using Peak View Software (AB SCIEX, Framingham, MA, United States).

Animals and Grouping

Adult male Wistar rats (240 ± 20 g) were obtained from Beijing Charles River Co. Ltd (Beijing, China; certification number: SCXK (Jing): 2016-0006). Rats were acclimated for 5 days and

provided access to water and standard laboratory animal diet *ad libitum*. They were randomly divided into four groups as follows: sham, IR, AEGE, and nimodipine (Nim), with 15 rats/group. The AEGE and Nim groups received AEGE (200 mg/kg/d) or Nim (15 mg/kg/d), respectively, orally for 15 days. The sham and IR groups received 0.9% sodium chloride orally for 15 days.

All experimental procedures were performed in accordance with the ethical principles for laboratory animals of the State Key Laboratory (Reference number: BCTG-2016-18). Experiments were reviewed and approved by the Animal Care Committee of the Jiangxi University of Chinese Medicine.

Establishment of IR Model

Rats were anesthetized using an intraperitoneal 10% injection of chloral hydrate (350 mg/kg). Cerebral ischemia-reperfusion injury was established following the method by Longa et al. (1989). Briefly, the external carotid artery was ligated and the common carotid artery was embolized through the internal carotid artery to the middle cerebral artery using a thread coated with silicone at the head end. Two hours after the induction of ischemia, the thread was pulled out to ensure the establishment of reperfusion. Rats in the sham group underwent a similar surgery, but without insertion of the monofilament.

Pharmacodynamics of AEGE

Neurobehavioral Assessment and Evaluation of Cerebral Infarction

After 24 h of reperfusion, the behavioral score of rats was evaluated using a 0–4 point scoring system as follows: no observable neurological dysfunction was marked as 0 points; toe curled up powerless was marked as 1 point; inclined to crawl in the opposite direction was marked as 2 points; turned autonomously to the opposite side upon being stimulated with slight sound was marked as 3 points; fell to the opposite side and had no spontaneous activity for a long time was marked as 4 points.

After neurobehavioral evaluation, the rats were anesthetized using chloral hydrate. Blood was collected from the posterior abdominal aorta. The animals were euthanized by decapitation and the brain tissues were collected.

Brain tissues of 3 rats/group were randomly selected for triphenyl tetrazolium chloride (TTC) staining. The entire brain tissue was sectioned into five 2 mm-thick coronal slices. These sections were incubated at 37°C for 16 min in 1% TTC solution (Solarbio, Beijing, China) and fixed with 4% paraformaldehyde for 3–5 h. The total brain slices and infarcted area were stained and imaged using Image-Pro Plus 6.0 (Media Cybernetics, Bethesda, MD, United States) and the percentage of the infarcted area was calculated.

H&E Staining

The brain tissues of 2 rats from each group were randomly selected for H&E staining. The portion between the root of the crossed optic nerve and the quadrigeminal body of the brain was placed in 4% paraformaldehyde at 4°C for about 24 h. After the fixed brain slices were dehydrated and embedded to prepare continuous paraffin

sections, HE (Solarbio, Beijing, China) staining was performed and the samples were observed using fluorescence microscopy (Leica, Weztlar, Germany).

Biochemical Evaluation

The brain tissues of 7 rats from each group were randomly selected for biochemical evaluation. The blood on the surface of the brain was washed with saline, and the excess saline was blotted using filter paper. Next, the coronal sections around the bregma point were collected (1 mm). Coronal brain tissues were weighed after sectioning. Brain tissue was added to precooled saline in a 1:9 ratio, homogenized, and centrifuged for 10 min (4,000 rpm). The activities of SOD, GSH-Px, and MDA in brain tissue were measured using the respective assay kits (Jiancheng Bioengineering, Nanjing, China). The IL-10, IL-1 β , and TNF- α levels in brain tissue were determined using ELISA (Neobioscience Technology, Shenzhen, China).

Metabolomics Analysis

Plasma Pretreatment and UPLC-Q/TOF-MS Analysis

The plasma samples of 10 rats in the sham, IR, and AEGE group were randomly selected for metabolomics analysis. Blood was collected from the abdominal aorta and loaded into an Eppendorf tube containing heparin sodium. The supernatant was obtained by centrifugation at 4,000 rpm for 10 min. Plasma supernatants were treated with methanol containing 2-chloro-L-phenylalanine (10 μ g/ml) in a 4:1 ratio (methanol: plasma supernatant, v/v, 250 μ l). After centrifugation at 4°C (4,000 rpm, 10 min), the supernatant was collected for analysis. A 50- μ l aliquot of each centrifuged supernatant was uniformly mixed to yield a quality control (QC) sample.

A Shimadzu UHPLC (ESI) system and an AB Sciex quadrupole time-of-flight mass spectrometer (TripleTOF 5600) were used for LC-MS analysis. An ACQUITY UPLC C18 column (100 mm \times 2.1 mm, 1.7 μ m, Waters) was used for all analyses. The mobile phase was a mixture of 0.1% formic acid in water (A) and acetonitrile (B). The proportion of mobile phase B was as follows: 2–30%, 0–3 min; 30–60%, 3–5 min; 60–80%, 5–15 min; 80–100%, 15–16 min; 100%, 16–19 min; 100–2%, 19–20 min; 2%, 20–25 min. The injection volume was 2 μ l, the flow rate 0.3 ml/min, and the column temperature was 40°C. TOF-MS and TOF-MS/MS were performed synchronously. Mass spectra were acquired in the positive and negative ion modes. The parameters of the positive ion mode were set as follows: ion spray voltage floating, 5,500 V; collision gas, 40 eV. The parameters of the negative ion mode were set as follows: ion spray voltage floating, –4,500 V; collision gas, –40 eV. The turbo spray temperature was 550°C and the TOF-MS mass ranged from m/z 50–1,250 Da.

During analysis of the sample sequence, a QC sample was run after every five injections to validate the analytical methodology (Zhang et al., 2017). QC (n = 6) and plasma samples were analyzed using LC-MS. Data quality was evaluated based on the relative SDs (RSDs) of the retention times and intensities of 10 typical peak (including internal standard) of the QC samples.

Data Analysis

Raw data of plasma samples were analyzed using MarkerView 2.0 (AB SCIEX, Framingham, MA, United States). Before chemometric analysis, the data obtained for each sample were normalized using internal standards (2-chloro-L-phenylalanine). The features were subjected to statistical analysis only when detection frequencies of any group reached 100% and the RSD was less than 30%. The missing values were replaced by half minimum of abundances of features. The pre-processed data were analyzed using principal component analysis (PCA) and orthogonal partial least squares discriminant analysis (OPLS-DA) using SIMCA 14.1 (Umetrics, Umeå, Sweden). Additionally, the model was considered to qualify when the cumulative values of R^2 (score of raw data interpreted by the model) and Q^2 (predictive power of the model) were greater than or equal to 0.5; OPLS-DA was performed using a permutation test (200 permutations) to avoid overfitting.

Features with variable importance in projection (VIP) scores >1 in the OPLS-DA model and p -values < 0.05 in t -test were selected and their corresponding metabolites identified. Human Metabolome database (HMDB) was used as a tool for the identification of differential metabolites using LC-MS. Associated metabolic pathways were established using the Kyoto Encyclopedia of Genes and Genomes (KEGG) and MetaboAnalyst 3.0, in addition to other online tools.

Transcriptomics Studies

Library Preparation for Transcriptome Sequencing

The brain tissues of 3 rats from the sham, IR, and AEGE groups were randomly selected for transcriptome analysis. Total RNA was extracted from about 150 mg of brain tissue using a MirVana total RNA extraction kit (Ambion, Carlsbad, CA, United States). RNA concentration was measured using Qubit® RNA Assay Kit and a Qubit® 2.0 Fluorometer (Life Technologies, Carlsbad, CA, United States). RNA integrity was assessed using an RNA Nano 6,000 Assay Kit of the Bioanalyzer 2,100 system (Agilent Technologies, CA, United States). A total amount of 1.5 µg of RNA per sample was used as the follow-up test material for RNA-sample preparation. Whole transcriptome profiling was performed using NEBNext® Ultra™ RNA Library Prep Kit for Illumina® (NEB, Ipswich, MA, United States) according to the manufacturer's protocol.

Clustering, Sequencing, and Quantification of Gene Expression

Clustering of index-coded samples was performed using a CBOT Cluster Generation system using HiSeq 4,000 PE Cluster Kit (Illumina). Next, RNA sequencing (150 bp, pair-ends) was performed using standard Illumina HiSeq 4000 platform protocols. All downstream analyses were based on clean data with high quality. Gene FPKM was calculated by adding the FPKM of each genome transcript. The differential expression of the two conditions was analyzed using DESeq2R software package (1.26.0). For genes with FPKM values ≥ 1 in at least one sample, the significantly different expressions between

groups were determined according to the criteria as follows: $p < 0.05$ and $|\log_2\text{FoldChange}| \geq 0.58$.

GO and KEGG Enrichment Analysis of Differentially Expressed Genes

Functional Annotation Bioinformatics Microarray Analysis (DAVID) database (Huang et al., 2009) was used to obtain Gene Ontology (GO) enrichment analysis of DEGs. GO terms ($p < 0.05$) were considered significantly enriched by DEGs. The enrichment of DEGs in KEGG pathways was tested using KEGG Orthology Based Annotation System v3.0 software; p -values were calculated using one-way ANOVA based on the normalized dataset. KEGG terms ($p < 0.05$) were considered significantly enriched by DEGs.

Western Blotting

Western blotting was used to determine the protein expression of the key genes measured using transcriptomic analysis. About 100 mg of brain tissue was lysed with 1 ml of RIPA buffer (Beyotime, Shanghai, China). The protein concentration of the brain homogenate was measured using a bicinchoninic acid assay kit (Thermo Scientific, MA, United States). Protein samples were resolved using sodium dodecyl sulfate polyacrylamide-gel electrophoresis and transferred onto polyvinylidene difluoride membranes (Millipore, Schwalbach, Germany). Then, the proteins were immunoblotted with their corresponding primary and secondary antibodies. A chemiluminescence assay kit was used to determine the intensity of each band using a Tanon 6600 luminous imaging workstation (Tanon, Shanghai, China). Protein expression was determined using Image-Pro Plus 6.0.

Statistical Analysis

All experimental data were analyzed using Student's t -test or one-way ANOVA test with SPSS version 21.0 software (IBM, Armonk, NY, United States) package to calculate statistical significance. $p < 0.05$ was considered statistically significant.

RESULTS

Identification of Chemical Constituents in AEGE

The total negative ion chromatograms of AEGE are shown in **Supplementary Figure S1**. A total of 18 components were characterized (**Supplemental Table S1**) and their chemical structures are shown in **Supplementary Figure S2**. Four major active components, isofraxidin, eleutheroside E, gastrodin and parishin A, were identified by comparison with the standards, whereas the others were identified by checking their characteristic product ions (**Supplementary Figure S1**).

Pharmacodynamic Effects of AEGE Neurobehavioral Scores and Evaluation of Cerebral Infarction

The neurobehavioral scores of the rats in the IR group were significantly higher ($p < 0.05$) than those in the sham group. The

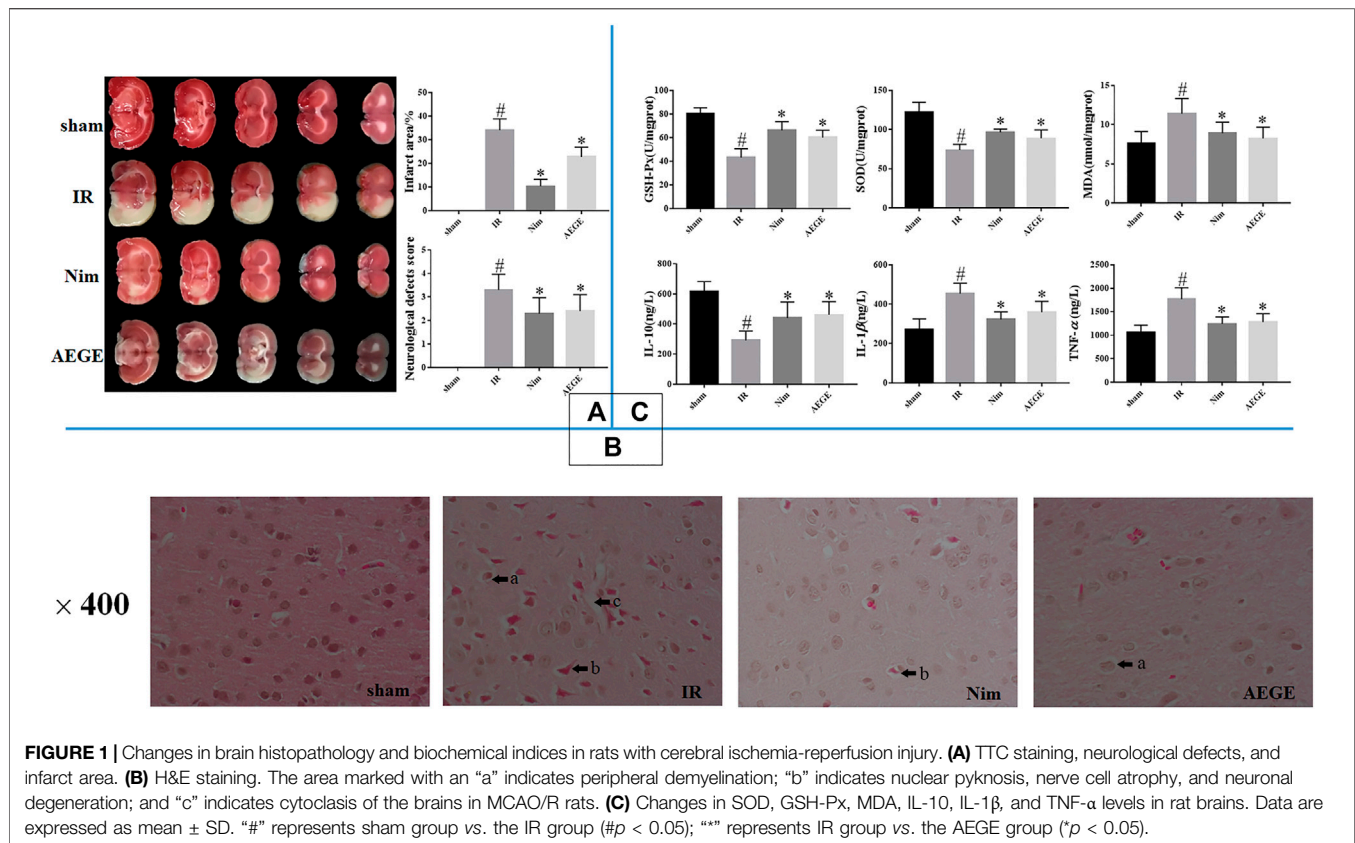


FIGURE 1 | Changes in brain histopathology and biochemical indices in rats with cerebral ischemia-reperfusion injury. **(A)** TTC staining, neurological defects, and infarct area. **(B)** H&E staining. The area marked with an “a” indicates peripheral demyelination; “b” indicates nuclear pyknosis, nerve cell atrophy, and neuronal degeneration; and “c” indicates cytotoxicity of the brains in MCAO/R rats. **(C)** Changes in SOD, GSH-Px, MDA, IL-10, IL-1β, and TNF-α levels in rat brains. Data are expressed as mean ± SD. “#” represents sham group vs. the IR group ($p < 0.05$); “*” represents IR group vs. the AEGE group ($p < 0.05$).

cerebral infarction area was consistent with these scores. TTC staining (Figure 1A) and scoring scales indicated the successful establishment of the IR model. The rats in the AEGE group showed significantly lower scores ($p < 0.05$) and infarction areas ($p < 0.05$) compared to those in the IR group. These findings indicated that AEGE and Nim had a therapeutic effect on nerve injury and CIR injury.

HE Staining

HE staining (Figure 1B) showed no neuronal damage or inflammatory cell infiltration in the cerebral cortex of rats in the sham group. However, the ischemic cortex of the brains exhibited cytotoxicity, nuclear pyknosis, nerve-cell atrophy, neuronal degeneration, and peripheral demyelination in the IR group. Treatment with AEGE and Nim improved the histopathological features caused due to CIR injury. The neuronal cells were restored to normal, and there were only a few nerve cells that exhibited peripheral demyelination and nerve-cell atrophy.

Biochemical Evaluation

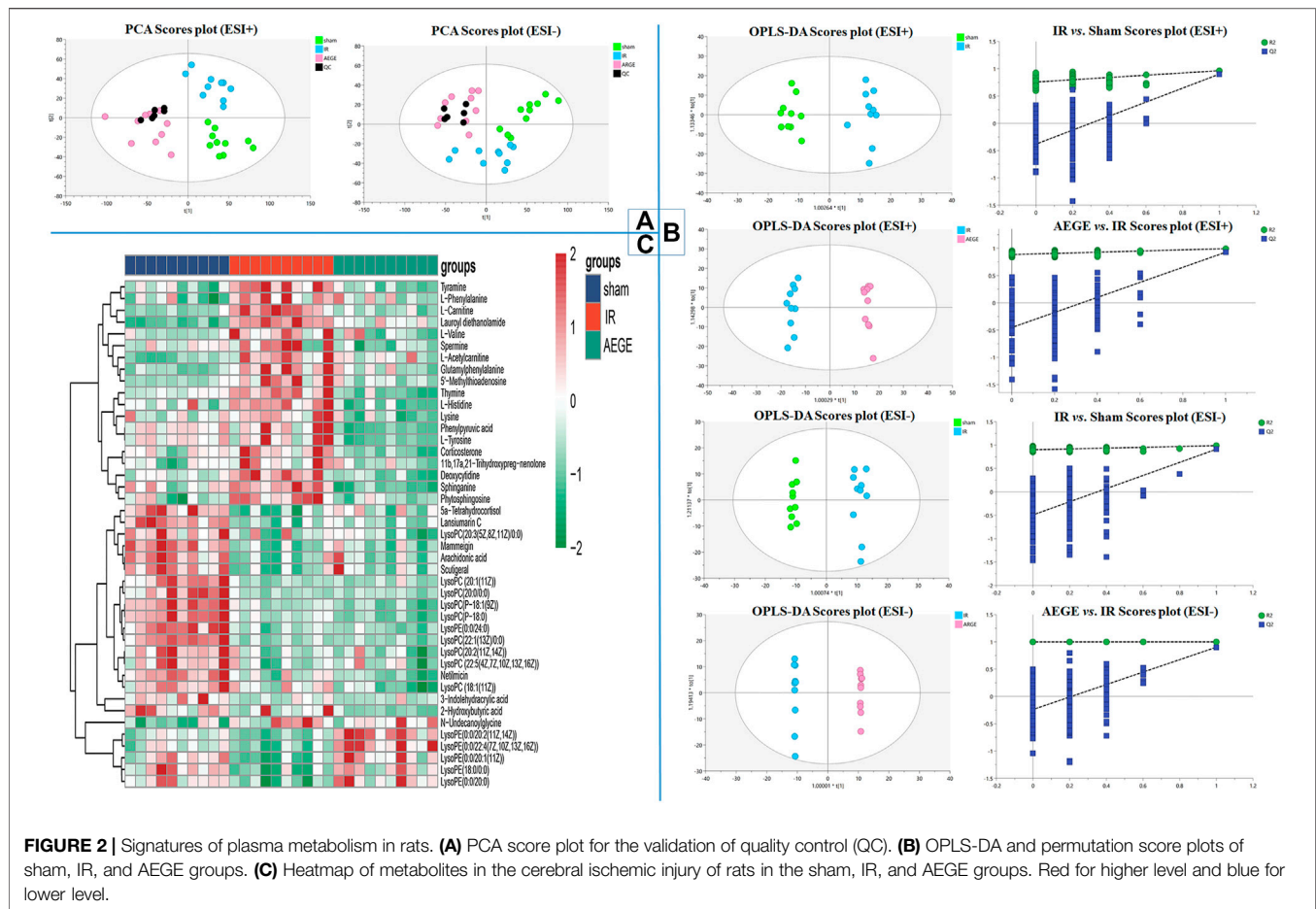
SOD and GSH-Px activity in the brain tissue of IR rats decreased significantly ($p < 0.05$), whereas there was a significant increase in MDA levels ($p < 0.05$) compared to the sham group. Compared to that in the IR group, GSH-Px and SOD activity increased significantly ($p < 0.05$) and MDA level decreased significantly ($p < 0.05$) in the AEGE group (Figure 1C).

In rats with IR injury, IL-10 expression was found to decrease significantly ($p < 0.05$), and the levels of IL-1β and TNF-α were significantly elevated ($p < 0.05$) compared to the corresponding values in the sham group. A significant decrease in TNF-α and IL-1β levels ($p < 0.05$) and a significant increase in IL-10 level ($p < 0.05$) was observed in the AEGE group (Figure 1C) compared to that in the IR group. These findings suggested that AEGE may be efficacious in treating cerebral ischemia-reperfusion injury by reducing oxidative stress and inflammation.

Metabolomics Studies

The 10 typical ion peaks in the QC samples showed low RSD in the peak intensity and retention times in the positive and negative ion modes (Supplementary Figure S3; Supplemental Table S3). The clustering of QC samples and significant separation between the sham, IR, and AEGE groups in PCA (Figure 2A) confirmed the robustness and reproducibility of the test method. Moreover, OPLS-DA modes both exhibited well-verifiable parameters (Supplemental Table S4). The permutation test with 200 iterations showed that the OPLS-DA models were not overfitted (Figure 2B).

The metabolites ($VIP > 1.0$, $p < 0.05$) were considered as potential differential metabolites. Combined with the primary parent ion information and secondary ion fragment information collected using high-resolution mass spectrometry, differential metabolites were identified by matching Peakview1.2 with the



substance molecules in HMDB, and combined using the standard sample atlas information.

Using this protocol, 43 differential metabolites (Table 1) were identified among the control, model, and AEGE groups. To better capture the changes in metabolism, a heatmap was constructed to represent the graphical view using all groups (Figure 2C). The changes in the levels of observed metabolites were divided into four scenarios as follows: 1) After administration of AEGE, the levels of metabolites, including L-phenylalanine, tyramine, deoxycytidine, sphinganine, 5'-methylthioadenosine, corticosterone, thymine, L-histidine, and phytosphingosine, returned to the same level as that in the sham group. 2) The metabolite levels in the IR vs. sham groups were not significantly upregulated or decreased; however, the levels decreased significantly after administration of AEGE. The types of metabolites in this category are more complex and there may be some positive feedback regulation that is considered normal. Examples include phenylpyruvic acid, L-tyrosine, and spermine. 3) The metabolite levels in the IR vs. sham groups were significantly upregulated or decreased; however, these levels were not significantly upregulated or decreased after the administration of AEGE. Examples include 3-indolehydracrylic acid, N-undecanoylglycine, and netilmicin. 4) The metabolite levels in the IR group were significantly

downregulated compared to those in the sham group; however, after the administration AEGE, these levels were still significantly downregulated. This phenomenon was called abnormal regulation. The metabolites mainly comprise lipids and fatty acids, such as LysoPC [20:1 (11Z)/0:0], LysoPC (P-18:0), and LysoPC (P-16:0/0:0).

Forty-three differential metabolites were enriched using the MetaboAnalyst 4.0 database to obtain the enrichment map of the metabolic pathways. The main pathways were identified for the following: phenylalanine, tyrosine, and tryptophan biosynthesis; phenylalanine metabolism; histidine metabolism; sphingolipid metabolism; pyrimidine metabolism; cysteine and methionine metabolism; tyrosine metabolism; steroid-hormone biosynthesis (Supplementary Figure S4). The levels of nine potential biomarkers, including L-phenylalanine, tyramine, deoxycytidine, sphinganine, 5'-methylthioadenosine, corticosterone, thymine, L-histidine, and phytosphingosine were significantly different in the plasma of rats in the IR group (Figure 3).

Transcriptomics Studies

A total of 2,326 DEGs were identified, which included 1,423 upregulated and 903 downregulated genes when the IR and sham groups were compared. A total of 1,453 DEGs were

TABLE 1 | Potential biomarkers of cerebral ischemic injury post-treatment with AEGE.

M/Z	Rt	Formula	Name	Adduct	HMDB	IR vs. sham	AEGE vs. IR
100.0756	2.02	C ₅ H ₁₁ NO ₂	L-Valine	+H-H ₂ O	HMDB0000883	↑	↓
120.0806	2.01	C ₈ H ₁₁ NO	Tyramine	+H-H ₂ O	HMDB0000306	↑***	↓***
127.0498	1.74	C ₅ H ₆ N ₂ O ₂	Thymine	+H	HMDB0000262	↑***	↓***
146.059	1.92	C ₉ H ₇ NO	Lysine	+H	HMDB0000182	↑*	↓***
147.0443	1.22	C ₉ H ₈ O ₃	Phenylpyruvic acid	+H-H ₂ O	HMDB0000205	↑	↓***
162.1109	0.92	C ₇ H ₁₅ NO ₃	L-carnitine	+H	HMDB0000062	↑***	↓***
178.0595	0.84	C ₈ H ₉ N ₃ O ₂	L-Histidine	+Na	HMDB0000177	↑***	↓***
182.08	1.2	C ₉ H ₁₁ NO ₃	L-Tyrosine	+H	HMDB0000158	↑	↓***
188.0698	6.75	C ₁₁ H ₁₁ NO ₃	3-Indolehydracrylic acid	+H-H ₂ O	HMDB0059765	↓*	↓
203.2234	0.81	C ₁₀ H ₂₆ N ₄	Spermine	+H	HMDB0001256	↑	↓***
204.1232	1.22	C ₉ H ₁₇ NO ₄	L-acetylcarnitine	+H	HMDB0000201	↑***	↓*
226.1788	15.89	C ₁₃ H ₂₅ NO ₃	N-Undecanoylglycine	+H-H ₂ O	HMDB0013286	↑	↓
250.0795	1.21	C ₉ H ₁₃ N ₃ O ₄	Deoxycytidine	+Na	HMDB0000014	↑***	↓***
288.2544	9.05	C ₁₆ H ₃₃ NO ₃	Lauroyl diethanolamide	+H	HMDB0032358	↑***	↓***
295.1275	3.3	C ₁₄ H ₁₈ N ₂ O ₅	Glutamylphenylalanine	+H	HMDB0029156	↑***	↓***
298.0962	2.72	C ₁₁ H ₁₅ N ₅ O ₃ S	5'-methylthioadenosine	+H	HMDB0001173	↑***	↓***
302.3049	8.96	C ₁₈ H ₃₉ NO ₂	Sphinganine	+H	HMDB0000269	↑	↓***
318.3026	8.98	C ₁₈ H ₃₉ NO ₃	Phytosphingosine	+H	HMDB0004610	↑***	↓***
329.2121	7.06	C ₂₁ H ₃₀ O ₄	Corticosterone	+H-H ₂ O	HMDB0001547	↑*	↓***
347.2222	7.05	C ₂₁ H ₃₂ O ₅	11b,17a,21-trihydroxypreg-nenolone	+H-H ₂ O	HMDB0006760	↑*	↓*
476.3109	9.42	C ₂₁ H ₄₁ N ₅ O ₇	Netilmicin	+H	HMDB0015090	***↑	↓
506.3621	10.18	C ₂₆ H ₅₂ NO ₆ P	LysoPC [P-18:1 (9Z)]	+H	HMDB0010408	***↑	↓
508.3734	11.45	C ₂₆ H ₅₄ NO ₆ P	LysoPC(P-18:0)	+H	HMDB0013122	***↑	↓*
522.3512	10.58	C ₂₆ H ₅₂ NO ₇ P	LysoPC [18:1 (11Z)]	+H	HMDB0010385	↑	↓
546.3526	15.24	C ₂₈ H ₅₂ NO ₇ P	LysoPC [20:3 (5Z,8Z,11Z)/0:0]	+H	HMDB0010393	↓*	↓
548.3694	11.46	C ₂₈ H ₅₄ NO ₇ P	LysoPC [20:2 (11Z,14Z)]	+H	HMDB0010392	↓	↓
550.3856	13.13	C ₂₈ H ₅₆ NO ₇ P	LysoPC [20:1 (11Z)]	+H	HMDB0010391	↓***	↑
552.3995	15.09	C ₂₈ H ₅₈ NO ₇ P	LysoPC(20:0/0:0)	+H	HMDB0010390	↓***	↑
566.4153	16.61	C ₂₉ H ₆₀ NO ₇ P	LysoPE (0:0/24:0)	+H	HMDB0011497	↓***	↓
570.3534	11.46	C ₃₀ H ₅₂ NO ₇ P	LysoPC [22:5 (4Z,7Z,10Z,13Z,16Z)]	+H	HMDB0010402	↓	↑
578.4174	15.68	C ₃₀ H ₆₀ NO ₇ P	LysoPC [22:1 (13Z)/0:0]	+H	HMDB0010399	↓***	↓
103.0406	1.59	C ₄ H ₈ O ₃	2-Hydroxybutyric acid	-H	HMDB0000008	↓	↓*
164.0702	2.00	C ₉ H ₁₃ NO ₃	L-phenylalanine	-H ₂ O-H	HMDB0000068	↑	↓*
303.2339	14.95	C ₂₀ H ₃₂ O ₂	Arachidonic acid	-H	HMDB0001043	↓***	↑
347.221	15.26	C ₂₁ H ₃₄ O ₅	5a-Tetrahydrocortisol	+H-H ₂ O	HMDB0000526	↓***	↑
353.1403	14.55	C ₂₁ H ₃₂ O ₅	Lansiumarin C	-H	HMDB0034838	↓***	↑
371.2212	14.95	C ₂₃ H ₃₂ O ₄	Scutigeral	-H	HMDB0030012	↓***	↓
403.1574	14.94	C ₂₅ H ₂₄ O ₅	Mammeigin	-H	HMDB0030785	↓***	↑
480.3112	10.16	C ₂₃ H ₄₈ NO ₇ P	LysoPE (18:0/0:0)	-H	HMDB0011130	↓***	↑
504.3122	9.84	C ₂₅ H ₄₈ NO ₇ P	LysoPE [0:0/20:2 (11Z,14Z)]	-H	HMDB0011483	↓	↑***
506.3291	10.95	C ₂₅ H ₅₀ NO ₇ P	LysoPE [0:0/20:1 (11Z)]	-H	HMDB0011482	↓	↑***
508.3408	12.78	C ₂₅ H ₅₂ NO ₇ P	LysoPE (0:0/20:0)	-H	HMDB0011481	↓	↑***
528.3108	9.61	C ₂₇ H ₄₈ NO ₇ P	LysoPE [0:0/22:4 (7Z,10Z,13Z,16Z)]	-H	HMDB0011493	↓	↑***

p* < 0.05.*p* < 0.01.****p* < 0.001.

identified, of which 507 were upregulated and 946 were downregulated when the AEGE and IR groups were compared; among them, the expression levels of 494 genes were restored after treatment with AEGE. All genes were used to construct volcano maps (**Figure 4A**). It was found that many genes were upregulated in the IR group, whereas, after treatment with AEGE, the expression of most genes was significantly downregulated. The general trend in the number of DEGs is shown in **Figure 4B** and was classified using the KEGG database. Following AEGE administration, the expression levels of amino acid-, carbohydrate-, and lipid-related genes partially returned to a level similar to that of the sham group.

The cellular processes and functions of the significantly altered genes can be understood by using the GO database. At the level of biological processes, genes were involved in the positive regulation of apoptosis. At the level of cellular components, the significantly changed genes mainly existed in the cytoplasm. At the molecular-function level, the genes were involved in the positive regulation of ATP binding, protein homodimerization, and identical protein binding (**Supplementary Figure S5**).

The KEGG database was used to analyze the biological pathways mediated by the identified genes in more depth. A total of 116 pathways were found to be significantly enriched when the sham and IR groups were compared (**Supplemental**

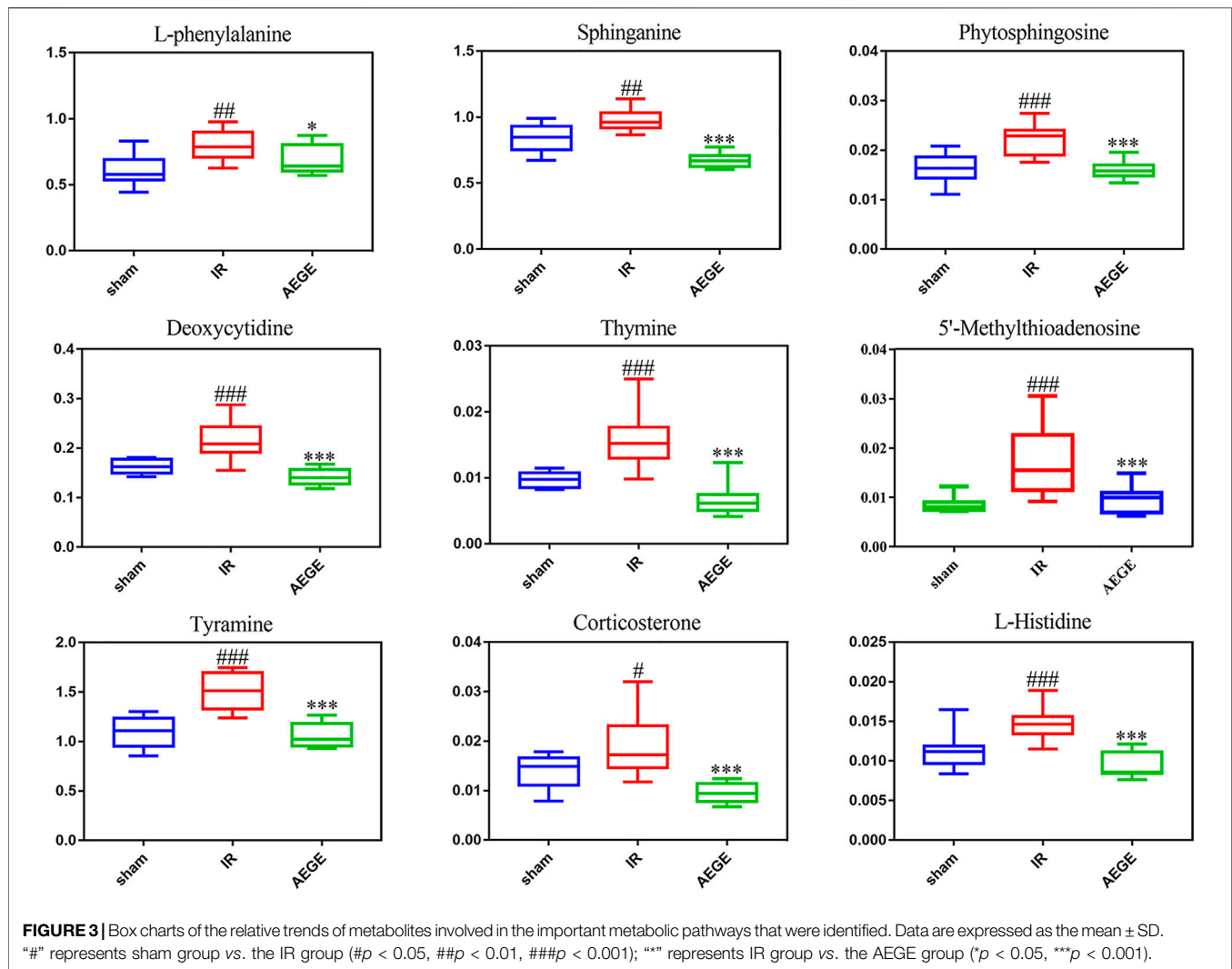


Table S5), whereas 28 pathways were found to be significantly enriched when the AEGE and IR groups were compared (Supplemental Table S6). Combined with metabolomic analysis, we found that the pathways of the DEGs were well associated with those of the metabolites produced during phenylalanine, pyrimidine, methionine, and sphingolipid metabolism. When the control, model, and AEGE groups were compared, the expression of six genes, including Tk1, Pold1, Rrm2, Pah, Mtap, and LOC100912604, was found to be restored (Figure 4C). Compared to the sham group, the expression levels of Hpd, Ddc, Degs2, Sgpp2, Asah2, Nme6 decreased significantly, whereas that of Sphk1 was significantly upregulated in the IR group. Following AEGE treatment, the expression of AK9 was significantly upregulated compared to that in the IR group.

Validation of Changes in Protein Expression

Integrated analysis indicated that the treatment of CIR with AEGE is related to phenylalanine, pyrimidine, methionine, and

sphingolipid metabolism. The protein expression of the key genes in rat brains was evaluated using western blotting (Figure 5). Compared to the sham group, the expression level of Pold1, Tk1, Mtap, Rrm2, and Pah increased significantly, whereas that of LOC100912604 decreased significantly in the brain tissue of rats in the IR group. After the administration of AEGE, the protein levels returned to a level similar to that in the sham group. The protein expression of the key genes analyzed using western blot was highly consistent with the results obtained using transcriptomics analysis.

DISCUSSION

Several studies have reported that oxidative stress and inflammation lead to apoptosis, autophagy, and necrosis after CIR. The decreased activities of SOD and GSH-Px and the increased levels of MDA in the brain tissue of IR rats may lead to weakened activity of antioxidant enzymes in

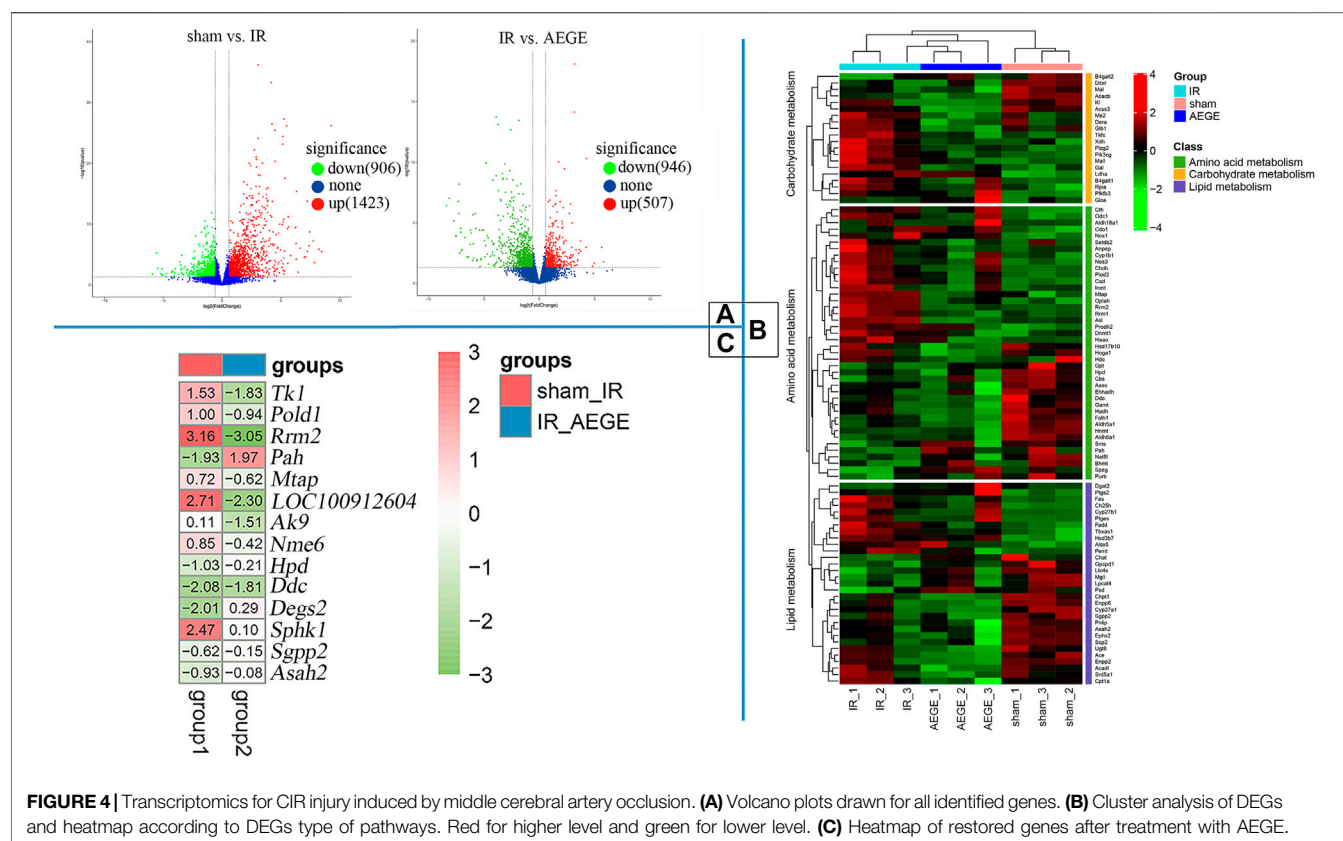


FIGURE 4 | Transcriptomics for CIR injury induced by middle cerebral artery occlusion. **(A)** Volcano plots drawn for all identified genes. **(B)** Cluster analysis of DEGs and heatmap according to DEGs type of pathways. Red for higher level and green for lower level. **(C)** Heatmap of restored genes after treatment with AEGE.

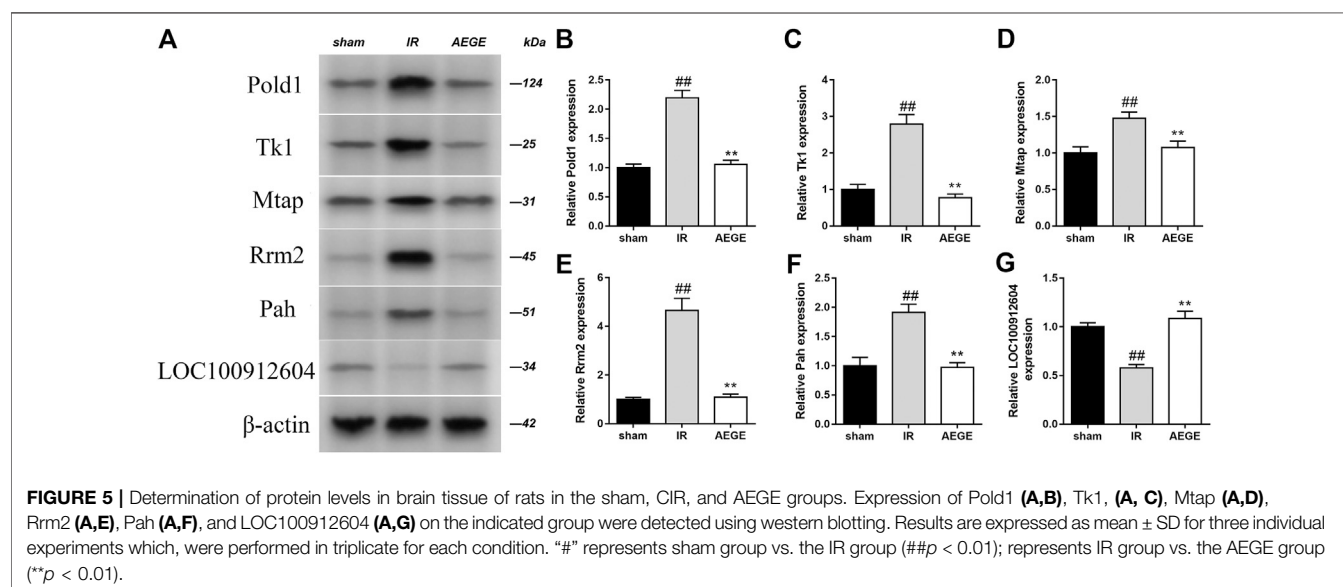


FIGURE 5 | Determination of protein levels in brain tissue of rats in the sham, CIR, and AEGE groups. Expression of Pold1 (A,B), Tk1 (A, C), Mtap (A,D), Rrm2 (A,E), Pah (A,F), and LOC100912604 (A,G) on the indicated group were detected using western blotting. Results are expressed as mean \pm SD for three individual experiments which, were performed in triplicate for each condition. “#” represents sham group vs. the IR group (## $p < 0.01$); represents IR group vs. the AEGE group (** $p < 0.01$).

the rat brain, which in turn can disrupt the balance between the antioxidant enzyme system and free oxygen radicals (Zhan and Yang, 2006). The activities of inflammatory cytokines, IL-1 β and TNF- α , in the brain tissue of IR rats increases significantly, whereas that of IL-10 decreases significantly.

This results in the induction of neutrophil adhesion, migration, and activation, and leads to an increase in inflammation and destruction of the brain tissue (Zhang et al., 1998). Therefore, it is believed that rats administered AEGE as a prophylactic might be less susceptible to CIR

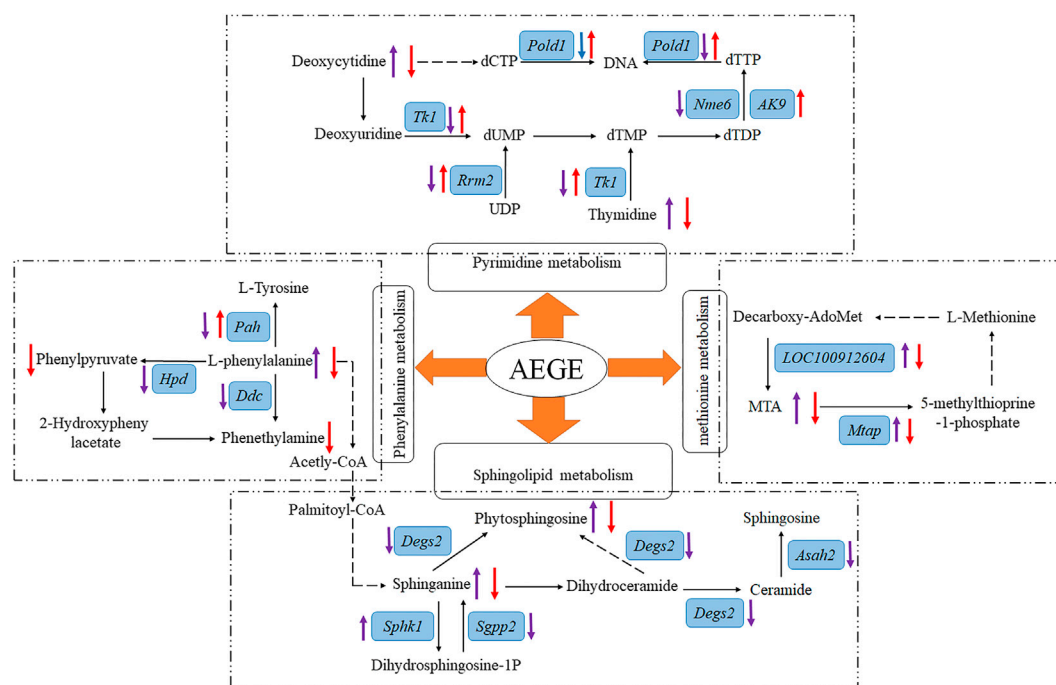


FIGURE 6 | Overview of metabolic pathway analysis. After treatment with AEGE, the concentration or expression of metabolites and genes (blue background and italic) were changed (“↑” means upregulated; “↓” means downregulated; purple arrow represents the ratio of IR to sham groups; red arrow represents the ratio of AEGE to IR groups). Dashed arrow indicates multiple steps in the pathway.

injury. This may be owing to the antioxidant and anti-inflammatory mechanisms of AEGE.

To further establish the relationship between the results from transcriptomic and metabolomics studies, data of the potential metabolites and the altered genes were integrated. The main metabolic pathways of the following metabolites were identified: phenylalanine, pyrimidine, methionine, and sphingolipids. AEGE could treat CIR injury by affecting these pathways at both transcriptional and metabolic levels. Details of the metabolic pathways are shown in **Figure 6**.

L-phenylalanine is an essential aromatic amino acid that plays a key role in the biosynthesis of other amino acids (Pardridge, 1998). When present in sufficiently high levels, phenylalanine acts as a neurotoxin that disrupts or attacks neural cells and tissues. Plasma L-phenylalanine levels can be increased in rats with traumatic brain injury (Vuille-Dit-Bille et al., 2012). Phenylpyruvic acid is a keto-acid, which is an intermediate or catabolic byproduct of phenylalanine metabolism. Tyrosine is an amino acid synthesized from phenylalanine in the presence of phenylalanine hydroxylase. We found the metabolite levels of L-phenylalanine to be significantly higher and the expression levels of Pah, Ddc, and Hpd genes to be significantly lower than those in the IR group. However, the levels of the metabolites, phenylpyruvic acid, and L-tyrosine, were not significantly different compared to those in the sham group. This may have occurred because

of the decrease in L-phenylalanine metabolism due to CIR, which led to the accumulation of L-phenylalanine, causing subsequent damage to the brain cells. After administration of AEGE, the levels of L-phenylalanine, phenylpyruvic acid, and L-tyrosine decreased significantly, and the expression of the Pah gene increased significantly. The expression trend of Pah protein analyzed using western blot was consistent with the results obtained using transcriptomics. Therefore, it could be inferred that AEGE can decrease L-phenylalanine levels. Reduced levels of L-phenylalanine may reduce the oxygen consumption of the brain, energy production, and storage, all of which are beneficial in brain recovery through phenylalanine metabolism.

Phytosphingosine exerted strong cytotoxic effects, modulated the *Caenorhabditis elegans* muscarinic acetylcholine receptor-mediated signal transduction pathway, and induced cell death (Lee et al., 2001). Sphinganine is a bioactive compound involved in cell proliferation, differentiation, transcription, autophagy, and apoptosis, all of which are relevant to inflammatory disease (Merrill et al., 2009). In this study, we found that sphinganine and phytosphingosine accumulated significantly in rats in the IR group, causing damage to brain cells. Moreover, we found that the expression of Degs2, Sgpp2, and Asah2 was significantly decreased, and that of the *Sphk1* gene was increased significantly in the brain tissue of rats with IR. This could likely be a protective mechanism of the body to

defend itself against high concentrations of sphinganine and phytosphingosine, to convert sphinganine to the less toxic dihydrosphingosine-1P, and reduce the conversion of sphinganine to phytosphingosine. After treatment with AEGE, the levels of phytosphingosine and sphinganine decreased significantly compared to that in the IR group. This reduction may be attributed to the regulation of phenylalanine metabolism by AEGE, which led to the decrease in acetyl-CoA levels. Therefore, the therapeutic effects of AEGE may be achieved by regulating the levels of sphingomyelin and sphingosine in sphingolipid metabolism by regulating phenylalanine metabolism.

Deoxycytidine is one of the principal nucleosides of DNA and is composed of cytosine and deoxyribose. Thymine is one of the pyrimidine bases of living matter. Exogenous uridine and cytidine play a role in maintaining brain function in rats with CIR injury (Löffler et al., 2018). In the IR group, the levels of deoxycytidine and thymine increased significantly, and the expression of Tk1, Pold1, Rrm2, and Nme6 genes decreased significantly compared to that in the sham group. The consistent trends of the two metabolites might be closely related to the enzymes controlled by the genes integrated with DNA. Following AEGE treatment, the expression of Tk1, Pold1, Rrm2, and AK9 were found to be significantly upregulated. Therefore, it could be reasonably deduced that AEGE regulates the balance between dCTP and dTTP through genes including Tk1, Pold1, Rrm2, AK9, and Tyms. Moreover, the expression trend of Tk1, POLD1, and Rrm2 proteins, which were verified using western blotting was the same as that obtained using metabolomics analysis. This result explains the decrease of blood deoxycytidine and thymine levels after treatment with AEGE. Collectively, these findings suggested that AEGE could improve the disorder in pyrimidine metabolism caused by CIR injury.

5'-Methylthioadenosine (MTA) can yield 5-methylthiopurine-1-phosphate and adenine through the metabolism of S-methyl-5'-thioadenosine phosphorylase (Mtap), which is an important step in the methionine- and purine-recovery pathways. MTA affects the regulation of gene expression and plays a role in proliferation, differentiation, and apoptosis (Ansorena et al., 2002). Protein methionine oxidation potentiates the activation of NF- κ B and contributes to CIR injury (Gu et al., 2016). In this study, we found that LOC100912604, Mtap, and MTA were significantly upregulated, which may have accelerated the metabolism and oxidation of methionine after CIR. After treatment with AEGE, LOC100912604, Mtap, and MTA were significantly downregulated, which restored methionine metabolism and reduced the damage to brain cells resulting from methionine oxidation. The expression trend of Mtap analyzed using western blotting was consistent with the results of transcriptomics analysis. Thus, AEGE intervention may regulate methionine metabolism and likely contribute to its therapeutic effects.

The main limitation of this study concerning the metabolomics component is one which is common to all

metabolomic investigations - identification of metabolites. Because of the unavailability to obtain the reference compounds, identifying them remained an enormous difficulty.

CONCLUSION

In summary, rats pretreated with AEGE suffered less severe CIR injury. Our findings revealed that AEGE significantly reduced the area of cerebral infarction caused by CIR injury. The mechanism of AEGE in alleviating CIR was via the reduction of oxidative stress and inflammation.

Results of transcriptomic and metabolomic studies indicated that six metabolites, namely, sphinganine, thymine, phytosphingosine, L-phenylalanine, deoxycytidine, 5'-methylthioadenosine; and six genes, namely, Tk1, Pold1, Rrm2, Pah, Mtap, and LOC100912604, were significantly altered in the IR group. The representative proteins in the altered pathways were determined using Western blot. These metabolites and genes could be regulated after treatment with AEGE, suggesting that the therapeutic effect of AEGE in CIR may be related to the regulation of phenylalanine and pyrimidine metabolic pathways, sphingolipid metabolism, and methionine metabolism.

Although this new prescription of ASE combined with GEB is seldom used in a clinical setting, it provides useful clues for the further development of this herbal combination.

DATA AVAILABILITY STATEMENT

The datasets generated for this study can be found in the Sequence Read Archive, <https://www.ncbi.nlm.nih.gov/gds/?term=GSE160500>.

ETHICS STATEMENT

The animal study was reviewed and approved by the Animal Care Committee of the Jiangxi University of Chinese Medicine. All standard biosecurity and institutional safety procedures have been adhered to in all the experiment procedures in this article.

AUTHOR CONTRIBUTIONS

BL, RC, and ZL conceived and designed the experiments; BL wrote manuscript; QW, ZL, SY and YF were involved in data acquisition; BL and RC have made statistical analyses. All authors read and approved the final manuscript.

FUNDING

This work was supported by National Natural Science Foundation of China (No. 81960701) and Natural Science

Foundation of Jiangxi Province (No. 20171ACB20039), Jiangxi Province talent Project (No. (2016)332), Nanchang innovative talent team (No. (2018)274), Nanchang Key Laboratory of active ingredients of traditional Chinese medicine and natural medicine (2019-NCZDSY-011).

REFERENCES

- Ansorena, E., García-Trevijano, E. R., Martínez-Chantar, M. L., Huang, Z.-Z., Chen, L., Mato, J. M., et al. (2002). S-adenosylmethionine and methylthioadenosine are antiapoptotic in cultured rat hepatocytes but proapoptotic in human hepatoma cells. *Hepatology* 35, 274–280. doi:10.1053/jhep.2002.30419
- Bai, J., and Lyden, P. D. (2015). Revisiting cerebral postischemic reperfusion injury: new insights in understanding reperfusion failure, hemorrhage, and edema. *Int. J. Stroke* 10, 143–152. doi:10.1111/ijis.12434
- Bai, Y., Tohda, C., Zhu, S., Hattori, M., and Komatsu, K. (2011). Active components from Siberian ginseng (*Eleutherococcus senticosus*) for protection of amyloid β (25–35)-induced neuritic atrophy in cultured rat cortical neurons. *J. Nat. Med.* 65, 417–423. doi:10.1007/s11418-011-0509-y
- Boese, A. C., Lee, J.-P., and Hamblin, M. H. (2020). Neurovascular protection by peroxisome proliferator-activated receptor α in ischemic stroke. *Exp. Neurol.* 331, 113323. doi:10.1016/j.expneurol.2020.113323
- Du, Z., Shu, Z., Lei, W., Li, C., Zeng, K., Guo, X., et al. (2018). Integration of metabonomics and transcriptomics reveals the therapeutic effects and mechanisms of baoyuan decoction for myocardial ischemia. *Front. Pharmacol.* 9, 514. doi:10.3389/fphar.2018.00514
- Green, A. R. (2008). Pharmacological approaches to acute ischaemic stroke: reperfusion certainly, neuroprotection possibly. *Br. J. Pharmacol.* 153, S325–S338. doi:10.1038/sj.bjp.0707594
- Gu, S. X., Blokhin, I. O., Wilson, K. M., Dhanesha, N., Doddapattar, P., Grumbach, I. M., et al. (2016). Protein methionine oxidation augments reperfusion injury in acute ischemic stroke. *JCI. Insight.* 1, 7. doi:10.1172/jci.insight.86460
- Huang, D. W., Sherman, B. T., and Lempicki, R. A. (2009). Systematic and integrative analysis of large gene lists using DAVID bioinformatics resources. *Nat. Protoc.* 4, 44–57. doi:10.1038/nprot.2008.211
- Huang, N.-K., Lin, C.-C., Lin, Y.-L., Huang, C.-L., Chiou, C.-T., Lee, Y.-C., et al. (2019). Morphological control of mitochondria as the novel mechanism of *Gastrodia elata* in attenuating mutant huntingtin-induced protein aggregations. *Phytomedicine* 59, 152756. doi:10.1016/j.phymed.2018.11.016
- Jhong, M.-C., Tang, N.-Y., Liu, C.-H., Huang, W.-H., Hsu, Y.-T., Liu, Y.-L., et al. (2013). Relationship between Chinese medicine pattern types, clinical severity, and prognosis in patients with acute cerebral infarct. *Explore* 9, 226–231. doi:10.1016/j.explore.2013.04.002
- Johnson, C. H., Ivanisevic, J., and Siuzdak, G. (2016). Metabolomics: beyond biomarkers and towards mechanisms. *Nat. Rev. Mol. Cell Biol.* 17, 451–459. doi:10.1038/nrm.2016.25
- Lee, J. S., Min, D. S., Park, C., Park, C. S., and Cho, N. J. (2001). Phytosphingosine and C2-phytoceramide induce cell death and inhibit carbachol-stimulated phospholipase D activation in Chinese hamster ovary cells expressing the *Caenorhabditis elegans* muscarinic acetylcholine receptor. *FEBS. Lett.* 499, 82–86. doi:10.1016/s0014-5793(01)02527-3
- Liu, R.-L., Xiong, Q.-J., Shu, Q., Wu, W.-N., Cheng, J., Fu, H., et al. (2012). Hyperoside protects cortical neurons from oxygen-glucose deprivation-reperfusion induced injury via nitric oxide signal pathway. *Brain Res.* 1469, 164–173. doi:10.1016/j.brainres.2012.06.044
- Lloyd-Jones, D., Adams, R., Carnethon, M., De Simone, G., Ferguson, T. B., Flegal, K., et al. (2009). Heart disease and stroke statistics--2009 update: a report from the American heart association statistics committee and stroke statistics subcommittee. *Circulation* 119, e21–181. doi:10.1161/circulationaha.108.191261
- Löffler, M., Carrey, E. A., and Zameitat, E. (2018). New perspectives on the roles of pyrimidines in the central nervous system. *Nucleosides, Nucleotides and Nucleic Acids* 37, 290–306. doi:10.1080/15257770.2018.1453076
- Longa, E. Z., Weinstein, P. R., Carlson, S., and Cummins, R. (1989). Reversible middle cerebral artery occlusion without craniectomy in rats. *Stroke* 20, 84–91. doi:10.1161/01.str.20.1.84
- Lu, Y., Hsiang, F., Chang, J. H., Yao, X. Q., Zhao, H., Zou, H. Y., et al. (2018). Houshiheisan and its components promote axon regeneration after ischemic brain injury. *Neural Regen. Res.* 13, 1195–1203. doi:10.4103/1673-5374.235031
- Merrill, A. H., Stokes, T. H., Momin, A., Park, H., Portz, B. J., Kelly, S., et al. (2009). Sphingolipidomics: a valuable tool for understanding the roles of sphingolipids in biology and disease. *J. Lipid Res.* 50, S97–S102. doi:10.1194/jlr.R800073-JLR200
- Mozaffarian, D., Benjamin, E. J., Go, A. S., Arnett, D. K., Blaha, M. J., Cushman, M., et al. (2016). Heart disease and stroke statistics-2016 update A report from the American heart association. *Circulation* 133, E38–E360. doi:10.1161/cir.0000000000000350
- Pardridge, W. M. (1998). Blood-brain barrier carrier-mediated transport and brain metabolism of amino acids. *J. Neurochem. Res.* 23, 635–644. doi:10.1023/a:1022482604276
- Pei, B., Yang, M., Qi, X., Shen, X., Chen, X., and Zhang, F. (2016). Quercetin ameliorates ischemia/reperfusion-induced cognitive deficits by inhibiting ASK1/JNK3/caspase-3 by enhancing the Akt signaling pathway. *Biochem. Biophysical Res. Commun.* 478, 199–205. doi:10.1016/j.bbrc.2016.07.068
- Peng, Z., Wang, S., Chen, G., Cai, M., Liu, R., Deng, J., et al. (2015). Gastrodin alleviates cerebral ischemic damage in mice by improving anti-oxidant and anti-inflammation activities and inhibiting apoptosis pathway. *Neurochem. Res.* 40, 661–673. doi:10.1007/s11064-015-1513-5
- Soares, B. P., Chien, J. D., and Wintermark, M. (2009). MR and CT monitoring of recanalization, reperfusion, and penumbra salvage: everything that recanalizes does not necessarily reperfuse!. *Stroke* 40, S24–S27. doi:10.1161/strokeaha.108.526814
- Tang, C., Wang, L., Cheng, M., Zhang, X., Liu, X., and Xiao, H. (2014). Rapid and sensitive analysis of parishin and its metabolites in rat plasma using ultra high performance liquid chromatography-fluorescence detection. *J. Chromatogr. B* 973, 104–109. doi:10.1016/j.jchromb.2014.08.020
- Tohda, C., Ichimura, M., Bai, Y., Tanaka, K., Zhu, S., and Komatsu, K. (2008). Inhibitory effects of *Eleutherococcus senticosus* extracts on amyloid β (25–35)-induced neuritic atrophy and synaptic loss. *J. Pharmacol. Sci.* 107, 329–339. doi:10.1254/jphs.08046fp
- Vuille-Dit-Bille, R. N., Ha-Huy, R., and Stover, J. F. (2012). Changes in plasma phenylalanine, isoleucine, leucine, and valine are associated with significant changes in intracranial pressure and jugular venous oxygen saturation in patients with severe traumatic brain injury. *Amino Acids* 43, 1287–1296. doi:10.1007/s00726-011-1202-x
- Wang, Z., Gerstein, M., and Snyder, M. (2009). RNA-Seq: a revolutionary tool for transcriptomics. *Nat. Rev. Genet.* 10, 57–63. doi:10.1038/nrg2484
- Wu, B., Xiao, X., Li, S., and Zuo, G. (2019). Transcriptomics and metabonomics of the anti-aging properties of total flavones of *Epimedium* in relation to lipid metabolism. *J. Ethnopharmacology* 229, 73–80. doi:10.1016/j.jep.2018.09.039
- Xie, Y., Zhang, B., and Zhang, Y. (2015). Protective effects of *Acanthopanax polysaccharides* on cerebral ischemia-reperfusion injury and its mechanisms. *Int. J. Biol. Macromolecules* 72, 946–950. doi:10.1016/j.ijbiomac.2014.09.055
- Yu, S.-S., Zhao, J., Zheng, W. P., and Zhao, Y. (2010). Neuroprotective effect of 4-hydroxybenzyl alcohol against transient focal cerebral ischemia via anti-apoptosis in rats. *Brain Res.* 1308, 167–175. doi:10.1016/j.brainres.2009.10.037
- Zhan, C., and Yang, J. (2006). Protective effects of isoliquiritigenin in transient middle cerebral artery occlusion-induced focal cerebral ischemia in rats. *Pharmacol. Res.* 53, 303–309. doi:10.1016/j.phrs.2005.12.008

SUPPLEMENTARY MATERIAL

The Supplementary Material for this article can be found online at: <https://www.frontiersin.org/articles/10.3389/fphar.2021.619076/full#supplementary-material>.

- Zhang, B., Zhang, H., Du, C., Ng, Q. X., Hu, C., He, Y., et al. (2017). Metabolic responses of the growing *Daphnia* similis to chronic AgNPs exposure as revealed by GC-Q-TOF/MS and LC-Q-TOF/MS. *Water Res.* 114, 135–143. doi:10.1016/j.watres.2017.02.046
- Zhang, Q., and Zhao, Y.-H. (2014). Therapeutic angiogenesis after ischemic stroke: Chinese medicines, bone marrow stromal cells (BMSCs) and their combinational treatment. *Am. J. Chin. Med.* 42, 61–77. doi:10.1142/s0192415x14500049
- Zhang, Z., Chopp, M., Goussev, A., and Powers, C. (1998). Cerebral vessels express interleukin 1 β after focal cerebral ischemia. *Brain Res.* 784, 210–217. doi:10.1016/s0006-8993(97)01317-6
- Zhou, R., Zhu, Y., Yang, W., Zhang, F., Wang, J., Yan, R., et al. (2020). Discovery of herbal pairs containing *Gastrodia elata* based on data mining and the Delphi expert questionnaire and their potential effects on stroke through network Pharmacology. *Evidence-Based Complement. Altern. Med.* 2020, 1. doi:10.1155/2020/42635912020
- Conflict of Interest:** The authors declare that the research was conducted in the absence of any commercial or financial relationships that could be construed as a potential conflict of interest.
- Copyright © 2021 Lin, Chen, Wang, Li, Yang and Feng. This is an open-access article distributed under the terms of the Creative Commons Attribution License (CC BY). The use, distribution or reproduction in other forums is permitted, provided the original author(s) and the copyright owner(s) are credited and that the original publication in this journal is cited, in accordance with accepted academic practice. No use, distribution or reproduction is permitted which does not comply with these terms.



Identification, Biological Activities and Biosynthetic Pathway of *Dendrobium* Alkaloids

Zongmin Mou¹, Yi Zhao^{2,3}, Fei Ye⁴, Yana Shi^{5,6}, Edward J. Kennelly^{2,3}, Suiyun Chen^{1*} and Dake Zhao^{1*}

¹Biocontrol Engineering Research Center of Plant Disease and Pest, Biocontrol Engineering Research Center of Crop Disease and Pest, School of Ecology and Environmental Science, Yunnan University, Kunming, China, ²Department of Biological Sciences, Lehman College and The Graduate Center, City University of New York, Bronx, NY, United States, ³Ph.D. Programs in Biochemistry, Biology, and Chemistry, The Graduate Center, City University of New York, New York, NY, United States, ⁴Kunming Municipal Hospital of Traditional Chinese Medicine, Kunming, China, ⁵College of Agriculture and Biotechnology, Yunnan Agricultural University, Kunming, China, ⁶Institute of Medicinal Plants, Yunnan Academy of Agricultural Sciences, Kunming, China

OPEN ACCESS

Edited by:

Gudrun S. Ulrich-Merzenich,
University Hospital Bonn, Germany

Reviewed by:

Jen-Tsung Chen,
National University of
Kaohsiung, Taiwan
Jiangjie Lu,
Hangzhou Normal University, China
Xiaoyu Ding,
Nanjing Normal University, China

*Correspondence:

Suiyun Chen
chensuiyun@ynu.edu.cn
Dake Zhao
zhaodk2012@ynu.edu.cn

Specialty section:

This article was submitted to
Ethnopharmacology,
a section of the journal
Frontiers in Pharmacology

Received: 14 September 2020

Accepted: 01 April 2021

Published: 20 April 2021

Citation:

Mou Z, Zhao Y, Ye F, Shi Y,
Kennelly EJ, Chen S and Zhao D (2021)
Identification, Biological Activities and
Biosynthetic Pathway of
Dendrobium Alkaloids.
Front. Pharmacol. 12:605994.
doi: 10.3389/fphar.2021.605994

Dendrobium is a genus of flowering plants belonging to the Orchidaceae family with more than 1,400 species. Many *Dendrobium* species have been used as medicinal plants in several Asian countries for thousands of years. Alkaloids were reported as the major biological markers due to their complex chemical compositions and various types. In this review, we summarized the structural types of alkaloids, their pharmacological activities, as well as the mechanisms of biological activities. More than sixty alkaloids were isolated and identified from the *Dendrobium* genus. Moreover, the pharmacological effects of *Dendrobium* alkaloids as hepatic lipid and gluconeogenesis regulation, as neuroprotection, and as anti-tumor, anti-inflammatory, anti-diabetes, and anti-virus factors were described. Besides, the total chemical synthesis of dendrobine is provided, while the biosynthetic pathway of dendrobine has been proposed based on the functions of associated genes. For applications of these invaluable herbs, more researches on the extraction of biological markers from compounds are needed. Further confirmation of the proposed biosynthetic pathways is anticipated as well.

Keywords: alkaloids, orchidaceae, *Dendrobium*, anti-inflammatory, antitumor, mechanisms, biosynthetic pathway

INTRODUCTION

Apart from Asteraceae, the orchid family is the second-largest flowering family, which has 28,000 species distributed in about 736 genera (Chase et al., 2015), among which *Dendrobium* is one of the largest genera. It contains more than 1,500 species (www.theplantlist.org), most of which are epiphytic or lithophytic, and it is widespread in South, East, and Southeast Asia, like China, Japan, Philippines, Vietnam, India, and Indonesia. Some species are also found in New Guinea, Australia, and the islands of the Pacific (Zhu et al., 2009). The plants of *Dendrobium* species have been used as traditional or folk medicine in many Asian countries for thousands of years. For instance, there are 96 *Dendrobium* species in China, and about 30 species, known as shí hú (石斛) or shí hú lán (石斛兰), have been widely used as ethnic medicine for tonifying the stomach, nourishing Yin (to enhance the production of body fluids, such as blood, saliva, tears, etc.), and clearing heat and toxic matter (Yang et al., 2006; Flora of China, 2020). The earliest written record of the medicinal usage of *Dendrobium* was found in the ancient text “Shen Nong’s Herbal Classic” 2000 years ago, in which it was considered to be a “superior grade” herbal medicine. Hundreds of years later, *Dendrobium* was

TABLE 1 | The ethnomedicine use of *Dendrobium* in some countries.

Country	<i>Dendrobium</i> species	Local name	Ethnomedicine use	References
China	<i>Dendrobium nobile</i> Lindl.	shí hú (石斛)	Used as a tonic and antipyretic for treating human disorders	Lam et al. (2015)
	<i>Dendrobium chrysotoxum</i> Lindl.	shí hú lán (石斛兰)	Used for clearing heat and toxic matter, and enhancing immunity	Lin et al. (2018)
	<i>Dendrobium fimbriatum</i> Hook.	huáng cǎo (黄草)		Yang et al. (2006)
	<i>Dendrobium officinale</i> Kimura et Migo	xīān cǎo (仙草)		Yuan et al. (2018)
	<i>Dendrobium aphyllum</i> (Roxb.) C.E.C.Fisch			Wang et al. (2020)
	<i>Dendrobium huoshanense</i> Z. Z. Tang et S. J. Cheng			
	<i>Dendrobium findlayanum</i> C. S. P. Parish et Rchb. f.			
	<i>Dendrobium loddigesii</i> Rolfe			
Japan	<i>Dendrobium moniliforme</i> (L.) Sw.	Fu-ran	Gives long life to men	Cakova et al. (2020)
Indian	<i>Dendrobium macraei</i> Lindl. (jeevanti)	Charaka samhita	Used as an astringent to the bowels, as anaphrodisiac, and in asthma and bronchitis	Lam et al. (2015)
	<i>Dendrobium alpestre</i> royle (jewanti)	Ayurved Jeevanti		
Thailand	<i>Dendrobium draconis</i> Rchb. F.	Unknown	Employed as a blood tonic	Ng et al. (2012)

documented in detail in “Compendium of Materia Medica” in Ming Dynasty (1590 AD). Nowadays, *Dendrobium nobile* Lindl., *Dendrobium chrysotoxum* Lindl., *Dendrobium fimbriatum* Hook., *Dendrobium officinale* Kimura et Migo, and *Dendrobium huoshanense* Z. Z. Tang et S. J. Cheng are included in Chinese Pharmacopoeia (2020 edition). Among these five species, *Dendrobium nobile* Lindl. is one of the 50 fundamental herbs used in traditional Chinese medicine (TCM). Generally, the fibrous stems of *Dendrobium* are employed as the officinal parts in ethnopharmacology, persevered by dry processing (Chinese Pharmacopoeia Commission, 2020). These stems are usually used either alone or mixed with other tonic Chinese herbs, like xī yáng shēn (American Ginseng) and gǒu qǐ zǐ (Barbary Wolferry Fruit) (Lin et al., 2018). Aside from China, *Dendrobium* species have also been used as ethnomedicines in Japan, Indian, and Thailand (Table 1). Given their high medicinal value and wide ethno-applications, the *Dendrobium* genus was recognized as a prized folk medicine (Ng et al., 2012).

Due to the important pharmacological activities and economical value of *Dendrobium* genus, up to now, many phytochemical and pharmacological researches have been implemented. The active constituents in *Dendrobium* are polysaccharides, alkaloids, flavonoids, amino acids, bibenzyls, and several trace elements (He et al., 2020). The polysaccharides from *Dendrobium* exhibit immunomodulatory and hepatoprotective activities; and the alkaloids are antioxidant, anticancer, and neuroprotective, while other compounds display anti-angiogenesis, anti-cytotoxicity, and anti-mutagenesis effects (Ng et al., 2012; Xu et al., 2013). Alkaloids are the earliest identified category of compounds in *Dendrobium* (Chen and Chen, 1935). More importantly, *Dendrobium* alkaloids are the key constituents that responsible for their pharmacological activities, making them potential candidates for new drugs. Therefore, some important bioactive markers such as dendrobine (20) have attracted many scientists to

investigate their chemical, pharmaceutical, and biological mechanisms, as well as biogenetic pathways (Li Q. et al., 2017).

Dendrobium alkaloids with complex chemical structures consist of pyrrole, indolizidine, terpenoid alkaloids, organic amine alkaloids, indole, quinazoline, and others (Xu et al., 2013). In accordance with other genera of Orchidaceae plants, indolizidine alkaloids and organic amine alkaloids are the major constituents of this genus (Lam et al., 2015). These chemicals are considered as active ingredients for effects like anti-inflammatory, cytotoxic, antitumor, cytoprotection, gluconeogenesis regulation, and preventing neuronal apoptosis (Ng et al., 2012). For instance, *Dendrobium nobile* Lindl. is a famous TCM recorded in Chinese Pharmacopoeia (2020 edition). The alkaloids of *Dendrobium nobile* Lindl. (DNLA) are considered to have beneficial effects on liver metabolism, hepatic lipid homeostasis, neuronal activity, and resistance effects on tumors, cancers, and virus based on previous studies (Table 2). Dendrobine (20), a sesquiterpene alkaloid, makes up 92.6% of the DNLA (Xu et al., 2017). Dendrobine (20) is the first identified active alkaloid of *Dendrobium nobile* Lindl. (Chen and Chen, 1935), and is regarded as the standard agent for qualitative and quantitative evaluation of *Dendrobium nobile* Lindl. (Li R. et al., 2017).

In this review, we aim to summarize the structural types, pharmacological activities, and the mechanisms of biological activities of *Dendrobium* alkaloids. Additionally, the proposed biogenetic pathways of dendrobine (20) are also included.

STRUCTURAL IDENTIFICATION OF DENDROBIUM ALKALOIDS

Alkaloids are representatives of the first category of compounds extracted from *Dendrobium* (Xu et al., 2013). *Dendrobium* alkaloids were isolated by the traditional alkaloid extraction method given their basic chemical structure. Dried powders of

TABLE 2 | Summary of the pharmacological of alkaloids isolated from *Dendrobium nobile* Lindl.

No	Organ	Alkaloids content of crude extract	Constituents of alkaloid extract	Pharmacological activities	References
1	Stem	79.8%	Dendrobine (20), 92.6% Dendrobine-N-oxide (22), 3.3% Nobilonine (45), 2.0% Dendroxine (24), 0.9% 6-Hydroxy-nobilonine (46), 0.32% 13-Hydroxy-14-oxodendrobine (26), 0.07%	Beneficial effects on liver glucose and lipid metabolism gene expressions Protective effects on CCl ₄ -induced acute liver injury	Xu et al. (2017) Li et al. (2019)
2	Stem	79.8%	Dendrobine (20), 92.6%	Protective effects on hepatic lipid homeostasis and acute liver injury	Huang S. et al. (2019); Zhou et al. (2020)
3	Stem	Unkown	Mixed fat-soluble alkaloids	Anti-tumor efficacy in human colorectal cancer	He et al. (2017)
4	Unkown	96.1%	Dendrobine (20), 90.7% Dendramine (23), 2.31% 3-Hydroxy-2-oxodendrobine (26), 1.29% Nobilonine, (45), 4.47%	Protection from OGD/RP-induced neuronal damages	Wang et al. (2010)
5	Stem	96.1%	Dendrobine (20), 90.7% Nobilonine (45), 4.47% Dendramine (23), 2.31% 3-Hydroxy-2-oxodendrobine (26), 1.29%	Protection of brain impairment	Li et al. (2011)
6	Unkown	54.5%	Dendrobine (20), 30.5%	Attenuation of LPS-induced hyperphosphorylation of tau protein and protection against LPS-induced apoptosis	Yang et al. (2014)
7	Unkown	79.8%	Dendrobine (20) Dendrobine-N-oxide (22) Nobilonine (45) Dendroxine (24) 6-Hydroxy-nobilonine (46) 13-Hydroxy-14-oxodendrobine (26)	Prevention of neuronal apoptosis and synaptic loss Regulation of α - and β -secretase in hippocampal neurons	Nie et al. (2016) Huang J. et al. (2019)
8	Dendrobine standard	>98%	Dendrobine (20), >98%	Anticancer activity toward non-small cell lung cancer cells	Song et al. (2019)
9	Dendrobine standard	98%	Dendrobine (20), 98%	Anti-influenza a virus	Li et al. (2017)

Dendrobium spp. were liquid-liquid extracted with various solvents, such as ethanol, methanol, or chloroform, then fractionated successively with water, petroleum ether, ethyl acetate, n-butyl alcohol, etc. (Yang et al., 2020). Subsequently, these fractions were purified on different silica gel column chromatography systems with various polarity ranges of solvents (Morita et al., 2000). Moreover, high performance liquid chromatography (HPLC) and ultra-performance liquid chromatography (UPLC) coupled with mass spectrometry were developed to discover new compounds of *Dendrobium* (Xu et al., 2020). Up to now, more than sixty alkaloids (Figures 1–5, 1–63) have been identified from this genus. The chemical structures include pyrrole, indolizidine, terpenoid, amine, and indole alkaloids. These compounds were mainly isolated from the whole plants, stems, or leaves of *Dendrobium nobile* Lindl., *Dendrobium officinale* Kimura et Migo, *Dendrobium findlayanum* C. S. P. Parish et Rchb. f., *Dendrobium chrysanthum* Wall. ex Lindl., *Dendrobium crepidatum* Lindl. ex Paxton, *Dendrobium anosmum* Lindl., *Dendrobium devonianum* Paxton, *Dendrobium*

friedericksianum Rchb. f., *Dendrobium hildebrandii* Rolfe, *Dendrobium loddigesii* Rolfe, *Dendrobium lohohense* Tang et F. T. Wang, *Dendrobium moniliforme* (L.) Sw., *Dendrobium pierardii* R. Br., *Dendrobium primulinum* Lindl., and *Dendrobium wardianum* R. Warner (Inubushi et al., 1964; Lüning et al., 1965; Elander et al., 1969; Ekevag et al., 1973; Begum et al., 2010; Lam et al., 2015; Hu et al., 2016; Hu et al., 2016; Xu et al., 2019).

Pyrrole Alkaloids

Most pyrrole alkaloids from Orchidaceae were found in *Dendrobium*, *Pleione*, and *Liparis* plants. Till now, only five pyrroles were reported in *Dendrobium*, and all of them are simple phthalide-pyrrolidine alkaloids (Figure 1). Shihunine (1), a water-soluble phthalide-type alkaloid, was the first pyrrole alkaloid from *Dendrobium lohohense* Tang et F. T. Wang in 1968 (Inubushi et al., 1964). Shihunidine (2) was also isolated from the same species by Li et al. (1991). Cis-trans isomerizations of dendrochrysin (3 and 4) and dendrochrysanines (5 and 6), the other four pyrrole isomers

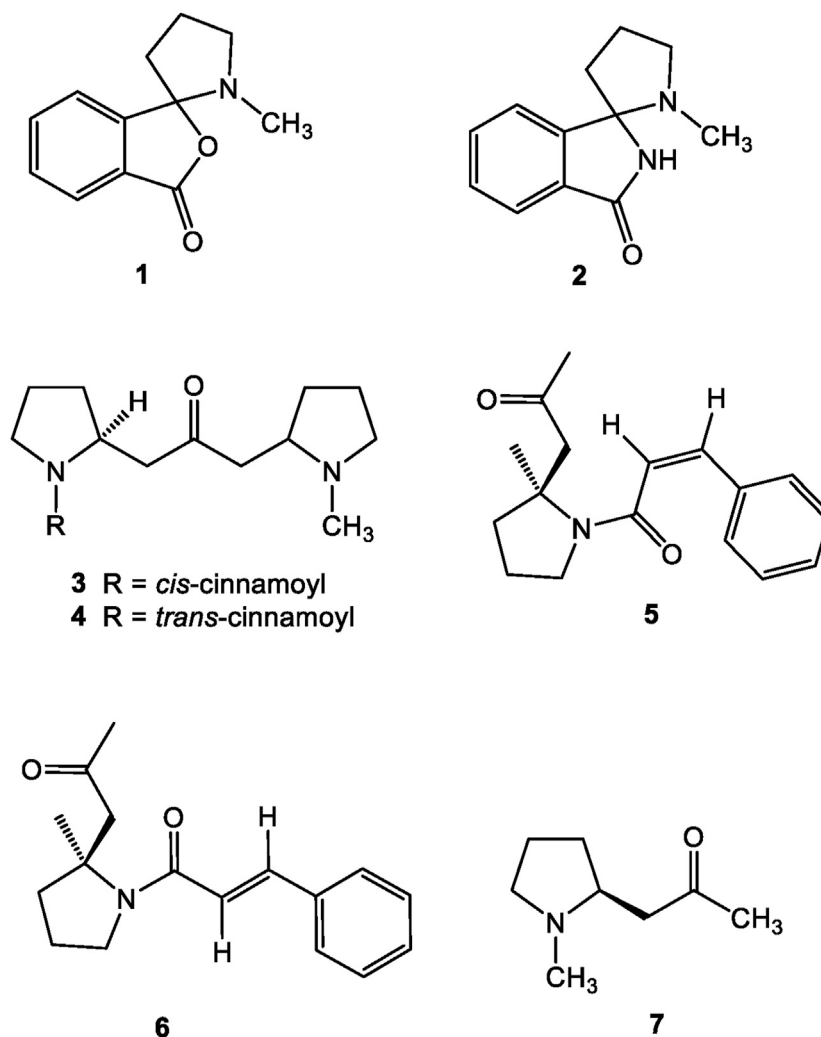


FIGURE 1 | Structures of pyrrole alkaloids reported in *Dendrobium*.

alkaloids, were isolated from *Dendrobium chrysanthum* Wall. ex Lindl. (Ekevag et al., 1973; Yang et al., 2005), while hygrine (7) was produced in *Dendrobium primulinum* Lindl. (Lüning et al., 1965).

Indolizidine Alkaloids

Indolizidine alkaloids are important constituents of *Dendrobium* (Xu et al., 2019). Twelve indolizidine alkaloids were observed in *Dendrobium*, most of which were from *Dendrobium crepidatum* Lindl. et Paxton (Figure 2, 8–19). Dendroprimine (8) is a simple indolizidine alkaloid reported in *Dendrobium primulinum* Lindl. (Lüning et al., 1965). Other indolizidine alkaloids such as crepidine (9), crepidamine (10), isocrepidamine (11), and isodendrocrepine (12) were found in *Dendrobium crepidatum* Lindl. et Paxton (Elander et al., 1973; Hu et al., 2020). The other three alkaloids of this type (±)-homocrepidine A [(±)-13] (±)-dendrocrepidamine A [(±)-14], and homocrepidine B (15) were first identified from the same *Dendrobium* species by Hu et al. (2016; 2020). Then the absolute configurations of the new

pairs enantiomeric octahydroindolizine compounds (±)-homocrepidine A [(±)-13] and (±)-dendrocrepidamine A [(±)-14], were verified by single-crystal X-ray diffraction (Hu et al., 2016; Hu et al., 2020). Recently, four new indolizidine alkaloids, crepidatamines A to D (16–19), were purified from *Dendrobium crepidatum* Lindl. et Paxton by Xu et al. (2019; 2020).

Terpenoid Alkaloids

Terpenoid alkaloids are another important secondary metabolites principally isolated from *Dendrobium* (Xu et al., 2013). The types of alkaloids are various based on their mono-, sesqui-, di-, and tri-terpenoid skeletons. Dendrobine (20) was the first terpenoid-alkaloid elucidated from *Dendrobium nobile* Lindl. in 1932 (Chen and Chen 1935). Subsequently, a total of 25 dendrobine-type alkaloids were found in *Dendrobium nobile* Lindl., *Dendrobium findlayanum* C. S. P. Parish et Rchb. f., *Dendrobium wardianum* R. Warner, and *Dendrobium moniliforme* (L.) Sw., most of which are sesquiterpenoid alkaloids (Figure 3, 20–42, 51–52).

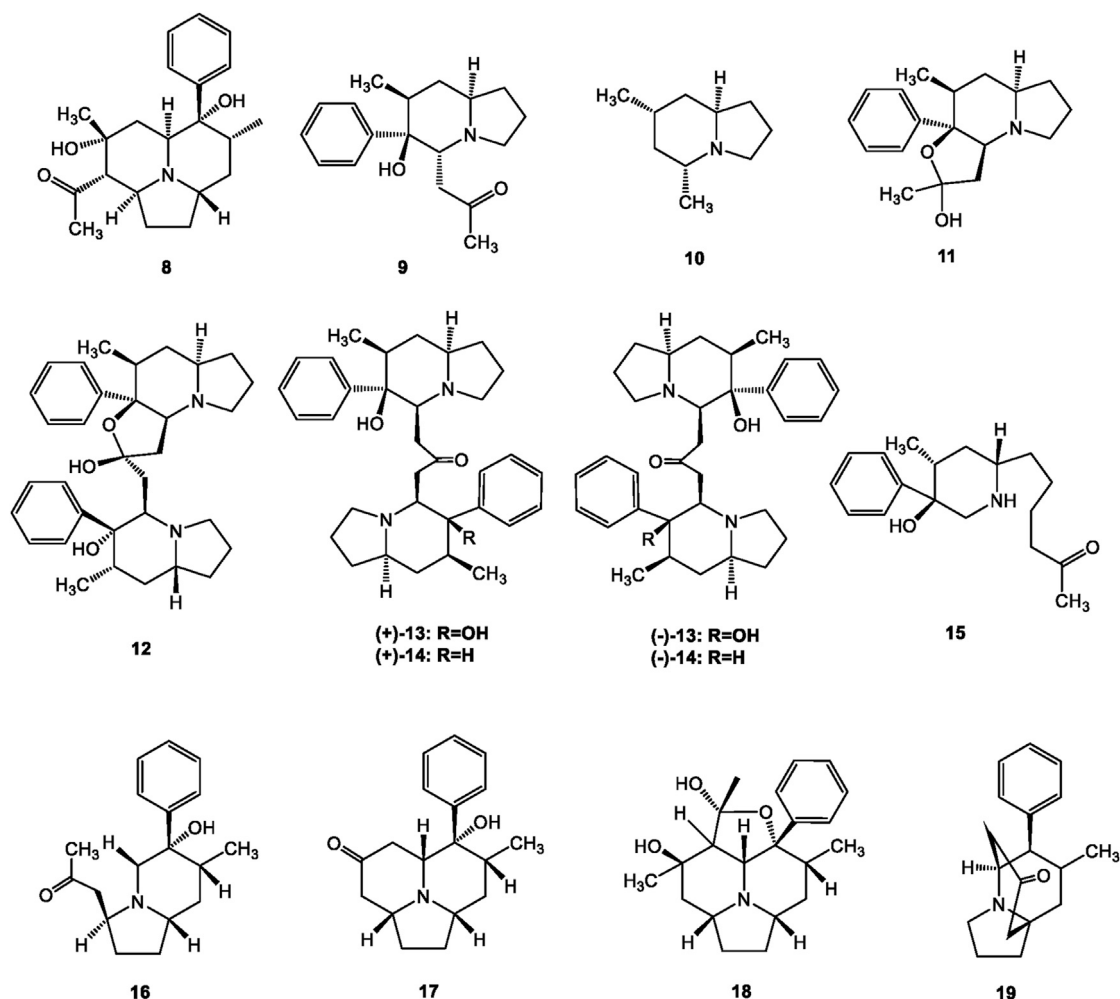


FIGURE 2 | Structures of indolizidine alkaloids reported in *Dendrobium*.

Interestingly, dendrobine-type alkaloids are a class of characteristic picrotoxanes with highly complex structures, which are only distributed in *Dendrobium* genus (Begum et al., 2010; Meng et al., 2017). All of these dendrobine-type alkaloids contain basic skeletons comprising one picrotoxane-type sesquiterpenoid combined with a five-membered C2-C9-linked N-heterocycle and C3-C5-linked lactonic ring (Xu et al., 2013).

Two thirds of terpenoid alkaloids in the genus *Dendrobium* were isolated from the certain species of *Dendrobium nobile* Lindl. Mubironines A-C (27–29) were identified from the whole plant (Morita et al., 2000), and the absolute components of these three compounds were confirmed by single-crystal X-ray diffraction. Dendroterpene A and B (30–31) were found from the stems recently (Wang P. et al., 2019). Other terpenoid alkaloids from *Dendrobium nobile* Lindl., compounds 20–26 and 32–41 have been reported over eighty years (Chen and Chen, 1935; Shhosuke and Yoshimasa, 1964; Inubushi and Nakano, 1965; Okamoto et al., 1966a; Okamoto et al., 1966b; Granelli et al., 1970;

Elander and Leander, 1971; Hedman and Leander, 1972; Okamoto et al., 1972; Glomqvist et al., 1973; Wang et al., 1985; Meng et al., 2017; Wang Q. et al., 2019; Liu et al., 2020; Yang et al., 2020). A total of eleven terpenoid alkaloids were purified from another three *Dendrobium* species. Dendrofindline B (42) was isolated from *Dendrobium findlayanum* C. S. P. Parish et Rchb. f. (Liu et al., 2020). Besides, seven new seco-dendrobines, findlayines A-F (43–48), and dendrofindline A (49) were identified from the same species. (Yang et al., 2018; Liu et al., 2020; Yang et al., 2020). In 2007, Liu et al. (2007) reported the isolation and structural identification of moniline (50) from the stems and leaves of *Dendrobium moniliforme* (L.) Sw.. Dendrowardine (51) and wardianumine A (52) were purified from *Dendrobium wardianum* R. Warner by Liu and Zhao. (2003) and Zhang et al. 2017, respectively.

Amine Alkaloids

Amine alkaloids are a class of widely spread natural amines with basic nitrogen but cannot form a ring in the skeleton. Most

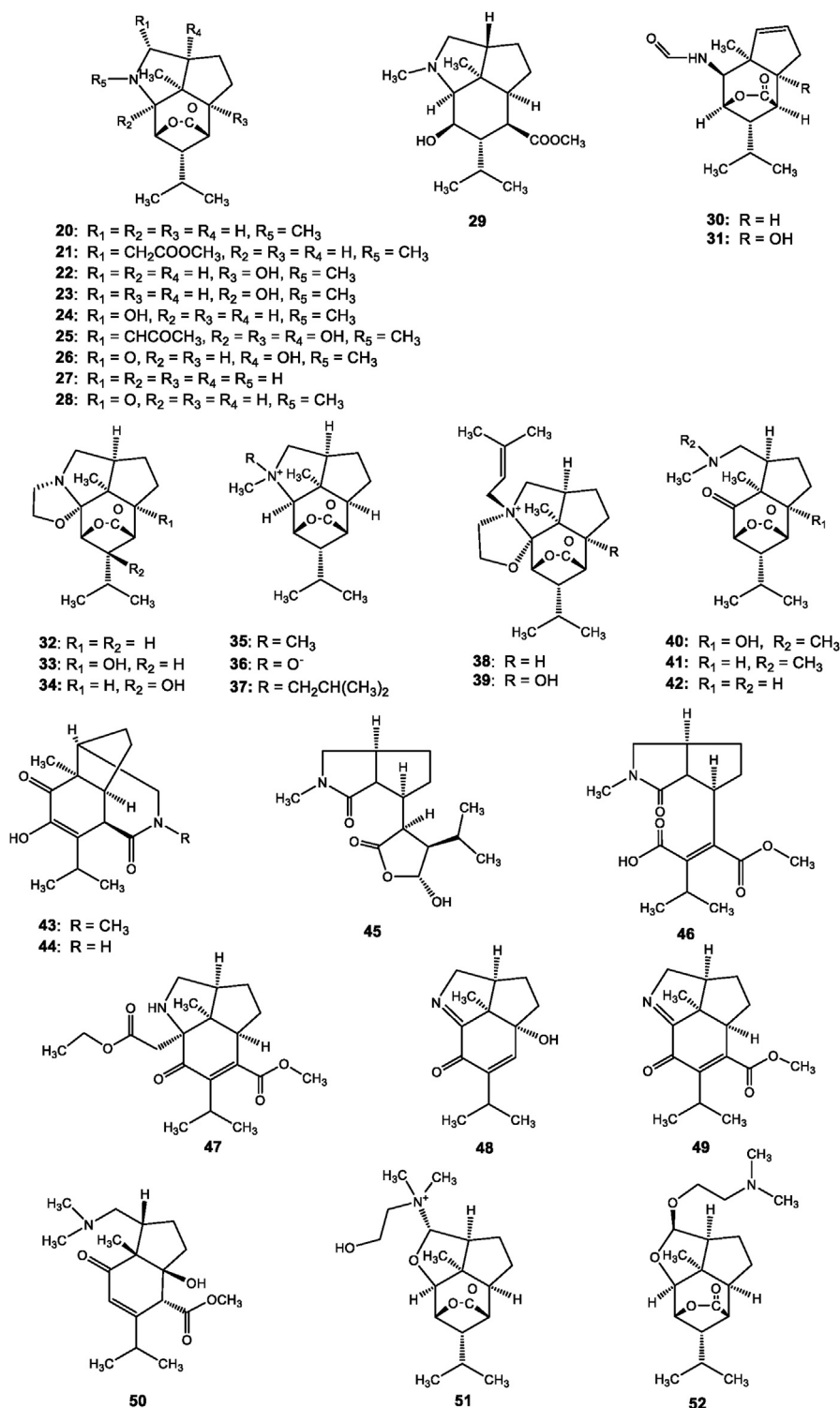


FIGURE 3 | Structures of terpenoid alkaloids reported in *Dendrobium*.

amines in *Dendrobium* are amides (**Figure 4**, 53–61). For example, *N*-*cis*-p-coumaroyltyramine (53) and *N*-*cis*-feruloyltyramine (54) were identified from the stems of

Dendrobium devonianum Paxton (Zhang et al., 2013). Pierardine (61) was isolated from *Dendrobium pierardii* R. Br. (Elander et al., 1969).

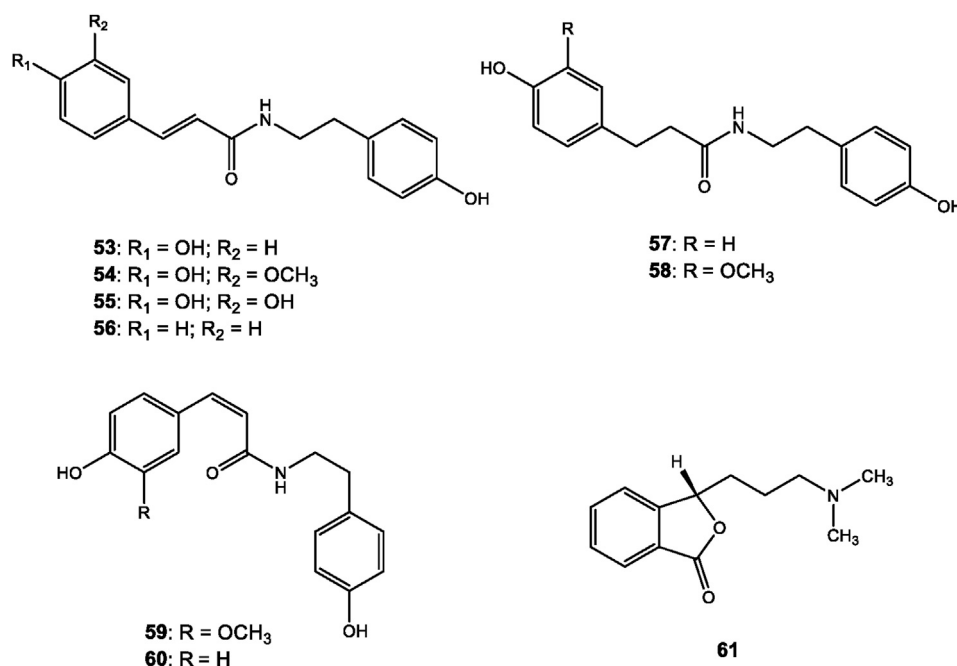


FIGURE 4 | Structures of organic amine alkaloids reported in *Dendrobium*.

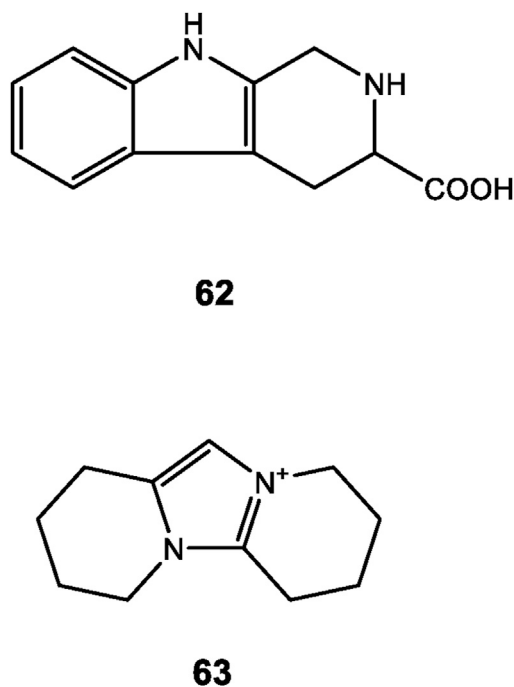


FIGURE 5 | Structures of indole and other alkaloids reported in *Dendrobium*.

Indole and Other Types of Alkaloids

2,3,4,9-tetrahydro-1H-pyrido [3,4-b] indole-3-carboxylic acid (62) was the only reported indole alkaloid from *Dendrobium devonianum* Paxton (Zhang et al., 2013) (Figure 5). Moreover,

anosmines (63) are another type of alkaloids isolated from two species of *Dendrobium*, whose structures were confirmed by X-ray crystallography (Hemscheidt and Spenser, 1993).

Metabolic Analysis of *Dendrobium*

At present, metabolomics has been widely utilized in the field of medicinal plants, such as bioactive components identification, drug metabolism, toxicology, and investigation on metabolic pathways, etc. (Liang et al., 2009). Alkaloids are regarded as chemical markers in quantitative analysis of *Dendrobium*. Generally, the metabolic profiling of *Dendrobium* alkaloid compounds was established by liquid chromatography coupled to single (LC-MS) and tandem (LC-MS/MS) mass spectrometry, in combination with multivariate data analyses, where secondary metabolites can be accurately quantified based on their fingerprint chromatograms. For example, the comparative metabolite analysis of *Dendrobium officinale* Kimura et Migo and *Dendrobium huoshanense* Z. Z. Tang et S. J. Cheng showed that the accumulation of alkaloids was species-specific (Song et al., 2020). Ten potential anti-inflammatory alkaloid components were detected from the extraction of *Dendrobium aphyllum* (Roxb.) C. E. C. Fisch by UPLC-MS (Wang P. et al., 2019), while eight water-soluble metabolites containing rare imidazolium alkaloids and anosmines (4) were identified by the screening of *Dendrobium nobile* Lindl., *Dendrobium officinale* Kimura et Migo, and *Dendrobium loddigesii* Rolfe, using chromatography along with spectroscopic techniques (Chen et al., 2018). Besides, DNLA was reported to improve hepatic lipid homeostasis based on the results of UPLC-MS of 48 kinds of hepatic bile acids in the livers of high fat diet (HFD)-fed mice (Huang S. et al., 2019). Furthermore, the combination of

metabolomic and transcriptomic technologies revealed the possible pathways in alkaloid biosynthesis of *Dendrobium officinale* Kimura et Migo (Guo et al., 2013).

PHARMACOLOGICAL ACTIVITIES

Dendrobium alkaloids are active components with anti-inflammatory, antitumor, and anti-viral effects, which can also regulate hepatic lipid and gluconeogenesis, and protect from hyperglycemia. For a better understanding of the bioactivities of *Dendrobium* alkaloids, previous studies on pharmacological efficacy are summarized.

Anti-inflammatory Activity

Inflammation induced by endotoxin such as lipopolysaccharide (LPS), is an immune defense response of organisms to tissue injury and microbial agents (Guha and Mackman, 2001). Most anti-inflammatory activities were tested with the LPS-induced RAW264.7 model by evaluating the indices of nitric oxide (NO) production and the expression of inducible NO synthase (Chen et al., 2018). The anti-inflammatory activities of *Dendrobium* alkaloids have been reported. For example, anosmines (63) that were presented in four *Dendrobium* species exhibited inhibitory activity against NO production and inflammation in LPS-activated RAW264.7 cells without cytotoxic activity (Chen et al., 2018). Besides (+)-homocrepidine A [(+)-13] isolated from *Dendrobium crepidatum* Lindl. ex Paxton was evaluated for its anti-inflammatory activity (NO inhibition) with LPS-induced RAW 264.7 macrophages, and the half maximal inhibitory concentration (IC₅₀) value was 3.6 μ M. However, the other enantiomeric isomer (–)-homocrepidine A [(–)-13], displayed an IC₅₀ value of 22.8 μ M, which was almost 7 times less active than [(+)-13]. Besides, their racemic mixtures (\pm)-homocrepidine A [(\pm)-13], showed a moderate inhibitory effect (IC₅₀ = 5.0 μ M). Similar pharmacological activities were observed in (\pm)-dendrocrepidamine A [(\pm)-14] (Hu et al., 2020). Compared with the enantiomers of racemic indolizidine and their racemic mixtures, homocrepidine B (15) also displayed moderate anti-inflammatory activity with the IC₅₀ value of 27.6 μ M (Hu et al., 2016). Furthermore, the total alkaloids, mainly consisted of six indolizidine-type compounds from the same *Dendrobium* species, showed protective effects against the LPS-induced acute lung injury in mice by the down-regulation of the TLR4-mediated MyD88/MAPK signaling pathway (Hu et al., 2018). Taken together, the pharmacological investigations of *Dendrobium* alkaloids on anti-inflammatory shed light on scientific guidance for the source of this genus.

Improved Regulation of Hepatic Lipid Homeostasis and Gluconeogenesis

The liver is quite essential to the regulation of lipid and glucose homeostasis. On the other hand, the disruption of homeostasis will result in metabolic disorders of the liver, including fatty liver and diabetes, which are the most common chronic liver disease all

over the world (Rinella, 2015). DNLA was found to impact the regulation of liver glucose and the expressions of lipid metabolism genes in mice livers by increasing the expressions of *PGC1 α* , *Glut2*, *Cpt1 α* , *Acox*, *ATGL/Pnpla2*, and *FoxO1* genes, and decreasing the mRNA transcription from the *Srebp1* gene (Xu et al., 2017). Moreover, excessive accumulation of hepatic lipids is responsible for liver metabolic dysfunction. Modulation of bile acids has been reported as an effective intervention strategy for maintaining hepatic lipid homeostasis (Chiang, 2013). DNLA exerted protective effects on hepatic lipid homeostasis by enhancing taurine-conjugated bile acids and decreasing the cholic acid/chenodeoxycholic acid ratio (Huang S. et al., 2019). To be specific, DNLA decreased four types of bile acids and increased five types of bile acids among 48 kinds of hepatic bile acids in the livers of high-fat diet (HFD)-fed mice (Huang S. et al., 2019). On the other hand, DNLA regulated hepatic gluconeogenesis by mediating the hepatic antioxidant components through hepatic metallothionein and the gene expression of the nuclear factor erythroid 2-related factor 2 antioxidant pathway, which plays critical roles in host defense against abnormal gluconeogenesis (Xu et al., 2017). The mechanisms were further elucidated that DNLA improved mitochondrial function and inhibited mitochondrial apoptotic cell death (Zhou et al., 2020). Overall, considering the beneficial effects of *Dendrobium* alkaloids on liver metabolism, *Dendrobium* alkaloids could be used as natural compounds in the development of new treatments for hyperlipidemia and hyperglycaemia.

Anti-tumor Activity

It was reported that *Dendrobium* alkaloids could inhibit tumor cell growth and mediate apoptosis. (He et al., 2017; Song et al., 2019; Wang et al., 2014). Specifically, the alkaloid extracts of *Dendrobium candidum* Wall. ex Lindl. were reported to significantly inhibit the growth of transplanted Lewis tumors, meanwhile, the mixed alkaloids could improve the spleen index and regulate the expressions of TNF- α and IL-2 (Wang et al., 2014). Moreover, the fat-soluble alkaloids extracted from *Dendrobium nobile* Lindl. were found to induce the apoptosis of human colorectal cancer HT-29 cells with an IC₅₀ value of 0.72 mg/ml at 48 h, where the cell cycle was arrested in G2 phase. Besides, the extraction decreased the mitochondrial membrane potential ($\Delta\Psi$ m) and induced ROS accumulation by increasing expression levels of apoptotic proteins, such as Caspase-9, Caspase-3, and intracellular cytochrome C (He et al., 2017), which may be related to the mitochondria-mediated apoptotic pathway. The combined treatment using sesquiterpene alkaloids, dendrobine (20) and cisplatin, was also effective for inhibiting the non-small cell lung cancer cells (NSCLC) *in vitro* and *in vivo*, where the cytotoxicity was induced by the simulation of c-jun NH₂-terminal kinase (JNK)/p38 stress signaling pathways, and the expression change of pro-apoptotic proteins Bax and Bim further led to the apoptosis (Figure 6, revised from song et al., 2019, created with BioRender.com). Besides, dendrobine (20) also mediated apoptotic cell death by the mitochondrial-mediated pathway (Song et al., 2019). On the whole, due to the distinct association with cell death signaling pathways, dendrobine (20)

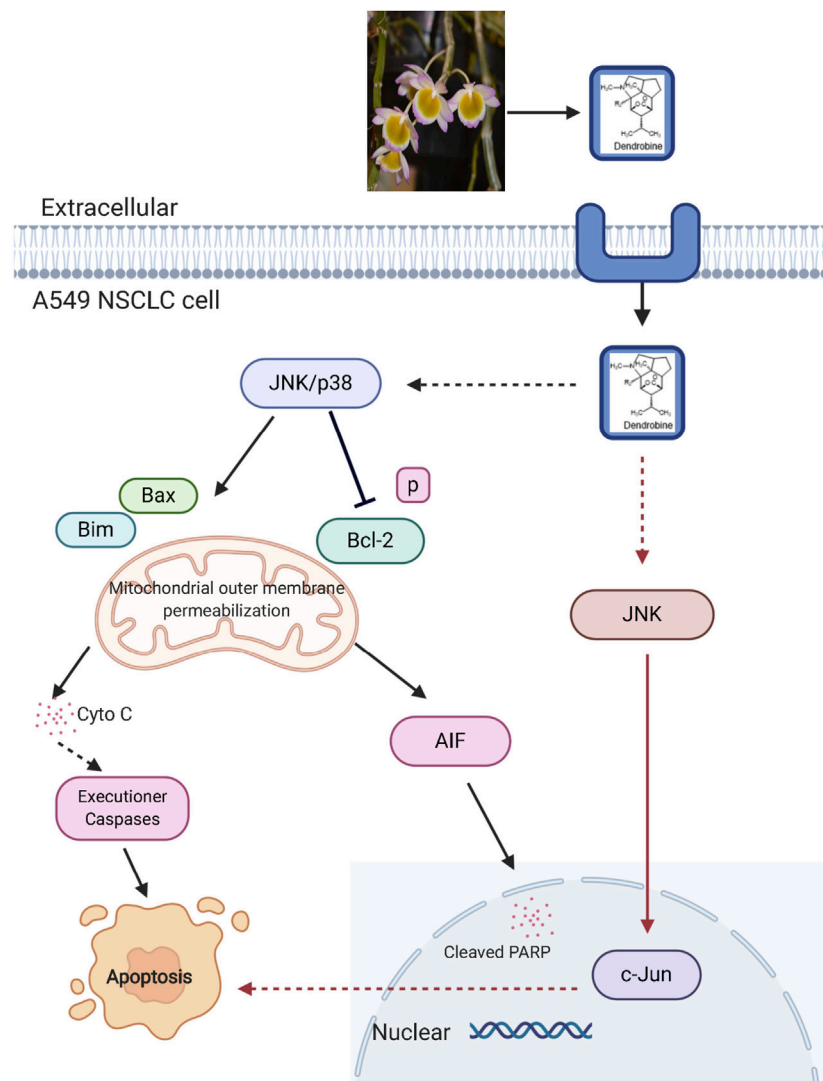


FIGURE 6 | Signaling pathway involved in dendrobine induced apoptosis in cancer cells. JNK, c-Jun N-terminal kinase; p38, p38 mitogenactivated protein kinase; Cyto C, cytochrome C; AIF, apoptosis inducing factor; Bcl-2, B-cell lymphoma two; Bim, Bcl-2 interacting mediator of cell death; PARP, poly ADP-ribose polymerase.

can be regarded as a potential agent for the development of novel anti-NSCLS strategies especially when combined with cisplatin. (Song et al., 2019).

Renal Protective and Anti-Diabetic Effects

In China, the dried stems of some *Dendrobium* species including *Dendrobium huoshanense* Z. Z. Tang et S. J. Cheng, *Dendrobium officinale* Kimura et Migo, and *Dendrobium nobile* Lindl. have been used to nourish kidney and improve the symptoms of diabetes (Cakova et al., 2020). For instance, shihunidine (2) and shihunine (1) isolated from *Dendrobium loddigesii* Rolfe displayed inhibitory effects on Na^+/K^+ -ATPase of the rat kidney (Li et al., 1991). Li et al. (2019) recently reported that DNLA showed vital hypoglycemic effects in diabetic rats. The shihunine (1) extracts from *Dendrobium loddigesii* Rolfe at the dose of 50 mg/kg decreased the triglycerides level by 43.7%, compared

with the non-treated db/db mice, and inhibited the expression of cleaved cysteine aspartic acid-specific protease 3. The result of western blot analysis also verified the agonistic effects of shihunine (1) extracts on the expressions of adenosine monophosphate-activated protein kinase phosphorylation and glucose transporter four in the liver or adipose tissues. Moreover, in clinical application, *Dendrobium* combined with other herbs, such as *Astragalus* spp. and *Schisandra* Michx., was applied for the therapy of diabetes (Cakova et al., 2020).

Neuro-Protective Activity

It was reported that *Dendrobium* alkaloids exerted beneficial effects on neuronal systems (Wang et al., 2010; Li et al., 2011), among which *Dendrobium nobile* Lindl. was most extensively studied on the treatment of central nervous system disorders. DNLA, containing dendrobine (20), dendrobine-N-oxide (22),

nobilonine (45), dendroxine (24), 6-hydroxy-nobilonine (46), and 3-hydroxy-2-oxodendrobine (also referred as 13-hydroxy-14-oxodendrobine) (26), was known as the active components of *Dendrobium nobile* Lindl. (Wang et al., 2010; Xu et al., 2017; Nie et al., 2018). Investigation on the mechanisms underlying the neuroprotective effects of DNLA revealed that DNLA prominently improved the neurobehavioral performance and prevented LPS-induced elevation in tumor necrosis factor receptor one via inhibition of phosphorylated p38 mitogen-activated protein kinases and the downstream nuclear factor kappa-B signal pathway (Li et al., 2011; Ng et al., 2012). Moreover, DNLA decreased the level of intracellular amyloid β peptide ($A\beta$) by improving impaired autolysosomal proteolysis in amyloid precursor protein/presenilin one mice (Nie et al., 2018), and regulating α - and β -secretase in hippocampal neurons of Sprague-Dawley rats (Huang J. et al., 2019). The reduction of $A\beta$ attenuated $A\beta_{25-35}$ -induced spatial learning and memory impairments by increasing the protein expression of neurotrophic factors, such as brain-derived neurotrophic factor, ciliary neurotrophic factor, and glial cell line-derived neurotrophic factor (Nie et al., 2016; Nie et al., 2018). Furthermore, DNLA lowered the LPS-induced hyperphosphorylation of tau protein and prevented neuronal apoptosis in rat brains (Yang et al., 2014). Given the neuro-protective effect of *Dendrobium* alkaloids, they could be promising therapeutic agents for the treatment of neurodegenerative disorders, such as Alzheimer's disease (Cakova et al., 2020).

Anti-influenza A Virus Activity

Dendrobine (20) displayed antiviral activity against influenza A viruses, including A/FM-1/1/47 (H1N1), A/Puerto Rico/8/34 H274Y (H1N1), and A/Aichi/2/68 (H3N2) in the antiviral assay, plaque assay, time-of-addition assay, and pseudovirus neutralization assay, with IC_{50} values of 3.39 ± 0.32 , 2.16 ± 0.91 , and 5.32 ± 1.68 μ g/ml, respectively. The low IC_{50} values of dendrobine (20) indicated that this compound could be applied as potential promising agents to treat influenza virus infection (Li R. et al., 2017). More importantly, the anti-virus test using dendrobine (20) provided valuable information for the full application of the TCM named “shí hú” (Li R. et al., 2017).

CHEMICAL SYNTHESIS AND BIOSYNTHETIC PATHWAY OF DENDROBINE

Dendrobine (20) is the first identified sesquiterpene alkaloid from *Dendrobium nobile* Lindl., which is recommended as the exclusive chemical marker for the quality control of this species by Chinese Pharmacopoeia (2015 and 2020 edition). The rule suggested that the mass fraction of dendrobine (20) should be greater than 0.4% in the medicinal *Dendrobium nobile* Lindl..

Chemical Synthesis of Dendrobine

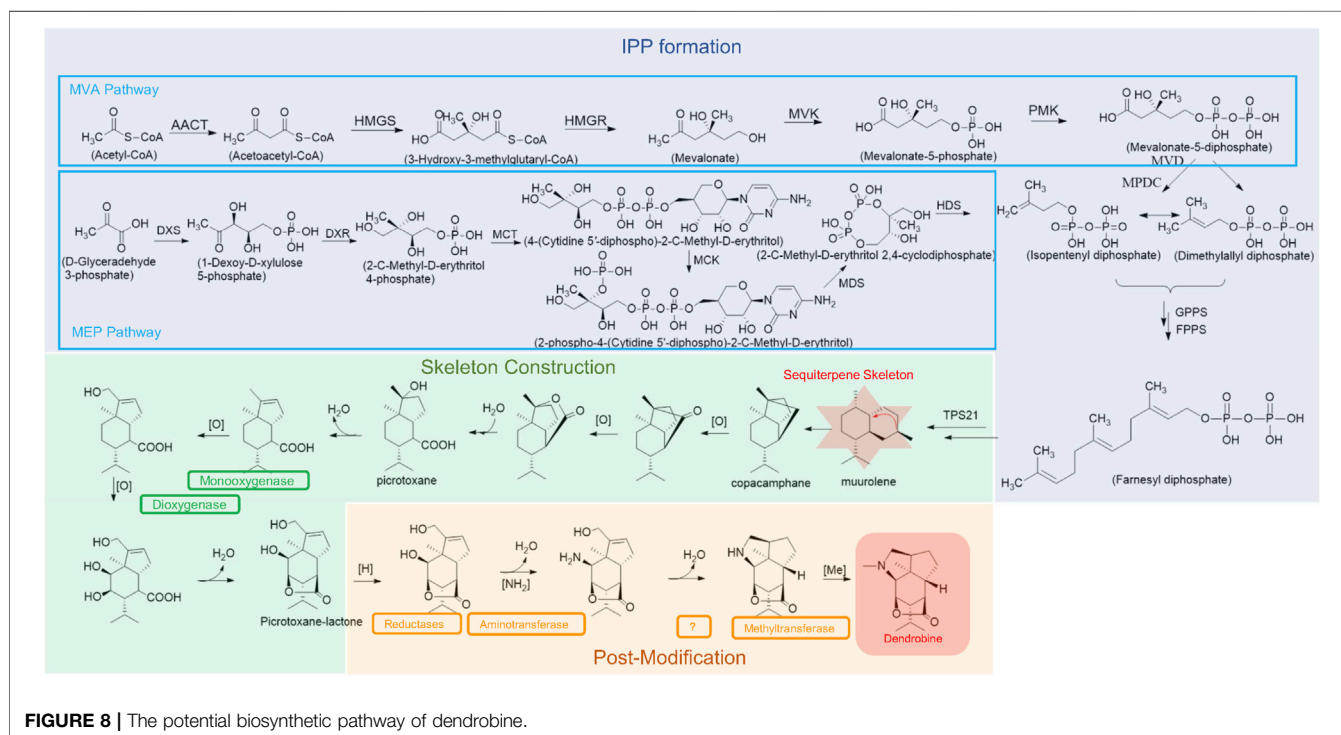
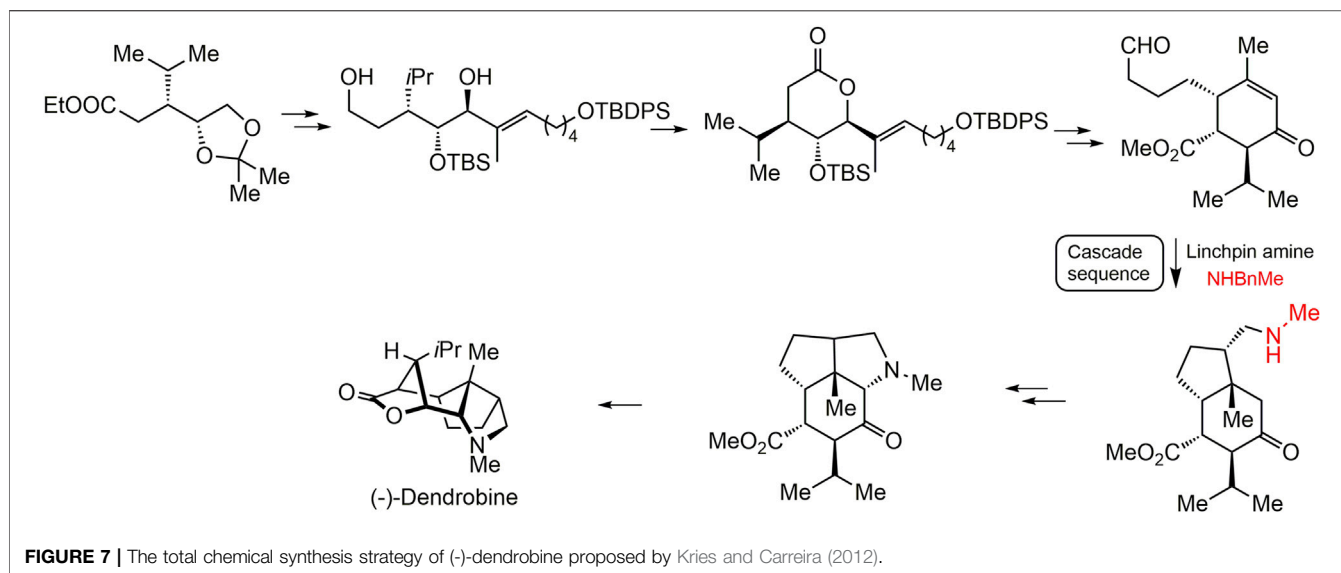
Dendrobine (20) with a complicated tetracyclic ring system and seven contiguous stereocenters displayed remarkable bioactivities. Up to now, several cases are available on the total

chemical synthesis of dendrobine (20). Connolly and Heathcock (1985) first synthesized dendrobine (20) in 1985. Several decades later, Kreis and Carreira (2012) achieved the total chemical synthesis based on 18 cascaded reactions with a key amine group, and the main synthesis pathway is summarized in **Figure 7** (Kreis and Carreira, 2012). Other three dendrobine-alkaloids (–)-dendrobine (20) (–)-mubironine B (27), and (–)-dendroxine (24) were also obtained by total synthesis (Guo et al., 2018). Despite the advances of these total synthesis methods, it remains challenging to overcome the compound yield after a series of reactions (Li Q. et al., 2017).

Biosynthesis of Dendrobine

Dendrobine (20) belongs to the class of terpenoid indole alkaloids (TIAs) (Wang et al., 2020). The biogenetic pathway of TIAs is conservative among alkaloid-producing plants (Li Q. et al., 2017). Based on the results of transcriptome and metabolomic analysis, the putative dendrobine (20) biosynthetic pathway was proposed, and a series of key metabolic genes were labeled in **Figure 8** (Guo et al., 2013; Li Q. et al., 2017; Chen et al., 2019).

Three core stages were involved in the biogenetic pathway, including the formation of isopentenyl diphosphate (IPP), the construction of sesquiterpene skeleton, and the process of post-modification. Firstly, the mevalonate (MVA) and 2-C-methyl-D-erythritol 4-phosphate (MEP) pathways were considered as the upstream of dendrobine (20) biosynthetic pathway, mainly for the synthesis of IPP (Chen et al., 2019). Three key enzyme-coding genes involved in the MVA pathway, *acetyl-CoA C-acetyltransferase* (AAT) gene, *phosphomevalonate kinase* (PMK) gene, and *diphosphomevalonate decarboxylase* (MVD) gene, were observed to be positively associated with dendrobine (20) accumulation in *Dendrobium nobile* Lindl. through large-scale transcriptome sequencing, and then validated through qRT-PCR analysis (Li Q. et al., 2017). In contrast, *hydroxymethylglutaryl-CoA synthase* (HMGS) gene and *3-hydroxy-3-methylglutaryl coenzyme A reductase* (HMGR) gene were found to be less effective in dendrobine (20) biosynthesis in the same species (Li Q. et al., 2017), though HMGS and HMGR both played significant roles in alkaloid biosynthesis in *Dendrobium officinale* Kimura et Migo (Chen et al., 2019). The result shows that HMGS and HMGR may differently contribute to the production of dendrobine (20) in *Dendrobium* spp.. In the MEP pathway, rate-determining genes *1-deoxy-D-xylulose-5-phosphate synthase* (DXS) and *1-deoxy-D-xylulose-5-phosphate reductoisomerase* (DXR) isolated from protocorms of *Dendrobium officinale* Kimura et Migo were largely up-regulated by the methyl jasmonate (MeJA) treatment, suggesting their significant roles in the sesquiterpene biosynthesis based on the analysis of KEGG enrichment and relative expression (Fan et al., 2016; Chen et al., 2019). The crucial impacts of DXS and DXR in *Dendrobium officinale* Kimura et Migo were later confirmed by the high correlations between total alkaloid contents and their transcripts (Chen et al., 2019), furthermore, DXS was a leaf-specific expression gene accounting for high alkaloids content in leaves (Shen et al., 2017).



IPP is an important downstream product of MVA and MEP pathways, which is the precursor for the construction of synthetic terpenes. IPP formed the skeleton of muurolene-type sesquiterpene initially catalyzed by TPS21 enzyme (Li Q. et al., 2017), then this sesquiterpene was further oxidized by monooxygenases and/or dioxygenase to produce picrotoxane-lactone. Cytochromes P450s (CYP450s) is a complex superfamily of monooxygenase, and they are vital for the formation of sesquiterpene alkaloids (dendrobine). At present, some CYP450s have been discovered in a few

Dendrobium species (Coon, 2005; Guo et al., 2013; Li Q. et al., 2017; Yuan et al., 2018; Chen et al., 2019). For instance, 59 full-length CYP450s candidate genes involved in the dendrobine (20) biosynthesis were identified and characterized in *Dendrobium officinale* Kimura et Migo through tissue-specific transcriptomic analysis, phylogenetic analysis, and further gene expression pattern induced by MeJA treatment (Chen et al., 2019). In *Dendrobium huoshanense* Z. Z. Tang et S. J. Cheng, 229 genes were identified as putative CYP450s, 7.8% of which were CYP71 family members

associated with hydroxylation steps of alkaloid biosynthesis (Yuan et al., 2018). However, the family members and expression patterns of CYP450s remain unclear in most *Dendrobium* plants. It is worth mentioning that all other 25 dendrobine-type alkaloids (20–42, 51–52) identified from *Dendrobium* were believed to share similar biosynthesis pathways due to the mutual sesquiterpene backbone of these alkaloids (Guo et al., 2013; Chen et al., 2019).

Following the generation of sesquiterpene skeleton, dendrobine (20) was finally synthesized by the post-modification of picrotoxane-lactone with a series of enzymes, including reductases, aminotransferases, and methyltransferases (Guo et al., 2013; Yuan et al., 2018). In *Dendrobium nobile* Lindl., the expression level of *methyltransferase-like protein 23* (*METTL23*) gene, *histone-lysine N-methyltransferase ATX4* (*ATX4*) gene, and *alanine aminotransferase 2* (*AAT2*) gene were enhanced after inoculation with MF23 (*Mycena* sp.), which was positively related with the content of dendrobine (20), implying their important roles in dendrobine (20) biosynthesis (Li Q. et al., 2017). Transcription factors play vital roles in modulating the expression of dendrobine (20) biosynthesis genes, such as C3H, bHLH, bZIP, MYB, and WRKY in *Dendrobium officinale* Kimura et Migo (Yuan et al., 2018).

Although the common biosynthesis pathway for most TIAs through the construction of strictosidine backbone exists in many plants (Wang et al., 2018), no enzyme involved in strictosidine formation has been verified in dendrobine (20) biosynthesis. However, due to the complex dendrobine (20) metabolism, accurate identification of genetic networks from a large number of candidate genes is needed in the future.

The metabolism of dendrobine (20) was affected by abiotic and biotic stresses. For example, light intensity was reported to influence the content of dendrobine (20) (Li J. L. et al., 2017). MeJA, a signaling molecule in the biosynthesis of alkaloids, could induce the accumulation of *Dendrobium* alkaloids by an active precursor supply (Chen et al., 2019). Besides, symbiosis with mycorrhizal fungus could stimulate the biosynthesis of dendrobine (20) by regulating the expressions of genes

involved in the MVA pathway (Li Q. et al., 2017). Other relevant factors need to be further elucidated.

CONCLUSION

In this paper, we summarized the structural types, pharmacological activities, and mechanisms of *Dendrobium* alkaloids, as well as the suggested biogenetic pathway of dendrobine (20), which is an important type of sesquiterpene alkaloids. Despite the advances of the investigation on alkaloids, more emphasis should be laid on the discovery of more novel skeletons in *Dendrobium* genus based on abundant alkaloid metabolites, and the improvement of isolation methods. Moreover, many current studies on *Dendrobium* were only focused on their crude extracts, or the activity of mixtures, which necessitates the need for figuring out the typical pharmacological activity of pure *Dendrobium* alkaloids. Additionally, further investigation on novel pharmacological activities of these alkaloids should be implemented. Meanwhile, in-depth researches on the biological mechanisms of these activities are also desired. Finally, although the biosynthetic pathway of dendrobine (20) has been proposed, further confirmation is anticipated.

AUTHOR CONTRIBUTIONS

DZ and SC contributed to the conception of the review. YZ and EK helped collect and perform the chemical analysis of compounds. FY helped to analyze the pharmacological activities of alkaloids. ZM and YS contributed to the mechanisms and biosynthetic pathways of alkaloids and wrote the manuscript.

FUNDING

This work was supported financially by the National Natural Science Foundation of China (No. 31960082; No. 81560622).

REFERENCES

- Begum, S. A., Sahai, M., Ray, A. B., Gössinger, E., Luzhetskaya, M., Härle, J., et al. (2010). *Progress in the Chemistry of Organic Natural Products: Picrotoxanes*. Vienna, Austria: Springer.
- Cakova, V., Bonte, F., and Lobstein, A. (2020). *Dendrobium*: Sources of Active Ingredients to Treat Age Related Pathologies. *Aging Dis.* 2, 827–849. 10.14336/AD.2017.0214.
- Chase, M. W., Cameron, K. M., Freudenstein, J. V., Pridgeon, A. M., Salazar, G., Van den Berg, C., et al. (2015). An Updated Classification of Orchidaceae. *Bot. J. Linn. Soc.* 177, 151–174. doi:10.1111/boj.12234
- Chen, H., Li, X., Xu, Y., Lo, K., Zheng, H., Hu, H., et al. (2018). Study on the Polar Extracts of *Dendrobium Nobile*, *D. Officinale*, *D. Loddigesii*, and *Flickingeria Fimbriata*: Metabolite Identification, Content Evaluation, and Bioactivity Assay. *Molecules* 23, 1185. doi:10.3390/molecules23051185
- Chen, K. K., and Chen, A. L. (1935). The Alkaloid of Chin-Shih-Hu. *J. Biol. Chem.* 111, 653–658. doi:10.1016/s0021-9258(18)75010-2
- Chen, Y., Wang, Y., Lyu, P., Chen, L., Shen, C., and Sun, C. (2019). Comparative Transcriptomic Analysis Reveal the Regulation Mechanism Underlying MeJA-Induced Accumulation of Alkaloids in *Dendrobium Officinale*. *J. Plant Res.* 132, 419–429. doi:10.1007/s10265-019-01099-6
- Chiang, J. Y. L. (2013). Bile Acid Metabolism and Signaling. *Compr. Physiol.* 3, 1191–1212. doi:10.1002/cphy.c120023
- Chinese Pharmacopoeia Commission (2020). *Pharmacopoeia of the People's Republic of China*. Beijing, China: China Medical Science Press, 263.
- Connolly, P. J., and Heathcock, C. H. (1985). An Approach to the Total Synthesis of Dendrobine. *J. Org. Chem.* 50, 4135–4144. doi:10.1021/jo00221a033
- Coon, M. J. (2005). Cytochrome P450: Nature's Most Versatile Biological Catalyst. *Annu. Rev. Pharmacol. Toxicol.* 45, 1–25. doi:10.1146/annurev.pharmtox.45.120403.100030
- Ekevag, U., Elander, M., Gawell, L., Leander, K., Lüning, B., and Swahn, C.-G. (1973). Studies on Orchidaceae Alkaloids. XXXIII. Two New Alkaloids, N-Cis- and N-Trans-Cinnamoylnorcuskygrine from *Dendrobium Chrysanthum* Wall. *Acta Chem. Scand.* 27, 1982–1986. doi:10.3891/acta.chem.scand.27-1982
- Elander, M., Leander, K., Klæboe, P., Cyvin, S. J., Lagerlund, I., and Ehrenberg, L. (1971). Studies on Orchidaceae Alkaloids. XXI. 6-hydroxynobiline, a New

- Alkaloid from *Dendrobium Hildebrandii* Rolfe. *Acta Chem. Scand.* 25, 717–720. doi:10.3891/acta.chem.scand.25-0717
- Elander, M., Leander, K., Luning, B., Holme, T., Lindberg, A. A., and Craig, J. C. (1969). Studies on Orchidaceae Alkaloids. XIV. A Phthalide Alkaloid from *Dendrobium Pierardii* Roxb. *Acta Chem. Scand.* 23, 2177–2178. doi:10.3891/acta.chem.scand.23-2177
- Elander, M., Leander, K., Rosenblom, J., Ruusa, E., Luning, B., and Swahn, C. G. (1973). Studies on Orchidaceae Alkaloids. XXXII. Crepidine, Crepidamine and Dendrocrepine, Three Alkaloids from *Dendrobium Crepidatum* Lindl. *Acta Chem. Scand.* 27, 1907–1913. doi:10.3891/acta.chem.scand.27-1907
- Fan, H., Wu, Q., Wang, X., Wu, L., Cai, Y., and Lin, Y. (2016). Molecular Cloning and Expression of 1-Deoxy-D-Xylulose-5-Phosphate Synthase and 1-Deoxy-D-Xylulose-5-Phosphate Reductoisomerase in *Dendrobium Officinale*. *Plant Cell Tiss. Organ. Cult.* 125, 381–385. doi:10.1007/s11240-016-0945-1
- Flora of China (2020). Flora of China. Available at: www.efloras.org (Accessed March 27, 2021).
- Glomqvist, L., Brandänge, S., Gawell, L., Leander, K., and Luning, B. (1973). Studies on Orchidaceae Alkaloids. XXXVII. Dendrowardine, a Quaternary Alkaloid from *Dendrobium Wardianum* Wr. *Acta Chem. Scand.* 27, 1439–1441. doi:10.3891/acta.chem.scand.27-1439
- Graneli, I., Leander, K., Luning, B., Liaaen-Jensen, S., Lamvik, A., Sunde, E., et al. (1970). Studies on Orchidaceae Alkaloids. XVI. A New Alkaloid, 2-Hydroxydendrobine, from *Dendrobium findlayanum* Par. et Rchb. f. *Acta Chem. Scand.* 24, 1209–1212. doi:10.3891/acta.chem.scand.24-1209
- Guha, M., and Mackman, N. (2001). LPS Induction of Gene Expression in Human Monocytes. *Cell Signal.* 13, 85–94. doi:10.1016/s0898-6568(00)00149-2
- Guo, X., Li, Y., Li, C., Luo, H., Wang, L., Qian, J., et al. (2013). Analysis of the *Dendrobium Officinale* Transcriptome Reveals Putative Alkaloid Biosynthetic Genes and Genetic Markers. *Gene* 527, 131–138. doi:10.1016/j.gene.2013.05.073
- Guo, L., Frey, W., and Plietker, B. (2018). Catalytic Enantioselective Total Synthesis of the Picrotoxane Alkaloids (–)-Dendrobine, (–)-Mubironine B, and (–)-Dendroxine. *Org. Lett.* 20, 4328–4331. doi:10.1021/acs.orglett.8b01782
- He, L., Luo, J., Wang, Y. Y., Shi, Y. J., and Ren, J. W. (2017). Fat-soluble Alkaloids Extracted from *Dendrobium Nobile* Lindl Induced Apoptosis of Human Colorectal Cancer HT-29 Cells. *Sci. Tech. Food Ind.* 38, 170–174.
- He, L., Su, Q., Bai, L., Li, M., Liu, J., Liu, X., et al. (2020). Recent Research Progress on Natural Small Molecule Bibenzyls and its Derivatives in *Dendrobium* Species. *Eur. J. Med. Chem.* 204, 112530. doi:10.1016/j.ejmech.2020.112530
- Hedman, K., Leander, K., Liaaen-Jensen, S., Tricker, M. J., and Svensson, S. (1972). Studies on Orchidaceae Alkaloids. XXVII. Quaternary Salts of the Dendrobine Type from *Dendrobium Nobile* Lindl. *Acta Chem. Scand.* 26, 3177–3180. doi:10.3891/acta.chem.scand.26-3177
- Hemscheidt, T., and Spenser, I. D. (1993). Biosynthesis of Anosmine: Incorporation of the Intact Six-Carbon Chain of Lysine and of Picecolic Acid. *J. Nat. Prod.* 56, 1281–1287. doi:10.1021/np50098a012
- Hu, Y., Zhang, C., Zhao, X., Wang, Y., Feng, D., Zhang, M., et al. (2016). (±)-Homocrepidine A, a Pair of Anti-inflammatory Enantiomeric Octahydroindolizine Alkaloid Dimers from *Dendrobium Crepidatum*. *J. Nat. Prod.* 79, 252–256. doi:10.1021/acs.jnatprod.5b00801
- Hu, Y., Ren, J., Wang, L., Zhao, X., Zhang, M., Shimizu, K., et al. (2018). Protective Effects of Total Alkaloids from *Dendrobium Crepidatum* against LPS-Induced Acute Lung Injury in Mice and its Chemical Components. *Phytochemistry* 149, 12–23. doi:10.1016/j.phytochem.2018.02.006
- Hu, Y., Yang, H., Ding, X., Liu, J., Wang, X., Hu, L., et al. (2020). Anti-inflammatory Octahydroindolizine Alkaloid Enantiomers from *Dendrobium Crepidatum*. *Bioorg. Chem.* 100, 103809. doi:10.1016/j.bioorg.2020.103809
- Huang, J., Huang, N., Zhang, M., Nie, J., Xu, Y., Wu, Q., et al. (2019). *Dendrobium* Alkaloids Decrease A β by Regulating α - and β -secretases in Hippocampal Neurons of SD Rats. *PeerJ* 7, e7627. doi:10.7717/peerj.7627
- Huang, S., Wu, Q., Liu, H., Ling, H., He, Y., Wang, C., et al. (2019). Alkaloids of *Dendrobium Nobile* Lindl. Altered Hepatic Lipid Homeostasis Regulation of Bile Acids. *J. Ethnopharmacol.* 241, 111976. doi:10.1016/j.jep.2019.111976
- Inubushi, Y., Ishii, H., Yasui, B., Konita, T., and Harayama, T. (1964). Isolation and Characterization of Alkaloids of the Chinese Drug “Chin-Shih-Hu”. *Chem. Pharm. Bull.* 12, 1175–1180. doi:10.1248/cpb.12.1175
- Inubushi, Y., and Nakano, J. (1965). Structure of Dendrine. *Tetrahedron Lett.* 6, 2723–2728. doi:10.1016/s0040-4039(01)99532-2
- Kreis, L. M., and Carreira, E. M. (2012). Total Synthesis of (–)-Dendrobine. *Angew. Chem. Int. Ed.* 51, 3436–3439. doi:10.1002/anie.201108564
- Lam, Y., Ng, T. B., Yao, R. M., Shi, J., Xu, K., Sze, S. C., et al. (2015). Evaluation of Chemical Constituents and Important Mechanism of Pharmacological Biology in *Dendrobium* Plants. *Evid. Based Complement. Alternat Med.* 2015, 841752. doi:10.1155/2015/841752
- Li, M. F., Hirata, Y., Xu, G. J., Niwa, M., and Wu, H. M. (1991). Studies on the Chemical Constituents of *Dendrobium Loddigesii* Rolfe. *Yao Xue Xue Bao* 26, 307–310.
- Li, Y., Li, F., Gong, Q., Wu, Q., and Shi, J. (2011). Inhibitory effects of *Dendrobium* alkaloids on memory impairment induced by lipopolysaccharide in rats. *Planta Med.* 77, 117–121. doi:10.1055/s-0030-1250235
- Li, J. L., Zhao, Z., Liu, H. C., Luo, C. L., and Wang, H. L. (2017). Influence of Light Intensity and Water Content of Medium on Total Dendrobine of *Dendrobium Nobile* Lindl. *Asian Pac. J. Trop. Med.* 10, 1095–1100. doi:10.1016/j.apjtm.2017.10.015
- Li, Q., Ding, G., Li, B., and Guo, S. X. (2017). Transcriptome Analysis of Genes Involved in Dendrobine Biosynthesis in *Dendrobium Nobile* Lindl. Infected with Mycorrhizal Fungus MF23 (*Mycena* sp.). *Sci. Rep.* 7, 7–16. doi:10.1038/s41598-017-00445-9
- Li, R., Liu, T., Liu, M., Chen, F., Liu, S., and Yang, J. (2017). Anti-influenza A Virus Activity of Dendrobine and its Mechanism of Action. *J. Agric. Food Chem.* 65, 3665–3674. doi:10.1021/acs.jafc.7b00276
- Li, X. W., Huang, M., Lo, K., Chen, W. L., He, Y. Y., Xu, Y., et al. (2019). Anti-diabetic Effect of a Shihunine-Rich Extract of *Dendrobium Loddigesii* on 3T3-L1 Cells and Db/db Mice by Up-Regulating AMPK-GLUT4-Ppara. *Molecules* 24(14):2673. doi:10.3390/molecules24142673
- Liang, X. M., Jin, Y., Wang, Y. P., Jin, G. W., Fu, Q., and Xiao, Y. S. (2009). Qualitative and Quantitative Analysis in Quality Control of Traditional Chinese Medicines. *J. Chromatogr. A* 1216, 2033–2044. doi:10.1016/j.chroma.2008.07.026
- Lin, X., Shi, H., Cui, Y., Wang, X., Zhang, J., Yu, W., et al. (2018). *Dendrobium* Mixture Regulates Hepatic Gluconeogenesis in Diabetic Rats via the Phosphoinositide-3-Kinase/protein Kinase B Signaling Pathway. *Exp. Ther. Med.* 16, 204–212. doi:10.3892/etm.2018.6194
- Liu, G. Y., Tan, L., Cheng, L., Ding, L. S., Zhou, Y., Deng, Y., et al. (2020). Dendrobine-type Alkaloids and Bibenzyl Derivatives from *Dendrobium Findlayanum*. *Fitoterapia* 142, 104497. doi:10.1016/j.fitote.2020.104497
- Liu, Q. F., and Zhao, W. M. (2003). A New Dendrobine-type Alkaloid from *Dendrobium Nobile*. *Chin. Chem. Lett.* 14, 278–279.
- Liu, W. H., Hua, Y. F., and Zhan, Z. J. (2007). Moniline, a New Alkaloid from *Dendrobium Moniliforme*. *J. Chem. Res.* 2007, 317–318. doi:10.3184/030823407X218048
- Luning, B., Leander, K., Gröndahl, N. J., Guthrie, C., and Hinton, M. (1965). Studies on Orchidaceae Alkaloids. III. The Alkaloids in *Dendrobium Primulinum* Lindl. And *Dendrobium Chrysanthum* Wall. *Acta Chem. Scand.* 19, 1607–1611. doi:10.3891/acta.chem.scand.19-1607
- Meng, C. W., He, Y. L., Peng, C., Ding, X. J., Guo, L., and Xiong, L. (2017). Picrotoxane Sesquiterpenoids from the Stems of *Dendrobium Nobile* and Their Absolute Configurations and Angiogenesis Effect. *Fitoterapia* 121, 206–211. doi:10.1016/j.fitote.2017.07.017
- Morita, H., Fujiwara, M., Yoshida, N., and Kobayashi, J. I. (2000). New Picrotoxinin-type and Dendrobine-type Sesquiterpenoids from *Dendrobium Snowflake* ‘Red Star’. *Tetrahedron* 56, 5801–5805. doi:10.1016/s0040-4020(00)00530-5
- Ng, T. B., Liu, J., Wong, J. H., Ye, X., Wing Sze, S. C., Tong, Y., et al. (2012). Review of Research on *Dendrobium*, a Prized Folk Medicine. *Appl. Microbiol. Biotechnol.* 93, 1795–1803. doi:10.1007/s00253-011-3829-7
- Nie, J., Jiang, L., Lu, Y., and Shi, J. (2018). *Dendrobium Nobile* Lindl. Alkaloids Decreases the Level of Intracellular β -amyloid by Improving Impaired Autolysosomal Proteolysis in APP/PS1 Mice. *Front. Pharmacol.* 9, 1479. doi:10.3389/fphar.2018.01479
- Nie, J., Tian, Y., Zhang, Y., Lu, Y. L., Li, L. S., and Shi, J. S. (2016). *Dendrobium* Alkaloids Prevent A β_{25-35} -induced Neuronal and Synaptic Loss via Promoting Neurotrophic Factor Expression in Mice. *PeerJ* 4, e2739. doi:10.7717/peerj.2739
- Okamoto, T., Natsume, M., Onaka, T., Uchimar, F., and Shimizu, M. (1972). Further Studies on the Alkaloidal Constituents of *Dendrobium Nobile*

- (Orchidaceae)-Structure Determination of 4-Hydroxy-Dendroxine and Nobilomethylene. *Chem. Pharm. Bull.* 20, 418–421. doi:10.1248/cpb.20.418
- Okamoto, T., Natsume, M., Onaka, T., Uchimar, F., and Shimizu, M. (1966a). The Structure of Dendramine (6-Oxydendrobine) and 6-Oxydendroxine the Fourth and Fifth Alkaloid from *Dendrobium Nobile*. *Chem. Pharm. Bull.* 14, 676–680. doi:10.1248/cpb.14.676
- Okamoto, T., Natsume, M., Onaka, T., Uchimar, F., and Shimizu, M. (1966b). The Structure of Dendroxine the Third Alkaloid from *Dendrobium Nobile*. *Chem. Pharm. Bull.* 14, 672–675. doi:10.1248/cpb.14.672
- Rinella, M. E. (2015). Nonalcoholic Fatty Liver Disease: a Systematic Review. *Jama* 313, 2263–2273. doi:10.1001/jama.2015.5370
- Shen, C., Guo, H., Chen, H., Shi, Y., Meng, Y., Lu, J., et al. (2017). Identification and Analysis of Genes Associated with the Synthesis of Bioactive Constituents in *Dendrobium Officinale* Using RNA-Seq. *Sci. Rep.* 7, 187. doi:10.1038/s41598-017-00292-8
- Shhosuke, Y., and Yoshimasa, H. (1964). Structures of Nobile and Dendrobine. *Tetrahedron Lett.* 5, 79–87. doi:10.1016/S0040-4039(00)90333-2
- Song, C., Jiao, C., Jin, Q., Chen, C., Cai, Y., and Lin, Y. (2020). Metabolomics Analysis of Nitrogen-Containing Metabolites between Two *Dendrobium* Plants. *Physiol. Mol. Biol. Plants* 26, 1425–1435. doi:10.1007/s12298-020-00822-1
- Song, T. H., Chen, X. X., Lee, C. K. F., Sze, S. C. W., Feng, Y. B., Yang, Z. J., et al. (2019). Dendrobine Targeting JNK Stress Signaling to Sensitize Chemotoxicity of Cisplatin against Non-small Cell Lung Cancer Cells *In Vitro* and *In Vivo*. *Phytomedicine* 53, 18–27. doi:10.1016/j.phymed.2018.06.018
- Wang, H., Zhao, T., and Che, C. T. (1985). Dendrobine and 3-Hydroxy-2-Oxidendrobine from *Dendrobium Nobile*. *J. Nat. Prod.* 48, 796–801. doi:10.1021/np50041a014
- Wang, J., Ge, Y., Zhou, C., Tong, Y., and Ren, Z. (2014). Study on the Mechanism of Extracts from Fresh *Dendrobium Candidum* against Lewis Lung Cancer. *Chin. J. Mod. Appl. Pharm.* 31, 953–957.
- Wang, P., Chen, X., Wang, H., Huang, S., Cai, C., Yuan, J., et al. (2019). Four New Picrotoxane-type Sesquiterpenes from *Dendrobium Nobile* Lindl. *Front. Chem.* 7, 812. doi:10.3389/fchem.2019.00812
- Wang, Q., Gong, Q., Wu, Q., and Shi, J. (2010). Neuroprotective Effects of *Dendrobium* Alkaloids on Rat Cortical Neurons Injured by Oxygen-Glucose Deprivation and Reperfusion. *Phytomedicine* 17, 108–115. doi:10.1016/j.phymed.2009.05.010
- Wang, Q., Liang, J., Brennan, C., Ma, L., Li, Y., Lin, X., et al. (2019). Anti-inflammatory Effect of Alkaloids Extracted from *Dendrobium Aphyllum* on Macrophage RAW 264.7 Cells through NO Production and Reduced IL-1, IL-6, TNF- α and PGE2 Expression. *Int. J. Food Sci. Technol.* 55, 1255–1264. doi:10.1111/ijfs.14404
- Wang, Z., Zhao, M., Cui, H., Li, J., and Wang, M. (2020). Transcriptomic Landscape of Medicinal *Dendrobium* Reveals Genes Associated with the Biosynthesis of Bioactive Components. *Front. Plant Sci.* 11, 391. doi:10.3389/fpls.2020.00391
- Xu, J., Han, Q. B., Li, S. L., Chen, X. J., Wang, X. N., Zhao, Z. Z., et al. (2013). Chemistry, Bioactivity and Quality Control of *Dendrobium*, a Commonly Used Tonic Herb in Traditional Chinese Medicine. *Phytochem. Rev.* 12, 341–367. doi:10.1007/s11101-013-9310-8
- Xu, X., Li, Z., Yang, R., and Zhou, H. (2020). Crepidatamines A and B, Two New Indolizidine Alkaloids from *Dendrobium Crepidatum* Lindl. *ex Paxt. Sci. Rep.* 24, 3071. doi:10.3390/molecules24173071
- Xu, X., Li, Z., Yang, R., Zhou, H., and Li, B. (2019). Crepidatamines C and D, Two New Indolizidine Alkaloids from *Dendrobium Crepidatum* Lindl. *ex Paxt. Molecules* 24, 3071. doi:10.3390/molecules24173071
- Xu, Y. Y., Xu, Y. S., Wang, Y., Wu, Q., Lu, Y. F., Liu, J., et al. (2017). *Dendrobium Nobile* Lindl. Alkaloids Regulate Metabolism Gene Expression in Livers of Mice. *J. Pharm. Pharmacol.* 69, 1409–1417. doi:10.1111/jphp.12778
- Yang, D., Cheng, Z. Q., Hou, B., Yang, L., Zi, C. T., Dong, F. W., et al. (2020). Two Unusual Dendrobine-type Alkaloids from *Dendrobium Findlayanum*. *Fitoterapia* 144, 104607. doi:10.1016/j.fitote.2020.104607
- Yang, D., Cheng, Z. Q., Yang, L., Hou, B., Yang, J., Li, X. N., et al. (2018). Secodendrobine-type Alkaloids and Bioactive Phenolics from *Dendrobium Findlayanum*. *J. Nat. Prod.* 81, 227–235. doi:10.1021/acs.jnatprod.7b00150
- Yang, L., Wang, Z., and Xu, L. (2006). Simultaneous Determination of Phenols (Bibenzyl, Phenanthrene, and Fluorenone) in *Dendrobium* Species by High-Performance Liquid Chromatography with Diode Array Detection. *J. Chromatogr. A* 1104, 230–237. doi:10.1016/j.chroma.2005.12.012
- Yang, L., Zhang, C., Yang, H., Zhang, M., Wang, Z., and Xu, L. (2005). Two New Alkaloids from *Dendrobium Chrysanthum*. *Heterocycles* 65, 633–636. 10.3987/COM-04-10251.
- Yang, S., Gong, Q., Wu, Q., Li, F., Lu, Y., and Shi, J. (2014). Alkaloids Enriched Extract from *Dendrobium Nobile* Lindl. Attenuates Tau Protein Hyperphosphorylation and Apoptosis Induced by Lipopolysaccharide in Rat Brain. *Phytomedicine* 21, 712–716. doi:10.1016/j.phymed.2013.10.026
- Yuan, Y., Yu, M., Jia, Z., Song, X., Liang, Y., and Zhang, J. (2018). Analysis of *Dendrobium Huoshanense* Transcriptome Unveils Putative Genes Associated with Active Ingredients Synthesis. *BMC Genomics* 19, 978. doi:10.1186/s12864-018-5305-6
- Zhang, A. L., Yu, M., Xu, H. H., and Si, J. P. (2013). Constituents of *Dendrobium Devonianum* and Their Antioxidant Activity. *Zhongguo Zhong Yao Za Zhi* 38, 844–847.
- Zhang, C., Liu, S. J., Yang, L., Yuan, M. Y., Li, J. Y., Hou, B., et al. (2017). Sesquiterpene Amino Ether and Cytotoxic Phenols from *Dendrobium Wardianum* Warner. *Fitoterapia* 122, 76–79. doi:10.1016/j.fitote.2017.08.015
- Zhou, J., Zhang, Y., Li, S., Zhou, Q., Lu, F., Shi, J., et al. (2020). *Dendrobium Nobile* Lindl. Alkaloids-Mediated Protection against CCl₄-Induced Liver Mitochondrial Oxidative Damage Is Dependent on the Activation of Nrf2 Signaling Pathway. *Biomed. Pharmacother.* 129, 100351. doi:10.1016/j.biopha.2020.110351
- Zhu, G., J. Z., Wood, J., and Wood, H. (2009). *Flora of China*. Beijing, China: Science Press, 367–397.

Conflict of Interest: The authors declare that the research was conducted in the absence of any commercial or financial relationships that could be construed as a potential conflict of interest.

Copyright © 2021 Mou, Zhao, Ye, Shi, Kennelly, Chen and Zhao. This is an open-access article distributed under the terms of the Creative Commons Attribution License (CC BY). The use, distribution or reproduction in other forums is permitted, provided the original author(s) and the copyright owner(s) are credited and that the original publication in this journal is cited, in accordance with accepted academic practice. No use, distribution or reproduction is permitted which does not comply with these terms.



Andrographolide Against Lung Cancer-New Pharmacological Insights Based on High-Throughput Metabolomics Analysis Combined with Network Pharmacology

Wen Luo^{1,2†}, Li Jia^{2†}, Jia-Wen Zhang², Dong-Jie Wang², Qiu Ren³ and Wei Zhang^{2*}

¹Respiratory Department, National Clinical Research Center for Infectious Disease, Shenzhen Third People's Hospital, The Second Affiliated Hospital, School of Medicine, Southern University of Science and Technology, Shenzhen, China, ²Department of Respiratory and Critical Care, First Affiliated Hospital, Harbin Medical University, Harbin, China, ³Department of Respiratory Medicine, Heilongjiang Provincial Hospital, Harbin, China

OPEN ACCESS

Edited by:

Michael Heinrich,
UCL School of Pharmacy,
United Kingdom

Reviewed by:

Chun Yang,
Nanjing Medical University, China
Lei Chen,
Fujian Agriculture and Forestry
University, China

*Correspondence:

Wei Zhang
weipozams@163.com

[†]These authors have contributed
equally to this work

Specialty section:

This article was submitted to
Ethnopharmacology,
a section of the journal
Frontiers in Pharmacology

Received: 20 August 2020

Accepted: 29 March 2021

Published: 21 April 2021

Citation:

Luo W, Jia L, Zhang J-W, Wang D-J,
Ren Q and Zhang W (2021)
Andrographolide Against Lung
Cancer-New Pharmacological Insights
Based on High-Throughput
Metabolomics Analysis Combined with
Network Pharmacology.
Front. Pharmacol. 12:596652.
doi: 10.3389/fphar.2021.596652

Andrographolide (Andro) has known to treat various illnesses such as colds, diarrhea, fever and infectious diseases. However, the effect mechanism of Andro is still unclear. Therefore, we used high-throughput metabolomics analysis to discover biomarkers, metabolic profiles and pathways to reveal the pharmacological action and effective mechanism of Andro against lung cancer. The metabolic effects of Andro on lung cancer animal was explored by ultra-performance liquid chromatography-triple-time of flight/mass spectrometry (UPLC-TOF/MS) analysis. Our results showed that Andro exhibited significant protective effects against lung cancer. Compared with control group, a total of 25 metabolites biomarkers was identified in urine of model animals, which 18 of them were regulated toward the normal direction after Andro treatment, and network pharmacology analysis showed that they were related with 570 proteins. Biological pathways analysis showed that the 11 metabolism pathways were regulated by Andro treatment in lung cancer mouse, and amino acid metabolism and arachidonic acid metabolism have great potential as target pathways for Andro against lung cancer. It revealed that high-throughput metabolomics combined with network pharmacology analysis provides deeply insight into the therapeutic mechanisms of natural product for promoting medicine development and disease treatment.

Keywords: target, metabolic pathway, urine biomarker, untargeted metabolomics, lung cancer, liquid chromatography

INTRODUCTION

Lung cancer accounting for 20% of all cancer death has been the major murderer for many years, which mostly because it is asymptomatic in primary stage and typically perceived at advanced stages (de Groot et al., 2018; Barta et al., 2019; Kim et al., 2020). The risk factors of lung cancer were related with cigarette smoking, E-cigarettes, biomass fuels, chronic obstructive pulmonary disease, occupational exposures, ambient air pollution, diet and nutrition as well as genetic factors (Trédaniel et al., 1994; Malhotra et al., 2016; Woodard et al., 2016; Sheng et al., 2018). Low-dose chest tomography chest X-rays and sputum cytology screening have been made in clinical

practice for early diagnosis, which possesses high rates of positive findings and is appropriate for diagnosis of lung cancers with low threats (Woznitza et al., 2017; New and Keith, 2018). Currently, there are three main treatment methods for lung cancer, which are chemotherapy, radiation therapy and surgery (Wibowo et al., 2016; Azar et al., 2017; Saad and Mathew, 2020). However, chemotherapy brings out adverse effects to a certain extent resulting from a long period management (Gridelli et al., 2011). Radiation therapy is only suitable for patients with small cell lung cancer, and it must be combined with some painkillers during the process of treatment (Forde et al., 2014; Postow et al., 2015; Verma and Simone, 2019). There is an imperative demand to find an emerging method with low side effects and intense activity for lung cancer treatment.

Andrographis paniculata (Burm. f.) Nees is a well-known medicinal plant in Southeastern Asian countries, has been widely applied as immunostimulant and anti-inflammatory drugs in clinic practice for many years (Puri et al., 1993). Andrographolide (Andro) is known to possess ability to treat the common cold, myocardial ischemia, respiratory tract infections, diarrhea, inflammation and infectious diseases (Zhu H. L. et al., 2011; Hossain et al., 2014; Wintachai et al., 2015; Ding et al., 2017). Some studies reported that it protected against acute lung injury exerted by reducing expression of myeloperoxidase and neutrophil-derived proteases, increasing in adhesion molecules (Zhu et al., 2013; Yang et al., 2014; Peng et al., 2016a; Gao et al., 2018). It also increases Nrf2 activity to protect against cigarette smoke-induced oxidative lung injury (Guan et al., 2013; Peng et al., 2016b). Andro ameliorates lung inflammation and fibrosis by inhibition of AIM2 inflammasome-mediated pyroptosis, activation of heme oxygenase-1 (Zhu Z. T. et al., 2011; Yang et al., 2013; Gao et al., 2019). The antimicrobial mechanism of Andro is related with up-regulation of human β -defensin-2 in human lung epithelial cells (Shao et al., 2012; Tan et al., 2016). It can down-regulate PI3K/Akt signaling pathway in lung cancer cells during in the process of proliferation, migration and invasion (Lee et al., 2010; Lin et al., 2011; Luo et al., 2013; Luo et al., 2014; Lim et al., 2015). Cisplatin-mediated anticancer effects was enhanced by Andro through blockade of autophagy and activation of the Akt/mTOR pathway (Mi et al., 2016; Yuwen et al., 2017).

Metabolomics method can be used to discover the biomarker and pathways related to disease processes and elucidate the mechanism of drugs (Johnson et al., 2016; Zhang et al., 2014; Zhang A. et al., 2017; Qiu et al., 2020). The untargeted metabolomics has ability to undertake simultaneous assessment of metabolites without any sample knowledge for hypothesis generation (Liang et al., 2014; Wang et al., 2014; Wu and Feng, 2016; Varma et al., 2018; Zhang et al., 2019a; Xie et al., 2019). The major disadvantage of untargeted metabolomics is that sample analysis generate lots of data leading to the majority of biological features are unidentifiable (Ribbenstedt et al., 2018; Zhang Y. et al., 2017; Ren, et al., 2018). At present, the combined analytical platform includes the ultra-performance liquid chromatography (UPLC) or gas chromatography in tandem with mass spectrometry (MS) and nuclear magnetic resonance spectroscopy (NMR) (French et al., 2018; Sun et al., 2018; Zhang

et al., 2018; Zhang et al., 2019b). These techniques allow for characteristic fingerprints of objects, predictive algorithms with pattern recognition statistical approaches to explain biological effect (Xia et al., 2013; Liang et al., 2015; Zhang et al., 2020). In this work, the untargeted metabolomics strategy based on UPLC-TOF/MS was used to explore the potential biomarkers and related metabolic pathways and to reveal the anticancer effect of Andro.

EXPERIMENTAL

Animals and Feeding

Animal care and experimental procedures were performed in accordance with the criteria outlined in the "Guide for the Care and Use of Laboratory Animals" prepared by the National Academy of Sciences. A total of forty-seven male C57BL/6 mice (6–8 weeks old, 20 ± 2 g weight) in SPF grade were purchased from Envigo Laboratory Animal Co., Ltd (Suzhou, China, catalog no. SCXK 2019-0002), which were bred and maintained in pathogen-free cages with 12 h light/dark cycles from 9:00–21:00, temperatures of $24^{\circ}\text{C} \pm 2^{\circ}\text{C}$, humidity of $50 \pm 5\%$, and food and water ad libitum.

Reagents

Pentobarbital sodium, sodium chloride solution and neutral buffered formalin were purchased from Xinxiang Sanwei Disinfectant Co., Ltd. (Tianjin, China). Andro (97.5% purity) was provided by Northern Biotechnology Research Institute (Beijing, China) and its chromatographic fingerprint of HPLC is shown in **Supplementary Figure S1**. Cisplatin was purchased from APiChem Technology (Hangzhou, China) and used as the positive drug. Interleukin-6 (IL-6), interleukin-2 (IL-2) and interleukin-10 (IL-10) were purchased from Toronto Research Chemicals (Toronto, Canada). Interleukin-1 beta (IL-1 β) was obtained from Origene Technologies, Inc (Beijing, China). Tumor necrosis factor- α (TNF- α) and nuclear transcription factor- κ B (NF- κ B) were bought from Biotechnology Bioengineering Co., Ltd. (Shanghai, China). Immunoglobulin G (IgG), immunoglobulin A (IgA) and immunoglobulin M (IgM) were purchased from Bioworld Technology, Inc (St Louis Park, MN, United States). Vascular endothelial growth factor (VEGF) was purchased from Jackson ImmunoResearch (West Grove, PA, United States). Hypoxia-inducible transcription factor-1 α (HIF-1 α) and matrix metallo proteinase-2 (MMP-2) were purchased from BIOSS (Beijing, China). Interferon- γ (TFN- γ), transforming growth factor- β (TGF- β), toll like receptor 4 (TLR4) and myeloid differentiation factor 88 (MYD88) were provided from Bioswarm Biotechnology Co., Ltd. (Hangzhou, China). Methanol, acetonitrile and formic acid were of chromatographic grade and purchased from Fisher Chemical Company (Geel, Belgium). Pure water was brought from the A.S. Watson Group Ltd. (Hong Kong, China). Chromatographic grade leucine enkephalin were purchased from Invitrogen Life Technologies (Carlsbad, CA, United States).

Instrument

High-performance ultra-performance liquid chromatography-Triple-time of flight/mass spectrometry (UPLC-Triple-TOF/MS)

system used in this research consisted of a ACQUITY H-CLASS UPLC (Waters Corp., Milford, MA, USA) and a Triple TOF™ 5,600 + Mass Spectrometer detector equipped with positive and negative modes of electrospray source (AB SCIEX, Foster City, CA, United States). H3018DR cryogenic high-speed centrifuge (Sigma Laborzentrifugen GmbH, Osterode am Harz, Germany); Normal-temperature centrifuge (Scientific Industries Inc., Bohemia, NY, United States)); WH-861 Vortex Shaker (Tanon Science and Technology Co. Ltd. China); CS-6400 automatic biochemical analyzer (Vital Scientific, Eppendorf, Germany)); BCD-206TAS Low-temperature refrigerator (Haier Company, China); AE240 mettler electronic balance (Mettler Toledo, Columbus, Ohio, United States).

Grouping, Model establishment and Administration

After seven days of adaptive feeding, C57BL/6 mice were divided into four groups in the light of the principle of weight uniformity: normal control group (NC, $n = 10$), lung cancer model group (LC, $n = 13$), cisplatin-treated group (LC + Cis, $n = 12$) and Andro-treated group (LC + Andro, $n = 12$). Lewis lung carcinoma cells were obtained from the Cancer Center of West China Medical University (Sichuan, China), then were cultured and generated in Dulbecco's modified Eagle's medium (Thermo Fisher Scientific, Inc., Waltham, MA, United States) containing 10% fetal bovine serum (Thermo Fisher Scientific, Inc.). Under 37°C and 5% CO₂ saturated humidity, the medium was changed every other day. Cells were every digested by trypsin, and the logarithmic phase cells were collected for experiment. A single dose 1×10^7 /ml Lewis lung cancer cells 0.2 ml were inoculated subcutaneously into the light axillary of C57BL mice. Tumors with a diameter of approximately 1–1.5 cm were formed in the right armpit of the modeled mice (10 days following injection), which the mice were considered as successfully established in xenografts manner (Li et al., 2016; Zhang Y. et al., 2019; Zhao et al., 2019). From the first day of modeling, mouse in NC and LC group were received dosage of 0.2 ml/10 g physiological saline via intragastric administration, mouse in LC + Cis group and LC + Andro group were respectively received dosage of 4.0 mg/kg/day cisplatin and 10.0 µMol/molar/kg/day Andro in intragastric administration way for twenty-eight days.

Sample Collection and Preparation

Urine Sample

After the final time of Andro administration, each mice in NC, LC, LC + Cis and LC + Andro group was individually fed in metabolic cages to gather urine for 24 h. The urine samples were centrifuged at 10,000 g for 15 min at 4°C, and then the supernatant liquid were delivered into a new eppendorf tube stored in –80°C refrigerator until metabolomics study. Prior to analysis, urine samples were thawed at 4°C until no ice was visible in the sample. Subsequently, 100 µL of aliquots of the urine samples were added 400 µL methanol in order to precipitate the proteins. The solution mixture was vibrated for 60 s and centrifuged at 12,000 g for 15 min, which gained supernatant was evaporated to dryness at 60°C under a stream of nitrogen. The

residue was dissolved again in 150 µL of methanol followed by vibrated for 30 s and centrifuging at 12,000 rpm for 10 min. 10 µL clear supernatant from each mice were mixed into a new eppendorf tube as quality control (QC) sample and the remained samples were passed through a 0.22 µm PTFE filter for UPLC-Triple-TOF/MS analysis.

Serum Sample

At 24 h after the final time of Andro treatment, mouse in NC, LC, LC + Cis and LC + Andro group were mildly anesthetized with sodium pentobarbital (50 mg/kg, i.p.). The blood samples of the animals were respectively collected from the abdominal aorta by a syringe, which were placed 10 min for coagulation and centrifuged at 3500 g for 15 min at 4°C. The obtained supernatant serum was delivered into a clean plastic tube and stored under –80°C until blood biochemical analysis.

Tumors Tissue Sample

Mice in each group were sacrificed by cervical spine removal, and the axillary subcutaneous tumor tissue was quickly and completely peeled off on ice. After weighting, the tumor samples were placed in liquid nitrogen and stored in a refrigerator at –80°C for tissue biochemical analysis.

Biochemical Indexes Detection

Prior to analysis, serum and tumor samples were thawed at 4°C until no ice was visible in the sample. According to the manufacturer's instructions, serum biochemical parameters level of IL-6, IL-1β, TNF-α, VEGF, HIF-1α, MMP-2, IgG, IgA, IgM, IL-2 and TFN-γ were evaluated using ELISA kits. Tumor tissue samples were homogenized and dissolved by corresponding solution based on the manufacturer's instructions of kits, then the IL-10, TGF-β, TLR4, MYD88 and NF-κB level were measured by automatic biochemical analyzer.

Metabolomics Analyses

Chromatography and Mass Spectrometry Conditions

All urine samples were analyzed using the UPLC-Triple-TOF/MS system following the manufacturer's instructions. An Acquity UPLC HSS C18 column (1.7 µm, 2.1 × 100 mm²) from Waters Corporation (Massachusetts, United States) was used for chromatographic separation. The column oven was kept at 33°C, and the temperature of the sample manager was maintained at 15°C. The flow rate was set 0.3 ml/min and the injection volume was 3 µL. 10 and 90% acetonitrile aqueous solutions were applied as weak and strong wash solvents respectively in the analyzed process. The mobile phase consisted of A (0.1% formic acid–water) and B (0.1% formic acid–acetonitrile). UPLC elution conditions were run as following: 0–1.5 min, 8% B; 1.5–4 min, 8–35% B; 4–8 min, 35–70% B; 8–9 min, 70–90% B; 9–11 min 90–8% B; 11–13 min 8% B. QC samples were sampled six times before analysis, and then was injected once every eight experimental samples. Using the Triple-TOF/MS model, the electrospray ionization (ESI) source was operated in both positive and negative modes. 50 to 1200 Da mass spectrum data were collected in MSE centroid mode. Accurate mass determination using leucine-enkephalin (m/z 556.2771 in ESI⁺ and 554.2615 in ESI[–]) was considered as external reference for Lock Spray™ injected at a

flow of 10 $\mu\text{L}/\text{min}$ in order to ensure the mass reproducibility and accuracy. The optimized MS parameters in the positive-ion detection mode are as follows: source temperature, 140°C; desolvation temperature, 460°C; desolvation gas flow 800 L/h; capillary voltage, 2.6 kV; cone voltage, 45 V; cone gas flow, 55 L/h; collision energy, 15–55 eV. The negative ion mode parameters was the same as the positive-ion detection mode, except for being negative in the capillary voltage 2.0 kV and cone gas flow 45 L/h. In addition, the air curtain gas was set 40 psi; 55 psi of atomizing gas and 55 psi of auxiliary atomizing gas.

Metabolome Data Interpretation

MarkerLynx XS Version 4.1 software (Waters Co., Milford, MA, United States) was used to command the instrument system, perform the sample list and obtain raw data in m/zXML format, and then XCMS (www.bioconductor.org/) was applied to extract the peak data, peak matching, peak alignment, and export before multivariate statistical analysis of variables. Three-dimensional data matrix including sample identity (ID), molecular mass (MS), peak area, and standardized ion strength was saved after data preprocessing by unit variance scaling and the mean-centered method. The exported data were imported to SIMCA-P software (Version 14.1, Umetrics, Umea, Sweden) for multivariate analysis such as principal component analysis (PCA) and orthogonal projections to latent structures discriminant analysis (OPLS-DA). PCA is an unsupervised method of pattern recognition approach that have ability to gain the overview and classification showing maximum variation and pattern recognition between. A score plot of the OPLS-DA model as supervised method was employed to visualize the metabolic difference between two different groups. S-plots generated from the OPLS-DA predictive results probe into the potential biomarkers that made a remarkable contribution to the metabolic distinction, which ion with the variable importance in the projection (VIP) value above 1.0 were considered significant. Meanwhile, data between two different groups were dissected by two-way analysis of variance to test the significance of differences, which significant differences meet p values less than 0.05 in test were considered significant. Afterward, the potential ions were verified by the raw MS data in chromatogram and accurate masses of quasimolecular ions were exported into biochemical databases online including METLIN (<http://metlin.scripps.edu/>), SMPD (<http://www.smpdb.ca/>), HMDB (<http://www.hmdb.ca/>) and KEGG (<http://www.kegg.com/>) (5 ppm as the accepted mass error) to confirm the structure of biomarkers. Next, the biomarkers were further identified by comparing the retention time and the tandem mass spectrometry (MS/MS) fragments of metabolites with those of the chemical standards. Adducts were obtained with the mass tolerance at 10 ppm. MetaboAnalyst 5.0 (<http://www.metaboanalyst.ca/>) was used to seek out vital potential metabolic pathways enrichment and topological analysis and network establishment. The metabolic correlation protein analysis of Andro efficacy was performed by Cytoscape 3.7.1 and Gene Cards (<https://www.genecards.org/>).

Statistical Analysis

During the experiments, all the tests were carried out at least three times using independent samples. All data are presented as mean \pm standard deviation, which statistical analysis was

conducted using SPSS software, version 12.0 software (SPSS, Inc., Chicago, IL, United States). The Student's t -test was applied to compare the difference between two individual groups, then P -values ≤ 0.05 were considered to indicate a statistically significant and P -values ≤ 0.01 were considered to indicate statistical significant. All statistical analyses were conducted on GraphPad Prism 6.05 software.

RESULTS

Effect of Andro on Biochemical Index

The mouse in NC group with smooth and shiny hair present normal feeding, drinking, excretion and weight gain in active state. In LC group, mouse with dirty and messy fur have a decreasing drinking, feeding and increasing excretion, moist cage, and weight reduction. Compared with LC group, the general states of the mouse in LC + Andro and LC + Cis is being made better.

As shown in **Figure 1**, compared with the NC group, the serum content of IL-6, IL-1 β , TNF- α , VEGF, HIF-1 α and MMP-2 from the LC group were increased, and IgG, IgA, IgM, IL-2 and TFN- γ level were decreased. Meanwhile, IL-10, TGF- β , TLR4, MYD88 and NF- κ B in tumor tissue were increased, indicating that the LC model of mouse was successfully developed. After therapeutic period, Andro could remarkably reduce IL-6, IL-1 β , TNF- α , VEGF, MMP-2 level in blood and IL-10, TGF- β , NF- κ B level of tumor tissue with significantly statistical implications ($p < 0.01$). The content of serum MMP-2, tumor tissue TLR4, MYD88 were also reduced by Andro treatment with statistical implications ($p < 0.05$). In addition, the level of IgG, IgA, IgM, IL-2 and TFN- γ in LC + Andro groups was significantly higher than those in the model group. Among them, the blood IgG, IL-2 and TFN- γ possess significantly statistical implications ($p < 0.01$) compared with LC group. Mouse in LC + Cis and LC + Andro group showed similar trends in biochemical indicators, indicating that Andro has a certain therapeutic effect on lung cancer, mainly by blocking the body's inflammatory response, promoting the regulation of the immune system, inhibiting the generation of cardiovascular disease, and preventing the proliferation, differentiation and metastasis of cancer cells.

Metabolic Profiling Analysis

Under the abovementioned condition, urinary sample from different groups could present in excellent peak shape, temperate intensity and clearly separation. In the initial stage, nine chromatographic peak were selected in overlaid chromatograms of the QC, which the relative standard deviation (RSD) of the peak area and retention time are respectively less than 5% indicating that the detection method possesses well repeatability. Due to spectra complication, the discrimination between each group were not clearly highlighted. Multivariate statistical analysis was applied to discern the discrepancy of metabolic components among the four groups. In **Figures 2A,B**, the positive and negative mode plots of urinary samples are shown that four group exhibit the obvious separation and did not exceed the limit indicating metabolic differences among the different four groups is significant and anomalous

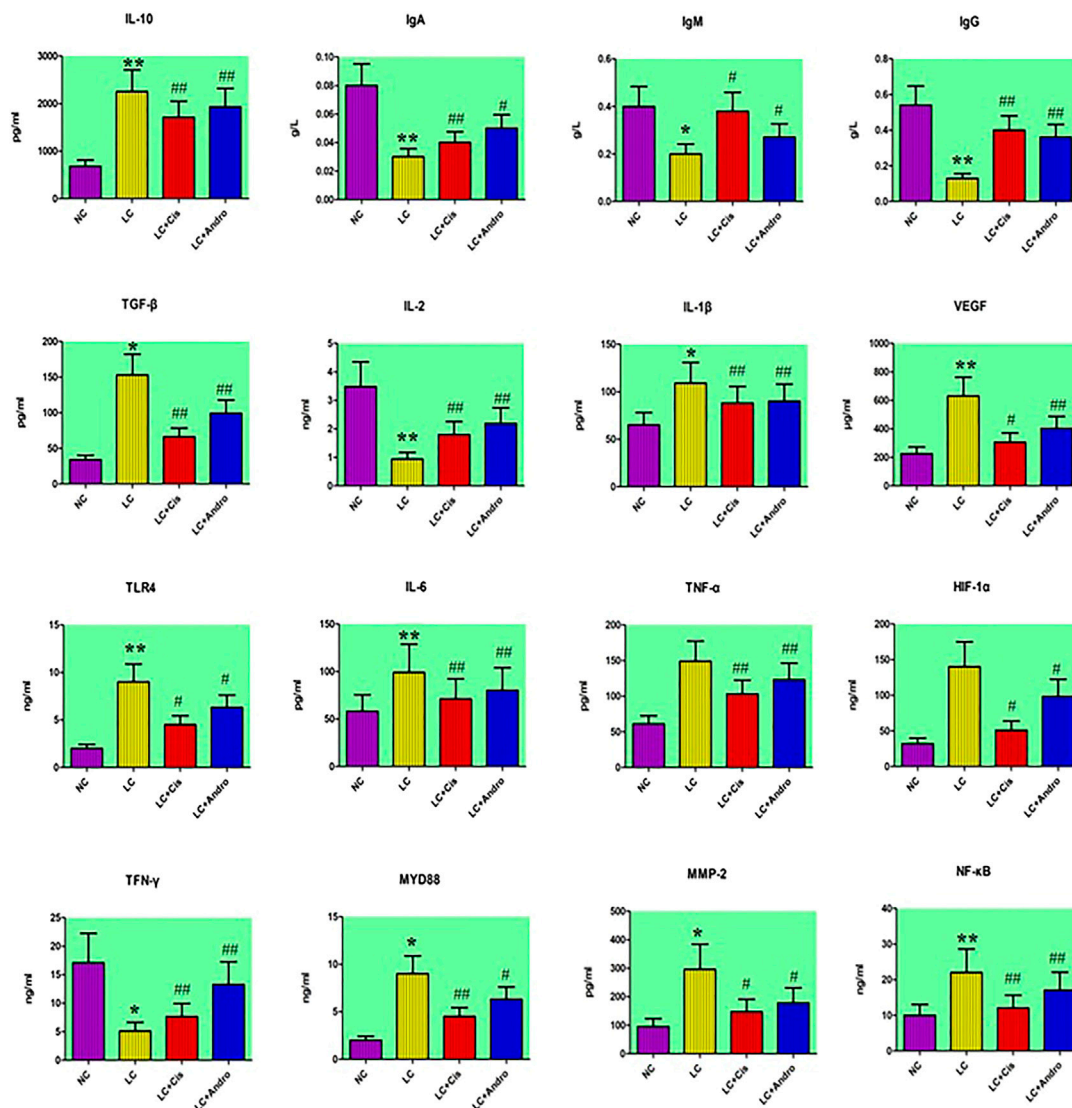


FIGURE 1 | The changes of chemical indexes content in different groups after Andro administration. “*” LC group vs NC group, $p < 0.05$; “***” LC group vs NC group, $p < 0.01$; “#” LC + Cis or LC + Andro group vs LC group, $p < 0.05$; “##” LC + Cis or LC + Andro group vs LC group, $p < 0.01$.

sample was not existed in the clustering of data. The samples from the NC group clustered together and remained relatively far from those from the LC groups. In addition, the clustering of LC + Cis group and LC + Andro group remained relatively far from LC group and close to NC group. Compared with LC + Andro group, the clustering of LC + Cis group is more close to NC group. The results suggested that metabolic state of LC mouse could be regulated by Andro treatment and the further multivariate analysis was necessary to explore potential relationships.

Biomarkers Screening, Discovery and Identification

Firstly, the data of NC and LC group were separately compared in both ion mode as shown in **Figures 3A,B**, which there are evident

separation between the clustering of NC group and LC groups, and the dispersion within the group is relatively clear. Secondly, a cross validation test that was performed the calculation of the R^2 and Q^2 values to evaluate the goodness of fit of the OPLS models, which R^2 close to 1 is the requisite condition for a good model, and Q^2 more than 0.5 represent good predictability of the model. In **Figures 4A,B** goodness of fit test was carried out to assess the predictability of the model indicating that the model have a well goodness. The clustering of LC group can be obviously separated from NC group (R^2Y (cum) = 0.970 and Q^2 (cum) = 0.791 in the ESI+ model, and R^2Y (cum) = 0.982 and Q^2 (cum) = 0.738 in the ESI- model) as shown **Figures 4B,C**. The mass-to-charge ratio with large dispersion in the statistical analysis of the loading plot acts a vital role in the separation between groups, the loading plot generated from OPLS-DA model as shown in **Figures 5A,B** bring

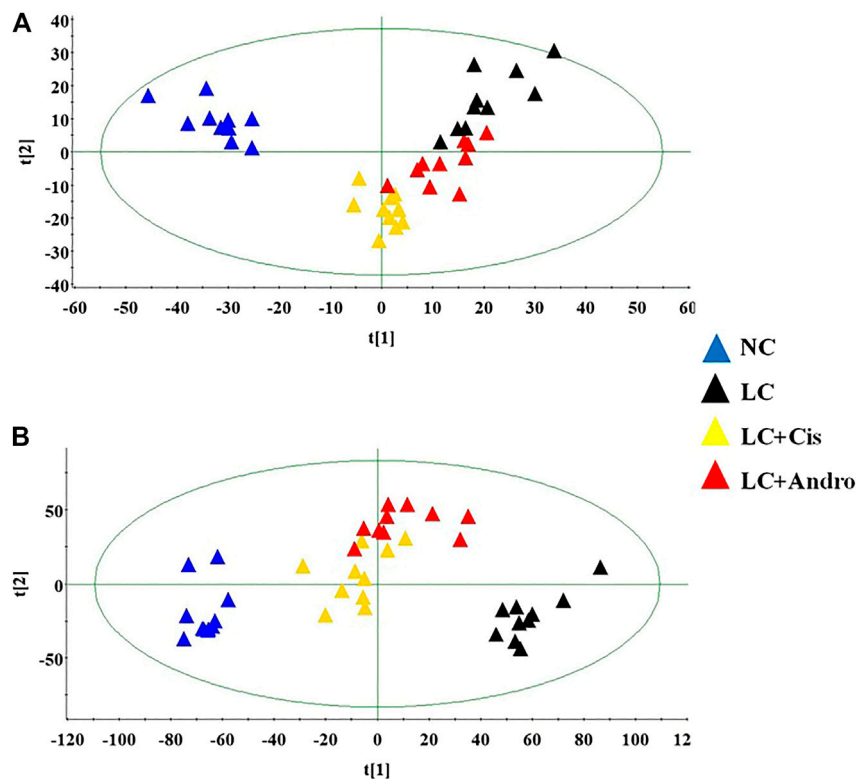


FIGURE 2 | The score plot of the PCA model among NC, LC, LC + Cis and LC + Andro group in positive ion mode (A); The score plot of the PCA model among NC, LC, LC + Cis and LC + Andro group in negative ion mode (B).

out the ions with major differences in abundance between NC group and LC group. From the **Figures 5C,D** of volcano plot, the VIP value was larger, the contribution was greater. Potential metabolite marker selection need to simultaneously satisfy the strength of both contribution and variable reliability from the same OPLS-DA model, which the value of the VIP score is more than 1.0 and *p* value is less than 0.05 in Student's *t*-test.

Combined with the retention time, exact mass-to-charge ratio of the variables and online databases, 25 urine metabolites including valine, inositol phosphate, alanine, thymine, proline, L-glutamine, pyridoxic acid, 3-hydroxybutyric acid, arginine, arachidonic acid, xanthurenic acid, glucose, isoleucine, p-cresol sulfate, kynurenic acid, tyrosine, chenodeoxycholic acid, creatinine, phenylpyruvic acid, coproporphyrin III, 12,13-EpOME, glycyl-threonine, 9 (S)-HPODE, 3-oxohexadecanoic acid, lactic acid were identified as biomarkers associated with the metabolic disturbances in animals with the lung cancer. The basic information such as molecular formula, compound name, corresponding *m/z*, VIP value was listed in **Supplementary Table S1**. Among them, specific content changes of 18 metabolites were determined to be changed trend back to NC group level after treatment with Andro, which eight metabolites including 12,13-EpOME, creatinine, inositol phosphate, lactic acid, thymine, arginine, coproporphyrin III and arachidonic acid were down-regulated in the urine, and ten metabolites including alanine, L-glutamine, isoleucine, 3-hydroxybutyric acid, proline, valine,

tyrosine, xanthurenic acid, kynurenic acid and p-cresol sulfate were up-regulated as shown in heatmap of **Supplementary Figure S2A**. Detailed the comparisons of metabolite relative peak area in NC, LC, LC + Andro and LC + C is group are shown in **Supplementary Figure S2B**, which Andro treatment has a greater influence on the content of isoleucine, 3-hydroxybutyric acid, arginine, coproporphyrin III, alanine, L-glutamine, lactic acid, arachidonic acid with significantly statistical implications (*p* < 0.01).

Metabolic Pathways Regulated by Andro

The changes in the levels of potential biomarkers suggested that the metabolic disturbances in mouse with lung cancer were relieved by Andro referring to phenylalanine, tyrosine and tryptophan biosynthesis, arachidonic acid metabolism, tyrosine metabolism, arginine and proline metabolism, alanine, aspartate and glutamate metabolism, porphyrin and chlorophyll metabolism, pyruvate metabolism, arginine biosynthesis, pyrimidine metabolism, phosphatidylinositol signaling system and inositol phosphate metabolism after Pareto method to standardize the data. As shown in **Figure 6A**, the impacts on the pathways phenylalanine, tyrosine and tryptophan biosynthesis and arachidonic acid metabolism were stronger, where the metabolic pathway with the influence value greater than or equal to 0.30 can be selected as the potential key metabolic pathway of drugs. From KEGG global metabolic network of

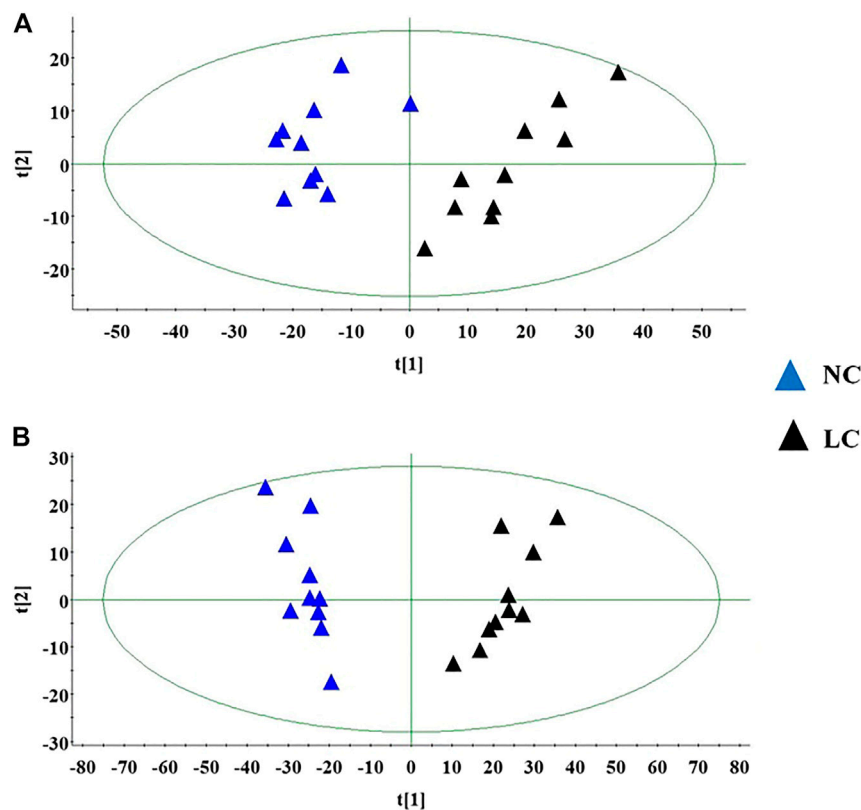


FIGURE 3 | The score plot of the PCA model between NC and LC group in positive ion mode (A); The score plot of the PCA model between NC and LC group in negative mode (B).

Figure 6B, potential metabolites regulated after Andro administration were closed with valine, leucine and isoleucine biosynthesis, alanine, aspartate and glutamate metabolism, phenylalanine, tyrosine and tryptophan biosynthesis, etc.

The Target Prediction

A total of 570 proteins were predicted and closely related with metabolites regulated by Andro, which mainly involves amino acid metabolism and arachidonic acid metabolism. ASS1, TAT, ALDH4A1, PTPN11 and JAK2 in **Figure 7** has higher correlation degree considered as potentially important markers for further study.

DISCUSSION

In this study, the biochemical analysis and pathological studies have shown that Andro treatment can enhance the immune system function of lung cancer model animals, inhibit inflammation reaction, tumor cell growth and metastasis. TNF- α is an inflammatory factor with multiple types of biological effects, which is secreted by activated macrophages, monocytes and T cells to mediate the process of inflammation and directly participate in the process of lung tissue injury and apoptosis (Inui et al., 2018). IL-6 secreted by monocytes and

macrophages is an inflammatory mediator involved in the immune regulation of infection and tumors (Zhao et al., 2018). IgM with a large molecular weight cannot pass through blood vessel walls, and can be used for early diagnosis of body infections (Macpherson et al., 2008; Liu and May 2016; Hansen et al., 2019; Zhou et al., 2019). TLR4 is a member of the Toll-like receptor superfamily that plays a biological role in the form of binding to ligands (Zhang J. et al., 2019). Tumor cells can release a large number of cytokines in the process of immune remodeling, such as IL-10 and TGF- β , the latter can weaken the killing activity of cytotoxic T lymphocytes and natural killer cells, evading immune surveillance and promote tumor metastasis (Solinas et al., 2010; Wei et al., 2010; Bellomo et al., 2016; Anguiano-Hernandez et al., 2019; Dong et al., 2019).

A flow chart for the experiments was shown in **Figure 8**. According to urine metabolomics analysis, Andro can regulate 18 of 25 biomarkers associated with the pathogenesis of lung cancer, including alanine, L-glutamine, isoleucine, 3-hydroxybutyric acid, 12,13-EpOME, arginine, proline, valine, tyrosine, creatinine, inositol phosphate, lactic acid, thymine, xanthurenic acid, kynurenic acid, p-cresol sulfate, coproporphyrin III, arachidonic acid, which is mainly related to phenylalanine, tyrosine and tryptophan biosynthesis, arachidonic acid metabolism, arachidonic acid metabolism, arginine and proline metabolism, alanine, aspartate and

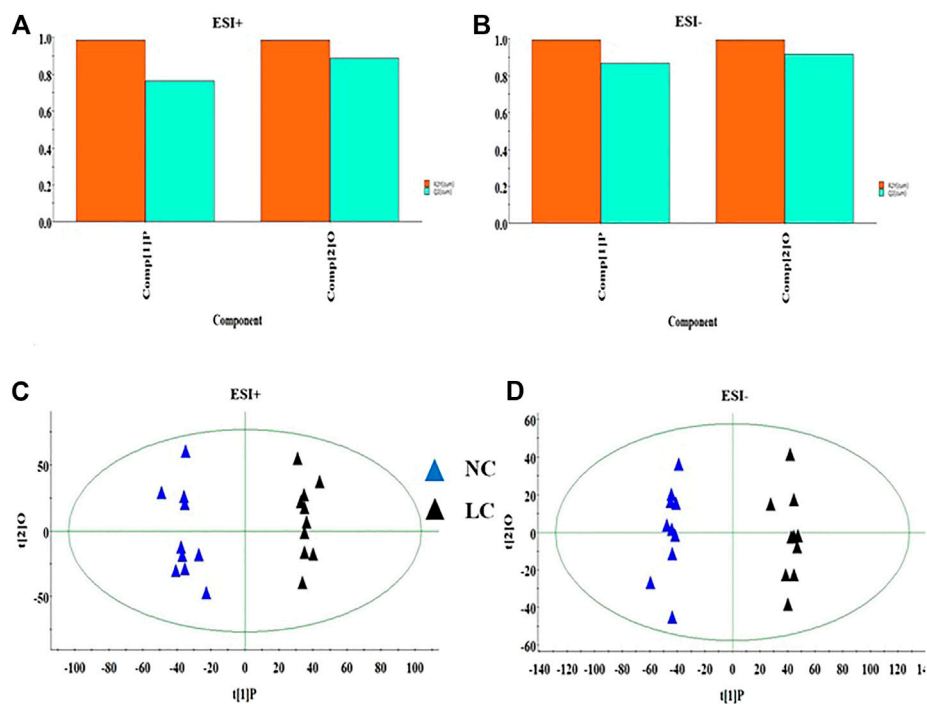


FIGURE 4 | The goodness of fit test for OPLS model in ESI+ and ESI- mode (A,B). OPLS-DA analysis of the data derived from the ESI+ and ESI- mode between NC and LC group (C,D).

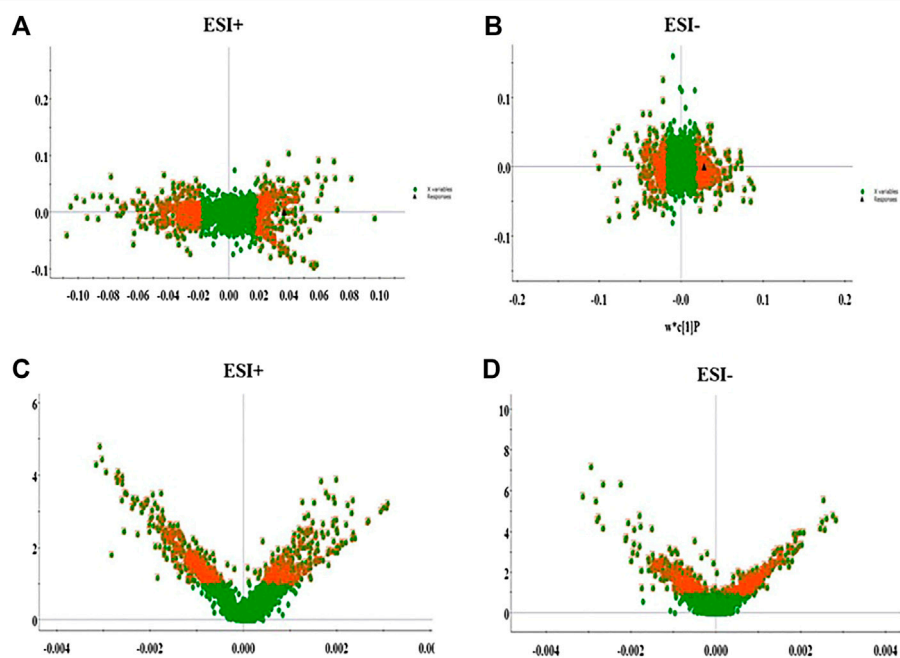


FIGURE 5 | The loading plot for OPLS model between NC and LC group in ESI+ and ESI- mode (A,B). VIP plot for OPLS model between NC and LC group in ESI+ and ESI- mode (C,D).

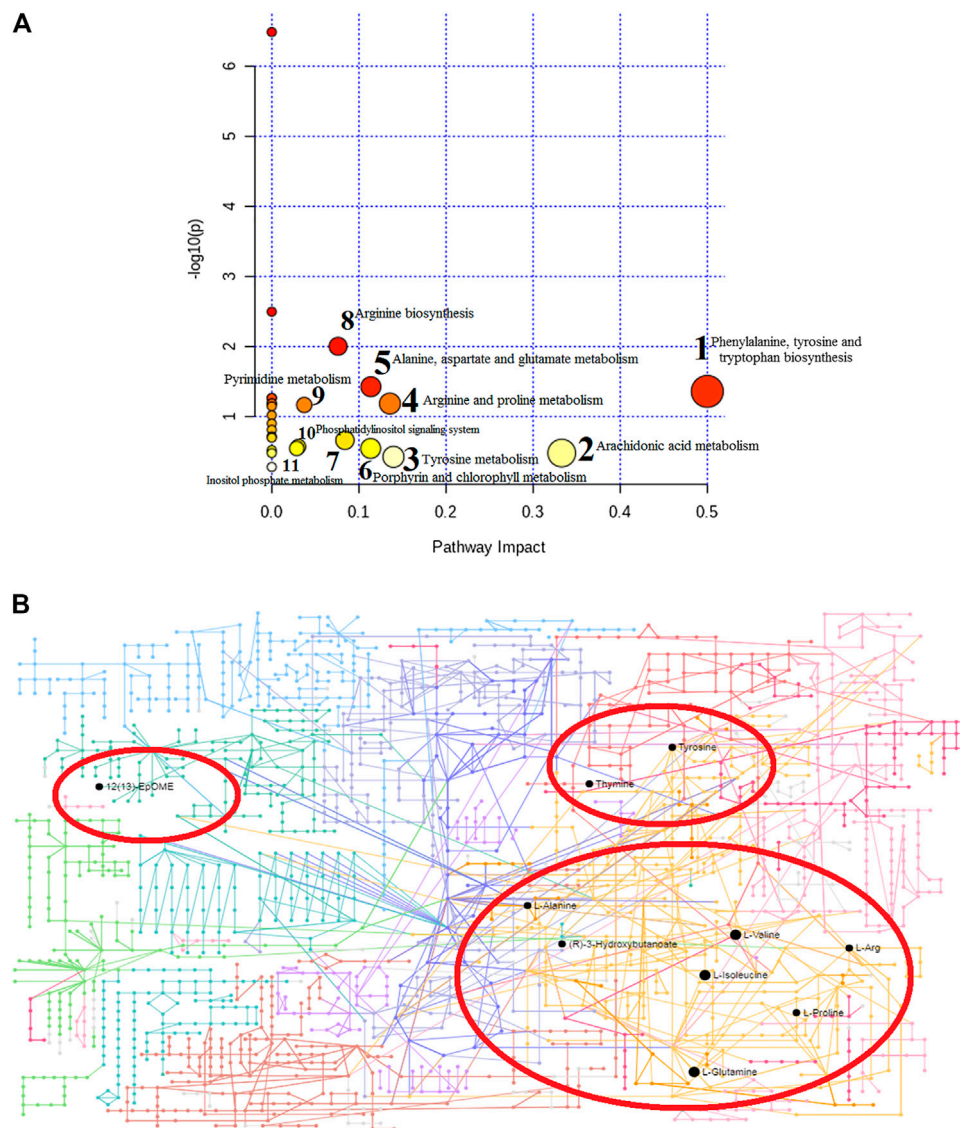


FIGURE 6 | Metabolic pathway analysis of identified 18 differential metabolites after Andro treatment, and impact value more than zero of pathways name (A); KEGG global metabolic network potential metabolites in model mouse after Andro administration (B).

glutamate metabolism, porphyrin and chlorophyll metabolism, pyruvate metabolism, arginine biosynthesis, pyrimidine metabolism, phosphatidylinositol signaling system and inositol phosphate metabolism. In the light of the impact value of the metabolic pathway, the pharmacological action and effective mechanism of Andro mainly acts on the amino acid metabolism pathway and arachidonic acid metabolic pathway to protect against lung cancer.

Amino acid metabolism not only plays an important role in the body's anabolism, but also plays an important role in the proliferation, apoptosis and invasion of tumor cells. Some amino acids are considered as tumor markers and present abnormal expression in patients with different tumors of lung cancer, skin cancer, prostate cancer, colon and breast cancer (Zhang et al., 2013; Liang et al., 2016; Nan et al., 2016; Lukey et al., 2017).

However, the abnormal state is not much different from normal people in chronic wasting diseases. During the process of tumors growth in the lung, it not only affects the human respiratory and circulatory system, but also causes changes in the body's energy metabolism even the overall metabolic state leading to some amino acid metabolism-related enzymes alteration in the body. The abnormal expression of amino acids metabolism provides energy for tumor tissues, constructs related proteins required for their growth and development, then it can also escape the tumor cell killing effect and immune surveillance of the host immune system (Vettore et al., 2020). Amino acids can also be used as signal molecules to participate in various signal pathways of tumor cells, which regulate themselves to take part in the formation of cellular energy-related metabolic regulation signal pathways, and control cell proliferation, growth and Invasion

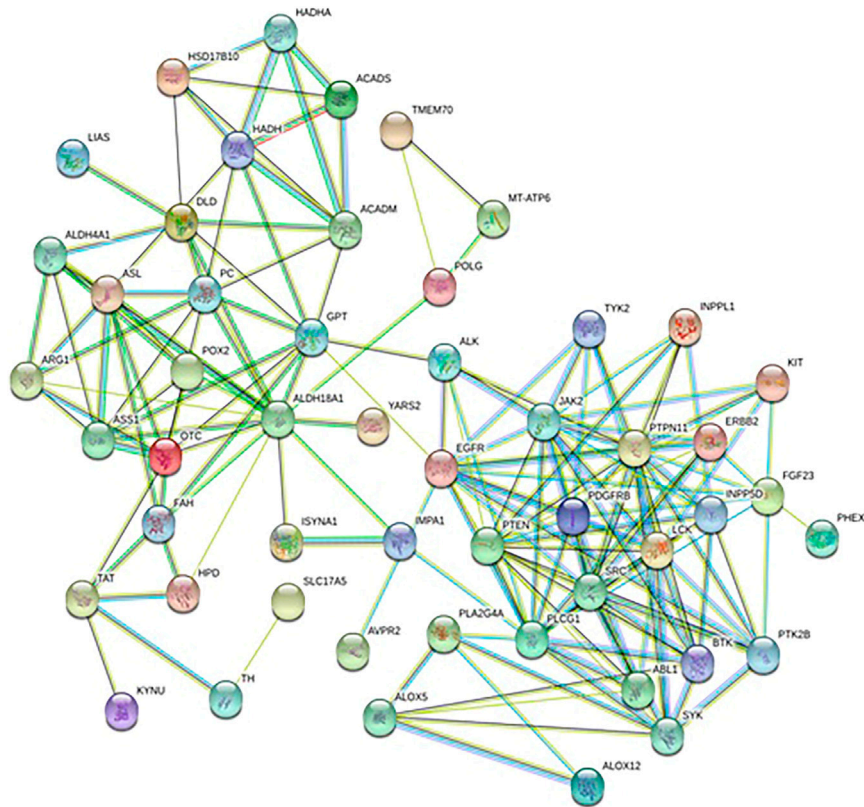


FIGURE 7 | Protein-protein correlation analysis of differentiated metabolites involved in Andro treatment protecting against lung cancer mouse.

ability as downstream proteins of proto-oncogenes (Liang et al., 2017; Sivanand and Vavder Heiden, 2020). Alanine is a non-essential amino acid produced by glycogen in the human body, which is produced by the conversion of carbohydrate pyruvate or the decomposition of DNA, dipeptide carnosine and goose serotonin. It can be converted into pyruvate and tricarboxylic acid cycle intermediates, and then converted into glucose through gluconeogenesis, as an energy source to meet the huge energy demand consumed by various metabolic activities of tumor cells. When branched chain amino acid is insufficient, alanine level is usually decreased, which may be related to muscle metabolism. Alanine can promote energy synthesis in cells and provide sufficient energy for cell growth (Deberardinis et al., 2008). It is an inhibitory neurotransmitter in the brain as the same as GABA, taurine and glycine. In addition, tumor cells also use glutamine as another source of energy. As the main substrate of aerobic metabolism of tumor cells in mitochondria, the proliferating tumor cells need to consume a large amount of glutamine (Bathe et al., 2011). Some clinical trials have demonstrated that patients receiving glutamine supplementation have higher nitrogen balance, and polymorphonuclear neutrophil granulocytes producing cysteyleukotrienes, lymphocyte recovery and intestinal permeability have been improved. Glutamine is converted to glutamate by the reaction of glutaminase and amidase. The glutamate product can be directly incorporated into GSH, or enter the Krebs cycle as

2-oxoglutarate through transamination or oxidative deamination reactions. Subsequently, the OAA formed in the Krebs cycle is transamination to aspartic acid, which is removed from the Krebs cycle for pyrimidine biosynthesis (Deberardinis et al., 2008; Bathe et al., 2011). This study revealed that the levels of alanine and glutamine in the model group were reduced, and Andro could restore the level of alanine and glutamine content to the control group trend by regulating alanine, aspartate and glutamate metabolism, and pyrimidine metabolism. Arginine, as an essential amino acid, is synthesized in the urea cycle of adults. It helps to process ammonia and can be converted into glucose and glycogen when needed. Arginine can activate AMP kinase, and then stimulate skeletal muscle fatty acid oxidation and muscle glucose uptake leading to the increasing level of the insulin secreted by pancreatic β cells. It also is involved in the metabolism of nitric oxide that is a vasodilator and free radical used by nitro-oxidative stress, apoptosis, cell cycle, angiogenesis, invasion and metastasis. Therefore, arginine deprivation may provide a potential treatment for lung cancer (Yang et al., 2009; Grimm et al., 2013). In our study, it was found that the arginine content in the urine of lung cancer mice reduced after Andro treatment, which was related to the regulation of arginine and proline metabolism as well as arginine biosynthesis. Proline is a non-essential amino acid synthesized from glutamic acid. It is an important part of collagen and has potential endogenous excitotoxin/neurotoxin activity, which can act as a neurotoxin

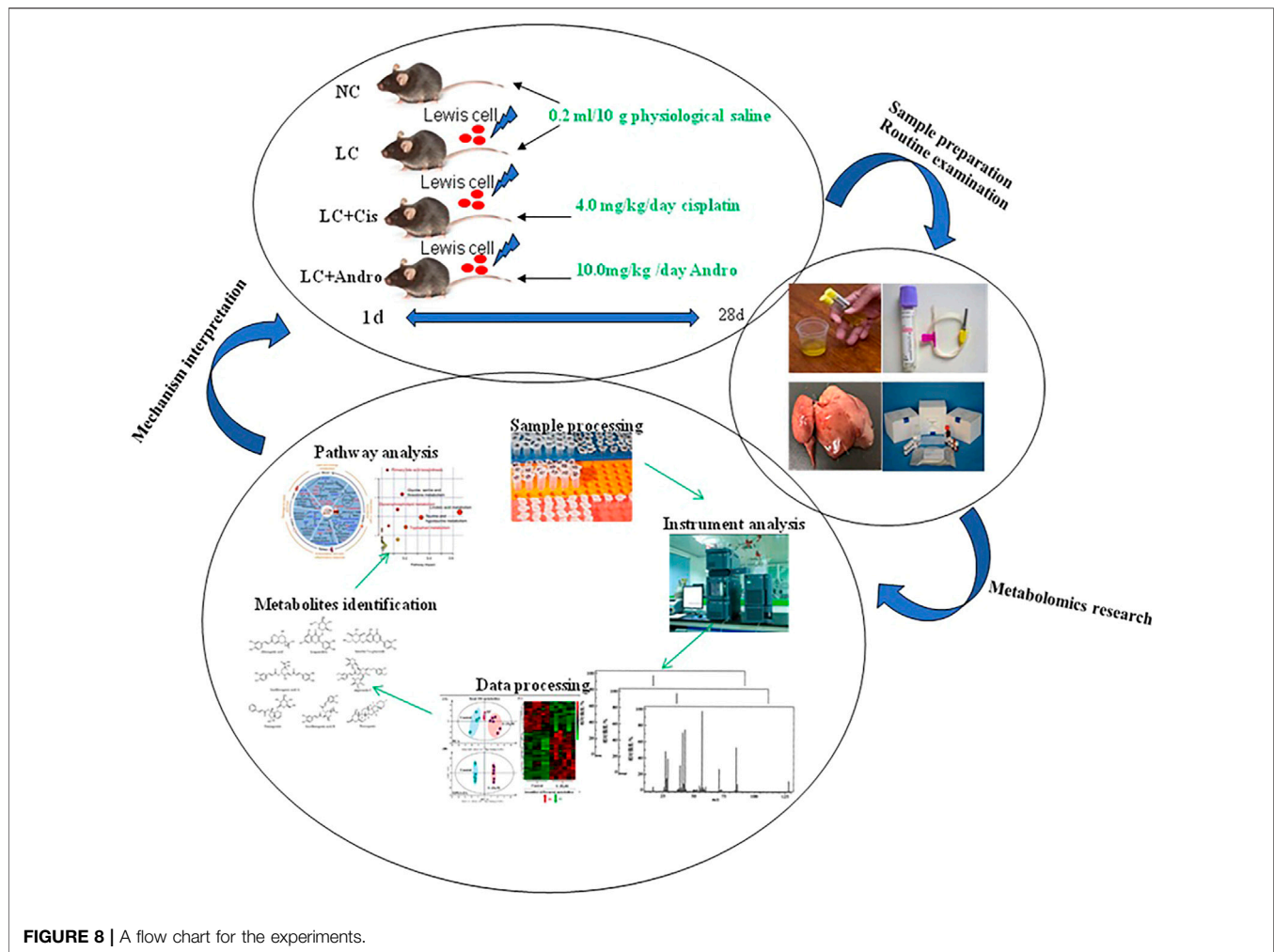


FIGURE 8 | A flow chart for the experiments.

and metabolic toxin to damage nerve cells and nerve tissue causing adverse health effects when it keeps at a high level for a long time. According to reports, the plasma concentration of proline in the model group was significantly reduced compared with the control group, and the rapid increase of proline dehydrogenase transcription by the tumor suppressor p53 triggered the degradation of this amino acid in cancer (Zhao et al., 2014; Phang et al., 2015). After Andro treatment, the proline content in the urine of lung cancer mice was increased mediated by regulating arginine and proline metabolism. Tyrosine, like other amino acids, is a component of protein and an alternative energy source for cell function. The liver is the main organ where tyrosine degradation occurs, producing intermediates or precursors for gluconeogenesis and ketone production. The degradation of tyrosine is catalyzed by a series of enzymatic reactions, which tyrosine metabolism disorders are related to many diseases, such as Huntington's disease and esophageal cancer. In the catalytic reaction of phenylalanine hydroxylase, tyrosine can be metabolized to phenylalanine. The lack of polycyclic aromatic hydrocarbons or the decrease of liver activity can cause phenylalanine metabolism disorder and acute liver damage. The decreasing level of tyrosine in urine of

the model group can infer that the liver function in the lung cancer body is abnormal (Wiggins et al., 2015; Herman et al., 2019). Andro can adjust phenylalanine, tyrosine and tryptophan biosynthesis, and tyrosine metabolism to promote tyrosine level close to normal state.

Tumor cell membrane phospholipids can release arachidonic acid (AA) through the action of phospholipase A2 (PLA2), then it was catalyzed to produce eicosanoids such as prostaglandins (PGE), leukotrienes and hydroxyeicosatetraenoic acid (HETEs) through the key enzymes from arachidonic acid metabolism network such as cyclooxygenase (COX), lipoxygenase (LOX) and cytochrome P450 monooxygenase, and further activates downstream signaling pathways such as PI3K/Akt. Thus, arachidonic acid plays an important role in the regulation of tumor cell proliferation and apoptosis. COX-2 is often over-expressed in tumor cells, which results in the accumulation of a large amount of PGE2 in tumor tissues (Łuczaj et al., 2015). PGE2 can inhibit tumor cell apoptosis, promote cell division, angiogenesis, tumor invasion and metastasis by binding to special receptors on the cell membrane. In addition, cPLA2 catalyzes membrane phospholipids to produce AA and lysophospholipids, which directly or indirectly participate in

tumorigenesis and development (Clay et al., 1999; Sabino et al., 2002). This study found that the content of AA in the model group mice was increased, indicating that lung cancer caused severe inflammation in the body and may exist cancer cell division, angiogenesis, tumor invasion and metastasis. Andro can reduce AA levels by regulating arachidonic acid metabolism. Metabolite products such as lactic acid level is significantly increased in cancer patients, while glucose level is significantly decreased due to the continuous existence of the Warburg effect, which is the result of abnormal metabolism in tumor cells, that is, the strong Glucose metabolism. Cancer cell metabolism mainly involves the final conversion of glucose to lactate through enzyme-catalyzed anaerobic fermentation (Fan et al., 2009; Rocha et al., 2010; Rocha et al., 2011). Lactic acid is also the cyclic carbon source of tricarboxylic acid (TCA) for non-small cell lung cancer to maintain tumor metabolism in the body. Therefore, the elevated lactate levels found in the serum of patients with non-small cell lung cancer can be attributed to the large number of cell proliferations. Our research has found that the lactic acid content in the urine of lung cancer mice was increased, which showed that the tumor metabolism in cancer animals was accelerated. After Andro treatment, the abnormal lactic acid content was reduced mainly achieved by regulating pyruvate metabolism. In the human body, thymine participates in numerous enzymatic reactions, which thymine and deoxyribose 1-phosphate can be biosynthesized from thymidine through interaction with thymidine phosphorylase. In addition, it can be also converted to dihydrothymine (Jordan et al., 2010; Faubert et al., 2017).

Thymine is a potentially toxic compound that is associated with numerous diseases, such as thymidine treatment, periodontal detection depth, colorectal cancer and temporomandibular joint disease in human. It is also associated with innate metabolic disease of β -uropropionase deficiency (Xu et al., 2016). Pathway analysis results have shown that Andro can reduce abnormally elevated levels of thymine in urine by regulating pyrimidine metabolism. As a kind of porphyrin, coproporphyrin III enters mitochondria, where it is oxidized and decarboxylated to form protoporphyrin IX. It is catalyzed by iron chelatase, which combines Fe^{2+} with protoporphyrin-IX to form heme. Drug toxicity can cause liver damage and hemoglobin synthesis dysfunction resulting to the increasing level of the synergistic porphyrin III in the urine, which in turn causes abnormal bilirubin metabolism and increases the level of DBIL (Bröer, 2008; Deja et al., 2014). The level of coproporphyrin III in the urine of lung cancer mice is elevated, which shows that lung cancer may cause liver damage and hemoglobin synthesis dysfunction. After Andro treatment, the abnormal content of coproporphyrin III was changed to the horizontal direction of the control group. Inositol, as a reactant of tumor cell energy metabolism and lipid metabolism, is significantly increased when the body's immune function is low and tumor cell proliferation. Tumor energy, carbohydrates, and lipid metabolism in patients are more active, and their immune function protecting against tumor cells proliferation is faster.

Some studies have added two other characteristics of cancer, namely reprogramming energy metabolism and evading immune destruction. In tumors from animal model, various energy metabolism pathways such as such as inositol phosphate metabolism, oxidative phosphorylation and purine metabolism and citrate cycle have changed. Inositol phosphate metabolism is altered in cancers body, and then they regulate chromatin remodeling (Steger et al., 2003; Hanahan and Weinberg, 2011). Andro can reduce inositol phosphate content in the urine of model mice by phosphatidylinositol signaling system and Inositol phosphate metabolism indicating that Andro can inhibit the energy, carbohydrate and lipid metabolism of tumor cells. Branched-chain amino acids (BCAA) such as valine, isoleucine and leucine possess similar structures with different metabolic pathways. Valine deficiency is marked by impaired brain nerve function, and isoleucine deficiency is marked by muscle tremors. Studies have reported that glycine, valine and methionine in the serum of lung cancer patients are significantly lower than those in healthy controls, which are considered to be essential in the development of primary tumor types (Khunger et al., 2018). 3-Hydroxybutyric acid, also known as β -hydroxybutyric acid, is a typical partial degradation product of branched-chain amino acids released from muscles for liver and kidney gluconeogenesis (Hashim et al., 2019). 12,13-EpOME is a very hydrophobic long-chain fatty acid. During the occurrence and development of tumors, a large amount of energy and raw materials are needed to meet the needs of their own growth due to the rapid metabolism of tumor cells, which will lead to an increase in fatty acid oxidation products in the body and a decrease in fatty acid content. This study found that the level of 12,13-EpOME in urine was increased, indicating that there may be serious abnormalities in lipid metabolism in cancer bodies. Xanthine acid as a metabolite of tryptophan catabolism is the substrate of methyltransferase in the tryptophan metabolism pathway. Xanthine is a product of the purine degradation pathway and will be converted to uric acid under the action of xanthine oxidase. p-Cresol sulfate that causes nephrotoxicity and vascular toxicity by activating the renal renin-angiotensin-aldosterone system (RAAS), and leads to renal tubular cell stress response cells and renal fibrosis is a uremic toxin (Battelli et al., 2018; Battelli et al., 2019). Creatinine is a breakdown product of creatine phosphate in muscles. The loss of water molecules in creatine leads to the formation of creatinine. Creatinine is transferred to the kidneys through plasma, and then cleared from the body through glomerular filtration and partial renal tubular excretion (Evans et al., 2019). ALK rearrangements result from inversions or translocations on chromosome 2 that fuse variable regions of a partner gene with exon 20 of the ALK gene (Shaw et al., 2009; Gainor et al., 2013; Tsao et al., 2016).

As an integral part of systems biology, metabolomics has developed rapidly in recent years. At this stage, metabolomics research in lung cancer is mainly focused on metabolic pathways of blood, urine, tissue cells, and breathing gas,

while sputum and pleural effusion are rarely reported in the literature, and further research is needed (Crutchfield et al., 2016; Dakappagari et al., 2017; Li et al., 2018). Since the existing analytical instruments, analytical techniques, and data processing methods are not perfect, and specimen preparation lacks uniform standards, metabolomics technology still needs further development. With the continuous insight into metabolomics research, HMDB improvement, the successful docking of various omics data and the verification of multiple biological models, panoramic information on the transcription, protein and metabolic levels of various tumors such as lung cancer could be obtained, and more molecular markers for early diagnosis, efficacy and prognosis evaluation will be discovered providing a theoretical basis for improving the clinical diagnosis and treatment of lung cancer.

CONCLUSION

This study discovers biomarkers, metabolic profiles and pathways as potential targets for insight into the pharmacological action and effective mechanism of Andro against lung cancer by high-throughput metabolomics analysis combined with network pharmacology. Andro can regulate 18 of 25 biomarkers associated with the pathogenesis of lung cancer, such as alanine, L-glutamine, isoleucine and 3-hydroxybutyric acid. Andro embodies the characteristics of enhancing the immune system function, inhibiting inflammation reaction, tumor cell growth and metastasis as well as balancing visceral metabolism, which was involved in amino acid metabolism, arachidonic acid metabolism, porphyrin and chlorophyll metabolism, pyruvate metabolism, pyrimidine metabolism, phosphatidylinositol signaling system and inositol phosphate metabolism. Andro were shown to address multiple relevant targets and signaling pathways in the Lewis lung cancer model. Due to generating the majority of biological data. Further, it could expand the number

of biological samples and perform clinical biological verification in the research process of lung cancer.

DATA AVAILABILITY STATEMENT

The original contributions presented in the study are included in the article/**Supplementary Material**, further inquiries can be directed to the corresponding authors.

ETHICS STATEMENT

The animal study was reviewed and approved by the Ethics Committee of Harbin Medical University.

AUTHOR CONTRIBUTIONS

WL and WZ designed the experiments; WL, LJ, J-WZ, D-JW, QR, WZ performed the experiment and analyzed the data; WL wrote the paper and WZ revised it. All the authors approved the final manuscript.

ACKNOWLEDGMENTS

This work was supported by grants from the Basic Scientific Research Projects of Heilongjiang Provincial Colleges and Universities (2020-KYYWF-1445).

SUPPLEMENTARY MATERIAL

The Supplementary Material for this article can be found online at: <https://www.frontiersin.org/articles/10.3389/fphar.2021.596652/full#supplementary-material>.

REFERENCES

- Anguiano-Hernandez, Y. M., Contreras-Mendez, L., Contreras-Mendez, L., Hernandez-Cueto, M. d. l. A., Alvarado-Yaah, J. E., Muñoz-Medina, J. E., et al. (2019). Modification of HIF-1 α , NF- κ B, IGFBP-3, VEGF and adiponectin in diabetic foot ulcers treated with hyperbaric oxygen. *Uhm* 46 (1), 35–44. doi:10.22462/01.03.2019.4
- Azar, F. E., Azami-Aghdash, S., Pournaghi-Azar, F., Mazdaki, A., Rezapour, A., Ebrahimi, P., et al. (2017). Cost-effectiveness of lung cancer screening and treatment methods: a systematic review of systematic reviews. *BMC Health Serv. Res.* 17 (1), 413. doi:10.1186/s12913-017-2374-1
- Barta, J. A., Powell, C. A., and Wisnivesky, J. P. (2019). Global epidemiology of lung cancer. *Ann. Glob. Health* 85 (1), 8. doi:10.5334/aogh.2419
- Bathe, O. F., Shaykhutdinov, R., Kopciuk, K., Weljie, A. M., McKay, A., Sutherland, F. R., et al. (2011). Feasibility of identifying pancreatic cancer based on serum metabolomics. *Cancer Epidemiol. Biomarkers Prev.* 20, 140–147. doi:10.1158/1055-9965.epi-10-0712
- Battelli, M. G., Bortolotti, M., Polito, L., and Bolognesi, A. (2019). Metabolic syndrome and cancer risk: the role of xanthine oxidoreductase. *Redox Biol.* 21, 101070. doi:10.1016/j.redox.2018.101070
- Battelli, M. G., Bortolotti, M., Polito, L., and Bolognesi, A. (2018). The role of xanthine oxidoreductase and uric acid in metabolic syndrome. *Biochim. Biophys. Acta (Bba) - Mol. Basis Dis.* 1864 (8), 2557–2565. doi:10.1016/j.bbdis.2018.05.003
- Bellomo, C., Caja, L., and Moustakas, A. (2016). Transforming growth factor β as regulator of cancer stemness and metastasis. *Br. J. Cancer* 115 (7), 761–769. doi:10.1038/bjc.2016.255
- Bröer, S. (2008). Apical transporters for neutral amino acids: physiology and pathophysiology. *Physiology* 23, 95–103. doi:10.1152/physiol.00045.2007
- Clay, C. E., Namen, A. M., Atsumi, G.-i., Willingham, M. C., High, K. P., Kute, T. E., et al. (1999). Influence of J series prostaglandins on apoptosis and tumorigenesis of breast cancer cells. *Carcinogenesis* 20 (10), 1905–1911. doi:10.1093/carcin/20.10.1905
- Crutchfield, C. A., Thomas, S. N., Sokoll, L. J., and Chan, D. W. (2016). Advances in mass spectrometry-based clinical biomarker discovery. *Clin. Proteomics* 13, 1. doi:10.1186/s12014-015-9102-9
- Dakappagari, N., Zhang, H., Stephen, L., Amaravadi, L., and Khan, M. U. (2017). Recommendations for clinical biomarker specimen preservation and stability assessments. *Bioanalysis* 9 (8), 643–653. doi:10.4155/bio-2017-0009
- de Groot, P. M., Wu, C. C., Carter, B. W., and Munden, R. F. (2018). The epidemiology of lung cancer. *Transl. Lung Cancer Res.* 7 (3), 220–233. doi:10.21037/tlcr.2018.05.06

- Deberardinis, R. J., Sayed, N., Ditsworth, D., and Thompson, C. B. (2008). Brick by brick: metabolism and tumor cell growth. *Curr. Opin. Genet. Development* 18, 54–61. doi:10.1016/j.gde.2008.02.003
- Deja, S., Porebska, I., Kowal, A., Zabek, A., Barg, W., Pawelczyk, K., et al. (2014). Metabolomics provide new insights on lung cancer staging and discrimination from chronic obstructive pulmonary disease. *J. Pharm. Biomed. Anal.* 100, 369–380. doi:10.1016/j.jpba.2014.08.020
- Ding, Y., Chen, L., Wu, W., Yang, J., Yang, Z., and Liu, S. (2017). Andrographolide inhibits influenza A virus-induced inflammation in a murine model through NF- κ B and JAK-STAT signaling pathway. *Microbes Infect.* 19 (12), 605–615. doi:10.1016/j.micinf.2017.08.009
- Dong, G., Lin, X. H., Liu, H. H., Gao, D. M., Cui, J. F., Ren, Z. G., et al. (2019). Intermittent hypoxia alleviates increased VEGF and pro-angiogenic potential in liver cancer cells. *Oncol. Lett.* 18 (2), 1831–1839. doi:10.3892/ol.2019.10486
- Evans, T. R. J., Kudo, M., Finn, R. S., Han, K.-H., Cheng, A.-L., Ikeda, M., et al. (2019). Urine protein:creatinine ratio vs 24-hour urine protein for proteinuria management: analysis from the phase 3 REFLECT study of lenvatinib vs sorafenib in hepatocellular carcinoma. *Br. J. Cancer* 121 (3), 218–221. doi:10.1038/s41416-019-0506-6
- Fan, T. W., Lane, A. N., Higashi, R. M., Farag, M. A., Gao, H., Bousamra, M., et al. (2009). Altered regulation of metabolic pathways in human lung cancer discerned by ^{13}C stable isotope-resolved metabolomics (SIRM). *Mol. Cancer* 8, 41. doi:10.1186/1476-4598-8-41
- Faubert, B., Li, K. Y., Cai, L., Hensley, C. T., Kim, J., Zacharias, L. G., et al. (2017). Lactate metabolism in human lung tumors. *Cell* 171, 358–371. doi:10.1016/j.cell.2017.09.019
- Forde, P. M., Kelly, R. J., and Brahmer, J. R. (2014). New strategies in lung cancer: translating immunotherapy into clinical practice. *Clin. Cancer Res.* 20, 1067–1073. doi:10.1158/1078-0432.ccr-13-0731
- French, C. D., Willoughby, R. E., Pan, A., Wong, S. J., Foley, J. F., Wheat, L. J., et al. (2018). NMR metabolomics of cerebrospinal fluid differentiates inflammatory diseases of the central nervous system. *Plos Negl. Trop. Dis.* 12 (12), e0007045. doi:10.1371/journal.pntd.0007045
- Gainor, J. F., Varghese, A. M., Ou, S.-H. I., Kabraji, S., Awad, M. M., Katayama, R., et al. (2013). ALK rearrangements are mutually exclusive with mutations in EGFR or KRAS: an analysis of 1,683 patients with non-small cell lung cancer. *Clin. Cancer Res.* 19 (15), 4273–4281. doi:10.1158/1078-0432.ccr-13-0318
- Gao, F., Liu, X., Shen, Z., Jia, X., He, H., Gao, J., et al. (2018). Andrographolide sulfonate attenuates acute lung injury by reducing expression of myeloperoxidase and neutrophil-derived proteases in mice. *Front. Physiol.* 9, 939. doi:10.3389/fphys.2018.00939
- Gao, J., Peng, S., Shan, X., Deng, G., Shen, L., Sun, J., et al. (2019). Inhibition of AIM2 inflammasome-mediated pyroptosis by Andrographolide contributes to amelioration of radiation-induced lung inflammation and fibrosis. *Cell Death Dis* 10 (12), 957. doi:10.1038/s41419-019-2195-8
- Gridelli, C., Bennouna, J., de Castro, J., Dingemans, A.-M. C., Griesinger, F., Grossi, F., et al. (2011). Randomized phase IIb trial evaluating the continuation of bevacizumab beyond disease progression in patients with advanced non-squamous non-small-cell lung cancer after first-line treatment with bevacizumab plus platinum-based chemotherapy: treatment rationale and protocol dynamics of the AvaALL (MO22097) trial. *Clin. Lung Cancer* 12 (6), 407–411. doi:10.1016/j.clcc.2011.05.002
- Grimm, E. A., Sikora, A. G., and Ekmekcioglu, S. (2013). Molecular pathways: inflammation-associated nitric-oxide production as a cancer-supporting redox mechanism and a potential therapeutic target. *Clin. Cancer Res.* 19, 5557–5563. doi:10.1158/1078-0432.ccr-12-1554
- Guan, S., Tee, W., Ng, D., Chan, T., Peh, H., Ho, W., et al. (2013). Andrographolide protects against cigarette smoke-induced oxidative lung injury via augmentation of Nrf2 activity. *Br. J. Pharmacol.* 168 (7), 1707–1718. doi:10.1111/bph.12054
- Hanahan, D., and Weinberg, R. A. (2011). Hallmarks of cancer: the next generation. *Cell* 144, 646–674. doi:10.1016/j.cell.2011.02.013
- Hansen, I. S., Baeten, D. L. P., and den Dunnen, J. (2019). The inflammatory function of human IgA. *Cell. Mol. Life Sci.* 76 (6), 1041–1055. doi:10.1007/s00018-018-2976-8
- Hashim, N. A. A., Ab-Rahim, S., Suddin, L. S., Saman, M. S. A., and Mazlan, M. (2019). Global serum metabolomics profiling of colorectal cancer. *Mol. Clin. Oncol.* 11 (1), 3–14. doi:10.3892/mco.2019.1853
- Herman, S., Niemelä, V., Emami Khoonsari, P., Sundblom, J., Burman, J., Landtblom, A. M., et al. (2019). Alterations in the tyrosine and phenylalanine pathways revealed by biochemical profiling in cerebrospinal fluid of Huntington's disease subjects. *Sci. Rep.* 9 (1), 4129. doi:10.1038/s41598-019-40186-5
- Hossain, M. S., Urbi, Z., Sule, A., and Hafizur Rahman, K. M. (2014). Andrographis paniculata (Burm. f.) Wall. ex Nees: a review of ethnobotany, phytochemistry, and pharmacology. *Scientific World J.* 2014, 274905. doi:10.1155/2014/274905
- Inui, T., Watanabe, M., Nakamoto, K., Sada, M., Hirata, A., Nakamura, M., et al. (2018). Bronchial epithelial cells produce CXCL1 in response to LPS and TNF α : a potential role in the pathogenesis of COPD. *Exp. Lung Res.* 44 (7), 323–331. doi:10.1080/01902148.2018.1520936
- Johnson, C. H., Ivanisevic, J., and Siuzdak, G. (2016). Metabolomics: beyond biomarkers and towards mechanisms. *Nat. Rev. Mol. Cell Biol.* 17, 451–459. doi:10.1038/nrm.2016.25
- Jordan, K. W., Adkins, C. B., Su, L., Halpern, E. F., Mark, E. J., Christiani, D. C., et al. (2010). Comparison of squamous cell carcinoma and adenocarcinoma of the lung by metabolomic analysis of tissue-serum pairs. *Lung Cancer* 68, 44–50. doi:10.1016/j.lungcan.2009.05.012
- Khunger, A., Khunger, M., and Velcheti, V. (2018). Dabrafenib in combination with trametinib in the treatment of patients with BRAF V600-positive advanced or metastatic non-small cell lung cancer: clinical evidence and experience. *Ther. Adv. Respir. Dis.* 12, 1753466618767611. doi:10.1177/1753466618767611
- Kim, D., Lee, Y. S., Kim, D. H., and Bae, S. C. (2020). Lung cancer staging and associated genetic and epigenetic events. *Mol. Cell* 43 (1), 1–9. doi:10.14348/molcells.2020.2246
- Lee, Y. C., Lin, H. H., Hsu, C. H., Wang, C. J., Chiang, T. A., and Chen, J. H. (2010). Inhibitory effects of andrographolide on migration and invasion in human non-small cell lung cancer A549 cells via down-regulation of PI3K/Akt signaling pathway. *Eur. J. Pharmacol.* 632 (1–3), 23–32. doi:10.1016/j.ejphar.2010.01.009
- Li, Q., Hu, K., Tang, S., Xu, L.-F., and Luo, Y.-C. (2016). Anti-tumor activity of tanshinone IIA in combined with cyclophosphamide against Lewis mice with lung cancer. *Asian Pac. J. Trop. Med.* 9 (11), 1084–1088. doi:10.1016/j.apjtm.2016.09.003
- Li, Y.-F., Qiu, S., Gao, L.-J., and Zhang, A.-H. (2018). Metabolomic estimation of the diagnosis of hepatocellular carcinoma based on ultrahigh performance liquid chromatography coupled with time-of-flight mass spectrometry. *RSC Adv.* 8 (17), 9375–9382. doi:10.1039/c7ra13616a
- Liang, Q., Liu, H., Xie, L.-x., Li, X., and Zhang, A.-H. (2017). High-throughput metabolomics enables biomarker discovery in prostate cancer. *RSC Adv.* 7 (5), 2587–2593. doi:10.1039/c6ra25007f
- Liang, Q., Liu, H., Zhang, T., Jiang, Y., Xing, H., and Zhang, A.-h. (2016). Discovery of serum metabolites for diagnosis of progression of mild cognitive impairment to Alzheimer's disease using an optimized metabolomics method. *RSC Adv.* 6 (5), 3586–3591. doi:10.1039/c5ra19349d
- Liang, Q., Wang, C., Wang, C., Li, B., and Zhang, A.-h. (2015). Metabolomics of alcoholic liver disease: a clinical discovery study. *RSC Adv.* 5 (98), 80381–80387. doi:10.1039/c5ra13417j
- Liang, Q., Yu, Q., Wu, H., Zhu, Y.-Z., and Zhang, A.-h. (2014). Metabolite fingerprint analysis of cervical cancer using LC-QTOF/MS and multivariate data analysis. *Anal. Methods* 6 (12), 3937–3942. doi:10.1039/c4ay00399c
- Lim, J. C., Jeyaraj, E. J., Sagincedu, S. R., Wong, W. S., and Stanslas, J. (2015). SRS06, a new semisynthetic andrographolide derivative with improved anticancer potency and selectivity, inhibits nuclear factor- κ B nuclear binding in the A549 non-small cell lung cancer cell line. *Pharmacology* 95 (1–2), 70–77. doi:10.1159/000370313
- Lin, H.-H., Tsai, C.-W., Chou, F.-P., Wang, C.-J., Hsuan, S.-W., Wang, C.-K., et al. (2011). Andrographolide down-regulates hypoxia-inducible factor-1 α in human non-small cell lung cancer A549 cells. *Toxicol. Appl. Pharmacol.* 250 (3), 336–345. doi:10.1016/j.taap.2010.11.014
- Liu, H., and May, K. (2016). Disulfide bond structures of IgG molecules: structural variations, chemical modifications and possible impacts to stability and biological function. *MAbs* 4 (1), 17–23. doi:10.4161/mabs.4.1.18347
- Lukey, M. J., Katt, W. P., and Cerione, R. A. (2017). Targeting amino acid metabolism for cancer therapy. *Drug Discov. Today* 22 (5), 796–804. doi:10.1016/j.drudis.2016.12.003
- Luo, W., Liu, Y., Zhang, J., Luo, X., Lin, C., and Guo, J. (2013). Andrographolide inhibits the activation of NF- κ B and MMP-9 activity in H3255 lung cancer cells. *Exp. Ther. Med.* 6 (3), 743–746. doi:10.3892/etm.2013.1196

- Luo, X., Luo, W., Lin, C., Zhang, L., and Li, Y. (2014). Andrographolide inhibits proliferation of human lung cancer cells and the related mechanisms. *Int. J. Clin. Exp. Med.* 7 (11), 4220–4225.
- Macpherson, A. J., McCoy, K. D., Johansen, F.-E., and Brandtzaeg, P. (2008). The immune geography of IgA induction and function. *Mucosal Immunol.* 1 (1), 11–22. doi:10.1038/mi.2007.6
- Malhotra, J., Malvezzi, M., Negri, E., La Vecchia, C., and Boffetta, P. (2016). Risk factors for lung cancer worldwide. *Eur. Respir. J.* 48 (3), 889–902. doi:10.1183/13993003.00359-2016
- Mi, S., Xiang, G., Yuwen, D., Gao, J., Guo, W., Wu, X., et al. (2016). Inhibition of autophagy by andrographolide resensitizes cisplatin-resistant non-small cell lung carcinoma cells via activation of the Akt/mTOR pathway. *Toxicol. Appl. Pharmacol.* 310, 78–86. doi:10.1016/j.taap.2016.09.009
- Nan, Y., Zhou, X., Liu, Q., Zhang, A., Guan, Y., Lin, S., et al. (2016). Serum metabolomics strategy for understanding pharmacological effects of ShenQi pill acting on kidney yang deficiency syndrome. *J. Chromatogr. B* 1026, 217–226. doi:10.1016/j.jchromb.2015.12.004
- New, M., and Keith, R. (2018). Early detection and chemoprevention of lung cancer. *F1000Res* 7, 61. doi:10.12688/f1000research.12433.1
- Peng, S., Gao, J., Liu, W., Jiang, C., Yang, X., Sun, Y., et al. (2016b). Andrographolide ameliorates OVA-induced lung injury in mice by suppressing ROS-mediated NF- κ B signaling and NLRP3 inflammasome activation. *Oncotarget* 7 (49), 80262–80274. doi:10.18632/oncotarget.12918
- Peng, S., Hang, N., Liu, W., Guo, W., Jiang, C., Yang, X., et al. (2016a). Andrographolide sulfonate ameliorates lipopolysaccharide-induced acute lung injury in mice by down-regulating MAPK and NF- κ B pathways. *Acta Pharmaceutica Sinica B* 6 (3), 205–211. doi:10.1016/j.apsb.2016.02.002
- Phang, J. M., Liu, W., Hancock, C. N., and Fischer, J. W. (2015). Proline metabolism and cancer. *Curr. Opin. Clin. Nutr. Metab. Care* 18, 71–77. doi:10.1097/mco.0000000000000121
- Postow, M. A., Callahan, M. K., and Wolchok, J. D. (2015). Immune checkpoint blockade in cancer therapy. *Jco* 33, 1974–1982. doi:10.1200/jco.2014.59.4358
- Puri, A., Saxena, R., Saxena, R. P., Saxena, K. C., Srivastava, V., and Tandon, J. S. (1993). Immunostimulant agents from *Andrographis paniculata*. *J. Nat. Prod.* 56 (7), 995–999. doi:10.1021/np50097a002
- Qiu, S., Zhang, A.-h., Guan, Y., Sun, H., Zhang, T.-l., Han, Y., et al. (2020). Functional metabolomics using UPLC-Q/TOF-MS combined with ingenuity pathway analysis as a promising strategy for evaluating the efficacy and discovering amino acid metabolism as a potential therapeutic mechanism-related target for geniposide against alcoholic liver disease. *RSC Adv.* 10 (5), 2677–2690. doi:10.1039/c9ra09305b
- Ren, J.-L., Zhang, A.-H., Kong, L., and Wang, X.-J. (2018). Advances in mass spectrometry-based metabolomics for investigation of metabolites. *RSC Adv.* 8 (40), 22335–22350. doi:10.1039/c8ra01574k
- Ribbenstedt, A., Ziarrusta, H., and Benskin, J. P. (2018). Development, characterization and comparisons of targeted and non-targeted metabolomics methods. *PLoS One* 13 (11), e0207082. doi:10.1371/journal.pone.0207082
- Rocha, C. M., Barros, A. S., Gil, A. M., Goodfellow, B. J., Humpfer, E., Spraul, M., et al. (2010). Metabolic profiling of human lung cancer tissue by 1H high resolution magic angle spinning (HRMAS) NMR spectroscopy. *J. Proteome Res.* 9, 319–332. doi:10.1021/pr9006574
- Rocha, C. M., Carrola, J., Barros, A. S., Gil, A. M., Goodfellow, B. J., Carreira, I. M., et al. (2011). Metabolic signatures of lung cancer in biofluids: NMR-based metabolomics of blood plasma. *J. Proteome Res.* 10, 4314–4324. doi:10.1021/pr200550p
- Saad, J., and Mathew, D. (2020). *Nonsteroidal anti-inflammatory drugs (NSAID) toxicity*, Treasure island, FL: (StatPearls Publishing).
- Sabino, M. C., Ghilardi, J. R., Feia, K. J., Jongen, J. L., Keyser, C. P., Luger, N. M., et al. (2002). The involvement of prostaglandins in tumorigenesis, tumor-induced osteolysis and bone cancer pain. *J. Musculoskelet. Neuronal Interact* 2 (6), 561–562.
- Shao, Z.-J., Zheng, X.-W., Feng, T., Huang, J., Chen, J., Wu, Y.-Y., et al. (2012). Andrographolide exerted its antimicrobial effects by upregulation of human β -defensin-2 induced through p38 MAPK and NF- κ B pathway in human lung epithelial cells. *Can. J. Physiol. Pharmacol.* 90 (5), 647–653. doi:10.1139/y2012-050
- Shaw, A. T., Yeap, B. Y., Mino-Kenudson, M., Digumarthy, S. R., Costa, D. B., Heist, R. S., et al. (2009). Clinical features and outcome of patients with non-small-cell lung cancer who harbor EML4-ALK. *Jco* 27 (26), 4247–4253. doi:10.1200/jco.2009.22.6993
- Sheng, L., Tu, J. W., Tian, J. H., Chen, H. J., Pan, C. L., and Zhou, R. Z. (2018). A meta-analysis of the relationship between environmental tobacco smoke and lung cancer risk of nonsmoker in China. *Medicine (Baltimore)* 97 (28), e11389. doi:10.1097/md.00000000000011389
- Sivanand, S., and Vander Heiden, M. G. (2020). Emerging roles for branched-chain amino acid metabolism in cancer. *Cancer Cell* 37 (2), 147–156. doi:10.1016/j.ccell.2019.12.011
- Solinas, G., Schiarea, S., Liguori, M., Fabbri, M., Pesce, S., Zammataro, L., et al. (2010). Tumor-conditioned macrophages secrete migration-stimulating factor: a new marker for M2-polarization, influencing tumor cell motility. *J.I.* 185 (1), 642–652. doi:10.4049/jimmunol.1000413
- Steger, D. J., Haswell, E. S., Miller, A. L., Wente, S. R., and O'Shea, E. K. (2003). Regulation of chromatin remodeling by inositol polyphosphates. *Science* 299, 114–116. doi:10.1126/science.1078062
- Sun, H., Yang, L., Li, M. X., Fang, H., Zhang, A. H., and Song, Q. (2018). UPLC-G2Si-HDMS untargeted metabolomics for identification of metabolic targets of Yin-Chen-Hao-Tang used as a therapeutic agent of dampness-heat jaundice syndrome. *J. Chromatogr. B Analyt Technol. Biomed. Life Sci.* 1081–1082, 41–50. doi:10.1016/j.jchromb.2018.02.035
- Tan, W. S. D., Peh, H. Y., Liao, W., Pang, C. H., Chan, T. K., Lau, S. H., et al. (2016). Cigarette smoke-induced lung disease predisposes to more severe infection with nontypeable *Haemophilus influenzae*: protective effects of andrographolide. *J. Nat. Prod.* 79 (5), 1308–1315. doi:10.1021/acs.jnatprod.5b01006
- Trédaniel, J., Boffetta, P., Saracci, R., and Hirsch, A. (1994). Exposure to environmental tobacco smoke and risk of lung cancer: the epidemiological evidence. *Eur. Respir. J.* 7 (10), 1877–1888. doi:10.1183/09031936.94.07101877
- Tsao, A. S., Scagliotti, G. V., Bunn, P. A., Jr, Carbone, D. P., Warren, G. W., Bai, C., et al. (2016). Scientific advances in lung cancer 2015. *J. Thorac. Oncol.* 11 (5), 613–638. doi:10.1016/j.jtho.2016.03.012
- Varma, V. R., Oommen, A. M., Varma, S., Casanova, R., An, Y., Andrews, R. M., et al. (2018). Brain and blood metabolite signatures of pathology and progression in Alzheimer disease: a targeted metabolomics study. *Plos Med.* 15 (1), e1002482. doi:10.1371/journal.pmed.1002482
- Verma, V., and Simone, C. B., 2nd (2019). Approaches to stereotactic body radiation therapy for large (≥ 5 centimeter) non-small cell lung cancer. *Transl Lung Cancer Res.* 8 (1), 70–77. doi:10.21037/tlcr.2018.06.10
- Vettore, L., Westbrook, R. L., and Tennant, D. A. (2020). New aspects of amino acid metabolism in cancer. *Br. J. Cancer* 122 (2), 150–156. doi:10.1038/s41416-019-0620-5
- Wang, X., Zhang, A., Yan, G., Han, Y., and Sun, H. (2014). UHPLC-MS for the analytical characterization of traditional Chinese medicines. *Trac Trends Anal. Chem.* 63, 180–187. doi:10.1016/j.trac.2014.05.013
- Wei, J., Barr, J., Kong, L.-Y., Wang, Y., Wu, A., Sharma, A. K., et al. (2010). Glioblastoma cancer-initiating cells inhibit T-cell proliferation and effector responses by the signal transducers and activators of transcription 3 pathway. *Mol. Cancer Ther.* 9 (1), 67–78. doi:10.1158/1535-7163.mct-09-0734
- Wibowo, E., Pollock, P. A., Hollis, N., and Wassersug, R. J. (2016). Tamoxifen in men: a review of adverse events. *Andrology* 4 (5), 776–788. doi:10.1111/andr.12197
- Wiggins, T., Kumar, S., Markar, S. R., Antonowicz, S., and Hanna, G. B. (2015). Tyrosine, phenylalanine, and tryptophan in gastroesophageal malignancy: a systematic review. *Cancer Epidemiol. Biomarkers Prev.* 24 (1), 32–38. doi:10.1158/1055-9965.epi-14-0980
- Wintachai, P., Kaur, P., Lee, R. C., Ramphan, S., Kuadkitkan, A., Wikan, N., et al. (2015). Activity of andrographolide against chikungunya virus infection. *Sci. Rep.* 5, 14179. doi:10.1038/srep14179
- Woodard, G. A., Jones, K. D., and Jablons, D. M. (2016). Lung cancer staging and prognosis. *Cancer Treat. Res.* 170, 47–75. doi:10.1007/978-3-319-40389-2_3
- Woznitza, N., Devaraj, A., Janes, S. M., Duffy, S. W., Bhowmik, A., Rowe, S., et al. (2017). Impact of radiographer immediate reporting of chest X-rays from general practice on the lung cancer pathway (radioX): study protocol for a randomised control trial. *Trials* 18 (1), 521. doi:10.1186/s13063-017-2268-x

- Wu, H., and Feng, F. (2016). Untargeted metabolomic analysis using LC-TOF/MS and LC-MS/MS for revealing metabolic alterations linked to alcohol-induced hepatic steatosis in rat serum and plasma. *RSC Adv.* 6, 28279–28288. doi:10.1039/c5ra27910k
- Xia, J., Broadhurst, D. I., Wilson, M., and Wishart, D. S. (2013). Translational biomarker discovery in clinical metabolomics: an introductory tutorial. *Metabolomics* 9, 280–299. doi:10.1007/s11306-012-0482-9
- Xie, J., Zhang, A.-h., Qiu, S., Zhang, T.-l., Li, X.-n., Yan, G.-l., et al. (2019). Identification of the perturbed metabolic pathways associating with prostate cancer cells and anticancer affects of obacunone. *J. Proteomics* 206, 103447. doi:10.1016/j.jprot.2019.103447
- Xu, X., Watt, D. S., and Liu, C. (2016). Multifaceted roles for thymine DNA glycosylase in embryonic development and human carcinogenesis. *Acta Biochim. Biophys. Sin (Shanghai)* 48 (1), 82–89. doi:10.1093/abbs/gmv141
- Yang, D., Zhang, W., Song, L., and Guo, F. (2013). Andrographolide protects against cigarette smoke-induced lung inflammation through activation of heme oxygenase-1. *J. Biochem. Mol. Toxicol.* 27 (5), 259–265. doi:10.1002/jbt.21483
- Yang, G.-Y., Taboada, S., and Liao, J. (2009). Induced nitric oxide synthase as a major player in the oncogenic transformation of inflamed tissue. *Methods Mol. Biol.* 512, 119–156. doi:10.1007/978-1-60327-530-9_8
- Yang, N., Liu, Y.-Y., Pan, C.-S., Sun, K., Wei, X.-H., Mao, X.-W., et al. (2014). Pretreatment with andrographolide Pills Attenuates lipopolysaccharide-induced pulmonary microcirculatory disturbance and acute lung injury in rats. *Microcirculation* 21 (8), 703–716. doi:10.1111/micc.12152
- Yuwen, D., Mi, S., Ma, Y., Guo, W., Xu, Q., Shen, Y., et al. (2017). Andrographolide enhances cisplatin-mediated anticancer effects in lung cancer cells through blockade of autophagy. *Anticancer Drugs* 28 (9), 967–976. doi:10.1097/cad.0000000000000537
- Zhang, A.-h., Sun, H., and Wang, X.-j. (2013). Recent advances in metabolomics in neurological disease, and future perspectives. *Anal. Bioanal. Chem.* 405 (25), 8143–8150. doi:10.1007/s00216-013-7061-4
- Zhang, A. H., Ma, Z. M., Sun, H., Zhang, Y., Liu, J. H., Wu, F. F., et al. (2019a). High-throughput metabolomics evaluate the efficacy of total lignans from *acanthophanax senticosus* stem against ovariectomized osteoporosis rat. *Front. Pharmacol.* 10, 553. doi:10.3389/fphar.2019.00553
- Zhang, A.-H., Sun, H., Yan, G.-L., Han, Y., Zhao, Q.-Q., and Wang, X.-J. (2019b). Chinmedomics: a powerful approach integrating metabolomics with serum pharmacochimistry to evaluate the efficacy of traditional Chinese medicine. *Engineering* 5, 60–68. doi:10.1016/j.eng.2018.11.008
- Zhang, A.-h., Sun, H., Yan, G.-l., Yuan, Y., Han, Y., and Wang, X.-j. (2014). Metabolomics study of type 2 diabetes using ultra-performance LC-ESI/quadrupole-TOF high-definition MS coupled with pattern recognition methods. *J. Physiol. Biochem.* 70 (1), 117–128. doi:10.1007/s13105-013-0286-z
- Zhang, A. H., Ma, Z. M., Kong, L., Gao, H. L., Sun, H., Wang, X. Q., et al. (2020). High-throughput lipidomics analysis to discover lipid biomarkers and profiles as potential targets for evaluating efficacy of Kai-Xin-San against APP/PS1 transgenic mice based on UPLC-Q/TOF-MS. *Biomed. Chromatogr.* 34 (2), e4724. doi:10.1002/bmc.4724
- Zhang, A., Sun, H., and Wang, X. (2018). Mass spectrometry-driven drug discovery for development of herbal medicine. *Mass. Spec. Rev.* 37 (3), 307–320. doi:10.1002/mas.21529
- Zhang, J., Xu, R., Wu, L., and Jiang, J. (2019). Expression and function of Toll-like receptors in peripheral blood mononuclear cells in patients with ankylosing spondylitis. *Mol. Med. Rep.* 20 (4), 3565–3572. doi:10.3892/mmr.2019.10631
- Zhang, Y., Zhang, X., Yue, Q., Wen, Z., and Zhang, M. (2019). [Ethanol extract of *Rhodiola rosea* L. regulates the number of tumor infiltrating T cells to enhance antitumor effect in Lewis lung cancer-bearing mice]. *Xi Bao Yu Fen Zi Mian Yi Xue Za Zhi* 35 (2), 103–108.
- Zhang, Y., Liu, P., Li, Y., and Zhang, A.-H. (2017). Exploration of metabolite signatures using high-throughput mass spectrometry coupled with multivariate data analysis. *RSC Adv.* 7 (11), 6780–6787. doi:10.1039/c6ra27461g
- Zhang, A., Sun, H., Yan, G., and Wang, X. (2017). Recent developments and emerging trends of mass spectrometry for herbal ingredients analysis. *Trac Trends Anal. Chem.* 94, 70–76. doi:10.1016/j.trac.2017.07.007
- Zhao, L., Zhong, Y., Liang, J., Gao, H., and Tang, N. (2019). Effect of *Astragalus* polysaccharide on the expression of VEGF and EGFR in mice with Lewis transplantable lung cancer. *J. Coll. Physicians Surg. Pak* 29 (4), 392–394. doi:10.29271/jcpsp.2019.04.392
- Zhao, M., Liu, Y., Liu, R., Qi, J., Hou, Y., Chang, J., et al. (2018). Upregulation of IL-11, an IL-6 family cytokine, promotes tumor progression and correlates with poor prognosis in non-small cell lung cancer. *Cell Physiol Biochem* 45 (6), 2213–2224. doi:10.1159/000488166
- Zhao, Q., Cao, Y., Wang, Y., Hu, C., Hu, A., Ruan, L., et al. (2014). Plasma and tissue free amino acid profiles and their concentration correlation in patients with lung cancer. *Asia Pac. J. Clin. Nutr.* 23, 429–436. doi:10.6133/apjcn.2014.23.3.13
- Zhou, J., Deng, Y., Li, F., Yin, C., Shi, J., and Gong, Q. (2019). Icariside II attenuates lipopolysaccharide-induced neuroinflammation through inhibiting TLR4/MyD88/NF- κ B pathway in rats. *Biomed. Pharmacother.* 111 (3), 315–324. doi:10.1016/j.biopha.2018.10.201
- Zhu, H. L., Huang, C. L., Wang, W. J., Zhan, X. Q., and Fan, X. M. (2011). [Effects of andrographolide on the concentration of cytokines in BALF and the expressions of type I and III collagen mRNA in lung tissue in bleomycin-induced rat pulmonary fibrosis]. *Xi Bao Yu Fen Zi Mian Yi Xue Za Zhi* 27 (7), 725–729.
- Zhu, T., Wang, D. X., Zhang, W., Liao, X. Q., Guan, X., Bo, H., et al. (2013). Andrographolide protects against LPS-induced acute lung injury by inactivation of NF- κ B. *PLoS One* 8 (2), e56407. doi:10.1371/journal.pone.0056407
- Zhu, Z. T., Jiang, X. S., Wang, B. C., Meng, W. X., Liu, H. Y., and Tian, Y. (2011). Andrographolide inhibits intimal hyperplasia in a rat model of autogenous vein grafts. *Cell Biochem Biophys* 60 (3), 231–239. doi:10.1007/s12013-010-9144-6
- Łuczaj, W., Moniuszko, A., Rusak, M., Zajkowska, J., Pancewicz, S., and Skrzydlewska, E. (2015). Peroxidative metabolism of arachidonic acid in the course of Lyme arthritis. *Ann. Agric. Environ. Med.* 22 (3), 433–437. doi:10.5604/12321966.1167708

Conflict of Interest: The authors declare that the research was conducted in the absence of any commercial or financial relationships that could be construed as a potential conflict of interest.

Copyright © 2021 Luo, Jia, Zhang, Wang, Ren and Zhang. This is an open-access article distributed under the terms of the Creative Commons Attribution License (CC BY). The use, distribution or reproduction in other forums is permitted, provided the original author(s) and the copyright owner(s) are credited and that the original publication in this journal is cited, in accordance with accepted academic practice. No use, distribution or reproduction is permitted which does not comply with these terms.



Huanglong Antitussive Granule Relieves Acute Asthma Through Regulating Pulmonary Lipid Homeostasis

Hua Yan^{1†}, Guiying Qian^{2†}, Rui Yang¹, Zichen Luo^{1,3}, Xianzheng Wang¹, Tong Xie^{1*}, Xia Zhao^{1*} and Jinjun Shan^{1,3}

¹Jiangsu Key Laboratory of Pediatric Respiratory Disease, Institute of Pediatrics, Affiliated Hospital of Nanjing University of Chinese Medicine, Nanjing, China, ²Changshu Hospital Affiliated to Nanjing University of Chinese Medicine, Changshu, China, ³Jiangsu Engineering Research Center for Efficient Delivery System of TCM, School of Pharmacy, Nanjing University of Chinese Medicine, Nanjing, China

OPEN ACCESS

Edited by:

Adolfo Andrade-Cetto,
National Autonomous University of
Mexico, Mexico

Reviewed by:

Amit Krishna De,
Indian Science Congress Association,
India
Jia Liu,
Institute of Basic Research in Clinical
Medicine, China

*Correspondence:

Tong Xie
xietong@njucm.edu.cn
Xia Zhao
zhaoxiahy@njucm.edu.cn

[†]These authors have contributed
equally to this work

Specialty section:

This article was submitted to
Ethnopharmacology,
a section of the journal
Frontiers in Pharmacology

Received: 21 January 2021

Accepted: 25 March 2021

Published: 23 April 2021

Citation:

Yan H, Qian G, Yang R, Luo Z, Wang X,
Xie T, Zhao X and Shan J (2021)
Huanglong Antitussive Granule
Relieves Acute Asthma Through
Regulating Pulmonary
Lipid Homeostasis.
Front. Pharmacol. 12:656756.
doi: 10.3389/fphar.2021.656756

Background: Asthma is a respiratory disease with chronic airway inflammatory, and individuals with asthma exacerbations is one of the most frequent causes of hospitalization. Huanglong antitussive granule (HL Granule), a Chinese proprietary herbal medicine, has been proved to be effective in the clinical treatment of pulmonary disease. This study is devoted to the pharmacodynamics of HL Granule in acute asthma and the possible mechanism from the perspective of lipidomics.

Methods: Mice were divided into four groups, control group, acute asthma model group, HL Granule treatment and montelukast sodium treatment group. Acute asthma was induced by ovalbumin (OVA). Histopathology, pulmonary function and enzyme linked immunosorbent assay (ELISA) were used to validated model and effect of HL Granule. Lipids were detected by ultra-high-performance liquid chromatography coupled to hybrid Quadrupole-Exactive Orbitrap mass spectrometry (UHPLC-Q-Exactive Orbitrap MS) and identified by MS-DAIL and built-in Lipidblast database. Differentially expressed lipids recalled in HL Granule treatment group were extracted for heatmap, enrichment analysis and correlation analysis.

Results: HL Granule was effective in decreasing airway hyperresponsiveness (AHR), airway inflammatory and the levels of IL-4 and IL-5. A total of 304 and 167 lipids were identified in positive and negative ion mode, respectively. Among these, 104 and 73 lipids were reserved in HL Granule group ($FDR < 0.05$), including acylcarnitine (ACar), fatty acid (FA), lysophosphatidylcholine (LPC), phosphatidylcholine (PC), lysophosphatidylethanolamine

Abbreviations: ACar, acylcarnitine; AHR, airway hyperresponsiveness; BALF, bronchoalveolar lavage fluid; Cer, ceramide; DG, diglyceride; ELISA, Enzyme linked immunosorbent assay; FA, fatty acid; HL Granule, Huanglong antitussive granule; LC-MS, liquid chromatography-mass spectrometry; LPC, lysophosphatidylcholine; LPE, lysophosphatidylethanolamine; OVA, ovalbumin; PC, phosphatidylcholine; PCe, ether-linked phosphatidylcholine; PE, phosphatidylethanolamine; PEE, ether-linked phosphatidylethanolamine; Penh, enhance pause; PG, phosphatidylglycerol; PI, phosphatidylinositol; PS, phosphatidylserine; SM, sphingomyelin; TG, triglyceride; TIC, total ion chromatograms; UHPLC-Q-Exactive Orbitrap MS, ultra-high-performance liquid chromatography coupled to hybrid Quadrupole-Exactive Orbitrap mass spectrometry

(LPE), phosphatidylethanolamine (PE), phosphatidylglycerol (PG), phosphatidylinositol (PI), phosphatidylserine (PS), diglyceride (DG), triglyceride (TG), sphingomyelin (SM) and ceramide (Cer). Furthermore, 118 and 273 correlations among 47 and 96 lipids in the positive and negative were observed, with ether-linked phosphatidylethanolamine (PEe) and phosphatidylcholine (PCe) ($FDR < 0.001$, Spearman correlation coefficient $r^2 > 0.75$).

Conclusion: HL Granule might improve pulmonary lipid homeostasis and could be used as an alternative or supplementary therapy in clinical for the treatment of asthma.

Keywords: acute asthma, treatment, huanglong antitussive granule, lipidomics, pulmonary lipids

INTRODUCTION

Asthma is a common chronic respiratory disease, characterized by respiratory symptoms and airflow limitation that vary over time, with different degrees of chronic airway inflammation and remodeling (Papi et al., 2018). In patients with asthma, acute exacerbation is defined as the changes of previous state, including symptoms, such as wheezing, shortness of breath, chest tightness and cough that recurrence or aggravation with decreasing respiratory function (Kostakou et al., 2019). Environmental determinants, such as allergen, polluted air, smoking, respiratory tract infection, etc. are known to induce asthma (Khreis et al., 2017; Neophytou et al., 2018; Mikhail and Grayson, 2019). Among them, infection is the main cause of acute asthma in children of any age, followed by allergy in school-age children (Dondi et al., 2017). Epidemiological studies show that the global prevalence of asthma is increasing (Lundbäck et al., 2016). The prevalence continues in low-and middle-income countries with lower incidence before, such as China, while may have reached a stable period in high-income countries with high incidence, such as Europe (Lundbäck et al., 2016; Huang et al., 2019; Rodriguez et al., 2019). Acute asthma is mainly a disease occurring in early childhood and the most common cause of hospitalization in children. There were 640,000 children visiting the pediatric emergency department every year, causing serious social and economic burden (Pardue Jones et al., 2016; Saglani et al., 2019). Moreover, acute asthma not only affects the quality of life in children, but also may develop into respiratory failure, even life-threatening if seriously. In Europe, about 15,000 people die a year due to asthma (Ferguson et al., 2017).

Currently, the interventions available for acute asthma remain relatively limited. The commonly used drugs for asthma are β_2 -adrenergic agonists, corticosteroids (ICSs) and leukotriene modifiers, usually montelukast sodium (Ramsahai et al., 2019). Montelukast sodium, a highly selective leukotriene receptor antagonist, has significantly contributed to asthma control, e.g., reducing asthma severity, especially early wheezing and disease control, over the past 20 years, and was demonstrated decreased peripheral blood eosinophil and induced inhibition of both early and late phase bronchoconstriction in asthma patients. In clinical practice, many doctors prefer montelukast sodium over ICSs (Valentovic, 2007; Lee and Kim, 2020). However, the United States Food and Drug Administration (FDA) recently reminded a black box warning of montelukast sodium, which is severe neuropsychiatric adverse reactions and has been added to

the latest Global Initiative of Asthma (GINA) (Glockler-Lauf et al., 2019; Global Strategy for Asthma Management and Prevention Global Initiative for Asthma (GINA), 2020). At present, traditional Chinese medicine (TCM), whether used alone or in combination with conventional asthma medication, has been widely applied to asthma treatment in China. Furthermore, TCM may propose possible explanations to explain asthma heterogeneity. TCM emphasizes the holistic concept and dialectical treatment that the human body is an organic whole, and a disease may have different treatments with different syndrome differentiations. In present study, HL Granule, a Chinese proprietary herbal medicine, has been widely used in various respiratory diseases, such as asthmatic bronchitis, cough variant asthma and other diseases with cough and wheeze (Naiming, 2004; Wenjin, 2018; Yin, 2019). According to the theory of TCM, the reason that asthma recurrent episodes is the phlegm *in vivo* all the time, which induces asthma on the premise of deficiency of healthy qi. HL Granule has the effect of tonifying kidney Qi, cleaning lung, relieving cough, calming panting, as well as ameliorating expectoration of phlegm., which is composed with *Astragalus atripilosulus* (Huangqi), *Epimedium brevicornu* (Yinyanghuo), *Platycodon grandiflorum* (Jiegeng), *Pheretima* (Dilong), *Belamcanda chinensis* (Shegan), *Houttuynia cordata* (Yuxingcao), *Ephedra sinica* (Mahuang), *Crataegus pinnatifida* (Shanzha) and *Lepidium apetalum* (Tinglizi) (**Supplementary Table S1**). However, no study has explored the efficacy and mechanism of HL Granule in the treatment of asthma. Therefore, in the study, we focused on the pharmacodynamics and possible mechanism of HL Granule while treating acute asthma, and explored the possibility of HL Granule as a supplementary or alternative therapy for montelukast sodium.

Lipidomics is a branch of metabolomics and the separate discipline that studies lipids systematically. Lipids are one of the most important components of living organisms, which can be divided into eight categories, including fatty acids, glycerides, phospholipids, sphingolipids, glycolipids, polyketide, sterols and isoamylenol ester (Fahy et al., 2011; Zhang et al., 2018). Changes in various biological processes will cause changes in lipids. Meanwhile, lipid changes are involved in various biological processes, including energy metabolism, cell membrane-related functions, signal molecules, inflammatory reactions, biomacromolecule-recognition signals, etc. (Barrera et al., 2013). Most of the intracellular life activities occur at the metabolic level, which reflect the environment of cells, and the

fluctuation of metabolites represent the complete pathophysiological characteristics including the interaction between heredity and environment (Kelly et al., 2017), while asthma is a complex disease that involves the interplay of genes and environmental factors. Studies have shown that lipid metabolism of asthmatic patients in bronchoalveolar lavage fluid (BALF) is disturbed (Kang et al., 2014). Lipids with significant changes, on the one hand, may be used as biomarkers (Ackerman et al., 2016; Trinh et al., 2016); on the other hand, play an important role in innate immunity and inflammation (MacEyka and Spiegel, 2014; O'Donnell et al., 2018). Therefore, the pharmacodynamic mechanism of HL Granule in an acute model of asthma was studied on the basis of lipidomics.

In present study, firstly, we detected pulmonary function, histopathology and inflammatory factors to evaluate the model and the curative effect of HL Granule. Afterward, on the basis of established stable and effective lipid analysis method (Yang et al., 2019), we used liquid chromatography-mass spectrometry (LC-MS) technology to research the changes of lipids in the lung tissue. Lastly, we constructed a lipid map of acute asthma and analyzed the regulatory effect of HL Granule on disordered lipids to explore the possible pharmacodynamic mechanism of HL Granule in the treatment of acute asthma.

METHODS AND MATERIALS

Chemicals and Regents

HL Granule (Lot No, 190107121) was purchased from Shanxi Dongke Pharmaceutical (Shanxi, China). Montelukast Sodium Oral Granule (Lot No, 829966) was purchased from Mercksharp and DohmeCorp (Inc. Kenilworth, NJ, United States). Standards of astragaloside IV (Lot No, 140321), icariin (Lot No, 18012906), irisflorelin (Lot No, 20041001), citric acid (Lot No, 19061002), quercetin 3-O- β -D-glucose-7-O- β -D-gentiobioside (Lot No, 19112806), deapio-platycodin D (Lot No, 19070307), platycodin D2 (Lot No, 19070306), deapio-platycodin D2 (Lot No, 19070308) and polygalacin D (Lot No, 170623) were from Chengdu Pufei De Biotech (Chengdu, China). Standards of astragalosid I (Lot No, 120525), astragaloside II (Lot No, 120528), calycosin (Lot No, 120615), calycosin-7-O-beta-D-glucoside (Lot No, 120819) and platycodin D (Lot No, 120826) were from Chengdu Herbpurify (Chengdu, China). Standards of ephedrine hydrochloride (Lot No, 171241-200506) and pseudoephedrine hydrochloride (Lot No, 171237-200806) were from National Institutes for Food and Drug control (Beijing, China). Standards of 3-O- β -D-glucopyranosyl platycodigenin (Lot No, P27A9S60106), platycodin D3 (Lot No, P28M8F32837) and platycoside E (Lot No, P06M10S81977) were from Shanghai Yuanye Biotech (Shanghai, China). The standard of deapio-platycoside E/platycoside g1 (Lot No, FY37239B0234) was purchased from Nantong Feiyu Biotech (Nantong, China). Ovalbumin (OVA) was obtained from Sigma-Aldrich (St. Louis, MO, United States).

High performance liquid chromatography (HPLC) grade acetonitrile, methanol, formic acid, ammonium formate and

ammonium acetate were purchased from Merck (LiChrosolv, Merck, Darmstadt, Germany). MS grade isopropanol was from ROE Scientific (United States). Standards of lysoPE (17:1) (Lot No, LM171LPE-11), SM (17:0) (Lot No, 170SM-13), TG (17:0/17:1/17:0 D5) (Lot No, 170/171/170TG(DG)-10) and PE (17:0/17:0) (Lot No, LM170PE-19) were obtained from Avanti Polar Lipids (AL, United States).

Components' Detection of HL Granule

HL Granule was dissolved in double distilled water, and ultrasound extracted for 30 min by methanol. The extraction was centrifuged by 12,000 rpm/min at 4°C for 10 min, and supernatant was injected into the instrument for components' detection. Chromatographic separation was performed on Waters ACQUITY UPLC H-CLASS system (Waters, Milford, MA, United States) with a AQUITY UPLC HSS T3 column (2.1 \times 100 mm, 1.8 μ m, United States). The column compartment was maintained at 35°C. The mobile phase was consisted of solvent A (0.1% formic acid in water) and solvent B (0.1% formic acid in acetonitrile). Gradient conditions were as follows: 0 min, 10% B, 0–23 min, 10%–90% B, 23–24 min, 90% B, 24–26 min, 90%–10% B, 26–30 min, 10% B, at a flow rate of 0.2 ml/min.

Mass spectrometry data was acquired by LTQ ORBITRAP XL mass spectrometer system (Thermo Scientific, United States) both in the positive and negative ionization mode. The temperature of the heated capillary was 270°C and that of the ESI probe was 300°C. The flows of sheath gas and auxiliary gas were set to 40 and 10 units, respectively. The scan range of the Orbitrap analyzer was m/z 500–1800 and MSⁿ data were acquired by LTQ in data dependent acquisition mode. Both of the positive and negative adopted the same MS parameters.

Experimental Animals

Female C57BL/6J mice (6 weeks old) were purchased from Nanjing Qinglongshan animal farm (Certificate number 201909516, Jiangsu, China). All the animal experiments were approved by the Animal Care and Use Committee of Nanjing University of Chinese medicine (Permit number: 201903A018). Before experiments, mice were housed in a facility free of specific pathogens and had one-week adjustment period.

Mice were divided into four groups, ten mice per group: control group, acute asthma model group, HL Granule treatment group and montelukast sodium treatment group. Acute asthma model was induced by ovalbumin (OVA). In detail, on the first and 14th day, mice were sensitized by intraperitoneal (IP) injection with 0.2 ml sensitizing solutions, containing 20 μ g OVA and 1 mg aluminum hydroxide. From day 20, mice inhaled 3% (wt/vol) atomized OVA for 30 min by using an ultrasonic nebulizer (Yuwell, Nanjing, China) for four consecutive days. On the 19th day, model mice were divided into three groups according to different treatments, i.e., model group, HL Granule group and montelukast sodium group, and individually oral gavaged with double distilled water (0.1 ml/10 g) (model group), HL Granule (9.1 g/kg/d) (HL Granule group), and montelukast sodium (1.52 mg/kg/d) (montelukast sodium group)

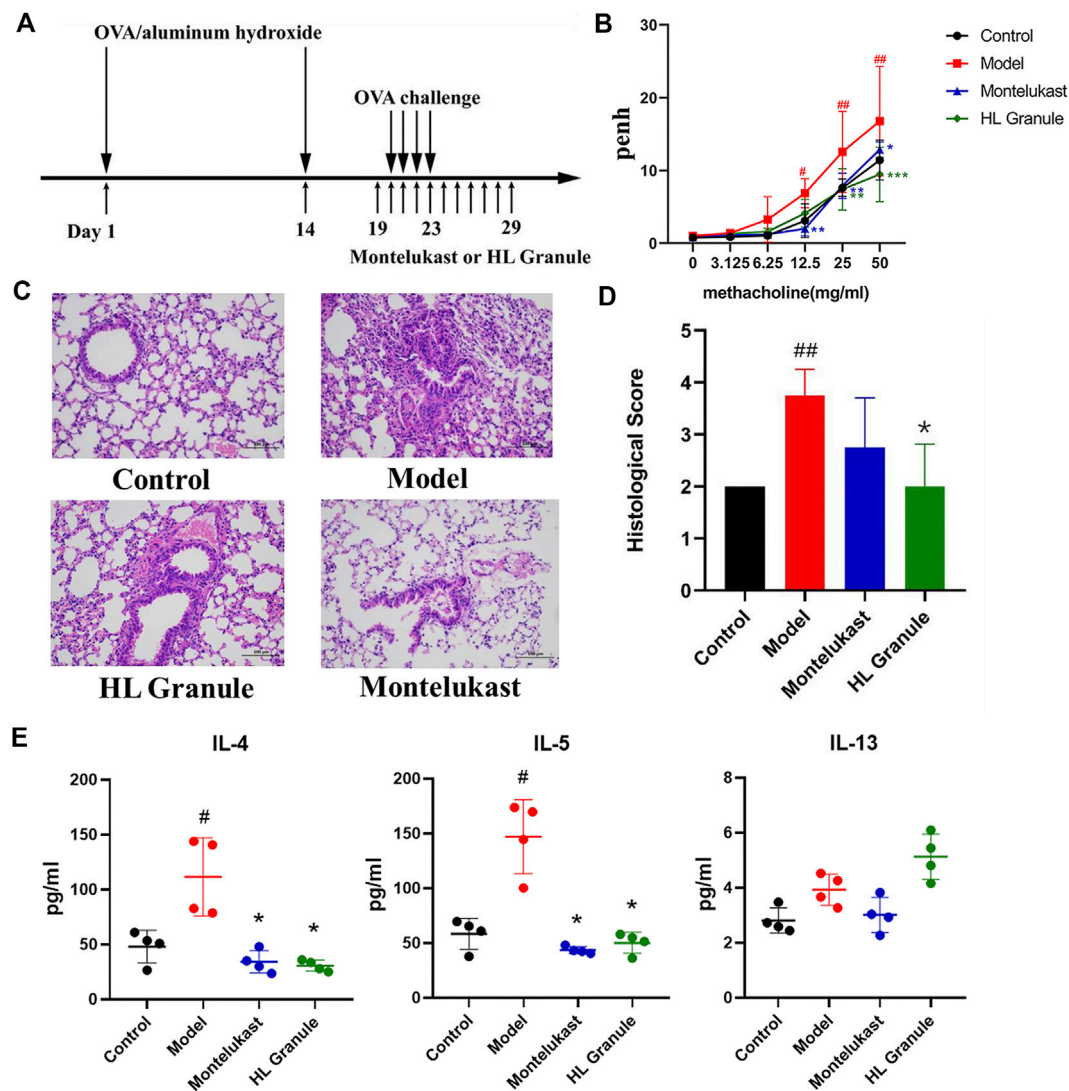


FIGURE 1 | The protective effect of HL Granule on acute asthma in mice. **(A)** The flowchart of induced and treatment in the model of acute asthma. The model of acute asthma was established and sensitized by intraperitoneal injection of 0.2 ml OVA, followed by atomization of 3% OVA. **(B)** Penh in each group. The data was collected in response to gradient concentration (0, 3.125, 6.25, 12.5, 25, and 50 mg/ml) of inhaled MCh. **(C, D)** Representative HE staining pictures (x200, C) and histological scores, $n = 4$. **(E)** The expressions of IL-4, IL-5 and IL-13 in BALF by Elisa. Results are presented as mean \pm SD, statistics in **(B)** was using two-way ANOVA, $n = 3$; statistics in D and E were using Kruskal-Wallis test, $n = 4$; # $p < 0.05$, ## $p < 0.01$ compared to control group; * $p < 0.05$, compared to model group.

at 24 h intervals for seven consecutive days. Throughout the experiment, control group was given IP injections and inhalation of saline following the same procedure as acute asthma model, and was administered by gavage with double distilled water (0.1 ml/kg) from day 19–25. The procedure has been summarized in **Figure 1A**.

Histopathology and Biochemical Analysis

Histopathology. Lung tissue sections were stained with hematoxylin and eosin (HE) to investigate the pathological changes. Histological scores were graded from 0 (normal) to 4 (severe) based on Inflammatory cell infiltrated in peribronchiolar and alveolar wall, degeneration, necrosis or exfoliation of

bronchial epithelium, the integrity of alveolar wall, mucus secretion and goblet cell proliferation.

Pulmonary function analysis. Pulmonary function was evaluated by Whole Body Plethysmography (Emka Technologies, France) after the last administration. The airway was stimulated with increasing concentrations of aerosolized methacholine (MCh) (0, 3.125, 6.25, 12.5, 25, 50 mg/ml). Then, enhanced pause (Penh) was determined to evaluate the bronchoconstriction function.

Enzyme linked immunosorbent assay (ELISA). ELISA kits were used to detect the expression of Interleukin-4 (IL-4), Interleukin-5 (IL-5) (Biolegend, San Diego, CA) and Interleukin-13 (IL-13) (Yi Fei Xue Biotechnology, China) in BALF.

Statistical Analysis

Data are expressed as mean \pm standard deviation (SD) in scatter plots and column bar graphs. Box-whisker Plot shows median, lower, and upper quartiles, as well as minimum and maximum values. GraphPad Prism 8.0.2 (GraphPad Software, United States) was used to analyze data by Mann-Whitney non parametric test for two unmatched groups and one-way ANOVA or two-way ANOVA for multiple comparisons. Enrichment *p*-values are given by the Kolmogorov-Smirnov-test. *p* < 0.05 is considered significant.

Untargeted Lipidomics Analysis With UHPLC-Q-Exactive Orbitrap MS

Lipid Extraction for Detection. A total of 20 mg lung tissue was used to extract lipids by the MTBE/MeOH/H₂O system. First, tissue homogenate was extracted by 225 μ l ice methanol solution containing internal standards (LPE (17:1), SM (17:0), TG (17:0/17:1/17:0) and PE (17:0/17:0), 5 μ g/ml). After vortexing for 10 s, 750 μ l MTBE was added, and the mixture was vortex for 10 min. Subsequently, 188 μ l of deionized water was added and the mixture was vortexed for 20 s. After centrifuging 2 min by 14,000 rpm at 4°C, the upper phase was dried in a vacuum concentrator. Finally, the upper phase lipid was reconstituted in the mixed solvent of methanol: toluene (9:1, v/v) for lipidomic analysis.

Quality Control Samples. The preparation was carried out by mixing equal aliquots of 5 μ l from each sample, and their pretreatment was carried out in the same manner as the samples. Five QCs were injected before samples, while one QC injection was inserted regularly after every 10 samples.

Chromatographic separation conditions. Untargeted lipidomics analysis of lung tissue was performed on an Ultra-high-performance liquid chromatography (Thermo Fisher Scientific, United States) coupled to hybrid Quadrupole-Exactive Orbitrap mass spectrometry (Thermo Fisher Scientific, United States). A reversed phase Waters Acquity UPLC CSH C18 (100 mm \times 2.1 mm, 1.7 μ m) maintained at 60°C was used for the chromatographic separation of lipids. The flow rate was set at 0.3 ml/min. Mobile phase A were ACN/H₂O (6:4, v/v), and B IPA/ACN (9:1, v/v), both containing 10 mM ammonium formate and 0.1% formic acid for positive ionization mode. For the negative ionization mode, 10 mM ammonium acetate was used as buffer system. The elution gradient started with 15% B for 4 min, and then increased from 15 to 48% B in 1 min, from 48 to 82% B in 17 min, and from 82 to 99% B in 1 min, and maintained for 1 min, back to 15% B at 24.2 min and maintained for 5.8 min to equilibrate column.

Mass Spectrometer Conditions. The mass spectrometer was operated with the following parameters: spray voltage 3.5 kV (positive) and 3.0 kV (negative). For both ionization modes, the sheath gas and aux gas were separately maintained at 35 and 15 arbitrary units, while the capillary temperature and the heater temperature were 325 and 300°C, respectively. The MS/MS data was acquired by data dependent method and top 10 abundant ions were used for fragmentation. The normalized collision energy (NCE) was set 25, 35, and 45 eV, respectively.

Data processing of lipidomics. Data deconvolution, lipid identification and alignment were analyzed by MS-DIAL 3.3 (MS-DIAL software, Japan). The output data matrix was exported for further statistical analysis. MetaboAnalyst 4.0 (metaboanalyst.ca/faces/ModuleView.xhtml) was used for multivariate analysis. Principal component analysis and heatmap were performed for cluster and visulation. Furthermore, lipid metabolites enrichment analysis was based on ChemRICH (<http://chemrich.fiehnlab.ucdavis.edu/>) (Barupal and Fiehn, 2017). The differentially expressed lipids were screened using the Kruskal-Wallis test and Mann-Whitney test by R 3.6.3. Correlation analysis was conducted using Spearman correlation and visualized with Cytoscape 3.8.2 (Cytoscape software, United States).

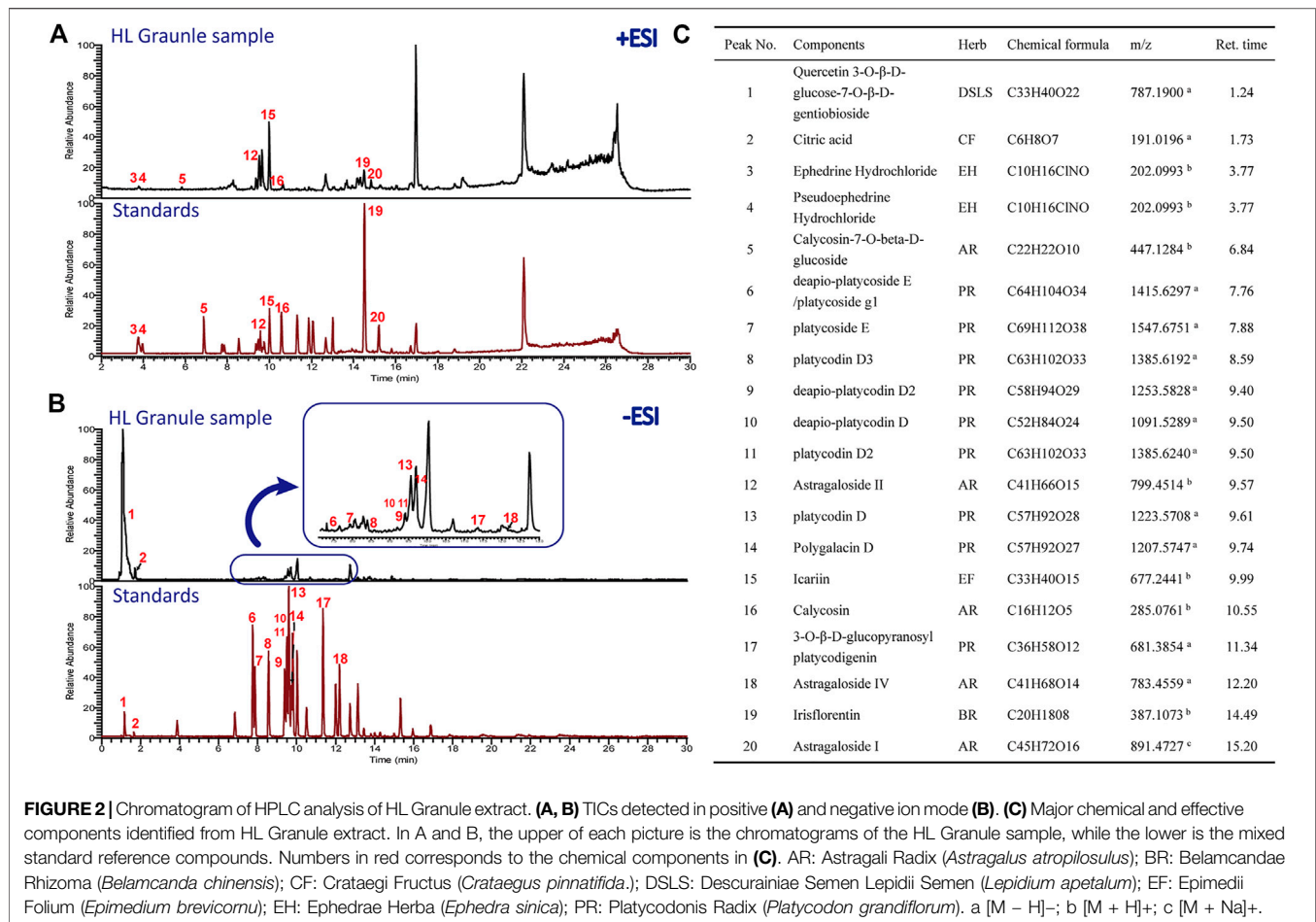
RESULTS

Quality Control of HL Granule by UHPLC-ESI/LTQ-Orbitrap-MS

The chemical profile of HL Granule was firstly analyzed by UPLC-ESI/LTQ-Orbitrap-MS. Both of the positive and negative ionizations were used. A total of 20 components belonging to seven crude materials were qualitative identified based on the standard compounds (**Figure 2**). Flavones and saponins in *Astragalus atropilosulus*, saponins in *Platycodon grandiflorum*, and alkaloids in *Ephedra sinica* were considered as the effective components. The typical total ion chromatograms (TICs) are shown in **Figure 2**. The results laid a foundation for the effectiveness and safety of HL Granule used in this study for asthma treatment.

Curative Effect of HL Granule in The Treatment of Acute Asthma in Mice

To develop an acute asthma like symptoms, OVA was used for sensitization and challenge (**Figure 1A**). At the end of the challenge period, airway hyperresponsiveness (AHR) was evaluated by calculating the enhance pause (Penh). The results showed that Penh increased significantly in model group (*p* < 0.05, 12.5 mg/ml methacholine; *p* < 0.01, 25 mg/ml, 50 mg/ml methacholine), and HL Granule could reverse AHR (*p* < 0.01, 25 mg/ml, 50 mg/ml methacholine, **Figure 1B**). The results suggested that HL Granule inhibited the bronchoconstriction and improved AHR. Then, inflammatory cell infiltration and airway remodeling were observed by histopathological examination. The results demonstrated that the inflammatory cell infiltration around the trachea and alveolar wall were more serious in the model group without airway remodeling, while HL Granule and montelukast sodium could relieve the inflammatory cell infiltration (**Figure 1C**). The HE staining was scored semi-quantitatively based on inflammatory cell infiltrated, mucus secretion and goblet cell proliferation mainly in airway and alveoli. Histopathological scores confirmed that HL Granule ameliorated OVA induced inflammatory changes and significantly reduced total leukocyte counts (**Figure 1D**).



Moreover, the curative effect of HL Granule was slightly better than montelukast sodium in alleviating lung pathology (Figure 1D).

T helper 2 (Th2) cell-mediated immunity is considered as an important role in the pathogenesis of asthma. Eosinophils and CD4⁺ cells producing interleukin-5 (IL-5) are frequently found in the blood and lung lavage fluid. To observe the Th2 cell mediated immunity, the levels of IL-4, IL-5, and IL-13 in BALF were analyzed in acute asthma model and the curative effect of HL Granule. The results showed that the levels of IL-4 and IL-5 increased significantly in asthmatic mice ($p < 0.05$). Administration of HL Granule significantly reduced IL-4 and IL-5 in BALF by 65.9 and 72.5% compared with those of the OVA groups ($p < 0.05$) (Figure 1E). In summary, the results suggested that HL Granule could be used in acute asthma treatment, and might be considered for replacing montelukast sodium as an adjuvant treatment of asthma. However, there was no significant change to IL-13.

Lipidomic Profiling of HL Granule Treatment of Acute Asthma

Lipids play a central role in lung physiology and pathology. The role of lipids in lung and respiratory disease has attracted more

attention in recent years, including cystic fibrosis, asthma and COPD, which are all associated with abnormal metabolism. To examine the lipid changes of OVA induced asthmatic mice, the lipid profile of lung tissue was analyzed. A total of 304 and 167 lipid molecular species sorted into five lipid categories and 22 lipid subclasses were confidently annotated based on the database matching in the positive and negative ion mode (Figure 3A). The most commonly identified lipid species in the developing method belonged to glycerophospholipids, which were dominant with 57.89% in total. Glycerophospholipids were found in the highest amounts in the membranes of all cells. Glycerolipids were account for 18.00%, which are considered as the quantities in fat stores. Additionally, sphingolipids were minor components, and only account for 5.98%. In summary, glycerophospholipids, sphingolipids, fatty acyls and glycerolipids were all important lipids in lung tissue of acute asthma.

Then, pooled QC samples were used to monitor the analytical performance. In order to evaluate and remove the systematic error, different normalization methods were applied after peak picking up and lipid annotation. The results showed the QC samples were clustered together by the random forest (SERRF) method, indicating that a robust data matrix can be obtained by the SERRF method (Figures 3B,C). Then, PCA models were applied to the

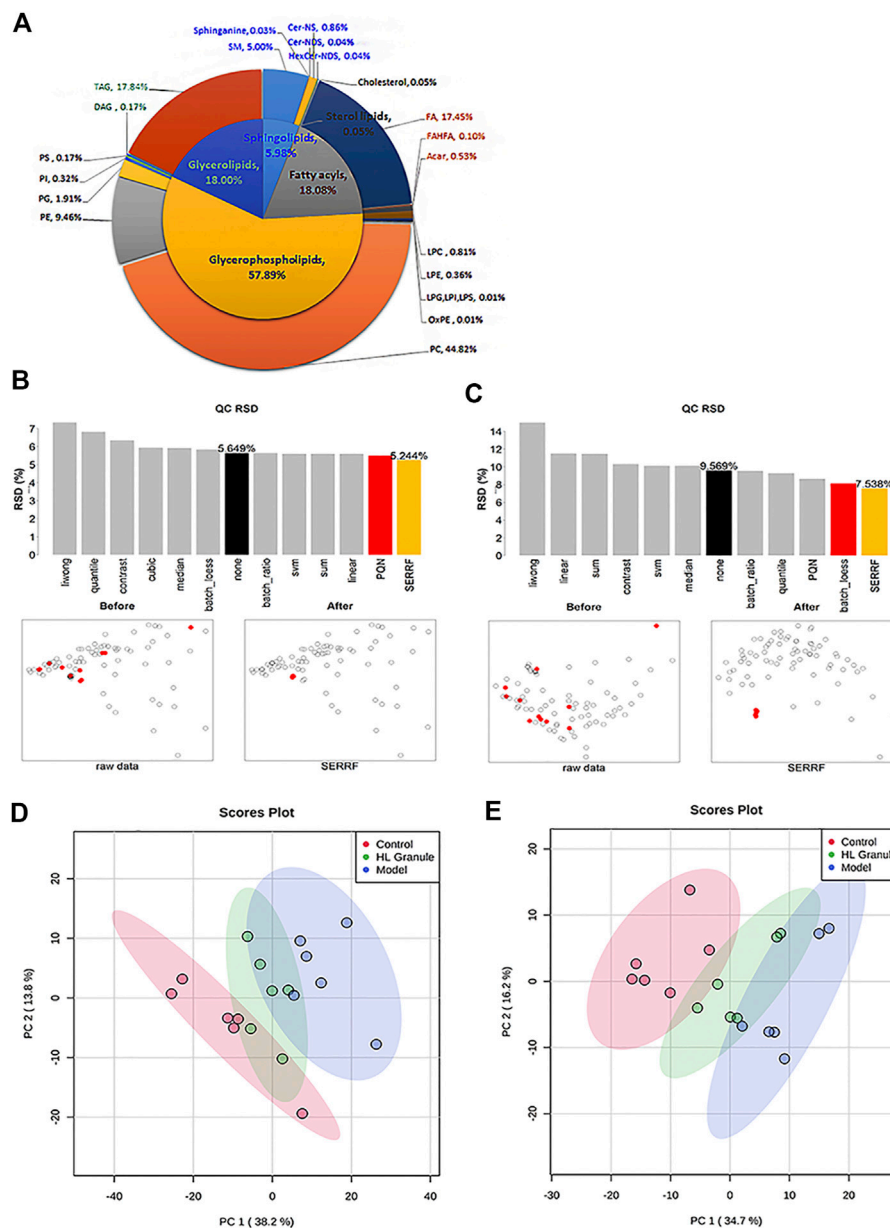


FIGURE 3 | lipids related to HL Granule treatment of acute asthma. **(A)** Double pie chart of lipids detected in lung tissue of acute asthma mice in positive and negative ion mode. **(B, C)** RSD and scatter plots of lipids in samples and QCs after normalization in positive **(B)** and negative ion mode **(C)**. **(D, E)** PCA of lipids in lung of mice in positive **(D)** and negative ion mode **(E)**, $n = 6$.

positive and negative lipidomic data respectively. For the positive lipidomic data, the first two components explained about 50% variables (PC1 = 38.2%, PC2 = 13.8%). For the negative lipidomic data, the first two components explained about 50.9% variables (PC1 = 34.7%, PC2 = 16.2%). The PCA score plots indicated that the component one can distinguish the observations of control and acute asthma obversions (**Figures 3D,E**). Remarkably, all the observations of HL Granule treatment appeared to cluster from the model group to the control group, suggesting that HL Granule could regulate lipids disorder in lung tissue of OVA

induced asthmatic mice. The score plot from negative data showed the same cluster profiles.

Characterization of Differentially Expressed Lipids

To compare the inter groups, the Kruskal Wallis test was used. Correspondingly, to verify the hypothesis about the irrelevance of differences between two groups, the Mann-Whitney test was used. A total of 162 lipids in the positive and 109 lipids in the negative were significantly changed after the OVA induced asthma,

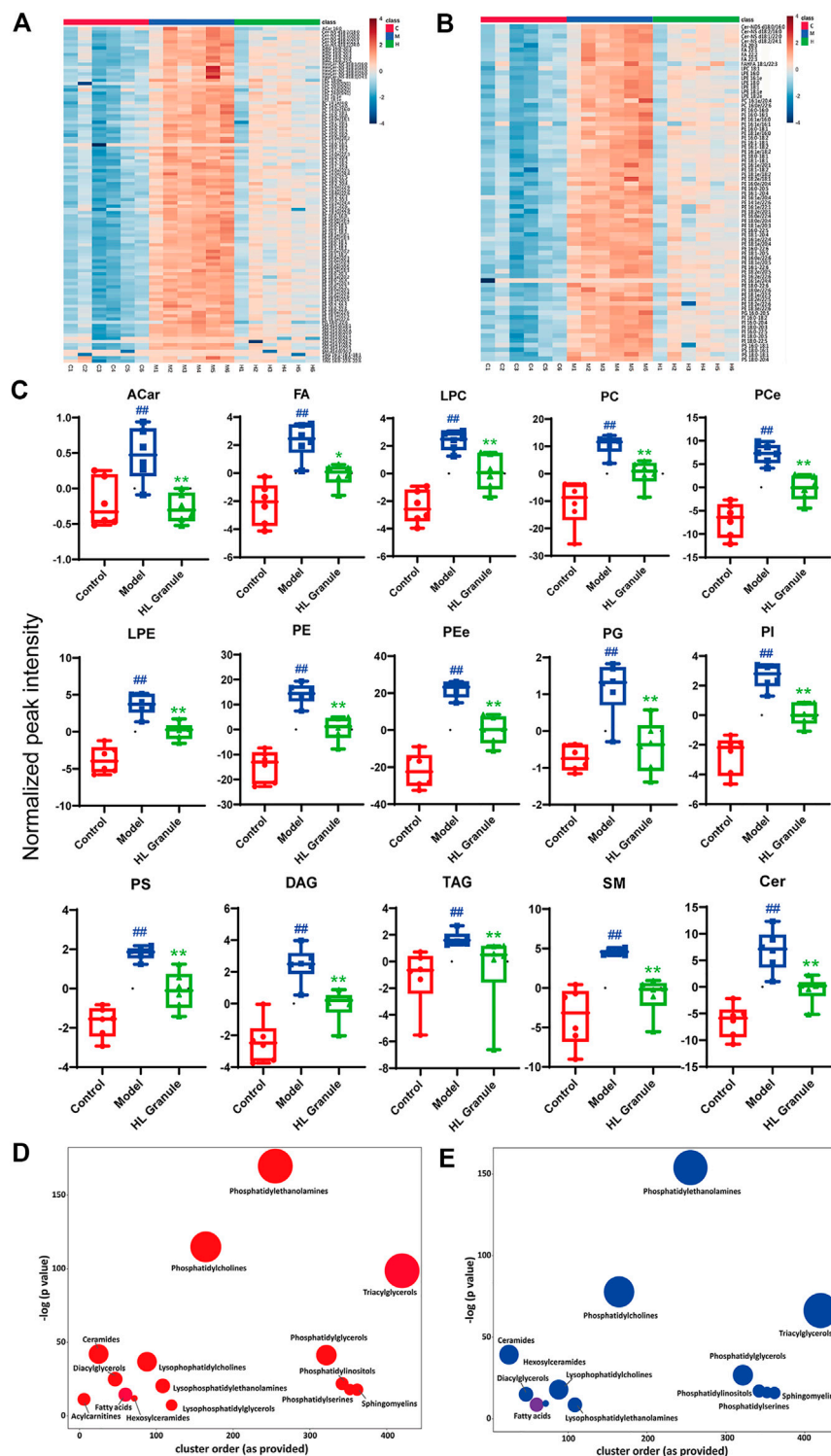


FIGURE 4 | Summary of differentially expressed lipids. **(A, B)** Heatmaps of differentially expressed lipids in positive **(A)** and negative **(B)** ion mode, $n = 6$. Each column represents a sample, each row represents a differential lipid, and each block represents the corresponding intensity value, red to blue of the corresponding lipid in each sample, representing the value from large to small. Differentially expressed lipids were reversed in HL Granule group compared to model group ($FDR < 0.05$). **(C)** Box-whisker Plot of differentially expressed lipid subclasses, in positive and negative ion mode, $n = 6$. **(D, E)** Enrichment statistics plot of significantly regulated lipids between model and control groups **(D)** as well as HL Granule and model groups **(E)**, $n = 6$. Each node reflects a significantly altered cluster of lipids. Enrichment p -values are given by the Kolmogorov-Smirnov-test. Node sizes represent the total number of lipids in each cluster set. The node color scale shows the proportion of increased (red) or decreased (blue) compounds. Purple-color nodes have both increased and decreased lipids. Results in (C) extends from 25th to 75th percentile and the line represents the median, the Mann-Whitney test was used between two groups, $n = 6$; # $p < 0.01$ compared to control group; ** $p < 0.01$, compared to model group.

including acylcarnitine (ACar), fatty acid (FA), lysophosphatidylcholine (LPC), phosphatidylcholine (PC), lysophosphatidylethanolamine (LPE), phosphatidylethanolamine (PE), phosphatidylglycerol (PG), phosphatidylinositol (PI), Phosphatidylserine (PS), diglyceride (DAG), triglyceride (TAG), sphingomyelin (SM) and ceramide (Cer). The lipids were considered upregulated if fold change (FC) > 2 and FDR < 0.05, and downregulated if FC < 0.5. The results from nonparametric tests showed that the lipid levels of OVA groups were significantly increased compared to control groups. Whereas, treatment of HL Granule significantly reduced the lipid levels. The differentially expressed lipids were illustrated by heatmaps (Figures 4A,B, Supplementary Tables S2, S3). Each square represents the intensity value of a specific lipid in a sample. The transition in color from red to blue represents the intensity value becoming smaller. The darker the red is, the larger the value is, and vice versa. As shown in heatmaps, under the condition of FDR < 0.05, a total of 104 lipids upregulated in the model group were reversed, including ACar, LPC, PC, LPE, PE, PG, DG, TG, SM and Cer, in positive ion mode (Figure 4A, Supplementary Table S2). In negative ion mode, a total of 73 lipids were found downregulated (FDR < 0.05), including FA, LPC, PC, LPE, PE, PI, PS, and Cer (Figure 4B, Supplementary Table S3). Box-whisker Plots of 15 major subclasses of differentially expressed lipids were shown, which confirmed the significant altered in lipids among control, model and HL Granule groups in lung tissue (Figure 4C). HL Granule could significantly downregulate the up-regulated lipids in model group by regulating the disorder of ACar, FA, LPC, PC, LPE, PE, PG, PI, PS, DG, TG, SM, Cer, as well as ether-linked phosphatidylethanolamine (PEe) and phosphatidylcholine (PCe) in acute asthma.

Enrichment analysis helps to gain mechanistic insight into metabolite lists. As shown in Figures 4D,E, each node represents a significantly changed lipid group ($p < 0.05$) and the node size reflects the total number of lipids contained in each lipid group. The results showed that phospholipids, sphingolipids, fatty acids and glycolipids changed significantly. Among them, phospholipids, including PE, PC, and TG, contained the higher number of lipids and changed more significantly, suggesting that lipids were important in acute asthma, especially phospholipids. More specifically, compared with the control group, 15 lipid classes in the model group changed significantly (Figure 4D). Apart from fatty acids and triglycerides with partial downregulation, the other lipid classes showed an overall upward trend. After HL Granule treatment, 13 of them were recalled ($p < 0.05$) with overall downregulation and partial upregulation in fatty acids (Figure 4E).

Combined with the results of lipid molecular species and lipid subclasses, we speculated that HL Granule might regulate phospholipids, sphingolipids, fatty acids and glycolipids, especially phospholipids in lung tissue to relieve acute asthma. Therefore, we speculated that HL Granule may improve acute asthma by regulating lipids homeostasis in lung tissue.

Correlation of the Differentially Expressed Lipids

Spearman correlation was conducted for all differentially expressed lipids. On the basis of FDR < 0.001 and Spearman

correlation coefficient $r^2 > 0.75$, 118 and 273 notable correlations among 47 and 96 lipids in the positive and negative were observed, with PEe and PCe. As shown in Figure 5A, of the 118 edges, PE (16:0e/20:3), PC (18:0/20:5), PE (18:1e/20:4), PC (14:0e/22:5) and PC (16:0e/22:6) showed significant correlation (edges ≥ 12). PC and PE are the most abundant phospholipids in all mammalian cell membranes, which can contain ether-bonds at the sn-1 position and are thus sub-classified into alkylacyl phospholipids. Furthermore, as shown in Figure 5B, Cer-NS (d18:1/16:0), Cer-NS (d18:1/22:0), Cer-NS (d18:1/24:1), FA (22:5), PG (16:0-16:1), PS (18:0-20:3) exhibited suggestive correlation (edges ≥ 14). Indubitable, correlation between different classes of phospholipids existed. Additionally, polyunsaturated fatty acids showed more correlation with ceramide non hydroxyfatty acid-sphingosine (Cer-NS). Although the relationship between FA and Cer remains unclear in pulmonary disease, C16:0 ceramide has been identified as the principal mediator of obesity-derived insulin resistance and impaired fatty acid oxidation (Raichur et al., 2014). The high level of correlation between the lipids implied that HL Granule may regulate lipid homeostasis by interaction between lipids.

DISCUSSION

HL Granule is composed of nine traditional Chinese medicines, and it has been shown that several herbs functions well in the treatment of acute asthma. Theoretically, *Ephedra sinica* is considered to be effective, which may have the effects of dispersing external wind and calming latent wind. It was found that Mahuang-Tang, Mahuang-Xixin-Fuzi decoction and Shegan-Mahuang Decoction, which are consisted of *Ephedra sinica* and *Belamcanda chinensis*, mitigated airway inflammation and asthmatic airway hyperresponsiveness (He et al., 2018; Gan et al., 2020; Lin et al., 2020). *Lepidium apetalum*, *Platycodon grandiflorum* and *Pheretima* were also found effective in asthma by alleviating airway inflammation (Huang et al., 2016; Kim et al., 2019a; Lee et al., 2020). Recent evidence suggested that formononetin and calycosin, two flavonoids predominantly representing in *Astragalus atripilosulus*, could alleviate allergic asthma by protecting epithelial integrity via regulating and activating G protein coupled estrogen receptor (Yuan et al., 2020). For supplementary therapy, the coadministration of budesonide and the extracts of *Epimedium brevicornu* in asthma were better than budesonide individual treatment (Ma et al., 2020). Thus, it is considerable to treat asthma with a combination consisting of HL Granule, which was confirmed by our experiments.

Th2 cell-mediated immunity has dominated in the past 30 years of research on the pathogenesis of asthma. IL-4, IL-5 and IL-13 are signature cytokines in Th2 cell mediated immunity. Clinically, serum IL-4, IL-5 and IL-13 levels increased significantly in patients with acute asthma (Lee et al., 2001). Thus, we combined pulmonary function, histopathology, IL-4, IL-5, and IL-13 to observe the therapeutic effect of HL Granule. The results suggested that HL Granule could improve lung

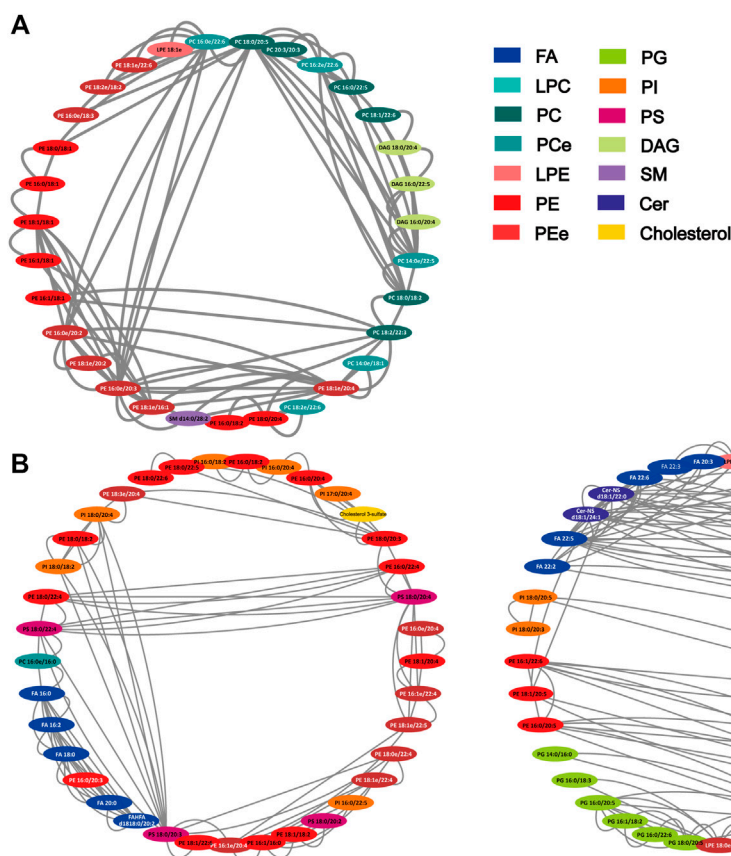


FIGURE 5 | Correlation network of differentially expressed lipids. **(A)** positive ion mode (47 nodes, 118 edges); **(B)** negative ion mode (96 nodes, 273 edges). The network was generated by Cytoscape 3.8.2 with attribute circle layout. Nodes were screened by FDR value <0.001 and Spearman correlation coefficient $r^2 > 0.75$. Edges represent the value of r^2 between two nodes.

function, reduce the inflammatory infiltration of lung tissue, especially around the airway, and decrease IL-4 and IL-5 expressions to relieve acute asthma, although airway remodeling was not obvious. However, some studies have shown that the thickness of airway smooth muscle, which is an important change in airway remodeling, is related to the severity of asthma, not to asthma progression (Hirota and Martin, 2013). Moreover, IL-13 induces excessive mucus production and goblet cell metaplasia (Kuperman et al., 2002). In our model, few mucus and goblet cells were observed by pathological results, which may be one of the reasons for no significant changes to IL-13.

Lipidomics is considered to be an indispensable tool for the researches of many diseases and physiological processes, and has been used to study inflammation-related diseases (Zhang et al., 2018). Clinical findings elucidated that lipid metabolism disorders are frequently observed in asthma patients (Kang et al., 2014; Gai et al., 2019). Therefore, regulating lipid homeostasis for asthma treatment is crux. Presently, there are few studies on the mechanism of regulating lipids on therapeutic drugs for asthma. In our study, we have studied the mechanism of HL Granule regulating lipid homeostasis.

Several studies show a significant treatment of asthma by components from traditional Chinese Medicine according to the regulation of lipid homeostasis. Metabolomics combined with network pharmacology clarified that *Astragalus atopilosulus* regulated arachidonic acid metabolism and ether lipid metabolism (Wang et al., 2019). *Platycodon grandiflorum* and *Crataegus pinnatifida* ethanol extracts, as well as *Ephedra sinica* methanol extracts may also improve lipid metabolism (Lee et al., 2017; Kim et al., 2019b; Lee et al., 2019). Remarkably, ephedrine, astragaloside IV, calycosin and icariin, which were detected and identified in present study, may be linked to lipids alterations. The chronic-effect study of ephedrine determined that brown adipose tissue (BAT) activity was significantly reduced after a 28 days ephedrine treatment (Carey et al., 2013; Carey et al., 2015). Studies in liver found that astragaloside IV attenuated lipid accumulation in an AMPK-dependent manner (Zhou et al., 2017), while hairy calycosin could effectively control the lipid peroxidation, reduce the levels of serum free fatty acid, and improve the steatosis (Liu et al., 2019). In addition, many studies have shown that the metabolites of icariin have a lipid-lowering effect, which has attracted widespread attention in recent years (Wang et al., 2020). Thus, HL Granule has

advantages in regulating lipid homeostasis. However, further studies are needed to explore the detailed mechanism among them.

To explore the mechanism of HL Granule in regulating lipid homeostasis, we used high-resolution lipidomics analysis based on UHPLC-Q-Exactive Orbitrap MS to recognize potential disease-related lipid changes in lung tissue. The method allows to detect a total of 304 and 167 lipids in positive and negative ion mode, of which 162 and 109 lipids in the model group were upregulated (FDR < 0.05, Fold change >2 or Fold change <0.5). Among them, HL Granule could reverse 104 and 73 lipids with statistical difference (FDR < 0.05). In the lung lipidomics, we identified at least thirteen types of lipids are regulated by HL Granule, including ACar, FA, LPC, PC, LPE, PE, PG, PI, PS, DG, TG, SM, and Cer. The observation suggested that HL Granule improved lipid homeostasis of acute asthmatic. The study enables us to understand the new pathway and pharmacological mechanism of HL Granule in the pathogenesis of asthma mediated by pulmonary lipid disorders.

Lung tissue contains 3–4% lipids in wet weight, and about 60% of the lipids are phospholipids (Rouser et al., 1969; Toshima and Akino, 1972). Phospholipids are important parts of cell membrane structure, and some pulmonary phospholipids are the main components of pulmonary surfactant in alveoli. In present study, phospholipids were disordered with the largest number in the lung tissue of acute asthma. The comprehensive analysis of heredity and metabolites suggests that PC increased in patients with asthma (Ried et al., 2013), which is consistent with our results, and HL Granule could downregulate the levels of PC. PE synthesis is critical for mitochondrial and endoplasmic reticulum function. The increased PE levels observed in the model groups might be reflective of an increased mitochondrial energy production. This assumption would be further supported by the increased levels of acylcarnitine levels. Additionally, our work reveals the levels of ether phospholipids are increased significantly in the model groups. Ether phospholipids in the plasma membrane act as the substrates for the lipid peroxidation and resulting in the further cell death (Zou et al., 2020). The downregulation of PEE levels suggested the protective effects of HL Granule. It has long been known that ether-linked phospholipids are abundantly present in neutrophils (Nagan and Zoeller, 2001), which could be rapidly recruited and are largely present in the airways of allergic eosinophilic asthmatic patients (Radermecker et al., 2018). A recent data suggested PEE and PCE were associated with ferroptosis sensitivity, which was involved in various pulmonary diseases (Zou et al., 2020).

PG predominantly observed in the lung tissue. The increased levels of PGs might inhibit Toll-like receptor (TLR)-mediated inflammation, and improved mitochondrial activity and inflammation (Chen et al., 2018; Choudhary et al., 2019). In present study, HL Granule downregulated partial PG and PE levels, suggesting a protective of the OVA induced asthma. PIs are the ubiquitous component of eukaryotic cells that participate in signal processes. Especially, glycerophosphoinositol 4-phosphate controls actin dynamics in cell systems (Corda et al., 2002). The literature reported that the PI antagonized the activation of

homologous ligands of TLR 2 and TLR 4, influencing innate immunity and the transcription of many pro-inflammatory genes (Voelker and Numata, 2019). PS is also one of the most abundant lipids in plasma membrane, and recent literatures reported that the exposed PS on the outer leaflet of the plasma membrane is the functional ligand for the signal pathway (Gong et al., 2017). Proteins interacting with PS are involved in almost all aspects of cellular regulation by activating protein kinases and transcription. Phagocytes recognized PS on apoptotic cells which were then cleared through CD36 and oxLPL receptors (Zhang et al., 2018). In the experimental model of allergic airway inflammation, apoptotic cells and inflammatory dendritic cells that express PS inhibitory immune receptor CD300a increased significantly after intraperitoneal injection of alum combined with OVA (Miki et al., 2015). It could be the reason for the increase of PS in the model group, and HL Granule might affect PS related proteins or cells.

Lysophospholipids (LPs) are produced by hydrolysis of phospholipids according to phospholipase A2 (PLA2). LPs exist in all types of cells, as a second messenger molecule to regulate intracellular signaling pathways. LPs also participate in many biological functions, including inflammation (Arifin and Falasca, 2016). In present study, we mainly changed LPC and LPE. Although some studies showed that some LPCs decreased in fasting serum (Ried et al., 2013). However, increasing level of LPC usually played a pathogenic role in the inflammatory injury of asthma (Bansal et al., 2016). LPC also induced migration of lymphocytes and macrophages, inhibited activation and migration of eosinophils, increased production of pro-inflammatory cytokines, aggravated oxidative stress and promotes apoptosis, thus accumulating inflammation and promoting the development of diseases (Knuplez et al., 2020; Liu et al., 2020). In the study, the upregulated LPCs were recalled by HL Granule which may be one of the reasons for its improvement of inflammation in acute asthma.

Sphingolipid serve as receptors for multiple pathogens and play key roles in immune signaling. Several studies reported that the asthma associated ORMDL3 (ORMDL Sphingolipid Biosynthesis Regulator 3) gene regulated the sphingolipid biosynthesis, and the altered sphingolipids modulate the T cells' metabolism. Our data revealed significant correlation between the ceramide non-hydroxyfatty acid sphingosine (Cer-NS) and long chain fatty acids, suggested the sphingolipid metabolism was involved in the therapeutic action of HL Granule. The accumulation of ceramides is reported to be associated with apoptosis (Hannun and Obeid, 2018). The decreased ceramides of HL Granule suggested the possible anti-apoptosis effect. Moreover, the produced SMs from ceramides on the plasma are supposed to be an acute response to extracellular stimuli. Additionally, plasma ultra-long-chain SM (d18:1/24:0) might work for regulating the activation of macrophages and inflammatory response (Sakamoto et al., 2017).

A research showed that long-chain polyunsaturated fatty acids could be converted into lipid mediators during inflammation to modulate bronchoconstriction and airway inflammation (Fussbroich et al., 2019). The key enzymes of fatty acid oxidation are involved in the OVA induced asthma, which

could significantly reduce allergen-induced AHR, the number of inflammatory cells, and the production of asthma-related cytokines and chemokines (Al-Khami et al., 2017). HL Granule could downregulate the levels of long-chain fatty acids, and further studies are required to identify the specific mechanisms. Correlation analysis revealed that the alteration of long chain fatty acids is highly correlated with that of ceramide levels. The results suggested the biosynthesis of ceramide from the fatty acids was involved in the protection of asthma by HL Granule. In addition, a specific ceramide species, C16:0 ceramide was recently identified regulating FAO and impairing fatty acid oxidation in obesity (Raichur et al., 2014). Our results show that HL Granule downregulated the level of acyl carnitine, which has the potential to activate inflammation. We also identified that DG and TG increased uniformly in the lung tissue, and HL Granule could regulate these upregulated lipids.

In summary, our research confirmed that HL Granule could be used in acute asthma treatment, but one deserved attention, is that different doses of HL Granule in the treatment, including variable treatment dose, optimal treatment dose, toxicities underwent dose, and so on, should be focused on in next studies. Additionally, there are few studies on lung lipids and asthma at present, and our exploration of the effect of HL Granule on acute asthma by regulating pulmonary lipid homeostasis is also preliminary. Further researches are needed to verify and reveal the role and interaction of lipids in asthma and drug intervention.

CONCLUSION

In conclusion, we established an acute model of asthma with AHR, airway inflammation, and increasing levels of IL-4 and IL-5, which could be effectively reduced by the treatment of HL Granule. A total of 304 and 167 lipids were detected and identified in positive and negative ion mode in lung tissue, of which 162 and 109 lipids were significantly upregulated in model group ($FDR < 0.05$, $FC > 2$ or $FC < 0.5$). 104 and 73 lipids could be reversed by HL Granule, with statistical difference ($FDR < 0.05$), including ACar, FA, LPC, PC, LPE, PE, PG, PI, PS, DG, TG, SM, and Cer. Notably, 118 and 273 correlations among 47 and 96 lipids in the positive and negative were observed, with P_E and P_C ($FDR < 0.001$, Spearman correlation coefficient $r^2 > 0.75$). Therefore, we found that lipid disorders play an important role in asthma. HL Granule may regulate pulmonary lipid homeostasis for the treatment of acute asthma. Furthermore, our study has significance for clinical guides. In view of the side effects of drugs used in the treatment of asthma such as montelukast sodium, HL Granule could be used as an alternative or supplementary therapy in clinic.

REFERENCES

Ackerman, S. J., Park, G. Y., Christman, J. W., Nyenhuis, S., Berdyshev, E., and Natarajan, V. (2016). Polyunsaturated lysophosphatidic acid as a potential asthma biomarker. *Biomarkers Med.* 10, 123–135. doi:10.2217/bmm.15.93

DATA AVAILABILITY STATEMENT

The raw data supporting the conclusion of this article will be made available by the authors, without undue reservation, to any qualified researcher.

ETHICS STATEMENT

The animal study was reviewed and approved by the Animal Care and Use Committee of Nanjing University of Chinese Medicine (Permit number: 201903A018).

AUTHOR CONTRIBUTIONS

HY and GQ were responsible for acquisition, analysis, and interpretation of data and had written the first draft of the manuscript, JS provided information for research design. RY, ZL, and XW participated in the analysis and provided experimental support. TX and XZ designed this study and edited the final manuscript.

FUNDING

This work was supported by the leading academics training program of Chinese medicine in Jiangsu Province, China (No. SLJ0224), Postgraduate Research & Practice Innovation Program of Jiangsu Province, China (No. KYCX20_1535), Natural Science Foundation of Jiangsu Province (BK20181426), the Natural Science Research of Jiangsu Higher Education Institutions of China (18KJA360004), Changshu Municipal Health Committee Supported the Project (CSWS201932), Suzhou Municipal Science and Technology Bureau Supporting Project (SYSD2019020).

ACKNOWLEDGMENTS

We thank Shanxi Dongke Pharmaceutical for providing HL Granule and Montelukast Sodium Oral Granule.

SUPPLEMENTARY MATERIAL

The Supplementary Material for this article can be found online at: <https://www.frontiersin.org/articles/10.3389/fphar.2021.656756/full#supplementary-material>.

Al-Khami, A. A., Ghoni, M. A., Del Valle, L., Ibba, S. V., Zheng, L., Pyakurel, K., et al. (2017). Fuelling the mechanisms of asthma: increased fatty acid oxidation in inflammatory immune cells may represent a novel therapeutic target. *Clin. Exp. Allergy* 47, 1170–1184. doi:10.1111/cea.12947

Arifin, S., and Falasca, M. (2016). Lysophosphatidylinositol signalling and metabolic diseases. *Metabolites* 6, 6. doi:10.3390/metabo6010006

- Bansal, P., Gaur, S. N., and Arora, N. (2016). Lysophosphatidylcholine plays critical role in allergic airway disease manifestation. *Sci. Rep.* 6. doi:10.1038/srep27430
- Barrera, N. P., Zhou, M., and Robinson, C. V. (2013). The role of lipids in defining membrane protein interactions: insights from mass spectrometry. *Trends Cell Biol.* 23, 1–8. doi:10.1016/j.tcb.2012.08.007
- Barupal, D. K., and Fiehn, O. (2017). Chemical Similarity Enrichment Analysis (ChemRICH) as alternative to biochemical pathway mapping for metabolomic datasets. *Sci. Rep.* 7, 14567. doi:10.1038/s41598-017-15231-w
- Carey, A. L., Formosa, M. F., Van Every, B., Bertovic, D., Eikelis, N., Lambert, G. W., et al. (2013). Ephedrine activates brown adipose tissue in lean but not obese humans. *Diabetologia* 56, 147–155. doi:10.1007/s00125-012-2748-1
- Carey, A. L., Pajtak, R., Formosa, M. F., Van Every, B., Bertovic, D. A., Anderson, M. J., et al. (2015). Chronic ephedrine administration decreases brown adipose tissue activity in a randomised controlled human trial: implications for obesity. *Diabetologia* 58, 1045–1054. doi:10.1007/s00125-015-3543-6
- Chen, W.-W., Chao, Y.-J., Chang, W.-H., Chan, J.-F., and Hsu, Y.-H. H. (2018). Phosphatidylglycerol incorporates into cardiolipin to improve mitochondrial activity and inhibits inflammation. *Sci. Rep.* 8. doi:10.1038/s41598-018-23190-z
- Choudhary, V., Uaratanawong, R., Patel, R. R., Patel, H., Bao, W., Hartney, B., et al. (2019). Phosphatidylglycerol inhibits toll-like receptor-mediated inflammation by danger-associated molecular patterns. *J. Invest. Dermatol.* 139, 868–877. doi:10.1016/j.jid.2018.10.021
- Corde, D., Iurisci, C., and Berrie, C. P. (2002). Biological activities and metabolism of the lysophosphoinositides and glycerophosphoinositols. *Biochim Biophys Acta* 1582, 52–69. doi:10.1016/S1388-1981(02)00137-3
- Dondi, A., Calamelli, E., Piccinno, V., Ricci, G., Corsini, I., Biagi, C., et al. (2017). Acute asthma in the pediatric emergency department: infections are the main triggers of exacerbations. *Biomed. Res. Int.* 2017, 1. doi:10.1155/2017/9687061
- Fahy, E., Cotter, D., Sud, M., and Subramaniam, S. (2011). Lipid classification, structures and tools. *Biochim. Biophys. Acta* 1811, 637–647. doi:10.1016/j.bbalip.2011.06.009
- Ferguson, J. E., Patel, S. S., and Lockey, R. F. (2017). Acute asthma, prognosis, and treatment. *J. Allergy Clin. Immunol.* 139, 438–447. doi:10.1016/j.jaci.2016.06.054
- Fussbroich, D., Zimmermann, K., Göpel, A., Eickmeier, O., Trischler, J., Zielen, S., et al. (2019). A specific combined long-chain polyunsaturated fatty acid supplementation reverses fatty acid profile alterations in a mouse model of chronic asthma. *Lipids Health Dis.* 18. doi:10.1186/s12944-018-0947-6
- Gai, X. Y., Zhang, L. J., Chang, C., Guo, C. L., Abulikemu, M., Li, W. X., et al. (2019). Metabolomic analysis of serum glycerophospholipid levels in eosinophilic and neutrophilic asthma. *Biomed. Environ. Sci.* 32, 96–106. doi:10.3967/bes2019.013
- Gan, W., Huang, Q., Wang, M., Wang, J., Hui, Y., Zhao, K., et al. (2020). A randomized controlled trial study protocol of modified Mahuang-Fuzi-Xixin decoction in the treatment of patients with mild bronchial asthma during acute exacerbation. *Medicine (Baltimore)* 99, e21858. doi:10.1097/MD.00000000000021858
- Global Strategy for Asthma Management and Prevention Global Initiative for Asthma (GINA) (2020). Available at: www.ginasthma.org.
- Glockler-Lauf, S. D., Finkelstein, Y., Zhu, J., Feldman, L. Y., and To, T. (2019). Montelukast and neuropsychiatric events in children with asthma: a nested case-control study. *J. Pediatr.* 209, 176–182. doi:10.1016/j.jpeds.2019.02.009
- Gong, Y.-N., Guy, C., Olason, H., Becker, J. U., Yang, M., Fitzgerald, P., et al. (2017). ESCRT-III acts downstream of MLKL to regulate necroptotic cell death and its consequences. *Cell* 169, 286–300. doi:10.1016/j.cell.2017.03.020
- Hannun, Y. A., and Obeid, L. M. (2018). Sphingolipids and their metabolism in physiology and disease. *Nat. Rev. Mol. Cell Biol.* 19, 175–191. doi:10.1038/nrm.2017.107
- He, Y., Lou, X., Jin, Z., Yu, L., Deng, L., and Wan, H. (2018). Mahuang decoction mitigates airway inflammation and regulates IL-21/STAT3 signaling pathway in rat asthma model. *J. Ethnopharmacology* 224, 373–380. doi:10.1016/j.jep.2018.06.011
- Hirota, N., and Martin, J. G. (2013). Mechanisms of airway remodeling. *Chest* 144, 1026–1032. doi:10.1378/chest.12-3073
- Huang, C.-Q., Li, W., Wu, B., Chen, W.-M., Chen, L.-H., Mo, G.-W., et al. (2016). Pheretima aspergillum decoction suppresses inflammation and relieves asthma in a mouse model of bronchial asthma by NF- κ B inhibition. *J. Ethnopharmacology* 189, 22–30. doi:10.1016/j.jep.2016.05.028
- Huang, K., Yang, T., Xu, J., Yang, L., Zhao, J., Zhang, X., et al. (2019). Prevalence, risk factors, and management of asthma in China: a national cross-sectional study. *The Lancet* 394, 407–418. doi:10.1016/S0140-6736(19)31147-X
- Kang, Y. P., Lee, W. J., Hong, J. Y., Lee, S. B., Park, J. H., Kim, D., et al. (2014). Novel approach for analysis of bronchoalveolar lavage fluid (BALF) using HPLC-QTOF-MS-based lipidomics: lipid levels in asthmatics and corticosteroid-treated asthmatic patients. *J. Proteome Res.* 13, 3919–3929. doi:10.1021/pr5002059
- Kelly, R. S., Dahlin, A., McGeachie, M. J., Qiu, W., Sordillo, J., Wan, E. S., et al. (2017). Asthma metabolomics and the potential for integrative omics in research and the clinic. *Chest* 151, 262–277. doi:10.1016/j.chest.2016.10.008
- Khreis, H., Kelly, C., Tate, J., Parslow, R., Lucas, K., and Nieuwenhuijsen, M. (2017). Exposure to traffic-related air pollution and risk of development of childhood asthma: a systematic review and meta-analysis. *Environ. Int.* 100, 1–31. doi:10.1016/j.envint.2016.11.012
- Kim, S.-B., Seo, Y.-S., Kim, H. S., Lee, A. Y., Chun, J. M., Moon, B. C., et al. (2019a). Anti-asthmatic effects of lepidii seu Descurainiae Semen plant species in ovalbumin-induced asthmatic mice. *J. Ethnopharmacology* 244, 112083. doi:10.1016/j.jep.2019.112083
- Kim, Y. J., Ryu, R., Choi, J.-Y., and Choi, M.-S. (2019b). Platycodon grandiflorusRoot ethanol extract induces lipid excretion, lipolysis, and thermogenesis in diet-induced obese mice. *J. Med. Food* 22, 1100–1109. doi:10.1089/jmf.2019.4443
- Knuplez, E., Curcic, S., Theiler, A., Bärnthaler, T., Trakaki, A., Trieb, M., et al. (2020). Lysophosphatidylcholines inhibit human eosinophil activation and suppress eosinophil migration in vivo. *Biochim. Biophys. Acta Mol. Cell Biol. Lipids* 1865, 158686. doi:10.1016/j.bbalip.2020.158686
- Kostakou, E., Kaniaris, E., Filiou, E., Vasileiadis, I., Katsaounou, P., Tzortzaki, E., et al. (2019). Acute severe asthma in adolescent and adult patients: current perspectives on assessment and management. *J. Clin. Med.* 8, 1283. doi:10.3390/jcm8091283
- Kuperman, D. A., Huang, X., Koth, L. L., Chang, G. H., Dolganov, G. M., Zhu, Z., et al. (2002). Direct effects of interleukin-13 on epithelial cells cause airway hyperactivity and mucus overproduction in asthma. *Nat. Med.* 8, 885–889. doi:10.1038/nm734
- Lee, Y. J., and Kim, C.-K. (2020). Montelukast use over the past 20 years: monitoring of its effects and safety issues. *Clin. Exp. Pediatr.* 63, 376–381. doi:10.3345/cep.2019.00325
- Lee, Y. C., Lee, K. H., Lee, H. B., and Rhee, Y. K. (2001). Serum levels of interleukins (IL)-4, IL-5, IL-13, and interferon- γ in acute asthma. *J. Asthma* 38, 665–671. doi:10.1081/JAS-100107544
- Lee, J.-J., Lee, H.-J., and Oh, S.-W. (2017). Antiobesity effects of sansa (Crataegi fructus) on 3T3-L1 cells and on high-fat-high-cholesterol diet-induced obese rats. *J. Med. Food* 20, 19–29. doi:10.1089/jmf.2016.3791
- Lee, S.-E., Lim, C., Lim, S., Lee, B., and Cho, S. (2019). Effect of Ephedrae Herba methanol extract on high-fat diet-induced hyperlipidaemic mice. *Pharm. Biol.* 57, 676–683. doi:10.1080/13880209.2019.1666883
- Lee, S., Han, E. H., Lim, M.-K., Lee, S.-H., Yu, H. J., Lim, Y. H., et al. (2020). Fermented platycodon grandiflorum extracts relieve airway inflammation and cough reflex sensitivity in Vivo. *J. Med. Food* 23, 1060–1069. doi:10.1089/jmf.2019.4595
- Lin, C.-C., Wang, Y.-Y., Chen, S.-M., Liu, Y.-T., Li, J.-Q., Li, F., et al. (2020). Shagan-Mahuang Decoction ameliorates asthmatic airway hyperresponsiveness by downregulating Th2/Th17 cells but upregulating CD4+FoxP3+ Tregs. *J. Ethnopharmacology* 253, 112656. doi:10.1016/j.jep.2020.112656
- Liu, X., Xie, Z.-H., Liu, C.-Y., and Zhang, Y. (2019). Effect of Chinese herbal monomer hairy calycosin on nonalcoholic fatty liver rats and its mechanism. *Comb. Chem. High Throughput Screen.* 22, 194–200. doi:10.2174/138620732266619041112814
- Liu, P., Zhu, W., Chen, C., Yan, B., Zhu, L., Chen, X., et al. (2020). The mechanisms of lysophosphatidylcholine in the development of diseases. *Life Sci.* 247, 117443. doi:10.1016/j.lfs.2020.117443
- Lundbäck, B., Backman, H., Lötvall, J., and Rönmark, E. (2016). Is asthma prevalence still increasing? *Expert Rev. Respir. Med.* 10, 39–51. doi:10.1586/17476348.2016.1114417

- Ma, Z., Tang, X., Gao, Y., Wang, H., Yu, P., and Liu, R. (2020). Combined extracts of *Epimedii Folium* and *ligustri lucidi fructus* with budesonide attenuate airway remodeling in the asthmatic rats by regulating apoptosis and autophagy. *Evidence-Based Complement. Altern. Med.* 2020, 1. doi:10.1155/2020/2319409
- MacEyk, M., and Spiegel, S. (2014). Sphingolipid metabolites in inflammatory disease. *Nature* 510, 58–67. doi:10.1038/nature13475
- Mikhail, I., and Grayson, M. H. (2019). Asthma and viral infections. *Ann. Allergy Asthma Immunol.* 123, 352–358. doi:10.1016/j.anai.2019.06.020
- Miki, H., Nakahashi-Oda, C., Sumida, T., and Shibuya, A. (2015). Involvement of CD300a phosphatidylserine immunoreceptor in aluminum salt adjuvant-induced Th2 responses. *J. Immunol.* 194, 5069–5076. doi:10.4049/jimmunol.1402915
- Nagan, N., and Zoeller, R. A. (2001). Plasmalogens: biosynthesis and functions. *Prog. Lipid Res.* 40, 199–229. doi:10.1016/S0163-7827(01)00003-0
- Naiming, X. (2004). Analysis of therapeutic effect of Huanglong antitussive granule on diseases with cough and asthma. *Mod. Tradit. Chin. Med.* 06, 27–28.
- Neophytou, A. M., Oh, S. S., White, M. J., Mak, A. C. Y., Hu, D., Huntsman, S., et al. (2018). Secondhand smoke exposure and asthma outcomes among African-American and Latino children with asthma. *Thorax* 73, 1041. doi:10.1136/thoraxjnl-2017-211383
- O'Donnell, V. B., Rossjohn, J., and Wakelam, M. J. O. (2018). Phospholipid signaling in innate immune cells. *J. Clin. Invest.* 128, 2670–2679. doi:10.1172/JCI97944
- Papi, A., Brightling, C., Pedersen, S. E., and Reddel, H. K. (2018). Asthma. *The Lancet* 391, 783–800. doi:10.1016/S0140-6736(17)33311-1
- Pardue Jones, B., Fleming, G. M., Otilio, J. K., Asokan, I., and Arnold, D. H. (2016). Pediatric acute asthma exacerbations: evaluation and management from emergency department to intensive care unit. *J. Asthma* 53, 607–617. doi:10.3109/02770903.2015.1067323
- Radermecker, C., Louis, R., Bureau, F., and Marichal, T. (2018). Role of neutrophils in allergic asthma. *Curr. Opin. Immunol.* 54, 28–34. doi:10.1016/j.coi.2018.05.006
- Raichur, S., Wang, S. T., Chan, P. W., Li, Y., Ching, J., Chaurasia, B., et al. (2014). CerS2 haploinsufficiency inhibits β -oxidation and confers susceptibility to diet-induced steatohepatitis and insulin resistance. *Cel Metab.* 20, 687–695. doi:10.1016/j.cmet.2014.09.015
- Ramsahai, J. M., Hansbro, P. M., and Wark, P. A. B. (2019). Mechanisms and management of asthma exacerbations. *Am. J. Respir. Crit. Care Med.* 199, 423–432. doi:10.1164/rccm.201810-1931CI
- Ried, J. S., Baurecht, H., Stücker, F., Krumsiek, J., Gieger, C., Heinrich, J., et al. (2013). Integrative genetic and metabolite profiling analysis suggests altered phosphatidylcholine metabolism in asthma. *Allergy* 68, 629–636. doi:10.1111/all.12110
- Rodriguez, A., Brickley, E., Rodrigues, L., Normansell, R. A., Barreto, M., and Cooper, P. J. (2019). Urbanisation and asthma in low-income and middle-income countries: a systematic review of the urban-rural differences in asthma prevalence. *Thorax* 74, 1020–1030. doi:10.1136/thoraxjnl-2018-211793
- Rouser, G., Simon, G., and Kritchevsky, G. (1969). Species variations in phospholipid class distribution of organs: I. Kidney, liver and spleen. *Lipids* 4, 599–606. doi:10.1007/BF02531047
- Saglani, S., Fleming, L., Sonnappa, S., and Bush, A. (2019). Advances in the aetiology, management, and prevention of acute asthma attacks in children. *Lancet Child. Adolesc. Health* 3, 354–364. doi:10.1016/S2352-4642(19)30025-2
- Sakamoto, H., Yoshida, T., Sanaki, T., Shigaki, S., Morita, H., Oyama, M., et al. (2017). Possible roles of long-chain sphingomyelins and sphingomyelin synthase 2 in mouse macrophage inflammatory response. *Biochem. Biophys. Res. Commun.* 482, 202–207. doi:10.1016/j.bbrc.2016.11.041
- Toshima, N., and Akino, T. (1972). Alveolar and tissue phospholipids of rat lung. *Tohoku J. Exp. Med.* 108, 253–263. doi:10.1620/tjem.108.253
- Trinh, H. K. T., Kim, S.-C., Cho, K., Kim, S.-J., Ban, G.-Y., Yoo, H.-J., et al. (2016). Exploration of the sphingolipid metabolite, sphingosine-1-phosphate and sphingosine, as novel biomarkers for aspirin-exacerbated respiratory disease. *Sci. Rep.* 6. doi:10.1038/srep36599
- Valentovic, M. (2007). Montelukast. *xPharm: the comprehensive pharmacology reference. Elsevier* 1–4. doi:10.1016/B978-008055232-3.62201-9
- Voelker, D. R., and Numata, M. (2019). Phospholipid regulation of innate immunity and respiratory viral infection. *J. Biol. Chem.* 294, 4282–4289. doi:10.1074/jbc.AW118.003229
- Wang, D., Li, R., Wei, S., Gao, S., Xu, Z., Liu, H., et al. (2019). Metabolomics combined with network pharmacology exploration reveals the modulatory properties of Astragali Radix extract in the treatment of liver fibrosis. *Chin. Med.* 14. doi:10.1186/s13020-019-0251-z
- Wang, M., Gao, H., Li, W., and Wu, B. (2020). Icaritin and its metabolites regulate lipid metabolism: from effects to molecular mechanisms. *Biomed. Pharmacother.* 131, 110675. doi:10.1016/j.biopha.2020.110675
- Wenjin, L. (2018). Clinical observation of Huanglong antitussive granule combined with western medicine in the treatment of infantile cough variant asthma. *J. Sichuan Tradit. Chin. Med.* 36 (01), 95–97.
- Yang, R., Zhang, Y., Qian, W., Peng, L., Lin, L., Xu, J., et al. (2019). Surfactant lipidomics of alveolar lavage fluid in mice based on ultra-high-performance liquid chromatography coupled to hybrid quadrupole-exactive orbitrap mass spectrometry. *Metabolites* 9, 80. doi:10.3390/metabo9040080
- Yin, J. (2019). Observation on the efficacy of Huanglong Antitussive Granule combined with budesonide aerosol inhalation in the treatment of pediatric asthmatic bronchitis. *Electron. J. Clin. Med. Lit.* 6 (A4), 186. doi:10.16281/j.cnki.jocml.2019.a4.129
- Yuan, W. Y., Li, L. Q., Chen, Y. Y., Zhou, Y. J., Bao, K. F., Zheng, J., et al. (2020). Frontline Science: two flavonoid compounds attenuate allergic asthma by regulating epithelial barrier via G protein-coupled estrogen receptor: probing a possible target for allergic inflammation. *J. Leukoc. Biol.* 108, 59–71. doi:10.1002/JLB.3HI0220-342RR
- Zhang, C., Wang, K., Yang, L., Liu, R., Chu, Y., Qin, X., et al. (2018). Lipid metabolism in inflammation-related diseases. *Analyst* 143, 4526–4536. doi:10.1039/c8an01046c
- Zhou, B., Zhou, D.-L., Wei, X.-H., Zhong, R.-Y., Xu, J., and Sun, L. (2017). Astragaloside IV attenuates free fatty acid-induced ER stress and lipid accumulation in hepatocytes via AMPK activation. *Acta Pharmacol. Sin.* 38, 998–1008. doi:10.1038/aps.2016.175
- Zou, Y., Henry, W. S., Ricq, E. L., Graham, E. T., Phadnis, V. V., Maretich, P., et al. (2020). Plasticity of ether lipids promotes ferroptosis susceptibility and evasion. *Nature* 585, 603–608. doi:10.1038/s41586-020-2732-8

Conflict of Interest: The authors declare that the research was conducted in the absence of any commercial or financial relationships that could be construed as a potential conflict of interest.

Copyright © 2021 Yan, Qian, Yang, Luo, Wang, Xie, Zhao and Shan. This is an open-access article distributed under the terms of the Creative Commons Attribution License (CC BY). The use, distribution or reproduction in other forums is permitted, provided the original author(s) and the copyright owner(s) are credited and that the original publication in this journal is cited, in accordance with accepted academic practice. No use, distribution or reproduction is permitted which does not comply with these terms.



Pharmacokinetic Profile and Oral Bioavailability of Diosgenin, Charantin, and Hydroxychalcone From a Polyherbal Formulation

Ruchira Salunkhe*, Chhaya Gadgoli, Archana Naik and Nikita Patil

Saraswathi Vidya Bhavan's College of Pharmacy, Dombivli, India

Background: Diosgenin, charantin, and hydroxychalcone are utilized for standardization of popular antidiabetic herbal drugs *Trigonella foenum-graecum* L. belonging to family Fabaceae, *Momordica charantia* L. belonging to family Cucurbitaceae, and *Cinnamomum verum* J. Presl belonging to family Lauraceae. However, no reports on the bioavailability of these markers were available. The present study was undertaken to determine the bioavailability and pharmacokinetic profile of the markers and formulations containing the herbs.

Methods: The pharmacokinetic profile and absolute bioavailability of the pure active markers were determined in male Wistar rats by administering individually the doses of 1.5 mg/kg i.v. and 15 mg/kg p.o., followed by estimation of serum levels of the markers at 0, 10, 30, 60, 120, and 240 mins till 24 h time points by a validated bioanalytical HPTLC method. Two standardized antidiabetic capsule formulations containing spray dried hydroalcoholic extracts of seeds of *Trigonella foenum-graecum* L. (42.8 mg equivalent to 0.95% w/w of diosgenin), fresh fruits of *Momordica charantia* L. (21.4 mg equivalent to 0.4% w/w of charantin), and bark of *Cinnamomum verum* J. Presl (10.71 mg equivalent to 0.079 %w/w hydroxychalcone) were prepared. In one formulation, piperine 1.5 mg was added along with the other herbal extracts mentioned. Bioavailability and pharmacokinetic profile of these two formulations were determined in male Wistar rats through estimating serum levels of active markers diosgenin, charantin, and hydroxychalcone at 0, 10, 30, 60, 120, and 240 mins till 24 h later oral administration of the formulations (Formulation without piperine F1 and formulation with Piperine F2).

Results: Plasma concentrations were found to decline mono-exponentially following intravenous administration, and the mean elimination half-life ($t_{1/2}$) was observed to be 7.93, 8.21, and 4.66 h, respectively. The absolute oral bioavailability of pure markers was observed to be $9.0 \pm 0.2\%$, $8.18 \pm 0.36\%$, and $10.54 \pm 0.52\%$ by the dose normalization method. The oral bioavailabilities of the formulations with respect to diosgenin, charantin, and hydroxychalcone were found to be 9.78, 10.743, and 8.07%, respectively. The formulation containing piperine indicated a significant ($p < 0.01$) increase in the bioavailabilities of all the marker compounds.

OPEN ACCESS

Edited by:

Chandra Kant Katiyar,
Emami, India

Reviewed by:

Pardeep Kumar,
Jawaharlal Nehru University, India
Shiv Bahadur,
GLA University, India

*Correspondence:

Ruchira Salunkhe
ruchira.karpe@gmail.com

Specialty section:

This article was submitted to
Ethnopharmacology,
a section of the journal
Frontiers in Pharmacology

Received: 14 November 2020

Accepted: 11 March 2021

Published: 29 April 2021

Citation:

Salunkhe R, Gadgoli C, Naik A and
Patil N (2021) Pharmacokinetic Profile
and Oral Bioavailability of Diosgenin,
Charantin, and Hydroxychalcone From
a Polyherbal Formulation.
Front. Pharmacol. 12:629272.
doi: 10.3389/fphar.2021.629272

Conclusion: In conclusion, diosgenin and charantin have low bioavailabilities as compared to hydroxychalcone. The bioavailabilities of all the three marker compounds can be increased exponentially with the addition of piperine.

Keywords: diosgenin, charantin, hydroxychalcone, bioavailability, pharmacokinetics, antidiabetic, herbal formulations

INTRODUCTION

The seeds of *Trigonella foenum-graecum* L, fruits of *Momordica charantia* L, and the bark of *Cinnamomum verum* J. Presl have been reported to possess antidiabetic activity (Rajesh et al., 2016; Mahmoud et al., 2017; Geberemeskel et al., 2019). Around 75% of herbal formulations available in Indian market for treatment of diabetes contain these herbs. Diosgenin from seeds of *T. foenum-graecum* is reported to have antidiabetic activity in the long-term use by restoration of pancreatic β -cells, downregulation of enzymes involved in hepatic gluconeogenesis and glucose export, upregulation of hepatic glucokinase, and increase in the amounts of hepatoprotective and antioxidant enzymes (Jesus et al., 2016). Charantin from fruits of *M. charantia* acts through stimulating peripheral and skeletal muscle glucose utilization, inhibition of adipocyte differentiation, suppression of key gluconeogenic enzymes, stimulation of key enzyme of the HMP pathway, and preservation of islet β cells and their functions (Nagappan et al., 2018). Hydroxychalcone from the bark of *C. verum* acts by mimicking the effect of insulin through enhancing glucose uptake and phosphorylation of insulin receptor in adipocytes; moreover, hydroxychalcone was also reported as a potential dietary PPAR γ ligand (Eissa et al., 2017).

The pharmacological actions of any drug are dependent on the serum levels of the same. The appropriate serum levels of a drug are dependent on its absorption and distribution metabolism of the drug. The bioavailability of a drug is defined as measurement of the rate and extent to which a drug reaches at the site of action (Kumar and Sanjita, 2013). In case of extracts of herbs or herbal drugs, it is challenging to determine bioavailability due to presence of many constituents. There is very little or no data available revealing pharmacokinetics and bioavailability of phytoconstituents and the formulations containing herbal extracts thereof. Such studies not only help in understanding the efficacy of formulations but also helpful in improving efficacy of formulation through adapting various ways of increasing bioavailability of phytoconstituents.

Herbal drugs are prone to content variations in each harvest and geographical source and hence need serious efforts to be put in standardizing with respect to that of bioavailability and pharmacokinetic study of the herbal formulations. In the present study, three active phytoconstituents viz diosgenin, charantin, and hydroxychalcone were studied for their bioavailabilities and pharmacokinetic parameters in albino rats, as the scientific data regarding their bioavailabilities and pharmacokinetic parameters could not be traced (**Figure 1**).

MATERIALS AND METHODS

Chemicals and Reagents

The seeds of *Trigonella foenum-graecum* L. and the bark of *Cinnamomum verum* J. Presl were purchased from the commercial supplier, batch number; 204480093, Sanjeevani Ayurvedic Stores, Angel park, shop number 4, Kalamboli, Navi Mumbai, Maharashtra, India. The fruits of *Momordica charantia* L. were purchased from the local market Kalamboli, Navi Mumbai, Maharashtra, India. Seeds of *T. foenum-graecum*, fresh fruits of *M. charantia*, bark of *C. verum* were authenticated by Dr. Harshad Pandit from Guru Nanak Khalsa College Matunga, Mumbai. The voucher specimen numbers rbs p 014060319 (*Trigonella foenum graecum* L.), rbs p 013960219 (*Momordica charantia* L.), rbs p 013980219 (*Cinnamomum verum* J. Presl), and rbs p 014040319 (*Piper nigrum* L.) are deposited, respectively. The active marker compounds diosgenin, charantin, and hydroxychalcone were isolated in the laboratory of Saraswathi Vidya Bhavan's College of Pharmacy, Mumbai, India and were characterized using chromatographic and spectral techniques by SAIF (Sophisticated Analytical Instrumentation Facilities), IIT Bombay. Solvents viz. chloroform, glacial acetic acid, and methanol were of analytical reagent (AR) grade. All other reagents used were of laboratory reagent (LR) grade and were used without further purification. For chromatographic analysis the HPLC grade solvents were utilized.

Isolation of Marker Compounds

Isolation of Steroidal Sapogenins (Diosgenin and Charantin)

Diosgenin and charantin are aglycone parts of the steroidal saponin obtained from methanolic extracts of seeds of *T. foenum-graecum* L. and fruits of *M. charantia* L., respectively by suitably modifying the reported methods (Sonal and Pratima, 2015; Chen et al., 2017). In brief, the plant materials (50 gm) were defatted with petroleum ether 100 ml (60–80°C), followed by extraction of the marc with polar solvent like methanol (200 ml), to get the glycoside enriched extract. Aglycones of these glycosides were obtained by refluxing the methanolic extracts with 2 M HCl. The aglycones released in this process were then partitioned into the organic phase consisting of diethyl ether (100 ml). The organic phases were then saponified with 10 ml of 10% alcoholic potassium hydroxide to get the aglycone in almost pure form. The aglycones were then purified by recrystallization.

Isolation of Hydroxychalcone

The bark powder of *C. verum* J. Presl (100 gm) was extracted in acetone (150 ml) at 50°C for 1.5 h. The extract was concentrated

at the reduced pressure and the precipitate formed in resulting solution was dissolved using small amount of methanol. The methanolic extract was then fractionated using Sephadex LH-20 column. The yield obtained from polyphenol hydroxychalcone was 0.32 gm % w/w, and as it was not adequate for the experiments, simulated reaction was carried out using cinnamaldehyde (2 gm) and catechin (1 gm) in 50 ml acetone. The reactants were heated at 100°C for 50 mins to get the product having structurally similar polyphenolic present in the cinnamon bark (Tanaka et al., 2008). The synthesized product and the isolated marker compound were confirmed for their identity using spectral studies.

Characterization of the isolated marker compounds was done using TLC, UV-visible spectroscopy, NMR, HPLMS, and elemental analysis and comparing the data with the respective reference standards.

Formulation of Capsules

Two capsule formulations F1 and F2 (Table 1) were prepared by incorporating the spray dried hydroalcoholic extracts of seeds of *T. foenum-graecum*, fresh fruits of *M. charantia*, and the bark of *C. zeylanicum*. The F2 formulation contained 1.5 mg of piperine. The extracts utilized for formulations were standardized for the content of diosgenin, charantin, and hydroxychalcone using the HPTLC method (Table 2).

The dose for each extract was selected based upon the content of these extracts in the marketed formulation quanto diab-forte (*T. foenum-graecum* extract 400 mg, *M. charantia* extract 200 mg, and *C. zeylanicum* extract 100 mg, respectively), which is utilized for the treatment of diabetes. The piperine content of 1.5 mg is added owing to the amount of the piperine utilized in the herbal formulations (Wadhwa et al., 2014; Mhaske et al., 2018).

The preparation of extracts for formulation of the capsules is described below.

Preparation of Extracts

In case of *T. foenum-graecum* L, the dried seeds were powdered and defatted using petroleum ether (100 ml) for 1 h, followed by extraction of the marc (50 gm), by refluxing it using 70% v/v hydroalcoholic solution. The extract (100 ml) was concentrated to 10 ml and then spray dried (Yield 4 gm).

For preparation of extract of fruits of *M. charantia* L, 50 gm of fresh fruits were grinded in the mixer and then it was extracted using 70% v/v hydroalcoholic solution (100 ml) for 3 h. The

extract (150 ml) was concentrated to 10 ml, followed by spray drying (Yield 3 gm).

Extraction of cinnamon bark (50 gm) was carried out by refluxing the powder using 70% v/v hydroalcoholic solution, followed by reducing the extract (100 ml) to 10 ml followed by spray drying (Yield 7 gm).

Determination of Content of Marker Compounds

The contents of diosgenin, charantin, and hydroxychalcone were determined from spray dried extracts of *T. foenum-graecum* L, *M. charantia* L, and *C. verum* J. Presl, respectively using the HPTLC method. The optimized chromatographic conditions are given in (Table 2).

The calibration curves were prepared for individual marker compounds in the range of 0.4 to 1.4 µg/ml.

The samples for analysis were prepared by dissolving 10 mg of individual spray dried extract in 10 ml of methanol to give the stock solution of 1 mg/ml (Solution A). 1 ml of Solution A was diluted to 10 ml with methanol to get a solution of 100 µg/ml (Solution B). Further dilutions were made in methanol. The samples were loaded on HPTLC plates and developed the chromatograms using the conditions described in (Table 2). The contents of the marker compounds were determined by extrapolating from respective calibration curves (Table 3).

Preparation and Evaluation of Formulations

The standardized spray dried extracts were mixed in the proportions indicated in Table 1 and granules of the same were prepared using the wet granulation method. The dough was formed using microcrystalline cellulose (Avicel) and 60% v/v, followed by addition of required quantity of talc, and then powder blend was passed through sieve number 10 to produce the granules. The granules were gently spread and dried at 45°C in oven for 3 hrs followed by sieving through sieve number 20 supported on 40 and added 10% w/w fines. The granules were then filled in hard gelatin capsules, followed by evaluation of capsules for the content uniformity through determination of content of the marker compounds using the HPTLC method.

Sample Preparation

Granules from 10 capsules were mixed, and a weight of the powder equivalent to 75 mg and was transferred to 100 ml volumetric flask. About 20 ml of methanol (HPLC grade) was added and sonicated for 15 mins or till dissolution of

TABLE 1 | Composition of the herbal formulations developed in laboratory.

Sr no	Ingredients	Composition per capsule	
		Formulation 1	Formulation 2 (mg)
1	<i>Trigonella foenum-graecum</i> extract	42.8 mg	42.8
2	<i>Momordica charantia</i> extract	21.4 mg	21.4
3	<i>Cinnamomum zeylanicum</i> extract	10.71 mg	10.71
4	70% v/v aqueous ethanol solution	0.11 ml	0.11
5	Microcrystalline cellulose	51 mg	51
6	Piperine	—	1.5

TABLE 2 | HPTLC conditions.

Application mode	Camag Linomat V using 100 µl Hamilton syringe
Development mode	CAMAG twin trough chamber
Plate material	Silica gel 60F254 pre-coated HPTLC plates
Application bandwidth	6 mm
Developing solvent	Chloroform: glacial acetic acid: methanol: water (4:3:2:1) v/v
Chamber saturation time	10 min
Developing distance	90 min
Development time	20 min
Detecting wave length	342 nm
Lamp	UV
Scanner	CAMAG TLC scanner II
Integrator	WIN CATS V 1.2.2

extracts. The volume was then made to the mark using methanol (HPLC grade) (Stock A). The stock solution A was filtered and 1 ml aliquot of the filtrate was further diluted to 100 ml using methanol (HPLC grade). The solutions were further filtered through 0.45 µ syringe membrane and loaded on HPTLC plate for development of chromatogram and analyzed for the content of respective markers.

Bioanalytical Method Development and Validation

The bioanalytical method was developed for the study of the bioavailabilities and the pharmacokinetic parameters of the marker compounds viz. diosgenin, charantin, and hydroxychalcone.

Animals

All animal experiments were approved by the Institutional Animal Ethics Committee (IAEC) and were in accordance with the Committee for the Purpose of Control and Supervision of Experiments on Animals (CPCSEA registration number: SVBCP/IAEC/M ph/18-19/65). Healthy Wistar male rats weighing 180–220 gm were procured from registered breeder Bharat Serum Pvt. Ltd.; Mumbai, India. Experimental animals were maintained on standard pelleted laboratory animal feed and water ad libitum. Animals were maintained at $22 \pm 2^\circ\text{C}$ and $55 \pm 5\%$ relative humidity in the light controlled (12 h light/12 h dark) room.

Analysis of the Marker Compounds in Plasma

Plasma concentrations of active marker compounds were determined using validated high-performance thin layer chromatography (HPTLC) with the UV detection method.

Preparation of Plasma Sample

The plasma samples (150 µl) were deproteinized by adding mixture of methanol: dichloromethane (1:1), followed by vortex mixing at 3000 rpm for 5 min. The supernatant was separated and further extracted with about 1.5 ml of ethyl acetate by mixing on vortex mixer at 3000 rpm for 10 min. The ethyl acetate layer was then collected and evaporated to dryness, followed by reconstitution with mobile phase (200 µl) containing chloroform: glacial acetic acid: methanol: water ((4.0: 3.0:2.0:1.0) v/v and 100 µl was applied on a HPTLC plate. The optimized HPTLC conditions for development and quantification of the constituents is given in **Table 2**.

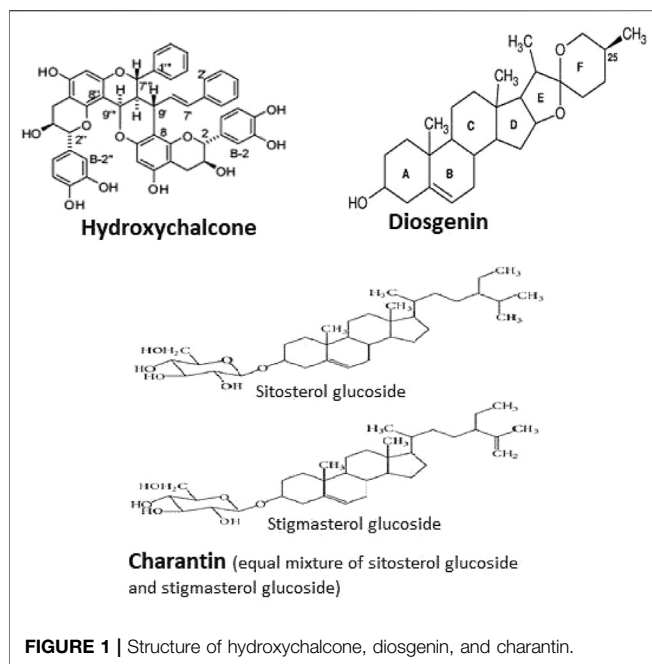
Preparation of Standard Solutions

Stock solutions of diosgenin, charantin, and hydroxychalcone were prepared by weighing 10 mg of each reference standard and dissolving in methanol (50 ml), followed by making up the volume to 100 ml with methanol to get the concentration of each marker as 100 ppm. The solution was then suitably diluted and 100 µl of the solution of the marker compounds was spiked in 100 µl plasma to get the concentration and prepared the solutions with concentrations in the range of 0.4–1.4 µg/ml of each marker compound. These were then utilized for preparation of calibration curve. The HPTLC analysis of samples and the

TABLE 3 | Content of diosgenin, charantin, and hydroxychalcone in the 70% v/v ethanolic extracts of *T foenum-graecum*, *M charantia*, and *C zeylanicum*, respectively.

Names of marker compounds in 70% v/v hydroalcoholic extracts	Mean retention time \pm SD (mins)	Mean content of markers per 10 mg of extract \pm SD (mean percent w/w)
Diosgenin from <i>T foenum-graecum</i>	1.742 \pm 0.04	0.11 \pm 0.005
Charantin from <i>M charantia</i>	3.942 \pm 0.02	0.045 \pm 0.02
Hydroxychalcone from <i>C zeylanicum</i>	7.717 \pm 0.06	0.024 \pm 0.03

Results are presented as mean \pm SD ($n = 3$).



0.0072 $\mu\text{g/ml}$, respectively and linearity in the calibration curve were demonstrated up to an upper limit of 1.11, 1.13, 1.12 $\mu\text{g/ml}$, respectively. Intra- and inter-day precision and accuracy were determined as per ICH guidelines.

Method Validation

The validation of the analytical method was executed as per “Guidance for industry: Bioanalytical Method Validation” from the United States Food and Drug Administration (Guidance for Industry, Bioanalytical Method Validation, 2001).

Calibration Curve

For calibration curve, the stock solution containing all the three markers in the concentration of 100 ppm of each was diluted suitably and spiked in blank plasma to get different concentrations in the range of 0.4–1.4 $\mu\text{g/ml}$, followed by extraction as described in Section *Analysis of the marker compounds in Plasma*. The standard solution after extraction were applied on HPLTLC plates and developed using the conditions described in **Table 2**. The calibration curves were constructed individually by plotting peak area of diosgenin, charantin, and hydroxychalcone against the concentrations of the marker compounds using linear regression. The experiment was carried out in triplicate (**Figure 2**).

Selectivity

Selectivity of the analytical method was determined by recording the retardation factors of the marker compounds through HPTLC as described in **Table 2**. The blank plasma was also

standard solutions were carried out using the parameter described (**Table 2**).

The retarding factors (Rf) values for diosgenin, charantin, and hydroxychalcone were found to be 0.72, 0.61, 0.30, respectively. The lower limit of quantification of the method was 0.33, 0.090,

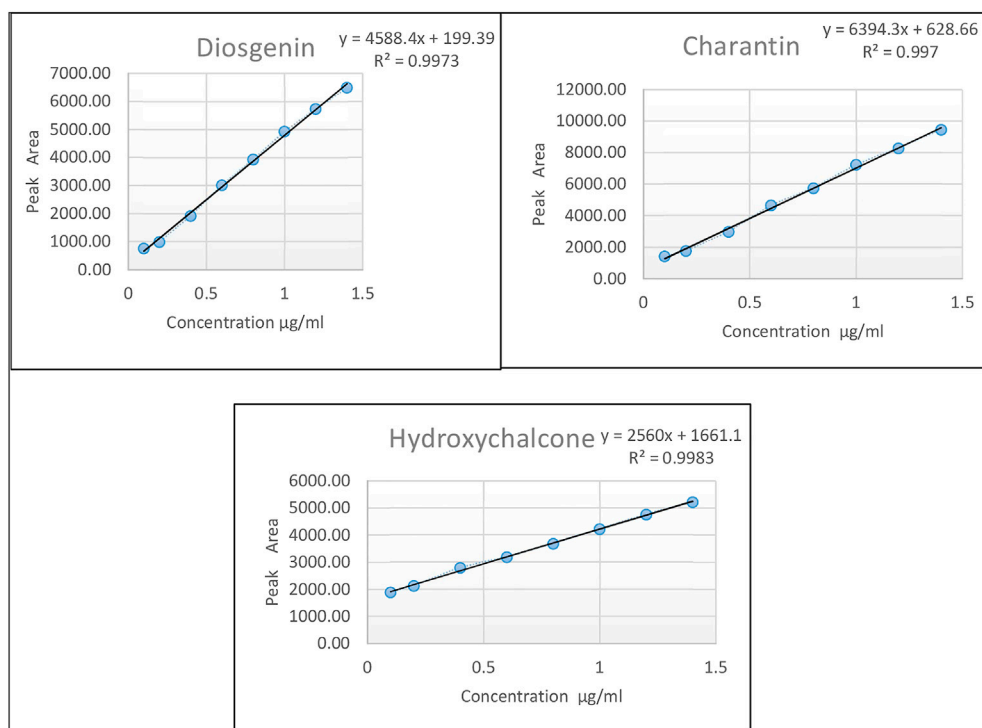


FIGURE 2 | Calibration curves of the marker compounds viz., diosgenin, charantin, and hydroxychalcone, respectively.

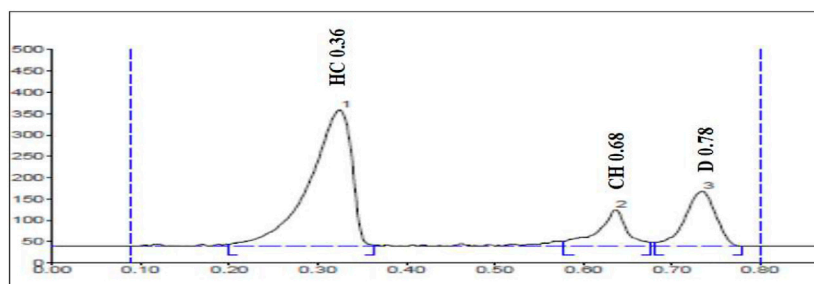


FIGURE 3 | Chromatogram of plasma sample spiked with the markers HC (Hydroxychalcone), CH (Charantin), and D (Diosgenin) in the concentration of 0.2 µg/ml.

subjected to chromatographic analysis as described in **Table 2**. The third chromatogram was run by spiking the plasma with LLOQ (0.2 µg/ml) of marker solutions. The interference at the Rf values was determined by comparing the area response in the blank matrix against the mean response of the extracted LLOQ

(0.2 µg/ml) samples. Also, interference at the Rf was evaluated by comparing the area response in the blank matrix against the mean response of extracted LLOQ (0.2 µg/ml) samples. The % interference was calculated by taking the ratio of “Area at the Rf of analyte to the Mean area (n = 5) at the Rf of analyte in the

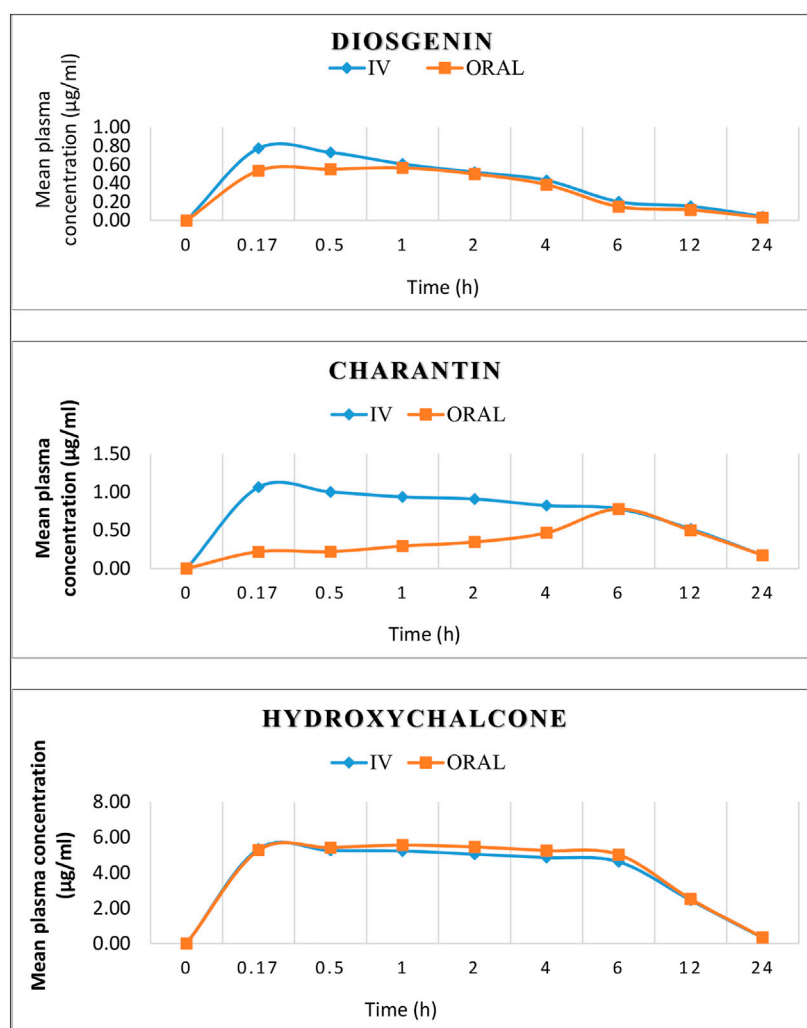


FIGURE 4 | Mean concentration–time profiles of diosgenin, charantin, and hydroxychalcone after i.v. (1.5 mg/kg) and oral (15 mg/kg) administration.

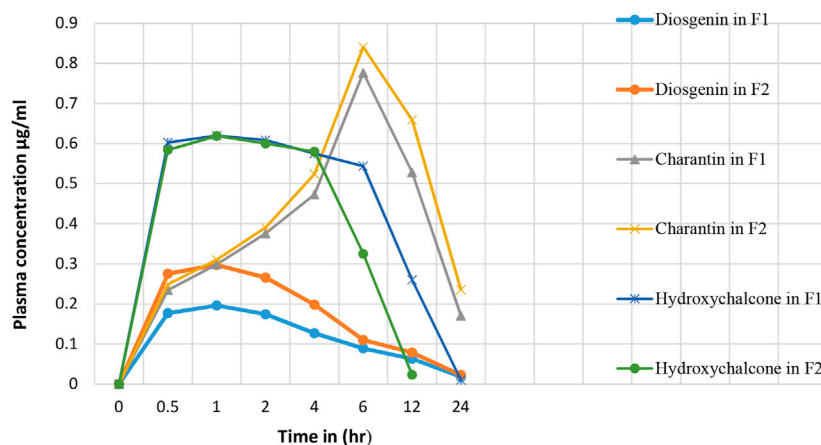


FIGURE 5 | Effect of piperine in herbal formulation on the plasma drug concentration of diosgenin, charantin, and hydroxychalcone.

LLOQ.” The selectivity of the method was calculated using the following formula

$$\% \text{ interference} = \frac{\text{area at Rf of analyte}}{\text{mean Area at Rf of analyte}} \times 100.$$

Accuracy and Precision

Accuracy studies were performed in terms of recoveries of hydroxychalcone, charantin, and diosgenin from spiked plasma. For this quality control samples, LQC–lower-concentration quality control sample (0.4 ppm) and MQC–medium concentration quality control samples (0.8 ppm) of all reference standard drugs were analyzed ($n = 3$), and % accuracy was calculated by comparing the average measured concentrations using the calibration curves to known concentrations.

The inter- and intra-day precision for the analytical method was determined by analyzing the quality control samples of all the marker compounds at LQC (0.4 PPM), MQC (0.8 PPM), and HQC (1.2 ppm) using the HPTLC method described above. For intra-day precision, RSD (Relative Standard Deviation) was calculated for analysis of the quality control samples in six replicates. In case of inter-day precision, RSD for analysis of the quality control samples carried out for three consecutive days was calculated. The analysis was carried out in six replicates.

Recovery and Stability

The extraction recoveries (ER) of diosgenin, charantin, and hydroxychalcone from plasma were determined at three different concentrations low-, middle-, and high-concentration range. Also unextracted dilution was prepared at concentration representing a 100% were applied/spotted and analyzed. The mean absolute % recovery was calculated by taking the ratio of “Mean peak area response of extracted samples at LQC/MQC/HQC” to the “Mean peak area response of unextracted samples at LQC/MQC/HQC.”

The mean absolute % recovery was calculated by taking the ratio of “Mean peak area response of extracted samples at MQC (0.8 µg/ml) level” to the “Mean peak area response of unextracted samples”. Overall recovery for analyte was calculated by taking the average of mean of absolute % recovery at LQC (0.4 µg/ml), MQC (0.8 µg/ml), and HQC (1.2 µg/ml) with SD and % CV for analyte are also reported.

Sample stability was determined by analyzing samples for quality control for analyte’s stock stability in solvent, refrigerator stock solution stability, freeze and thaw stability, and bench top stability.

Pharmacokinetic Studies

The pharmacokinetic studies were carried out in male Wistar rats. Initially the absolute bioavailabilities of individual marker compounds were determined, followed by determination of bioavailability of the formulations F1 and F2 with respect to the marker compounds.

Determination of Absolute Bioavailability of Marker Compounds

Absolute bioavailabilities of marker compounds viz. diosgenin, charantin, and hydroxychalcone were determined in male Wistar rats. The animals weighing 300–350 gm were fasted overnight before the dosing with free access to drinking water throughout the experimental period. For the purpose of dosing all the three marker compounds viz, diosgenin, charantin, and hydroxychalcone were suspended in water to make the dose of 15 mg/kg per oral to be administrated to the groups of three rats. The animals were divided into two groups with six animals in each group. The first group received the marker compounds in the dose of 1.5 mg/kg i.v. *via* lateral tail vein, while the second group received the marker compounds in the dose of 15 mg/kg p.o. The rats were anesthetized using ether and blood samples were collected through puncturing the retro-orbital plexus at 0, 0.17, 0.5, 1, 2, 4, 6, 12, and 24 h time points. Blood samples were centrifuged to separate plasma and stored at -20°C until bioanalysis.

Determination of Bioavailability of Formulations

Bioavailabilities of the two formulations viz. F1 containing the standardized spray dried extracts of seeds of *T. foenum-graecum*, fresh fruits of *M. charantia*, and the bark of *C. verum*. The F2 containing the spray dried extracts as mentioned in F1 along with the piperine (1.5 mg) were determined by administering the formulations in the dose of 75 mg/kg b.w. p.o. to the two groups (each group n = 6) of male Wistar rats weighing 300–350 gm, fasted overnight. For administration of the formulations, these were suspended in water with 2% w/v and Tween 80, and administered through oral gavage. The blood samples were collected through puncturing the retro-orbital plexus at 0, 0.17, 0.5, 1, 2, 4, 6, 12, and 24 h time points. Blood samples were centrifuged to separate plasma and stored at -20°C until bioanalysis.

Pharmacokinetic Parameters (Jagannath et al., 2004; Michal et al., 2017)

The pharmacokinetic parameters were calculated for both the individual marker compounds as well as the formulations (F1 and F2).

Non-compartmental analysis of data was performed using statistical moment theory. The peak plasma concentration (C_{\max}) and the corresponding time (T_{\max}) were directly obtained from the raw data.

The area under the plasma concentration vs. time curve upto the last quantifiable point, $\text{AUC}_{(0-t)}$, was calculated by the linear and log-linear trapezoidal rule summation:

$$\text{AUC}_{(0-t)} = \sum \frac{C_0 + C_t}{2} \times T_t - T_0.$$

C = Plasma drug concentration at time t.

T = Time required to attain C.

The $\text{AUC}_{(0-t)}$ was extrapolated to infinity (i.e., $\text{AUC}_{(0-\infty)}$) by adding the quotient of $C_{\text{last}}/K_{\text{el}}$,

$$\text{AUC}_{(t-\infty)} = \frac{C_{\text{last}}}{K_{\text{el}}},$$

Where C_{last} represents the last measurable time concentration and K_{el} represents the elimination rate constant.

K_{el} was calculated by the linear regression of the log-transformed concentrations of the last three data points in the terminal phase.

$$K_{\text{el}} = -\text{slope} \times 2.303.$$

Slope was obtained from log-transformed concentrations of the last three data points in the terminal phase.

The half-life of the elimination phase was obtained from using the relationship,

$$t_{1/2} = \frac{0.693}{K_{\text{el}}}.$$

Clearance was calculated using the relationship $\text{Cl} = \text{Vd} \times K_{\text{el}}$

Vd = Apparent volume of distribution

K_{el} = Elimination rate constant

Apparent volume of distribution was calculated using relationship

$$\text{Vd} = \frac{\text{Dose Administered}}{\text{Plasma concentration}}.$$

Absolute oral bioavailability (F) was calculated using relationship $F = \{[\text{AUC}_{(\text{oral})}/\text{AUC}_{(\text{iv})}] \times [\text{Dose}_{(\text{iv})}/\text{Dose}_{(\text{oral})}]\} \times 100$.

Statistical Analysis

The results are expressed as mean \pm standard deviation (SD). Data were statistically analyzed using Student's t test. A p value of less than 0.05 was considered as statistically significant.

RESULTS AND DISCUSSION

Isolation and Characterization of Marker Compounds

Isolation of marker compounds viz, diosgenin, charantin, and hydroxychalcone were done as per the procedure given in Section *Isolation of Marker compounds*. Identity of the isolated marker compounds was determined using chromatographic and spectral studies. The spectroscopic data of the marker compounds were compared with the standard marker compounds for the confirmation of the structures.

Formulation of Capsule

For formulation of capsules, the content of diosgenin, charantin, and hydroxychalcone were determined in the spray dried extracts of *T. foenum graecum* L, *M. charantia* L, and *C. verum* J. Presl, respectively using the HPTLC method.

Standardization of Extracts

The extracted samples were loaded on HPTLC plates and developed the chromatograms using the conditions described in (Table 2). The contents of the marker compounds were determined by extrapolating from respective calibration curves.

These standardized extracts were then utilized for preparation of polyherbal formulation.

Evaluation of Polyherbal Formulation

The evaluation of capsules was done for the content uniformity through determination of content of the marker compounds using the HPTLC method; results are represented in Table 4.

Validation of Bioanalytical Method

The validation was executed as per "Guidance for industry: Bioanalytical Method Validation" from the United States Food and Drug Administration (Guidance for Industry, Bioanalytical Method Validation, 2001). The results of validation parameters are given as follows.

Selectivity

The selectivity of the method was evaluated by analyzing blank plasma samples prior to spiking. The representative chromatograms

TABLE 4 | Contents of diosgenin, charantin, and hydroxychalcone in polyherbal formulation determined using the optimized HPTLC method.

Name of the hydroalcoholic extracts present in formulation	Mean. Wt. of each capsule (n = 3)	Mean retention time (n = 3)	Mean content of markers (mg) in the formulation 75 mg (n = 3)	Mean % w/w content (n = 3)
<i>T. foenum-graecum</i> , (D)	197.52 ± 0.07	1.742 ± 0.04	1.0280 ± 0.02	0.95 ± 0.01
<i>M. charantia</i> , (CH)		3.942 ± 0.02	0.5240 ± 0.01	0.4 ± 0.01
<i>C. zeylanicum</i> , (HC)		7.717 ± 0.06	0.0822 ± 0.005	0.079 ± 0.002

Results are expressed as mean ± SD (n = 3). D: Diosgenin, CH: Charantin HC: Hydroxychalcone.

of the plasma sample spiked at 0.2 µg/ml of all the three marker compounds and compared with the blank plasma sample. The results presented in **Figure 3** indicate that the chromatogram of the marker compounds was free of interfering peaks at the R_f values of diosgenin (D), charantin (CH), and hydroxychalcone (HC). Thus, it indicated the method selectivity **Table 5**.

Linearity of Calibration Curves

Linearity for the calibration curve of each marker compound was observed in the range of 0.4–1.4 µg/ml with the regression equations for the marker compounds as given below: the regression equation for diosgenin was $Y = 1527.8 X + 65.653$ ($R^2 = 0.9955$); the regression equation for charantin was $Y = 2139.3 X + 203.2$ ($R^2 = 0.9953$); the regression equation for hydroxychalcone was $Y = 811.26 X + 599.29$ ($R^2 = 0.9952$),

Where X was the concentrations of analytes in rat plasma and Y was the peak areas.

Precision

Precision studies were performed for inter-day and intra-day variation in developed method by applying quality control samples through HPTLC analysis using optimized chromatographic conditions, as given in **Table 2**. The % RSD values of the results of determination of concentrations at LQC, MQC, and HQC levels for hydroxychalcone, charantin, and diosgenin are found within the limit that is lower than 10% as shown in the **Table 6**, and the accuracy was within 85–120% for samples for quality control. The results demonstrated that the method qualifies the precision and accuracy criteria.

Extraction Recovery and Stability

The mean % recoveries for diosgenin, charantin, and hydroxychalcone were found to be 94.25, 88.02, and 93.70%, respectively, at all three levels of quality control samples.

The percent recovery of diosgenin, charantin, and hydroxychalcone are observed within the acceptance criteria of 85–120%, indicates the accuracy of the HPTLC method utilized (ICH Guideline M10 On Bioanalytical Method Validation, 2019).

The stability experiments were carried out to evaluate the degradations of the marker compounds under different experimental conditions. The results presented in **Table 7** indicate that there is no significant degradation of diosgenin, charantin, and hydroxychalcone in plasma under different experimental conditions.

As per the acceptance criteria, % ratio (Stability/comparison) should be within 85–115%; from the above results, it was

concluded that all the marker compounds were within the acceptance criteria for stability study **Table 7**.

Pharmacokinetic Study

Determination of Absolute Bioavailability of Marker Compounds

The above validated bioanalytical HPTLC method was successfully and completely applied to evaluate pharmacokinetics in male Wistar rats. Initially the bioavailability of marker compounds was determined by administering the pure marker compounds individually to Wistar rats by oral (dose 15 mg/kg b.w per oral) and parenteral (dose 1.5 mg/kg b.w i.v.) routes, followed by determination of content of the same in plasma at different time points by the HPTLC method. The results of the absolute bioavailability studies of the individual marker compounds are presented in **Table 8**.

The nature of the plasma curves following intravenous administration suggested a mono-exponential decline in the plasma concentration vs. time curves of the active marker compounds **Figure 4**.

Results presented in **Table 8** reveal that the highest absolute bioavailability is obtained for hydroxychalcone (10.54%), when calculated by the dose normalization method probably due to polar nature, while the other two markers being steroidal, the bioavailability was between 8–9%.

Elimination rate constant (K_{el}) indicates the rate at which a drug is removed from the body, which is found to be 0.09 and 0.08 h⁻¹, 0.08 and 0.084 h⁻¹, and 0.14 and 0.148 h⁻¹ for i.v. and oral routes of administration for diosgenin, charantin, and hydroxychalcone, respectively. The similar K_{el} values for i.v. and oral routes of administration for marker compounds over the concentration range encountered in clinical settings indicate the first order elimination.

Plasma half-life ($t_{1/2}$) indicates the time required for reducing the concentration of drug to the half of its concentration; it also

TABLE 5 | Selectivity study of diosgenin, charantin, and hydroxychalcone spiked at 0.2 µg/ml in rat plasma.

Marker compounds	Parameters		
	Area	SD	% Interference
Diosgenin (0.2 µg/ml)	2035.38	29.25	1.43
Charantin (0.2 µg/ml)	1157.03	20.58	1.77
Hydroxychalcone (0.2 µg/ml)	2465.03	40.78	1.65

TABLE 6 | Precision of diosgenin, charantin, and hydroxychalcone in rat plasma.

Marker compounds	Concentration (µg/ml)	Intra-day assay	Inter-day assay
		%RSD	%RSD
Diosgenin	0.4	0.91	0.90
	0.8	1.42	1.39
	1.2	0.44	1.00
Charantin	0.4	1.50	0.77
	0.8	0.51	1.50
	1.2	0.21	1.15
Hydroxychalcone	0.4	0.91	1.06
	0.8	0.49	0.33
	1.2	1.25	0.73

(n = 3).

indicates whether the accumulation of the drug occurs under a multiple dosage regimen and it is essential to decide on the appropriate dosing intervals. $t_{1/2}$ was found to be 7.5638 and 7.9300 h i.v. and oral, respectively for diosgenin, 8.33 and 8.2 h for charantin, and 4.68 and 4.65 h for hydroxychalcone i.v. and oral, respectively, indicating there was no statistically significant difference in the values for intravenous as well as oral routes of administration due to first order elimination.

Volume of distribution (Vd) is theoretical volume that would contain the total amount of administered drug at the same concentration in plasma. It represents the degree at which drug is distributed in the body tissue rather than plasma. Higher Vd indicates greater amount of tissue distribution and low protein binding. The highest volume of distribution was observed for diosgenin (2.5 ml/kg) followed by charantin (1.4 ml/kg) and least was observed for hydroxychalcone (0.27 ml/kg), indicating high protein binding of hydroxychalcone and ultimately low $t_{1/2}$ and lower clearance of drug from the body. In case of diosgenin and charantin, as those are steroidal sapogenin, they have higher lipid solubility and have lower molecular weight compared to that of hydroxychalcone which is water soluble and having higher molecular weight; hence diosgenin and charantin have high volume of distribution and ultimately have high $t_{1/2}$ values.

Drug clearance (Cl) is concerned with the rate at which a drug is removed from the body. It refers to the amount of the drug

eliminated per unit time from the body. Clearance is related to the total drug concentration in the plasma (free + protein-bound) and not the free concentration. As per the results obtained, clearance for the hydroxychalcone was found to be 0.0417 ml/h/kg which is the least, followed by diosgenin (0.22 ml/h/kg) and charantin (0.11 ml/h/kg), indicating higher AUC for hydroxychalcone and the highest residence time of the drug in the systematic circulation and that slower will be the decline in plasma concentration of hydroxychalcone.

AUC represents the total drug exposure with respect to the time. Assuming the linear kinetics with elimination rate constant, one can show that AUC is equivalent to the total amount of drug observed in the body. AUC for the diosgenin was found to be 4.47 and 4.95 µg h/ml for i.v. and oral administration, respectively. AUC for charantin and hydroxychalcone was found to be 12.48 and 15.26 µg h/ml and 72.99 and 69.25 µg h/ml with i.v. and p.o. administrations, respectively. Higher AUC value of hydroxychalcone indicates more time hydroxychalcone will remain in the systematic circulation giving higher bioavailability.

T_{max} represents the time taken by a substance to reach the maximum concentration (C_{max}) in the blood. Hydroxychalcone, being a weakly acidic compound due to presence of the phenolic groups, remains unionized at gastric pH and hence indicated very fast absorption after oral administration with short T_{max} of 1h. Charantin being nonpolar steroidal compound takes long time for its absorption which is revealed from the highest T_{max} value of

TABLE 7 | Stability data for diosgenin, charantin, and hydroxychalcone in rat plasma.

Marker compounds	Concentration (µg/ml)	Room temperature standard stock solution stability (%)	Refrigerator standard stock solution stability (%)	Freeze thaw stability (%)	Short-term room temperature stability (%)
Diosgenin	0.4	85.18 ± 0.45	91.73 ± 0.46	87.06	98.64
	0.8	84.86 ± 1.23	90.24 ± 1.13	94.52	97.90
	1.2	85.03 ± 2.16	89.56 ± 2.21	97.86	98.25
Charantin	0.4	86.79 ± 2.99	85.79 ± 2.43	74.01	95.25
	0.8	86.02 ± 3.49	88.13 ± 2.13	88.12	90.25
	1.2	88.39 ± 1.52	90.14 ± 2.02	97.85	96.54
Hydroxychalcone	0.4	87.59 ± 2.33	90.03 ± 1.56	63.73	63.76
	0.8	85.15 ± 1.67	94.16 ± 1.32	70.63	79.32
	1.2	87.00 ± 1.23	91.23 ± 1.84	79.32	79.02

Results are presented as mean ± SD (n = 3).

6 h. Although diosgenin is the nonpolar steroidal compound, it takes 1 h to reach the T_{\max} due to higher number of OH groups in compound making it more polar as compared to the charantin. The results of pharmacokinetic parameters presented in **Table 9**, indicate that almost same C_{\max} values of diosgenin, charantin, and hydroxychalcone, 0.57 and 0.61 $\mu\text{g/ml}$, 0.71 and 1.06 $\mu\text{g/ml}$, and 5.42 and 5.35 $\mu\text{g/ml}$, respectively, for i.v. and oral routes of administration were found.

Mean residence time (MRT) is the average time the drug stays at the site of action. MRT for the marker compounds viz, diosgenin, charantin, and hydroxychalcone was found to be 8.20 and 9.94 h, 14.75 and 11.98 h, and 7.87 and 7.90 h for i.v. and oral routes of administration, respectively. MRT is inversely proportional to the AUC of the drug.

Rate of absorption (K_a) determines the time required for the administered drug to the reach an effective plasma concentration and may, thus, affect the onset of drug effect. K_a influences both the peak plasma concentration (C_{\max}) and time it takes to reach the peak (T_{\max}). Highest K_a value of 1.5 h^{-1} was obtained in hydroxychalcone followed by diosgenin (1.1 h^{-1}) and the least of case of charantin, 0.46 h^{-1} . As the rate of absorption is 0.46 h^{-1} , which is less compared to that of diosgenin and hydroxychalcone, it has higher T_{\max} value of 6 h.

Bioavailability is the measurement of the rate and the extent to which drug reaches at the site of action. Absolute bioavailability compares the bioavailability of active drug in systemic circulation following non-intravenous administration, with the bioavailability of the same drug following intravenous administration. The absolute bioavailability of the drug, when administered by extra vascular route is usually less than one (i.e., $F < 100\%$). In the present study, absolute bioavailability of diosgenin, charantin, and hydroxychalcone was found to be 9, 8.18, and 10.54%, respectively. Various physiological factors reduce the availability of the drugs prior to their entry into the systemic circulation. Higher absolute bioavailability for

hydroxychalcone may be due to its higher tissue binding, high molecular weight, higher water solubility, and higher volume of distribution. On the other hand, diosgenin and charantin are the steroidal sapogenins having higher lipid solubility, hence have least volume of distribution, which affects their bioavailability.

Determination of Bioavailability of Formulations

The polyherbal formulations were prepared using the alcoholic extracts. The extracts contain several constituents that can influence the bioavailability and pharmacokinetic parameters of the marker compounds. Piperine is used in the current study as it is known for the enhancement of bioavailability of drug component from ancient time and in the traditional system of medicine Ayurveda (Chen et al., 2017; Mhaske et al., 2018).

Results presented in **Table 10** indicate the values of pharmacokinetic parameters obtained due to oral administration of the formulations F1 and F2 calculated with respect to the marker compounds viz. diosgenin, charantin, and hydroxychalcone. The elimination rate constants K_{el} values of the individual marker compounds in all the formulations were found to be similar when compared with the pure molecules diosgenin, charantin, and hydroxychalcone, respectively. Significant reduction ($p < 0.01$) in the clearance rate of all the three marker compounds is observed in formulation F2 as compared to the formulation F1, indicating availability of the marker compounds for activity due to inhibition of CYP enzymes by piperine **Figure 5** (Volak et al., 2008).

There is a significant increase ($p < 0.01$) in the $AUC_{0-\infty}$ values of individual marker compounds in case of administration of the formulations F2 as compared to F1, indicating availability of significantly higher concentrations of the phytoconstituents for action. This is due to the bioenhancing effect of piperine through inhibition of CYP2D6 and CYP3A4 (ICH Guideline M10 on Bioanalytical Method Validation, 2019).

TABLE 8 | Mean (\pm SD) pharmacokinetic parameters and absolute bioavailabilities for diosgenin, charantin, and hydroxychalcone in rats after a single dose administration.

Parameters	Diosgenin		Charantin		Hydroxychalcone	
	Oral single dose administration (15 mg/kg per oral) ($\mu\text{g/ml}$)	IV single-dose administration (1.5 mg/kg i.v.) ($\mu\text{g/ml}$)	Oral single-dose administration (15 mg/kg per oral) ($\mu\text{g/ml}$)	IV single-dose administration (1.5 mg/kg i.v.) ($\mu\text{g/ml}$)	Oral single-dose administration (15 mg/kg per oral) ($\mu\text{g/ml}$)	IV single-dose administration (1.5 mg/kg i.v.) ($\mu\text{g/ml}$)
K_{el} (h^{-1})	0.0917 \pm 0.003	0.0875 \pm 0.004	0.0832 \pm 0.0005	0.0844 \pm 0.001	0.1481 \pm 0.001	0.1488 \pm 0.001
$t_{1/2}$ (h)	7.5638 \pm 0.21	7.9300 \pm 0.37	8.3328 \pm 0.05	8.2090 \pm 0.13	4.6806 \pm 0.04	4.6565 \pm 0.04
Vd (ml/kg)	—	2.5397 \pm 0.57	—	1.4108 \pm 0.001	—	0.2799 \pm 0.0004
Cl (ml/h/kg)	2.5143 \pm 0.09	0.2221 \pm 0.05	5.9268 \pm 0.31	0.1191 \pm 0.002	0.4199 \pm 0.01	0.0417 \pm 0.0004
AUC_{∞}^0 ($\mu\text{g}\cdot\text{h/ml}$)	4.4753 \pm 0.06	4.9575 \pm 0.44	12.4872 \pm 0.11	15.2678 \pm 0.03	72.9944 \pm 0.49	69.2514 \pm 0.09
C_{\max} ($\mu\text{g/ml}$)	0.5773 \pm 0.012	0.6122 \pm 0.1	0.7725 \pm 0.009	1.0633 \pm 0.001	5.4245 \pm 0.2	5.3583 \pm 0.002
T_{\max} (h)	1	—	6	—	1	—
$AUMC_{\infty}^0$ ($\mu\text{g}\cdot\text{h}^2/\text{ml}$)	36.700 \pm 0.77	17.3937 \pm 2.10	176.7245 \pm 1.83	182.9438 \pm 1.74	574.5756 \pm 1.08	547.3199 \pm 1.21
MRT (h)	8.2008 \pm 0.15	9.9420 \pm 0.90	14.1521 \pm 0.07	11.9823 \pm 0.10	7.8716 \pm 0.04	7.9034 \pm 0.01
K_a (h^{-1})	1.1 \pm 0.10	—	0.4617 \pm 0.02	—	1.5 \pm 0.16	—
Absolute bioavailability (%)	9.0 \pm 0.2		8.18 \pm 0.36		10.54 \pm 0.52	

Results are presented as mean \pm SD ($n = 6$) (K_{el} -elimination rate constant, $t_{1/2}$ -plasma half-life, Cl-drug clearance, AUC-area under curve, C_{\max} -maximum concentration of the drug, T_{\max} -the time taken by a substance to reach the C_{\max} , AUMC-A under the moment curve, MRT-mean residence time, and K_a -rate of absorption).

TABLE 9 | Relative bioavailabilities of diosgenin, charantin, and hydroxychalcone in the formulation without piperine (F1), formulation with piperine (F2), and oral pure drug administration.

Diosgenin:					
Formulations	AUC _{0-∞} (μg.h/ml)	Dose (mg/kg p.o)	Relative bioavailability		
			Standard	Sample	Relative bioavailability
F2	1.9838	0.68	F2	F1	0.7346
Oral pure drug administration	4.4753	15	Oral pure drug administration	F1	9.7782
			Oral pure drug administration	F2	13.3113
Charantin:					
Formulations	AUC _{0-∞} (μg.h/ml)	Dose (mg/kg p.o)	Relative bioavailability		
			Standard	Sample	Relative bioavailability
F2	1.6009	0.179	F2	F1	0.6836
Oral pure drug administration	12.4872	15	Oral pure drug administration	F1	10.7433
			Oral pure drug administration	F2	15.7160
Hydroxychalcone:					
Formulations	AUC _{0-∞} (μg.h/ml)	Dose (mg/kg p.o)	Relative bioavailability		
			Standard	Sample	Relative bioavailability
F2	1.4294	0.0364	F2	F1	0.8523
Oral pure drug administration	72.994	15	Oral pure drug administration	F1	8.0701
			Oral pure drug administration	F2	9.4692

(F1-Formulation without piperine, F2-Formulation containing Piperine).

$t_{1/2}$ represents the time required to reduce the concentration of the drug to be half of C_{max} value due to the elimination process. This value in turn also indicates the time for which the drug remains in the body. There was no significant difference in $t_{1/2}$. The highest MRT values of 13.33 and 14.41 h were observed for charantin in F1 and F2, respectively.

Absorption rate constant K_a values for marker compound was found to be significantly increased ($p < 0.05$) for diosgenin and charantin in F2 as compared to F1, indicating more availability through improved absorption rate constant. In case of charantin, there was a decrease in the value of K_a of the formulation F2 as compared to the formulation F1, indicating increased rate of permeation due to piperine in F2.

Relative bioavailability measures the bioavailability of a formulation of certain drug when compared with another

formulation of the same drug. Relative bioavailability is one of the measures used to assess bioequivalence between two drug products. From the results of bioavailabilities of the markers viz. diosgenin, charantin, and hydroxychalcone from the formulations F1 and F2, the relative bioavailabilities for these were calculated and the results are presented in **Table 9**.

Results presented in **Table 9** indicate that the relative bioavailability of diosgenin in the formulation F1 when calculated with reference to F2 was found to be 0.73. When the relative bioavailability for F1 was compared to that of pure oral drug, it was found to be 9.77. Relative bioavailability for the formulation F2 when compared to the pure drug was found to be 13.31. Hence, it can be concluded that there is a 13-fold increase in the bioavailability of diosgenin due to presence of piperine.

TABLE 10 | Effect of piperine on the pharmacokinetic parameters of the marker compounds viz, diosgenin, charantin, and hydroxychalcone after administration of the herbal formulations.

Parameters	Diosgenin		Charantin		Hydroxychalcone	
	F1 (75 mg/kg per oral) (μg/ml)	F2 (75 mg/kg per oral) (μg/ml)	F1 (75 mg/kg per oral) (μg/ml)	F2 (75 mg/kg per oral) (μg/ml)	F1 (75 mg/kg per oral) (μg/ml)	F2 (75 mg/kg per oral) (μg/ml)
K_{el} (h^{-1})	0.0900 ± 0.004	0.0890 ± 0.001	0.0896 ± 0.0003	0.0844 ± 0.003	0.1450 ± 0.002	0.1412 ± 0.005
$t_{1/2}$ (h)	7.7088 ± 0.32	7.7838 ± 0.117	7.7316 ± 0.025	8.2130 ± 0.25	4.7801 ± 0.08	4.9129 ± 0.169
Cl (mg/h/kg)	0.3456 ± 0.02	0.2199 ± 0.004	0.5553 ± 0.006	0.4548 ± 0.02	0.0685 ± 0.001	0.0350 ± 0.001
AUC _{0-∞} (μg.h/ml)	1.9838 ± 0.02	2.7006 ± 0.006	1.6009 ± 0.034	2.3419 ± 0.05	1.4294 ± 0.01	1.6772 ± 0.003
C_{max} (μg/ml)	0.1962 ± 0.002	0.2975 ± 0.002	0.1008 ± 0.002	0.1506 ± 0.002	0.0954 ± 0.002	0.1517 ± 0.0001
T_{max} (h)	1	1	6	6	1	1
AUMC _{0-∞}	19.7230 ± 0.25	26.1961 ± 0.40	21.3542 ± 0.54	33.7730 ± 1.58	12.490 ± 0.20	12.7395 ± 0.27
MRT (h)	9.9420 ± 0.03	9.700 ± 0.15	13.3383 ± 0.05	14.4165 ± 0.38	8.7378 ± 0.08	7.5954 ± 0.15
K_a (h^{-1})	1.0 ± 0.02	1.1 ± 0.03	0.73 ± 0.04	0.41 ± 0.04	1.2 ± 0.09	1.5 ± 0.24

Results are presented as mean ± SD ($n = 6$), (K_{el} -Elimination rate constant, $t_{1/2}$ - plasma half-life, Cl-drug clearance, AUC- area under curve, C_{max} -maximum concentration of the drug, T_{max} -the time taken by a substance to reach the C_{max} , AUMC- A under the moment curve, MRT-mean residence time, and K_a -rate of absorption).

As per the results for charantin, the relative bioavailability of the charantin in F1 when compared to that of F2 was found to be 0.68. Relative bioavailability of F1 when compared to that of the oral pure drug was found to be 10.74. At the same time, when relative bioavailability of F2 was compared to that of pure drug, it was found to be 15.71. Relative bioavailability of the formulation has been increased due to piperine.

The relative bioavailability of the hydroxychalcone in F1 when compared with that of F2 was found to be 0.85. When relative bioavailability of F1 was compared with that of oral pure drug, it was found to be 8.07. When F2 was compared with that of the pure drug, it was found to be 9.46. Hence, it was observed that there was an increase in the relative bioavailability of formulation due to presence of piperine.

Results of the relative bioavailability as presented in **Table 10** clearly indicate that there was an increase in the bioavailability of the formulation due to incorporation of piperine. Piperine was known for the enhancement of bioavailability of the drug components from the ancient times. When relative bioavailability was studied, it was found that there was a 13- to 15-fold increase ($p < 0.01$) in the bioavailability of the marker compounds in the formulation F2 due to piperine.

CONCLUSION

In conclusion, a bioanalytical HPTLC method has been developed and validated for the first time for evaluation of pharmacokinetics and absolute bioavailabilities of marker compounds diosgenin, charantin, and hydroxychalcone in single oral and intravenous administrated rats. The absolute

bioavailabilities of marker compounds were found to be in the range of 8 to 10% which is increased by about 15% in formulation due to incorporation of piperine.

Further studies can be carried out at various dose levels and measures can be taken for improving the bioavailability.

DATA AVAILABILITY STATEMENT

The original contributions presented in the study are included in the article/**Supplementary Material**; further inquiries can be directed to the corresponding author.

ETHICS STATEMENT

The animal study was reviewed and approved by the Institutional Animal Ethics Committee (IAEC). CPCSEA registration number: SVBCP/IAEC/M ph/18-19/65.

AUTHOR CONTRIBUTIONS

RS: isolation, characterization, HPTLC method development, bioavailability studies, and pharmacokinetic studies. CG: research guide. AN: research guide. NP: bioanalytical method development and validation.

SUPPLEMENTARY MATERIAL

The Supplementary Material for this article can be found online at: <https://www.frontiersin.org/articles/10.3389/fphar.2021.629272/full#supplementary-material>

REFERENCES

- Chen, Z., Lei, Y. L., Wang, W. P., Lei, Y. Y., Liu, Y. H., Hei, J., et al. (2017). Effects of saponin from *Trigonella foenum-graecum* seeds on dyslipidemia. *Iran J. Med. Sci.* 42 (6), 577–585.
- Eissa, L. A., Elsherbiny, N. M., and Maghmomeh, A. O. (2017). Effect of 2-hydroxychalcone on adiponectin level in type 2 diabetes induced experimentally in rats. *Egypt. J. Basic Appl. Sci.* 4 (1), 1–8. doi:10.1016/j.ejbas.2016.12.002
- Geberemeskel, G. A., Debebe, Y. G., and Nguse, N. A. (2019). Antidiabetic effect of fenugreek seed powder solution (*Trigonella foenum-graecum* L.) on hyperlipidemia in diabetic patients. *J. Diabetes Res.* 2019, 8507453. doi:10.1155/2019/8507453
- Guidance for Industry, Bioanalytical Method Validation (2001). *US department of health and human services, Food and drug administration*. Rockville, MD, United States: Center for Drug Evaluation and Research (CDER), Center for Veterinary Medicine (CVM), 1–2.
- ICH Guideline M10 on Bioanalytical Method Validation (2019). *Committee for Human Medicinal Products*. London and European medicine agency.
- Jagannath, K., Chaluvadi, M. R., Mullangi, R., Mamidi, N. V. S. R., and Srinivas, N. R. (2004). Intravenous Pharmacokinetics, oral bioavailability and Dose proportionality of Ragaglitazar, a novel PPAR- α activator in rats. *Biopharma. Drug dispos.* 25, 323–328. doi:10.1002/bdd.413
- Jesus, M., Martins, A. P. J., Gallardo, E., and Silvestre, S. (2016). Diosgenin: recent highlights on Pharmacology and analytical methodology. *J. Anal. Methods Chem.* 2016, 4156293. doi:10.1155/2016/4156293
- Kumar, A. S., and Sanjita, D. (2013). A review article on bioavailability and bioequivalence studies. *Int. J. Pharm. Technol. Res.* 5 (4), 1711–1721.
- Mahmoud, M. F., El Ashry, F. E. Z. Z., El Maraghy, N. N., and Fahmy, A. (2017). Studies on the antidiabetic activities of *Momordica charantia* fruit juice in streptozotocin-induced diabetic rats. *Pharm. Biol.* 55 (1), 758–765. doi:10.1080/13880209.2016.1275026
- Mhaske, D. B., Sreedharan, S., and Mahadik, K. R. (2018). Role of piperine as an effective bioenhancer in drug absorption. *Pharm. Anal. Acta* 9, 7. doi:10.4172/2153-2435.1000591
- Michal, S., Piotr, B., Katarzyna, S., Ewelina, H., and Ewa, P. (2017). Assessment of physical properties of granules with paracetamol and caffeine. *Saudi Pharm. J.* 25, 900–905. doi:10.1016/j.jsps.2017.02.009
- Nagappan, K., Anoop, K., Kowmudi, G., and Sailaja, M. (2018). Charantin: a neglected antidiabetic compound from *Momordica charantia* L. *Int. J. Pharm. Sci. Rev. Res.* 51 (2), 35–40.
- Rajesh, P., Sonia, S. S., Reddy, Y. V., and Kumar, M. S. (2016). Anti-Diabetic profile of cinnamon powder extract in experimental diabetic animal. *Int. J. Pharm. Sci. Res.* 7 (2), 824–828. doi:10.13040/IJPSR.0975-8232.7(2).824-28
- Sonal, D., and Pratima, T. (2015). Charantin: an important lead compound from *Momordica charantia* for the treatment of diabetes. *J. Pharmacognosy Phytochem.* 3 (6), 163–166.

- Tanaka, T., Matsuo, Y., Yamada, Y., and Kouno, I. (2008). Structure of polymeric polyphenols of cinnamon bark deduced from condensation products of Cinnamaldehyde with Catechin and procyanidins. *J. Agric. Food Chem.* 56, 5864–5870. doi:10.1021/jf800921r
- Volak, L. V., Ghirmai, S., Cashman, J. R., and Court, M. H. (2008). Curcuminoids inhibit multiple human cytochromes P450, UDP-glucuronosyltransferase, and sulfotransferase enzymes, whereas piperine is a relatively selective CYP3A4 inhibitor. *Drug Metab. Dispos.* 36, 1594–1605. doi:10.1124/dmd.108.020552
- Wadhwa, S., Singhal, S., and Rawat, S. (2014). Bioavailability enhancement by piperine: a review. *Asian J. Biomed. Pharm. Sci.* 04 (36), 1–8.

Conflict of Interest: The authors declare that the research was conducted in the absence of any commercial or financial relationships that could be construed as a potential conflict of interest.

Copyright © 2021 Salunkhe, Gadgoli, Naik and Patil. This is an open-access article distributed under the terms of the Creative Commons Attribution License (CC BY). The use, distribution or reproduction in other forums is permitted, provided the original author(s) and the copyright owner(s) are credited and that the original publication in this journal is cited, in accordance with accepted academic practice. No use, distribution or reproduction is permitted which does not comply with these terms.



Anti-Myocardial Ischemia Reperfusion Injury Mechanism of Dried Ginger-Aconite Decoction Based on Network Pharmacology

Feng Xie, Yuan-Yuan Wu, Guang-Jing Duan, Bin Wang, Feng Gao, Pei-Feng Wei, Lin Chen, A-Ping Liu and Min Li*

School of Pharmacy, Shaanxi University of Chinese Medicine, Xi'an, China

OPEN ACCESS

Edited by:

Sayed Ahmad,
Jamia Hamdard University, India

Reviewed by:

Shijun Xu,
Chengdu University of Traditional
Chinese Medicine, China
Mohd Shahid,
Chicago State University,
United States

*Correspondence:

Min Li
413159921@qq.com

Specialty section:

This article was submitted to
Inflammation Pharmacology,
a section of the journal
Frontiers in Pharmacology

Received: 24 September 2020

Accepted: 08 April 2021

Published: 06 May 2021

Citation:

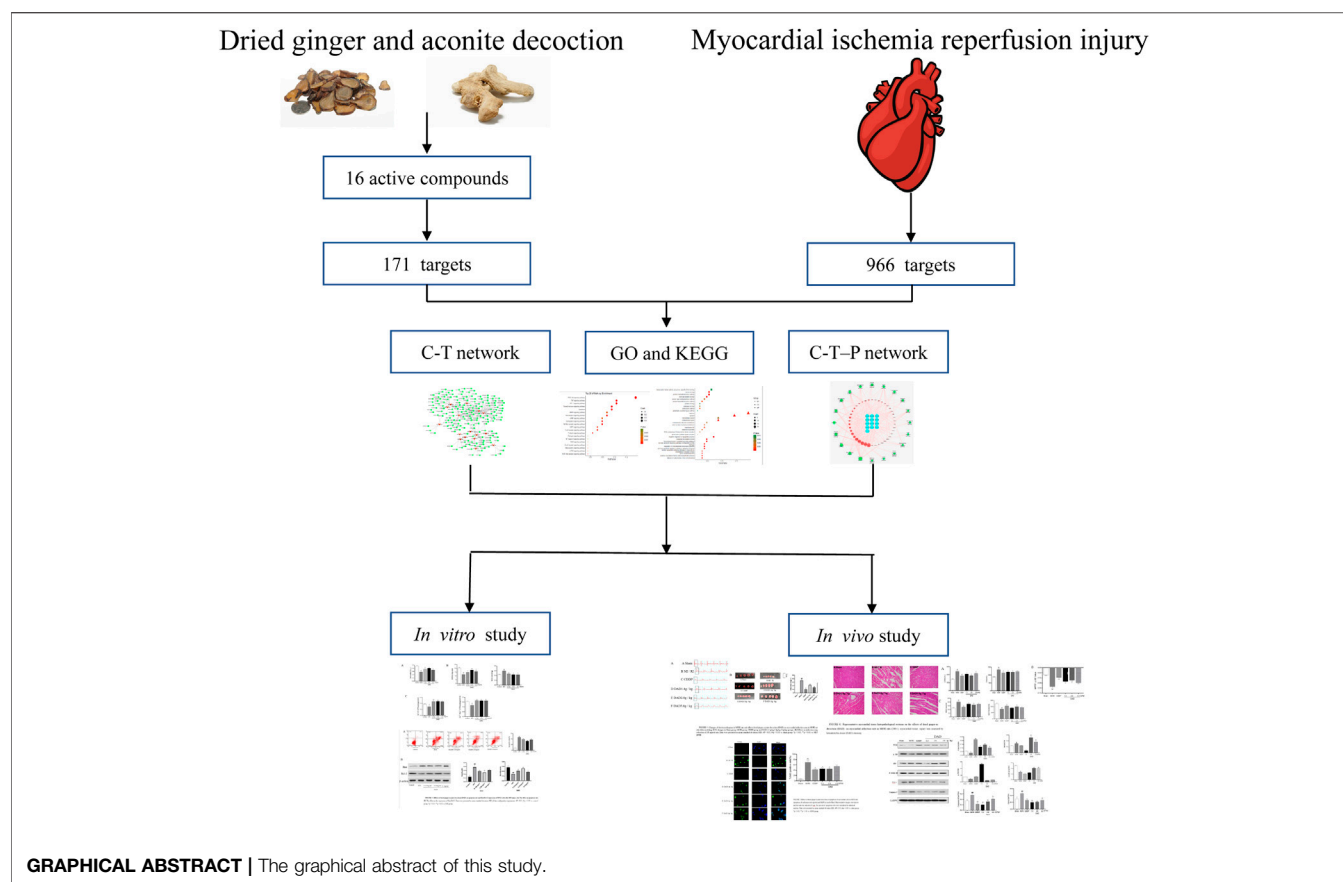
Xie F, Wu Y-Y, Duan G-J, Wang B,
Gao F, Wei P-F, Chen L, Liu A-P and
Li M (2021) Anti-Myocardial Ischemia
Reperfusion Injury Mechanism of Dried
Ginger-Aconite Decoction Based on
Network Pharmacology.
Front. Pharmacol. 12:609702.
doi: 10.3389/fphar.2021.609702

Dried ginger-aconite decoction (DAD) is a traditional Chinese medicine (TCM) formula that has been extensively used in the treatment of myocardial ischemia reperfusion injury (MI/RI). However, its specific mechanism against MI/RI has not been reported yet. Therefore, this paper studies the potential active components and mechanism of DAD against MI/RI based on network pharmacology and experimental verification. Sixteen active components of DAD were screened according to oral bioavailability and drug similarity indices. Through Cytoscape 3.7.0, a component-target network diagram was drawn, and potential active components of DAD against MI/RI were determined. Protein-protein interaction (PPI) and compound-target-pathway (C-T-P) networks were established through the software to discover the biological processes, core targets and core pathways of DAD against MI/RI. High Performance Liquid Chromatography (HPLC) analysis identified the presence of potentially active core components for network pharmacological prediction in DAD. It was found that DAD might have played a therapeutic role in anti-MI/RI by activating the PI3K/Akt/GSK-3 β signaling pathway in order to reduce mitochondrial hypoxia injury and myocardial cell apoptosis. The network pharmacological prediction was validated by Hypoxia/reoxygenation(H/R) model *in vitro* and ligation model of the ligation of the left anterior descending branch *in vivo*. It was verified that DAD had activated PI3K/AKT/GSK-3 β to reduce myocardial apoptosis and play a therapeutic function in MI/RI.

Keywords: dried ginger-aconite decoction, myocardial ischemia reperfusion injury, network pharmacology, energy metabolism, tcm

INTRODUCTION

Myocardial ischemia-reperfusion injury (MI/RI) denotes the further destruction of the cardiac structure, and the further aggravation of metabolic dysfunction or even irreversible damage of the myocardial cell, following the restoration of blood supply of ischemic and anoxic myocardial tissue, which mainly involves re-expansion of myocardial infarction area and life-threatening arrhythmia (Lee et al., 2002; Raedschelders et al., 2012; Inoue, 2016). A common clinical cardiovascular disease, it has since developed into a killer ailment with high morbidity and mortality (Hausenloy and Yellon, 2013; Heusch, 2017). It typically occurs among the middle-aged and elderly population; however, as social competition becomes increasingly fierce, pressure on the youth has also increased, as they are



also prone to develop myocardial ischemic diseases (Ingram et al., 2013; Han et al., 2018). Some studies indicate that 18 million people die of cardiovascular diseases every year globally, of which MI/RI incidence accounts for around 50% (Wei, 2017). MI/RI pathogenesis involves the interaction of multiple mechanisms, including vasoconstrictor release, non-reperfusion, deep inflammatory response, apoptosis and necrosis (Chen et al., 2020; Li et al., 2020a; Samiotis et al., 2021). Albeit not quite effective, the current treatment methods for MI/RI are percutaneous coronary intervention and the use of related thrombolytic drugs; nevertheless, MI/RI still has a high mortality rate worldwide. Therefore, research and attention on the mechanism of MI/RI have a considerable significance for its prevention and treatment.

Traditional Chinese medicine (TCM) plays an indispensable role in the prevention and treatment of MI/RI. It spans a long history, including Yi Qi Huoxue decoction, Gualou Xiebai Baijiu decoction and Si Ni decoction (Deng et al., 2017; Zheng and Bao, 2017; Gao et al., 2019). It has been extensively used in MI/RI treatment, and dried ginger-aconite decoction (DAD), which comprises two kinds of Chinese herbal medicines, is one such medicine. Composed of aconite and dried ginger, DAD is recorded in the *Treatise on Febrile and Miscellaneous Disease*. Considering the efficacy of Yang for resuscitation, DAD is used to clinically treat ischemic heart diseases (Xu, 1986). Previous studies have indicated that DAD has a protective effect on the hearts of

rats with MI/RI, and such effect is closely associated with its antioxidant and apoptosis effect (Shi et al., 2014). However, its bioactive compounds and their pharmacological mechanisms are still relatively unclear.

Network pharmacology integrates biological systems and multi-directional pharmacological approaches, incorporates biological networks and drug action networks, transcends the constraints of single-target beliefs, and begins from multi-target research strategies in order to achieve a comprehensive network analysis of drug effects (Xu et al., 2014; Chen et al., 2017; Zhang et al., 2018a). It is a significant approach to study the mechanisms of the multi-components, multi-targets and multi-pathways of TCM (Hopkins, 2008; Li and Zhang, 2013). The varied components of DAD are complex. Previous studies have determined that DAD can treat MI/RI by reducing the apoptosis of cardiomyocytes; however, the exact mechanism remains vague. Therefore, a comprehensive method is applied in this study to illustrate the molecular mechanisms of DAD. Network pharmacology is used to predict the active components and mechanisms of DAD in MI/RI treatment. HPLC is applied to determine whether DAD contains certain components for network pharmacological prediction. Afterward, *in vivo* and *in vitro* experiments are conducted to validate its mechanism on network pharmacological prediction. A graphical abstract of this study is presented in Graphical Abstract.

MATERIALS AND METHODS

Materials

Aconitum abietetorum W.T.Wang and L.Q.Li (No. 51078020190334YC) and *Zingiber officinale* Roscoe (No. 51078020191020YC) were obtained from Jiangyou City, Sichuan Province, China. The geographical location of Jiangyou is within 31°32'26"–32°19'18" north and 104°31'35"–105°17'30" east. Material authentication for TCM identification was carried out by Professor Gang Zhang of Shaanxi University of Chinese Medicine. The samples were deposited at the Herbal Medicine Museum of the same university.

Fetal bovine serum (FBS) was purchased from BI (United States). Phosphate buffer saline (PBS) and Dulbecco's modified Eagle medium (DMEM) were procured from Gibco (United States). Penicillin streptomycin mixture and Cell Counting Kit-8 (CCK-8) from Shanghai Biyuntian Co., Ltd. (Shanghai, China). Dimethyl sulfoxide (DMSO) and trypsin were also procured from Gibco (United States). The assay kits for malondialdehyde (MDA), superoxide dismutase (SOD) apoptosis, atpase, creatine kinase (CK), mitochondrial permeability transition pore (MPTP), lactate dehydrogenase (LDH) and glutathione peroxidase (GSH-PS) were all obtained from Boster Biological Technology Co., Ltd. (Wuhan, China). Cyt-C, β -action, GADPH, Casp9, PI3K, AKT, Bax, Bcl-2 and phosphorylated(P)-AKT, GSK3 β were also purchased from Boster Biological Technology Co., Ltd. (Wuhan, China). 6-gingerol (202,003), aconitine (No. A0608), mesaconitine (A0196) and hypaconitine (A0609) were all purchased from Chengdu Munst Biotechnology Co., Ltd. Standard purity was set as more than 98%. Methanol and triethylamine were purchased from Shaanxi Weitong Chemical Co., Ltd.

Dried ginger-aconite decoction Preparation

Aconite and dried ginger were mixed at a 1:1 ratio. They were soaked in water for 0.5 h, then were boiled twice for 1 h each time. The filtrates were collected via gauzes, combined and concentrated to 1 g/ml to obtain the extract. For this study, 100 g of aconite and 100 g of dried ginger were prepared. Both components were completely immersed in water for 0.5 h. Then, 1.6 L water was added, letting the mixture boil for 1 h twice. The extract was then collected, filtered with gauze, and concentrated to 200 ml. The supernatant was obtained after centrifugation of the solution at 3,000 r/min, sterilized with 0.22 μ m aqueous microporous membrane, and sealed.

Network Pharmacology

Screening of Dried ginger-aconite decoction Active Components and Collection of Targets

The chemical constituents of aconite and dried ginger were examined from the Traditional Chinese Medicine Integrated Database (TCMSP, <https://tcmsp.com/tcmsp.php>) and the Comparative Toxicogenomic Database (CTD, <http://ctdbase.org/>), with aconite and dried ginger as the keywords. Active components of DAD were screened via oral bioavailability (OB)

and drug-like quality (DL) (Cao et al., 2018), with DL \geq 0.18 and OB \geq 30% as the thresholds.

The primary compounds of aconite and dried ginger are alkaloids and volatile oil, both of which are irreplaceable and have good pharmacological activity. Thus, the following nine compounds were supplemented: deoxyaconitine, aconitine, hypaconitine, mesaconitine, 6-gingerol, 8-gingerol, 10-gingerol, 6-shogaol, and zingerone. The targets of all active compounds were obtained and imported into the Universal Protein (UniProt) database (<https://www.uniprot.org/>) to standardize their names.

Predicting Targets of DAD Against MI/RI

With "myocardial ischemia-reperfusion injury" as the keywords, MI/RI targets in the Disgenet database (<https://www.disgenet.org/>) limited to "*Homo sapiens*" were obtained. The interactions of the DAD and MI/RI targets were considered as the potential therapeutic targets. The protein-protein interaction (PPI) of the common targets was accomplished in the string database (<https://string-db.org/>); the parameter organism was set to *Homo sapiens*, while the other basic settings were set as default. Using the Cytoscape 3.7.0 software, compound-target (C-T) and PPI were constructed.

Pathway and Functional Enrichment Analysis

The database for Annotation, Visualization and Integrated Discovery (DAVID) v6.8 (www.david.ncicrf.gov/) provides a comprehensive set of functional annotation tools for researchers to understand the biological meanings behind extensive lists of genes. It was employed to undertake pathway enrichment analyses using the Gene Ontology (GO) and the Kyoto Encyclopedia of Genes and Genomes (KEGG) databases. Pathway terms with $p < 0.05$ were deemed significant. Using the Cytoscape 3.7.0 software, compound-target-pathway (C-T-P) was constructed.

In vitro Experiment

HPLC Method for Component Analysis

DAD was filtered through a 0.22 μ m nylon membrane prior to HPLC analysis. An HPLC System (Thermo, United States) was used to separate the components of DAD. All components were separated by Waters Bridge C18 (4.6 mm \times 150 mm, 5 μ m) and a C18 guard. Flowrate was set at 1.0 mL min⁻¹. The column temperature was 30°C. The wavelength was set at 237 nm. The mobile phases were (A) methanol and (B) triethylamine aqueous solution, with gradient elution of 0–15 min (A: B = 30:70), 15–40 min (A:B = 65:35) and baseline (A:B = 30:70).

Grouping and Modeling

Rat myocardial cells (H9C2) were purchased from Wuhan Punosai Life Science and Technology Co., Ltd. (Wuhan, China). The cells were cultured in DMEM with 10% FBS, 100 U/ml penicillin and 100 μ l/ml streptomycin. They were maintained inside a humidified incubator with 95% air and 5% CO₂ at 37°C. They were subjected to experimental procedures when they reached an 80% confluence level of population. They were classified into five groups: control group, Hypoxia/reoxygenation(H/R) group, DAD low-dose group

(0.125 mg/ml), DAD medium-dose group (0.25 mg/ml), and DAD high-dose group (0.5 mg/ml). For all experiments, the cells were rendered quiescent by serum starvation for 24 h before treatment. Following pretreatment with DAD at varied doses for 24 h, the cells for all groups—except for the control group and the H/R group—were incubated in DMEM and glucose-free DMEM, respectively and then placed inside a hypoxia chamber (Stem Cell Technologies, San Diego, CA, United States). The chamber was flushed with 95% (v/v) N₂ and 5% (v/v) CO₂ at a flowrate of 15 L/min for 10 min, and maintained at 37°C to induce hypoxia injury. After hypoxia for 12 h, reoxygenation was conducted by replacing the medium to DMEM that contained 4.5 mM glucose (pH 7.4) and by subsequent incubation in a CO₂ incubator (5% (v/v) CO₂, 95% (v/v) air) for 2 h (Wang et al., 2018).

Survival Rate of H9C2 Cells

CCK8 assay was applied to determine the influence of DAD on the survival rate of H9C2 cells that were damaged by oxygen. The cells were briefly seeded onto 96-well plates and then cultured until they adhered. Afterward, the cells were treated with DAD at varied concentrations (0.125 mg/ml, 0.25 mg/ml, 0.5 mg/ml). Model group and control group were given DMEM (without glucose) and DMEM, respectively. Model according to the above method. Afterward, 10 µl of CCK-8 was added, and the mixture was incubated for another 2 h. Absorbance was recorded at 450 nm, and the experiments were performed in parallel in triplicate.

Detection of Apoptosis Rate

The H/R damaged cells in each group were digested with 0.25% trypsin and centrifuged at 1,500 r/min for 5 min. The supernatant was discarded and the cells were collected. The collected cells were then resuspended with PBS (pH 7.2), washed with PBS twice, and centrifuged at 1,500 r/min for 5 min, before the supernatant was discarded. The precipitated cells were resuspended with 500 µl of binding buffer, then 5 µl of annexin V-FITC and 5 µl of PI staining solution was added. After mixing, the cells were incubated at room temperature in the dark for 5–15 min. Finally, the apoptosis for each group was detected by flow cytometry (NovoCyte 452180529501, Thermo, United States).

Biochemical Testing

After H/R injury, the cells in each group were obtained. According to the manufacturer's protocols, the SOD, MDA, Na⁺-K⁺-ATP and Ca²⁺-Mg²⁺-ATP levels were detected by their respective commercial kits.

In vivo Experiment

Establishment and Grouping of MI/RI in Rat Models

Sixty Sprague-Dawley male rats were purchased from Chengdu Da Shuo Experimental Co., Ltd. (Sichuan, China). They were housed in a specific-pathogen-free (SPF) environment. The rats in DAD low-dose, DAD medium-dose and DAD high-dose groups were orally administered with 1.4 g/kg, 2.8 g/kg and 5.6 g/kg DAD once daily, respectively. Those in the positive control group were orally administered with 0.09 g/kg per day

of compound danshen dripping pills (CDDP), and those in the model, and sham group were orally administered with the same volume of 0.9% NaCl. A week later, all rats were operated, with the sham group only opening the chest without ligation. Left thoracotomy and pericardiectomy, followed by left anterior descending coronary artery ligation, were performed. After 40 min of ischemia, the ligature was opened for reperfusion for 2 h. The serum and heart tissue samples were prepared for future experiment. All animal experiments were performed in accordance with the Animal Care and Use Committee of the Institute of Materia Medica, China (No. TCM-2019-194,040-E08).

Detection of Myocardial Infarction Area in MI/RI Rats

Prior to the experiment, 2% TTC was placed in a 37°C thermostat for 0.5 h. Four rats were randomly selected from each group. Their hearts were removed, flushed with PBS, and rapidly frozen at -20°C. The specimens were uniformly cut into 1 mm slices under the line of ligature and placed in a 37°C, 2% TTC solution to dye for 20 min, and then fixed with 10% formaldehyde solution. Ultimately, the myocardial infarction area was white and the non-infarction area was red. The infarct area was calculated using ImageJ software (Media Cybernetics, Inc., Rockville, MD, United States). The applied equation was as follows,

$$\text{Infarction Range} = \frac{\text{Infarction Range}}{\text{Left Ventricular Area}} \times 100\%.$$

Immunohistochemical Staining

Immediately after reperfusion, the heart was removed and rinsed in precooled saline. The myocardium from the anterior wall of the left ventricle was removed. The heart was then fixed with precooled 4% paraformaldehyde and rinsed with water for 12 h. The specimens were dehydrated afterward. They were then immersed in xylene, and hematoxylin-eosin (H-E) staining was conducted after routine paraffin-embedded staining. Then, the slices were sealed with conventional resin, and the pathological changes in the myocardium were observed under an optical microscope (Olympus BX 41, Japan).

Myocardial Tissue Apoptosis Detection

After MI/RI modeling, the heart tissue was removed. The tissue sections were washed in a phosphate buffer solution, and fixed in a 4% paraformaldehyde solution. They were then cut into paraffin sections with a thickness of 4 µm, and proteinase K was added. After a strict color rendering according to the kit instructions, five visual fields were randomly selected for shooting, and the color images of ten independent fields were randomly captured and digitized. The cells with clear nuclear markers were defined as TUNEL positive. Image J software was used for recording, and the apoptosis rate was calculated. The applied equation was as follows:

$$\text{Apoptosis index} = \frac{\text{Number of TUNEL positive cells}}{\text{Total number of cardiomyocytes}} \times 100\%.$$

Biochemical Testing

After reperfusion, the rats were intraperitoneally anesthetized using chloral hydrate (30 mg/kg), and the blood samples were

TABLE 1 | Information on the 16 active compounds in the DAD.

Herbal name	TCMSP ID	Compound	OB	DL
Aconite	MOL002395	Deoxyandrographolide	56.3	0.31
Aconite	MOL002398	Karanjin	69.56	0.34
Aconite	MOL002424	aconitine	7.87	0.23
Aconite	MOL000538	hypoconitine	31.39	0.26
Aconite	MOL002089	mesaconitin	8.7	0.25
Aconite	MOL002388	Delphin_qt	57.76	0.28
Aconite	MOL002392	Deltoin	46.69	0.37
Dried ginger	MOL002467	6-gingerol	35.64	0.16
Dried ginger	MOL002459	10-gingerol	19.14	0.28
Dried ginger	MOL002495	6-shogaol	31	0.14
Dried ginger	MOL002516	zingeron	25.23	0.05
Dried ginger	MOL000359	sitosterol	36.91	0.75
Dried ginger	MOL002464	1-Monolinolein	37.18	0.3
Dried ginger	MOL002501	[(1S)-3-[(E)-but-2-enyl]-2-methyl-4-oxo-1-cyclopent-2-enyl] (1R,3R)-3-[(E)-3-methoxy-2-methyl-3-oxoprop-1-enyl]-2,2-dimethylcyclopropane-1-carboxylate	62.86	0.3
Dried ginger	MOL002514	Sexangularetin	35.64	0.16
Dried ginger	MOL000358	beta-sitosterol	36.91	0.75

obtained from the abdominal aorta. The samples were left standing at room temperature for 30 min and then centrifuged at 3,000 r/min for 15 min. The serum was collected and stored at -80°C until used. Based on the manufacturer's protocols, the GSH-Sp, MDA, CK and LDH levels were detected by the respective commercial kits.

Detection of MPTP Open Holes in Myocardial Tissues

The fresh myocardial tissue just removed was rinsed with PBS; the excess water on the surface of the myocardial tissue was absorbed using a filter paper. The proper part of the entire heart tissue was taken; its mass was accurately measured, and the tissue homogenate was prepared using a mass-to-volume ratio of 1:9. The entire operation needed to be conducted in an ice bath. Finally, the tissue homogenate was centrifuged for 3,500 r/min for 10 min. The supernatant was collected and stored at -80°C for later use. The openness of the MPTP holes in the homogenate was determined according to the kit instructions.

Western Blot Analysis (*in vivo* and *in vitro*)

The myocardial tissue and the H9C2 cells were lysed by RIPA buffer (Shanghai Weiao Biological Technology Co., Ltd., China) containing cocktail protease inhibitors (1:100) and a protein phosphatase inhibitor (1:50) for 30 min on ice. The protein concentration in the supernatants was determined by BCA assay (Shanghai Weiao Biological Technology Co., Ltd., China). Protein samples were loaded with 10% SDS-polyacrylamide gel (Shanghai Weiao Biological Technology Co., Ltd. China), and then electrophoretically transferred onto PVDF (Millipore, Billerica, MA, United States). The membranes were blotted with 5% fat-free milk in a TBST buffer for 2 h at room temperature and then incubated at 4°C overnight with the following primary antibodies: anti-Caspase-9 (1:600), anti-Bax (1:500), anti-Bcl-2 (1:500), anti-Cyt-c (1:500), anti-PI3K (1:500), anti-Akt (1:1,000), anti-p-Akt (1:1,000), anti-p-GSK-3 β (1:1,000), and anti-GAPDH (1:1,000). The membrane was rinsed thrice on the second day and then incubated with HRP-conjugated secondary antibodies for 1 h at room

temperature. The blots were imaged under an enhanced chemiluminescence (ECL) system. The target band molecular weights and the net optical density were analyzed using the AlphaEase FC software (Alpha Innotech, United States).

Statistical Analysis

All data were expressed as mean \pm standard deviation (SD). GraphPad Prism 7 software was employed to ascertain statistically significant differences. The differences among multiple groups were assessed using one-way analysis of variance (ANOVA). The difference between the means was considered statistically significant when $p < 0.05$.

RESULTS

Network Pharmacology

DAD Active Compounds and Target Screening

From aconite and dried ginger, 16 compounds (Table 1) were retrieved from the TCMSP database, and 171 targets were retrieved from the TCMSP and CTD databases (Figure 1A). A total of 966 targets of MI/RI were obtained from the DisGeNet databases. A total of 80 targets (Table 2) were obtained through the intersection of the 966 MI/RI targets and the 171 putative targets of aconite and dried ginger. These 80 mutual targets were identified as potential therapeutic targets for DAD against MI/RI (Figure 1B). The C-T network included 187 nodes (16 for potential bioactive components and 171 for protein targets). Among the bioactive components, aconitine (DAD, degree = 48), 6-ginger (DAD, degree = 31) and mesaconitine (DAD, degree = 25), hypoconitine (DAD, degree = 24) exhibited the greatest correlation with MI/RI. These could be the key components of DAD against MI/RI.

PPI Network Analysis

To examine the potential interactions of the 80 targets, String 11.0 database was used to build a PPI network. The minimum

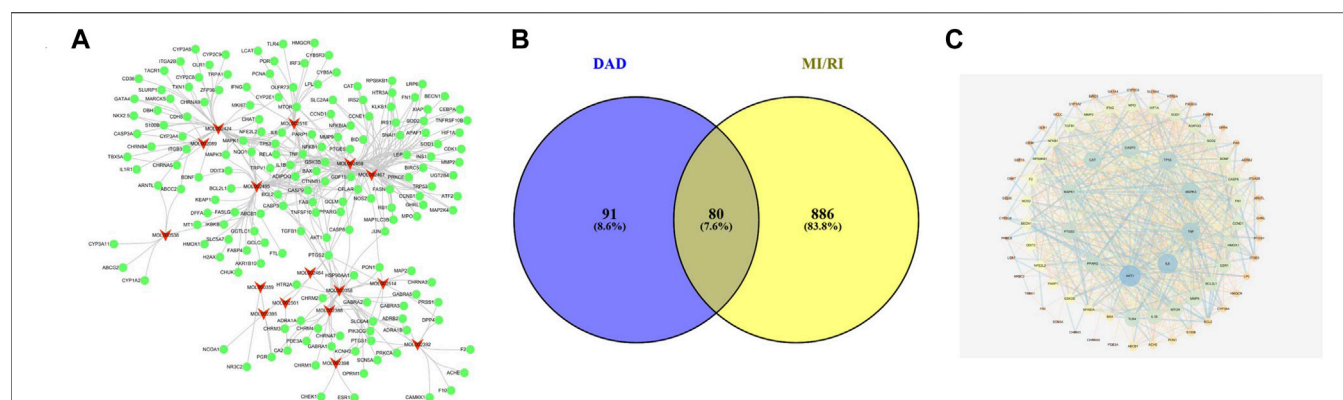


FIGURE 1 | The networks of dried ginger and aconite decoction anti-MI/RI. **(A)** The compound-target network of DAD. The red nodes represent active compounds and the green nodes represent targets. The target surrounding the active components are proportional to their degree. **(B)** Overlap of DAD and MI/RI targets. The blue circles represent DAD targets and the yellow circles represent MI/RI targets. The shaded area is the target of DAD anti-MI/RI. **(C)** The protein-protein interaction network of protein targets obtained from STRING database and constructed by Cytoscape. The colors of the nodes are illustrated from blue to yellow to orange in descending order of degree values.

TABLE 2 | Targets information of DAD anti-MI/RI.

Target name	Full name of the target	Uniprot ID
MAPK3	Mitogen-activated protein kinase 3	P27361
CYP2C9	Cytochrome P450 2C9	P11712
CYP2C8	Cytochrome P450 2C8	P10632
CYP3A4	Cytochrome P450 3A4	P08684
ARNTL	Aryl hydrocarbon receptor nuclear translocator-like protein 1	O00327
CD36	Platelet glycoprotein 4	P16671
GATA4	Transcription factor GATA-4	P43694
ITGA2B	Integrin alpha-IIb	P08514
ITGB3	Integrin beta-3	P05106
MTOR	Serine/threonine-protein kinase mtor	P42345
OLR1	Ox-LDL receptor 1	P78380
S100B	Protein S100-B	P04271
TNF	Tumor necrosis factor	P01375
BAX	Apoptosis regulator BAX	Q07812
BCL2	Apoptosis regulator Bcl-2	P10415
BDNF	BDNF	P23560
CASP3	Caspase-3	P42574
MAPK1	Mitogen-activated protein kinase 1	P28482
CHAT	SH2 domain-containing protein 3C	Q8N5H7
CHRNA5	Neuronal acetylcholine receptor subunit alpha-5	P30532
IL1B	Interleukin-1 beta	P01584
IL6	Interleukin-6	P05231
NFKB1	Nuclear factor NF-kappa-B p105 subunit	P19838
TP53	Cellular tumor antigen p53	P04637
TRPA1	Transient receptor potential cation channel subfamily a member 1	O75762
ABCB1	ATP-dependent translocase ABCB1	P08183
CYP1A2	Cytochrome P450 1A2, EC 1.14.14.1	P05177
GSK3B	Glycogen synthase kinase-3 beta, GSK-3 beta	P49841
CCND1	G1/S-specific cyclin-D1	P24385
PPARG	PPAR-gamma	P37231
PTGS2	Prostaglandin G/H synthase 2	P35354
BIRC5	Baculoviral IAP repeat-containing protein 5	O15392
GDF15	Growth/differentiation factor 15	Q99988
CASP8	Caspase-8	Q14790
NOS2	Nitric oxide synthase, inducible	P35228
CAT	Catalase	P04040
MMP2	72 kDa type IV collagenases	P08253
ADIPOQ	Adiponectin	Q15848
MMP9	Matrix metalloproteinase-9	P14780
MPO	Myeloperoxidase	P05164
PARP1	Poly [ADP-ribose] polymerase 1	P09874

(Continued on following page)

TABLE 2 | (Continued) Targets information of DAD anti-MI/RI.

Target name	Full name of the target	Uniprot ID
SOD1	Superoxide dismutase [Cu-Zn]	P00441
SOD2	Superoxide dismutase [Mn], mitochondrial	P04179
AKT1	RAC-alpha serine/threonine-protein kinase	P31749
BECN1	Beclin-1	Q14457
FAS	Tumor necrosis factor receptor superfamily member 6	P25445
FN1	Fibronectin	P02751
GHRL	Appetite-regulating hormone	Q9UBU3
HIF1A	Hypoxia-inducible factor 1-alpha	Q16665
NFKBIA	NF-kappa-B inhibitor alpha	P25963
PRKCE	Protein kinase C epsilon type	Q02156
RPS6KB1	Ribosomal protein S6 kinase beta-1	P23443
NFE2L2	Nuclear factor erythroid 2-related factor2	Q16236
HMOX1	Heme oxygenase 1	P09601
DDIT3	DNA damage-inducible transcript 3 protein	P35638
GCLC	Glutamate--cysteine ligase catalytic subunit	P48506
FABP4	Fatty acid-binding protein	P15090
GCLM	Glutamate--cysteine ligase regulatory subunit	P48507
BCL2L1	Bcl-2-like protein 1	Q07817
HMGCR	3-hydroxy-3-methylglutaryl-coenzyme a reductase	P00347
IFNG	Interferon gamma	P01579
LCAT	Phosphatidylcholine-sterol acyltransferase	P04180
LPL	Lipoprotein lipas	P06858
TGFB1	Transforming growth factor beta-1 proprotein	P01137
TLR4	Toll-like receptor 4	O00206
PTGS1	Prostaglandin G/H synthase 1	P23219
PIK3CG	PI3K-gamma	P48736
F2	Prothrombin	P00734
SCN5A	Sodium channel protein type 5 subunit alpha	Q14524
F10	Coagulation factor X	P00742
ACHE	Acetylcholinesterase, AChE, EC 3.1.1.7	P22303
ADRB2	Beta-2 adrenergic receptor	P07550
DPP4	Dipeptidyl peptidase 4	P27487
ESR1	Estrogen receptor	P03372
NR3C2	Mineralocorticoid receptor	P08235
CHRM3	Muscarinic acetylcholine receptor M3	P20309
PDE3A	cGMP-inhibited 3',5'-cyclic phosphodiesterase A	Q14432
HTR2A	5-hydroxytryptamine receptor 2A	P28223
SLC6A4	Sodium-dependent serotonin transporter	P31645
PON1	Serum paraoxonase/arylesterase 1	P27169

combined score between the targets was set as the medium confidence (0.400). The PPI network of the potential target was saved as a TSV file and then entered into Cytoscape 3.7.0 for visualization (**Figure 1C**). In the PPI network, targets with high degrees played a significant role in central correlation. The top 5 targets, which were ranked in terms of degree value, were acquired as the core targets. These targets were AKT1 (degree = 47), IL6 (degree = 41), TNF (degree = 38), MAPK3 (degree = 36) and TP53 (degree = 30).

GO Enrichment Analysis

The biological function of DAD against MI/RI was identified by GO enrichment of the 80 potential therapeutic targets. A total of 158 GO items were obtained from the GO enrichment analysis of 80 potential therapeutic targets, including 118 biological processes (BP), 22 cell components (CC) and 18 molecular functions (MF) ($p < 0.05$). To realize a brief

demonstration, only the top 10 significant GO entries were selected for further analysis. The top ten analyses for BP, CC and MF were selected respectively (**Figure 2A**), which indicated that DAD might regulate cell apoptosis, inflammation and mitochondrial energy metabolism to exert its therapeutic effects against MI/RI.

Pathway Enrichment

To examine the potential pathways of DAD on MI/RI, a pathway enrichment of the 80 potential therapeutic targets was conducted. The top 20 significantly enriched pathways are presented in **Figure 2B**. Among the potential pathways, PI3K/AKT signaling was the most prominently enriched based on the gene numbers. To further clarify and elucidate the molecular mechanism of DAD treatment on MI/RI, a C-T-P network diagram was drawn based on the top 20 signaling pathways, as well as the targets and compounds involved (**Figure 2C**). After integrating drug target

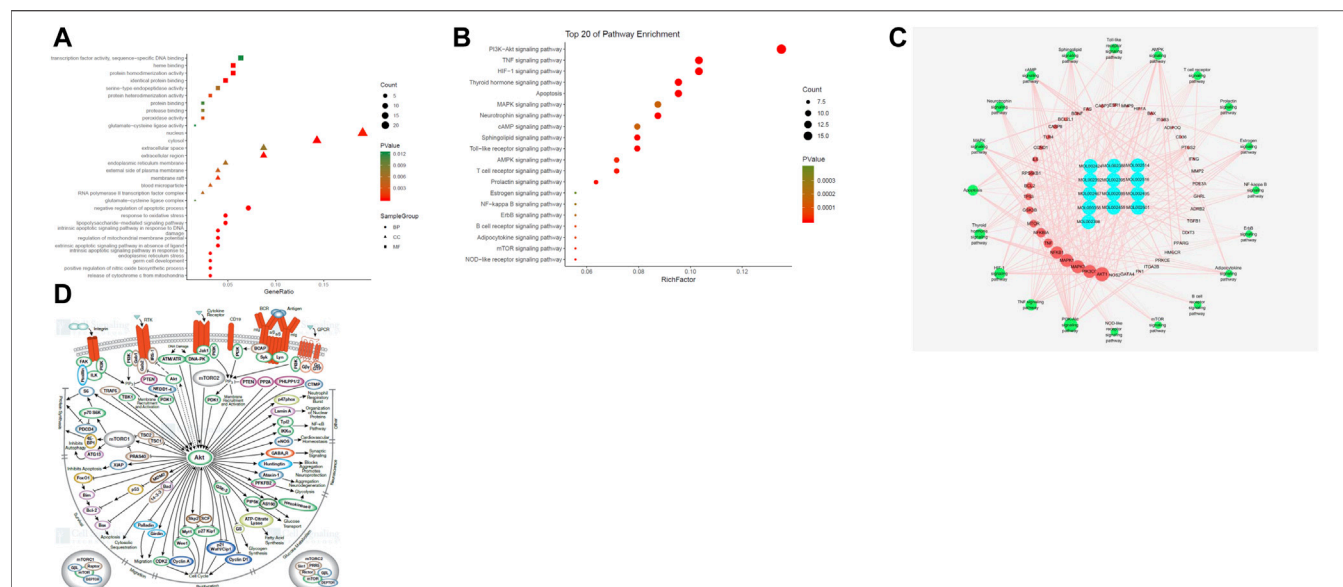


FIGURE 2 | (A) The gene ontology (GO) enrichment analysis for key targets. **(B)** The KEGG pathway enrichment analysis of key targets. **(C)** The compound-target-pathway network constructed by Cytoscape. The blue nodes represent active components in DAD, the red nodes represent putative targets, the green nodes represent the signaling pathways. Node's size is proportional to their degree. **(D)** PI3K/Akt signaling pathway network (PI3K/Akt signaling pathway network is derived from <https://www.cellsignal.cn/pathways/pathways-akt-signaling>)

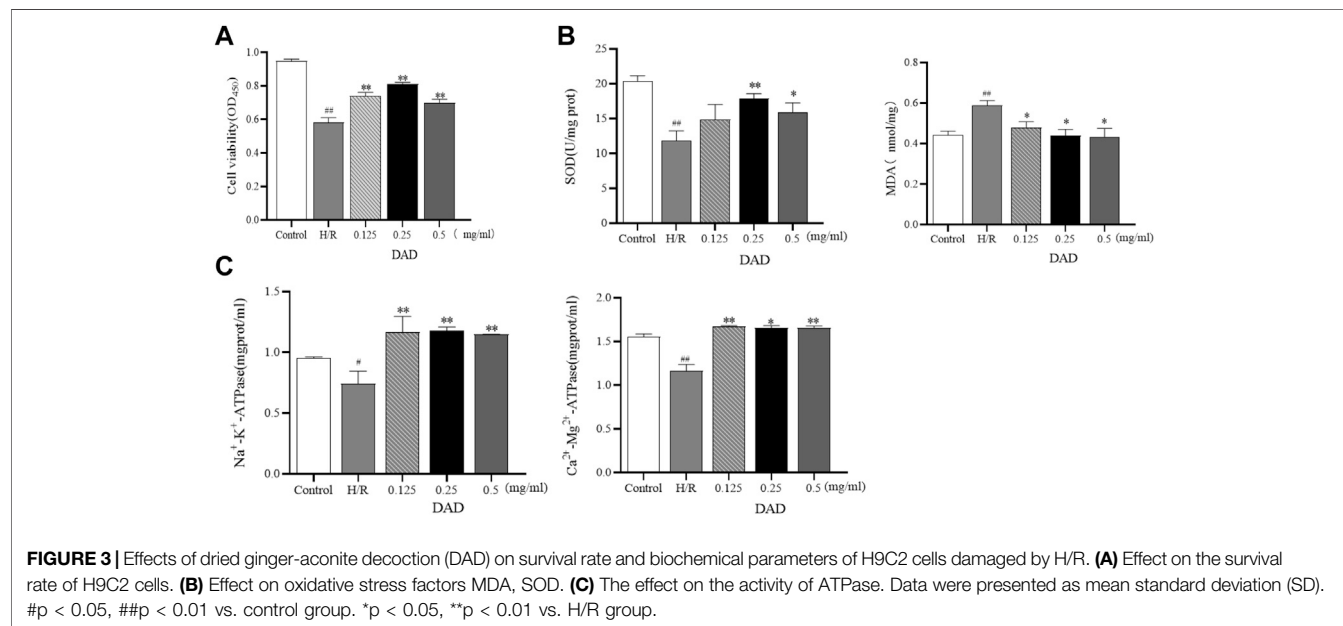


FIGURE 3 | Effects of dried ginger-aconite decoction (DAD) on survival rate and biochemical parameters of H9C2 cells damaged by H/R. **(A)** Effect on the survival rate of H9C2 cells. **(B)** Effect on oxidative stress factors MDA, SOD. **(C)** The effect on the activity of ATPase. Data were presented as mean standard deviation (SD). #p < 0.05, ##p < 0.01 vs. control group. *p < 0.05, **p < 0.01 vs. H/R group.

predictions, pathway and function enrichments, and network analyses, AKT1, PI3K, MAPK3, MAPK1, NFKB, TNF, NFKBA, MTOR, GSK3 β and TP53 were identified. These targets were highly associated with apoptosis and inflammation. Likewise, they were considered as the key targets of DAD against MI/RI. Interestingly, of the aforementioned targets, only GSK3 β was downstream of the PI3K/AKT signaling pathway (Figure 2D). Thus, it was speculated that the anti-MI/RI effect of DAD might be

associated with its regulation of apoptosis and mitochondrial energy metabolism by targeting PI3K/AKT/GSK3 β signaling pathways with their relevant activators.

In vitro Experiments

HPLC Analysis

Network pharmacology predicted that aconitine, 6-ginger, mesaconitine and hypaconitine in DAD were the potential active components of anti-MI/RI in DAD. The phytochemical composition

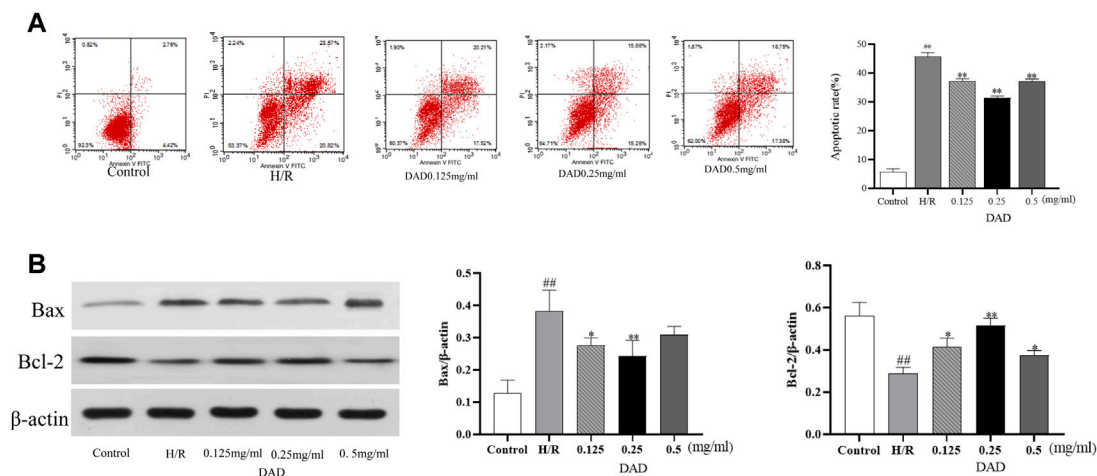


FIGURE 4 | Effects of dried ginger-aconite decoction (DAD) on apoptosis rate and Bax/Bcl-2 expression of H9C2 cells after H/R injury. **(A)** The effect on apoptosis rate. **(B)** The effect on the expression of Bax/Bcl-2. Data were presented as mean standard deviation (SD) of three independent experiments. # $p < 0.05$, ## $p < 0.01$ vs. control group. * $p < 0.05$, ** $p < 0.01$ vs. H/R group.

of DAD was assessed using HPLC. As shown in **Supplementary Figure S1**, DAD contained aconitine, 6-ginger, mesaconitine.

H9C2 Cells' Survival Test Results

The effects of DAD were initially assessed based on the cell viability of the H9C2 cells damaged by H/R. It was found that the exposure of H9C2 cells to H/R injury had led to a decrease in cells ($p < 0.01$). Compared to the control group, the survival rate of the H/R group was only 58%. When the H9C2 cells were pretreated with 0.125–0.5 mg/ml DAD, cell viability was significantly restored ($p < 0.01$). DAD (0.25 mg/ml) had the greatest effect on cell survival rate, which increased by 25% ($p < 0.01$), compared to the H/R group (**Figure 3A**). These data suggest that DAD pretreatment may provide protection against H/R-induced cardiomyocyte injury.

Results of Biochemical Testing

The outcome of cardiomyocyte hypoxia was insufficient oxygen as required by the mitochondria, which would lead to mitochondrial damage, reduced ATP production and aggravated oxidative damage of the cardiomyocytes. SOD is an oxygen free radical scavenger in human body (Khatua et al., 2012; Ling et al., 2019). The final product of oxidative damage is MDA, which can damage the mitochondria. The change in MDA can reflect the degree of oxidative damage of the cells (Mao et al., 2008; Radmanesh et al., 2017). The enzymatic activities of $\text{Na}^+\text{-K}^+\text{-ATP}$ and $\text{Ca}^{2+}\text{-Mg}^{2+}\text{-ATP}$ indirectly reflect changes in the amount of ATP (Zhu et al., 2019). After pretreatment with varied DAD doses, the MDA levels of H9C2 cells damaged by H/R could be reduced to varied degrees, as well as increased the activities of SOD, $\text{Na}^+\text{-K}^+\text{-ATP}$ and $\text{Ca}^{2+}\text{-Mg}^{2+}\text{-ATP}$. In the administration group (**Figure 3B–C**), DAD (0.25 mg/mg) manifested the best therapeutic effect ($p < 0.05$). These results imply that the protective effect of DAD on H/R-damaged H9C2 is related to the mitochondria.

Effect of DAD on the Apoptosis Rate of H9C2 Cells With H/R Injury

As discussed, ischemia and hypoxia aggravate the oxidative damage of cardiomyocytes and eventually induce the apoptosis of cardiomyocytes. H/R injury significantly increased the apoptosis rate of the H9C2 cells, which increased by 35% compared to the control group ($p < 0.01$). After DAD preconditioning, the apoptosis rate of the H9C2 cells damaged by H/R significantly decreased, while the apoptosis rate of the DAD group (0.25 mg/kg) decreased by 18% ($p < 0.01$) compared to the H/R group (**Figure 4A**).

Western Blot Analysis

Network pharmacological analysis implied that the molecular mechanism of the anti-MI/RI effect of DAD might be associated with apoptosis. The mammalian BCL-2 family member Bcl-2 was an anti-apoptotic protein, while Bax protein induced apoptosis by enhancing cytochrome c (Cyt-C) release from the mitochondria (Aamazadeh et al., 2020; Lin et al., 2020). Therefore, the two targets of Bax and Bcl-2 (Bax and Bcl-2 belonged to the targets of DAD in anti-MI/RI) were validated *in vitro*. Compared to the control group, the expression of Bax had significantly increased and the expression of Bcl-2 had significantly decreased after the H9C2 cells were damaged by H/R ($p < 0.01$). Compared to the H/R group, the expression of Bax in the H9C2 cells damaged by H/R had significantly decreased, while the expression of BCL2 had significantly increased when the H9C2 cells were pretreated by DAD ($p < 0.01$). In the administration group (**Figure 4B**), DAD (0.25 mg/mg) manifested the best therapeutic effect. *In vitro* studies were found consistent with network pharmacology, with DAD being shown to resist MI/RI by reducing myocardial cell apoptosis. *In vitro* studies were found consistent with network pharmacology, with DAD being shown to resist MI/RI by reducing myocardial cell apoptosis.

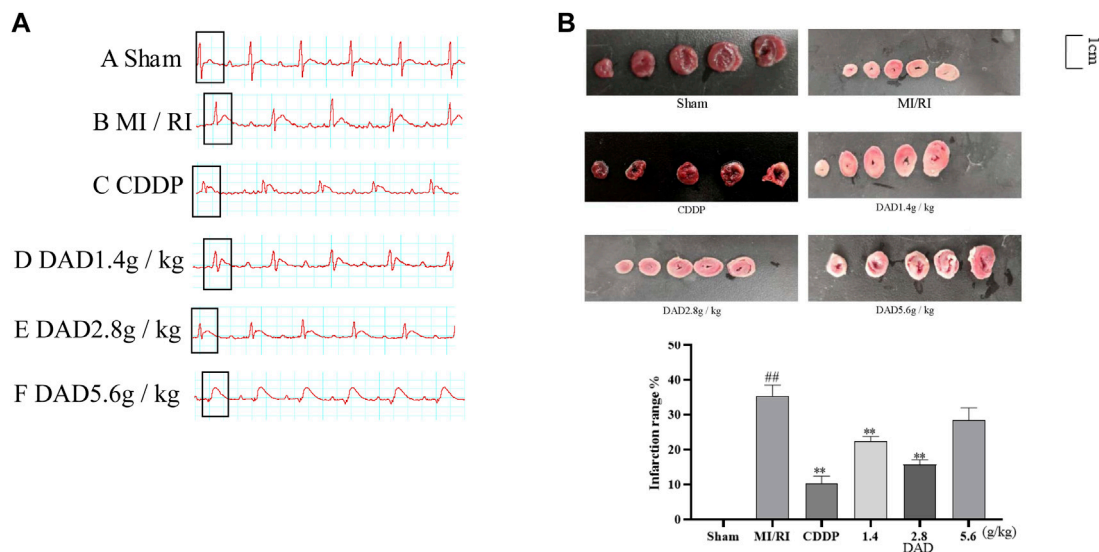


FIGURE 5 | Changes of electrocardiogram in MI/RI rats and effects dried ginger-aconite decoction (DAD) on myocardial infarction area in MI/RI rats. **(A)** After modeling, ECG changes in Sham group, MI/RI group, CDDP group and DAD (1.4 g/kg, 2.8 g/kg, 5.6 g/kg) groups. **(B)** Effects on infarction range reduction of I/R injured rats. Data were presented as mean standard deviation (SD). [#] $p < 0.05$, ^{##} $p < 0.01$ vs. sham group. ^{*} $p < 0.05$, ^{**} $p < 0.01$ vs. MI/RI group.

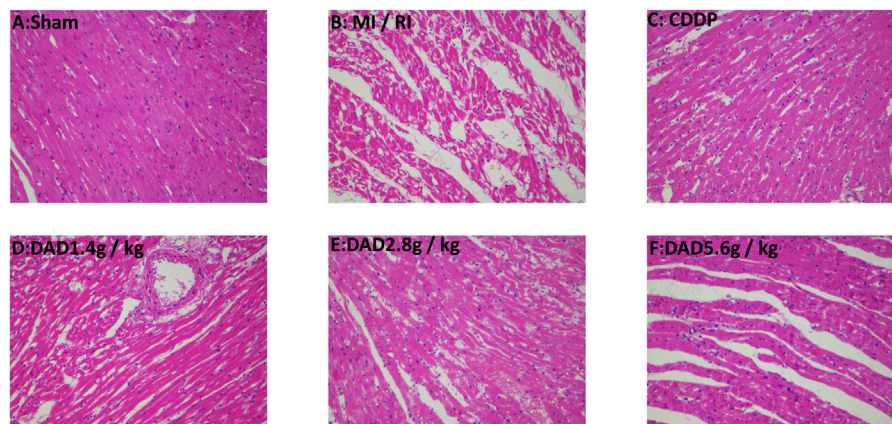


FIGURE 6 | Representative myocardial tissue histopathological sections on the effects of dried ginger-aconite decoction on myocardial infarction size in MI/RI rats (200 \times). Myocardial tissue injury was assessed by hematoxylin-eosin (H&E) staining.

In vivo Experiments

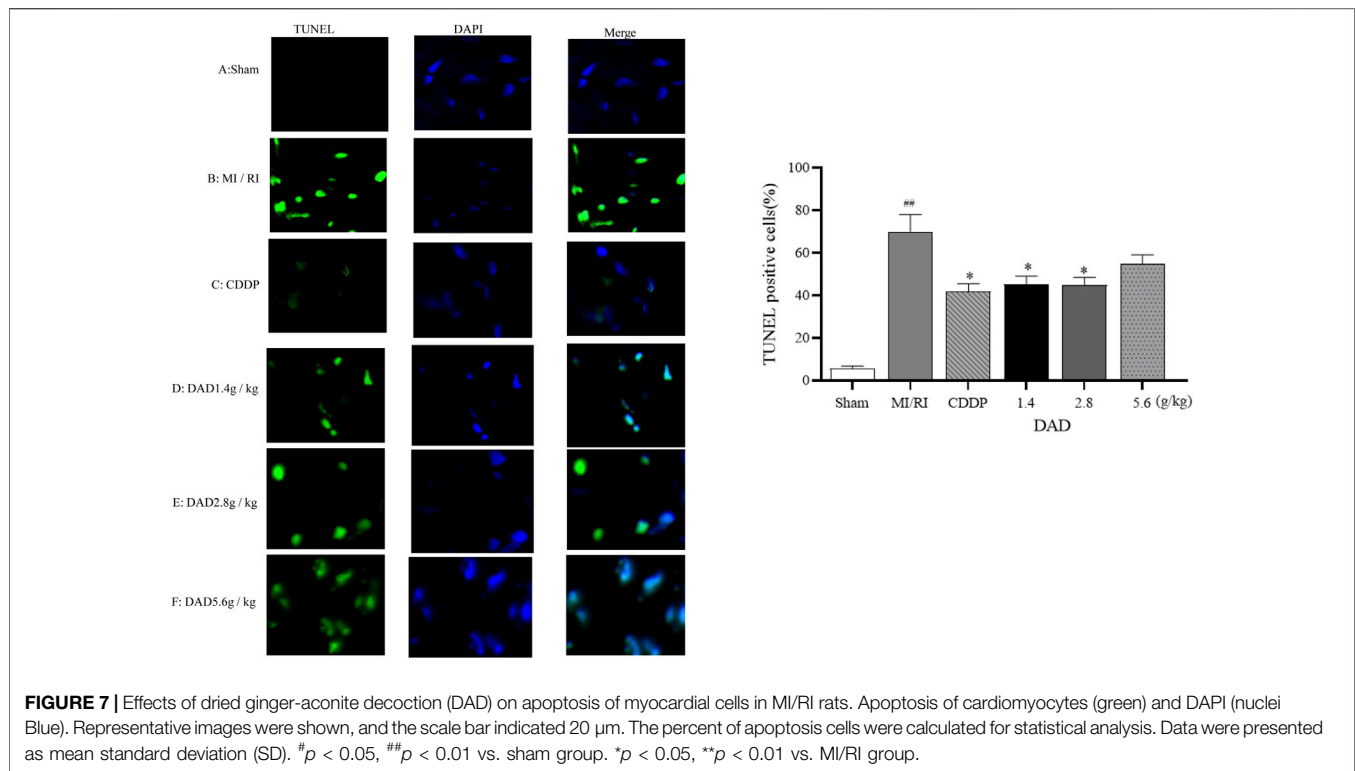
Results of ECG and Myocardial Infarction Area in MI/RI Rats

The electrocardiogram test results (Figure 5A) of rats presented that the ST segment was elevated after reperfusion for each group compared to the sham operation group, indicating that the model had been successfully established. Compared to the sham group, the MI/RI group had significantly increased the infarct size (45%) of the myocardial tissue (Figure 5B), ($p < 0.01$). Compared to the MI/RI group, the infarct size of the myocardial tissue for each administration group had significantly reduced. The lowest infarct size was 9.2% in the CDDP (positive) group. Among the three DAD groups ($p < 0.01$), the MI area of rats in the DAD (2.8 g/kg) medium dose group was the lowest (19.3%) ($p < 0.01$).

Meanwhile, although the high dose of DAD (5.6 g/kg) did not manifest a significant reduction in infarct size, a protective trend of infarct size reduction could be perceived.

Histopathological Examinations

The degree of myocardial injury could be determined by histopathological examinations (Zhou et al., 2020). In the sham group, the myocardial tissue was intact, with a clear texture and regular arrangement of the myocardial fibers, and without apparent cell swelling and fracture; the nuclei material was evenly distributed, without apparent pathological changes. In contrast, in the MI/RI group, the texture of the myocardial tissue was blurred, the shape of the myocardial fiber was disordered, the myocardial tissue was faulted, the interstitium was severely



swollen, the nuclear morphology was changed, and some of the nuclei had disappeared. DAD treatment (1.4, 2.8 and 5.6 g/kg groups) partially attenuated the myocardial tissue histopathological damages, with the greatest improvement realized in the 2.8 g/kg group (Figure 6).

Effect of DAD on Myocardial Cell Apoptosis in MI/RI Rats

TUNEL assay was applied to evaluate the effects of DAD on the apoptosis of myocardial tissue cells in MI/RI rats. Compared to that of the sham operation group, the apoptosis rate (70%) of the MI/RI group had significantly increased ($p < 0.01$). DAD (1.4, 2.8 and 5.6 g/kg) treatment had significantly mitigated the increased percentage of apoptotic cells compared to the model group ($p < 0.01$). Among the three DAD groups, the 2.8 g/kg group exhibited the lowest apoptosis rate (45%). Meanwhile, although a high dose of DAD (5.6 g/kg) did not significantly reduce the apoptosis rate, a decreasing trend in such rate was observed (Figure 7).

Results of Biochemical Testing

Myocardial enzymes are vital indicators in the clinical detection of heart health (Radhiga et al., 2012; Xiang-Qian et al., 2019). The activity of the LDH and CK enzyme sharply increased after myocardial injury. The expressions of LDH and CK significantly increased in the MI/RI group ($p < 0.01$), suggesting that serious heart damage might occur. After treatment, the activities of CK and LDH decreased in each dose group of DADs (1.4, 2.8 and 5.6 g/kg), while the activities

of the 2.8 g/kg group had significantly decreased ($p < 0.01$) (Figure 8A). Oxidative stress injury is a key mechanism of I/R injury. Under ischemia and hypoxia conditions, the mitochondria of cardiomyocytes are damaged, the permeability of the mitochondria membrane is transformed (Figure 8B), and reactive oxygen species are released into the cytoplasm through the damaged mitochondria. SOD and GSH-Px are known as free-radical scavengers *in vivo*. Remarkably, after MI/RI, mitochondrial swelling degree and MDA had increased alongside a decreased GSH-Px activity. After treatment with varied DAD (1.4, 2.8 and 5.6 g/kg), the degree of mitochondrial swelling and the degree of elevated MDA level among MI/RI rats were reduced, while the activity of GSH-Px, SOD were restored (Figure 8C). Among the three DAD groups, DAD (2.8 g/kg) manifested the best therapeutic effect ($p < 0.05$).

Promotion of PI3K/AKT/GSK-3 β by DAD

As a unique molecular target in the mitochondria, Cyt-C can activate apoptosis factors such as CASP9 and can lead to the apoptosis of damaged myocardium (Gao et al., 2016). Considering that the anti-MI/RI mechanism of DAD has been shown to be associated with apoptosis *in vitro*, the network pharmacologically predicted pathway and the related mitochondrial targets *in vivo* were further validated, namely the PI3K/AKT/GSK-3 β pathway and the mitochondrial targets-Cyt-C and CASP9. Western blot analysis presented that the expression of PI3K/AKT/GSK-3 β was inhibited ($p < 0.05$), and that the expression of Cyt-C and CASP9 was significantly increased in the MI/RI group compared to the

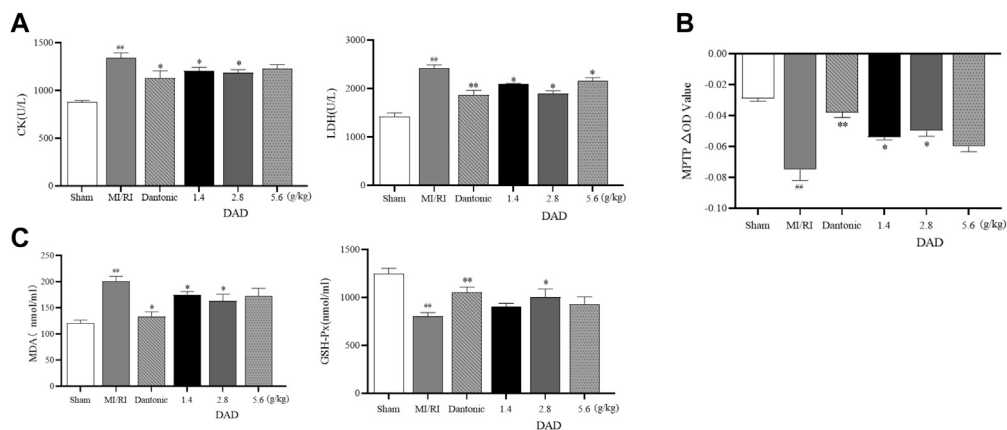


FIGURE 8 | Effects of dried ginger-aconite decoction (DAD) on biochemical indices and MPTP conversion pores in MI/RI rats. **(A)** Effects on activities of myocardial enzymes CK, and LDH. **(B)** Effects on mitochondrial transformation pore MPTP. **(C)** Effect on oxidative stress factors MDA, and GSH-Px. Data were presented as mean standard deviation (SD). # $p < 0.05$, ## $p < 0.01$ vs. sham group. * $p < 0.05$, ** $p < 0.01$ vs. MI/RI group.

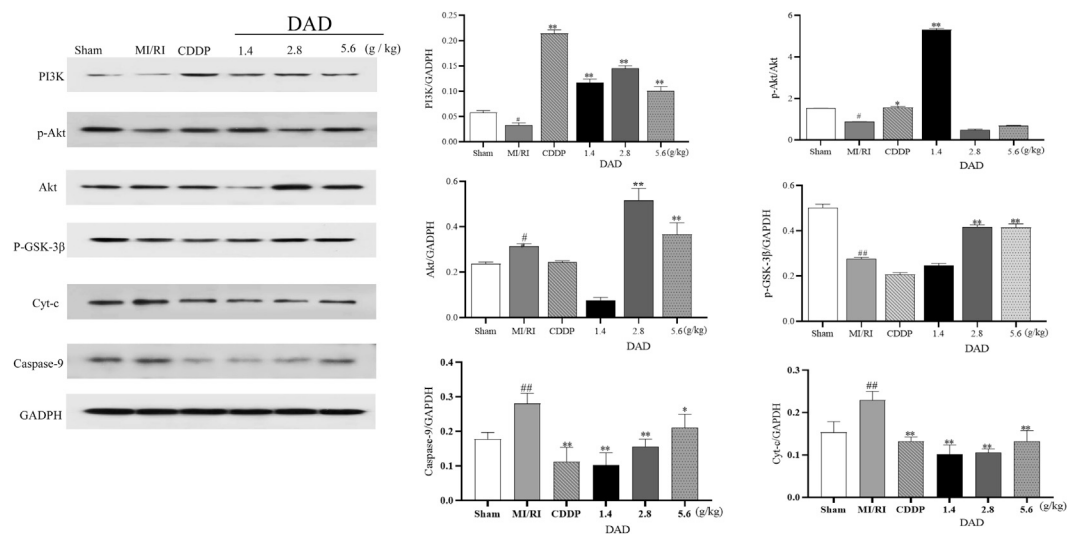


FIGURE 9 | Experimental validation of key signaling pathways and mitochondrial key targets *in vivo*. Dried ginger-aconite decoction (DAD) activates the PI3K/Akt/GSK-3β signaling pathway and inhibits the expression of Cyt-C and CASP9. Data were presented as mean standard deviation (SD) of three independent experiments. # $p < 0.05$, ## $p < 0.01$ vs. sham group. * $p < 0.05$, ** $p < 0.01$ vs. MI/RI group.

sham group ($p < 0.05$). After DAD intervention, the expression of PI3K/AKT/GSK-3β was significantly activated, and the expressions of Cyt-C and CASP9 were significantly decreased in the DAD groups compared to the MI/RI group (Figure 9). Among the three DAD groups, DAD (2.8 g/kg) manifested the best therapeutic effect ($p < 0.05$).

DISCUSSION

MI/RI is not only a primary cause of death among patients with cardiovascular and cerebrovascular diseases, but can also seriously affect the prognosis of patients with ischemic heart diseases. While the effects of DAD against MI/RI have been

demonstrated, its exact mechanism is vague. In this case, pharmacological approaches are adopted to explore relevant molecular pharmacological mechanisms and validate them empirically.

Sixteen active components and 171 targets of DAD were obtained using OB and DL parameters as significant evaluation indices and supplements of significant components. A higher degree of the compound in the C-T network denotes a greater significance. This study found that the degree values of aconitine, 6-ginger, hypaconitine and mesaconitine were among the top. These could be the key components of DAD against MI/RI. The HPLC method was used to determine the above components in DAD that were predicted by network pharmacology. We found that DAD contained aconitine, 6-

ginger, mesaconitine, which was consistent with the results of network pharmacology.

Through network pharmacology, it was found that BP that was highly correlated with DAD anti-MI/RI was the negative regulation of the apoptotic process, the lipopolysaccharide-mediated signaling pathways, the regulation of mitochondrial membrane potential, the inherent apoptotic signaling pathway as a response to DNA damage, the external apoptotic signaling pathway lacking ligand, and release of cytochrome C from mitochondria. An analysis of the C-T-P network revealed that DAD anti-MI/RI acted on multiple targets and signaling pathways. The core targets of the active compounds in DAD were determined, namely AKT1, PIK3G, MAPK3, MAPK1, NFKB, TNF, NFKBA, MTOR, GSK3 β and TP53. As with BP, these targets were associated with apoptosis and inflammation. Various studies have likewise confirmed that apoptosis is the key mechanism of anti-MI/RI (Zhang et al., 2018b; Li et al., 2020b). Apoptosis plays a vital function in MI/RI prognosis. Studies have determined that the inhibition of myocardial cell apoptosis during MI/RI can mitigate the enlargement of the infarct area and can effectively protect cardiac functions (Geng et al., 2020). Significantly, PI3K/AKT/GSK-3 β , an apoptotically-related signaling pathway, has the highest anti-MI/RI correlation in DAD (Chen et al., 2017). Therefore, DAD may play an anti-MI/RI function by inhibiting myocardial apoptosis through the PI3K/AKT/GSK-3 β signaling pathway. To further validate this hypothesis, *in vivo* and *in vitro* experiments are conducted to validate its mechanism on network pharmacological prediction.

Mitochondria is the energy factory of the cells and is also the site of ATP synthesis (Wang et al., 2020). On a physiological level, a stable mitochondria provides ATP to the body; when it is damaged (i.e., by hypoxia injury), it can produce superoxides and reactive oxygen species, leading to adverse stimuli like calcium overload and oxidative stress, and further inducing apoptosis and necrosis in cells (Latini et al., 2015). The abnormal openness of MPTP, as a key regulator of mitochondrial functions, can induce mitochondrial structure disorders, which influence mitochondrial functions and eventually result to cell apoptosis. Under normal physiological conditions, MPTP remains closed, while Ca²⁺ overload and excessive oxidative stress can induce it to open (Tait and Green, 2010). Cyt-C generally exists in the space between the inner and outer membranes of the mitochondria, and cannot cross the outer membrane to reach the cytoplasm under physiological conditions (Joseph and Levine, 2015). When the MPTP is abnormally open and causes damage to the mitochondrial membrane structure, Cyt-C is released from the mitochondria into the cytoplasm and acts as a vital pro-apoptotic factor. It binds to the apoptotic protease activator 1 in the synergistic role of deoxyadenosine triphosphate. Caspase-9 is activated, eventually leading to apoptosis (Mace et al., 2014). Interestingly, *in vitro* studies have depicted that DAD reduces apoptosis and increases ATPase activity in H/R-damaged H9C2 cells. Meanwhile, *in vivo* studies have presented that DAD can reduce myocardial injury in MI/RI rats, with the rate of apoptosis of myocardial cells, the oxidative damage, the degree of mitochondrial MPTP opening, and the expressions of Cyt-C and CASP9 likewise all reduced. Therefore, as predicted by

network pharmacological analysis, it was verified that DAD could reduce cardiomyocyte apoptosis both *in vivo* and *in vitro*.

The PI3K/AKT/GSK-3 β signaling pathway is a fundamental pathway in MI/RI. Phosphatidylinositol 3-kinase (PI3K, a lipid kinase) can specifically catalyze the phosphorylation of the phosphatidylinositol-3 hydroxyl group (Stokes and Condliffe, 2018). It phosphorylates PIP2 to produce PIP3 firstly (Zhang et al., 2017), and then activates AKT (Chen et al., 2014). Activated AKT can yield a series of phosphorylation cascade reactions and can regulate significant downstream effector molecules such as Glycogen synthase kinase-3 β (GSK-3 β) to exert their biological functions (Ya-Fei et al., 2010). GSK-3 β is a serine/threonine kinase (Sun et al., 2011; Barré and Perkins, 2014), and is the most extensively studied downstream target of AKT. It can promote cardiomyocyte apoptosis through an intrinsic mitochondrial pathway (Yan et al., 2011); meanwhile, phosphorylated GSK3 β has no biological activity, which can reduce myocardial cell apoptosis. (Jun et al., 2011). The PI3K/AKT/GSK-3 β signaling pathway plays a vital function in the growth, survival, apoptosis and proliferation of cells. Recent studies have presented that the activation of this signaling pathway can reduce body damage caused by hypoxia (Kaneko et al., 2016; Li et al., 2018; Jing et al., 2019). Interestingly, *in vivo* studies have indicated that DAD can activate the expression of the said signaling pathway.

The innovation of this study involves the prediction of active components, BP and mechanism of action of DAD against MI/RI using network pharmacology. This study has demonstrated that DAD plays an anti-MI/RI role by activating PI3K/AKT/GSK3 β to reduce cardiomyocyte apoptosis. Nevertheless, the limitations of this study should be acknowledged. Firstly, DAD at its highest concentration has either no or minimal effect against MI/RI. In the dose-setting process, the clinical equivalent dose was selected as the medium-dose group. In **Figures 3, 5–9**, dose dependence was not found, which might be because the concentration gradient established was not large enough. Future studies may focus on the study of the “dose-effect” relationship of DAD in regulating SOD and MDA, as well as other indices. Moreover, most TCMs can play multiple therapeutic roles, and network pharmacology can predict DAD anti-MI/RI by inflammation relevant signaling pathways. Thus, further studies may explore inflammation-related signaling pathways and regulators. In addition, the active compounds neutralized in DAD have been identified by network pharmacology. However, the compounds that exert therapeutic effects are still unknown and deserve further study. Overall, the aforementioned limitations should continue to be studied in order to clarify the therapeutic mechanisms of DAD.

CONCLUSION

In this study, a comprehensive strategy that involved network pharmacological analysis, HPLC technology and experimental verification was adopted to determine the potential active components and molecular mechanisms of DAD against MI/RI. Based on the TCMSP database and on core compounds, 16

active compounds of DAD were obtained. The presence of four of these components was identified in DAD by HPLC, in which the components were potential therapeutic ingredients as predicted by network pharmacology. Through the analysis of BP, hub targets and hub signaling pathways and experimental verification, it was concluded that DAD could play an anti-MI/RI role by inhibiting myocardial apoptosis via PI3K/AKT/GSK3 β . The experimental results were consistent with the network pharmacological predictions. Relatively, this study evidently clarified the anti-MI/RI mechanism of DAD, which could provide a certain basis for future studies on DAD.

DATA AVAILABILITY STATEMENT

The original contributions presented in the study are included in the article/**Supplementary Material**, further inquiries can be directed to the corresponding author.

ETHICS STATEMENT

All animal experiments were carried out in accordance with the Animal Care and Use Committee of the Institute of Materia Medica, China (No. TCM-2019- 040-E08).

REFERENCES

- Aamazadeh, F., Ostadrahimi, A., Rahbar Saadat, Y., and Barar, J. (2020). Bitter Apricot Ethanolic Extract Induces Apoptosis through Increasing Expression of Bax/Bcl-2 Ratio and Caspase-3 in PANC-1 Pancreatic Cancer Cells. *Mol. Biol. Rep.* 47, 1895–1904. doi:10.1007/s11033-020-05286-w
- Barré, B., and Perkins, N. D. (2014). Retraction Notice to: the Skp2 Promoter Integrates Signaling through the NF- κ B, P53, and Akt/GSK3 β Pathways to Regulate Autophagy and Apoptosis. *Mol. Cell* 55, 524–538. doi:10.1016/j.molcel.2010.03.018
- Cao, H., Li, S., Xie, R., Xu, N., Qian, Y., Chen, H., et al. (2018). Exploring the Mechanism of Dangguiliuhuang Decoction against Hepatic Fibrosis by Network Pharmacology and Experimental Validation. *Front. Pharmacol.* 9, 187. doi:10.3389/fphar.2018.00187
- Chen, C., Li, G., Geng, F., Zhang, Z., Li, J., Yang, M., et al. (2014). Berberine Reduces Ischemia/reperfusion-Induced Myocardial Apoptosis via Activating AMPK and PI3K-Akt Signaling in Diabetic Rats. *Apoptosis* 19, 946–957. doi:10.1007/s10495-014-0977-0
- Chen, L., Cheng, L., Wei, X., Yuan, Z., Wu, Y., Wang, S., et al. (2017). Tetramethylpyrazine Analogue CXCI95 Protects against Dopaminergic Neuronal Apoptosis via Activation of PI3K/Akt/GSK3 β Signaling Pathway in 6-OHDA-Induced Parkinson's Disease Mice. *Neurochem. Res.* 42, 1–10. doi:10.1007/s11064-016-2148-x
- Chen, W., Lv, L., Nong, Z., Chen, X., and Chen, C. (2020). Hyperbaric Oxygen Protects against Myocardial Ischemia Reperfusion Injury through Inhibiting Mitochondria Dysfunction and Autophagy. *Mol. Med. Rep.* 22, 4254–4264. doi:10.3892/mmr.2020.11497
- Deng, X., Xing, X., Sun, G., Xu, X., Wu, H., Li, G., et al. (2017). Guanxin Danshen Formulation Protects against Myocardial Ischemia Reperfusion Injury-Induced Left Ventricular Remodeling by Upregulating Estrogen Receptor β . *Front. Pharmacol.* 8, 777. doi:10.3389/fphar.2017.00777
- Gao, C.-K., Liu, H., Cui, C.-J., Liang, Z.-G., Yao, H., and Tian, Y. (2016). Role of microRNA-195 in Cardiomyocyte Apoptosis Induced by Myocardial Ischemia-Reperfusion Injury. *J. Genet.* 95, 99–108. doi:10.1007/s12041-016-0616-3

AUTHOR CONTRIBUTIONS

FX, G-JD, and Y-YW performed the experiments, analyzed the data and wrote the manuscript. ML, BW, and P-FW designed the study. FG, LC, and A-PL revised the article. All authors have read and agreed to the final version of the manuscript.

FUNDING

This research was financially supported by National Natural Science Foundation of China, China, (81373988); Project of science and Technology Department of Shaanxi Province (2017JM8080); Project of Shaanxi Provincial Administration of traditional Chinese Medicine (JCPT007); Project of Education Department of Shaanxi Province (20JC012); and Subject Innovation Team of Shaanxi University of Chinese Medicine, China, (2019-QN02). The person in charge of the project is ML.

SUPPLEMENTARY MATERIAL

The Supplementary Material for this article can be found online at: <https://www.frontiersin.org/articles/10.3389/fphar.2021.609702/full#supplementary-material>

- Gao, Y., Song, G., Cao, Y. J., Yan, K. P., Li, B., Zhu, X. F., et al. (2019). The Guizhi Gancao Decoction Attenuates Myocardial Ischemia-Reperfusion Injury by Suppressing Inflammation and Cardiomyocyte Apoptosis. *Evid. Based Complement. Alternat Med.* 2019, 1947465. doi:10.1155/2019/1947465
- Geng, Z., Zhu, X., Han, X., and Xin, X. (2020). Effect of Dexmedetomidine Post-treatment on Oxidative Stress and Apoptosis Induced by Myocardial Ischemiareperfusion Injury in Rats. *Trop. J. Pharm. Res.* 19, 571–575. doi:10.4314/tjpr.v19i3.16
- Han, C., Li, F., Liu, Y., Ma, J., Yu, X., Wu, X., et al. (2018). Modified Si-Ni-San Decoction Ameliorates Central Fatigue by Improving Mitochondrial Biogenesis in the Rat Hippocampus. *Evid. Based Complement. Alternat Med.* 2018, 9452127. doi:10.1155/2018/9452127
- Hausenloy, D. J., and Yellon, D. M. (2013). Myocardial Ischemia-Reperfusion Injury: a Neglected Therapeutic Target. *J. Clin. Invest.* 123, 92–100. doi:10.1172/jci62874
- Heusch, G. (2017). Critical Issues for the Translation of Cardioprotection. *Circ. Res.* 120, 1477–1486. doi:10.1161/circresaha.117.310820
- Hopkins, A. L. (2008). Network Pharmacology: the Next Paradigm in Drug Discovery. *Nat. Chem. Biol.* 4, 682–690. doi:10.1038/nchembio.118
- Ingram, T. E., Fraser, A. G., Bleasdale, R. A., Ellins, E. A., Margulescu, A. D., Halcox, J. P., et al. (2013). Low-dose Sodium Nitrite Attenuates Myocardial Ischemia and Vascular Ischemia-Reperfusion Injury in Human Models. *J. Am. Coll. Cardiol.* 61, 2534–2541. doi:10.1016/j.jacc.2013.03.050
- Inoue, T. (2016). Ischemia-reperfusion Injury Is Still a Big Hurdle to Overcome for Treatment of Acute Myocardial Infarction. *J. Cardiol.* 67, 305–306. doi:10.1016/j.jjcc.2015.09.002
- Jing, Z., Qiang, L., Ling, H., and Neonatology, D. O. (2019). The Effect of PI3K/Akt/GSK-3 β Signaling Pathway on the Injury of Neurons after Hypoxia-Ischemia In Vitro. *Chongqing Med.* 48, 18–22.
- Joseph, E. K., and Levine, J. D. (2015). Caspase Signalling in Neuropathic and Inflammatory Pain in the Rat. *Eur. J. Neurosci.* 20, 2896–2902. doi:10.1111/j.1460-9568.2004.03750.x
- Jun, H. O., Kim, D. H., Lee, S. W., Lee, H. S., and Kim, K. W. (2011). Clusterin Protects H9c2 Cardiomyocytes from Oxidative Stress-Induced Apoptosis via

- Akt/GSK-3 β Signaling Pathway. *Exp. Mol. Med.* 43. doi:10.3858/emmm.2011.43.1.006
- Kaneko, T., Dehari, H., Sasaki, T., Igarashi, T., Ogi, K., Okamoto, J.-Y., et al. (2016). Hypoxia-induced Epithelial-Mesenchymal Transition Is Regulated by Phosphorylation of GSK3- β via PI3 K/Akt Signaling in Oral Squamous Cell Carcinoma. *Oral Surg. Oral Med. Oral Pathol. Oral Radiol.* 122, 719–730. doi:10.1016/j.oooo.2016.06.008
- Khatua, T. N., Padiya, R., Karnewar, S., Kuncha, M., Agawane, S. B., Kotamraju, S., et al. (2012). Garlic Provides Protection to Mice Heart against Isoproterenol-Induced Oxidative Damage: Role of Nitric Oxide. *Nitric Oxide* 27, 9–17. doi:10.1016/j.niox.2012.03.004
- Latini, R., Staszewsky, L., and Ottani, F. (2015). [Controversies on the Role of Mitochondria in Coronary Reperfusion Damage as Potential Therapeutic Target]. *G Ital. Cardiol. (Rome)* 16, 544–548. doi:10.1714/2028.22036
- Lee, Y.-M., Chen, H.-R., Hsiao, G., Sheu, J.-R., Wang, J.-J., and Yen, M.-H. (2002). Protective Effects of Melatonin on Myocardial Ischemia/reperfusion Injury In Vivo. *J. Pineal Res.* 33, 72–80. doi:10.1034/j.1600-079x.2002.01869.x
- Li, J., Cheng, R., and Wan, H. (2020a). Overexpression of TGR5 Alleviates Myocardial Ischemia/reperfusion Injury via AKT/GSK-3 β Mediated Inflammation and Mitochondrial Pathway. *Biosci. Rep.* 40, BSR20193482. doi:10.1042/bsr20193482
- Li, Q., Yang, J., Zhang, J., Liu, X. W., Yang, C. J., Fan, Z. X., et al. (2020b). Inhibition of microRNA-327 Ameliorates Ischemia/reperfusion Injury-induced Cardiomyocytes Apoptosis through Targeting Apoptosis Repressor with Caspase Recruitment Domain. *J. Cell Physiol.* 235, 3753–3767. doi:10.1002/jcp.29270
- Li, S., and Zhang, B. (2013). Traditional Chinese Medicine Network Pharmacology: Theory, Methodology and Application. *Chin. J. Nat. Medicines* 11, 110–120. doi:10.1016/s1875-5364(13)60037-0
- Li, Y., Ruan, X., Chen, T., Gao, J., and Wang, X. (2018). Anti-apoptotic Effect of Suxiao Jiuxin Pills against Hypoxia-Induced Injury through PI3K/Akt/GSK3 β Pathway in HL-1 Cardiomyocytes. *J. Chin. Med. Assoc.* 81, 816–824. doi:10.1016/j.jcma.2018.02.002
- Lin, H., Wu, T., Peng, L., Su, W., Wang, Y., Li, X., et al. (2020). Lnc-MAP6-1:3 Knockdown Inhibits Osteosarcoma Progression by Modulating Bax/Bcl-2 and Wnt/ β -Catenin Pathways. *Int. J. Med. Sci.* 17, 2248–2256. doi:10.7150/ijms.47405
- Ling, Z., Le, J. L., Yu, L. J., Xin, J., Zhi, L. L., Liang, Z. Y., et al. (2019). Possible Involvement of Alpha B-Crystallin in the Cardioprotective Effect of N-Butanol Extract of Potentilla Anserina L. On Myocardial Ischemia/reperfusion Injury in Rat. *Phytomedicine: Int. J. phytotherapy phytopharmacology* 55, 320–329. doi:10.1016/j.phymed.2018.10.024
- Mace, P. D., Riedl, S. J., and Salvesen, G. S. (2014). Caspase Enzymology and Activation Mechanisms. *Methods Enzymol.* 544, 161–178. doi:10.1016/b978-0-12-417158-9.00007-8
- Mao, W. P., Zhang, N. N., and Wei, C. J. (2008). Cadmium Induced Mitochondrial Damage in HEK 293 Cell. *Chin. J. Public Health* 19, 305–307.
- Radhiga, T., Rajamanickam, C., Senthil, S., and Pugalendi, K. V. (2012). Effect of Ursolic Acid on Cardiac Marker Enzymes, Lipid Profile and Macroscopic Enzyme Mapping Assay in Isoproterenol-Induced Myocardial Ischemic Rats. *Food Chem. Toxicol.* 50, 3971–3977. doi:10.1016/j.fct.2012.07.067
- Radmanesh, E., Dianat, M., Badavi, M., Goudarzi, G., and Mard, S. A. (2017). The Cardioprotective Effect of Vanillic Acid on Hemodynamic Parameters, Malondialdehyde, and Infarct Size in Ischemia-Reperfusion Isolated Rat Heart Exposed to PM10. *Iran J. Basic Med. Sci.* 20, 760–768. doi:10.22038/IJBMS.2017.9007
- Raedschelders, K., Ansley, D. M., and Chen, D. D. Y. (2012). The Cellular and Molecular Origin of Reactive Oxygen Species Generation during Myocardial Ischemia and Reperfusion. *Pharmacol. Ther.* 133, 230–255. doi:10.1016/j.pharmthera.2011.11.004
- Samiotis, I., Papakonstantinou, N. A., Dedeilias, P., Vasileiadis, I., and Kotanidou, A. (2021). Dantrolene Induces Mitigation of Myocardial Ischemia-Reperfusion Injury by Ryanodine Receptor Inhibition. *Semin. Thorac. Cardiovasc. Surg.* S1043-0679, 00012. doi:10.1053/j.semctvs.2021.01.004
- Shi, Q., Peng, F., Li, J., and Zhao, Y. (2014). Protective Effect of Ganjiang Fuzi Decoction on Myocardial Ischemia-Reperfusion Injury in Rats. *Agric. Sci. Tech.* 15, 1370–1373.
- Stokes, C. A., and Condliffe, A. M. (2018). Phosphoinositide 3-kinase δ (PI3K δ) in Respiratory Disease. *Biochem. Soc. Trans.* 46, 361–369. doi:10.1042/bst20170467
- Sun, D., Shen, M., Li, J., Li, W., Zhang, Y., Zhang, Z., et al. (2011). Cardioprotective Effects of Tanshinone IIA Pretreatment via Kinin B2 Receptor-Akt-GSK-3 β Dependent Pathway in Experimental Diabetic Cardiomyopathy. *Cardiovasc. Diabetol.* 10, 4. doi:10.1186/1475-2840-10-4
- Tait, S. W. G., and Green, D. R. (2010). Mitochondria and Cell Death: Outer Membrane Permeabilization and beyond. *Nat. Rev. Mol. Cell Biol.* 11, 621–632. doi:10.1038/nrm2952
- Wang, J., Toan, S., and Zhou, H. (2020). New insights into the role of mitochondria in cardiac microvascular ischemia/reperfusion injury[J]. *Angiogenesis* 23, 299–314. doi:10.1007/s10456-020-09720-2
- Wang, W., Huang, X., Shen, D., Ming, Z., Zheng, M., and Zhang, J. (2018). Polyphenol Epigallocatechin-3-Gallate Inhibits Hypoxia/reoxygenation-Induced H9C2 Cell Apoptosis. *Minerva Med.* 109, 95–102. doi:10.23736/S0026-4806.17.05349-6
- Wei, J. (2017). Progress in Treatment of Acute Myocardial Infarction. *J. Clin. Rational Drug Use* 010, 180–181.
- Xiang-Qian, M., Xing, Y., Zu-Feng, H., Ying-Li, B., and Laboratory, D. O. (2019). Characteristics of Echocardiography and Myocardial Enzymes in Patients with Acute Pulmonary Embolism. *J. Community Med.* doi:10.1109/icfsfpe48751.2019.9055758
- Xu, H., Zhang, Y., Lei, Y., Gao, X., Zhai, H., Lin, N., et al. (2014). A Systems Biology-Based Approach to Uncovering the Molecular Mechanisms Underlying the Effects of Dragon's Blood Tablet in Colitis, Involving the Integration of Chemical Analysis, ADME Prediction, and Network Pharmacology. *PLoS One* 9, e101432. doi:10.1371/journal.pone.0101432
- Xu, X. (1986). Discussion on the Application of Aconite. *J. Beijing Traditional Chin. Med.* 1986, 33–36.
- Ya-Fei, M. A., Liu, X. W., and Qiao, X. (2010). The Anti-apoptotic Effect of Puerarin on Myocardial Ischemia-Reperfusion Injury Mediated by PI3K/Akt Signaling Pathway in Rats. *Chin. J. Gerontol.* 34, 1673–1676.
- Yan, L., Wei, X., Tang, Q.-Z., Feng, J., Zhang, Y., Liu, C., et al. (2011). Cardiac-specific Mindin Overexpression Attenuates Cardiac Hypertrophy via Blocking AKT/GSK3 β and TGF- β 1-Smad Signalling. *Cardiovasc. Res.* 92, 85–94. doi:10.1093/cvr/cvr159
- Zhang, M., Jang, H., Gaponenko, V., and Nussinov, R. (2017). Phosphorylated Calmodulin Promotes PI3K Activation by Binding to the SH2 Domains. *Biophysical J.* 113, 1956–1967. doi:10.1016/j.bpj.2017.09.008
- Zhang, R., Xu, L., Zhang, D., Hu, B., Luo, Q., Han, D., et al. (2018b). A20% Ginkgolide B%Inflammation%Myocardial Ischemia/reperfusion injury%NF-Kb. *Front. Immunol.* 9, 2844. doi:10.1038/aps.2017.117
- Zhang, Y.-q., Guo, Q.-y., Li, Q.-y., Ren, W.-q., Tang, S.-h., Wang, S.-s., et al. (2018a). Main Active Constituent Identification in Guanxinjing Capsule, a Traditional Chinese Medicine, for the Treatment of Coronary Heart Disease Complicated with Depression. *Acta Pharmacol. Sin.* 39, 975–987. doi:10.1038/aps.2017.117
- Zheng, Q., and Bao, Y. M. (2017). [Regulatory Effects of Traditional Chinese Medicine on Autophagy in Myocardial Ischemia Reperfusion Injury]. *Zhongguo Zhong Yao Za Zhi* 42, 2925–2929. doi:10.19540/j.cnki.cjmm.20170714.010
- Zhou, S., Ai, Z., Li, W., You, P., Wu, C., Li, L., et al. (2020). Deciphering the Pharmacological Mechanisms of Taohoe-Chengqi Decoction Extract against Renal Fibrosis through Integrating Network Pharmacology and Experimental Validation In Vitro and In Vivo. *Front. Pharmacol.* 11, 425. doi:10.3389/fphar.2020.00425
- Zhu, S.-M., Zhao, Y.-Z., Li, Y. Z., Guo, H., Wang, L., and Tian, P. (2019). Correlation of Lipid Peroxidation and ATP Enzyme on Erythrocyte Membrane with Fetal Distress in the Uterus in Patients with Intrahepatic Cholestasis of Pregnancy. *Eur. Rev. Med. Pharmacol. Sci.* 23, 2318–2324. doi:10.26355/eurrev_201903_17371

Conflict of Interest: The authors declare that the research was conducted in the absence of any commercial or financial relationships that could be construed as a potential conflict of interest.

Copyright © 2021 Xie, Wu, Duan, Wang, Gao, Wei, Chen, Liu and Li. This is an open-access article distributed under the terms of the Creative Commons Attribution License (CC BY). The use, distribution or reproduction in other forums is permitted, provided the original author(s) and the copyright owner(s) are credited and that the original publication in this journal is cited, in accordance with accepted academic practice. No use, distribution or reproduction is permitted which does not comply with these terms.



Estimation of Andrographolides and Gradation of *Andrographis paniculata* Leaves Using Near Infrared Spectroscopy Together With Support Vector Machine

Dilip Sing¹, Subhadip Banerjee², Shibu Narayan Jana², Ranajoy Mallik¹, Sudarshana Ghosh Dastidar¹, Kalyan Majumdar¹, Amitabha Bandyopadhyay¹, Rajib Bandyopadhyay^{1*} and Pulok K. Mukherjee^{2,3}

¹Department of Instrumentation and Electronics Engineering, Jadavpur University, Salt Lake Campus, Kolkata, India, ²School of Natural Product Studies, Jadavpur University, Kolkata, India, ³Institute of Bioresources and Sustainable Development, Imphal, India

OPEN ACCESS

Edited by:

Salvador Cañigual,
University of Barcelona, Spain

Reviewed by:

Subhash Chandra Mandal,
Government of West Bengal, India
Manel Alcalá,
Universitat Autònoma de Barcelona,
Spain

*Correspondence:

Rajib Bandyopadhyay
bandyopadhyay.rajib@gmail.com

Specialty section:

This article was submitted to
Ethnopharmacology,
a section of the journal
Frontiers in Pharmacology

Received: 16 November 2020

Accepted: 01 April 2021

Published: 06 May 2021

Citation:

Sing D, Banerjee S, Jana SN, Mallik R, Dastidar SG, Majumdar K, Bandyopadhyay A, Bandyopadhyay R and Mukherjee PK (2021) Estimation of Andrographolides and Gradation of *Andrographis paniculata* Leaves Using Near Infrared Spectroscopy Together With Support Vector Machine. *Front. Pharmacol.* 12:629833. doi: 10.3389/fphar.2021.629833

Andrographis paniculata (Burm. F) Nees, has been widely used for upper respiratory tract and several other diseases and general immunity for a historically long time in countries like India, China, Thailand, Japan, and Malaysia. The vegetative productivity and quality with respect to pharmaceutical properties of *Andrographis paniculata* varies considerably across production, ecologies, and genotypes. Thus, a field deployable instrument, which can quickly assess the quality of the plant material with minimal processing, would be of great use to the medicinal plant industry by reducing waste, and quality grading and assurance. In this paper, the potential of near infrared reflectance spectroscopy (NIR) was to estimate the major group active molecules, the andrographolides in *Andrographis paniculata*, from dried leaf samples and leaf methanol extracts and grade the plant samples from different sources. The calibration model was developed first on the NIR spectra obtained from the methanol extracts of the samples as a proof of concept and then the raw ground samples were estimated for gradation. To grade the samples into three classes: good, medium and poor, a model based on a machine learning algorithm - support vector machine (SVM) on NIR spectra was built. The tenfold classification results of the model had an accuracy of 83% using standard normal variate (SNV) preprocessing.

Keywords: near infrared spectroscopy, minimal processing, medicinal plant, *Andrographis paniculata*, quality grading, support vector machine

INTRODUCTION

Andrographis paniculata (Burm. F) Nees, popularly known as the “king of bitters,” is an herbaceous plant in the family Acanthaceae. In China, India, Thailand, and Malaysia, this plant has been widely used for treating sore throat, flu, and upper respiratory tract infections (Jayakumar et al., 2013). Its major constituents are the group of diterpenoids designated as andrographolides. Andrographolides have a broad range of therapeutic activities, such as anti-inflammatory (Shen et al., 2002), antibacterial, antitumor, antidiabetic, antimalarial, and hepatoprotective (Trivedi and Rawal,

2001; Jayakumar et al., 2013; Dai et al., 2019). Clinical trials suggest that *Andrographis paniculata* has a strong treating capacity of viral respiratory infections (Hu et al., 2018).

The genotype and agroecology of *Andrographis paniculata* determine the nature and quantity of the active molecules like andrographolides and hence the pharmacological activities (Jayakumar et al., 2013). It is important to estimate the most important active molecules, the andrographolides and classify *Andrographis paniculata* plants with respect to this group of marker molecule. Traditional classifications based on visual inspection of the morphological traits do not consider the active molecules at all. Thus, estimations of active molecules for pharmacognosy, physicochemical studies are mainly based on analytical techniques like high performance liquid chromatography (HPLC), high performance thin layer chromatography (HPTLC), LC-MS/MS (Mukherjee et al., 2015). These techniques are time-consuming, complicated, labor-intensive, and expensive; moreover, they produce considerable quantities of wastes (Borraz-Martínez et al., 2019). Any field level quality control system should be able to handle a large number of samples fast, at a relatively low cost and reasonably dependable accuracy and precision.

Use of NIR Spectra for detection and estimation of specific chemical constituents has proved its worth in diverse fields of application. Its advantages are low cost, speed and simplicity of detection, need for minimal sample preparation and even nondestructive use of samples, feasibility of use at the field level and the feasibility of mechanizing the detection/estimation system for large number of samples. NIR spectroscopy uses liquid and solid samples without any pretreatment. Even when sample extracts are used, NIR spectroscopy obviates the use of further costly chemicals, equipment and time that are required in standard techniques like HPLC. NIR spectroscopy has been successfully used in several areas, like, in the tea leaf quality assessment (Hazarika et al., 2018), in food safety assessment (Cen and He, 2007; Lee and Herrman, 2016; Kusumaningrum et al., 2018) environmental chemistry, microfluidics, biomolecules (Cho et al., 2009), cancer diagnostic agents, and forensic science (Muehlethaler et al., 2016) as well as explosive detection.

In this study, the feasibility of using NIR spectra for estimating andrographolides in *Andrographis paniculata* plant samples and grading the samples based on the estimates was investigated. The performance of NIR spectrum-based technique was examined both in samples of dry powdered leaves and methanol extracts of leaves. Methanol extracts were required for estimation through HPLC, the gold standard (Mukherjee, 2019). If NIR spectrum can estimate andrographolides with reasonable accuracy compared to HPLC, that itself will be a big advantage in saving cost, time, and make mechanization of large scale estimates feasible.

We also attempted to grade the *Andrographis paniculata* samples based on the content of andrographolides (IP 2014). As only a small portion of the spectra responds to the andrographolides, a low cost portable spectrometer with customized range can be employed for simple gradation of the samples without the need for highly accurate estimation, and is likely to be used as a ready-to-apply tool by the traders for

breeding and improvement of cultivars for obtaining higher drug yield (Raina et al., 2013).

MATERIALS AND METHODS

Plant Material

Plant material (leaves) of *Andrographis paniculata* was collected from West Medinipur, East Medinipur, Purulia, South 24 Parganas, Hooghly, and Kolkata district of West Bengal, India. Plant material were identified and authenticated by Dr S. Rajan, Field botanist, the medicinal plant collection unit, Ooty, Tamil Nadu, Govt. of India. The voucher specimens of 18 samples (specimen no. SNPS/JU/2018/12–29) were deposited at School of Natural Product Studies, Jadavpur University, Kolkata, India for future reference.

Based on the content of andrographolides, *Andrographis paniculata* samples were graded into 3 categories: good quality, medium quality and poor quality. Plants having high andrographolides content (>2.50%) (Raina et al., 2013) were considered to be of good quality and placed in grade I; those with <1%, the non-acceptable level according to the Indian Pharmacopodia (IP 2014), were placed in grade III. The intermediate types ($\geq 2.5\%$ and $\leq 1\%$) were placed in grade II.

Chemical Analysis

Chemicals and Reagents

Andrographolides standard (>95% HPLC) was obtained from Sigma Aldrich. Methanol (HPLC grade), glacial acetic acid (HPLC grade), petroleum ether and ethyl acetate (analytical grade) and all other solvents (AR grade) were procured from Merck, India. Quantitative estimation was performed with Empowers software using the external standard calibration method.

Extraction

The air-dried (at room temperature) samples of 18 plants were powdered to a moderately coarse texture (180–355 μm) by a mechanical grinder. Methanolic extracts were made from the powdered samples (50 g in 80 ml of methanol) using rotary shaker at 150 rpm for 10 mins. Each sample was extracted thrice. The extracts were filtered and dried by vacuum evaporation using a rotary evaporator at 50°C and high pressure. The dried extract (10 mg) was dissolved in methanol and filtered through 0.22 μm membranes to get the stock solution (10 mg/ml). The stock solution was diluted to get 1 mg/ml sample concentration for HPLC.

High Performance Liquid Chromatography Analysis

The Reverse phase HPLC (RP-HPLC) system (Waters, United States of America) equipped with a rheodyne 7725i injector having 20 μL loop, 3 Lines degasser (Volume 400 μL), LC-30AD pump, C18 column (5 μm particle size, 250 \times 4.6") UV/Vis detector was used for the analysis. The method developed was isocratic with the mobile phase of Methanol: Water (1% acetic acid) - 60:40 v/v/v. A Milli-Q academic water purification system (Bedford, MA, United States of America) equipped with

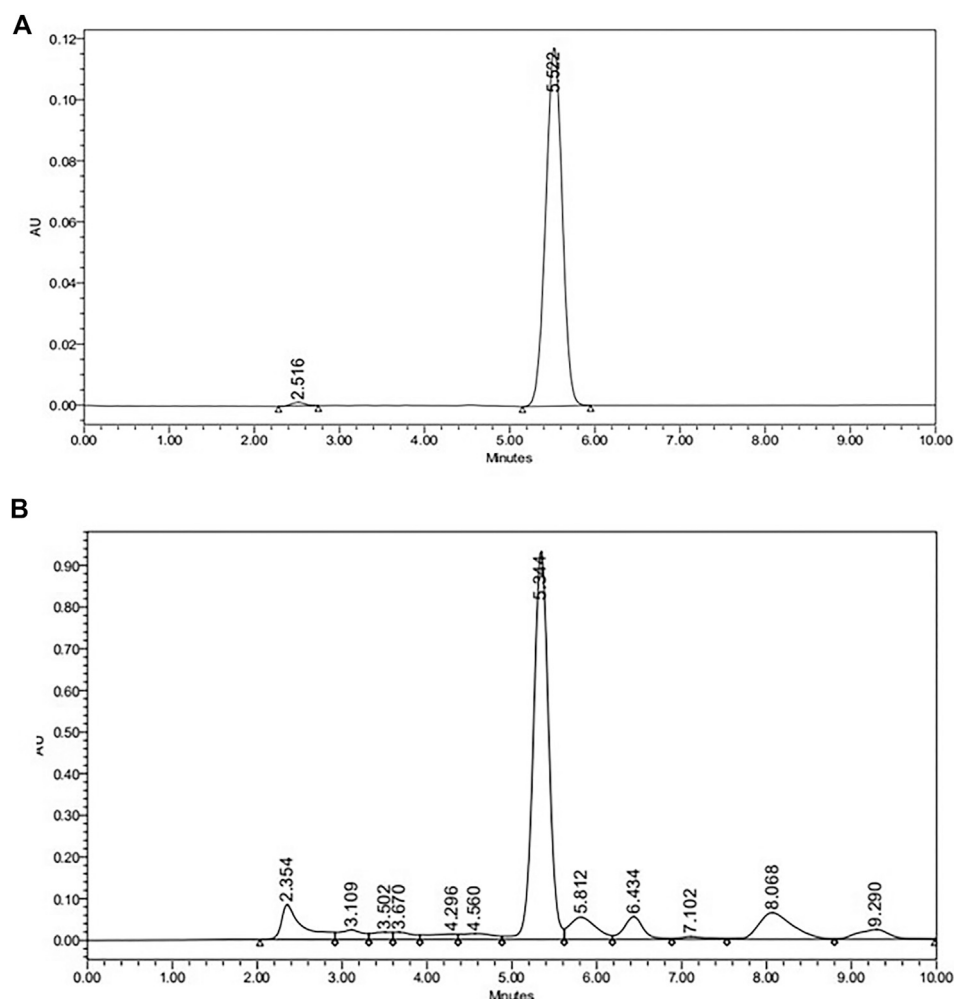


FIGURE 1 | HPLC chromatogram of (A) Andragrapholides Standard (B) *Andrographis paniculata* extract sample.

0.22 μm Millipak express filter. The pH of the solvent B was adjusted at 2.4 by using 1% (v/v) glacial acetic acid for better ionization. The mobile phase was filtered through 0.45 mm pore size (Millipore) membrane filter followed by sonication to degas the solvent. Whatman syringe filters (NYL 0.45 μm) were used for the filtration of the sample. The temperature of the column was kept at 25°C and the injection volume was 20 μL . The total run time was set at 10 min. The flow rate was set at 1.0 ml/min and the λ_{max} was set at 230 nm for maximum absorption of the compound. Quantitative estimation was performed with Empower 2 software programs using the external calibration method. Typical chromatograms of andrographolides standard and an *Andrographis paniculata* extract sample are shown in Figure 1.

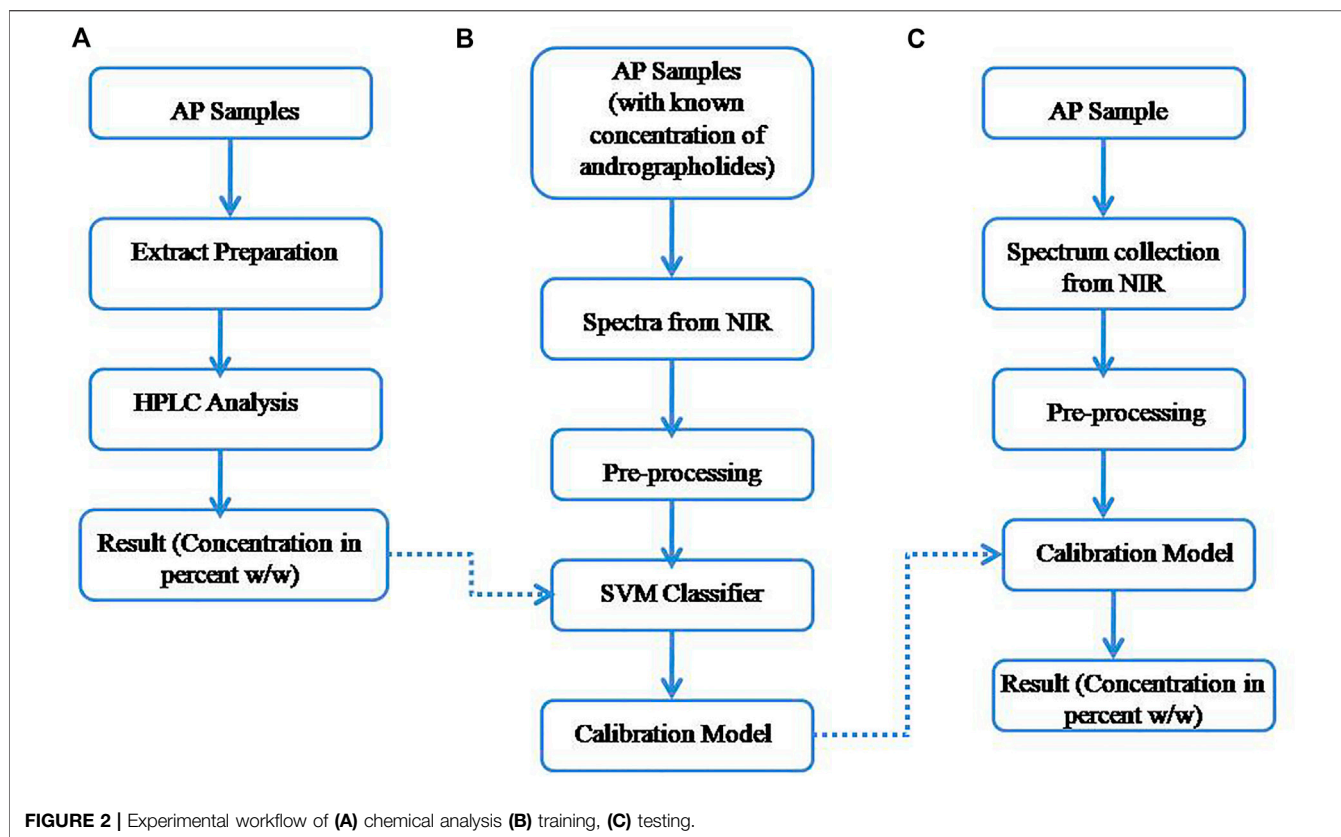
Method Validation

The RP-HPLC method was validated on the basis of the International Conference on Harmonization guidelines (ICH Q2 (R1) Guideline) (ICH Harmonized Tripartite Guideline, 2005). Method specificity was determined by

comparing the retention time of both the standard and test samples. Limit of Detection (LOD) and Limit of Quantification (LOQ) were calculated based on the equation: $\text{LOD} = 3.3 \sigma/S$ and $\text{LOQ} = 10 \sigma/S$, where σ is the residual standard deviation of regression and S is the slope of the calibration curve. The accuracy of the method was determined as percent recovery by the assay of known added amount of analyte in the sample. The samples were spiked with three different concentrations of standard compounds in triplicate. The precision of the analytical method was assessed by measuring six replicates of each of three different concentrations of the reference compounds. The results were represented as %RSD of intra-day and inter-day analysis.

Experimental Setup and Near Infrared Spectroscopy Spectra Acquisition

A DWARF-Star NIR spectrometer (StellarNet Inc., United States of America) coupled with an upward looking



diffuse reflectance accessory RFX-3D was used to acquire the diffuse reflectance spectra of the medicinal plant samples. The scanning range was from 900 to 1700 nm, and a RS50 (50 mm diameter White reflectance standard, halon>97%) was used as a calibration reference. The sample (after drying and grinding) was placed in a standard quartz plate of 1 mm thickness at the top of RFX-3D. RFX-3D was integrated with a 5 W halogen bulb and three fiber connectors to the spectrometer each positioned 120° in a circle to eliminate the need to rotate for coarse grain or non-uniform samples. Each sample was scanned 16 times with integration time of 300 ms and then the averaged spectrum was used for analysis. The S/N ratio was 4,000:1, wave-number accuracy was within $\pm 0.01 \text{ cm}^{-1}$, and the resolution was set as the resolving resolution of 2.5 nm. The temperature was kept at about 25°C during the whole experiment. **Figure 2** explains the workflow of the chemical analysis, and the training, and testing steps with NIR spectrum.

In the Stellarnet spectrometer used in our study, the data points were collected from 900 to 1700.5 nm with a gap of 1.75 nm. Thus there were $(1700.5 - 900) / 1.75 = 459$ points for each spectrum. Fifteen (15) replicates were taken for each sample; thus, in total, $459 \times 18 \times 15$ spectral data points were obtained for 18 samples.

DATA ANALYSIS

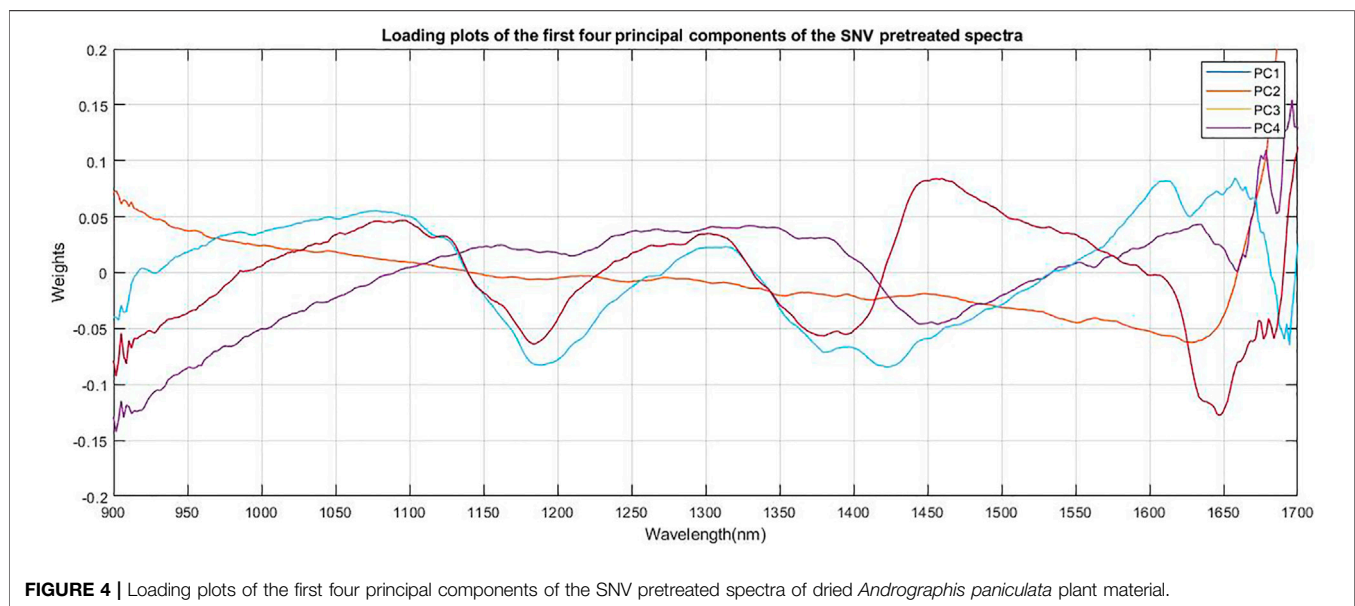
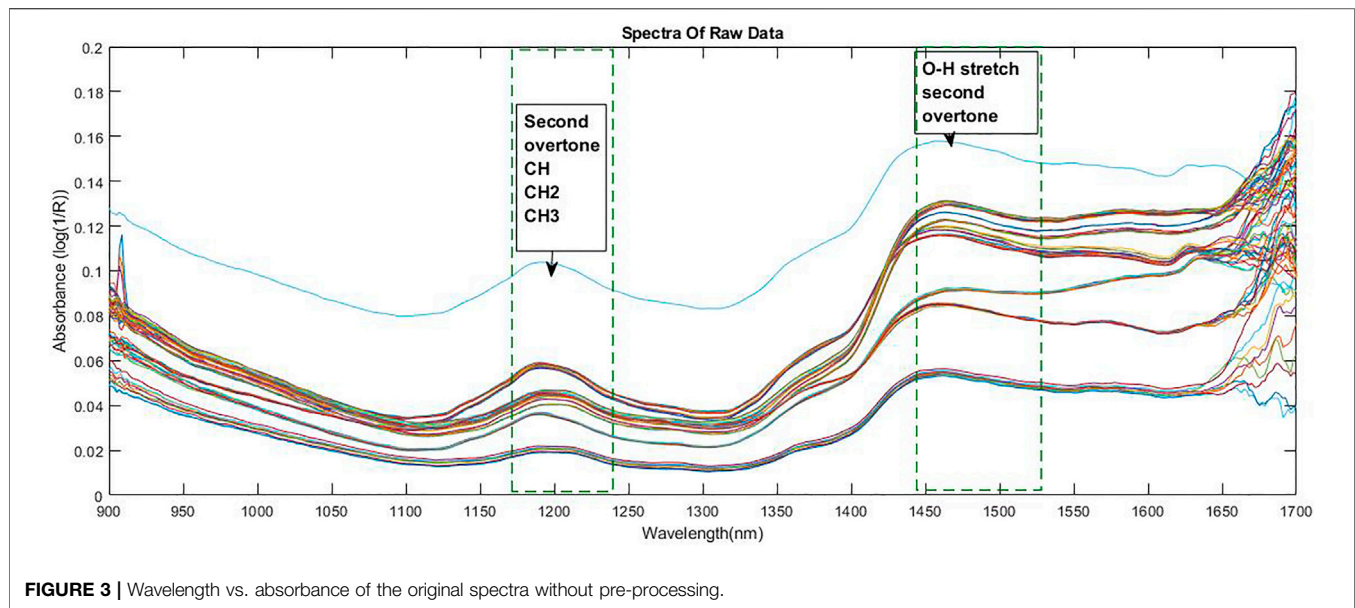
Both raw and pretreated spectral data obtained from the NIR instrument with the *Andrographis paniculata* samples were analyzed. To reduce the effect of scattering, data was pretreated with standard normal variate (SNV) method. The chemometric methods - principal component analysis (PCA), linear discriminant analysis (LDA) and support vector machine (SVM) were applied for clustering and classification.

Preprocessing

In order to reduce the effect of base line variation, and scattering of light, standard normal variate (SNV) preprocessing technique was used on NIR spectra. The method removes the offset by subtracting the mean value of the full spectrum and brings all the spectra to the same scale dividing by the standard deviation of the spectrum (Barnes et al., 1989).

Principal Component Analysis

Principal component analysis (PCA) (Pearson, 1901) was used in order to visualize the multivariate data, by transforming the data along orthogonal axes, and the first two axes were plotted to observe the discrimination between the samples. Here, each point in the PCA plot corresponds to one spectrum.



Linear Discriminant Analysis

For reduction of features, Linear Discriminant Analysis (Fisher, 1936) was also used to visualize the samples in a lesser dimension hyper-plane. LDA maximizes separation between the samples. Only the first two axes were considered for visualizing the data. Class information was used to plot the data. PCA and LDA were implemented in Matlab V10.0 (Mathworks Co., United States of America).

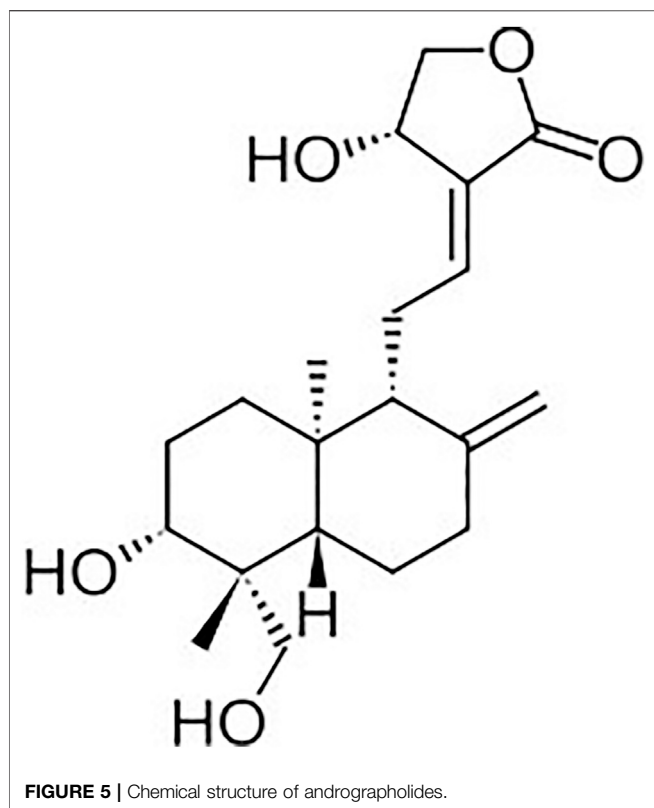
Support Vector Machine

Support vector machine (SVM) is a machine learning algorithm (Cortes and Vapnik, 1995). We have used radial basis function (RBF) as the kernel function. In this study, the two parameters of

SVM - γ (RBF kernel width) and c (SVM cost factor) were obtained based on the minimal classification error through a two-dimension grid search coupled with a leave-ten-out cross validation.

Full-spectrum data was directly used as the input of SVM to build the gradation model. The search range for γ was set from 10^{-6} to 10 with 15 values spaced uniformly for c from 10^{-3} to 100 with 11 values spaced uniformly. The optimal parameter combination of γ and c were obtained as 0.0001 and 100, respectively.

Support vector machine (SVM) was implemented in R studio. The accuracy of classification was estimated on the basis of the tenfold cross-validation method, where nine subsets were used for training and one subset for testing.



RESULTS AND DISCUSSION

Interpretation of Spectroscopic Characterization

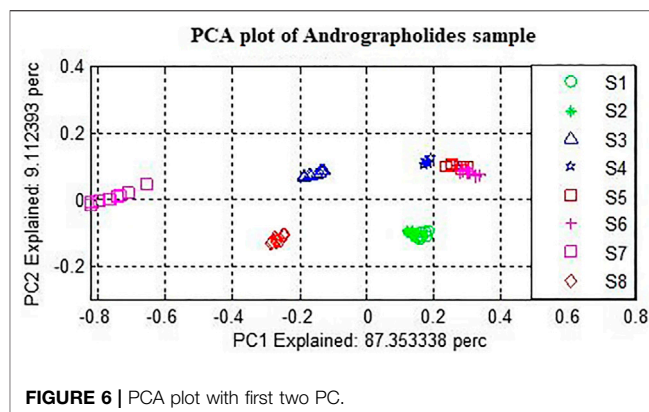
Original and Preprocessed Spectra

The graphical representation of the wavelength vs. absorbance of the raw spectra without any pre-processing is shown in **Figure 3**. The spectra obtained using the dried leaf powder shows absorption peaks at 1200 nm (C-H Second overtone region due to presence of CH₂, CH) and 1472 nm (O-H second overtone region due to presence of R-OH group) (Reuben et al., 2018).

Loading Plot

The loading plot of the spectra is shown in **Figure 4**. The relative contributions of each PC to the explained variation were large for the first few components, with 97.2% of the variation explained by the first four components for andrographolides (PC1 = 55.89%, PC2 = 21.82%, PC3 = 15.94%, and PC4 = 3.56%).

The first two principal components (PCs) showed strong absorption peaks at 1100 and 1300 nm (C-H Second overtone region due to presence of CH₃). The loading plot of PC2 (**Figure 4**) showed another absorption peak at 1450 nm (O-H Second overtone region due to presence of R-OH group) and loading plot of PC1 showed another absorption peak at 1650 nm (C-H first overtone region due to presence of CH₃). The loading plot of PC4 (**Figure 4**) had major



absorption peaks at 1400 nm (O-H second overtone, associated with water) and 1650 nm (C-H first overtone region due to presence of CH₃, CH₂, CH). These are all related to the most abundant structural groups present in the andrographolides (**Figure 5**).

Plot of Principal Component Analysis

PCA was performed on the raw and preprocessed spectra to examine the qualitative differences among the three varieties of the samples. **Figure 6** presents the PCA score plot derived from the raw spectra of *Andrographis paniculata* samples. The first and second principal components (PCs) accounted for 90.67% and 7.89% of the total variance, respectively. Samples of the same variety have been observed to appear as clusters, and no overlaps were observed among the three samples.

Plot of Linear Discriminant Analysis

Figure 7 displays the Linear Discrimination Analysis plot applied to the whole data matrix after preprocessing using Standard Normal Variate (SNV). The discrimination is better than PCA.

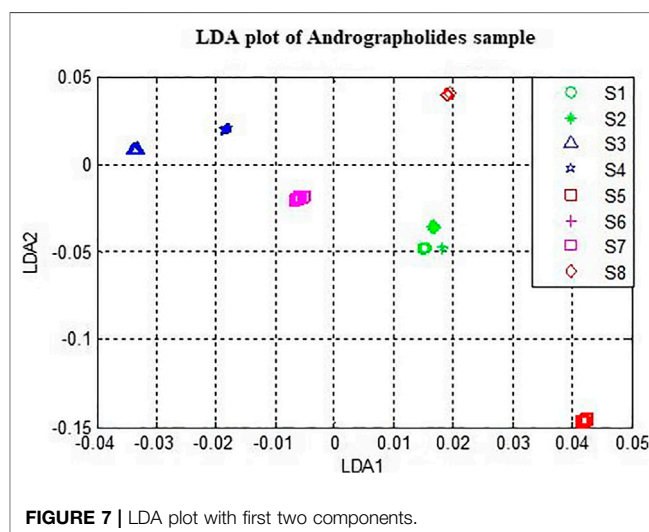


TABLE 1 | Result of HPLC and NIR and the grades of the 18 samples.

Serial no	Sample ID	HPLC method (w/w %)	Prediction by NIR		Grade
			Extract (w/w %)	Powder (w/w %)	
1	SNPS/JU/12	2.50	2.45	2.25	II
2	SNPS/JU/13	2.20	2.10	2.00	II
3	SNPS/JU/14	1.5	1.45	1.44	II
4	SNPS/JU/15	0.53	0.47	0.41	III
5	SNPS/JU/16	0.54	0.54	0.49	III
6	SNPS/JU/17	0.55	0.50	0.44	III
7	SNPS/JU/18	0.93	0.90	0.89	III
8	SNPS/JU/19	2.90	2.89	2.46	I
9	SNPS/JU/20	2.65	2.62	2.52	I
10	SNPS/JU/21	1.71	1.70	1.65	II
11	SNPS/JU/22	2.57	2.54	2.32	I
12	SNPS/JU/23	2.72	2.62	2.52	I
13	SNPS/JU/24	2.68	2.31	2.14	I
14	SNPS/JU/25	2.30	2.28	2.29	II
15	SNPS/JU/26	1.57	1.80	2.07	II
16	SNPS/JU/27	1.79	2.24	2.05	II
17	SNPS/JU/28	1.59	1.54	1.44	II
18	SNPS/JU/29	2.03	2.13	2.12	II
	Correlation coefficient with respect to HPLC results		0.97	0.94	
	"t" value		0.27	1.78	
	"p" value		0.79	0.09	

TABLE 2 | Result of 10-fold cross-validation.

Cross validation folds	% Classification on SNV preprocess data
1	75
2	95
3	90
4	75
5	80
6	90
7	81
8	75
9	81
10	85
Average	83

Support Vector Machine Model

For analysis on the spectra obtained from the ethanol extracts of 18 samples, the support vector model was used for regression on the data pretreated with SNV data. The results of HPLC analysis, NIR predicted values and the corresponding grades are shown in **Table 1**. The of correlation coefficients and paired two tailed "t" statistic results of three pairs of among three sets of estimates: NIR estimates of methanol extract, NIR estimates of powdered samples, and the estimates from HPLC analysis, are given in **Table 1**.

Eighteen data patterns were considered for the tenfold cross-validation method. In this method, a total of ten train-test trials were conducted, and the total data set was divided into ten subsets. Out of these ten subsets, one subset (10% of data) was used as the test set, and the other nine subsets (90% of data) were used as the training set. The classification rates were then

averaged over these folds for estimating the classifier performance. The classification rate and the total misclassified pattern on 18 NIR data are shown in **Table 2**.

From the results of the tenfold cross-validation method, the average classification rate is found to vary from 75% to 95% and the average accuracy is obtained as 83% with SNV preprocessing. This result is quite encouraging, even though the data set is quite small with respect to the number of classes.

CONCLUSION

In this paper, a methodology has been proposed to grade *Andrographis paniculata* samples using NIR spectroscopy and SVM classifier based on the content of marker molecules, andrographolides. Relative accuracies of estimating the andrographolides by NIR spectra of methanol extracts of the samples, and powdered leaf samples were compared taking the estimates obtained from HPLC analysis as the standard. The accuracy of estimation based on extracts was a little higher than the powder leaf samples. But it did not change the grading pattern of the samples. Support vector machine was used to grade the samples into three classes—Class I (best quality), Class II (intermediate quality) and Class III (poor quality). The average classification accuracy of tenfold cross validation of SVM was obtained as 83%. Thus, NIR based estimation of powdered leaf samples combined with SVM classifier can be a low-cost solution to grade the samples rapidly. A small range portable NIR instrument would serve as a field-lab deployable instrument for gradation of *Andrographis paniculata* samples by the industry.

DATA AVAILABILITY STATEMENT

The raw data supporting the conclusions of this article will be made available by the authors, without undue reservation.

AUTHOR CONTRIBUTIONS

DS: Conceptualization, Methodology Development, Coding, Writing. SB: Data curation, HPLC analysis. SNJ: Sample collection, and extraction. RM: Coding and data analysis. NIR

data analysis. Investigation. SGD: Coding and data analysis. NIR data analysis. KM: Conceptualization, Methodology Development. AB: Improving data interpretation, Reviewing and Editing. RB: Validation, Supervision, Writing, Reviewing and Editing. PM: Conceptualization, Supervision, Reviewing and Editing.

FUNDING

Funded by National Medicinal Plant Board, Ministry of Ayush, Govt. of India.

REFERENCES

- Barnes, R. J., Dhanoa, M. S., and Lister, S. J. (1989). Standard Normal Variate Transformation and De-Trending of Near-Infrared Diffuse Reflectance Spectra. *Appl. Spectrosc.* 43 (5), 772–777. doi:10.1366/0003702894202201
- Borraz-Martínez, S., Simó, J., Gras, A., Mestre, M., and Boqué, R. (2019). Multivariate Classification of Prunus Dulcis Varieties Using Leaves of Nursery Plants and Near Infrared Spectroscopy. *Sci. Rep.* 9 (1), 1–9. doi:10.1038/s41598-019-56274-5
- Cen, H., and He, Y. (2007). Theory and Application of Near Infrared Reflectance Spectroscopy in Determination of Food Quality. *Trends Food Sci. Technol.* 18: 72–83. doi:10.1016/j.tifs.2006.09.003
- Cho, H., Lee, B., Liu, G. L., Agarwal, A., and Lee, L. P. (2009). Label-Free and Highly Sensitive Biomolecular Detection Using SERS and Electrokinetic Preconcentration. *Lab. A Chip* 9 (23), 3360–3363. doi:10.1039/b912076a
- Cortes, C., and Vapnik, V. (1995). Support-vector networks. *Mach. Learn.* 20, 273–297. doi:10.1007/BF00994018
- Dai, Y., Chen, S. R., Chai, L., Zhao, J., Wang, Y., and Wang, Y. (2019). Overview of Pharmacological Activities of Andrographis Paniculata and its Major Compound Andrographolide. *Crit. Rev. Food Sci. Nutr.* 59 (Sup1), S17–S29. doi:10.1080/10408398.2018.1501657
- Fisher, R. A. (1936). The Use of Multiple Measurements in Taxonomic Problems. *Ann. Eugenics* 7 (2), 179–188. doi:10.1111/j.1469-1809.1936.tb02137.x
- Hazarika, A. K., Chanda, S., Sabhapondit, S., Sanyal, S., Tamuly, P., Tasrin, S., et al. (2018). Quality Assessment of Fresh Tea Leaves by Estimating Total Polyphenols Using Near Infrared Spectroscopy. *J. Food Sci. Technol.* 55 (12), 4867–4876. doi:10.1007/s13197-018-3421-6
- Hu, X. Y., Wu, R. H., Martin, L., Blondel, C., Lai, L. Y. W., Stuart, B., et al. (2018). Correction: Andrographis Paniculata (Chuān Xīn Lián) for Symptomatic Relief of Acute Respiratory Tract Infections in Adults and Children: A Systematic Review and Metaanalysis. *PLoS One* 13 (11), 1–30. doi:10.1371/journal.pone.0207713
- Jayakumar, T., Hsieh, C. Y., Lee, J. J., and Sheu, J. R. (2013). Experimental and Clinical Pharmacology of Andrographis Paniculata and its Major Bioactive Phytoconstituent Andrographolide. *Evid.-Based Complement. Altern. Med.* 2013, 846740. doi:10.1155/2013/846740
- ICH Harmonised Tripartite Guideline (2016). “Validation of analytical procedures: text and methodology” in International Conference on Harmonisation of Technical Requirements for Registration of Pharmaceuticals for Human Use, Chicago, USA.
- Kusumaningrum, D., Lee, H., Lohumi, S., Mo, C., Kim, M. S., and Cho, B. K. (2018). Non-Destructive Technique for Determining the Viability of Soybean (Glycine Max) Seeds Using FT-NIR Spectroscopy. *J. Sci. Food Agric.* 98 (5), 1734–1742. doi:10.1002/jsfa.8646
- Lee, K. M., and Herrman, T. J. (2016). Determination and Prediction of Fumonisin Contamination in Maize by Surface-Enhanced Raman Spectroscopy (SERS). *Food Bioproc. Technol.* 9 (4), 588–603. doi:10.1007/s11947-015-1654-1
- Muehlethaler, C., Leona, M., and Lombardi, J. R. (2016). Towards a Validation of Surface-Enhanced Raman Scattering (SERS) for Use in Forensic Science: Repeatability and Reproducibility Experiments. *Forensic Sci. Int.* 268, 1–13. doi:10.1016/j.forsciint.2016.09.005
- Mukherjee, P. K., Bahadur, S., Chaudhary, S. K., Amit, K., and Mukherjee, K. (2015). Quality Related Safety Issue-Evidence-Based Validation of Herbal Medicine Farm to Pharma. *Evid.-Based Validation Herbal Med.* 2015, 1–28. doi:10.1016/B978-0-12-800874-4.00001-5
- Mukherjee, P. K. (2019). *Quality Control and Evaluation of Herbal Drugs*. Alpharetta, GA: Elsevier Science.
- Pearson, K. (1901). LIII. On Lines and Planes of Closest Fit to Systems of Points in Space. *Lond. Edinb. Dublin Philos. Mag. J. Sci.* 2 (11), 559–572. doi:10.1080/14786440109462720
- Raina, A. P., Veena Gupta, N. S., and Dutta, M. (2013). Andrographis Paniculata (Burm. f.) Wall. Ex Nees (Kalmegh), a Traditional Hepatoprotective Drug from India. *Genet. Resour. Crop Evol.* 60 (3), 1181–1189. doi:10.1007/s10722-012-9953-0
- Reuben, N. O., Perez, P. A., Josiah, M. A., and Mouazen Abdul, M. (2018). Towards Enhancing Sustainable Reuse of Pre-Treated Drill Cuttings for Construction Purposes by Near-Infrared Analysis: A Review. *J. Civil Eng. Construction Technol.* 9 (3), 19–39. doi:10.5897/jcct2018.0482
- Shen, Y. C., Chen, C. F., and Chiou, W. F. (2002). Andrographolide Prevents Oxygen Radical Production by Human Neutrophils: Possible Mechanism(s) Involved in its Anti-Inflammatory Effect. *Br. J. Pharmacol.* 135 (2), 399–406. doi:10.1038/sj.bjp.0704493
- Trivedi, N. P., and Rawal, U. M. (2001). Hepatoprotective and Antioxidant Property of Andrographis Paniculata (Nees) in BHC Induced Liver Damage in Mice. *Indian J. Exp. Biol.* 39 (1), 41–46.

Conflict of Interest: The authors declare that the research was conducted in the absence of any commercial or financial relationships that could be construed as a potential conflict of interest.

Copyright © 2021 Sing, Banerjee, Jana, Mallik, Dastidar, Majumdar, Bandyopadhyay, Bandyopadhyay and Mukherjee. This is an open-access article distributed under the terms of the Creative Commons Attribution License (CC BY). The use, distribution or reproduction in other forums is permitted, provided the original author(s) and the copyright owner(s) are credited and that the original publication in this journal is cited, in accordance with accepted academic practice. No use, distribution or reproduction is permitted which does not comply with these terms.



***In-Vitro* α -amylase, α -glucosidase Inhibitory Activities and *In-Vivo* Anti-Hyperglycemic Potential of Different Dosage Forms of Guduchi (*Tinospora Cordifolia* [Willd.] Miers) Prepared With Ayurvedic Bhavana Process**

Rohit Sharma^{1*}, Rajesh Bolleddu², Jayanta K. Maji³, Galib Ruknuddin⁴ and Pradeep K. Prajapati⁴

¹Department of Ras Shastra and Bhaishajya Kalpana, Faculty of Ayurveda, Institute of Medical Sciences, Banaras Hindu University, Varanasi, India, ²Central Ayurveda Research Institute, CCRAS, Ministry of AYUSH, Government of India, Kolkata, West Bengal, India, ³Society for Research and Initiatives for Sustainable Technologies and Institutions (SRISTI), Ahmedabad, India, ⁴Department of Ras Shastra and Bhaishajya Kalpana, All India Institute of Ayurveda, University of Delhi, New Delhi, India

OPEN ACCESS

Edited by:

Chandra Kant Katiyar,
Emami, India

Reviewed by:

Aline Carvalho Pereira,
Universidade Federal De Lavras, Brazil
Johanna Mahwahwatse Bapela,
University of Pretoria, South Africa

*Correspondence:

Rohit Sharma
rohitsharma@bhu.ac.in

Specialty section:

This article was submitted to
Ethnopharmacology,
a section of the journal
Frontiers in Pharmacology

Received: 15 December 2020

Accepted: 07 April 2021

Published: 10 May 2021

Citation:

Sharma R, Bolleddu R, Maji JK, Ruknuddin G and Prajapati PK (2021) *In-Vitro* α -amylase, α -glucosidase Inhibitory Activities and *In-Vivo* Anti-Hyperglycemic Potential of Different Dosage Forms of Guduchi (*Tinospora Cordifolia* [Willd.] Miers) Prepared With Ayurvedic Bhavana Process. *Front. Pharmacol.* 12:642300. doi: 10.3389/fphar.2021.642300

Guduchi (*Tinospora cordifolia* [Willd.] Miers) is a flagship rejuvenating herb of Ayurveda with reported anti-diabetic potential. In the present study, different dosage forms of *Guduchi* stem (growing on neem tree) were developed by adopting Ayurvedic pharmaceutical process of *Bhavana* (levigation). *Guduchi Churna* (GC) was subjected to 07 times *Bhavana* separately with its own extracted juice, decoction and potable water, and dosage forms namely *Svarasa Bhavita Guduchi Churna* (SBGC), *Kwatha Bhavita Guduchi Churna* (KBGC), and *Jala Bhavita Guduchi Churna* (JBGC) were prepared. The present study was aimed to evaluate the role of *Bhavana* on the potentiation of therapeutic properties of *Guduchi*. Sequential solvent extracts (5, 10, 15 and 25%) of GC, SBGC, KBGC and JBGC were prepared in different solvents [phosphate buffer, hexane, dichloromethane (DCM), chloroform] and screened for the α -amylase and α -glucosidase inhibitory activity. The results revealed that phosphate buffer and DCM extracts of SBGC exhibited strong α -amylase inhibitory potential (>80% inhibition at 25% concentration) followed by KBGC, JBGC and GC with reference to the standard acarbose. In α -glucosidase inhibitory activity, maximum inhibition was observed in DCM and chloroform extracts of SBGC (>85% inhibition at 25% concentration), followed by KBGC (>80% inhibition at 25% concentration), JBGC and GC. *In vivo* anti-hyperglycemic studies were carried out by oral glucose tolerance test in Swiss albino mice. Test drugs (JBGC, KBGC, SBGC) treated groups showed marginal decrease of blood glucose levels in normo glycemic mice. However, the blood glucose level in test drug JBGC, KBGC and SBGC treated groups was still within normal range in overnight fasted mice. In oral glucose tolerance test, among all dosage forms SBGC (51.08%) produced pronounced anti-hyperglycemic effect followed by KBGC (42.57%) at a dose of 520 mg/kg. The GC, JBGC, KBGC and SBGC samples

were also standardized using berberine (a well established anti-diabetic compound) as a marker compound by HPTLC fingerprint analysis. Findings of the present study indicate that SBGC and KBGC can be used in the treatment of diabetes mellitus and gives supporting evidence to Ayurvedic claims that the *Bhavana* process has pharmaceutico-therapeutic significance in Ayurvedic drug development.

Keywords: *tinospora cordifolia*, *guduchi*, *bhavana*, α -amylase, α -glucosidase, anti-hyperglycemic, hypoglycemic

INTRODUCTION

Diabetes mellitus (DM) is a chronic metabolic disorder caused by a failure in insulin production or a decrease in insulin sensitivity and function, affecting the lipid and carbohydrate metabolism. Hyperglycemia, an inevitable ramification of diabetes, is linked with several deleterious effects associated with this disease (Sharma et al., 2015a). DM is exponentially growing worldwide and leading cause of morbidity and mortality in low- and middle-income countries (Olowoyo et al., 2018). Based on current report of International Diabetes Federation (IDF) the global number of diabetic people (aged 18–99 years) will increase to 693 million by 2045 (Cho et al., 2018). Most of the conventional anti-diabetic drugs are reported to have side effects in long term use and have certain limitations, and options from natural products especially herbal medicine are being searched to meet the need (Sharma et al., 2015a).

Guduchi (*Tinospora cordifolia* Willd. Miers.; Family: Menispermaceae) is a renowned, deciduous, extensively spreading, climbing, herbaceous vine, distributed throughout the tropical Indian subcontinent and China, ascending to an altitude of 300 m. Mainly three *Tinospora* species are available in India, namely *T. cordifolia*, *T. malabarica*/*T. sinensis* and *T. crispa*. Though these species are closely related with their morphology and chemical properties, amongst them, the level of berberine (a well established anti-diabetic compound) is reported higher in *T. cordifolia*. The name - *T. cordifolia* is ascribed to the Ayurvedic plant *Guduchi* in Ayurvedic Pharmacopoeia of India and the traditional practitioners also consider *T. cordifolia* as the genuine source for *Guduchi* (Srinivasan et al., 2008; Nidhi et al., 2013). *Guduchi* is traditionally used in Indian Ayurveda medicine to treat wide range of diseases such as fever, diabetes, urinary disorders, anemia, jaundice, asthma, stress, allergy, skin disorders, arthritis, liver disorders etc., (Saha and Ghosh, 2012; Sharma et al., 2014a). Several reports substantiate its high anti-diabetic potential (Sharma et al., 2015a). Time by time its different traditional formulations like *Churna* (fine powder), *Kwatha* (decoction), *Satva* (sedimented starchy aqueous extract) and *Ghana* (solidified aqueous extract) were developed according to its need, and their anti-diabetic potential is evident from several studies (Sharma et al., 2013a; Sharma et al., 2013b; Sharma et al., 2015b; Gade, 2017).

Bhavana (levigation or wet-grinding of powdered drugs with juice/decoction/solution of plant, animal or mineral origin) is a unique traditional method of transformation of raw material/substances and process of herbal drug manufacturing, affecting the physicochemical and biological properties of a dosage form.

Bhavana is one of the most commonly carried out pharmaceutical process in Ayurveda, having multi-dimensional pharmaceutico-therapeutic implications and various popular traditional herbal or herbo-mineral formulations are being prepared by this process. *Bhavana* process is claimed to make quicker and augmented action with possible reduction in therapeutic dose of the drug under process (Sharma and Prajapati, 2015; Sharma et al., 2017). *Churnakriya* is a type of *Bhavana*, wherein *Bhavana* of juice/decoction of the same drug is given usually with the motto of augmentation of properties of the drug being levigated and, hence, to potentiate the therapeutic action (Acharya, 2004). By adopting *Churnakriya* method of *Bhavana*, the potency of single herbs like *Guduchi* can be improved.

To the best of our knowledge, to date, there is no scientific evidence on the inhibitory effects of any dosage form or formulation of *Guduchi* on carbohydrate hydrolyzing enzymes. Also, no reports are available exploring anti-hyperglycemic potential of *Bhavita* dosage form of *Guduchi*. Considering all these, the present study was planned to validate the classical uses of *Guduchi* and its preparations in diabetes and understand the role of *Bhavana* in herbal drug potentiation, especially whether *Bhavana* process could augment the therapeutic potential of *Guduchi Churna* (GC) to manage glycemic levels. GC was subjected to 07 times *Bhavana* separately with its own extracted juice, decoction and potable water, and the dosage forms namely *Svarasa Bhavita Guduchi Churna* (SBGC), *Kwatha Bhavita Guduchi Churna* (KBGC), and *Jala Bhavita Guduchi Churna* (JBGC) were prepared. The third trial preparation JBGC was prepared (by subjecting *Bhavana* to GC with potable water) to obtain the same particle size reduction as in first two groups and to understand the effect of *Bhavana*. These preparations were comparatively evaluated for *in-vitro* α -amylase, α -glucosidase inhibitory activities and *in-vivo* anti-hyperglycemic potential with High Performance Thin Layer Chromatography (HPTLC) profiling.

MATERIALS AND METHODS

Preparation of Test Formulations

JBGC, KBGC and SBGC samples were prepared by adopting classical Ayurvedic pharmaceutical guidelines of *Bhavana* process (Sharma and Prajapati, 2015; Sharma et al., 2017) in the department of Rasa Shastra and Bhaishajya Kalpana, Institute for Postgraduate Teaching and Research in Ayurveda, Gujarat Ayurved University, Jamnagar, Gujarat, India.

For preparation of *Guduchi Churna* (#80 sieve), *Guduchi Svarasa*, and *Guduchi Kwatha*, mature fresh medium sized



FIGURE 1 | Unit operating process of Svarasa Bhavita Guduchi Churna (SBGC), Kwatha Bhavita Guduchi Churna (KBGC), and Jala Bhavita Guduchi Churna (JBGC) samples preparation by traditional Bhavana method. **(A)**- (1) fresh Guduchi stems (2) chopped/crushed, **(B)**- (1) expressed juice (for SBGC batch) (2) decoction was prepared (for KBGC batch), **(C)**- wet grinding of Guduchi Churma with liquid media (Guduchi juice for SBGC batch, Guduchi decoction for KBGC batch, and potable water for JBGC batch) in edge-runner, **(D)**- soft and fine mass formed during grinding, **(E)**- observation of Subhavitā Lakṣhaṇa (Confirmatory tests for completion of levigation), **(F)**- wet granulation, **(G)**- hot air over drying, **(H)**- dry granules, **(I)**- preparation of tables.

diameter (1.6–2.0 cm) stems of *Guduchi*, climbing on neem (*Azadirachta indica*) tree were collected in monsoon season from the same vicinity (from non polluted, wild area of ‘Moti Panchasara’ village of Jamnagar district, Gujarat) to avoid any phyto-geographical differences. The physical impurities and outer exfoliating skin were removed and washed thoroughly with potable water. The collected plant material was authenticated (voucher specimen no- Phm/6,198) by the concerned authority in the Pharmacognosy laboratory of the institute.

Fresh *Guduchi* stems were taken to prepare different dosage forms as per classical Ayurvedic guidelines i.e., *Sadaiva ardra prayojyeta* (always use in fresh state) (Shastri, 2005; Sharma et al., 2012). *Guduchi* stems growing with the support of neem tree were selected, because it is believed to be the best as the synergy between these plants enhances its efficacy (Kinghorn, 2003; Bhalerao et al., 2012). Medium diameter or thumb sized stems from the same plant with uniform maturity was selected for study, as this is advocated to use for preparing *Guduchi*-based formulations (Acharya, 2008). Ayurvedic guidelines advocate collecting stems of medicinal plants in rainy/spring season. These ancient claims are supported by recent reports that the

concentration or percentage of total alkaloids and the anti-diabetic biomarkers, tinosporaside and berberine of *Guduchi* are bit higher in rainy/monsoon season (Sharma et al., 2013c; Choudhry et al., 2014). Therefore the same harvesting time was selected for *Guduchi* collection.

In pharmaceutical process, three different batches of SBGC, KBGC, and JBGC were prepared. GC was subjected to 07 times *Bhavana* separately in edge-runner with *Guduchi Svarasa* (fresh expressed juice of *Guduchi* stems) - for SBGC batch, *Guduchi Kwatha* (decoction of *Guduchi* stems) - for KBGC batch) and potable water - for JBGC batch. The whole unit operating process involved in the preparation of SBGC, KBGC, and JBGC is exemplified in **Figure 1**. The whole pharmaceutical process of 07 times *Bhavana* for each formulation SBGC, KBGC, and JBGC was completed in the same season therefore excluding possibility of major changes in environmental conditions. The duration of wet grinding for each cycle of *Bhavana* was kept constant to 9 h so as to maintain homogeneity in pharmaceutical processing among the batches of three formulations. The finished products were collected, weighed and their compressed tablets (500 mg each) were prepared and stored in air-tight sterile glass containers along with small pieces of cotton in them.

In-Vitro α -Amylase and α -Glucosidase Inhibitory Studies

Chemicals and Reagents

Soluble starch (Merck), 3, 5-dinitrosalicylic acid (DNSA) (S D fine-chem Ltd.), phosphate buffer (0.02 M), hexane, dichloro methane (DCM) (S D fine-chem Ltd.), chloroform (S D fine-chem Ltd.), porcine pancreatic α -amylase (PPA) (Sigma-Aldrich) and acarbose (Bayer pharma) were used.

Test Materials

From the tablets of preparations, 5, 10, 15 and 25% of GC, JBGC, KBGC and SBGC solutions were prepared in different solvents (phosphate buffer, hexane, dichloro methane, chloroform).

α -Amylase Inhibitory Activity

The α -amylase inhibitory activity was determined according to the standard methods (Kumar et al., 2010; Sudha et al., 2011). 200 μ L of phosphate buffer was mixed with 200 μ L of α -amylase solution and 500 μ L of various concentrations of test samples (5–25%) separately, were incubated at room temperature for 15 min and followed by addition of 200 μ L of starch solution (1%) in all test tubes and further incubated for 10 min at 37°C. The enzymatic reaction was stopped by adding 400 μ L of freshly prepared DNS reagent and placing in boiling water bath for 5 min. The mixture was allowed to cool, diluted with 15 ml of distilled water and absorbance was determined at 540 nm (Double beam systonic spectrometer-2201). The control samples were also prepared accordingly without any plant extracts and were compared with the test samples containing various concentrations of the plant extracts prepared with different solvents. The results were expressed as % inhibition.

α -Glucosidase Inhibitory Activity

The α -glucosidase inhibitory activity was determined using the standard method (Chougale et al., 2009; Tripathi, 2014). The enzyme solution was prepared by dissolving 0.5 mg α -glucosidase in 10 ml phosphate buffer (pH 7.0) containing 20 mg bovine serum albumin. It was diluted further to 1:10 with phosphate buffer just before use. Test sample solutions (5,10,15, and 25%) were prepared and 5 μ L each of the sample solutions or DMSO (sample blank) were then added to 250 μ L of 20 mM *p*-nitrophenyl- α -D -glucopyranoside and 495 μ L of 100 mM phosphate buffer (pH 7.0). It was pre-incubated at 37°C for 5 min and the reaction started by addition of 250 μ L of the enzyme solution, after which it was incubated at 37°C for exactly 15 min 250 μ L of phosphate buffer was added instead of enzyme for blank. The reaction was then stopped by addition of 1000 μ L of 200 mM Na₂CO₃ solution and the amount of *p*-nitrophenol released was measured by reading the absorbance of sample against a sample blank (containing DMSO with no sample) at 400 nm using UV visible spectrophotometer. The results were expressed as % inhibition.

Data Analysis

Experimental data of α -amylase and α -glucosidase inhibitory activity was expressed by multivariate analysis, principal

component analysis (PCA) with the help of Unscrambler software (Sharma et al., 2013c).

In Vivo Anti-Hyperglycemic Studies

Experimental Animals

Swiss albino mice of either sex weighing 30 \pm 5 g were obtained from animal house attached to Pharmacology laboratory of Institute for Postgraduate Teaching and Research in Ayurveda, Gujarat Ayurved University, Jamnagar, Gujarat, India, for experiments and maintained under standard experimental and husbandry conditions.

The animals were housed in each cage made of poly-propylene with stainless steel top grill. The dry wheat (post hulled) waste was used as bedding material and was changed every morning. The animals were exposed to 12 h light and 12 h dark cycle with the relative humidity of 50–70% and the ambient temperature during the period of experimentation was 22 \pm 03°C. Animals were fed with Amrut brand rat pellet feed supplied by Pranav Agro Mills Pvt. Limited and drinking water *ad libitum*. The experiments were carried out after obtaining permission from Institutional Animal Ethics Committee (IAEC Approval number: IAEC/13/2013/01/PhD).

Dose Selection and Schedule

The clinical dose of *Bhavita Guduchi Churna* was taken based on available references as 4 g/day (Sharma et al., 2014c; Shingadiya et al., 2017). The dose for experimental study was calculated by extrapolating the human dose to animals (520 mg/kg) based on the body surface area ratio by referring to the tables of Paget and Barnes (Paget and Barnes, 1964). The test drugs were suspended in distilled water with suitable concentration and administered according to the body weight of the animals by oral route with the help of gastric oral cannula.

Instruments Used

One touch Glucometer (Lifeline Surgicals, New Delhi, India) with *Ez Smart* strips, weighing scale, disposable needle and syringe, mono pan balance and mortar and pestle.

Experimental Study

The hypoglycemic activity and anti-hyperglycemic activities were carried out by modifying previously described method of Pilkhwai et al. (2010). The selected mice were acclimatized for 7 days prior to experiments. The animals were divided randomly into relevant groups of six animals each. Then both activities were evaluated for the test drugs as per the following protocols:

Hypoglycaemic Activity

Swiss albino mice of either sex were randomly divided into five groups of six animals each. The first group received distilled water and served as water control group (10 ml/kg, po). Second group served as standard control group to which glibenclamide (0.65 mg/kg) was administered. Third, fourth and fifth groups were received JBGC, KBGC and SBGC respectively in the dose of 520 mg/kg, orally.

The animals were fasted overnight prior to the experiment and in the morning the fasting initial reading of blood sugar level

(BSL) was measured with the help of One Touch Ez Smart CE0537 Glucometer, by using One Touch Ez Gluco test strips as per user's guideline by collecting the blood sample from tail vein under aseptic conditions. Then the water, test drug and standard drug were administered to respective groups. The BSL was recorded after 1, 2, 3 and 5 h of test drug administration for assessing the hypoglycemic effect after drug administration.

Anti-Hyperglycaemic Activity

The selected animals were randomly divided into five groups of six animals each. First group served as glucose control group to which glucose solution (5 g/kg, po) was administered. Second group served as standard control group to which glibenclamide (0.65 mg/kg, po) was administered. Third, fourth and fifth groups were received JBGC, KBGC and SBGC respectively in the dose of 520 mg/kg, oral.

Animals were fasted overnight prior to the experiment and in the morning the fasting initial BSL was measured as mentioned in hypoglycemic activity. Test drugs and reference standard drug were given to the respective group of animals as per the body weight. After 1 h of drug administration, glucose (5 g/kg, po) solution was administered to all groups orally by dissolving it in distilled water. Thereafter BSL was recorded at 30, 60, 90 and 120 min of post glucose overload for accessing the anti-hyperglycemic activity of test drug (Malalavidhane et al., 2000; Sachdewa et al., 2001; Kingsley et al., 2013).

Statistical Analysis

Results were presented as Mean \pm SEM, difference between the groups was statistically determined by Student paired 't' test with initial values of respective groups and unpaired 't' test with control group. The data also assessed through Anova followed by Dunnet's multiple 't' test. The level of significance set at $p < 0.05$. The level of significance was noted and interpreted accordingly.

High Performance Thin Layer Chromatography Studies

All chemicals utilized were of analytical grade and acquired from Merck Ltd. Berberine chloride hydrate, CAS number - 14,050-10G; purity 90% was purchased from Sigma Aldrich (St. Louis, MO, United States). 5 g of each GC, SBGC, KBGC and JBGC formulation was refluxed with 50 ml of methanol for around 2 h. The subsequent solutions were filtered and concentrated using a rotary evaporator. The resultant extracts i.e., 240 mg (GC); 137 mg (SBGC); 200 mg (KBGC) and 100 mg (JBGC) were transferred in to 50 ml volumetric flask. The standard Berberine chloride hydrate 10 mg was dissolved in 10 ml methanol and finally standard concentration 1000 μ g/ml was made. The calibration curve prepared with different volumes of standard stock solution (1, 2, 3, 4, 5, 7 μ L) were spotted on HPTLC plate (20 \times 10 cm) for berberine chloride hydrate followed by spotting (3, 4, 2, 1.8 μ L) GC, JBGC, SBGC and KBGC respectively sample stock solutions in triplicate. Samples were applied as bands 4 mm wide keeping 12-mm distance from the left edge using Camag Linomat V applicator with a 100 μ L test syringe at a steady application rate of 150 nL s⁻¹. The mobile

phase used was n-hexane, ethyl acetate, glacial acetic acid and methanol (10:1.1:1.1:2.5, v/v). After development, the plates were dried and observed in CAMAG TLC Visualizer at 254 nm. The developed plate was then scanned at 254 nm using CAMAG TLC densitometric Scanner 3 incorporated with WinCATS 1.4.8 programming (Doshi et al., 2014; Kamboj and Saluja, 2017).

RESULTS

α -Amylase Inhibitory Activity

The test formulations in different solvents were studied for inhibitory activity of α - amylase enzyme (Figure 2). It is evident from graphs that maximum α - amylase inhibition was demonstrated by SBGC, followed by KBGC, JBGC and GC formulations in comparison to the standard acarbose. In phosphate buffer saline SBGC formulation showed maximum activity (87%) which is comparable with acarbose (90%).

α -Glucosidase Inhibitory Activity

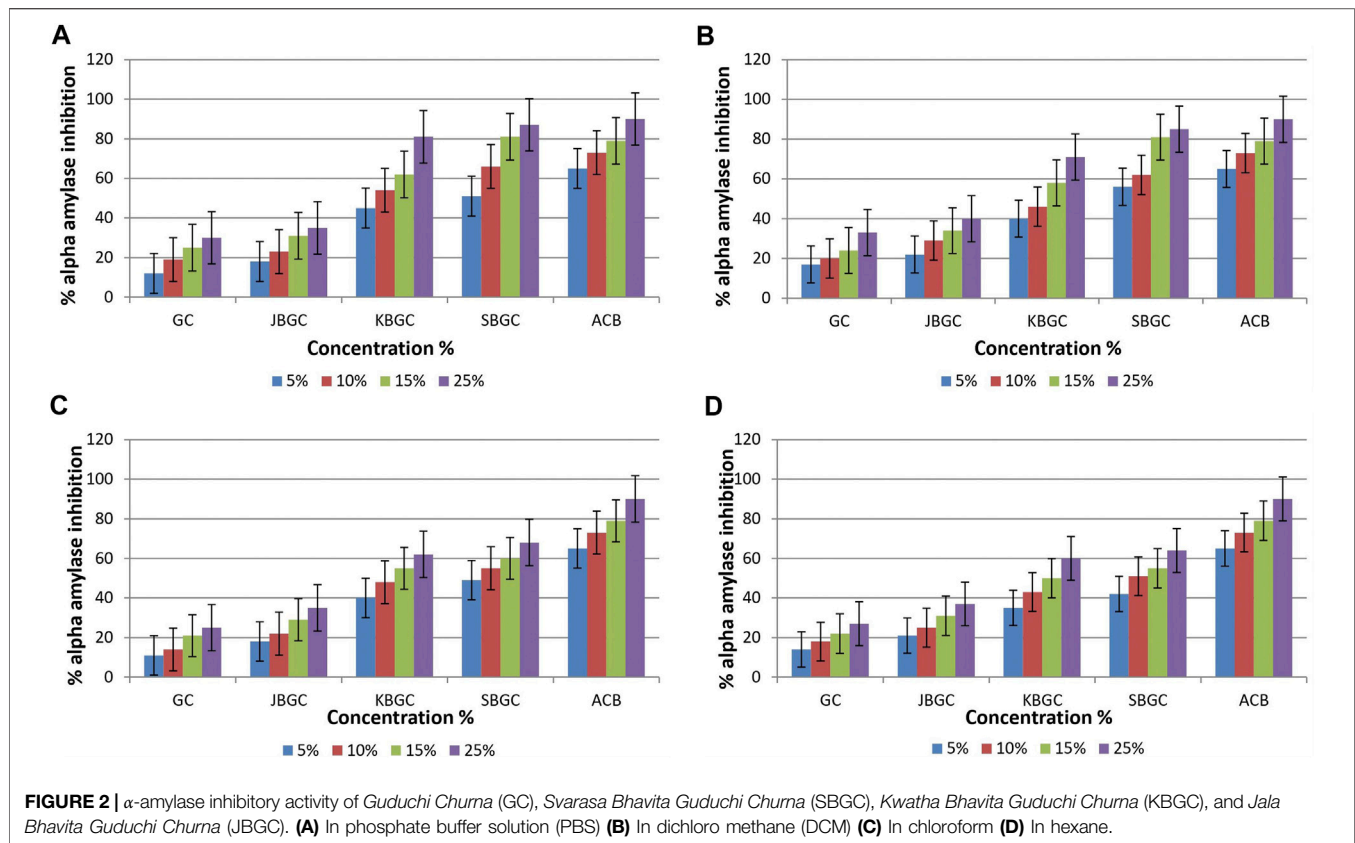
Data with respect to effect of GC, JBGC, KBGC and SBGC on α -glucosidase inhibitory activity are represented in Figure 3. It is evident from the graphs that maximum inhibition was demonstrated by DCM and chloroform extracts of SBGC, followed by KBGC, JBGC and GC in comparison to standard acarbose. Maximum inhibition (89%) was reported by SBGC formulation at 25% solution of DCM.

Differences Among the High, Medium and Low α -Amylase Inhibitory Activity Groups

To better screen the fuzziness and integrity of the various concentration and polarity codified *Guduchi* samples differentiating their α -amylase inhibitory activity (Figure 4), in the experimental samples, % of inhibitory outcome were separated five groups, high ($\leq 54\%$), medium ($\leq 43\%$) and very low ($\geq 21\%$). An overview of the differences in the respective concentrations (5, 10, 15 and 25%) samples was obtained using unsupervised PCA, which takes into account all variables (Figures 4A, Figures 4B). The 1st and 2nd principal components explained 91 and 1% of the total variance respectively. In score plot, we can observe clear separation between SBGC and KBGC, while there was not clear separation of GC and JBGC because of α -amylase activity as a continuous variable. The SBGC samples have high content of active marker compounds may have great potential for preventing postprandial hyperglycemia followed by KBGC, JBGC and GC medicaments in comparison to standard acarbose.

Differences Among the High, Medium and Low α -Glucosidase Inhibitory Activity

The experimental findings of the various concentration and polarity codified *Guduchi* samples differentiating their α -glucosidase inhibitory activity (Figure 5), in the experimental samples, % of inhibitory outcome were separated five groups, high ($\leq 52.4\%$), medium ($\leq 39\%$) and very low ($\geq 14\%$). An overview of



the differences in the respective concentrations (5, 10, 15 and 25%) samples was obtained using unsupervised PCA, which takes into account all variables (Figures 5A, Figures 5B). The first and 2nd principal components explained 99 and 1% of the total variance respectively. In score plot, we can observe clear separation of between GC and KBGC, while there was not clear separation of SBGC and JBGC because of α -glucosidase activity as a continuous variable. Furthermore, DCM and chloroform extract of SBGC with a high amount of active marker compounds may have more synergy and supra additive therapeutic effect, followed by KBGC, JBGC and GC in comparison to standard acarbose.

Hypoglycemic Activity

Table 1 and Figure 6 represent the results of SBGC, KBGC, JBGC formulations on glucose concentration in normal fasted mice. All test formulations has produced a marginal hypoglycemia during the experimental studies. However the glucose concentrations were restored to that of pretreatment level (0 h). GB treated group leads to significant decrease in blood glucose level at almost all the time intervals in comparison to control group and maximum protection was observed at 3rd hour with 45.20%.

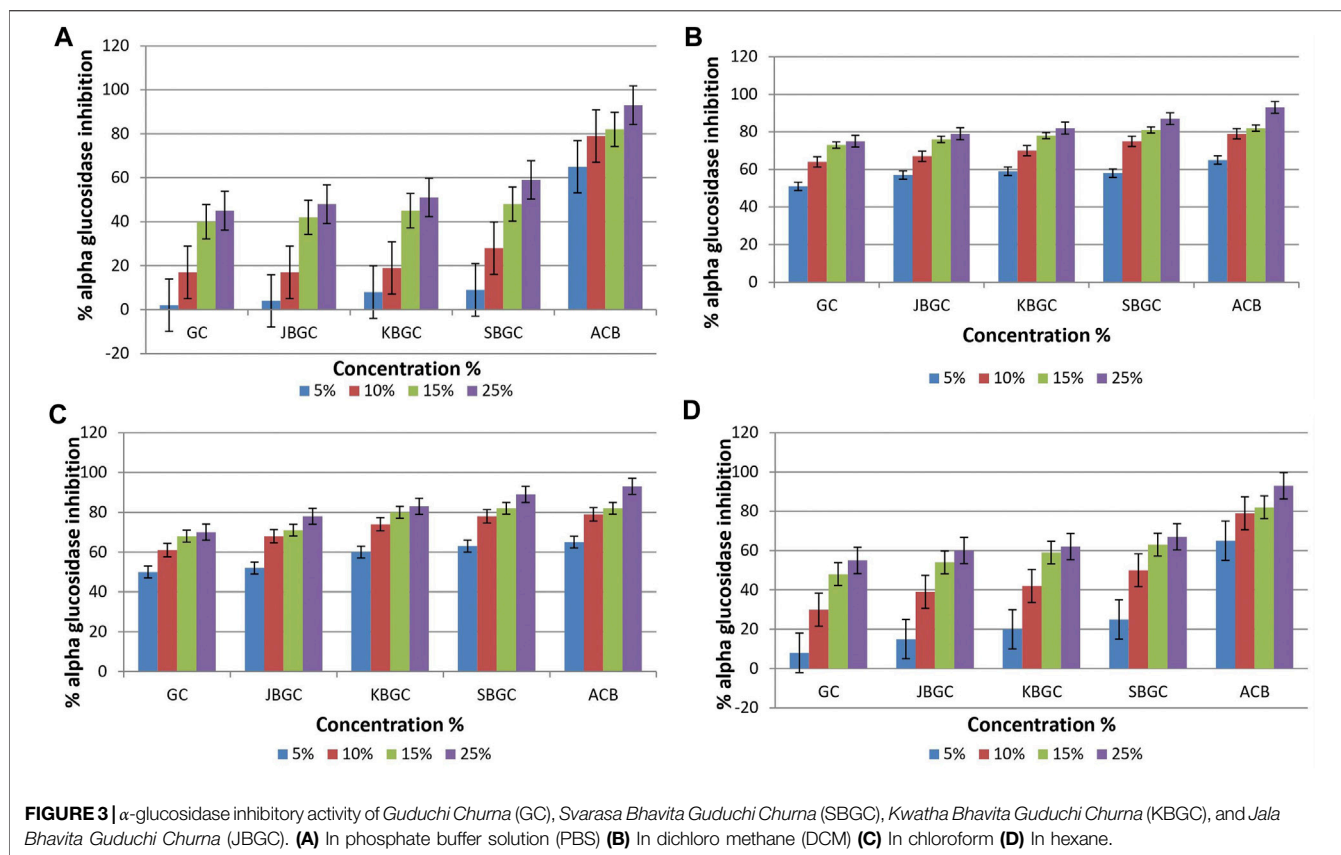
Anti-Hyperglycemic Activity

The effects of JBGC, KBGC and SBGC formulations in glucose tolerance test in mice are presented in Table 2 and Figure 7. All formulations are shown significant activity at an oral dose of 520 mg/kg. The maximum protection was observed at 90 min

after glucose load. Among all formulations SBGC and KBGC were produced maximum protection at 90 min. Glibenclamide was used as standard and produced maximum protection at 90 min with percentage protection of 62.60%. The maximum glucose concentration was observed at 60 min with glucose concentration of 236.6 mg/dl. The percentage protection at 90 min produced by JBGC, KBGC and SBGC is 38.46, 42.06 and 56.56 respectively when tested at dose of 520 mg/kg, these results are comparable in activity produced by glibenclamide at a dose of 0.65 mg/kg. SBGC produced significant anti-hyperglycemic effect at all-time intervals in comparison to control group. Overall, SBGC produced pronounced anti-hyperglycemic effect followed by KBGC and JBGC.

High Performance Thin Layer Chromatography Studies

The developed mobile phase consisting of n-hexane, ethyl acetate and methanol (10:1.1:1.1:2.5, v/v) gave better, sharp and well defined peak resolution for standard (berberine chloride hydrate-a well-known anti-diabetic compound) as well as a test samples. The developed HPTLC method resolved the standard compound at R_F value of nearly about 0.28 ± 0.02 for berberine chloride hydrate for confirming the presence in coded extract visualized by band parallel to standard spot along with other resolved components in the developed TLC plate. The TLC plates were scanned at 254 nm and to identify of berberine chloride hydrate



in the sample chromatogram was confirmed by three-dimensional (3D) chromatogram (**Figure 8**) obtained after densitometric scanning. The calibration curve was linear range of (200–1,400 ng/spot) for berberine chloride hydrate. The linear regression of the berberine chloride hydrate standard was determined with $R^2 \pm SD = 0.991 \pm 3.21\%$ with regression line; $y = 7.336x + 459.8$. The quantification of berberine chloride hydrate in the respective codified samples is depicted in **Table 3**. The peak corresponding to berberine chloride hydrate and berberine from the codified samples solution had the same retardation factor ($R_F = 0.28 \pm 0.02$).

DISCUSSION

This study was carried out not only to validate the traditional uses of *Guduchi* and its preparations in diabetes (Sharma et al., 2014b) but also to initiate search for newer pharmacophores with specificity toward pancreatic α -amylase or α -glucosidase. Structurally as well as mechanistically, PPA is closely related to HPA (human pancreatic α -amylase) (Brayer et al., 1995). Hence, sequential solvent extracts of different formulations of *Guduchi* viz. GC, JBGC, KBGC and SBGC were screened for the presence of PPA inhibitors, the lead extracts quantified for PPA inhibition under *in-vitro* conditions. Primary screening for α -amylase inhibition was performed based on starch-iodine color complex formation. Different extracts of GC, JBGC,

KBGC and SBGC were prepared in various solvents such as phosphate buffer, DCM, chloroform and hexane extracts. All these extracts were screened, and all of them tested positive for PPA inhibition by chromogenic DNSA method. It was noted that phosphate buffer and DCM extracts of SBGC exhibited strong PPA inhibitory potential (>80% inhibition, in 15 and 25% concentrations) followed by KBGC, JBGC and GC. In α -glucosidase inhibitory activity, maximum inhibition was shown by DCM and chloroform extracts of SBGC (>85% inhibition, in 15 and 25% concentrations), followed by KBGC (>80% inhibition, in 15 and 25% concentrations), JBGC and GC.

In both α -amylase and α -glucosidase inhibitory activities, a dose/concentration dependent effect was observed on increasing the concentrations of the extract solution, suggesting a competitive type of inhibition. Our results suggests that extracts of GC, JBGC, KBGC and SBGC act effectively as PPA inhibitors leading to a reduction in starch hydrolysis and hence eventually to lowered glucose levels. Also, a good discrimination among respective codified samples is easily obtained from PCA analysis, may be due to supra-additive active metabolite load in context of α -amylase and α -glucosidase inhibitory activity. Our study shows that SBGC followed by KBGC were effectively inhibiting α -amylase and α -glucosidase enzyme and therefore it may be used as hypoglycemic agents in the management of post prandial hyperglycemia. The study suggests that one of the targets for hypoglycaemic property of *Guduchi* is α -amylase and α -glucosidase inhibition, where SBGC demonstrated a highly

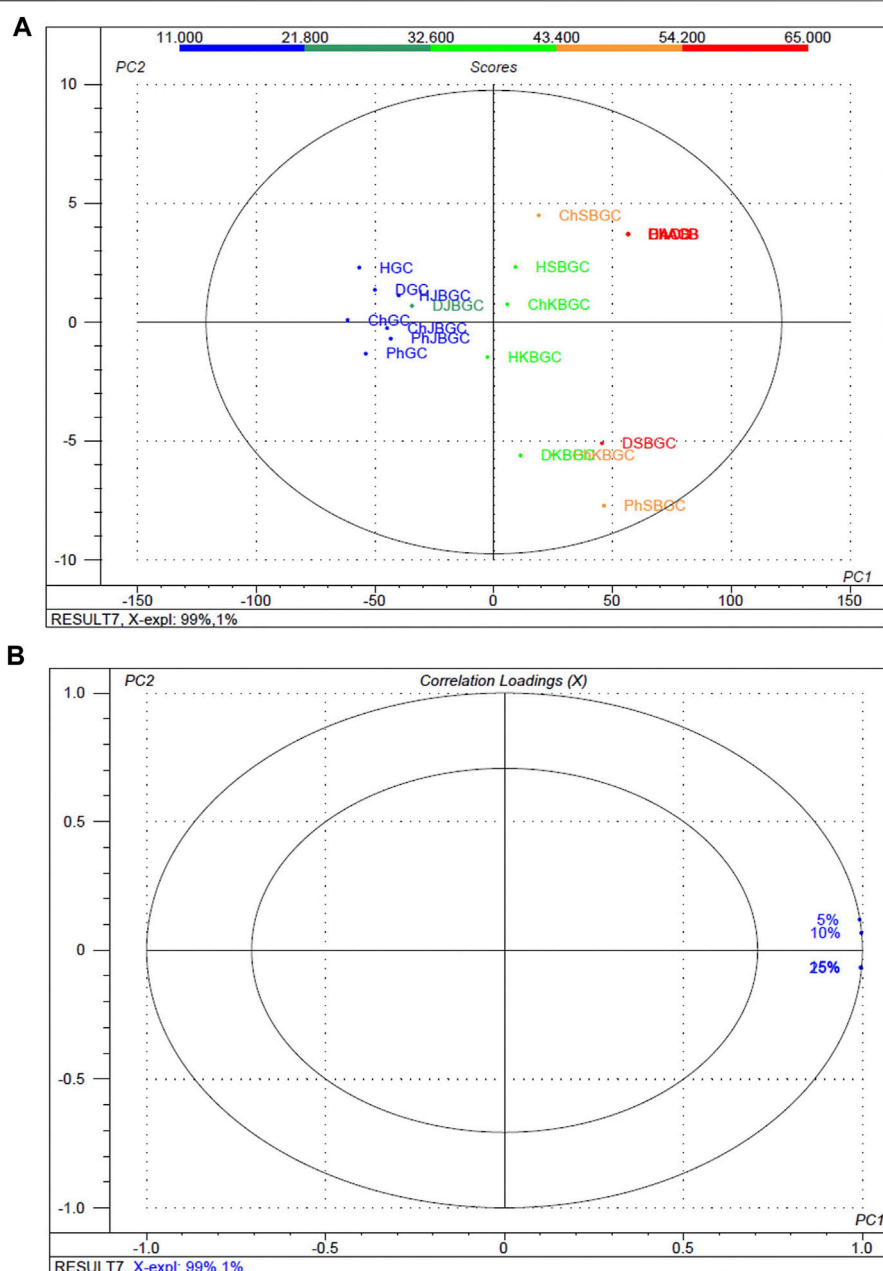


FIGURE 4 | Multivariate statistical analysis of codified different polarity *Guduchi* samples (Ph: phosphate buffer solution, D: dichloro methane, Ch: chloroform, and H: hexane) based on an unsupervised PCA model. **(A)** Unsupervised PCA score plot **(B)** Loading plot of α -amylase inhibitory activity of GC, JBGC, KBGC, SBGC formulations and various concentrations.

promising and effective strategy for diabetes, which may serve as a lead for isolation and characterization of compounds responsible for it.

Taking leads from encouraging enzyme inhibitory results, *in-vivo* experiments were carried out to understand the effects of extracts on glycemic levels of experimental animals. An ideal antihyperglycemic agent should decrease the elevated blood glucose levels and should maintain the normal blood glucose levels (Venkatesh et al., 2003). The decrease in blood glucose levels below the normal i.e., hypoglycemia, is the major side effect of insulin and oral hypoglycemic agents. In the

present investigation, all extracts were tested for their hypoglycemic activity and the results showed partial hypoglycemia in normal mice, where as glibenclamide showed maximum protection (45.20%) at 3rd hour.

Glucose tolerance test is a preliminary method to assess the ability of drug to reduce the increased blood glucose levels or not (Kingsley et al., 2013). In this screening method, the animals are loaded with challenging dose of glucose (5 g/kg) after 60 min of test, standard drug administration. After glucose load, the raise in

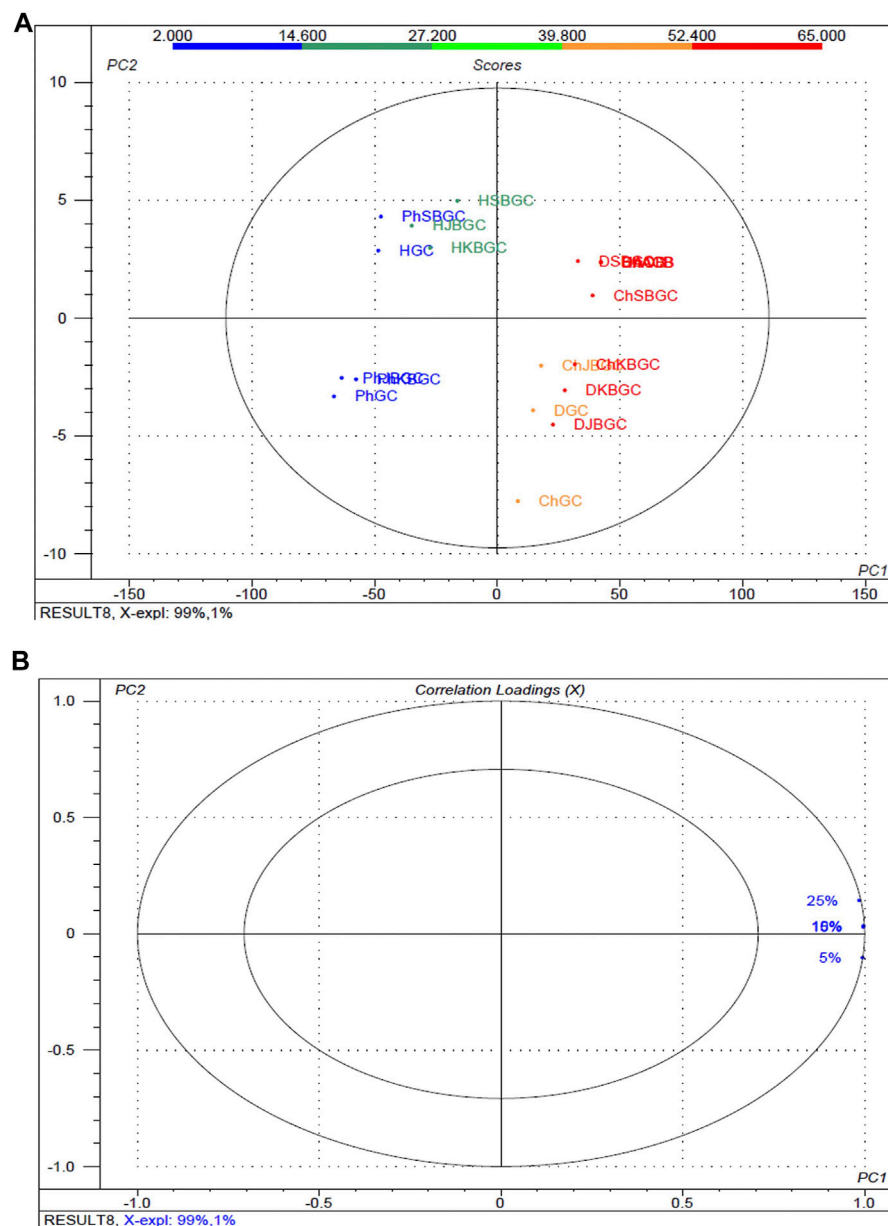


FIGURE 5 | Multivariate statistical analysis of codified different polarity *Guduchi* samples (Ph: phosphate buffer solution, D: dichloro methane, Ch: chloroform, and H: hexane) based on an unsupervised PCA model. **(A)** Unsupervised PCA score plot and **(B)** Loading plot of α -glucosidase activity of GC, JBGC, KBGC, SBGC formulations and various concentrations. The ellipse represents the Hotelling T^2 with 95% confidence.

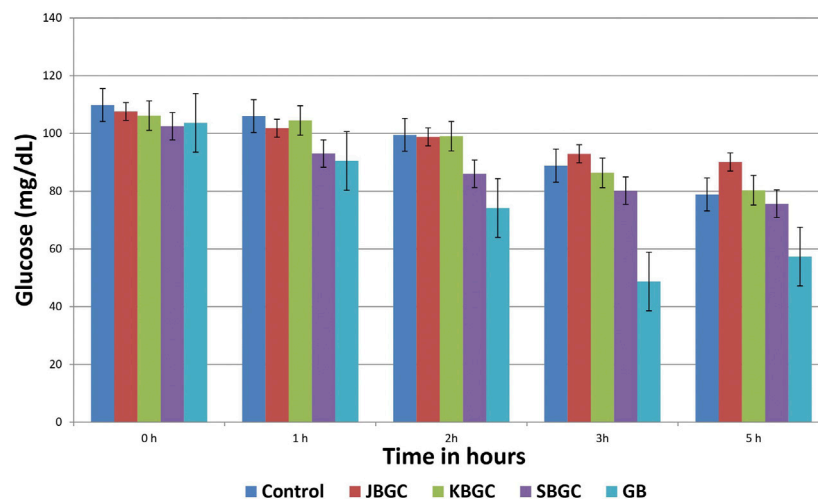
glucose concentration is observed from 30 min and reached maximum at 60 min and decreased by 120 min. SBGC, KBGC, and JBGC extracts produced significant activity at 90 min, however, the maximum significant ($p < 0.01$) activity was produced at 520 mg/kg by SBGC, KBGC, and JBGC is 56.56, 42.06 and 38.46 respectively. SBGC produced significant anti-hyperglycemic effect at all-time intervals in comparison to control group. Overall, SBGC produced pronounced anti-hyperglycemic effect followed by KBGC and JBGC. The standard glibenclamide (10 mg/kg) produced a significant maximum protection at 90 min (62.60%). The observed

promising results of the test drugs on glycemic levels could be due to the increased concentration of the anti-diabetic phytoconstituents during *Bhavana* process. It also has been reported that the anti-diabetic activity of this plant is primarily due to improving the entry of glucose into the peripheral tissues and organs like the liver and decreasing the activity of phosphorylase in the liver, thereby it may prevent the release of glucose into the blood (Puranik et al., 2010). The same mechanism may be involved in the observed activity profile; however further detailed studies are needed to understand the exact pharmacodynamics involved.

TABLE 1 | Effect of JBGC, KBGC and SBGC on blood sugar level in normal overnight fasted Swiss albino mice at various time intervals.

Blood glucose level (mg/dl)					
Groups	Initial (mg/dl)	1 h (mg/dl)	2 h (mg/dl)	3 h (mg/dl)	5 h (mg/dl)
WC	109.83 ± 2.24	106.00 ± 2.80	99.50 ± 1.70*	88.83 ± 1.90*	78.83 ± 1.85*
JBGC	107.60 ± 1.32	101.80 ± 1.49 (4.12)	98.80 ± 4.85* (0.7)	92.92 ± 2.65**	90.10 ± 2.39*
KBGC	106.16 ± 3.05	104.50 ± 1.46* (1.41)	99.00 ± 3.59* (0.5)	86.33 ± 4.01* (2.81)	80.33 ± 2.42*
SBGC	102.50 ± 1.01	93.00 ± 3.51** (12.26)	86.00 ± 5.46* (13.56)	80.16 ± 3.92* (9.76)	75.66 ± 4.520* (4.02)
GB	103.64 ± 4.82	90.5 ± 2.32* (14.62)	74.17 ± 1.25* (25.45)	48.67 ± 2.26* (45.20)	57.33 ± 4.84** (27.27)

WC, Water control; JBGC, Jala Bhavita Guduchi Churna; KBGC, Kwatha Bhavita Guduchi Churna; SBGC, Svarasa Bhavita Guduchi Churna; GB, Glibenclamide as standard control. * $p < 0.05$, ** $p < 0.01$ are in comparison with initial blood glucose levels of the mice (0 h) in the respective group. Figures in parenthesis indicate the percentage decrease. Values are mean ± S.E.M; n = 6.

**FIGURE 6 |** Effect of Svarasa Bhavita Guduchi Churna (SBGC), Kwatha Bhavita Guduchi Churna (KBGC), and Jala Bhavita Guduchi Churna (JBGC) on BSL in normal fasted mice.**TABLE 2 |** Effect of JBGC, KBGC and SBGC on blood sugar level in glucose overloaded Swiss albino mice at various time intervals.

Blood glucose level (mg/dl)					
Groups	0 min	30 min	60 min	90 min	120 min
GC	86.66 ± 2.84**	180.83 ± 3.84**	236.6 ± 4.49**	189.0 ± 2.3**	134.5 ± 2.89**
JBGC	80.1 ± 1.62**	160.9 ± 2.89** (11.11)	184.6 ± 2.62** (21.99)	116.3 ± 1.26** (38.46)	93.4 ± 3.42** (30.55)
KBGC	84.4 ± 3.97**	143.8 ± 4.56** (20.47)	165.8 ± 3.12** (29.94)	109.5 ± 3.15** (42.06)	88.8 ± 1.94** (33.97)
SBGC	79.6 ± 4.58**	131.2 ± 1.97** (27.44)	116.7 ± 4.23** (50.67)	82.1 ± 1.59** (56.56)	82.2 ± 3.04** (38.88)
GB	82.42 ± 5.12**	104.17 ± 2.68** (42.39)	101.5 ± 3.58** (57.10)	70.67 ± 1.36** (62.60)	61.33 ± 2.33** (54.40)

GC, Glucose control; JBGC, Jala Bhavita Guduchi Churna; KBGC, Kwatha Bhavita Guduchi Churna; SBGC, Svarasa Bhavita Guduchi Churna; GB, Glibenclamide as standard control. * $p < 0.05$, ** $p < 0.01$ are in comparison with initial blood glucose levels of the mice (0 h) in the respective group. Figures in parenthesis indicate the percentage decrease. Values are mean ± S.E.M; n = 6.

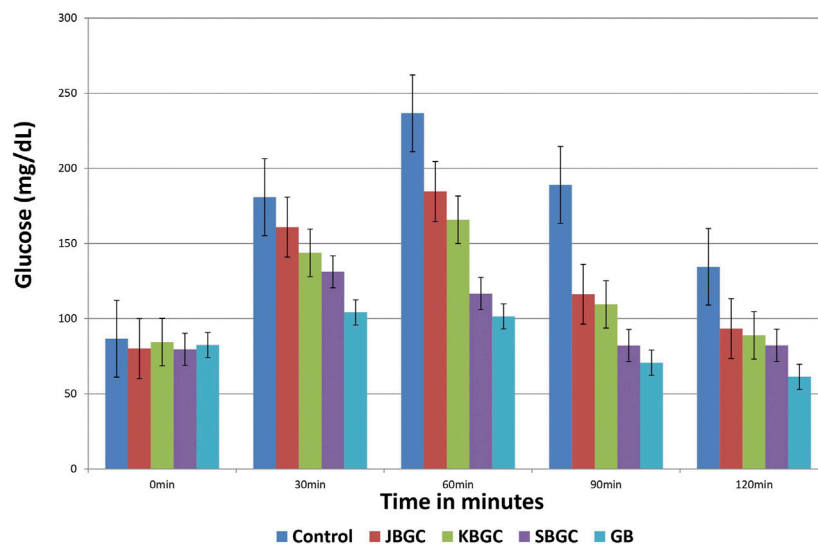


FIGURE 7 | Effect of Svarasa Bhavita Guduchi Churna (SBGC), Kwatha Bhavita Guduchi Churna (KBGC), and Jala Bhavita Guduchi Churna (JBGC) on BSL in glucose overloaded mice.

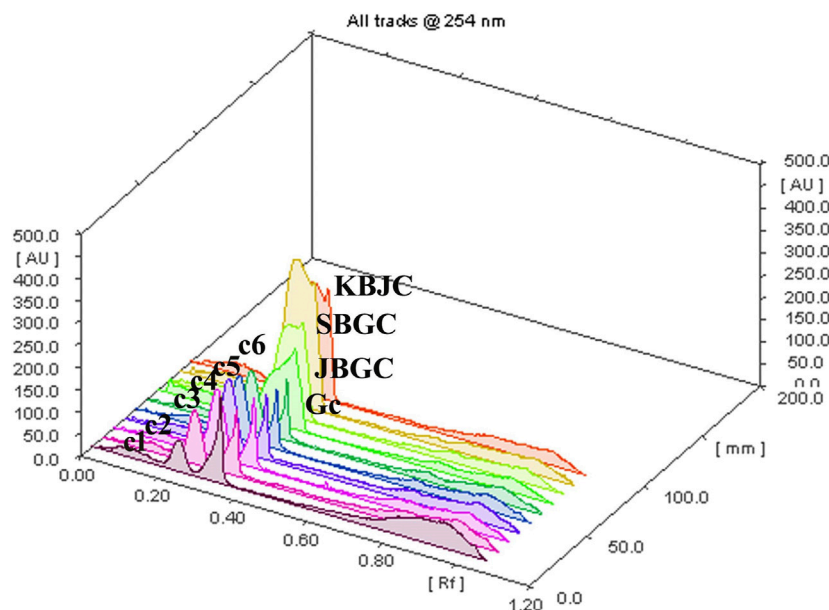


FIGURE 8 | TLC plate scanned at 254 nm showing berberine chloride hydrate in the 3D samples chromatogram.

In view of the potential anti-diabetic importance of *Guduchi*, and promising results obtained in present study from *in-vitro* and *in-vivo* investigations, an attempt has been made to chromatographically quantify the berberine level in *Bhavita Guduchi* samples (SBGC, KBGC, and JBGC). The isoquinoline alkaloid 'berberine' has been tested and used successfully in experimental and human diabetes. It is reported to exhibit significant antioxidant and anti-hyperglycemic activity, inhibits FOXO 1 (Forkhead Box O1 Protein), which integrates insulin signaling with mitochondrial function, and activates AMPK (AMP-activated protein kinase), thus decreases

the levels of blood sugar, cholesterol and maintains the blood pressure (Sharma and Batra, 2013). Berberine salts are also reported as bioavailability enhancer (Cui et al., 2019). On the flip side, isolation of another anti-diabetic compound Tinosporaside, an 18-norclerodane glucoside, is a tedious and more reductionist way to sample cleanup (Puratchimani and Jha, 2007), which would be a distortion of Ayurvedic holistic principle. In the present study, HPTLC method was developed for the determination of berberine chloride hydrate in *Guduchi* formulations, which showed the presence of berberine chloride hydrate in SBGC (32%) > KBGC (25.3%) > JBGC

TABLE 3 | The berberine chloride hydrate present in different codified samples.

Samples (coded methanolic extract)	Conc ⁿ prepared (mg/ml)	Spotting volume (μL)	Berberine chloride hydrate determined (ng/spot)	Extractive value (%)	% Marker in extract	% Of marker in raw powder (g)
GC	2.74	3	963.44	2.74	11.72	0.32
JBGC	2	4	2024.63	2	25.30	0.51
SBGC	4	2	2,563.14	4	32	1.28
KBGC	4.8	1.8	1,222.23	4.8	14.14	0.59

GC, Guduchi Churna; JBGC, Jala Bhavita Guduchi Churna; KBGC, Kwatha Bhavita Guduchi Churna; SBGC, Svarasa Bhavita Guduchi Churna; GB, Glibenclamide as standard control.

(14.14%) > GC (11.72%) respectively in increasing way. In HPTLC, increased berberine level in *Bhavita* samples (in comparison to GC) signifies the role of *Bhavana* in increasing the concentration of phyto-constituents. The obtained HPTLC results also corroborate with the findings of *in-vitro* and *in-vivo* experiments, wherein *Bhavita* samples exhibited better results than crude *Guduchi Churna*, and specifically SBGC showed better activity profile among all other samples. The increased berberine level after *Bhavana* could be having the role as bioavailability enhancer or imparting a supra-additive effect. Therefore further investigations are required to understand the kinetic chemistry of *Bhavana* in adding of myriad of bioactive phytoconstituents or active metabolites during wet grinding process and its possible role in improving the absorption and bioavailability of drugs.

In Ayurvedic classics, only *Svarasa* (extracted juice) dosage form of *Guduchi* is mentioned to be used for diabetes and in Ayurvedic pharmaceuticals the *Svarasa* dosage form is said to be more potent than *Kwatha* (decoction) (Sharma et al., 2014b). Also, the *Svarasa* is extracted whole juice that may have more extractive principles of the plant, while decoction is only aqueous soluble extract of the botanical. However owing to very short shelf life of *Svarasa* (3 h) (Gupta et al., 2011), other dosage forms of *Guduchi* (viz. *Churna* or *Kwatha*) are popular among traditional practitioners. Thus better activity profile of SBGC in present *in-vitro* and *in-vivo* experiments validates and substantiate the Ayurvedic claims to use *Guduchi Svarasa* in diabetes; and to prepare the *Svarasa Bhavita* dosage form appears to be an effective way to preserve the properties of *Svarasa*. Hence further shelf-life studies are required for better understanding.

Present findings endorse the use of these formulations of *Guduchi* to manage glycemic levels in type 2 diabetes management. Further *in-vivo* antidiabetic as well as clinical studies are warranted to substantiate these findings. More extensive works are also needed to explore these formulations for their antioxidant, cytoprotective, and immunomodulatory roles in the management of other pathological metabolic cascades involved in diabetes.

CONCLUSION

In this study, better α -amylase, α -glucosidase inhibitory activities and significant anti-hyperglycemic effect of SBGC and KBGC ascertain definite role of *Bhavana* in augmentation of bioefficacy of drugs and suggest promising potential of these *Guduchi* formulations for the management of type 2 diabetes. This corroborate with findings of HPTLC study, wherein the percentage of anti-diabetic compound 'berberine' was found increased in *Bhavita* samples (maximum in

SBGC, followed by KBGC and JBGC). The obtained results provide new leads to researchers to investigate these formulations apropos their pharmacokinetic and pharmacodynamic mechanistic roles, bioactivities on other therapeutic parameters as well as at clinical levels. This traditional Ayurvedic pharmaceutical concept of *Bhavana* can be utilized further in invention of new chemical moieties in the field of drug discovery and development.

DATA AVAILABILITY STATEMENT

The original contributions presented in the study are included in the article/Supplementary Material, further inquiries can be directed to the corresponding author.

ETHICS STATEMENT

The animal study was reviewed and approved by Institutional Animal Ethics Committee, Institute for Postgraduate Teaching and Research in Ayurveda, Gujarat Ayurved University, Jamnagar, Gujarat, India (IAEC Approval number: IAEC/13/2013/01/PhD).

AUTHOR CONTRIBUTIONS

RS, GR and PP designed the study protocol. RS performed the Pharmaceutical study. RS and JM performed the experiments and analyzed the data. RS and RB wrote the manuscript. GR and PP contributed to the critical reading and revision of the manuscript. All authors contributed to the article and approved the submitted version.

ACKNOWLEDGMENTS

The authors are thankful to Head, Pharmacology laboratory, Dr. B. Ravishankar, Dr. Mukesh Nariya, and Head, Pharmaceutical chemistry laboratory, Dr. V. J. Shukla of I.P.G.T. and R.A. (currently I.T.R.A.), Gujarat Ayurved University, Jamnagar, for providing full support to conduct the study. The authors are also grateful to the authorities of Department of Rasa Shastra and Bhaishajya Kalpana, the Institute, and Gujarat Ayurved University, for providing the facilities and granting permission to undertake the present study. The authors kindly acknowledge Banaras Hindu University for the seed grant under IOE for the year 2020–2021.

REFERENCES

- Acharya, Y. T. (2008). *Siddha Yoga Sangraha, Jwaradhikar*, Ch. 1. 13th edition. Nagpur: Shri Baidhnath Ayurved Bhavan Ltd. 4.
- Acharya, Y. T. (2004). *Sushruta Samhita of Sushruta, Chikitsa Sthana*, Ch. 10, Ver. 10-12, Reprint edition, Varanasi: Chaukhambha Krishanadas Academy. 415.
- Bhalerao, B. M., Kasote, D. M., Nagarkar, B. E., Jagtap, S. D., Vishwakarma, K. S., Pawar, P. K., et al. (2012). Comparative Analysis of Radical Scavenging and Immunomodulatory Activities of *Tinospora Cordifolia* Growing with Different Supporting Trees. *Acta Biol. Szeged*. 56, 65–71.
- Brayer, G. D., Luo, Y., and Withers, S. G. (1995). The Structure of Human Pancreatic Amylase at 1.8 Å Resolution and Comparisons with Related Enzymes. *Protein Sci.* 4, 1730–1742. doi:10.1002/pro.5560040908
- Cho, N. H., Shaw, J. E., Karuranga, S., Huang, Y., da Rocha Fernandes, J. D., Ohlrogge, A. W., et al. (2018). IDF Diabetes Atlas: Global Estimates of Diabetes Prevalence for 2017 and Projections for 2045. *Diabetes Res. Clin. Pract.* 138, 271–281. doi:10.1016/j.diabres.2018.02.023
- Choudhry, N., Singh, S., Siddiqui, M. B., and Khatoun, S. (2014). Impact of Seasons and Dioecy on Therapeutic Phytoconstituents of *Tinospora Cordifolia*, a Rasayana Drug. *Biomed. Res. Int.* 2014, 1–11. doi:10.1155/2014/902138
- Chougale, A. D., Ghadyale, V. A., Panaskar, S. N., and Arvindekar, A. U. (2009). Alpha Glucosidase Inhibition by Stem Extract of *Tinospora Cordifolia*. *J. Enzyme Inhib. Med. Chem.* 24, 998–1001. doi:10.1080/14756360802565346
- Cui, H. X., Hu, Y. N., Li, J. W., Yuan, K., and Guo, Y. (2019). Preparation and Evaluation of Antidiabetic Agents of Berberine Organic Acid Salts for Enhancing the Bioavailability. *Molecules* 24, 103. doi:10.3390/molecules24112156
- Doshi, G., Chaskar, P., Une, H., and Zine, S. (2014). Solicitation of HPLC and HPTLC Techniques for Determination of Rutin from *Polalthia Longifolia* Thwaites. *Phcog Res.* 6, 234–239. doi:10.4103/0974-8490.132601
- Gade, P. (2017). Effectiveness of Guduchi Kwatha (*Tinospora Cordifolia* in Prameha (DM Type II). *J. Indian Sys. Med.* 5, 227.
- Gupta, A., Jaiswal, M., and Prajapati, P. K. (2011). Shelf Life of Ayurvedic Dosage Forms-Traditional View, Current Status and Prospective Need. *Indian J. Tradit. Knowl.* 10, 672–677.
- Kamboj, A., and Saluja, A. K. (2017). Development of Validated HPTLC Method for Quantification of Stigmasterol from Leaf and Stem of *Bryophyllum Pinnatum*. *Arabian J. Chem.* 10, S2644–S2650. doi:10.1016/j.arabjc.2013.10.006
- Kinghorn, A. D. (2003). *Quality Standards of Indian Medicinal Plants*. New Delhi: Indian Council of Medical Research, 212.
- Kingsley, R. B., Mishra, M., Brindha, P., and Subramoniam, A. (2013). Anti-diabetic Activity of Active Fractions of *Stereospermum Tetragonum* DC and Isolation of Active Principles. *J. Young Pharm.* 5, 7–12. doi:10.1016/j.jyp.2012.09.002
- Kumar, B. D., Mitra, A., and Manjunatha, M. (2010). A Comparative Study of Alpha-Amylase Inhibitory Activities of Common Antidiabetic Plants of Kharagpur 1 Block. *Int. J. Green. Pharm.* 4, 115–121. doi:10.4103/0973-8258.63887
- Malalavidhane, T. S., Wickramasinghe, S. M. D. N., and Jansz, E. R. (2000). Oral Hypoglycaemic Activity of *Ipomoea Aquatica*. *J. Ethnopharmacol.* 72, 293–298. doi:10.1016/s0378-8741(00)00217-8
- Nidhi, P., Swati, P., and Krishnamurthy, R. (2013). Indian *Tinospora* Species: Natural Immunomodulators and Therapeutic Agents. *Int. J. Pharm. Biol. Chem. Sci.* 2, 1–9. doi:10.9734/bpi/bsbvtv2
- Olowoyo, P., Jenkins, C., Feng, W., an Bayona, H., Mohan, S., Joshi, R., et al. (2018). Gaps in Guidelines for the Management of Diabetes in Low-And Middle-Income versus High-Income Countries. A Systematic Review. *Diabetes Care* 41, 1097. doi:10.2337/dc17-1795
- Paget, G. E., and Barnes, J. M. (1964). “Evaluation of Drug Activities,” in *Pharmacometrics*. Editors D. R. Lawrence and A. L. Bacharach (New York: Academic Press), 161.
- Pilkhwil, S. S., Sah, M. L., Juyal, V., and Pandey, S. (2010). Hypoglycemic Activity of Aqueous Extract of *Urtica Parviflora* Roxb in Normoglycemic Rats. *Int. J. Phytomed.* 2, 47–51. doi:10.5138/ijpm.2010.0975.0185.02009
- Puranik, N., Kammar, K. F., and Sheela, D. (2010). Anti-diabetic Activity of *Tinospora Cordifolia* (Willd.) in Streptozotocin Diabetic Rats; Does it Act like Sulfonylureas?. *Turk. J. Med. Sci.* 40, 265–270. doi:10.3906/sag-0802-40
- Puratchamani, V., and Jha, S. (2007). HPTLC Standardization of *Tinospora Cordifolia* Using Tinosporaside. *Indian J. Pharm. Sci.* 69, 578. doi:10.4103/0250-474X.36951
- Sachdewa, A., Raina, D., Srivastava, A. K., and Khemani, L. D. (2001). Effect of Aegle Marmelos and *Hibiscus Rosa Sinensis* Leaf Extract on Glucose Tolerance in Glucose Induced Hyperglycemic Rats (Charles Foster). *J. Environ. Biol.* 22, 53–57.
- Saha, S., and Ghosh, S. (2012). *Tinospora Cordifolia*: One Plant, Many Roles. *Anc. Sci. Life* 31 (4), 151–159. doi:10.4103/0257-7941.107344
- Sharma, A., and Batra, A. (2013). Berberine a Novel Antidiabetic Drug. *Int. J. Res. Rev. Pharm. Appl. Sci.* 3, 216–230. doi:10.5958/j.2231-1750.3.2.008
- Sharma, R., Amin, H., Ruknuddin, G., and Prajapati, P. K. (2014a). Therapeutic Vistas of Guduchi (*Tinospora Cordifolia*): A Medico-Historical Memoir. *J. Res. Educ. Ind. Med. XX*, 113–128.
- Sharma, R., Amin, H., Galib, R., and Prajapati, P. K. (2014b). Antidiabetic Appraisal of Guduchi (*Tinospora Cordifolia* (Willd.) Miers): Insightful Exposition of Ayurvedic Claims. *Rasamruta* 6, 1–14.
- Sharma, R., Amin, H., Galib, P. K., and Prajapati, P. K. (2015a). Antidiabetic Claims of *Tinospora Cordifolia* (Willd.) Miers: Critical Appraisal and Role in Therapy. *Asian Pac. J. Trop. Biomed.* 5, 68–78. doi:10.1016/S2221-1691(15)30173-8
- Sharma, R., Amin, H., Ruknuddin, G., and Prajapati, P. (2015b). Efficacy of Ayurvedic Remedies in Type 2 Diabetes: A Review through Works Done at Gujarat Ayurved University, Jamnagar. *J. Med. Nutr. Nutraceut* 4, 63–69. doi:10.4103/2278-019X.151812
- Sharma, R., Galib, R., and Prajapati, P. K. (2017). Antimicrobial Evaluation of Svarasa Bhavita Guduchi Churna (Levigated Powder of *Tinospora Cordifolia* (Willd.) Miers with its Juice. *Ayurscientifica* 1, 25–30.
- Sharma, R., Galib, R., Shukla, V. J., and Prajapati, P. K. (2014c). *Role of Bhavana Sanskara on Guduchi Churna and its Effect on Type 2 Diabetes Mellitus*. Jamnagar: Gujarat Ayurved University, IPGT and RA, 116–117. [Thesis].
- Sharma, R., Kumar, V., Ashok, B., Galib, R., Prajapati, P., and Ravishankar, B. (2013b). Hypoglycemic and Anti-hyperglycemic Activity of Guduchi Satva in Experimental Animals. *Ayu* 34, 417–420. doi:10.4103/0974-8520.127726
- Sharma, R., Kumar, V., Galib, R., Prajapati, P., Ravishankar, B., and Ashok, B. (2013a). Evaluation of Hypoglycaemic and Anti-hyperglycaemic Activities of Guduchi Ghana in Swiss Albino Mice. *Int. J. Green. Pharm.* 7, 145–148. doi:10.4103/0974-8520.12772610.4103/0973-8258.116397
- Sharma, R., and Prajapati, P. K. (2015). Liquid Media's in Bhavana Samskara: A Pharmaceutico-Therapeutic Prospect. *J. Phytopharmacol.* 4, 49–57.
- Sharma, R., R. G., Prajapati, P., and Amin, H. (2013c). Seasonal Variations in Physicochemical Profiles of Guduchi Satva (Starchy Substance from *Tinospora Cordifolia* [Willd.] Miers). *J. Ayurveda Integr. Med.* 4, 193–197. doi:10.4103/0975-9476.123685
- Sharma, R., Shukla, V. J., Ravishankar, B., and Prajapati, P. K. (2012). *The effect of two different dosage forms of Guduchi i.e. Satva and Ghana WSR antihyperglycemic effect on madhumeha (NIDDM)*. Jamnagar: Gujarat Ayurved University, IPGT and RA, 132–133. [dissertation].
- Shastri, P. (2005). *Sharangadhara Samhita of Sharangadhara, Prathama Khanda, with the Commentary of Adhamalla's Dipika and Kasiram's Gudhartha Dipika*. 6th edition. 1/45. Varanasi: Chaukhamba Orientalia. 11.
- Shingadiya, R. K., Bedarkar, P. B., Pargiri, B. J., and Prajapati, P. K. (2017). Effect of Churnakriya in the Management of Several Lifestyle Disorders: A Review through Research Workcarried Out at RSBK Department, Jamnagar, India. *Int. J. Res. Ayurveda Pharm.* 8, 68–72. doi:10.7897/2277-4343.08285
- Srinivasan, G., Unnikrishnan, K., Rema Shree, A., and Balachandran, I. (2008). HPLC Estimation of Berberine in *Tinospora Cordifolia* and *Tinospora Sinensis*. *Indian J. Pharm. Sci.* 70, 96–99. doi:10.4103/0250-474x.40341

- Sudha, P., Zinjarde, S. S., Bhargava, S. Y., and Kumar, A. R. (2011). Potent α -amylase Inhibitory Activity of Indian Ayurvedic Medicinal Plants. *BMC Complement. Altern. Med.* 11, 5. doi:10.1186/1472-6882-11-5
- Tripathi, Y. B. (2014). Insulin Secreting and α -glucosidase Inhibitory Activity of Hexane Extract of *Annona Squamosa* Linn. In Streptozotocin (STZ) Induced Diabetic Rats. *Indian J. Exp. Biol.* 52, 623–629.
- Venkatesh, S., Madhava Reddy, B., Dayanand Reddy, G., Mullangi, R., and Lakshman, M. (2003). Antihyperglycemic Activity of *Helicteres Isora* Roots in Alloxan-Induced Diabetic Rats. *Pharm. Biol.* 41, 347–350. doi:10.1076/phbi.41.5.347.15937

Conflict of Interest: The authors declare that the research was conducted in the absence of any commercial or financial relationships that could be construed as a potential conflict of interest.

Copyright © 2021 Sharma, Bolleddu, Maji, Ruknuddin and Prajapati. This is an open-access article distributed under the terms of the Creative Commons Attribution License (CC BY). The use, distribution or reproduction in other forums is permitted, provided the original author(s) and the copyright owner(s) are credited and that the original publication in this journal is cited, in accordance with accepted academic practice. No use, distribution or reproduction is permitted which does not comply with these terms.



Metabolite Profiling of the Indian Food Spice Lichen, *Pseudevernia furfuracea* Combined With Optimised Extraction Methodology to Obtain Bioactive Phenolic Compounds

Rishu Kalra^{1,2}, Xavier A. Conlan², Carlos Areche³, Rahul Dilawari⁴ and Mayurika Goel^{1*}

¹TERI-Deakin Nanobiotechnology Centre, Sustainable Agriculture Division, The Energy and Resources Institute, Gurugram, India,

²Centre for Chemistry and Biotechnology, School of Life and Environmental Sciences, Deakin University, Geelong, VIC, Australia,

³Departamento de Química, Facultad de Ciencias, Universidad de Chile, Nuñoa, Chile, ⁴CSIR-Institute of Microbial Technology, Chandigarh, India

OPEN ACCESS

Edited by:

Sayeed Ahmad,
Jamia Hamdard University, India

Reviewed by:

Washim Khan,
University of Mississippi, United States
Souaibou Yaouba,
Université de Lorraine, France

*Correspondence:

Mayurika Goel
mayurika.goel@teri.res.in
mayurikagoel@gmail.com

Specialty section:

This article was submitted to
Ethnopharmacology,
a section of the journal
Frontiers in Pharmacology

Received: 15 November 2020

Accepted: 04 March 2021

Published: 10 May 2021

Citation:

Kalra R, Conlan XA, Areche C,
Dilawari R and Goel M (2021)
Metabolite Profiling of the Indian Food
Spice Lichen, *Pseudevernia furfuracea*
Combined With Optimised Extraction
Methodology to Obtain Bioactive
Phenolic Compounds.
Front. Pharmacol. 12:629695.
doi: 10.3389/fphar.2021.629695

Pseudevernia furfuracea (L.) Zopf (*Parmeliaceae*) is a well-known epiphytic lichen commonly used in Indian spice mixtures and food preparations such as curries. This study is an attempt to find the best extraction methodology with respect to extractive yield, total polyphenolic content (TPC), total flavonoid content and antioxidant activities of lichen *P. furfuracea*. Two phenolic compounds, atraric acid and olivetoric acid were isolated and quantified in their respective extracts with the aid of reverse phase high performance liquid chromatography (RP-HPLC). The highest concentration of both the compounds, atraric acid (4.89 mg/g DW) and olivetoric acid (11.46 mg/g DW) were found in 70% methanol extract. A direct correlation was also observed between the concentrations of these compounds with the free radical scavenging potential of the extracts which might contribute towards the antioxidant potential of the extract. Moreover, scanning electron microscopy and HPLC analysis which was used to study the effect of pre-processing on extraction process highlighted the capacity of a mixer grinder technique for improved separation of surface localized metabolites and enrichment of the fraction. An investigation of the chemical profile of the bioactive extract 70% methanol extract using UHPLC-DAD-MS lead to tentative identification of forty nine compounds. This extract was also assessed towards HEK 293 T cell line for cytotoxicity analysis. Concentration range of 0.156 to 100 µg/ml of PF70M extract exhibited no significant cell death as compared to control. Further, the active extract showed protective effect against hydroxyl radical's destructive effects on DNA when assessed using DNA nicking assay. Based upon this, it can be concluded that optimization of extraction solvent, sample pre-processing and extraction techniques can be useful in extraction of specific antioxidant metabolites.

Keywords: lichen, antioxidants, atraric acid, olivetoric acid, UHPLC-MS, metabolomics profiling, *Pseudevernia furfuracea*, spatial localization

INTRODUCTION

Bioactive secondary metabolites of natural origin are extremely useful in food, pharmaceutical, agrochemical, nutraceutical and cosmeceutical industries due to their multifaceted biological activities such as antioxidant, antimicrobial, anticancer and antifungal (Goel et al., 2011; Sisodia et al., 2013; Goel et al., 2014; Newman and Cragg, 2016; Goel et al., 2020). Related to this, natural product derived antioxidants have been shown to exhibit strong protective effects against a variety of chronic health problems by postponing the damage caused by oxidative stress (Liu 2003). Antioxidants and their associated benefits is currently a subject of intensive research due to an increase in lifestyle disorders associated with stress and in line with this some lichens have been explored for their antioxidant potential through the last decade (Manojlovic et al., 2012; Kosanic et al., 2013; Kosanić et al., 2014; Kumar et al., 2014; Zugic, 2016).

Lichens are the microbial association defined by a stable symbiotic relationship between a mycobiont (fungal partner) and a photobiont (photoautotrophic partner, usually a green alga or cyanobacterium) (Calcott et al., 2018). Traditionally, some of the lichens are consumed for their culinary qualities, and used for their preservative and medicinal properties (Upreti et al., 2005). *Pseudevernia furfuracea* is well-known foliose lichen, commercially used in the spice mixture, food preparation like curries and as preservative in food and herbal preparations (Güvenç et al., 2012; Kosanic et al., 2013; Aoussar et al., 2017). Despite a decade of study, the potential of lichens to yield novel unique metabolites have not been fully realised. However an increase in technological capacity has recently rekindled the attention of pharmaceutical industries and researchers to determine potential of lichens antioxidants (Crittenden, 1991; Nash, 1996). The ethnopharmacological importance and consumption of the lichens as a functional food has resulted in investigations focusing upon the discovery and identification of the naturally occurring compounds responsible for their bioactivity. Phenolic polyketides present in lichens have been reported to have strong antioxidant properties (Hidalgo et al., 1994; Odabasoglu et al., 2006). Moreover, it has been well documented that extraction procedures used to isolate these compounds are vital for determining extractive yield and total polyphenols and thus antioxidant potential of the extracts (Spigno and De Faveri, 2007; Ismail et al., 2019). Factors such as extraction solvents, sample processing techniques, particle size, extraction techniques have been shown to have an influence on extraction efficiency and subsequent bioactivity (Cacace and Mazza, 2003; Ng et al., 2012). Therefore, it was rationalized that the extraction procedure is an important prerequisite for the comprehensive exploration of the beneficial effects of the species.

This study is designed to determine the effect of different extraction solvents, different extraction techniques and different grinding methods on obtaining polyphenolic and flavonoid rich fractions and evaluation of their antioxidant potential from lichen. The purpose of the study was to find best extraction methodology with respect to extractive yield and antioxidant activities of obtained extracts in order to inform the food industry

at large. The main factors selected for their presumed influence on the extraction efficiency and antioxidant potential are polarity of solvent, grinding or processing method and extraction methods. Separation of the metabolites rich portion from the lichen matrix was afforded by a grinding method prior to the determination of spatial localization of metabolites responsible for bioactivity in sample. Moreover, two key metabolites were isolated and quantified in different extracts and was found to be directly correlated with the free radical scavenging potential. In order to fully understand the fundamental process which influences the sample processing techniques, scanning electron microscopy was used to identify the separated fractions obtained after grinding and residual components left after extraction process. Finally, UHPLC-DAD-MS was used to study the qualitative composition of active extract and as such this work forms a platform for the advancement of lichen based food in future products and to enable a better understanding of food research where lichen forms a part of the diet.

MATERIALS AND METHODS

Material

Lichen material was collected from a local vendor (Khari baoli, New Delhi, India) in November 2017. Khari baoli market is one of Asia's largest wholesale spice market selling all kinds of spice. Sample *Pseudevernia furfuracea* is being sold as a part of spice mixture (Figure 1). The sample was then washed in distilled water, dried at room temperature ($25 \pm 5^\circ\text{C}$). The sample was identified by Prof. Prem Lal Uniyal and a voucher specimen (DUH 1401) was deposited in the herbarium of University of Delhi, Delhi, India.

Chemicals and Reagents

2,2-Diphenyl-1-picrylhydrazyl (DPPH) radical, 2,2-azinobis (3-ethylbenzothiazoline-6-sulphonic acid) (ABTS), folin-Ciocalteu reagent, gallic acid, quercetin, aluminum chloride anhydrous, 2-thiobarbituric acid (TBA), deoxyribose, ethylenediaminetetraacetic acid (EDTA) disodium dihydrate, ascorbic acid, alamar blue and trolox were procured from Sigma-Aldrich (Sigma Aldrich India Pvt Ltd., Bangalore, India). Potassium persulphate and sodium bicarbonate were purchased from Sisco Research Laboratories Pvt. Ltd. (Maharashtra, India). Ferric chloride, hydrogen peroxide, orthophosphoric acid were purchased from Fischer Scientific (Mumbai India). All the solvents methanol, acetone, hexane, ethyl acetate, dichloromethane, and dimethyl sulphoxide were purchased from Merck Millipore (KGaA, Darmstadt, Germany). Chemicals and solvents used were of analytical and HPLC grade, respectively.

Grinding of the Lichen Samples

The raw sample was dried in an oven at 40°C before grinding and divided into two portions; the first portion of sample (200 g) was chopped with the help of scissors to get fine pieces. These fine pieces were then crushed with the help of pestle mortar and resulted into homogenised powder. Other portion of the raw



FIGURE 1 | *Pseudevernia furfuracea* as it is sold in the spice market khari baoli (New Delhi, India).

sample (50 g) was ground up with a mixer-grinder (Philips, HL-1606) at maximum rotation speed for 15 min. This process led to the separation of sample into two portions, cortex powder and medulla pieces. Both the fractions were analysed and tested separately for their surface morphology, bioactive contents and bioactivity assays.

Extraction of Lichen Samples

Lichen sample was extracted using three variables parameters which include different extraction solvents, different grinding methods and different extraction methods. **Figure 2** explaining the complete experimental design for the preparation of different extracts gives a clear overview of all the different extraction.

To analyse the effect of different extraction solvent, direct extraction was done using hexane, ethyl acetate, acetone, methanol, 70% methanol, water. On the other hand, in case of sequential extraction, solvents of increasing polarity (hexane followed by dichloromethane, ethyl acetate, methanol and 50% methanol) were used in serial manner (**Figure 2**). To understand the effect of pre-processing on extraction process, differently grounded sample as mentioned above (*Grinding of the Lichen Samples*) were extracted separately using optimized solvent (70% methanol) and reflux method. All the extractions were done in triplicate using reflux apparatus at 60°C. Similarly, different extraction methods including maceration, sonication, reflux

and soxhlet were used to access the effect of methodology on extraction yield and metabolic profiling.

Extraction yield in all the methods was calculated by following formula:

$$\text{Total Yield (\%)} = \left(\frac{\text{Total extract mass}}{\text{Mass of lichen}} \right) \times 100$$

Determination of Total Polyphenol and Total Flavonoid Contents

Total polyphenol content (TPC) and total flavonoid content (TFC) of the lichen extracts were measured using previously reported Folin-Ciocalteu's method (Singleton Vernon et al., 1999) and aluminum chloride method (Ordonez et al., 2006), respectively. The total polyphenol content of the extracts was expressed as mg of gallic acid equivalent (GAE)/g of dry lichen material on the basis of calibration curve of gallic acid (20–200 µg/ml; $R^2 = 0.99$). The total flavonoid content of the extracts was expressed as mg of quercetin equivalent (QE)/g of dry lichen material on the basis of calibration curve of quercetin (1–100 µg/ml; $R^2 = 0.99$). The absorbance for each methodology was determined using UV-Visible spectrophotometer-2450 (Shimadzu).

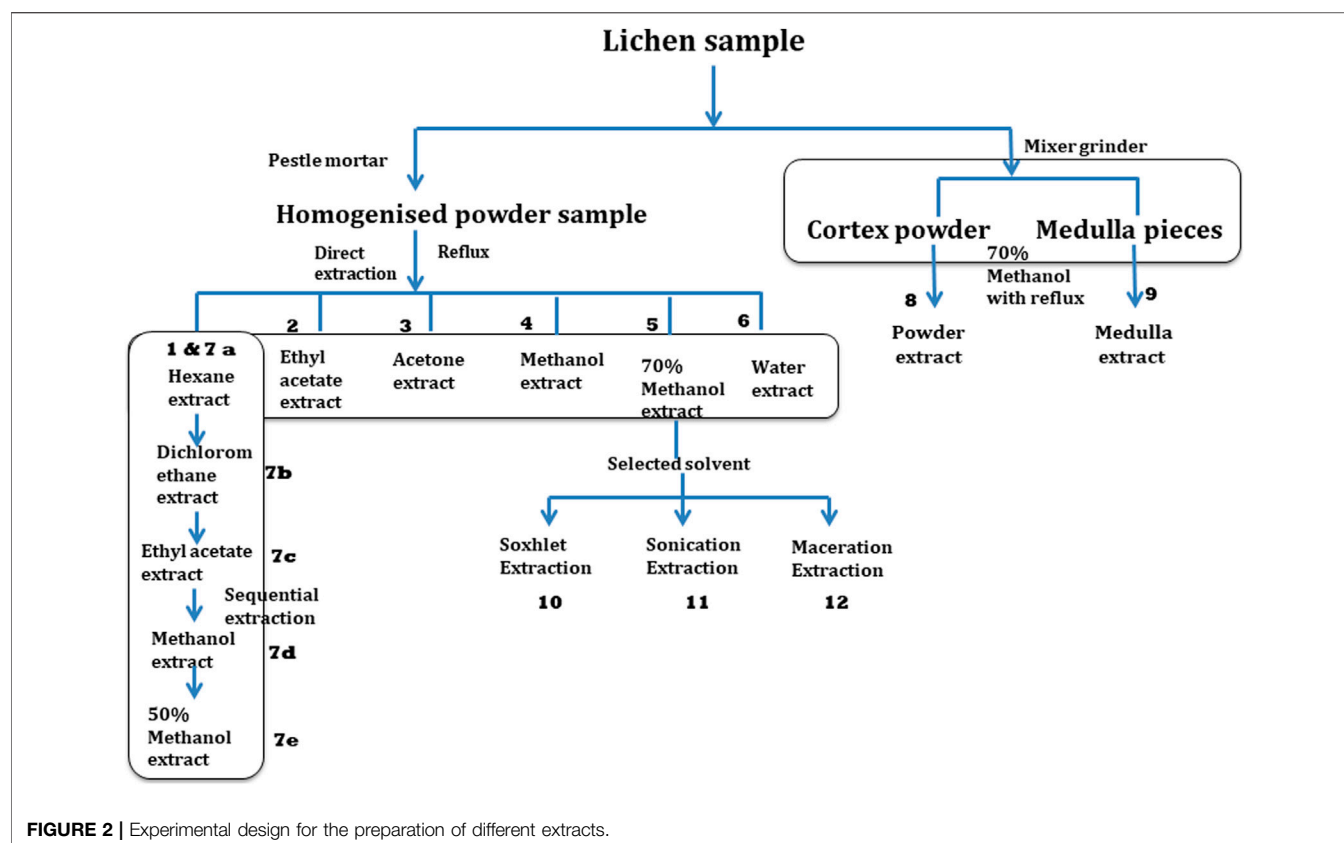


FIGURE 2 | Experimental design for the preparation of different extracts.

Evaluation of Free Radical Scavenging Potential

Free radical scavenging potential of the extract were evaluated by ABTS⁺ radical cation decolourisation assay, DPPH radical scavenging assay, hydroxyl radical scavenging potential using trolox as the standard.

ABTS Radical Scavenging Potential

The ABTS assay was performed in line with the previously described protocol by Re *et al.*, with slight modification as follows (Re *et al.*, 1999). The ABTS⁺ radical cation was prepared by mixing 7 mM ABTS aqueous solution with 2.45 mM potassium persulfate (final concentration) and allowing the mixture to stand in the dark at room temperature for 12–16 h before use. The working solution was prepared by diluting the stock solution with ethanol for an initial absorbance of about 0.70 ± 0.02 at 745 nm. Free radical scavenging potential was assessed by mixing different concentration (5–100 µg/ml) of sample and standard Trolox (1–20 µM; 0.25–5 µg/ml) with ABTS⁺ working standard to make a final volume of 1 ml. The decrease in absorbance was measured exactly after 6 min at 30°C. The half maximal inhibitory concentration (IC₅₀) for test samples and Trolox was calculated by plotting the scavenging capacity against the concentration. The results were expressed as Trolox Equivalent Antioxidant Capacity (TEAC) µM Trolox/g DW.

1, 1-Diphenyl-2-picrylhydrazyl Radical-Scavenging Potential

Free radical scavenging potential of the samples was tested using a previously developed DPPH radical-scavenging protocol (Brand-Williams *et al.*, 1995). The 0.2 mM solution of DPPH was prepared in 70% methanol and stirred overnight in the dark at room temperature before use. Free radical scavenging potential was assessed by mixing different concentration (10–300 µg/ml) of samples and standards Trolox (5–50 µM; 1.25–12.5 µg/ml) with DPPH solution to make a final volume of 1 ml. These samples were shaken well and kept in dark for 30 min at room temperature. The decrease in absorbance was measured (at room temperature) after 30 min at 517 nm. The results were expressed as Trolox Equivalent Antioxidant Capacity (TEAC) µM Trolox/g DW as mentioned above in ABTS assay.

Hydroxyl Radical Scavenging Potential

This assay was performed by previously described protocol described by Li (2013). Hydroxyl radical was generated by the Fenton reaction (Fe³⁺-ascorbate-EDTA-H₂O₂ system). Samples (10–50 µg/ml) and standard Trolox (1–25 µM; 0.25–6.25 µg/ml) were mixed with 400 µL of phosphate buffer (0.2 M, pH 7.4) followed by 50 µL of deoxyribose (50 mM), 50 µL of Na₂EDTA (1 mM), 50 µL of FeCl₃ (3.2 mM) and 50 µL of H₂O₂ (50 mM). Addition of 50 µL of ascorbic acid (1.8 mM) initiates the reaction. Total volume of the reaction mixture was adjusted to 800 µL with buffer. The reaction mixture was incubated at 50°C for 20 min.

followed by addition of 250 μ l of trichloroacetic acid (10%, w/w) for the termination of reaction. Chromogen was developed by addition of 150 μ l of TBA (5%, in 1.25% NaOH aqueous solution) and incubated at 105°C for 15 min. The mixture was cooled and absorbance was measured at 532 nm. The results were expressed as Trolox Equivalent Antioxidant Capacity (TEAC) μ M Trolox/g DW as mentioned above in ABTS assay.

Antioxidant Activity Using DNA Nicking Assay

Antioxidant activity of bioactive extract was also assessed by DNA damage protection assay. Analysis was performed using supercoiled pBSK plasmid DNA according to the method of Zhao et al. (2014) with slight modifications (Zhao et al., 2014). A mixture of plasmid DNA (0.5 μ g) and active extract PF70M in concentration range of 25–200 μ g/ml was incubated at room temperature for 10 min followed by addition of equal volume of Fenton's reagent (30 mM H_2O_2 , 80 mM $FeCl_3$, and 50 mM ascorbic acid). Reaction mixtures were then allowed incubated for 30 min at 37°C. The DNA was examined on 1% agarose gel using ethidium bromide staining. Curcumin was found as positive control.

Isolation and Quantification of Metabolites by High Performance Liquid Chromatography

The isolation of metabolites was performed using column chromatography (CC) over silica gel (100–200#). The extracts was eluted using hexane/ethyl acetate (95:5 to 70:30, v/v) as eluent and yielded nine major fractions (A–I). Fraction B was further subjected to CC over silica gel (60–120#), using hexane/ethyl acetate (95:5 to 28:20, v/v) lead to isolation of pale yellow crystals (compound 1). Fractions F was subjected to preparative TLC and lead to isolation of pale yellow amorphous powder (compound 2). Both the isolated compounds were identified with the help of NMR and mass spectral analysis.

Chemical analysis of the lichen extracts was performed using a Waters HPLC system consisting of a 600 quaternary gradient pump with an online vacuum degasser, a 717 auto-sampler, and 2996 diode array detector. Separation of the compounds of interest was achieved using a reversed phase C_{18} Luna column (Phenomenex, Lorange, CA, United States, 150 mm \times 4.6 mm, 5 μ m) and a 10 μ l injection volume. A five point calibration curve from standard solutions was prepared by 10 μ l injections of 5–100 μ g/ml. Commercial standards of lichen compounds were not available therefore abovementioned isolated compounds were used as standards for the quantification. An HPLC gradient was applied: A (0.8% orthophosphoric acid in water) and B (acetonitrile). The following gradient was used at a flow rate of 1 ml/min: initial, 100% A in 0–5 min; 100% B in 5–45 min, 100% A in 45–60 min. Presence of compounds in the extracts was confirmed by comparison of retention time and ultraviolet and visible (UV-Vis) absorption spectra (Chowdhary et al., 2019).

UHPLC-DAD-MS Analysis

A Thermo Scientific Dionex Ultimate 3000 UHPLC system hyphenated with a Thermo high resolution Q Exactive focus mass spectrometer (Thermo, Bremen, Germany) were used for analysis. Mass calibration for the Orbitrap™ was performed once a week, in both negative and positive modes, to warrant a working mass accuracy lowers than or equal to 5 ppm. UHPLC and mass parameters were used as per previously described method for the analysis of lichen samples (Salgado et al., 2018). An HPLC gradient having eluent (A) 0.1% formic acid in water, eluent (B) 0.1% formic acid in acetonitrile was performed. The following gradient was used at a flow rate of 1 ml/min: 5% B in 0–5 min; 30% B in 5–10 min, 30% B in 15 min, 70% B in 20 min, 70% B in 25 min, 5% B in 35 min, 12 min for column equilibration before each injection. The injection volume was 10 μ L. Analysis was performed on UHPLC C_{18} column (Acclaim, 150 mm \times 4.6 mm ID, 2.5 mm, Thermo Fisher Scientific, Bremen, Germany) operated at 25°C. The MS conditions were as follows: Spray voltage 2500 V (for ESI-); aux. gas unit flow rate 20; aux gas heater temperature 500°C; capillary temperature 400°C; sheath gas flow rate 75 units. Full scan range was set in negative mode with the resolving power of 70,000 FWHM (full width half maximum) at m/z 200. For the compounds of interest, a scan range of m/z 100–1000 was chosen; the automatic gain control (AGC) set at 3×10^6 and the injection time set to 200 ms. Scan-rate was set at 2 scans s^{-1} . A mixture of taurocholic acid sodium salt, buspyrone hydrochloride, and sodium dodecil sulfate (Sigma-Aldrich, Darmstadt, Germany), plus Ultramark 1621 (Alpha Aesar, Stevensville, MI, United States) dissolved in a mixture of acetic acid, acetonitrile, water and methanol, was used as calibration solution to ensure a working mass accuracy lower than or equal to 5 ppm. For confirmation purposes, a targeted MS/MS analysis was performed using the mass inclusion list, with a 30 s time window, with the Orbitrap spectrometer operating in negative mode at 17,500 FWHM (m/z 200). The AGC target was set to 2×10^5 , with the maximum injection time of 20 ms. The precursor ions were filtered by the quadrupole which operates at an isolation window of m/z 2. The fore vacuum, high vacuum and ultrahigh vacuum were maintained at approximately 2 mbar, from 105 and below 1010 mbar, respectively. Collision energy (HCD cell) was operated at 30 kv. Detection was based on calculated exact mass of target compounds, as shown in Table 3.

Cell Cytotoxicity/Viability Assay

The cytotoxicity for most bioactive extract (PF70M) extract was assessed toward HEK 293 T cell line using Alamar Blue (Resazurin), a cell metabolic activity reagent (Sigma) (Rampersad et al., 2012). The log phase cells were harvested and cell count was adjusted to (1×10^4 /well) in DMEM containing 10% fetal bovine serum (FBS) and incubated for 12 h under 5% CO_2 at 37°C in 96-well microplates. Next day, cells were incubated with varying concentrations of PF70M extract at 37°C for 24 h. Following this, 0.02% Alamar blue reagent was added and the cells were further incubated for 6–8 h under 5% CO_2 at 37°C. Fluorescence was measured with excitation wavelength at 545 nm and emission wavelength at 590 nm in Elisa plate reader (Power Wave HT Microplate Spectrophotometer–BioTek).

TABLE 1 | Extraction yield, total phenolics and antioxidant potential of *P. furfuracea* using different extraction solvents, grinding method and extraction method.

Experiment number	Extraction solvent/method/grinding technique	Extractive yield \pm SE (wt%)	TPC ^a (mg GAE/g DW)	TFC ^b (mg QE/g DW)	TEAC ^c (μ M TROLOX/g DW)	Atraric acid ^d (mg/g DW)	Olivetoric acid ^d (mg/g DW)
1 and 7a	Hexane/reflux/pestle mortar	1.38 \pm 0.44	0.70 \pm 0.10	0.02 \pm 0.00	1.66 \pm 0.00* 0.45 \pm 0.01** 19.33 \pm 0.21***	Nd	Nd
2	Acetone/reflux/pestle mortar	4.04 \pm 0.32	5.92 \pm 0.38	0.22 \pm 0.04	6.91 \pm 0.16* 5.33 \pm 0.07** 99.12 \pm 1.14***	0.63	1.95
3	Ethylacetate/reflux/pestle mortar	3.7 \pm 0.44	9.80 \pm 0.60	0.10 \pm 0.00	7.62 \pm 0.04* 4.65 \pm 0.06** 64.77 \pm 0.74***	1.20	1.44
4	Methanol/reflux/pestle mortar	7.83 \pm 0.68	21.43 \pm 0.11	0.24 \pm 0.00	25.97 \pm 0.69* 13.94 \pm 0.26** 260.31 \pm 7.60***	0.72	2.56
5	70% methanol/reflux/pestle mortar	9.81 \pm 0.41	32.38 \pm 0.29	0.38 \pm 0.00	38.30 \pm 1.53* 19.10 \pm 0.60** 353.06 \pm 9.58***	2.41	11.46
6	Water/reflux/pestle mortar	9.55 \pm 0.95	5.84 \pm 0.10	0.16 \pm 0.01	5.22 \pm 0.00* 3.02 \pm 0.09** 80.30 \pm 5.47***	0.08	Nd
7	Sequential extraction	15.19 \pm 0.24					
7b	Dichloro methane/reflux/pestle mortar	2.64 \pm 0.27	5.39 \pm 0.10	0.07 \pm 0.00	7.10 \pm 0.04* 2.45 \pm 0.07** 42.03 \pm 0.19***	0.15	0.42
7c	Ethyl acetate/reflux/pestle mortar	2.23 \pm 0.26	5.88 \pm 0.07	0.03 \pm 0.00	4.96 \pm 0.15* 2.96 \pm 0.03** 32.56 \pm 0.79***	0.14	0.69
7d	Methanol/reflux/pestle mortar	4.9 \pm 0.11	10.65 \pm 0.11	0.06 \pm 0.00	13.39 \pm 0.24* 4.81 \pm 0.11** 75.08 \pm 1.42***	0.97	3.39
7e	50% methanol/reflux/pestle mortar	4.28 \pm 0.56	3.86 \pm 0.08	0.11 \pm 0.00	6.12 \pm 0.02* 2.40 \pm 0.05** 59.16 \pm 1.00***	0.43	0.69
8	70% methanol/reflux/mixer grinder (cortex powder portion)	8.92 \pm 0.08	28.07 \pm 0.16	0.35 \pm 0.00	23.90 \pm 0.05* 14.06 \pm 0.13** 302.39 \pm 6.40***	2.61	6.69
9	70% methanol/reflux/mixer grinder (medulla pieces)	5.25 \pm 0.19	14.87 \pm 0.03	0.11 \pm 0.00	15.26 \pm 0.09* 6.52 \pm 0.03** 99.32 \pm 1.76***	1.01	6.49
10	70% methanol/soxhlet/pestle mortar	11.06 \pm 0.26	41.73 \pm 2.37	0.44 \pm 0.00	47.57 \pm 0.16* 22.48 \pm 0.04* 388.33 \pm 3.31***	4.89	8.35
11	70% methanol/sonication/pestle mortar	6.72 \pm 0.42	18.39 \pm 0.48	0.14 \pm 0.00	20.16 \pm 0.03* 7.38 \pm 0.08** 127.58 \pm 1.22***	4.04	6.03
12	70% methanol/maceration/pestle mortar	7.04 \pm 0.30	17.54 \pm 0.00	0.12 \pm 0.00	23.28 \pm 0.08* 8.25 \pm 0.14** 176.15 \pm 1.13***	0.21	6.83

^aData expressed as mg of gallic acid equivalent (GAE)/g of lichen dry material.

^bData expressed as mg of quercetin equivalent (QE)/g of lichen dry material.

^cData expressed as μ M of Trolox equivalent/g of lichen dry material (*) TEAC assayed by ABTS method, (**) TEAC assayed by DPPH method, (***) TEAC assayed by OH scavenging method.

^dAmount represented in μ g/g of the dry lichen material, nd-peak not detected.

The percent difference between treated and un-treated cells was calculated by following formula:

$$\% \text{Viability} = \left(\frac{\text{RFU of treated sample}}{\text{RFU of untreated}} \right) \times 100$$

Where RFU stands for relative fluorescence unit.

Statistical Analysis

Results are expressed as mean of triplicate data \pm standard error and Pearson correlation between polyphenol contents, flavonoid content, atraric acid and olivetoric acid concentration and antioxidant potential was established by IBM SPSS statistical software.

RESULTS AND DISCUSSION

Effect on Extractive Yield Different Solvent Treatment

The percentage extractive yield obtained from the solvent treatments ranged from 1.38 ± 0.44 to $15.19 \pm 0.24\%$ and the full data can be viewed in **Table 1**. The maximum extractive yield was obtained in 70% methanol followed by water and methanol and the key driver behind the increased extraction efficiency with 70% methanol is principally due to extraction of wide range of compounds (polar to non-polar) present in *Pseudevernia furfuracea*. The optimum extraction yield observed from the successive extraction is likely due to the better mass transfer from the substrate, which is clearly visible in the scanning electron microscopy (SEM) image (Supplementary Figure S1). The residue (a dense layer of platelets like crystals) left after each extraction can be observed and these crystals were washed off successively after each extraction. These findings suggest better extraction efficiency from the substrate and thus the driver of the highest extractive yield in the successive extraction (Supplementary Figure S1). Nevertheless, taking into consideration, other factors such as time, resources required and nature of metabolites directed toward bioactivity, 70% methanol was found to be the most appropriate solvent for the efficient and rapid extraction of bioactive phenolic constituents.

Different Grinding Techniques

As lichen metabolites are not homogeneously distributed in the sample matrix, different types of grinding methods or sample processing technique may influence extraction yield, TPC, metabolites concentration and subsequently the antioxidant potential of extract. To understand this effect, two different grinding methods, a pestle mortar and a mixer grinder were assessed. Samples crushed in mortar pestle resulted in a homogenised powder and was considered as a whole thallus sample for extraction, represented in experiment 5 (**Figure 2**) affording the extraction yield of $9.81 \pm 0.41\%$. Whereas the total extractive yield obtained from the mixer grinder method ($14.17 \pm 0.19\%$) which is the sum total of extractive yield of cortex powder sample ($8.92 \pm 0.08\%$) and medulla pieces ($5.25 \pm 0.11\%$) is far more than the yield obtained from sample ground using mortar pestle which generated the homogenous powder.

Different Extraction Techniques

The extraction techniques chosen for their putative influence on extraction efficiency with a single optimized solvent were identified as soxhlet, reflux, sonication and maceration. With the optimum solvent (70% methanol), the extractive yield was found to be best with soxhlet extraction ($11.03 \pm 0.26\%$), followed by reflux ($9.81 \pm 0.41\%$), then maceration ($7.04 \pm 0.30\%$) and finally sonication ($6.72 \pm 0.42\%$). The higher yield obtained with the soxhlet extraction may be attributed to the application of warm solvent and exhaustive extraction with fresh solvent in every siphon.

Determination of Total Polyphenolic Content and Total Flavonoid Contents

The total polyphenolic content of the extracts prepared with solvents of different polarities, different extraction and grinding methods were determined from regression equation of calibration curve and expressed in gallic acid equivalents. In terms of solvent influence the 70% methanol extract led to the maximum TPC (32.38 ± 0.29 mg of GAE/g of dry lichen material) followed by methanol, ethyl acetate, acetone, water and hexane. These results indicate that polar solvents such as the water component of the 70% methanol and methanol assist in the extraction of polyphenolics due to the hydroxyl moieties on the phenols. With the sequential extraction the methanol extract showed the maximum TPC, followed by ethyl acetate, dichloromethane, 50% methanol and finally hexane. The low amount of TPC achieved in the 50% extract might be attributed to extraction of major polyphenol beforehand by methanol in the sequence.

Importantly, processing of the sample with different grinding methods led to separation of fractions providing one fraction rich in total polyphenol and flavonoid content. The sample ground with the mortar and pestle gave a uniform powder mixture (whole thallus) that produced a higher TPC content (32.38 ± 0.29 mg of GAE/g of dry lichen material). On the other hand the sample ground in the mixer grinder gave two separate fractions; cortex powder having almost similar TPC content (28.06 ± 0.16 mg of GAE/g of dry lichen material) as obtained in whole thallus sample and the medulla pieces providing lower TPC content (14.87 ± 0.03 mg of GAE/g of dry lichen material).

In another set of experiments, comparison of extraction of total polyphenols with the optimized extraction solvent mixture (70% Methanol) was also carried out using four commonly used extraction techniques (soxhlet, reflux, sonication and maceration). **Table 1** shows the result of total polyphenol content obtained by four different extraction procedures. The results indicate that the maximum yield of total polyphenolics was achieved by soxhlet extraction followed by reflux, sonication and maceration. Exhaustive extraction of total polyphenols in soxhlet extracts is because of the repeated and continuous washing of the crude material and application of heat during extraction as compared to other extraction methods.

The total flavonoid content of the extracts prepared with solvents of different polarities, different grinding and extraction methods were determined from the regression equation of calibration curve obtained from quercetin and expressed in quercetin equivalents. The different solvents exhibited substantial differences in the TFC as depicted in **Table 1**. The TFC ranged from 0.02 ± 0.00 mg of QE/g of dry lichen material for hexane to 0.38 ± 0.00 mg of QE/g of dry lichen material for 70% methanol extract. In case of sequential extraction, 50% methanol extract has maximum flavonoid content (0.11 ± 0.00 mg QE/g) followed by dichloromethane, methanol and ethylacetate. The mixer grinder processing of samples led to an improved separation of fractions rich in flavonoids. The TFC content of the cortex powder fraction (0.35 ± 0.00 mg QE/g) is almost equivalent to the whole

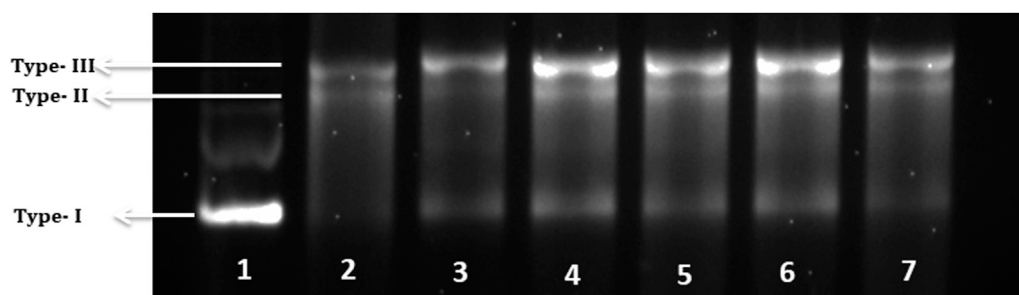


FIGURE 3 | DNA Nicking assay showing protective effect of PF70M extract against hydroxyl radical generated by Fenton's reagent. Lane 1: Native plasmid DNA pBSK without treated with Fenton's reagent; Lane 2: DNA treated with Fenton's reagent; Lane 3: DNA treated with Fenton's reagent and 25 $\mu\text{g/ml}$ Curcumin; Lane 4–7: DNA treated with Fenton's reagent and *Pseudevernia furfuracea* 70% methanol extract (200, 100, 50 and 25 $\mu\text{g/ml}$, respectively).

thallus sample (0.38 ± 0.00 mg QE/g) whereas medulla pieces provided a lower TFC content (0.11 ± 0.00 mg of QE/g of dry lichen material). When considering the different extraction methods the maximum TFC were afforded by soxhlet extraction (0.44 ± 0.00 mg of QE/g of dry lichen material) followed by reflux, sonication and maceration.

Free Radical Scavenging Potential

To evaluate the free radical scavenging potential of different extracts, three types of assays were employed. The chemical composition of different extracts will have an influence depending on the test employed and therefore more than one assay was performed to get a thorough understanding of the extract's antioxidant potential. Antioxidant potential of the different samples were expressed as μM of Trolox equivalents per gram of dry lichen material as it is a more significant and descriptive expression. The results of antioxidant potential of different extract by ABTS, DPPH and OH scavenging assay are summarized in **Table 1**. Among the various solvents used, extracts obtained with 70% methanol exhibit higher antioxidant potential with highest TEAC value. With the different grinding techniques, the TPC, TFC and antioxidant potential obtained from cortex powder is comparable to the homogenised powder. Separation of surface metabolites in cortex powder portions provides an enriched fraction targeted to specific metabolites and also in terms of TPC, TFC and antioxidant potential. When comparing the different extraction methods, it was also observed that the extraction of the metabolites having maximum TPC, TFC and highest antioxidant potential was found *via* soxhlet extraction.

Antioxidant Potential

Lastly, a DNA nicking assay was used to understand the protective effect of specific extract against hydroxyl radical's destructive effects on DNA. Hydroxyl radicals generated using Fenton's reaction mixture resulted in degradation of supercoiled form of plasmid DNA (Lane 1, Type 1) into single stranded nicked and double stranded linear forms of DNA (Lane 2, Type II and III) (**Figure 3**). Results showed that presence of curcumin in 25 $\mu\text{g/ml}$ concentrations (Lane 3) protect the DNA in supercoiled form. Similarly, presence of PF70M extract at different

concentrations (200–25 $\mu\text{g/ml}$, Lane 4–7, respectively) in the reaction mixture diminished the DNA damage. Thus, concentration-dependent intensification of native supercoiled DNA (Type 1) was observed.

Correlation of Antioxidant Potential With Total Polyphenolic Content and Total Flavonoid Content

The redox potential of the components such as polyphenols, phenolic acids and flavonoids is the determining factor for the antioxidant property of any food or herbal entity (Tembo et al., 2017). A statistical significant relationship was established between total polyphenol contents, total flavonoid content and TEAC values obtained from DPPH, ABTS and hydroxyl scavenging assays (**Table 2**). As a correlation between the TPC and antioxidant potential are marginally better when compared to the correlation between the TFC and antioxidant potential we suggest here that the phenolic compounds play a more significant role towards antioxidant potential than the flavonoids.

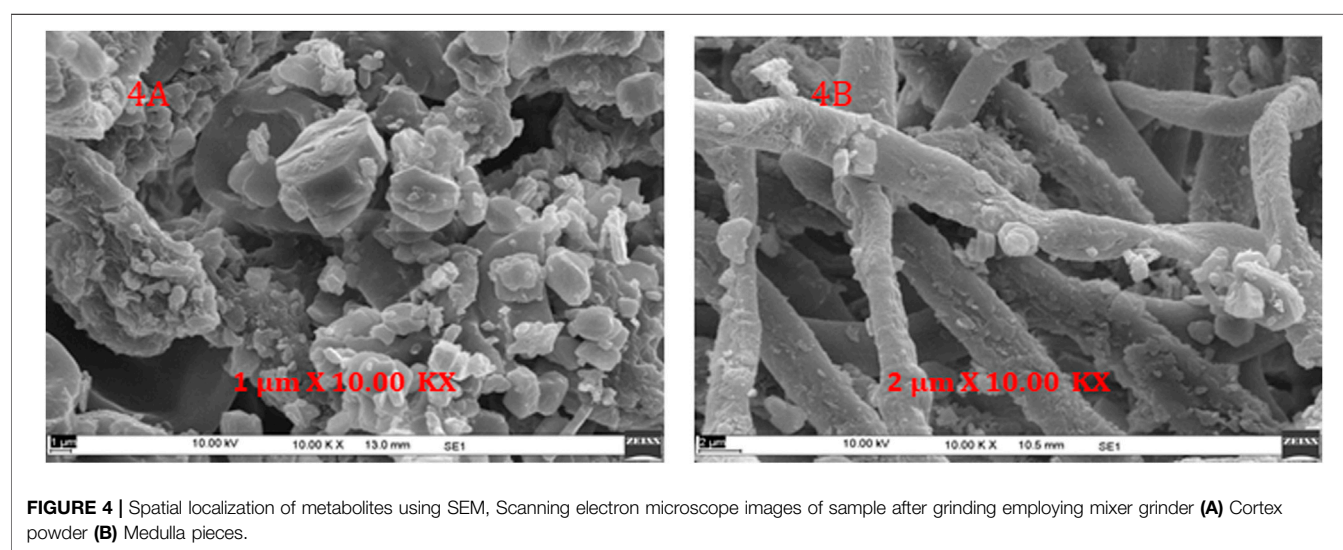
Spatial Localization of Metabolites Using High Performance Liquid Chromatography and Scanning Electron Microscopy Surface Morphology Using Scanning Electron Microscopy

As discussed earlier, samples ground in the mixer grinder lead to separation of fine powder (cortex) and coarser segments (medulla). These two portions were examined using SEM (EVO MA10, Carl Zeiss) to have a clear understanding of their surface morphology. This approach also helped to understand the spatial localization of some surface metabolites in sample. Microscopic observation of the two portions identifies some crystals like structure present on the surface (**Figure 4**). This result is consistent with the findings of Komaty et al., who have discussed the separation of cortex powder from medulla pieces and thus obtained atranorin localized on the cortex portion of *P. furfuracea* (Komaty et al., 2016).

TABLE 2 | Values of Pearson's correlation coefficients (*r*) for the TPC, TFC, TEAC (DPPH), TEAC (ABTS), TEAC (OH radical scavenging), Atraric acid and Olivetoric acid concentration.

Correlations	TPC content (mg GAE/DW)	TFC content (mg QE/DW)	TEAC ABTS (μM Trolox/DW)	TEAC DPPH (μM Trolox/DW)	TEAC OH radical scavenging (μM Trolox/DW)	Atraric acid conc (mg/g DW)	Olivetoric acid conc (mg/g DW)
TPC content (mg GAE/DW)	1	0.874**	0.979**	0.979**	0.962**	0.873**	0.867**
TFC content (mg QE/DW)	0.874**	1	0.842**	0.920**	0.936**	0.846**	0.701**
TEAC ABTS (μM Trolox/DW)	0.979**	0.842**	1	0.972**	0.950**	0.824**	0.870**
TEAC DPPH (μM Trolox/DW)	0.979**	0.920**	0.972**	1	0.986**	0.863**	0.819**
TEAC OH radical scavenging (μM Trolox/DW)	0.962**	0.936**	0.950**	0.986**	1	0.827**	0.808**
Atraric acid conc (mg/g DW)	0.873**	0.846**	0.824**	0.863**	0.827**	1	0.672**
Olivetoric acid conc (mg/g DW)	0.867**	0.701**	0.870**	0.819**	0.808**	0.672**	1

**Correlation is significant at the 0.01 level (2-tailed)



Determination of Atraric Acid and Olivetoric Acid by High Performance Liquid Chromatography

To further confirm this in our study, both of these portions were treated separately for extraction and identification of their respective metabolites. Characterisation of the some constituents in the extracts was performed with the two secondary metabolites that has been isolated namely atraric acid and olivetoric acid. These metabolites were characterized using NMR and mass spectroscopic data. Typical chromatograms of the standard compounds are shown in **Figure 5**. The calibration curves of atraric acid and olivetoric acid also showed good linearity ($R^2 = 0.9994$ and 0.9971 , respectively). Quantification of these metabolites in all the extracts obtained using different extraction solvents, techniques and grinding methods was carried out using regression equation obtained from their calibration plots and results are presented in **Table 1**. In the case of different solvent extraction, the maximum concentration of both the compounds were found in the 70% methanol extract, matching the trend observed in total phenolic content study. With the different extraction methods,

the maximum concentration of atraric acid was achieved *via* soxhlet extraction and interestingly the concentration of olivetoric acid was higher in the reflux process. This highlights the importance of taking holistic approaches towards sample extract optimisation.

The concentrations of both the compounds were observed to be higher in the homogenised powder followed by the cortex powder and the medulla. A marginal difference of olivetoric acid was found between cortex powder and medulla pieces highlighting presence of olivetoric acid in both the portions equally and cannot be separated by this method. Interestingly the concentration of the atraric acid which has been reported as hydrolysis derivative of atranorin when come in contact with methanol or processed in the presence of methanol (Oettl et al., 2014) was found to be more concentrated in the powder compared to the cortex (**Figure 5**) thus highlighting the surface localization of atranorin and can be easily separated from the sample by simple pre-processing.

A good correlation was found between concentration of both compounds and TEAC obtained from ABTS, DPPH and OH

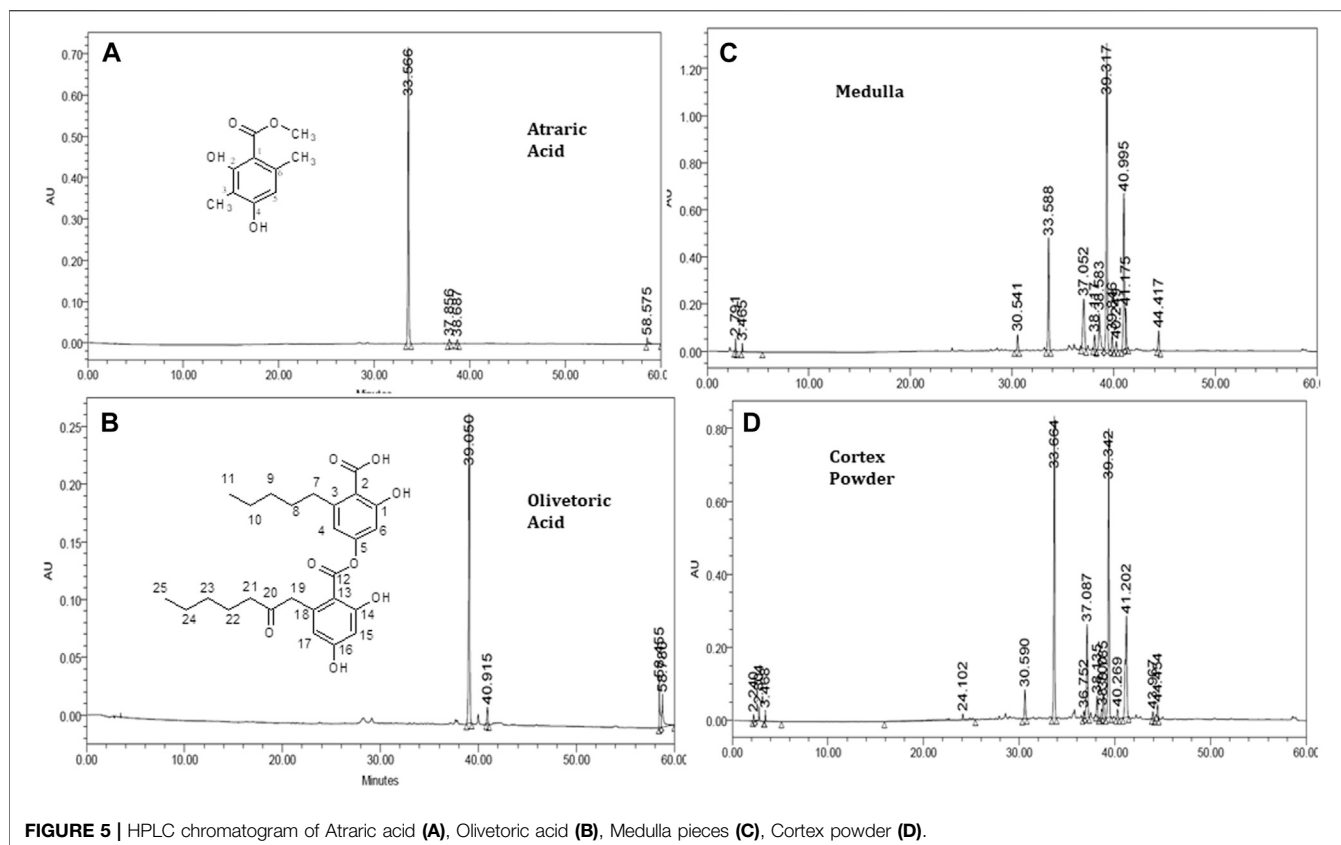


FIGURE 5 | HPLC chromatogram of Atraric acid (A), Olivetoric acid (B), Medulla pieces (C), Cortex powder (D).

scavenging assay in all the three parameters (Table 2). These results indicate that these two metabolites might contribute strongly toward the antioxidant potential of this lichen.

Based on this information the importance of the lichen *Pseudevernia furfuracea* have been shown to have key metabolites that contribute strongly to the antioxidant profile of the food product. Lichens in general are underutilised in western food cuisine and this work shows that they may have an important place to in food products. In generally lichens have not been well studied in terms of their potential as a healthy food product and this highlights them as a viable avenue which could even lead to large scale production of them. For this to occur and for the successful application of them into food products it is clear that the way in which the sample is processed and if required the approach to biomolecule extraction is particularly important.

Identification Data (Nuclear Magnetic Resonance and Mass Spectra) of Compounds

Both the compounds were identified on the basis of nuclear magnetic resonance (NMR) data and high resolution mass spectrometry (HRMS) data reported previously.

Atraric acid (1): Pale yellow crystal, $^1\text{H-NMR}$ (CDCl_3) δ : 2.16 (3H, s, 3-Me), 2.52 (3H, s, 6-Me), 3.95 (3H, s, $-\text{C}=\text{OOCH}_3$), 6.28 (1H, s, H-5), 12.40 (1H, s, 4-OH), 12.88 (1H, s, 2-OH); $^{13}\text{C-NMR}$ (CDCl_3) δ : 176.54 ($-\text{C}=\text{O}$), 166.74 (C-4), 164.06 (C-2), 143.42 (C-

6), 114.05 (C-1), 112.45 (C-3), 107.53 (C-5), 54.56 (C- OCH_3), 26.86 (Me-C6), 10.48 (Me-C3). (+)HRMS: 197.0807 $[\text{M} + \text{H}]^+$. Obtained data was in good agreement with reported literature (Gormann et al., 2003).

Olivetoric acid (2): Pale yellow amorphous powder, $^1\text{H-NMR}$ (CDCl_3) δ : 0.93 (6H, t, 11-Me and 25-Me), 1.3 (8H, m, H-9, 10, 23, 24), 1.5 (2H, dd, H-7), 2.4 (2H, t, H-21), 2.8 (2H, bs, H-19), 6.5 (4H, d, H-4, 6, 15, 17), 10.0 (1H, s, 16-OH), 10.5 (2H, s, 1-OH, 14-OH); $^{13}\text{C-NMR}$ (CDCl_3) δ : 163.21 (C-14), 162.69 (C-1), 158.39 (C-16), 142.06 (C-5), 132.72 (C-18), 104.13 (C-2), 103.02 (C-13), 100.92 (C-15), (+) HRMS: 473.54 $[\text{M} + \text{H}]^+$.

Composition of 70% Methanol Extract of *Pseudevernia furfuracea* Using UHPLC-DAD-MS

Electrospray Orbitrap is a rapid and state of art tool for the characterization of metabolites in various food and herbal commodity. Considering the metabolites profiling of 70% methanol extract, it has been subjected to UHPLC/ESI/MS/MS analysis to investigate the whole biochemical composition of stated extract. Figure 6 shows the total ion current chromatograms (TIC) of 70% methanol extract and Table 3 presented the list of all the compounds tentatively identified on the basis of their m/z of molecular ion $[\text{M}-\text{H}]^-$ and respective mass information extracted through their MS and MS/MS spectra. Sixty five peaks were detected using UHPLC/ESI/MS/MS in the negative

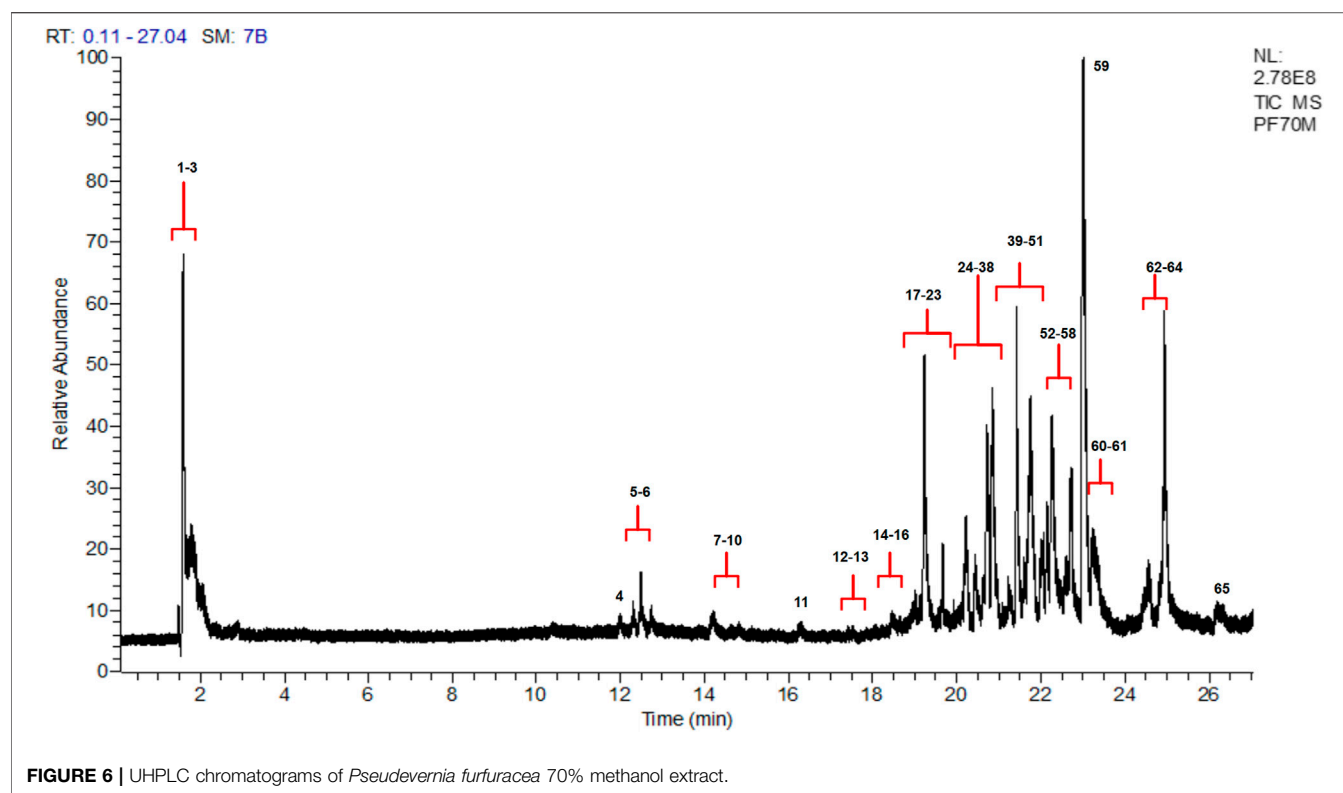


FIGURE 6 | UHPLC chromatograms of *Pseudevernia furfuracea* 70% methanol extract.

mode. Of the forty nine compounds identified in this species the majority were depsides, depsidones, depsons, lipids, pulvinic acid derivative, diphenylether derivatives and dibenzofurans. Eight depsides moieties namely decarboxyhamnolic acid, boninic acid, epiphorellic acid II, 4-O-methylolivetic acid, dihydropicrolicenic acid, haemathamnolic acid isomer, squamatic acid and 2, 2' -di-O-methylantraic acid, respectively were tentatively identified. Few of these compounds are in congruent with previous reported data (Torres-Benítez et al., 2017).

Along with depsides, eight depsidones moieties were identified namely menegazziaic acid (Salgado et al., 2018), loxodellonic acid, 3-hydroxyphysodic acid, methylphysodic acid (Le Pogam et al., 2015), physodic acid, acido-nor-8'-metilconstictico, physodic acid isomer and derivative physodic acid, respectively. Two depsons moieties identified as picrolicenic acid isomer and picrolicenic acid, both having $[M-H]^-$ ions at m/z 441.1920 were also detected.

Two dibenzofuran (DBF) corresponding to peak 9 and 55 were identified as methyl porphyrlate and haemophaein, respectively. Besides, DBF, two pulvinic acid derivative namely pulvinic acid and vulpinic acid corresponding peak 33 and 61 were also identified. β -Alectoronic acid and 2'-O-methylphysodone belongs to category of diphenyl ether has also been detected. Peak 37 was identified as loxodinol (diphenyl ether) (Torres-Benítez et al., 2017).

As is often the case with biological samples several components are not fully elucidated however the mass spectral information generated here forms the basis for their further investigation.

Cytotoxicity Assay

PF70M extracts were tested for their toxic effect on HEK 293T cells by *in vitro* viability test method using Alamar blue as described in methods. The data obtained was plotted as bar graph depicting the percent difference between treated and untreated cells to evaluate the level of cellular viability (Figure 7). The results showed that after treatment with varying concentrations (0.156–100 $\mu\text{g/ml}$) of PF70M extracts there was no significant cell death as compared to control cells as shown in Figure 7 suggesting its safe application to host cells.

Conclusion

The chemical composition of lichen extracts mainly depends upon the method used for the extraction of metabolites. Studying various extraction processes using different solvents, methods and pre-processing techniques, we have found that 70% methanol extract using soxhlet method and mixer grinder technique is the most efficient combination for the enrichment of powder fraction targeting specific metabolites. Extract obtained using this combination resulted in a fraction rich in polyphenolic and flavonoids compounds that accounted for the significant antioxidant potential. The findings of the present work suggest that this lichen used in the form of spice mixture has also potential antioxidant effect. Also the safety of the active extract could be proved with the cytotoxicity and DNA damage protection assays. The antioxidant potential of the detected metabolites obtained from profiling of the active extract should be further explored in suitable cell based and *in vivo* models. Also, detailed studies for elucidation of mechanism

TABLE 3 | Biochemical composition of 70% methanol extract by UHPLC-DAD-MS analysis the negative ion mode.

Peak	Tentative identification	Molecular formula	Retention time (min.)	Theoretical mass (m/z)	Measured mass (m/z)	Accuracy (ppm)	Metabolite type	MS ions (ppm)
1	Arabic acid	C ₅ H ₉ O ₆	1.59	165.0399	165.0401	−1.2	Acid	147.0294; 113.0237; 129.0187
2	Atracic acid ^a	C ₈ H ₁₁ O ₇	1.58	195.0505	195.0508	−1.5	Acid	165.0401
3	Glucosylglycolate	C ₈ H ₁₃ O ₈	1.67	237.0610	237.0619	−3.8	Acid	207.0511; 147.0296
4	Derivative 2,4-Diformyl-3,5-dihydroxytoluene o	C ₉ H ₇ O ₆	11.99	211.0243	211.0247	−1.9	A	179.0349; 167.0336; 149.0239
5	2,6-Diformyl-3,5-dihydroxytoluene	C ₈ H ₇ O ₄	12.31	167.0344	167.0347	−1.8	A	123.0445
6	Orsellinic acid	C ₁₀ H ₉ O ₆	12.48	225.0399	225.0404	−2.2	A	181.0504; 167.0345; 149.0240
7	2,4-Dicarboxy-3-hydroxy-5-methoxytoluene	—	14.19	—	—	—	—	371.1017; 339.0755; 278.1034; 141.0917; 135.1196; 301.2022
8	Unknown	—	14.19	—	—	—	—	—
9	9,10,12,13-Tetrahydroxyhexadecanoic acid	C ₁₆ H ₃₁ O ₆	14.26	319.2121	319.2128	−2.2	L	—
10	Methyl porphyrilate	C ₁₇ H ₁₁ O ₇	14.82	327.0505	327.0513	−2.4	DBF	283.0612; 181.0498
11	9,10,12,13,14-Pentahydroxytricosenoic acid	C ₂₃ H ₄₃ O ₇	15.18	431.3009	431.3015	−1.4	L	—
12	Hexahydroxytetracosanoic acid	C ₂₄ H ₄₇ O ₈	16.27	463.3271	463.3277	−1.3	L	389.1244
13	9,10,12,13-tetrahydroxynonadecanoic acid	C ₁₉ H ₃₇ O ₆	17.55	361.2590	361.2598	−2.2	L	—
14	Menegazziaic acid	C ₁₈ H ₁₃ O ₉	17.87	373.0560	373.0567	−1.9	D	329.0671; 167.0344; 149.0240; 151.0398
15	Hexahydroxytetracosenoic acid	C ₂₄ H ₄₅ O ₈	18.46	461.3114	461.3121	−1.5	L	417.2859; 375.5755
16	9,10,12,13,14-Pentahydroxytricosanoic acid	C ₂₃ H ₄₅ O ₇	18.66	433.3165	433.3171	−1.4	L	329.0671; 389.2546
17	9,10,12,13-Tetrahydroxyeicosanoic acid	C ₂₀ H ₃₉ O ₆	18.95	375.2747	375.2754	−1.9	L	361.2609
18	Unknown	—	19.01	—	—	—	—	467.2780; 413.2912; 375.2755; 135.0389; 119.0173
19	9,10,12,13,14-Pentahydroxytetracosanoic acid	C ₂₄ H ₄₇ O ₇	19.13	447.3322	447.3328	−1.3	L	433.3170
20	Unknown	—	19.22	—	—	—	—	481.2937; 445.3171; 389.2911; 181.3367; 109.1143
21	Olivetonic acid, 2,4-Dihydroxy-6-(2'-oxo-n-heptyl)-benzoic acid	C ₁₄ H ₁₇ O ₅	19.65	265.1076	265.1083	−2.6	A	247.0972; 221.1182
22	Loxodellic acid	C ₂₃ H ₂₃ O ₈	19.74	427.1393	427.1400	−1.6	D	235.0975; 385.0932; 343.0970; 249.0767; 195.0662
23	9,10,12,13-Tetrahydroxypentacosanoic acid	C ₂₄ H ₄₅ O ₇	19.88	445.3165	445.3173	−1.8	L	417.3225
24	Hexahydroxyhexacosanoic acid	C ₂₆ H ₅₁ O ₈	19.93	491.3584	491.3589	−1.0	L	445.3173; 345.2437
25	9,10,12,13-tetrahydroxydocosanoic acid	C ₂₂ H ₄₃ O ₆	20.04	403.3060	403.3068	−2.0	L	375.2755
26	Unknown	—	20.13	—	—	—	—	309.0983; 265.1081; 237.0767; 190.0540; 103.0760
27	9,10,12,13-Tetrahydroxydocosanoic acid	C ₂₂ H ₄₃ O ₆	20.23	403.3060	403.3067	−1.7	L	387.3123
28	Unknown	—	20.25	—	—	—	—	451.2832; 403.3066; 345.2437; 110.2839; 108.2998

(Continued on following page)

TABLE 3 | (Continued) Biochemical composition of 70% methanol extract by UHPLC-DAD-MS analysis the negative ion mode.

Peak	Tentative identification	Molecular formula	Retention time (min.)	Theoretical mass (m/z)	Measured mass (m/z)	Accuracy (ppm)	Metabolite type	MS ions (ppm)
28	9,10,11,12,13,14,15-Hexahydroxycosaenoic acid	C ₂₆ H ₄₉ O ₈	20.43	489.3427	489.3432	-1.0	L	429.3227
29	Decarboxyathamnic acid	C ₁₈ H ₁₅ O ₉	20.55	375.0716	375.0724	-2.1	d	167.0345; 209.0455
30	9,10,12,13,14-Pentahydroxyhexacosanoic acid	C ₂₆ H ₅₁ O ₇	20.66	475.3635	475.3641	-1.3	L	431.3376; 447.3331
31	Hexahydroxyxooctacosenoic acid	C ₂₈ H ₅₃ O ₉	20.66	533.3690	533.3694	-0.7	L	475.3640
32	9,10,12,13-tetrahydroxytricosanoic acid	C ₂₃ H ₄₅ O ₆	20.72	417.3216	417.3224	-1.9	L	403.3067
33	Pulvinic acid	C ₁₈ H ₁₁ O ₅	20.80	307.0606	307.0615	-2.9	PAD	263.0715; 117.0342
34	Boninic acid	C ₂₅ H ₃₁ O ₈	20.85	459.2019	459.2026	-1.5	d	415.2128; 237.1130; 281.1033; 253.1078; 223.0974
35	Unknown	—	20.85	—	—	—	—	509.3247; 459.2026; 415.2129; 345.2437; 109.2090
36	Epiphorellin acid II	C ₂₆ H ₃₁ O ₉	20.92	487.1968	487.1974	-1.2	d	443.2076; 235.0977; 251.0930; 429.1917
37	Loxodinol	C ₂₅ H ₂₉ O ₉	20.98	473.1812	473.1819	-1.5	DE	429.1920; 237.0768
38	Unknown	—	20.98	—	—	—	—	263.0927; 243.0066; 221.0816; 209.0454; 104.0931
39	Olivetolcarboxylic acid	C ₁₂ H ₁₅ O ₄	21.08	223.0970	223.0975	-2.2	A	179.1074; 207.1027
40	4-O-Methylolivetoric acid	C ₂₇ H ₃₃ O ₈	21.20	485.2175	485.2182	-1.4	d	441.2286; 279.1240
41	6-ethyl-6-n-pentylpentadecan-4,5,7,8,15-pentol-15-acetate	C ₂₄ H ₄₇ O ₆	21.20	431.3373	431.3381	-1.9	Aliphatic compounds	417.3233
42	Unknown	—	21.24	—	—	—	—	501.2130; 485.2180; 455.1588; 431.3380; 345.2438
43	9-Hydroxydocosapentaenoic acid	C ₂₂ H ₃₃ O ₃	21.32	345.2430	345.2439	-2.6	L	301.2536
44	Unknown	—	21.38	—	—	—	—	419.0988; 265.1083; 151.0396; 123.0446; 105.0337
45	Dihydricpicrolinonic acid	C ₂₅ H ₃₁ O ₇	21.42	443.2070	443.2077	-1.6	d	399.2177; 221.1184; 151.0394
46	Haemathamnic acid isomer	C ₁₉ H ₁₅ O ₁₀	21.51	403.0665	403.0673	-2.0	d	371.0412; 209.0455; 359.0778
47	Unknown	—	21.61	—	—	—	—	468.2028; 443.2077; 210.1328; 144.2105; 122.3307
48	Unknown	—	21.67	—	—	—	—	261.0770; 233.0817; 223.0975; 179.1075; 151.0398
49	3-Hydroxyphysodic acid	C ₂₆ H ₂₉ O ₉	21.69	485.1812	485.1817	-1.0	D	441.1926; 247.0976
50	Acido-nor-8'-methylconstictico	C ₂₁ H ₁₉ O ₁₁	21.69	447.0927	447.0933	-1.3	D	209.0455; 403.1052
51	Squamatic acid	C ₁₉ H ₁₇ O ₉	21.74	389.0873	389.0880	-1.8	d	193.0140; 163.0396; 149.0239; 119.0497; 121.0289
52	Methylphysodic acid	C ₂₇ H ₃₁ O ₈	22.06	483.2019	483.2023	-0.8	D	453.0593; 345.2436
53	Picrolinonic acid isomer	C ₂₅ H ₂₉ O ₇	22.15	441.1913	441.1920	-1.6	Depsone	—
54	Physodic acid	C ₂₆ H ₂₉ O ₈	22.25	469.1862	469.1866	-0.9	D	425.1969; 247.0973; 451.1762

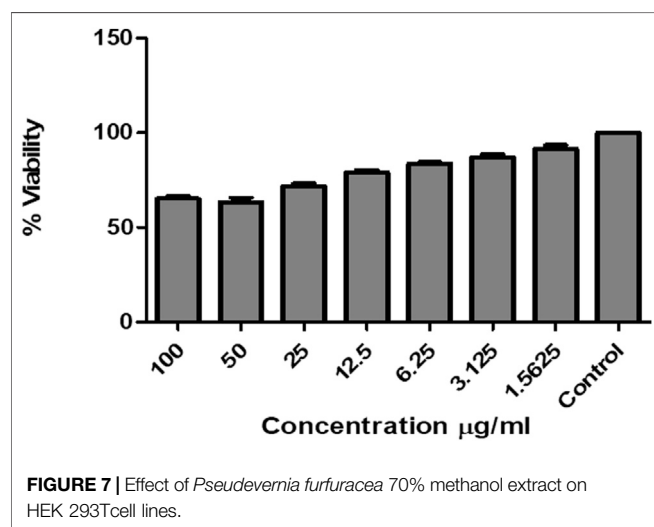
(Continued on following page)

TABLE 3 | (Continued) Biochemical composition of 70% methanol extract by UHPLC-DAD-MS analysis the negative ion mode.

Peak	Tentative identification	Molecular formula	Retention time (min.)	Theoretical mass (m/z)	Measured mass (m/z)	Accuracy (ppm)	Metabolite type	MS ions (ppm)
55	Haemophaein	C ₂₇ H ₃₁ O ₇	22.42	467.2070	467.2076	−1.3	DBF	247.0975; 425.1970; 451.1762
56	β-Alectoronic acid	C ₂₈ H ₃₁ O ₉	22.60	511.1968	511.1971	−0.6	DE	369.1351; 247.0975; 263.0927; 467.2073
57	2,2'-Di-O-methylanizic acid	C ₂₆ H ₃₃ O ₇	22.67	457.2226	457.2234	−1.7	d	265.1080; 413.2310; 427.2128; 443.2079
58	Physodic acid isomer	C ₂₆ H ₂₉ O ₈	22.73	469.1862	469.1868	−1.3	D	247.0976; 425.1968
59	Derivative physodic acid	C ₂₅ H ₂₉ O ₆	23.00	425.1964	425.1973	−2.1	D	381.2068; 177.0945
60	Unknown	—	23.23	—	—	—	—	423.0492 395.0543 409.0699 163.0394 119.0497
61	Vulpinic acid	C ₁₉ H ₁₃ O ₅	23.49	321.0763	321.0771	−2.5	PAD	—
62	Picroliconic acid	C ₂₅ H ₂₉ O ₇	24.55	441.1913	441.1920	−1.6	Depsone	359.1863
63	9-Hydroxydicosapentaenoic acid isomer	C ₂₂ H ₃₃ O ₃	24.69	345.2430	345.2438	−2.3	L	301.2538
64	2'-O-Methylphysodone	C ₂₆ H ₃₁ O ₆	24.92	439.2121	439.2126	−1.1	DE	—
65	Unknown	—	26.25	—	—	—	—	555.2851 537.2493 389.2700 239.2504 119.2575

^aIsolated, identified and quantified.

Where A = Aromatic; L = Lipid; D = depsidone; d = depside; DE = diphenylether; DBF = dibenzofuran; PAD = pulvinic acid derivative.



behind these activities can further contribute in the better utilization of this lichen.

DATA AVAILABILITY STATEMENT

The raw data supporting the conclusions of this article will be made available by the authors, without undue reservation, to any qualified researcher.

AUTHOR CONTRIBUTIONS

RK contributed toward the execution of the experiments, drafting and editing of the article. XC contributed in the language corrections and editions. CA helped in getting the UPLC-MS/MS (Metabolite profiling) analysis done. RD contributed in the cytotoxicity assay. MG contributed towards the Design of study, plan of experiments, guidance, critical revision, final edition and approval of the article.

FUNDING

The research activities of the authors are supported by the The Energy and Resources Institute, India and Deakin University, Australia. RK is supported by Deakin University HDR scholarship (Candidate ID—218121642).

ACKNOWLEDGMENTS

The authors are grateful to Mr. Chandrakant Tripathi for assistance with electron microscopy imaging. The authors acknowledge Prof Prem Lal Uniyal, Department of Botany, University of Delhi for the identification of sample. The authors also acknowledge the financial support received from the Science and Engineering Research Board, Govt. of India (ECR/2016/001018).

REFERENCES

- Aoussar, N., Manzali, R., Nattah, I., Rhallabi, N., Vasiljevic, P., Bouksaim, M., et al. (2017). Chemical composition and antioxidant activity of two lichens species (*Pseudevernia furfuracea* L. and *Evernia prunastri* L.) collected from Morocco. *J. Mater. Environ. Sci.* 8 (6), 1968–1976.
- Brand-Williams, W., Cuvelier, M. E., and Berset, C. (1995). Use of a free radical method to evaluate antioxidant activity. *LWT - Food Sci. Technology* 28 (1), 25–30. doi:10.1016/S0023-6438(95)80008-5
- Cacace, J. E., and Mazza, G. (2003). Optimization of extraction of anthocyanins from black currants with aqueous ethanol. *J. food sci.* 68 (1), 240–248. doi:10.1111/j.1365-2621.2003.tb14146.x
- Calcott, M. J., Ackerley, D. F., Knight, A., Keyzers, R. A., and Owen, J. G. (2018). Secondary metabolism in the lichen symbiosis. *Chem. Soc. Rev.* 47 (5), 1730–1760. doi:10.1039/c7cs00431a
- Chowdhary, K., and Kaushik, N. (2019). UPLC-MS and dereplication-based identification of metabolites in antifungal extracts of fungal endophytes. *Proc. Natl. Acad. Sci. India, Sect. B Biol. Sci.* 89 (4), 1379–1387. doi:10.1007/s40011-018-1060-3
- Crittenden, P., and Porter, N. (1991). Lichen-forming fungi: potential sources of novel metabolites. *Trends Biotechnol.* 9 (1), 409–414. doi:10.1016/0167-7799(91)90141-4
- Goel, M., Kalra, R., Ponnann, P., Jayaweera, J. A. A. S., and Kumbukgolla, W. W. (2021). Inhibition of penicillin-binding protein 2a (PBP2a) in methicillin resistant *Staphylococcus aureus* (MRSA) by combination of oxacillin and a bioactive compound from *Ramalina roesleri*. *Microb. Pathogenesis* 150, 104676. doi:10.1016/j.micpath.2020.104676
- Goel, M., Rani, A., Dureja, P., and Uniyal, P. (2014). Investigation of allelopathic potentiality of the himalyan lichen *parmelia reticulata* tayl. Against *phalaris minor* retz. *APCBEE Proced.* 9, 140–144. doi:10.1016/j.apcbee.2014.01.025
- Goel, M., Sharma, P. K., Dureja, P., Rani, A., and Uniyal, P. L. (2011). Antifungal activity of extracts of the lichens *Parmelia reticulata*, *Ramalina roesleri*, *Usnea longissima* and *Stereocaulon himalayense*. *Arch. Phytopathology Plant Prot.* 44 (13), 1300–1311. doi:10.1080/03235408.2010.496549
- Gormann, R., Kaloga, M., Li, X.-C., Ferreira, D., Bergenthal, D., and Kolodziej, H. (2003). Furanonaphthoquinones, atraric acid and a benzofuran from the stem bark of *Newbouldia laevis*. *Phytochemistry* 64 (2), 583–587. doi:10.1016/s0031-9422(03)00277-2
- Güvenç, A., Küpeli Akkol, E., Süntar, İ., Keleş, H., Yıldız, S., and Çalış, İ. (2012). Biological activities of *Pseudevernia furfuracea* (L.) Zopf extracts and isolation of the active compounds. *J. Ethnopharmacology* 144 (3), 726–734. doi:10.1016/j.jep.2012.10.021
- Hidalgo, M. E., Ferná'ndez, E., Quilhot, W., and Lissi, E. (1994). Antioxidant activity of depsides and depsidones. *Phytochemistry* 37 (6), 1585–1587. doi:10.1016/s0031-9422(00)89571-0
- Ismail, B. B., Pu, Y., Guo, M., Ma, X., and Liu, D. (2019). LC-MS/QTOF identification of phytochemicals and the effects of solvents on phenolic constituents and antioxidant activity of baobab (*Adansonia digitata*) fruit pulp. *Food Chem.* 277, 279–288. doi:10.1016/j.foodchem.2018.10.056
- Komaty, S., Letertre, M., Dang, H. D., Jungnickel, H., Laux, P., Luch, A., et al. (2016). Sample preparation for an optimized extraction of localized metabolites in lichens: application to *Pseudevernia furfuracea*. *Talanta* 150, 525–530. doi:10.1016/j.talanta.2015.12.081
- Kosanic, M., Manojlovic, N., Jankovic, S., Stanojkovic, T., and Rankovic, B. (2013). *Evernia prunastri* and *Pseudevernia furfuracea* lichens and their major metabolites as antioxidant, antimicrobial and anticancer agents. *Food Chem. Toxicol.* 53, 112–118. doi:10.1016/j.fct.2012.11.034
- Kosanić, M., Ranković, B., Stanojković, T., Rančić, A., and Manojlović, N. (2014). Cladonia lichens and their major metabolites as possible natural antioxidant, antimicrobial and anticancer agents. *LWT Food Sci. Technol.* 59 (1), 518–525. doi:10.1016/j.lwt.2014.04.047
- Kumar, J., Dhar, P., Tayade, A. B., Gupta, D., Chaurasia, O. P., Upreti, D. K., et al. (2014). Antioxidant capacities, phenolic profile and cytotoxic effects of saxicolous lichens from trans-Himalayan cold desert of Ladakh. *PLoS One* 9 (6), e98696. doi:10.1371/journal.pone.0098696
- Le Pogam, P., Schinkovitz, A., Legouin, B., Le Lamer, A.-C., Boustie, J., and Richomme, P. (2015). Matrix-free UV-laser desorption ionization mass spectrometry as a versatile approach for accelerating dereplication studies on lichens. *Anal. Chem.* 87 (20), 10421–10428. doi:10.1021/acs.analchem.5b02531
- Li, X. (2013). Solvent effects and improvements in the deoxyribose degradation assay for hydroxyl radical-scavenging. *Food Chem.* 141 (3), 2083–2088. doi:10.1016/j.foodchem.2013.05.084
- Liu, R. H. (2003). Health benefits of fruit and vegetables are from additive and synergistic combinations of phytochemicals. *Am. J. Clin. Nutr.* 78 (3 Suppl. 1), 517S–520S. doi:10.1093/ajcn/78.3.517S
- Manojlovic, N., Rankovic, B., Kosanic, M., Vasiljevic, P., and Stanojkovic, T. (2012). Chemical composition of three *Parmelia* lichens and antioxidant, antimicrobial and cytotoxic activities of some their major metabolites. *Phytomed* 19 (13), 1166–1172. doi:10.1016/j.phymed.2012.07.012
- Nash, T. H. (1996). *Lichen biology*. Cambridge, U. K: Cambridge University Press.
- Newman, D. J., and Cragg, G. M. (2016). Natural products as sources of New drugs from 1981 to 2014. *J. Nat. Prod.* 79 (3), 629–661. doi:10.1021/acs.jnatprod.5b01055
- Ng, L., Ang, Y., Khoo, H., and Yim, H. (2012). Influence of different extraction parameters on antioxidant properties of *Carica papaya* peel and seed. *Res. J. Phytochem.* 6 (3), 61–74. doi:10.3923/rjphyto.2012.61.74
- Odabasoglu, F., Cakir, A., Suleyman, H., Aslan, A., Bayir, Y., Halici, M., et al. (2006). Gastroprotective and antioxidant effects of usnic acid on indomethacin-induced gastric ulcer in rats. *J. Ethnopharmacology* 103 (1), 59–65. doi:10.1016/j.jep.2005.06.043
- Oettl, S. K., Hubert, J., Nuzillard, J. M., Stuppner, H., Renault, J. H., and Rollinger, J. M. (2014). Dereplication of depsides from the lichen *Pseudevernia furfuracea* by centrifugal partition chromatography combined to ¹³C nuclear magnetic resonance pattern recognition. *Anal. Chim. Acta* 846, 60–67. doi:10.1016/j.aca.2014.07.009
- Ordóñez, A., Gómez, J., Vattuone, M., and Lslá, M. (2006). Antioxidant activities of *Sechium edule* (jacq.) swartz extracts. *Food Chem.* 97 (3), 452–458. doi:10.1016/j.foodchem.2005.05.024
- Rampersad, S. N. (2012). Multiple applications of Alamar Blue as an indicator of metabolic function and cellular health in cell viability bioassays. *Sensors* 12 (9), 12347–12360. doi:10.3390/s120912347
- Re, R., Pellegrini, N., Proteggente, A., Pannala, A., Yang, M., and Rice-Evans, C. (1999). Antioxidant activity applying an improved ABTS radical cation decolorization assay. *Free Radic. Biol. Med.* 26 (9–10), 1231–1237. doi:10.1016/S0891-5849(98)00315-3
- Salgado, F., Alborno, L., Cortéz, C., Stashenko, E., Urrea-Vallejo, K., Nagles, E., et al. (2018). Secondary metabolite profiling of species of the genus *Usnea* by UHPLC-ESI-OT-MS-MS. *Molecules* 23 (1), 54. doi:10.3390/molecules23010054
- Singleton, V. L., Orthofer, R., and Lamuela-Raventós, R. M. (1999). [14] Analysis of total phenols and other oxidation substrates and antioxidants by means of folin-cicalteu reagent. *Methods Enzymol.* 299, 152–178. doi:10.1016/S0076-6879(99)90017-1
- Sisodia, R., Geol, M., Verma, S., Rani, A., and Dureja, P. (2013). Antibacterial and antioxidant activity of lichen species *Ramalina roesleri*. *Nat. Product. Res.* 27 (23), 2235–2239. doi:10.1080/14786419.2013.811410
- Spigno, G., and De Faveri, D. M. (2007). Antioxidants from grape stalks and marc: influence of extraction procedure on yield, purity and antioxidant power of the extracts. *J. Food Eng.* 78 (3), 793–801. doi:10.1016/j.jfoodeng.2005.11.020
- Tembo, D. T., Holmes, M. J., and Marshall, L. J. (2017). Effect of thermal treatment and storage on bioactive compounds, organic acids and antioxidant activity of baobab fruit (*Adansonia digitata*) pulp from Malawi. *J. Food Compos. Anal.* 58, 40–51. doi:10.1016/j.jfca.2017.01.002
- Torres-Benítez, A., Rivera-Montalvo, M., Sepúlveda, B., Castro, O., Nagles, E., Simirgiotis, M., et al. (2017). Metabolomic analysis of two *parmotrema* lichens: *P. robustum* (degl.) hale and *P. andinum* (mull. Arg.) hale using UHPLC-ESI-OT-MS-MS. *Molecules* 22 (11), 1861. doi:10.3390/molecules22111861

- Upreti, D. K., Divakar, P. K., and Nayaka, S. (2005). Commercial and Ethnic Use of Lichens in India. *Econ. Bot.* 59 (3), 269–273. doi:10.1663/0013-0001(2005)059[0269:caeul]2.0.co;2
- Zhao, J., Ma, D., Luo, M., Wang, W., Zhao, C., Zu, Y., et al. (2014). *In vitro* antioxidant activities and antioxidant enzyme activities in HepG2 cells and main active compounds of endophytic fungus from pigeon pea [*Cajanus cajan* (L.) Millsp.]. *Food Res. Int.* 56, 243–251. doi:10.1016/j.foodres.2013.12.028
- Zugic, A., Jeremic, I., Isakovic, A., Arsic, I., Savic, S., and Tadic, V. (2016). Evaluation of anticancer and antioxidant activity of a commercially available CO₂ supercritical extract of old man's beard (*usnea barbata*). *PLoS One* 11, e0146342. doi:10.1371/10.1371/journal.pone.0146342

Conflict of Interest: The authors declare that the research was conducted in the absence of any commercial or financial relationships that could be construed as a potential conflict of interest.

Copyright © 2021 Kalra, Conlan, Areche, Dilawari and Goel. This is an open-access article distributed under the terms of the Creative Commons Attribution License (CC BY). The use, distribution or reproduction in other forums is permitted, provided the original author(s) and the copyright owner(s) are credited and that the original publication in this journal is cited, in accordance with accepted academic practice. No use, distribution or reproduction is permitted which does not comply with these terms.



Polyphenolic-Rich Compounds From *Dillenia pentagyna* (Roxb.) Attenuates the Doxorubicin-Induced Cardiotoxicity: A High-Frequency Ultrasonography Assisted Approach

OPEN ACCESS

Edited by:

Chandra Kant Katiyar,
Emami, India

Reviewed by:

Haci Ahmet Deveci,
University of Gaziantep, Turkey
Mikhail Olugbemi Nafiu,
University of Ilorin, Nigeria
Kely De Picoli Souza,
Federal University of Grande
Dourados, Brazil
Sayeed Ahmad,
Jamia Hamdard University, India

*Correspondence:

Ranadeep Gogoi
gogoiranadeep@
niperguwahati.ac.in
V. G. M. Naidu
vgmnaidu@gmail.com

Specialty section:

This article was submitted to
Ethnopharmacology,
a section of the journal
Frontiers in Pharmacology

Received: 01 November 2020

Accepted: 15 April 2021

Published: 17 May 2021

Citation:

Tene K, Kalyan Kumar M,
Basveshwar G, Eswara Rao P,
Jagadeesh Kumar G, kumar P,
Pemmaraju DB, Murty USN, Gogoi R
and Naidu VGM (2021) Polyphenolic-
Rich Compounds From *Dillenia*
pentagyna (Roxb.) Attenuates the
Doxorubicin-Induced Cardiotoxicity: A
High-Frequency Ultrasonography
Assisted Approach.
Front. Pharmacol. 12:624706.
doi: 10.3389/fphar.2021.624706

Kalyani Tene¹, M. Kalyan Kumar², G. Basveshwar², P. Eswara Rao², G. Jagadeesh Kumar², Pramod kumar³, Deepak B. Pemmaraju², U. S. N. Murty², Ranadeep Gogoi^{1,4*} and V. G. M. Naidu^{2*}

¹Department of Biotechnology, National Institute of Pharmaceutical Education and Research- Guwahati, Assam, India,

²Department of Pharmacology and Toxicology, National Institute of Pharmaceutical Education and Research-Guwahati, Assam, India, ³Department of Pharmaceutical Analysis, National Institute of Pharmaceutical Education and Research Guwahati, Assam, India, ⁴Biological Sciences and Technology Department, CSIR-North-East Institute of Science and Technology, Assam, India

Cardiovascular complications are the foremost concern in patients undergoing anticancer therapy. There is an unmet need to address the problems arising from the drug-induced toxicity for the long-term benefit of the patients undergoing chemotherapy. Alternative medicines are gaining their prosperity in addressing the various drug-induced organ toxicity. *Dillenia pentagyna* Roxb (DP) is an ethnomedicinal plant rich in flavonoids and phenolic contents. In India & Nepal, DP is a common ingredient of traditional medicines used to treat multiple ailments like inflammation, cancer, and diabetes. However, its protective role against doxorubicin (Dox) induced cardiotoxicity remains unexplored. Herein, we investigated the potential effects of various extracts/fractions obtained from the DP's bark against Dox-induced cardiotoxicity, both *in-vitro* and *in-vivo*. The anti-oxidant content of the extracts/fractions was evaluated by using DPPH, ABTS and FRAP chemical assays. The results indicated that the hydroalcoholic (HA) extract of DP has intense anti-oxidant potential. Further fractionation of DP revealed that the phenolic-rich fraction (F1) has a high anti-oxidant potential. The protective effect of extract/fraction was also investigated in the H9c2 cell line following the Dox-induced cardiotoxicity model. We observed that the pre-treatment of extract/fraction in cardiomyocytes had exhibited increased cell viability. Fluorescence-based chemical assays indicated a decreased ROS levels in the treated groups in comparison to the Dox control group. The effect of DP was evaluated further in balb/c mice by the Dox-induced cardiotoxicity model. Non-

Abbreviations: DPPH, 2,2-diphenyl-1-picryl-hydrazyl; ABTS, 2,2'-azino-bis(3-ethylbenzo) thiazoline-6-sulfonic acid; TPC, Total phenolic acid; RIPA buffer; MTT, 3-(4,5-dimethylthiazol-2-yl)-2,5-diphenyl tetrazolium bromide; FRAP, ferric reducing antioxidant power; CM-H2DCFDA, chloromethyl derivative of 2', 7' -dichlorofluorescein (DCF); ROS, Reactive oxygen species; FACS, fluorescence-activated cell sorting; DMSO, dimethylsulfoxide; ESI, electrospray ionization; ATCC, American type culture collection; NCCS, National center for cell science; SOD-2, superoxide dismutase; Keap-1, Kelch-like ECH-associated protein 1; Nrf-2, nuclear factor erythroid 2-related factor 2; HO-1, hemoxygenase; RSA, radical scavenging assay; BSA, bovine serum albumin; LCMS-QTOF, Liquid chromatography-quadrupole time of flight; HFUS- high frequency ultrasonography.

invasive techniques like high-frequency ultrasonography and electrocardiogram revealed that the mice pre-treated with DP had improved cardiac functionality (left ventricular ejection fraction and stroke volume) and normalized the electrocardiograms compared to the Dox control group. Further, biochemical analysis with the cardiac tissues revealed that the cytoprotective proteins like HO-1, SOD-2, and Nrf-2 were elevated in the DP treated groups compared to the Dox control group. Overall, our results suggested that the bioactive extract/fractions of DP helped alleviate the Dox-induced cardiotoxicity. LC-QTOF-ESI-MS analysis of DP and F1 indicated that polyphenolic anti-oxidant compounds like gallic acid, syringic acid, and sinapic acid could be responsible for the potent -cardioprotective effect. Future understanding of the pharmacokinetics and pharmacodynamic parameters can help translate from the bench to the bedside.

Keywords: doxorubicin, oxidative stress, cardioprotection, ultrasonography, *dillenia pentagyna roxb*

INTRODUCTION

Cancer is one of the significant public health concerns affecting nearly 18 million people, thereby leading to 9.6 million deaths worldwide (Bray et al., 2018). Current treatment strategies for cancer include targeted therapy (Ex: immunotherapy), photodynamic/thermal treatment, radiation, and chemotherapy. Among them, chemotherapeutic drugs have shown a better prognosis in reducing the tumor burden and increasing cancer patients' overall life expectancy. Modern cancer therapies had increased the number of survivors. However, there is a surge in cardiac complications in patients undergoing various cancer therapies contributing to increased morbidity and mortality (Tan and Scherrer-Crosbie, 2014). Multiple drugs and therapies like Doxorubicin, Paclitaxel, monoclonal antibodies (Trastuzumab), and tyrosine kinase inhibitors (Imatinib), causes cardiotoxicity (Brown et al., 2015). Doxorubicin (Dox) is a widely used drug reported to induce oxidative stress-mediated necrosis in the cardiomyocytes (Xu et al., 2020). A single regime of Dox at a dose of 60–75 mg/m² for every three weeks is being used in the clinical application (Rugo et al., 2016). Increased dosage of Dox leads to its accumulation in cardiolipin (a phospholipid located in the inner mitochondrial membrane) of cardiomyocytes leading to the disruption of the electron transport chain, ultimately leading to the generation of ROS (Huang et al., 2015). Reports indicated that the Dox also reduces the functional capacity of the Nrf-2 gene, which is a critical regulator of the redox system (Wang et al., 2019). This affects the reduction of anti-oxidant enzymes like glutathione (GSH), and catalase (Peoples et al., 2019). Few Nrf-2 activators have been developed (Cuadrado et al., 2019); however, limitations like interference with drug's oncologic efficacy and low bioavailability had hindered their complete translation. Therefore, creating safe and highly effective therapeutics to mitigate the toxicity associated with the chemotherapeutic drugs will benefit cancer patients.

Plants are considered a vast source of natural anti-oxidants from ancient times. Many such sources have even become part of our dietary lifestyle due to polyphenols, vitamins, mineral content. They have high nutritional value and therefore gained

importance in drug discovery over time. *Dillenia pentagyna* Roxb (DP) belongs to the family Dilleniaceae, commonly known as Nepali elephant apple, is a highly valued medicinal plant distributed in Asian countries. Fruits of it are edible and are cooked as a dish by the tribal people of North-East and central parts of India. The plant's bark and fruits have been traditionally used for treating inflammatory diseases, chest pain, and cancer (Sharma et al., 2001). The plant's seed and bark are also used against cancer by the Koch-Rajbanshi tribes of northeastern states in India (Yadav and Srivastava, 2014). Fruits of the plant possess flavonoid glycosides like naringenin 7-galactosyl and dihydroquercetin 5- galactoside (Saiful Yazan and Armania, 2014).

Preliminary *in-vitro* studies on the bark showed anti-oxidant content due to the presence of lupeol, betulin, and betulinic acids. Despite the therapeutic properties, the plant or its parts were not scientifically explored for beneficial effects in managing drug-induced oxidative stress-mediated diseases/toxicity. In this regard, the current study intends to evaluate *Dillenia pentagyna* Roxb (DP) extract/purified fractions ameliorative effect against Dox-induced cardiotoxicity in both *in-vitro* and *in-vivo* studies. High-frequency ultrasonography assisted real-time monitoring of cardiac functional parameters was attempted. To the best of our knowledge, we are the first to understand the potential of DP against Dox-induced cardiotoxicity using high-frequency ultrasonography (HFUS).

MATERIALS AND METHODS

Chemicals

Doxorubicin (Dox), DPPH, ABTS, NBT, DTNB, and Lactate dehydrogenase (LDH) assay kit were purchased from Sigma Chemicals (St. Louis, MO, United States). Ascorbic acid was purchased from Hi-media. Creatine Kinase-MB (CK-MB) was procured from Accurex (Mumbai, India). Normal goat serum, Alexa Flour 488 goat anti-rabbit, and Hoescht's 33,258 were procured from Invitrogen. All primary (Nrf-2, SOD-2, Keap-1, and HO-1) and secondary antibodies used in this study were obtained from Cell Signalling Technology (Beverly, Massachusetts United States). LC-MS grade water and

acetonitrile were purchased from M/s JT Baker, United States. Ammonium acetate and formic acid were brought from M/s Sigma Aldrich, United States. All the chemicals were used as such without any modification and derivatization.

Cell Lines and Maintenance

Rat cardiomyocytes (H9c2 cell line) were procured from NCCS, Pune and colon cancer cell line (HCT-116) was procured from ATCC, United States. The cells were cultured in DMEM, and RPMI medium respectively enriched with fetal bovine serum (10% v/v), L-Glutamine (1%), and anti-anti (antibiotic and antimycotic) (100 U/ml) and was maintained at 37°C in a humidified air containing 5% CO₂ in a sterile condition.

Animals

25–30 g male Balb/c mice were used to evaluate the bioactive DP's cardio-protective activity (hydro-alcoholic). Animals were procured from Palamur Biosciences (Hyderabad, India). All experiments were performed by following the Committee for the Purpose of Control and Supervision of Experiments on Animals (CPCSEA), India. The study was approved by the Institutional Animal Ethics Committee (IAEC), Guwahati, India (NIPS/NIPER/18/029). The animals have been housed in individually ventilated cages (IVC) under standard conditions (temperature 23 ± 1°C, 12 h light/dark cycle). Acute oral toxicity study was performed for the maximum dose of 2000 mg/kg for seven days as per Organization for Economic Co-operation and Development (OECD) guidelines.

Plant Material Collection

The bark of *Dillenia pentagyna* Roxb. was collected from Auxiguri village, Baksa district (91° 20.47' E and 26° 39.49' N), Assam in the month of April. The plant was authenticated from Bodoland University Herbarium, Kokrajhar, with accession number (BUH 0000142).

Preparation of Bioactive Extract

Bark was shade dried at room temperature and pulverized into fine powder through a grinding mill (MF 10 B S000, IKA, Germany). The fine powder was extracted with successive solvents with low polarity to high polarity index. The powder was first defatted with the hexane and macerated twice with each solvent for 24 h in an incubator shaker. The solvents were followed as chloroform (CH), ethyl acetate (EA), ethanol (EOH), and hydro-alcohol (HA) (1:1). The extracts were filtered using Whatman filter paper Grade-1 and subjected to dryness using a rotary evaporator (IKA RV 10, Germany).

IN-VITRO ANTI-OXIDANT ASSAYS

All the extracts were tested for preliminary anti-oxidant potential by using the following assays.

DPPH Radical Scavenging Assay

All the extracts and fractions of DP were tested for their free radical scavenging properties using a Spectramax I3X (Molecular

Devices, United States). 20 µl aliquot of different concentrations of the extracts, fractions (1,000, 500, 250, 125, 62.5 and 31.25 µg/ml) and the respective standard (Ascorbic acid 200, 100, 50, 25 and 12.5 µg/ml) were added to 200 µl of DPPH in methanol (0.2 mM). After 20 min of incubation, the absorbance of each solution was read at 517 nm. Results were expressed in percentage free radical scavenging activity (% RSA) with reference to ascorbic acid (Sridhar and Charles, 2019), and IC₅₀ values were calculated.

ABTS Radical Scavenging Assay

All the extracts and fractions of DP were tested to scavenge the cation radicals. To 20 µl of various concentrations of the test samples (1,000, 500, 250, 125, 62.5 and 31.25 µg/ml) or standard 200, 100, 50, 25 and 12.5 µg/ml, 200 µL of ABTS solution was added and incubated for 20 min. The resulting absorbance of these solutions was measured spectrophotometrically at 734 nm using Spectramax I3X. Analyses were done in percentage radical scavenging activity (% RSA). Ascorbic acid was employed as the reference standard (Abramovič et al., 2017), and IC₅₀ values were calculated.

FRAP Assay

All the extracts and fractions of DP were tested for their ability to reduce Fe⁺³ to Fe⁺², which can be observed from light green to blue color at an absorbance of 700 nm. Ascorbic acid was used as a reference standard. 0.2 ml of each test sample of different dilutions (1,000, 500, 250, 125 and 62.5 µg/ml) was added to 0.2 ml of PBS and 0.2 ml of 1% ferric chloride. The reaction was incubated for 20 min at 50 °C, and the reaction was stopped by adding 0.2 ml of 10% trichloroacetic acid, 0.5 ml of distilled water, and 0.2 ml of 0.1% ferric chloride. Absorbance was measured against a blank solution containing all the reagents except the test samples or standard. The value of FRAP was expressed in mg ascorbic acid equivalent (AAE)/Gram of extract (Müller et al., 2011).

Total Phenolic Content

Total phenolic content of all the extracts and fractions of DP were estimated by the Folin–Ciocalteu method. Bioactive fractions 100 µl (1 mg/ml) and mixed thoroughly with 0.2 ml of Folin–Ciocalteu followed by adding 0.75 ml of sodium carbonate solution 75% (w/v) and incubated for 30 min and read at 765 nm. Results were expressed as mg of Gallic acid Equivalent (GA)/Gram of extract (Alizadeh Behbahani and Shahidi, 2019).

METHOD DEVELOPMENT FOR SEPARATION OF THE ACTIVE CONSTITUENTS

Flash Chromatography was used for the separation of active components. Solvent optimization was carried out initially using thin-layer chromatography (TLC) on Silica gel 60 F₂₅₄ (Merck, Germany) A range of solvents with different polarity indexes was used, and finally, methanol and water (9:1 ratio) was found to be optimal to separate maximum constituents. Later, the crude

extract was loaded onto the flash chromatography apparatus (Biotage Isolera one, Sweden), and the chemical components were eluted using the mobile gradient phase by reverse phase chromatography. The solvents used are methanol (A) and water (B) (A: B) 100–90% with a flow rate of 20 ml/min using a Sfar C18 30gD Duo 30um cartridge. Three fractions (named Fraction F1, F2, and F3) were collected and evaluated for *in-vitro* anti-oxidant potential, and further biological activity screening was performed.

In-vitro Cardioprotective Studies

Cell Viability

Cells were seeded at the density of 1×10^4 /well and incubated for 12 h. Bioactive fractions were treated with different concentrations (6.25, 12.5, 25, and 50 µg/ml) for 24 h. MTT assay assessed cell viability followed by treatment with bioactive extract/fraction with or without Dox treatment. 0.5 mg/ml MTT was added to the cells and incubated for 4 h. DMSO was added to dissolve the insoluble formazan crystals and read the plate at 570 nm by Spectramax I3X (Van Meerloo et al., 2011).

Measurement of ROS and Superoxide Anion Radicals

Cells were plated 1×10^6 /well and pre-treated with bioactive fractions for 2 h, and Dox 40 µM was given for 24 h. Cellular ROS generation was determined qualitatively by CM-H2DCFDA and evaluated using a fluorescence microscope (EVOS FL Auto two, Invitrogen). The fluorescein intensity was quantitatively assessed by a Flow cytometer (Life Technologies, Thermo fisher scientific, Singapore). Cellular Superoxide radical generation was defined by Mitosox red. H9c2 cells were subjected to the same treatment as ROS and superoxide radical was evaluated by a confocal microscope (Leica, Germany). Results were expressed as mean fluorescence intensity (MFI).

Bioactive Fraction/s and Dox on Cancer Cell Line

Cells were seeded at the density of 5×10^3 cells/well and incubated for 12 h. Bio-active fractions were treated with different concentrations 3.125, 6.25, 12.5, 25 and 50 µg/ml for 24 h. Extracts were treated along with Dox (2.5 µM) for 24 h, and an MTT reagent was used to assess the cell viability. 0.5 mg/ml MTT was added to the cells and incubated for 4 h. DMSO was added to dissolve the insoluble formazan crystals, and the plate was read at 570 nm by Spectramax I3X (Molecular Devices, United States of America).

In-vivo Studies

Experimental Design

Mice were divided into four groups, each group consisting of six animals. Group 1: Normal saline control. Group 2: disease control, received an intraperitoneal injection of Dox 2.5 mg/kg six times in two weeks. Group 3: Treated with the bioactive DP (100 mg/kg) per oral (p.o) daily once for fourteen days and an intraperitoneal injection of Dox 2.5 mg/kg six times in two weeks. Group 4: Given DP (200 mg/kg) (p.o) daily once for fourteen days and an i. p injection of Dox 2.5 mg/kg six times in two weeks of the study. Body weights of the mice were recorded at periodic

intervals during the study to evaluate the treatment's effect (Rugo et al., 2016).

Electrocardiographic Recording (ECG) and Analysis

The ECG was performed for different groups on day 14th (end of the experiment). Briefly, mice were anesthetized with 4% isoflurane and maintained anesthesia with 1–2% isoflurane and followed by insertion of electrodes through a needle in the right hind limb, right forelimb, left forelimb. The ECG was recorded for each mice and data was collected by AD Instrument, Australia. T wave elevation, *p* duration, and ST heights were analyzed using Lab Chart 8 software (AD Instrument, Australia) (Sheibani et al., 2020).

Analysis of the Cardiac Parameters by High-Frequency Ultrasonography Imaging

The animals underwent imaging to evaluate the cardiac functional parameters. The animals were anesthetized with 4% isoflurane in an anesthesia chamber and placed on a heating pad, and anesthesia was maintained using 1.5% isoflurane by a nasal mask throughout the experiment. Echocardiography was performed using a high-frequency (30 MHz) small animal imaging system (Vevo LAZR-X 3100, FUJIFILM Visual Sonics). The transducer used was MX400 with a mouse small cardiology application and the parasternal long-axis view (Gangrade et al., 2020; Tene et al., 2020). Cardiac functions like cardiac output, fractional shortening, and ejection fraction were calculated from B mode where left ventricular region of the heart was focused in a two-dimensional manner. Similarly, systolic volume, diastolic volume, left ventricular mass, left ventricular posterior wall thickness systolic (LVPW; s) left ventricular posterior wall thickness diastolic (LVPW; d) were measured for each animal from the M-mode image. Measurements were performed using digital image analysis software (Vevo Lab 3.1.1).

Assessment of Anti-Oxidant Enzymes

Serum was collected and stored at -20°C . CK-MB, LDH assays were measured with corresponding assay kits from Accurex and Sigma. Heart tissue was homogenized with Tissue lyser II (Qiagen, Germany) using 0.05M PBS pH 7.4 and centrifuged at 12,000 rpm at 4°C for 10 min, and the supernatant was collected and anti-oxidant parameters GSH (Owen and Butterfield, 2010), catalase, MDA was measured. Results were expressed per mg protein (Ohkawa et al., 1979).

Tissue Processing

The mice were sacrificed by cervical dislocation under mild anesthesia and the heart from each mice was collected. Organs were fixed and stored in neutral 10% formalin solution for 24 h. Tissues were dehydrated in grades of alcohol and embedded in paraffin blocks. Sections (5 µm) were cut by using a microtome and placed on slides and stained with hematoxylin and eosin (H&E) staining. A light microscope analyzed the stained segments under 20x magnification (Koul et al., 2014).

Western Blot Analysis

The effect of DP in modulating the ROS mediated by the Dox induction was evaluated by western blot analysis of the homogenized H9c2 cells and heart tissue lysate. The cells and heart tissues were briefly collected and washed with ice-cold 1X PBS, followed by RIPA lysis buffer protein extraction (Battu et al., 2018). The supernatant was collected, and the protein concentration was determined by using the Bradford reagent at 595 nm. Equal protein concentrations were subjected to SDS-PAGE (10 and 12% Tris-Glycine gel) with a pre-stained protein molecular weight marker (Bio-Rad). The separated proteins were transferred to nitrocellulose membrane (Bio-rad) followed by blocking in 3% BSA (Hi-media) for 1 h at room temperature. Blocked membranes were incubated with the specific primary antibodies (Nrf-2, Keap-1, SOD-2, HO-1, α -tubulin, and β -actin) overnight at 4°C, washed three times with TBST followed by incubation with secondary antibody for 1 h at room temperature. Blots were developed by using Clarity substrate solution (Peroxide solution and enhancer solution (1:1) on a Chemiluminescence 17-200255 (Fusion F_x Vilber 363 Lourmat) and densitometric analysis by ImageJ software (Bethesda, Maryland, United States).

LC-MS/MS Characterization

Hydroalcoholic extract of *Dillenia pentagyna* Roxb. and its fraction F1 was used for UHPLC-QTOF-ESI-MS analysis. Dried samples were mixed with methanol and water on an equal ratio (1:1). Samples were vortexed and sonicated for uniform mixing. Samples were filtered by a 0.22 μ m syringe filter to remove the foreign article and to avoid cone choking during analysis. Plant metabolites identification was performed using UHPLC-QTOF (Agilent 1,290 Infinity II Binary pump, well plate autosampler, thermostatted column compartment, and Agilent 6545XT AdvanceBio QTOF LC/MS/MS. Agilent Poroshell 120 EC C18, 2.7 μ m, 2.1 \times 100 mm column was used in this study with 45°C. The autosampler temperature was kept at 6°C to avoid any degradation during the analysis. The mobile phase was used in gradient mode as A and B. A is composed of 95:5 Water: Acetonitrile with 0.1% formic acid and 10 mM Ammonium Acetate, and B is composed of 95:5 Acetonitrile: Water with 0.1% formic acid and 10 mM Ammonium Acetate. The flow rate was kept at 0.4 ml per minute. Mobile phase B was changed concerning time such as 0.00 min-2% B, 3 min-2%B, 15 min-95%B, 20 min-95%B, 20.1 min-2%B, 25 min-2% B, and the stop time was 25-min. QTOF MS was run in both positive and negative mode using the Agilent Jet stream option. Source conditions were composed of gas temperature-275°C, drying gas (nitrogen)-8 L per minute, nebulizer gas (nitrogen) -35psi, sheath gas temperature -300°C, sheath gas flow-11 L per minute. Fragmentation, capillary voltage, and nozzle voltage were set at 150, 3500, and 1000 V, respectively. The mass range was kept 100-1700 m/z with one spectrum per second acquisition rate time.

Statistics

Mean \pm SEM values were used for the expression of data unless mentioned otherwise. Statistical analyses of data were performed using the One Way ANOVA (GraphPad Software Inc., CA,

United States) followed by Tukey's post hoc test unless specified. Values of $p < 0.05$ were considered statistically significant.

RESULTS

Identification and Purification of the Anti-Oxidant Fractions

The bark powder obtained from the *Dillenia pentagyna* Roxb (DP) was subjected to polarity guided extraction and identified that the DP hydroalcoholic extract has a potent anti-oxidant property (**Supplementary Figure S1**). The generalized scheme of the study is depicted in the **Figure 1**. The DP hydroalcoholic extract was subjected to fractionation to obtain different fractions (F1, F2, and F3) (**Supplementary Figure S2**). Further analysis identified that fraction F1 has shown high anti-oxidant molecule content (DPPH, ABTS, and FRAP) compared to the respective control (DP), (**Figures 2A–C**). The total phenolic content analysis indicated that the bioactive DP and fraction F1 have high total phenolic content, as shown in **Figure 2D**.

Bioactive DP Hydroalcoholic Extract and Its Fraction F1 Alleviates the Dox-Induced Toxicity in Cardiomyocytes

Pre-treatment with the bioactive fractions (DP and F1) has shown no remarkable changes in the morphology of the H9c2 cardiomyocytes. The MTT assay result indicated that the cardiomyocytes treated with Dox exhibited $43.61 \pm 1.61\%$ of viability. In contrast, pre-treatment with the bioactive DP has alleviated the Dox's toxic effect in H9c2 cells in a dose-dependent manner. A similar protection effect was observed when the cardiomyocytes were treated with the fraction F1, as shown in **Figures 2E,F**, respectively, Maximum protection was observed at the higher concentration of the DP and F1 (12.5 μ g/ml). Meanwhile, bioactive extracts alone (without Dox) did not cause significant cytotoxicity (**Supplementary Figures S2A,B**).

Bioactive Fraction Attenuates the Dox-Induced ROS Production *In-vitro*

Dox causes cellular and mitochondrial damage by intracellular ROS generation. Hence, to evaluate the bioactive DP's role in modulating the cellular ROS generation, we have assessed the quantitative total cellular ROS level using a fluorescent dye DCFDA by FACS. **Figure 3A** represents the distribution of the DCFDA stained cell populations. As evidenced in **Figure 3B**, there is a right shift of the cell population in the Dox control group, indicating an overall increase in ROS level compared to the control group. When pre-treated with the bioactive DP and its fraction F1, the cardiomyocytes have shown ROS levels equivalent to the control group. The fluorescent microscope images also indicated a high fluorescence in the Dox group and basal amounts of intracellular ROS in the cardiomyocytes pre-treated with the bioactive DP and fraction F1, as shown in **Figure 3C**. The quantified bar graph represents their mean fluorescence

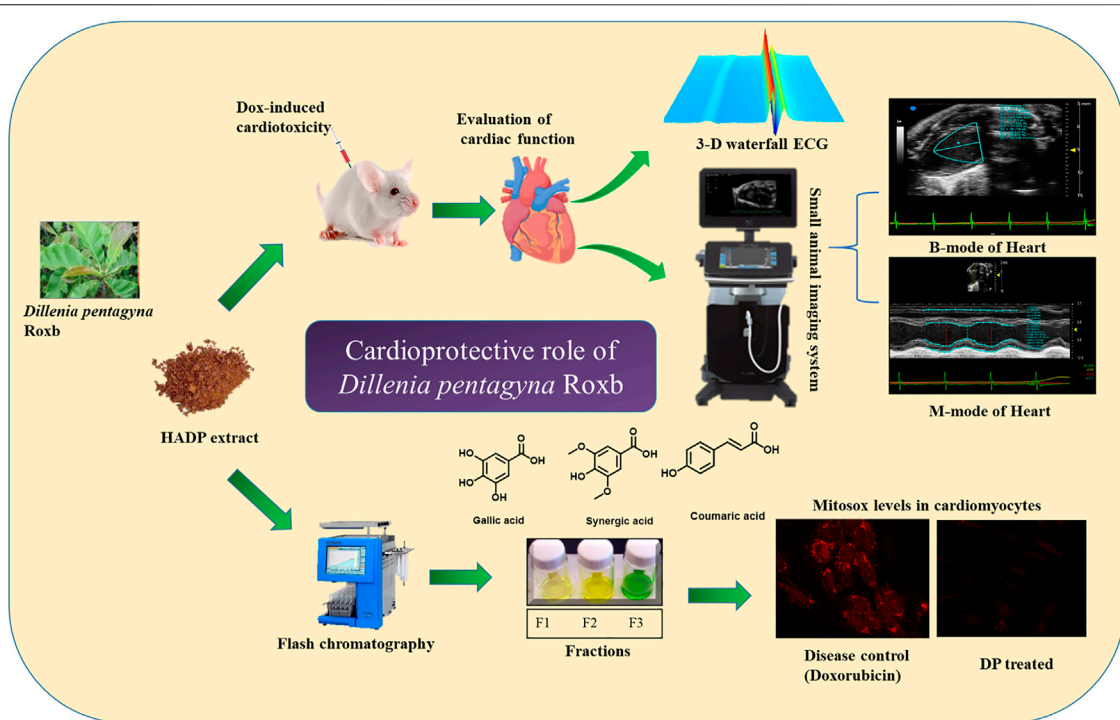


FIGURE 1 | Schematic representation of the proposed study design cardioprotective mechanism by the hydroalcoholic extract of DP.

intensities (MFI) in **Figure 3D**. The Dox-treated group of cardiomyocytes has higher mean fluorescence intensity (MFI: 204 ± 2.0) than the control group (140 ± 9.0).

Whereas the pre-treatment with DP ($12.5 \mu\text{g/ml}$) and F1 ($12.5 \mu\text{g/ml}$) had significantly reduced the ROS levels (143.5 ± 1.5 and 150 ± 2.0 , respectively). Mitochondrial superoxide was assessed using Mitosox red by a confocal microscope. The mean fluorescent intensity in Dox control remarkably increased compared with the control group, where pre-treatment with bioactive fractions attenuated the superoxide generation in mitochondria in **Figures 3E,F**. The results indicated that the cardiomyocytes, upon pre-treatment with the bioactive DP and its fraction F1 even after the induction with Dox, have successfully alleviated the increased ROS levels.

Bioactive Fraction Did Not Compromise the Anticancer Activity of Dox

Both the DP hydroalcoholic extract and fraction F1 were co-treated with Dox ($2.5 \mu\text{M}$) in a cancer cell line (HCT116) to understand if they have any interference. We observed that the cancer cell death was similar in the groups treated with Dox alone and Dox combined with the DP hydroalcoholic extract and fraction (Supplementary Figures S3C,D). Overall, the results indicate that the DP hydroalcoholic extract and fraction F1 had not compromised the Dox anticancer property. However, considering the scalability, cost of production, and effort to green technology contribution, we have opted for the DP hydroalcoholic extract for the *in-vivo* studies.

In-vivo Cardioprotective Role of the Bioactive DP

Acute toxicity studies indicated that the bioactive DP was safe at a dose of 2000 mg/kg in mice, where no toxicity was observed for 14 days a single administration. Therefore, by following the OECD guidelines 425, we have chosen $1/20^{\text{th}}$ (i.e., 100 mg/kg) and $1/10^{\text{th}}$ (200 mg/kg) of the maximum tolerable dose for further studies.

Bioactive DP Hydroalcoholic Extract Attenuated the Myocardial Injury In-vivo

The cardioprotective effect of the bioactive fraction was evaluated in a Dox-induced cardiotoxicity mice model (**Figure 4A**). Electrocardiogram measurements were performed in the various groups to assess the impact of the bioactive DP. A significant decrease in the heart rate (bradycardia) was evidenced in the Dox treated group (394.3 ± 27.43) in comparison to the control mice (499.04 ± 40.49). However, the bioactive DP hydroalcoholic extract treated groups (382.7 ± 59.4 & 447.04 ± 74.7) have significantly improved heart rate than the Dox group. The heart rate of the DP hydroalcoholic extract-treated group was near to the control mice. In **Figure 4B** representative 3D and ECG images of T-wave elevation were observed in the Dox group. T-wave and ST height elevation was found in the disease control, where it was normalized in the treatment groups, as shown in **Figures 4C–E**.

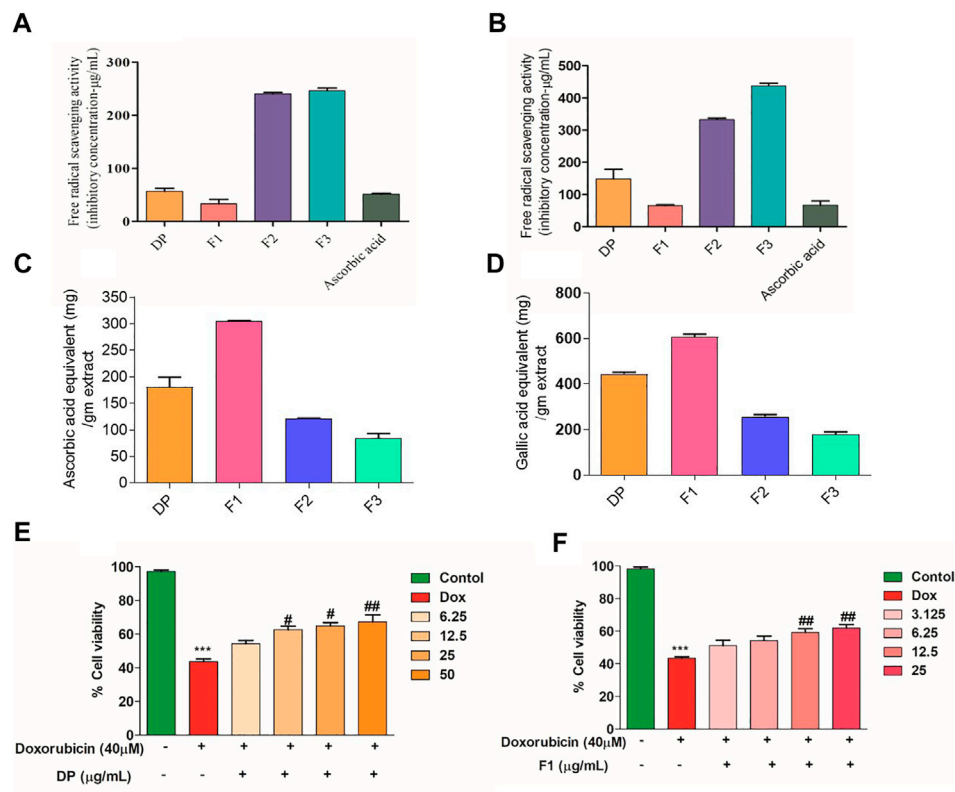


FIGURE 2 | IC₅₀ values of the bioactive fractions in various antioxidant assays. **(A)** ABTS and **(B)** DPPH assay compared with ascorbic acid. **(C)** FRAP assay (equivalent ascorbic acid/gm extract) **(D)** Total phenolic content (Gallic acid equivalent/gm extract). **(E, F)** Cell viability of cardiomyocytes (H9c2) pre-treatment with DP and Fraction F1 along with Dox. Values were expressed as Mean ± SEM (*n* = 3). The data were analyzed by One Way ANOVA using Graph Pad Prism. ****p* < 0.001, and ***p* < 0.01 represents Control vs Dox control. ##*p* < 0.01 and ###*p* < 0.001 represents Dox control vs Treatment groups.

Bioactive DP Hydroalcoholic Extract Alleviates Functional Heart Parameters

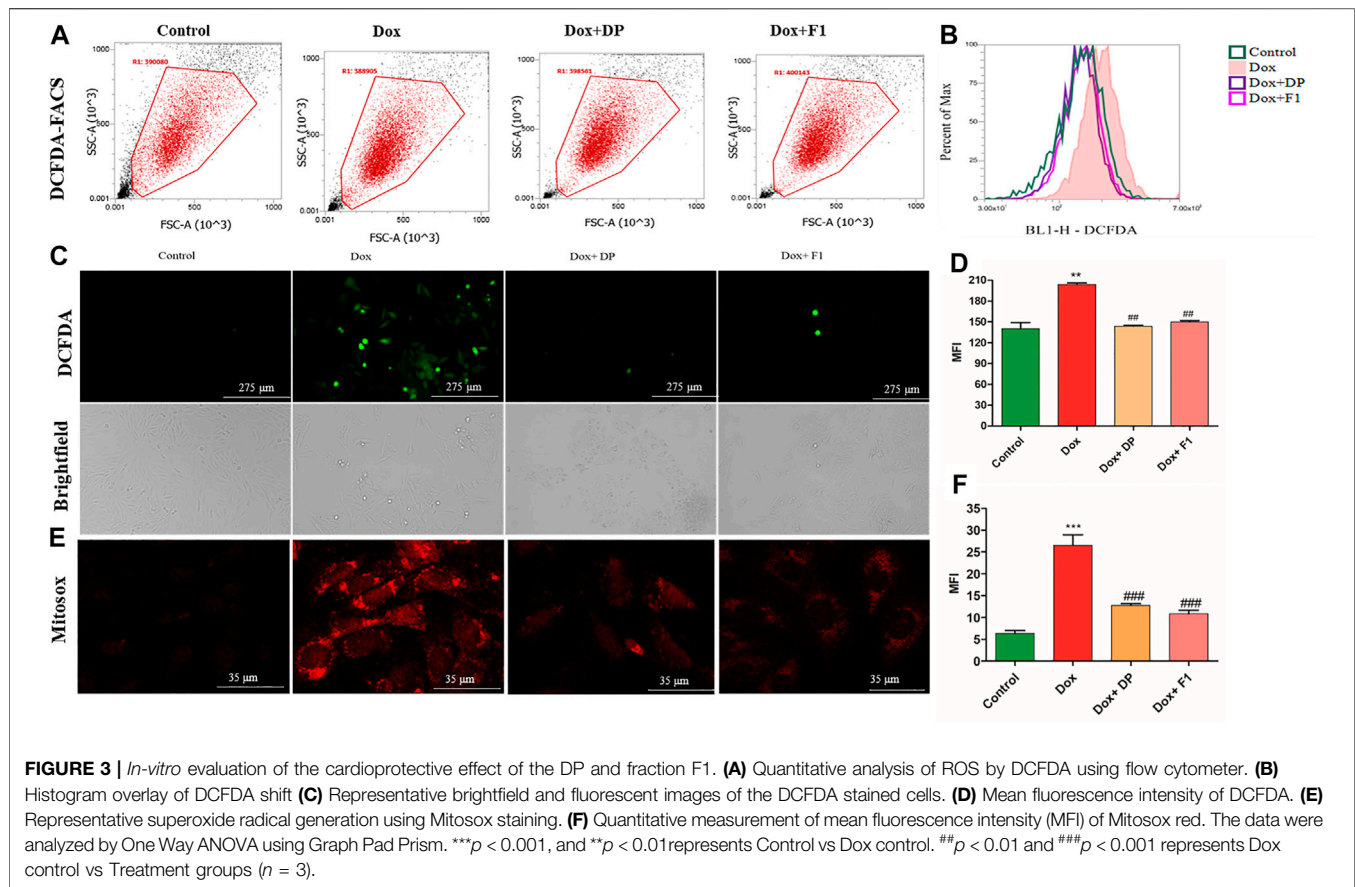
Figure 4F shows the representative M-mode images obtained from the parasternal long-axis view images by using a high-frequency ultrasonography-based electrocardiograph imaging system. The left ventricular (LV) posterior wall thickness, ejection fraction, fractional shortening, cardiac output, and stroke volume of the Dox treated group was decreased compared to the control group (Figures 4D–M). Simultaneously, the bioactive DP hydroalcoholic extract-treated groups have restored cardiac parameters and were found to be near the control group.

Bioactive DP Hydroalcoholic Extract Alleviates Functional Heart Parameters

The mice's body weights at the end of the study indicated that the disease control group had shown remarkably reduced body weights compared to the control group. The DP (100 and 200 mg/kg) pre-treated groups had maintained the body weight to its initial values, as shown in Figure 5A. The heart index (HI), a ratio of heart weight to body weight, was lower in the Dox treated group when compared to the control group. The DP pre-treated group has values almost

near the normal saline group, as shown in Figure 5B. Further, key biomarker enzymes for tissue damage in the heart, i.e., Creatine Kinase isoenzyme-MB (CK-MB) and lactate dehydrogenase (LDH) levels were analyzed. The Dox alone treated mice group has shown an increase in both the enzymes' levels than the control group. This reveals that the Dox treated group elevated oxidative stress where lipid peroxidation causes tissue damage followed by enzymatic heart levels (LDH and CK-MB) increase.

Meanwhile, bioactive DP group mice have significantly reduced the levels compared to the control group, as shown in Figures 5C,D. This indicates the protective role of the bioactive DP in alleviating Dox-induced cardiac tissue damage. Also, the levels of anti-oxidant key regulators GSH and catalase were remarkably increased in the treatment groups, as shown in Figures 5E,F. The tissue MDA and nitric oxide (NO) levels were significantly elevated in the Dox treated groups compared to the control group. Bioactive DP treated groups have decreased the levels in a dose-dependent manner, as shown in Figures 5G,H. Histopathological study of the heart tissue in normal control mice exhibited apparent integrity of the myocardial cell membrane with no evident inflammatory cell infiltration, as shown in Figure 5I. The Dox treated mice group showed necrosis and filtration of the lymphocytes, macrophages, and inflammatory cells along with the vacuolization. In some of the myocytes, the myofibrils were disorganized and evident with clear



space, indicating intracellular edema. Pre-treatment of the bioactive DP (100 and 200 mg/kg) prevented the entry of the inflammatory cells and vacuole changes caused by the Dox treatment.

Bioactive Fractions Attenuate Dox-Induced Cardiotoxicity by Activating Nrf-2 Expression

Nrf-2, a key anti-oxidant transcription factor, plays a vital role in maintaining redox homeostasis under oxidative stress. **Figure 5J** showed treatment with DP alleviated the Dox-induced cardiotoxicity by activating the Nrf-2 expression where the subsequent downstream protein levels were increased *in-vitro*. We found that Keap-1 protein levels were decreased, and Nrf-2 levels were raised in the treatment group in a dose-dependent manner compared with Dox control *in-vivo* (**Figure 5K**). The quantitative analysis SOD-2 and HO-1 protein levels were increased in the treatment group compared with the Dox control group in both *in-vitro* and *in-vivo* shown in **Figures 5L,M**. Overall, results indicated that the bioactive fraction attenuated the Dox-induced cardiotoxicity by the Nrf-2 pathway.

LC-MS (LC-QTOF-ESI-MS) Analysis

Hydroalcoholic extract of DP and the fraction F1 were subjected to characterize the lead compounds responsible for the biological activity. Mass accuracy measurements were observed to be within

the limit of ± 10 PPM. The obtained mass of the molecules/metabolites present in the sample matches with the available literature, as shown in **Tables 1–4**. Chromatogram for the hydroalcoholic extract of DP and its fraction F1 have been portrayed in **Figure 6A**. The samples were screened for identification hits based on screening scores and the targeted identification of plant metabolites using a find-by-formula algorithm. However, it may be concluded that most of the molecules have been observed for the formate and acetate adduct form. Polyphenolic compounds gallic acid, benzoic acid, syringic acid, coumaric acid, protocatechuic aldehyde, mellein, 2-hydroxy xanthone, sinapic acid are active chemical constituents in the hydroalcoholic extract and its fraction F1 as detected in the LC-QTOF-ESI-MS, negative mode (**Tables 1, 3**). However, coumaric acid, cinnamic acid, and umbelliferone are the common active chemical constituents in the hydroalcoholic extract and fraction F1 in the LC-QTOF-ESI-MS analysis in the positive mode, as portrayed in **Tables 2, 4** and represented and the structures illustrated in **Figure 6B**. The proposed cardio protective mechanism of HC has been represented in the **Figure 7**.

DISCUSSION AND CONCLUSION

Recent progress in cancer therapy has increased patients' life expectancy and elevated the cardiac complications in them.

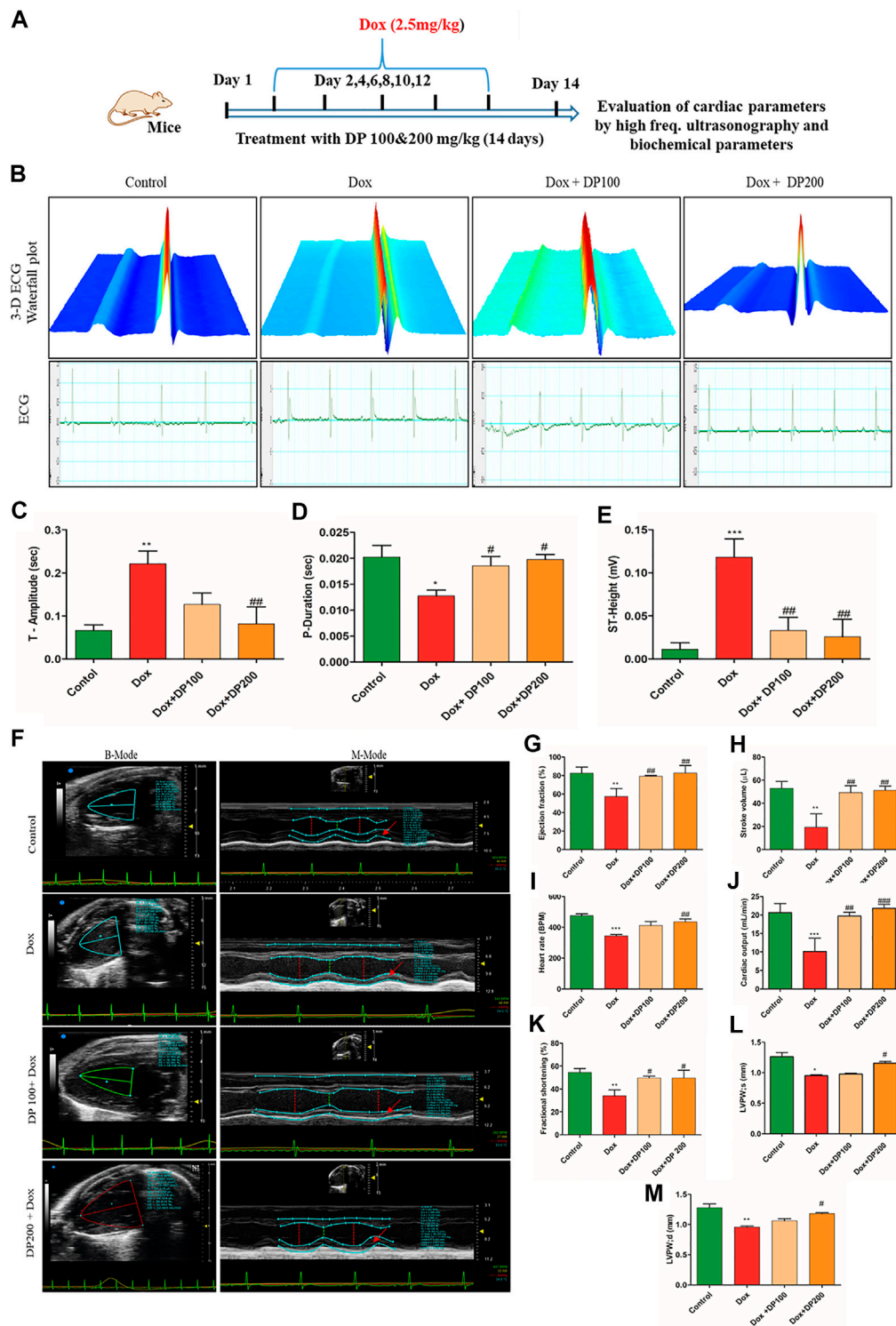


FIGURE 4 | Effect of DP extracts on the electrocardiogram. **(A)** Representative study design for cardioprotective model. **(B)** 3-D representative images of the electrocardiogram with elevated T-wave (I) Control (II) Dox control (III) Dox + DP100 and (IV) Dox + DP 200 **(C)** P-Duration **(D)** T- Amplitude **(E)** ST- Height, where $n = 5$. Effect of DP extract on *in-vivo* cardiac parameters by Vevo Lazer X 3100. **(F)** Representative images of M-Mode (I) control (II) Dox control (III) Dox + DP 100 and (IV) Dox + DP200. **(G)** Ejection fraction. **(H)** Stroke volume. **(I)** Heart rate. **(J)** Cardiac output **(K)** Fractional shortening **(L)** left ventricular posterior wall thickness (systole) **(M)** left ventricular posterior wall thickness (diastole), where $n = 4$. The data were analyzed by One Way ANOVA using Graph Pad Prism. *** $p < 0.001$, ** $p < 0.01$, * $p < 0.05$ represents normal control vs disease control (Dox). # $p < 0.05$ ## $p < 0.01$ and ### $p < 0.001$ represents disease control (Dox) vs treatment groups.

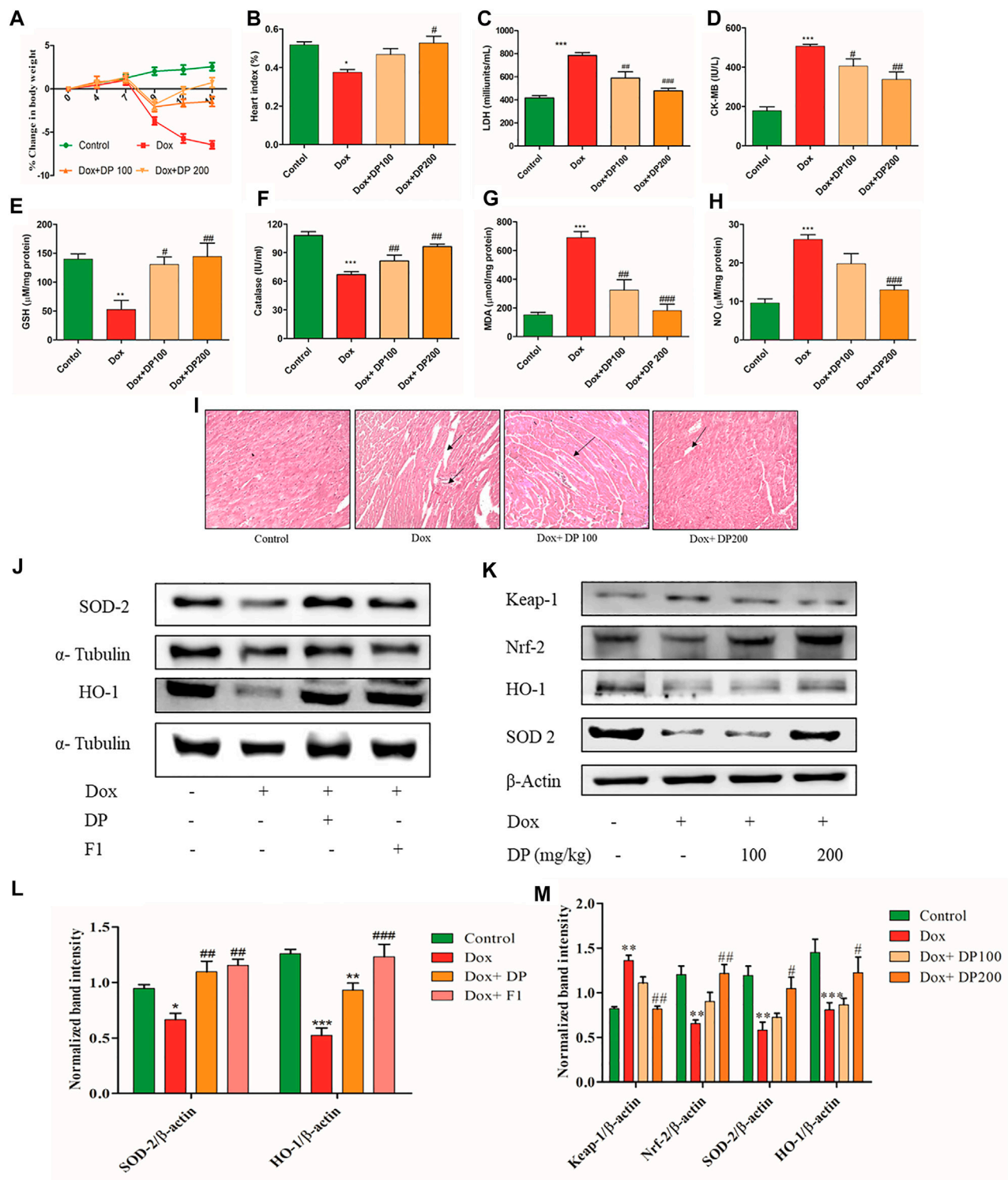


FIGURE 5 | Effect of DP extract on (A) percentage change in body weight (B) Heart index (C) LDH (D) CK-MB (E) GSH (F) catalase (G) MDA and (H) Nitric oxide, where $n = 5$. (I) Histopathology H&E staining of cardiac tissue. (J) *In-vitro* western blot analysis of protein levels of SOD-2 and HO-1 in H9c2 cell line (K) *In-vivo* western blot analysis of SOD-2, Keap-1, Nrf-2, and HO-1. (L) Quantitative analysis of relative protein levels of SOD-2 and HO-1. (M) Quantitative analysis of relative protein levels of KEAP-1, Nrf-2 SOD-2, and HO-1 expression respectively. The data were analyzed by One Way ANOVA and Two Way ANOVA using Graph Pad Prism. *** $p < 0.001$, ** $p < 0.01$, * $p < 0.05$ represents normal control vs disease control (Dox). # $p < 0.05$ ## $p < 0.01$ and ### $p < 0.001$ represents disease control (Dox) vs treatment groups ($n = 3$).

TABLE 1 | QTOF-ESI-MS data of identified plant metabolites from hydroalcoholic extract of DP in negative mode $[M-H]^-$ with the possible molecular formula.

S. No.	Retention time	Name	Molecular formula	Mean measured mass (Da) m/z	Mass (Da)	Diff (Tgt, ppm)	Reference
1	1.035	Gallic acid	C ₇ H ₆ O ₅	169.01	170.12	0.57	Uddin et al. (2020)
2	6.33	Benzoic acid	C ₇ H ₆ O ₂	167.03	122.12	3.47	Yang et al. (2018)
3	6.364	Syringic acid	C ₉ H ₁₀ O ₅	197.04	198.17	3.68	Ding et al. (2017)
4	6.081	Coumaric acid	C ₉ H ₈ O ₃	163.04	164.16	1.21	Rafiee et al. (2020)
5	6.364	Protocatechuic aldehyde	C ₇ H ₆ O ₃	197.04	138.12	5.28	Jiang et al. (2019)
6	5.914	Paeonol	C ₉ H ₁₀ O ₃	165.05	166.17	2.53	Ding et al. (2016)
7	6.447	Hesperetin	C ₁₆ H ₁₄ O ₆	347.07	302.27	6.71	
8	7.063	Mellein	C ₁₀ H ₁₀ O ₃	237.07	178.18	0.83	
9	6.214	Scopoletin	C ₁₀ H ₈ O ₄	237.04	192.16	4.86	
10	0.636	2-Hydroxyxanthone	C ₁₃ H ₈ O ₃	257.04	212.20	-3.27	
11	6.663	Herniarin	C ₁₀ H ₈ O ₃	235.06	176.16	3.61	
12	6.397	Sinapic acid	C ₁₁ H ₁₂ O ₅	223.06	224.21	1.95	Bin Jordan et al. (2020)
13	6.43	Naringenin	C ₁₅ H ₁₂ O ₅	317.06	272.26	5.75	

TABLE 2 | QTOF-ESI-MS data of identified plant metabolites from hydroalcoholic extract of DP in positive mode $[M+H]^+$ with possible molecular formula.

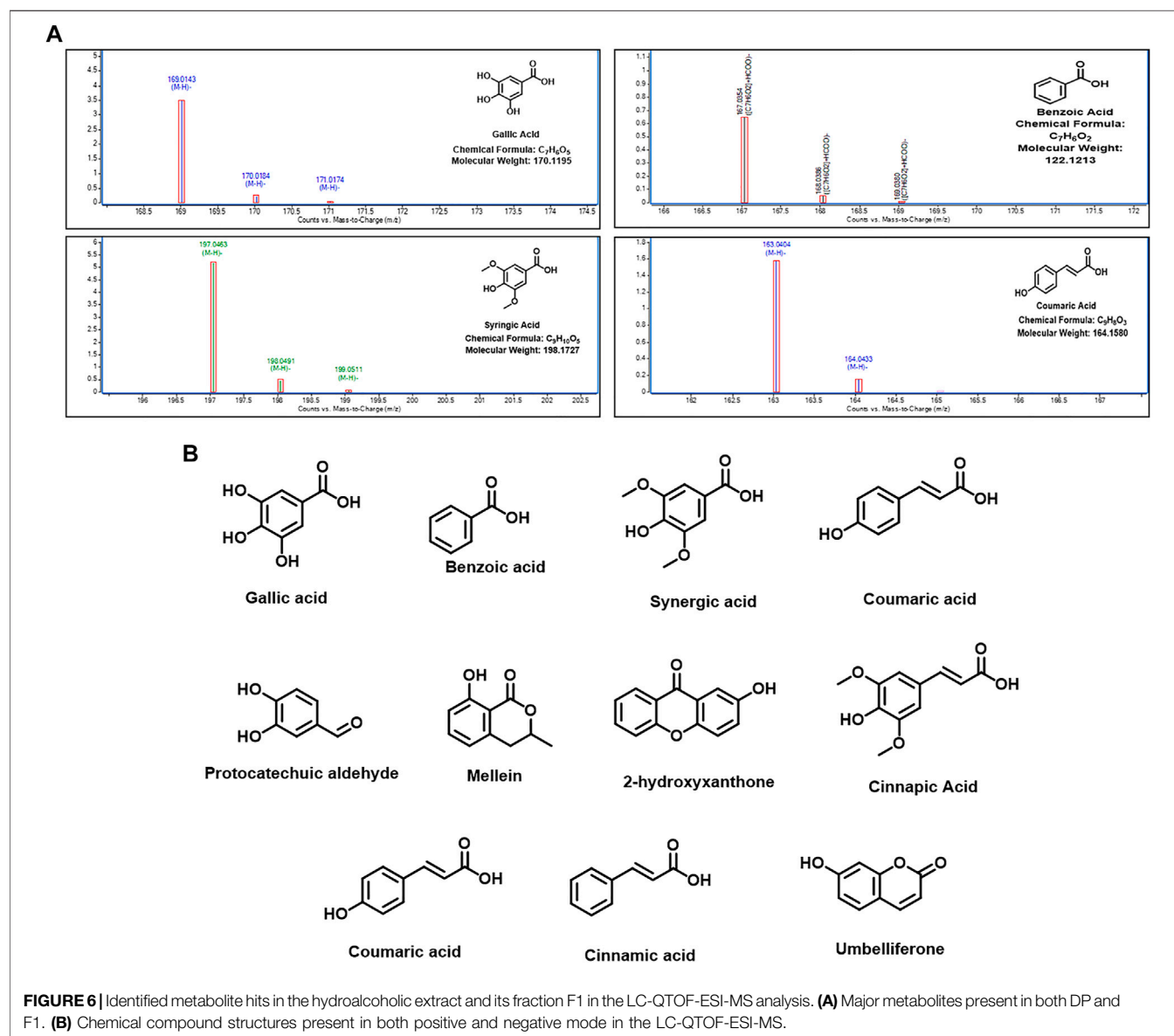
Peak no.	Retention time	Name	Molecular formula	Mean measured mass (Da) m/z	Mass (Da)	Diff (Tgt, ppm)	
1	21.107	Coumaric acid	C ₉ H ₈ O ₃	165.05	192.17	1.45	
2	0.995	Cinnamic acid	C ₉ H ₈ O ₂	149.05	148.16	2.38	
3	5.857	Herniarin	C ₁₀ H ₈ O ₃	177.05	176.16	-2.91	
4	16.279	Umbelliferone	C ₉ H ₆ O ₃	163.03	162.12	2.49	Luo et al. (2018)

TABLE 3 | QTOF-ESI-MS data of identified plant metabolites from fraction F1 in negative mode $[M-H]^-$ with a possible molecular formula.

S. NO.	Retention time	Name	Molecular formula	Mean measured mass (Da) m/z	Mass (Da)	Diff (Tgt, ppm)
1	6.958	Benzoic acid	C ₇ H ₆ O ₂	167.03	122.12	4.43
2	1.047	Gallic acid	C ₇ H ₆ O ₅	169.01	170.12	3.23
3	7.308	Ellagic acid	C ₁₄ H ₆ O ₈	301.00	302.0077	4.83
4	7.008	Syringic acid	C ₉ H ₁₀ O ₅	197.04	198.21	4.31
5	3.046	Protocatechuic aldehyde	C ₇ H ₆ O ₃	137.18	138.12	3.18
6	6.709	Coumaric acid	C ₉ H ₈ O ₃	163.04	164.0481	4.4
7	8.241	Dihydroquercetin	C ₁₅ H ₁₂ O ₇	303.05	304.25	4.74
8	7.358	Epi-catechin-3-gallate (ECG)	C ₂₂ H ₁₈ O ₁₀	441.08	442.40	4.76
9	10.672	Hispidulin	C ₁₆ H ₁₂ O ₆	299.05	462.40	5.29
10	0.831	2-Hydroxyxanthone	C ₁₃ H ₈ O ₃	257.04	212.20	-4.78
11	1.83	2,3-Dihydroxybenzoic acid	C ₇ H ₆ O ₄	153.01	154.12	3.73
12	10.838	Cirsilineol	C ₁₈ H ₁₆ O ₇	343.08	344.30	3.56
13	1.813	Catechol	C ₆ H ₆ O ₂	109.03	110.10	3.98
14	11.721	Formononetin	C ₁₆ H ₁₂ O ₄	327.08	268.26	5.16
15	6.909	Hydroxycaffeic acid	C ₉ H ₈ O ₅	241.03	196.16	2.96
16	10.072	Cirsimaritin	C ₁₇ H ₁₄ O ₆	359.07	314.29	5.34
17	10.072	Rosmarinic acid	C ₁₈ H ₁₆ O ₈	359.07	360.31	4.66
18	6.942	Umbelliferone	C ₉ H ₆ O ₃	207.03	162.14	5.62
19	0.648	5,6-Dihydroxy-7,8,3',4'-tetramethoxyflavone	C ₁₉ H ₁₈ O ₈	419.09	406.34	2.27
20	6.692	Eriodictyol 7-O-glucoside	C ₂₁ H ₂₂ O ₁₁	509.13	450.39	5.96
21	10.672	Dihydroxyflavone	C ₁₅ H ₁₀ O ₄	299.05	254.24	5.83
22	12.387	Glycyrrin	C ₂₂ H ₂₂ O ₆	427.14	382.40	3.03
23	6.709	Citropten	C ₁₁ H ₁₀ O ₄	265.07	206.19	3.97
24	7.341	Caffeic acid	C ₉ H ₈ O ₄	225.04	180.16	3.42
25	7.441	Sinapic acid	C ₁₁ H ₁₂ O ₅	223.06	224.06	4
26	7.441	Mellein	C ₁₀ H ₁₀ O ₃	223.06	178.18	5.03

TABLE 4 | QTOF-ESI-MS data of identified plant metabolites from fraction F1 in positive mode $[M+H]^+$ with the possible molecular formula.

Peak no.	Retention time	Name	Molecular formula	Mean measured mass (Da) m/z	Mass (Da)	Diff (Tgt, ppm)
1	21.107	Coumaric acid	$C_9H_8O_3$	165.05	192.17	1.45
2	5.857	Herniarin	$C_{10}H_8O_3$	177.05	176.16	-2.91
3	16.279	Umbelliferone	$C_9H_6O_3$	163.03	162.12	2.49



Doxorubicin (Dox) is a widely known chemotherapeutic drug, which induces oxidative stress, leading to free radicals, subsequently causing oxidative damage to the cardiomyocytes (Pugazhendhi et al., 2018). Dox-induced cardiotoxicity model has been successfully demonstrated in various cultured cell lines (Chan et al., 1996), isolated heart cultures, whole animal models, and humans (Singal

et al., 1987). Identification and evaluation of safer bioactive molecules/fractions, which help alleviate the existing chemotherapeutic drugs' cardiotoxic effect, would benefit cancer patients.

Dillenia pentagyna Roxb. is a nutritionally and medicinally valued plant distributed widely in South Asian countries. The fruits and bark of the plant were used for the treatment of various

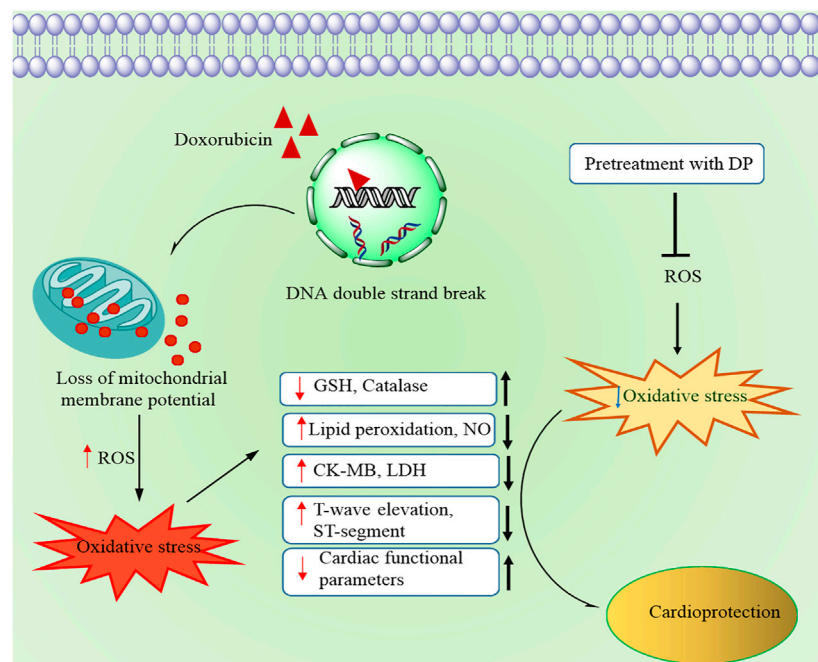


FIGURE 7 | Schematic representation of the proposed cardioprotective mechanism by the hydroalcoholic extract of DP

ailments. In the current study, we intend to evaluate the anti-oxidant role in alleviating the Dox-induced cardiotoxicity both *in-vitro* and *in-vivo*. The preliminary anti-oxidant tests suggested that the *Dillenia pentagyna* Roxb's hydroalcoholic extract had high anti-oxidant chemical compounds. Therefore, the bioactive DP was further subjected to fractionation to obtain a purified bioactive fraction (Fraction-1).

However, anti-oxidant chemical tests indicated that both the DP and Fraction-1 have an equivalent amount of anti-oxidant compounds, and fraction F1 has high phenolic content than the crude DP. The pretreatment with DP and F1 has shown the increased cell viability in H9c2 cells indicating the protective activity. Multiple pieces of evidence revealed that the reactive oxygen species (ROS) has a direct implication in the pathogenesis of Dox-induced cardiotoxicity (Hwang et al., 2008; Sun et al., 2015). *In-vitro* DCFDA and Mitosox staining revealed that the Dox treated cardiomyocytes (H9c2) have high levels of reactive oxygen species, which is evident by the fluorescence signal in both the flow cytometric and microscopic analysis. Simultaneously, the cells treated with the bioactive DP have shown a less amount of fluorescence, indicating the reduced ROS. The previous reports suggest that anti-oxidants can modulate the anticancer drug efficacy in cancer treatment (Conklin, 2004). However, the treatment with DP and F1 and Dox on the cancer cell line did not compromise the anticancer activity of Dox in the cancer cell line.

When evaluated by the ECG, the cardioprotective activity of the bioactive DP evidenced normalization of ECG changes, most notably ST height and T-wave elevation. An altered ECG was due to the propagation of lipid peroxidation in the Dox treated mice group as the bioactive fractions reduced lipid peroxidation, which could be responsible for the normalized T-wave elevation and ST-

height. Electrocardiographic (ECG) imaging is a non-invasive method to study the various cardiac parameters. In the current study, we have used the electrocardiography-based imaging technique to study the bioactive DP's cardioprotective effect in Dox-induced cardiotoxicity models. The application of such techniques provides reliable information about the cardiac profile. Dox causes a decrease in left ventricular wall thickness (Prathumsap et al., 2020), cardiac functional parameters ejection fraction, fractional shortening, stroke volume, cardiac output, and heart rate. Our findings of increased cardiac functional parameters indicated that DP had reduced the toxic effects of Dox-induced cardiotoxicity. In our study, *in vivo* anti-oxidant markers like GSH and catalase were also elevated, indicating the endogenous anti-oxidant defense system. Cardiac tissue biomarkers like Creatine kinase isoenzyme-MB (CKMB), Lactate dehydrogenase (LDH) were released when damage to the cardiomyocytes. We found that the Dox treatment has increased their levels in the Dox group, whereas the pre-treatment significantly decreased the levels with bioactive DP, indicating the attenuation of the cardiac damage by Dox. The same was further supported by estimating tissue-based lipid peroxidation end product MDA and the nitrite levels. We found that the levels were significantly decreased, indicating that treatment with DP inhibited lipid peroxidation.

Nuclear factor (erythroid-derived 2)-like 2 (Nrf-2), a redox-sensitive transcription factor regulating various cellular responses to electrophilic/oxidative stress. It has previously been revealed the role of Nrf-2 in the detoxification process in cardiac cells (Howden, 2013). Therefore, growing evidence suggested that Nrf-2 may target Dox-induced cardiotoxicity treatment (Tomlinson et al., 2019; Zhang et al., 2020). Our study results indicated that treatment

with the bioactive DP increased the expression of Nrf-2 a critical anti-oxidant regulator of oxidative stress, by decreasing its negative regulator Keap-1 expression. The downstream proteins expression like SOD-2 and HO-1 were elevated, indicating the rise of anti-oxidant enzyme expression that counteracts the produced ROS in H9c2 cell line and *in vivo* anti-oxidant enzyme expression that neutralizes the produced ROS in H9c2 cell line and *in-vivo* evident from the western blot analysis. This proves that the bioactive DP ameliorated Dox-induced oxidative stress.

It is evident from this study that identified metabolite hits gallic acid, benzoic acid, syringic acid, coumaric acid, protocatechuic aldehyde, mellein, 2-hydroxy xanthone, sinapic acid, coumaric acid, cinnamic acid, and umbelliferone are phenolic containing chemical constituents present in hydroalcoholic extract DP and its F1 fraction in the LC-QTOF-ESI-MS. Therefore, it may be concluded that hydroalcoholic extract and its fraction F1 are enriched with polyphenols and have shown good cardioprotective activity in the preclinical screening model.

Taken together, our data showed convincing evidence that pre-treatment with DP and F1 alleviated the cardiotoxicity *in-vitro*. *In-vivo* mice model also indicated that the DP caused no significant effect to the body weights, meanwhile restoring the cardiac parameters nearly equal to the normal control group. Pretreatment with DP attenuated the Dox-induced cardiotoxicity by reducing the oxidative stress, and the Nrf-2 pathway mediated the cardioprotection. Further *in-vivo* studies are required to understand the role of fraction F1, and extensive studies have to be performed to know the exact molecules involved in the protective effect of the DP against Dox-induced cardiotoxicity.

DATA AVAILABILITY STATEMENT

The original contributions presented in the study are included in the article/**Supplementary Material**, further inquiries can be directed to the corresponding authors.

REFERENCES

- Abramović, H., Grobin, B., Poklar, N., and Cigić, B. (2017). The methodology applied in DPPH, ABTS and folin-ciocalteu assays has a large influence on the determined antioxidant potential. *Acta Chim. Slov.* 64, 491–499. doi:10.17344/acs.2017.3408
- Alizadeh Behbahani, B., and Shahidi, F. (2019). Melissa officinalis essential oil: chemical compositions, antioxidant potential, total phenolic content and antimicrobial activity. *Nutr. Food Sci. Res.* 6, 17–25. doi:10.29252/nfsr.6.1.17
- Battu, S., Afroz, S., Giddaluru, J., Naz, S., Huang, W., Khumukcham, S. S., et al. (2018). Amino acid starvation sensing dampens IL-1 β production by activating ribocustering and autophagy. *PLoS Biol.* 16, e2005317. doi:10.1371/journal.pbio.2005317
- Bin Jordan, Y. A., Ansari, M. A., Raish, M., Alkharfy, K. M., Ahad, A., Al-Jenoobi, F. I., et al. (2020). Sinapic acid ameliorates oxidative stress, inflammation, and apoptosis in acute doxorubicin-induced cardiotoxicity via the NF- κ B-mediated pathway. *Biomed. Res. Int.* 2020, 3921796.
- Bray, F., Ferlay, J., Soerjomataram, I., Siegel, R. L., Torre, L. A., and Jemal, A. (2018). Global cancer statistics 2018: GLOBOCAN estimates of incidence and mortality worldwide for 36 cancers in 185 countries. *CA Cancer J. clin.* 68, 394–424. doi:10.3322/caac.21492

ETHICS STATEMENT

The animal study was reviewed and approved by the Institutional Animal Ethics Committee (IAEC), Guwahati, India (NIPS/NIPER/18/029).

AUTHOR CONTRIBUTIONS

VN, RG: Design and guidance for the whole experiment. KT, KK, and JK performed experiments. BG, EP: operation of the animal experiment. KT, DP: Interpretation of data and drafted, edited the manuscript. PK provided phytochemical analysis. UM, VN: acquired funding.

FUNDING

The authors would also like to recognize the National Mission on Himalayan Studies (NMHS) Ref No: GBPI/NMHS-2017-18/HSF-02, India, for supporting our research. The authors would also like to acknowledge Agilent Technologies, Bangalore, for their technical support.

ACKNOWLEDGMENTS

The authors would like to acknowledge the Department of Pharmaceuticals (DOP), Ministry of Chemicals and Fertilizers, India.

SUPPLEMENTARY MATERIAL

The Supplementary Material for this article can be found online at: <https://www.frontiersin.org/articles/10.3389/fphar.2021.624706/full#supplementary-material>

- Brown, S.-A., Sandhu, N., and Herrmann, J. (2015). Systems biology approaches to adverse drug effects: the example of cardio-oncology. *Nat. Rev. Clin. Oncol.* 12, 718–731. doi:10.1038/nrclinonc.2015.168
- Chan, E. M., Thomas, M. J., Bandy, B., and Tibbits, G. F. (1996). Effects of doxorubicin, 4'-epirubicin, and antioxidant enzymes on the contractility of isolated cardiomyocytes. *Can. J. Physiol. Pharmacol.* 74, 904–910. doi:10.1139/y96-091
- Conklin, K. A. (2004). Cancer chemotherapy and antioxidants. *J. Nutr.* 134, 3201S–3204S. doi:10.1093/jn/134.11.3201S
- Cuadrado, A., Rojo, A. I., Wells, G., Hayes, J. D., Cousin, S. P., Rumsey, W. L., et al. (2019). Therapeutic targeting of the NRF2 and KEAP1 partnership in chronic diseases. *Nat. Rev. Drug Discov.* 18, 295–317. doi:10.1038/s41573-018-0008-x
- Ding, S. K., Wang, L. X., Guo, L. S., Luo, P., Du, J. J., Zhao, Z. L., et al. (2017). Syringic acid inhibits apoptosis pathways via downregulation of p38MAPK and JNK signaling pathways in H9c2 cardiomyocytes following hypoxia/reoxygenation injury. *Mol. Med. Rep.* 16 (2), 2290–2294.
- Ding, Y., Li, Q., Xu, Y., Chen, Y., Deng, Y., Zhi, F., et al. (2016). Attenuating oxidative stress by paeonol protected against acetaminophen-induced hepatotoxicity in mice. *PLoS One* 11 (5), e0154375.
- Gangrade, A., Gawali, B., Jodi, P. K., Naidu, V. G., and Mandal, B. B. (2020). Photo-electro active nanocomposite silk hydrogel for spatiotemporal controlled release of chemotherapeutics: an *In Vivo* approach towards suppressing

- solid tumor growth. *ACS Appl. Mater. Inter.* 12 (25), 27905–27916. doi:10.1021/acsami.0c02470
- Howden, R. (2013). Nrf2 and cardiovascular defense oxid. *Med. Cel. Longevity* 2013, 104308. doi:10.1155/2013/104308
- Huang, Q., Zhou, H. J., Zhang, H., Huang, Y., Hinojosa-Kirschenbaum, F., Fan, P., et al. (2015). Thioredoxin-2 inhibits mitochondrial reactive oxygen species generation and apoptosis stress kinase-1 activity to maintain cardiac function. *Circulation* 131, 1082–1097. doi:10.1161/circulationaha.114.012725
- Hwang, J.-T., Kwon, D. Y., Park, O. J., and Kim, M. S. (2008). Resveratrol protects ROS-induced cell death by activating AMPK in H9c2 cardiac muscle cells. *Genes Nutr.* 2, 323–326. doi:10.1007/s12263-007-0069-7
- Jiang, L., Zeng, H., Ni, L., Qi, L., Xu, Y., Xia, L., et al. (2019). HIF-1 α preconditioning potentiates antioxidant activity in ischemic injury: the role of sequential administration of dihydrotanshinone I and protocatechuic aldehyde in cardioprotection. *Antioxid. Redox Signal.* 31 (3), 227–242.
- Koul, A., Goyal, R., and Bharati, S. (2014). Protective effect of *Azadirachta indica* A. Juss against doxorubicin-induced cardiac toxicity in tumour bearing mice. *Indian J. Exp. Biol.* 52 (4), 323–331.
- Luo, H., Fan, Z., Xiang, D., Jiang, Z., Zhang, W., Gao, L., et al. (2018). The protective effect of umbelliferone ameliorates myocardial injury following ischemia-reperfusion in the rat through suppression NLRP3 inflammasome and upregulating the PPAR- γ . *Mol. Med. Rep.* 17 (2), 3404–3410.
- Müller, L., Fröhlich, K., and Böhm, V. (2011). Comparative antioxidant activities of carotenoids measured by ferric reducing antioxidant power (FRAP), ABTS bleaching assay (aTEAC), DPPH assay and peroxyl radical scavenging assay. *Food Chem.* 129, 139–148. doi:10.1016/j.foodchem.2011.04.045
- Ohkawa, H., Ohishi, N., and Yagi, K. (1979). Assay for lipid peroxides in animal tissues by thiobarbituric acid reaction. *Anal. Biochem.* 95, 351–358. doi:10.1016/0003-2697(79)90738-3
- Owen, J. B., and Butterfield, D. A. (2010). “Measurement of oxidized/reduced glutathione ratio,” in *Protein Misfolding and Cellular Stress in Disease and Aging* (New York, NY: Springer), 269–277. doi:10.1007/978-1-60761-756-3_18
- Peoples, J. N., Saraf, A., Ghazal, N., Pham, T. T., and Kwong, J. Q. (2019). Mitochondrial dysfunction and oxidative stress in heart disease. *Exp. Mol. Med.* 51, 1–13. doi:10.1038/s12276-019-0355-7
- Prathumsap, N., Shinlapawittayatorn, K., Chattipakorn, S. C., and Chattipakorn, N. (2020). Effects of doxorubicin on the heart: From molecular mechanisms to intervention strategies. *Eur. J. Pharmacol.* 866, 172818. doi:10.1016/j.ejphar.2019.172818
- Pugazhendhi, A., Edison, T. N. J. I., Velmurugan, B. K., Jacob, J. A., and Karuppusamy, I. (2018). Toxicity of doxorubicin (Dox) to different experimental organ systems. *Life Sci.* 200, 26–30. doi:10.1016/j.lfs.2018.03.023
- Rafiee, Z., Moaiedi, M. Z., Gorji, A. V., and Mansouri, E. (2020). *p*-Coumaric acid mitigates doxorubicin-induced nephrotoxicity through suppression of oxidative stress, inflammation and apoptosis. *Arch. Med. Res.* 51 (1), 32–40.
- Rugo, H. S., Olopade, O. I., Demichele, A., Yau, C., van 't Veer, L. J., Buxton, M. B., et al. (2016). Adaptive randomization of veliparib-carboplatin treatment in breast cancer. *N. Engl. J. Med.* 375, 23–34. doi:10.1056/nejmoa1513749
- Saiful Yazan, L., and Armanian, N. (2014). Dilleniaceae: a review of the traditional uses, active constituents and pharmacological properties from pre-clinical studies. *Pharm. Biol.* 52, 890–897. doi:10.3109/13880209.2013.872672
- Sharma, H. K., Chhangte, L., and Dolui, A. K. (2001). Traditional medicinal plants in Mizoram, India. *Fitoterapia* 72, 146–161. doi:10.1016/s0367-326x(00)00278-1
- Sheibani, M., Nezamoleslami, S., Faghir-Ghanesefat, H., Hossein Emami, A., and Dehpour, A. R. (2020). Cardioprotective effects of dapson against doxorubicin-induced cardiotoxicity in rats. *Cancer Chemother. Pharmacol.* 85, 563–571. doi:10.1007/s00280-019-04019-6
- Singal, P., Deally, C., and Weinberg, L. (1987). Subcellular effects of adriamycin in the heart: a concise review. *J. Mol. Cell. Cardiol.* 19, 817–828. doi:10.1016/s0022-2828(87)80392-9
- Sridhar, K., and Charles, A. L. (2019). *In vitro* antioxidant activity of Kyoho grape extracts in DPPH and ABTS assays: Estimation methods for EC50 using advanced statistical programs. *Food Chem.* 275, 41–49. doi:10.1016/j.foodchem.2018.09.040
- Sun, L., Fan, H., Yang, L., Shi, L., and Liu, Y. (2015). Tyrosol prevents ischemia/reperfusion-induced cardiac injury in H9c2 cells: involvement of ROS, Hsp70, JNK and ERK, and apoptosis. *Molecules* 20, 3758–3775. doi:10.3390/molecules20033758
- Tan, T. C., and Scherrer-Crosbie, M. (2014). Cardiac complications of chemotherapy: role of imaging. *Curr. Treat. Options Cardiovasc. Med.* 16, 296. doi:10.1007/s11936-014-0296-3
- Tene, K., Kumar, K., Pemmaraju, D. B., Kumar, J., Shantanu, P. A., Gogoi, R., et al. (2020). Ameliorative effect of *Dillenia indica* fruits against doxorubicin-induced cardiomyocyte toxicity. *Adv. Traditional Med.* doi:10.1007/s13596-020-00510-1
- Tomlinson, L., Lu, Z. Q., Bentley, R. A., Colley, H. E., Murdoch, C., Webb, S. D., et al. (2019). Attenuation of doxorubicin-induced cardiotoxicity in a human *in vitro* cardiac model by the induction of the NRF-2 pathway. *Biomed. Pharmacother.* 112, 108637. doi:10.1016/j.biopha.2019.108637
- Uddin, S. J., Afroz, M., Zihad, S. M. N. K., Rahman, M. S., Akter, S., Khan, I. N., et al. (2020). A systematic review on anti-diabetic and cardioprotective potential of gallic acid: a widespread dietary phytoconstituent. *Food Rev. Int.*, 1–20.
- Van Meerloo, J., Kaspers, G. J. L., and Cloos, J. (2011). “Cell sensitivity assays: the MTT assay,” in *Cancer Cell Culture*. (New York, NY: Springer), 237–245. doi:10.1007/978-1-61779-080-5_20
- Wang, P., Geng, J., Gao, J., Zhao, H., Li, J., Shi, Y., et al. (2019). Macrophage achieves self-protection against oxidative stress-induced ageing through the Mst-Nrf2 axis. *Nat. Commun.* 10, 1–16. doi:10.1038/s41467-019-08680-6
- Xu, S., Wang, Y., Yu, M., Wang, D., Liang, Y., Chen, Y., et al. (2020). LongShengZhi capsule inhibits doxorubicin-induced heart failure by anti-oxidative stress. *Biomed. Pharmacother.* 123, 109803. doi:10.1016/j.biopha.2019.109803
- Yadav, R. K., and Srivastava, S. K. (2014). Monitoring *in vitro* phytochemical analysis of some diabetic plants and its utilization. *Ann. Phytomedicine* 3, 35–39.
- Yang, X.-J., Dang, B., and Fan, M.-T. J. M. (2018). Free and bound phenolic compound content and antioxidant activity of different cultivated blue highland barley varieties from the Qinghai-Tibet Plateau. *Molecules* 23 (4), 879.
- Zhang, X., Hu, C., Kong, C.-Y., Song, P., Wu, H.-M., Xu, S.-C., et al. (2020). FNDC5 alleviates oxidative stress and cardiomyocyte apoptosis in doxorubicin-induced cardiotoxicity via activating AKT. *Cell Death Differ* 27, 540–555. doi:10.1038/s41418-019-0372-z

Conflict of Interest: The authors declare that the research was conducted in the absence of any commercial or financial relationships that could be construed as a potential conflict of interest.

Copyright © 2021 Tene, Kalyan Kumar, Basveshwar, Eswara Rao, Jagadeesh Kumar, kumar, Pemmaraju, Murty, Gogoi and Naidu. This is an open-access article distributed under the terms of the Creative Commons Attribution License (CC BY). The use, distribution or reproduction in other forums is permitted, provided the original author(s) and the copyright owner(s) are credited and that the original publication in this journal is cited, in accordance with accepted academic practice. No use, distribution or reproduction is permitted which does not comply with these terms.



***Turbina oblongata* Protects Against Oxidative Cardiotoxicity by Suppressing Lipid Dysmetabolism and Modulating Cardiometabolic Activities Linked to Cardiac Dysfunctions**

Ochuko L. Erukainure¹, Chika I. Chukwuma², Motlalepula G. Matsabisa^{1*}, Miranda T. Javu¹, Veronica F. Salau³, Neil A. Koorbanally⁴ and Md. Shahidul Islam³

¹Department of Pharmacology, Faculty of Health Sciences, School of Clinical Medicine, University of the Free State, Bloemfontein, South Africa, ²Center for Quality of Health and Living, Faculty of Health and Environmental Sciences, Central University of Technology, Bloemfontein, South Africa, ³Department of Biochemistry, School of Life Sciences, University of KwaZulu-Natal, Durban, South Africa, ⁴School of Chemistry and Physics, University of KwaZulu-Natal, Durban, South Africa

OPEN ACCESS

Edited by:

Michael Heinrich,
UCL School of Pharmacy,
United Kingdom

Reviewed by:

Ramesh Bhonde,
Dr. D. Y. Patil Vidyapeeth, India
Bianca Seminotti,
Federal University of Rio Grande do
Sul, Brazil

*Correspondence:

Motlalepula G. Matsabisa
matsabisamg@ufs.ac.za

Specialty section:

This article was submitted to
Ethnopharmacology,
a section of the journal
Frontiers in Pharmacology

Received: 27 September 2020

Accepted: 26 April 2021

Published: 20 May 2021

Citation:

Erukainure OL, Chukwuma CI,
Matsabisa MG, Javu MT, Salau VF,
Koorbanally NA and Islam MS (2021)
Turbina oblongata Protects Against
Oxidative Cardiotoxicity by
Suppressing Lipid Dysmetabolism and
Modulating Cardiometabolic Activities
Linked to Cardiac Dysfunctions.
Front. Pharmacol. 12:610835.
doi: 10.3389/fphar.2021.610835

Cardiotoxicity leading to cardiovascular dysfunction and ultimately cardiac failure remains a major global health issue irrespective of race, age and country. Several factors including lipotoxicity, oxidative imbalance, exacerbated angiotensin-converting enzyme (ACE) activity and altered bioenergetics have been implicated in the pathophysiology of cardiovascular diseases. *Turbina oblongata* (E. Mey. ex Choisy) A. Meeuse is among the medicinal plants commonly used traditionally in the treatment and management of various ailments including cardiovascular dysfunctions in South Africa. In the present study, *T. oblongata* was investigated for its cardioprotective mechanism on oxidative-mediated cardiotoxicity by determining its effect on redox imbalance, purinergic and cholinergic dysfunction, and ACE activity as well as lipid dysmetabolism and pathways in iron-induced oxidative cardiac injury. Oxidative injury was induced *ex vivo* in freshly isolated heart by incubating with 0.1 mM FeSO₄. Treatment was done by co-incubating with *T. oblongata* extract or gallic acid which served as the standard antioxidant. Induction of oxidative cardiac injury led to significant depleted levels of glutathione, triglyceride, HDL-cholesterol, superoxide, catalase and ENTPDase activities, with concomitant elevated levels of malondialdehyde, cholesterol, LDL-cholesterol, ACE, acetylcholinesterase, ATPase and lipase activities. These levels and activities were significantly reversed following treatment with *T. oblongata*. Induction of oxidative injury also caused alterations in lipid metabolites, with concomitant activation of beta oxidation of very long chain fatty acids, plasmalogen synthesis and mitochondrial beta-oxidation of long chain saturated fatty acids pathways. Some of the altered metabolites were restored following treatment with *T. oblongata*, with concomitant inactivation of beta oxidation of very long chain fatty acid pathway. These results indicate the cardioprotective effect of *T. oblongata* against oxidative-mediated cardiotoxicity. This is evidenced by its ability to mitigate lipotoxicity and modulate dysregulated cardiometabolic activities as portrayed by

its antioxidative activity and suppressive effects on ACE, acetylcholinesterase and lipase activities, while modulating cardiac lipid dysmetabolism.

Keywords: cardiotoxicity, lipid dysmetabolism, metabolomics, *turbina oblongata*, cardiometabolism

INTRODUCTION

Cardiovascular dysfunctions leading to cardiovascular failure has been linked to global early mortalities, with oxidative stress arising from disordered cardiac bioenergetics playing a triggering role (Poulter, 2003; Wold et al., 2005; Li et al., 2019). This is often depicted by cardiac lipid dysmetabolism which is characterized by hyperlipidemia as well as defects in beta-oxidation pathway and mitochondrial oxidative phosphorylation (Antozzi and Zeviani, 1997). Fatty acids (FAs) have been reported as a major energy source for the heart, as they are estimated to meet over 70% of the heart's energy needs (Drosatos and Schulze, 2013). Alteration in cardiac FAs and their metabolism leading to lipotoxicity has been implicated among the pathomechanism of cardiovascular dysfunctions (Erukainure et al., 2020b; Salau et al., 2020b). Exacerbated activities of cardiac lipase and angiotensin-converting enzyme (ACE), as well as altered cardiac supply of triglycerides from the liver and accumulation of cholesterol in the heart are major contributing factors of lipotoxicity. Lipotoxicity has been linked to increased production and accumulation of free radicals leading to oxidative stress, when the latter overwhelms the cardiac endogenous antioxidant system (Jiménez-González et al., 2020). This crosstalk between lipotoxicity and oxidative stress presents pathogenic mechanisms and progression of cardiotoxicity and other cardiovascular dysfunctions, ultimately leading to heart failure.

Turbina oblongata is among the medicinal plants commonly used traditionally in the treatment and management of various ailments in South Africa. It is a perennial herb belonging to the Convolvulaceae family and widely distributed in Botswana, Swaziland, Malawi, Tanzania, Zimbabwe and South Africa (Srivastava and Rauniyar, 2020). In South Africa, the plant is commonly found in all provinces except the Western Cape and it is locally referred to as *ubhoqo* (Semenya et al., 2018; Srivastava and Rauniyar, 2020). Its other synonyms are *Ipomoea atherstonei*, *Ipomoea lambtoniana*, *Ipomoea oblongata* and *Ipomoea randii* (Foden and Potter, 2005). The plant leaves have been reported for their wound healing properties and anticancer activities (Hutchings et al., 1996; Kose et al., 2015). The plant is also traditionally used in the treatment of diarrhea, respiratory infections, hypertension, impotency, renal disease, and sexually transmitted infections (Srivastava and Rauniyar, 2020). These properties can be attributed to its phytochemical constituents which have been reported to consist of flavonoids, terpenoids, glycosides, steroids, anthocyanins, and alkaloids.

The present study investigated the cardioprotective mechanism of *T. oblongata* on oxidative-mediated cardiotoxicity by reporting its effect on redox imbalance,

purinergic and cholinergic dysfunction, ACE activity and lipid dysmetabolism in iron-induced oxidative cardiac injury.

MATERIALS AND METHODS

Plant Material and Extraction

Turbina oblongata was collected from Eastern Cape Province, South Africa (GPS coordinates: 32°44'20.1"S 26°54'58.3"E). The plant sample was identified and authenticated at the Geo Potts herbarium (BLFU), University of the Free State (specimen voucher number: BLFU MGM0019).

The plant sample was air-dried after washing and was blended to fine powder. The powdered sample (100 g in a 1:5 mass:solvent ratio in ml) was subjected to sequential extraction using solvents of increasing polarity vis-à-vis hexane, dichloromethane (DCM), methanol and dichloromethane (MeOH:DCM; 1:1, v/v) and methanol (MeOH). Each extraction was carried out at ambient room temperature for 24 h. After extraction, each extract was filtered and subsequently concentrated *in vacuo* with an R-215 rotary evaporator (Buchi, Switzerland). Concentrated samples were collected into glass vials and stored at 4°C.

Enzyme Inhibitory Activity

The concentrated extract samples were investigated for their anti-hypertensive activities by determining their ability to inhibit the activity of ACE *in vitro* (Shalaby et al., 2006). Based on the ACE inhibitory activities, the DCM extract was selected for further evaluation for its anti-hypertensive potential by determining its ability to inhibit the activity of renin using modified standard method (Udenigwe et al., 2009). The DCM extract, based on its activity on ACE and Renin, was chosen for further *ex vivo* studies.

Induction of Oxidative Cardiac Injury *Ex Vivo*

Hearts harvested from Sprague Dawley rats were homogenized in 50 mM sodium phosphate buffer (pH 7.5; with 1% Triton X-100). The homogenates were then centrifuged at 15,000 rpm at 4°C for 10 min to obtain the tissue supernatants.

A 100 µl of the cardiac tissue supernatant was incubated with 0.1 mM FeSO₄ (pro-oxidant) and different concentrations (30, 60, 120 and 240 µg/ml) of the DCM extract of *T. oblongata* at 37°C for 30 min according to previously published methods (Erukainure et al., 2020a; Salau et al., 2020b). Reaction samples without the extract served as the negative control (untreated), while reaction sample without the pro-oxidant and extract served as the normal control. Gallic acid was used as the standard antioxidative drug.

The study was conducted under the approved guidelines of the Animal Ethics Committee of the University of KwaZulu-Natal, Durban, South Africa (Protocol approval number: AREC/020/017D).

Determination of Oxidative Stress Parameters

Reduced Glutathione Level

This was determined according to Ellman's method (Ellman, 1959). Briefly, 100 μ l of the reaction samples was deproteinized with 300 μ l of 10% TCA and centrifuged at 3,500 rpm for 5 min. 200 μ l of the mixture was added to 50 μ l of Ellman's reagent in a 96-well plate and incubated for 5 min. Absorbance was measured at 415 nm and GSH level was extrapolated from a GSH standard curve.

Superoxide Dismutase Enzyme Activity

This was determined with slight modification of a previously established method (Kakkar et al., 1984). Briefly, 15 μ l of the reaction samples was mixed with 170 μ l of 0.1 mM diethylenetriaminepentaacetic acid (DETAPAC) in a 96-well plate. Then 15 μ l of 1.6 mM 6-hydroxydopamine (6-HD) was added to the mixture and swirled. Absorbance was immediately read at 492 nm for 3 min at 1 min interval.

Catalase Activity

Catalase activity was determined using a previously established protocol (Aebi, 1984). Briefly, 100 μ l of the reaction samples was mixed with 340 μ l of 50 mM phosphate buffer (pH 7.0). Thereafter, 150 μ l of 2 M hydrogen peroxide was added to the mixture and incubated for 5 min. Absorbance was measured at 240 nm at 1 min interval for 3 min.

Lipid Peroxidation

Lipid peroxidation was carried out by measuring the malondialdehyde (MDA) level of the reaction samples using a previously established method (Chowdhury and Soulsby, 2002). In brief, a reaction mixture made up of equal volumes (100 μ l) of the reaction samples and 8.1% SDS solution, 1 ml of 0.25% thiobarbituric acid (TBA) and 375 μ l of 20% acetic acid was boiled for 1 h. Absorbance was measured at 532 nm and MDA levels were extrapolated from a MDA standard curve.

Determination of ACE Activity

ACE activity was determined spectrophotometrically by a slight modification of Holmquist's method (Holmquist et al., 1979), using N-[3-(2-Furyl) acryloyl]-L-phenylalanyl-glycyl-glycine (FAPGG) as substrate. Briefly, 200 μ l of the reaction samples were incubated with 1 ml of 0.5 mM FAPGG for 10 min at 37°C. Absorbance was measured at 345 nm at 2 min intervals. ACE activity was measured as the rate of reaction ($\Delta A/\text{min}$) as expressed below:

$$\text{ACE activity} = \frac{(\text{AI} - \text{AF})\text{Sample} - (\text{AI} - \text{AF})\text{Blank}}{\text{Time interval (min)}}$$

Where AI = initial absorbance; AF = final absorbance.

Determination of Cholinergic Enzymes Activity

Cholinergic enzyme activity was determined by analyzing the acetylcholinesterase activity of the reaction samples using the

Ellman's procedure (Ellman et al., 1961). A reaction containing 20 μ l of the reaction samples, 10 μ l of Ellman's reagent (3.3 mM, pH 7.0) and 50 μ l of phosphate buffer (0.1 M, pH 8) was incubated for 20 min at 25°C. Then 10 μ l of 0.05 M acetylcholine iodide was added to the reaction samples and absorbance was measured at 412 nm at 3 min intervals.

Determination of Purinergic Enzymes Activities

The purinergic enzyme activities of the reaction samples were determined by analyzing the activities of adenylypyrophosphatase (ATPase) (Adewoye et al., 2000; Erukainure et al., 2017) and ecto-nucleoside triphosphate diphosphohydroase (ENTPDase) (Akomolafe et al., 2017) respectively.

ATPase Activity

Briefly, a reaction mixture containing 100 μ l of the reaction samples, 100 μ l of 5 mM KCl, 650 μ l of 0.1 M Tris-HCl buffer, and 20 μ l of 50 mM ATP was incubated in a shaker for 30 min at 37°C. Then 1.25% ammonium molybdate and 500 μ l of a distilled water were added to terminate the reaction. Thereafter, a 500 μ l of a freshly prepared 9% ascorbic acid was added to the mixture and allowed to stand for 30 min. Absorbance was measured at 660 nm.

ENTPDase Activity

Briefly, 20 μ l of the reaction samples was incubated with a mixture containing 200 μ l of the reaction buffer (1.5 mM CaCl_2 , 5 mM KCl, 0.1 mM EDTA, 10 mM glucose, 225 mM sucrose and 45 mM Tris-HCl) for 10 min at 37°C. 20 μ l of 50 mM ATP was then added to the reaction mixture and further incubated in a shaker for 20 min at 37°C. Reaction was halted by adding 200 μ l of 10% TCA, followed by 200 μ l of 1.25% ammonium molybdate and a freshly prepared 9% ascorbic acid. The mixture was allowed to stand on ice for 10 min. Absorbance was read at 600 nm.

Determination of Lipase Activity

The lipase activity of the reaction samples was determined by a little modification of a previously established method (Kim et al., 2010). A 100 μ l of the reaction samples was incubated with 169 μ l of Tris buffer (100 mM Tris-HCl and 5 mM CaCl_2 , pH 7.0) at 37°C for 15 min 5 μ l of 10 mM *p*-NPB (*p*-nitrophenyl butyrate in dimethyl formamide) was added to the mixture and further incubated for 15 min at 37°C. Absorbance was measured at 405 nm at 1 min interval. Lipase activity was expressed as the rate of reaction ($\Delta A/\text{min}$).

Determination of Cardiac Lipid Profile

Cardiac tissue supernatants were incubated overnight (12 h) with 0.1 mM FeSO_4 and 240 $\mu\text{g}/\text{ml}$ of *T. oblongata* DCM extract or gallic acid as described above. The samples were centrifuged at 15,000 rpm for 10 min at 4°C. The supernatants were immediately assayed for lipid profile levels including, total cholesterol, triglycerides, and HDL-cholesterol using an Automated Chemistry Analyzer (Labmax Plenno, Labtest Co. Ltd., Lagoa Santa, Brazil) with commercial assay kits according to manufacturer's manual.

TABLE 1 | IC50 values for ACE and renin inhibitory activities of *T. oblongata* extracts.

Activities	HEX	MEOH	DCM:MEOH (1:1)	DCM ($\mu\text{g/ml}$)	Aqueous	Captopril	Aliskiren
ACE inhibition	ND	364	167	81.1	ND	1.31	ND
Renin inhibition	ND	ND	ND	127	ND	ND	13.4

HEX, hexane extract; MEOH, methanol extract; DCM:MEOH, dichloromethane and methanol extract; DCM, dichloromethane extract. ND = not determined.

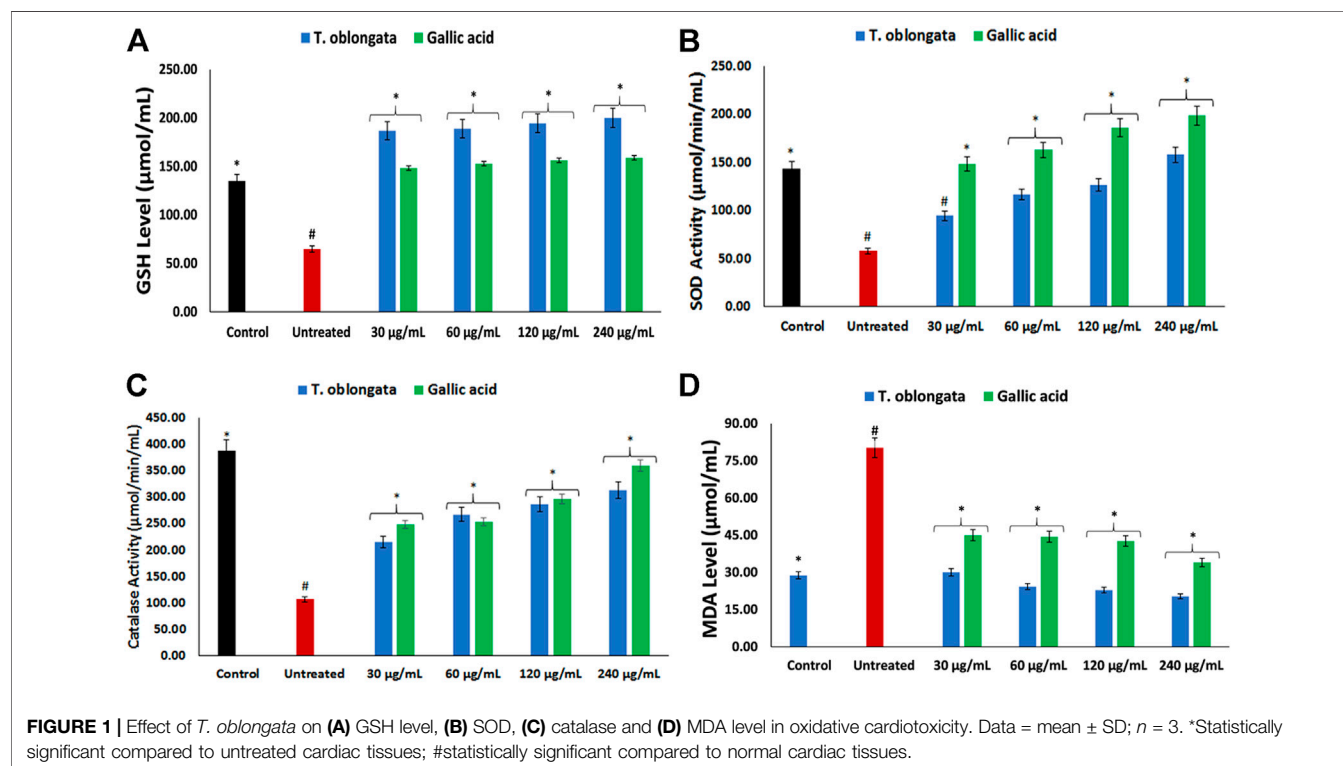


FIGURE 1 | Effect of *T. oblongata* on (A) GSH level, (B) SOD, (C) catalase and (D) MDA level in oxidative cardiotoxicity. Data = mean \pm SD; $n = 3$. *Statistically significant compared to untreated cardiac tissues; #statistically significant compared to normal cardiac tissues.

Metabolite Extraction and Profiling

As described above, the reaction mixture was prepared and incubated overnight (12 h). Lipid metabolites were then extracted from the samples and subjected to GC-MS metabolic profiling (Ralston-Hooper et al., 2011) with slight modification. Briefly, cold chloroform was mixed with the reaction samples in a ratio of 5:1 and vortexed for 1 min. The mixture was incubated on ice for 20 min and centrifuged at 15,000 rpm for 10 min at 4°C to yield two liquid phases. The lower phase (chloroform) layer containing the lipid metabolites and other non-polar metabolites was collected and subsequently profiled with GC-MS.

GC-MS Analysis of Lipid Metabolites

The chloroform layer which contains the lipid and other non-polar metabolites were analyzed with GC-MS (Agilent technologies 6,890 series GC coupled with (an Agilent) 5,973 Mass Selective Detector and driven by Agilent Chemstation software). The operating parameters include: Column: HP-5MS capillary column (30 m \times 0.25 mm ID, 0.25 μm film

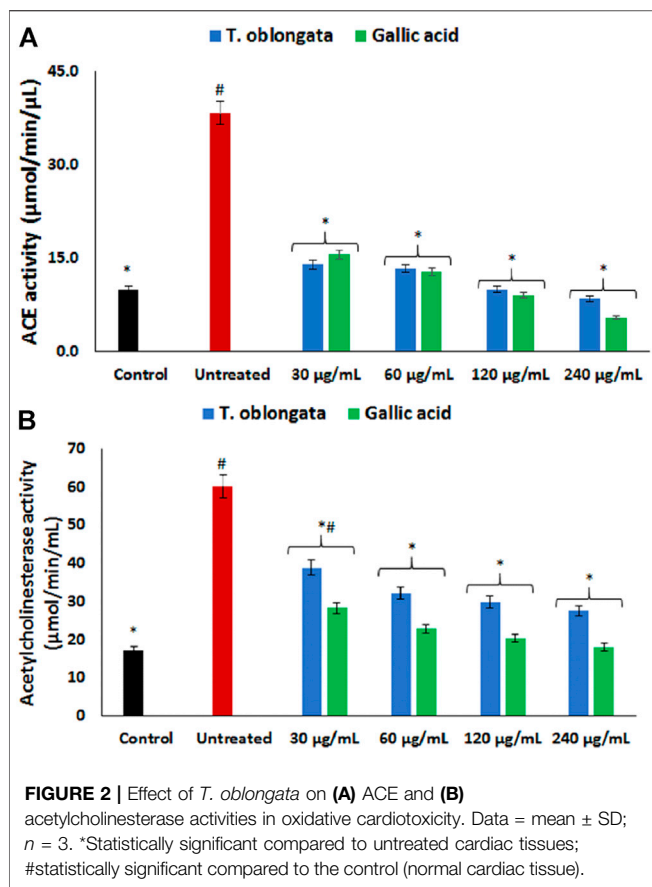
thickness, 5% phenylmethylsiloxane); Carrier gas: ultra-pure helium; Flow rate: 1.0 ml min⁻¹ and a linear velocity of 37 cm s⁻¹; Injector temperature: set at 250°C. Initial oven temperature: 60°C, programmed to 280°C at the rate of 10°C min⁻¹. Injection: 1 μl made in split mode at a split ratio of 20:1; Electron ionization mode: 70 eV; Electron multiplier voltage: at 1859 V; Ion source temperature: 230°C; Quadrupole temperature: 150°C; Solvent delay: 4 min; Scan range: 50–70 amu. Lipid metabolites were identified using an inbuilt NIST library.

Metabolic Pathway Analysis

To identify the relevant pathways involved in lipid metabolism in the protective role of *T. oblongata* on oxidative cardiotoxicity, the identified lipid metabolites were subjected to pathway enrichment analysis using the MetaboAnalyst 4.0 online server (Chong et al., 2018).

High-Performance Liquid Chromatography

HPLC-diode array detection analysis was performed on the DCM extract using an Agilent 1,100 series (Agilent, Waldbronn,



Germany) instrument equipped with photo diode array, autosampler, column thermostat and degasser. A Phenomenex: Luna 5 μ m C₁₈ (2) (150 \times 4.6 mm; 5 μ m particle size) column was used as the stationary phase. Water containing 0.1% of formic acid (A) and acetonitrile (B) served as mobile phases at a flow rate of 1 ml/min. Gradient elution was applied as follows: Initial ratio 95% A: 5% B, keeping for 10 min, changed to 90% A: 10% B in 10 min, changed to 70% A: 30% B in 10 min, to 50% A: 50% B in 10 min, maintaining for 0.5 min and back to initial ratio in 0.5 min. Temperature was set to 30°C. Extract or standards were dissolved in HPLC grade methanol (2 mg/ml) and the injection volume was 20.0 μ L. Chromatograms were recorded at 254 nm.

Statistical Analysis

One-way analysis of variance (ANOVA) was used in analyzing the data and presented as mean \pm SD. Significant differences between means at $p < 0.05$ were obtained with the Tukey's HSD-multiple range post-hoc test. Statistical analyses were done using IBM Statistical Package for the Social Sciences (SPSS) for Windows, version 23.0 (IBM Corp., Armonk, NY, United States). The GC-MS identified metabolites were subjected to statistical analysis (distinct changes and distribution) using the MetaboAnalyst 4.0 online server (Chong et al., 2018). Graphs were prepared using Microsoft Excel Spreadsheet and MetaboAnalyst 4.0 online server.

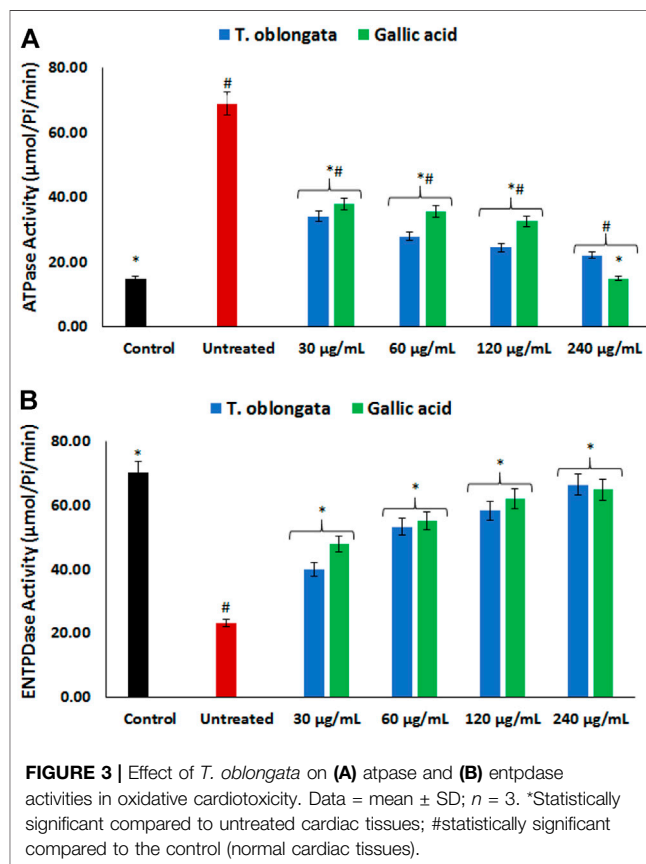
RESULTS

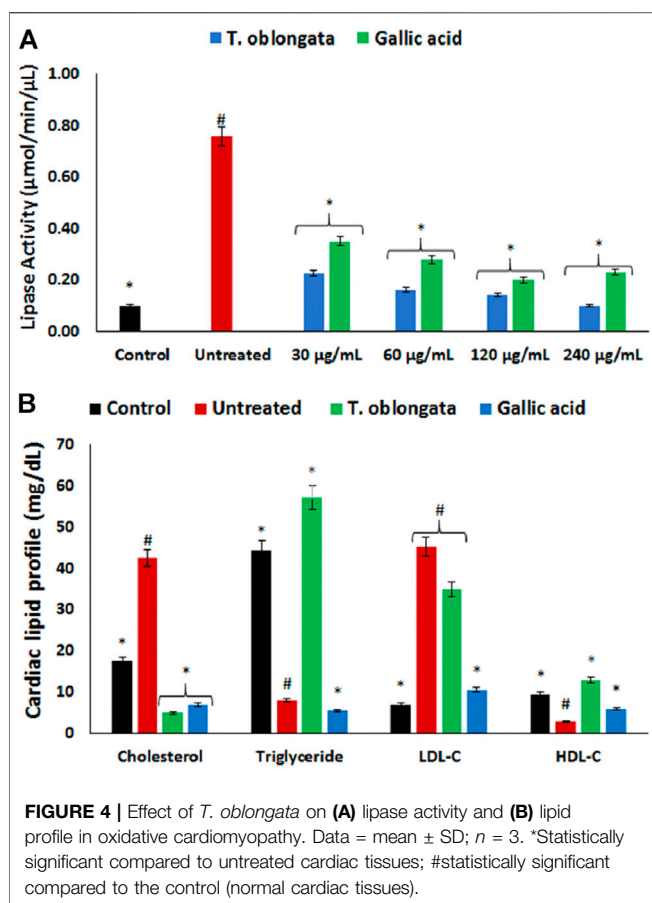
Except for MEOH:DCM and DCM extracts, the extracts had no inhibitory effect on ACE activity as shown in **Supplementary Figure S1A**. The MEOH:DCM and DCM extracts significantly ($p < 0.05$) inhibited the enzyme activity in a dose dependent manner. This is further depicted by their IC₅₀ values of 167 and 81.1 μ g/ml, respectively (**Table 1**) and compared favourably with that of the standard ACE-inhibitor captopril oil (**Supplementary Figure S1B**).

The DCM extract having displayed the best ACE inhibitory activity, and was recommended for further investigated for its renin inhibitory activity. The extract significantly ($p < 0.05$) inhibited the ACE activity dose dependently (**Supplementary Figure S2A**), with an IC₅₀ value of 127 μ g/ml (**Table 1**). This activity compared favorably with that of Aliskiren (**Supplementary Figure S2B** and **Table 1**).

Induction of oxidative cardiac injury led to significant ($p < 0.05$) decreased levels of GSH, SOD and catalase activity, with concomitant elevated level of MDA as depicted in **Figures 1A–D**. Following treatment with the DCM extract, these levels and activities were significantly ($p < 0.05$) reversed to near normal. Except for GSH level, these reversals were dose-dependent and compared favourably with gallic acid.

ACE activity was significantly ($p < 0.05$) elevated in cardiac tissues following the induction of oxidative cardiac injury as shown in **Figure 2A**. Treatment with the DCM extract led to





significant ($p < 0.05$) depletion in the activity dose-dependently, depicting an inhibitory effect.

As shown in **Figure 2B**, induction of oxidative cardiac injury led to significant ($p < 0.05$) elevation of cardiac acetylcholinesterase activity. The activity was significantly ($p < 0.05$) reversed dose-dependently to near normal following treatment with the DCM extract. The reversed activity compared favorably with that of gallic acid.

As depicted in **Figures 3A,B**, there was a significant ($p < 0.05$) elevation in cardiac ATPase activity, with concomitant decreased ENTPDase activity following the induction of oxidative cardiac injury. Treatment with the DCM extract led to significant ($p < 0.05$) reversion of these activities to near normal dose-dependently and compared favorably with gallic acid.

There was a significant ($p < 0.05$) elevation in cardiac lipase activity following the induction of oxidative cardiac injury as shown in **Figure 4A**. The activity was significantly ($p < 0.05$) inhibited dose-dependently after treatment with the DCM extract, and compared favorably with gallic acid.

Induction of oxidative cardiac injury led to significant ($p < 0.05$) elevation of cardiac levels of cholesterol and LDL-C, with concomitant decreased levels of triglycerides and HDL-C as shown in **Figure 4B**. Following treatment with the DCM extract, there was a significant depletion in cardiac level of cholesterol with concomitant elevation of triglyceride and HDL-C levels. Although the level of LDL-C was reduced in the treated tissues, it was however not statistically significant.

GC-MS analysis of the extracted lipid metabolites revealed the presence of unsaturated fatty acid, saturated fatty acid, fatty ester, fatty alcohol, fatty amide, glycerol and steroids in the cardiac tissue as shown in **Table 1**. Induction of cardiac tissue led to the complete depletion of octadecadienoic acid (Z,Z)-; cis-10-heptadecenoic acid; eicosanoic acid; n-heptadecanol-1 and retinal; with concomitant generation of 14-pentadecenoic acid; octadecanoic acid; tetracosanoic acid; cis-11,14-eicosadienoic acid, methyl ester; n-tetracosanol-1 and glycerol 1-palmitate. Treatment with the DCM extract led to the depletion of oxidative generated 14-pentadecenoic acid; tetracosanoic acid; cis-11,14-eicosadienoic acid, methyl ester; n-tetracosanol-1 and glycerol 1-palmitate, with concomitant generation of 9,12-Octadecadienoic acid (Z,Z)-; cis-11-eicosenoic acid; malonic acid, 2-hexyl tetradecyl ester; 1-(+)-Ascorbic acid 2,6-dihexadecanoate; pentanoic acid, heptadecyl ester; 13-tetradecen-1-ol acetate; oleamide and pseduosarsasapogenin-5,20-dien methyl ether. Non lipid metabolites consisting of ursane-3,12-diol; betulin and 28-hydroxylup-20(29)-ene-3,21-dione were also identified in cardiac tissues treated with the DCM extract.

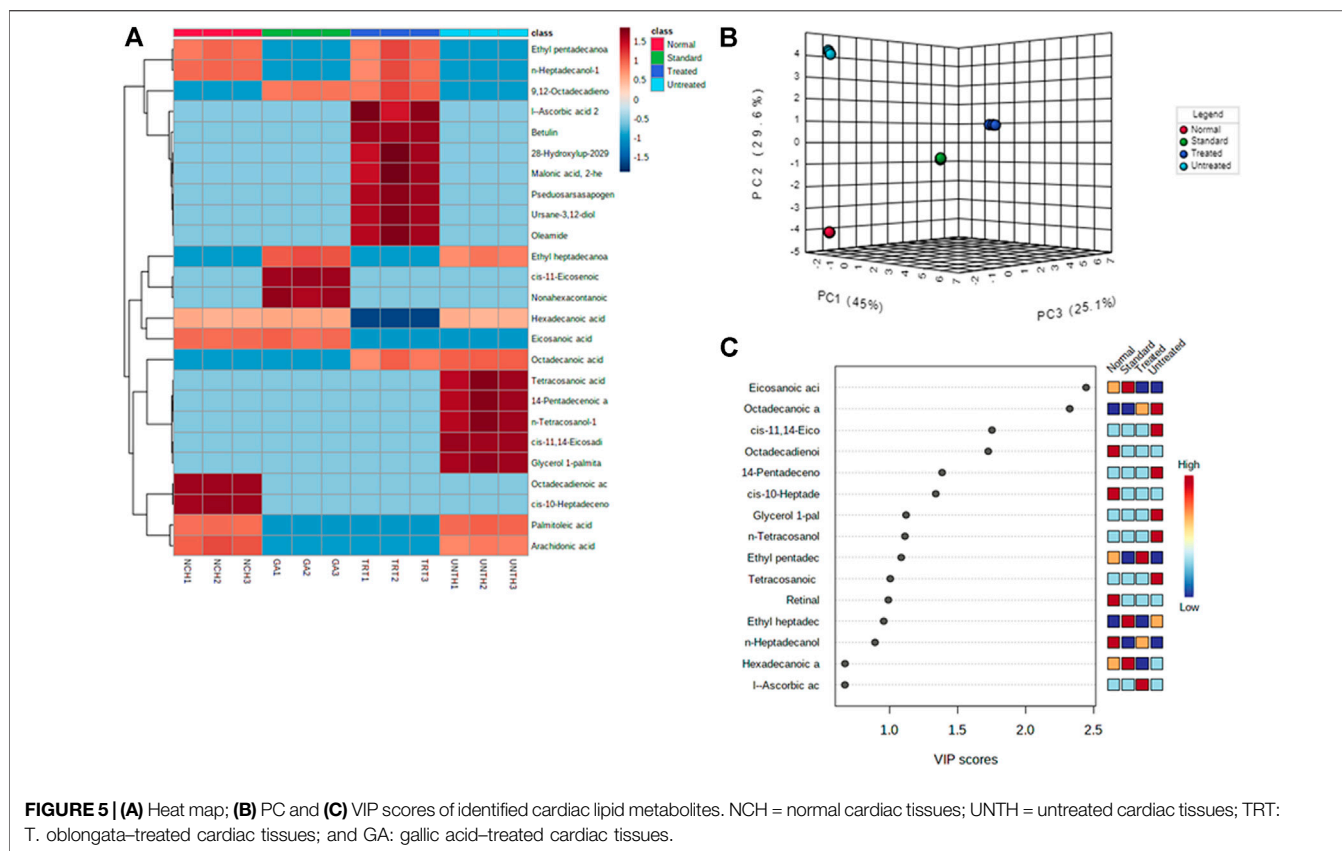
Distinct changes and distribution of the cardiac metabolites were observed for all the experimental groups as portrayed by the negative values and heat intensity of the heat map following clustering analysis (**Figure 5A**). This is also supported by the distinctive changes between the pair wise score plots between the selected principal components (PCs) of metabolites from the treated tissues and that of the untreated (**Figure 5B**). This is further corroborated by the distribution of the important identified features (metabolites) and their respective concentrations in each experimental group by Partial Least Squares - Discriminant Analysis (PLS-DA) as shown in **Figure 5C**.

Pathway enrichment of the identified cardiac lipid metabolites revealed an inactivation of retinol metabolism pathway, with concomitant activation of beta oxidation of very long chain fatty acids, plasmalogen synthesis and mitochondrial beta-oxidation of long chain saturated fatty acids pathways as depicted in **Figure 6** and **Table 2**. Treatment with the DCM extract did not reactivate the retinol metabolism pathway but inactivated oxidative-activated beta oxidation of very long chain fatty acids. It further inactivated arachidonic acid metabolism, glycerolipid metabolism, fatty acid elongation in mitochondria, fatty acid biosynthesis, fatty acid metabolism and steroidogenesis pathways. The oxidative-activated pathways were inactivated in cardiac tissues treated with gallic acid.

To determine the bioactive compound that may be responsible for the studied biological activity of the DCM extract, the extract was subjected to HPLC analysis. As depicted in **Figure 7**, quercetin was identified as the active compound in the extract.

DISCUSSION

Cardiotoxicity is a major global health issue as it has been implicated in the pathogenesis of cardiovascular dysfunction which may lead to cardiac failure if not well treated and managed (Poulter, 2003; Wold et al., 2005; Li et al., 2019).



Several factors including lipotoxicity, oxidative imbalance, exacerbated ACE activity and altered bioenergetics have been implicated in the pathophysiology of cardiovascular diseases. The high cost associated with its treatment coupled with the side effect of synthesized drugs are of major concerns to health practitioners. This has led to an increased paradigm shift to natural products for cheap and affordable drugs with little or no side effects. The present study reports the cardioprotective effect of *T. oblongata* and the possible mechanism and pathways by which it brings about its effect.

Oxidative stress has been implicated as a major mechanism in the pathogenesis and progression of cardiotoxicity and other cardiological dysfunctions (Fearon and Faux, 2009; Angsutararux et al., 2015). This has been attributed to suppressed endogenous antioxidant activity owing to increased free radical productions in the cardiac tissues. In the present study, the depleted GSH level, SOD and catalase activities (Figures 1A–C) depicts an onset of oxidative stress following induction of oxidative cardiac injury. This is further evidenced by the elevated cardiac MDA level (Figure 1D) which indicates a peroxidative effect on the cardiac lipids following the induction of oxidative cardiac injury. These altered activities and levels correspond with previous reports on the occurrence of oxidative stress after induction of oxidative injury in isolated hearts (Erukainure et al., 2020a; Salau et al., 2020b). The onset of oxidative stress can be attributed to iron-catalyzed Fenton's and Haber-Weiss reactions following the incubation of heart tissues with Fe^{2+} . The exacerbated GSH

level, SOD and catalase activities, with concomitant suppressed MDA level in cardiac tissues treated with the DCM extract of *T. oblongata* indicate an antioxidative and anti-peroxidative effect of the extract. This corroborates previous reports on the antioxidant cardioprotective effect of plants (Wattanapitayakul et al., 2005; Adegbola et al., 2017). The antioxidative activity of the extract may be attributed to the identified flavonoid, quercetin (Figure 7). Quercetin is among the common flavonoids found in most fruits, herbs and vegetables, and has been reported for its potent antioxidant and cardioprotective properties (Zhang et al., 2011; Chen et al., 2013).

Increased ACE activity has been implicated in the pathophysiology of cardiotoxicity and other cardiovascular dysfunctions (Ferrario and Strawn, 2006; Salau et al., 2020b). The enzyme catalyzes the hydrolysis of angiotensin I to angiotensin II, with the latter possessing a vasoconstrictive effect leading to hypertension, myocyte death and hypertrophy (Fiordaliso et al., 2000; Agunloye et al., 2019). The increased ACE activity following the induction of oxidative cardiac injury (Figure 2A), therefore suggests an exacerbated cardiac level angiotensin II. The depleted ACE activity following treatment with the DCM extract of *T. oblongata* indicates an ACE-inhibitory effect of the extract, thus depicting reduced cardiac levels of angiotensin II. This corroborates the ability of the extract to inhibit ACE activity *in vitro* (Table 1 and Supplementary Figure S1). ACE-inhibitors have been reported as potent therapies in the treatment and management of

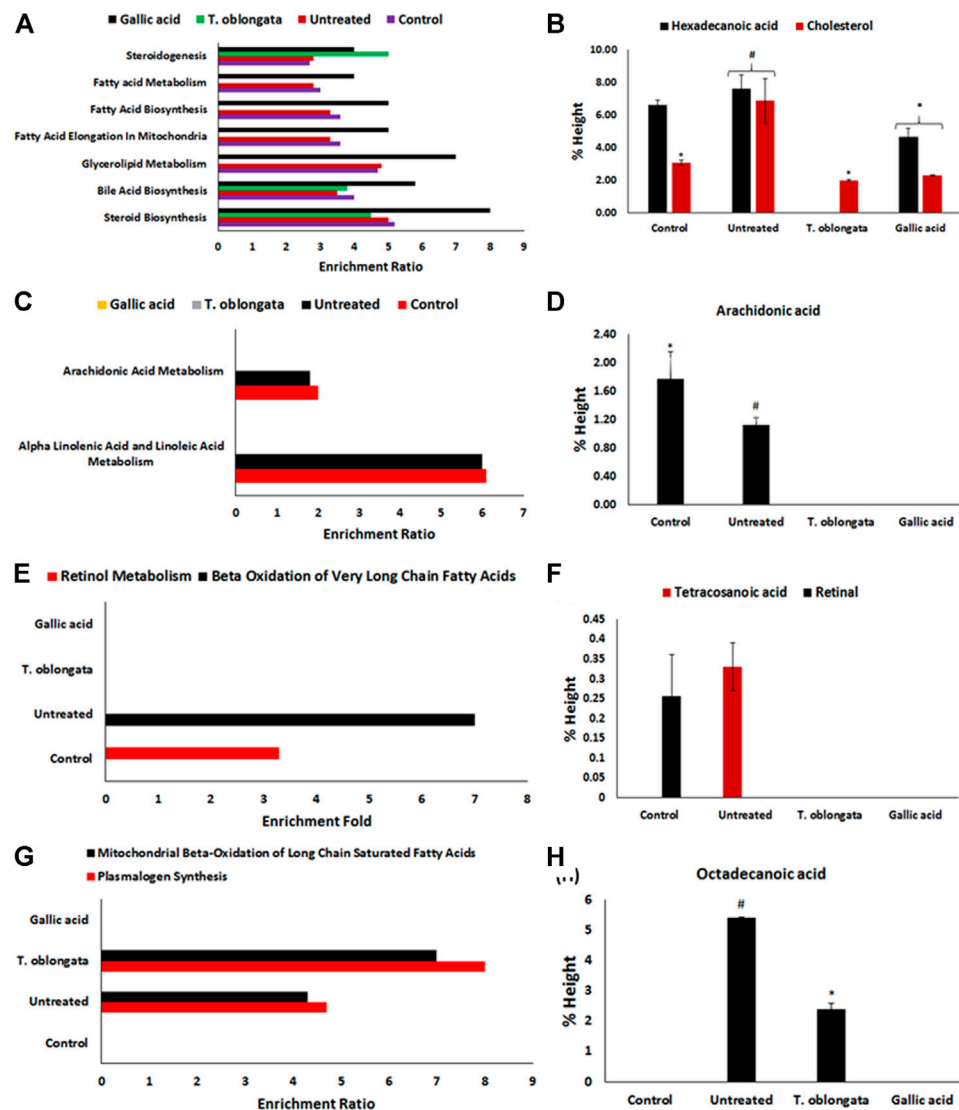


FIGURE 6 | (A) Fold enrichment for steroid biosynthesis, bile acid biosynthesis, glycerolipid metabolism, fatty acid elongation in mitochondria, fatty acid biosynthesis, fatty acid metabolism and steroidogenesis pathways and their **(B)** metabolites concentrations; **(C)** fold enrichment for alpha linolenic acid and linoleic acid metabolism, and arachidonic acid metabolism pathways and their **(D)** metabolites; **(E)** fold enrichment for beta oxidation of very long chain fatty acids and retinol metabolism pathways and their **(F)** metabolites; **(G)** fold enrichment for plasmalogen synthesis and mitochondrial beta-oxidation of long chain saturated fatty acids and their **(H)** metabolites.

cardiovascular diseases, which may be part of the possible mechanism by which the extract protect against oxidative-mediated cardiotoxicity. This corroborates previous reports on the use medicinal plants as ACE inhibitors (Khan and Kumar, 2019; Le et al., 2020). The ACE inhibitory activity of the extract may be attributed to the presence of quercetin, which has also been reported for its ACE inhibitory activity (Huang et al., 2017; Luo et al., 2017).

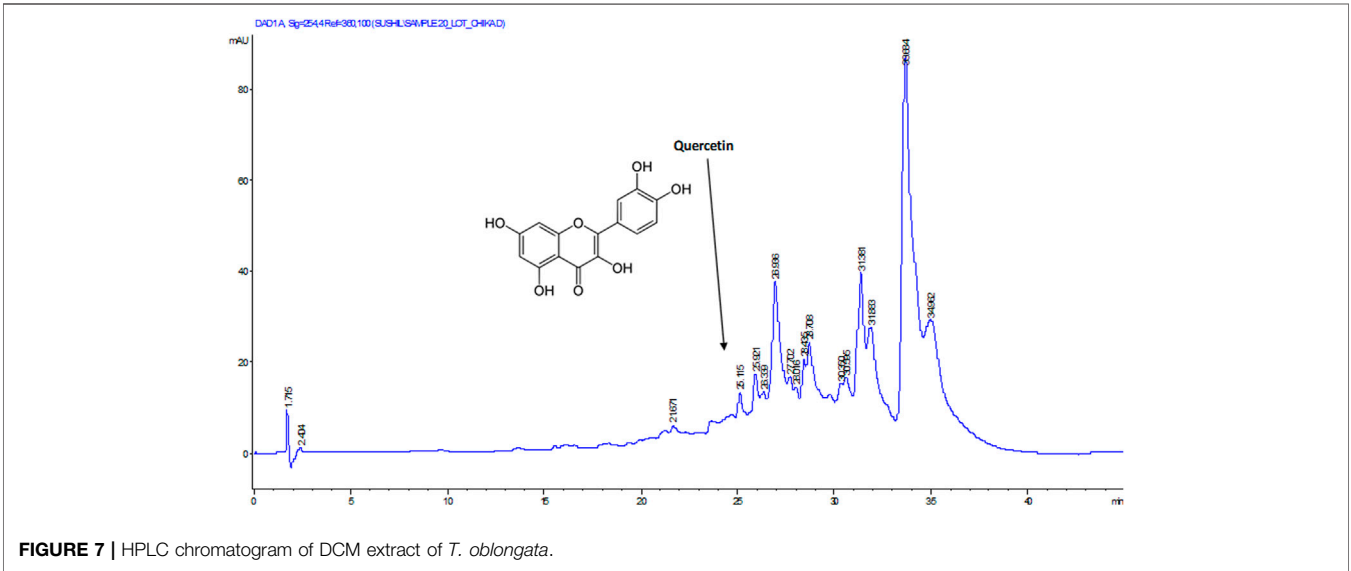
The elevated acetylcholinesterase activity following the induction of oxidative cardiac injury (Figure 2B) suggests a decreased cardiac level of acetylcholine, thus depicting a cholinergic dysfunction. This can be attributed to the fact the enzyme catalyzes the hydrolysis of acetylcholine to acetate and

choline. Acetylcholine is important in muscular contraction and also facilitates vasodilation *via* the muscarinic receptors (Kellogg et al., 2005; Agunloye et al., 2019), thus indicating that decreased concentrations could have detrimental effect on the normal physiological function of the heart. Several studies have reported acetylcholinesterase inhibition as a therapeutic mechanism in the treatment and management of cardiotoxicity and other cardiovascular dysfunctions (Gavioli et al., 2014; Roy et al., 2014; Wu et al., 2017). The decreased acetylcholinesterase in the treated cardiac tissues therefore suggests a therapeutic effect against oxidative-mediated cardiotoxicity. This corresponds with several reports on the ability of medicinal plants to inhibit cardiac

TABLE 2 | Identified pathways in experimental cardiac tissues.

Pathways	Normal	Untreated	<i>T. Oblongata</i>	Gallic acid
Steroid biosynthesis	X	X	X	X
Bile acid biosynthesis	X	X	X	X
Alpha linolenic acid and linoleic acid metabolism	X	X	–	–
Glycerolipid metabolism	X	X	–	X
Fatty acid elongation in mitochondria	X	X	–	X
Fatty acid biosynthesis	X	X	–	X
Retinol metabolism	X	–	–	–
Fatty acid metabolism	X	X	–	X
Steroidogenesis	X	X	X	X
Arachidonic acid metabolism	X	X	–	–
Beta oxidation of very long chain fatty acids	–	X	–	–
Plasmalogen synthesis	–	X	X	–
Mitochondrial beta-oxidation of long chain saturated fatty acids	–	X	X	–

X = detected; – = not detected.



acetylcholinesterase activities (Agunloye et al., 2019; Salau et al., 2020b). Purinergic enzyme activities have been reported to play an important role in the normal physiological activities of the heart. These enzymes phospho-hydrolyze adenosine triphosphate (ATP) and adenosine monophosphate (AMP) to produce the endogenous signaling nucleotide, adenosine which has been reported as a potent dilator and an important factor in bioenergetics (Das and Maulik, 1996; Burnstock, 2017). The increased ATPase and decreased ENTPDase activities following the induction of oxidative cardiac injury (**Figures 3A,B**) indicate a decreased cardiac level of ATP and adenosine. These levels in the untreated cardiac tissues corresponds with previous reports on altered purinergic activities in oxidative injuries (Salau et al., 2020a; Erukainure et al., 2020b). The increased ATPase activity suggests a diminished cardiac level of ATP and depicts an altered bioenergetic activity as ATP is an important energy-signaling

molecule. Altered cardiac bioenergetics have been implicated in the pathophysiology of oxidative stress, cardiotoxicity and other cardiovascular dysfunctions (Das and Maulik, 1996). Both ATP and adenosine have been reported for their vasodilatory activities in coronary vessels (Kirby et al., 2010). The decreased ATPase and elevated ENTPDase activities following treatment with *T. oblongata* DCM extract therefore indicates an improved purinergic activity which may suggest improved bioenergetics. The normal heart function depends on lipids as its energy fuel for its physiological functions *via* hydrolysis of cardiac triglyceride by lipase to fatty acids (Ritterhoff and Tian, 2017). The heart does not produce triglyceride and thus depends on its supply from the liver. The elevated lipase activity following the induction of oxidative cardiac injury (**Figure 4A**) therefore suggests an incessant breakdown of cardiac triglyceride, which corroborates with the depleted cardiac level of triglyceride (**Figure 4B**). The elevated lipase activity and reduced triglyceride level in the untreated cardiac tissues suggests

TABLE 3 | GC-MS identified lipid metabolites in experimental cardiac tissues.

Classes	Compounds	Control	Untreated	<i>T. oblongata</i>	Gallic acid
Unsaturated fatty acid	Palmitoleic acid	1.84 ± 0.18	2.62 ± 0.16	ND	ND
	Octadecadienoic acid (Z,Z)-	3.56 ± 0.12	ND	ND	ND
	cis-10-Heptadecenoic acid	0.87 ± 0.10	ND	ND	ND
	Eicosanoic acid	5.19 ± 0.10	ND	ND	3.49 ± 0.29
	Arachidonic acid	1.78 ± 0.38	1.12 ± 0.10	ND	ND
	14-Pentadecenoic acid	ND	1.34 ± 0.29	ND	ND
	Octadecanoic acid		5.42 ± 0.01	2.38 ± 0.21	ND
	9,12-Octadecadienoic acid (Z,Z)-	ND	ND	1.48 ± 0.15	0.73 ± 0.11
	cis-11-Eicosenoic acid	ND	ND	ND	1.01 ± 0.10
	Hexadecanoic acid	6.60 ± 0.33	7.60 ± 0.87	ND	4.68 ± 0.50
Saturated fatty acid	Tetracosanoic acid	ND	0.33 ± 0.06	ND	ND
	Ethyl hexadecanoate	1.28 ± 0.24	1.11 ± 0.21	1.39 ± 0.27	1.68 ± 0.27
Fatty ester	Ethyl pentadecanoate	2.78 ± 0.61	2.44 ± 0.50	2.84 ± 0.57	2.72 ± 0.52
	cis-11,14-Eicosadienoic acid, methyl ester	ND	5.06 ± 0.40	ND	ND
	Ethyl heptadecanoate	ND	ND	ND	ND
	Malonic acid, 2-hexyl tetradecyl ester	ND	ND	0.15 ± 0.01	ND
	l-(+)-Ascorbic acid 2,6-dihexadecanoate	ND	ND	11.96 ± 9.16	ND
	Pentanoic acid, heptadecyl ester	ND	ND	0.17 ± 0.01	ND
	Pentadecanol	0.37 ± 0.03	1.59 ± 0.30	0.32 ± 0.02	0.85 ± 0.10
Fatty alcohol	n-Heptadecanol-1	0.86 ± 0.07	ND	0.72 ± 0.09	ND
	n-Tetracosanol-1	ND	0.49 ± 0.09	ND	ND
	13-Tetradecen-1-ol acetate	ND	ND	0.20 ± 0.03	ND
	Oleamide	ND	ND	0.26 ± 0.03	ND
Fatty amide	Glycerol 1-palmitate	ND	0.50 ± 0.03	ND	ND
Glycerol	Retinal	0.26 ± 0.11	ND	ND	ND
Steroids	Cholesterol	3.08 ± 0.18	6.87 ± 1.36	1.99 ± 0.04	2.29 ± 0.02
	Pseudo-sarsapogenin-5,20-dien methyl ether	ND	ND	0.34 ± 0.06	ND
Non-lipid	Ursane-3,12-diol	ND	ND	0.35 ± 0.04	ND
	Betulin	ND	ND	0.38 ± 0.13	ND
	28-Hydroxylup-20(29)-ene-3,21-dione	ND	ND	0.40 ± 0.01	ND
	Nonahexacontanoic acid	ND	ND	ND	0.32 ± 0.02

Values = mean ± SD; n = 3. ND = not detected.

abnormality in FA supply and utilization. This may further indicate a suppressed ATP level which also corroborates the increased ATPase activity (**Figure 3A**). This may therefore portray a metabolic dependence on aerobic glycolysis for cardiac energy (ATP) supply (Stanley, 2001; Salau et al., 2020b). The depleted lipase activity and elevated triglyceride level in cardiac tissues treated with *T. oblongata* extract therefore indicate an arrest of incessant lipolysis of triglyceride and improved lipid utilization, which also suggests an improved cardiac bioenergetic.

The elevated cholesterol and LDL-C, with concomitant depleted HDL-C following the induction of oxidative cardiac injury (**Figure 4B**) indicates a disrupted cardiac lipid spectrum and insinuate a cardiac lipotoxic effect which has been linked to the pathophysiology of cardiotoxicity (Poulter, 2003). High concentrations of cholesterol and LDL-C have also been implicated in vasoconstriction and linked to most cardiovascular dysfunctions (Lamping et al., 1994; Pfister and Campbell, 1996; Kopkan et al., 2009). The decreased cholesterol and LDL-C levels as well as elevated HDL-C level on treatment with *T. oblongata* therefore indicates an antilipemic effect of the extract against oxidative-disrupted cardiac lipid profile. This correlates with previous reports on the ability of medicinal plants to maintain cardiac lipid spectrum in oxidative-mediated cardiotoxicity (Erukainure et al., 2020a).

An occurrence of cardiac lipotoxicity on induction of oxidative cardiac injury was further depicted by dysregulated lipid metabolic pathways and altered lipid metabolites (**Tables 2, 3** and **Figures 5, 6**). Dysregulated lipid metabolism in the heart leading to free fatty acids (FFAs) have been implicated among the pathophysiology of cardiotoxicity and other cardiovascular dysfunctions (Antozzi and Zeviani, 1997; Ventura-Clapier et al., 2004). The elevated cardiac level of cholesterol in the untreated tissues corroborates that of the cardiac lipid spectrum (**Figure 4A**) and the major metabolites for steroid biosynthesis, bile acid biosynthesis and steroidogenesis pathways (**Figures 6A,B**). The inactivation of retinol metabolism in the untreated cardiac tissue can be attributed to the complete depletion of retinal (**Figures 6E,F**) and corroborates previous reports linking the downregulation of the pathway to impaired cardiac lipid metabolism and heart failure (Osorio et al., 2002; Lee et al., 2014). The activation of beta oxidation of very long chain fatty acids and mitochondrial beta-oxidation of long chain saturated fatty acids pathways can be attributed to the metabolites octadecanoic acid and tetracosanoic acid (**Figures 6E–H**). The incessant activation of these pathways has been implicated in increased production of NADH, FADH₂ and acetyl-CoA (Marín-García and Goldenthal, 2002). Acetyl-CoA is further broken down in the tricarboxylic acid (TCA) cycle to generate NADH, FADH₂ and ATP. High concentrations of these

electron carriers have been reported to cause a high mitochondrial membrane potential leading to the inhibition of the electron transport (Brownlee, 2001; Du et al., 2001). This automatically reduces oxygen (O_2) to superoxide (O_2^-). Thus, it can be insinuated that the continuous production of O_2^- and concomitant low SOD activity (Figure 1B) in the untreated tissues may be an oxidative mechanism on induction of oxidative cardiac injury.

Inactivation of beta oxidation of very long chain fatty acids in tissues treated with *T. oblongata* DCM extract therefore suggests a decreased production of the electron carriers which depicts a suppressed production of O_2^- . This corroborates the absence of tetracosanoic acid and the high SOD activity. The inactivation of alpha linolenic acid and linoleic acid metabolism, glycerolipid metabolism, fatty acid elongation in mitochondria, fatty acid biosynthesis, and fatty acid metabolism suggests a possible hypolipidemic mechanism by which the extract mitigates oxidative-mediated lipid dysmetabolism in oxidative-mediated cardiotoxicity.

As depicted in Figure 7, quercetin was identified as an active component of the DCM fraction of *T. oblongata*. Quercetin ranks among the most popular phenolics as it is commonly found in fruits, vegetables, and herbs (Zhang et al., 2011). Its potent antioxidant properties have been reported and has been exploited in the treatment and management of various oxidative-mediated ailments such as diabetes, cardiovascular diseases, and cancer (Zhang et al., 2011; Georgiev et al., 2014; Patel et al., 2018). The studied activities of *T. oblongata* in the present study may therefore be attributed to the presence of quercetin, which may also work in synergy with other unidentified phytochemicals.

CONCLUSION

These results indicate the cardioprotective effect of *T. oblongata* against oxidative-mediated cardiotoxicity. This is evidenced by the ability of its DCM extract to mitigate lipotoxicity and modulate dysregulated cardiometabolic activities as shown by its antioxidant activity and suppressive effects on ACE, acetylcholinesterase and lipase activities, while modulating cardiac lipid dysmetabolism. The presence of quercetin in the extract may contribute to these activities. However, further *in vivo* studies are recommended to identify the molecular mechanism

that maybe involved in the cardioprotective effect of the extract and its bioactive compounds.

DATA AVAILABILITY STATEMENT

The original contributions presented in the study are included in the article/Supplementary Material, further inquiries can be directed to the corresponding author.

ETHICS STATEMENT

The animal study was reviewed and approved by the animal ethical committee of the University of KwaZulu-Natal, Durban, South Africa.

AUTHOR CONTRIBUTIONS

Conceptualization: MM, MJ, CC and OLE; Plant material and Indigenous Usage: MJ and MM; Experiments: OE; CC; VS; and MI. Metabolomics: OE and NK; Original manuscript draft: OE; CC and VS; Manuscript editing: all authors; Funding and Supervision: MM.

FUNDING

This work was supported by research funding from the National Research Foundation; and the Department of Science and Innovation (DSI) through the IKS-Based Technology Innovations. OE is thankful to the University of the Free State, Bloemfontein, South Africa for Incentives for Rated Researchers (2019060769); and the National Research Foundation (NRF) for Scarce Skills Postdoctoral Research Grant (UID: 132822).

SUPPLEMENTARY MATERIAL

The Supplementary Material for this article can be found online at: <https://www.frontiersin.org/articles/10.3389/fphar.2021.610835/full#supplementary-material>

REFERENCES

- Adegbola, P., Aderibigbe, I., Hammed, W., and Omotayo, T. (2017). Antioxidant and Anti-inflammatory Medicinal Plants Have Potential Role in the Treatment of Cardiovascular Disease: a Review. *Am. J. Cardiovasc. Dis.* 7 (2), 19–32.
- Adewoye, O. E., Bolarinwa, A. F., and Olorunsogo, O. O. (2000). Ca⁺⁺, Mg⁺⁺-ATPase Activity in Insulin-dependent and Non-insulin Dependent Diabetic Nigerians. *Afr. J. Med. Med. Sci.* 29 (3–4), 195–199.
- Aebi, H. (1984). “[13] Catalase In Vitro,” in *Meth. Enzymol* (Elsevier), 105, 121–126. doi:10.1016/s0076-6879(84)05016-3
- Agunloye, O. M., Oboh, G., Ademiluyi, A. O., Ademosun, A. O., Akindahunsi, A. A., Oyagbemi, A. A., et al. (2019). Cardio-protective and Antioxidant Properties of Caffeic Acid and Chlorogenic Acid: Mechanistic Role of Angiotensin Converting Enzyme,

- Cholinesterase and Arginase Activities in Cyclosporine Induced Hypertensive Rats. *Biomed. Pharmacother.* 109, 450–458. doi:10.1016/j.biopha.2018.10.044
- Akomolafe, S. F., Akinyemi, A. J., Ogunsuyi, O. B., Oyeleye, S. I., Oboh, G., Adeoyo, O. O., et al. (2017). Effect of Caffeine, Caffeic Acid and Their Various Combinations on Enzymes of Cholinergic, Monoaminergic and Purinergic Systems Critical to Neurodegeneration in Rat Brain-In Vitro. *NeuroToxicology* 62, 6–13. doi:10.1016/j.neuro.2017.04.008
- Angsutararux, P., Luanpitpong, S., and Issaragrisil, S. (2015). Chemotherapy-induced Cardiotoxicity: Overview of the Roles of Oxidative Stress. *Oxid. Med. Cel. Longev.* 2015, 795602. doi:10.1155/2015/795602
- Antozzi, C., and Zeviani, M. (1997). Cardiomyopathies in Disorders of Oxidative Metabolism. *Cardiovasc. Res.* 35, 184–199. doi:10.1016/s0008-6363(97)00141-7
- Brownlee, M. (2001). Biochemistry and Molecular Cell Biology of Diabetic Complications. *Nature* 414 (6865), 813–820. doi:10.1038/414813a

- Burnstock, G. (2017). Purinergic Signaling in the Cardiovascular System. *Circ. Res.* 120 (1), 207–228. doi:10.1161/circresaha.116.309726
- Chen, J.-Y., Hu, R.-Y., and Chou, H.-C. (2013). Quercetin-induced Cardioprotection against Doxorubicin Cytotoxicity. *J. Biomed. Sci.* 20 (1), 95. doi:10.1186/1423-0127-20-95
- Chong, J., Soufan, O., Li, C., Caraus, I., Li, S., Bourque, G., et al. (2018). MetaboAnalyst 4.0: towards More Transparent and Integrative Metabolomics Analysis. *Nucleic Acids Res.* 46 (W1), W486–W494. doi:10.1093/nar/gky310
- Chowdhury, P., and Soulsby, M. (2002). Lipid Peroxidation in Rat Brain Is Increased by Simulated Weightlessness and Decreased by a Soy-Protein Diet. *Ann. Clin. Lab. Sci.* 32, 188–192.
- Das, D., and Maulik, N. (1996). “Bioenergetics, Ischemic Contracture and Reperfusion Injury,” in *Myocardial Ischemia: Mechanisms, Reperfusion, Protection* (Springer), 76, 155–173. doi:10.1007/978-3-0348-8988-9_10
- Drosatos, K., and Schulze, P. C. (2013). Cardiac Lipotoxicity: Molecular Pathways and Therapeutic Implications. *Curr. Heart Fail. Rep.* 10 (2), 109–121. doi:10.1007/s11897-013-0133-0
- Du, X. L., Edelstein, D., Dimmeler, S., Ju, Q., Sui, C., and Brownlee, M. (2001). Hyperglycemia Inhibits Endothelial Nitric Oxide Synthase Activity by Posttranslational Modification at the Akt Site. *J. Clin. Invest.* 108 (9), 1341–1348. doi:10.1172/jci11235
- Ellman, G. L., Courtney, K. D., Andres, V., Jr., and Featherstone, R. M. (1961). A New and Rapid Colorimetric Determination of Acetylcholinesterase Activity. *Biochem. Pharmacol.* 7, 88–95. doi:10.1016/0006-2952(61)90145-9
- Ellman, G. L. (1959). Tissue Sulfhydryl Groups. *Arch. Biochem. Biophys.* 82, 70–77. doi:10.1016/0003-9861(59)90090-6
- Erukainure, O. L., Mopuri, R., Oyeode, O. A., Koorbanally, N. A., and Islam, M. S. (2017). Dacryodes Edulis Enhances Antioxidant Activities, Suppresses DNA Fragmentation in Oxidative Pancreatic and Hepatic Injuries; and Inhibits Carbohydrate Digestive Enzymes Linked to Type 2 Diabetes. *Biomed. Pharmacother.* 96, 37–47. doi:10.1016/j.biopha.2017.09.106
- Erukainure, O. L., Chukwuma, C. I., Matsabisa, M. G., Salau, V. F., Koorbanally, N. A., and Islam, M. S. (2020a). *Buddleja Saligna* Willd (Loganiaceae) Inhibits Angiotensin-Converting Enzyme Activity in Oxidative Cardiopathy with Concomitant Modulation of Nucleotide Hydrolyzing Enzymatic Activities and Dysregulated Lipid Metabolic Pathways. *J. Ethnopharmacology* 248, 112358. doi:10.1016/j.jep.2019.112358
- Erukainure, O. L., Salau, V. F., Oyenih, A. B., Mshicileli, N., and Islam, M. S. (2020b). Strawberry Fruit (*Fragaria X Ananassa* Cv. Romina) Extenuates Iron-Induced Cardiac Oxidative Injury via Effects on Redox Balance, Angiotensin-Converting Enzyme, Purinergic Activities, and Metabolic Pathways. *J. Food Biochem.* 44 (8), e13315. doi:10.1111/jfbc.13315
- Fearon, I. M., and Faux, S. P. (2009). Oxidative Stress and Cardiovascular Disease: Novel Tools Give (Free) Radical Insight. *J. Mol. Cell Cardiol.* 47, 372–381. doi:10.1016/j.yjmcc.2009.05.013
- Ferrario, C. M., and Strawn, W. B. (2006). Role of the Renin-Angiotensin-Aldosterone System and Proinflammatory Mediators in Cardiovascular Disease. *Am. J. Cardiol.* 98, 121–128. doi:10.1016/j.amjcard.2006.01.059
- Fiordaliso, F., Li, B., Latini, R., Sonnenblick, E. H., Anversa, P., Leri, A., et al. (2000). Myocyte Death in Streptozotocin-Induced Diabetes in Rats Is Angiotensin II-Dependent. *Lab. Invest.* 80, 513–527. doi:10.1038/labinvest.3780057
- Foden, W., and Potter, L. (2005). *Ipomoea Oblongata* E.Mey. Ex Choisy. National Assessment. Red List of South African plants version 2020.1. [Online]. Available: <http://redlist.sanbi.org/species.php?species=1625-89> (Accessed August 13, 2020).
- Gavioli, M., Lara, A., Almeida, P. W. M., Lima, A. M., Damasceno, D. D., Rocha-Resende, C., et al. (2014). Cholinergic Signaling Exerts Protective Effects in Models of Sympathetic Hyperactivity-Induced Cardiac Dysfunction. *PLoS One* 9, e100179. doi:10.1371/journal.pone.0100179
- Holmquist, B., Bünning, P., and Riordan, J. F. (1979). A Continuous Spectrophotometric Assay for Angiotensin Converting Enzyme. *Anal. Biochem.* 95, 540–548. doi:10.1016/0003-2697(79)90769-3
- Huang, W.-Y., Fu, L., Li, C.-Y., Xu, L.-P., Zhang, L.-X., and Zhang, W.-M. (2017). Quercetin, Hyperin, and Chlorogenic Acid Improve Endothelial Function by Antioxidant, Antiinflammatory, and ACE Inhibitory Effects. *J. Food Sci.* 82, 1239–1246. doi:10.1111/1750-3841.13706
- Hutchings, A., Scott, A., Lewis, G., and Cunningham, A. (1996). Zulu Medicinal Plants. *Pietermaritzburg*. South Africa: University of Natal Press.
- Jiménez-González, S., Marín-Royo, G., Jurado-López, R., Bartolomé, M. V., Romero-Miranda, A., Luaces, M., et al. (2020). The Crosstalk between Cardiac Lipotoxicity and Mitochondrial Oxidative Stress in the Cardiac Alterations in Diet-Induced Obesity in Rats. *Cells* 9, 451. doi:10.3390/cells9020451
- Kakkar, P., Das, B., and Viswanathan, P. (1984). A Modified Spectrophotometric Assay of Superoxide Dismutase. *Indian J. Biochem. Biophys.* 21 (2), 130–132.
- Kellogg, D. L., Jr, Zhao, J. L., Coey, U., and Green, J. V. (2005). Acetylcholine-induced Vasodilation Is Mediated by Nitric Oxide and Prostaglandins in Human Skin. *J. Appl. Physiol.* 98, 629–632. doi:10.1152/jappphysiol.00728.2004
- Khan, M. Y., and Kumar, V. (2019). Mechanism & Inhibition Kinetics of Bioassay-Guided Fractions of Indian Medicinal Plants and Foods as ACE Inhibitors. *J. Traditional Complement. Med.* 9, 73–84. doi:10.1016/j.jtcme.2018.02.001
- Kim, Y. S., Lee, Y. M., Kim, H., Kim, J., Jang, D. S., Kim, J. H., et al. (2010). Anti-obesity Effect of Morus Bombycis Root Extract: Anti-lipase Activity and Lipolytic Effect. *J. Ethnopharmacology* 130, 621–624. doi:10.1016/j.jep.2010.05.053
- Kirby, B. S., Crecelius, A. R., Voyles, W. F., and Dineno, F. A. (2010). Vasodilatory Responsiveness to Adenosine Triphosphate in Ageing Humans. *J. Physiol.* 588, 4017–4027. doi:10.1113/jphysiol.2010.197814
- Kopkan, L., Khan, M. A. H., Lis, A., Awayda, M. S., and Majid, D. S. A. (2009). Cholesterol Induces Renal Vasoconstriction and Anti-natriuresis by Inhibiting Nitric Oxide Production in Anesthetized Rats. *Am. J. Physiology-Renal Physiol.* 297, F1606–F1613. doi:10.1152/ajprenal.90743.2008
- Kose, L. S., Moteetee, A., and Van Vuuren, S. (2015). Ethnobotanical Survey of Medicinal Plants Used in the Maseru District of Lesotho. *J. Ethnopharmacol.* 170, 184–200. doi:10.1016/j.jep.2015.04.047
- Lamping, K. G., Piegors, D. J., Benzuly, K. H., Armstrong, M. L., and Heistad, D. D. (1994). Enhanced Coronary Vasoconstrictive Response to Serotonin Substitutes after Removal of Dietary Cholesterol in Atherosclerotic Monkeys. *Arterioscler Thromb.* 14, 951–957. doi:10.1161/01.atv.14.6.951
- Le, X. T., Phi, X. T., Phi, X. T., Nguyen, D. T. T., Pham, H. T. N., Nguyen Van, T., et al. (2020). Angiotensin-converting Enzyme Inhibitory Activity of Some Vietnamese Medicinal Plants. *Vjste* 62, 77–82. doi:10.31276/vjste.62(2).77-82
- Lee, S.-A., Jiang, H., Trent, C. M., Yuen, J. J., Narayanasamy, S., Curley, R. W., Jr, et al. (2014). Cardiac Dysfunction in β -carotene-15,15'-dioxygenase-deficient Mice Is Associated with Altered Retinoid and Lipid Metabolism. *Am. J. Physiology-Heart Circulatory Physiol.* 307, H1675–H1684. doi:10.1152/ajpheart.00548.2014
- Li, T., Chen, L., Yu, Y., Yang, B., Li, P., and Tan, X. Q. (2019). Resveratrol Alleviates Hypoxia/reoxygenation Injury induced Mitochondrial Oxidative Stress in Cardiomyocytes. *Mol. Med. Rep.* 19, 2774–2780. doi:10.3892/mmr.2019.9943
- Luo, J., Zhang, C., Liu, Q., Ou, S., Zhang, L., and Peng, X. (2017). Combinative Effect of Sardine Peptides and Quercetin Alleviates Hypertension through Inhibition of Angiotensin I Converting Enzyme Activity and Inflammation. *Food Res. Int.* 100, 579–585. doi:10.1016/j.foodres.2017.07.019
- Marín-García, J., and Goldenthal, M. J. (2002). Fatty Acid Metabolism in Cardiac Failure: Biochemical, Genetic and Cellular Analysis. *Cardiovasc. Res.* 54, 516–527. doi:10.1016/s0008-6363(01)00552-1
- Osorio, J. C., Stanley, W. C., Linke, A., Castellari, M., Diep, Q. N., Panchal, A. R., et al. (2002). Impaired Myocardial Fatty Acid Oxidation and Reduced Protein Expression of Retinoid X Receptor- α in Pacing-Induced Heart Failure. *Circulation* 106, 606–612. doi:10.1161/01.cir.0000023531.22727.c1
- Pfister, S. L., and Campbell, W. B. (1996). Reduced Pulmonary Artery Vasoconstriction to Methacholine in Cholesterol-Fed Rabbits. *Hypertension* 27, 804–810. doi:10.1161/01.hyp.27.3.804
- Poulter, N. (2003). Global Risk of Cardiovascular Disease. *Heart* 89, ii2–ii5. doi:10.1136/heart.89.suppl_2.ii2
- Ralston-Hooper, K., Jannasch, A., Adamec, J., and Sepúlveda, M. (2011). “The Use of Two-Dimensional Gas Chromatography–Time-Of-Flight Mass Spectrometry (GCx GC–ToF-MS) for Metabolomic Analysis of Polar Metabolites,” in *Metabolic Profiling*. Editor T. O. Metz (Springer), 708, 205–211. doi:10.1007/978-1-61737-985-7_12
- Ritterhoff, J., and Tian, R. (2017). Metabolism in Cardiomyopathy: Every Substrate Matters. *Cardiovasc. Res.* 113, 411–421. doi:10.1093/cvr/cvx017
- Roy, A., Guatimosim, S., Prado, V. F., Gros, R., and Prado, M. A. M. (2014). Cholinergic Activity as a New Target in Diseases of the Heart. *Mol. Med.* 20, 527–537. doi:10.2119/molmed.2014.00125

- Salau, V. F., Erukainure, O. L., Ibeji, C. U., Olasehinde, T. A., Koorbanally, N. A., and Islam, M. S. (2020a). Vanillin and Vanillic Acid Modulate Antioxidant Defense System via Amelioration of Metabolic Complications Linked to Fe 2+-induced Brain Tissues Damage. *Metab. Brain Dis.* 35 (5), 727–738. doi:10.1007/s11011-020-00545-y
- Salau, V. F., Erukainure, O. L., and Islam, M. S. (2020b). Caffeic Acid Protects against Iron-Induced Cardiotoxicity by Suppressing Angiotensin-Converting Enzyme Activity and Modulating Lipid Spectrum, Gluconeogenesis and Nucleotide Hydrolyzing Enzyme Activities. *Biol. Trace Elem. Res.* 199 (3), 1052–1061. doi:10.1007/s12011-020-02227-3
- Semenya, S. S., Madamombe-Manduna, I., Mashele, S. S., and Polori, K. L. (2018). Ethno-medical Botany and Some Biological Activities of *Ipomoea Oblongata* Collected in the Free State Province, South Africa. *J. Biol. Sci.* 18, 441–449. doi:10.4314/ahs.v18i4.29
- Shalaby, S. M., Zakora, M., and Otte, J. (2006). Performance of Two Commonly Used Angiotensin-Converting Enzyme Inhibition Assays Using FA-PGG and HHL as Substrates. *J. Dairy Res.* 73, 178–186. doi:10.1017/s0022029905001639
- Srivastava, D., and Rauniyar, N. (2020). *Medicinal Plants of Genus Ipomoea. Beau Bassin*. Mauritius: LAP LAMBERT Academic Publishing.
- Stanley, W. C. (2001). Cardiac Energetics during Ischaemia and the Rationale for Metabolic Interventions. *Coron. Artery Dis.* 12 (Suppl. 1), S3–S7.
- Udenigwe, C. C., Lin, Y.-S., Hou, W.-C., and Aluko, R. E. (2009). Kinetics of the Inhibition of Renin and Angiotensin I-Converting Enzyme by Flaxseed Protein Hydrolysate Fractions. *J. Funct. Foods* 1, 199–207. doi:10.1016/j.jff.2009.01.009
- Ventura-Clapier, R., Garnier, A., and Veksler, V. (2004). Energy Metabolism in Heart Failure. *J. Physiol.* 555, 1–13. doi:10.1113/jphysiol.2003.055095
- Wattanapitayakul, S. K., Chularojmontri, L., Herunsalee, A., Charuchongkolwongse, S., Niumsukul, S., and Bauer, J. A. (2005). Screening of Antioxidants from Medicinal Plants for Cardioprotective Effect against Doxorubicin Toxicity. *Basic Clin. Pharmacol. Toxicol.* 96, 80–87. doi:10.1111/j.1742-7843.2005.pto960112.x
- Wold, L. E., Ceylan-Isik, A. F., and Ren, J. (2005). Oxidative Stress and Stress Signaling: Menace of Diabetic Cardiomyopathy. *Acta Pharmacologica Sinica* 26, 908–917. doi:10.1111/j.1745-7254.2005.00146.x
- Wu, S. J., Li, Y. C., Shi, Z. W., Lin, Z. H., Rao, Z. H., Tai, S. C., et al. (2017). Alteration of Cholinergic Anti-inflammatory Pathway in Rat with Ischemic Cardiomyopathy—Modified Electrophysiological Function of Heart. *J. Am. Heart Assoc.* 6 (9), e006510. doi:10.1161/JAHA.117.006510
- Zhang, M., Swarts, S. G., Yin, L., Liu, C., Tian, Y., Cao, Y., et al. (2011). *Antioxidant Properties of Quercetin*. Boston, United States: Springer, 283–289. doi:10.1007/978-1-4419-7756-4_38

Conflict of Interest: The authors declare that the research was conducted in the absence of any commercial or financial relationships that could be construed as a potential conflict of interest.

Copyright © 2021 Erukainure, Chukwuma, Matsabisa, Javu, Salau, Koorbanally and Islam. This is an open-access article distributed under the terms of the Creative Commons Attribution License (CC BY). The use, distribution or reproduction in other forums is permitted, provided the original author(s) and the copyright owner(s) are credited and that the original publication in this journal is cited, in accordance with accepted academic practice. No use, distribution or reproduction is permitted which does not comply with these terms.



A Critical Review and Scientific Prospective on Contraceptive Therapeutics from Ayurveda and Allied Ancient Knowledge

Narendra Bhatt^{1*} and Manasi Deshpande²

¹CRIA Consultant Pvt. Ltd. Mumbai, Mumbai, India, ²Department of DravyagunaVigyan, Bharati Vidyapeeth Deemed to be University, College of Ayurved, Pune, India

OPEN ACCESS

Edited by:

Javier Echeverria,
University of Santiago, Chile

Reviewed by:

Mattan Levi,
Tel Aviv University, Israel
Parveen Bansal,
Baba Farid University of Health
Sciences, India

*Correspondence:

Narendra Bhatt
dmsbhatt@gmail.com

Specialty section:

This article was submitted to
Ethnopharmacology,
a section of the journal
Frontiers in Pharmacology

Received: 15 November 2020

Accepted: 11 May 2021

Published: 03 June 2021

Citation:

Bhatt N and Deshpande M (2021) A
Critical Review and Scientific
Prospective on Contraceptive
Therapeutics from Ayurveda and Allied
Ancient Knowledge.
Front. Pharmacol. 12:629591.
doi: 10.3389/fphar.2021.629591

Commonly used synthetic or prescribed hormonal drugs are known to interfere with the endocrine system and may have adverse reproductive, neurological, developmental, and metabolic effects in the body. These may also produce adverse effects such as polycystic ovarian disorder, endometriosis, early puberty, infertility or toxicity to gonads, testicular germ cell cancer, breast or prostate cancer, brain developmental problems, and even birth defects. Globally, the emergence of renewed interest in natural products for reproductive health is on the rise, which offers opportunities for new contraceptive developments. The search for alternate, safer contraceptive products or agents of natural origin is of scientific interest. Ayurvedic classical texts offer knowledge and information about the reproductive function and therapeutics including those for enhancement and limiting male and female fertility. Review of ancient, medieval, and recent—including texts on erotica that provide information on approaches and large numbers of formulations and drugs of plant, mineral or animal origin—claimed to have sterilizing, contraceptive, abortifacient, and related properties is presented. Few among these are known to be toxic and few are not so common. However, most of the formulations, ingredients, or modes of administration have remained unattended to, due to issues related to consumer compliance and limitations of standardization and lack of appropriate validation modalities. Several of these ingredients have been studied for their phytoconstituents and for the variety of pharmacological activities. Efforts to standardize several classical dosage forms and attempts to adapt to modern technologies have been made. List of formulations, ingredients, and their properties linked with known constituents, pharmacological, biological, and toxicity studies have been provided in a series of tables. The possible effectiveness and safety of selected formulations and ingredients have been examined. Suggestions based on new drug delivery systems integrated with advances in biotechnology, to provide prospects for new therapeutics for contraception, have been considered. Ayurveda is built on a holistic paradigm of biological entity rather than limited gonadal functions. Graphic presentation of a few carefully chosen possibilities has been depicted. New approaches to standardization and ethnopharmacological validation of natural contraceptive therapeutics may offer novel mechanisms and modalities and therapeutic opportunities to satisfy unmet needs of contraception.

Keywords: natural contraceptive, herbal contraceptive, ayurved contraceptive, reproductive health and traditional medicine, contraceptive traditions

INTRODUCTION

The world population is expected to reach more than 11 billion by 2050 (Census of India, 2011). Population in the world is currently (2020) growing at a rate of around 1.05% per year. The current average population increase is estimated at 81 million people per year and current world population is 7.9 billion as of March 2021 (World Population Clock, 2021). This burgeoning population particularly in developing countries is a matter of concern for social, economic, and environmental reasons in terms of providing food, shelter, and life. The challenge of dealing with an ever-increasing population has been dealt with largely by conventional medicine using different methods of contraception such as oral contraceptive pills, intrauterine contraceptive devices, and barrier devices. These devices, techniques, and drugs seem to have been efficiently practiced for contraception but with many reported adverse effects as well as failure resulting in unwanted pregnancy. (Dutta, 2013).

BIRTH CONTROL HISTORY

Technically, birth control can be defined as the methods, procedures, or practices that are implemented to prevent conception leading to pregnancy in women. The term can be associated with contraception and family planning where knowledge about birth control is equally important.

The Egyptian Ebers Papyrus from 1550 BCE and the Kahun Papyrus from 1850 BCE have some of the earliest documented descriptions of birth control: the use of honey, acacia leaves, and lint to be placed in the vagina to block sperm. (Lipsey et al., 2005; Cuomo, 2010).

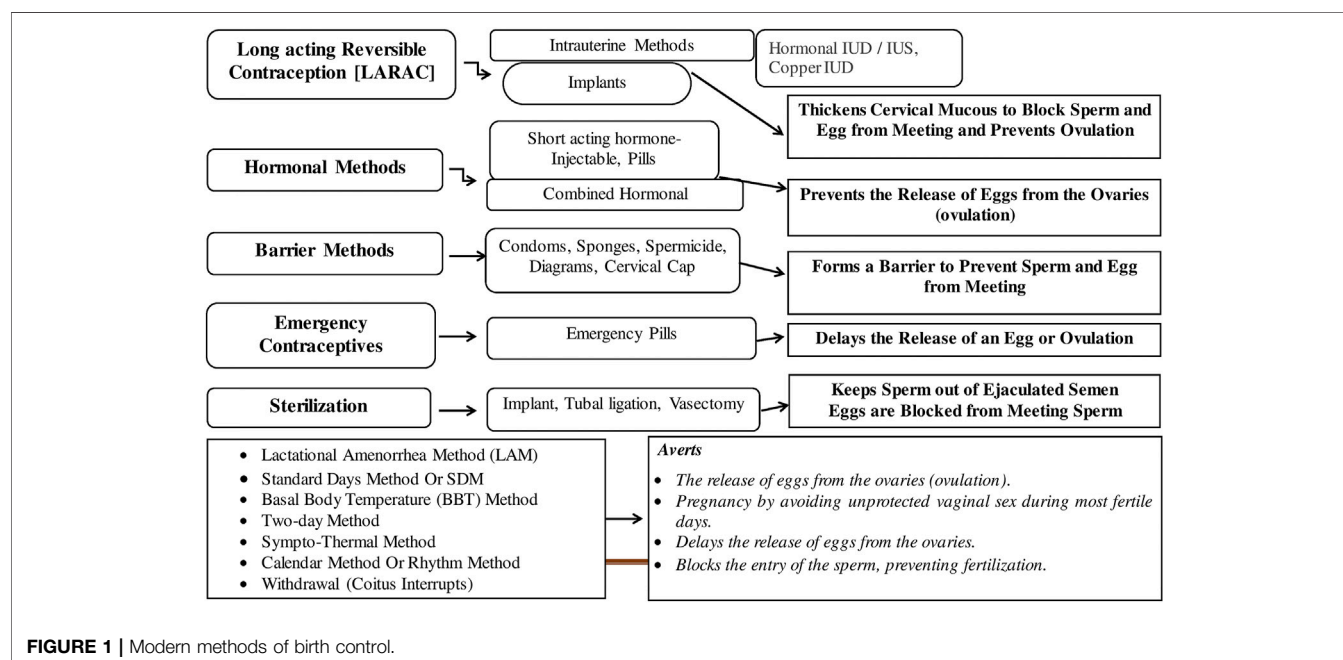
In medieval Europe, any effort to halt pregnancy was deemed immoral by the Catholic Church, (Cuomo, 2010), although it is believed that women of the time still used a number of birth control measures such as coitus interrupts and inserting lily root and rue into the vagina. Women in the middle ages were also persuaded to tie weasel—a small wild animal—testicles around their thighs during sex to prevent pregnancy. The oldest condoms discovered to date were recovered in the ruins of Dudley Castle in England and date back to 1640. They were made of animal gut and were most likely used to prevent the spread of sexually transmitted diseases during the English Civil War (Jon, 2012). Casanova, living in 18th-century Italy, described the use of a lambskin covering to prevent pregnancy; however, condoms only became widely available in the 20th century (Cuomo, 2010).

Modern Methods to Control Fertility (World Health Organization, 2020)

Several methods currently used to curb for contraception are presented (Figure 1).

ADVERSE EFFECTS

Commonly used synthetic or prescribed hormonal drugs are known to interfere with the endocrine system and may have adverse reproductive, neurological, developmental, and metabolic effects in the body. These may cause polycystic ovarian disorder, endometriosis, early puberty, infertility, toxicity to gonads, testicular germ cell cancer, breast or prostate cancer, brain developmental problems, and even birth defects. The search for alternate and safer means/drugs to prevent



birth is an open-ended area of scientific research. It is always an appealing idea to further research to develop contraceptive drugs of natural origin that have high efficacy without any adverse effects on the reproductive system.

UNMET NEEDS

According to a recent report from the Guttmacher Institute, 214 million women of reproductive age in the developing world who want to avoid pregnancy are not using a modern contraceptive method. These women are considered to have an “unmet need” for modern contraception, with 59 million relying on traditional methods such as abstinence and withdrawal and 155 million simply using no contraception at all. (Elizabeth et al., 2020).

India's total fertility rate (TFR) may have declined significantly over the years, but there remain significant challenges in family planning according to new research. In an Economic and Political Weekly article, Purushottam M. Kulkarni of Jawaharlal Nehru University suggested that there is a significant unmet need for contraception in India. Data from National Family Health Surveys (NFHS) have shown that while there was a decline in the unmet need for contraceptive services from 1992-93 (NFHS-1) through to 2005-06 (NFHS-3), and between 2005-06 and 2015-16 (NFHS-4), there has not been any significant improvement in access to contraception. (Mint, 2020).

SIGNIFICANCE OF REVIEW

Despite obvious success, the rise in population continues to remain a medical challenge due to reasons of social, economic, personal, and biological consequences. Though well-established contraceptive drugs and measures have been utilized, the long term and excessive use of hormonal contraceptives are of serious concerns due to their probable adverse effects. There is need to explore the alternative or new possibilities.

The search for an effective and safe contraceptive agent remains a challenge. Contraceptive drugs of natural origin are of all-time research interests. Traditional systems of medicine like Ayurveda address all issues related to health and illnesses based on the principle of equilibrium between the biosphere and cosmosphere, which include reproductive phenomenon. Ayurvedic pharmacopoeia has formulations and ingredients that are attributed to affect coitus, spermatogenesis, and ovulation, uterine, fetal, and placental activities. These include emmenagogues, ecboic drugs, contraceptives, uterine sedatives for females, and depurate or drugs that hamper male sexual and reproductive capabilities, affect fluidity or motility of the seminal fluid, destroy sperms, or impede libido.

A large number of drugs are known to have sterilizing, contraceptive, and abortifacients properties. However, these indigenous means and drugs were extensively used even in rural or tribal cultures until the 20th century, when there has been no noteworthy systematic or scientific efforts to study these aspects except for a few intermittent studies. While the list of such ingredients is quite big, unusually small scientific data are

available about the nature of their active components and about their mechanisms of action.

As biotechnology-based advances open up new vistas in biomedical research, it will be of interest to examine the subject of contraception once again, as in Ayurveda, in the light of present-day pharmacology for future possibilities.

A thoughtful attempt has been made here to explore Ayurvedic and scientific aspects of formulations and ingredients as described in multiplicity of classical texts covering different facets of contraception.

METHODOLOGY

Ancient classical texts, medieval compendia, and other pertinent texts were assessed for enlisting different methods used for contraception and to enlist formulations and ingredients used for a variety of activities that could be pharmacologically linked to contraception. Specific search was undertaken for any existing review that could add to information on the subject. A systematic review of published articles on the subjects related to contraception was undertaken. The description of methods used in the experimental animal models, and the antifertility effect of active ingredients, their doses, safety, and toxicity were examined. Ninety-four plants and six minerals are reported in this review having a variety of contraceptive activities.

Flowchart of the systematic review process to search for contraceptive plants is presented. (Figure 2).

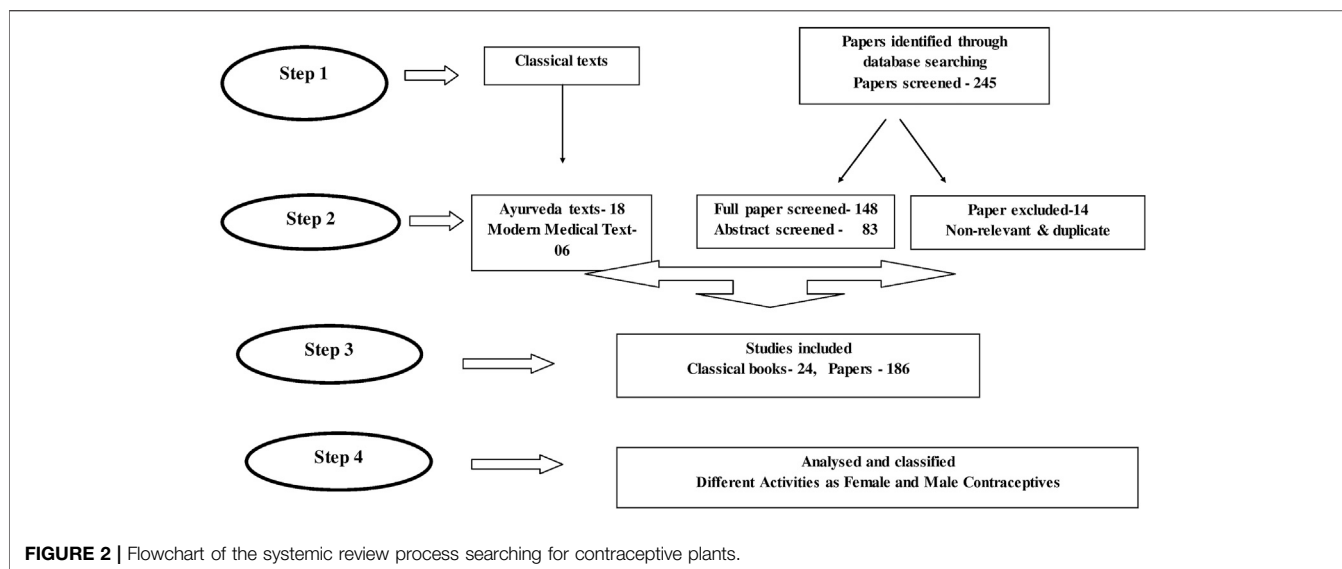
CONTRACEPTIVES IN AYURVEDA AND MEDIEVAL SANSKRIT LITERATURE

Ayurvedic literature is rife with thousands of formulations and has about 1100 ingredients attributed with well-defined therapeutic approaches including reproduction. There are references to temporary or permanent sterilization. Search for contraception from traditional knowledge of Ayurveda has been of interest to the Central Drug Research Institute, Council of Scientific and Industrial Research under Ministry of Science and Technology, and the Central Council for Research in Ayurvedic Sciences under Ministry of Health (now Ministry of AYUSH), bodies under the Government of India. Several other private and industry organizations had undertaken studies in the past. However, there is a need to revive research interest in Ayurveda in reproductive biology for safe, low-cost, user-friendly, and reliable therapeutic solutions to satisfy different contraception requirements.

Vedic Period (1500-500 BCE)

Regulated sexual life or abstinence from sex was considered the ideal method of contraception in *Vedic* times. The emphasis was more on propensity of the right, healthy progeny. Indirect references to contraception can be found in the *Atharva Veda*.

The use of drugs leading to impotence as punishment meted out to a person committing social sins or to an enemy or infliction



of injury to two cords situated near the scrotum or the scrotum itself, to put an end to one's desire for progeny were in practice. These can be considered as references for use of drugs to prevent conception, vasectomy, and castration, respectively (Satvalekar, 1958a).

A mechanical device made of stone to obstruct multiple channels of *Yoni*—the vaginal cavity to prevent conception has been mentioned. This could be considered as the earliest form of an intrauterine contraceptive device. Similarly, artificially induced changes to make the vaginal cavity rough or dry, besides its mechanical obstruction for futile coitus have been mentioned (Satvalekar, 1958b). This reference reflects some chemical changes to be produced artificially, probably in the cervical mucus obstructing the entry of sperms, or in the endometrium influencing the implantation of the zygote and a mechanical barrier in the vaginal canal. (Tewari and Chaturvedi, 1981). In *Brhadaranyaka Upanishad*, a breath exercise is advised during coitus to avoid conception (Dash and Basu, 1968).

Samhita Period: (300-500 BCE)

Though *Charak Samhita*, *Sushrut Samhita*, and *Ashtang Sangraha–Bruhatryee*, the three ancient most Ayurveda treatises, have elaborated the subject of reproduction extensively, there are no direct references to contraception.

Kshetra—the female reproductive system as the field, *ambu*—the nutrient fluids, *bija*—the sperm or ovum as the seed, *rutukal*—the ideal ovulatory period, *marga*—the female canal, *Vayu*—the neural system, and *hrid*—the psychological status are considered the essential factors for conception. Any or more of these factors if influenced artificially can lead to a failure of conception. The *shukravaha srotas* and *aartavavaha srotas* representing seminal and menstrual flows, respectively, are among the 13th intrinsic and interdependent biological pathways or channels (that could be explained based on now prevalent means of system biology). This early knowledge could pave the way for the development of different kinds of contraceptive

methods prevailing in the present scenario, and all of them influence one or the other factors that have been explained in the ancient classics (Vagbhatt, 2000; Sushrut, 2002).

Contraceptive activities in the context of Ayurvedic principle of fertility are explained in **Figure 3**.

Medieval Period (1000 AD to 1900 AD)

Rajamartanda written in the 11th century is probably one of the earliest texts to mention a specific prescription for contraceptives. Compendia texts like *Bhava Prakash*, *Yoga Ratnakara*, *Bhaishajya Ratnavali*, *Gadanigrah*, and several others prescribe many herbal and herbo-mineral contraceptive preparations for local and oral use by men and women.

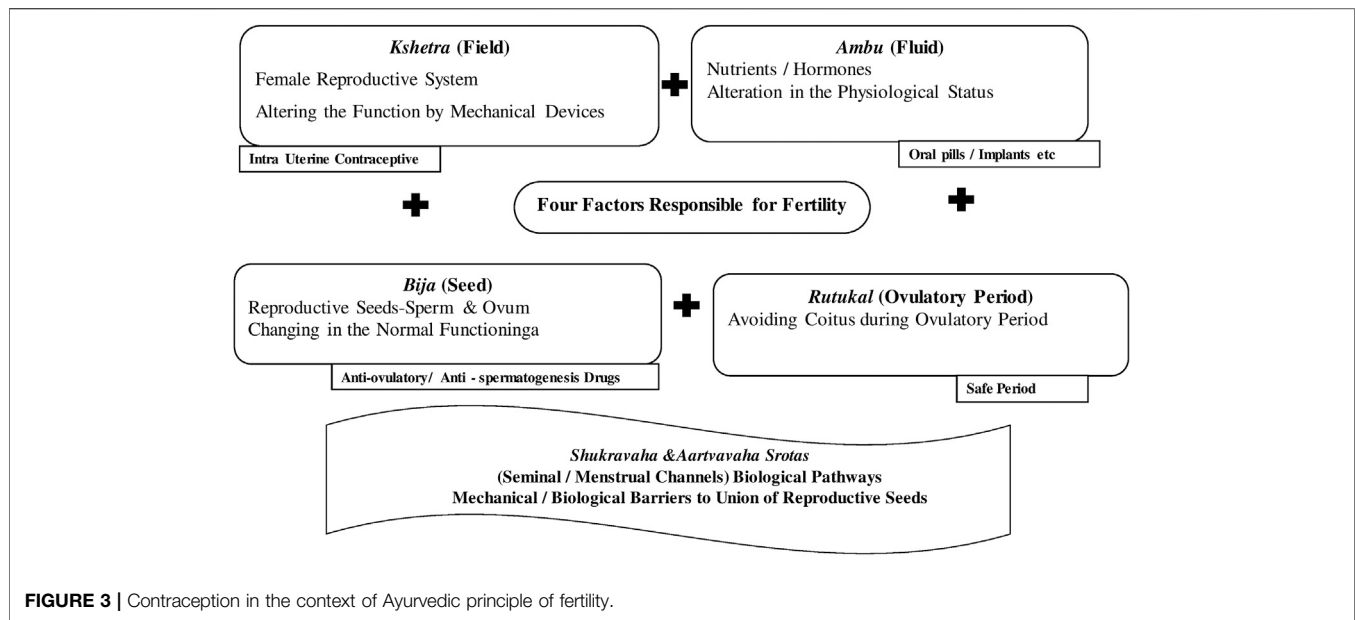
By the 11th century, the oriental connectivity that had sociocultural effects also brought in practices to prevent conception or induce abortion. References to oral and local contraceptives are found in *Bruhad Yoga Tarangini* and *RatiRahasya* [AD800], *RasaPrakashSudhakar* [AD1300], *Panchasayaka*, *Smaradeepika* and *RasaRatnaSamuccchay* [AD1400], *RatiManjiri* [AD1500], *Kandarpchudamani* [AD1577], *AnnangaRang*, *Bhavprakash* and *YogaRatnakar* [AD1600], *YogaRatnaSamuccchaya* [AD 1800], and *Brihan Nighantu Ratnakar* and *BhaishajyaRatnaval i*[AD 1900].

The subject of contraceptives in ancient times dealt not only with medieval medicine but also with art and the literary works of poets, playwrights, and philosophers. Like *Kama Sutra*, the famous text on erotica, a large number of books in the 19th century contain various recipes for contraception and for inducing abortions and diverse birth control practices.

Some of the most prescribed practices and recipes for preventing conception are as follows.

1. Local Contraceptives for Females

Vaginal fumigation or application before coitus with (1) moistened *Saindhava lavana* (Rock salt) with *Til* (Sesame) oil. (Jugnu and Sharma, 2011), (2) wood of *Neem* (*Azadirachta*



indica A. Juss.) before coitus (Tripathi, 1969), and (3) powdered root of *Dhattura* (*Datura metel* L.) plucked on the 14th day (dark night) of the lunar month [Indradev, 1998] or tying the waist with roots (Lakmipatishashtri, 1983).

2. Oral Contraceptives

- Powder of *Pippali* (*Piper longum* L.) and *Vidanga* (*Embelia ribes* Burm.f.) with *Tankana* (*Borax*) taken in equal quantity in fertile phase with milk (Lakmipatishashtri, 1983).
- Flowers of *Japa* (*Hibiscus rosa-sinensis* L.): immediately after the delivery of a child (Bhavamisra, 1961; Lakmipatishashtri, 1983) or with *Kanji* (fermented drink) along with 48 grams of old jaggery to be taken for 3 days in the fertile phase. (Lakmipatishashtri, 1983).
- Root of *Tanduliyaka* (*Amaranthus spinosus* L.) with *Tandulodaka* (rice water) to be taken after menstruation for 3 days. (Lakmipatishashtri, 1983).
- Powders of *Talisa patra* (*Abies spectabilis* (D. Don) Mirb.) and *Gairika* (*Red Ochre*, Fe_2O_3) in equal parts to be consumed on the 4th day of menstruation with water. (Lakmipatishashtri, 1983).
- Aqueous extract of *Rasanjana* (Extract of *Berberis aristata* DC.), *Hemavati* (*Sweta - Vacha*) (*Iris × germanica* L.), and *Vayastha* (*Terminalia chebula* Retz.) with cold water. (Rajeshwaradatta, 2001).
- Powders of *Amla* (*Phyllanthus emblica* L.), *Arjuna* (*Terminalia arjuna* (Roxb. ex DC)), and *Abhaya* (*Terminalia chebula* Retz.) with water. (Rajeshwaradatta, 2001).
- Paste made of the root of *Chitraka* (*Plumbago zeylanica* L.) mixed with *Nirgundi* (*Vitex negundo* L.) juice given orally in the dose of one 12 gm with honey. (Lakmipatishashtri, 1983).
- Powder of seeds of *Sarshapa* (*Brassica rapa* L.) with *Tanduliyam* (*Amaranthus spinosus* L.) and *Sarkara*

(Sugar candy) pounded with *Tandulodaka* (rice water) given with milk. (Jugnu and Sharma, 2011).

- Ashes of *Sehund stem* (*Euphorbia neriifolia* L.), 12 g daily. (Kuchimara, 2007).
- Rhizome of *Haridra* (*Curcuma longa* L.) daily during the 3 days of menstruation followed by an additional 3 days (Kuchimara, 2007).
- Powders of *Krishna Jeeraka* (*Carum carvi* L.), *Karchooram* (*Hedychium spicatum* Sm.), *Nagakesara* (*Mesua ferrea* L.), *Haritaki* (*Terminalia chebula* Retz.), *Kalonji* (*Nigella sativa* L.), and *Kayaphala* (*Myrica nagi* Thunb.) made into pills in the size of ziziphus fruit for 7 days. (Kuchimara, 2007).

3. Abortifacient

- Root of *Sweta Aparajita* (*Clitoria ternatea* L.), *Kakadani* (*Sarngesta*) (*Cardiospermum halicacabum* L.) or *Punarnava* (*Boerhavia diffusa* L.) with oil of *Eranda* (*Ricinus communis* L.)—*Patradanda* (stem of leaf) to be inserted in the vagina (Rajamartanda, 1966; Tripathi, 1969; Lakmipatishashtri, 1983).
- *Devalaya Churna* (scrapped lime powder from the wall of temple) 12 g with water. (Lakmipatishashtri, 1983; Indradev, 1998).
- Seeds of *Grnjana* (Carrot) (*Daucus carota* L.) with roots of *Tuvari* (*Cajanus cajan* (L.) Huth) and *Sindura* (lead oxide).
- *Ghotipurisa* (feces of mare) mixed with *Kanji*, filtered, and mixed with rock salt, *Ugra* (*Apium graveolens* L.), and *Asuri Taila* (Oil of *Brassica juncea* (L.) Czern.) with *Visha* (*Aconitum chasmanthum* Stapf ex Holmes) (Lakmipatishashtri, 1983).

Plant and mineral drugs mentioned as contraceptives in the Ayurvedic classical texts are given in **Table 1**.

It is observed that 79 plant drugs and six mineral drugs are used as abortifacients, oral contraceptives, or as local applications

TABLE 1 | List of plant and metal drugs as contraceptives in Ayurveda classics. Vertical column numbers indicate *AartavJanan*—Emmenagogue (1), *Aparapatan*—placental expulsion (2), *Garbhanuloman/Garbhapatkar*—Abortifacient or *Garbhastravakar*—expel Fetus (3), *Garbhanirodhak Contraceptives* (4), *Garbhashayasancochak*—Ecboic (5), *Shandhyakar/Pumstvopadhatin*—drugs that hamper male sexual or reproductive capability (6), and *Shukrashodhan*—Depurates (7).

Sr. No.	Sanskrit name	Botanical name	(1)	(2)	(3)	(4)	(5)	(6)	(7)
	<i>Aguru</i>	<i>Aquilaria malaccensis</i> Lam.		✓					
	<i>Ahiphen</i>	<i>Papaver somniferum</i> L.						✓	
	<i>Amalaki</i>	<i>Phyllanthus emblica</i> L.				✓			
	<i>Ashok</i>	<i>Saraca asoca</i> (Roxb.) J.J.de Wilde	✓				✓		
	<i>Asuri</i>	<i>Brassica juncea</i> (L.) Czern			✓				
	<i>Arjuna</i>	<i>Terminalia arjuna</i> (Roxb. ex DC.) Wight & Arn.				✓			
	<i>Bhanga</i>	<i>Cannabis sativa</i> L.						✓	✓
	<i>Bhurjapatra</i>	<i>Betula utilis</i> D. Don		✓	✓				
	<i>Chandan</i>	<i>Santalum album</i> L.						✓	
	<i>Chavya</i>	<i>Piper retrofractum</i> Vahl		✓					
	<i>Chirbilva</i>	<i>Holoptelea integrifolia</i> (Roxb.) Planch.			✓				
	<i>Chitraka</i>	<i>Plumbago zeylanica</i> L.	✓	✓	✓	✓			
	<i>Chuka</i>	<i>Rumex acetosa</i> L.						✓	
	<i>Devdaru</i>	<i>Cedrus deodara</i> (Roxb. ex D. Don) G. Don	✓	✓					
	<i>Dhanyak</i>	<i>Coriandrum sativum</i> L.						✓	
	<i>Dhattura</i>	<i>Datura metel</i> L.				✓		✓	
	<i>Ela</i>	<i>Elettaria cardamomum</i> (L.) Maton		✓	✓				
	<i>Eranda</i>	<i>Ricinus communis</i> L.			✓				
	<i>Eshvari</i>	<i>Aristolochia indica</i> L.			✓		✓		
	<i>Gmjana</i>	<i>Daucus carota</i> L.			✓				
	<i>Haridra</i>	<i>Curcuma longa</i> L.				✓			
	<i>Haritaki</i>	<i>Terminalia chebula</i> Retz.				✓			
	<i>Harmal</i>	<i>Peganum harmala</i> L.					✓		
	<i>Hemavati</i>	<i>Iris germanica</i> L.				✓			
	<i>Hingu</i>	<i>Ferula assa-foetida</i> L.			✓				
	<i>Hirabol</i>	<i>Commiphora myrrha</i> (Nees) Engl.					✓		
	<i>Japa</i>	<i>Hibiscus rosa-sinensis</i> L.				✓			
	<i>Karchuram</i>	<i>Hedychium spicatum</i> Sm.				✓			
	<i>Kadamb</i>	<i>Neolamarckia cadamba</i> (Roxb.) Bosser							✓
	<i>Kakadani (Sarngesta)</i>	<i>Cardiospermum halicacabum</i> L.			✓				
	<i>Kakamachi</i>	<i>Solanum nigrum</i> L.						✓	
	<i>Karpas</i>	<i>Gossypium herbaceum</i> L.	✓				✓		
	<i>Karpur</i>	<i>Cinnamomum camphora</i> (L.) J. Presl						✓	
	<i>Kasani</i>	<i>Cichorium intybus</i> L.						✓	
	<i>Kayaphala</i>	<i>Myrica nagi</i> Thunb.				✓			✓
	<i>Ketaki</i>	<i>Pandanus tectorius</i> Parkinson ex Du Roi			✓				
	<i>Krishna Jeeraka</i>	<i>Carum carvi</i> L.			✓	✓			
	<i>Kulattha</i>	<i>Vigna unguiculata</i> (L.) Walp.	✓	✓				✓	
	<i>Kushtha</i>	<i>Aucklandia costus</i> Falc	✓	✓	✓				✓
	<i>Langali</i>	<i>Gloriosa superba</i> L.			✓		✓		
	<i>Lodhra</i>	<i>Symplocos racemosa</i> Roxb.					✓		
	<i>Mandukparni</i>	<i>Centella asiatica</i> (L.) Urb.		✓					
	<i>Mocharas</i>	<i>Bombax ceiba</i> L.					✓		
	<i>Nagakesara</i>	<i>Mesua ferrea</i> L.				✓			
	<i>Nagdamani</i>	<i>Artemisia nilagirica</i> (C. B. Clarke) Pamp.			✓				
	<i>Neem</i>	<i>Azadirachta indica</i> A. Juss.				✓	✓		
	<i>Nimbu</i>	<i>Citrus × aurantium</i> L.						✓	
	<i>Nilophar</i>	<i>Nymphaea alba</i> L.						✓	
	<i>Nirgundi</i>	<i>Vitex negundo</i> L.			✓	✓		✓	
	<i>Pippali</i>	<i>Piper longum</i> L.		✓		✓			
	<i>Punarnava</i>	<i>Boerhavia diffusa</i> L.			✓				
	<i>Rasanjana</i>	<i>Berberis aristata</i> DC.				✓			
	<i>Rason</i>	<i>Allium cepa</i> L.						✓	
	<i>Sarshapa</i>	<i>Brassica rapa</i> L.					✓		
	<i>Sehund</i>	<i>Euphorbia nerifolia</i> L.					✓		
	<i>Shal-sarjarasa</i>	<i>Shorea robusta</i> Gaertn.	✓						
	<i>Shallaki</i>	<i>Boswellia serrata</i> Roxb.					✓		
	<i>Shan</i>	<i>Dioscorea polystachya</i> Turcz.	✓						
	<i>Shigru</i>	<i>Moringa oleifera</i> Lam.			✓				
	<i>Shinshapa</i>	<i>Dalbergia sissoo</i> Roxb. ex DC.			✓				
	<i>Shyonak</i>	<i>Oroxylum indicum</i> (L.) Kurz					✓		

(Continued on following page)

TABLE 1 | (Continued) List of plant and metal drugs as contraceptives in Ayurveda classics. Vertical column numbers indicate *AartavJanan*—Emmenagogue (1), *Aparapatan*—placental expulsion (2), *Garbhanuloman/Garbhapatkar*—Abortifacient or *Garbhastravakar*—expel Fetus (3), *Garbhanirodhak Contraceptives* (4), *Garbhashayasancochak*—Ecboic (5), *Shandhyakar/Pumstvopadhatin*— drugs that hamper male sexual or reproductive capability (6), and *Shukrashodhan*—Depurates (7).

Sr. No.	Sanskrit name	Botanical name	(1)	(2)	(3)	(4)	(5)	(6)	(7)
	<i>Sitab</i>	<i>Ruta graveolens</i> L.					✓	✓	✓
	<i>Sitaphal</i>	<i>Annona squamosa</i> L.			✓	✓			
	<i>Sunthi</i>	<i>Zingiber officinale</i> Roscoe		✓					
	<i>Sweta Aparajita</i>	<i>Clitoria ternatea</i> L.			✓				
	<i>Talisa patra</i>	<i>Abies spectabilis</i> (D. Don) Mirb.	✓	✓		✓			
	<i>Tanduliyaka</i>	<i>Amaranthus spinosus</i> L.				✓			
	<i>Tintidika</i>	<i>Tamarindus indica</i> L.						✓	
	<i>Tilataila</i>	Sesame oil				✓			
	<i>Tuvari</i>	<i>Cajanus cajan</i> (L.) Huth			✓				
	<i>Ugra</i>	<i>Apium graveolens</i> L.			✓				
	<i>Ulatakambal</i>	<i>Abroma augusta</i> (L.) L.f.	✓				✓		
	<i>Unnab</i>	<i>Ziziphus jujuba</i> Mill.						✓	
	<i>Upakunchika</i>	<i>Nigella sativa</i> L.		✓		✓	✓		
	<i>Ushir</i>	<i>Chrysopogon zizanioides</i> (L.) Roberty							✓
	<i>Vacha</i>	<i>Acorus calamus</i> L.			✓				
	<i>Vansha</i>	<i>Bambusa bambos</i> (L.) Voss	✓					✓	
	<i>Vidanga</i>	<i>Embelia ribes</i> Burm.f.	✓	✓		✓			
	<i>Visha</i>	<i>Aconitum chasmanthum</i> Stapf ex Holmes			✓				
Minerals/Metals									
	<i>Devalaya Churna</i>	Scrapped lime powder from the wall of temple				✓			
	<i>Gairika</i>	Red Ochre, Fe_2O_3				✓			
	<i>Nausagar</i>	NH_4Cl						✓	
	<i>Saindhava lavana</i>	Rock salt				✓			
	<i>Sindura</i>	Lead oxide			✓	✓			
	<i>Tankana</i>	Borax				✓			

along with *Kanji* (fermented drink), *Tandulodaka* (rice water), *Sarkara* (sugar candy), milk, and honey.

POTENTIAL INGREDIENTS HAVING ANTIFERTILITY OR CONTRACEPTIVE PROPERTIES

This literature survey revealed that there are about more than 94 indigenous medicinal plants having scientific evidence of acting as contraceptives. Some of the remarkable plant drugs with parts used, their chemical constituents, and pharmacological activities are described in **Table 2**. This compiled information will provide useful reference for new drug designing models, acting either as male or female contraceptives.

Pharmacologically, there are about 67 medicinal plants which possess antifertility activity in females and 56 medicinal plants in males. Several plants have shown to help contraception from the female and male perspectives.

In various experimental animal models, these herbal extracts have shown minimal side effects in comparison to the chemically synthesized contraceptives, which usually contain various combinations of hormones. These plant extracts have active phytoconstituents, which are responsible for the antifertility effects such as antioovulation, anti-implantation, and others.

CLINICAL STUDIES

Some of the plants that have demonstrated interesting antifertility activity in clinical trials are as follows.

Embelia ribes Burm.f.

Single drug was administered in a dose of 2°g for 5°days followed by 1°g daily for another 10°days. After observing the effect on 2051 cycles in 45 women over 4°years, it was reported that the plant protected 95% of women from pregnancy (Tewari et al., 1976).

Hibiscus rosa-sinensis L.

Red petals of the plant *Rudrapushpaka* collected between October and December. The extract was administered to 30 sexually active women at a dose of 750°mg/day from day 7 to day 22 of the reproductive cycle. It was observed that no one had become pregnant (Tewari, 1974).

Neem oil

A study was conducted on neem seed oil as local application for the reproductive female [246 women in the fertile age-group, 4 dropped out] as a method of family planning for a period of 12–36 cycles. In nine cases, there was conception due to drug failure and in four cases, there was conception due to drug omission. Neem seed oil may be used as an external barrier as

TABLE 2 | Medicinal plants and their phytoconstituents validated for various female/male contraceptive activities. Different contraceptive activities studied on medicinal plants could be categorized as follows. Female contraceptive activities: (2A) anti-implantation activity, (2B) abortifacient, (2C) antifertility, (2D) antioviulatory, and (2E) antiestrogenic activity. Male contraceptive activities: (2F) antispermatogenic, (2G) spermicidal, and (2H) antiandrogenic activity.

Sr. No.	Botanical name, family, Sanskrit name, parts	Chemical composition	Extract	Mode of action in experimental studies	Reference
A Anti-implantation activity					
1.	<i>Abies spectabilis</i> (D. Don) Mirb. Pinaceae Talisa Patra, leaf	Flavonoids, bioflavonoids, glycosides, phytosterols	Benzene, alcoholic	Anti-implantation activity	Anonymous (1996)
2.	<i>Abroma augusta</i> (L.) L.f. Malvaceae Pishach karpas, roots	L-rhamnose, L-arabinose, D-xylose, D-mannose, D-galactose, D-glucose, D-galacturonic acid, and D-glucuronic acid	Alcoholic	Anti-implantation	Maurya et al. (2004), Pokharkar et al. (2010), Kalita et al. (2011)
3.	<i>Adhatoda vasica</i> Nees synonym of <i>Justicia adhatoda</i> L. Acanthaceae Vasa, leaves	Alkaloids, tannins, saponins, and phenolics flavonoids	Aqueous	Anti-implantation	Pokharkar et al. (2010); Kaur et al. (2011); Raj et al. (2011)
4.	<i>Ailanthus excelsa</i> Roxb Simaroubaceae Maharukha, leaves	Sitosterol, quassinoids, and ailantic acid	Ethanollic	Anti-implantation decreased of implant sites	Priya et al. (2012); Tamboli and Konadawar (2013)
5.	<i>Allium cepa</i> L. Amaryllidaceae Palandu, onion, bulb	Kampferol, β -sitosterol, ferulic acid, and myritic acid	Ethanollic	Anti-implantation inhibition of implant sites	Thakare et al. (2009); Ola-Mudathir et al. (2008)
6.	<i>Aloe barbadensis</i> Mill. Synonym of aloe vera (L.) Burm.f. Asphodelaceae Kumari, leaves	Water, polysaccharides, pectin, cellulose, hemicellulose, and glucomannan	Ethanollic and aqueous	Anti-implantation	Shah et al. (2017), Shah et al. (2016)
7.	<i>Areca catechu</i> L. Areaceae Poogaphala, Nuts	Alkaloids—pilocarpine, arecaidine, and arecoline	Petroleum ether, alcoholic, and aqueous	Anti-implantation	Garg and Garg (1970); Garg and Garg (1971)
8.	<i>Cassia fistula</i> L. Fabaceae Aragvadha, fruits, bark	Alkaloid	Aqueous	Anti-implantation, decreased glycogen content in uterus, and antifertility	Yadav and Jain (2009)
9.	<i>Carica papaya</i> L. Caricaceae, Papaya unripe fruit pulp, seeds, latex	Papain, caricacin, carposamine, and oleanolic glycoside	Pet ether, alcohol, and aqueous ethanol	60 % anti-implantation activity, abortifacient in albino rats	Garg and Garg (1970); Garg and Garg (1971); Das (1980); Sinha and Nathawat (1989); Changamma and Lakshman (2013)
10.	<i>Centratherum anthelminticum</i> (L.) Gamble Asteraceae Vanya Jeeraka, seeds	Glycosides, carbohydrates, phenolic compounds, tannins, flavonoids, proteins, saponins, and sterols	Ethanol	Postcoital anti-implantation activity	Sharma et al. (1994)
11.	<i>Citrus × aurantium</i> L. Rutaceae Bijaura, seeds	Citroflavonoids, glucosides, and triterpenoids	Petroleum ether	Anti-implantation, antioviulatory, abortifacients increased ovarian weight, decreased Graafian follicles, and irregular estrous cycle	Patil and Patil (2013)
12.	<i>Embelia ribes</i> Burm.f. Primulaceae Vidang, berries	Embelin, volatile oil, and fixed oil	Isolated embelin	Anti-implantation and postcoital antifertility activity	Prakash (1981); Nand (1981); Dixit and Joshi (1983)

(Continued on following page)

TABLE 2 | (Continued) Medicinal plants and their phytoconstituents validated for various female/male contraceptive activities. Different contraceptive activities studied on medicinal plants could be categorized as follows. Female contraceptive activities: (2A) anti-implantation activity, (2B) abortification, (2C) antifertility, (2D) antioviulatory, and (2E) antiestrogenic activity. Male contraceptive activities: (2F) antispermatogetic, (2G) spermicidal, and (2H) antiandrogenic activity.

Sr. No.	Botanical name, family, Sanskrit name, parts	Chemical composition	Extract	Mode of action in experimental studies	Reference
13.	<i>Gloriosa superba</i> L. Colchicaceae Langli Root	Colchicine (superbine)	Hydroalcoholic extract at two different doses	Antifertility, anti-implantation activity in postcoital study, abortifacient activity	Latha et al. (2013)
14.	<i>Grewia asiatica</i> L. Malvaceae, seeds	Potassium, calcium, phosphorus, copper, zinc, and magnesium	Aqueous	Anti-implantation and abortification activity	Kamboj and Dhawan (1982)
15.	<i>Hibiscus rosa-sinensis</i> L. Malvaceae Japa Flowers	Cyclopeptide alkaloid	Ethanol and benzene extract	Anti-implantation, antioviulatory, increased uterine weight, secretion of estrogenic by atretic follicles, postcoital antifertility	Neeru and Sharma (2008); Vasudeva and Sharma (2008); Hadimur et al. (2014), Pal et al. (1985)
16.	<i>Mesua ferrea</i> L. Calophyllaceae Nagakeshara, flowers	Mesuol, mamegin, mesuaferronea, and mameuisin	Aqueous	Anti-implantation activity	Seshadri and Pillai (1981); Munshi et al. (1977)
17.	<i>Michelia champaca</i> L. Magnoliaceae Champaka, Anthers	Essential oil	Benzene and hydroalcoholic extract	Postcoital anti-implantation activity	Sharma et al. (1994); Taprial et al. (2013)
18.	<i>Momordica charantia</i> L. Cucurbitaceae Karwellaka roots, leaves	Glycosides, saponins, alkaloids, fixed oils, triterpenes, proteins, and steroids	Aqueous	Uterine stimulant activity, Antifertility, estrogenic activity	Jamwal and Anand (1962); Saksena (1971)
19.	<i>Plumbago zeylanica</i> L. Plumbaginaceae Chitrak, root	Plumbagin	Plumbagin-free alcohol	Anti-implantation and abortifacient activity	Gupta et al. (2011)
20.	<i>Ricinus communis</i> L. Euphorbiaceae Erand, castor bean Seed	Ricine and isoquinoline	Aqueous	Anti-implantation, increase in diameter of the uterus, and decrease in uterine hormones	Makonnen et al. (1999)
21.	<i>Rubia cordifolia</i> L. Rubiaceae Manjishtha Root	Munjistin, purpurin, and pseudopurpurin	Ethanol extract	Anti-implantation	Maurya et al. (2004)
22.	<i>Sapindus trifoliatus</i> L. Sapindaceae Arishtak Fruits, pulp, and seeds	Essential oil	Butanol	Antizygotic, blastocytotoxic, or anti-implantation activity	Pal et al. (2013); Bodhankar et al. (1974)
23.	<i>Sesbania sesban</i> (L.) Merr. Fabaceae Sesban Leaves	Alkaloids, flavonoids, glycosides, tannin, anthraquinone, steroid, phlobatannins, and terpenoids	Extract and powder	Inhibit the ovarian function, change the uterine structure, and prevent the implantation	Singh (1990a); Samajdar and Ghosh (2017)
B Abortification activity					
1.	<i>Abroma augusta</i> (L.) L.f. Malvaceae <i>Pishach karpas</i> , roots	L-rhamnose, L-arabinose, D-xylose, D-mannose, D-galactose, D-glucose, D-galacturonic acid, and D-glucuronic acid	Alcoholic	Abortification activity	Pokharkar et al. (2010); Kalita et al. (2011)

(Continued on following page)

TABLE 2 | (Continued) Medicinal plants and their phytoconstituents validated for various female/male contraceptive activities. Different contraceptive activities studied on medicinal plants could be categorized as follows. Female contraceptive activities: (2A) anti-implantation activity, (2B) abortification, (2C) antifertility, (2D) antioviulatory, and (2E) antiestrogenic activity. Male contraceptive activities: (2F) antispermatogenic, (2G) spermicidal, and (2H) antiandrogenic activity.

Sr. No.	Botanical name, family, Sanskrit name, parts	Chemical composition	Extract	Mode of action in experimental studies	Reference
2.	<i>Abrus precatorius</i> L. Papilionaceae Gunja, Seeds	Abrin, abrasine, precasine, and precol	Aqueous	Abortifacient activity or antifertility agent with a risk of DNA damage	Sarwat et al. (2009); Kaur et al. (2011); Shrivastava et al. (2007); Azmeera et al. (2012); Priya et al. (2012)
3.	<i>Achyranthes aspera</i> L. Amaranthaceae Apamarga Whole plant, Stem bark, Root	Fatty acids, oleonic acid, bisdesmosidic, triterpenoid alkaloids, D-glucuronic, betaine, and achyranthine	Benzene, ethanolic, and chloroform	Abortifacient activity in rabbits	Raj et al. (2011); Vasudeva and Sharma (2006)
4.	<i>Adhatoda vasica</i> Nees synonym of <i>Justicia adhatoda</i> L. Acanthaceae, Vasa, Leaves	Alkaloids, tannins, saponins, phenolics, and flavonoids	Aqueous	Abortification activity	Pokharkar et al. (2010); Kaur et al. (2011); Raj et al. (2011)
5.	<i>Aegle marmelos</i> (L.) Corrêa. Rutaceae Bilva, whole plant, leaves	Marmelosin, luvangetin, psoralen, tannins, and marmin	Aqueous extract	Abortifacient activity in albino rats	Gangadhar and Lalithakumari (1995); Sathiyaraj et al. (2010)
6.	<i>Annona squamosa</i> L. Annonaceae Custard apple Seeds, leaves, and bark	Atropine alkaloids, and anonaine	Ethyl acetate extract	Abortifacient induces early abortion	Jain and Dixit (1992)
7.	<i>Areca catechu</i> L. Arecaceae Poogaphala, nuts	Alkaloids—pilocarpine, arecaidine, and arecoline	Petroleum ether, alcoholic, and aqueous	Abortifacient activity in albino rats and antifertility activity	Garg and Garg (1970); Garg and Garg (1971); Shrestha et al. (2010)
8.	<i>Barleria prionitis</i> L. Acanthaceae Saireyak, Roots	Acbarlerin, barlerin, β -sitosterol, flavanol glycoside, and iridoids	Methanol extract	Abortifacient	Gupta et al. (2000)
9.	<i>Carica papaya</i> L. Caricaceae Papaya unripe fruit pulp, seeds, and latex	Papain, caricacin, carpasemine, and oleanolic glycoside,	Pet ether, alcohol, and aqueous ethanol	Abortifacient in albino rats and antifertility	Garg and Garg (1970), Garg and Garg (1971); Das (1980); Sinha and Nathawat (1989); Changamma and Lakshman (2013)
10.	<i>Citrus × aurantium</i> L. Rutaceae Bijaura, Seeds	Citroflavonoids, glucosides, and triterpenoids	Petroleum ether	Abortifacient, increased ovarian weight, decreased Graafian follicles, and irregular estrous cycle	Patil and Patil (2013)
11.	<i>Daucus carota</i> L. Apiaceae Grinjanak, seed	Essential oil	Petroleum, ether, benzene, alcohol, and water	Abortifacient activity	Garg (1975); Jansen and Wolhimuth (2014); Shah and Varute (1980)
12.	<i>Gloriosa superba</i> L. Colchicaceae Langli Root	Carbohydrates, flavonoids, steroids, alkaloids, tannins, and glycosides	Ether, chloroform, and ethyl alcohol extracts	Abortifacient activity and significant reduction in number of implants and number of pups born	Malpani and Mahurkar (2018)
13.	<i>Grewia asiatica</i> L. Malvaceae, seeds	Potassium, calcium, phosphorus, copper, zinc, and magnesium	Aqueous	Abortification activity	Kamboj and Dhawan (1982)
14.	<i>Lepidium sativum</i> L. Brassicaceae Chandrasur Mature explants	Lepidine	Methanolic	Abortifacient and antioviulatory	Pande et al. (2002)

(Continued on following page)

TABLE 2 | (Continued) Medicinal plants and their phytoconstituents validated for various female/male contraceptive activities. Different contraceptive activities studied on medicinal plants could be categorized as follows. Female contraceptive activities: (2A) anti-implantation activity, (2B) abortification, (2C) antifertility, (2D) antiovarulatory, and (2E) antiestrogenic activity. Male contraceptive activities: (2F) antispermato-genic, (2G) spermicidal, and (2H) antiandrogenic activity.

Sr. No.	Botanical name, family, Sanskrit name, parts	Chemical composition	Extract	Mode of action in experimental studies	Reference
15.	<i>Ricinus communis</i> L. Euphorbiaceae Erand, Castor bean Seed	Ricinine and isoquinoline	Aqueous extract	Abortifacient	Makonnen et al. (1999), Sandhyakumary et al. (2003)
16.	<i>Woodfordia fruticosa</i> (L.) Kurz Lythraceae Dhataki, flowers	Tannins, flavonoids, anthraquinone glycosides, and polyphenols	Aqueous and ethanol	Abortifacient	Pathak et al. (2005)
C Antifertility activity					
1.	<i>Abrus precatorius</i> L. Papilionaceae Gunja, Seeds	Abrin, abrasine, precasine, and precol	Aqueous	Antifertility agent with a risk of DNA damage	Sarwat et al. (2009); Kaur et al. (2011); Shrivastava et al. (2007); Azmeera et al. (2012); Priya et al. (2012)
2.	<i>Acacia leucophloea</i> (Roxb.) Willd. Leguminosae—Fabaceae Shwet babul, roots	N-hexacosanol, beta-amyrin, beta-sitosterol, and tannin	Alcoholic	Antifertility activity	Dheeraj (2011)
3.	<i>Annona squamosa</i> L. Annonaceae Custard apple Seeds, leaves, and bark	Atropine alkaloids and anonaine	Ethyl acetate extract	Abortifacient—induces early abortion	Jain and Dixit (1992)
4.	<i>Areca catechu</i> L. Arecaceae Poogaphala, Nuts	Alkaloids—pilocarpine, arecaine, and arecoline	Nut oil Ethanol extract	Antifertility activity in female albino rats, antiovarulatory, and ovarian weight decreased due to imbalance in gonadotrophins	Garg et al. (1974); Shrestha et al. (2010)
5.	<i>Azadirachta indica</i> A. Juss Meliaceae Nimba Leaves, flower, and seed	Azadirachtin, nimbolin, nimbin, nimbidin, nimbidol, sodium nimbin, and gedunin	Female albino rabbits Seed oil	Antifertility and functional sterility	Vyas and Purohit (2018)
6.	<i>Carica papaya</i> L. Caricaceae Papaya unripe fruit pulp, seeds, and latex	Papain, caricacin, carposmine, and oleanolic glycoside	Pet ether, alcohol, aqueous, and ethanol	Antifertility	Garg and Garg (1970); Garg and Garg (1971); Das (1980); Sinha and Nathawat (1989); Changamma and Lakshman (2013)
7.	<i>Cissampelos pareira</i> L. Menispermaceae, Patha Leaves and stem	Berberine	Leaf extract	Altered the estrous cycle pattern in female mice, Antifertility	Ganguly et al. (2007); Samatha et al. (2011)
8.	<i>Cuminum cyminum</i> L. Apiaceae Jeerak, seeds	Cuminal and cuminic alcohol	Extract	Antifertility effect in female albino rat	Priya et al. (2012); Sharma J et al. (2001)
9.	<i>Crataeva nurvala</i> Buch-Ham. Capparaceae Varuna Dried stem bark	Alkaloids, triterpene, tannins, saponins, flavonoids, sterols, glucosylinate, lupeol, and diosgenin	Ethanol, aqueous	Antifertility effects estrogenic activity	Bhaskar et al. (2009)
10.	<i>Curcuma longa</i> L. Zingiberaceae Haldi, rhizome	Curcumin and flavanoids	Ethanol, aqueous	Propylene glycol solution, antifertility, antiovarulatory—suppression of GnRH	Ghosh et al. (2011); Bhagat and Purohit (1986)

(Continued on following page)

TABLE 2 | (Continued) Medicinal plants and their phytoconstituents validated for various female/male contraceptive activities. Different contraceptive activities studied on medicinal plants could be categorized as follows. Female contraceptive activities: (2A) anti-implantation activity, (2B) abortification, (2C) antifertility, (2D) antioviulatory, and (2E) antiestrogenic activity. Male contraceptive activities: (2F) antispermatogenic, (2G) spermicidal, and (2H) antiandrogenic activity.

Sr. No.	Botanical name, family, Sanskrit name, parts	Chemical composition	Extract	Mode of action in experimental studies	Reference
11.	<i>Daucus carota</i> L. Apiaceae Grinjanak, Seed	Essential oil	Petroleum, ether, benzene, alcohol, and water	Antifertility activity	Garg (1975); Jansen and Wolhlmuth (2014); Shah and Varute (1980)
12.	<i>Desmodium gangeticum</i> (L.) DC. Fabaceae Shaliparni, Root	Lavonoid glycosides, pterocarpanoids, lipids, glycolipids, and alkaloids	Gangeticum	Antifertility effect	Pillai et al. (1982)
13.	<i>Embelia ribes</i> Burm.f. Primulaceae Vidang, Berries	Embelin, volatile oil, fixed oil, resin, tannin, christembine (alkaloid), and phenolic acids	Isolated embelin	Anti-implantation and postcoital antifertility activity	Prakash (1981b)
14.	<i>Ferula jaeschkeana</i> Vatke Apiaceae Heengupatri, Dried leaves	Flavonoids, alkaloids, terpenoids, cardiac glycosides, saponins, and phenolics	Hexane	Duration-dependent luteolytic changes in the corpora lutea	Pathak et al. (1995)
15.	<i>Gloriosa superba</i> L. Colchicaceae Langli, Root	Colchicine (superbine)	Hydroalcoholic extract at two different doses 30 and 60 mg/kg	Antifertility, anti-implantation activity in postcoital study	Latha et al. (2013)
16.	<i>Hibiscus rosa-sinensis</i> L. Malvaceae Japa Flowers	Cyclopeptide alkaloid	Ethanol and benzene extract	Anti-implantation, antioviulatory, secretion of estrogenic by atretic follicles, and postcoital antifertility	Neeru and Sharma (2008)
17.	<i>Lawsonia inermis</i> L. Lythraceae Madayantika Leaves	Lawson, esculetin, fraxetin, isoplumbagin, scopoletin, betulin, betulinic acid, hennadiol, lupeol, lacoumarin, quinone, and naphthaquinone	Powder	Preventing pregnancy in 60% of the animals tested	Munshi et al. (1977)
18.	<i>Lepidium sativum</i> L. Brassicaceae Chandrasur Mature explants	Lepidine	Methanolic	Abortifacient and antioviulatory	Pande et al. (2002)
19.	<i>Melia azedarach</i> L. <i>Meliaceae</i> , MalaVembu seed and leaves	Triterpenoids	Seed extract	Antifertility effect, increased preimplantation, postimplantation, and total prenatal mortalities	Mandal and Dhariwal (2007)
20.	<i>Momordica charantia</i> L. Cucurbitaceae Karwellaka Roots and leaves	Glycosides, saponins, alkaloids, fixed oils, triterpenes, proteins, and steroids	Aqueous	Uterine stimulant activity, antifertility, and estrogenic activity	Jamwal and Anand (1962); Saksena (1971)
21.	<i>Nigella sativa</i> L. Ranunculaceae Krishna jeerak, Seeds	Fixed oil, volatile oil, and alkaloids	Hexane	Antifertility activity in rats, postcoital contraceptive	Keshri et al. (1995)
22.	<i>Piper betle</i> L. Piperaceae Betel leaf, Pan Petiol	Eugenol, eugenol acetate, piper betol, piperol, and methyl eugenol phytol	Alcoholic	Antifertility, antiestrogenic effects in female rats	Sharma et al. (2007)
23.	<i>Piper longum</i> L. Piperaceae Pippali Root and ruits	Piperine	Powder, hexane fraction, and benzene	Antifertility activity—prolonged the length of the extort cycle, drastic reduction in the number of implantation sites, marked suppression in the ovarian cytokines and nitric acid level	Laxmi et al. (2006); Kholkute et al. (1979)

(Continued on following page)

TABLE 2 | (Continued) Medicinal plants and their phytoconstituents validated for various female/male contraceptive activities. Different contraceptive activities studied on medicinal plants could be categorized as follows. Female contraceptive activities: (2A) anti-implantation activity, (2B) abortifacient, (2C) antifertility, (2D) antiovarian, and (2E) antiestrogenic activity. Male contraceptive activities: (2F) antispermatozoicidal, (2G) spermicidal, and (2H) antiandrogenic activity.

Sr. No.	Botanical name, family, Sanskrit name, parts	Chemical composition	Extract	Mode of action in experimental studies	Reference
24.	<i>Trichosanthes cucumerina</i> L. Cucurbitaceae Snake gourd, Fruit	Cucurbitacin B, cucurbitacin E, isocucurbitacin B, E, sterols 2 β -sitosterol stigmasterol	Aqueous	Affected the normal estrous cycle, significantly reduced the number of healthy follicles, corpora lutea, and increased the number of regressing follicles. Reduced serum FSH and LH levels	Devendra et al. (2009)
25.	<i>Zingiber officinale</i> Roscoe Zingiberaceae Sunthi Rhizome	Monocyclic, phenols, sesquiterpenes, essential oil, oleoresins, and proteolytic enzymes	Aqueous, ethanol extracts	Antifertility activity	Pathak et al. (2005)
D Antiovarian activity					
1.	<i>Achyranthes aspera</i> L. Amaranthaceae Apamarga Whole plant, Stem bark, Root	Fatty acids, oleonic acid, bisdesmosidic, triterpenoid alkaloids, D-glucuronic, betaine, and achyranthine	Benzene, ethanolic, chloroform	Antiadulatory, anti-implantation, hormonal disturbance in uterus, and expulsion of ovary	Shibeshi et al. (2006); Vasudeva and Sharma (2006)
2.	<i>Areca catechu</i> L. Areaceae Poogaphala, Nuts	Alkaloids—pilocarpine, arecaidine, and arecoline	Ethanolic extract	Antiovarian, ovarian weight decreased due to imbalance in gonadotrophins	Shrestha et al. (2010)
3.	<i>Azadirachta indica</i> A. Juss. Meliaceae Nimba Leaves, flower, and seed	Azadirachtin, nimbin, nimbidin, nimbidol, sodium nimbin, and gedunin	Alcoholic extract flower in Sprague–Dawley rats	Disrupted the estrous cycle and caused a partial block in ovulation	Gbotolorun et al. (2003); Vyas and Purohit (2018)
4.	<i>Butea monosperma</i> (Lam.) Kuntze Fabaceae Palash, bark, and flowers	Kino-tannic acid, gallic acid, and pyrocatechin	Aqueous extract	Inhibit ovulation	Shrivastava et al. (2007), Sinha and Nathawat (1989)
5.	<i>Calotropis procera</i> (Aiton) W.T. Aiton Apocynaceae Arka, Root	Steroidal alkaloid	Calotropin, aqueous ethanol	Antiovarian prolonged di-estrous stage with temporary inhibition of ovulation	Gupta et al. (1990); Abdelgader and Elsheikh (2018); Sharma and Jacob (2001a); Pokharkar et al. (2010)
6.	<i>Catunaregam spinosa</i> (Thunb.) Tirveng. Rubiaceae Madanphal, Fruits, seeds, and pulp	Saponins, valeric acid resin, wax, and coloring matter	Ethanolic extract, isolated oleic acid	Antiovarian effect in rabbits, antiimplantation activity in albino rats	Malhi and Trivedi (1972); Pillai et al. (1977)
7.	<i>Citrus × aurantium</i> L. Rutaceae Bijaura, Seeds	Citroflavonoids, glucosides, and triterpenoids	Petroleum ether	Anti-implantation, antiovarian, abortifacient, increased ovarian weight, decreased Graafian follicles, irregular estrous cycle	Patil and Patil (2013)
8.	<i>Curcuma longa</i> L. Zingiberaceae Haldi, rhizome	Curcumin and flavonoids	Ethanol, aqueous	Propylene glycol solution antifertility, antiovarian, decreased ovarian weight, suppression of GnRH	Ghosh et al. (2011)
9.	<i>Hibiscus rosa-sinensis</i> L. Malvaceae Japa, Flowers	Cyclopeptide alkaloid	Ethanol, benzene extract	Anti-implantation, antiovarian, increased uterine weight, secretion of estrogenic by atretic follicles, postcoital antifertility	Neeru and Sharma (2008)

(Continued on following page)

TABLE 2 | (Continued) Medicinal plants and their phytoconstituents validated for various female/male contraceptive activities. Different contraceptive activities studied on medicinal plants could be categorized as follows. Female contraceptive activities: (2A) anti-implantation activity, (2B) abortification, (2C) antifertility, (2D) antioviulatory, and (2E) antiestrogenic activity. Male contraceptive activities: (2F) antispermatogetic, (2G) spermicidal, and (2H) antiandrogenic activity.

Sr. No.	Botanical name, family, Sanskrit name, parts	Chemical composition	Extract	Mode of action in experimental studies	Reference
10.	<i>Musa paradisiaca</i> L. Musaceae, Banana, stem	Alkaloids and flavonoids	Ethanollic	Antioviulatory suppressed ovulation due to inhibition in secretion of GnRH	Soni et al. (2013)
11.	<i>Papaver somniferum</i> L. Papaveraceae <i>Ahiphen</i> , Latex	Noscapine alkaloid	Alcoholic extract	Antioviulatory decreased production of gonadotrophin	Kumar and Sachin (2013)
12.	<i>Plumbago rosea</i> L. Plumbaginaceae <i>Raktachitrak</i> , Leaves	Plumbagin, sitosterol glycoside, tannins, and fatty alcohol	Acetone, ethanolic	Antioviulatory inhibition of ovulation with irregular estrous cycle	Sheeja et al. (2011)
13.	<i>Semecarpus anacardium</i> L.f. Anacardiaceae Bhallatak Fruits	Alkaloids	Aqueous and ethanolic	Reversible antioviulatory activity	Sushma et al. (2016)
14.	<i>Taxus baccata</i> L. Taxaceae <i>Talishpatra</i> Common Yew Leaves	Pseudo alkaloids	Leaf extract	Antioviulatory, inhibited secretion of ovarian hormones	Priya et al. (2012); Kaur et al. (2011)
15.	<i>Vitex negundo</i> L. Lamiaceae <i>Nirgundi</i> , roots, and seeds	Casticin, isoorientin, chrysophenol D, luteolin, p-hydroxybenzoic acid, and D-fructose	Aqueous	Antioviulatory activity	Lal et al. (1992)
E Antiestrogenic activity					
1.	<i>Allium sativum</i> L. Amaryllidaceae <i>Rason</i> , Bulb	Sulfur-containing compounds	Alcohol	Ecobolic in mice and rats, estrogenic activity in female albino rats	Tewari et al. (1971); Ola-Mudathir et al. (2008)
2.	<i>Cyperus rotundus</i> L. Cyperaceae <i>Musta</i> , Rhizome	Cyperene, humulen, selinene, zierone, campholenicopaene, and limonene	Aqueous	Antiestrogenic property	Gediya et al. (2011)
3.	<i>Glycyrrhiza glabra</i> L. Fabaceae <i>Yashtimadhu</i> , Roots	Triterpene glycyrrhizin acid and glycoside	Water	Estrogenic activity	Ahmad et al. (2011)
4.	<i>Guilandina bonduc</i> L. sy. <i>Caesalpinia bonduc</i> (L.) Roxb. Leguminosae <i>Karanja</i> , seeds	Phytosterinin, β -sitosterol, flavonoids, bonducillin, aspartic acid, arginine, and citrulline β -carotene	Aqueous	Antiestrogenic activity	Salunke et al. (2011)
5.	<i>Nelumbo nucifera</i> Gaertn. Nelumbonaceae <i>Kamala</i> , Lotus Seeds	Hydrocarbons	Ethanollic extract	Antiestrogenic, decreased ovarian weight, estrogens inhibition	Mutreja et al. (2008)
6.	<i>Sesamum indicum</i> L. Pedaliaceae <i>Tila</i> , seeds	Oil, protein, and carbohydrate	Extract	Estrogenic effect in female albino rats	Priya et al. (2012)
7.	<i>Vitex negundo</i> L. Lamiaceae <i>Nirgundi</i> , roots and seeds	Casticin, isoorientin, chrysophenol D, luteolin, p-hydroxybenzoic acid, and D-fructose	Aqueous	Antioviulatory activity	Lal et al. (1992)

(Continued on following page)

TABLE 2 | (Continued) Medicinal plants and their phytoconstituents validated for various female/male contraceptive activities. Different contraceptive activities studied on medicinal plants could be categorized as follows. Female contraceptive activities: (2A) anti-implantation activity, (2B) abortification, (2C) antifertility, (2D) antioviulatory, and (2E) antiestrogenic activity. Male contraceptive activities: (2F) antispermatogetic, (2G) spermicidal, and (2H) antiandrogenic activity.

Sr. No.	Botanical name, family, Sanskrit name, parts	Chemical composition	Extract	Mode of action in experimental studies	Reference
F Antispermatogetic activity					
1.	<i>Abru sprecaorius</i> L. Papilionaceae <i>Gunja</i> , seeds	Abrin, abrasine, precasine, and precol	Aqueous	Reduced sperm motility, density, antispermatogetic effect, reduced activity of testicular enzyme, post-testicular antifertility effect	Bajaj et al. (1981); Dixit et al. (1987); Kulshreshtha and Mathur (1990); Sinha (1990)
2.	<i>Aegle marmelos</i> (L.) Corrêa. Rutaceae <i>Bilva</i> , whole plant and leaves	Marmelosin, luvangetin, psoralen, tannins, and marmin	Aqueous extract	Inhibit spermatogenesis and sperm motility male rat reproduction, affecting the sexual behavior and epididymal sperm concentration	Sur et al. (1999); Sur et al. (2002)
3.	<i>Albizia lebbeck</i> (L.) Benth. Fabaceae <i>Shirish</i> , Pods	Melacacidin, D-catechin, β -sitosterol, albiziahexoside, betulinic acid, and echinocystic acid glycosides	Methanolic extract	Spermatogenic arrest in male albino rats	Gupta et al. (2004); (Gupta et al. 2005a)
4.	<i>Andrographis paniculata</i> (Burm.f.) Nees Acanthaceae <i>Kirattikta</i> , leaves	Andrographolide, Andrographidoids A, B, C, D, E, diterpenoid, and lactone	Water extract	Antispermatogetic	Akbarsha et al. (1990); Akbarsha and Murugaian (2000)
5.	<i>Ananas comosus</i> (L.) Merr. Bromeliaceae <i>Custard apple</i> , seeds	Atropine alkaloids and anonaine	Water	Antispermatogetic activity	Satyawati (1983)
6.	<i>Annona squamosa</i> L. Annonaceae <i>Custard apple</i> Seeds, leaves, and bark	Atropine alkaloids and anonaine	Ethyl acetate extract	Antispermatogetic activity	Jain and Dixit (1992)
7.	<i>Areca catechu</i> L. Arecaceae <i>Poogaphala</i> , Nuts	Alkaloids—pilocarpinearecaidine, arecoline	Water	No abnormality in Leydig cell and interstitium tissue	Ave Olivia et al. (2020)
8.	<i>Aristolochia indica</i> L. Aristolochiaceae <i>Ishwari</i> , roots	Aristolochic acid, ceryl alcohol, β -sitosterol, stigmast-4-en-3-one, friedelin, and cycloeucalenol	Aristolochic acid	Antispermatogetic	Gupta et al. (1996)
9.	<i>Azadirachta indica</i> A. Juss. Meliaceae <i>Nimba</i> Leaves, flower, and seed	Azadirachtin, nimbolin, nimbin, nimbidin, nimbidol, sodium nimbinat, and gedunin	Aqueous, alcoholic	Decrease in the weight of seminal vesicles, ventral prostate, reduction in epithelial height, nuclear diameter, and the secretory materials in the lumen	Gediya et al. (2011)
10.	<i>Bacopa monnieri</i> (L.) Wettst. Plantaginaceae <i>Brahmi</i> , whole plant	Bacosides and saponins	Aqueous extract	Reversible suppression of spermatogenesis and fertility, without producing apparent toxic effects	Singh et al. (2013)
11.	<i>Balanites roxburghii</i> Planch. Zygophyllaceae <i>Ingudi</i> , Fruit pulp	Saponin, furanocoumarin, and flavonoid	Methanol, palmitine hydroxide	Antispermatogetic activity	Dixit et al. (1981), Agarwal and Dixit (1982)
12.	<i>Berberis aristata</i> DC. Berberidaceae <i>Daruharidra</i> , Roots	Berberine and berbamine	Palmitine hydroxide	Antispermatogetic action	Gupta and Dixit (1989)

(Continued on following page)

TABLE 2 | (Continued) Medicinal plants and their phytoconstituents validated for various female/male contraceptive activities. Different contraceptive activities studied on medicinal plants could be categorized as follows. Female contraceptive activities: (2A) anti-implantation activity, (2B) abortification, (2C) antifertility, (2D) antioviulatory, and (2E) antiestrogenic activity. Male contraceptive activities: (2F) antispermatogetic, (2G) spermicidal, and (2H) antiandrogenic activity.

Sr. No.	Botanical name, family, Sanskrit name, parts	Chemical composition	Extract	Mode of action in experimental studies	Reference
13.	<i>Butea monosperma</i> (Lam.) Kuntze Fabaceae Palash, bark, and flowers	Kino-tannic acid, gallic acid, and pyrocatechin	Aqueous extract	Antispermatogetic effect	Wati and Verute (1988)
14.	<i>Calotropis procera</i> (Aiton) W.T. Aiton Apocynaceae Arka, root	Steroidal alkaloid	Calotropin, aqueous ethanol	Antispermatogetic, antiandrogenic activities, and/or endocrine disrupting effects, functional alteration in genital organ	Gupta et al. (1990); Abdelgader and Elsheikh (2018); Sharma and Jacob (2001b) Pokharkar et al. (2010)
15.	<i>Carica papaya</i> L. Caricaceae Papaya, unripe fruit pulp, seeds, latex	Papain, caricacin, carposmine, oleanolic glycoside,	Pet ether, Alcohol, aqueous Ethanol	Antispermatogetic activity reduced spermatogenesis, inhibition in steroidal hormones	Changamma and Lakshman (2013)
16.	<i>Celastrus paniculatus</i> Willd. Celastraceae Jyotishmati, seeds	Alkaloids, tannins, saponins, steroid, terpenoid, flavonoids, phlobatannin, cardiac, and glycoside	Seed	Antispermatogetic activity	Bidwai et al. (1990)
17.	<i>Cichorium intybus</i> L. Asteraceae, Chicory Whole plant	Inulin, sesquiterpene lactones, vitamins, minerals, fat, and mannitol,	Aqueous	Antispermatogetic activity	Roy and Venkatakrishna (1983)
18.	<i>Cinnamomum camphora</i> (L.) J.Presl Lauraceae Karpur Camphor, leaves and resin	Essential oil—camphor, linalool, and cineole	Leaf	Inhibition of spermatogenesis	Singh (1990b)
19.	<i>Cuminum cyminum</i> L. Apiaceae Jeerak, seeds	Cuminal and cuminic alcohol	Extract	Antispermatogetic effect	Priya et al. (2012); Sharma J et al. (2001)
20.	<i>Embelia ribes</i> Burm.f. Primulaceae Vidang, berries	Embelin, volatile oil, and fixed oil	Isolated embelin	Inhibition of spermatozoa motility	Prakash (1981); Nand (1981); Dixit et al. (1983); Gupta et al. (1989)
21.	<i>Euphorbia neriifolia</i> L. Milk brush Euphorbiaceae Latex, Whole plant	β -amyrin acetate, lupenone, 3-acetoxy-20-lupanol, cycloart-25-en-3 β , 24 ζ -diol, and cycloart	Ethanol	Antispermatogetic effect	Mali (1999)
22.	<i>Hibiscus rosa-sinensis</i> L. Malvaceae Japa Flowers	Cyclopeptide alkaloid	Ethanol, benzene extract	Spermatogenic elements of testis and epididymal sperm count., androgenic activity	Reddy et al. (1997); Gupta et al. (1985)
23.	<i>Momordica charantia</i> L. Cucurbitaceae Karwellaka Roots and leaves	Glycosides, saponins, alkaloids, fixed oils, triterpenes, proteins, and steroids	Aqueous	Antispermatogetic, antisteroidogenic activity	Naseem et al. (1998)
24.	<i>Ocimum sanctum</i> L. Lamiaceae, Tulsi, leaves	Carvacrol, sesquiterpene, hydrocarbon, and caryophyllene	Benzene extract	Decreased sperm count, weight of testis, and sperm motility	Pandey and Madhuri (2010)

(Continued on following page)

TABLE 2 | (Continued) Medicinal plants and their phytoconstituents validated for various female/male contraceptive activities. Different contraceptive activities studied on medicinal plants could be categorized as follows. Female contraceptive activities: (2A) anti-implantation activity, (2B) abortification, (2C) antifertility, (2D) antioviulatory, and (2E) antiestrogenic activity. Male contraceptive activities: (2F) antispermatogetic, (2G) spermicidal, and (2H) antiandrogenic activity.

Sr. No.	Botanical name, family, Sanskrit name, parts	Chemical composition	Extract	Mode of action in experimental studies	Reference
25.	<i>Piper betle</i> L. Piperaceae <i>Betel leaf, Pan</i> Petiole	Eugenol, eugenol acetate, piper betol, piperol, methyl eugenol, and phytol	Alcoholic extract	Reduced sperm motility	Adhikary et al. (1989); Sarkar et al. (2000)
26.	<i>Piper nigrum</i> L. Piperaceae <i>Marich, Black pepper</i> Fruit	Piperine	Fruit powder—suspended in sterile distilled water containing milk powder	Alterations in the male reproductive organs, reversible after cessation of treatment	Mishra and Singh (2009), Malini et al. (1999)
27.	<i>Plumbago zeylanica</i> L. Plumbaginaceae <i>Chitrak, Root</i>	Plumbagin	Ethnol	Antispermatogetic	Purohit et al. (2008)
28.	<i>Pterocarpus santalinus</i> L.f. Fabaceae <i>Raktachandan</i> Stem bark	Santalin A, B, savinin, calocedrin, pterolinus K, L, and pterostilbenes	Water	Semen coagulating activity	Dhawan et al. (1980)
29.	<i>Pueraria tuberosa</i> (Willd.) DC. Fabaceae, <i>Varahikand</i> , rhizome	Puerarin, genistein, and daidzein	Methanol	Inhibition of spermatogenesis	Gupta et al. (2004), Gupta et al. (2005b)
30.	<i>Semecarpus anacardium</i> L.f. Anacardiaceae <i>Bhallatak, Marking nut</i> , Seeds	Bhilwanols, phenolic compounds, biflavonoids, and sterols glycosides	Ethanol	Reduction in the number of primary spermatocytes, secondary spermatocytes, and spermatids	Gupta et al. (2013); Sharma et al. (2003)
31.	<i>Terminalia arjuna</i> (Roxb. ex DC.) Wight & Arn. Combretaceae <i>Arjuna</i> , Bark	Tannins, triterpenoid saponins, flavonoids, gallic acid, ellagic acid, and phytosterols	Crude form	Inhibition of spermatogenesis	Jha and Dixit (1986), Lal and Udupa (1993)
32.	<i>Tylophora asthmatica</i> (L. f.) Wight & Arn. Apocynaceae <i>Khadki Rasna</i> Leaf and stem	Aempferol, quercetin, tyloindane, cetyl-alcohol, tannins, glucose, calcium salts, and potassium chloride	Pure alkaloid	Antispermatogetic activity	Dikshith et al. (1990)
G Spermicidal activity					
1.	<i>Acacia concinna</i> (Willd.) DC. Leguminosae-Mimosoideae <i>Shikekai</i> , stem bark	Hexacosanol, spinasterone, oxalic, tartaric, citric, succinic, ascorbic acid, alkaloids calyctomine, and nicotine	Alcoholic	Spermicidal and semen coagulating activity	Kamboj and Dhawan (1982)
2.	<i>Achyranthes aspera</i> L. Amaranthaceae <i>Apamarga</i> Whole plant, Stem bark, Root	Fatty acids, oleonic acid, bisdesmosidic, triterpenoid alkaloids, D-glucuronic, betaine, and achyranthine	Benzene, ethanolic, and chloroform	Spermicidal	Raj et al. (2011); Shibeshi et al. (2006); Vasudeva and Sharma (2006)
3.	<i>Astonia scholaris</i> (L.) R.Br. Apocynaceae <i>Saptaparna</i> , stem bark	Erythrodiol, uvaol, betulin, oleanolic acid ursolic acid, and β -amyrin	Water extract	Decline germ cell population	Gupta et al. (2003), 2004)
4.	<i>Azadirachta indica</i> A. Juss. Meliaceae <i>Nimba</i> Leaves, flower, and seed	Azadirachtin, nimbolin, nimbin, nimbidin, nimbidol, sodium nimbin, and gedunin	Aqueous and Alcoholic	Spermicidal effect on number of spermatozoa and level of fructose	Gediya et al. (2011), Kasturi et al. (1997)
5.	<i>Bambusa bambos</i> (L.) Voss Poaceae, <i>Vansha</i> Tender stem	Balarenone, barlerin, barlerinoside, verbascoside, acetylbarlerin, and lupulinoside	Ethanol	Reduced sperm motility	Vanithakumar et al. (1989)

(Continued on following page)

TABLE 2 | (Continued) Medicinal plants and their phytoconstituents validated for various female/male contraceptive activities. Different contraceptive activities studied on medicinal plants could be categorized as follows. Female contraceptive activities: (2A) anti-implantation activity, (2B) abortification, (2C) antifertility, (2D) antioviulatory, and (2E) antiestrogenic activity. Male contraceptive activities: (2F) antispermatogetic, (2G) spermicidal, and (2H) antiandrogenic activity.

Sr. No.	Botanical name, family, Sanskrit name, parts	Chemical composition	Extract	Mode of action in experimental studies	Reference
6.	<i>Cannabis sativa</i> L. Cannabaceae Bhang, leaves	Cannabinoids, terpenes, and sesquiterpenes	Butin	Testicular lesions	Dixit and Joshi (1982)
7.	<i>Citrullus colocynthis</i> (L.) Schrad. Cucurbitaceae Indrawaruni Bitter apple, fruits	Carbohydrate, protein, amino acid, tannins, saponins, phenolics, and cardicglycoloids	Ethanol	Impairment of sperm	Chaturvedi and Dixit (1997)
8.	<i>Daucus carota</i> L. Apiaceae Grinjanak, Seed	Essential oil	Petroleum, ether, benzene, alcohol, and water	Spermicidal activity	Garg (1975); Jansen and Wolhmuth (2014); Shah and Varute (1980)
9.	<i>Embelia ribes</i> Burm.f. Primulaceae Vidang, Berries	Embelin	Embelin in 50 and 100 ^{mg} /kg doses	Reversible contraception like activity in male dogs	Nand (1981); Dixit and Bhagava (1983)
10.	<i>Mentha arevensis</i> L. Lamiaceae Pudina, leaves	Alkaloids, steroids, and glycosides	Petroleum ether	Spermicidal Decreased weight of testis, sperm motility, and viability	Sharma and Jacob (2001a)
11.	<i>Myristica fragrans</i> Houtt Myristicaceae Nutmeg, Jatiphal, seeds	Myristicin, elemicin, myristic acid, alpha-pinene, terpenes, beta-pinene, and trimyristin	Ethanol	Premature ejaculation	Mishra and Shukla (1980)
12.	<i>Strychnos potatorum</i> L.f. Loganiaceae Nirmali, Seeds	Strychnine	Seed extract	suppressive effects on male fertility	Gupta et al. (2006)
13.	<i>Terminalia bellirica</i> (Gaertn.) Roxb. Combretaceae Bibhitak Fruits	Phenolic acids, saponins, lignans, triterpenoids, resveratrol glycosides, arjungenin, β -sitosterol, and stigmasterol	Aqueous	Spermicidal activity in rat semen, human semen	Kaur et al. (2011)
14.	<i>Tinospora cordifolia</i> (Willd.) Hook.f. & Thomson Menispermaceae Amrita Giloe Stem	Berberine, palmatine D, choline D, diterpene, terpenoids alkaloids, and steroids	Aqueous	Spermicidal Reduced weight of testis, sperm count	Gupta and Sharma (2003)
15.	<i>Trigonella foenum-graecum</i> L., Fabaceae Methika, Seeds	Water, carbohydrates, protein, fat, and calcium	Aqueous	Spermicidal activity in human and rat semen	Priya et al. (2012)
16.	<i>Withania somnifera</i> (L.) Dunal Solanaceae Ashwagandha Stem and root	Withanolides	Stem, ethanolic	Reversible spermicidal and infertilizing effect	Singh et al. (2013); Mali (1999)
H Antiandrogenic activity					
1.	<i>Aloe barbadensis</i> Mill. Synonym of <i>Aloe vera</i> (L.) Burm.f. Asphodelaceae Kumari, leaves	Water, polysaccharides, pectin, cellulose, hemicellulose, and glucomannan	Extract	Antiandrogenic activity on monkeys	Dixit et al. (1983)

(Continued on following page)

TABLE 2 | (Continued) Medicinal plants and their phytoconstituents validated for various female/male contraceptive activities. Different contraceptive activities studied on medicinal plants could be categorized as follows. Female contraceptive activities: (2A) anti-implantation activity, (2B) abortification, (2C) antifertility, (2D) antioviulatory, and (2E) antiestrogenic activity. Male contraceptive activities: (2F) antispermatogenic, (2G) spermicidal, and (2H) antiandrogenic activity.

Sr. No.	Botanical name, family, Sanskrit name, parts	Chemical composition	Extract	Mode of action in experimental studies	Reference
2.	<i>Aristolochia indica</i> L. Aristolochiaceae <i>Ishwari</i> , roots	Aristolochic acid, ceryl alcohol, β -sitosterol, stigmast-4-en-3-one, friedelin, and cycloeucalenol	Aristolochic acid	Antiandrogenic effects on langur monkey	Gupta et al. (1996)
3.	<i>Andrographis paniculata</i> (Burm.f.) Nees Acanthaceae <i>Kirattikta</i> , leaves	Andrographolide, andrographidoids A, B, C, D, E, diterpenoid, and lactone	Water extract	Antiandrogenic	Akbarsha et al. (1990); Akbarsha and Murugaian (2000)
4.	<i>Azadirachta indica</i> A. Juss., Meliaceae <i>Nimba</i> Leaves, flower, and seed	Azadirachtin, nimbolin, nimbin, nimbidin, nimbidol, sodium nimbin, and gedunin	Seed oil	Antiandrogenic	Sharma et al. (1987); Sinha et al. (1984); Roop et al. (2005)
5.	<i>Cuscuta reflexa</i> Roxb Convolvulaceae <i>Amarwel</i> , whole plants	Alkaloids	Methanolic	Antisteroidogenic	Gupta et al. (2003)
6.	<i>Curcuma longa</i> L. Zingiberaceae <i>Haldi</i> , rhizome	Curcumin and flavanoids	Ethanol, aqueous	Antiandrogenic	Bhagat and Purohit (1986)
7.	<i>Foeniculum vulgare</i> Mill Apiaceae <i>Common fennel</i> , seeds	Anethole, alpha pinene, beta myrcene—pinene, bitter fenchone, camphene, and estragole	Alcoholic	Antiandrogenic	Farooq et al. (1997)
8.	<i>Hibiscus rosa-sinensis</i> L. Malvaceae <i>Japa</i> , Flowers	Cyclopeptide alkaloid	Ethanol and Benzene extract	Spermatogenic elements of testis and epididymal sperm count., androgenic activity	Reddy et al. (1997); Gupta et al. (1985)
9.	<i>Mucuna urens</i> (L.) Medik. Fabaceae <i>Horase been</i> , <i>Kapikacchu</i> Seeds	L-DOPA, with trace amounts of serotonin, nicotine, and bufotenine	Water	Effect on gonads and sex accessory glands	Udoh and Ekpenyong (2001)
10.	<i>Nicotiana tabacum</i> L. Solanaceae <i>Tobacco</i> , leaves	Lipid constituents, free fatty acids, triglycerides, and sterol esters free sterols	Nicotine	Antiandrogenic	Londonkar et al. (1998)
11.	<i>Plumbago zeylanica</i> L. Plumbaginaceae <i>Chitrak</i> , root	Plumbagin	Plumbagin-free alcohol	Antiandrogenic	Bhargava (1984)
12.	<i>Ruta graveolens</i> L. Rutaceae, <i>Rue</i> , leaves	Volatile oil	Aqueous extracts	Adverse effects on territorial aggression and sexual behavior in male albino rats	Khoury and Akawi (2005)
13.	<i>Semecarpus anacardium</i> L.f. Anacardiaceae <i>Bhallatak</i> , <i>Marking nut</i> , Seeds	Bhilwanols, phenolic compounds, biflavonoids, and sterols glycosides	Aqueous extracts	Antiandrogenic	Singh (1985)

a cost-effective herbal contraceptive for its spermicidal property and is considered safe for regular use. (Achintya, 2018).

***Ricinus communis* L.**

The seeds of *Ricinus communis* Linn RICOM-1013-J, administered as a single oral dose of 2.3–2.5°g once/12°months acted as protection against pregnancy in 50 women volunteers. The study revealed very minimal side effects. The antifertility and contraceptive efficacy of RICOM-1013-J is due to hormonal mechanisms (Isichei et al., 2000). Goncim et al. (2010) stated that one seed of *Ricinus communis* L. taken orally can prevent ovulation in humans and the anticonceptive effect may be due in part to the prevention of ovulation.

Compound Formulation

A study was conducted on a combination of *Ashoka* (*Saraca indica* L.), *Vidanga* (*Embelia ribes* Burm.f.), *Laksha* (*lac*), and *Kramuk* (*Areca nut*) on 834 young, healthy patients in active reproductive age below 40°years. The drug was administered from the 5th°day of LMP for a period of 15°days in a daily dose schedule of 1°gm (2 tablets) at bedtime with milk. Results suggested that the failure rate of treatment 1.19/HWY is comparable to both steroidal oral contraceptive pills and intrauterine device. It does not affect the hypothalamo-pituitary axis and did not have any other adverse effects. It can be a good alternative for lactating women (Palep and Jukar, 2003).

Central Council for Research in Ayurveda and Siddha had taken up a number of studies to evaluate the efficacy of Ayurvedic formulations like *K Capsule*, *Ayush AC-IV*, *Pippalyadi yoga* (in three different doses), *Ayush AC II*, *Talisadi yoga*, *Vidangadi yoga*, etc., which were proved as safe and effective in different clinical studies. Besides this, the council also tried the efficacy of *neem oil*—as a local contraceptive and found encouraging results (Galib et al., 2008).

TERATOGENIC EFFECT

Ayurveda classical texts have references to congenital birth [*anmabalapravrita*] disorders as per the etiopathology and clinical presentation. Some congenital malformations in the fetus may occur but the mechanism is still not clear.

Teratogen is an agent or factor that causes malformation in the embryo. One of the causes of malformation may be toxic substances such as drugs and environmental toxins in pregnancy.

Herbal drugs with appropriate dose and duration may not cause teratogenic effect but in the case of excess dose with improper mode of administration, for a longer duration than therapeutically advised, teratogenic effect may be seen. Scientific validation of their safe use in pregnancy is hardly documented. Teratogenic effects of some of the medicinal plans have been mentioned in **Table 3**.

It is observed that drugs having contraceptive and abortifacient action have potent teratogenic effect in experimental models. There are several studies of teratogenicity on other herbal drugs which are not showing teratogenic effects in low doses and may cause

teratogenic effects in high doses, for example, *Ashwagandha* (*Withania somnifera* (L.) Dunal), *Punarnava* (*Boerhavia diffusa* L.), *Narangi* (*Citrus aurantium* L), *Nimba* (*Azadirachta indica* A. Juss.), *Jatamansi* (*Nardostachys jatamansi* (D.Don) DC.), (*Bala* *Abutilon indicum* L.) Sweet), and *Yastimadhu* (*Glycyrrhiza glabra* L.) (Jati, 2018).

Different contraceptive activities in the abovementioned 94 plant ingredients are categorized in **Table 4**.

DISCUSSION

Presently, scientifically established methods of contraception and contraceptive drugs are used extensively. The synthetic contraceptive drugs known to interfere with the endocrine system and natural hormones may produce reproductive, neurological, developmental, and metabolic adverse effects that are serious at times. Search for safer drugs and preference for natural origin contraceptive drugs and methods are of research interests. Necessarily, the objectives for research of novel contraceptives from nature would be the assurance regarding effectiveness, safety, and user compliance. There are many plants known to have antifertility activity both in male and female. Some of these plants had spermicidal and altered hormone levels.

The classical Ayurvedic texts offer substantial knowledge on reproductive biology for healthy progeny and medieval Ayurvedic and specific Sanskrit texts provide information about methods and a broad range of therapeutics and ingredients that are described for use in contraception. These include local and oral contraceptives, abortifacients, and other methods of antifertility and birth control. These formulations and ingredients are a valuable source for extended research in the field of contraception.

In this study, 94 indigenous medicinal plants have been reviewed. Chemotaxonomically, it is of interest to note that the maximal number of plants having abortifacient and contraceptives are from *Fabaceae*, *Acanthaceae*, *Euphorbiaceae*, and *Liliaceae* families.

Ingredients, Phytoconstituents, and Contraceptive Activities

Certain alkaloids, glycosides, saponins, tannins, terpenoids, and other phytoconstituents are known to disrupt ovarian functions and estrous cyclicity through interplay of ovarian and extra ovarian hormones. Alkaloids are a major group of secondary metabolites bitter in taste that stimulate the central nervous system or directly work on the human brain. These are antiparasitic, antiplasmodial, anticorrosive, antioxidative, antibacterial, anti-HIV, and have insecticidal activities. In a review, it has been suggested that maximum alkaloids containing plant drugs have been reported to have an antifertility, antioviulatory, anti-implantation, abortifacient effect on animals (Choudhury and Jadhav, 2013).

A majority of these medicinal ingredients used either in formulations or singly over centuries have also been studied for a variety of pharmacological, biological, and therapeutic activities.

***Achyranthes aspera* L.**

A plant known to have antimicrobial, hypolipidemic, and has antifertility qualities is also used to treat asthma and cough.

Fruits of *Annona squamosa* L.

A known insecticidal, antioviulatory, and abortifacient plant that is hematinic, cooling, a sedative, stimulant, expectorant, and tonic. Its seeds are abortifacient and insecticidal and are used to destroy lice in the hair.

***Calotropis gigantea* L.**

Calotropis gigantea L. having certain antifertility glycosides and cardenolides is used for colic pain, flatulence, asthma, cough, and whooping cough and has wound healing, anticancer, and hypoglycaemic effects. *Calotropis Madar* rootbark is used for

abortive purposes and in India is used as an antidote and in the treatment of elephantiasis, leprosy, and chronic eczema.

Camphor

Camphor, the well-known aromatic, has hormone-modulating, contraceptive, abortifacient, and lactation-inhibiting properties in women. It has a dose-dependent effect in human sperm motility and viability. Camphor can pass the placental barrier and affect embryo development. Camphor-containing compounds have shown uterotrophic, anticonvulsant, nicotinic receptor blocking, anti-implantation, antiestrogenic, as well as estrogenic activities and can reduce serum triglyceride and thyroid hormone.

Flowers of *Hibiscus rosa-sinensis* L. containing quercetin-7-O-galactoside, polyphenolic compounds, and kaempferol, having antispermatogenic compounds, is prescribed for contraception

TABLE 3 | List of drugs with teratogenic effect

Sr. No.	Name of plants	Phytoconstituent	Dose and duration	Teratogenic effect
1	<i>Asparagus racemosus</i> Willd. Root	Shatavarin, Racemosol	1000 ^o mg/kg/body weight for 60-day Charles foster rat pups Methanolic extract	Prenatal study—increased resorption of fetus, gross malformation i.e., swelling in legs, IUGR with small placental size. Postnatal study—decreased number of pups per litter and increased mortality of pups and delayed developmental parameters Goel et al. (2006)
2	<i>Datura metel</i> L. Leaves	Atropine alkaloids	500 ^o mg/body kg wt rats, ethanolic extract	Teratogenic in the late stage of pregnancy Azeez and Philip (2013)
3	<i>Gloriosa superba</i> L. Tuber	Colchicine	1-3 ppm and 4-5 ppm Hydroalcoholic extract	Antifertility activity scarcely produced abnormal embryos. Induce high percentage of abnormalities. Badwaik (2011)
4	<i>Lawsonia inermis</i> L.	Flavonoid and phenolic compounds	100 ^o mg/kg body wt. BALB/c mice between 8-12 ^o wk hydroalcoholic extract	90% embryo, more extra ribs anencephaly, exencephaly, skeletal abnormalities, height and weight loss in embryos Lobat (2015)
5	<i>Luffa operculata</i> (L.) Cogn. Tea, decoction	Glycosides, saponins, resin, free sterols, aliphatic esters, quinones	After ingestion of a variable amount of tea made with dried fruit, decoction	Abortion, reduction in birth rate Barilli et al. (2005)
6	<i>Plumbago zeylanica</i> L.	Plumbagin	100 ^o mg/body kg wt orally with 0.5 ^o ml of distilled water in mice	Stunted growth, subcutaneous, and deep hemorrhage, kinking of tail, protrusion of back of head Srivastava (2017)
7	<i>Ruta graveolens</i> L.	Essential oil	5, 10, and 20% w/v or plain water (control) orally for 4 days	Changes in the blastocyst formation, reducing the number, and delaying the development of embryos Gutiérrez-Pajares et al. (2003)
8	<i>Sena (Senna) alexandrina</i> Mill-Fabaceae	Sennosides	Extract	embryotoxic effect De Freitas et al. (2005) Increase blood flow to the uterus and its attachments, increasing the risk of fetal loss, and may pass spasms in the infant Schulz et al. (2002)
9	<i>Zingiber officinale</i> Roscoe	Carbohydrates (50–70%), lipids (3–8%), terpenes, and phenolic compounds	Orally at 0, 250, 500, 1000, or 2000 ^o mg/kgbw/day—five groups	High dose significantly reduced the number of live fetuses, increased fetal death, and resorption. Reda et al. (2018)
10	<i>Pipalyadi gutika</i>	Piperine	5 times to one and five times to the other than the recommended dose for humans Rats	Fetus—LBW, smaller in length, developmental defects of soft tissues, skeletons, herniation of intestines into umbilical cord, Mother—less weight gain during gestation Chaudhury et al. (2001)
11	<i>Vishamustivati [VV]</i> & <i>Shuddha Tankana [ST]</i>	-	175 ^o mg/kg of aqueous solutions of VisamustiVati, 300 ^o mg/kg aqueous solutions of SuddhaTankana, orally from day 1 to day 7 of post mating period	VV and ST shows positive Teratological effect on new-borns, gross remarkable external morphological and skeletal defects Jati (2018)

TABLE 4 | List of medicinal plants with one or more contraceptive activities.

Sr. No	Plant name	Anti-implantation	Abortification	Antifertility	Antioviulatory	Antiestrogenic activity	Antispermatogetic	Spermicidal	Antiandrogenic activity
1	<i>Abies spectabilis</i> (D.Don) Mirb.	✓							
2	<i>Abroma augusta</i> (L.) L.f.	✓	✓						
3	<i>Abrus precatorius</i> L.		✓	✓			✓		
4	<i>Acacia concinna</i> (Willd.) DC.							✓	
5	<i>Acacia leucophloea</i> (Roxb.) Willd.			✓					
6	<i>Achyranthes aspera</i> L.		✓		✓			✓	
7	<i>Adhatoda vasica</i> Nees	✓	✓						
8	<i>Aegle marmelos</i> (L.) Corrêa.		✓				✓	✓	
9	<i>Ailanthus excelsa</i> Roxb	✓							
10	<i>Albizia lebbeck</i> (L.) Benth.						✓		
11	<i>Allium cepa</i> L.	✓							
12	<i>Allium sativum</i> L.					✓			
13	<i>Aloe barbadensis</i> Mill.	✓							✓
	Synonym of <i>Aloe vera</i> (L.) Burm.f.								
14	<i>Alstonia scholaris</i> (L.) R.Br.						✓		✓
15	<i>Andrographis paniculata</i> (Burm.f.) Nees						✓		✓
16	<i>Ananas comosus</i> (L.) Mer							✓	
17	<i>Annona squamosa</i> L.		✓				✓		
18	<i>Areca catechu</i> L.	✓	✓	✓	✓		✓		
19	<i>Aristolochia indica</i> L.						✓	✓	
20	<i>Azadirachta indica</i> A. Juss.			✓	✓		✓	✓	✓
21	<i>Bacopa monnieri</i> (L.) Wettst.						✓		
22	<i>Balanites roxburghii</i> Planch.						✓		
23	<i>Bambusa bambos</i> (L.) Voss							✓	
24	<i>Barleria prionitis</i> L.		✓						
25	<i>Berberis aristata</i> DC						✓		
26	<i>Butea monosperma</i> (Lam.) Kuntze				✓		✓		
27	<i>Calotropis procera</i> (Aiton) Dryand.				✓		✓		
28	<i>Cannabis sativa</i> L.							✓	
29	<i>Carica papaya</i> L.	✓	✓	✓			✓		
30	<i>Cassia fistula</i> L.	✓							
31	<i>Catunaregam spinosa</i> (Thunb.) Tirveng.								
32	<i>Celastrus paniculatus</i> Willd.						✓		
33	<i>Centratherum anthelminticum</i> (L.) Gamble	✓							
34	<i>Cichorium intybus</i> L.						✓		
35	<i>Cinnamomum camphora</i> (L.) J. Presl						✓		
36	<i>Cissampelos pareira</i> L.			✓					
37	<i>Citrullus colocynthis</i> (L.) Schrad.							✓	
38	<i>Citrus × aurantium</i> L.	✓	✓		✓				
39	<i>Crateva nurvala</i> Buch. -Ham			✓					
40	<i>Cuminum cyminum</i> L.			✓			✓		
41	<i>Cuscuta reflexa</i> Roxb								✓
42	<i>Curcuma longa</i> L.			✓					✓
43	<i>Cyperus rotundus</i> L.					✓			
44	<i>Daucus carota</i> L.		✓	✓				✓	
45	<i>Desmodium gangeticum</i> (L.) DC.			✓					
46	<i>Embelia ribes</i> Burm.f.	✓	✓				✓	✓	
47	<i>Euphorbia nerifolia</i> L.						✓		

(Continued on following page)

TABLE 4 | (Continued) List of medicinal plants with one or more contraceptive activities.

Sr. No	Plant name	Anti-implantation	Abortification	Antifertility	Antiovolatory	Antiestrogenic activity	Antispermatogetic	Spermicidal	Antiandrogenic activity
48	<i>Ferula jaeschkeana</i> Vatke			✓					
49	<i>Foeniculum vulgare</i> Mill								✓
50	<i>Gloriosa superba</i> L.	✓	✓	✓					
51	<i>Glycyrrhiza glabra</i> L.					✓			
52	<i>Grewia asiatica</i> L.	✓	✓						
53	<i>Guilandina bonduc</i> L. Sy. <i>Caesalpinia bonducella</i> (L.) Fleming					✓			
54	<i>Hibiscus rosa-sinensis</i> L.	✓		✓	✓		✓		✓
55	<i>Lawsonia inermis</i> L.			✓					
56	<i>Lepidium sativum</i> L.		✓	✓					
57	<i>Melia azedarach</i> L.			✓					
58	<i>Mentha arevensis</i> L.							✓	
59	<i>Mesua ferrea</i> L.	✓							
60	<i>Michelia champaca</i> L.	✓							
61	<i>Momordica charantia</i> L.	✓		✓			✓		
62	<i>Mucuna urens</i> (L.) Medik								✓
63	<i>Musa paradisiaca</i> L.				✓				
64	<i>Myristica fragrans</i> Houtt							✓	
65	<i>Nelumbo nucifera</i> Gaertn.					✓			
66	<i>Nicotiana tabacum</i> L.								✓
67	<i>Nigella sativa</i> L.			✓					
68	<i>Ocimum sanctum</i> L.						✓		
69	<i>Papaver somniferum</i> L.				✓				
70	<i>Piper betle</i> L.			✓			✓		
71	<i>Piper longum</i> L.			✓			✓		
72	<i>Piper nigrum</i> L.			✓			✓		
73	<i>Plumbago rosea</i> L.				✓				
74	<i>Plumbago zeylanica</i> L.	✓					✓		✓
75	<i>Pterocarpus santalinus</i> L.f.						✓		
76	<i>Pueraria tuberosa</i> (Willd.) DC						✓		
77	<i>Ricinus communis</i> L.	✓	✓						
78	<i>Ruta graveolens</i> L.								✓
79	<i>Sapindus trifoliatus</i> L.	✓							
80	<i>Semecarpus anacardium</i> L.f.				✓		✓		✓
81	<i>Sesbania sesban</i> (L.) Merr	✓							
82	<i>Sesamum indicum</i> L.					✓			
83	<i>Strychnos potatorum</i> L.f.							✓	
84	<i>Taxus baccata</i> L.				✓				
85	<i>Terminalia arjuna</i> (Roxb. ex DC.) Wight & Arn						✓		
86	<i>Terminalia bellirica</i> (Gaertn.) Roxb							✓	
87	<i>Tinospora cordifolia</i> (Willd.) Hook.f. & Thomson							✓	
88	<i>Trichosanthes cucumerina</i> L.			✓					
89	<i>Trigonella foenum-graecum</i> L.							✓	
90	<i>Tylophora asthmatica</i> (L. f.) Wight & Arn						✓		
91	<i>Vitex negundo</i> L.				✓	✓			
92	<i>Withania somnifera</i> (L.) Dunal							✓	
93	<i>Woodfordia fruticosa</i> (L.) Kurz		✓						
94	<i>Zingiber officinale</i> Roscoe			✓					

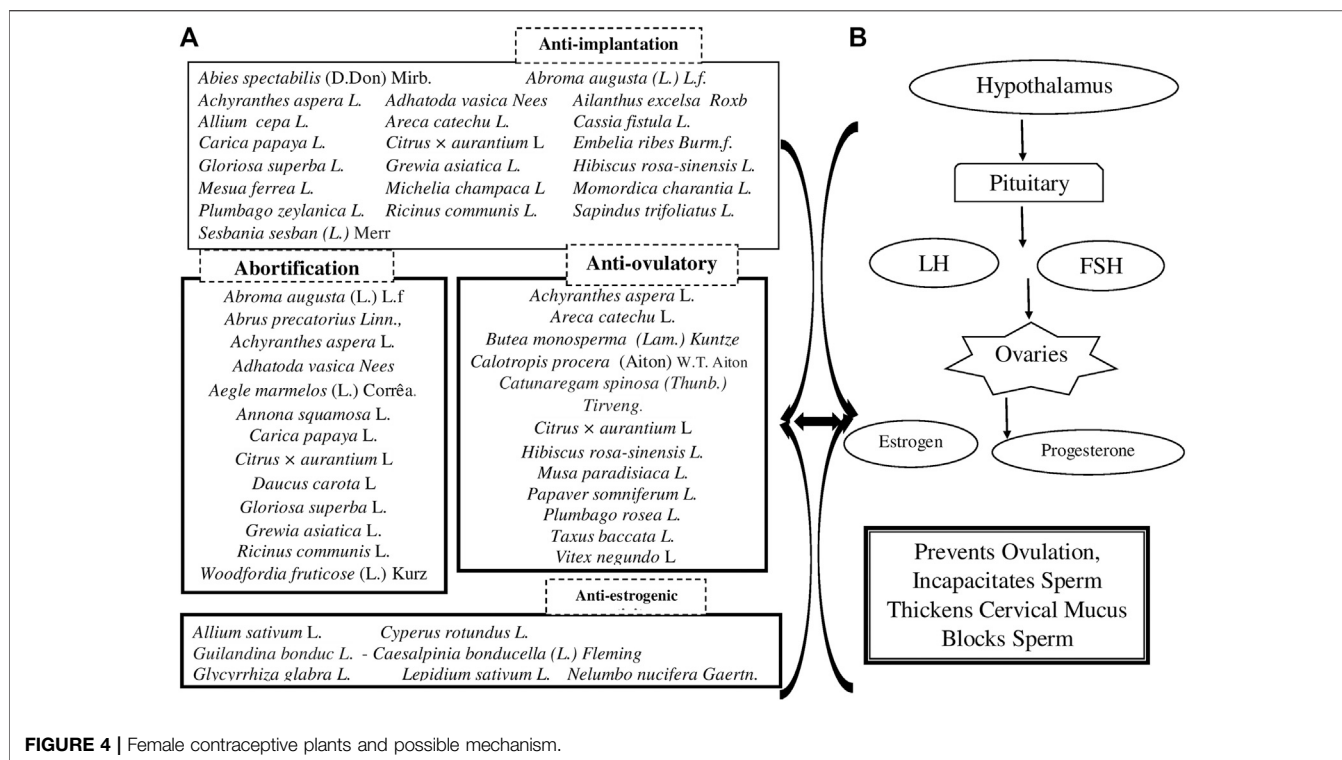


FIGURE 4 | Female contraceptive plants and possible mechanism.

and is used to treat bacterial infection, hyperlipidemia, and depression and act as an antioxidant.

Two of the most bitter stimulant plants, *Momordica charantia* L. and *Azadirachta indica* A. Juss., produce an irregular pattern of estrous cycle with prolonged diestrus phase. Steroids, triterpenoids, reducing sugars, alkaloids, phenolic compounds, flavonoids, and tannins in the plant cause reduction in the number of normal follicles because of atresia which occur due to disruption of the process of follicle selection. *Azadirachta* arrests spermatogenesis and androgen depletion.

Roots of *Plumbago zeylanicum* L. have been used as an abortifacient, internally or as an irritant to the uterus. This acid and stimulant root increases appetite helps indigestion and is used for dyspepsia, piles, and skin diseases. It induces sweating, its powder is occasionally taken as snuff to relieve headache, and it helps in the adhesion of tissues in the body and is antidiarrheal.

Tinospora cordifolia (Willd.) Hook.f. and Thomson, an immunomodulator plant used to treat tuberculosis, fever, and wounds, has antifertility qualities. It is used for antioxidant, hypoglycaemic, and cardioprotective activities.

Excessive use of substances having pungent, bitter, and astringent tastes is contraindicated for sexual functions. Excess consumption of bitter taste leads to loss of strength and energy, astringent taste affects the sperm count, and can even reduce the sex drive while strongly pungent ingredients like pepper exhibit spermicidal or abortifacients effects.

Prolonged consumption of these tastes may lead to emaciation of the body.

Mechanism of Action Female Contraceptives

Medicinal plants may induce infertility in distinct ways. They may affect the ovarian, uterine, and hormone production functions and interfere with implantation or sperm production. These drugs are of natural origin, hydrophilic, and lipophilic; can traverse paracellularly through the vaginal mucosa; and exhibit its efficacy as contraceptive, by altering the vaginal pH. These drugs may variably act locally to bring changes in the cervical mucus and alter decidual embedding and thereby act as anti-implantation agents, or may inhibit propulsion of sperm in the fallopian tubes by altering tubal mechanism or may act on hormones as antioovulation agents. They may act through rapid expulsion of the fertilized ova from the fallopian tube or inhibit implantation due to disturbance of the estrogen progesterone balance or induce fetal abortion by inhibition of nutrition to the uterus and the embryo.

Moreover, plants with estrogenic property can directly influence pituitary action by peripheral modulation of luteinizing hormone (LH) and follicle stimulating hormone (FSH), decreasing their secretions and blocking ovulation (Brinker, 1997). Plants with antiestrogenic activities intercept in the process of development of ovum and endometrium and on the other hand, plants have abortifacient effects (Gark et al., 1978; Prakash et al., 1985).

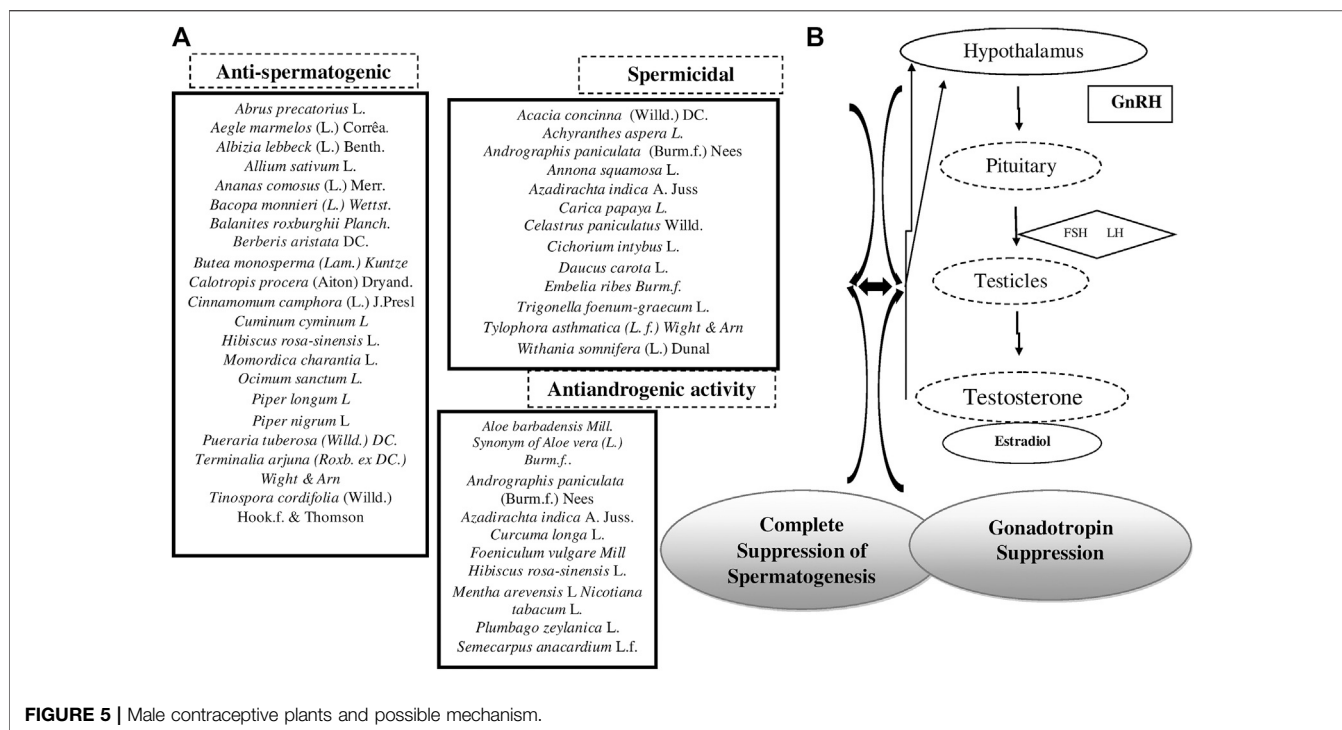


FIGURE 5 | Male contraceptive plants and possible mechanism.

The site of action of antifertility agents in females comprises the hypothalamus, the anterior pituitary, the ovary, the oviduct, the uterus, and the vagina. The mammalian uterus is the main site of antifertility effects (Williamson et al., 1996). Typical estrogenic compounds possess the ability to increase the uterine wet weight and induce cornification and opening of vagina in immature rats, which results in anti-implantation effects (Turner, 1971).

Antifertility plants prevent fertilization; these drugs obstruct the formation of gametes and interfere with the process of fertilization. Antioviulatory plants induce infertility by suppressing ovulation. *Anti-implantation* plants prevent the attachment or penetration of fertilized ovum into the uterus. *Butea monosperma* (Lam.) Kuntze, *Ocimum sanctum* L., *Calotropis procera* (Aiton) W.T. Aiton, *Mentha arvensis*, and *Lawsonia inermis* L—all have anti-implantation activity. Abortifacient plants cause early expulsion of the fetus. These act during the first five weeks of pregnancy as they block the action of progesterone so that the uterus sloughs off the embryo. *Abrus precatorius* L., *Annona squamosa* L., *Calotropis procera* (Aiton) W.T. Aiton, *Carica papaya* L., *Dhatura metel* L., *Momordica charantia* L., and *Catunaregam spinosa* (Thunb.) Tirveng are medicinal plant drugs which can be used as abortifacients. Stimulant, irritant, and bulk forming characteristics of these drugs facilitate abortion along with hormonal regulation and modulation of genital functioning. These ingredients are considered stimulants and are hot in nature and hence should be used for a short duration.

It observed that large numbers of antifertility plant extracts are known to exhibit estrogenic activity in rats (Dahanukar et al., 2000). Estrogenic substance may cause the expulsion of ova from the tube, disruption of luteotrophic activity of the blastocyst, and disrupt the functional equilibrium between the endogenous

estrogen and progesterone, which may result in failure in fertility. Increase in the wet weight of uterus of substance-treated ovariectomized immature rats may indicate that the substance has an estrogenic effect (Mukherjee, 2002).

The hypothalamus has threshold requirement for estrogen to cause a massive release of LH by the pituitary gland. This surge of LH is the trigger, which initiates the rupture of the follicle (ovulation) (Bullock et al., 1995). It is known that an increase in the serum progesterone level prevents pregnancy through inhibition of ovulation and alteration of cervical mucus.

Most of the plants possess inhibition of implantation or reduction of estrogen level and increment of progesterone level as the possible mechanism of antifertility effect.

The anti-implantation effect may be due to the disturbance of endocrine–endometrial synchrony that is dependent on estrogen and progesterone balance. Factors other than the hormones such as histamine, prostaglandins, proteolytic enzyme NOS, alkaline phosphatase, interleukins, and leukemia-inhibitory factors, which are important for implantation, may also be affected by the various plant extracts (Gupta, 1994; Garg et al., 1978; Novaro et al., 1997; Prakash et al., 1989; Dimitriadis et al., 2003; Yang et al., 1994).

Male Contraceptives

Male contraceptive drugs may inhibit spermatogenesis or act on male hormones when used orally or may be spermistatic or spermicidal when used intravaginally. Male contraceptives might work to suppress sperm production by antispermatogetic or prevent maturation of sperm or prevent the flow of sperm through the vas deferens or deposition of the sperm (Soni et al., 2015).

Plant extracts have also shown promising antifertility effects when administered to male rats. The various effects on male reproductive system to induce antifertility action shown by plants includes antispermato-genic effect, post-testicular antifertility effect, spermicidal effect, sperm-immobilizing effect, antiandrogenic effect, etc.

Antispermato-genic activity indicates interference in the steroidogenesis when the cholesterol level rises and sudanophilic lipid accumulates (Mandal et al., 2010). Some of the plant extracts kill the viability and work on Sertoli cells and have various effects on spermatogenesis, such as reducing the nuclear and cytoplasmic volume and vacuolizing Sertoli cells (Sharma RS et al., 2001) or acts through Leydig cells (Dufau et al., 1984). Some plant extracts act by unbalancing the hormones or through their antimotility activity (Verma and Yadav, 2021).

Spermicidal are contraceptive substances that destroy the sperm when inserted vaginally prior to intercourse. The spermicidal agents consist of a surfactant that destroys the sperm cell membrane. Lipid peroxidation may play an important role in disrupting the sperm membrane physiology that may or may not be accompanied with a detrimental effect on the defense system of the human spermatozoa against the ROS.

Antiandrogens, also known as androgen antagonists or testosterone blockers, prevent androgens like testosterone and dihydrotestosterone (DHT) from mediating their biological effects in the body. *Andrographis paniculata* (Burm.f.) Nees, *Azadirachta indica* A. Juss., *Curcuma longa* L., *Hibiscus rosa-sinensis* L., and *Plumbago zeylanica* L. act by blocking the androgen receptor (AR) and/or inhibiting or suppressing androgen production. They can be considered as the functional opposites of AR agonists, for instance, androgens and anabolic steroids (AAS) like testosterone, DHT, and nandrolone and selective androgen receptor modulators (SARMs) like enobosarm.

Figures 4, 5 provide group of these plants 3 (a) and 4 (a) with probable female and male contraceptive activities 3 (b) and 4 (b), respectively.

Limitations/Challenges

A major limitation is the contradictory reports or non-reproducibility of published data, which can provide useful leads. At times, failure of reproducibility of contraceptive activity of a plant or its constituent is observed. This could be due to the multiple factors at different levels that are known to affect the reproductive process. The other reason could be the variable effect of the herbal contraceptive/s in animals as against when used in humans.

The contraceptives of natural origin are not used much in practice, the main factor being the lack of standardization and reliable validation studies. The information has thus remained fragmented. Studies have consequently been scarce. Interest has waned due to the complexity and enormity of the large and long-term study requirements covering multiple variables.

Analytical methods, information on phytoconstituents, availability of markers, and their activities have now provided

new standardization approaches to herbal products that assure higher safety and stability.

The solution to this is to investigate the efficacy of these herbs in humans themselves, after ascertaining their safety in animal models. There is also a need to record the conditions under which the plants are used by indigenous people, including the time and place of collection, proper botanical authentication, and schedule of administration. Advances in biology offer adaptable and promising experimental models to examine the effectiveness of natural products for altering reproductive functions and contraception

CONTRACEPTION AND NEW TECHNOLOGIES FOR NATURAL PRODUCTS

There is a need to use new contraceptive methods to minimize the side effects. The following technological advances are relevant in the context of this review for discovery and development of novel contraceptives of natural origin.

- o Ayurveda recommends fumigation as a method and as a therapeutic procedure to treat various diseases, including microbial infections. Ayurvedic methods of sterilization with fumigation can be alternated as a modern contraceptive with the help of nanotechnology. Natural novel bioactive compound drugs could be developed with novel drug-delivery systems.

- o A team in the University of Washington has developed an electrically spun cloth with nanometer-sized fibers that get dissolved to release drugs, thus providing a platform for cheap, discrete, and reversible protection ("Drug-Eluting Fibers for HIV-1 Inhibition and Contraception").

- o Pharmacy on a chip is one of the most exciting parts of the drug-delivery system. It is a chip implanted into the body which releases drugs at set intervals. It would release the hormones estrogen and progesterone over a specific period to stop the release of eggs from the ovaries and thus prevent pregnancy.

- o Nanotechnology-based condom systems have the potential to prevent the spread of HIV and STIs.

- o Transdermal drug delivery (TDD) is an alternative method of drug administration for drugs whose delivery by conventional oral, topical, intravenous, and intramuscular methods is of limited efficacy. Recent advances in TDD involve the use of nanoparticles (NPs), which exhibit great potential to enhance drug permeation across the skin.

- o Skin patches containing microneedles is a painless and minimally invasive method of TDD in which micron-sized pores are created in the epidermis to allow delivery of drugs to the blood vessels present in the dermal layer of the skin.

- o Researchers report on a technique for administering contraceptive hormones through special backings on jewelry such as earrings, wristwatches, rings, or necklaces. The contraceptive hormones are contained in patches applied to portions of the jewelry in contact with the skin, allowing the drugs to be absorbed into the body (Georgia Institute of Technology, 2019).

Possibilities for new means of drug development

- Developing newer biotechnology-based cellular or molecular models that could better replicate reproductive processes.
- Methods that act after ovulation and interfere with sperm delivery or function in the male or in the female genital tract or both ought to be adopted.
- Design of nonhormonal contraceptive agents—as an alternative option to hormonal formulations—with the help of herbals.
- New delivery mechanisms that can act both short and long term; the possibilities are to develop herbal pessary, jelly, patches, and condoms, or mechanical devices with natural ingredients to optimize the effects.
- Methods which limit the side effects associated with systemic exposure should be developed in lower dosage forms to ensure efficacy.
- Technologies that markedly improve the cost, acceptability, and deliverability of contraceptives.
- Personalized contraception-human genome could minimize the side effects while maximizing health benefits at the individual level.

CONCLUSION

Fertility and contraception are continued subjects of biomedical research and innovation. Alternatives to unmet needs for safer contraception methods and drugs are searched for. Many Ayurvedic medicinal ingredients and compound formulations are claimed to inhibit male and female fertility as mentioned in the classical literature. Several of these validated drugs possess

spermicidal, antispermatogetic, antioviulatory, anti-implantation, antiestrogenic, and abortifacient activity. The Indian system of medicine, Ayurveda, offers highly promising opportunities when analytical, biological, technological, and clinical advances are collectively integrated with therapeutic rationale based on Ayurvedic principles. A plethora of available data, information, and knowledge on these ingredients could be the subject of newer research interests.

These medicinal ingredients need further reexamination and critical evaluation to explore their lesser known or unknown pharmacological and biological activity/activities and effects. Present-day biotechnological methods could be usefully utilized to evaluate their contraceptive efficacies. There is a need to revive and stimulate new research programs and projects that will not only benefit the need of contraception but will also throw new light on reproductive biology.

AUTHOR CONTRIBUTIONS

The corresponding author Dr. NB contributed to the concept, initial compilation, structure of the review, and final editing of the text and figures. Co-author Dr. MD contributed to compiling and comparing pharmacological data and the preparation of tables and figures.

ACKNOWLEDGMENTS

We sincerely thank Dr. Vandana Kozarekar for reference review and edit support.

REFERENCES

- Abdelgader, A., and Elsheikh, A. (2018). Antiandrogenic Activity of *Calotropis Procera* Latex in Rats. *Asian Pac. J. Reprod.* 7, 129–135. doi:10.4103/2305-0500.233574
- Achintya, M. (2018). Evaluation of Contraceptive Properties of Neem Oil - A Prospective Study. *Sci. Cult.* 84 (1–2), 67–70.
- Adhikary, P., Banerji, J., Chowdhury, D., Das, A. K., Deb, C. C., Mukherjee, S. R., et al. (1989). Antifertility Effect of Piper Betle Linn. Extract on Ovary and Testis of Albino Rats. *Indian J. Exp. Biol.* 27, 868–870.
- Agarwal, M., and Dixit, V. P. (1982). *Effect of Balanites Roxburghii on Male Reproductive Tract of Langur Monkey*. Allahabad: 52nd Annual Session of National Academy Science, 56.
- Ahmad, S., Jamal, Y., and Mannan, A. (2011). Review of Some Medicinal Plants with Anti-fertility Activities. *Unani Res.* 1 (2), 24–28. doi:10.5530/ur.2.2011.6
- Akbarsha, M. A., Manivannan, B., Hamid, K. S., and Vijayan, B. (1990). Antifertility Effect of Andrographis Paniculata (Nees) in Male Albino Rat. *Indian J. Exp. Biol.* 28 (5), 421–426.
- Akbarsha, M. A., and Murugaian, P. (2000). Aspects of the Male Reproductive Toxicity/male Antifertility Property of Andrographolide in Albino Rats: Effect on the Testis and the Cauda Epididymal Spermatozoa. *Phytother. Res.* 14 (6), 432–435. doi:10.1002/1099-1573(200009)14:6<432::aid-ptr622>3.0.co;2-i
- Anonymous (1996). *Pharmacological Investigations of Certain Medicinal Plants and Compound Formulations Used in Ayurveda and Siddh*. New Delhi: Central Council of Research in Ayurved and Siddha, 474.
- Ave Olivia, R., Purwakanthi, A., and Dewi, H. (2020). Antifertility Effect of Betel Nut (Areca Catechu L) in Male Rat. *MEDISAINS* 18 (2), 52–57. doi:10.30595/medisains.v18i2.7588
- Azeez, O. I., and Philip, A. A. (2013). Retarded Hippocampal Development Following Prenatal Exposure to Ethanolic Leaves Extract of *Datura Metel* in Wistar Rats. *Niger. Med. J.* 54 (6), 411–414. doi:10.4103/0300-1652.126299
- Azmeera, M., Elumalai, A., Eswaraiah, M. C., and Mathangi, N. (2012). An Updated Review on Anti-fertility Plants. *Inter. J. Pharmacother.* 2 (1), 4–6.
- Badwaik, H., Giri, T. K., Tripathi, D. K., Singh, M., and Khan, A. H. (2011). A Review on Pharmacological Profile for Phytomedicine Known as *Gloriosa Superb* Linn. *Res. J. Pharmacognosy Phytochemistry* 3 (3), 103–107.
- Bajaj, A., Mathur, R. S., Wadhwa, M., and Bahel, S. (1981). Effect of Steroidal Fraction of *Abrus precatorius* on Testes of Albino Rats. *Geobios* 8, 29–31.
- Barilli, S., Santos, S., and Montanari, T. (2005). Effect of decocyte of northern buchinha fruits (*Luffa operculata* Cogn.) on female reproduction and embryonic and fetal development. *XVII Scientific Initiation Hall. Book of Abstracts* (Porto Alegre: Pro-Rectory of Research, UFRGS), 539.
- Bhagat, M., and Purohit, A. (1986). *Kinetics of the Testicular Cell Population Following Various Curcuma Longa Rhizome Extract Administration in Male Albino Rats, A Morphometric Approach*, in: *National Entellus*. India: National Symposium on the Use of Primates in Biochemical Research Jaipur, 53.
- Bhargava, S. K. (1984). Effects of Plumbagin on Reproductive Function of Male Dog. *Indian J. Exp. Biol.* 22, 153–156.
- Bhaskar, V. H., V. H., Profulla, B. R., Kumar, M., and Sangameswaran, B. (2009). Evaluation of the Antifertility Activity of Stem Bark of *Crataeva nurvalabuch-Hum*. *Afr. J. Biotechnol.* 8 (22), 6453–6456. doi:10.5897/ajb09.303
- Bhavamisra, B. P. (1961). in *Varanasi. Chowkhambha Sanskrit Series, IInd Part Chikitsa*. 3rd, 7033–7034.
- Bidwai, P. P., Wangoo, D., and Bhullar, N. (1990). Antispermatogetic Action of *Celastrus paniculatus* seed Extract in the Rat with Reversible Change in the Liver. *J. Ethnopharmacol* 28 (3), 293–303. doi:10.1016/0378-8741(90)90080-d

- Bodhankar, S. L., Garg, S. K., and Mathur, V. S. (1974). Antifertility Screening of Plants. Part IX. Effect of Five Indigenous Plants on Early Pregnancy in Female Albino Rats. *Indian J. Med. Res.* 62, 831–837.
- Brinker, F. (1997). Inhibition of Endocrine Function by Botanical Agents, Antigonadotropic Activity. *Br. J. Phytother* 4, 123–145.
- Bullock, J., Boyle, J., and Wang, M. B. (1995). in *Physiology*. Editor J. Velker 3rd edn. (Lippincott Williams & Wilkins), 497–519.
- Census of India (2011). Population Projections for India and States 2011 – 2036. Available at: https://nhm.gov.in/New_Updates_2018/Report_Population_Projection_2019 (Accessed November 6, 2020).
- Changamma, C., and Lakshman, J. (2013). Antispermatogetic Effect of Carica Papaya Seed Extract on Steroidogenesis in Albino Rats. *Int. J. Pharm. Pharm. Sci.* 5 (1), 67–69.
- Chaturvedi, M., and Dixit, V. P. (1997). Antifertility Effect of *Citrullus colocynthis* Schrad in Male Albino Rats. *Indian J. Environ. Sci.* 1 (2), 89–92.
- Chaudhury, M. R., Chandrasekaran, R., and Mishra, S. (2001). Embryotoxicity and Teratogenicity Studies of an Ayurvedic Contraceptive--Pippaliyadi. *J. Ethnopharmacol.* Feb 74 (2), 189–193. doi:10.1016/s0378-8741(00)00354-8
- Choudhury, P. K., and Jadhav, S. (2013). Pharmacological Action of Plant Alkaloids in Female Reproductive System of Test Animals And/or Human Beings: A Review. *Int. J. Pharm. Sci. Rev. Res.* 23 (2), 98–107.
- Cuomo, Amy. (2010). "Birth Control," in *Encyclopedia of Motherhood*. Editor A. O'Reilly (Thousand, Oaks, Calif: Sage Publications), 121–126.
- Dahanukar, S. A., Kulkarni, R. A., and Rege, N. N. (2000). Pharmacology of Medicinal Plants and Natural Products. *Indian J. Pharmacol.* 32, S81–S118.
- Das, R. P. (1980). Effect of Papaya Seeds on the Genital Organs and Fertility of Male Rats. *Indian J. Exp. Biol.* 18, 408–409.
- Dash, B., and Basu, R. (1968). Methods for sterilization and Contraception in Ancient and Medieval period. *IJHS* 3910, 9–24.
- De Freitas, T. G., Augusto, P., and Montanari, T. (2005). Effect of Ruta Graveolens L. On Pregnant Mice. *Contraception* 71 (1), 74–77. doi:10.1016/j.contraception.2004.07.014
- Devendra, N. K., Vijaykumar, B., Malashetty, Y., Seetharam, N., Suresh, P., and Patil, S. B. (2009). Effect of Ethanol Extract of Whole Plant of *Trichosanthes cucurbitina* Var. *Cucurbitina* L. On Gonadotropins, Ovarian Follicular Kinetics and Oestrous Cycle for Screening of Antifertility Activity in Albino Rats. *Int. J. Morphol.* 27 (1), 173–182. doi:10.4067/S0717-95022009000100030
- Dhawan, B. N., Dubey, M. P., Mehrotra, B. N., Rastogi, R. P., and Tandon, J. S. (1980). Screening of Indian Plants for Biological Activity: Part-IX. *Indian J. Exp. Biol.* 18, 594–602.
- Dheeraj, A. (2011). Anti-fertility Activity of *Acacia Leucophloea*. *Scholars Res. Libr.* 3 (3), 411–413.
- Dikshith, T. S. S., Raizada, R. B., and Mulchandani, N. B. (1990). Toxicity of Pure Alkaloid of *Tylophora asthmatica* in Male Rats. *Indian J. Exp. Biol.* 28 (3), 208–212.
- Dimitriadis, E., Robb, D. L., Liu, Y. X., Enders, A. C., et al. (2003). IL-11 and IL-11R α Immunolocalisation at Primate Implantation Sites Supports a Role for IL-11 in Placentation and Fetal Development. *Reprod. Biol. Endocrinol.* 1 (1), 34. doi:10.1186/1477-7827-1-34
- Dixit, V. P., Bhargava, S. K., and Gupta, R. A. (1981). Hyperglycemia Induced Testicular Dysfunction after Chronic Administration of *Balanites roxburghii* Planch Fruit Pulp Extract in Dog (*Canis Indicus*). *Indian J. Exp. Biol.* 19, 918–921.
- Dixit, V. P., and Bhargava, S. K. (1983). Reversible Contraception like Activity of Embelin in Male Dogs (*Cannus Indicus* Linn.). *Andrologia* 15 (5), 486–494. doi:10.1111/j.1439-0272.1983.tb00174.x
- Dixit, V. P., and Joshi, S. (1983). Effect of Aloe Barbadensis and Clofibrate in Triton Induced Hyperlipidaemic presbyitis Monkeys. *Ind. J. Med. Res.* 78, 417–421.
- Dixit, V. P., and Joshi, S. (1982). Effects of Chronic Administration of Garlic (*Allium Sativum* Linn) on Testicular Function. *Indian J. Exp. Biol.* 20, 534–536.
- Dixit, V. P., Joshi, S., and Kumar, A. (1983). Possible Antispermatogetic Activity of *Gloriosa Superba* (EtOH-Extract) in Male Gerbil (*Meriones hurriane* Jerdon): A Preliminary Study. *Comp. Physiol.* 8, 17–22.
- Dixit, V. P., Sinha, R., and Gupta, I. (1987). Inhibition of Sperm Production and Sperm Dynamics in *Abrus precatorius* Treated Males. *The Indian Zoologist* 11 (1-2), 115–118.
- Dufau, M. L., Winters, C. A., Hattori, M., Aquilano, D., Baranao, J. L., Nozu, K., et al. (1984). Hormonal Regulation of Androgen Production by the Leydig Cell. *J. Steroid Biochem.* 20, 161–173. doi:10.1016/0022-4731(84)90203-6
- Dutta, D. C. (2013). *Text Book of Gynaecology Including Contraception*. 6th edition. New Delhi: Jaypee Brothers medical publisher.
- Elizabeth, S., Ann, B., Jacqueline, E. D., Taylor, R., Lori, S. A., Naomi, L-D., et al. (2020). Report- Adding it up: Investing in Sexual and Reproductive Health 2019. Available at: <https://www.guttmacher.org/report/adding-it-up-investing-in-sexual-reproductive-health-2019-executive-summary/resources> (Accessed November 10, 2020).
- Farooq, T., Vanitha Kumari, G., Bhuvaneswari, G., and Malini, T. (1997). Effects of Anethole on Accessory Sex Tissue of Albino Rats. *J. Res. Ayurv Siddha* 15, 161–170.
- Galib, A. C., Kar, M. M., Rao and Ala, N. (2008). Concepts of Contraception in Ancient India & Status in Present Scenario. *J. Ind. Inst. Hist. Med.* XXXVIII, 79–88.
- Gangadhar, R., and Lalithakumari, K. (1995). Abortifacient Activity of the Aqueous Extract of the Leaves of *Aegle Marmelos* (Bel) in Albino Rats. *Indian Drugs* 32, 129–131.
- Ganguly, M., Borthakur, M. K., Devi, N., and Mahanta, R. (2007). Antifertility Activity of T Methanolic Leaf Extract of *Cissampelos Pareira* in Female Albino Mice. *J. Ethnopharmacology* 111 (3), 688. doi:10.1016/j.jep.2007.01.023
- Garg, S. K., Mathur, V. S., and Chaudhary, R. R. (1978). Screening of Indian Plants for Antifertility Activity. *Indian J. Exp. Biol.* 16, 1077. doi:10.1007/bf00930383
- Garg, S. K. (1975). Antifertility Effect of Some Chromatographic Fractions of *Daucus Carota*. *Indian J. Pharmacol.* 7, 40–42.
- Garg, S. K. (1974). Antifertility Effect of Oil from Few Indigenous Plants on Female Albino Rats. *Planta Med.* 26, 391. doi:10.1055/s-0028-1099405
- Garg, S. K., and Garg, G. P. (1970). A Preliminary Report on the Smooth Muscle Stimulating Property of Some Indigenous Plants on Isolated Rat Uterus. *Bull. P. G. Chandigarh* 4, 162.
- Garg, S. K., and Garg, G. P. (1971). Antifertility Effects of *Areca Catechu* Linn. And *Carica Papaya* Linn. in Female Albino Rats. *Indian J. Pharmac* 3, 23.
- Garg, S. K., Mathur, V. S., and Chaudhury, R. R. (1978). Screening of Indian Plants for Anti-fertility Activity. *Indian J. Exp. Biol.* 16 (10), 1077–1079.
- Gbotolorun, S. C., Osinubi, A. A., Noronha, C. C., and Okanlawon, A. O. (2008). Antifertility Potential of Neem Flower Extract on Adult Female Sprague-Dawley Rats. *Afr. Health Sci. Sep.* 8 (3), 168–173.
- Gediya, S., Ribadiya, C., Soni, J., Shah, N., and Jain, H. (2011). Herbal Plants Used as Contraceptives. *Int. J. Curr. Pharm. Rev. Res.* 2 (1), 47–53.
- Georgia Institute of Technology (2019). Contraceptive Jewelry Could Offer a New Family Planning Approach Science Daily. Available at: www.sciencedaily.com/releases/2019/03/190326105705.htm (Accessed November 14, 2020).
- Ghosh, A. K., Das, A. K., and Patra, K. K. (2011). Studies on Antifertility Effect of Rhizome of *Curcuma Longa* linn. *Asian J. Pharm. Life Sci.* 1 (4), 349–353.
- Goel, R. K., Prabha, T., Kumar, M. M., Dorababu, M., Prakashand Singh, G. (2006). Teratogenicity of *Asperaguscacemosus* Wild. Root, an Herbal Medicine. *Indian J. Exp. Biol.* 44 (7), 570–573.
- Goncim, H. Y., Mador, E. S., and Ogunranti, J. O. (2010). *Ricinus Communis* Var *Minor* Inhibits Follicular Development and Possibly Ovulation in Human Subjects as Shown by Ultrasound Follicle Tracking. *Clinical Medicine Insights*. January: Reproductive Health.
- Gupta, A. K., Bindal, M. C., Gupta, S. K., Prakash, D., and Vedpal (2013). Aphrodisiac Activity of *Semecarpus Anacardium* Nut. *Int. Res. J. Pharm.* 4, 202–204.
- Gupta, I., Tank, R., and Dixit, V. P. (1985). Fertility Regulation in Males: Effect of *Hibiscus Rosa-Sinensis* and *Malvaviscus* Flower Extract on Male Albino Rats. *Proc. Nat. Acad. Sci. India* 55 (B), 262–267.
- Gupta, M., Mazumder, U. K., Pal, D. K., and Bhattacharya, S. (2003). Anti-steroidogenic Activity of Methanolic Extract of *Cuscuta reflexa* Roxb. Stem and *Corchorus Olitorius* Linn. Seed in Mouse Ovary. *Indian J. Exp. Biol.* 41, 641–644.
- Gupta, R. S., Choudhary, R., Yadav, R. K., Verma, S. K., and Dobhal, M. P. (2005a). Effect of Saponins of *Albizia Lebbeck* (Linn.) Benth. Bark on the Reproductive System of Male Albino Rats. *J. Ethnopharmacol* 96 (1-2), 31–36. doi:10.1016/j.jep.2004.07.025
- Gupta, R. S., and Dixit, V. P. (1989). Testicular Cell Population Dynamics Following Palmitine Hydroxide Treatment in Male Dogs. *J. Ethnopharmacol* 25, 151–157. doi:10.1016/0378-8741(89)90016-0
- Gupta, R. S., Dobhal, M. P., and Dixit, V. P. (1996). Morphometric and Biochemical Changes in Testes of Presbyitis Entellus Dufresne (Langur

- Monkey) Following Aristolochic Acid Administration. *Ann. Biol.* 12 (2), 328–334.
- Gupta, R. S., Kachhawa, J. B., and Chaudhary, R. (2004). Antifertility Effects of Methanolic Pod Extract of Albizia Lebbeck (L) Benth in Male Rats. *Asian J. Androl.* 6 (2), 155–159.
- Gupta, R. S., Kumar, P., and Dixit & Dhobhal, V. P. M. P. (2000). Antifertility Studies of Root Extract of Barleria prionitis Linn. In Male Albino Rats with Special Reference to Testicular Cell Population Dynamics. *J. Ethnopharmacol.* 70 (2), 111–117. doi:10.1016/S0378-8741(99)00150-6
- Gupta, R. S., and Sharma, A. (2003). Antifertility Effect of Tinospora Cordifolia Willd. Stem Extract in Male Rats. *Indian J. Exp. Biol.* 41, 885–889.
- Gupta, R. S., Sharma, N., and Dixit, V. P. (1990). Calotropin, A Novel Compound for Fertility Control. *Ancient Sci. Life* 9 (4), 224–230.
- Gupta, R. S., Sharma, R., Sharma, A., Choudhary, R., Bhatnagar, A. K., and Joshi, Y. C. (2005b). Antifertility Effects of Pueraria Tuberosa Root Extract in Male Rats. *Pharm. Biol.* 42 (8), 603–609. doi:10.1080/13880200490902491
- Gupta, R. S., Kanwar, M., Rehwani, H., Verma, S. K., and Dobhaal, M. P. (2006). Contraceptive Efficacy of Strychnos potatorum Seed Extract in Male Albino Rats. *Asian J. Exp. Sci.* 20 (1), 181–187.
- Gupta, S., Dheeraj, A., Sharma, N. K., Jhade, D., and Bharti, A. (2011). Effect of Plumbagin Free Alcohol Extract of Plumbago Zeylanica Linn. Root on Reproductive System of Female Wister Rats. *Asian Pac. J. Trop. Med.* 4 (12), 978–984. doi:10.1016/S1995-7645(11)60230-7
- Gupta, S. S. (1994). Prospects and Perspectives of Natural Plants Products in Medicine. *Indian J. Pharmacol.* 26, 1–12.
- Gupta, S., Sanyal, S. N., and Kanwar, U. (1989). Antispermato-genic Effect of Embelin, a Plant Benzoquinone, on Male Albino Rats *In Vivo* and *In Vitro*. *Contraception* 39, 307–320. doi:10.1016/0010-7824(89)90063-2
- Gutiérrez-Pajares, J. L., Zúñiga, L., and Pino, J. (2003). Ruta Graveolens Aqueous Extract Retards Mouse Preimplantation Embryo Development. *Reprod. Toxicol.* 17 (6), 667–672. doi:10.1016/j.reprotox.2003.07.002
- Hadimur, K., Revansiddppa, S. S., Lone, N. D., Veena, K., and Neelamma, P. (2014). Anti-implantation and Pregnancy Interruption Activity of Japaku-suma (Hibiscus Rosa Sinensis) & its Combinations in Albino Rats. *Br. J. Med. Health Res.* 1 (3), 11–18. doi:10.7897/2277-4343.04316
- Indradev, T. (1998). *Rasaratnasamuccaya of Rasavagbhata*. 1st Edition. Varanasi, India: Chaukhambha Sanskrit Bhavan, 95–96.
- Isichei, C. O., Das, S. C., Ogunkeye, O. O., Okwuasaba, F. K., Uguru, V. E., Onoruvwe, O., et al. (2000). Preliminary Clinical Investigation of the Contraceptive Efficacy and Chemical Pathological Effects of RICOM-1013-J of Ricinus communis Var Minor on Women Volunteers. *Phytother. Res.* 14 (1), 40–42. doi:10.1002/(sici)1099-1573(200002)14:1
- Jain, G. C., and Dixit, V. P. (1982). *Effect of Annona Squamosa Ethanol Extract and Testicular Function of Dogs (Canis Indicus Linn.)*, II Annual Session of Science, 22.
- Jamwal, K. S., and Anand, K. K. (1962). Preliminary Screening of Some Reputed Abortifacient Indigenous Plants. *Indian J. Pharm.* 2, 218–220.
- Jansen, G. C., and Wolhlumuth, H. (2014). Carrot Seed for Contraception: A Review. *Aust. J. Herbal Med.* 26, 10–17.
- Jati, K. P., Mahapatra, A. K., and Rajagopala, S. (2018). *Teratogenic Effect of Herbal Drugs - A Review*. *IJAAR Volume III Issue X Sep -Oct*, 1516–1523.
- Jha, R. K., and Dixit, V. P. (1986). Inhibition of Spermatogenesis after Chronic Administration of *Terminelia Arjuna* and *Sapindustrifoliatus* (50% EtOH Extract) in Male Albino Rats. *Proc. Nat. Acad. Sci.* 56 (3), 94–99.
- Jon, K. (2012). A History of Birth Control Methods. Planned Parenthood Report. January, Federation of America. Available at: https://www.plannedparenthood.org/files/2613/9611/6275/History_of_BC_Methods.pdf (Accessed November 20, 2020).
- Jugnu, S., and Sharma, B. (2011). *Rajamartanda. Ancient Sanskrit Medical Text of Maharaja Bhoja with Sanskrit Text: English Transliteration and Commentary in English*. Varanasi: Chaukhambha Orientalia. StreeRogadhikara, 16 to 18 and 31.
- Kalita, J. C., Chakrabarty, A., and Tanti, B. (2011). Assessment of Antifertility Activity of Some Traditionally Used Plants by Different Ethnic Communities in Three Districts of Assam, India. *J. Herbal Med. Toxicol.* 5 (2), 65–72.
- Kamboj, V. P., and Dhawan, B. N. (1982). Research on Plants for Fertility Regulation in India. *J. Ethnopharmacology* 6 (2), 191–226. doi:10.1016/0378-8741(82)90004-6
- Kasturi, M., Nazeer, A. R., Pathan, K. M., Parveen, D. S., and Manivannan, B. (1997). Effects of Azadirachtaindica Leaves on the Seminal Vesicles and Ventral Prostate in Albino Rats. *Indian J. Physiolpharmacol* 41, 234–240.
- Kaur, R., Sharma, A., Kumar, R., and Kharb, R. (2011). Rising Trends towards Herbal Contraceptives. *J. Nat. Product. Plant Resour.* 1 (4), 5–12.
- Keshri, G., Singh, M. M., Lakshmi, V., and Kamboj, V. P. (1995). Post-coital Contraceptive Efficacy of the Seeds of Nigella Sativa in Rats. *Indian J. Physiolpharmacol* 39, 59–62.
- Kholkute, S. D., Kekere, M. B., and Munshi, S. R. (1979). Antifertility Effect of Fruits of Piper Longum on Female Rats. *Indian J. Exp. Biol.* 17, 289–290.
- Khoury, N. A., and Akawi, Z. E. (2005). Antiandrogenic Activity of Ruta Graveolens L in Male Albino Rats with Emphasis on Sexual and Aggressive Behaviour. *Neuroendocrinology Lett.* 26 (6), 823.
- Kuchimara (2007). *Kuchimaratantra, Text with English Translation by Goli Penchalaprasada*. Varanasi: Chaoukhambha Krisandas Academy.
- Kulshreshtha, S. S., and Mathur, R. S. (1990). Effect of Steroidal Fraction of Seeds of Abrus precatorius Linn. On Rat Testis. *Indian J. Exp. Biol.* 28, 752–756.
- Kumar, C. P., and Sachin, J. (2013). Pharmacological Action of Plant Alkaloids in Female Reproductive System of Test Animals And/or Human Beings: A Review. *Int. J. Pharm. Sci. Rev. Res.* 23, 98–107.
- Lakmipatishashtri (1983). “Varanasi. Yogaratnakara – Yonivyapat,” in *Chikitsa Yonivyapad/Garbhsnivaran* 1, 4–6. 3rd ed. (Chowkhambha Sanskrit Series).
- Lal, B., and Udupa, K. N. (1993). A Preliminary Study of Antifertility Effect of an Indigenous Drug – Arjuna (Terminalia Arjuna). *JRAS* 14 (1), 165–169.
- Lal, B., Udupa, K. N., and Tripathi, V. K. (1992). Study of the Antifertility Effect of Nigundi [Vitex Nigundo]- A Preliminary Trails. *J. Res. Ayurved Siddha* 13 (1–2), 89–93.
- Latha, K. P., Kirana, H., and Girish, H. N. (2013). Anti Implantation Activity of the Hydrocoloholoc Tuber Extract of Gloriosa Superb Linn in Female Albino Rats. *Int. J. Adv. Pharm. Biol. Chem.* 2 (3), 443–448.
- Laxmi, V., Kumar, R., Agarwal, S. K., and Dhar, J. D. (2006). Antifertility Activity of Piper Longum in Female Rats. *NAT. Prores* 20 (3), 235–239. doi:10.1080/14786410500045465
- Lipsey, R. G., Carlaw, K., and Bekar, C. (2005). *Historical Record on the Control of Family Size. Economic Transformations: General Purpose Technologies and Long-Term Economic Growth*. Oxford University Press, 335–340.
- Lobat, J., Neda, S., Najmeh, S., Mehrnoosh, S., Soleiman, K., Hedayatollah, S., et al. (2015). Antioxidant Activity and Teratogenicity Evaluation of Lawsonia Inermis in BALB/c Mice. *J. Clin. Diagn. Res.* 9 (5), FF01–FF04. doi:10.7860/JCDR/2015/12290.5911
- Londonkar, R. L., Srinivasreddy, P., Somanathreddy, P., and Patil, S. B. (1998). Nicotine Induced Inhibition of Activities of Accessory Reproductive Ducts in Male Rats. *J. Ethnopharmacol* 60 (30), 215–221. doi:10.1016/S0378-8741(97)00148-7
- Makonnen, E., Zerihun, L., Assefa, G., and Rostom, A. A. (1999). Antifertility Activity of Ricinus communis Seed in Female guinea Pigs. *East. Afr. Med. J.* 76, 335–337.
- Malhi, B. S., and Trivedi, V. P. (1972). Vegetable Antifertility Drugs of India. *Q. J. Crude Drug Res.* 12 (3), 1922–1928. doi:10.3109/13880207209068244
- Mali, P. C. (1999). Antifertility Activity of *Euphorbia neriifolia* Linn. Root Extract in Male Rats. *Indian J. Environ. Sci.* 3 (2), 85–190.
- Malini, T., Manimaran, R. R., Arunkumar, J., Arulhas, M. M., and Govindarajulu, P. (1999). Effects of Piperine on Testis of Albino Rats. *J. Ethnopharmacology* 64 (3), 219–225. doi:10.1016/S0378-8741(98)00128-7
- Malpani, A., and Mahurkar, N. (2018). Antifertility Activity of Different Extracts of Tuberous Roots of Gloriosa Superba Linn. *In female Wistar albino rats Indian Drugs* 55 (7), 67–71.
- Mandal, R., and Dhaliwal, P. K. (2007). Antifertility Effect of Melia Azedarach Linn. (Dharek) Seed Extract in Female Albino Rats. *Indian J. Exp. Biol.* 45, 853–860.
- Mandal, T. K., and Das, N. S. (2010). Testicular Toxicity in Cannabis Extract Treated Mice: Association with Oxidative Stress and Role of Antioxidant Enzyme Systems. *Toxicol. Ind. Health* 26, 11–23. doi:10.1177/0748233709354553
- Maurya, R., Srivastava, S., Kulshreshtha, D. K., and Gupta, C. M. (2004). Traditional Remedies for Fertility Regulation. *Curr. Med. Chem.* 11 (11), 1431–1450. doi:10.2174/0929867043365215

- Mint (2020). The Unmet Need for Contraception in India. Available at: <https://www.livemint.com/news/india/the-unmet-need-for-contraception-in-india-11581350642826.html> (Assessed November 5, 2020).
- Mishra, R. K., and Singh, S. K. (2009). Antispermato-genic and Antifertility Effects of Fruits of *Piper Nigrum* L. In Mice. *Indian J. Exp. Biol.* 47, 706–714.
- Misra, D. N., and Shukla, G. D. (1980). Vitafix in Premature Ejaculation A Controlled Trial. *Indian Pract.* 33, 81.
- Mukherjee, P. (2002). *An Approach to Evaluation of Botanicals*. 1st edn. New Delhi, India: Business Horizons; Quality Control Herbal Drugs.
- Munshi, S. R., Shetye, T. A., and Nair, R. K. (1977). Antifertility Activity of Three Indigenous Plant Preparations. *Plant Med.* 31, 73–75. doi:10.1055/s-0028-1097494
- Mutreja, A., Agarwal, M., Kushwaha, S., and Chauhan, A. (2008). Effect of *Nelumbo nucifera* Seeds on the Reproductive Organs of Female Rats. *Iranian J. Reprod. Med.* 6 (1), 7–11.
- Nand, O. P. (1981). Antifertility Investigation on Embelin- an Oral Contraceptive of Plant Origin. *Plant Med.* 41 (3), 259–266. doi:10.1055/s-2007-971712
- Naseem, M. Z., Patil, S. R., Patil, S. R., and Patil, S. B. (1998). Antispermato-genic and Androgenic Activities of *Momordica Charantia* (Karela) in Albino Rats. *Jethnopharmacol* 61 (1), 9–16. doi:10.1016/s0378-8741(98)00006-3
- Neeru, V., and Sharma, S. K. (2008). Post-coital Antifertility Activity of Hibiscus Rosa-Sinensis Linn. Roots. *Evid. Based Complement. Alternat Med.* 5 (1), 91–94. doi:10.1093/ecam/nem003
- Novaro, V., Gonzalez, E., Jawerbaum, A., Rettori, V., Canteros, G., and Gimeno, M. F. (1997). Nitric Oxide Synthase Regulation during Embryonic Implantation. *Reprod. Fertil. Develop.* 9 (5), 557–564. doi:10.1071/r97005
- Ola-Mudathir, K. F., Suru, S. M., Fafunso, M. A., Obioha, U. E., and Faremi, T. Y. (2008). Protective roles of onion and garlic extracts on cadmium-induced changes in sperm characteristics and testicular oxidative damage in rats. *Food Chem. Toxicol.* 46 (12), 3604–3611. doi:10.1016/j.fct.2008.09.004
- Pal, R., Arup, M., and Achintya, S. (2013). Exploring post Coital Antifertility Activity with Toxicological and Hormonal Profiling of *Sapindustrifoliatus* Linn. *Int. Res. J. Pharm. Appl. Sci.* 3 (5), 53–60.
- Pal, A. K., Bhattacharya, K., Kabir, S. N., and Pakrashi, A. (1985). Flowers of *Hibiscus rosa-sinensis*, a potential source of contragestative agent: II. Possible mode of action with reference to anti-implantation effect of the benzene extract. *Contraception* 32 (5), 517–529. doi:10.1016/0010-7824(85)90021-6
- Palep, H. S., and Jukar, S. R. (2003). Effectiveness of Indigenous Oral Contraceptive. Available at: https://www.bhj.org.in/journal/2003_4502_april/effectiveness_310.htm (Accessed October 15, 2020).
- Pande, D., Malik, S., Bora, M., and Srivastav, P. (2002). A rapid protocol for in vitro micropropagation of *Lepidium sativum* linn. and enhancement in the yield of lepidine. *In Vitro Cell Dev Biol -Plant* 38, 451–455. doi:10.1079/IVP2002322
- Pandey, G., and Madhuri, S. (2010). Pharmacological Activities of *Ocimum Sanctum* (Tulsi): A Review. *Int. J. Pharm. Sci. Rev. Res.* 5 (1), 61.
- Pathak, A. K., Mallurwar, V. R., Kondalkar, A. K., and Soni, S. (2005). A Review of Plants with Anti-fertility Activity. *Nig J. Nat. Prod. Med.* 09, 4–10. doi:10.4314/njnp.v9i1.11824
- Pathak, S., Jonathan, S., and Prakash, A. O. (1995). Timely Administration of Extract of *Ferulajaeschkeana* Causes Luteolysis in the Ovary of Cyclic Guinea pig. *Indian J. Physiol Pharmacol* 39, 395–399.
- Patil, S. J., and Patil, S. B. (2013). Antioviulatory Activity of Petroleum Ether Extract of Chromatographic Fractions of Citrus Medica Seeds in Albino Rats. *Int. J. Med. Sci.* 13 (6), 410–417. doi:10.3923/jms.2013.410.417
- Pillai, N. R., Alam, M., and Purushothaman, K. K. (1982). Studies on Antifertility Activity of Oleanolic Acid 3 α -Glucoside (RDG-D). *J. Res. Indian Med. Yoga Homeop* 12, 26–29.
- Pillai, N. R., Alam, M., and Purushothaman, K. K. (1977). Studies on the Antifertility Activity of Oleanolic Acid 3- β -glucoside (RDG-1). *J. Res. Indian Med. Yoga Homeopath.* 12, 26–29. doi:10.1016/0360-1323(77)90003-8
- Pokharkar, R. D., Saraswat, R. K., and Kotkar, S. (2010). Survey of Plants Having Antifertility Activity from Western Ghat Area of Maharashtra State. *J. Herbal Med. Toxicol.* 4 (2), 71–75.
- Prakash, A. O., Kushwah, K., and Pathak, S. (1989). Effect of Ethanolic Extract of *Ferula Jaeschkeana* Vatke on the Biochemical Constituents in Vital Organs of Pregnant Rats. *Indian J. Pharmacol.* 21, 129–134.
- Prakash, A. O., Saxena, V., Shukla, S., and Mathur, R. (1985). Contraceptive Potency of *Pueraria Tuberosa* D.C. And its Hormonal Status. *Acta Eur. Fertil.* 16 (1), 59–65.
- Prakash, S. S. (1981). Anti-fertility Investigations on Embellin. *Planta Med.* 41, 259–266. doi:10.1055/s-2007-971712
- Priya, G., Saravanan, K., and Renuka, C. (2012). Medicinal Plants with Potential Antifertility Activity- A Review of Sixteen Years of Herbal Medicine Research (1994–2010). *Int. J. PharmTech Res.* 4 (1), 481–494.
- Purohit, A., Vyas, S. K., and Vyas, K. B. (2008). Contraceptive Efficacy of *Plumbago Zeylanica* Root Extract (50% Etoh) in Male Albino Rats with Special Emphasis on Testicular Cell Population Dynamics. *Anc Sci. Life Jan* 27 (3), 31–35.
- Raj, A., Singh, A., Sharma, A., Singh, N., Kumar, P., and Bhatia, V. (2011). Antifertility Activity of Medicinal Plants on Reproductive System of Female Rat. *Int. J. BioEngineering Sci. Technol.* 02 (03), 44–50.
- Rajeshwaradatta, S. (2001). *Bhaishiya Ratnavali of Govindadass with 'Vidyotini' Hindi Commentary*. 14th Edition. Varanasi: Chaukhambha Sanskrit Sansthan. VerseYoniviyipad 67/27, 28, 30–32.
- Reda, H., El, M., and Azza, A. (2018). Attia Ginger Causes Subfertility and Abortifacient in Mice by Targeting Both Estrous Cycle and Blastocyst Implantation without Teratogenesis. *Phytomedicine* 50, 300–308. doi:10.1016/j.phymed.2018.01.021
- Reddy, M. C., Murthy, R. K. D., and Saraswati, B. P. (1997). Antispermato-genic and Androgenic Activities of Various Extracts of *Hibiscus Rosa-Sinensis* in Albino Mice. *Indian J. Exp. Biol.* 35, 1170–1174.
- Roop, J. K., Dhaliwal, P. K., and Guraya, S. S. (2005). Extracts of *Azadirachta indica* and *Melia Azadarach* Seeds Inhibit Folliculogenesis in Albino Rats. *Braz. J. Med. Bio. Res.* 38 (6), 943–947. doi:10.1590/s0100-879x2005000600017
- Roy, C. A., and Venkatakrishna, B. H. (1983). Impairment of Spermatogenesis by *Cichorium Intybus* Plant Extract. *Naturwiss enschaften* 70, 365–369.
- Saksena, S. K. (1971). Study of Antifertility Activity of the Leaves of *Momordica linn* (Karela). *Indian J. Physiol. Pharmacol.* 15 (2), 79–80.
- Salunke, K. R., Ahmed, R. N., and Marigoudar, S. R. L. (2011). Effect of Graded Doses of *Caesalpinia Bonducella* Seed Extract on Ovary and Uterus in Albino Rats. *J. Basic Clin. Physiol. Pharmacol.* 22 (1-2), 49–53. doi:10.1515/jbcp.2011.006
- Samajdar, S., and Ghosh, A. K. (2017). Pharmacological effects of *Sesbania sesban* Linn : An overview. *PharmaTutor* 5 (7), 16–21.
- Samatha, J., and Bhattacharya, S. (2011). Cissampelos Pareira: A Promising Anti-fertility Agents. *Int. J. Res. Ayurveda Pharm.* 2 (2), 439–442.
- Sandhyakumary, K., Bobby, R. G., and Indira, M. (2003). Antifertility Effects of *Ricinus communis* Linn. On Rats. *Phytother Res.* 17 (5), 508–511. doi:10.1002/ptr.1308
- Sarkar, M., Gangopadhyay, P., Basak, B., Chakrabarty, K., Banerji, J., Adhikary, P., et al. (2000). The Reversible Antifertility Effect of *Piper Bette* Linn. On Swiss Albino Male Mice. *Contraception* 62, 271–274. doi:10.1016/s0010-7824(00)00177-3
- Sarwat, J., Salma, R., Mir, A. K., Mushtaq, A., Muhammad, Z., Muhammad, A., et al. (2009). Antifertility Effects of Ethanolic Seed Extract of *Abrusprecatorius* L. On Sperm Production and DNA Integrity in Adult Male Mice. *J. Med. Plants Res.* 3 (10), 809–814.
- Sathiyaraj, K., Sivaraj, A., Madhumitha, G., Vinoth kumar, P., Mary saral, A. M., Devi, K., et al. (2010). Antifertility Effect of Aqueous Leaf Extract of *Aegle Marmelos* on Male Albino Rats. *Int. J. Curr. Pharm. Res.*, 2 (1), 26–29.
- Satvarekar, S. D. (1958b). *Atharva Veda Ka Svadhyaya, Part II, (Kand VI – 138 / 1, 4, 5)*. 2nd. Pardi: Swadhyaya Mandal.
- Satvarekar, S. D. (1958a). *Atharva Veda Ka Svadhyaya, Part II, (Kand VI – 37 / 2,3)*. 2nd edition. Pardi: Swadhyaya Mandal.
- Satyawati, G. V. (1983). *Indian Plants and Plant Products with Antifertility Effect [A Review of Edition Literature between 1975-1982]*. New Delhi: ICMR.
- Schulz, V., Hänsel, R., and Tyler, V. (2001). *Rational phytotherapy: a physician's guide to herbal medicine*. Psychology Press.
- Seshadri, C., and Pillai, S. R. (1981). Antifertility Activity of a Compound Ayurvedic Preparation. *J. Sci. Res. Pl Med.* 2 (1&2), 1–3.
- Shah, N. V., and Varute, A. J. (1980). Effect of *Daucus Carrota* Seed Extract on Male Reproductive Organs of Albino Rats (testisII). in: All India Symposium in Life Sciences. Nagpur 91, 217.

- Shah, S. K., Jhade, D., and Chouksey, R. (2017). Pharmacological Evaluation and Antifertility Activity of Aloe Barbadensis Linn on Female Wistar Rats. *Int. J. Phytomedicine* 9 (2), 253–260.
- Shah, S. K., Jhade, D., and Chouksey, R. (2016). Antifertility Activity of Ethanolic and Aqueous Extracts of Aloe Vera Mill on Female Wistar Rats: Rising Approaches of Herbal Contraception. *J. Pharm. Sci. Res.* 8 (9), 952–957.
- Sharma, A., Verma, P. K., and Dixit, V. P. (2003). Effect of Semecarpus Anacardium Fruits on Reproductive Function of Male Albino Rats. *Asian J. Androl.* 5, 121–124.
- Sharma J, J., Sharma, S., and Jain, R. (2001). "Antifertility Activity of Cuminum Cyminum on Reproductive Organs of Male Albino Rats (*Rattus norvegicus*)," in *National Symposium Reproductive Biology and Comparative Endocrinology Vadodara* (Gujarat, 69).
- Sharma, J. D., Jha, R. K., Gupta, I., and Jain, P. (1987). Antiandrogenic Properties of Neem Seed Oil Azadirachta indica in Rat and Rabbit. *Ancient Sci. Life* 1, 30–38.
- Sharma, J. D., Sharma, L., and Yadav, P. (2007). Antifertility Efficacy of Piper Betel Linn. (Petiol) on Female Albino Rats. *Asian J. Exp. Sci.* 21 (1), 145–150.
- Sharma, N., and Jacob, D. (2001b). Inhibition of Fertility and Functional Alteration in the Genital Organs of Male Swiss Albino Mouse after Administration of Calotropis Procerca Flower Extract. *Pharm. Biol.* 39 (6), 403–407. doi:10.1076/pbbi.39.6.403.5882
- Sharma, N., and Jacob, D. (2001a). Antifertility Investigation and Toxicological Screening of the Petroleum Ether Extract of the Leaves of Mentha Arevensis L. In Male Albino Mice. *J. Ethnopharmacology* 75 (1), 5–12. doi:10.1016/s0378-8741(00)00362-7
- Sharma, R. S., Rajalakshmi, M., and Jeyaraj, D. A. (2001). Current Status of Fertility Control Methods in India. *J. Biosci.* 26, 391–305. doi:10.1007/bf02704741
- Sharma, S., Mehta, B. K., and Gupta, D. N. (1994). Screening of post-coital Anti-implantation Activity of Machelachampaka (Anthers) and Centrathurmanthelminticum (Seeds). *Indian Drugs* 31, 280–281.
- Sheeja, E., Joshi, S. B., and Jain, D. C. (2011). Anti-ovulatory and Estrogenic Activity of Plumbago Rosea Leaves in Female Albino Rats. *Indian J. Pharmacol.* 41 (6), 273–277. doi:10.4103/0253-7613.59927
- Shibeshi, W., Makonnen, E., Zerihun, L., and Debella (2006). Effect of Achyranthes aspera L. on fetal abortion, uterine and pituitary weights, serum lipids and hormones. *Afr. Health Sci.* 6 (2), 108–112. doi:10.5555/afhs.2006.6.2.108
- Shrestha, J., Shanbhag, T., Shenoy, S., Amuthan, A., Prabhu, K., Sharma, S., et al. (2010). Antiovarulatory and Abortifacient Effects of Areca Catechu (Betel Nut) in Female Rats. *Indian J. Pharmacol.* 42 (5), 306–311. doi:10.4103/0253-7613.70350
- Shrivastava, S., Dwivedi, S., Dubey, D., and Kapoor, S. (2007). Traditional Herbal Remedies from Madhya Pradesh Used as Oral Contraceptives- A Field Survey. *Int. J. Green Pharm.* 1 (1), 18–22.
- Singh, A. R., Singh, K. P., and Shekhawat, S. (2013). Spermicidal Activity and Antifertility Activity of Ethanolic Extract of Withaniasomnifera in Male Albino Rats. *Int. J. Pharm. Sci. Rev. Res.* 21 (2), 227–232.
- Singh, S. P. (1990b). Effect of Cinnamomum Camphora Leaf Extract on Testicular Function of House Sparrow (*Passer domesticus* L.). *Indian J. Phy Nat. Sci.* 10, 22–25.
- Singh, S. P. (1985). Regulation of Fertility in Male through an Indigenous Plant *Semecarpus Anacardium* Linn. *J. Res. Edu Indian Med.* 4 (384), 9–20.
- Singh, S. P. (1990a). Fertility Control of Female through Sesbania Sesbanseeds. *J. Res. Educ. Indian Med.* 9 (4), 227–232. doi:10.1071/sr9900227
- Sinha, K. C., Rair, S. S., Bardhan, J., Thomas, P., Jain, A. K., and Jain, R. K. (1984). Anti-implantation Effect of Neem Oil. *Indian J. Med. Res.* 80, 708–710.
- Sinha, R. (1990). Post-testicular Antifertility Effects of Abrusprecatoriusseed Extract in Albino Rats. *J. Ethnopharmacol* 28 (2), 13–81. doi:10.1016/0378-8741(90)90027-q
- Sinha, R. K., and Nathawat, G. S. (1989). Anti-fertility Effects of Some Plants Used by the Street Herbal Vendors for Birth Control. *Ancient Sci. Life* (2), 66–68.
- Soni, P., Siddiqui, A. A., Dwivedi, J., and Soni, V. (2013). Antiovarulatory and Estrogenic Activity of Stem of Musa Paradisiaca in Female Albino Rats. *J. Appl. Pharm. Sci.* 3 (08), 102–106. doi:10.5667/tang.2013.0011
- Soni, P. K., Luhadia, G., Sharma, D. K., and Mali, P. C. (2015). Antifertility Activates of Traditional Medicinal Plants in Male with Emphasis on Their Mode Action: a Review. *J. Glob. Biosci.* 4, 1165–1179.
- Srivastava, A., Srivastava, V. K., and Singh, G. (2017). Study of Teratogenic Effects of Chitrak (Plumbago Zeylanica) an Ayurvedic Drug on Developing Mice Embryo. *J. Adv. Res. Ayur. Yoga Unani Sidd. Homeo.* 4 (1&2), 46–50. doi:10.24321/2394.6547.201711
- Sur, T. K., Pandit, S., and Pramani, K. T. (1999). Antispermato-genic Activity of Leaves of Aegle Marmelos Corr. In Albino Rats: A Preliminary Report. *Biomedicine* 19, 199–202.
- Sur, T. K., Pandit, S., Pramanik, T., and Bhattacharyya, D. (2002). Effect of Aegle Marmelos Leaf on Rat Sperm motility: an Invitro Study. *Indian J. Pharmacol.* 34, 276–277.
- Sushma, Y., Kulkarni, G., and Singh, S. (2016). Antifertility Activity of Aqueous and Ethanolic Extracts of Semecarpus Anacardium Fruit in Female Albino Rats. *Int. J. Pharm. Sci. Res.* 7 (3), 1235–1239.
- Sushrut (2002). *Susrutsamhita with Nibandhasangraha of Dalhans [Ayurved Classical Text]*. 7th Edition. Varanasi, India: Chaukhambha Orientalia.
- Tamboli, S. A., and Konadawar, M. S. (2013). Anti-Implantation Activity of the Leaf Extract of Ailanthus ExcelsaRoxb. *Int. J. Pharm. Pharm. Sci.* 5 (Suppl. 4), 128–129.
- Taprial, S., Kashyap, D., Mehta, V., Kumar, S., and Kumar, D. (2013). Antifertility effect of hydroalcoholic leaves extract of Michelia champaca L.: an ethno medicine used by Bhatra women in Chhattisgarh state of India. *J. Ethnopharmacol.* 147 (3), 671–675. doi:10.1016/j.jep.2013.03.003
- Tewari, P. V. (1974). Preliminary Clinical Trial on Flowers of Hibiscus Rosasinensis as an Oral Contraceptive. *J. Res. Indian Med. Yoga Homeopath* 9, 96–98.
- Tewari, P. V., Sharma, S. K., and Basu, K. (1976). Clinical Trial of an Indigenous Drug as an Oral Contraceptive. *J. Natl. Integrated Med. Assoc.* 18, 117–118.
- Tewari, P. V., and Chaturvedi, C. (1981). Method of Population Control in Ayurvedic Classics. *Ancient Sci. Life*, 1, 72–79.
- Tewari, P. V., Mapa, H. C., and Chaturvedi, C. (1971). *J. Res. Indian Med.* 6 (2), 112.
- Thakare, V. N., Kothavade, P. S., Dhote, V. V., and Deshpande, A. D. (2009). Antifertility Activity of Ethanolic Extract of Allium cepa Linn in Rats. *Int. J. Pharm Tech Res.* 1 (1), 73–78.
- Tripathi, I. (1969). *Gadanigraha of Sodhal with 'Vidyotini' Hindi Commentary*. 1st Edition. Verse- Uttarardha; Pradaradhikar: Varanasi. Chaukhambha Sanskrit series, 60–62.
- Turner, D. C. (1971). *General Endocrinology*. 4th ed. Tokyo: WB Saunders Company, Topan Company Ltd.
- Udoh, P., and Ekpenyong, J. (2001). Effect of *Mucuna Urens*(horse Eyes Bean) on the Gonads of Male guinea Pigs. *Phytother Res.* 15 (2), 99–102. doi:10.1002/ptr.699
- Vagbhatt (2000). *Ashtanghridaya with Sarvagasundara of Arundatta and Hemadri [Ayurved Classical Text]*. Varanasi: Krishnadas Academy. Verse-Sharira 1/8.
- Vanithakumari, G., Manonayagi, S., Padma, S., and Malini, T. (1989). Antifertility Effect of Bambusaarundinaceae Shoot Extracts in Male Rats. *J. Ethnopharmacology* 25, 173–180. doi:10.1016/0378-8741(89)90019-6
- Vasudeva, N., and Sharma, S. K. (2008). Post-coital Antifertility Activity of Hibiscus Rosa-Sinensis Linn. Roots. *Adv. Access Publ.* 5 (1), 91–94. doi:10.1093/ecam/nem003
- Vasudeva, N., and Sharma, S. K. (2006). Post-Coital Antifertility Activity of *Achyranthes aspera* linn. Root. *J. Ethnopharmacology* 107 (2), 179–181. doi:10.1016/j.jep.2006.03.009
- Verma, S., and Yadav, A. (2021). Rising trends towards the development of oral herbal male contraceptive: an insight review. *J. Pharm. Sci.* 7, 23. doi:10.1186/s43094-020-00154-7
- Vyas, V., and Purohit, A. (2018). Contraceptive Effect O F Neem Seed Oil and its Active Fractions on Female Albino Rabbits. *Asian J. Pharm. Clin. Res.* 11 (12), 421–424. doi:10.22159/ajpcr.2018.v11i12.28188
- Wati, B. T., and Verute, A. T. (1988). Butea Monosperma Leaf Extract Induced Alterations in the Testicular Function of Albino Rats: A Histological and Biochemical studyInternational Symposium on Recent Advances in Male Reproduction. *Hyderabad* 12 (14), 16.
- Williamson, E. M., Okpako, D. T., and Evans, F. J. (1996). *Pharmacological Methods in Phytotherapy Research: Selection Preparation and Pharmacological Evaluation of Plant Material*. London: John Wiley & Sons, 191–212.
- World Health Organization (2020). Contraceptives. Available at: <https://www.who.int/news-room/fact-sheets/detail/family-planning-contraception> (Accessed November 8, 2020).
- World Population Clock (2021). World Population Clock: 7.9 Billion People. Worldometer. Available at: <https://www.worldometers.info> (Accessed March 28, 2021).

Yadav, R., and Jain, G. C. (2009). Antifertility Effect of Aqueous Extract of Seeds of Cassia Fistula in Female Rats. *Adv. Contraception* 15, 293–301. doi:10.1023/a:1006784224191

Yang, Z. M., Le, S. P., Chan, D. B., and Harper, M. J. (1994). Temporal and Spatial Expression of Leukemia Inhibitory Factor in Rabbit Uterus during Early Pregnancy. *Mol. Reprod. Develop.* 38 (2), 148–152. doi:10.1002/mrd.1080380205

Conflict of Interest: Author NB is Owner / Director of the company CRIA Consultants Pvt. Ltd., Mumbai (India).

The remaining author declares that the research was conducted in the absence of any commercial or financial relationships that could be construed as a potential conflict of interest.

Copyright © 2021 Bhatt and Deshpande. This is an open-access article distributed under the terms of the Creative Commons Attribution License (CC BY). The use, distribution or reproduction in other forums is permitted, provided the original author(s) and the copyright owner(s) are credited and that the original publication in this journal is cited, in accordance with accepted academic practice. No use, distribution or reproduction is permitted which does not comply with these terms.



Yeast-Host Interactions: *Anadenanthera colubrina* Modulates Virulence Factors of *C. albicans* and Inflammatory Response *In Vitro*

Carolina Medeiros de Almeida Maia^{1,2}, Silvana Pasetto²,
Cassiano Francisco Weege Nonaka¹, Edja Maria Melo de Brito Costa^{1*} and
Ramiro Mendonça Murata^{2*}

¹Department of Dentistry, Postgraduate Program in Dentistry, State University of Paraíba, Campina Grande, Brazil, ²Department of Foundational Sciences, School of Dental Medicine, East Carolina University, Greenville, NC, United States

OPEN ACCESS

Edited by:

Gudrun S. Ulrich-Merzenich,
University Hospital Bonn, Germany

Reviewed by:

Rodnei Dennis Rossoni,
Sao Paulo State University, Brazil
Melyssa Negri,
State University of Maringá, Brazil

*Correspondence:

Ramiro Mendonça Murata
muratar16@ecu.edu
Edja Maria Melo de Brito Costa
edjacosta@gmail.com

Specialty section:

This article was submitted to
Ethnopharmacology,
a section of the journal
Frontiers in Pharmacology

Received: 16 November 2020

Accepted: 25 May 2021

Published: 08 June 2021

Citation:

Maia CMdeA, Pasetto S,
Nonaka CFW, Costa EMMdeB and
Murata RM (2021) Yeast-Host
Interactions: *Anadenanthera colubrina*
Modulates Virulence Factors of *C.*
albicans and Inflammatory Response
In Vitro.
Front. Pharmacol. 12:629778.
doi: 10.3389/fphar.2021.629778

Oral candidiasis is one of the most common fungal infections in humans. Its incidence has increased widely, as well as the antifungal resistance, demanding for the search for novel antifungal therapeutic agents. *Anadenanthera colubrina* (Vell.) Brenan is a plant species that has been proven to possess pharmacological effects, including antifungal and anti-inflammatory activities. This study evaluated *in vitro* the effects of standardized *A. colubrina* extract on virulence factors of *Candida albicans* and its regulation on immune response through *C. albicans*-host interaction. Antifungal activity was evaluated by Broth Microdilution Method against reference *Candida* strains (*C. albicans*, *C. glabrata*, *C. tropicalis*; *C. dubliniensis*). Anti-biofilm effect was performed on *C. albicans* mature biofilm and quantified by CFU/mL/g of biofilm dry weight. Proteolytic enzymatic activities of proteinase and phospholipase were assessed by Azocasein and Phosphatidylcholine assays, respectively. Cytotoxicity effect was determined by Cell Titer Blue Viability Assay on Human Gingival Fibroblasts. Co-cultured model was used to analyze *C. albicans* coexisting with HGF by Scanning Electron Microscopy and fluorescence microscopies; gene expression was assessed by RT-PCR of *C. albicans* enzymes (SAP-1, PLB-1) and of host inflammatory cytokines (IL-6, IL-8, IL-1 β , IL-10). Cytokines secretion was analysed by Luminex. The extract presented antifungal effect with MIC < 15.62 μ g/ml against *Candida* strains. Biofilm and proteolytic activity were significant reduced at 312.4 μ g/ml (20 \times 15.62 μ g/ml) extract concentration. Cell viability was maintained higher than 70% in concentrations up to 250 μ g/ml (LD₅₀ = 423.3 μ g/ml). Co-culture microscopies demonstrated a substantial decreased in *C. albicans* growth and minimal toxicity against host cells. Gene expressions of SAP-1/PLB-1 were significantly down-regulated and host immune response was modulated by a significant decreased on IL-6 and IL-8 cytokines secretion. *A. colubrina* had antifungal activity on *Candida* strains, antibiofilm, and anti-proteolytic enzyme effects against *C. albicans*. Presented low cytotoxicity to the host cells and modulatory effects on the host immune response.

Keywords: phytotherapy, antifungal agents, oral candidiasis, *Candida albicans*, biofilm, virulence factors, immune response

INTRODUCTION

Oral candidiasis is one of the most common fungal infections in humans (Hertel et al., 2016; Rosa-García et al., 2020) and is caused by yeasts from the genus *Candida* (Williams and Lewis, 2011), a polymorphic fungus and a commensal microorganism that colonizes the human oral cavity in healthy people (Nikou et al., 2019). However, under circumstances where host immunity is impaired, *Candida* spp. can switch its harmless phenotype to a pathogenic form capable of breaching mucosal barriers (Dantas et al., 2016), causing from superficial mucosal infection to deep seated invasive and life-threatening disseminated disease (Lewis and Williams, 2017; Nikou et al., 2019), which is related to a high mortality rate (58–81%) (Vaezi et al., 2017).

Candida albicans is the species most often associated to oral candidiasis (Prieto et al., 2016; Pappas et al., 2018), accounting for up to 95% of the cases (Vila et al., 2020). Its overgrowth and invasion of superficial tissues is dependent on the host's defenses and the virulence factors of the fungus (Tooyama et al., 2015; Millsop and Faze, 2016; Hellstein and Marek, 2019), such as, adherence to oral epithelial or medical devices surfaces; biofilm formation; destruction of host tissue through secretion of proteolytic enzymes; evasion of host defenses invasion mechanisms and development of drug resistance (Höfs et al., 2016; Vila et al., 2020).

Considering the continuing rise of resistant *Candida* spp. strains and the limited number of antifungal agents, novel therapeutic strategies have been directed toward the identification of bioactive compounds that target virulence factors and pathogenic mechanisms to prevent *C. albicans* transition from harmless commensal to pathogen (Francisconi et al., 2020; Vila et al., 2020).

In this regard, natural products from plants are considered a potential source for the development of new antifungal therapies. Between the years of 1940 and 2014, 40% of all molecules accepted by FDA (US Food and Drug Administration) were natural products (Newman and Cragg, 2016). *Anadenanthera colubrina* (Vell.) Brenan, popularly known as Angico, is a plant species that can be found in Brazil, from the Northeastern to the Southeastern regions. It is a woody species typical of the Caatinga Brazilian biome (Silva et al., 2019) and its use by the traditional communities of Brazilian semiarid as a medicinal plant is common, which includes the treatment of inflammation in general (Araújo et al., 2014; Araújo et al., 2015). Recent researches have shown that *A. colubrina* has promising therapeutic properties, such as antifungal (Lima et al., 2014; Silva et al., 2019), anti-proliferative (Lima et al., 2014), anti-inflammatory (Guarneire et al., 2019; Cardoso-Junior et al., 2020), antioxidant (Araújo et al., 2019; Cardoso-Junior et al., 2020), and anti-HIV (Maia et al., 2021).

Some studies regarding the antifungal effects of *A. colubrina* have suggested an inhibitory activity among *Candida* species, mainly on *C. albicans* biofilms. (Lima et al., 2014; Silva et al., 2019). Lima et al. (2014) demonstrated *in vitro* the strong antifungal activity of *A. colubrina* extract against *C. albicans* in planktonic culture and also its potential in inhibit the formation of *C. albicans* biofilm. Therefore, *A. colubrina* extract toxicity and

therapeutic action were evaluated *in vivo* on *Galleria mellonella* model, having not affected the viability of the larvae at doses below 100 mg/kg and high potential for the treatment of *C. albicans* infection (Silva et al., 2019). These recent findings suggest that *A. colubrina* extract is a strong *Candidate* for development of a new agent for the treatment of oral candidiasis.

Despite this therapeutic potential, there is little information available about how this plant species can regulate the expression of virulence factors of *Candida* co-cultured with humans cells and the host immune response during the fungal infection as well. Therefore, the present study aimed to evaluate *in vitro* the modulatory effects of *A. colubrina* extract on major virulence factors related to the pathogenicity of *C. albicans* infection through the interaction between host and pathogen.

MATERIAL AND METHODS

Plant Material and Standardized Extraction Procedures

The plant material was collected during the month of September in the semi-arid region of Paraíba state, Brazil (7° 22' 25" S, 35° 59' 32" W). Botanical specimens of *Anadenanthera colubrina* (Vell.) Brenan were deposited in the Manuel de Arruda Câmara Herbarium (ACAM) at the State University of Paraíba (UEPB), Campus I, Campina Grande, Paraíba, Brazil, under no 1936/ACAM. This research was conducted under authorization number SisGen A289DF4. A hydroethanolic standardized extract was obtained according to the method described by Carvalho et al. (2011). Briefly, hydroethanolic extract (80%, v/v) of the plant bark was obtained by maceration for 48 h using the proportion of 10 mg of the plant for each 25 ml of 80% ethyl alcohol. Three filtrations of the material were performed, followed by vacuum concentration (Tecnal TE-211, Piracicaba, SP) and lyophilization (Martin Christ 1-2 LDplus, Germany). An extraction yield of 31.7% was obtained.

Considering the same standardized extract (same batch of plant material and same extraction process) used in this research and used by Lima et al. (2014), Rocha et al. (2017), Lima et al. (2018—*data not published*) and Silva et al. (2019), the presence of polyphenol, tannins and flavonoids, compounds with straight relationship with *A. colubrina* extract pharmacological activity, were also recently monitored by gas chromatograph (GC) coupled to mass spectrometer (MS) with electron impact ionization (EI) (model GCMS-QP2010 Ultra, Shimadzu) according to the method described by Maia et al. (2021), using the same standardized material.

Susceptibility Test

The antimicrobial activity of *A. colubrina* extract was assessed by Broth Microdilution Method against the following *Candida* spp: *C. albicans* ATCC® 90028, *C. albicans* ATCC® MYA-2876, *C. glabrata* ATCC® MYA-275, *C. tropicalis* ATCC® MYA-750; *C. dubliniensis* ATCC® MYA-646, with the determination of the minimum inhibitory concentration (MIC) and minimum fungicidal concentration (MFC), according to CLSI guidelines (M27-A2) (Clinical and Laboratory Standards Institute (CLSI),

2002). The assay was performed in 96 well-plates (Greiner Bio-One North America, Inc. Monroe, NC) containing 100 μ L/well of RPMI-1640 culture medium (Lonza Bioscience, Walkersville, MD). One hundred microliters of the extract were added to the initial well (8,000 μ g/ml), followed by serial microdilution, obtaining concentrations between 2,000 and 15.62 μ g/ml. Inoculum concentration was standardized using a spectrophotometer (SpectraMax M3, Molecular Devices, Sunnyvale, CA), by first measuring the absorbance in the range of 0.08–0.1 at 625 nm, which yielded a yeast stock solution equivalent to 5×10^6 CFU/mL that was then diluted in RPMI-1640 medium to a final concentration of 5×10^3 CFU/mL. Next, 100 μ L of yeast suspension was added to each well, resulting in a final concentration of 2.5×10^3 CFU/mL. The plates were incubated for 24 h at 37°C in 5% CO₂ (VWR Symphony 5.3 A, Radnor, PA). Fluconazole (512 μ g/ml) (Alfa Aesar, Tewksbury, MA) was used as positive control. The vehicle control used was Dimethyl Sulfoxide 1% (DMSO, BDH Solvents, Dawsonville, GA). The MIC was defined as the lowest concentration of the sample capable of inhibiting visible microbial growth, as confirmed by the change in the color of the RPMI-1640 medium. For the determination of the MFC, an aliquot of 10 μ L from each well with concentrations equal to or higher than the MIC was sub-cultivated in Sabouraud Dextrose Agar medium (BD Difco, Franklin Lakes, NJ) and incubated at 37°C, in 5% CO₂, for 48 h. The MFC was defined as the smallest concentration that inhibited visible growth on the agar plates. All of the assays were performed in triplicates and repeated at least three different times for reproducibility (Seleem et al., 2016b).

Biofilm Assay

An inoculum of 1×10^6 CFU/mL of *C. albicans* (ATCC[®] MYA-2876) was grown for 24 h in a sterile 24-well plate (Greiner Bio-One North America, Inc. Monroe, NC, United States) using Yeast Nitrogen Base Medium (YNB, Sigma Aldrich, San Luis, MO) with 50 mM of glucose (VWR Life Science, Radnor, PA) for 24 h at 37°C in 5% CO₂ to establish initial biofilm growth. Total volume of 1 ml of inoculum was pipetted in each well. After 24 h of incubation, the biofilms were treated once daily with 100 μ L of *A. colubrina* extract at concentrations equivalents to 156.2 μ g/ml (10×15.62 μ g/ml) and 312.4 μ g/ml (20×15.62 μ g/ml), which remained incubated with the biofilm suspended in medium overnight. The vehicle control used was 1% DMSO, while positive control was Fluconazole (10xMIC). Before each treatment, biofilms were washed with Phosphate Buffer Solution (PBS, Lonza Bioscience, Walkersville, MD) and replenished with 900 μ L of fresh YNB medium in addition to 100 μ L of the corresponding treatment, yielding a total volume of 1 ml in each well. After 72 h of treatments, adhered biofilms were collected by scraping the bottom of each well plate and suspending in PBS, which was then centrifuged at 10,000 rpm for 5 min. Biomass (dry weight) of each biofilm sample was obtained by discarding the supernatant and placing the samples in a speed vacuum to dry for 40 min. Colony formation unit (CFU) was determined by submitting the biofilm suspension to serial dilutions (10^{-1} , 10^{-2} , 10^{-3} , 10^{-4}) and plating 10 μ L of these dilutions on Sabouraud Dextrose Agar

plates, which were incubated at 37°C in 5% CO₂. After 24 h of incubation, the number of *C. albicans* colonies was counted and the data was normalized based on the CFU/ml/dry weight of biofilm sample (Santana et al., 2013; Seleem et al., 2016a; Seleem et al., 2016b; Chen et al., 2018).

Proteinase and Phospholipase Enzyme Secretion Assay

Proteinase and phospholipase enzyme secretion assays were conducted as previously performed by Santana et al. (2013), Chen et al. (2018). Biofilms of *C. albicans* were grown for 24 h in YNB Medium with 50 mM of glucose at 37°C in 5% CO₂ and treated with *A. colubrina* extract (156.2 μ g/ml– 10×15.62 μ g/ml and 312.4 μ g/ml– 20×15.62 μ g/ml). Trypsin (Gibco, Invitrogen) was used as standard. The vehicle control used was 1% DMSO. After 72 h of biofilm maturation, the enzyme secretion assays were performed on biofilms suspended in PBS, which were sonicated for 15 s at 20% amplitude with pulses at 5 s and 10 s intervals (FB120; Fischer Scientific, Pittsburgh, PA, United States). The proteinase enzyme activity was determined by mixing the supernatant of the biofilm solution with 1% azocasein (Sigma Aldrich, San Luis, MO) at 9:1 (v/v) for 1 h at 37°C in 5% CO₂. Then, 500 μ L of 10% trichloroacetic acid (VWR) was added to stop the reaction. The solution was centrifuged for 5 min at 10,000 rpm and 500 μ L of the supernatant was combined with 500 μ L of 0.5 M NaOH (Macron Fine Chemicals, Avantor VWR Life Science, Radnor, PA), which was incubated for 15 min at 37°C in 5% CO₂. Absorbance was read in a spectrophotometer at 440 nm (Pande et al., 2006; Gonçalves et al., 2012; Santana et al., 2013; Chen et al., 2018). The phospholipase enzyme activity was determined by mixing the supernatant of the biofilm solution (pH corrected to 7.5) with phosphatidylcholine substrate (Sigma Aldrich, San Luis, MO) at 9:1 (v/v) for 1 h at 37°C in 5% CO₂ and reading the absorbance in a spectrophotometer at 630 nm (Taniguchi et al., 2009). The rates of absorbance shifts (Δ OD) for the repetitions were adjusted by the blank. One enzyme unity was arbitrarily established as the absorbance shift, by minute of reaction, by biomass, multiplied by one thousand ($U = \Delta$ ODnm \times min $^{-1} \times 1,000$). The specific enzyme activity was defined as the amount of enzyme that elicited an increase of 0.001 units of absorbance/minute of digestion by biofilm dry weight (g) (Taniguchi et al., 2009; Santana et al., 2013; Chen et al., 2018).

Cytotoxicity Assay

The *in vitro* cytotoxic effect of *A. colubrina* extract was performed on oral fibroblasts cells (HGF-1 ATCC[®] CRL-2014) and determined by a resazurin fluorometric method (Cell Titer Blue Viability Assay, Promega Corp, Madison, WI). Oral fibroblast cells were cultured in Dulbecco's modified Eagle's medium (DMEM, Lonza, Walkersville, MD) with 10% fetal bovine serum (FBS Gibco, Invitrogen, Waltham, MA) at 37°C in 5% CO₂. Fibroblast cells (1×10^5 cells/mL) were first seeded in each well of a 24-well plate in DMEM with 10% FBS, and the plates were incubated for 24 h at 37°C in 5% CO₂. The *A. colubrina* extract was diluted in DMSO 1%, with final concentration inside the wells of 0.1%, and then added to the

cultured cells wells (2,500–0.25 µg/ml). The plates were incubated for 24 h at 37°C in 5% CO₂. Resazurin (30 µL) was added to each well, and the cells were incubated for 3 h. The fluorescence of the supernatant was read in a microplate reader with excitation of 555 nm, emission of 585 and 570 nm cut off (O'Brien et al., 2000).

Co-Culture Model Fluorescence Microscopy

A co-culture model was conducted by culturing fibroblast cells and *C. albicans* together in a sterile 24-well plate, as adapted by Wong et al. (2014), Oliveira Silva et al. (2018). First, oral fibroblast cells were seeded in DMEM with 10% FBS at 37°C in 5% CO₂ for 24 h. The medium was then replaced with an inoculum of 5×10^3 to 2.5×10^3 CFU/mL *C. albicans* (MYA 2876) grown in DMEM without FBS. Fibroblast cells and *C. albicans* were treated with 33.28 µg/ml of *A. colubrina* extract. The plate was then incubated at 37°C in 5% CO₂ for 24 h. The vehicle control tested was 0.1% DMSO and the positive control was Fluconazole (10 µg/ml). The distribution of dead and live fibroblast cells was examined using the viability/cytotoxicity Live/Dead Assay Kit for mammalian cell type (Molecular Devices, Sunnyvale, CA), which contains a mixture of Calcein AM and EthDIII (Ethidium Homodimer III). Calcofluor white (Sigma Aldrich, San Luis, MO) was used to stain *C. albicans*. Fluorescent images of the double staining were captured using fluorescence microscopy (Keyence All-in-One BZ-X810 Fluorescence Microscope, Itasca, IL).

Co-Culture Model Scanning Electron Microscopy

Co-culture model was conducted by culturing fibroblast cells and *C. albicans* together in a sterile petri dish (Greiner Bio-One North America, Inc. Monroe, NC), following the same protocol above described for co-culture plating and treatments. After the period of incubation, the samples were washed twice with PBS and fixed in glutaraldehyde 3% (v/v) at room temperature for 12 h. The dehydrated cells were submitted to sequential baths of ethanol at concentrations of 50, 70, 90% and absolute ethanol twice, then coated with gold/palladium alloy in a Metalizer (Desk V Denton Vacuum, Moorestown, NJ) and observed using a Scanning Electron Microscope (Zeiss EVO LS10 SEM, Oberkochen, Alemanha) (Bersan et al., 2014; Freires et al., 2014).

Co-Culture Model Quantitative Real-Time PCR

Following the same protocol above described for co-culture plating, RNA was isolated from fibroblast cells and *C. albicans* after 8 h of treatment with *A. colubrina* extract. The fibroblast cells RNA and *C. albicans* RNA were isolated and purified using RNeasy® Mini Kit (Qiagen, Hilden, Germany) and RiboPure™-Yeast Kit (Invitrogen, ThermoFischer Scientific, Rockford, IL) respectively. SpectraDrop Micro-Volume Starter Kit (Molecular Devices, Sunnyvale, CA) was used to quantify the total RNA extracted. Real-time PCR was conducted by using QuantiFast®

SYBR® Green RT-PCR One Step Kit (Qiagen, Hilden, Germany). The *C. albicans* primers for the genes: *Secreted Aspartyl Proteinases-1* (SAP-1), *Phospholipase B-1* (PLB-1), and *ACT-1* (*housekeeping*) at 10 µM were used. ACT-1 was the gene used to normalize SAP-1 and PLB-1 genes expression. The following host inflammatory cytokines genes were selected: IL-6 (Qiagen Gene ID#: 3570), IL-8 (Qiagen Gene ID#: 3576); IL-10 (Qiagen Gene ID#: 3587); IL-1β (Qiagen Gene ID#: 3553) and GAPDH (*housekeeping*) (Qiagen Gene ID#: 2597). All data from cytokines genes expression were normalized using the housekeeping gene GAPDH. PCR amplification was performed by using 25 µL reaction mix per well in 0.2 ml 8-Strip PCR tubes. The reactions were conducted in thermocycler (QuantStudio 3 Real Time PCR System, ThermoFischer Scientific, Rockford, IL) at 50°C for 10 min (Reverse Transcription Step); 95°C for 5 min (PCR Initial Activation Step); followed by 40 cycles of 10 s at 95°C (Denaturation Step) and 30 s at 60°C (Annealing/Extension Step). Analysis of relative gene expression was achieved according to the ΔΔCt method (Seleem et al., 2016a; Seleem et al., 2016b; Chen et al., 2018).

Host Inflammatory Cytokines Analysis Using Luminex

As previously described, co-culture models were performed using fibroblasts cells, *C. albicans* (MYA2876), and the tested groups of *A. colubrina* extract (33.28 µg/ml), positive control (Fluconazole 10 µg/ml) and 0.1% DMSO (vehicle control). After 8 h of incubation, the supernatants of the co-culture were collected, centrifuged for 10 min at 1,000 rpm, and assayed immediately using Human Magnetic Premixed Multi-Analyte Luminex Assay Kit (R&D Systems, Mienneapolis, MN) for secretion of pro-inflammatory cytokines IL-6, IL-8, IL-1β, and anti-inflammatory IL-10. Culture supernatants and cytokine capture bead cocktails were incubated during the overnight period. The samples were then incubated for 1 h with biotin-labeled antibody and for 30 min in a dilution of streptavidin-PE. Data were obtained by Luminex 200 Milliplex System and analyzed with Milliplex Analyst software (Allin et al., 2016).

Statistical Analysis

Data were expressed as the mean ± SEM using one-way analysis of variance (ANOVA) and Dunnett's multiple comparison tests in relation to the vehicle, using GraphPad Prism software (version 8.02). Results were considered significant if *p*-values were less than 0.05.

RESULTS

Phytochemical Analysis

Standardization of plant inputs for the pharmaceuticals industry plays an important role in product outcomes. The quality of the botanical material, as well as the adequate processing of the fresh material, including drying, transportation, storage, and the use of appropriate and reproducible extraction techniques have a straight outcome on health benefits and economic issues. Previous studies were conducted to determine the best

TABLE 1 | Phytochemical compounds identified in the hydroalcoholic bark extract of *A. colubrina* by GC-MS (Maia et al., 2021).

	Compound	RT	RI	Area (%)
1	2-Piperidinecarboxylic acid, 1TMS	8.404	1,267	0.06
2	Butanedioic acid, 2TMS	9.079	1,319	0.02
3	Glyceric acid, 3TMS	9.380	1,343	0.01
4	Isoeugenol, 1TMS	11.065	1,482	0.03
5	Malic acid, 3TMS	11.248	1,498	0.15
6	Erythritol, 4TMS	11.422	1,513	0.01
7	Erythronic acid, 4TMS	12.151	1,574	0.02
8	4-Hydroxybenzoic acid, 2TMS	12.918	1,636	0.02
9	D-Ribose, 2,3,4,5-tetrakis-O-(trimethylsilyl)-, O-methyloxime	13.285	1,664	0.01
10	Xylitol, 5TMS	14.295	1740	0.90
11	Xylitol, 5TMS	14.370	1745	0.1
12	β-D-Xylopyranose, 4TMS	14.510	1755	0.02
13	D-(+)-Galactopyranose, 5TMS	16.390	1884	0.02
14	D-Glucopyranose, 5TMS	16.930	1920	1.37
15	D-Glucopyranose, 5TMS	17.100	1930	0.04
16	D-Mannitol, 6TMS	17.560	1960	0.18
17	Gallic acid, 4TMS	17.800	1975	0.02
18	Palmitic acid, 1TMS	18.965	2047	0.07
19	Myo-inositol, 6TMS	20.220	2,125	0.27
20	Stearic acid, 1TMS	22.210	2,246	0.02
21	Sucrose, 8TMS	29.378	2,705	48.08
22	Catechin, 5TMS	32.458	2,920	0.52

TABLE 2 | Minimum Inhibitory Concentration (MIC) and Minimum Fungicidal Concentration (MFC) of *A. colubrina* extract against *Candida* strains.

Candida strain	A. colubrina			Fluconazole		
	MIC (μg/ml)	MFC (μg/ml)	MFC/MIC ratio	MIC (μg/ml)	MFC (μg/ml)	MFC/MIC ratio
<i>Candida albicans</i> ATCC [®] 90028	<15.62	>2,000	>4	<1	64–128	>4
<i>Candida albicans</i> ATCC [®] MYA-2876	<15.62	2,000	>4	<1	64–128	>4
<i>Candida glabrata</i> ATCC [®] MYA-275	<15.62	>2,000	>4	8	>128	>4
<i>Candida tropicalis</i> ATCC [®] MYA-750	<15.62	250	>4	4	>128	>4
<i>Candida dubliniensis</i> ATCC [®] MYA-646	<15.62	>2,000	>4	<1	32–64	>4

Note: MFC/MIC <4: fungicidal profile/MFC/MIC >4: fungistatic profile.

conditions for *A. colubrina* extract preparation (Lima et al., 2014; Rocha et al., 2017; Lima et al., 2018—data not published; Maia et al., 2021) The presence of polyphenol content of 53.1% (Lima et al., 2014) and 53.18% (Rocha et al., 2017) gallic acid equivalents; tannins (8.7% catechin equivalents) and flavonoids (0.3% quercetin equivalents) (Lima et al., 2014), compounds with straight relationship with *A. colubrina* extract activity were also recently monitored by GC-MS analysis (Maia et al., 2021). These results, presented in **Table 1**, suggest the maintenance of the same phytochemical profile of the standardized extract.

In Vitro Antifungal Activity

MIC and MFC values for *A. colubrina* extract and for the standard antifungal on *Candida* spp. are illustrated in **Table 2**. For the extract, the MIC were lower than 15.62 μg/ml and the MFC ranged from 250 μg/ml to higher than 2,000 μg/ml, while MIC and MFC of Fluconazole ranged from lower than 1 to 8 μg/ml and from 32 to higher than 128 μg/ml, respectively. The extract demonstrated strong antifungal activity against all *Candida* strains tested, based on the classification proposed by Holetz et al. (2002). According to the parameters stated by

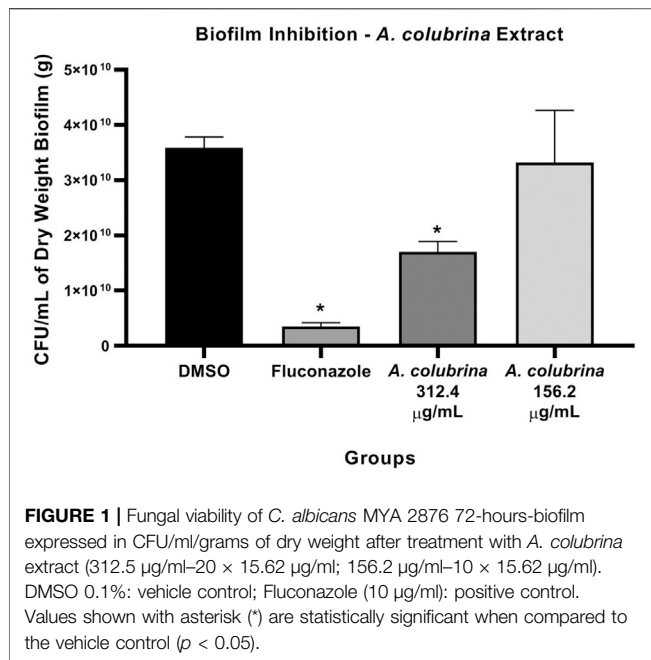
Siddiqui et al. (2013), the ratio MFC/MIC found demonstrated a fungistatic effect of the extract against the species tested.

Biofilm Inhibition

Biofilm assay showed that the treatments with *A. colubrina* extract at 312.4 μg/ml, equivalent to 20 × 15.62 μg/ml for *C. albicans* MYA 2876, and with Fluconazole at 10 μg/ml (10MIC) had significant reduction ($p < 0.05$) in fungal load, expressed as CFU/ml/g of biofilm dry weight, in comparison to the vehicle control group (DMSO 0.1%) (**Figure 1**).

Proteinase and Phospholipase Enzymes Secretion

Phospholipase enzyme activity was significant reduced ($p < 0.05$) after the treatments with *A. colubrina* at 156.2 μg/ml (10 × 15.62 μg/ml) and 312.4 μg/ml (20 × 15.62 μg/ml), when compared to the vehicle (DMSO 0.1%). On the other hand, the proteinase enzyme activity was significant decreased ($p < 0.05$) by the extract only at 312.4 μg/ml (20 × 15.62 μg/ml) in comparison to the vehicle control group (**Figures 2A,B**).



Co-Culture Model of Fibroblasts and *C. albicans* Cytotoxicity

The *A. colubrina* extract presented LD₅₀ of 432.3 µg/ml and a non-toxic profile on gingival fibroblast cell culture up to a concentration of 250 µg/ml, with cell viability remaining higher than 70%, when compared to the vehicle and the cell control groups, as shown in **Figure 3**.

Proteolytic Enzymes Gene Expression

Similar to the profile obtained from the biofilm proteinase and phospholipase assays, the gene expression of SAP-1 and PLB-1 secreted by *C. albicans* MYA 2876, grown as immature biofilm in

a co-culture model, was significantly down-regulated ($p < 0.05$) after the exposure to *A. colubrina* extract at 33.28 µg/ml, when compared to the vehicle control group (**Figures 4A,B**).

Fluorescence Microscopy

In the co-culture model of fibroblasts coexisting with *C. albicans*, samples treated with *A. colubrina* extract showed a considerable decrease in *Candida* growth distribution in comparison with the vehicle control, as indicated by the sparse and less dense accumulation of *C. albicans* (blue color) among viable fibroblast cells (green color) in fluorescent images. In addition, fibroblasts viability was not significantly affected by the treatment with the extract, since there was no significant increase in the dead fibroblast population, indicated by the red fluorescent color, suggesting that *A. colubrina* was effective against *C. albicans* with minimal effects or toxicity on fibroblast cells (**Figures 5A–C**).

Scanning Electron Microscopy

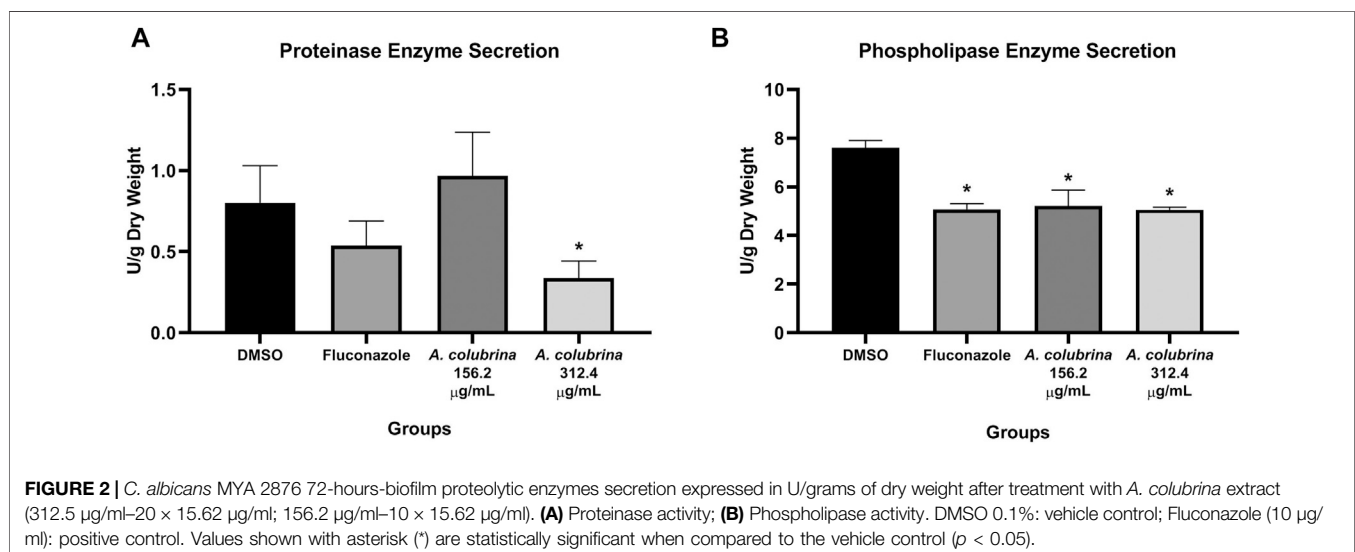
As seen in **Figures 6A–C**, the pattern was similar to the arrangement observed on Fluorescence Microscopy. The SEM showed density reduction of *C. albicans* biofilm, and de-structuring of hyphae morphology, in comparison to the vehicle control group.

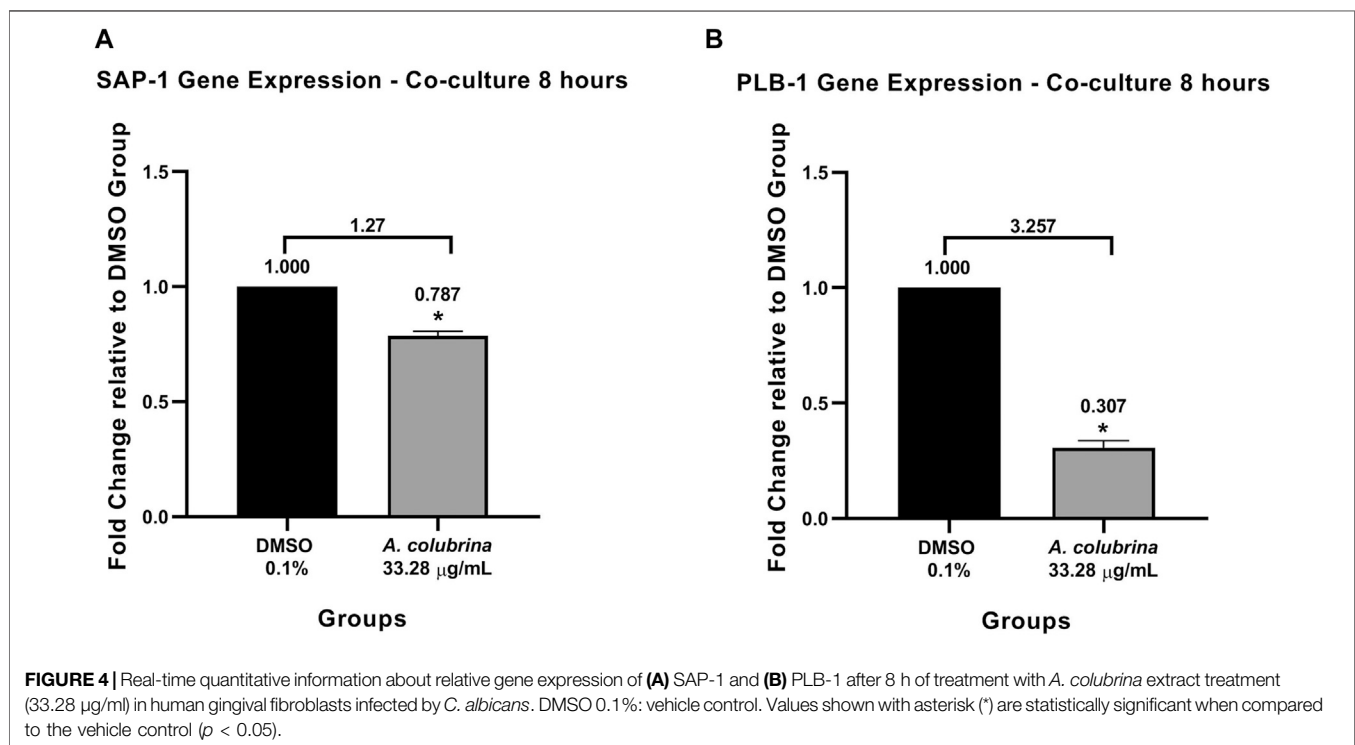
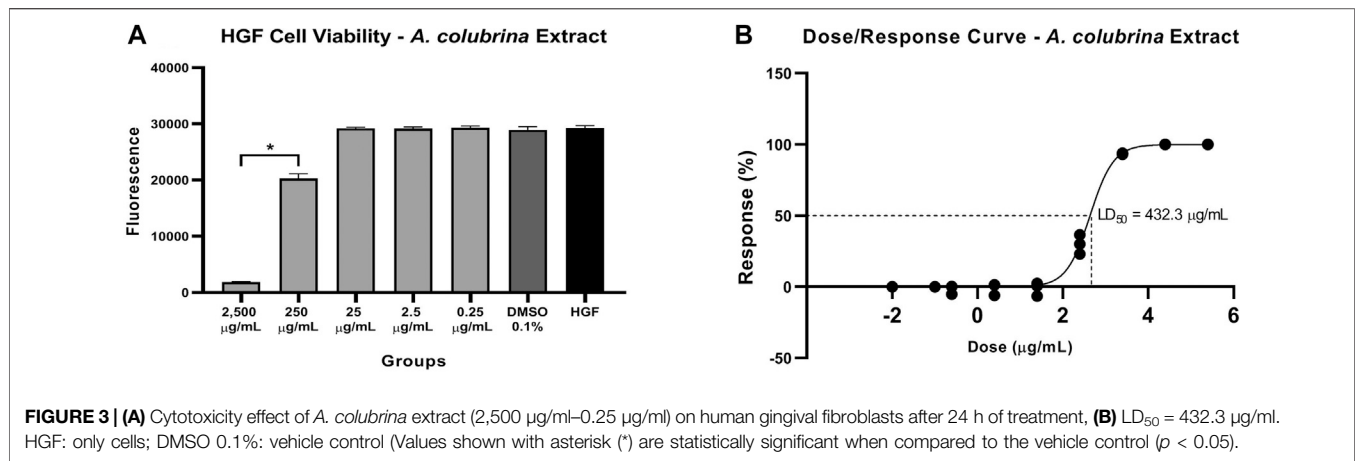
Pro and Anti-inflammatory Cytokines Gene Expression

The *A. colubrina* extract at 33.28 µg/ml presented a modulatory effect on the gene expression of host inflammatory cytokines in a co-culture model. The gene expression of IL-6, IL-1β, and IL-10 were up-regulated after host cells exposure to the extract, while IL-8 gene expression was down-regulated. However, the *A. colubrina* concentration tested showed no statistical difference ($p > 0.05$) on the gene expression of the host cytokines in comparison to the vehicle control group (**Figures 7A–D**).

Pro and Anti-inflammatory Cytokines Secretion

Co-culture supernatants were assessed for expression of pro-inflammatory IL-6, IL-8, and IL-1β as well as anti-inflammatory





cytokine IL-10, following treatments with *A. colubrina* extract (33.28 µg/ml). The extract has resulted in a significant reduction ($p < 0.05$) in the expression of IL-6 and IL-8 when compared to the vehicle control group. On the other hand, there was no detection of modulatory effect on the expression of IL-1β and IL-10 cytokines upon treatment with the extract (**Figure 8**).

DISCUSSION

Recently, the traditional therapeutic use of *A. colubrina* by popular communities in Brazilian culture has encouraged comprehensive studies about its biological properties to be conducted (Damascena et al., 2014; Lima et al., 2014; Barreto et al., 2016; Mota et al., 2017;

Guarneire et al., 2019; Silva et al., 2019; Cardoso-Junior et al., 2020; Maia et al., 2021). In this study, we evaluated the *A. colubrina* extract effects on virulence factor of *C. albicans* and its modulatory effects on host immune response during the fungal infection.

In a previous study, we evaluated the phytochemical composition of the *A. colubrina* extract (Lima et al., 2014), in which was found that the extract presents in its composition a high total polyphenol content (53.18% gallic acid equivalents); tannins (8.77% catechin equivalents) and flavonoids (0.28% quercetin equivalents). This chemical profile seems to support the biological activities evaluated here and discussed ahead, since these classes of compounds are related to a wide range of properties, including antifungal (Ramirez et al., 2013; Kanchanapiboon et al., 2020) and immune response

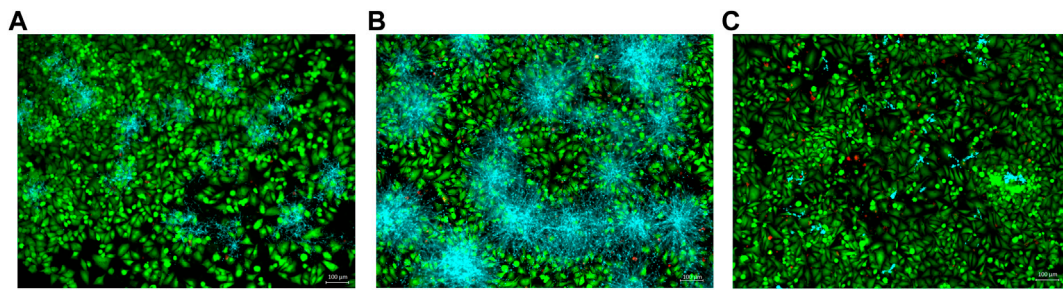


FIGURE 5 | Co-culture fluorescence microscopy after 24 h of treatment with *A. colubrina* extract. **(A)** *A. colubrina* extract (33.28 µg/ml); **(B)** Vehicle control (DMSO 0.1%) and **(C)** Positive control (Fluconazole-10 µg/ml). Scale bar set at 100 µm at 100x magnification power.

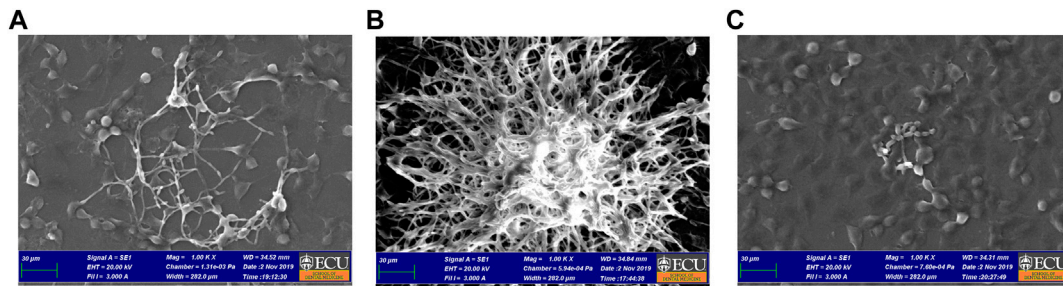


FIGURE 6 | Co-culture SEM after 24 h of treatment with *A. colubrina* extract. **(A)** *A. colubrina* extract (33.28 µg/ml); **(B)** Vehicle control (DMSO 0.1%) and **(C)** positive control (Fluconazole-10 µg/ml). Scale bar set at 30 µm at 1,000x magnification power.

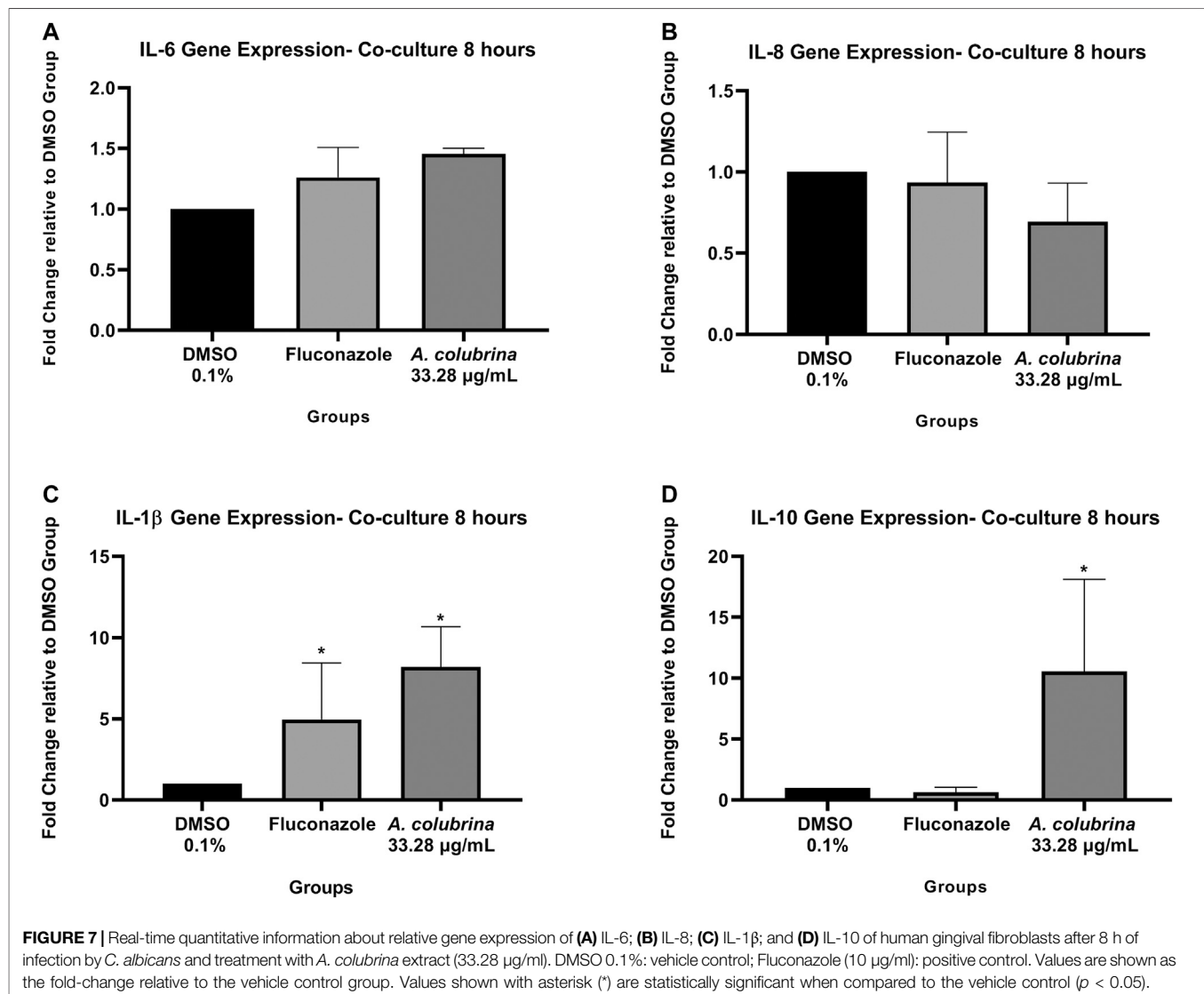
modulatory effects (Fu et al., 2013; Ji et al., 2019; Cardoso Junior et al., 2020).

A. colubrina extract has been reported to present *in vitro* antifungal properties against *Candida* spp. and anti-biofilm properties, mainly on *C. albicans* biofilms (Lima et al., 2014; Silva et al., 2019). The susceptibility assay from our study showed a strong anti-*Candida* effect (Holetz et al., 2002) of *A. colubrina*, exerting a fungistatic profile (Siddiqui et al., 2013) over all the strains tested in planktonic form. *Candida* spp. is not only an important component of oral microbiota, living as a common commensal in immunocompetent individuals (Qin et al., 2016), but also display an important role in shaping the oral microbiome (Xu and Dongari-Bagtzoglou, 2015; Bertolini et al., 2019). Thus, total elimination of yeast from the body is neither desirable nor feasible (Bhattacharya et al., 2020) and its growth inhibition instead its elimination might be positive regarding the infection control, by preventing the rise of pathogenic strains that could lead to more severe infections and antifungal resistance (Ford et al., 2015).

One of the major virulence factors related to *C. albicans* pathogenesis, with significant clinical implications, resides in its ability to form biofilms (Fox et al., 2015; Wall et al., 2019). In oral cavity, hyphae formation and adherence to oral epithelial cells and other abiotic surfaces, such as dentures, leads to the development of this structured community of surface-associated microbial populations embedded in an extracellular matrix (Ghannoum et al., 2015; Hirota et al., 2017). In our study, biofilms treated with *A. colubrina* at 312.4 µg/ml (20×15.62 µg/ml) showed

significant decrease in fungal viability in comparison to the vehicle group, by reducing the CFU/mL/g parameter and altering the biofilm composition and structure integrity. For this biofilm assay model, we used *C. albicans* MYA 2876, considering the MFC result of this strain after the treatment with the extract. In addition, higher concentrations of *A. colubrina*, equivalent to 156.2 µg/ml (10×15.62 µg/ml) and 312.4 µg/ml (20×15.62 µg/ml), were used against *C. albicans* MYA 2876 strain, due to biofilm structured and stable environment, which is tolerant to antifungal agents' diffusion (Tsui et al., 2016).

Once biofilm is established, the expression of *C. albicans* virulence factors increases (Jabra-Rizk, 2011) also giving rise to the release of extracellular hydrolytic enzymes by the biofilms into the local environment, contributing to candidiasis progression (Vila et al., 2020). Most notable of the secreted enzymes frequently implicated in the pathogenicity of *C. albicans* are Secreted Aspartyl Proteinases (SAPs) and Secreted Phospholipases (PLs), which are involved in host tissue invasion, nutrient acquisition, immune evasion, and organ damage (Jabra-Rizk, 2011; Sorgo et al., 2013; Swidergall and Filler, 2017). In order to evaluate the modulating effect of *A. colubrina* extract over this critical virulence factor, we demonstrated that phospholipase enzyme activities was significant reduced using the extract both at 156.2 µg/ml (10×15.62 µg/ml) and 312.4 µg/ml (20×15.62 µg/ml) concentrations, while proteinase activity was decreased only by the highest concentration. These results suggest that both antifungal and anti-biofilm activities of *A.*

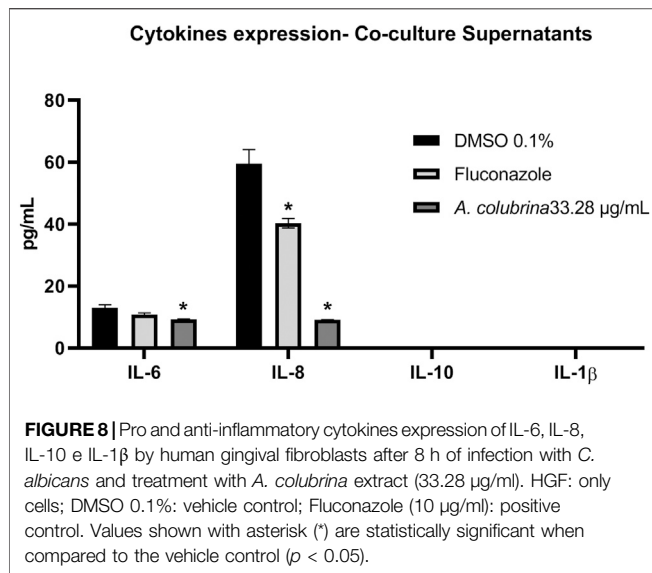


colubrina could involve the inhibition of proteolytic enzymes expression as mechanism of action, considering that during *C. albicans* penetration, these enzymes affect epithelial junctions and enable degradation of cell membrane components, facilitating fungal adhesion and biofilm formation to both oral epithelium or abiotic surfaces (Naglik et al., 2011).

To confirm the results obtained over proteolytic enzyme secretion, we assessed gene expression of SAP-1 (PLB-1) after treatment with *A. colubrina* at 33.28 μg/ml on co-culture models of immature biofilm of *C. albicans* coexisting with fibroblasts. We demonstrated a significant down-regulation on the gene expression of both enzymes in comparison to the vehicle group. These findings are consistent to the enzymatic secretion results, considering that fungal infections usually present a higher gene expression of SAPs and PLs. Proteinases were shown to induce degradation of a variety of host factors, such as E-cadherin, present in epithelial cell junction, increasing the hyphae capacity for colonization and penetration into host tissues, and factors involved in the innate and adaptive immune responses, allowing *C.*

albicans to overcome the host immune defenses (Kumar et al., 2017). On the other hand, phospholipases expression displays an active role in epithelial adherence and tissue invasion, since their catalytic action results in disruption of epithelial cell membrane allowing the penetration of yeasts into host cell cytoplasm (Sanità et al., 2014). Thus, our results suggest that the *A. colubrina* can act by interfering with yeast invasion mechanisms, which could prevent the development of candidiasis.

The cytotoxicity assay was conducted on human gingival fibroblasts ($LD_{50} = 432.3 \mu\text{g/ml}$) in order to verify the therapeutic safety level previously, regarding further *in vivo* and human clinical researches. *A. colubrina* extract maintained the cell viability higher than 70% at concentrations up to 250 μg/ml, representing a relatively low cytotoxic activity. This finding is consistent with results recently reported, which verified the low toxicity of the bark extract of *A. colubrina* on human cells lines, such macrophages (Silva et al., 2019; Cardoso-Junior et al., 2020), keratinocytes and also on tumoral cell strains (Lima et al., 2014). These data corroborate to the results found in this study related to



the low toxic potential effect of this product, shown to be pharmacological safe *in vitro*, by maintaining the cell viability.

Considering the purpose to evaluate the regulating effects of *A. colubrina* extract on *C. albicans*-host interaction, we used a co-culture model to provide comprehensions about the complex system of an immature *C. albicans* biofilm coexisting with fibroblast cells incubated with the tested extract. Recent studies had been conducted in order to evaluate *in vitro* the modulatory effects of natural compounds on the interaction between *C. albicans* and the host using a co-culture model (Seleem et al., 2016a; Seleem et al., 2016b; Chen et al., 2018). Moreover, co-cultures have demonstrated to be an effective tool to stimulate physiological conditions and induce interactions between the cells that triggers important host response pathways (Serrano et al., 2017).

Microscope images obtained from the co-culture model were helpful to evaluate qualitatively the distribution of *C. albicans* and fibroblasts in response to *A. colubrina* and the controls groups. The pattern imaging observed through fluorescence microscopy demonstrated a considerable reduction in *C. albicans* growth without affecting significantly the fibroblasts viability, showing a strong antifungal effect with minimal toxicity. Similarly, the arrangement observed on co-culture SEM imaging in a higher magnification and topographic view, showed significant alterations of the biofilm structure treated with *A. colubrina*. When compared to the vehicle group, it is possible to observe structural alterations, such as notable decrease of the density biofilm and de-structuring of the hyphae morphology in the areas where the extract was able to penetrate. In addition, hyphae decreased, indicating a potential reduction of the biofilm virulence, since the formation of hyphae is associated to tissue invasion.

Host immune defense against *C. albicans* infection requires a wide range of complex molecular mechanisms involving the recognition of fungal cell wall components, the activation of host immune cell signaling cascades and the release of cytokines and chemokines (Brown et al., 2012; Pappas et al., 2018). Some reviews were recently published regarding the

interplay between *C. albicans* and host cells and the immune response during *C. albicans* mucosal infection (Höfs et al., 2016; Naglik et al., 2017; Nikou et al., 2019; Swidergall, 2019; Vila et al., 2020), serving as a guidelines to improve our understanding that relies on this complex interaction.

Therefore, to evaluate the modulatory activity of *A. colubrina* on the host pro-inflammatory response during the *Candida* infection, we employed a transcriptomic approach in conjunction with a proteomic profiling, regarding the analysis for the host cells' gene expression and the release of pro-inflammatory and anti-inflammatory cytokines. We choose a panel of inflammatory markers according to the host immune response mechanisms upon *Candida* recognition, considering the activation of transmembrane Toll Like Receptors (TRLs) (Salvatori et al., 2016; Pappas et al., 2018), which triggers signaling pathways and results at the release of pro-inflammatory cytokines, mainly IL-1α, IL-1β, IL-6, IL-8, and CCL5 (RANTES) by the host cells (Hebecker et al., 2014; Verma et al., 2017; Verma et al., 2018).

The assessment of gene expression demonstrated that *A. colubrina* affects the expression of host inflammatory cytokines by down-regulating IL-8 gene expression and up-regulating IL-6, IL-1β, and IL-10 gene expression. However, there was no statistical difference when compared to vehicle control group. On the other hand, the analysis for expression of host pro-inflammatory and anti-inflammatory cytokines was found significant reduction on the secretion of pro-inflammatory cytokines IL-6 and IL-8, suggesting a modulatory role of *A. colubrina* on the host pro-inflammatory response, which could help to eradicate the fungal infection. A possible reason for the differences between gene expression and production profile of IL-1β, IL-6 and IL-10 is based on a negative feedback mechanism modulating gene expression. Cytokines gene expression may play an important role in regulating the release of them. However, as indicated by the significant reduction in expression of these molecules, there may be a negative feedback inhibition mechanism involving the transcription and translation processes, which regulates their respective gene expression. However, this hypothesis needs to be confirmed through further molecular studies.

As mentioned before, IL-6 and IL-8 play a crucial role in innate immune response. While IL-8 is a known neutrophil recruiter from the circulating blood to the site of infection (Höfs et al., 2016), IL-6 is related to immune response to microorganisms and its expression is directly influenced by the secretion of other pro-inflammatory cytokines, especially IL-1 (Tanaka et al., 2014). Some reports state that *C. albicans* infection is crucial for the modulation and release of IL-1α, IL-6, and IL-8, promoting a higher production of these cytokines (Feller et al., 2014; Figueira et al., 2020; Mo et al., 2020). In this regard, our findings suggest that *A. colubrina* might reduce pro-inflammatory IL-6 and IL-8 cytokines expression during the fungal infection, due its strong antifungal activity, which modulates some putative virulence factors of the *C. albicans*, such as biofilm formation and proteolytic enzyme secretion, reducing the fungus pathogenicity. In addition, the low cytotoxicity of the extract on the host cells does not induce an inflammatory response.

This is the first study reporting the effects of *Anadenanthera colubrina* (Vell.) Brenan on *Candida albicans*-Host interaction. *A. colubrina* extract demonstrated anti-*Candida*, antibiofilm and anti-proteolytic enzyme activities against *C. albicans*, with relatively low cytotoxicity to the host cells. Furthermore, presented modulatory effects on the host immune response, as indicated by its regulation of IL-6 and IL-8 pro-inflammatory cytokines secretion. In this regard, *A. colubrina* could be considered as a potential source for an anti-*Candida* formulation. Further investigations about the regulation activity of *A. colubrina* on others *C. albicans* key virulence factors, including expression of cell surface adhesins, proteolytic degradation of host immune factors and invasion and destruction of host tissue mechanisms, must to be conducted in order to reinforce and establish the extract effects over molecular and signaling pathways in *Candida* pathogenesis.

DATA AVAILABILITY STATEMENT

The raw data supporting the conclusions of this article will be made available by the authors, without undue reservation, to any qualified researcher.

REFERENCES

- Allin, N., Cruz-Almeida, Y., Velsko, I., Vovk, A., Hovemcamp, N., Harrison, P., et al. (2016). Inflammatory Response Influences Treatment of Localized Aggressive Periodontitis. *J. Dent Res.* 95 (6), 635–641. doi:10.1177/0022034516631973
- Araújo, D. R. C., Silva, L. C. N., Silva, A. G., Araújo, J. M., Macêdo, A. J., Correia, M. T. S., et al. (2014). Comparative Analysis of Anti-*Staphylococcus aureus* Action of Leaves and Fruits of *Anadenanthera Colubrina* Var. *Cebil* (Griseb.) Altschul. *Afr. J. Microbiol. Res.* 8, 2690–2696. doi:10.5897/AJMR2014.6901
- Araújo, D. R. C., Silva, T. D., Harand, W., Lima, C. S. A., Ferreira Neto, J. P., Ramos, B. A., et al. (2019). Bioguided Purification of Active Compounds from Leaves of *Anadenanthera Colubrina* Var. *Cebil* (Griseb.) Altschul. *Biomolecules*. 9 (10), 590. doi:10.3390/biom9100590
- Araújo, T. A. S., Castro, V. T. N. A., Solon, L. G. S., Silva, G. A., Almeida, M. G., Costa, J. G. M., et al. (2015). Does Rainfall Affect the Antioxidant Capacity and Production of Phenolic Compounds of an Important Medicinal Species?. *Ind. Crop Prod.* 76, 550–556. doi:10.1016/j.indcrop.2015.07.008
- Barreto, H. M., Coelho, K. M. R. N., Ferreira, J. H. L., dos Santos, B. H. C., de Abreu, A. P. L., Coutinho, H. D. M., et al. (2016). Enhancement of the Antibiotic Activity of Aminoglycosides by Extracts from *Anadenanthera Colubrina* (Vell.) Brenan Var. *Cebil* against Multi-Drug Resistant Bacteria. *Nat. Product. Res.* 30 (11), 1289–1292. doi:10.1080/14786419.2015.1049177
- Bersan, S. M., Galvão, L. C., Góes, V. F., Sartoratto, A., Figueira, G. M., Rehder, V. L., et al. (2014). Action of Essential Oils from Brazilian Native and Exotic Medicinal Species on Oral Biofilms. *BMC Complement. Altern. Med.* 14, 151. doi:10.1186/1472-6882-14-451
- Bertolini, M., Ranjan, A., Thompson, A., Diaz, P. I., Sobue, T., Maas, K., et al. (2019). *Candida Albicans* Induces Mucosal Bacterial Dysbiosis that Promotes Invasive Infection. *Plos Pathog.* 15 (4), e1007717. doi:10.1371/journal.ppat.1007717
- Bhattacharya, S., Sae-Tia, S., and Fries, B. C. (2020). Candidiasis and Mechanisms of Antifungal Resistance. *Antibiotics* 9 (6), 312. doi:10.3390/antibiotics9060312
- Brown, G. D., Denning, D. W., and Levitz, S. M. (2012). Tackling Human Fungal Infections. *Science* 336 (6082), 647. doi:10.1126/science.1222236
- Carvalho, D. D. C., Alves, E., Barbosa Camargos, R., Ferreira Oliveira, D., Soares Scolfaro, J. R., de Carvalho, D. A., et al. (2011). Plant Extracts to Control *Alternaria alternata* in Murcott Tangor Fruits. *Revista Iberoamericana de Micología* 28, 173–178. doi:10.1016/j.riam.2011.05.001

AUTHOR CONTRIBUTION

Conceptualization: RM, EC, CN, and CM. Investigation and Data curation: CM and SP. Formal analysis: RM, EC, CM, and SP. Writing—original draft: CM. Writing—review and editing: CM, SP, CN, EC, and RM.

FUNDING

Research reported in this publication was supported by Brazilian Coordination of Improvement of Higher Education Personnel–CAPES (PDSE–Call 47/2017), by the National Institutes of Health–NIH under award number UNC/CFAR P30AI50410 and funds from ECU, Division of Research, Economic Development, and Engagement.

ACKNOWLEDGMENTS

The authors thank to Brazilian Coordination of Improvement of Higher Education Personnel–CAPES (PDSE–Call 47/2017).

- Chen, E., Benso, B., Seleem, D., Ferreira, L. E. N., Pasetto, S., Pardi, V., et al. (2018). Fungal-Host Interaction: Curcumin Modulates Proteolytic Enzyme Activity of *Candida Albicans* and Inflammatory Host Response In Vitro. *Int. J. Dentistry* 2018, 1–7. doi:10.1155/2018/2393146
- Clinical and Laboratory Standards Institute (CLSI) (2002). *Reference Method for Broth Dilution Antifungal Susceptibility Testing of Yeast. Approved standard M27-A2*. Wayne: Clinical and Laboratory Standards Institute.
- da Silva Dantas, A., Lee, K. K., Raziunaite, I., Schaefer, K., Wagener, J., Yadav, B., et al. (2016). Cell Biology of *Candida Albicans*-Host Interactions. *Curr. Opin. Microbiol.* 34, 111–118. doi:10.1016/j.mib.2016.08.006
- Damascena, N. P., Souza, M. T. S., Almeida, A. F., Cunha, R. S., Damascena, N. P., Curvello, R. L., et al. (2014). Antioxidant and Orofacial Anti-nociceptive Activities of the Stem Bark Aqueous Extract of *Anadenanthera colubrina* (Velloso) Brenan (Fabaceae). *Nat. Product. Res.* 28 (10), 753–756. doi:10.1080/14786419.2013.877902
- Feller, L., Khammissa, R. A. G., Chandran, R., Altini, M., and Lemmer, J. (2014). Oral Candidosis in Relation to Oral Immunity. *J. Oral Pathol. Med.* 43 (8), 563–569. doi:10.1111/jop.12120
- Figueira, L. M. D., Ricomini Filho, A. P., Silva, W. J., Cury, A. A. D. B., and Ruiz, K. G. S. (2020). Glucose Effect on *Candida Albicans* Biofilm during Tissue Invasion. *Arch. Oral Biol.* 117, 104728. doi:10.1016/j.archoralbio.2020.104728
- Ford, C. B., Funt, J. M., Abbey, D., Issi, L., Guiducci, C., Martinez, D. A., et al. (2015). The Evolution of Drug Resistance in Clinical Isolates of *Candida Albicans*. *Elife* 4, e00662. doi:10.7554/eLife.00662.001
- Fox, E. P., Bui, C. K., Nett, J. E., Hartooni, N., Mui, M. C., Andes, D. R., et al. (2015). An Expanded Regulatory Network Temporally Controls *Candida Albicans* Biofilm Formation. *Mol. Microbiol.* 96 (6), 1226–1239. doi:10.1111/mmi.13002
- Francisconi, R. S., Huacho, P. M. M., Tonon, C. C., Bordini, E. A. F., Correia, M. F., Sardi, J. d. C. O., et al. (2020). Antibiofilm Efficacy of tea Tree Oil and of its Main Component Terpinen-4-Ol against *Candida Albicans*. *Braz. Oral Res.* 34, e050. doi:10.1590/1807-3107bor-2020.vol34.0050
- Freires, I. d. A., Murata, R. M., Furlatti, V. F., Sartoratto, A., Alencar, S. M. d., Figueira, G. M., et al. (2014). *Coriandrum Sativum* L. (Coriander) Essential Oil: Antifungal Activity and Mode of Action on *Candida* spp., and Molecular Targets Affected in Human Whole-Genome Expression. *Plos One* 9 (6), e99086. doi:10.1371/journal.pone.0099086
- Fu, R.-H., Liu, S.-P., Chu, C.-L., Lin, Y.-H., Ho, Y.-C., Chiu, S.-C., et al. (2013). Myricetin Attenuates Lipopolysaccharide-Stimulated Activation of Mouse Bone Marrow-Derived Dendritic Cells through Suppression of IKK/NF- κ B

- and MAPK Signalling Pathways. *J. Sci. Food Agric.* 93 (1), 76–84. doi:10.1002/jsfa.5733
- Ghannoum, M., Roilides, E., Katragkou, A., Petraitis, V., and Walsh, T. J. (2015). The Role of Echinocandins in Candida Biofilm-Related Vascular Catheter Infections: *In Vitro* and *In Vivo* Model Systems. *Clin. Infect. Dis.* 61, S618–S621. doi:10.1093/cid/civ815
- Gonçalves, L. M., Del Bel Cury, A. A., Sartoratto, A., Garcia Rehder, V. L., and Silva, W. J. (2012). Effects of Undecylenic Acid Released from Denture Liner on *Candida* Biofilms. *J. Dent Res.* 91 (10), 985–989. doi:10.1177/0022034512458689
- Guarneire, G. J., Cardoso Junior, O., Marques Lima, N., Aguiar Santos, E., Aguiar Schulze, C., Pereira Silva, W., et al. (2019). Effect of Anadenanthera Colubrina Protease Inhibitors as an Antiinflammatory Mediator. *Nat. Product. Res.* 35, 1690–1695. doi:10.1080/14786419.2019.1624962
- Hebecker, B., Naglik, J. R., Hube, B., and Jacobsen, I. D. (2014). Pathogenicity Mechanisms and Host Response during Oral *Candida Albicans* Infections. *Expert Rev. Anti-infective Ther.* 12 (7), 867–879. doi:10.1586/14787210.2014.916210
- Hellstein, J. W., and Marek, C. L. (2019). Candidiasis: Red and white Manifestations in the Oral Cavity. *Head Neck Pathol.* 13 (1), 25–32. doi:10.1007/s12105-019-01004-6
- Hertel, M., Schmidt-Westhausen, A. M., and Strietzel, F.-P. (2016). Local, Systemic, Demographic, and Health-Related Factors Influencing Pathogenic Yeast Spectrum and Antifungal Drug Administration Frequency in Oral Candidiasis: a Retrospective Study. *Clin. Oral Invest.* 20, 1477–1486. doi:10.1007/s00784-015-1631-0
- Hirota, K., Yumoto, H., Sapaar, B., Matsuo, T., Ichikawa, T., and Miyake, Y. (2017). Pathogenic Factors in Candida Biofilm-Related Infectious Diseases. *J. Appl. Microbiol.* 122 (2), 321–330. doi:10.1111/jam.13330
- Höfs, S., Mogavero, S., and Hube, B. (2016). Interaction of Candida Albicans with Host Cells: Virulence Factors, Host Defense, Escape Strategies, and the Microbiota. *J. Microbiol.* 54 (3), 149–169. doi:10.1007/s12275-016-5514-0
- Holetz, F. B., Pessini, G. L., Sanches, N. R., Cortez, D. A. G., Nakamura, C. V., and Dias Filho, B. P. (2022). Screening of Some Plants Used in the Brazilian Folk Medicine for the Treatment of Infectious Diseases. *Mem. Inst. Oswaldo Cruz* 97 (7), 1027–1031. doi:10.1590/S0074-02762002000700017
- Jabra-Rizk, M. A. (2011). Pathogenesis of Polymicrobial Biofilms. *Tomycj* 5, 39–43. doi:10.2174/1874437001105010039
- Ji, R., Sun, H., Peng, J., Ma, X., Bao, L., Fu, Y., et al. (2019). Rosmarinic Acid Exerts an Antagonistic Effect on Vascular Calcification by Regulating the Nrf2 Signalling Pathway. *Free Radic. Res.* 53 (2), 187–197. doi:10.1080/10715762.2018.1558447
- Junior, O. C., Lima, N. M., Silva, M. G. A., Aguiar, V. B., Carli, G. P., Scherrer, E. C., et al. (2020). *In Vitro* and *In Vivo* Evaluation of Anti-inflammatory Activity and Free Radical Scavenging Potential of Leaves Extract from *Anadenanthera Colubrina*. *Nat. Product. Res.* 1–5, 1–5. doi:10.1080/14786419.2020.1727472
- Kanchanapiboon, J., Kongsu, U., Pattamadilok, D., Kamponchaidet, S., Wachisunthon, D., Poonsatha, S., et al. (2020). Boesenbergia Rotunda Extract Inhibits *Candida Albicans* Biofilm Formation by Pinostrobin and Pinocembrin. *J. Ethnopharmacology* 261, 113193. doi:10.1016/j.jep.2020.113193
- Kumar, R., Breindel, C., Saraswat, D., Cullen, P. J., and Edgerton, M. (2017). *Candida Albicans* Sap6 Amyloid Regions Function in Cellular Aggregation and Zinc Binding, and Contribute to Zinc Acquisition. *Sci. Rep.* 7 (1), 2908. doi:10.1038/s41598-017-03082-4
- Lewis, M. A. O., and Williams, D. W. (2017). Diagnosis and Management of Oral Candidosis. *Br. Dent J.* 223 (9), 675–681. doi:10.1038/sj.bdj.2017.886
- Lima, R. d. F., Alves, É. P., Rosalen, P. L., Ruiz, A. L. T. G., Teixeira Duarte, M. C., Góes, V. F. F., et al. (2014). Antimicrobial and Antiproliferative Potential of *Anadenanthera colubrina* (Vell.) Brenan. *Evidence-Based Complement. Altern. Med.* 2014, 1–7. doi:10.1155/2014/802696
- Maia, C. M. d. A., Pasetto, S., Raimundo e Silva, J. P., Tavares, J. F., Costa, E. M. M. d. B., and Murata, R. M. (2021). *Anadenanthera Colubrina* (Vell.) Brenan as an Inhibitor of HIV-1 BaL Infection. *Nat. Product. Res.* 1–5. doi:10.1080/14786419.2021.1892097
- Millsop, J. W., and Fazel, N. (2016). Oral Candidiasis. *Clin. Dermatol.* 34 (4), 487–494. doi:10.1016/j.clindermatol.2016.02.022
- Mo, F., Ma, J., Yang, X., Zhang, P., Li, Q., and Zhang, J. (2020). *In Vitro* and *In Vivo* Effects of the Combination of Myricetin and Miconazole Nitrate Incorporated to Thermosensitive Hydrogels, on *C. Albicans* Biofilms. *Phytomedicine* 71, 153223. doi:10.1016/j.phymed.2020.153223
- Mota, G. S., Sartori, C. J., Miranda, I., Quilhó, T., Mori, F. A., and Pereira, H. (2017). Bark Anatomy, Chemical Composition and Ethanol-Water Extract Composition of *Anadenanthera Peregrina* and *Anadenanthera Colubrina*. *Plos One* 12 (12), e0189263. doi:10.1371/journal.pone.0189263
- Naglik, J. R., König, A., Hube, B., and Gaffen, S. L. (2017). Candida Albicans -epithelial Interactions and Induction of Mucosal Innate Immunity. *Curr. Opin. Microbiol.* 40, 104–112. doi:10.1016/j.mib.2017.10.030
- Naglik, J. R., Moyes, D. L., Wächter, B., and Hube, B. (2011). Candida Albicans Interactions with Epithelial Cells and Mucosal Immunity. *Microbes Infect.* 13 (12–13), 963–976. doi:10.1016/j.micinf.2011.06.009
- Newman, D. J., and Cragg, G. M. (2016). Natural Products as Sources of New Drugs from 1981 to 2014. *J. Nat. Prod.* 79, 629–661. doi:10.1021/acs.jnatprod.5b01055
- Nikou, S.-A., Kichik, N., Brown, R., Ponde, N., Ho, J., Naglik, J., et al. (2019). *Candida Albicans* Interactions with Mucosal Surfaces during Health and Disease. *Pathogens* 8 (2), 53. doi:10.3390/pathogens8020053
- O'Brien, J., Wilson, I., Orton, T., and Pognan, F. (2000). Investigation of the Alamar Blue (Resazurin) Fluorescent Dye for the Assessment of Mammalian Cell Cytotoxicity. *Eur. J. Biochem.* 267, 5421–5426. doi:10.1046/j.1432-1327.2000.01606.x
- Pande, M., Dubey, V. K., Yadav, S. C., and Jagannadham, M. V. (2006). A Novel Serine Protease Cryptolepin from *Cryptolepis Buchananii*: Purification and Biochemical Characterization. *J. Agric. Food Chem.* 54 (26), 10141–10150. doi:10.1021/jf062206a
- Pappas, P. G., Lionakis, M. S., Arendrup, M. C., Ostrosky-Zeichner, L., and Kullberg, B. J. (2018). Invasive Candidiasis. *Nat. Rev. Dis. Primers* 4, 18026. doi:10.1038/nrdp.2018.26
- Prieto, D., Correia, I., Pla, J., and Román, E. (2016). Adaptation of *Candida Albicans* Commensalism in the Gut. *Future Microbiol.* 11 (4), 567–583. doi:10.2217/fmb.16.1
- Qin, Y., Zhang, L., Xu, Z., Zhang, J., Jiang, Y.-y., Cao, Y., et al. (2016). Innate Immune Cell Response upon *Candida Albicans* Infection. *Virulence* 7 (5), 512–526. doi:10.1080/21505594.2016.1138201
- Rocha, E., Medeiros, A., Castro, R., Rosalen, P., Saraiva, K., Godoy, G., et al. (2017). Antifungal Activity, Phytochemical Characterization and Thermal Profile of *Anadenanthera Colubrina* (Vell.) Brenan. *Pesqui. Bras. Odontopediatria Clin. Integr.* 17 (1), 1–14. doi:10.4034/PBOCL.2017.171.12
- Rosa-García, E., Olade-Hernández, M. J., Irigoyen-Camacho, M. E., Mondragón-Padilla, A., Mendoza-Juache, A., and Sánchez-Vargas, L. O. (2020). Antifungal Susceptibility of Oral Isolates of *Candida* Species from Chronic Kidney Disease Patients on Chronic Dialysis. *J. Mycol. Med.* 101009, 1–6. doi:10.1016/j.mycmed.2020.101009
- Salvatori, O., Puri, S., Tati, S., and Edgerton, M. (2016). Innate Immunity and Saliva in *Candida Albicans*-Mediated Oral Diseases. *J. Dent Res.* 95 (4), 365–371. doi:10.1177/0022034515625222
- Sanitá, P. V., Zago, C. E., Pavarina, A. C., Jorge, J. H., Machado, A. L., and Vergani, C. E. (2013). Enzymatic Activity Profile of a Brazilian Culture Collection of *Candida Albicans* Isolated from Diabetics and Non-diabetics with Oral Candidiasis. *Mycoses* 57 (6), a-n. doi:10.1111/myc.12162
- Santana, I. L., Gonçalves, L. M., Vasconcellos, A. A. d., da Silva, W. J., Cury, J. A., and Cury, A. A. D. B. (2013). Dietary Carbohydrates Modulate *Candida Albicans* Biofilm Development on the Denture Surface. *Plos One* 8 (5), e64645. doi:10.1371/journal.pone.0064645
- Selem, D., Benso, B., Noguti, J., Pardi, V., and Murata, R. M. (2016a). *In Vitro* and *In Vivo* Antifungal Activity of Lichochalcone-A against *Candida Albicans* Biofilms. *Plos One* 11 (6), e0157188. doi:10.1371/journal.pone.0157188
- Selem, D., Chen, E., Benso, B., Pardi, V., and Murata, R. M. (2016b). *In Vitro* Evaluation of Antifungal Activity of Monolaurin against *Candida Albicans* Biofilms. *Peer J.* 4, e2148. doi:10.7717/peerj.2148
- Serrano, R., González-Menéndez, V., Rodríguez, L., Martín, J., Tormo, J. R., and Genilloud, O. (2017). Co-culturing of Fungal Strains against *Botrytis Cinerea* as

- a Model for the Induction of Chemical Diversity and Therapeutic Agents. *Front. Microbiol.* 8, 649. doi:10.3389/fmicb.2017.00649
- Siddiqui, Z. N., Farooq, F., Musthafa, T. N. M., Ahmad, A., and Khan, A. U. (2013). Synthesis, Characterization and Antimicrobial Evaluation of Novel Halopyrazole Derivatives. *J. Saudi Chem. Soc.* 17 (2), 237–243. doi:10.1016/j.jscs.2011.03.016
- Silva, D. R., Rosalen, P. L., Freires, I. A., Sardi, J. d. C. O., Lima, R. F., Lazarini, J. G., et al. (2019). *Anadenanthera Colubrina* Vell Brenan: Anti-Candida and Antibiofilm Activities, Toxicity and Therapeutical Action. *Braz. Oral Res.* 33, e023. doi:10.1590/1807-3107bor-2019.vol33.0023
- Silva, V. d. O., Pereira, L. J., Pasetto, S., da Silva, M. P., Meyers, J. C., and Murata, R. M. (2018). Effects of Monolaurin on Oral Microbe-Host Transcriptome and Metabolome. *Front. Microbiol.* 9, 2638. doi:10.3389/fmicb.2018.02638
- Sorgo, A. G., Heilmann, C. J., Brul, S., de Koster, C. G., and Klis, F. M. (2013). Beyond the wall: Candida albicans secret(e)s to survive. *FEMS Microbiol. Lett.* 338 (1), 10–17. doi:10.1111/1574-6968.12049
- Swidergall, M. (2019). *Candida Albicans* at Host Barrier Sites: Pattern Recognition Receptors and beyond. *Pathogens* 8 (1), 40. doi:10.3390/pathogens8010040
- Swidergall, M., and Filler, S. G. (2017). Oropharyngeal Candidiasis: Fungal Invasion and Epithelial Cell Responses. *Plos Pathog.* 13 (1), e1006056. doi:10.1371/journal.ppat.1006056
- Tanaka, T., Narazaki, M., and Kishimoto, T. (2014). IL-6 in Inflammation, Immunity, and Disease. *Cold Spring Harbor Perspect. Biol.* 6 (10), a016295. doi:10.1101/cshperspect.a016295
- Taniguchi, L., de Fátima Faria, B., Rosa, R. T., de Paula e Carvalho, A., Gursky, L. C., Elifio-Espósito, S. L., et al. (2009). Proposal of a Low-Cost Protocol for Colorimetric Semi-quantification of Secretory Phospholipase by *Candida Albicans* Grown in Planktonic and Biofilm Phases. *J. Microbiol. Methods* 78 (2), 171–174. doi:10.1016/j.mimet.2009.05.012
- Tooyama, H., Matsumoto, T., Hayashi, K., Kurashina, K., Kurita, H., Uchida, M., et al. (2015). *Candida* Concentrations Determined Following Concentrated Oral Rinse Culture Reflect Clinical Oral Signs. *BMC Oral Health* 15, 150. doi:10.1186/s12903-015-0138-z
- Tsui, C., Kong, E. F., and Jabra-Rizk, M. A. (2016). Pathogenesis of *Candida Albicans* biofilm. *Pathog. Dis.* 74 (4), ftw018. doi:10.1093/femspd/ftw018
- Vaezi, A., Fakhim, H., Khodavaisy, S., Alizadeh, A., Nazeri, M., Soleimani, A., et al. (2017). Epidemiological and Mycological Characteristics of Candidemia in Iran: A Systematic Review and Meta-Analysis. *J. de Mycologie Médicale* 27 (2), 146–152. doi:10.1016/j.mycmed.2017.02.007
- Verma, A. H., Richardson, J. P., Zhou, C., Coleman, B. M., Moyes, D. L., Ho, J., et al. (2017). Oral Epithelial Cells Orchestrate Innate Type 17 Responses to *Candida Albicans* through the Virulence Factor Candidalysin. *Sci. Immunol.* 2 (17), eaam8834. doi:10.1126/sciimmunol.aam8834
- Verma, A. H., Zafar, H., Ponde, N. O., Hepworth, O. W., Sihra, D., Aggor, F. E. Y., et al. (2018). IL-36 and IL-1/IL-17 Drive Immunity to Oral Candidiasis via Parallel Mechanisms. *J. Immunol.* 201 (2), 627–634. doi:10.4049/jimmunol.1800515
- Vila, T., Sultan, A. S., Montelongo-Jauregui, D., and Jabra-Rizk, M. A. (2020). Oral Candidiasis: A Disease of Opportunity. *J. Fungi.* 6 (1), 15. doi:10.3390/jof6010015
- Wall, G., Montelongo-Jauregui, D., Vidal Bonifacio, B., Lopez-Ribot, J. L., and Uppuluri, P. (2019). *Candida Albicans* Biofilm Growth and Dispersal: Contributions to Pathogenesis. *Curr. Opin. Microbiol.* 52, 1–6. doi:10.1016/j.mib.2019.04.001
- Williams, D., and Lewis, M. (2011). Pathogenesis and Treatment of Oral Candidosis. *J. Oral Microbiol.* 3, 5771. doi:10.3402/jom.v3i0.5771
- Wong, S. S., Kao, R. Y., Yuen, K. Y., Wang, Y., Yang, D., Samaranayake, L. P., et al. (2014). *In Vitro* and *In Vivo* Activity of a Novel Antifungal Small Molecule against *Candida* Infections. *PLoS One* 9 (1), e85836. doi:10.1371/journal.pone.0085836
- Xu, H., and Dongari-Bagtzoglou, A. (2015). Shaping the Oral Mycobiota: Interactions of Opportunistic Fungi with Oral Bacteria and the Host. *Curr. Opin. Microbiol.* 26, 65–70. doi:10.1016/j.mib.2015.06.002

Conflict of Interest: The authors declare that the research was conducted in the absence of any commercial or financial relationships that could be construed as a potential conflict of interest.

Copyright © 2021 Maia, Pasetto, Nonaka, Costa and Murata. This is an open-access article distributed under the terms of the Creative Commons Attribution License (CC BY). The use, distribution or reproduction in other forums is permitted, provided the original author(s) and the copyright owner(s) are credited and that the original publication in this journal is cited, in accordance with accepted academic practice. No use, distribution or reproduction is permitted which does not comply with these terms.



Dendrobium Officinale Polysaccharide Attenuates Insulin Resistance and Abnormal Lipid Metabolism in Obese Mice

Jian Qu^{1†}, Shengyu Tan^{2†}, Xinyan Xie³, Wenqiang Wu³, Haihong Zhu¹, Hang Li¹, Xiaobo Liao⁴, Jiaojiao Wang¹, Zhi-Ang Zhou⁴, Song Huang^{3*} and Qiong Lu^{1*}

¹Department of Pharmacy, The Second Xiangya Hospital, Central South University, Changsha, China, ²Department of Geriatrics, The Second Xiangya Hospital of Central South University, Changsha, China, ³Mathematical Engineering Academy of Chinese Medicine, Guangzhou University of Chinese Medicine, Guangzhou, China, ⁴Department of Cardiovascular Surgery, The Second Xiangya Hospital, Central South University, Changsha, China

OPEN ACCESS

Edited by:

Sayed Ahmad,
Jamia Hamdard University, India

Reviewed by:

Ye Huang,
Xiyuan Hospital CACMS, China
Alexandre Abilio De Souza Teixeira,
University of São Paulo, Brazil

*Correspondence:

Song Huang
huangnn421@163.com
Qiong Lu
christy_lu@csu.edu.cn

[†]These authors have contributed
equally to this work

Specialty section:

This article was submitted to
Ethnopharmacology,
a section of the journal
Frontiers in Pharmacology

Received: 28 January 2021

Accepted: 01 June 2021

Published: 14 June 2021

Citation:

Qu J, Tan S, Xie X, Wu W, Zhu H, Li H,
Liao X, Wang J, Zhou Z-A, Huang S
and Lu Q (2021) Dendrobium Officinale
Polysaccharide Attenuates Insulin
Resistance and Abnormal Lipid
Metabolism in Obese Mice.
Front. Pharmacol. 12:659626.
doi: 10.3389/fphar.2021.659626

Objectives: Dendrobium officinale polysaccharide (DOP) is the main active ingredient in a valuable traditional Chinese medicine, which exerts several pharmacological activities including hepatoprotection and hypoglycemic effects. However, the effects of DOP on obesity-associated insulin resistance (IR) and lipid metabolism remain unknown. This study aimed to investigate the role of DOP in IR and abnormal lipid metabolism in obese mice.

Methods: IR models were established using 3T3-L1 adipocytes, C2C12 myocytes, and primary cultured hepatocytes exposed to palmitate acid. After treatment with DOP, insulin-stimulated glucose uptake, glucose release, and AKT phosphorylation was detected. Fasting blood glucose, fasting serum insulin, the glucose tolerance test (GTT), and the insulin tolerance test (ITT) were measured to evaluate IR of obese mice. Lipid analysis was conducted to evaluate the effects of DOP on lipid metabolism in obese mice.

Results: *In vitro*, DOP treatment ameliorated palmitic acid-induced IR in adipocytes, myocytes, and hepatocytes. DOP regulated cellular insulin sensitivity via the peroxisome proliferator-activated receptor- γ (PPAR- γ). Furthermore, administration of DOP significantly reduced the IR and visceral adipose tissue (VAT) inflammation of diet-induced obese (DIO) and the genetically-induced obesity mice (ob/ob) mouse models. In addition, DOP treatment attenuated the high-fat diet (HFD)-induced liver lipid accumulation by reducing liver triglycerides (TG), plasma free fatty acid (FFA), serum cholesterol (TC), and low-density lipoprotein cholesterol (LDL-C) levels, while increasing HDL-C levels.

Conclusion: DOP could improve obesity-associated IR and abnormal lipid metabolism through its activities on PPAR- γ , and may serve as a potential therapeutic agent for obesity-associated insulin resistance and lipid metabolism disorder.

Keywords: abnormal lipid metabolism, Dendrobium officinale polysaccharide, insulin resistance, obesity, peroxisome proliferator-activated receptor- γ

Abbreviations: DIO, Diet-induced obese; DOP, Dendrobium officinale polysaccharide; FFA, Free fatty acid; GTT, Glucose tolerance test; HDL-C, High-density lipoprotein cholesterol; HFD, High-fat diet; HOMA-IR, Homeostasis model assessment of insulin resistance; IR, Insulin resistance; ITT, Insulin tolerance test; LDL-C, Low-density lipoprotein cholesterol; PPAR- γ , Peroxisome proliferator-activated receptor- γ ; TC, Serum cholesterol; TG, Triglycerides; VAT, Visceral adipose tissue.

INTRODUCTION

With rapid economic growth, obesity is becoming an increasing health concern worldwide. Understandably, obesity was defined as a disease by the Obesity Society (TOS) in 2008 (Belkina and Denis, 2010; Jastreboff et al., 2019). Obesity is characterized by increased circulating fatty acid levels resulting from excessive lipolysis and absorption of basal adipose tissue, which in turn promote the development of ectopic lipid deposition and insulin resistance (IR) (Crowe et al., 2009). Consistently, studies have shown that obesity is a risk factor for metabolic syndrome, which includes IR and dyslipidemia, impaired fasting blood glucose, and hyperinsulinemia (Laaksonen et al., 2002; Meigs et al., 2006). In addition, obesity increases the risk and mortality of many diseases Council of the Obesity (2008), González-Domínguez et al. (2020), especially type 2 diabetes, cardiovascular disease, hypertension, and dyslipidemia (De Lorenzo et al., 2019).

IR refers to the reduction of insulin sensitivity and response to insulin target organs and tissues (liver, adipose tissue, skeletal muscle) due to varied reasons (Samuel and Shulman, 2012). This leads to a decrease in glucose uptake and utilization. Therefore, the body will compensatively secrete excess insulin to maintain the stability of blood sugar, leading to hyperinsulinemia, which in turn leads to dyslipidemia. Dyslipidemia manifests as increased total cholesterol (TC), triglycerides (TG), and free fatty acids (FFA), normal or slightly increased low-density lipoprotein cholesterol (LDL-C), and decreased high-density lipoprotein cholesterol (HDL-C) (Klop et al., 2013). Moreover, the symptoms of IR are impaired glucose absorption in muscles and increased gluconeogenesis in the liver during fasting and postprandial conditions, leading to hyperglycemia (Møller and Kaufman, 2005). Insulin-sensitive tissues (adipose tissue, heart, and liver) are significantly affected by obesity at biomolecular and functional levels (Barazzoni et al., 2018). Excessive fat accumulation can change the function of adipose organs and leads to obesity-related diseases (Ling and Rønn, 2019). In addition, a close relationship between the mechanisms implicated in lipid metabolic disorders and IR has also been reported (Savage et al., 2007). Further, obesity and IR are closely related to inflammation of metabolic tissues, including the liver, muscle, and adipose tissue (Winer et al., 2016; Wu and Ballantyne, 2017; Ghorpade et al., 2018). Excessive fat accumulation and abnormal lipid metabolism caused by obesity induce the transformation of macrophages from the anti-inflammatory M2 polarized state to the pro-inflammatory M1 polarized state, leading to VAT inflammation, thus promoting the development of obesity-related IR (Xu et al., 2003; Lumeng et al., 2007; Kojta et al., 2020). At the same time, IR further aggravates lipid metabolism disorders, leading to a series of metabolic disorders such as diabetes and cardiovascular diseases. The specific manifestations of visceral adipose tissue (VAT) inflammation are increased levels of pro-inflammatory cytokines such as tumor necrosis factor (TNF)- α and interleukin (IL)-6 Hotamisligil et al. (1993), Kern et al. (2001), and decreased levels of anti-inflammatory cytokines IL-10 and IL-4 in obesity-related IR patients (Esposito et al., 2003). Therefore, the prevention or treatment of IR and lipid

metabolism disorders may be an effective way to inhibit obesity-related diseases.

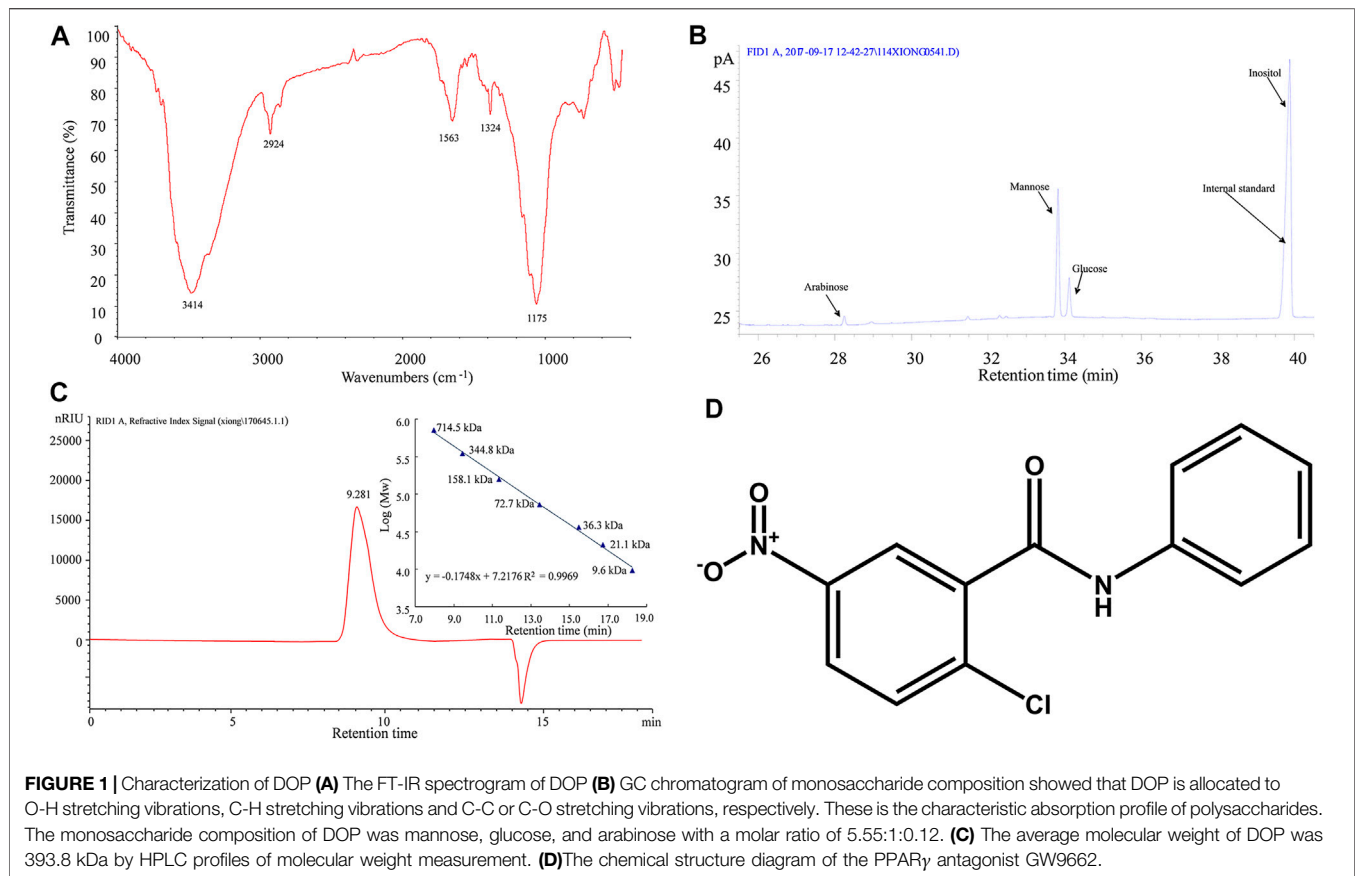
Dendrobium officinale Kimura et Migo is a valuable traditional Chinese medicine that has been used to treat diabetes, obesity, rheumatoid arthritis, and many other diseases. It has been reported that *Dendrobium officinale Kimura et Migo* can inhibit the effects of oxidative stress and pro-inflammatory cytokines (Teixeira da Silva et al., 2015). Oxidative stress and inflammation may also lead to obesity-related IR (Xu et al., 2003; Gortan Cappellari et al., 2016). *Dendrobium officinale polysaccharide (DOP)* is the main active component of *Dendrobium officinale Kimura et Migo*, which exerts pharmacological activities including antioxidation, lowering blood lipids and blood sugar levels, and hepatoprotection (Huang et al., 2016). In type 2 diabetic rats, DOP treatment reduced hepatic lipid metabolism disorders and alleviated symptoms of hepatic lipid accumulation (Yang et al., 2020). These studies indicated that DOP is expected to be a novel therapeutic agent for obesity-related diseases including IR and abnormal lipid metabolism. However, to date, there are almost no available mechanistic studies investigating mechanistic studies on the effects of DOP in IR and abnormal lipid metabolism. Meanwhile, the mechanism of DOP in obesity-related IR and abnormal lipid metabolism is still unclear.

The purpose of this study was to explore the effects and mechanisms of action of DOP on obesity-related IR and lipid metabolism disorders. First, at the cellular level, we measured glucose uptake, glucose output, and Akt phosphorylation in insulin-stimulated hepatocytes, muscle cells, and adipocytes, respectively. The results showed that DOP treatment could improve IR-induced obesity. Subsequently, we conducted a mechanism study and found that DOP mainly acted on peroxisome proliferator-activated receptor- γ (PPAR- γ) signaling to regulate insulin sensitivity in diet-induced obesity (DIO) mice. We evaluated how DOP could improve IR in DIO mice by assessing fasting blood glucose and fasting serum insulin levels, the glucose tolerance test (GTT), the insulin tolerance test (ITT), and the inflammation related indicators of VAT. Furthermore, lipid analysis showed that DOP attenuated the abnormal lipid metabolism in DIO mice. We also validated the therapeutic effects of DOP in the genetically-induced obesity mice (ob/ob mice) model. Overall, we expect that our study can provide a basis for the clinical application of DOP in obesity-related IR and lipid metabolism disorders.

MATERIALS AND METHODS

Animal Models

To establish a diet-induced obese (DIO) mice model, two-month-old male C57BL6 mice were fed a high-fat diet (HFD, 60% fat, 20% protein, and 20% carbohydrate) for 3 months. Ob/ob mice are a classical experimental model of obesity-induced IR as evidenced by a plethora of studies. Ob/ob mice harbor a recessive mutation in leptin and are characterized by hyperphagia, obesity, hyperinsulinemia, insulin-resistance (IR), and hyperglycemia; thus, they are commonly used as a model for



studies of diabetes and obesity. Ob/ob mice were purchased from Hunan SJA Laboratory Animal Co., Ltd. (license number: SCXK 2019-0004). All animals were housed under 12-h light/dark cycles and were provided unrestricted access to food and water unless otherwise specified.

For *in vivo* DOP treatment, after 3 months of a HFD, the DIO mice were divided into two groups, the control group and the experimental group, the control group received normal saline (NS) orally, and the experimental group was administrated DOP (150 mg/kg) orally, once daily for 3 months. The DOP involved in this study was prepared by the laboratory of Mathematical Engineering Academy of Chinese Medicine, Guangzhou University of Chinese Medicine (Liang et al., 2018; Liang et al., 2019). The proportion of total polysaccharides in the DOP was 93.80%. Moreover, the FT-IR spectrogram showed that DOP has an intense and broad absorption peak around 3414 cm⁻¹, a weak absorption peak at 2924 cm⁻¹ and 1324 cm⁻¹, and an asymmetrical extension at 1175 cm⁻¹ (Figure 1A). And GC chromatogram of monosaccharide composition showed that DOP had the characteristic absorption profile of polysaccharides. DOP is composed of mannose, glucose, and arabinose with a molar ratio of 5.55:1:0.12 (Figure 1B). Meanwhile, the average molecular weight of DOP determined by HPLC profiles of molecular weight measurement was 393.8 kDa (Figure 1C). The structure composition of DOP showed that its

formulation was identical to the DOP prepared by Hua (Hua et al., 2004).

All protocols pertaining to animal care and experiments were reviewed and approved by the Institutional Animal Care and Use Committee of the Laboratory Animal Research Center at Xiangya Medical School of Central South University, China.

Cell Culture and Treatment

Primary hepatocytes, C2C12 myoblasts, and 3T3-L1 preadipocytes were cultured in a humidified incubator at 37°C and supplemented with 5% CO₂. Standard protocols were utilized to induce differentiation of these cells. To establish IR models, primary hepatocytes, C2C12, myoblasts and 3T3-L1 preadipocytes were treated with 0.5 mmol/L palmitate acid (PA; Sigma) for 24 h. Glucose levels in the medium were measured to determine whether the IR model was successful. For *in vitro* DOP treatment, 200 µg/ml DOP was added to the culture medium for 48 h.

Cell Viability

The Cell Counting Kit-8 (CCK-8) was used to assess the viability of 3T3-L1 adipocytes after DOP treatment, as per the manufacturer's protocol. Absorbance was measured at 450 nm *via* a microplate reader (Thermo Electron Corp).

TABLE 1 | Primer sequences used for real-time PCR analysis.

Gene	Forward primer	Reverse primer
Actin (mouse)	GGCTGTATTCCCTCCATCG	CCAGTTGGTAACAATGCCATGT
PPAR- γ (mouse)	GGAAAGACAACGGACAAATCAC	TACGGATCGAACTGGCAC
TNF α (mouse)	TATGGCTCAGGTCCTCACTC	CTCCCTTGCAGAACTCAGG
IL-6	AGTTGCCTTCTTGGGACTGA	CAGAATTGCCATTGCACAAC
IL-10	GCCCTTCCTATGTGTGTTTG	TTGAGTTTCCGTACTGTTTGAGG
IL-4	CCCCAGCTAGTTGTCATCCTG	CAAGTGATTTTTGTCGCATCCG

Glucose Uptake and Glucose Output Assay

The glucose uptake and glucose output assays were performed as described previously (Su et al., 2019). The medium glucose levels were measured by a Glucose Assay Kit (Abcam, ab65333) according to the manufacturer's instructions.

Western Blot and qRT-PCR Analysis

Western blotting analysis was conducted as previously described (Li et al., 2009). Primary antibodies p-AKT (CST9272s; Dilution 1:1,000) and AKT (CST9272s; Dilution 1:1,000) were purchased from Cell Signaling Technology, and PPAR- γ (ab209350, Dilution 1:1,000) was purchased from Abcam. All primary antibodies were incubated at 4°C overnight, the secondary antibodies were diluted to 1:5,000, and specific proteins were visualized by ECL Plus. For qRT-PCR analysis, the total RNA from cultured cells were isolated by TRIzol (Thermo Fisher Scientific). The list of primers used for real-time PCR analysis are described in Table 1.

Blood Glucose, Serum Insulin, Insulin Tolerance Test, Glucose Tolerance Test, and HOMA-IR Index

The measurement of blood glucose levels and serum insulin, and the performance of the ITT and GTT, have been reported previously (Ying et al., 2017; Xiao et al., 2020). The following formula was used to calculate the homeostasis model assessment of IR (HOMA-IR) index: [fasting blood glucose levels (mmol/L)] \times [fasting serum insulin levels (μ U/ml)]/22.5 (Su et al., 2019).

Lipid Analysis

Approximately, 0.1 g liver was homogenized in phosphate-buffered saline (PBS) solution (1:9 ratio). The mixture was centrifuged at 2,500 rpm for 10 min at 4°C after which the supernatant was collected. The cytoplasm of L02 cells was collected with 2% Triton X-100. Hepatic and hepatocellular TG were quantified using chemical reagent kits from Nanjing Jiancheng Bioengineering Institute (Nanjing, China). In addition, serum lipids including TC, TG, LDL-C, and HDL-C levels were determined using kits from Nanjing Jiancheng Bioengineering Institute (Nanjing, China). Plasma-free fatty acid (FFA) levels were measured enzymatically using a kit from WAKO Chemicals. Absorbance values of all samples were measured using a spectrophotometric system.

Hematoxylin and Eosin Staining and Oil Red O Staining

Livers samples (4–5 micron in thickness) were placed in cassettes and submerged in 10% formalin solution overnight. Samples were processed in a dehydrating ethanol gradient, followed by xylene incubation and paraffin embedding. Serial 8- μ m sections were used for hematoxylin and eosin (H&E) staining and Oil Red O staining.

Quantification and Statistical Analysis

All data are presented as mean \pm SD. For comparisons between two groups, a two-tailed Student's t-test was used. Comparisons between multiple groups were performed using ANOVA followed by Bonferroni's post-hoc correction. A *p*-value < 0.05 was considered statistically significant.

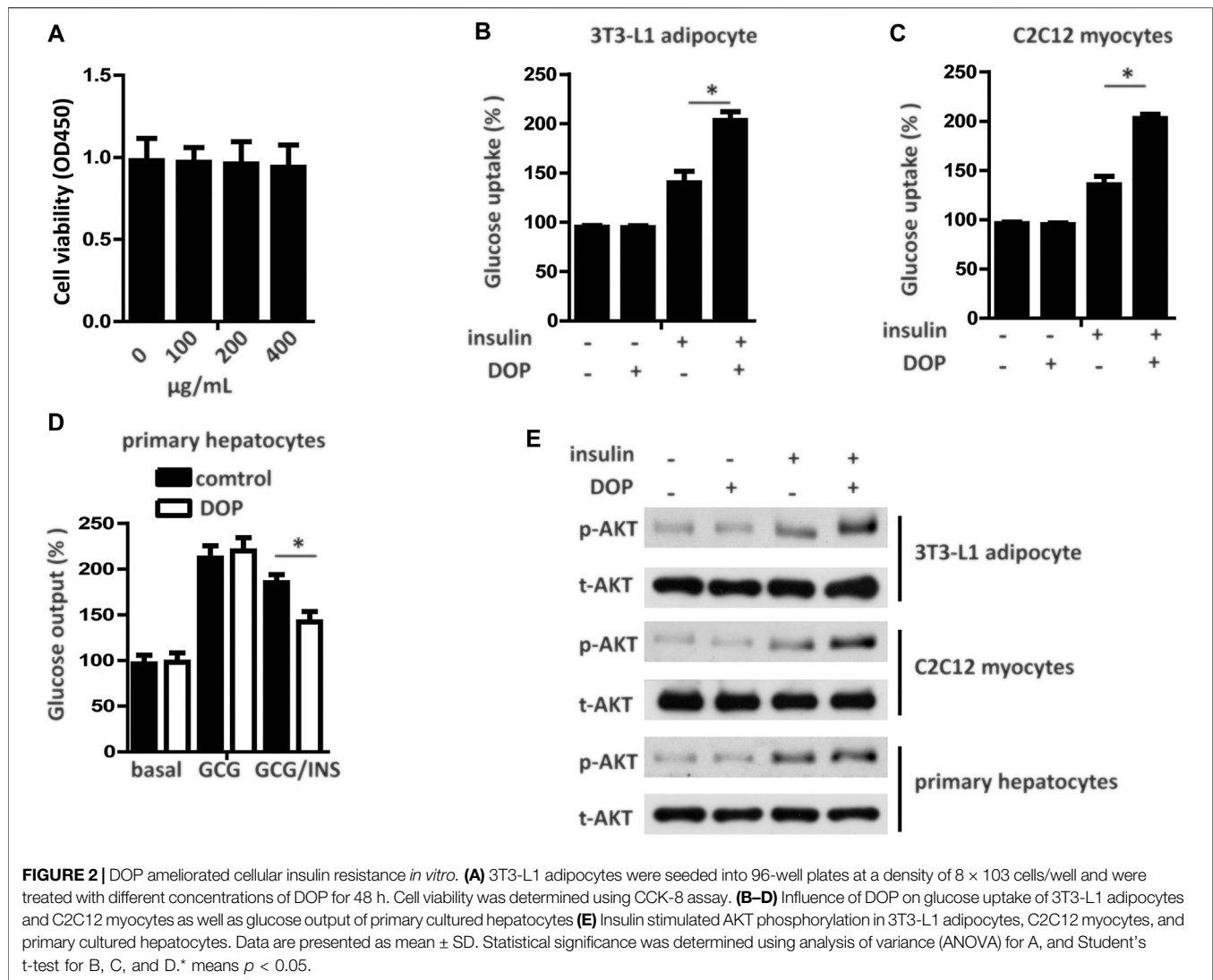
RESULTS

DOP Ameliorated Cellular Insulin Resistance *In Vitro*

The cytotoxicity of DOP was assessed by the CCK-8 assay, which revealed DOP did not affect cell viability at concentrations of 100, 200, and 400 μ g/ml (Figure 2A). To explore whether DOP participated in the regulation of insulin sensitivity, we treated PA-induced adipocytes, myocytes, and hepatocytes with DOP. As expected, DOP treatment significantly promoted the insulin-stimulated glucose uptake of 3T3-L1 adipocytes and C2C12 myocytes (Figures 2B,C), while the glucose output of primary cultured hepatocytes decreased (Figure 2D). In addition, the insulin-stimulated AKT phosphorylation of 3T3-L1 adipocytes, C2C12 myocytes, and primary cultured hepatocytes was increased following DOP treatment (Figure 2E). Taken together, these results suggested that DOP ameliorated cellular IR of adipocytes, myocytes, and hepatocytes *in vitro*.

DOP Regulated Cellular Insulin Sensitivity by Activating PPAR- γ

Pharmacological activation of PPAR- γ has emerged as an effective method for treating diabetes. We found that the transcript levels of PPAR- γ mRNA in 3T3-L1 adipocytes, C2C12 myocytes, and primary cultured hepatocytes treated with DOP were elevated (Figures 3A–C). Western blotting analysis further confirmed that DOP could promote the protein expression levels of PPAR- γ (Figure 3D). These



observations suggested that DOP increased the expression of PPAR- γ .

To validate whether DOP regulated cellular insulin sensitivity through the activation of PPAR- γ , we treated PA-induced adipocytes and myocytes with GW9662, a PPAR- γ antagonist. GW9662 is a potent and selective PPAR- γ antagonist with an IC₅₀ of 3.3 nM, showing 10 and 1000-fold selectivity over PPAR α and PPAR- δ , respectively. The chemical structure is shown in **Figure 1D**. The effects of DOP on 3T3-L1 adipocytes and C2C12 myocytes was abrogated by GW9662, which indicated that DOP failed to improve the insulin sensitivity if PPAR- γ was inhibited (**Figures 3E,F**). Taken together, these results indicated that DOP regulated cellular insulin sensitivity by activating PPAR- γ .

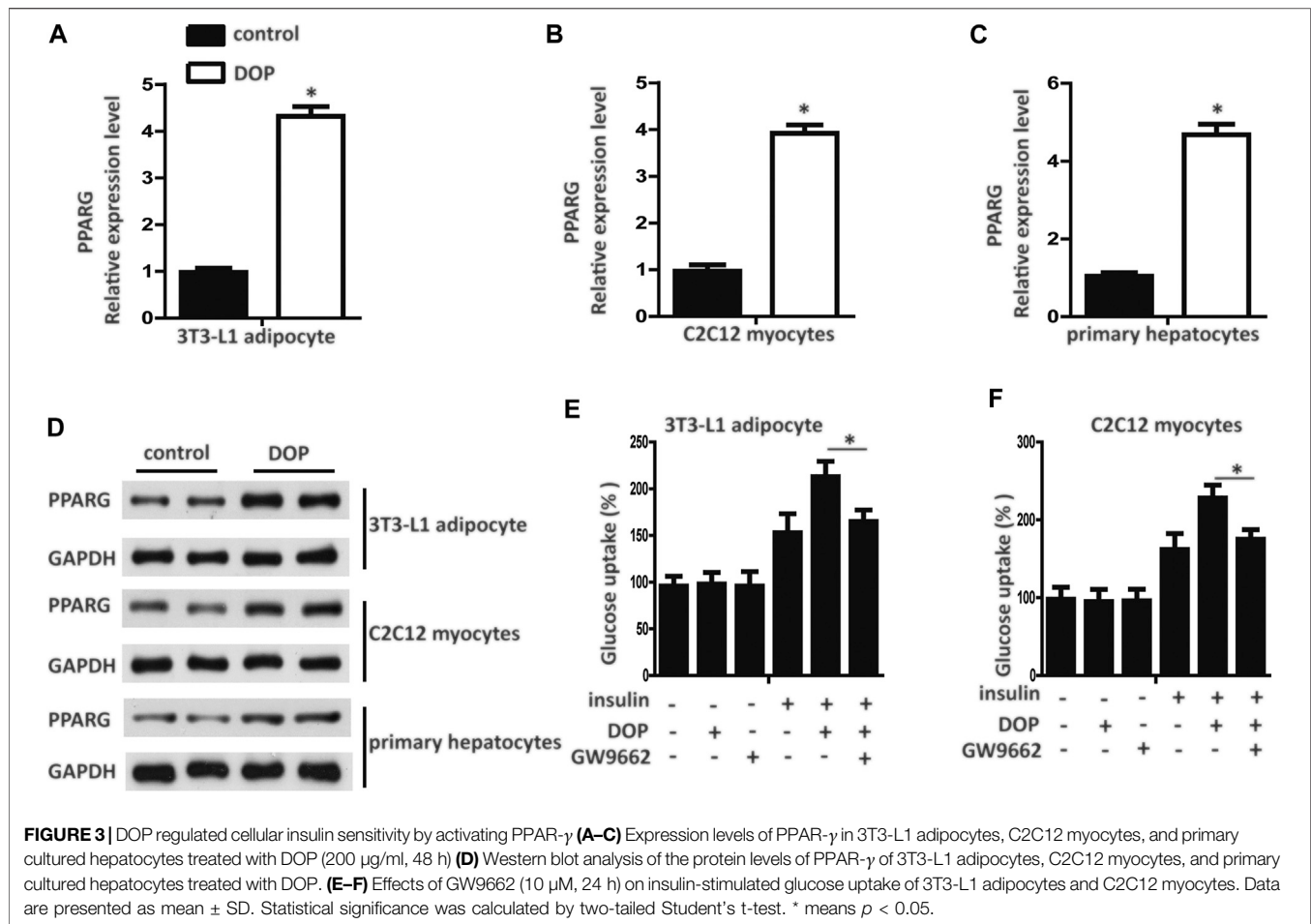
Administration of DOP Reduced the Insulin Resistance of Obese Mice

To explore the therapeutic potential of DOP on the IR of obese mice, we treated obese mice with normal saline (NS) or DOP.

Notably, mice treated with DOP had lower fasting blood glucose levels and fasting serum insulin (**Figures 4A,B**). The HOMA-IR index was also lowered in the DOP-treated group (**Figure 4C**). Moreover, DOP could also suppress VAT inflammation. The levels of pro-inflammatory cytokines IL-6 and TNF α were also decreased, while the anti-inflammatory cytokines IL-10 and IL-4 were increased (**Figure 4D**). Furthermore, the results of the GTT and ITT revealed that glucose tolerance and clearance in mice were increased after administration of DOP (**Figures 4E,F**). Together, these findings suggested that administration of DOP reduced IR and adipose tissue inflammation in obese mice.

DOP Impaired Lipid Metabolism Disorder in Obese Mice

To further explore the effect of DOP on lipid metabolism in obese mice, serum, and hepatic lipid levels were assayed. DOP-treated mice exhibited significantly lower TG levels in the liver when compared with untreated mice (**Figure 5A**). In addition, FFA,



serum TC, TG, and LDL-C levels in DOP-treated mice were also lower than in the control group (Figures 5B–E). Importantly, DOP treatment was effective in increasing HDL-C levels (Figure 5F). The H&E staining and Oil Red O staining of the liver samples indicated that compared with the control group, the lipid levels and volumes were decreased in DOP treatment group in ob/ob mice (Figure 5G). Taken together, these results showed that DOP could ameliorate lipid metabolism disorders in obese mice.

DOP Treatment Alleviated Insulin Resistance in Ob/Ob Mice

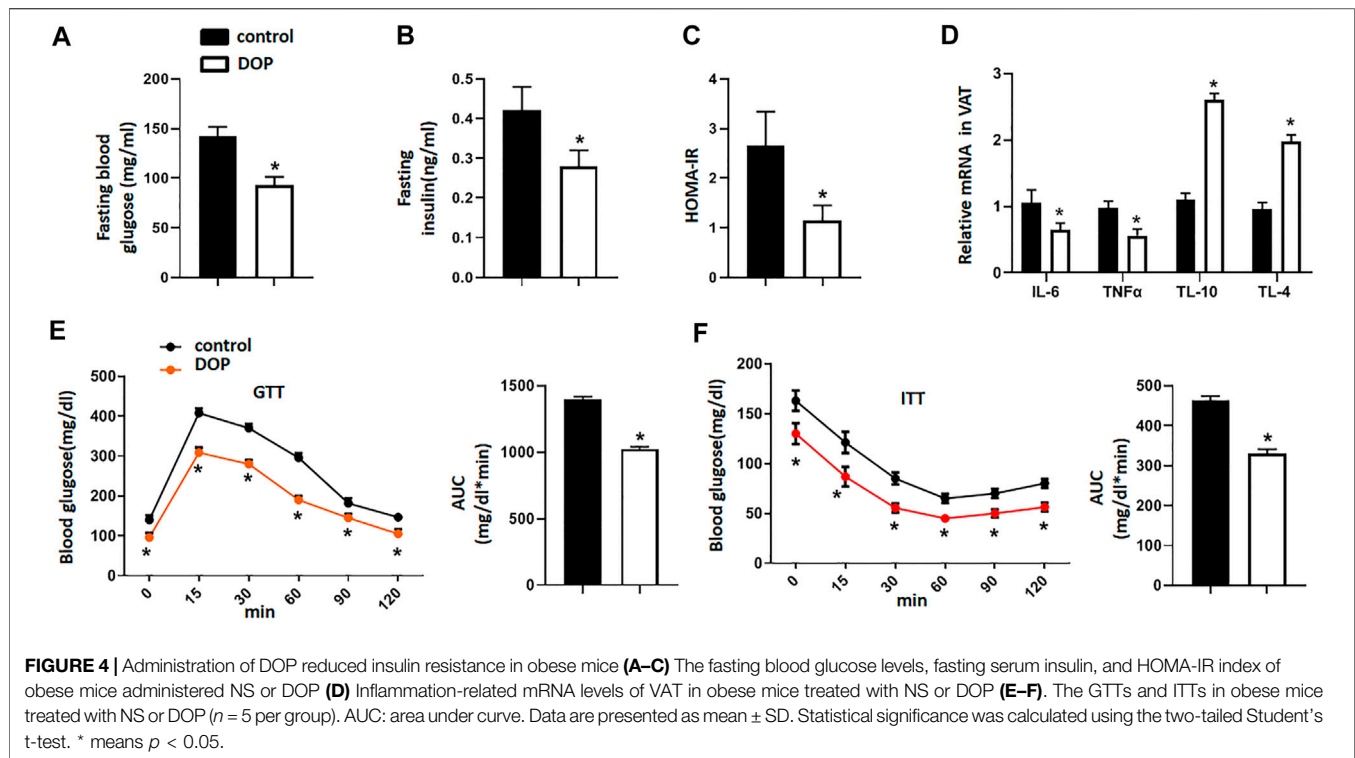
To further confirm the therapeutic effect of DOP, ob/ob mice were orally administered DOP as mentioned above. Similar to the observations in obese mice, ob/ob mice treated with DOP also exhibited decreased fasting blood glucose levels, fasting serum insulins, and a lower HOMA-IR index (Figures 6A–C). In addition, VAT inflammation was also restrained by DOP treatments exhibited by reduced levels of inflammatory cytokines (IL-6 and TNF α) and elevated expression of anti-inflammatory cytokines (IL-10 and IL-4) (Figure 6D). The results from the GTT and ITT indicated that the application of DOP could improve the glucose intolerance of ob/ob mice

(Figures 6E,F). Thus, all these results indicated that DOP treatment could alleviate IR and adipose tissue inflammation in ob/ob mice.

DISCUSSION

Obesity is the basis of IR, which is a potential cause of a complex metabolic syndrome, including hypertension, elevated fasting blood glucose, low HDLC, and elevated TG levels (Beale, 2013). Therefore, there is an urgent need to identify potential therapeutic agents and suitable targets to attenuate IR and abnormal lipid metabolism in obese patients. In this study, we confirmed the potential therapeutic target of PPAR- γ in obese mice and the role of DOP in attenuating IR and abnormal lipid metabolism.

IR is defined as the decreased sensitivity to insulin and response of insulin to target organs and tissues (liver, adipose tissue, skeletal muscle) (Samuel and Shulman, 2012). IR can lead to an increase in intracellular glucose concentration and a decrease in glucose uptake. However, for the liver, IR is characterized by an inability to inhibit liver glucose production and glycogen decomposition (Randle et al., 1963; Randle et al., 1964; Randle et al., 1965). AKT protein kinase in adipocytes,



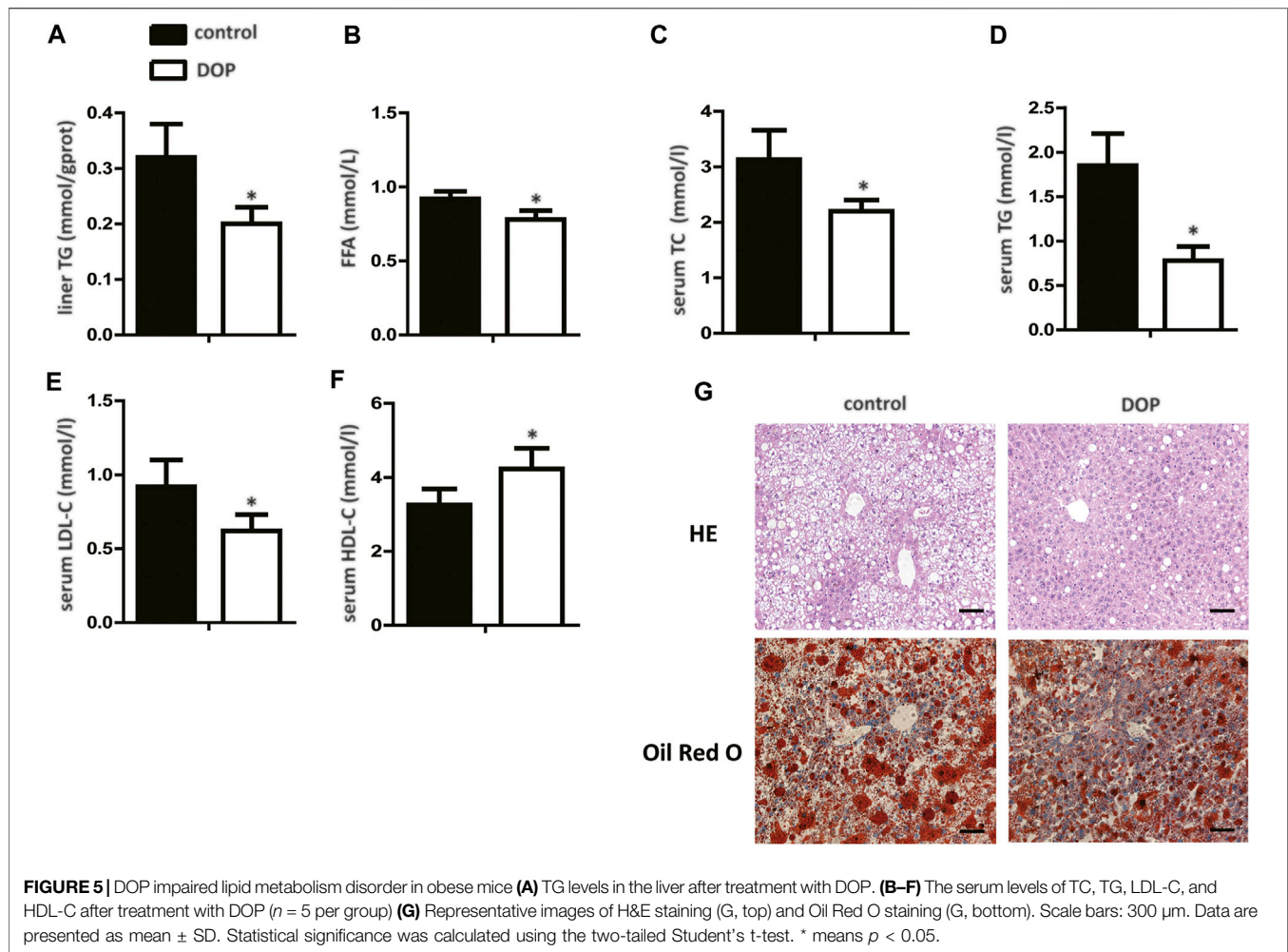
muscle cells, and liver cells is the key kinase regulating glucose homeostasis (Czech, 2017). Previous studies have found that fatty acid stimulation is an early event of IR (Lee et al., 2014). In this study, we used PA to treat adipocytes, myocytes, and hepatocytes to establish IR models of the three cell types. We then measured glucose uptake or output and insulin-stimulated AKT phosphorylation in these insulin-resistant cells with or without DOP treatment. As expected, DOP treatment significantly promoted the insulin-stimulated glucose uptake of 3T3-L1 adipocytes and C2C12 myocytes, while the glucose output from hepatocytes decreased. Therefore, it is likely that DOP is an agent for potential treatment or prevention of IR.

Multiple mechanisms are involved in the IR of type 2 diabetes. PPAR- γ is a subfamily of nuclear receptors. Activation of PPAR- γ has been reported to improve blood glucose control and systemic insulin sensitivity in patients with type 2 diabetes (Semple et al., 2006). The activation of nuclear receptor PPAR- γ in adipose tissue, liver, and muscle is a determinants of insulin sensitivity (Lu et al., 2011; Germoush et al., 2019). In accordance with previous studies, our results showed that DOP could up-regulate the expression of PPAR- γ in adipocytes, myocytes, and hepatocytes.

IR can lead to hyperinsulinemia and impaired fasting blood glucose (elevated fasting blood glucose). Further, ITT, and GTT are also effective methods to evaluate IR (Guerre-Millo et al., 2001). IR can be diagnosed clinically by a homeostasis model of IR (HOMA-IR) based on fasting blood glucose and fasting serum insulin levels (Yee et al., 2019). To further explore the therapeutic effects of DOP on IR, we conducted *in vivo* experiments using and obese IR mouse model. The results showed that the levels of

fasting blood glucose and fasting serum insulin in the DOP-treated group were significantly lower than those in the control group. Through the ITT and GTT, we found that the blood glucose concentration of mice treated with DOP decreased significantly, which indicated that DOP treatment could significantly increase the glucose tolerance of obese mice and clearance rate of insulin to blood glucose. Furthermore, an increase in obesity-induced lipid storage leads to adipose tissue dysfunction and promotes adipocyte secretion of pro-inflammatory cytokines, including TNF- α and IL-6. Moreover, due to the transformation of M2 macrophages to M1 in obesity tissues, the expression of anti-inflammatory cytokines IL-10 and IL-4 secreted by M2 macrophages is decreased (Taylor, 2021). Changes in the expression of these markers lead to VAT inflammation, which in turn promotes IR. However, our study showed that DOP treatment can reverse the changes in pro-inflammatory and anti-inflammatory cytokines caused by obesity. These results once again confirmed the therapeutic effects of DOP on obesity-induced IR.

Typical obesity-induced dyslipidemia includes elevation in TC, TG, and FFA levels; normal or mildly elevated LDL-C; and decreased HDL-C levels (Klop et al., 2013). Multiple studies have shown that these changes in lipid metabolism are closely related to IR (Reaven et al., 1988; Frayn, 1993; Boden et al., 1994; Ormazabal et al., 2018). Therefore, we analyzed the levels of serum and liver lipids in obese mice with or without DOP treatment. The FFA and serum TC, TG, and LDL-C levels were lower and the serum HDL-C levels were higher in DOP-treated mice than control mice. These results were similar to the study by Yang et al. study, whereby DOP treatment reduced the



metabolic disorder of liver lipids (fatty acids, TG, and glycerolipids) and reduced the symptoms of lipid accumulation in the liver of type 2 diabetic rats (Yang et al., 2020). Thus, we believe that DOP treatment can improve disorders of obesity-induced lipid metabolism.

Interestingly, only a handful of studies have been published in areas related to DOP and obesity to date. The present study investigated whether DOP could improve IR and lipid metabolism disorders in DIO mice. In order to better demonstrate the therapeutic effects of DOP, we used the ob/ob mouse, a genetic model of obesity. Leptin-deficient (ob/ob) mice are an excellent model of obesity and IR Tomita et al. (1992) and are characterized by elevated insulin and glucose levels and by elevated plasma TG and TC, dyslipidemia, and IR (Dubuc, 1976; Fellmann et al., 2013). Concordant with DIO mice, DOP treatment significantly improved glucose tolerance and insulin clearance of blood glucose in ob/ob mice. Remarkably, DOP has also been shown to inhibit VAT inflammation and liver lipid deposition in the ob/ob mouse model of hereditary obesity. Further, this model was used to further confirm the therapeutic effects of DOP on obesity-related IR and lipid metabolism disorders.

There is a limitation to be noted in our study. Hyperinsulinemic-euglycemic clamp studies are the “gold standard” for evaluating IR, but in our study, we did not adopt this method due to the limitations of the experimental conditions. Nonetheless, an important strength of our study is that it is the first to confirm that DOP can reduce IR and improve abnormal lipid metabolism in obese mice.

In conclusion, DOP can improve insulin sensitivity by up-regulating the expression of PPAR- γ , thus improving obesity-related IR. In addition, DOP can treat disorders of lipid metabolism in obese mice. To our knowledge, our study is the first to confirm that DOP can reduce IR and improve abnormal lipid metabolism in obese mice, which provides a novel therapeutic option for the treatment of obesity-related IR and lipid metabolism disorders.

DATA AVAILABILITY STATEMENT

The original contributions presented in the study are included in the article/Supplementary Material, further inquiries can be directed to the corresponding authors.

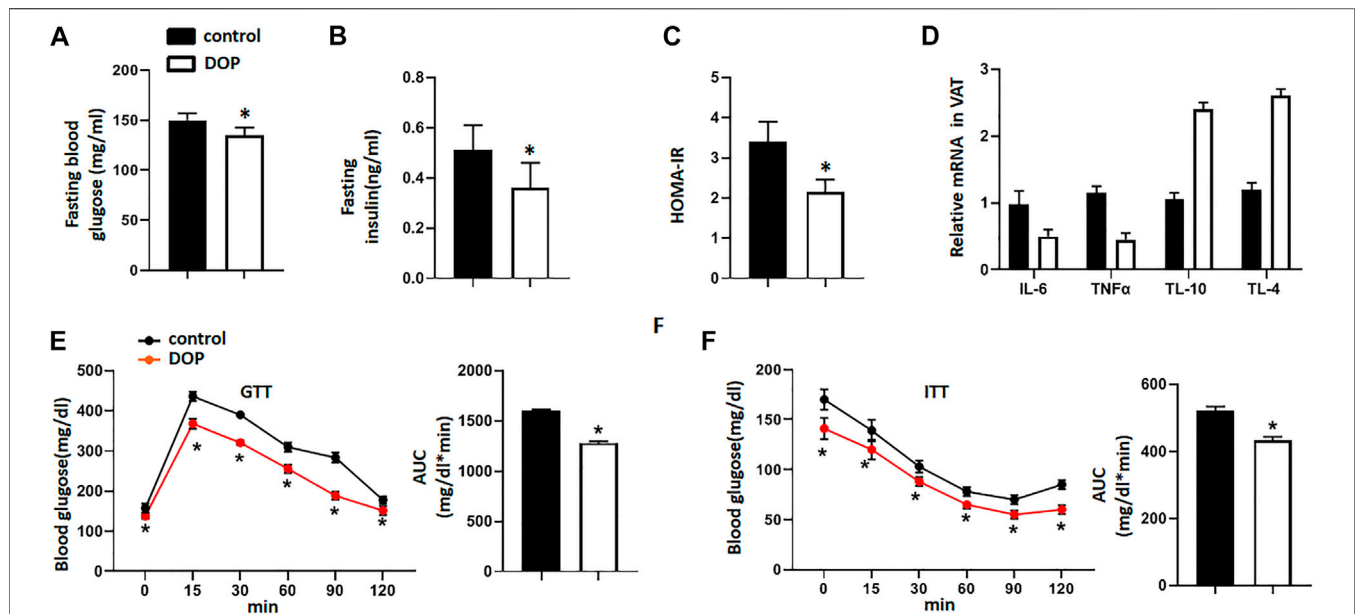


FIGURE 6 | DOP treatment alleviated insulin resistance in ob/ob mice (A–C) The fasting blood glucose levels, fasting serum insulin, and HOMA-IR index of ob/ob mice administered NS or DOP (D) Inflammation-related mRNA levels of VAT in ob/ob mice treated with NS or DOP (E–F). The GTTs and ITTs in ob/ob mice treated with NS or DOP ($n = 5$ per group). AUC: area under curve. Data are presented as mean \pm SD. Statistical significance was calculated using the two-tailed Student's *t*-test. * means $p < 0.05$.

ETHICS STATEMENT

The animal study was reviewed and approved by the Institutional Animal Care and Use Committee of the Laboratory Animal Research Center at Xiangya Medical School of Central South University, China.

AUTHOR CONTRIBUTIONS

Study design: QL, SH; Study conduct: XX, WW, HZ, HL, and JW; Data collection: XX, WW, ZZ, HL, HZ, and JW; Data analysis: QL, XX, XL, and JQ; Data interpretation: QL, XX, XL, and JQ; Drafting manuscript: XX and WW; Revising manuscript content:

QL, XX, ST; Approval of the final manuscript: QL, XX, WW, HZ, HL, XL, JW, ZZ, and SH are responsible for the integrity of the data analysis, and all authors take responsibility for and attest to the integrity of the data analysis. QL and SH are responsible for sharing the editors' comments with the other authors.

FUNDING

This work was supported by the Natural Science Foundation of Hunan Province (2020JJ4799) and National Science and Technology Major Project (Grant No:2020ZX09201-28).

REFERENCES

- Barazzoni, R., Gortan Cappellari, G., Ragni, M., and Nisoli, E. (2018). Insulin Resistance in Obesity: an Overview of Fundamental Alterations. *Eat. Weight Disord.* 23 (2), 149–157. doi:10.1007/s40519-018-0481-6
- Beale, E. G. (2013). Insulin Signaling and Insulin Resistance. *J. Invest. Med.* 61 (1), 11–14. doi:10.2310/JIM.0b013e3182746f95
- Belkina, A. C., and Denis, G. V. (2010). Obesity Genes and Insulin Resistance. *Curr. Opin. Endocrinol. Diabetes Obes.* 17 (5), 472–477. doi:10.1097/MED.0b013e32833c5c48
- Boden, G., Chen, X., Ruiz, J., White, J. V., and Rossetti, L. (1994). Mechanisms of Fatty Acid-Induced Inhibition of Glucose Uptake. *J. Clin. Invest.* 93 (6), 2438–2446. doi:10.1172/JCI117252
- Council of the Obesity, S. (2008). Obesity as a Disease: the Obesity Society Council Resolution. *Obesity (Silver Spring)* 16 (6), 1151. doi:10.1038/oby.2008.246
- Crowe, S., Wu, L. E., Economou, C., Turpin, S. M., Matzaris, M., Hoehn, K. L., et al. (2009). Pigment Epithelium-Derived Factor Contributes to Insulin Resistance in Obesity. *Cel Metab.* 10 (1), 40–47. doi:10.1016/j.cmet.2009.06.001
- Czech, M. P. (2017). Insulin Action and Resistance in Obesity and Type 2 Diabetes. *Nat. Med.* 23 (7), 804–814. doi:10.1038/nm.4350
- De Lorenzo, A., Gratteri, S., Gualtieri, P., Cammarano, A., Bertucci, P., and Di Renzo, L. (2019). Why Primary Obesity Is a Disease? *J. Transl Med.* 17 (1), 169. doi:10.1186/s12967-019-1919-y
- Dubuc, P. U. (1976). The Development of Obesity, Hyperinsulinemia, and Hyperglycemia in Ob/ob Mice. *Metabolism.* 25 (12), 1567–1574. doi:10.1016/0026-0495(76)90109-8
- Esposito, K., Pontillo, A., Giugliano, F., Giugliano, G., Marfella, R., Nicoletti, G., et al. (2003). Association of Low Interleukin-10 Levels with the Metabolic Syndrome in Obese Women. *J. Clin. Endocrinol. Metab.* 88 (3), 1055–1058. doi:10.1210/jc.2002-021437

- Fellmann, L., Nascimento, A. R., Tibiriça, E., and Bousquet, P. (2013). Murine Models for Pharmacological Studies of the Metabolic Syndrome. *Pharmacol. Ther.* 137 (3), 331–340. doi:10.1016/j.pharmthera.2012.11.004
- Frayn, K. N. (1993). Insulin Resistance and Lipid Metabolism. *Curr. Opin. Lipidol.* 4 (3), 197–204. doi:10.1097/00041433-199306000-00004
- Germoush, M. O., Elgebaly, H. A., Hassan, S., Kamel, E. M., Bin-Jumah, M., and Mahmoud, A. M. (2019). Consumption of Terpenoids-Rich Padina Pavonia Extract Attenuates Hyperglycemia, Insulin Resistance and Oxidative Stress, and Upregulates PPAR γ in a Rat Model of Type 2 Diabetes. *Antioxidants*. 9 (1), 22. doi:10.3390/antiox9010022
- Ghorpade, D. S., Ozcan, L., Zheng, Z., Nicoloso, S. M., Shen, Y., Chen, E., et al. (2018). Hepatocyte-secreted DPP4 in Obesity Promotes Adipose Inflammation and Insulin Resistance. *Nature*. 555 (7698), 673–677. doi:10.1038/nature26138
- González-Domínguez, Á., Visiedo-García, F. M., Domínguez-Riscart, J., González-Domínguez, R., Mateos, R. M., and Lechuga-Sancho, A. M. (2020). Iron Metabolism in Obesity and Metabolic Syndrome. *Int. J. Mol. Sci.* 21 (15), 5529. doi:10.3390/ijms21155529
- Gortan Cappellari, G., Zanetti, M., Semolic, A., Vinci, P., Ruozzi, G., Falcione, A., et al. (2016). Unacylated Ghrelin Reduces Skeletal Muscle Reactive Oxygen Species Generation and Inflammation and Prevents High-Fat Diet-Induced Hyperglycemia and Whole-Body Insulin Resistance in Rodents. *Diabetes*. 65 (4), 874–886. doi:10.2337/db15-1019
- Guerre-Millo, M., Rouault, C., Poulain, P., Andre, J., Poitout, V., Peters, J. M., et al. (2001). PPAR- γ Null Mice Are Protected from High-Fat Diet-Induced Insulin Resistance. *Diabetes*. 50 (12), 2809–2814. doi:10.2337/diabetes.50.12.2809
- Hotamisligil, G., Shargill, N., and Spiegelman, B. (1993). Adipose Expression of Tumor Necrosis Factor- α : Direct Role in Obesity-Linked Insulin Resistance. *Science*. 259 (5091), 87–91. doi:10.1126/science.7678183
- Hua, Y.-F., Zhang, M., Fu, C.-X., Chen, Z.-H., and Chan, G. Y. S. (2004). Structural Characterization of a 2-O-Acetylglucosaminan from *Dendrobium Officinale* Stem. *Carbohydr. Res.* 339 (13), 2219–2224. doi:10.1016/j.carres.2004.05.034
- Huang, K., Li, Y., Tao, S., Wei, G., Huang, Y., Chen, D., et al. (2016). Purification, Characterization and Biological Activity of Polysaccharides from *Dendrobium Officinale*. *Molecules*. 21 (6), 701. doi:10.3390/molecules21060701
- Jastreboff, A. M., Kotz, C. M., Kahan, S., Kelly, A. S., and Heymsfield, S. B. (2019). Obesity as a Disease: The Obesity Society 2018 Position Statement. *Obesity*. 27 (1), 7–9. doi:10.1002/oby.22378
- Kern, P. A., Ranganathan, S., Li, C., Wood, L., and Ranganathan, G. (2001). Adipose Tissue Tumor Necrosis Factor and Interleukin-6 Expression in Human Obesity and Insulin Resistance. *Am. J. Physiology-Endocrinology Metab.* 280 (5), E745–E751. doi:10.1152/ajpendo.2001.280.5.E745
- Klop, B., Elte, J., and Cabezas, M. (2013). Dyslipidemia in Obesity: Mechanisms and Potential Targets. *Nutrients*. 5 (4), 1218–1240. doi:10.3390/nu5041218
- Kojta, I., Chacińska, M., and Błachnio-Zabielska, A. (2020). Obesity, Bioactive Lipids, and Adipose Tissue Inflammation in Insulin Resistance. *Nutrients*. 12 (5), 1305. doi:10.3390/nu12051305
- Laaksonen, D. E., Lakka, H. M., Niskanen, L. K., Kaplan, G. A., Salonen, J. T., and Lakka, T. A. (2002). Metabolic Syndrome and Development of Diabetes Mellitus: Application and Validation of Recently Suggested Definitions of the Metabolic Syndrome in a Prospective Cohort Study. *Am. J. Epidemiol.* 156 (11), 1070–1077. doi:10.1093/aje/kwf145
- Lee, Y. S., Kim, J.-W., Osborne, O., Oh, D. Y., Sasik, R., Schenk, S., et al. (2014). Increased Adipocyte O₂ Consumption Triggers HIF-1 α , Causing Inflammation and Insulin Resistance in Obesity. *Cell*. 157 (6), 1339–1352. doi:10.1016/j.cell.2014.05.012
- Li, H., Xie, H., Liu, W., Hu, R., Huang, B., Tan, Y.-F., et al. (2009). A Novel microRNA Targeting HDAC5 Regulates Osteoblast Differentiation in Mice and Contributes to Primary Osteoporosis in Humans. *J. Clin. Invest.* 119 (12), 3666–3677. doi:10.1172/JCI39832
- Liang, J., Chen, S., Chen, J., Lin, J., Xiong, Q., Yang, Y., et al. (2018). Therapeutic Roles of Polysaccharides from *Dendrobium Officinale* on Colitis and its Underlying Mechanisms. *Carbohydr. Polym.* 185, 159–168. doi:10.1016/j.carbpol.2018.01.013
- Liang, J., Li, H., Chen, J., He, L., Du, X., Zhou, L., et al. (2019). *Dendrobium Officinale* Polysaccharides Alleviate colon Tumorigenesis via Restoring Intestinal Barrier Function and Enhancing Anti-tumor Immune Response. *Pharmacol. Res.* 148, 104417. doi:10.1016/j.phrs.2019.104417
- Ling, C., and Rönn, T. (2019). Epigenetics in Human Obesity and Type 2 Diabetes. *Cel. Metab.* 29 (5), 1028–1044. doi:10.1016/j.cmet.2019.03.009
- Lu, M., Sarraf, D. A., Talukdar, S., Sharma, S., Li, P., Bandyopadhyay, G., et al. (2011). Brain PPAR- γ Promotes Obesity and Is Required for the Insulin-Sensitizing Effect of Thiazolidinediones. *Nat. Med.* 17 (5), 618–622. doi:10.1038/nm.2332
- Lumeng, C. N., Bodzin, J. L., and Saltiel, A. R. (2007). Obesity Induces a Phenotypic Switch in Adipose Tissue Macrophage Polarization. *J. Clin. Invest.* 117 (1), 175–184. doi:10.1172/JCI29881
- Meigs, J. B., Wilson, P. W. F., Fox, C. S., Vasan, R. S., Nathan, D. M., Sullivan, L. M., et al. (2006). Body Mass Index, Metabolic Syndrome, and Risk of Type 2 Diabetes or Cardiovascular Disease. *J. Clin. Endocrinol. Metab.* 91 (8), 2906–2912. doi:10.1210/jc.2006-0594
- Moller, D. E., and Kaufman, K. D. (2005). Metabolic Syndrome: a Clinical and Molecular Perspective. *Annu. Rev. Med.* 56, 45–62. doi:10.1146/annurev.med.56.082103.104751
- Ormazabal, V., Nair, S., Elfeky, O., Aguayo, C., Salomon, C., and Zuñiga, F. A. (2018). Association between Insulin Resistance and the Development of Cardiovascular Disease. *Cardiovasc. Diabetol.* 17 (1), 122. doi:10.1186/s12933-018-0762-4
- Randle, P. J., Garland, P. B., Hales, C. N., and Newsholme, E. A. (1963). The Glucose Fatty-Acid Cycle its Role in Insulin Sensitivity and the Metabolic Disturbances of Diabetes Mellitus. *The Lancet*. 281 (7285), 785–789. doi:10.1016/s0140-6736(63)91500-9
- Randle, P. J., Garland, P. B., Newsholme, E. A., and Hales, C. N. (1965). The Glucose Fatty Acid Cycle in Obesity and Maturity Onset Diabetes Mellitus. *Ann. NY Acad. Sci.* 131 (1), 324–333. doi:10.1111/j.1749-6632.1965.tb34800.x
- Randle, P., Newsholme, E., and Garland, P. (1964). Regulation of Glucose Uptake by Muscle. 8. Effects of Fatty Acids, Ketone Bodies and Pyruvate, and of Alloxan-Diabetes and Starvation, on the Uptake and Metabolic Fate of Glucose in Rat Heart and Diaphragm Muscles. *Biochem. J.* 93 (3), 652–665. doi:10.1042/bj0930652
- Reaven, G. M., Hollenbeck, C., Jeng, C. Y., Wu, M. S., and Chen, Y. D. (1988). Measurement of Plasma Glucose, Free Fatty Acid, Lactate, and Insulin for 24 H in Patients with NIDDM. *Diabetes*. 37 (8), 1020–1024. doi:10.2337/diab.37.8.1020
- Samuel, V. T., and Shulman, G. I. (2012). Mechanisms for Insulin Resistance: Common Threads and Missing Links. *Cell*. 148 (5), 852–871. doi:10.1016/j.cell.2012.02.017
- Savage, D. B., Petersen, K. F., and Shulman, G. I. (2007). Disordered Lipid Metabolism and the Pathogenesis of Insulin Resistance. *Physiol. Rev.* 87 (2), 507–520. doi:10.1152/physrev.00024.2006
- Semple, R. K., Chatterjee, V. K., and O'Rahilly, S. (2006). PPAR and Human Metabolic Disease. *J. Clin. Invest.* 116 (3), 581–589. doi:10.1172/JCI28003
- Su, T., Xiao, Y., Xiao, Y., Guo, Q., Li, C., Huang, Y., et al. (2019). Bone Marrow Mesenchymal Stem Cells-Derived Exosomal MiR-29b-3p Regulates Aging-Associated Insulin Resistance. *ACS Nano*. 13 (2), 2450–2462. doi:10.1021/acsnano.8b09375
- Taylor, E. B. (2021). The Complex Role of Adipokines in Obesity, Inflammation, and Autoimmunity. *Clin. Sci. (Lond)*. 135 (6), 731–752. doi:10.1042/CS20200895
- Teixeira da Silva, J. A., Tsavkelova, E. A., Zeng, S., Ng, T. B., Parthibhan, S., Dobránszki, J., et al. (2015). Symbiotic *In Vitro* Seed Propagation of *Dendrobium*: Fungal and Bacterial Partners and Their Influence on Plant Growth and Development. *Planta*. 242 (1), 1–22. doi:10.1007/s00425-015-2301-9
- Tomita, T., Doull, V., Pollock, H. G., and Krizsan, D. (1992). Pancreatic Islets of Obese Hyperglycemic Mice (Ob/ob). *Pancreas*. 7 (3), 367–375. doi:10.1097/00006676-199205000-00015
- Winer, D. A., Luck, H., Tsai, S., and Winer, S. (2016). The Intestinal Immune System in Obesity and Insulin Resistance. *Cel. Metab.* 23 (3), 413–426. doi:10.1016/j.cmet.2016.01.003
- Wu, H., and Ballantyne, C. M. (2017). Skeletal Muscle Inflammation and Insulin Resistance in Obesity. *J. Clin. Invest.* 127 (1), 43–54. doi:10.1172/JCI88880
- Xiao, Y.-Z., Yang, M., Xiao, Y., Guo, Q., Huang, Y., Li, C.-J., et al. (2020). Reducing Hypothalamic Stem Cell Senescence Protects against Aging-Associated Physiological Decline. *Cel. Metab.* 31 (3), 534–548 e535. doi:10.1016/j.cmet.2020.01.002

- Xu, H., Barnes, G. T., Yang, Q., Tan, G., Yang, D., Chou, C. J., et al. (2003). Chronic Inflammation in Fat Plays a Crucial Role in the Development of Obesity-Related Insulin Resistance. *J. Clin. Invest.* 112 (12), 1821–1830. doi:10.1172/JCI1945110.1172/jci200319451
- Yang, J., Chen, H., Nie, Q., Huang, X., and Nie, S. (2020). Dendrobium Officinale Polysaccharide Ameliorates the Liver Metabolism Disorders of Type II Diabetic Rats. *Int. J. Biol. Macromolecules.* 164, 1939–1948. doi:10.1016/j.ijbiomac.2020.08.007
- Yee, H. Y., Yang, J. J., Wan, Y. G., Chong, F. L., Wu, W., Long, Y., et al. (2019). Molecular Mechanisms of Insulin Resistance and Interventional Effects of Chinese Herbal Medicine. *Zhongguo Zhong Yao Za Zhi.* 44 (7), 1289–1294. doi:10.19540/j.cnki.cjcmm.20181105.003
- Ying, W., Riopel, M., Bandyopadhyay, G., Dong, Y., Birmingham, A., Seo, J. B., et al. (2017). Adipose Tissue Macrophage-Derived Exosomal miRNAs Can Modulate *In Vivo* and *In Vitro* Insulin Sensitivity. *Cell.* 171 (2), 372–384 e312. doi:10.1016/j.cell.2017.08.035
- Conflict of Interest:** The authors declare that the research was conducted in the absence of any commercial or financial relationships that could be construed as a potential conflict of interest.
- Copyright © 2021 Qu, Tan, Xie, Wu, Zhu, Li, Liao, Wang, Zhou, Huang and Lu. This is an open-access article distributed under the terms of the Creative Commons Attribution License (CC BY). The use, distribution or reproduction in other forums is permitted, provided the original author(s) and the copyright owner(s) are credited and that the original publication in this journal is cited, in accordance with accepted academic practice. No use, distribution or reproduction is permitted which does not comply with these terms.



Variable Secondary Metabolite Profiles Across Cultivars of *Curcuma longa* L. and *C. aromatica* Salisb.

Poonam Kulyal, Satyabrata Acharya[†], Aditya B. Ankari[†], Praveen K. Kokkiripati, Sarada D. Tetali* and Agepati S. Raghavendra*

Department of Plant Sciences, School of Life Sciences, University of Hyderabad, Hyderabad, India

OPEN ACCESS

Edited by:

Sayeed Ahmad,
Jamia Hamdard University, India

Reviewed by:

Nicholas John Sadgrove,
Royal Botanic Gardens, Kew,
United Kingdom
Abdul Akbar,
Siksha 'O' Anusandhan University,
India

*Correspondence:

Sarada D. Tetali
stetali@uohyd.ac.in
Agepati S. Raghavendra
asrsl@uohyd.ernet.in
as_raghavendra@yahoo.com

[†]These authors have contributed
equally to this work

Specialty section:

This article was submitted to
Ethnopharmacology,
a section of the journal
Frontiers in Pharmacology

Received: 27 January 2021

Accepted: 24 May 2021

Published: 30 June 2021

Citation:

Kulyal P, Acharya S, Ankari AB,
Kokkiripati PK, Tetali SD and
Raghavendra AS (2021) Variable
Secondary Metabolite Profiles Across
Cultivars of *Curcuma longa* L. and *C.*
aromatica Salisb..
Front. Pharmacol. 12:659546.
doi: 10.3389/fphar.2021.659546

Background: *Curcuma* spp. (Zingiberaceae) are used as a spice and coloring agent. Their rhizomes and essential oils are known for medicinal properties, besides their use in the flavoring and cosmetic industry. Most of these biological activities were attributed to volatile and nonvolatile secondary metabolites present in the rhizomes of *Curcuma* spp. The metabolite variations among the species and even cultivars need to be established for optimized use of *Curcuma* spp.

Objectives: We compared the phytochemical profiles of rhizomes and their essential oils to establish the variability among seven cultivars: five of *Curcuma longa* L. (Alleppey Supreme, Duggirala Red, Prathibha, Salem, Suguna) and two of *C. aromatica* Salisb. (Kasturi Araku, Kasturi Avidi). The GC-MS and LC-MS-based analyses were employed to profile secondary metabolites of these selected cultivars.

Methods: Rhizomes of *Curcuma* spp. were subjected to hydro-distillation to collect essential oil and analyzed by GC-MS. The methanol extracts of fresh rhizomes were subjected to LC-MS analyses. The compounds were identified by using the relevant MS library databases as many compounds as possible.

Results: The essential oil content of the cultivars was in the range of 0.74–1.62%. Several compounds were detected from the essential oils and rhizome extracts by GC-MS and LC-MS, respectively. Of these, 28 compounds (13 from GCMS and 15 from LCMS) were common in all seven cultivars, e.g., α -thujene, and diarylheptanoids like curcumin. Furthermore, a total of 39 new compounds were identified from *C. longa* L. and/or *C. aromatica* Salisb., most of them being cultivar-specific. Of these compounds, 35 were detected by GC-MS analyses of essential oils, 1,2-cyclohexanediol, 1-methyl-4-(1-methylethyl)-, and santolina alcohol, to name a few. The other four compounds were detected by LC-MS of the methanolic extracts of the rhizomes, e.g., kaempferol-3,7-O-dimethyl ether and 5,7,8-trihydroxy-2',5'-dimethoxy-3',4'-methylene dioxisoflavanone.

Abbreviations: CU, curcumin; cvs, cultivars; DMC, demethoxy curcumin; BDMC, bisdemethoxycurcumin.

Conclusions: We identified and recorded the variability in the metabolite profiles of essential oils and whole rhizome extracts from the seven cultivars of *Curcuma longa* L. and *C. aromatica* Salisb. As many as 39 new metabolites were detected in these seven Indian cultivars of *Curcuma* spp. Many of these compounds have health benefits.

Keywords: *Curcuma longa* L., *Curcuma aromatica* Salisb, essential oil, metabolomics, secondary metabolites, GC-MS, LC-MS

INTRODUCTION

Turmeric (*Curcuma longa* L.) is a perennial rhizomatous herb that belongs to the family Zingiberaceae (Prasath et al., 2018). It has been used traditionally in India for its medicinal value and as a spice (Srinivasan et al., 2004; Aggarwal et al., 2007; Esatbeyoglu et al., 2012). In Ayurvedic medicine, turmeric is used internally (as a stomachic, tonic, and blood purifier) or externally (prevention and treatment of skin diseases) (Gounder and Lingamallu, 2012). Turmeric was scientifically validated for several pharmacological benefits, including antioxidant, anti-inflammatory, and chemoprotective properties (Miquel et al., 2002; Krup et al., 2013; Kanase and Khan, 2018; Umar et al., 2020). The rhizomes of turmeric are enriched with several bioactive metabolites, though the attention was mostly on curcuminoids. Besides curcumin (a curcuminoid), the essential oil of *C. longa* L. showed antimicrobial activity and ability to suppress aflatoxins production (Ferreira et al., 2013).

Out of 110 species of genus *Curcuma*, only ~20 species were used so far for phytochemical studies (Nahar and Sarker, 2007). *Curcuma longa* L. is popularly known as turmeric, while *C. aromatica* Salisb. and *C. caesia* Roxb. are known as wild turmeric and black turmeric, respectively. *C. longa* L. and a few other species, including *C. aromatica* Salisb., produce curcumin, a yellow colored curcuminoid. So far, at least 235 compounds, primarily phenolics, terpenoids, and alkaloids, were identified from *Curcuma* spp. (Li et al., 2011). About 70 varieties of *C. longa* L. are cultivated in India (Sasikumar, 2005; Parthasarathy and Chempakam, 2008), but very few are chemically profiled.

The essential oil of *Curcuma* spp. is used in traditional medicine for many ailments (Dosoky and Setzer, 2018). The volatile component of *C. longa*'s rhizome is responsible for its aromatic flavor and odor (Gounder and Lingamallu, 2012). Its essential oil is considered safe for human use (Tisserand and Young, 2013). The oils of *C. longa* L. and *C. aromatica* Salisb. have applications in the food and pharmaceutical industries due to their antioxidant, antibacterial, and anti-inflammatory properties (Dosoky and Setzer, 2018). The essential oil also improved the bioavailability of curcumin, thereby its bioactivity (Shishu and Maheshwari, 2010). Preliminarily clinical trials indicated that the essential oil from *C. longa* L. and *C. aromatica* Salisb. was helpful against cancer, asthma, and other ailments (Cheng et al., 1999; Joshi et al., 2003; Li Y. et al., 2009). Thus, there is a need to identify high-yielding cultivars containing curcuminoids and essential oil.

Since the pharmacological properties of *Curcuma* spp. are dependent on their chemical profiles, studies on the chemical constituents of turmeric/wild turmeric and their essential oils gained significance. Thin-layer chromatography (TLC)

is one of the methods employed to quantify curcumin (Setyaningsih et al., 2016) and other curcuminoids (Phattanawasin et al., 2009) in *Curcuma longa* L. A few different techniques used were HPTLC (Pathania et al., 2006; Paramasivam et al., 2009), nuclear magnetic resonance (NMR) spectroscopy (Li W. et al., 2009), and the HPLC method (Kulyal et al., 2016).

Our present study on metabolite profiles would pave the way for metabolomics by providing the identity of several metabolites. Metabolomics is a practical approach for the comprehensive profiling and comparison of metabolites in plant systems (De Vos et al., 2007). It is crucial for quality evaluation and scientific validation of medicinal plants and their products (Mukherjee et al., 2016). Mainly information on secondary metabolites of medicinal plants/spices is of great importance in health, food, and nutrition sectors, due to the antioxidant nature, color, or flavor of these secondary compounds (Beekwilder et al., 2005; Dixon et al., 2006; Hall, 2006). The quality of turmeric and other spices depends on factors, such as cultivation, collection, storage, milling, and processing, apart from genetics and adulteration issues. Therefore, metabolomics provides a practical approach for quality control (Mukherjee et al., 2016; Tetali et al., 2021).

Over the past decade, several methods suitable for large-scale analysis of metabolites in plant extracts were developed (Dixon et al., 2006; Hall, 2006). However, to date, no single analytical method can successfully detect the entire metabolome of higher plants, especially of medicinal and aromatic plants, as they are highly rich in chemically diverse metabolites (Tetali et al., 2021). The GC-MS and LC-MS techniques mutually complement each other in unraveling secondary metabolomes comprising a wide range of volatile and nonvolatile compounds. These compounds belonged to terpenes, phenolic acids, phenylpropanoids, saponins, alkaloids, polyamines, and their derivatives (Huhman and Sumner, 2002; Moco et al., 2006).

Essential oils from different *Curcuma* species, including *C. longa* L. and *C. aromatica* Salisb, were studied for their chemical constituents (Choudhury et al., 1996; Angel et al., 2014; Nampoothiri et al., 2015; Dosoky and Setzer, 2018) to establish their variability. Variation in the volatile compositions of *Curcuma* spp. such as *C. longa* L. and *C. zedoaria*, was done using GC-MS (Dosoky et al., 2019). A combination of GC-MS and LC-MS techniques was used for metabolite analysis of *C. domestica* L. (*C. longa* L.) (Herebian et al., 2009). In the present study, the volatile (essential oil) and nonvolatile (total extract) components of the fresh rhizome of the seven cultivars of *Curcuma* spp. were analyzed by the GC-MS and LC-MS techniques. The present study is the first report revealing such detailed

TABLE 1 | Essential oil content and total number of compounds detected by GC-MS in the rhizomes of *Curcuma* species.

Sl. No.	Cultivar (species)	Essential oil (%)	Identified (Reported in <i>Curcuma</i> spp. or another plant species)	Unidentified	
				Unknown	Not reported from any plant species
1	Alleppey Supreme (<i>C. longa</i> L.)	1.42	31	58	111
2	Duggirala Red (<i>C. longa</i> L.)	0.74	36	56	108
3	Prathibha (<i>C. longa</i> L.)	1.20	44	60	96
4	Salem (<i>C. longa</i> L.)	1.00	30	39	131
5	Suguna (<i>C. longa</i> L.)	0.80	35	51	114
6	Kasturi Araku (<i>C. aromatica</i> Salisb.)	0.78	29	64	107
7	Kasturi Avidi (<i>C. aromatica</i> Salisb.)	1.62	31	60	109

metabolite profiles of the selected cultivars to the best of our knowledge. These cultivars, except Alleppey Supreme, are typically cultivated in Telangana and Andhra Pradesh, and these states are among the largest producers of turmeric in India (Parthasarathy and Chempakam, 2008).

Most of the studies worldwide on *Curcuma* spp., for their curative properties, were with *C. longa* L., followed by *C. aromatica* Salisb, *C. aeruginosa* Roxb. (Simoh and Zainal, 2015), and *C. kwangsiensis* S. K. Lee & C. F. Liang (Zeng et al., 2009). Several cultivars exist within these species, which vary in their chemical profiles. The present article is the first attempt to characterize both volatile (essential oil) and nonvolatile (crude extract) components of fresh rhizomes of seven cultivars of *Curcuma* spp. by the GC-MS and LC-MS techniques. Our results using GC-MS and LC-MS analyses revealed high variability in their metabolite profiles of seven cultivars of genus *Curcuma*. We emphasize that such an approach could be exploited to distinguish cultivars for a specific application based on their metabolite profile.

MATERIALS AND METHODS

Materials and Reagents

LC-MS grade methanol, water, and acetonitrile were purchased from Fisher Scientific (Pittsburgh, PA, United States). Ammonium formate, formic acid, 4-fluoro-4'-hydroxy benzophenone (97%), and *n*-hexane were from Sigma-Aldrich, India. Anhydrous sodium sulfate (99.99%) was from Merck Millipore, India.

Fresh rhizomes of four cultivars of *Curcuma longa* L. (Duggirala Red, Prathibha, Salem, and Suguna) and two cultivars of *C. aromatica* Salisb. (Kasturi Araku and Kasturi Avidi) were collected from Turmeric Research Station, Kammarpally, Telangana State, India. Alleppey Supreme cultivar of *C. longa* L. was from the Indian Institute of Spices Research, Marikunnu (IISR) Kozhikode, Kerala, India. The mature rhizome samples were collected during the postharvest

season of turmeric (May–Jun) in 2011 and 2012 and cryopreserved at -80°C until extraction and analysis.

Isolation of Essential Oil by Hydrodistillation for GC-MS Analysis

50 g each of fresh turmeric rhizome of five cultivars of *C. longa* L. cvs. Alleppey Supreme, Duggirala Red, Prathibha, Salem, Suguna, and two cultivars of *C. aromatica* Salisb. cvs. Kasturi Araku and Kasturi Avidi were taken out from a -80°C freezer, made into pieces, and ground in a pestle with a mortar to a fine powder under liquid nitrogen. The powder was subjected to hydrodistillation in a Clevenger-type apparatus for 7 h. The essential oil obtained after distillation was dried over anhydrous sodium sulfate and kept at -80°C until GC-MS analysis.

GC-MS Running Conditions and Metabolite Identification

The chemical composition of the *Curcuma* spp. essential oil was analyzed by the GC-MS technique using Agilent 7890 A gas chromatograph coupled with a Leco Pegasus HT TOF mass spectrometer equipped with a $29.8\text{ m} \times 320\text{ }\mu\text{m}$ HP-5MS 5% phenyl methyl siloxane capillary column with $0.25\text{ }\mu\text{m}$ film thickness. The oven temperature was programmed at 65°C for 2 min and then increased from 65 to 90°C at $5^{\circ}\text{C}/\text{min}$ (held for 3 min). Then the temperature was increased from 90 to 103°C (held for 3 min) and from 103 to 150°C (held for 15 min) at $20^{\circ}\text{C}/\text{min}$ and $8^{\circ}\text{C}/\text{min}$, respectively. The temperature was raised finally from 150 to 280°C at $20^{\circ}\text{C}/\text{min}$. The injector, interphase, and ion source were maintained at 250°C , 280°C , and 250°C , respectively. The detector voltage was 1500 V. A solvent delay of 2 min was selected. One microliter (diluted with *n*-hexane; 1:10) of essential oil sample was injected into the GC-MS system using split mode (50: 1). Helium was used as a carrier gas at a flow rate of 1 ml/min. GC-MS data were measured at 70 eV; mass scan 40–1000 amu.

The compounds were identified by comparing their mass spectra with the data available in the literature, National

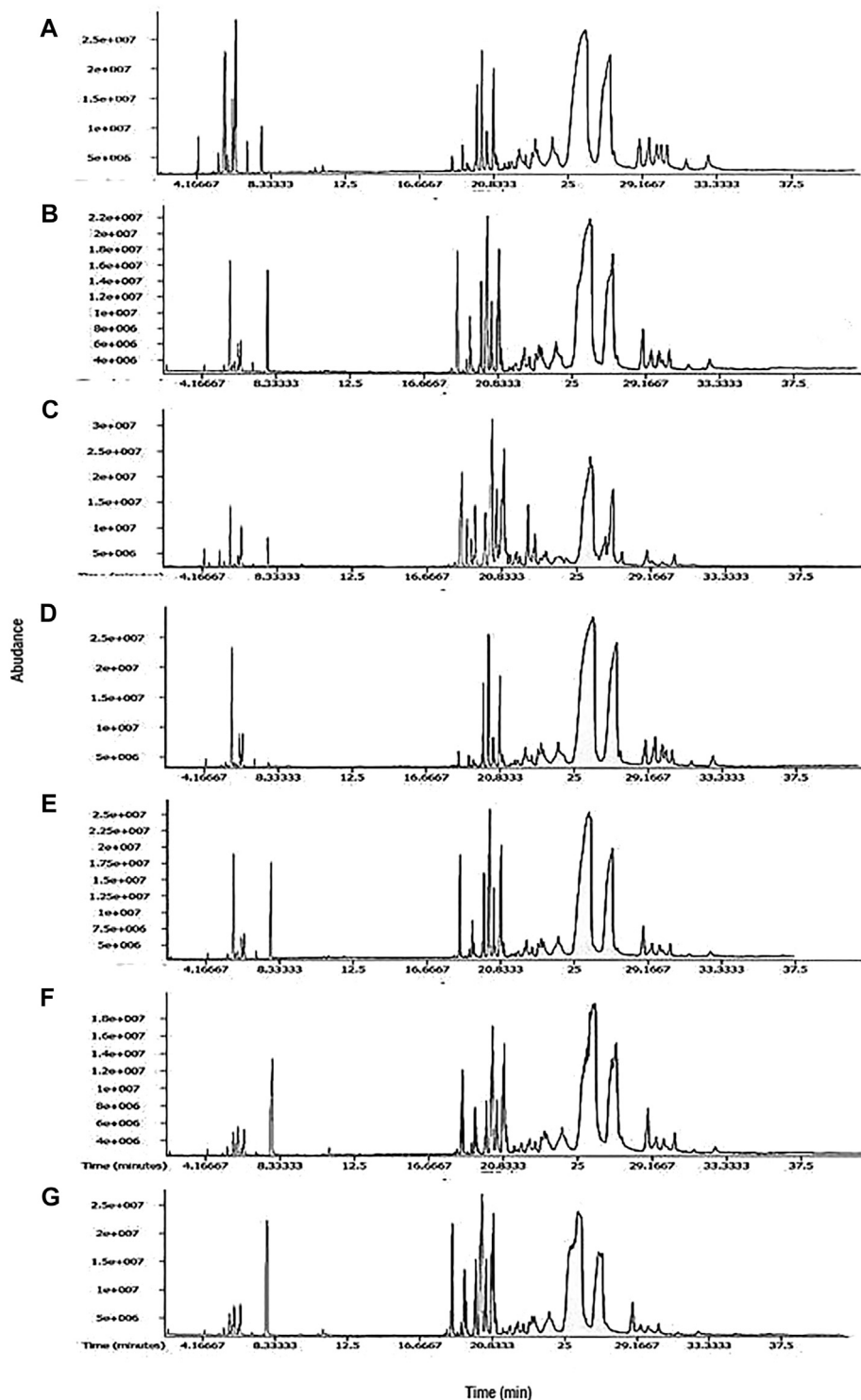


FIGURE 1 | Representative TIC chromatograms from GCMS of essential oil from cultivars (A) Alleppey Supreme, (B) Duggirala Red, (C) Prathibha, (D) Salem, (E) Suguna of *Curcuma longa* L. and cvs. (F) Kasturi Araku, (G) Kasturi Avidi of *C. aromatica* Salisb.

Institute of Standards Technology NIST, and Leco-Fiehn Rtx5 libraries. The compounds originated from the GC-MS data file were identified by matching most resembling spectra with the

NIST library. Each search produced a hit list of compounds according to match factor or similarity with the library spectra. All the compounds showing similarity more than 70% with the

TABLE 2 | Cultivar-specific compounds identified, in one of the seven cultivars of *Curcuma longa* L. or *C. aromatica* Salisb. by GC-MS in the essential oil from rhizomes. The structures of the compounds (serial numbers from 1 to 23) are given in **Figure 2** (panel numbers: 1–23), and this is the first report of these compounds from the genus *Curcuma* L. These compounds, however, were reported from genus other than *Curcuma* L. The compounds from serial numbers 24 to 41 are already reported in *Curcuma* species. Structures for few compounds (serial numbers 24–30) are given in **Figure 3** (panel numbers: 1–7). Abbreviations used: AS, Alleppey Supreme; DR, Duggirala Red; PR, Prathibha; SA, Salem; SU, Suguna; KAr, Kasturi Araku; KAv, Kasturi Avidi.

Sl. No.	Compound name	Cultivar	RT (Min)	Area/abundance	Formula	Mass	Mass fragmentations	Class of compound	Reported from plant species	References
1	1,2-Cyclohexanediol, 1-methyl-4-(1-methylethyl)-	AS	6.38	958955880	C ₁₀ H ₂₀ O ₂	172.146	43, 71, 111 154	Monoterpenoid	<i>Citrus medica</i> L. Leaf and peel essential oil	Bhuiyan et al. (2009)
2	Trans, trans-Octa-2,4-dienyl acetate	AS	8.22	84981	C ₁₀ H ₁₆ O ₂	168.115	43, 77, 79	Dienyl acetate	<i>Kaempferia galanga</i> L. Dried rhizomes	Othman et al. (2006)
3	Phenol, 2-methoxy-3-(2-propenyl)-	AS	17.05	200016	C ₁₀ H ₁₂ O ₂	164.083	77, 131 164	Phenolic monoterpenoid	<i>Dalbergia stevensonii</i> Standl. Wood extracts	Jiang et al. (2018)
4	3-Isopropyl-4-methyl-1-pentyn-3-ol	DR	13.59	805101	C ₉ H ₁₆ O	140.120	43, 97 107	Alcohol constituent	<i>Anethum sowa</i> Roxb. ex, Fleming Leaf and stem essential oil	Saleh-e-in et al. (2010)
5	5,9-Tetradecadiyne	DR	19.45	11283632	C ₁₄ H ₂₂	190.172	41, 105, 147	Unsaturated hydrocarbon	<i>Ferula vesceritensis</i> Coss. & Durieu ex Trab. Leaves	Zellagui et al. (2012)
6	Naphthalene, 5-butyl-1,2,3,4-tetrahydro-	DR	20.62	1290163	C ₁₄ H ₂₀	188.156	91, 145 188	Tetralin Type	<i>Meconopsis punicea</i> Maxim. and <i>M. delavayi</i> (Franch.) Franch. Ex Prain, essential oil	Yuan et al. (2003)
7	Santolina alcohol	DR	23.63	547909	C ₁₀ H ₁₈ O	154.135	59, 81 121	Tertiary alcohol	<i>Achillea filipendulina</i> Lam., aerial part	Sharopov and Setzer (2010)
8	2-Pentanone, 4-mercapto-4-methyl-	PR	5.32	1330293	C ₆ H ₁₂ OS	132.060	43, 55 132	Ketone	<i>Camellia sinensis</i> (L.) Kuntze	Kumazawa et al. (2005)
9	8-Methylene-3-oxatricyclo[5.2.0.0(2,4)]nonane-	PR	11.72	25554	C ₉ H ₁₂ O	136.08	40, 79, 92	Hydrocarbon	<i>Schisandra chinensis</i> (Turcz.) Baill., essential oil dried fruit	Wang et al. (2005)
10	7-Tetracyclo[6.2.1.0(3,8)0(3,9)]undecanol, 4,4,11,11 tetramethyl-	PR	19.16	21297856	C ₁₅ H ₂₄ O	220.182	77, 119 159	Sesquiterpene alcohol	<i>Cyperus articulatus</i> L., essential oil roots/rhizome	Metuge et al. (2014)
11	Bicyclo(2.2.1)hept-2-ene, 2,3-dimethyl-	PR	19.41	23461594	C ₉ H ₁₄	122.109	79, 94 122	Cyclic hydrocarbon	<i>Abies alba</i> Mill leaf and twig	Yang et al. (2009)
12	1H-3a,7-methanoazulene, 2,3,4,7,8,8a-hexahydro-3,6,8,8-tetramethyl-, [3R-(3a,3a,7a,8a)]-	PR	19.69	1483176	C ₁₅ H ₂₄	204.187	93, 119 161	Sesquiterpene	<i>Lindera aggregata</i> (Sims) Kosterm., essential oil	Hong (2011)
13	Cholesta-8,24-dien-3-ol, 4-methyl-, (3a,4a)-	PR	21.56	84686714	C ₂₈ H ₄₆ O	398.354	69, 105 119	Triterpenoid	<i>Parkia speciosa</i> Hassk. seed	Salman et al. (2006)
14	4-Ethylphenethylamine	PR	25.88	507899185	C ₁₀ H ₁₅ N	149.120	63, 120	Amine	<i>Psidium guajava</i> L. stem bark essential oil	Fasola et al. (2011)
15	Cyclohexanol, 2-methyl-5-(1-methylethenyl)-	PR	26.57	3965291	C ₁₀ H ₁₇ O	154.135	67, 107 136	Monoterpenoid	<i>Mentha spicata</i> L. aerial parts	Mohammed et al. (2017)
16	Cyclohexane, 1,2-dimethyl-3,5-bis(1-methylethenyl)-	PR	26.59	26170712	C ₁₄ H ₂₄	192.187	107, 149	Monoterpenoid	<i>Rhanterium adpressum</i> Coss. & Durieu Aerial parts	Kala et al. (2009)
17	5,8,11,14-Eicosatetraenoic acid, phenylmethyl ester, (all-Z)-	SA	5.39	15244294	C ₂₇ H ₃₈ O ₂	394.287	67, 91 205	Mster	<i>Petiveria alliacea</i> L., whole plant	Sathiyabalan et al. (2014)
18	11-Dodecen-2-one	SA	36.83	511982	C ₁₂ H ₂₂ O	182.167	43, 124 182	Ketone	<i>Ficus hispida</i> L. f Fresh male and female receptive figs, leaves	Song et al. (2001)
19	E-11-Tetradecenoic acid	SA	37.15	335669	C ₁₄ H ₂₆ O ₂	226.193	41, 55, 69	Fatty acid	<i>Coriandrum sativum</i> L., leaf oil	Bhuiyan et al. (2009)
20	2-Nonen-4-yn-1-ol, (Z)-	SU	10.68	287984	C ₉ H ₁₄ O	154.135	41, 67	Alcohol	<i>Alpinia speciosa</i> (J.C. Wendl.) K. Schum	Ho (2010)

(Continued on following page)

TABLE 2 | (Continued) Cultivar-specific compounds identified, in one of the seven cultivars of *Curcuma longa* L. or *C. aromatica* Salisb. by GC-MS in the essential oil from rhizomes. The structures of the compounds (serial numbers from 1 to 23) are given in Figure 2 (panel numbers: 1–23), and this is the first report of these compounds from the genus *Curcuma* L. These compounds, however, were reported from genus other than *Curcuma* L. The compounds from serial numbers 24 to 41 are already reported in *Curcuma* species. Structures for few compounds (serial numbers 24–30) are given in Figure 3 (panel numbers: 1–7). Abbreviations used: AS, Alleppey Supreme; DR, Duggirala Red; PR, Prathibha; SA, Salem; SU, Suguna; KAr, Kasturi Araku; KAv, Kasturi Avidi.

Sl. No.	Compound name	Cultivar	RT (Min)	Area/abundance	Formula	Mass	Mass fragmentations	Class of compound	Reported from plant species	References
21	3-Cyclohexen-1-one, 3,5,5-trimethyl-	SU	21.81	10709364	C ₉ H ₁₄ O	138.104	95, 138 96, 138	Cyclohexenone	Seeds and leaves <i>Crocus sativus</i> L. Dried saffron	D'Auria et al. (2006)
22	6,10-Dodecadien-1-yn-3-ol, 3,7,11-trimethyl-	SU	23.27	18320904	C ₁₅ H ₂₄ O	220.182	41,67, 95, 138	Sesquiterpenoid	<i>Hiptage benghalensis</i> (L.) Kurz, leaves	Venkataramani and Chinnagounder (2012)
23	3-Octen-5-yne, 2,7-dimethyl-, (Z)-	KAv	7.91	132889991	C ₁₀ H ₁₆	136.125	93, 121, 136	Monoterpene	<i>Litsea glutinosa</i> (Lour.) C.B. Rob Fruit oil	Chowdhury et al. (2008b)
24	Aromadendrene	PR	21.68	32839807	C ₁₅ H ₂₄	204.187	41,67,161	Hydrocarbon	<i>Curcuma purpurascens</i> Blume, rhizome, essential oil	Hong et al. (2014)
25	Isoborneol	PR	10.16	931077	C ₁₀ H ₁₈ O	154.135	41,67,95	Monoterpenoid	<i>Curcuma aromatica</i> Salisb, rhizome Essential oil	Sasikumar (2005)
26	β-Elementene	PR	17.87	8265459	C ₁₅ H ₂₄	204.187	41,67,193	Sesquiterpene	<i>Curcuma longa</i> L., rhizome Essential oil	Ma and Gang (2006)
27	α-Santalene	PR	19.15	167463111	C ₁₅ H ₂₄	204.187	41,94, 122	Sesquiterpene	<i>Curcuma longa</i> L., rhizome Essential oil	Chowdhury et al. (2008a)
28	2-Tridecanone	PR	36.82	145399		198.198	43,57	Ketone	<i>Curcuma albiflora</i> Thwaites, rhizome Essential oil	Herath et al. (2017)
29	Nonanoic acid	SU	37.82	1054190	C ₉ H ₁₈ O ₂	158.1307	41,60,129	Fatty acid	<i>Curcuma longa</i> L., rhizome Essential oil	Nieman et al. (2012)
30	Eucalyptol	KAr	6.34	73923505	C ₁₀ H ₁₈ O	154.135	51,71, 139	Monoterpene	<i>Curcuma longa</i> L., rhizome Essential oil	Chowdhury et al. (2008a)
31	Carvacrol	AS	15.46	800060	C ₁₀ H ₁₄ O	150.104	91, 135	Monoterpene	<i>Curcuma longa</i> L., rhizome, essential oil	Awasthi and Dixit (2009)
32	endo-Borneol	PR	25.95	762477	C ₁₀ H ₁₈ O	154.135	95, 140	Monoterpene	<i>Curcuma longa</i> L., rhizome Essential oil	Chowdhury et al. (2008a)
33	1,3,5-Cycloheptatriene, 3,7,7-trimethyl-	KAv	22.26	44959671	C ₁₀ H ₁₄	134.109.120	41,91,119	Cyclic hydrocarbon	<i>Curcuma longa</i> L., rhizome Essential oil	Chowdhury et al. (2008a)
34	p-Cymen-8-ol	KAr	11.08	28783214	C ₁₀ H ₁₄ O	150.104	51,91, 135	Monoterpenoid	<i>Curcuma longa</i> L., rhizome Essential oil	Chowdhury et al. (2008a)
35	Camphor	PR	9.68	7985363	C ₁₀ H ₁₆ O	152.120	41,95,152	Terpenoid ketone	<i>Curcuma longa</i> L., rhizome Essential oil	Leela et al. (2002)
36	α-Bisabolol	PR	22.60	26108003	C ₁₅ H ₂₆ O	222.198	41,69, 119	Sesquiterpenoid	<i>Curcuma longa</i> L., rhizome Essential oil	Chowdhury et al. (2008a)
37	α-Elementone	PR	22.99	5795701	C ₁₅ H ₂₂ O	218.167	67,119, 216	Sesquiterpene	<i>Curcuma longa</i> L., rhizome Essential oil	Singh et al. (2010)
38	Caryophyllene oxide	PR	21.85	84236617	C ₁₅ H ₂₄ O	220.182	21,96,138	Sesquiterpenoid oxide	<i>Curcuma longa</i> L., rhizome Essential oil	Chowdhury et al. (2008a)
39	Citral	KAr	10.81	4942325	C ₁₀ H ₁₆ O	152.120	69,119	Monoterpene	<i>Curcuma longa</i> L., rhizome Essential oil	Chowdhury et al. (2008a)
40	Neoisolongifolene, 8,9-dehydro-	KAr	20.92	956644398	C ₁₅ H ₂₄	204.187	44,131, 187	Bicyclic hydrocarbon	<i>Curcuma longa</i> L., rhizome Essential oil	Chowdhury et al. (2008a)
41	Sabinene hydrate	KAv	19.81	30005835	C ₁₀ H ₁₈ O	154.135	79,93,121	Monoterpene	<i>Zingiber Officinale</i> Roscoe, rhizome essential oil	Koo and Gang (2012)

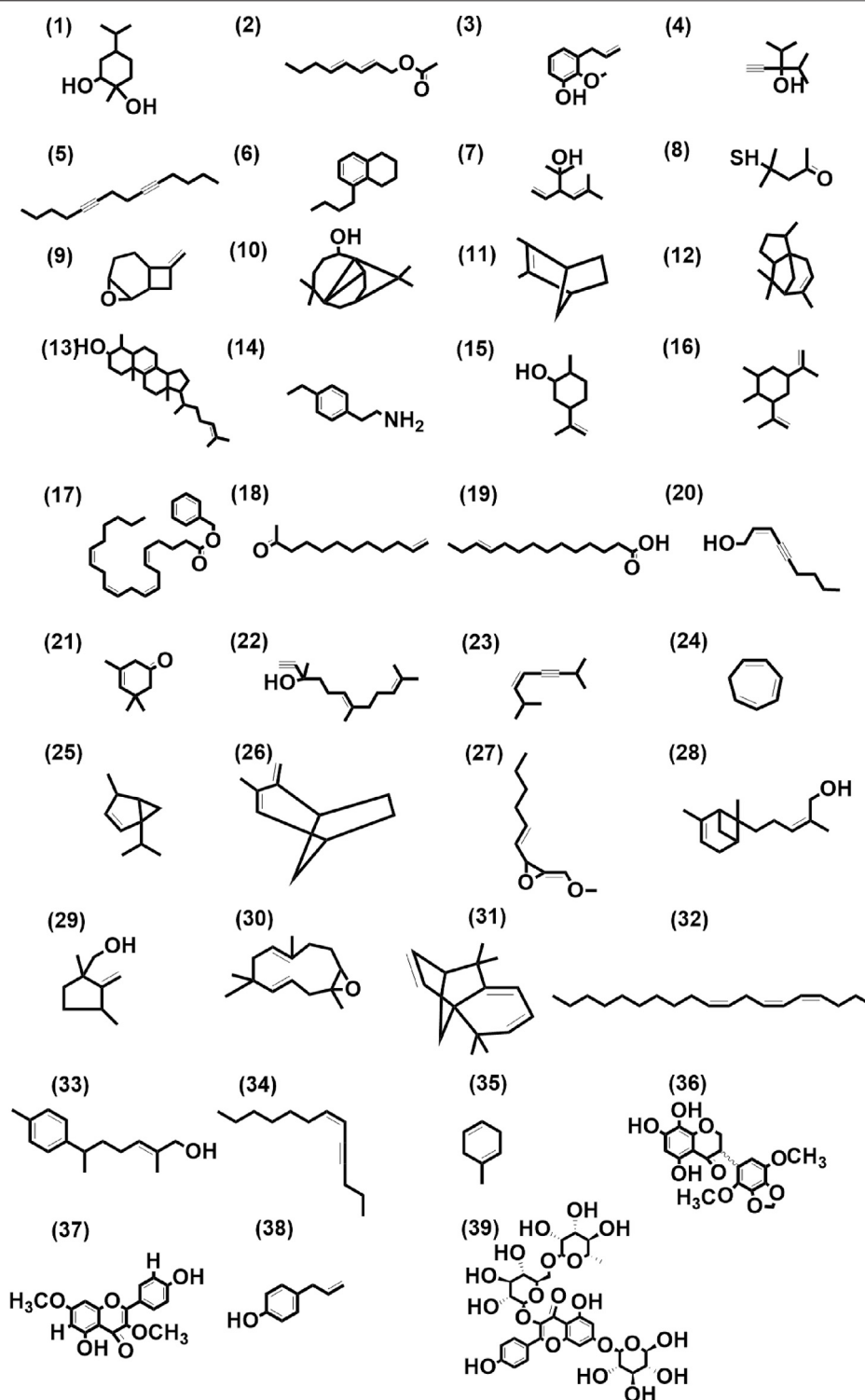


FIGURE 2 | Structures of first-time reported (total 39) from the genus *Curcuma*, identified from cultivars of *Curcuma longa* L. and *C. aromatica* Salisb. detected in essential oil (panel numbers 1–23 and 24–35 corresponding to serial numbers 1–23 and 1–12 of **Tables 2, 3** respectively) and rhizome extracts (panel numbers 36 and 37–39 corresponding to serial numbers 1 and 1–3 of **Tables 6, 7** respectively) by GC-MS and LC-MS, respectively. Details of all these compounds are given in **Supplementary Tables S3, S4**. (1) 1,2-Cyclohexanediol, 1-methyl-4-(1-methylethyl)-, (2) trans, trans-octa-2,4-dienyl acetate, (3) phenol, 2-methoxy-3-(2-propenyl)-, (4) 3-isopropyl-4-methyl-1-pentyn-3-ol, (5) 5,9-tetradecadiyne, (6) naphthalene, 5-butyl-1,2,3,4-tetrahydro-, (7) santolina alcohol, (8) 2-pentanone, 4-mercapto-4-methyl-, (9) 8-methylene-3-oxatricyclo[5.2.0.0(2,4)]nonane, (10) 7-tetracyclo[6.2.1.0(3,8)0(3,9)]undecanol, 4,4,11,11 tetramethyl-, (11) bicyclo(2.2.1)hept-

(Continued)

FIGURE 2 | 2-ene, 2,3-dimethyl-, (12) 1H-3a,7-methanoazulene, 2,3,4,7,8,8a-hexahydro-3,6,8,8-tetramethyl-, [3R-(3a,3aá,7á,8aá)]-, (13) cholesta-8,24-dien-3-ol, 4-methyl-, (3á,4á)-, (14) 4-ethylphenethylamine, (15) cyclohexanol, 2-methyl-5-(1-methylethenyl)-, (16) cyclohexane, 1,2-dimethyl-3,5-bis(1-methylethenyl)-, (17) 5,8,11,14-eicosatetraenoic acid, phenylmethyl ester, (all-Z)-, (18) 11-dodecen-2-one, (19) E-11-tetradecenoic acid, (20) 2-nonen-4-yn-1-ol, (Z)-, (21) 3-cyclohexen-1-one, 3,5,5-trimethyl-, (22) 6,10-dodecadien-1-yn-3-ol, 3,7,11-trimethyl-, (23) 3-octen-5-yne, 2,7-dimethyl-, (Z)-, (24) 1,3,5-cycloheptatriene, (25) bicyclo(3.1.0)hexane, 4-methyl-1-(1-methylethyl)-, didehydro deriv., (26) bicyclo(3.2.1)oct-2-ene, 3-methyl-4-methylene-, (27) oxirane, 2-(hexyn-1-yl)-3-methoxymethylene-, (28) bergamotol, Z- α -trans-, (29) (1,3-dimethyl-2-methylene-cyclopentyl)-methanol, (30) 12-oxabicyclo(9.1.0)dodeca-3,7-diene, 1,5,5,8-tetramethyl-, [1R-(1R*,3E,7E,11R*)]-, (31) isolongifolene, 4,5,9,10-dehydro-, (32) Z,Z,Z-4,6,9-nonadecatriene, (33) 6-(p-tolyl)-2-methyl-2-heptenol, (34) 6-tridecen-4-yne, (Z)-, (35) 1,4-cyclohexadiene, 1-methyl-, (36) kaempferol-3,7-O-dimethyl ether, (37) 5,7,8-trihydroxy-2',5'-dimethoxy-3',4'-methylene dioxysoflavanone, (38) chavicol, (39) kaempferol-3-O-rutinoside-7-O-glucoside.

NIST library were selected by the software (Software: Version 4.22 optimized for Pegasus®). Software searches (identifies) compound from their mass spectra and includes MS interpretation programs for analyzing mass spectra based on chemical structure, molecular formula, isotopic pattern, etc. The similarity of 70% or above between the m/z values of the compound detected in the respective cultivar and the MS-libraries' mass fragmentation pattern was considered as identification. Furthermore, mass spectra of all compounds were also matched with ranges available as per their CAS number. Compounds for which the CAS number was not generated, the PubChem CID was used. Compounds below the similarity level of 70% were not considered and grouped as unknown. The data obtained with the samples collected in 2012 are presented in this article.

Preparation of Rhizome Extracts for LC-MS Analysis

Samples for LC-MS analysis were prepared by grinding the fresh rhizome to a fine powder in a mortar and pestle under liquid nitrogen. 1 g of the rhizome powder was suspended in 2 ml of MeOH (LC-MS grade). The samples were sonicated for 30 min and centrifuged for 25 min at 1500 rpm, and the supernatants were separated by filtering through a 0.45- μ m Nylon filter disk. These extracts were freshly prepared for the analysis. A 200 μ l aliquot of the extract was diluted quantitatively with internal standard (IS) 200 μ l 4-fluoro-4'-hydroxy benzophenone solution. It was prepared freshly for each analysis by dissolving in methanol for a final concentration of 0.58 mg/ml. The samples were subjected to LC-MS analysis for the complete metabolite profile. The data obtained with the samples collected in 2012 were presented in this article.

LC-MS/MS Conditions and Metabolite Identification

LC-MS analyses of the crude extract of fresh rhizome of *Curcuma* spp. were performed according to Jiang et al. (2006) using Agilent 6520 Accurate Q-TOF (Agilent Santa Clara, CA), and the column used was Zorbax Eclipse XDB-C 18, 4.6 \times 50 mm, 1.8 μ m; Mobile phase: A) buffer (5 mM ammonium formate, 0.1% formic acid, in deionized and distilled H₂O) and B) acetonitrile; gradient (in buffer A): 0–2 min, 5% B; 2–57 min, 5–100% B; 57–60 min, 100% B; 60–65 min, 100–5% B; flow rate: 0.25 ml/min; temperature, 40°C; injection volume 5 μ l. For the MS detection, Agilent MSD-Trap-SL

was equipped with electrospray ionization (ESI) interface as the ion source. The acquisition parameters for the negative mode were: drying N₂ temperature, 350°C, 8 l/min; nebulizer pressure 40 psi; HV capillary 4000 V; skimmer 65.0 V; mass range measured: 110–1700 m/z; Spray voltage: 4 kV; scan rate 1.4. We analyzed the results in both the positive and the negative ion mode acquired by Agilent TOF/Q-TOF mass spectrometry and full MS scan, in the form of total ion current (TIC) chromatogram, and the metabolites were identified based on their MS/MS spectra and fragmentation rules reported previously (Jiang et al., 2006).

RESULTS

Essential Oil Content

The oil was obtained by hydro-distillation, in a Clevenger-type apparatus, of the fresh rhizomes of five cultivars (Alleppey Supreme, Duggirala Red, Prathibha, Salem, and Suguna) of *Curcuma longa* L. and two cultivars (Kasturi Araku and Kasturi Avidi) of *C. aromatica* Salisb. The yield of essential oil from the seven cultivars was in the range of 0.74–1.62% on a fresh weight basis, with the highest yield of 1.62% in cv. Kasturi Avidi (*C. aromatica* Salisb.) followed by cv. Alleppey Supreme (*C. longa* L.) with an amount of 1.42% and the lowest yield of 0.74% in cv. Duggirala Red (*C. longa* L.). The essential oil yields from the other five rhizomes were in between these values (Table 1). The oil yields of *C. longa* L. varieties were higher than those of *C. aromatica* Salisb.

GC-MS Analysis of Essential Oil

Essential oils of seven cultivars of *Curcuma* spp. were subjected to GC-MS analysis, and the results from one of such studies for each cultivar are presented in this article. The representative TIC chromatograms of these cultivars are shown in Figure 1. Several compounds were detected in each cultivar's essential oil (Table 1). Only a few of the identified compounds were confirmed based on their match with the compound profiles found in the NIST databases and Leco-Fiehn Rtx5 library. Up to 44 compounds were identified from the five cvs. of *C. longa* L. and 31 compounds from two cvs. of *C. aromatica* Salisb. (Table 1). Altogether 80 compounds were grouped into three categories: cultivar-specific (41), present in more than one cultivar (26), and common in all seven cultivars (13).

These 41 cultivar-specific compounds were detected in the essential oil of one of the cultivars of *C. longa* L. or *C. aromatica* Salisb. (Table 2). The essential oil of *C. longa* L. cv. Prathibha had the highest number of cultivar-specific compounds, whereas *C.*

TABLE 3 | Compounds detected in more than one cultivar of *C. longa* L. and *C. aromatica* Salisb. identified by GCMS in the essential oil from rhizomes. The structures of the compounds from serial numbers 1–12 are given in **Figure 2** (panel numbers: 24–35), and the compounds with SI.No. 13–18 are shown in **Figure 3**, with corresponding panel numbers: 8–13 respectively. Abbreviations used: AS, Alleppey Supreme; DR, Duggirala Red; PR, Prathibha; SA, Salem; SU, Suguna; KAr, Kasturi Araku; KAv, Kasturi Avidi.

SI No.	Compound name	Cultivar	RT (Min)	Area/abundance	Formula	Mass	Mass fragment ions	Class of compound	Reported from plant species	References
1	1,3,5-Cycloheptatriene	AS, PR, SA, SU, KAr, KAv	2.16	6243556	C ₇ H ₈	92.0626	65,91	Closed ring organic compound	<i>Ceropegia woodii</i> Schltr	Meng et al. (2010)
2	Bicyclo(3.1.0)hexane, 4-methyl-1-(1-methylethyl)-, dihydro deriv	DR, PR, SA, SU	5.70	89775296	C ₁₀ H ₁₆	136.1252	41, 77, 93	Monoterpene	<i>Zingiber Officinale</i> Roscoe	Tang et al. (2012)
3	Bicyclo(3.2.1)oct-2-ene, 3-methyl-4-methylene-	DR, SU, KAv	9.35	559996	C ₁₀ H ₁₆	134.1096	91, 105, 134	Monoterpene	<i>Seseli daucifolium</i> C.B. Clarke	Mohiuddin et al. (2012)
4	Oxirane, 2-(hexyn-1-yl)-3-methoxymethylene-	DR, KAr, KAv	9.75	71555	C ₁₀ H ₁₄ O ₂	166.0994	79, 110	Cyclic ether and epoxide	<i>Hyptis spicigera</i> Lam	Ladan et al. (2011)
5	Bergamotol, Z-α-trans-	AS, SA	20.90	39326774	C ₁₅ H ₂₄ O	220.182	91, 93, 119, 187	Sesquiterpene alcohol	<i>Pogostemon deccanensis</i> (Panigrahi) Press	Kumar et al. (2019)
6	(1,3-Dimethyl-2-methylene-cyclopentyl)-methanol	AS, DR, SA, SU, KAv	21.05	25037989	C ₉ H ₁₆ O	140.1201	67, 77, 94, 109	alcohol H	<i>Elsholtzia argyi</i> H. Lévy	Peng and Yang (2005)
7	12-Oxabicyclo[9.1.0]dodeca-3,7-diene, 1,5,5,8-tetramethyl-, [1R-(1R*,3E,7E,11R*)]-	DR, KAr	21.67	21304483	C ₁₅ H ₂₄ O	220.1827	67, 96, 109, 138	Epoxide	<i>Eugenia Caryophyllus</i> (Spreng.) Bullock & S.G. Harrison	Mani and Boominathan (2011)
8	Isolongifolene, 4,5,9,10-dehydro-	AS, DR, SA, SU, KAr	22.10	350003	C ₁₅ H ₂₀	200.1565	77, 91, 143, 157, 185	Polycyclic hydrocarbon	<i>Cymbopogon citratus</i> (DC.) Stapf	Tajidin (2012)
9	Z,Z,Z-4,6,9-Nonadecatriene	DR, KAv	22.33	169215573	C ₃₄ H ₁₉	262.2661	79, 93	Hydrocarbon	<i>Papaver somniferum</i> L.	Kumaravel et al. (2019)
10	6-(p-Tolyl)-2-methyl-2-heptenol	AS, SU, KAv	22.98	60406564	C ₁₅ H ₂₂ O	218.167	91, 119, 202	Aromatic alcohol	<i>Zingiber officinale</i> Roscoe	Choudhari and Kareppa (2013)
11	6-Tridecen-4-yne, (Z)-	DR, PR, SU	23.14	153999724	C ₁₃ H ₂₂	178.1722	43, 79, 94	Hydrocarbon	<i>Ambrosia trifida</i> L.	Wang et al. (2005)
12	1,4-Cyclohexadiene, 1-methyl-	KAr, KAv	23.15	156905042	C ₇ H ₁₀	94.0783	55, 79, 94	Aromatic alcohol	<i>Capsicum annuum</i> L.	Eggink et al. (2012)
13	Camphene	AS, DR, PR, SU	4.56	930505	C ₁₀ H ₁₆	136.125	93, 121	Monoterpene	<i>Curcuma longa</i> L.	Chowdhury et al. (2008a)
14	α-Phellandrene	AS, DR, SA, SU, KAr	5.72	2645357306	C ₁₀ H ₁₆	136.125	77, 93	Monoterpene	<i>Curcuma longa</i> L.	Chowdhury et al. (2008a)
15	Limonene	AS, SU, KAr, KAv	6.27	202198637	C ₁₀ H ₁₆	136.125	68, 93	Monoterpene	<i>Curcuma longa</i> L.	Singh et al. (2010)
16	α-Terpineol	AS, PR, SA, SU, KAr, KAv	11.25	35019844	C ₁₀ H ₁₈ O	154.135	59, 93, 121	Monoterpenoid	<i>Curcuma longa</i> L.	Gopalan et al. (2000)
17	β-Sesquiphellandren	DR, SA, SU, KAv	20.83	962609070	C ₁₅ H ₂₄	204.187	68, 79	Sesquiterpene	<i>Curcuma longa</i> L.	Chowdhury et al. (2008a)
18	Nerolidol	DR, PR, SA, SU, KAv	21.79	15626126	C ₁₅ H ₂₆ O	222.198	69, 93	Sesquiterpinol	<i>Curcuma longa</i> L.	Awasthi and Dixit (2009)
19	Bicyclo(4.1.0)hept-2-ene, 3,7,7-trimethyl-	DR, KAv	5.63	227551	C ₁₀ H ₁₆	136.125	93, 121	Monoterpene	<i>Curcuma longa</i> L.	Chowdhury et al. (2008a)
20	α-Terpinene	AS, DR, SA, KAr, KAv	6.00	28366949	C ₁₀ H ₁₆	136.125	93, 121, 136	Monoterpene	<i>Curcuma longa</i> L.	Chowdhury et al. (2008a)
21	cis-Ocimene	DR, PR, SA, SU, KAr, KAv	6.74	466438	C ₁₀ H ₁₆	136.125	41, 93	Monoterpene	<i>Curcuma longa</i> L.	Usman et al. (2009)
22	γ-Terpinene	AS, DR, PR, SA, SU, KAr	7.01	26650014	C ₁₀ H ₁₆	136.125	93, 119, 136	Monoterpene	<i>Curcuma longa</i> L.	<i>Curcuma longa</i> L. Usman et al. (2009)
23	Linalool	AS, DR, PR, SU	8.15	500594	C ₁₀ H ₁₈ O	154.135	71, 93, 121	Alcohol	<i>Curcuma longa</i> L.	<i>Curcuma longa</i> L. Leela et al. (2002)

(Continued on following page)

TABLE 3 | (Continued) Compounds detected in more than one cultivar of *C. longa* L. and *C. aromatica* Salisb. identified by GCMS in the essential oil from rhizomes. The structures of the compounds from serial numbers 1–12 are given in Figure 2 (panel numbers: 24–35), and the compounds with SI.No. 13–18 are shown in Figure 3, with corresponding panel numbers: 8–13 respectively. Abbreviations used: AS, Alleppey Supreme; DR, Duggirala Red; PR, Prathibha; SA, Salem; SU, Suguna; KAr, Kasturi Araku; KAv, Kasturi Avidi.

SI No.	Compound name	Cultivar	RT (Min)	Area/abundance	Formula	Mass	Mass fragment ions	Class of compound	Reported from plant species	References
24	Terpinene-4-ol	AS, DR, PR, SA, SU	10.83	2557284	C ₁₀ H ₁₈ O	154.135	73, 94, 154	Monoterpene	<i>Curcuma longa</i> L.	<i>Curcuma longa</i> L. Singh et al. (2010)
25	cis- α -Bisabolene	PR, KAr	20.40	11244271	C ₁₅ H ₂₄	204.187	67, 93, 161, 204	Sesquiterpene	<i>Curcuma longa</i> L.	<i>Curcuma longa</i> L. Chowdhury et al. (2008a)
26	Ar-Tumerone	DR, SA, KAv	25.87	328137262	C ₁₅ H ₂₀ O	216.151	83, 119, 173, 216	Sesquiterpene	<i>Curcuma longa</i> L.	<i>Curcuma longa</i> L. Chowdhury et al. (2008a)

TABLE 4 | Compounds common in the seven cultivars of *Curcuma* spp detected by GC-MS in essential oil obtained from rhizomes. The structures of the two compounds with serial numbers 10 and 13 are given in Figure 3 (panel numbers: 14–15 respectively).

SI No.	Compound name	RT (Min)	Area/abundance	Formula	Mass	Mass fragment ions	Class of compound	Reported from plant species	References
1	α -Thujene	4.13	9407392	C ₁₀ H ₁₆	136.125	93, 136	Monoterpenoid	<i>Curcuma longa</i> L.	Raina et al. (2005)
2	1s- α -Pinene	4.27	122103688	C ₁₀ H ₁₆	136.125	39, 41, 93	Monoterpenoid	<i>Curcuma longa</i> L.	Singh et al. (2002)
3	Sabinene	5.05	3901899	C ₁₀ H ₁₆	136.125	93, 136	Monoterpenoid	<i>Curcuma longa</i> L., leaves	Behura et al. (2002)
4	β or m-Cymene	6.20	338719033	C ₁₀ H ₁₄	134.109	65, 91, 119	Aromatic hydrocarbon	<i>Curcuma longa</i> L.	Singh et al. (2002)
5	Terpinolene	7.82	225186296	C ₁₀ H ₁₆	136.125	93, 121	Monoterpenoid	<i>Curcuma longa</i> L.	Leela et al. (2002)
6	trans- α -Bergamotene	18.86	2365810	C ₁₅ H ₂₄	204.187	69, 93, 119, 161	Sesquiterpene	<i>Curcuma longa</i> L.	Raina et al. (2005)
7	α -Caryophyllene	19.23	6097261	C ₁₅ H ₂₄	204.187	93, 121	Sesquiterpene	<i>Curcuma longa</i> L., leaves	Behura et al. (2002)
8	trans- β -Farnesene	19.37	211225438	C ₁₅ H ₂₄	204.187	69, 93, 133	Sesquiterpene	<i>Curcuma longa</i> L.	Singh et al. (2002)
9	Ar-Curcumene	19.88	482956678	C ₁₅ H ₂₂	202.172	132, 202	Sesquiterpene	<i>Curcuma longa</i> L.	Singh et al. (2002)
10	α -Zingiberene	20.25	1117738917	C ₁₅ H ₂₄	204.187	69, 93, 119, 204	Sesquiterpene	<i>Curcuma longa</i> L.	Chowdhury et al. (2008a)
11	Tumerone	22.16	67277186	C ₁₅ H ₂₂ O	218.167	83, 157	Sesquiterpene	<i>Curcuma longa</i> L.	Singh et al., 2002)
12	Curione	27.34	439832546	C ₁₅ H ₂₂ O	218.167	83, 120, 218	Sesquiterpene	<i>Curcuma longa</i> L.	Leela et al. (2002)
13	2-Heptadecanone	39.17	152911	C ₁₇ H ₃₄ O	254.261	43, 55, 71, 125	Ketone	<i>Curcuma angustifolia</i> Roxb	Srivastava et al. (2006)

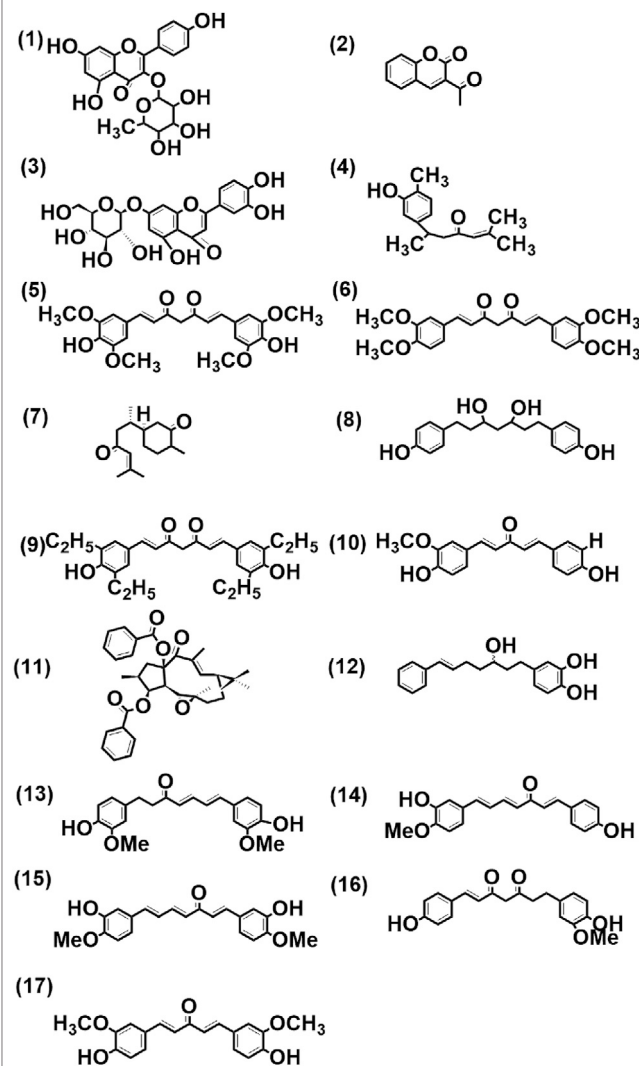
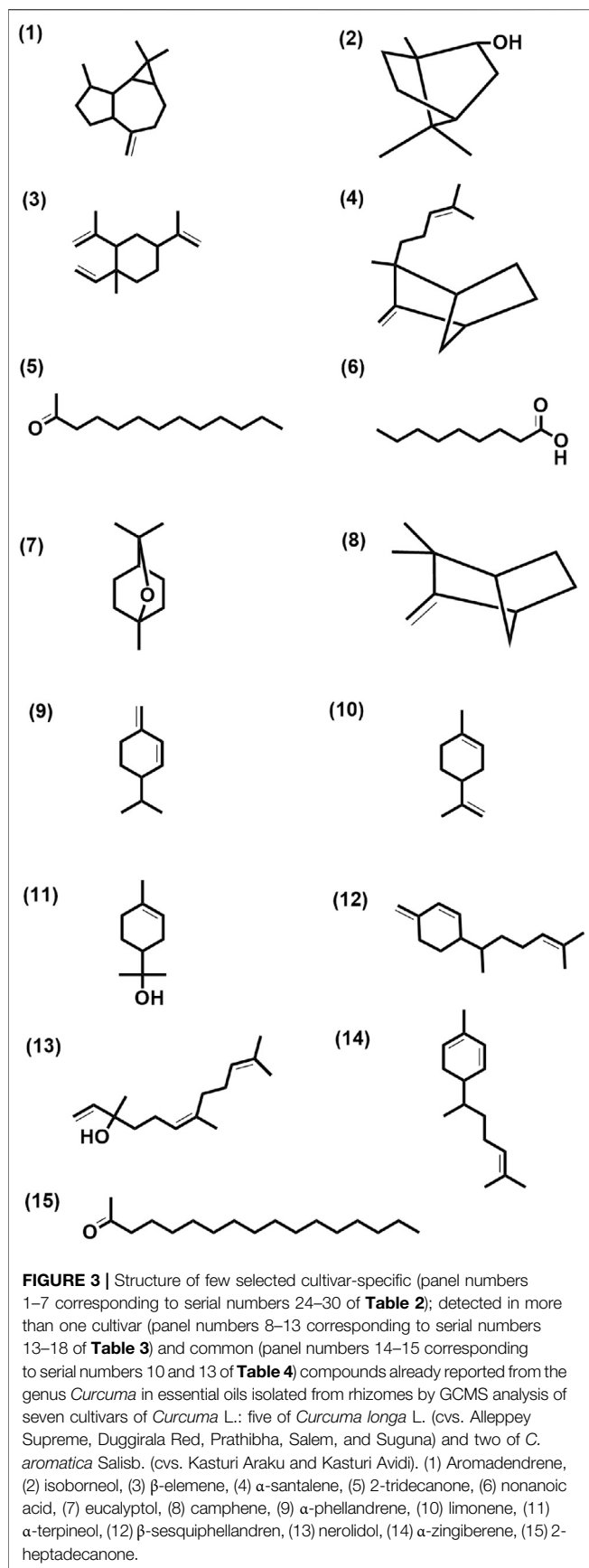


TABLE 5 | Total number of compounds detected by LC-MS from the rhizome extract of *C. longa* L. and *C. aromatica* Salisb.

Sl. No.	Cultivar (Species)	Total number of Metabolites detected	Metabolites identified	Unknown Metabolites
1	Alleppey Supreme (<i>C. longa</i> L.)	86	43	43
2	Duggirala Red (<i>C. longa</i> L.)	107	23	84
3	Prathibha (<i>C. longa</i> L.)	60	28	32
4	Salem (<i>C. longa</i> L.)	91	28	63
5	Suguna (<i>C. longa</i> L.)	96	30	66
6	Kasturi Avidi (<i>C. aromatica</i> Salisb.)	90	30	60
7	Kasturi Araku (<i>C. aromatica</i> Salisb.)	92	29	63

aromatica Salisb., cv. Kasturi Araku had the least (Table 2). Of these, 23 cultivar-specific compounds were reported for the first time from the genus *Curcuma*. The chemical structures of these 23 compounds (Table 2, Sl. Nos. 1–23) are presented in Figure 2 (panels 1–23). In addition to 41 cultivar-specific compounds, 26 compounds were present in more than one cultivar (Table 3). Among these, 12 were detected first time in the genus *Curcuma* (Table 3, Sl. Nos. 1 to 12; Figure 2, panels: 24–35). The remaining 14 were already known in *C. longa* L. A total of 13 compounds were common in all seven cultivars of *C. longa* L. and *C. aromatica* Salisb. (Table 4) and the representative structures of two of these compounds are given in Figure 3 (panel numbers 14–15, corresponding to serial numbers 10 and 13 respectively of Table 4). Most of these compounds belong to mono, di, and sesquiterpene. A summary of all 80 compounds identified by GC-MS in the essential oils of the seven cultivars is presented in Supplementary Table S1.

LC-MS Analysis of Methanol Extracts

Methanolic extracts of rhizomes from the seven cultivars of *Curcuma* spp. were subjected to LC-MS analysis. The results from one of such analyses for each cultivar are presented in this article. The use of “positive” and “negative” modes of LC-MS was quite helpful. TIC chromatograms of all seven cultivars of *Curcuma longa* L. and *C. aromatica* Salisb. were shown in Supplementary Figure S1A for negative mode and Supplementary Figure S1B for positive mode.

A typical LC-MS analysis of methanolic extracts from rhizomes of *C. longa* L. cv. Alleppey Supreme revealed the presence of up to 86 compounds. Out of these, 43 were identified, and the remaining 43 compounds remained unknown. The (–) ESI-LC-MS detected 30 known compounds, and the (+) ESI-LC-MS detected 23 known compounds with an overlap of 10 compounds, detected by both negative and positive ion modes. A similar assessment of data was done with all seven cultivars of *Curcuma* spp. (Table 5). Altogether 62 compounds were identified, as presented in Supplementary Table S2. These compounds were grouped into three categories: cultivar-specific,

detected in more than one cultivar, and common. There were 23 cultivar-specific compounds present in any one cultivar of *C. longa* L. or *C. aromatica* Salisb. (Table 6). 24 compounds were present in more than one cultivar of *C. longa* L. and/or *C. aromatica* Salisb. (Table 7). The remaining 15 were common in all seven cultivars (Table 8). Of these 15 common compounds found in the LC-MS/MS chromatograms, only one was a “Bisabolane” sesquiterpene (Parthasarathy et al., 2009) and all other 14 were diarylheptanoids. These were identified based on the MS/MS spectra reported by Jiang et al. (2006), including curcumin (CU), demethoxycurcumin (DMC), and bisdemethoxycurcumin (BDMC). Among the other diarylheptanoids, 1-(4-hydroxyphenyl)-7-(4-hydroxy-3-methoxyphenyl)-1,4,6-heptatrien-3-one; 1,5-bis(4-hydroxy-3-methoxyphenyl)-1,4-pentadien-3-one, etc., were common in all the cultivars of *C. longa* L. and *C. aromatica* Salisb. (Table 8). The structure of the five common compounds was given in Figure 4 (panels 13, 14–15, 16, and 17 corresponding to serial numbers 10, 5–6, 15, and 1, respectively, of Table 8). In addition to diarylheptanoids, several other classes (phenolic acids, flavonoids, ketonic sesquiterpenes, and fatty acid derivatives) were also detected in the turmeric rhizomes.

Compounds Reported First Time From the Genus *Curcuma* Using GC-MS and LC-MS Analysis

A total of 39 compounds were detected (Figure 2) for the first time from the genus *Curcuma*. Out of these, 35 and 4 compounds were identified respectively in the essential oils and whole rhizome extracts of *C. longa* L. and *C. aromatica* Salisb. by the GC-MS and LC-MS techniques. Details of the compounds, including the class of compound, molecular weight, are given in Tables 2, 3, 5, and 6; structures of all these compounds are shown in Figure 2 (panels: 1–39). The MS and MS/MS spectra of these compounds are presented in Supplementary Figure S2 (panels: 1–39). These compounds were reported earlier from plants belonging to any genus other than *Curcuma*, and this is the first report from genus

TABLE 6 | Cultivar-specific compounds identified by LC-MS in the rhizome extracts from one of the seven cultivars of *Curcuma longa* L. and *C. aromatica* Salisb. The structure of the compound with the serial number “1” is given in **Figure 2** (panel number: 36) and compounds with Sl. Nos. 2, 3–9 are given in **Figure 4** with the corresponding panel nos. 3, 5–11, respectively. Abbreviations used: AS, Alleppey Supreme; DR, Duggirala Red; PR, Prathibha; SA, Salem; SU, Suguna; KAr, Kasturi Araku; KAv, Kasturi Avidi.

Sl. No.	Compound name	Cultivar	RT (Min)	Area/abundance	Formula	Mass (m/z)	Mass fragment ions	Class of compound	Reported from plant species	References
1	Kaempferol-3,7-O-dimethyl ether	AS	12.77	25537	C ₁₇ H ₁₄ O ₆	313.0721 M-H	108; 123; 152; 153	Flavonoid	<i>Lumnitzera racemosa</i> Willd and <i>Artemisia vulgaris</i> L.	Nikolova (2006); DeSouza et al. (2010)
2	Luteolin-7-O-glucoside	AS	42.2	5324	C ₂₁ H ₂₀ O ₁₁	447.2733 M-H	167 110; 185; 279; 280	Flavonoid	<i>Curcuma Zedoaria</i> (Christm.) Roscoe	Mass bank ACCESSION: TY00-0145; Rahmatullah et al. (2012)
3	1,7-Bis(4-hydroxy-3,5-dimethoxyphenyl)-1,6-heptadiene-3,5-dione	PR	32.9	186331	C ₂₃ H ₂₄ O ₈	428.2 M-H	109; 123; 137; 159; 191; 209	Diarylheptanoid	<i>Curcuma longa</i> L.	Nurfina et al. (1997)
4	1,7-Bis(3,4-dimethoxy phenyl)-1,6-heptadiene-3,5-dione	PR	38.3	335360	C ₂₃ H ₂₄ O ₆	396.2 M-H	105; 107; 119; 129; 137; 145; 155; 195	Diarylheptanoid	<i>Curcuma longa</i> L.	Chen et al. (2006)
5	(6S)-2-Methyl-6-[(1R,5S)-(4-methene-5-hydroxyl-2-cyclohexen)-2-hepten-4-one	PR	40.2	229164	C ₁₅ H ₂₄ O ₂	236.1 M-H	105; 106; 107; 108; 109; 119; 120; 121; 133; 135	Bisabolane	<i>Curcuma longa</i> L.	Li et al. (2011)
6	1,7-Bis(4-hydroxyphenyl)-3,5-heptanediol	KAr	22.8	8120	C ₁₉ H ₂₄ O ₄	316.1 M-H	105; 106; 107; 119; 121; 147; 148	Diarylheptanoid	<i>Curcuma longa</i> L.	Ma and Gang (2006)
7	1,7-Bis(3,5-diethyl-4-hydroxyphenyl)-1,6-heptadiene-3,5-dione	KAr	60.6	129145	C ₂₇ H ₃₂ O ₄	420.3 M-H	106; 107; 119; 120; 121; 122; 123; 144; 145; 146; 147; 171; 172; 175; 187; 197; 201; 209; 211; 213; 223; 237; 239; 321; 323	Aromatic	<i>Curcuma longa</i> L.	Li et al. (2011)
8	1-(4-Hydroxy-3-methoxyphenyl)-5-(4-hydroxyphenyl)-1,4-pentadiene-3-one	KAv	28.8	8009	C ₁₈ H ₁₆ O ₄	296.1 M-H	105; 109; 117; 119; 133; 145; 159; 161; 171; 173; 181; 185; 1207; 209; 223; 233; 239; 251; 279	Diarylheptanoid	<i>Curcuma longa</i> L.	Park and Kim (2002)
9	(-)-(12E,2S,3S,4R, 5R,6R, 9S,11S, 15R)-3,15-Dibenzoyloxy-5,6-epoxylathyr-12-en-14-one	KAv	39.8	5683	C ₃₄ H ₃₈ O ₆	542.2 M-H	119; 145; 183; 211; 212; 237	Diterpenoid	<i>Euphorbia micractina</i> Boiss	Tian et al. (2011)
10	5'-methoxycurcumin	PR	35.56	388655	C ₂₂ H ₂₂ O ₇	398.1 M-H	117; 119; 129; 137; 145; 149; 161; 175; 207	Diarylheptanoid	<i>Curcuma longa</i> L.	Ravindran (2000)
11	Methyl-7-methoxycoumarin,4-	SU	34.4	67927	C ₁₁ H ₁₀ O ₃	190.1953	115; 116; 117; 119; 120	Coumarin	none	NIST CAS register No. 2555–28–4 Mass Bank ACCESSION: PR100013 Ma and Gang (2006)
12	Hydroferulic acid	KAr	16.8	13992	C ₁₀ H ₁₂ O ₆	195.10 M-H	109; 121; 122	Phenolic acid	<i>Curcuma longa</i> L.	
13	1,2,3,4-Tetraphenylbutane-2,3-diol	KAr	11.1	3926	C ₂₈ H ₂₆ O ₂	394.1 M-H	112; 129; 133; 180; 207; 243; 247; 263; 339	Aliphatic diol	none	Pubchem Compound ID: 344369
14	4-Hepten-3-one, 5-hydroxy-1,7-bis(4-hydroxyphenyl)-	PR	25.2	1418	C ₁₉ H ₂₀ O ₄	312.1 M-H	118; 119; 120; 146; 161	Diarylheptanoid	<i>Curcuma longa</i> L.	Jiang et al. (2006)
15	5,7-Dihydroxy-2-(4-hydroxyphenyl)-chroman-4-one	PR	26.8	12833	C ₁₅ H ₁₂ O ₅	272.0 M-H	107; 119; 120	Phenolic acids	none	Chromadex
16	Tetradecanoic acid/myristic acid	AS	29.47	2381	C ₁₄ H ₂₈ O ₂	228.0 M-H	128; 130; 143; 155; 158; 182; 183; 184; 210	Fatty acid	none	NIST CAS 544–63–8
17	1-(4-Hydroxy-3-methoxyphenyl)-7-(4-hydroxy-3,5-dimethoxyphenyl)-4,6-heptadiene-3-one	PR	32.0	194388	C ₂₂ H ₂₄ O ₆	384.1 M-H and M + H	150; 151; 158; 165	Diarylheptanoid	<i>Curcuma longa</i> L.	Jiang et al. (2006)
18	Tumerone	AS	35.3	6120	C ₁₅ H ₂₂ O	218.0 M-H		Bisabolane sesquiterpene	<i>Curcuma longa</i> L.	He (2000)

(Continued on following page)

TABLE 6 | (Continued) Cultivar-specific compounds identified by LC-MS in the rhizome extracts from one of the seven cultivars of *Curcuma longa* L. and *C. aromatica* Salisb. The structure of the compound with the serial number “*” is given in Figure 2 (panel number: 36) and compounds with Sl. Nos. 2, 3–9 are given in Figure 4 with the corresponding panel nos. 3, 5–11, respectively. Abbreviations used: AS, Alleppey Supreme; DR, Duggirala Red; PR, Prathibha; SA, Salem; SU, Suguna; KAr, Kasturi Arakur; KAv, Kasturi Avidi.

Sl. No.	Compound name	Cultivar	RT (Min)	Area/abundance	Formula	Mass (m/z)	Mass fragment ions	Class of compound	Reported from plant species	References
19	4-Methylene-5-hydroxybisabol-2,10-diene-9-one	PR	44.6	321246	C ₁₅ H ₂₂ O ₂	234.1 M + H	101; 103; 117; 129; 130; 131; 132; 133; 134; 145; 157; 146; 157; 158; 173; 201	Sesquiterpene	<i>Curcuma heyneana</i>	Sirat and Meng (2009)
20	1,7-Bis(3,4-dimethoxyphenyl)-4,4-dimethyl-1,6-heptadiene-3,5-dione	PR	54.4	9854	C ₂₃ H ₂₈ O ₆	447.2 M-H	129; 135 286; 298; 316; 317	Diarylheptanoid	Valeton & Zijl <i>Curcuma longa</i> L.	Liang et al. (2009)
21	25-Benzylpentacyclo-(22.3.1.0)-octacos-1(27),3(8),4(6),10(15),11,13;17(22),18,20,24(28),25-dodecaen	AS	54.96	42646	C ₃₈ H ₅₀	450.2 M + H	105; 107; 119; 121; 122	Cyclic diarylheptanoid	<i>Myrica rubra</i> (Lour.) Siebold & Zucc	Ishida et al. (2002)
22	Palmitic acid	SA	59.5	16809	C ₁₆ H ₃₂ O ₂	256.2 M-H	120; 166	Fatty acid	<i>Curcuma kwangsiensis</i> S.K. Lee & C.F. Liang	Jiang et al. (1989)
23	Stearic acid	SA	63.8	76820	C ₁₈ H ₃₆ O ₂	284.1 M-H	197; 199; 200	Fatty acid	<i>Curcuma longa</i> L.	Ma and Gang (2006)

Curcuma. Out of the total of 62 compounds detected by LC-MS analyses of rhizome extracts, four compounds were reported for the first time from the *Curcuma* genus. One was cultivar-specific (Table 6; Sl. Nos. 1; Figure 2, panels: 36), and three were present in more than one cultivar (Table 7; Sl. Nos. 1–3). The structures of these first-time reported compounds are given in Figure 2 (panels: 37–39), and their corresponding mass fragmentation spectra are shown in Supplementary Figure S2 (panels: 36–39).

A comprehensive table each for GCMS (Supplementary Table S3) and LCMS (Supplementary Table S4) shows the details of compound identification methods used in the present study for the first-time reported compounds from genus *Curcuma* and the previous literature. A list of 80 (GC-MS) and 62 (LC-MS) compounds can be seen in Supplementary Tables S5, S6 respectively.

DISCUSSION

In one of our previous studies, we reported that the HPLC method could be a valuable tool to differentiate the cultivars of *Curcuma* spp. based on their curcuminoids content ratios (Kulyal et al., 2016). Curcuminoids play a significant role in food, cosmetics, and medicinal compounds. But there are several other secondary metabolites such as terpenoids (e.g., mono-, sesqui-, di-, tri-, so on), alkenes, aromatic compounds, flavonoids, coumarins, etc. that are responsible for various biological activities. All these secondary metabolites are present in either the volatile essential oil or the nonvolatile fraction of the *Curcuma* spp. Employing untargeted metabolomics would be the ideal way to identify as many metabolites as possible. Therefore, in the present study, we analyzed these secondary compounds using GC-MS and LC-MS/MS.

Versatility of GC-MS and LC-MS Techniques to Identify a Large Number of Metabolites

GC-MS analysis is an appropriate technique for analyzing volatile compounds, whereas LC-MS is for detecting polar compounds, and thus, these two techniques are mutually complementary to each other. In the present study, several of the volatile compounds present in the cultivars of *C. longa* L. and *C. aromatica* Salisb. belonging to mono- and sesquiterpenoids were detected by GC-MS (Tables 2–4). On the other hand, LC-MS analysis detected phenolic (Tables 6–8) compounds, including several diarylheptanoids in the methanolic extracts of both *C. longa* L. and *C. aromatica* Salisb. (Figure 4). Electrospray ionization (ESI), coupled with LC/MS/MS, turned out to be a powerful tool in metabolite profiling and metabolomics research. Studies on chemical derivatization and quantification of several metabolites in turmeric powders and fresh rhizome extracts by LC-MS or LC-MS/MS were made. But the rapid screening within the cultivars of *C. longa* L. of fresh turmeric rhizome has not yet been reported. To the best of our knowledge, we were able to record the presence of several metabolites, which were not reported so far in the *C. longa* L. and *C. aromatica* Salisb. (Tables 2, 3, 6, 7, and Figure 2), using the available literature search, Metlin library, mass bank, and NIST library.

TABLE 7 | Compounds identified by LC-MS in rhizome extracts of more than one cultivar of *Curcuma longa* L. and *C. aromatica* Salisb. The compounds from serial numbers 1–3 are reported first time from the genus *Curcuma*, the structures of these compounds along with few others are given in **Figure 2** (panels: 37–39; panels 1–2, 4, 12 corresponding to serial numbers 4–5, 6, 7). Abbreviations used: AS, Alleppey Supreme; DR, Duggirala Red; PR, Prathibha; SA, Salem; SU, Suguna; KAR, Kasturi Araku; KAV, Kasturi Avidi.

Sl. No.	Compound name	Cultivar	RT (Min)	Area/abundance	Formula	Mass (m/z)	Mass fragment ions	Class of compound	Reported from plant species	References
1	5,7,8-Trihydroxy-2',5'-dimethoxy-3',4'-methylene dioxyisoflavanone	AS, DR, KAV	2.2	51978	C ₁₈ H ₁₈ O ₉	377.1059 M-H ⁺	101; 102; 113; 119; 161; 163; 228; 336	Flavonoid	<i>Terminalia ivorensis</i> A. Chev	Ogundare and Olajuyigbe (2012)
2	Chavicol	AS, SU	38.83	55821	C ₉ H ₂₀ O	135.0794 M + H ⁺	102; 115 116	Terpenoid	<i>Piper betle</i> L.	NIST CAS No: 501–92–8 Nagori et al. (2011)
3	Kaempferol-3-O-rutinoside-7-O-glucoside	PR, SA	33.2	3752	C ₃₃ H ₄₀ O ₂₀	755.2655 M-H ⁺	135; 161; 175; 176; 191; 439; 579; 755; 756	Flavonoid	<i>Lycopersicon esculentum</i> Mill	Le Gall et al. (2003)
4	Kaempferol-3-rhamnoside	AS, DR	10.76	5367	C ₂₁ H ₂₀ O ₁₀	431.9911 M-H	125; 142; 146; 150 176; 184 190; 293; 304; 308 311; 316; 343; 345	Flavonoid	<i>Curcuma Xanthorrhiza</i> Roxb	Ruslay et al. (2007)
5	3-Acetyl coumarin	AS, PR, SA, SU, KAV	34.65	289624	C ₁₁ H ₈ O ₃	188.0534	115; 116; 117; 118 141; 143	Coumarin	None	Pub Chem ID 24852845 NIST 3949–36–8
6	Turmeronol	AS, DR, SU	25.36	87260	C ₁₅ H ₂₀ O ₂	232.1436	103; 104; 105 107; 115; 117; 118 119; 120; 121; 128 129; 131; 141; 142; 143 119; 183; 184	Bisabolane sesquiterpene	<i>Curcuma longa</i> L.	Ma and Gang (2006)
7	7-(3,4-Dihydroxyphenyl)-5-hydroxy-1-phenyl-(1E)-1-heptene	AS, KAV	35.99	16570	C ₁₉ H ₂₂ O ₃	298.1 M-H		Diarylheptanoid	<i>Curcuma xanthorrhiza</i> Roxb	Suksamrarn et al. (1994)
8	1,7-Diphenyl-1,6-heptadiene-3,5-dione	AS, SA	2.49	9697	C ₁₉ H ₁₆ O ₂	276.0	115	Diarylheptanoid	Synthesized the compound	Sundaryono et al. (2003)
9	1-Hepten-3-one, 5-hydroxy-1,7-bis(3,4-dihydroxyphenyl)-	PR, SA, SU, KAR, KAV	21.2	1660	C ₁₉ H ₂₀ O ₆	344.1	107; 121; 134; 135; 136; 159; 161; 162; 177; 178	Diarylheptanoid	<i>Alnus japonica</i> (Thunb.) Steud	Sati et al. (2011)
10	4-(p-Hydroxyphenyl)-3-buten-2-one	AS, DR, SA, KAV	22.16	18641	C ₁₀ H ₁₀ O ₂	162.0	117; 118	Flavonoid	None	NIST CAS 3160–35–8
11	5-Hydroxy-7-(4-hydroxyphenyl)-1-phenyl-(1E)-1-heptene	AS, DR, PR, SA, KAR, KAV	23.11	6169	C ₂₀ H ₂₄ O ₄	328.1	107; 119; 133; 134; 135; 136; 159; 161; 162; 177; 178	Diarylheptanoid	<i>Curcuma xanthorrhiza</i> Roxb	Suksamrarn et al. (1994)
12	1-(4-Hydroxy-3-methoxyphenyl)-7-(4-hydroxy-3,5-dimethoxyphenyl)-4,6-heptadiene-3-one	AS, DR, SA, KAR, KAV	25.8	6408	C ₂₂ H ₂₄ O ₆	384.1	133; 134; 147; 148; 150; 151; 158; 165; 175; 176; 186; 187; 188; 189; 203; 204; 232	Diarylheptanoid	<i>Curcuma longa</i> L.	Jiang et al. (2006)
13	1,5-Bis(3,4-methylenedioxyphenyl)-1,4-pentadien-3-one	SU, KAV	26.0	9161	C ₁₉ H ₁₄ O ₅	322.0	115; 119; 121; 133; 143; 235; 237; 247; 263; 275	Diarylheptanoid	<i>Curcuma longa</i> L.	Jiang et al. (2006)
14	1-Hydroxy-1-(3,4-dihydroxyphenyl)-7-(4-hydroxy-3-methoxyphenyl)-6-hepten-3,5-dione	AS, KAV	26.7	45589	C ₂₀ H ₂₀ O ₇	372.1	103; 117; 131; 137; 143; 145; 149; 163; 177	Diarylheptanoid	<i>Curcuma longa</i> L.	Jiang et al. (2006)
15	1,7-Bis(4-hydroxyphenyl)-1-heptene-3,5-dione	AS, DR, PR, SA, SU, KAV	27.4	8495	C ₁₉ H ₁₈ O ₄	310.1	117; 118; 119; 145; 146; 161; 175; 176	Diarylheptanoid	<i>Curcuma longa</i> L.	Jiang et al. (2006)
16	1,7-Bis(4-hydroxyphenyl)-1,4,6-heptatrien-3-one	AS, DR, PR, SA, SU, KAV	30.0	7240	C ₁₉ H ₁₆ O ₃	292.1	115; 117; 119; 120; 143; 145	Diarylheptanoid	<i>Curcuma longa</i> L.	Li et al. (2011)
17	7-(4-Hydroxy-3-methoxyphenyl)-1-(4-hydroxy phenyl)-4,6-heptadien-3-one	AS, KAV	31.8	138675	C ₂₀ H ₂₀ O ₄	324.1	107; 117; 119; 120; 122; 123; 131; 135; 137; 145; 146; 147; 148; 163; 195; 223	Diarylheptanoid	<i>Curcuma longa</i> L.	Jiang et al. (2006)

(Continued on following page)

TABLE 7 | (Continued) Compounds identified by LC-MS in rhizome extracts of more than one cultivar of *Curcuma longa* L. and *C. aromatica* Salisb. The compounds from serial numbers 1–3 are reported first time from the genus *Curcuma*, the structures of these compounds along with few others are given in Figure 2 (panels: 37–39; panels 1–2, 4, 12 corresponding to serial numbers 4–5, 6, 7). Abbreviations used: AS, Alleppey Supreme; DR, Duggirala Red; PR, Prathibha; SA, Salern; SU, Suguna; KA, Kasturi Araku; KAV, Kasturi Avidi.

Sl. No.	Compound name	Cultivar	RT (Min)	Area/abundance	Formula	Mass (m/z)	Mass fragment ions	Class of compound	Reported from plant species	References
18	Coumaran	AS, DR, SA, SU	34.36	6563	C ₉ H ₈ O	120.0	116; 117; 118; 119	Coumarin	None	Chromadex
19	5,7-Dihydroxy-4-methylcoumarin	AS, SA, SU, KAV	34.57	92188	C ₁₀ H ₈ O ₄	192.17	113; 115; 116; 117; 118; 141	Coumarin	None	PubChem CID 5354284
20	1,7-Bis(3,4,5-trimethoxyphenyl)-1,6-heptadiene-3,5-dione	PR, SU, KA, KAV	35.82	4972	C ₂₅ H ₂₈ O ₈	456.3	280; 281; 298; 299	Diarylheptanoid	Synthesised the compound	Hahn et al. (2002)
21	Curione	AS, DR, PR, SU, KA, KAV	46.50	19540	C ₁₅ H ₂₂ O	218.0	101; 103; 117; 129; 130; 131; 132; 133; 134; 145; 157; 146; 157; 158; 173	Bisabolane sesquiterpene	<i>Curcuma longa</i> L.	He (2000)
22	Hydrocinnamic acid	SU, KA	35.1	3812	C ₉ H ₁₀ O ₂	150.0	103; 105; 133	Phenolic acid	<i>Curcuma longa</i> L.	Ma and Gang (2006)
23	Curcumenol	AS, SU, KA, KAV	36.67	34556	C ₁₅ H ₂₂ O ₂	234.1	105; 107; 109; 117; 123; 125; 133; 137	Sesquiterpene	<i>Curcuma heyneana</i> Valeton & Zijl	Sirat and Meng (2009)
24	Oleic acid	SA, KA	60.2	15974	C ₁₈ H ₃₄ O ₂	282.1	168; 257	Fatty acid	<i>Curcuma longa</i> L.	Ma and Gang (2006)

Cultivar Variability Based on Secondary Metabolites

Based on the presence or absence of metabolites identified by GC-MS and LC-MS analyses, there was a need to authenticate cultivar variability. Thus, the metabolite library can be constructed based on the cultivar-specific and compounds found in more than one cultivar. There are very few reports on cultivar-specific secondary metabolite variation. Out of a total of 142 compounds identified by both GC-MS and LC-MS, only 28 compounds (13 from GCMS and 15 from LCMS) were common (**Tables 4, 8**) present in all the cultivars of *C. longa* L. and *C. aromatica* Salisb. Ten of 13 common compounds (GCMS) were reported earlier from *C. longa* L. rhizome. Two compounds, namely sabinene and α-caryophyllene, were reported from the leaves of *C. longa* L. The remaining one compound, i.e., 2-heptadecanone, was detected for the first time from these two *Curcuma* species. This compound was earlier reported in the essential oil of *Curcuma angustifolia* Roxb. rhizome (Srivastava et al., 2006).

As per our analyses, 64 compounds (**Tables 2, 6**) out of 142 compounds were cultivar-specific. Of these 64 compounds, 41 were identified in essential oils by GC-MS (e.g., carvacrol, endo-borneol) and 23 (e.g., tumerone, methyl-7-methoxycoumarin,4-) in fresh rhizome extracts (LC-MS) of any one of the cultivars of *C. longa* L. or *C. aromatica* Salisb. In addition, 50 compounds (**Tables 3, 7**) were identified to be present in some of the cultivars, present in more than one cultivar but not common to all the cultivars of *C. longa* L. and *C. aromatica* Salisb. Out of these 50 compounds, 26 were identified in essential oils through GC-MS. For example, 1,3,5-cycloheptatriene was detected in all six cultivars except cv. Duggirala Red, whereas 12-oxabicyclo(9.1.0)dodeca-3,7-diene, 1,5,5,8-tetramethyl-, [1R-(1R*,3E,7E,11R*)]-, was detected only in cvs. Duggirala Red and Kasturi Araku. The rest 24 compounds were detected in rhizome extracts by LC-MS (e.g., chavicol detected in cvs. Alleppey Supreme and Suguna). The present extensive analyses of both essential oils and whole rhizome secondary metabolome of seven cultivars of *C. longa* L. and *C. aromatica* Salisb. established cultivar variability. Variability of the compounds within or/and in between the cultivars of *C. longa* L. and *C. aromatica* Salisb. will give a better understanding of their selection. The current study will help select cultivars for use in pharmacology or the food industry.

Discovery of First-Time Reported Metabolites in *C. longa* L. and *C. aromatica* Salisb.

In the present study, as many as 142 compounds were identified in the essential oils and rhizome extracts of *C. longa* L. and *C. aromatica* Salisb. Out of these, 39 compounds were identified for the first time in the genus *Curcuma*. However, these compounds were found in other plant genera. The structures of these compounds are shown in **Figure 2**, and corresponding details, including the class of compound, molecular weight, are given in **Tables 2, 3, 6**, and **7**. As an example, cv. Alleppey Supreme of *C. longa* L. showed three cultivar-specific compounds. Among these, 1,2-cyclohexanediol, 1-methyl-4-(1-methylethyl)- (oxygenated

TABLE 8 | Compounds commonly detected by LC-MS analysis of rhizomes extract of all seven cultivars of *Curcuma* spp.: five of *Curcuma longa* L. (cvs. Alleppey Supreme, Duggirala Red, Prathibha, Salem, and Suguna) and two of *C. aromatica* Salisb. (cvs. Kasturi Araku, Kasturi Avidi). The structures for the compounds in the serial numbers 10, 5, 6, 15, and 1 are given in **Figure 4** (panels 13, 14, 15, 16, and 17 respectively).

Sl. No.	Compound name	RT (Min)	Area/abundance	Formula	Mass (m/z)	Mass fragment ions	Class of compound	Reported from plant species	References
1	1,5-Bis(4-hydroxy-3-methoxyphenyl)-1,4-pentadien-3-one	23.5	3535	C ₁₉ H ₁₈ O ₅	325.1247	117; 118; 119; 120; 135; 143; 145; 146; 159; 161; 187	Diarylheptanoid	<i>Curcuma longa</i> L.	Li et al. (2011)
2	Ar-Turmerone	24.7	23545	C ₁₅ H ₂₀ O	216.1	103; 104; 105; 106; 107; 108; 115; 116; 117; 118; 119; 120	Bisabolane sesquiterpene	<i>Curcuma longa</i> L.	Parthasarathy and Chempakam (2008)
3	Tetrahydroxybisdemethoxycurcumin	25.4	4773	C ₁₉ H ₂₀ O ₄	311.1446	117; 118; 119; 120; 146; 161	Diarylheptanoid	<i>Curcuma longa</i> L.	Jiang et al. (2006)
4	Tetrahydrodemethoxycurcumin	25.9	7734	C ₂₀ H ₂₂ O ₅	341.1272	101; 113; 119	Diarylheptanoid	<i>Piper nigrum</i> L.	Ravindran (2000)
5	1-(4-Hydroxyphenyl)-7-(4-hydroxy-3-methoxyphenyl)-1,4,6-heptatrien-3-one	26.1	76458	C ₂₀ H ₁₈ O ₄	321.0938	115; 117; 119; 121; 132; 133; 134; 143; 145; 174; 235; 237; 247; 263; 264; 274; 275	Diarylheptanoid	<i>Curcuma longa</i> L.	Jiang et al. (2006)
6	1,7-Bis(4-hydroxy-3-methoxyphenyl)-1,4,6-heptatrien-3-one	26.3	64172	C ₂₁ H ₂₀ O ₅	351.1123	108; 115; 119; 136; 143; 148; 164; 195; 207; 223; 224; 235; 245; 251; 261; 262; 263; 279; 291; 307	Diarylheptanoid	<i>Curcuma longa</i> L.	Jiang et al. (2006)
7	Tetrahydroxycurcumin	26.5	81260	C ₂₀ H ₂₀ O ₇	371.1686	133; 134; 135; 148; 149; 175; 176; 177	Diarylheptanoid	<i>Curcuma longa</i> L.	Jiang et al. (2006)
8	1-(4-Hydroxy-3-methoxyphenyl)-7-(4-hydroxy-3,5-dimethoxyphenyl)-1,4,6-heptatrien-3-one	26.84	58571	C ₂₂ H ₂₂ O ₆	382.1	149; 159; 173; 197; 209; 211; 221; 233; 237; 239; 249; 261; 267; 277; 289; 293; 295; 305; 309	Diarylheptanoid	<i>Curcuma longa</i> L.	Jiang et al. (2006)
9	1,6-Heptadiene-3,5-dione, 1-(3,4-dihydroxyphenyl)-7-(4-hydroxy phenyl)-	31.6	5753	C ₁₉ H ₁₆ O ₅	324.1	134; 135; 136; 143	Diarylheptanoid	<i>Curcuma longa</i> L.	Jiang et al. (2006)
10	1-(3,4-Dihydroxyphenyl)-7-(4-hydroxy-3-methoxyphenyl)-hepta-1,6-diene-3,5-dione	32.3	16375	C ₂₀ H ₁₈ O ₆	353.1212	134; 135; 136; 150	Diarylheptanoid	<i>Curcuma longa</i> L.	Jiang et al. (2006)
11	Bisdemthoxycurcumin	34.5	1675644	C ₁₉ H ₁₆ O ₄	307.1132	117; 119; 120; 143; 145	Diarylheptanoid	<i>Curcuma longa</i> L.	Jiang et al. (2006)
12	Demethoxycurcumin	35.4	1302410	C ₂₀ H ₁₈ O ₅	337.1251	117; 119; 120; 132; 134; 143; 145; 158; 160; 175; 201	Diarylheptanoid	<i>Curcuma longa</i> L.	Jiang et al. (2006)
13	Dihydrocurcumin	35.8	5151	C ₂₁ H ₂₂ O ₆	369.1533	132; 134; 135; 149	Diarylheptanoid	<i>Curcuma longa</i> L.	Jiang et al. (2006) (Continued on following page)

TABLE 8 | (Continued) Compounds commonly detected by LC-MS analysis of rhizomes extract of all seven cultivars of *Curcuma* spp.: five of *Curcuma longa* L. (cvs. Alleppey Supreme, Duggirala Red, Prathibha, Salem, and Suguna) and two of *C. aromatica* Salisb. (cvs. Kasturi Araku, Kasturi Avidi). The structures for the compounds in the serial numbers 10, 5, 6, 15, and 1 are given in Figure 4 (panels 13, 14, 15, 16, and 17 respectively).

Sl. No.	Compound name	RT (Min)	Area/abundance	Formula	Mass (m/z)	Mass fragment ions	Class of compound	Reported from plant species	References
14	Curcumin	36.2	1503497	C ₂₁ H ₂₀ O ₆	367.1374	158; 160; 175 132; 133; 134; 135 149; 158; 160; 161 175	Diarylheptanoid	<i>Curcuma longa</i> L.	Jiang et al. (2006)
15	1-Heptene-3,5-dione, 1,7-bis-(4-hydroxy-3-methoxyphenyl)-	43.2	5078	C ₂₀ H ₂₀ O ₅	339.1473	117; 119; 120; 134 158	Diarylheptanoid	<i>Curcuma longa</i> L.	Jiang et al. (2006)

alcoholic monoterpenoid) was earlier reported from leaf and peel essential oil of *Citrus medica* L. (Rutaceae). This compound is used as a flavoring agent (Bhuiyan et al., 2009); trans, trans-octa-2,4-dienyl acetate, present in common Malaysian *Kaempferia galanga* L. (Zingiberaceae), was used for its food-flavoring property (Othman et al., 2006). Phenol, 2-methoxy-3-(2-propenyl)-, an allyl chain-substituted guaiacol was reported from rosewood extracts (Jiang et al., 2018).

The following four compounds were identified from cv. Duggirala Red (*C. longa* L.): 3-isopropyl-4-methyl-1-pentyn-3-ol (alcohol constituent) containing leaf and stem of *Anethum sowa* Roxb. ex, Fleming, used for flavoring of food, beverages and also for many medical preparations (Saleh-e-in et al., 2010); 5,9-tetradecadiyne (unsaturated hydrocarbon) was found to be a major component of *Ferula veseritensis* Coss. & Durieu ex Trab. leaf essential oil (Zellagui et al., 2012); naphthalene, 5-butyl-1,2,3,4-tetrahydro- (tetralin type of compounds) found in the essential oil of *Meconopsis punicea* Maxim. and *M. delavayi* (Franch.) Franch. Ex Prain (Slavík and Slavíková; Yuan et al., 2003); and santolina alcohol was reported from plant *Achillea filipendulina* Lam. (Sharopov and Setzer, 2010). A total of nine cultivar-specific compounds were detected in cv. Prathibha (*C. longa* L.) and the examples of these compounds and their source plants, respectively, are 7-tetracyclo[6.2.1.0(3.8)0(3.9)]undecanol, 4,4,11,11 tetramethyl- in *Cyperus articulatus* L. (Metuge et al., 2014); bicyclo(2.2.1)hept-2-ene, 2,3-dimethyl- in *Abies alba* Mill. (Yang et al., 2009). Cultivar-specific compounds of three each were detected in cvs. Salem (*C. longa* L.) and Suguna (*C. longa* L.) (Table 2). In *C. aromatica* Salisb., only one cultivar-specific compound was detected in cv. Kasturi Avidi, i.e., 3-octen-5-yne, 2,7-dimethyl-, (Z)-, and this compound was earlier reported from the medicinally important *Litsea glutinosa* (Lour.) C.B. Rob. fruit essential oil (Chowdhury et al., 2008a).

Some of the compounds identified in our study were present in more than one cultivar. For example, 6-(p-tolyl)-2-methyl-2-heptenol (Table 3) was detected in three cvs.: Alleppey supreme, Suguna of *C. longa* L., and Kasturi Avidi of *C. aromatica* Salisb. This compound was earlier reported from *Zingiber officinale* Roscoe (Zingiberaceae), used as a spice, food products, and beverages (Choudhary and Kareppa, 2013).

Limitations and Strengths of the Present Study

There is significant variability within and between the cultivars of *C. longa* L. and *C. aromatica* Salisb, which can be exploited to differentiate the cultivars of *Curcuma* spp. The feasibility of studies without using any standard compounds was pointed out by Núñez et al. (2020). Similarly, reference compounds were not used in our study to derive arithmetic indices under the experimental conditions. Despite the dilution made in the essential oil sample before injecting into the GC-MS system, the sample was still too concentrated. The high concentration of oil might have restricted the resolution due to overloading the detector. This could be the reason that we could not identify several compounds. We would ensure the further dilution of the oil sample in our future studies. However, the technology employed, GC-TOFMS and LC-QTOFMS, and MS-spectral database/literature search enabled us to establish the cultivar variability of *Curcuma* spp. The detailed information on the metabolite variability within or/and between the cultivars of *C. longa* L. and *C. aromatica* Salisb. may assist us in selecting the cultivars for a specific purpose, like culinary use, coloring, or pharmacological purpose. The studies such as the present one can help to select cultivars, particularly for use in pharmacology or the food industry. Metabolite variability poses a challenge in the use of turmeric in therapy. The practitioners need to be quite careful and use the identified cultivar and avoid mix-up. The caution applies to commercial/industrial use. Once standardized, the protocol should ensure the use of a specific cultivar. Our GC-MS and LC-MS-based metabolite identification is distinct from chemophenetic studies but is a complementary approach to characterize the *Curcuma* metabolome.

Importance of *Curcuma* spp. Metabolites for Human Health

Curcuminoids (CU, DMC, and BDMC) were identified as the main bioactive compounds of genus *Curcuma* and proved to have a broad spectrum of biological activities based on pharmacological studies. However, rhizomes and their essential oils of *Curcuma* spp. contained several other

TABLE 9 | Pharmacological activity of metabolites identified, other than major curcuminoids (curcumin, demethoxycurcumin, and bisdemethoxy curcumin), in *C. longa* L. and *C. aromatica* Salisb.

Sl. No.	Compound name	Source plant	Tested Compound/essential oil/extract	Pharmacological activity/health benefit of the compound or compound containing plant product	References (Activity assay or compound detection)
1	Carvacrol	<i>Curcuma longa</i> L.	Compound	Antibacterial	Suntres et al. (2015)
2	p-Cymene	<i>Curcuma longa</i> L.	Compound	Antioxidant	(De Oliveira et al. (2015)
				Anti-inflammatory, anticancer, and antimicrobial effects	Marchese et al. (2017)
3	Eucalyptol	<i>Curcuma longa</i> L.	Compound	Antitumor anti-inflammatory relevance to Alzheimer's disease	Murata et al. (2013); Islam et al. (2014)
4	α -Pinene	<i>Curcuma longa</i> L.	Compound	Anti-inflammatory and chondroprotective	Rufino et al. (2014)
5	α -Terpineol	<i>Curcuma longa</i> L.	Compound	Anti-inflammatory	De Oliveira et al. (2012)
6	Terpinolene	<i>Curcuma longa</i> L.	Compound	Anticancer	Okumura et al. (2012)
7	2-Heptadecanone	<i>Curcuma angustifolia</i> Roxb	Dried rhizome essential oil	As a coolant, demulscent	Srivastava et al. (2006)
8	Santolina alcohol	<i>Achillea filipendulina</i> Lam	Aerial part essential oil	Traditional herbal medicine	Sharopov and Setzer (2010)
9	Cyclohexanol, 2-methyl-5-(1-methylethenyl)-	<i>Mentha spicata</i> L.	Aerial parts essential oil	Antifungal	Mohammed et al. (2017)
10	Cyclohexane, 1,2-dimethyl-3,5-bis(1-methylethenyl)-	<i>Rhanterium adpressum</i> Coss. & Durieu	Aerial parts essential oil	Antifungal	Kala et al. (2009)
11	4-Ethylphenethylamine	<i>Psidium guajava</i> L.	Stem bark essential oil	Antioxidant	Fasola et al., 2011)
12	5,9-Tetradecadiyne	<i>Ferula vesceritensis</i> Coss. & Durieu ex Trab	Leaves essential oil	Antibacterial	Zellagui et al. (2012)
13	E-11-Tetradecenoic acid	<i>Coriandrum sativum</i> L.	Leaf essential oil	Spice, flavoring agent, antimicrobial	Bhuiyan et al. (2009)
14	6,10-Dodecadien-1-yn-3-ol, 3,7,11-trimethyl-	<i>Hiptage benghalensis</i> (L.) Kurz	Leaves essential oil	Treatment of skin diseases, cough, asthma, leprosy	Venkataramani and Chinnagounder (2012)
15	Chavicol	<i>Piper betle</i> L.	Leaf oil	Antifungal, antiseptic, and anthelmintic	Nagori et al. (2011)
16	1,2-Cyclohexanediol, 1-methyl-4-(1-methylethyl)-	<i>Citrus medica</i> L.	Leaf and peel essential oil	Antibiotic	Bhuiyan et al. (2009)
17	3-Isopropyl-4-methyl-1-pentyn-3-ol	<i>Anethum sowa</i> Roxb. ex, Fleming	Leaf and stem essential oil	Flavoring of food and beverages, antimicrobial, antioxidant	Saleh-e-in et al. (2010)
18	Bicyclo(2.2.1)hept-2-ene, 2,3-dimethyl-	<i>Abies alba</i> Mill	Leaf and twig essential oil	Radical scavenging activity	Yang et al. (2009)
19	2-Nonen-4-yn-1-ol, (Z)-	<i>Alpinia speciosa</i> (J.C. Wendl.) K. Schum	Seeds and leaves essential oil	As a food and herbal medicine, mosquito larvicidal activity	Ho (2010)
20	8-Methylene-3-oxatricyclo [5.2.0.0(2,4)]nonane	<i>Schisandra chinensis</i> (Turcz.) Baill	Dried fruit essential oil	Antioxidant	Wang et al. (2005)
21	3-Cyclohexen-1-one, 3,5,5-trimethyl-	<i>Crocus sativus</i> L.	Dried saffron oil	Antitumor	(D'Auria et al. (200
22	Ar-Turmerone α -Turmerone β -Turmerone α -Santalene Ar-Curcumene	<i>Curcuma longa</i> L.	Rhizome essential oil	Antioxidant	Singh et al. (2010)
23	7-Tetracyclo[6.2.1.0(3.8)0(3.9)]undecanol, 4,4,11,11 tetramethyl-	<i>Cyperus articulatus</i> L.	Roots/rhizome essential oil	Anti-onchocera activity	Metuge et al. (2014)
24	Cholesta-8,24-dien-3-ol, 4-methyl-, (3 α ,4 α)-	<i>Parkia speciosa</i> Hassk.	Seed essential oil	High nutritional and medicinal value	Salman et al. (2006)
25	3-Octen-5-yne, 2,7-dimethyl-, (Z)-	<i>Litsea glutinosa</i> (Lour.) C.B. Rob	Fruit essential oil	Antirheumatic	Chowdhury et al. (2008b)
26	5,8,11,14-Eicosatetraenoic acid, phenylmethyl ester, (all-Z)-	<i>Petiveria alliacea</i> L.	Whole plant essential oil	Used as folk medicine to enhance memory and in treatment of common cold, flu, other viral, or bacterial infections	Sathiyabalan et al. (2014)
27	Naphthalene, 5-butyl-1,2,3,4-tetrahydro-	<i>Meconopsis punicea</i> Maxim. and <i>M. delavayi</i> (Franch.) Franch. Ex Prain	Whole plant essential oil	As a traditional medicinal plant for anti-inflammatory and analgesic activity	Yuan et al. (2003)
28	1H-3a,7-methanoazulene, 2,3,4,7,8,8a-hexahydro-3,6,8,8-tetramethyl-, [3R-(3 α ,3 α ,7 α ,8 α)]-	<i>Lindera aggregata</i> (Sims) Kosterm	Root/tubers essential oil	Treatment of decubitus ulcer	Hong (2011)
29	trans, trans-Octa-2,4-dienyl acetate	<i>Kaempferia galanga</i> L.	Dried rhizomes	Spice, food-flavoring agent	Othman et al. (2006)

(Continued on following page)

TABLE 9 | (Continued) Pharmacological activity of metabolites identified, other than major curcuminoids (curcumin, demethoxycurcumin, and bisdemethoxy curcumin), in *C. longa* L. and *C. aromatica* Salisb.

Sl. No.	Compound name	Source plant	Tested Compound/ essential oil/extract	Pharmacological activity/health benefit of the compound or compound containing plant product	References (Activity assay or compound detection)
30	11-Dodecen-2-one	<i>Ficus hispida</i> L. f	Fresh male and female receptive figs	Vasorelaxant Hepatoprotective, anti-inflammatory, antipyretic	Song et al. (2001)
31	Kaempferol-3,7-O-dimethyl ether	<i>Lumnitzera racemosa</i> Willd and <i>Artemisia vulgaris</i> L.	Fresh twig methanolic extract; leaf methanolic extract	Antibacterial	Nikolova (2006); DeSouza et al. (2010)
32	5,7,8-Trihydroxy-2',5'-dimethoxy-3',4'-methylene dioxysoflavanone	<i>Terminalia ivorensis</i> A. Chev	Fresh sawdust	Antifungal	Ogundare and Olajuyigbe (2012)
33	Kaempferol-3-O-rutinoside-7-O-glucoside	<i>Lycopersicon esculentum</i> Mill	Methanolic extract of fruit	Antioxidant	Le Gall et al. (2002)
34	Phenol, 2-methoxy-3-(2-propenyl)-	<i>Dalbergia stevensonii</i> Standl	Wood extracts	Used as raw material for medical industries	Jiang et al. (2018)
35	2-Pentanone, 4-mercapto-4-methyl-	<i>Camellia sinensis</i> (L.) Kuntze	Tea leaves	Antioxidant	Kumazawa et al. (2005)

bioactive (volatile and nonvolatile) compounds. A summary of the pharmacological studies with the metabolites detected in the present study is given in **Table 9**. Some of the studies demonstrated therapeutic activity with the isolated metabolites, e.g., carvacrol (Suntres et al., 2015), p-cymene (De Oliveira et al., 2015), which are commonly found in essential oils of *Curcuma* spp. A few other reports correlated anti-inflammatory and antioxidant properties of *C. longa* L. essential oil with its chemical components α -tumerone, α -santalene (Singh et al., 2010) (**Table 9**). Several compounds detected in the present study in the essential oil or rhizome extracts of *C. longa* L. or *C. aromatica* Salisb. were also found in the essential oil of other medicinal plants, traditionally used for their health benefits. The examples of such compounds are 5,9-tetradecadiyne, a cultivar-specific compound of Duggirala Red (*C. longa* L.), earlier reported in *Ferula vesceritensis* Coss. & Durieu ex Trab. leaf essential oil, exhibiting antibacterial activity; 3-octen-5-yne, 2,7-dimethyl-, (Z)-, a hydrocarbon monoterpene, identified from cv. Kasturi Avidi (*C. aromatica* Salisb.) was earlier reported from fruit essential oil of the medicinally important plant, *Litsea glutinosa* (Lour.) C.B. Rob. (Chowdhury et al., 2008a). We suggest that the medicinal use of the genus *Curcuma* can be not only species but also cultivar-specific.

CONCLUDING REMARKS

Essential oils from spices and aromatic plants are enriched with bioactive metabolites, easily isolated and used, unlike the difficulties encountered with synthetic chemical products. The low mammalian toxicity and biodegradable nature of the natural secondary products provide an attractive option to develop them also for crop protection. Metabolomics is a practical and dynamic approach to make a comprehensive

study. Both GC-MS and LC-MS techniques should be used to characterize the metabolite profiles of as many cultivars as possible for building a reference library. Preparative LC can be helpful to collect individual metabolite fractions and establish their identity. Several metabolites detected in 7 selected cultivars of *Curcuma* spp. by GC-MS and LC-MS analyses are reported first time in *Curcuma* spp. We suggest that the seven Indian cultivars of *Curcuma* spp. employed in our study can be used as sources of such compounds. High-throughput analysis of cultivar-specific and first-time detected compounds in the present study may lead to new drug candidates. The metabolites validated for their medicinal or other users can be quantified using simple techniques such as HPLC or TLC to ensure their presence in the herbal preparations.

DATA AVAILABILITY STATEMENT

The datasets presented in this study can be found in online repositories. The names of the repository/repositories and accession number(s) can be found below: <https://www.ebi.ac.uk/metabolights/MTBLS2790>.

AUTHOR CONTRIBUTIONS

ST and AR planned and designed all the experiments. PK and PKK did the experiments and preliminary data interpretation related to GC-MS and LC-MS/MS, respectively. PK, ST, and AR re-analyzed the data and wrote the draft of the manuscript. SA prepared tables and reference search. AA drew the figures and helped in editing the manuscript. All the authors read and approved the final version of the manuscript.

FUNDING

Part of this study was supported by grants from DBT (BT/PR/11674/PBD/16/838/2008) sanctioned to Prof. A.S. Raghavendra (PI) and Prof. Sarada D. Tetali (co-PI) and the Institute of Eminence - University of Hyderabad (IoE-UoH) Research Chair Professor Grant to Prof. A.S. Raghavendra.

ACKNOWLEDGMENTS

The authors are indebted to Professors K. Uma Maheshwari (Turmeric Research Station, Kammarpally of Telangana State, India) and K. Nirmal Babu (Indian Institute of Spices Research, Marikunnu, Kozhikode, Kerala, India) for providing turmeric samples. PK and PKK acknowledge their research fellowships from the research project (BT/PR/11674/PBD/16/838/2008). SA is a recipient of a research fellowship from the University of Hyderabad and AA is a recipient of UGC-JRF (856/SC/CSIR-UGC/NET/Dec 2016). The authors are thankful to Prasanth Bitla, School of Life Sciences, University of Hyderabad, for acquisition of GC-MS and LC-MS data. The authors are thankful to DBT-CREBB, DBT-FIST, and UGC-SAP for supporting infrastructural facilities of the Department of Plant Sciences and School of Life Sciences. The authors also acknowledge the ChemDraw Ultra 12.0 software tool used to draw structures in **Figures 2, 3** and **4**.

SUPPLEMENTARY MATERIAL

The Supplementary Material for this article can be found online at: <https://www.frontiersin.org/articles/10.3389/fphar.2021.659546/full#supplementary-material>

Supplementary Figure 1 | (A) Representative TIC chromatograms from negative ion (–) ESI-HPLC from cultivars (A) Alleppey Supreme, (B) Duggirala Red, (C) Prathibha, (D) Salem, (E) Suguna of *Curcuma longa* L. and cvs. (F) Kasturi Araku, (G) Kasturi Avidi of *C. aromatica* Salisb. Peak labelled IS represents internal standard. **(B)** Representative TIC chromatograms from positive ion (+) ESI-HPLC from cultivars (A) Alleppey Supreme, (B) Duggirala Red, (C) Prathibha, (D) Salem, (E) Suguna of *Curcuma longa* L. and cvs. (F) Kasturi Araku, (G) Kasturi Avidi of *C. aromatica* Salisb. Peak labelled IS represents internal standard.

REFERENCES

- Aggarwal, B. B., Sundaram, C., Malani, N., and Ichikawa, H. (2007). "Curcumin: The Indian Solid Gold," in *The Molecular Targets and Therapeutic Uses of Curcumin in Health and Disease*. Editors B. B. Aggarwal, Y.-J. Surh, and S. Shishodia (Boston, MA: Springer US), 1–75. doi:10.1007/978-0-387-46401-5_1
- Angel, G. R., Menon, N., Vimala, B., and Nambisan, B. (2014). Essential Oil Composition of Eight Starchy *Curcuma* Species. *Ind. Crops Prod.* 60, 233–238. doi:10.1016/j.indcrop.2014.06.028
- Awasthi, P. K., and Dixit, S. C. (2009). Chemical Composition of Curcuma Longaleaves and Rhizome Oil from the plains of Northern India. *J. Young Pharm.* 1, 312. doi:10.4103/0975-1483.59319
- Beekwilder, J., Jonker, H., Meesters, P., Hall, R. D., Van Der Meer, I. M., and Ric de Vos, C. H. (2005). Antioxidants in Raspberry: On-Line Analysis Links

Supplementary Figure 2 | MS and MS/MS spectra of cultivar-specific compounds first time reported from genus *Curcuma*, identified from cultivars of *Curcuma longa* L. and *C. aromatica* Salisb. detected in essential oil (1–35) and rhizome extracts (36–39) by GC-MS (MS spectra) and LC-MS (MS/MS spectra) respectively. (Spectra 1–23 corresponds to panel numbers: 1–23 of **Figure 2** and serial numbers: 1–23 of Table 2. Spectra 24–35 corresponds to panel numbers: 24–35 of **Figure 2** and serial numbers: 1–12 of **Table 3**. Spectra 36 correspond to panel numbers 36 of **Figure 2** and serial number 1 of **Table 6**. Spectra 37–39 correspond to panel number 37–39 of **Figure 2** and serial number 1–3 of **Table 7**). (1) 1,2-Cyclohexanediol, 1-methyl-4-(1-methylethyl)-, (2) trans, trans-Octa-2,4-dienyl acetate, (3) Phenol, 2-methoxy-3-(2-propenyl)-, (4) 3-Isopropyl-4-methyl-1-pentyn-3-ol (5) 5,9-Tetradecadiyne, (6) Naphthalene, 5-butyl-1,2,3,4-tetrahydro-, (7) Santolina alcohol, (8) 2-Pentanone, 4-mercapto-4-methyl-, (9) 8-Methylene-3-oxatricyclo[5.2.0.0(2,4)]nonane, (10) 7-Tetracyclo[6.2.1.0(3,8)0(3,9)]undecanol, 4,4,11,11 tetramethyl-, (11) Bicyclo[2.2.1]hept-2-ene, 2,3-dimethyl-, (12) 1H-3a,7-Methanoazulene, 2,3,4,7,8,8a-hexahydro-3,6,8,8-tetramethyl-, [3R-(3a,3a, 7a, 8a)], (13) Cholesta-8,24-dien-3-ol, 4-methyl-, (3a,4a)-, (14) 4-Ethylphenethylamine, (15) Cyclohexanol, 2-methyl-5-(1-methylethenyl)-, (16) Cyclohexane, 1,2-dimethyl-3,5-bis(1-methylethenyl)-, (17) 5,8,11,14-Eicosatetraenoic acid, phenylmethyl ester, (all-Z)-, (18) 11-Dodecen-2-one, (19) E-11-Tetradecenoic acid, (20) 2-Nonen-4-yn-1-ol, (Z)-, (21) 3-Cyclohexen-1-one, 3,5,5-trimethyl-, (22) 6,10-Dodecadien-1-yn-3-ol, 3,7,11-trimethyl-, (23) 3-Octen-5-yne, 2,7-dimethyl-, (Z)-, (24) 1,3,5-Cycloheptatriene, (25) Bicyclo[3.1.0]hexane, 4-methyl-1-(1-methylethyl)-, dihydro deriv., (26) Bicyclo[3.2.1]oct-2-ene, 3-methyl-4-methylene-, (27) Oxirane, 2-(hexyn-1-yl)-3-methoxymethylene-, (28) Bergamotol, Z- α -trans-, (29) (1,3-Dimethyl-2-methylene-cyclopentyl)-methanol, (30) 12-Oxabicyclo[9.1.0]dodeca-3,7-diene, 1,5,5,8-tetramethyl-, [1R-(1R*,3E,7E,11R)]-, (31) Isologifolene, 4,5,9,10-dehydro-, (32) Z,Z,Z-4,6,9-Nonadecatriene, (33) 6-(p-Tolyl)-2-methyl-2-heptanol, (34) 6-Tridecen-4-yne, (Z)-, (35) 1,4-Cyclohexadiene, 1-methyl-, (36) Kaempferol-3,7-O-dimethyl ether, (37) 5,7,8-Trihydroxy-2',5'-dimethoxy-3',4'-methylene dioxysoflavanone, (38) Chavicol, (39) Kaempferol-3-O-rutinoside-7-O-glucoside.

Supplementary Table 1 | A list of secondary metabolites identified by GC-MS in the essential oil from the rhizomes of five cvs. of *C. longa* L. and two cvs. of *C. aromatica* Salisb. Abbreviations: AS, Alleppey Supreme; DR, Duggirala Red; PR, Prathibha; SA, Salem; SU, Suguna; KA, Kasturi Araku; KAV, Kasturi Avidi.

Supplementary Table 2 | A list of secondary metabolites identified by LC-MS in the rhizomes extract of five cvs. of *C. longa* L. and two cvs. of *C. aromatica* Salisb. Abbreviations used: AS, Alleppey Supreme; DR, Duggirala Red; PR, Prathibha; SA, Salem; SU, Suguna; KA, Kasturi Araku; KAV, Kasturi Avidi.

Supplementary Table 3 | Identification parameters of first-time reported compounds by GC-MS in the essential oil from the seven cultivars of *Curcuma* spp. along with the methods used in previous literature.

Supplementary Table 4 | Identification parameters of first-time reported compounds by LC-MS in the rhizome extracts of genus *Curcuma* along with the methods used in related previous literature.

Supplementary Table 5 | The list of 80 compounds identified by GCMS analysis.

Supplementary Table 6 | The list of 62 compounds identified by LCMS analysis.

- Antioxidant Activity to a Diversity of Individual Metabolites. *J. Agric. Food Chem.* 53, 3313–3320. doi:10.1021/jf047880b
- Behura, S., Sahoo, S., and Srivastava, V. K. (2002). Major Constituents in Leaf Essential Oils of *Curcuma Longa* L. And *Curcuma Aromatica* Salisb. *Curr. Sci.* 83, 1312–1313.
- Bhuiyan, M. N. I., Begum, J., Sardar, P. K., and Rahman, M. S. (2009). Constituents of Peel and Leaf Essential Oils of *Citrus Medica* L. *J. Sci. Res.* 1, 387–392. doi:10.3329/jsr.v1i2.1760
- Chen, W. F., Deng, S. L., Zhou, B., Yang, L., and Liu, Z. L. (2006). Curcumin and its Analogues as Potent Inhibitors of Low Density Lipoprotein Oxidation: H-Atom Abstraction from the Phenolic Groups and Possible Involvement of the 4-Hydroxy-3-Methoxyphenyl Groups. *Free Radic. Biol. Med.* 40, 526–535. doi:10.1016/j.freeradbiomed.2005.09.008
- Cheng, J. H., Wu, W. Y., Liu, W. S., Chang, G., Liu, Y. L., Yang, Z. G., et al. (1999). Treatment of 17 Cases of Patients with Primary Liver Cancer with *Curcuma Aromatica* Oil Infused via Hepatic Artery. *Shijie Huaren Xiaohua Zazhi* 7, 92.

- Choudhari, S. S., and Kareppa, B. M. (2013). Identification of Bioactive Compounds of *Zingiber Officinale* roscoe Rhizomes through Gas Chromatography and Mass Spectrometry. *Int. J. Pharm. Res. Dev* 5, 16–20.
- Choudhury, S. N., Ghosh, A. C., Saikia, M., Choudhury, M., and Leclercq, P. A. (1996). Volatile Constituents of the Aerial and Underground Parts of *Curcuma aromatica* Salisb. From India. *J. Essent. Oil Res.* 8, 633–638. doi:10.1080/10412905.1996.9701031
- Chowdhury, J. U., Bhuiyan, M. N. I., and Nandi, N. C. (2008b). Aromatic Plants of Bangladesh : Essential Oils of Leaves and Fruits of *Litsea Glutinosa* (Lour.) C.B. Robinson. *Bangladesh J. Bot.* 37, 81–83. doi:10.3329/bjb.v37i1.1568
- Chowdhury, J. U., Nandi, N. C., Bhuiyan, M. N. I., and Mobarok, M. H. (2008a). Essential Oil Constituents of the Rhizomes of Two Types of *Curcuma Longa* of Bangladesh. *Bangladesh J. Sci. Ind. Res.* 43, 259–266. doi:10.3329/bjsir.v43i2.970
- D'Auria, M., Mauriello, G., Racioppi, R., and Rana, G. L. (2006). Use of SPME-GC-MS in the Study of Time Evolution of the Constituents of Saffron Aroma: Modifications of the Composition during Storage. *J. Chromatogr. Sci.* 44, 18–21. doi:10.1093/chromsci/44.1.18
- De Oliveira, M. G., Marques, R. B., De Santana, M. F., Santos, A. B., Brito, F. A., Barreto, E. O., et al. (2012). α -Terpineol Reduces Mechanical Hypernociception and Inflammatory Response. *Basic Clin. Pharmacol. Toxicol.* 111, 120–125. doi:10.1111/j.1742-7843.2012.00875.x
- De Oliveira, T. M., De Carvalho, R. B., Da Costa, I. H., De Oliveira, G. A., De Souza, A. A., De Lima, S. G., et al. (2015). Evaluation of P-Cymene, a Natural Antioxidant. *Pharm. Biol.* 53, 423–428. doi:10.3109/13880209.2014.923003
- De Vos, R. C., Moco, S., Lommen, A., Keurentjes, J. J., Bino, R. J., and Hall, R. D. (2007). Untargeted Large-Scale Plant Metabolomics Using Liquid Chromatography Coupled to Mass Spectrometry. *Nat. Protoc.* 2, 778–791. doi:10.1038/nprot.2007.95
- DeSouza, L., Wahidulla, S., and Devi, P. (2010). Antibacterial Phenolics from the Mangrove *Lumnitzera Racemosa*. *Indian J. Mar. Sci.* 39, 294–298.
- Dixon, R. A., Gang, D. R., Charlton, A. J., Fiehn, O., Kuiper, H. A., Reynolds, T. L., et al. (2006). Applications of Metabolomics in Agriculture. *J. Agric. Food Chem.* 54, 8984–8994. doi:10.1021/jf061218t
- Dosoky, N. S., Satyal, P., and Setzer, W. N. (2019). Variations in the Volatile Compositions of *Curcuma* Species. *Foods* 8, 1–14. doi:10.3390/foods8020053
- Dosoky, N. S., and Setzer, W. N. (2018). Chemical Composition and Biological Activities of Essential Oils of *Curcuma* Species. *Nutrients* 10, 10–17. doi:10.3390/nu10091196
- Eggink, P. M., Maliepaard, C., Tikunov, Y., Haanstra, J. P. W., Pohn-Flament, L. M. M., de Wit-Maljaars, S. C., et al. (2012). Prediction of Sweet Pepper (*Capsicum annuum*) Flavor Over Different Harvests. *Euphytica* 187, 117–131. doi:10.1007/s10681-012-0761-6
- Esatbeyoglu, T., Huebbe, P., Ernst, I. M., Chin, D., Wagner, A. E., and Rimbach, G. (2012). Curcumin—from Molecule to Biological Function. *Angew. Chem. Int. Ed. Engl.* 51, 5308–5332. doi:10.1002/anie.201107724
- Fasola, T. R., Oloyede, G. K., and Aponjolosun, B. S. (2011). Chemical Composition, Toxicity and Antioxidant Activities of Essential Oils of Stem Bark of Nigerian Species of Guava (*Psidium Guajava* Linn.). *EXCLI J.* 10, 34–43. doi:10.17877/DE290R-1133
- Ferreira, F. D., Kimmelmeier, C., Arrotéia, C. C., Da Costa, C. L., Mallmann, C. A., Janeiro, V., et al. (2013). Inhibitory Effect of the Essential Oil of *Curcuma Longa* L. And Curcumin on Aflatoxin Production by *Aspergillus flavus* Link. *Food Chem.* 136, 789–793. doi:10.1016/j.foodchem.2012.08.003
- Gopalan, B., Goto, M., Kodama, A., and Hirose, T. (2000). Supercritical Carbon Dioxide Extraction of Turmeric (*Curcuma Longa*). *J. Agric. Food Chem.* 48, 2189–2192. doi:10.1021/jf9908594
- Hahm, E. R., Cheon, G., Lee, J., Kim, B., Park, C., and Yang, C. H. (2002). New and Known Symmetrical Curcumin Derivatives Inhibit the Formation of Fos-Jun-DNA Complex. *Cancer Lett.* 184, 89–96. doi:10.1016/S0304-3835(02)00170-2
- Hall, R. D. (2006). Plant Metabolomics: From Holistic hope, to Hype, to Hot Topic. *New Phytol.* 169, 453–468. doi:10.1111/j.1469-8137.2005.01632.x
- He, X. G. (2000). On-line Identification of Phytochemical Constituents in Botanical Extracts by Combined High-Performance Liquid Chromatographic-Diode Array Detection-Mass Spectrometric Techniques. *J. Chromatogr. A.* 880, 203–232. doi:10.1016/S0021-9673(00)00059-5
- Herath, H. M. I. C., Wijayasiriwardene, T. D. C. M. K., and Premakumara, G. A. S. (2017). Comparative GC-MS Analysis of All *Curcuma* Species Grown in Sri Lanka by Multivariate Test. *Ruhuna J. Sci.* 8, 103. doi:10.4038/rjs.v8i2.29
- Herebian, D., Choi, J. H., Abd El-Aty, A. M., Shim, J. H., and Spittler, M. (2009). Metabolite Analysis in *Curcuma Domestica* Using Various GC-MS and LC-MS Separation and Detection Techniques. *Biomed. Chromatogr.* 23, 951–965. doi:10.1002/bmc.1207
- Ho, J.-C. (2010). Chemical Composition and Bioactivity of Essential Oil of Seed and Leaf from *Alpinia speciosa* Grown in Taiwan. *Jnl Chin. Chem. Soc.* 57, 758–763. doi:10.1002/jccs.201000105
- Hong, L. (2011). *Radix Linderae* Essential Oil Improving the Immunity Activities and Preventing the Occurrence of Decubitus in Aged People. *J. Med. Plants Res.* 5, 3733–3738. doi:10.5897/JMPR.9001070
- Hong, S. L., Lee, G. S., Syed Abdul Rahman, S. N., Ahmed Hamdi, O. A., Awang, K., Aznam Nugroho, N., et al. (2014). Essential Oil Content of the Rhizome of *Curcuma Purpurascens* Bl. (Temu Tis) and its Antiproliferative Effect on Selected Human Carcinoma Cell Lines. *ScientificWorldJournal* 2014, 397430. doi:10.1155/2014/397430
- Huhman, D. V., and Sumner, L. W. (2002). Metabolic Profiling of Saponins in *Medicago Sativa* and *Medicago Truncatula* Using HPLC Coupled to an Electrospray Ion-Trap Mass Spectrometer. *Phytochemistry* 59, 347–360. doi:10.1016/S0031-9422(01)00432-0
- Ishida, J., Kozuka, M., Tokuda, H., Nishino, H., Nagumo, S., Lee, K. H., et al. (2002). Chemopreventive Potential of Cyclic Diarylheptanoids. *Bioorg. Med. Chem.* 10, 3361–3365. doi:10.1016/S0968-0896(02)00164-5
- Jiang, D. Q., Pu, Q. L., Huang, P., Huang, X. M., He, Y. Z., He, C. H., et al. (1989). [Studies on the Chemical Constituents of *Curcuma Kwangsiensis*]. *Yao Xue Xue Bao* 24, 357–359.
- Jiang, H., Timmermann, B. N., and Gang, D. R. (2006). Use of Liquid Chromatography-Electrospray Ionization Tandem Mass Spectrometry to Identify Diarylheptanoids in Turmeric (*Curcuma Longa* L.) Rhizome. *J. Chromatogr. A.* 1111, 21–31. doi:10.1016/j.chroma.2006.01.103
- Jiang, S. C., Ge, S. B., and Peng, W. (2018). Molecules and Functions of Rosewood: *Dalbergia stevenson*. *Arabian J. Chem.* 11, 782–792. doi:10.1016/j.arabjc.2017.12.032
- Joshi, J., Ghaisas, S., Vaidya, A., Vaidya, R., Kamat, D. V., Bhagwat, A. N., et al. (2003). Early Human Safety Study of Turmeric Oil (*Curcuma Longa* Oil) Administered Orally in Healthy Volunteers. *J. Assoc. Physicians India* 51, 1055–1060.
- Kala, A., Noureddine, G., Belkacemi, D., Segni, L., Zellagui, Amar., Samir, H., et al. (2009). Composition of the Essential Oil of *Rhanterium Adpressum* Coss. And Durieu. from Algeria. *Arch. Appl. Sci. Res.* 1, 115–118.
- Kanase, V., and Khan, F. (2018). An Overview of Medicinal Value of *Curcuma* Species. *Asian J. Pharm. Clin. Res.* 11, 40–45. doi:10.22159/ajpcr.2018.v11i12.28145
- Khan, A., Vaibhav, K., Javed, H., Tabassum, R., Ahmed, M. E., Khan, M. M., et al. (2014). 1,8-cineole (Eucalyptol) Mitigates Inflammation in Amyloid Beta Toxicated PC12 Cells: Relevance to Alzheimer's Disease. *Neurochem. Res.* 39, 344–352. doi:10.1007/s11064-013-1231-9
- Koo, H. J., and Gang, D. R. (2012). Suites of Terpene Synthases Explain Differential Terpenoid Production in Ginger and Turmeric Tissues. *PLoS One* 7, e51481. doi:10.1371/journal.pone.0051481
- Krup, V., Prakash, L. H., and A, H. (2013). Pharmacological Activities of Turmeric (*Curcuma Longa* linn): A Review. *J. Homeop Ayurv Med.* 02, 133. doi:10.4172/2167-1206.1000133
- Kulyal, P., Kuchibhatla, L. N., Uma Maheshwari, K., Nirmal Babu, K., Tetali, S. D., and Raghavendra, A. S. (2016). Highly Sensitive HPLC Method for Estimation of Total or Individual Curcuminoids in *Curcuma* Cultivars and Commercial Turmeric Powders. *Curr. Sci.* 111, 1816–1824. doi:10.18520/cs/v111/i11/1816-1824
- Kumar, V., Shriram, V., Bhagat, R., Khare, T., Kapse, S., and Kadoo, N. (2019). Phytochemical Profile, Anti-oxidant, Anti-inflammatory, and Anti-proliferative Activities of *Pogostemon Deccanensis* Essential Oils. *3 Biotech.* 9, 31. doi:10.1007/s13205-018-1560-0
- Kumazawa, K., Kubota, K., and Masuda, H. (2005). Influence of Manufacturing Conditions and Crop Season on the Formation of 4-Mercapto-4-Methyl-2-Pentanone in Japanese green tea (Sen-cha). *J. Agric. Food Chem.* 53, 5390–5396. doi:10.1021/jf050392z

- Kutti Gounder, D., and Lingamallu, J. (2012). Comparison of Chemical Composition and Antioxidant Potential of Volatile Oil from Fresh, Dried and Cured Turmeric (*Curcuma Longa*) Rhizomes. *Ind. Crops Prod.* 38, 124–131. doi:10.1016/j.indcrop.2012.01.014
- Ladan, Z., Amupitan, J. O., Oyewale, A. O., Okonkwo, E. M., Ladan, E. O., Odjobo, B., et al. (2011). Chemical Composition and Biological Activity of the Volatile Oils of *Hyptis Spicigera* against *Trypanosoma Brucei* Tbb Found in Northern Nigeria. *Afr. J. Pure Appl. Chem.* 5, 53–58.
- Le Gall, G., Colquhoun, I. J., Davis, A. L., Collins, G. J., and Verhoeven, M. E. (2003). Metabolite Profiling of Tomato (*Lycopersicon esculentum*) Using ¹H NMR Spectroscopy as a Tool to Detect Potential Unintended Effects Following a Genetic Modification. *J. Agric. Food Chem.* 51, 2447–2456. doi:10.1021/jf0259967
- Leela, N., Tava, A., Shafi, P. M., John, S. P., and Chempakam, B. (2002). Chemical Composition of Essential Oils of Turmeric (*Curcuma Longa* L.). *Acta Pharm.* 52, 137–141.
- Li, S., Yuan, W., Deng, G., Wang, P., Yang, P., and Aggrawal, B. (2011). Chemical Composition and Product Quality Control of Turmeric (*Curcuma Longa* L.). *Topharmacj* 5, 28–54. doi:10.2174/2210290601102010028
- Li, W., Wang, S., Feng, J., Xiao, Y., Xue, X., Zhang, H., et al. (2009a). Structure Elucidation and NMR Assignments for Curcuminoids from the Rhizomes of *Curcuma Longa*. *Magn. Reson. Chem.* 47, 902–908. doi:10.1002/mrc.2478
- Li, Y., Wo, J. M., Liu, Q., Li, X., and Martin, R. C. (2009b). Chemoprotective Effects of *Curcuma Aromatica* on Esophageal Carcinogenesis. *Ann. Surg. Oncol.* 16, 515–523. doi:10.1245/s10434-008-0228-0
- Liang, G., Shao, L., Wang, Y., Zhao, C., Chu, Y., Xiao, J., et al. (2009). Exploration and Synthesis of Curcumin Analogues with Improved Structural Stability Both *In Vitro* and *In Vivo* as Cytotoxic Agents. *Bioorg. Med. Chem.* 17, 2623–2631. doi:10.1016/j.bmc.2008.10.044
- Ma, X., and Gang, D. R. (2006). Metabolic Profiling of Turmeric (*Curcuma Longa* L.) Plants Derived from *In Vitro* Micropropagation and Conventional Greenhouse Cultivation. *J. Agric. Food Chem.* 54, 9573–9583. doi:10.1021/jf061658k
- Mani, P., and Boominathan, M. (2011). Comparative Studies of the Antimicrobial Activity of Crude Extracts and Fractions from *Eugenia Caryophyllus* against *Candida Albicans* Isolate from Chronic Disease Affected Patients. *Int. J. Institutional Pharm. Life Sci.* 1, 36–47.
- Marchese, A., Arciola, C. R., Barbieri, R., Silva, A. S., Nabavi, S. F., Tsetegho Sokeng, A. J., et al. (2017). Update on Monoterpenes as Antimicrobial Agents: A Particular Focus on P-Cymene. *Materials (Basel)* 10, 1–15. doi:10.3390/ma10080947
- Meng, X., Wang, Z., and Lv, H. (2010). Constituents and Bacteriostatic Activity of Volatile Matter from Four Flower Plant Species. *Indian J. Agric. Res.* 44, 157–167.
- Metuge, J. A., Nyongbela, K. D., Mbah, J. A., Samje, M., Fotso, G., Babiaka, S. B., et al. (2014). Anti-Onchocerca Activity and Phytochemical Analysis of an Essential Oil from *Cyperus Articulatus* L. *BMC Complement. Altern. Med.* 14, 223. doi:10.1186/1472-6882-14-223
- Miquel, J., Bernd, A., Sempere, J. M., Díaz-Alperi, J., and Ramírez, A. (2002). The Curcuma Antioxidants: Pharmacological Effects and Prospects for Future Clinical Use. A Review. *Arch. Gerontol. Geriatr.* 34, 37–46. doi:10.1016/s0167-4943(01)00194-7
- Moco, S., Bino, R. J., Vorst, O., Verhoeven, H. A., De Groot, J., Van Beek, T. A., et al. (2006). A Liquid Chromatography-Mass Spectrometry-Based Metabolome Database for Tomato. *Plant Physiol.* 141, 1205–1218. doi:10.1104/pp.106.078428
- Mohammed, L. M., M. Salah, T. F., and Qader, K. O. (2017). Chemical Composition and Antifungal Activity of *Mentha Spicata* L. Plant from Sulaimaniyah in Iraq. *Kjar* 2, 52–56. doi:10.24017/science.2017.1.11
- Mohiuddin, M., Chowdhury, M. J., Alam, M. K., and Hossain, M. (2012). Chemical Composition of Essential Oil of Four Flavouring Plants Used by the Tribal People of Bandarban hill District in Bangladesh. *Int. J. Med. Aromat. Plants* 2, 106–113.
- Mukherjee, P. K., Harwansh, R. K., Bahadur, S., Biswas, S., Kuchibhatla, L. N., Tetali, S. D., et al. (2016). Metabolomics of Medicinal Plants - A Versatile Tool for Standardization of Herbal Products and Quality Evaluation of Ayurvedic Formulations. *Curr. Sci.* 111, 1624–1630. doi:10.18520/cs/v111/i10/1624-1630
- Murata, S., Shiragami, R., Kosugi, C., Tezuka, T., Yamazaki, M., Hirano, A., et al. (2013). Antitumor Effect of 1, 8-cineole against colon Cancer. *Oncol. Rep.* 30, 2647–2652. doi:10.3892/or.2013.2763
- Muthukumar, P., Kumaravel, S., and Nimia, N. (2019). Phytochemical, GC-MS and FT-IR Analysis of *Papaver Somniferum* L. *Jpbs* 7, 1–8. doi:10.18231/jjpbs.2019.001
- Nagori, K., Singh, M. K., Alexander, A., Kumar, T., Dewangan, D., Badwaik, H., et al. (2011). *Piper Betle* L.: A Review on its Ethnobotany, Phytochemistry, Pharmacological Profile and Profiling by New Hyphenated Technique DART-MS (Direct Analysis in Real Time Mass Spectrometry). *J. Pharm. Res.* 4, 2991–2997. Available at: <http://jpronline.info/article/view/9266/4710>.
- Nahar, D. L., and Sarker, S. (2007). “Phytochemistry of the Genus Curcuma,” in *Turmeric: The Genus Curcuma*. Editors K. Ravindran, P. N., and K. N. Babu (Boca Raton, Florida: & Sivaraman), 71–106.
- Nampoothiri, S. V., Philip, R. M., Kankangi, S., Kiran, C. R., and Menon, A. N. (2015). Essential Oil Composition, α-Amylase Inhibition and Antiglycation Potential of Curcuma aromatica Salisb. *J. Essent. Oil Bearing Plants* 18, 1051–1058. doi:10.1080/0972060X.2014.908746
- Nieman, D. C., Cialdella-Kam, L., Knab, A. M., and Shanely, R. A. (2012). Influence of Red Pepper Spice and Turmeric on Inflammation and Oxidative Stress Biomarkers in Overweight Females: A Metabolomics Approach. *Plant Foods Hum. Nutr.* 67, 415–421. doi:10.1007/s11130-012-0325-x
- Nikolova, M. (2006). Intraspecific Variability in the Flavonoid Composition of *Artemisia Vulgaris* L. *Acta Bot. Croat.* 65, 13–18.
- Núñez, N., Vidal-Casanella, O., Sentellas, S., Saurina, J., and Núñez, O. (2020). Non-targeted Ultra-high Performance Liquid Chromatography-High-Resolution Mass Spectrometry (UHPLC-HRMS) Fingerprints for the Chemometric Characterization and Classification of Turmeric and Curry Samples. *Separations* 7, 32–13. doi:10.3390/separations7020032
- Nurfina, A. N., Reksahadiprodjo, M. S., Timmerman, H., Jenie, U. A., Sugiyanto, D., and Van Der Goot, H. (1997). Synthesis of Some Symmetrical Curcumin Derivatives and Their Antiinflammatory Activity. *Eur. J. Med. Chem.* 32, 321–328. doi:10.1016/S0223-5234(97)89084-8
- Ogundare, A. O., and Olajuyigbe, A. O. (2012). Bioactivity Guided Isolation of the Antifungal Components in Sawdust Extracts of *Piptadeniatrum Africanum*, and *Terminalia Ivorensis*. *Malays. J. Microbiol.* 8, 34–41. doi:10.21161/mjm.32611
- Okumura, N., Yoshida, H., Nishimura, Y., Kitagishi, Y., and Matsuda, S. (2012). Terpinolene, a Component of Herbal Sage, Downregulates AKT1 Expression in K562 Cells. *Oncol. Lett.* 3, 321–324. doi:10.3892/ol.2011.491
- Othman, R., Ibrahim, H., Mohd, M. A., Mustafa, M. R., and Awang, K. (2006). Bioassay-guided Isolation of a Vasorelaxant Active Compound from *Kaempferia Galanga* L. *Phytomedicine* 13, 61–66. doi:10.1016/j.phymed.2004.07.004
- Paramasivam, M., Poi, R., Banerjee, H., and Bandyopadhyay, A. (2009). High-performance Thin Layer Chromatographic Method for Quantitative Determination of Curcuminoids in *Curcuma Longa* Germplasm. *Food Chem.* 113, 640–644. doi:10.1016/j.foodchem.2008.07.051
- Park, S. Y., and Kim, D. S. (2002). Discovery of Natural Products from Curcuma Longa that Protect Cells from Beta-Amyloid Insult: a Drug Discovery Effort against Alzheimer's Disease. *J. Nat. Prod.* 65, 1227–1231. doi:10.1021/np010039x
- Parthasarathy, V. A., and Chempakam, B. (2008). in “Chemistry of Spices,” in Chemistry Of Spices. Editors V. A. Parthasarathy, B. Chempakam, and T. J. Zachariah (Cambridge: CABI). 1–445. doi:10.4327/jsnfs1949.32.267
- Pathania, V., Gupta, A. P., and Singh, B. (2006). Improved HPTLC Method for Determination of Curcuminoids from *Curcuma Longa*. *J. Liquid Chromatogr. Relat. Tech.* 29, 877–887. doi:10.1080/10826070500531417
- Peng, H. Y., and Yang, X. E. (2005). Volatile Constituents in the Flowers of *Elsholtzia Argyi* and Their Variation: A Possible Utilization of Plant Resources after Phytoremediation. *J. Zhejiang Univ. Sci. B* 6, 91–95. doi:10.1631/jzus.2005.B0091
- Phattanawasin, P., Sotanaphun, U., and Sriphong, L. (2009). Validated TLC-Image Analysis Method for Simultaneous Quantification of Curcuminoids in *Curcuma Longa*. *Chroma* 69, 397–400. doi:10.1365/s10337-008-0893-y
- Prasath, D., Kandianan, K., Leela, N. K., Aarthi, S., Sasikumar, B., and Babu, K. N. (2018). Turmeric. *Hortic. Rev.* 46, 99–184. doi:10.1002/9781119521082.ch3

- Rahmatullah, M., Azam, M. N. K., Pramanik, S., Sania, S., Rahman, S., and Jahan, R. (2012). Antihyperglycemic Activity Evaluation of Rhizomes of *Curcuma Zedoaria* (Christm.) roscoe and Fruits of *Sonneratia Caseolaris* (L). *Engl. Int. J. Pharmtech Res.* 4, 125–129.
- Raina, V. K., Srivastava, S. K., and Syamsundar, K. V. (2005). Rhizome and Leaf Oil Composition of *Curcuma Longa* from the Lower Himalayan Region of Northern India. *J. Essent. Oil Res.* 17, 556–559. doi:10.1080/10412905.2005.9698993
- Ravindran, P. N. (2000). in *Black Pepper: Piper Nigrum*. Editor P. N. Ravindran (London: CRC Press). doi:10.1201/9780203303870
- Rufino, A. T., Ribeiro, M., Judas, F., Salgueiro, L., Lopes, M. C., Cavaleiro, C., et al. (2014). Anti-inflammatory and Chondroprotective Activity of (+)- α -Pinene: Structural and Enantiomeric Selectivity. *J. Nat. Prod.* 77, 264–269. doi:10.1021/np400828x
- Ruslay, S., Abas, F., Shaari, K., Zainal, Z., Maulidiani Sirat, H., et al. (2007). Characterization of the Components Present in the Active Fractions of Health Gingers (*Curcuma Xanthorrhiza* and *Zingiber Zerumbet*) by HPLC-DAD-ESIMS. *Food Chem.* 104 (3), 1183–1191. doi:10.1016/j.foodchem.2007.01.067
- Saleh-e-in, M. M., Sultana, A., Husain, M., and Roy, S. K. (2010). Chemical Constituents of Essential Oil from *Anethum Sowa* L. Herb (Leaf and Stem) Growing in Bangladesh. *Bangladesh J. Sci. Ind. Res.* 45, 173–176. doi:10.3329/bjsir.v45i2.5721
- Salman, Z., Mohd Azizi, C. Y., Nik Norulaini, N. A., and Mohd Omar, A. K. (2006). “Gas Chromatography /Time-Of-Flight Mass Spectrometry for Identification of Compounds from *Parkia Speciosa* Seeds Extracted by Supercritical Carbon Dioxide,” in Proceedings of the 1st International Conference on Natural Resources Engineering & Technology, Putrajaya, Malaysia, July 24–25, 2006, 112–120.
- Sasikumar, B. (2005). Genetic Resources of Curcuma: Diversity, Characterization and Utilization. *Plant Genet. Resour.* 3, 230–251. doi:10.1079/PGR200574
- Sathiyabalan, G., Lincy, P., Muthukumarasamyand Mohan, V. (2014). GC-MS Analysis of Bioactive Components of *Petiveria Alliacea* L. Whole Plant (Phytolaccaceae). *Int. J. Pharma Res. Heal. Sci.* 2, 387–392.
- Sati, S. C., Sati, N., and Sati, O. P. (2011). Bioactive Constituents and Medicinal Importance of Genus *Alnus*. *Pharmacogn. Rev.* 5, 174–183. doi:10.4103/0973-7847.91115
- Setyaningsih, D., Murti, Y. B., Fudholi, A., Hinrichs, W. L. J., Mudjahid, R., Martono, S., et al. (2016). Validated TLC Method for Determination of Curcumin Concentrations in Dissolution Samples Containing *Curcuma Longa* Extract. *J. Ilmu Kefarmasian Indones.* 14, 147–157.
- Sharopov, F., and Setzer, W. (2010). Composition of the Essential Oil of *Achillea Filipendulina* Lam. From Tajikistan. *Der Pharma Chem.* 2, 134–138.
- Shishu and Maheshwari, M. (2010). Comparative Bioavailability of Curcumin, Turmeric and Biocurcumin in Traditional Vehicles Using Non-everted Rat Intestinal Sac Model. *J. Funct. Foods* 2, 60–65. doi:10.1016/j.jff.2010.01.004
- Simoh, S., and Zainal, A. (2015). Chemical Profiling of *Curcuma Aeruginosa* Roxb. Rhizome Using Different Techniques of Solvent Extraction. *Asian Pac. J. Trop. Biomed.* 5, 412–417. doi:10.1016/S2221-1691(15)30378-6
- Singh, G., Kapoor, I. P., Singh, P., de Heluani, C. S., de Lampasona, M. P., and Catalan, C. A. (2010). Comparative Study of Chemical Composition and Antioxidant Activity of Fresh and Dry Rhizomes of Turmeric (*Curcuma Longa* Linn.). *Food Chem. Toxicol.* 48, 1026–1031. doi:10.1016/j.fct.2010.01.015
- Singh, G., Singh, O. P., and Maurya, S. (2002). Chemical and Biocidal Investigations on Essential Oils of Some Indian *Curcuma* Species. *Prog. Cryst. Growth Characterization Mater.* 45, 75–81. doi:10.1016/S0960-8974(02)00030-X
- Sirat, H. M., and Meng, L. L. (2009). Chemical Components of the Rhizome Oil of *Curcuma Heyneana* Val. *Mjs* 28, 323–328. doi:10.22452/mjs.vol28no3.10
- Slavík, J., and Slavíková, L. (1977). Alkaloids of Some Himalayan Species of *Meconopsis* Genus. *Collect. Czech. Chem. Commun.* 42, 132–139. doi:10.1135/cccc19770132
- Song, Q., Yang, D., Zhang, G., and Yang, C. (2001). Volatiles from *Ficus Hispida* and Their Attractiveness to Fig Wasps. *J. Chem. Ecol.* 27, 1929–1942. doi:10.1023/a:1012226400586
- Srinivasan, K., Sambaiah, K., and Chandrasekhara, N. (2004). Spices as Beneficial Hypolipidemic Food Adjuncts: A Review. *Food Rev. Int.* 20, 187–220. doi:10.1081/FRI-120037160
- Srivastava, A. K., Srivastava, S. K., and Syamsundar, K. V. (2006). Volatile Composition of *Curcuma Angustifolia* Roxb. Rhizome from central and Southern India. *Flavour Fragr. J.* 21 (3), 423–426. doi:10.1002/ffj.1680
- Suksamrarn, A., Eiamong, S., Piyachaturawat, P., and Charoenpiboonsin, J. (1994). Phenolic Diarylheptanoids from *Curcuma Xanthorrhiza*. *Phytochemistry* 36, 1505–1508. doi:10.1016/S0031-9422(00)89751-4
- Sundaryono, A., Nourmamode, A., Gardrat, C., Grélier, S., Bravic, G., Chasseau, D., et al. (2003). Studies on the Photochemistry of 1,7-Diphenyl-1,6-Heptadiene-3,5-Dione, a Non-phenolic Curcuminoid Model. *Photochem. Photobiol. Sci.* 2, 914–920. doi:10.1039/b301229h
- Suntres, Z. E., Coccimiglio, J., and Alipour, M. (2015). The Bioactivity and Toxicological Actions of Carvacrol. *Crit. Rev. Food Sci. Nutr.* 55, 304–318. doi:10.1080/10408398.2011.653458
- Tajidin, N. E. (2012). Chemical Composition and Citral Content in Lemongrass (*Cymbopogon Citratus*) Essential Oil at Three Maturity Stages. *Afr. J. Biotechnol.* 11, 2685–2693. doi:10.5897/ajb11.2939
- Tang, J., Li, X., and Han, J. (2012). Analysis of Volatile Components in Rhizome Zingibers, *Zingiber Officinale* Roscoe and *Ginger Pee* by GC-MS and Chemometric Resolution. *J. Chin. Med. Res. Dev.* 1, 47–53. doi:10.9754/journal.wmc.2010.00662
- Tetali, S. D., Acharya, S., Ankari, A. B., Nanakram, V., and Raghavendra, A. S. (2021). Metabolomics of *Withania Somnifera* (L.) Dunal: Advances and Applications. *J. Ethnopharmacol.* 267, 113469. doi:10.1016/j.jep.2020.113469
- Tian, Y., Xu, W., Zhu, C., Lin, S., Li, Y., Xiong, L., et al. (2011). Lathyrane Diterpenoids from the Roots of *Euphorbia Micractina* and Their Biological Activities. *J. Nat. Prod.* 74, 1221–1229. doi:10.1021/np2001489
- Tisserand, R., and Young, R. (2013). *Essential Oil Safety-E-Book: A Guide for Health Care Professionals*. Churchill Livingstone, London: Elsevier Health Sciences.
- Umar, N. M., Parumasivam, T., Aminu, N., and Toh, S. M. (2020). Phytochemical and Pharmacological Properties of *Curcuma Aromatica* Salisb (Wild Turmeric). *J. App Pharm. Sci.* 10, 180–194. doi:10.7324/JAPS.2020.1010018
- Usman, L., Hamid, A. A., George, O., Ameen, O., Muhammad, N. O., Zubair, M., et al. (2009). Chemical Composition of Rhizome Essential Oil of *Curcuma longa* L. growing in Growing in North Central Nigeria. *World J. Chem.* 4, 178–181.
- Venkataramani, M., and Chinnagounder, S. (2012). Preliminary Phytochemical Screening and GC-MS Profiling of *Hiptage Benghalensis* (L.) Kurz. *J. Pharm. Res.* 5, 2895–2899.
- Wang, P., Liang, W., Kong, C., and Jiang, Y. (2005). Allelopathic Potential of Volatile Allelochemicals of *Ambrosia Trifida* L. On Other Plants. *Allelopath. J.* 15, 131–136.
- Yang, S. A., Jeon, S. K., Lee, E. J., Im, N. K., Jhee, K. H., Lee, S. P., et al. (2009). Radical Scavenging Activity of the Essential Oil of Silver Fir (*Abies alba*). *J. Clin. Biochem. Nutr.* 44, 253–259. doi:10.3164/jcbn.08-240
- Yuan, C., Nan, P., Shi, S., and Zhong, Y. (2003). Chemical Composition of the Essential Oils of Two Chinese Endemic *Meconopsis* Species. *Z. Naturforsch C J. Biosci.* 58, 313–315. doi:10.1515/znc-2003-5-603
- Zellagui, A., Gherraf, N., and Rhouati, S. (2012). Chemical composition and antibacterial activity of the essential oils of *Ferula vesicertensis* Coss et Dur. leaves, endemic in Algeria. *Org. Med. Chem. Lett.* 2, 31. doi:10.1186/2191-2858-2-31
- Zeng, J. H., Xu, G. B., and Chen, X. (2009). Application of the Chromatographic Fingerprint for Quality Control of Essential Oil from Guangxi *Curcuma Kwangsiensis*. *Med. Chem. Res.* 18, 158–165. doi:10.1007/s00044-008-9115-2

Conflict of Interest: The authors declare that the research was conducted in the absence of any commercial or financial relationships that could be construed as a potential conflict of interest.

Copyright © 2021 Kulyal, Acharya, Ankari, Kokkiripati, Tetali and Raghavendra. This is an open-access article distributed under the terms of the Creative Commons Attribution License (CC BY). The use, distribution or reproduction in other forums is permitted, provided the original author(s) and the copyright owner(s) are credited and that the original publication in this journal is cited, in accordance with accepted academic practice. No use, distribution or reproduction is permitted which does not comply with these terms.



Multielemental Analysis and *In Vitro* Evaluation of Free Radical Scavenging Activity of Natural Phytopigments by ICP-OES and HPTLC

S. M. Nandanwadkar*, P. J. Hurkadale*, C. M. Bidikar and M. M. Godbole

KLE Academy of Higher Education and Research, Belgaum, India

OPEN ACCESS

Edited by:

Sayed Ahmad,
Jamia Hamdard University, India

Reviewed by:

Sameer Ahmed Shamsuddin Mapari,
University of Mumbai, India

Kamal Y. T.,
King Khalid University, Saudi Arabia
Nasir Siddiqui,
King Saud University, Saudi Arabia

*Correspondence:

S. M. Nandanwadkar
wadkar1252@gmail.com
P. J. Hurkadale
pramodhurakadle@yahoo.com

Specialty section:

This article was submitted to
Ethnopharmacology,
a section of the journal
Frontiers in Pharmacology

Received: 24 October 2020

Accepted: 15 February 2021

Published: 06 July 2021

Citation:

Nandanwadkar SM, Hurkadale PJ,
Bidikar CM and Godbole MM (2021)
Multielemental Analysis and *In Vitro*
Evaluation of Free Radical Scavenging
Activity of Natural Phytopigments by
ICP-OES and HPTLC.
Front. Pharmacol. 12:620996.
doi: 10.3389/fphar.2021.620996

The phytopigments derived from ethnomedicinal plants employed as traditional medicines appear to be the simplest alternative for artificial radical colorants. This can be because of persistent use of synthetic dyes and their harmful impacts linked to human lives as well as to the ecosystem. The literature evidences clearly reveal the complications from growing demands of radical colorants from artificial origin. The planned analysis work hence focuses on screening of the fundamental composition of phytopigments, obtained from plant sources by subtle technique of ICP-OES, with axial plasma combined with nebulizer motor-assisted gas flow approach, utilizing microwave digester for complete digestion of phytopigments, thereby establishing the pigments being safe for consumption. Additionally, the observations from free radical scavenging activity using DPPH by HPTLC concluded that the natural pigments obtained from plant sources are rich in flavonoids with potent antioxidant property. Thus, an effort has been made through the developed ICP-OES methodology, to beat the distinct imprecise practice of food labeling, once natural pigments are utilized in a variety of additives, as food colorants with amounts of components detected as arsenic, lead, and metal, within specified limits of FSSAI, demonstrate and establish safety of natural foodstuff agents, as compared over hazardous synthetic azo dyes.

Keywords: phytopigments, ethnomedicinal plants, ICP-OES, complete digestion, DPPH-HPTLC

INTRODUCTION

Colors form an integral component of food and related consumer goods because of their intrinsic indispensable fundamental property of imparting unique characteristic hues to the product to which they are added. These food colors not only define nature of food but also are linked to human desires for types of food consumed; for example, yellow to light green for raw fruits with citrus flavor (acidic), whereas red and pink for ripe condition with sweet taste. Routine food colors are classified into tetrapyrroles, tetraterpenoids, flavonoids, etc. Some class of pigments were also further categorized into anthocyanins (from blue berries), betalains (from beetroot), and annatto (from bixin seeds).

On the basis of their source of origin, colors may be classified as follows:

1. Natural: bixin, anthocyanins, betanins, chlorophylls, curcumin, lycopene, etc.
2. Nature identical: orange, watermelon, etc.

3. Artificial colors: blue-1, blue-2, tartrazine, erythrosine, citrus red-2, indigo carmine, Ponceau 4R, etc.
4. Inorganic: TiO_2 (from metals) (Mortensen, 2006).

The recent advancements in technology for extraction and assessment of biological activities like antiaging phenomena as well as therapeutic efficacy like treating blood disorders, anemia, beneficial effect on lungs, free radical scavenging activity, and the newer phytopigments like anthocyanins, betanins, curcumins, indigotin, and isatin are the preferred choice of coloring agents in foods by public considering focal point of their safety as well as for manufacturers in regards to expanding their extensive business (Graham et al., 1990; Micozzi et al., 1990; Zhang et al., 1991; Sies et al., 1992; Van Poppel, 1993). In terms of food frauds, the establishment of accurate and rapid instrumental techniques for natural colorings is required, especially for the phytopigments like anthocyanins and betalains; oleo-resins like paprika and turmeric; carotenoids; and quinoids, that are off late frequently utilized in different foods and related consumer matrices (Fujii et al., 2001). Frugal, fast, and concurrent analytical techniques need to be established. Elemental estimation is another parameter of great significance for determining beneficial and toxic effects of plant pigments, like anthocyanin, betanin, paprika oleoresin, annatto, and turmeric oleoresin, that contain adequate basic components additionally for human well-being (Kohen and Nyska, 2002). Most recent innovations in Foodomics as well as farsighted toxicological studies have been applied for screening potential hazardous synthetic contaminants such as heavy metals and aflatoxins in early medication improvement/new drug lead molecule discoveries. Hence, such novel innovations would surely be utilized to add to the scientific evidence to plant pigments in regards to its safety (Jordan et al., 2010). The overall expanding enthusiasm for natural cycles just as the synthetic structure of plants for dietary, restorative, and ecological issues has led to advanced metal-related studies (Adriano, 2001). Recent dossiers and newer regulations regarding stringent food norms and laws prompt more noteworthy entry of toxic metals into the climate, with the indication that a critical aspect of the populace is currently routinely exposed to these toxic metals (Goyer, 1997). Plants are probable sources for micro- and macro-essential nutrients, since there are different take-up courses for fundamental components such as uptake of minerals, salts, and metals from soil (Barthwal et al., 2008). These components are utilized, for instance, keeping up osmotic balance, as basic parts in sugars and proteins, as segments of natural atoms associated with typical digestion (e.g., magnesium (Mg) in chlorophyll, phosphorous (P) in ATP, iron (Fe) in photosynthesis, copper (Cu) in root digestion, and zinc (Zn) for development), and as chemical activators (e.g., potassium (K) in tissue cells and layers, calcium (Ca) for stress reaction, (K) as development controller, and nickel (Ni); Hepler, 2005; Tanhan et al., 2007; Soetan et al., 2010; Wang et al., 2013). Adjacent to the fundamental components, a few metals, for example, arsenic (As), cadmium (Cd), and lead (Pb), are toxic to the creature even in exceptionally low levels, while other do not show any positive or negative impact. It is vital, particularly for spices, that they contain adequate fundamental components (micro-macro nutrients)

additionally for human well-being. Besides, micro-components in plants are associated with the arrangement cycles of dynamic synthetic elements, which permit their utilization for treating various disorders, for example, iron (Fe) supplement for blood-related disorders. The detrimental impact results from the reality that heavy metals migrate from soils, harvests, or plants, entering the food chain (Antonijević et al., 2012), or by therapeutic applications from medicaments (Cheng, 1955; Garcia et al., 2000; Başgel and Erdemoğlu, 2006; Adeyolanu et al., 2016). Considering the aforementioned points, the World Health Organization (WHO) has specified the permissible levels in crude plant material for the presence of heavy metals, thereby maintaining a stringent watch of negative effects on human well-being by plant utilization or its clinical use (WHO, 1991; Zeiner et al., 2015).

Antioxidant assays might depend on the probable type of anticancer agents (lipophilic or hydrophilic, and enzymatic or nonenzymatic) (Huang et al., 2005). The DPPH test by HPTLC is one of the reliable mainstreams and frequently preferred technique among diagnostic tools for identifying the presence of radical scavenging/antioxidant activity. The technique is basic, productive, moderately reasonable, and fast. The shading change occurs from purple color of the reagent to lemon yellow color components possessing free radical scavenging property, permitting the spectrophotometric assurance of the agent possessing possible free radical scavenging (antioxidant) activity (Molyneux, 2004; Kedare and Singh, 2011).

In the proposed research, an effort has been made to feature the biotherapeutic potential of phytopigments utilized in foods and related food merchandises, by chromatographic fingerprints *via* free radical activity, along with multielemental assessment using inductive coupled plasma-optical emission spectroscopy (ICP-OES), with a viewpoint to screen heavy metals such as lead, arsenic, and cadmium, in addition to micro- and macro-minerals like Mg, Fe, and Zn. Therefore, the novel strategy developed above would surely be employed in routine quality control for monitoring food.

EXPERIMENTAL

Reagents

Natural pigments like anthocyanins, betanins, curcumin oleoresin, paprika oleoresin, and annatto were procured from Neelikon Food Dyes Pvt. Ltd., Mumbai. 98% nitric acid-reagent grade (Fisher Scientific, Fair Lawn, NJ, United States). Hydrogen peroxide (H_2O_2)-30% reagent grade (J.T. Baker, Phillipsburg, NJ, United States). Micro laboratory cleaner (International Products Corporation, Trenton, NJ, United States). Distilled, deionized water, 18 MΩ (Continental Water Systems, San Antonio, TX, United States). For HPTLC analysis, n-butanol, glacial acetic acid, water, and DPPH (1,1-diphenyl-2-picrylhydrazyl) were of analytical grade and purchased from Merck and Sigma Chemical, Germany.

Apparatus

ICP AVIO 200 inductively coupled plasma optical emission spectrometer was purchased from Perkin-Elmer, Ahmedabad, Gujarat. Titan MPS microwave digester. Teflon® PFA microwave

TABLE 1 | Plasma specification and optimum conditions for ICP-OES.

Optimum conditions	Parameters
Plasma power	1,350–1,500 w
Gas flow	0.2 (nebulizer)/0.8 auxiliary (liters/minutes)
Coolant	15°C (55°F)
Nebulizer type	Cross flow
Nebulizer flow rate	0.2–0.8 (liters/minutes)
Pump speed	6.2 RPM
Stabilization time	60 s
No. of probes for each measuring	3
Plasma observation	Axial (low concentration), radial (high concentration)

vessels rated to 120 psi (CEM, Matthews, NC, United States). Lined digestion vessels rated to 200 psi (CEM, Matthews, NC, United States). Food processor was designed for home use. High-density polyethylene bottles, Nalgene®, or equivalent were purchased from Nalge Company, Rochester, NY, United States. The HPTLC system purchased from Camag was used for TLC analysis, and data interpretation was performed using digitally optimized vision CATS Software. Camag derivatizer was employed for derivatization to demonstrate free radical antioxidant activity using DPPH.

Instrumentation

A Titan MPS microwave digester 950 W power with temperature and pressure monitoring and control was utilized to digest all the samples. The microwave was aligned after the U.S. Environmental Protection Agency (EPA) calibration procedure that involves heating a known volume of water at specific powers (Hepler, 2005). Individual experience directs that the sample weights should be kept at or below the prescribed weights to minimize the potential for overpressuring and venting during the microwave digestion process. Samples containing high levels of sugars are apt to react more quickly and to generate more pressure. If these products are substituted for the materials analyzed in this work, using smaller sample sizes and lower powers are strongly recommended to prevent overpressuring.

The ICP-OES analysis was performed on the Perkin-Elmer ICP AVIO 200 inductively coupled plasma-optical emission spectrometer equipped with an axial standard torch using cross-flow nebulizer. Autosampler featuring a quartz sample probe to minimize sample cross contamination was used. The working specifications of ICP-OES Avio 200 and optimal conditions of plasma are given in **Table 1**. ICP AVIO 200 was used because of its extremely sensitive precision to detect metals at trace levels. Also, due to the simultaneous measurement, no reduction in sample throughput was observed from making measurements at multiple wavelengths of an element. Therefore, multiple emission lines were measured simultaneously for each element to verify analytical results. The analysis of different types of the samples of phytopigments was performed on different days and because each sample was in a different acid matrix, optimum background correction points (BGC) and peak windows were determined as a function of sample before the analysis was performed. The standard concentrations were matched to the anticipated levels in the diluted

samples (Fikarová, 2020). The Camag HPTLC system was employed for chromatographic analysis.

Sample Pretreatment for Inductive Coupled Plasma-Optical Emission Spectroscopy Analysis Using Avio 200 Perkin Elmer System

The phytopigments obtained from Neelikon Pvt Ltd. were pretreated using digestion mixture of concentrated nitric acid (HNO₃) and sulfuric acid (H₂SO₄), utilizing the Perkin Elmer Titan MPS microwave digester (Liu et al., 2020).

Digestion Procedure for Inductive Coupled Plasma-Optical Emission Spectroscopy Analysis

- Step 1: 10 gm of each selected phytopigments were accurately weighed into the Teflon PFA digestion vessels.
- Step 2: Concentrated, ultrapure HNO₃ and 2 mL concentrated, ultrapure H₂SO₄ were added to the sample.
- Step 3: Cap the vessel in the capping station.
- Step 4: Phytopigment powders were digested as per **Table 2**.
- Step 5: Cool for approximately five minutes and vent vessels.
- Step 6: Repeat Step 4 for juices containing pulp.
- Step 7: Cool for five minutes, vent, and open the vessels using the capping station.
- Step 8: Add 3 mL 30% H₂O₂ to the samples.
- Step 9: After effervescence subsides, transfer the samples into clean, acid-washed volumetric flasks, and dilute to 100 mL with double distilled water.
- Step 10: Transfer the samples to clean HDPE bottles.

Standard Preparation for HPTLC Analysis

Standard solutions of selected phytopigments (anthocyanins, betanins, turmeric oleoresin, paprika oleoresin, and annatto) were of 100 ppm using methanol.

Sample Preparation for HPTLC Analysis

Marketed food samples such as locally available jams, squashes, ice cream flavors, and chili powders, containing anthocyanins, betanins, paprika oleoresin, and annatto, were accurately weighed as per requirement (100 ppm) and mixed with a mixture of methanol and water (8:2 v/v). For turmeric samples, locally available turmeric powder was obtained from the market, and 10 ppm solution was prepared and further subjected to spectroscopic and chromatographic analyses by ICP-OES and HPTLC techniques.

Optimized Conditions for HPTLC

Chromatography was performed on 20 × 10 cm aluminum-coated silica gel 60 F₂₅₄ HPTLC plates (C.A.S. No. 105642, Merck, Darmstadt, Germany). Sample application was done using Camag Linomat V with 100 µL (Hamilton syringe, United States). Development was done using a solvent system of n-butanol: glacial acetic acid: water (4:4:1 v/v/v) up to 70 mm in twin-trough chamber with saturation of 10 min with 5 min

TABLE 2 | Microwave digestion parameters for phytopigment analysis.

Parameter	Stage 1	Stage 2	Stage 3	Stage 4	Stage 5
Power (%)	10	45	45	45	45
Power (watts)	51	366	366	366	366
Pressure (PSI)	20	40	80	120	160
Run time (min)	2	10	10	10	20
Time at parameter (min)	2	5	5	5	10
Temperature at parameter (°C)	0	75	85	100	120
Fan speed (% of maximum)	100	100	100	100	100

TABLE 3 | Quantification of heavy metals observed in selected phytopigments with prescribed limits.

Sl. no	Name of the color	Heavy metals			
		Arsenic (mg/kg) ≤ 1	Lead (mg/kg) ≤ 1	Cadmium (mg/kg) ≤ 1	Mercury (mg/kg) ≤ 2
1	Anthocyanins	0.11	0.103	0.043	<0.1
2	Paprika	0.014	0.120	0.042	0.013
3	Betanin	0.022	0.167	0.045	0.014
4	Turmeric	–	0.061	0.049	–
5	Annatto	–	2.864	0.033	–

TABLE 4 | ICP-OES results for selected phytopigments with reference values in mg/mL.

Phytopigment	Annatto	Anthocyanin	Betanins	Paprika	Turmeric
Minerals in highest quantity with observed amounts	Iron (Fe) 6.345 ± 0.40 mg/L, calcium (Ca) 4.868, and magnesium (Mg) 2.478	Iron (Fe) 20.58 ± 0.40 mg/L	Magnesium (Mg) 17.85 ± 0.4 mg/L with iron (Fe) 5.097 ± 0.40 mg/L and calcium (Ca) 5.368 ± 0.7 mg/L	Calcium (Ca) 5.958 ± 0.7 mg/L, iron (Fe) 0.278, and magnesium (Mg) 0.064 mg/L	Magnesium (Mg) 19.40 ± 0.40 mg/L and iron (Fe) 4.942 ± 0.40 mg/L mg/L

plate equilibrium. Spectrodensitometric scanning was performed post-derivatization using the DPPH reagent at 540 nm.

1,1-Diphenyl-2-picrylhydrazyl Radical Scavenging

After development, the plates were dried for 10 min using a Camag plate heater III. Derivatization was done using 0.5 mM arrangement of 1,1-diphenyl-2-picrylhydrazyl (DPPH) as the reagent in ethanol for 5 s (Anuyahong et al., 2020). HPTLC plates were dried at room temperature (23°C) for 90 s and then warmed for 30 s at 60°C in a dark room. Densitometric scanning was performed at 540 nm using a Camag TLC scanner four under programming control of vision CATS, v 2.5 Muttentz, Switzerland. Zones were recognized promptly as lemon yellow regions against light violet/purple zones (bands). Estimations were done in duplicate. Ascorbic acid was utilized as a positive control.

RESULTS AND DISCUSSION

For heavy metal analysis of phytopigments, nine references of heavy metal standards, Ba, Cd, Cr, Co, Cu, Pb, Ni, As, and Se, were calibrated for analysis of anthocyanins, betanins, and paprika oleoresin, from which toxic heavy metals, when subjected to ICP-OES analysis, particularly, Pb, As, and Cd,

were found to be well below the specified limits of the U.S. FDA and FSSAI regulations. The concentrations of As, Cd, Pb, and Hg were under the detection limit in each sample, which means that the investigated phytopigment samples of interest were free of toxic metals (Table 3). On a beneficial note, the nutritive profile of frequently used phytopigments was determined. Several studies have shown that the peel of beetroot was characterized by the largest betalain content (Kujala et al., 2002; Shing and Hathan, 2014; Slatnar et al., 2015; Sawicki et al., 2016). In this study, test sample of blue berry squashes and jams demonstrated anthocyanins with the highest content of iron (20.52 mg/L), and beetroot juices demonstrated betanins with the highest quantity of magnesium (17.85 mg/L), along with considerable amounts of iron (5.097 mg/L) and calcium (5.368 mg/L). Locally marketed turmeric samples reported turmeric oleoresins with the highest concentration of magnesium (19.40 mg/L) followed by the iron content of 4.942 mg/L, whereas chili powders demonstrated paprika oleoresin, reporting the calcium content of 5.958 mg/L. Element composition with respect to macro- and microelemental concentrations of different phytopigment parts is shown in Tables 4, 5. The results in the proposed study indicate that multielemental estimation of natural pigments was successfully performed by the ICP-OES technique, proving it to be a preferred and precise tool in routine quality control of food and related merchandized goods, ensuring and assuring

TABLE 5 | Elemental analysis of phytopigment analysis with respective wavelengths and observed experimental values by ICP-OES AVIO 200 with reference values in mg/mL.

Element	Wavelength	Experimental	Label
Ca	396.845	51.3 ± 0.7	<115
Cu	224.702	0.137 ± 0.03	
Fe	238.200	0.59 ± 0.40	
K	766.515	0.681 ± 7.3	
Mg	279.553	42.70 ± 0.4	57.5
Na	589.589	24.79 ± 0.02	
P	177.436	139.51 ± 1.3	
Zn	206.198	0.79 ± 0.2	

safety profile of food additives and contaminants in the form of heavy metals, if any.

The utilization of HPTLC and a sophisticated scanner with a photodiode detector makes possible utilization of selected phytopigments on TLC plates without prior preparation steps (Pozharitskaya et al., 2007a; Pozharitskaya et al., 2007b). In a similar fashion, chromatographic separation, *in situ* radical scavenging activity examination of selected phytopigments was done by online HPTLC-DAD and HPTLC-DPPH techniques simultaneously. In this study, a simple and rapid HPTLC densitometric method for the analysis of selected phytopigments was developed. Different trial compositions of the solvent systems were put to task in order to obtain high-resolution and reproducible peaks. From preliminary experiments, the best results were obtained using the mobile phase of n-butanol: glacial acetic acid: water (4:4:1, v/v/v). Selected phytopigment samples were applied directly onto the plates without any prechromatographic separations. The DPPH reagent has a unique absorption maximum in the range of 510 and 520 nm, which is diminished in the

presence of a compound capable of reducing it to its hydrazine form. The kinetic behavior of antioxidants is a significant factor in the assessment of antiradical activity. A reaction time of 30 s at 50°C was seen as the optimum antioxidant-DPPH response period. After chromatographic separation, *in situ* DPPH radical scavenging properties of phytopigments were controlled by an online HPTLC-DPPH technique. This is viewed as in **Figure 1**, by derivatized image of silica plates with DPPH radicals reducing light violet/purple bands to lemon yellow bands. These zones demonstrated antioxidant activity. The intensity of the lemon yellow color depended upon the amount and nature of radical scavenging activity in the sample.

DISCUSSION

The phytopigments were subjected to elemental estimation by the ICP-OES (AVIO-200 model) technique in accordance with pharmacopeial dossiers USP 231 and USP 233. The elemental characterization of selected natural pigments utilizing the Perkin Elmer TITAN MPS digester equipped with nebulizer and dual axial plasma assisted fast elemental analysis. The developed protocol was validated by performing calibration using heavy metal reference standards of mercury (Hg), lead (Pb), cadmium (Cd), arsenic (As), selenium (Se), chromium (Cr), copper (Cu), cobalt (Co), and antimony (Sb). The ICP-OES method designed for elemental analysis gave accurate and precise nutritional profile for selected phytopigments in regards to inherent micro-macro essential elements like iron (Fe), calcium (Ca), zinc (Zn), and phosphorus (P). The ICP-OES outcome determined that heavy metals like arsenic (As), cadmium (Cd), lead (Pb), and mercury (Hg) were reported ≤1 ppm as specified within herbal

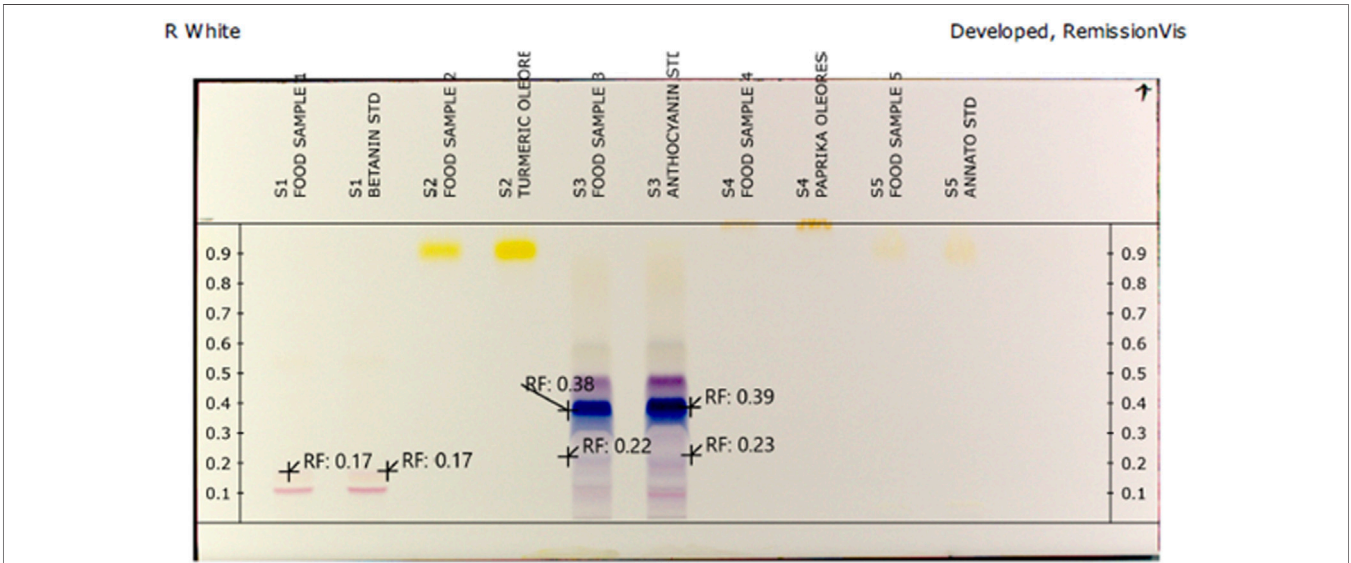


FIGURE 1 | HPTLC fingerprint of selected phytopigments exhibiting antioxidant property post-derivatization by the DPPH reagent.

pharmacopeia, labeling the selected phytopigments nonhazardous and safe for human consumption. The selected phytopigments reported essential minerals as follows: anthocyanins pigment reported the highest iron (Fe) content of 20.52 mg/L, and betanin pigment reported the highest magnesium (Mg) content of 17.85 mg/L, along with considerable amounts of iron (Fe) and calcium (Ca), of 5.097 mg/L and 5.368 mg/L, respectively; paprika oleoresin pigment reported only calcium (Ca) content of 5.958 mg/L. USP compliant DPPH assisted HPTLC protocol, developed for selected phytopigments, indicated that lemon yellow bands of phytopigments possess radical scavenging property with inherent chemical structure proving them to be antioxidant agents, suggesting them as future “Nutraceuticals.”

CONCLUSION

The microwave-assisted digestion using the Perkin Elmer Titan MPS digester gave a contamination-free sampling with minimal overall analysis time, providing faster, simpler, effective, and accurate estimation of elements. Toxic heavy metals, when subjected to the ICP-OES analysis, were within the specified limits of U.S. FDA and FSSAI regulations. On a beneficial note, the essential nutritive profile of frequently used phytopigments was determined. Annatto from butter had highest amounts of iron (Fe: 6.345 mg/L), calcium (Ca: 5.368 mg/L), and magnesium content (2.478 mg/L). Anthocyanins had the highest content of iron (Fe: 20.52 mg/L). Betanins had the highest quantity of magnesium (Mg: 17.85 mg/L) along with considerable amounts of iron (Fe: 5.097 mg/L) and calcium (Ca: 5.368 mg/L), with paprika oleoresin reporting calcium (Ca) content of 5.958 mg/L, whereas turmeric oleoresin from locally purchased turmeric powder demonstrated the highest content of magnesium (Mg: 19.40 mg/L), followed by the iron (Fe) content of 4.942 mg/L. The lemon yellow florescent bands indicated the presence of antioxidant property of the pigment.

The results in the proposed study indicate that multielemental estimation of phytopigments was successfully performed by the ICP-OES technique, proving it to be a preferred and precise tool as a routine quality control method ensuring and assuring safety profile of food additives and contaminants in the form of heavy metals, if any. The effect directed, antioxidant activity of the

phytopigments was proven by 2,2-diphenyl-1-picrylhydrazyl (DPPH) test, using the CAMAG HPTLC system, where DPPH was used as a derivatizing reagent.

This work portrays the screening and identification of essential nutrients like iron, calcium, and magnesium as well as heavy metals in accordance with guidelines of FSSAI for foods (food industries) may be performed simultaneously utilizing the ICP-OES technique. The radical analysis carried out by the HPTLC-DPPH assay demonstrated possible inherent antioxidant properties of selected phytopigments.

DATA AVAILABILITY STATEMENT

The original contributions presented in the study are included in the article/**Supplementary Material**; further inquiries can be directed to the corresponding author.

AUTHOR CONTRIBUTIONS

NSM: conceptualization, methodology, original draft preparation, software analysis and interpretation, supervision, investigation, and final draft check. 2. HP: editing and final draft check. 3. BCM: original draft preparation, visualization, image graphics reviewing, data curation, supervision, investigation, and final draft check. 4. GM: data curation, language corrections, and final draft check.

ACKNOWLEDGMENTS

The authors are grateful to M. G. Nandanwadkar, general manager, Chika Overseas, Gujarat, Vatva, Ahmedabad, India, for providing timely instrumental facilities. The author expresses sincere gratitude toward Anchrom Managing Directors, Mr. Dilip Charegaonkar and Mr. Akshay Charegaonkar, India Specific Application Lab Pvt. Ltd., Mulund, Mumbai.

SUPPLEMENTARY MATERIAL

The Supplementary Material for this article can be found online at: <https://www.frontiersin.org/articles/10.3389/fphar.2021.620996/full#supplementary-material>.

REFERENCES

- Adeyolanu, O. D., Kadiri, O. J., Are, K. S., and Oluwatosin, G. A. (2016). Lead and cadmium contents in a medicinal plant/spice grown in an urban city of Nigeria. *Cogent Food Agric.* 2 (1), 1136016. doi:10.1080/23311932.2015.1136016
- Adriano, D. C. (2001). *Trace elements in terrestrial environments: biogeochemistry, bioavailability, and risks of metals*. 2nd edn. New York, NY: Springer.
- Antoničević, M. M., Dimitrijević, M. D., Milić, S. M., and Nujkić, M. M. (2012). Metal concentrations in the soils and native plants surrounding the old flotation tailings pond of the Copper Mining and Smelting Complex Bor (Serbia). *J. Environ. Monit.* 14 (3), 866–877. doi:10.1039/c2em10803h

- Anuyahong, T., Chusak, C., and Adisakwattana, S. (2020). Incorporation of anthocyanin-rich riceberry rice in yogurts: effect on physicochemical properties, antioxidant activity and *in vitro* gastrointestinal digestion. *LWT* 129, 109571. doi:10.1016/j.lwt.2020.109571
- Barthwal, J., Nair, S., and Kakkar, P. (2008). Heavy metal accumulation in medicinal plants collected from environmentally different sites. *Biomed. Environ. Sci.* 21 (4), 319–324. doi:10.1016/S0895-3988(08)60049-5
- Başgel, S., and Erdemoglu, S. B. (2006). Determination of mineral and trace elements in some medicinal herbs and their infusions consumed in Turkey. *Sci. total Environ.* 359 (1–3), 82–89. doi:10.1016/j.scitotenv.2005.04.016
- Cheng, T. (1955). The effect of seed treatment with microelements upon the germination and early growth of wheat. *Sci. Sin.* 4, 129–135.

- Fikarová, K. (2020). *Development of novel approaches to automated sample preparation for pharmaceutical and environmental analysis*. Prague, Czechia: Univerzita Karlova, 1–113.
- Fujii, M., Shimizu, T., and Nakamura, M. (2001). *Natural colors for foods*. Chiba, Japan: Toyo.
- García, E., Cabrera, C., Lorenzo, M. L., and López, M. C. (2000). Chromium levels in spices and aromatic herbs. *Sci. Total Environ.* 247 (1), 51–56. doi:10.1016/S0048-9697(99)00467-2
- Goyer, R. A. (1997). Toxic and essential metal interactions. *Annu. Rev. Nutr.* 17 (1), 37–50. doi:10.1146/annurev.nutr.17.1.37
- Graham, S., Haughey, B., Marshall, J., Brasure, J., Zielesny, M., Freudenheim, J., et al. (1990). Diet in the epidemiology of gastric cancer. *Nutr. Cancer* 13, 19–34. doi:10.1080/01635589009514042
- Hepler, P. K. (2005). Calcium: a central regulator of plant growth and development. *Plant Cell* 17 (8), 2142–2155. doi:10.1105/tpc.105.032508
- Huang, D., Ou, B., and Prior, R. L. (2005). The chemistry behind antioxidant capacity assays. *J. Agric. Food Chem.* 53, 1841–1856. doi:10.1021/jf030723c
- Jordan, S. A., Cunningham, D. G., and Marles, R. J. (2010). Assessment of herbal medicinal products: challenges, and opportunities to increase the knowledge base for safety assessment. *Toxicol. Appl. Pharmacol.* 243 (2), 198–216. doi:10.1016/j.taap.2009.12.005
- Kedare, S. B., and Singh, R. P. (2011). Genesis and development of DPPH method of antioxidant assay. *J. Food Sci. Technol.* 48, 412–422. doi:10.1007/s13197-011-0251-1
- Kohen, R., and Nyska, A. (2002). Oxidation of biological systems: oxidative stress phenomena, antioxidants, redox reactions, and methods for their quantification. *Toxicol. Pathol.* 30 (6), 620–650. doi:10.1080/01926230290166724
- Kujala, T. S., Vienola, M. S., Klika, K. D., Lopenen, J. M., and Pihlaja, K. (2002). Betalain and phenolic compositions of our beetroot (*Beta vulgaris*) cultivars. *Eur. Food Res. Technol.* 214 (4), 505–510. doi:10.1007/s00217-001-0478-6
- Liu, B., Jia, Y., Jing, Y., and Yao, Y. (2020). Comparison analysis of wet digestion and stripping methods on recovery of lithium isotopes in the loaded phase. *Chem. Phys.* 539, 110962. doi:10.1016/j.chemphys.2020.110962
- Micozzi, M. S., Beecher, G. R., Taylor, P. R., and Khachik, F. (1990). Carotenoid analyses of selected raw and cooked foods associated with a lower risk for cancer. *J. Natl. Cancer Inst.* 82 (4), 282–285. doi:10.1093/jnci/82.4.282
- Molyneux, P. (2004). The use of the stable free radical diphenylpicrylhydrazyl (DPPH) for estimating antioxidant activity. *Songklanakarin J. Sci. Technol.* 26, 211–219.
- Mortensen, A. (2006). Carotenoids and other pigments as natural colorants. *Pure Appl. Chem.* 78 (8), 1477–1491. doi:10.1351/pac200678081477
- Pozharitskaya, O. N., Ivanova, S. A., Shikov, A. N., Makarov, V. G., and Galambosi, B. (2007). Separation and evaluation of free radical-scavenging activity of phenol components of green, brown, and black leaves of *Bergenia crassifolia* by using HPTLC-DPPH* method. *J. Sep. Sci.* 30, 2447–2451. doi:10.1002/jssc.200700178
- Pozharitskaya, O. N., Ivanova, S. A., Shikov, A. N., and Makarov, V. G. (2007a). Separation and evaluation of free radical-scavenging activity of phenol components of *Embolia officinalis* extract by using an HPTLC-DPPH* method. *J. Sep. Sci.* 30 (9), 1250–1254. doi:10.1002/jssc.200600532
- Sawicki, T., Bączek, N., and Wiczowski, W. (2016). Betalain profile, content and antioxidant capacity of red beetroot dependent on the genotype and root part. *J. Funct. Foods* 27, 249–261. doi:10.1016/j.jff.2016.09.004
- Shing, B., and Hathan, B. S. (2014). Chemical composition, functional properties and processing of beetroot - a review. *Int. J. Scientific Eng. Res.* 5 (1), 679–684.
- Sies, H., Stahl, W., and Sundquist, A. R. (1992). Antioxidant functions of vitamins. Vitamins E and C, beta-carotene, and other carotenoids. *Ann. N. Y. Acad. Sci.* 669 (1), 7–20. doi:10.1111/j.1749-6632.1992.tb17085.x
- Slatnar, A., Stampar, F., Veberic, R., and Jakopic, J. (2015). HPLC-MS(n) identification of betalain profile of different beetroot (*Beta vulgaris* L. ssp. *vulgaris*) parts and cultivars. *J. Food Sci.* 80 (9), C1952–C1958. doi:10.1111/1750-3841.12977
- Soetan, K. O., Olaiya, C. O., and Oyewole, O. E. (2010). The importance of mineral elements for humans, domestic animals and plants-A review. *Afr. J. Food Sci.* 4 (5), 200–222. doi:10.5897/AJFS.9000287
- Tanhan, P., Kruatrachue, M., Pokethitiyook, P., and Chaiyarat, R. (2007). Uptake and accumulation of cadmium, lead and zinc by Siam weed [*Chromolaena odorata* (L.) King & Robinson]. *Chemosphere* 68 (2), 323–329. doi:10.1016/j.chemosphere.2006.12.064
- Van Poppel, G. (1993). Carotenoids and cancer: an update with emphasis on human intervention studies. *Eur. J. Cancer* 29A (9), 1335–1344. doi:10.1016/0959-8049(93)90087-v
- Wang, M., Zheng, Q., Shen, Q., and Guo, S. (2013). The critical role of potassium in plant stress response. *Int. J. Mol. Sci.* 14 (4), 7370–7390. doi:10.3390/ijms14047370
- WHO (1991). *Guidelines for assessment of herbal medicines*. Geneva, Switzerland: World Health Organisation.
- Zeiner, M., Juranović Cindrić, I., Požgaj, M., Pirk, R., Šilić, T., and Stinger, G. (2015). Influence of soil composition on the major, minor and trace metal content of Velebit biomedical plants. *J. Pharm. Biomed. Anal.* 106, 153–158. doi:10.1016/j.jpba.2014.10.012
- Zhang, L. X., Cooney, R. V., and Bertram, J. S. (1991). Carotenoids enhance gap junctional communication and inhibit lipid peroxidation in C3H/10T1/2 cells: relationship to their cancer chemopreventive action. *Carcinog.* 12 (11), 2109–2114. doi:10.1093/carcin/12.11.2109

Conflict of Interest: The authors declare that the research was conducted in the absence of any commercial or financial relationships that could be construed as a potential conflict of interest.

Copyright © 2021 Nandanwadkar, Hurkadale, Bidikar and Godbole. This is an open-access article distributed under the terms of the Creative Commons Attribution License (CC BY). The use, distribution or reproduction in other forums is permitted, provided the original author(s) and the copyright owner(s) are credited and that the original publication in this journal is cited, in accordance with accepted academic practice. No use, distribution or reproduction is permitted which does not comply with these terms.



The Effects of Erchen Decoction on Gut Microbiota and Lipid Metabolism Disorders in Zucker Diabetic Fatty Rats

Tian Zhao¹, Libin Zhan^{1*}, Wen Zhou¹, Wanxin Chen¹, Jintong Luo¹, Lijing Zhang¹, Zebin Weng¹, Chunyan Zhao¹ and Shenlin Liu^{2,3*}

¹School of Traditional Chinese Medicine and School of Integrated Chinese and Western Medicine, Nanjing University of Chinese Medicine, Nanjing, China, ²Affiliated Hospital of Nanjing University of Chinese Medicine, Nanjing, China, ³Jiangsu Provincial Hospital of Traditional Chinese Medicine, Nanjing, China

OPEN ACCESS

Edited by:

Sayeed Ahmad,
Jamia Hamdard University, India

Reviewed by:

Bin Geng,
Chinese Academy of Medical
Sciences and Peking Union Medical
College, China
Štefan Zorad,
Slovak Academy of Sciences (SAS),
Slovakia

*Correspondence:

Libin Zhan
zlbj@njucm.edu.cn
Shenlin Liu
lsjsszyy@126.com

Specialty section:

This article was submitted to
Ethnopharmacology,
a section of the journal
Frontiers in Pharmacology

Received: 30 December 2020

Accepted: 13 July 2021

Published: 22 July 2021

Citation:

Zhao T, Zhan L, Zhou W, Chen W,
Luo J, Zhang L, Weng Z, Zhao C and
Liu S (2021) The Effects of Erchen
Decoction on Gut Microbiota and Lipid
Metabolism Disorders in Zucker
Diabetic Fatty Rats.
Front. Pharmacol. 12:647529.
doi: 10.3389/fphar.2021.647529

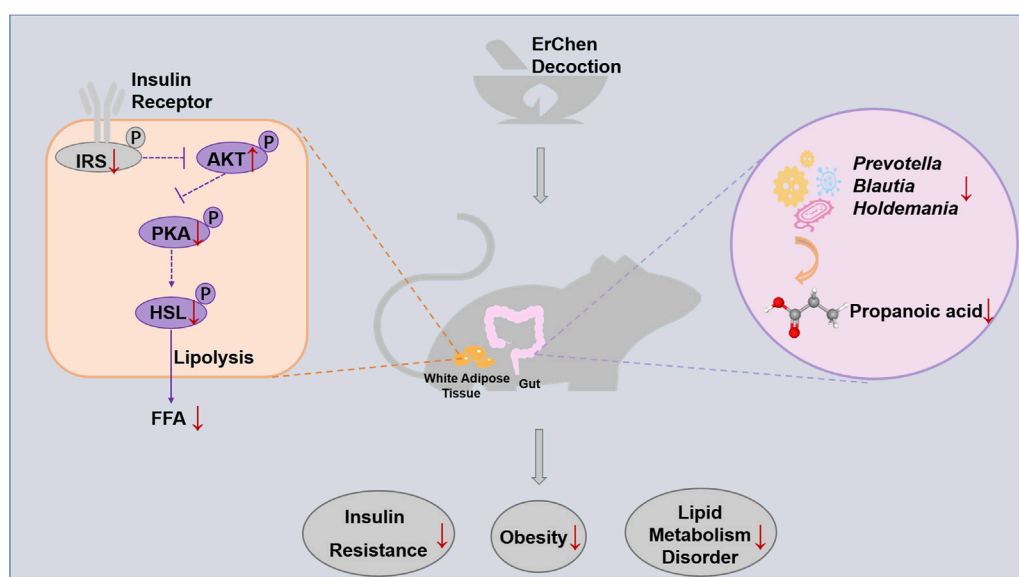
Obesity is a chronic metabolic disease caused by genetic and environmental factors that has become a serious global health problem. There is evidence that gut microbiota is closely related to the occurrence and development of obesity. Erchen Decoction (ECD), a traditional Chinese medicine, has been widely used for clinical treatment and basic research of obesity and related metabolic diseases in recent years. It can significantly improve insulin resistance (IR) and lipid metabolism disorders. However, there is no microbiological study on its metabolic regulation. In this study, we investigated the effects of ECD on obesity, especially lipid metabolism and the composition and function of gut microbiota in Zucker diabetic fatty (ZDF) rats, and explored the correlation between the biomarkers of gut microbiota and metabolite and host phenotype. The results showed that ECD could reduce body weight, improve IR and lipid metabolism, and reduce the concentration of free fatty acids (FFA) released from white adipose tissue (WAT) due to excessive lipolysis by interfering with the insulin receptor substrate 1 (IRS1)/protein kinase B (AKT)/protein kinase A (PKA)/hormone-sensitive triglyceride lipase (HSL) signaling pathway in ZDF rats. Additionally, ECD gradually adjusted the overall structure of changed gut microbiota, reversed the relative abundance of six genera, and changed the function of gut microbiota by reducing the content of propionic acid, a metabolite of gut microbiota, in ZDF rats. A potentially close relationship between biomarkers, especially *Prevotella*, *Blautia*, and *Holdemania*, propionic acid and host phenotypes were demonstrated through correlation analysis. The results suggested that the beneficial effects of ECD on obesity, especially lipid metabolism disorders, are related to the regulation of gut microbiota in ZDF rats. This provides a basis for further research on the mechanism and clinical application of ECD to improve obesity via gut microbiota.

Keywords: obesity, Erchen decoction, lipid metabolism disorders, insulin resistance, gut microbiota, short-chain fatty acids

INTRODUCTION

With the improvement of living standards and changes in lifestyles, the number of obese people is increasing sharply. The latest data has showed that, there were more than 1.9 billion adults worldwide who were overweight (about 39% of the total), and 650 million who were obese (about 13% of the total). 38 million children under the age of five were overweight or obese¹. Obesity is

¹World Health Organization. (2020). Obesity and overweight. <https://www.who.int/news-room/fact-sheets/detail/obesity-and-overweight>. [Accessed December 20, 2020].



GRAPHICAL ABSTRACT | Erchen Decoction could inhibit excessive lipolysis and improve lipid metabolism disorders by regulating the IRS1/AKT/PKA/HSL signaling pathway in white adipose tissue of ZDF rats. The delay in developing obesity was related to changes in gut microbiota composition and function in ZDF rats.

an important risk factor for many metabolic diseases (Saltiel and Olefsky, 2017), cardiovascular diseases (Luo et al., 2018), and even certain types of cancers (Majchrzak et al., 2019). At present, obesity, especially primary obesity, is considered to be a common disease. How to effectively prevent obesity and reduce the occurrence and development of related diseases has become a major research focus.

Adipose tissue is a main depot for storing and releasing energy and plays a key role in energy homeostasis, especially lipid metabolism balance. Dysfunction and metabolic disorder in adipose tissue is a characteristic pathological change in obesity and an important cause of local inflammation and systemic insulin resistance (IR) (Caprio et al., 2017). Insulin signaling is of crucial importance for maintaining adipose tissue function (Czech, 2017), whether from circulation or central insulin signaling (Scherer et al., 2011). Adipose tissue IR, especially an impaired insulin-signaling pathway, affects the key enzymes of lipolysis (Frühbeck et al., 2014), which leads to enhanced lipolysis as an important manifestation of metabolic disorders in adipose tissue.

Erchen Decoction (ECD), a traditional Chinese medicine formula, was first recorded in the Taiping Huimin Formula Bureau in the Song Dynasty, and is mainly used to treat phlegm dampness syndrome due to spleen dysfunction and dampness accumulation. Modern studies have found that ECD has beneficial weight loss, anti-inflammatory, and anti-oxidation effects, and significantly improves decreased insulin sensitivity (Zhang et al., 2017) and glucose and lipid metabolism disorders, especially lipid metabolism in metabolic diseases (Gao et al., 2015; Ding et al., 2018; Zhang et al., 2020b; Lee et al., 2020). In recent years, growing evidence has linked changes in gut microbiota with insulin sensitivity (Pedersen et al., 2016) and lipid metabolism (Kindt et al., 2018), and is now a target for obesity treatment

(Maruvada et al., 2017). The potential therapeutic mechanism of Chinese herbal medicines to ameliorate related metabolic diseases by improving the gut microbiota is also gradually being discovered (Gong et al., 2020). Previous studies have reported that the metabolism improvement of main traditional Chinese medicines (such as *Wolfiporia extensa* (Peck) Ginns (syn. *Poria cocos* (Schwein.) F.A.Wolf) and *Zingiber Officinale* Roscoe (Wang et al., 2020)) and their extracts (such as *Citrus reticulata* Blanco extract (Zhang et al., 2020c)) and active ingredients (such as glycyrrhiza polysaccharide (Zhang et al., 2018)) in ECD was closely related to the modulation of gut microbiota. A series of studies have been conducted on the effects by which ECD improves obesity. However, the role of ECD as a compound recipe in gut microbiota and whether the effect of ECD on improving IR or lipid metabolism disorders is related to changes in intestinal microbiota are still unclear.

The aim of this study was to observe whether ECD intervention could induce changes in IR and lipid metabolism disorders, delay the development of obesity, and affect the composition and function of gut microbiota in Zucker diabetic fatty (ZDF) rats, a spontaneous obesity model. More importantly, our goal was to determine the underlying correlation between the biological effects of ECD and the changes of gut microbiota and to provide a theoretical basis by which ECD improves obesity and related metabolic diseases via a gut microbiological mechanism.

MATERIALS AND METHODS

Preparation of ECD

ECD is composed of six components, as shown in Table 1. All herbs were purchased from Sanyue Chinese Traditional Medicine

TABLE 1 | The components of ECD.

Herbal name	Botanical Latin name	Place of origin	Part used	Amount used
Ban-Xia	<i>Pinellia ternata</i> (Thunb.) Makino	Jiangsu	dried tuber	15 g
Chen-Pi	<i>Citrus × aurantium</i> L.	Zhejiang	dried mature pericarp	15 g
Fu-Ling	<i>Wolfiporia extensa</i> (Peck) Ginns (syn. <i>Poria cocos</i> (Schwein.) F.A.Wolf)		dried sclerotia	9 g
Gan-Cao	<i>Glycyrrhiza uralensis</i> Fisch. ex DC.	Gansu	dried root and rhizome	4.5 g
Sheng-Jiang	<i>Zingiber Officinale</i> Roscoe	Jiangsu	fresh rhizome	7 pieces
Wu-Mei	<i>Prunus mume</i> (Siebold) Siebold and Zucc.	Fujian	dry near-mature fruit	1 piece

Co., Ltd. (Nantong, China) and prepared according to the Chinese Pharmacopoeia method (Chinese Pharmacopoeia Commission, 2015). The medicines were soaked in eight weight/volume (1:8, w/v) distilled water for 2 h. After boiling on high heat, they were simmered at low heat for 30 min. They were extracted twice, and the filtrate combined and concentrated until the final crude drug concentration was 0.23 g/ml for low dose, 0.46 g/ml for medium dose, and 0.92 g/ml for high dose. The medium dose is clinically effective dose of ECD. The samples were stored in a refrigerator at 4°C.

Chemical Composition of ECD Samples

High performance liquid chromatography (HPLC) was performed on a Waters 2,695 system (Waters Corporation, Milford, MA, United States), consisting of a binary solvent delivery manager, an auto-sampler, and a PDA detector. Chromatographic separations were performed on an Alltima C18 column (250 × 4.6 mm, 5 μm). Flow rate and column temperature were set at 1 ml min⁻¹ and 30°C, respectively. A mobile phase system consisting of 0.1% formic acid in H₂O (A)-acetonitrile (B) was applied with the following gradient program: 0–5 min, 95% A; 5–15 min, 95–75% A; 15–24 min, 75% A; 24–29 min, 75–65% A; 29–34 min, 65% A; 34–39 min, 65–55% A; 39–44 min, 55–50% A; 44–50 min, 50% A; 50–55 min, 50–30% A; 55–60 min, 30% A; 60–70 min, 30–10% A; 70–75 min, 10% A; 75–80 min, 10–0% A; 80–83 min, 0% A; 83–86 min, 0–95% A; 86–90 min, 95% A. The injection volume was 10 μL. Ultraperformance liquid chromatography-electrospray ionization-quadrupole-time of flight-mass spectrometry (UHPLC-ESI-Q-TOF-MS) was also performed on ECD samples. Details of the detection method are described in the supplementary materials.

Animal Model

We used 32 ZDF rats (*Fa/Fa*) with body weights of 130 ± 10 g, and six Zucker lean (ZL) rats (*Fa/+*) with body weights of 102 ± 12 g. All rats were 5 weeks old, male, with animal quality certificate No. SCXK (Beijing) 2016–0,006 provided by Vital River Laboratories (Beijing, China). They were raised in the specific pathogen-free animal experiment center at Nanjing University of Chinese medicine (Nanjing, China) at a temperature of 24 ± 2°C, humidity of 65 ± 5%, light/dark cycle of 12 h/12 h, and were provided food and water *ad libitum*. All animal experiments were approved by the Animal Ethics Committee of Nanjing University of Chinese Medicine (approval No. 201909A017). All studies were conducted in

accordance with the recommendations of Guide for the Care and Use of Laboratory Animals.

Experimental Design

After adaptive feeding, rats were randomly divided into five groups: control group (L, *n* = 6), model group (Z, *n* = 8), ECD low-dose group (EC-L, *n* = 8), medium-dose group (EC-M, *n* = 8), and high-dose group (EC-H, *n* = 8). Group L was fed with a normal diet (MD17121, Mediscience, China), and the others were given formula feed (Purina#5008, Lab diet, United States). Dietary composition is shown in **Supplementary Table 1**. From 5 to 9 weeks old, ECD treatment groups (EC-L, EC-M, and EC-H groups) were orally administered the low (2.28 g/kg), medium (4.57 g/kg), or high (9.14 g/kg) doses of ECD, and the L and Z groups were given high-pressure-sterilized water instead of ECD once a day with a volume of 1 ml/100 g. These dosages were calculated from the equivalent conversion of the body surface area between animals and humans.

Fresh fecal samples were collected into sterile tubes, avoiding contact with skin or urine of rats, at the end of adaptive feeding (5-week-old rats) and before the end of the experiment (9-week-old rats), then stored at –80°C before processing for 16S rRNA gene sequencing. The body weights, abdominal circumferences, and food intakes of rats in all five groups were measured weekly. At the age of 9 weeks, an insulin tolerance test (ITT) was performed by intraperitoneal injection of insulin (5 U/kg) after fasting for 6 h, and the area under the curve (AUC) was calculated.

After the experiment, the rats were fasted for 12 h and then anesthetized with isoflurane. Blood was taken from the abdominal aorta. The supernatant was collected after centrifugation at 4°C and 180 g for 10 min, and the levels of total cholesterol (TC), high-density lipoprotein cholesterol (HDL-C), low-density lipoprotein cholesterol (LDL-C), and triglycerides (TG) also with alanine aminotransferase (ALT), aspartate aminotransferase (AST), blood urea nitrogen (BUN) and creatinine (Cr) were measured by an automatic biochemical analyzer (Chemray 240, Rayto, China). Fasting serum insulin levels were determined by enzyme-linked immunosorbent assay (10–1,250–01, Mercodia, Sweden), and the Homeostasis Model Assessment-Insulin Resistance (HOMA-IR) index was calculated as follows: HOMA-IR = fasting plasma glucose (mmol/L) × fasting serum insulin (mIU/L)/22.5 (Matthews et al., 1985). The remaining samples were used for determination of fasting serum free fatty acids (FFA). The weights of perirenal WAT and epididymal WAT were measured, and the fat body ratio was calculated as follows: Fat body ratio = (perirenal or epididymal)

WAT weight (mg)/body weight (g) \times 100%; Total fat body ratio = (perirenal + epididymal) WAT weight (mg)/body weight (g) \times 100%. The epididymal WAT from the same part of each rat was collected for hematoxylin-eosin (HE) staining and western blotting. Cecal contents (fresh feces in the cecum) were collected for targeted metabolomics analysis. EC-M group was used as the representative of EC groups for subsequent HE staining, western blotting, FFA determination, gut microbiota sequencing, and short-chain fatty acids (SCFAs) content detection. Except the paraformaldehyde fixed WAT was stored at 4°C, all samples were stored at -80°C.

HE Staining

To detect the difference of cell morphology in WAT, the three most representative rats in groups L, Z, and EC were respectively selected and their WAT were dehydrated and embedded, and then prepared into 5- μ M paraffin sections (RM2245, Leica, Germany). After stained with HE staining solution (R20570-2, Yuanye, China), WAT was observed and photographed using a microscope (BX53, Olympus, Japan).

Western Blotting and FFA Determination

The four most representative rats in groups L, Z, and EC were respectively selected for western blotting and FFA determination. Epididymal WAT samples in three groups were homogenized in RIPA buffer (P0012B, Beyotime, Beijing, China) supplemented with a mixture of 100 \times protease inhibitor cocktail (5871s, CST, United States) and 100 \times phosphatase inhibitor cocktail (5870s, CST, United States) to obtain their protein samples. The same amounts of protein samples were subjected to sodium dodecyl sulfate-polyacrylamide gel electrophoresis (SDS-PAGE) and blotted with the following antibodies: phospho-Insulin Receptor Substrate 1 (IRS1) (Ser307) (#2381, CST, United States, 1:1,000), IRS1 (ab52167, Abcam, United Kingdom, 1:500), phospho-Protein Kinase B (AKT) (Ser473) (4058S, CST, United States, 1:1,000), AKT (9272S, CST, United States, 1:1,000), phospho-Protein Kinase A (PKA) $\alpha/\beta/\gamma$ (Thr197) (ab75991, Abcam, United Kingdom, 1:5,000), PKA $\alpha/\beta/\gamma$ (SC-390548, Santa Cruz, United States, 1:1,000), Phospho-hormone-sensitive triglyceride lipase (HSL) (Ser563) (AF2350, Affinity, United States, 1:2000), HSL (AF6403, Affinity, United States, 1:2000), adipose triglyceride lipase (ATGL) (A6245, Abclonal, 1:1,000) and β -actin (3700S, CST, United States, 1:1,000). The membranes were incubated with secondary antibodies conjugated to HRP (BA-1054/BA1050, Boster, Hubei, China, 1:2000). The immunoreactive bands were treated with chemiluminescence solution (ECL, Tanon, Shanghai, China) and detected by X-ray films. The blots were visualized with an Amersham Imager 600 (General Electric Company, United States).

According to the instruction of the determination kit (A042-2-1, Jiancheng, China), the concentrations of FFA in the serum samples of rats in groups L, Z, and EC were detected.

Gut Microbiota Sequencing and Data Analysis

The fecal samples of rats in L, Z, and EC groups at 5 and 9 weeks old were sequenced for the 16S rRNA gene (Shanghai Personal

Biotechnology Co., Ltd., Shanghai, China). According to the manufacturer's protocol, total microbial DNA was extracted from stool samples, and DNA was quantified by a Nanodrop. The quality of DNA extraction was detected by 1.2% agarose gel electrophoresis. The V3-V4 region of the 16S rRNA gene was amplified by polymerase Chain Reaction (PCR). The amplified products were quantified by fluorescence (Microplate reader, BioTek, FLx800), and the samples were mixed according to the corresponding proportions. The sequencing Library (TruSeq Nano DNA LT Library Prep Kit, Illumina company) was prepared, and double-ended sequencing (MiSeq PE300 sequencer) was performed with a Miseq Regent Kit V3 (600 cycles).

The analysis was carried out using Quantitative Insights into Microbial Ecology (QIIME2) and R language ggplot2 package software. The sequence denoising was performed by a DADA2 analysis process (Callahan et al., 2016). According to the distribution of amplitude sequence variables (ASVs) among the groups, the Simpson index at 5 and 9 weeks of age was evaluated to characterize alpha diversity, and a box plot was drawn using R script. The differences in beta diversity at 5 and 9 weeks of age were evaluated by principal coordinates analysis (PCoA) based on unweighted UniFrac distance, a classical multidimensional scaling (cMDS) analysis method (Ramette, 2007). Sample two-dimensional sorting graphs of PCoA were drawn by R script, and the significance of the differences was evaluated by adonis analysis. The number of common and unique ASVs between groups was shown by a Venn diagram. At the level of taxonomic composition, species at 5 and 9 weeks of age in each group was displayed at the phylum and genus levels to understand the overall microbial composition. At the genus level, the UPGMA algorithm was carried out to perform hierarchical clustering analysis based on the Bray-Curtis distance matrix to show the similarity of the microbial composition among groups. Linear discriminant analysis (LDA) effect size (LEfSe) analysis, a nonparametric Kruskal-Wallis and Wilcoxon rank sum test combined with LDA effect size (Segata et al., 2011), was applied to explore the difference between groups at 5 and 9 weeks of age, and measure the changes in microbiota during the development of obesity and ECD treatment. An LDA value distribution histogram was used to show the species significantly enriched and their degree of importance. A cladogram was constructed to display the taxonomic hierarchical distribution of biomarkers in each group. Random forest analysis was applied to show the order of importance of biomarkers among groups at 9 weeks of age. The functional potential was predicted and analyzed based on Phylogenetic Investigation of Communities by Reconstruction of Unobserved States (PICRUSt) 2. The abundance of secondary functional pathways in the KEGG pathway database (<http://www.genome.jp/kegg/pathway.html>) was calculated for gut microbiota of 9-week-old rats. The functional units were identified by PCoA based on Bray-Curtis similarity, and differential metabolic pathways were predicted by metagenomeSeq. Spearman correlation analysis was used to determine the correlation between biomarkers and differential metabolic pathways. A heat map was constructed

to investigate the potential relationship between the biomarkers and host phenotype.

The raw sequences of Miseq sequences from 44 fecal samples of rats have been submitted to NCBI Project under accession number PRJNA686642 with NCBI Sequence Read Archive under accession number SRP298569.

SCFAs Analysis

The targeted metabolism technology, ultraperformance liquid chromatography-tandem mass spectrometry (UPLC-MS/MS), was used to quantitatively detect SCFAs in the cecal contents of L, Z, and EC groups (Metabo-Profile, Shanghai, China). According to the manufacturer's protocol, approximately 10 mg of sample was put in a 1.5 ml tube, and 25 μ L of water and 185 μ L of acetonitrile:methanol (8:2) was added to extract metabolites. After high-speed centrifugation (18,000 g, 20 min), 15 μ L of internal standard was added to the 135 μ L supernatant, which was aliquoted and diluted. UPLC-MS/MS (Waters ACQUITY UPLC-Xevo TQ-S, Waters Corp., Milford, MA, United States) was used for SCFA detection. TargetLynx software (Waters Corp., Milford, MA, United States) was used to process the original data files generated by UPLC-MS/MS, and the peaks of each metabolite were integrated, calibrated, and quantified. Partial least squares discrimination analysis (PLS-DA) was applied to show the composition of SCFAs among groups. Integrated Metabolomic Analysis Platform v1.0 (Metabo-Profile, Shanghai, China) was used for statistical analysis. A heat map was constructed to show the potential relationship between the biomarker and host phenotype.

Statistical Analysis

The data of ZDF rat phenotypes was expressed as means \pm standard error of the mean (SEM). The statistical differences between groups were evaluated by analysis of variance (ANOVA) using GraphPad Prism 8.0 software (GraphPad, La Jolla, CA, United States), and the specific analysis method is shown in the legend of each figure. ImageJ v1.8.0 (Rawak Software Inc., Stuttgart, Germany) was used to analyze the number and cross-sectional area of adipocytes in WAT. The target protein bands were quantified with ImageQuant TL 1D software (GE Healthcare, United States). Spearman correlation analysis was conducted to evaluate correlations between the biomarkers in gut microbiota and SCFAs and host phenotype. Significant differences were accepted at p values of <0.05 .

RESULTS

The Chemical Composition of ECD

A characteristic HPLC chromatogram of an ECD sample is shown in **Figure 1**. ECD contained four compounds, liquiritin, hesperidin, glycyrrhizic acid, and 6-gingerol, which are flavonoids, saponins, and phenols, and is basically consistent with the results of previous studies (Lee et al., 2020). UHPLC-ESI-Q-TOF-MS total ion chromatogram and results of ECD sample are shown in **Supplementary Figure 1** and **Supplementary Table 2**. One hundred and twenty-six compounds in the

positive ion mode and 20 compounds in the negative ion mode were detected, including naringin and 8-gingerol that were not detected by HPLC. Nobiletin was found in the positive ion mode, and five compounds were found in both the positive ion and negative ion mode. Previous studies have predicted that hesperidin, naringin, nobiletin, glycyrrhizic acid, and 6-gingerol might be the main bioactive components and medicinal material bases of ECD intervention in metabolic diseases (Lee et al., 2018).

ECD Delayed the Development of Obesity in ZDF Rats

To observe the effects of ECD on obesity in ZDF rats, we compared the changes of body weight, abdominal circumference, and food intake in the five groups. The results revealed that the difference of body weight age-dependently increased in group Z comparison to group L. ECD treatment notably reduced the body weight of rats at 8 weeks old. At 9 weeks of age, the body weight gain compared with the baseline of the ECD-treated groups was significantly lower than that of group Z (**Figures 2A,B**). The weekly changes in abdominal circumference showed the same trend as that of body weight, with ECD treatment at 7 weeks of age significantly reducing the enlarged abdominal circumference (**Figure 2C**), which illustrated that ECD had intervention effects on abdominal obesity. However, the intervention effect of ECD was not realized through the control of food intake (**Figure 2D**).

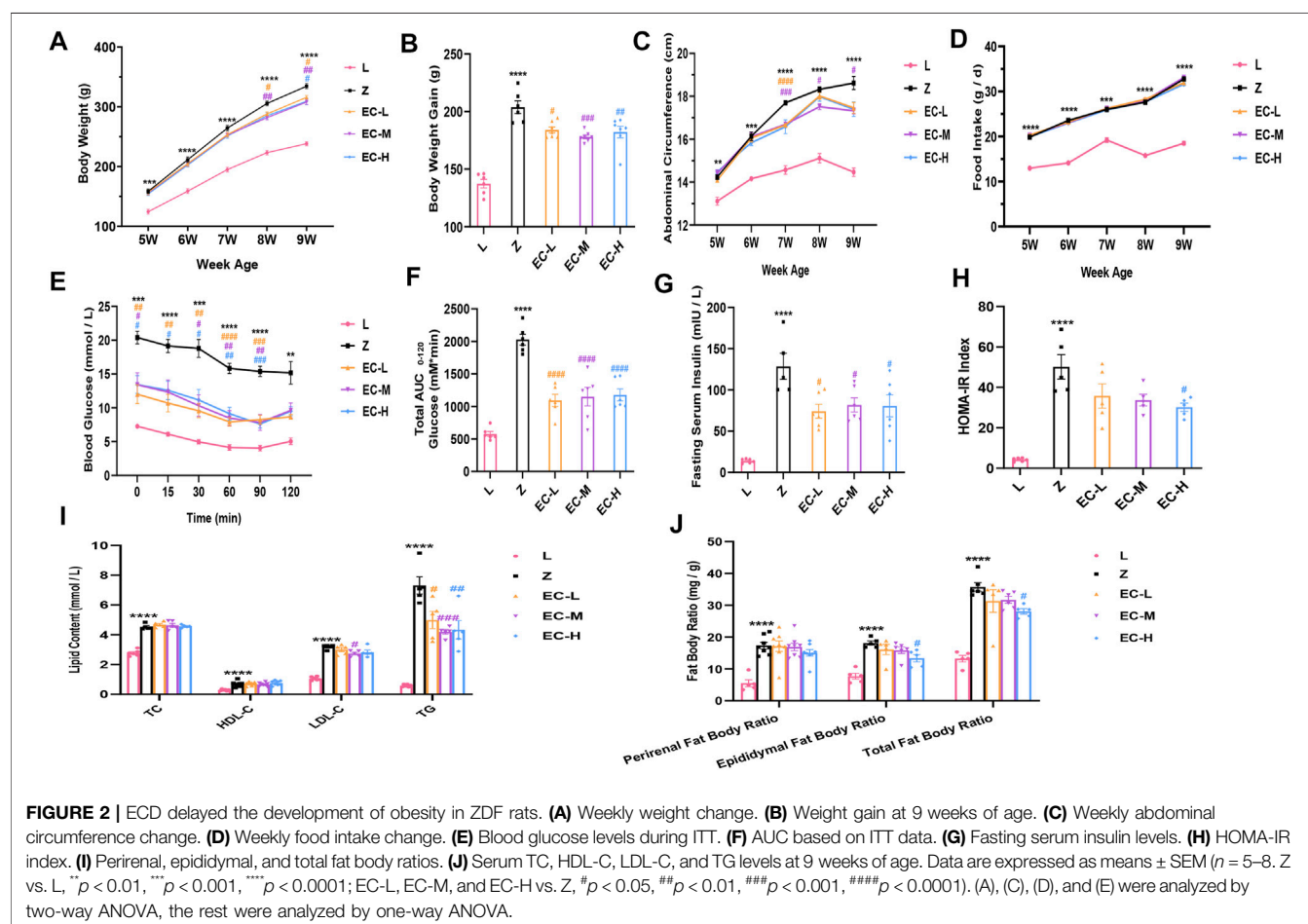
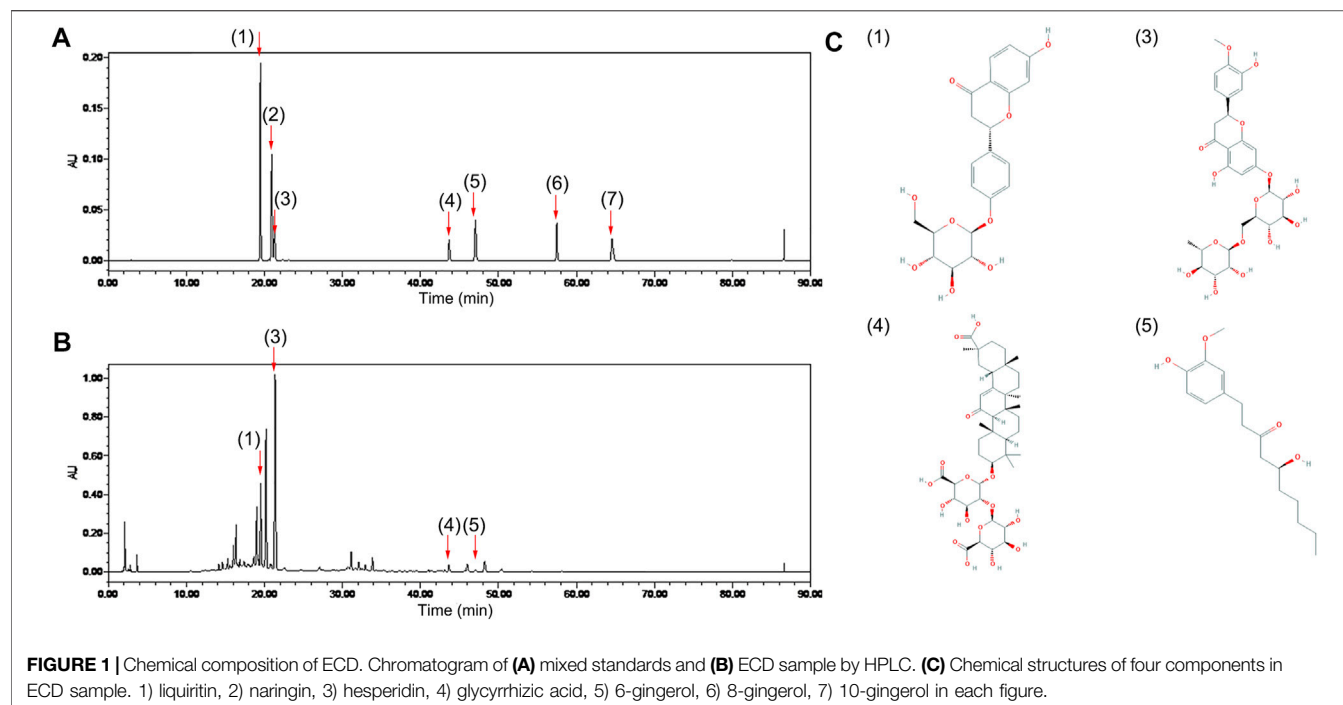
Insulin sensitivity was evaluated by ITT at 9 weeks of age. The results revealed a higher blood glucose level at each time point and AUC in group Z, while ECD treatment effectively improved insulin sensitivity (**Figures 2E,F**). Additionally, fasting serum insulin levels and HOMA-IR indexes increased significantly in group Z, while ECD treatment attenuated IR of ZDF rats (**Figures 2G,H**).

The fat body ratio and blood lipids were standardized at the end of the experiment. The results showed an obvious increase of fat body ratio and various indexes of blood lipids in group Z. ECD markedly reduced epididymal and total fat body ratio, serum LDL-C, and TG (**Figures 2I,J**), indicating that ECD could regulate abnormal lipid metabolism *in vivo*. These data illustrated that ECD could effectively prevent and treat obesity and improve IR and lipid metabolism disorders in ZDF rats as expected.

The dose used in group EC-M is a clinically effective dose, which had basically same effect while less negative impact on liver and kidney function of rats compared with group EC-H (mainly manifested in significantly elevated ALT and more notably higher Cr level in group EC-H, as shown in **Supplementary Figure 2**). Therefore, EC-M was taken as the representative of treatment groups for subsequent studies.

ECD Improved Insulin Signal Transduction and Decreased Lipolysis in WAT of ZDF Rats

WAT stores TG as an energy reserve and provides energy to tissues in the form of FFA. In pathological conditions, excessive



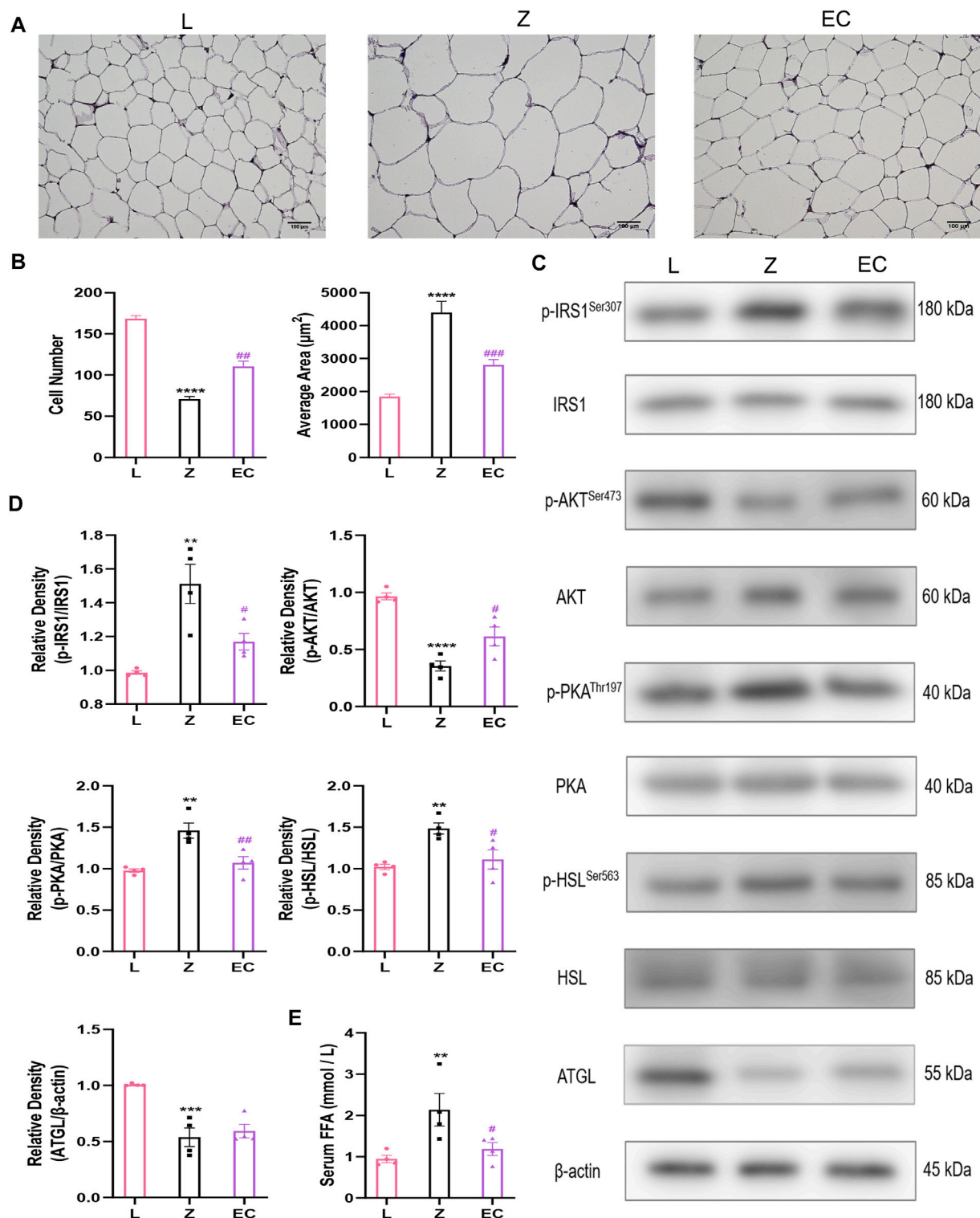


FIGURE 3 | ECD improved insulin signal transduction and decreased lipolysis in WAT of ZDF rats. **(A)** Representative image (bar: 100 μm) and **(B)** number and average area of adipocytes of WAT HE staining ($n = 3$. Z vs. L, **** $p < 0.0001$; EC vs. Z, ## $p < 0.01$, ### $p < 0.001$). **(C)** Representative bands and **(D)** relative protein expression of p-IRS1/IRS1, p-AKT/AKT, p-PKA/PKA, p-HSL/HSL, and ATGL. **(E)** Serum FFA concentration ($n = 4$. Z vs. L, ** $p < 0.01$, *** $p < 0.001$, **** $p < 0.0001$; EC vs. Z, # $p < 0.05$, ## $p < 0.01$). (B), (D), and (E) were analyzed by one-way ANOVA.

lipolysis is a characteristic pathological change of obesity. At the histological level, HE staining results showed that the adipocytes in group L were uniform in size, clear in boundary and tightly arranged. However, in the same field of vision, the number of adipocytes decreased, the diameter and cross-sectional area of adipocytes increased in group Z, while ECD treatment increased the number of adipocytes, reduced the area of adipocytes tended to be normal (**Figures 3A,B**). Insulin has an important regulatory effect on lipolysis. It activates insulin signaling by binding to receptors on adipocytes and regulates downstream PKA activity. HSL, a key enzyme in the process of hydrolyzing diacylglycerol into glycerol and FFA, is an important target for PKA control. The expressions of p-IRS1/IRS1, p-AKT/AKT, p-PKA/PKA, and p-HSL/HSL in the epididymal WAT of ZDF rats were determined by western blotting to explore the underlying effect of ECD on lipolysis. The results showed that there were no significant changes in total protein levels of IRS1, AKT, PKA, or HSL levels in the three groups. However, we observed the differences in phosphorylation with a significant increase in p-IRS1/IRS1, p-PKA/PKA, and p-HSL/HSL levels and downregulation of the level of p-AKT/AKT in group Z. Compared with group Z, ECD could regulate the phosphorylation status of these molecules in the opposite direction, thereby improve significantly the activity. ATGL is the rate-limiting enzyme which decomposes triacylglycerols to diacylglycerol, which provides substrate for HSL. Contrary to HSL, its activity does not seem to be regulated by phosphorylation (Zimmermann et al., 2004). Therefore, the expression of ATGL protein was also measured. Compared with group L, ATGL protein content in group Z was notably reduced, but ECD did not modify it. These results suggested that there might be abnormal lipolysis in WAT of ZDF rats, and the effect of ECD on the lipolysis relied more on the improvement of IRS1/AKT/PKA/HSL signaling pathway rather than on a direct regulation of HSL or ATGL (**Figures 3C,D**). The regulation of insulin on ATGL is not mediated by AKT (Yin et al., 2019) or PKA (Zimmermann et al., 2004), which may explain why ECD had no effect on ATGL. The level of lipolysis affects the content of FFA in the circulation. Thus, we compared the concentrations of fasting serum FFA in three groups to confirm the effect of ECD on lipolytic function of ZDF rats. Compared with group L, the FFA concentration of group Z increased, while ECD treatment significantly reduced the FFA concentration of ZDF rats (**Figure 3E**). The above results indicated that there were abnormal cell morphology and excessive lipolysis in WAT of ZDF rats, and ECD could possess protective effect on the morphology of adipocytes and reduce the release of FFA from excessive lipolysis of WAT by interfering with insulin signal transduction, which might be related to the improvement of IRS1/AKT/PKA/HSL signaling pathway.

ECD Modulated the Overall Structure and Composition of Gut Microbiota in ZDF Rats

To explore whether the biological effects of ECD were related to changes in gut microbiota, an important target for the development of obesity, fecal samples from rats at 5 and

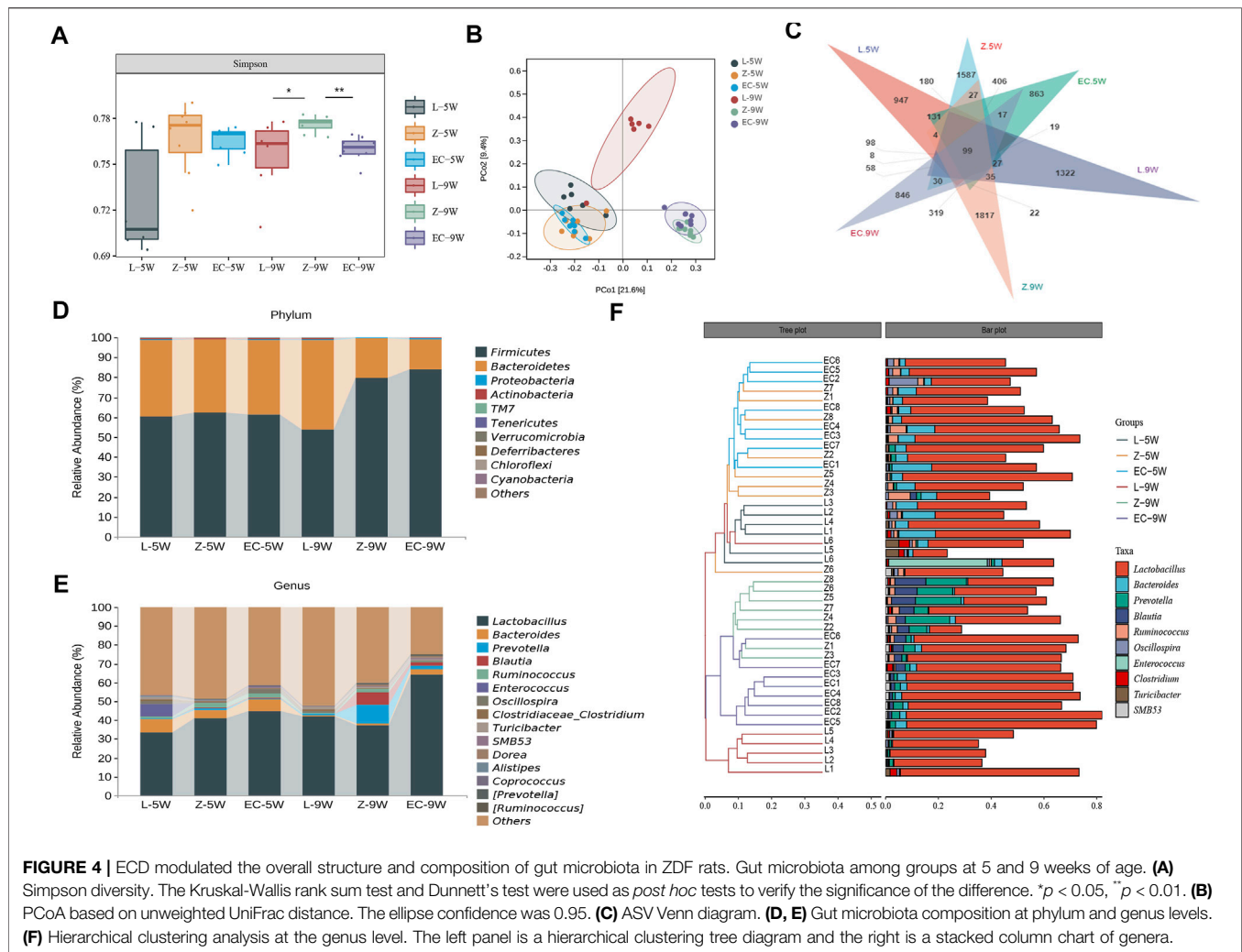
9 weeks of age were collected and the 16S-V3V4 regions of the gut microbiota were pair-end sequenced using the Illumina high-throughput sequencing platform. A total of 1,610,611 sequences were gathered after denoising, and 1,113,709 high-quality sequences were obtained after quality control from 44 samples. The 17,692 sequence abundances of each sample ensured that all samples were analyzed at the same level of sequencing depth after leveling.

We first assessed the changes in the structure of gut microbiota of rats. At 5 weeks of age, the Simpson index of ZDF rats was no different from that of the control. While at 9 weeks of age, the Simpson index of group Z was significantly higher than that of L, ECD intervention significantly reduced this index and changed the alpha diversity of gut microbiota in ZDF rats (**Figure 4A**). PCoA based on unweighted UniFrac distance (**Figure 4B**) illustrated that the bacterial structure of groups Z and L were separated significantly at 5 weeks of age. With the development of obesity, the bacterial structure of group Z changed (Z-5W vs. Z-9W: $R^2 = 0.322,165$, $p = 0.002$), and the difference between groups Z and L was more obvious at 9 weeks of age (L-5W vs. Z-5W: $R^2 = 0.127,367$, $p = 0.002$; L-9W vs. Z-9W: $R^2 = 0.321,536$, $p = 0.001$). ECD also gradually changed the bacterial structure of ZDF rats (EC-5W vs. EC-9W: $R^2 = 0.361,867$, $p = 0.002$). At 9 weeks, the bacterial structures of EC and Z groups could be distinguished significantly (Z-5W vs. EC-5W: $R^2 = 0.061437$, $p = 0.701$; Z-9W vs. EC-9W: $R^2 = 0.238,092$, $p = 0.001$).

We further observed the changes in the composition of gut microbiota of rats. We found that from 5 to 9 weeks of age, the shared ASVs between groups L and Z decreased from 890 to 312, and those between groups Z and EC decreased from 1,237 to 689 (**Figure 4C**), indicating that both the development of obesity and the intervention of ECD might cause some changes in the composition of rat gut microbiota. The top 10 phyla and top 15 genera in relative abundance of fecal microbiota in each group of rats at 5 and 9 weeks old are shown in **Figures 4D,E**, respectively. *Firmicutes* and *Bacteroidetes* were the two main phyla, followed by *Proteobacteria* and *Actinobacteria*, which was similar to the situation of human gut microbiota. At the genus level, *Lactobacillus* was the dominant genus in all stages of rats in each group. Hierarchical clustering analysis of the top 10 abundant genera of gut microbiota of each group at the two stages showed that the microbial composition of the EC group was similar to that of group Z at 5 weeks of age, while at 9 weeks of age, the microbial composition of the EC group was more similar to that of group L due to the intervention of ECD (**Figure 4F**). These results indicated that ECD gradually regulated the overall structure and genus composition of gut microbiota in ZDF rats.

ECD Regulated the Abundance of Biomarkers at the Genus Level of Gut Microbiota in ZDF Rats

To detect biomarkers at the genus level, we compared horizontally the composition of gut microbiota among three groups at 5 and 9 weeks of age, and compared vertically the changes of gut microbiota of each group from 5 to 9 weeks of age. The gut microbiota changed significantly with the development



of obesity and ECD treatment were explored. We found that the differences of gut microbiota at genus level were not significant at 5 weeks of age. However, from 5 to 9 weeks, the promotion of nine genera (*Prevotella*, *Blautia*, *Dorea*, *SMB53*, *Allobaculum*, *Coprobacillus*, *[Ruminococcus]*, *Holdemanella*, and *Sutterella*) and the reduction of five genera (*Akkermansia*, *Oscillospira*, *Adlercreutzia*, *Dehalobacterium*, and *f_Erysipelotrichaceae_g_Clostridium*) were established during the development of obesity, which had a significant difference in group Z comparison to L at 9 weeks of age, implying the potential relevance of these genera to obesity progression (Supplementary Table 3). At the same time, ECD treatment gradually changed the relative abundance of four genera mentioned above, including decreasing *Prevotella*, *Blautia*, *Coprobacillus* and *Holdemanella*, and increasing *Akkermansia*. In addition, ECD also gradually reduced the amount of *Ruminococcus*. At 9 weeks of age, the relative abundance of these genera in group EC were markedly different from group Z and tended to a normal level, which are the bacterial targets of ECD. LDA value distribution histogram and corresponding cladogram were used to show microbiota and their taxonomic

hierarchies with significant differences between groups at 9 weeks of age (Figures 5A,B). The relative abundances of ECD intervention biomarkers are shown in Figure 5C, and their LDA and p values are shown in Supplementary Table 4. The importance order of these genera is shown by random forest analysis. In particular, *Prevotella*, *Ruminococcus*, *Blautia* and *Holdemanella* have a greater impact on the formation of differences among groups (Figure 5D).

ECD Regulated the Function of Gut Microbiota in ZDF Rats

To observe whether the changes in the composition of gut microbiota further leads to functional changes, we further carried out the prediction of the function of microbiota, and detected the changes in the content of important microbiota metabolites, SCFAs. The function of gut microbiota in 9-week-old rats was mainly focused on genetic information processing and metabolism, especially energy metabolism and the metabolism of the three major energy substances, amino acids, carbohydrates, and lipid (Figure 6A). However, PCoA showed that there was a certain

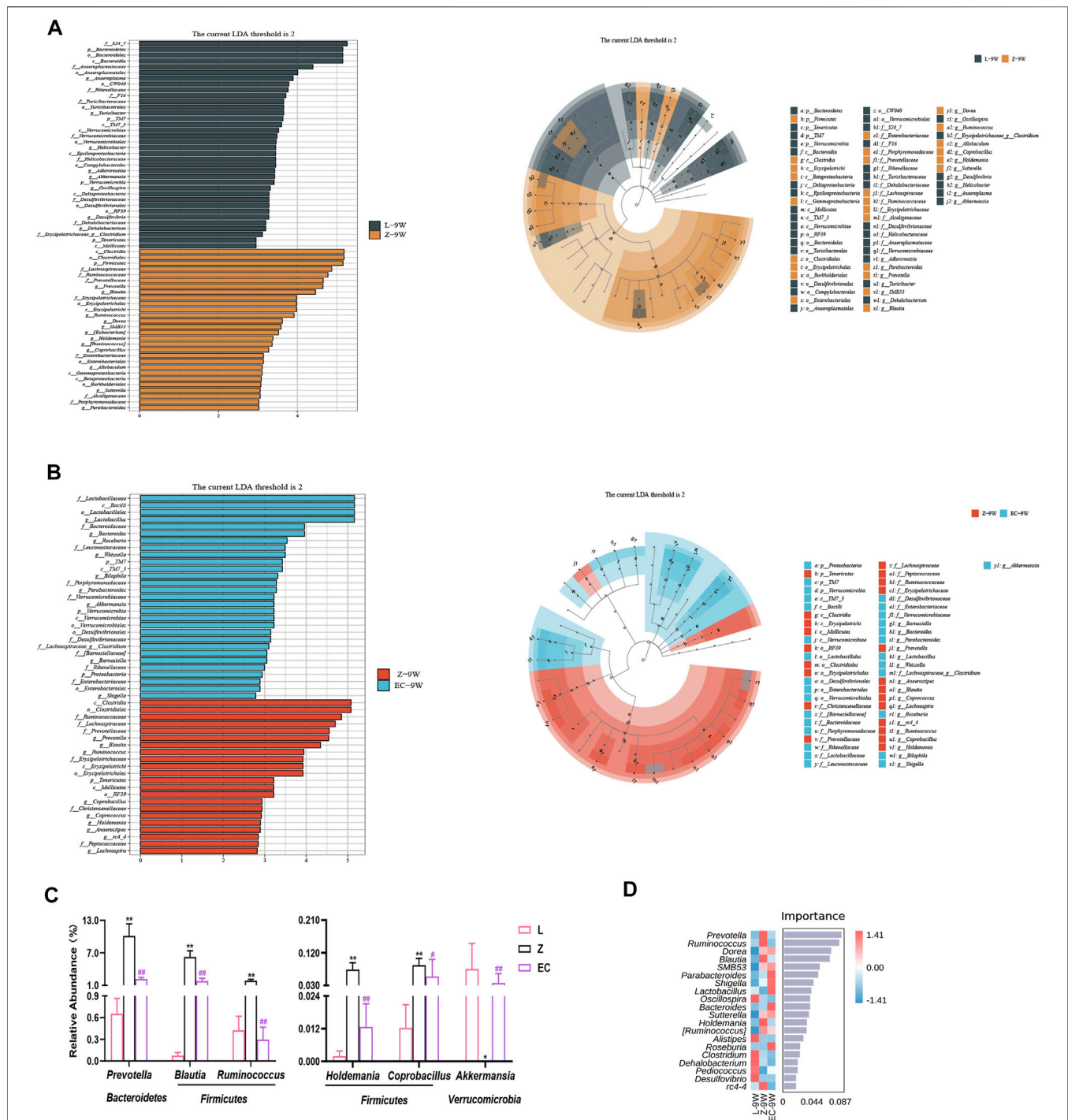
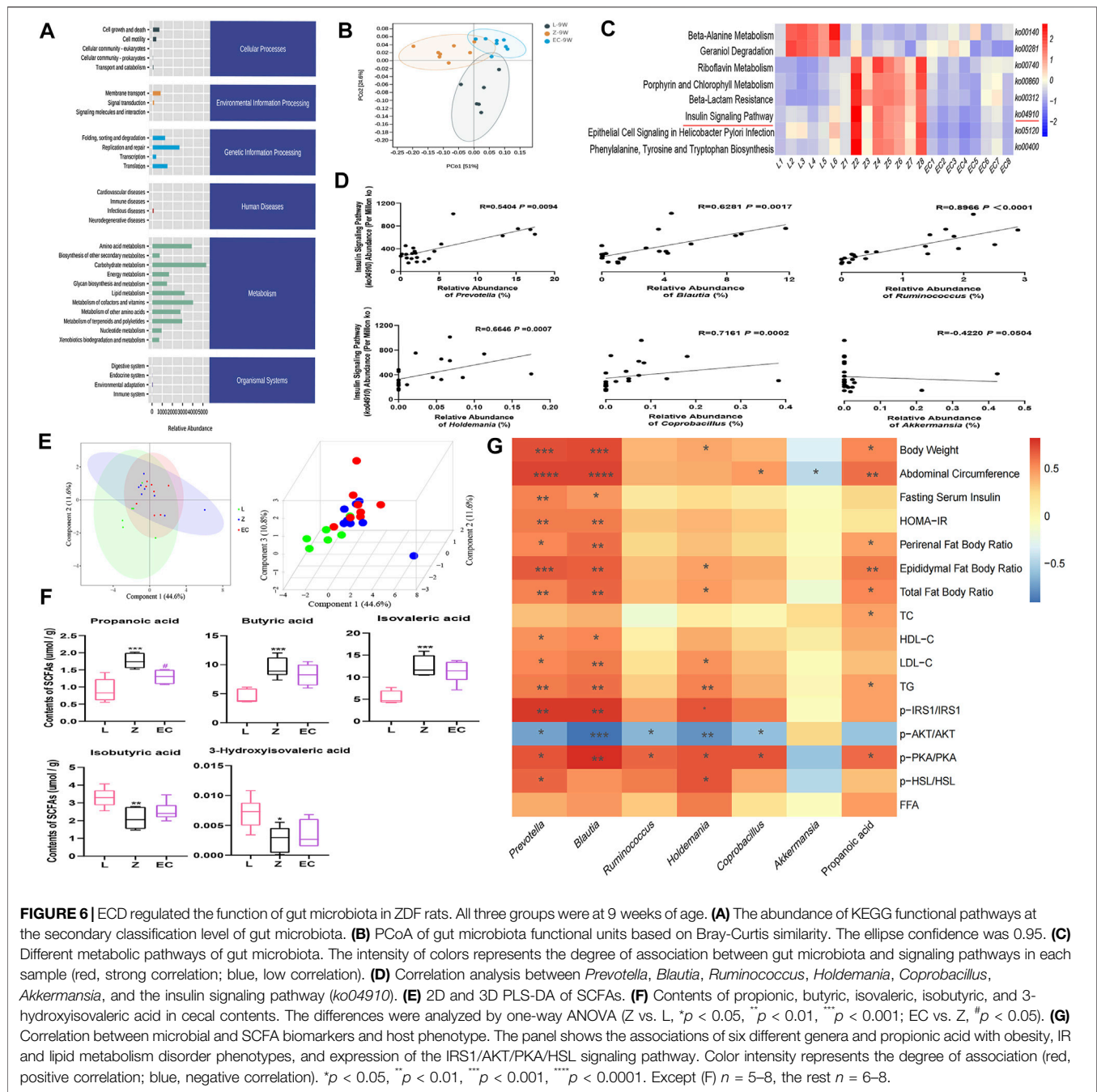


FIGURE 5 | ECD regulated the abundance of biomarkers at the genus level of gut microbiota in ZDF rats. All three groups were at 9 weeks of age. **(A)** LDA value distribution histogram and cladogram of biomarkers between groups L and Z. **(B)** LDA value distribution histogram and cladogram of biomarkers between groups Z and EC. LDA score threshold >2 in (A) and (B). **(C)** Relative abundances of *Prevotella*, *Blautia*, *Ruminococcus*, *Holdemania*, *Coprobacillus*, and *Akkermansia* among three groups. The *p*-value was determined by LEfSe analysis. **(D)** Random forest analysis of differential gut microbiota. The intensity of colors represents the abundance distribution of gut microbiota in each sample (red, the corresponding abundance was higher; blue, the corresponding abundance was lower).

separation of microbial functions among the three groups in rats. In the PC1 dimension, the functional composition of the EC group was more similar to that of group L, with a contribution rate of 51%

(Figure 6B). There were significant differences in eight signaling pathways, including the insulin signaling pathway (*ko04910*) (Figure 6C). Its abundance was significantly positively correlated



with the relative abundance of *Prevotella*, *Blautia*, *Ruminococcus*, *Holdemania*, and *Coprobacillus* (Figure 6D), implying a potential role for these ECD intervention biomarkers. The metabolites secreted, modified, and degraded by gut microbiota are important mediators of the host-microbiota dialogue, which participate in the regulation of host metabolism. SCFAs are metabolites that have a high concentration in the cecum, and mainly include acetic acid, propionic acid, and butyric acid. The metabolism of SCFAs in the cecum of groups at 9 weeks of age was analyzed. The results showed that ZDF and ZL rats were separated in their composition of SCFAs (Figure 6E). Compared with group L, there were significant changes

in the contents of five SCFAs in group Z, among which propionic, butyric, and isovaleric acid were notably increased, while isobutyric and 3-hydroxyisovaleric acid were obviously reduced. ECD treatment significantly reduced propionic acid and tended to reduce butyric and isovaleric acid while raising isobutyric and 3-hydroxyisovaleric acid in the cecum of rats (Figure 6F). *Prevotella* (De Vadder et al., 2016), *Blautia* (Reichardt et al., 2014) and *Ruminococcus* (Krautkramer et al., 2020) strains have been reported to produce propionic acid by fermentation. Therefore, ECD might reduce the abundance of these bacteria to reduce the content of propionic acid. Acetic acid is the fermentation product of

most intestinal bacteria. Butyric acid- and propionic acid-producing bacteria were almost different, which explains why there were no differences in acetic acid among the groups or a significant change in the content of butyric acid after the intervention.

ECD significantly improved IR and lipid metabolism disorders, especially in WAT of ZDF rats. Therefore, we analyzed the correlation between the six core genera and propionic acid, which changed after ECD intervention, and host phenotype (Figure 6G). We observed that *Prevotella* and *Blautia* were not only markedly correlated positively with obesity phenotypes such as body weight and abdominal circumference, but also with pathological manifestations such as IR and abnormal lipid metabolism, while *Holdemania* was mainly associated positively with lipid metabolism disorder-related indexes. *Prevotella*, *Blautia*, *Ruminococcus*, *Holdemania*, and *Coprobacillus* also showed different degrees of correlation with the expression of the IRS1/AKT/PKA/HSL signaling pathway in WAT. In addition, the content of the gut microbiota metabolite propionic acid was significantly positively correlated with body weight, abdominal circumference, and phenotypes related to lipid metabolism disorders. These results revealed a potentially close relationship between the host phenotype and biomarkers, especially *Prevotella*, *Blautia*, *Holdemania*, and propionic acid. These might be important targets for ECD to improve obesity, especially lipid metabolism disorders via gut microbiota. The regulation of the insulin signaling pathway might also play an important role.

DISCUSSION

In this study, we found for the first time that ECD changes the composition and function of gut microbiota in ZDF rats, which led them towards a healthier state. Interestingly, the changes in gut microbiota induced by ECD intervention were closely related to the improvement of IR and lipid metabolism disorders, especially in WAT, indicating that the beneficial effects of ECD on obesity, especially lipid metabolism disorders, were related to the regulation of gut microbiota in ZDF rats.

ZDF rats are characterized by obesity, IR, and hyperlipidemia due to mutations in the extracellular region of the leptin receptor (Habegger et al., 2014). Compared with traditional dietary model, this animal model has a shorter time interval and is stable, which makes it ideal to study obesity. We found that ECD treatment could help the negative effects of obesity, including weight loss, improvements in IR, and the regulation of dyslipidemia, which is consistent with previous studies (Gao et al., 2015; Zhang et al., 2017; Ding et al., 2018; Zhang et al., 2020b; Lee et al., 2020) and illustrates that ECD has a regulatory effect on obesity caused by genetic factors. However, the regulatory effects of ECD on TC and HDL-C in blood lipids are not currently consistent, which might be related to the different models and drug concentrations.

Previous studies have investigated the biological effects by which ECD modulates metabolism. ECD can promote the expression of CDKAL1 and improve the function of islet cells, thereby ameliorating insulin secretion (Gao et al., 2015). Moreover, the intervention effects by which ECD improves lipid metabolism include the inflammatory response (Lee et al., 2020) and lipid

transport (Ding et al., 2018). The lipid metabolic balance is the result of a combination of lipogenesis and lipolysis. Studies have found that ECD upregulates the expression of peroxisome proliferator-activated receptor gamma (PPAR γ) in visceral fat and skeletal muscle and lipoprotein lipase (LPL) in skeletal muscle (Zhang et al., 2020b), and reduces the lipid accumulation caused by IR by inhibiting the expression of IRS1 phosphorylation in the liver (Zhang et al., 2017). Adipose tissue is an important target organ for the treatment of obesity (Kusminski et al., 2016), as it expands in obese individuals. Due to homeostatic regulation and continuous low-level inflammation (Shiau et al., 2019), excessive fat leads to lipolysis, resulting in FFA releases to the circulation and liver, skeletal muscle, pancreas, and other tissues, which leads to lipid toxicity and IR throughout the body. In particular, visceral adipocyte hypertrophy results in decreased insulin sensitivity, a weakened insulin anti-lipolytic effect, and enhanced lipolytic activity in adipocytes (Roden and Shulman, 2019). Studies have found that the anti-lipolytic effect of insulin can be adjusted through the AKT/PKA/HSL signaling pathway (Yin et al., 2019), and inhibiting excessive lipolysis of adipose tissue (Park et al., 2020) is an important way to treat metabolic diseases. Consistent with previous results, we found that adipocytes expanded, IRS1 phosphorylation increased, AKT activity decreased, and insulin signal transduction was impaired, while PKA-mediated HSL activity was upregulated and the ability to release FFA into the circulation was enhanced in the WAT of ZDF rats. ECD not only changed the histological morphology, but also improved lipolysis in WAT by modulating the IRS1/AKT/PKA/HSL signaling pathway and reverting it to normal. Under the condition of basically the same food intake and calories, ECD changed the weight of ZDF rats, which might be related to the increase of energy consumption. Both previous studies and our studies have shown that ECD could improve the metabolic regulation of adipose tissue, which might be accompanied by changes in the function of mitochondria in adipose tissue, because the location (Brestoff et al., 2020) and activity (Joffin et al., 2021) of mitochondria in adipose tissue play a key role in the homeostasis of lipid metabolism.

Host genetics affect the composition of gut microbiota (Goodrich et al., 2014), and gut microbiota in turn regulate host energy homeostasis and glucose and lipid metabolism (Tremaroli and Backhed, 2012). In addition, environmental factors also importantly affect the gut microbiota (Rothschild et al., 2018). Many studies have revealed a close underlying connection between changes in gut microbiota and the occurrence and development of obesity. Targeting gut microbiota could improve insulin sensitivity (Udayappan et al., 2016), thereby regulating insulin-mediated lipid metabolism in adipocytes (Kimura et al., 2013) and improving host obesity. In our previous work, we observed the effects of fecal microbiota transplantation on the progression of obesity-susceptible diabetic mellitus (Zhang L. et al., 2020) and dynamic changes in fecal microbiota in the diabetic mellitus stage of ZDF rats (Zhou et al., 2019). We revealed a potential role for the gut microbial structure and composition in the disease progression of ZDF rats. At the same time, we found that the traditional Chinese medicine formula,

ECD could delay the development of obesity in ZDF rats. Based on this, here we investigated the intervention effect of ECD on gut microbiota in the obesity stage of ZDF rats. We found that ECD reversed the changed diversity, adjusted the overall structure, and shifted the composition of gut microbiota at the genus level to render them normal during the development of obesity, especially the relative abundances of *Prevotella*, *Blautia*, *Ruminococcus*, *Holdemania*, *Coprobacillus*, and *Akkermansia* in ZDF rats. Current studies indicate that the association of *Prevotella* and *Blautia* with host health or disease status is controversial. Some researchers believe that increased *Prevotella* abundance can promote glycogen storage (Kovatcheva-Datchary et al., 2015) and produce succinic acid to activate intestinal gluconeogenesis, which is related to the improvement of glucose metabolism and insulin tolerance (De Vadder et al., 2016). However, some studies have found that *Prevotella* can participate in the biosynthesis of branched-chain amino acids, which is an important risk factor for the decreased insulin sensitivity, glucose tolerance, and the occurrence of type 2 diabetes (De Filippis et al., 2019). In addition, high levels of *Prevotella* can activate immune and stromal cells to release more inflammatory mediators, promote chronic inflammation (Larsen, 2017), and participate in the disease process. In obese (Si et al., 2017) and non-alcoholic fatty liver disease (Zhu et al., 2013; Schwimmer et al., 2019) individuals, *Prevotella* is significantly enriched. We found that ECD intervention reduced the elevated *Prevotella* in ZDF rats, and in addition to insulin resistance, *Prevotella* abundance was markedly positively correlated with lipid metabolism disorders, while previous studies focused on carbohydrate and amino acid metabolic pathways (Petersen et al., 2017). *Blautia* is an important SCFA producing bacteria (Liu et al., 2015), with anti-inflammatory effects (Benítez-Páez et al., 2020) that aid in the recovery of intestinal mucosal damage (Zhou et al., 2017); it is inversely associated with visceral fat content (Ozato et al., 2019) and plays a beneficial therapeutic role in metabolic disorders (Rodríguez et al., 2020). However, some studies have suggested that higher *Blautia* is associated with increased intestinal permeability (Leclercq et al., 2014), and its abundance is positively correlated with metabolic diseases and related to cardiovascular disease predictors such as plasma glutamate and branched-chain amino acids (Ottosson et al., 2018). In metabolic diseases such as obesity (Stanislawski et al., 2017), diabetes (Egshatyan et al., 2016; Wei et al., 2018), and nonalcoholic steatohepatitis (Del Chierico et al., 2017), the abundance of *Blautia* is increased. This might be related to the decrease in the abundance of other SCFA producing bacteria (Becker et al., 2011), or the result of inflammatory responses in different disease stages (Tuovinen et al., 2013). Our results indicated that ECD reduced *Blautia*, which was remarkably enriched in ZDF rats, and its abundance was significantly positively correlated with the negative effects of insulin sensitivity and lipid metabolism. *Ruminococcus* can degrade resistant starches (Ze et al., 2012), thereby increasing intestinal energy absorption, which promotes weight gain in individuals (Cotillard et al., 2013). It also affects intestinal health by promoting oxidative stress (Hall et al., 2017) and

inflammatory responses (Rajilić-Stojanović et al., 2015; van den Munckhof et al., 2018), and is considered to be related to negative human health consequences (Hills et al., 2019). ECD reduced the relative abundance of this genus. Members of the *Erysipelotrichaceae* family are closely related to clinical indicators of impaired glucose and lipid metabolism and are important targets of metabolic diseases (Kaakoush, 2015; Lippert et al., 2017). Both *Holdemania* and *Coprobacillus* are members of the *Erysipelotrichaceae* family. *Holdemania* is related to the occurrence of inflammatory reaction (Barandouzi et al., 2020; Jang et al., 2020), elevated in patients with type 1 diabetes (Biaassoni et al., 2020), and is considered to be a predictor of hypertension (Hsu et al., 2020). *Coprobacillus* is an important butyric acid producer and can be cross-fed with *Anaerostipes*, *Roseburia*, and *Bifidobacterium* to maintain butyric acid concentrations in the colon (Muthuramalingam et al., 2020). It affects intestinal function and mediates related intestinal diseases (Kassinen et al., 2007) through the inflammatory response (Shi et al., 2018; Seo et al., 2019). Its abundance is also positively correlated with the expression of immune function related genes (Elderman et al., 2018). Through the influence of lipid metabolism (Kim et al., 2018), its abundance in the intestines of obese animals and humans is increased (Wang et al., 2018; Terzo et al., 2020). ECD effectively reduced the relative abundance of these two genera of *Erysipelotrichaceae* in ZDF rats, and we found that the relative abundance of *Holdemania* was significantly and positively correlated with abnormal lipid metabolism. *Akkermansia* is currently one of the most widely studied probiotics, and it might be suitable for treating metabolic syndrome. It can improve metabolic disorders in obese animals and humans, including decreased insulin sensitivity and glucose and lipid metabolism disorders (Anhê et al., 2015; Dao et al., 2016; Depommier et al., 2019). It restores intestinal barrier function (Desai et al., 2016) through the immunomodulatory effect of cell membrane protein AMUC-1100 binding to toll-like receptor 2 (Plovier et al., 2017) reducing macrophage infiltration, proinflammatory cytokines, and chemokine expression, therefore reducing the risk of cardiovascular disease (Li et al., 2016). ECD increased the relative abundance of *Akkermansia* that was decreased in ZDF rats. The inconsistency of current research results is not only related to differences in disease states, animal models, interventions, diets, etc., but also indicates that effects of microbiota cannot be generalized simply as beneficial or harmful. Differences at the species level might lead to different results, and disease phenotypes are often only related to a small number of strains (Truong et al., 2017). Therefore, it is necessary to further explore the changes of specific strains under each genus in future research.

Gut microbiota is an important endogenous factor in regulating WAT browning (Li et al., 2017) and brown adipose tissue activity (Quan et al., 2020), and it can regulate WAT inflammation (Virtue et al., 2019) and affect WAT function. Studies have showed that intestinal barrier injury in obese individuals can lead to the translocation of intestinal flora or flora components (Anhê et al., 2020), and the

number of bacteria in adipose tissue is related to immune cell infiltration, inflammation, and metabolic indicators, which affect the metabolic health of obese individuals (Massier et al., 2020). Treatment with obesity-related harmful strains increases the hypertrophy of adipocytes in obese mice, resulting in decreased insulin sensitivity and increased lipolysis in adipose tissue (Keskitalo et al., 2018). We found that the relative abundances of *Prevotella*, *Blautia*, and *Holdemania* were not only clearly positively correlated with the host phenotype, but also with the expression of the IRS1/AKT/PKA/HSL signaling pathway in WAT, suggesting that *Prevotella*, *Blautia*, and *Holdemania* might be important targets for ECD to enhance insulin sensitivity, thereby reducing excessive lipolysis in WAT of ZDF rats. However, the specific mechanism is still unclear, which is a direction worthy of attention in future research.

This study is the first to examine gut microbiota targets of ECD intervention. In addition to gut microbiota, their metabolite SCFAs may be an important pathway for exerting their metabolic effects (De Vadder et al., 2014). Although SCFAs are related to metabolism, the role of SCFAs in energy homeostasis is ambiguous at present (Canfora et al., 2015). Some animal and human studies have shown that obesity is associated with high levels of SCFAs (Freeland and Wolever, 2010; Kim et al., 2019). Gut microbiota ferment undigested carbohydrates (such as resistant starch and dietary fiber) and proteins in the small intestine to produce SCFAs, which increases energy absorption and then *de novo* synthesis of lipids and glucose in the whole body, providing about 10% of an individual's energy requirements, potentially leading to obesity (Turnbaugh et al., 2006). Consistently, propionic and butyric acid, the two most important SCFAs, increased significantly in the cecal contents of 9-week-old ZDF rats. This change might be the result of an increase in intestinal bacteria producing these two SCFAs or a decrease in bacteria utilizing them in the intestinal tract of ZDF rats. The changes may also be related to the fermentation or utilization rates of different gut microbiota, microbial cross-feeding, mucosal absorption and transport rate and other complex factors (Schwiertz et al., 2010; Fernandes et al., 2014). Studies have shown that butyric acid is the main energy source for intestinal epithelial cells and can increase lipid synthesis (Birt et al., 2013). The presence of propionic acid in feces is related to increased risk of type 2 diabetes (Sanna et al., 2019). Furthermore, both propionic and butyric acid can stimulate lipolysis in adipocytes (Rumberger et al., 2014). We found that the content of propionic acid was significantly positively correlated with the phenotypes of obesity and lipid metabolism disorders. Decreased propionic acid content could be used as an independent predictor of the improvement of insulin sensitivity (Tirosh et al., 2019). ECD administration reduced the concentration of propionic acid in ZDF rats, possibly by adjusting the gut microbiota to change the content of fermentation products. Studies have shown that *Blautia* strains ferment the deoxy sugars rhamnose and fucose to form propionic acid through the propylene glycol pathway (Reichardt et al., 2014). *Prevotella* (De Vadder et al., 2016) and

Ruminococcus (Krautkramer et al., 2020) produce succinate, an intermediate product of propionic acid, through the succinate pathway. Therefore, propionic acid might be an important medium for gut microbiota of ECD intervention and a subject for future research. Different SCFAs might exert their biological effects through synergy and antagonism (Li et al., 2020). In addition, the content of SCFAs in different intestinal segments is different (Cummings et al., 1987), and SCFAs in circulation are more closely related to peripheral insulin sensitivity, systemic lipolysis, and metabolic health (Müller et al., 2019). Therefore, the regulatory effect of ECD on SCFAs still needs to be further explored.

In conclusion, we found that ECD could regulate lipid metabolism, improve lipolysis in WAT, and modulate the composition and function of gut microbiota in ZDF rats. There was a significant correlation between biomarkers and host phenotype, suggesting that the beneficial effects of ECD on obesity, especially lipid metabolism disorders, were related to the modulation of gut microbiota. The limitations of this research were that, first of all, isoflurane anesthesia may aggravate the pre-existing IR (Fang et al., 2020), thereby affecting the judgment of the degree of IR in ZDF rats. Secondly, genetic levels and even more molecular experiments may be required to confirm the complex crosstalk among molecules for the changes in the lipolytic function of WAT. Moreover, the dietary factors cannot be ignored. The dietary components of ZL and ZDF rats were different (Supplementary Table 1), and the food intake of ZDF rats was much higher than that of ZL rats (Figure 2D), which led to different types and amounts of substrates fermented by gut microbiota, resulting in metabolic differences (Makki et al., 2018). Finally, the causal relationship between the regulation of gut microbiota by ECD and the improvement of lipid metabolism remains to be further explored.

CONCLUSION

We found that ECD delayed the development of obesity, inhibited excessive lipolysis by improving the activity of the IRS1/AKT/PKA/HSL signaling pathway in WAT of ZDF rats. In addition, ECD had an impact on the composition and function of obesity-related gut microbiota, reduced the content of *Prevotella*, *Blautia*, and *Holdemania*, and the metabolite propionic acid. These biomarkers were significantly positively correlated with host obesity phenotype, especially lipid metabolism disorders. This study provides new insights into the role of ECD in improving obesity and regulating lipid metabolism disorders via gut microbiota and helps to further clarify the mechanism of ECD in the treatment of obesity.

DATA AVAILABILITY STATEMENT

The raw sequences of Miseq sequences from 44 fecal samples of rats have been submitted to NCBI Project under accession number PRJNA686642 with NCBI Sequence Read Archive under accession number SRP298569.

ETHICS STATEMENT

The animal study was reviewed and approved by the recommendations of Guide for the Care and Use of Laboratory Animals.

AUTHOR CONTRIBUTIONS

LZ (2nd author) and SL designed and supervised the study, and provided guidance on data analysis and article writing. ZW completed the compound chemical composition test of compound. TZ, WZ, WC, and JL conducted the animal trial and sample collection. TZ performed staining and molecular experiment, conducted data analysis, figure and chart production, and completed the article writing. LZ (6th author) provided suggestions for experiment implementation and article writing. CZ provided assistance in the production of heat map. All authors approved the final article.

FUNDING

This work was supported by the Key Project of the National Natural Science Foundation of China (No.81730111), the

Traditional Chinese Medicine Leading Intelligence Project of Jiangsu Province (No. SLJ0227), the Postgraduate Research, and Practice Innovation Program of Jiangsu Province (No. KYCX20_1548), and a Project Funded by the Priority Academic Program Development of Jiangsu Higher Education Institutions (Integration of Chinese and Western Medicine).

ACKNOWLEDGMENTS

We would like to thank Shanghai Personal Biotechnology Co., Ltd. (Shanghai, China) for providing sequencing services and helpful discussions pertaining to the sequencing and data analysis, and Metabo-Profile Biotechnology Co., Ltd. (Shanghai, China) for providing the determination and analysis of short-chain fatty acids. The authors declare no competing interests.

SUPPLEMENTARY MATERIAL

The Supplementary Material for this article can be found online at: <https://www.frontiersin.org/articles/10.3389/fphar.2021.647529/full#supplementary-material>

REFERENCES

- Anhê, F. F., Jensen, B. A. H., Varin, T. V., Servant, F., Van Blerk, S., Richard, D., et al. (2020). Type 2 Diabetes Influences Bacterial Tissue Compartmentalisation in Human Obesity. *Nat. Metab.* 2 (3), 233–242. doi:10.1038/s42255-020-0178-9
- Anhê, F. F., Roy, D., Pilon, G., Dudonné, S., Matamoros, S., Varin, T. V., et al. (2015). A Polyphenol-Rich cranberry Extract Protects from Diet-Induced Obesity, Insulin Resistance and Intestinal Inflammation in Association with increased Akkermansia spp. Population in the Gut Microbiota of Mice. *Gut* 64 (6), 872–883. doi:10.1136/gutjnl-2014-307142
- Barandouzi, Z. A., Starkweather, A. R., Henderson, W. A., Gyamfi, A., and Cong, X. S. (2020). Altered Composition of Gut Microbiota in Depression: A Systematic Review. *Front. Psychiatry* 11, 541. doi:10.3389/fpsy.2020.00541
- Becker, N., Kunath, J., Loh, G., and Blaut, M. (2011). Human Intestinal Microbiota: Characterization of a Simplified and Stable Gnotobiotic Rat Model. *Gut Microbes* 2 (1), 25–33. doi:10.4161/gmic.2.1.14651
- Benítez-Páez, A., Gómez del Pugar, E. M., López-Almela, I., Moya-Pérez, Á., Codoñer-Franch, P., and Sanz, Y. (2020). Depletion of Blautia Species in the Microbiota of Obese Children Relates to Intestinal Inflammation and Metabolic Phenotype Worsening. *mSystems* 5 (2), e00857–19. doi:10.1128/mSystems.00857-19
- Biassoni, R., Di Marco, E., Squillario, M., Barla, A., Piccolo, G., Ugolotti, E., et al. (2020). Gut Microbiota in T1DM-Onset Pediatric Patients: Machine-Learning Algorithms to Classify Microorganisms as Disease Linked. *J. Clin. Endocrinol. Metab.* 105 (9), e3114–e3126. doi:10.1210/clinem/dgaa407
- Birt, D. F., Boylston, T., Hendrich, S., Jane, J.-L., Hollis, J., Li, L., et al. (2013). Resistant Starch: Promise for Improving Human Health. *Adv. Nutr.* 4 (6), 587–601. doi:10.3945/an.113.004325
- Brestoff, J. R., Wilen, C. B., Moley, J. R., Li, Y., Zou, W., Malvin, N. P., et al. (2021). Intercellular Mitochondria Transfer to Macrophages Regulates White Adipose Tissue Homeostasis and Is Impaired in Obesity. *Cel. Metab.* 33 (2), 270–282. doi:10.1016/j.cmet.2020.11.008
- Callahan, B. J., McMurdie, P. J., Rosen, M. J., Han, A. W., Johnson, A. J. A., and Holmes, S. P. (2016). DADA2: High-Resolution Sample Inference from Illumina Amplicon Data. *Nat. Methods* 13 (7), 581–583. doi:10.1038/nmeth.3869
- Canfora, E. E., Jocken, J. W., and Blaak, E. E. (2015). Short-chain Fatty Acids in Control of Body Weight and Insulin Sensitivity. *Nat. Rev. Endocrinol.* 11 (10), 577–591. doi:10.1038/nrendo.2015.128
- Caprio, S., Perry, R., and Kursawe, R. (2017). Adolescent Obesity and Insulin Resistance: Roles of Ectopic Fat Accumulation and Adipose Inflammation. *Gastroenterology* 152 (7), 1638–1646. doi:10.1053/j.gastro.2016.12.051
- Chinese Pharmacopoeia Commission (2015). *Pharmacopoeia of the People's Republic of China*, Vol. I. China: China Medical Science Press.
- Cotillard, A., Kennedy, S. P., Kong, L. C., Prifti, E., Pons, N., Le Chatelier, E., et al. (2013). Dietary Intervention Impact on Gut Microbial Gene Richness. *Nature* 500 (7464), 585–588. doi:10.1038/nature12480
- Cummings, J. H., Pomare, E. W., Branch, W. J., Naylor, C. P., and Macfarlane, G. T. (1987). Short Chain Fatty Acids in Human Large Intestine, portal, Hepatic and Venous Blood. *Gut* 28 (10), 1221–1227. doi:10.1136/gut.28.10.1221
- Czech, M. P. (2017). Insulin Action and Resistance in Obesity and Type 2 Diabetes. *Nat. Med.* 23 (7), 804–814. doi:10.1038/nm.4350
- Dao, M. C., Everard, A., Aron-Wisniewsky, J., Sokolowska, N., Prifti, E., Verger, E. O., et al. (2016). Akkermansia Muciniphila and Improved Metabolic Health during a Dietary Intervention in Obesity: Relationship with Gut Microbiome Richness and Ecology. *Gut* 65 (3), 426–436. doi:10.1136/gutjnl-2014-308778
- De Filippis, F., Pasolli, E., Tett, A., Tarallo, S., Naccarati, A., De Angelis, M., et al. (2019). Distinct Genetic and Functional Traits of Human Intestinal Prevotella Copri Strains Are Associated with Different Habitual Diets. *Cell Host & Microbe* 25 (3), 444–453. doi:10.1016/j.chom.2019.01.004
- De Vadder, F., Kovatcheva-Datchary, P., Goncalves, D., Vinera, J., Zitoun, C., Duchamp, A., et al. (2014). Microbiota-generated Metabolites Promote Metabolic Benefits via Gut-Brain Neural Circuits. *Cell* 156 (1–2), 84–96. doi:10.1016/j.cell.2013.12.016
- De Vadder, F., Kovatcheva-Datchary, P., Zitoun, C., Duchamp, A., Bäckhed, F., and Mithieux, G. (2016). Microbiota-Produced Succinate Improves Glucose Homeostasis via Intestinal Gluconeogenesis. *Cell Metab.* 24 (1), 151–157. doi:10.1016/j.cmet.2016.06.013
- Del Chierico, F., Nobili, V., Vernocchi, P., Russo, A., De Stefanis, C., Gnani, D., et al. (2017). Gut Microbiota Profiling of Pediatric Nonalcoholic Fatty Liver

- Disease and Obese Patients Unveiled by an Integrated Meta-omics-based Approach. *Hepatology* 65 (2), 451–464. doi:10.1002/hep.28572
- Depommier, C., Everard, A., Druart, C., Plovier, H., Van Hul, M., Vieira-Silva, S., et al. (2019). Supplementation with Akkermansia Muciniphila in Overweight and Obese Human Volunteers: a Proof-Of-Concept Exploratory Study. *Nat. Med.* 25 (7), 1096–1103. doi:10.1038/s41591-019-0495-2
- Desai, M. S., Seekatz, A. M., Koropatkin, N. M., Kamada, N., Hickey, C. A., Wolter, M., et al. (2016). A Dietary Fiber-Deprived Gut Microbiota Degrades the Colonic Mucus Barrier and Enhances Pathogen Susceptibility. *Cell* 167 (5), 1339–1353. doi:10.1016/j.cell.2016.10.043
- Ding, S., Kang, J., Tong, L., Lin, Y., Liao, L., and Gao, B. (2018). Erchen Decoction Ameliorates Lipid Metabolism by the Regulation of the Protein CAV-1 and the Receptors VLDLR, LDLR, ABCA1, and SRB1 in a High-Fat Diet Rat Model. *Evidence-Based Complement. Altern. Med.* 2018, 1–12. doi:10.1155/2018/5309490
- Egshatyan, L., Kashtanova, D., Popenko, A., Tkacheva, O., Tyakht, A., Alexeev, D., et al. (2016). Gut Microbiota and Diet in Patients with Different Glucose Tolerance. *Endocr. Connect.* 5 (1), 1–9. doi:10.1530/EC-15-0094
- Elderman, M., Hugenholtz, F., Belzer, C., Boekschoten, M., van Beek, A., de Haan, B., et al. (2018). Sex and Strain Dependent Differences in Mucosal Immunology and Microbiota Composition in Mice. *Biol. Sex. Differ.* 9 (1), 26. doi:10.1186/s13293-018-0186-6
- Fang, X., Xia, T., Xu, F., Wu, H., Ma, Z., Zhao, X., et al. (2020). Isoflurane Aggravates Peripheral and central Insulin Resistance in High-Fat Diet/streptozocin-Induced Type 2 Diabetic Mice. *Brain Res.* 1727, 146511. doi:10.1016/j.brainres.2019.146511
- Feng, Y.-L., Cao, G., Chen, D.-Q., Vaziri, N. D., Chen, L., Zhang, J., et al. (2019). Microbiome-metabolomics Reveals Gut Microbiota Associated with Glycine-Conjugated Metabolites and Polyamine Metabolism in Chronic Kidney Disease. *Cell. Mol. Life Sci.* 76 (24), 4961–4978. doi:10.1007/s00018-019-03155-9
- Fernandes, J., Su, W., Rahat-Rozenbloom, S., Wolever, T. M. S., and Comelli, E. M. (2014). Adiposity, Gut Microbiota and Faecal Short Chain Fatty Acids Are Linked in Adult Humans. *Nutr. Diabetes* 4 (6), e121. doi:10.1038/nutd.2014.23
- Freeland, K. R., and Wolever, T. M. S. (2010). Acute Effects of Intravenous and Rectal Acetate on Glucagon-like Peptide-1, Peptide YY, Ghrelin, Adiponectin and Tumour Necrosis Factor- α . *Br. J. Nutr.* 103 (3), 460–466. doi:10.1017/S0007114509991863
- Frühbeck, G., Méndez-Giménez, L., Fernández-Formoso, J.-A., Fernández, S., and Rodríguez, A. (2014). Regulation of Adipocyte Lipolysis. *Nutr. Res. Rev.* 27 (1), 63–93. doi:10.1017/S095442241400002X
- Gao, B.-Z., Chen, J.-C., Liao, L.-H., Xu, J.-Q., Lin, X.-F., and Ding, S.-S. (2015). Erchen Decoction Prevents High-Fat Diet Induced Metabolic Disorders in C57BL/6 Mice. *Evidence-Based Complement. Altern. Med.* 2015, 1–9. doi:10.1155/2015/501272
- Gong, S., Ye, T., Wang, M., Wang, M., Li, Y., Ma, L., et al. (2020). Traditional Chinese Medicine Formula Kang Shuai Lao Pian Improves Obesity, Gut Dysbiosis, and Fecal Metabolic Disorders in High-Fat Diet-Fed Mice. *Front. Pharmacol.* 11, 297. doi:10.3389/fphar.2020.00297
- Goodrich, J. K., Waters, J. L., Poole, A. C., Sutter, J. L., Koren, O., Blekhan, R., et al. (2014). Human Genetics Shape the Gut Microbiome. *Cell* 159 (4), 789–799. doi:10.1016/j.cell.2014.09.053
- Habegger, K. M., Al-Massadi, O., Heppner, K. M., Myronovych, A., Holland, J., Berger, J., et al. (2014). Duodenal Nutrient Exclusion Improves Metabolic Syndrome and Stimulates Villus Hyperplasia. *Gut* 63 (8), 1238–1246. doi:10.1136/gutjnl-2013-304583
- Hall, A. B., Yassour, M., Sauk, J., Garner, A., Jiang, X., Arthur, T., et al. (2017). A Novel Ruminococcus Gnavus Clade Enriched in Inflammatory Bowel Disease Patients. *Genome Med.* 9 (1), 103. doi:10.1186/s13073-017-0490-5
- Hills, R., Pontefract, B., Mishcon, H., Black, C., Sutton, S., and Theberge, C. (2019). Gut Microbiome: Profound Implications for Diet and Disease. *Nutrients* 11 (7), 1613. doi:10.3390/nu11071613
- Hsu, C.-N., Hou, C.-Y., Chang-Chien, G.-P., Lin, S., and Tain, Y.-L. (2020). Maternal N-Acetylcysteine Therapy Prevents Hypertension in Spontaneously Hypertensive Rat Offspring: Implications of Hydrogen Sulfide-Generating Pathway and Gut Microbiota. *Antioxidants* 9 (9), 856. doi:10.3390/antiox9090856
- Jang, J.-H., Yeom, M.-J., Ahn, S., Oh, J.-Y., Ji, S., Kim, T.-H., et al. (2020). Acupuncture Inhibits Neuroinflammation and Gut Microbial Dysbiosis in a Mouse Model of Parkinson's Disease. *Brain Behav. Immun.* 89, 641–655. doi:10.1016/j.bbi.2020.08.015
- Joffin, N., Paschoal, V. A., Gliniak, C. M., Crewe, C., Elnwasany, A., Szewda, L. I., et al. (2021). Mitochondrial Metabolism Is a Key Regulator of the Fibro-Inflammatory and Adipogenic Stromal Subpopulations in white Adipose Tissue. *Cell Stem Cell* 28 (4), 702–717. doi:10.1016/j.stem.2021.01.002
- Kaakoush, N. O. (2015). Insights into the Role of *Erysipelotrichaceae* in the Human Host. *Front. Cel. Infect. Microbiol.* 5, 84. doi:10.3389/fcimb.2015.00084
- Kassinen, A., Krogus-Kurikka, L., Mäkiuokko, H., Rinttilä, T., Paulin, L., Corander, J., et al. (2007). The Fecal Microbiota of Irritable Bowel Syndrome Patients Differs Significantly from that of Healthy Subjects. *Gastroenterology* 133 (1), 24–33. doi:10.1053/j.gastro.2007.04.005
- Keskitalo, A., Munukka, E., Toivonen, R., Hollmén, M., Kainulainen, H., Huovinen, P., et al. (2018). *Enterobacter cloacae* Administration Induces Hepatic Damage and Subcutaneous Fat Accumulation in High-Fat Diet Fed Mice. *PLoS One* 13 (5), e0198262. doi:10.1371/journal.pone.0198262
- Kim, J.-Y., Kwon, Y. M., Kim, I.-S., Kim, J.-A., Yu, D.-Y., Adhikari, B., et al. (2018). Effects of the Brown Seaweed Laminaria Japonica Supplementation on Serum Concentrations of IgG, Triglycerides, and Cholesterol, and Intestinal Microbiota Composition in Rats. *Front. Nutr.* 5, 23. doi:10.3389/fnut.2018.00023
- Kim, K. N., Yao, Y., and Ju, S. Y. (2019). Short Chain Fatty Acids and Fecal Microbiota Abundance in Humans with Obesity: A Systematic Review and Meta-Analysis. *Nutrients* 11 (10), 2512. doi:10.3390/nu11102512
- Kimura, I., Ozawa, K., Inoue, D., Imamura, T., Kimura, K., Maeda, T., et al. (2013). The Gut Microbiota Suppresses Insulin-Mediated Fat Accumulation via the Short-Chain Fatty Acid Receptor GPR43. *Nat. Commun.* 4, 1829. doi:10.1038/ncomms2852
- Kindt, A., Liebisch, G., Clavel, T., Haller, D., Hörmannspurger, G., Yoon, H., et al. (2018). The Gut Microbiota Promotes Hepatic Fatty Acid Desaturation and Elongation in Mice. *Nat. Commun.* 9 (1), 3760. doi:10.1038/s41467-018-05767-4
- Kovatcheva-Datchary, P., Nilsson, A., Akrami, R., Lee, Y. S., De Vadder, F., Arora, T., et al. (2015). Dietary Fiber-Induced Improvement in Glucose Metabolism Is Associated with Increased Abundance of *Prevotella*. *Cel. Metab.* 22 (6), 971–982. doi:10.1016/j.cmet.2015.10.001
- Krautkramer, K. A., Fan, J., and Bäckhed, F. (2020). Gut Microbial Metabolites as Multi-Kingdom Intermediates. *Nat. Rev. Microbiol.* 19, 77–94. doi:10.1038/s41579-020-0438-4
- Kusminski, C. M., Bickel, P. E., and Scherer, P. E. (2016). Targeting Adipose Tissue in the Treatment of Obesity-Associated Diabetes. *Nat. Rev. Drug Discov.* 15 (9), 639–660. doi:10.1038/nrd.2016.75
- Larsen, J. M. (2017). The Immune Response to Prevotellabacteria in Chronic Inflammatory Disease. *Immunology* 151 (4), 363–374. doi:10.1111/imm.12760
- Leclercq, S., Matamoros, S., Cani, P. D., Neyrinck, A. M., Jamar, F., Stärkel, P., et al. (2014). Intestinal Permeability, Gut-Bacterial Dysbiosis, and Behavioral Markers of Alcohol-Dependence Severity. *Proc. Natl. Acad. Sci. USA* 111 (42), E4485–E4493. doi:10.1073/pnas.1415174111
- Lee, A. Y., Park, W., Kang, T.-W., Cha, M. H., and Chun, J. M. (2018). Network Pharmacology-Based Prediction of Active Compounds and Molecular Targets in Yijin-Tang Acting on Hyperlipidaemia and Atherosclerosis. *J. Ethnopharmacology* 221, 151–159. doi:10.1016/j.jep.2018.04.027
- Lee, S. M., Lee, J., Kang, E., Kim, H.-L., Hwang, G.-S., and Jung, J. (2020). Lipidomic Analysis Reveals Therapeutic Effects of Yijin-Tang on High-Fat/high-Cholesterol Diet-Induced Obese Mice. *Phytomedicine* 74, 152936. doi:10.1016/j.phymed.2019.152936
- Li, G., Xie, C., Lu, S., Nichols, R. G., Tian, Y., Li, L., et al. (2017). Intermittent Fasting Promotes White Adipose Browning and Decreases Obesity by Shaping the Gut Microbiota. *Cel. Metab.* 26 (4), 672–685. doi:10.1016/j.cmet.2017.08.019
- Li, J., Lin, S., Vanhoutte, P. M., Woo, C. W., and Xu, A. (2016). Akkermansia Muciniphila Protects against Atherosclerosis by Preventing Metabolic Endotoxemia-Induced Inflammation in ApoE^{-/-} Mice. *Circulation* 133 (24), 2434–2446. doi:10.1161/CIRCULATIONAHA.115.019645
- Li, L., Pan, M., Pan, S., Li, W., Zhong, Y., Hu, J., et al. (2020). Effects of Insoluble and Soluble Fibers Isolated from Barley on Blood Glucose, Serum Lipids, Liver

- Function and Caecal Short-Chain Fatty Acids in Type 2 Diabetic and normal Rats. *Food Chem. Toxicol.* 135, 110937. doi:10.1016/j.fct.2019.110937
- Lippert, K., Kedenko, L., Antonielli, L., Kedenko, I., Gemeier, C., Leitner, M., et al. (2017). Gut Microbiota Dysbiosis Associated with Glucose Metabolism Disorders and the Metabolic Syndrome in Older Adults. *Beneficial Microbes* 8 (4), 545–556. doi:10.3920/BM2016.0184
- Liu, C., Li, J., Zhang, Y., Philip, A., Shi, E., Chi, X., et al. (2015). Influence of Glucose Fermentation on CO₂ Assimilation to Acetate in Homoacetogen *Blautia Coccoides* GA-1. *J. Ind. Microbiol. Biotechnol.* 42 (9), 1217–1224. doi:10.1007/s10295-015-1646-1
- Luo, J., Huang, L., Wang, A., Liu, Y., Cai, R., Li, W., et al. (2018). Resistin-Induced Endoplasmic Reticulum Stress Contributes to the Impairment of Insulin Signaling in Endothelium. *Front. Pharmacol.* 9, 1226. doi:10.3389/fphar.2018.01226
- Majchrzak, M., Brzecka, A., Daroszewski, C., Błasiak, P., Rzechonek, A., Tarasov, V. V., et al. (2019). Increased Pain Sensitivity in Obese Patients after Lung Cancer Surgery. *Front. Pharmacol.* 10, 626. doi:10.3389/fphar.2019.00626
- Makki, K., Deehan, E. C., Walter, J., and Bäckhed, F. (2018). The Impact of Dietary Fiber on Gut Microbiota in Host Health and Disease. *Cell Host & Microbe* 23 (6), 705–715. doi:10.1016/j.chom.2018.05.012
- Maruvada, P., Leone, V., Kaplan, L. M., and Chang, E. B. (2017). The Human Microbiome and Obesity: Moving beyond Associations. *Cell Host & Microbe* 22 (5), 589–599. doi:10.1016/j.chom.2017.10.005
- Massier, L., Chakaroun, R., Tabei, S., Crane, A., Didt, K. D., Fallmann, J., et al. (2020). Adipose Tissue Derived Bacteria Are Associated with Inflammation in Obesity and Type 2 Diabetes. *Gut* 69 (10), 1796–1806. doi:10.1136/gutjnl-2019-320118
- Matthews, D. R., Hosker, J. P., Rudenski, A. S., Naylor, B. A., Treacher, D. F., and Turner, R. C. (1985). Homeostasis Model Assessment: Insulin Resistance and β -cell Function from Fasting Plasma Glucose and Insulin Concentrations in Man. *Diabetologia* 28 (7), 412–419. doi:10.1007/BF00280883
- Müller, M., Hernández, M. A. G., Goossens, G. H., Reijnders, D., Holst, J. J., Jocken, J. W. E., et al. (2019). Circulating but Not Faecal Short-Chain Fatty Acids Are Related to Insulin Sensitivity, Lipolysis and GLP-1 Concentrations in Humans. *Sci. Rep.* 9 (1), 12515. doi:10.1038/s41598-019-48775-0
- Muthuramalingam, K., Singh, V., Choi, C., Choi, S. I., Kim, Y. M., Unno, T., et al. (2020). Dietary Intervention Using (1,3)/(1,6)- β -Glucan, a Fungus-Derived Soluble Prebiotic Ameliorates High-Fat Diet-Induced Metabolic Distress and Alters Beneficially the Gut Microbiota in Mice Model. *Eur. J. Nutr.* 59 (6), 2617–2629. doi:10.1007/s00394-019-02110-5
- Ottosson, F., Brunkwall, L., Ericson, U., Nilsson, P. M., Almgren, P., Fernandez, C., et al. (2018). Connection between BMI-Related Plasma Metabolite Profile and Gut Microbiota. *J. Clin. Endocrinol. Metab.* 103 (4), 1491–1501. doi:10.1210/je.2017-02114
- Ozato, N., Saito, S., Yamaguchi, T., Katashima, M., Tokuda, I., Sawada, K., et al. (2019). *Blautia* Genus Associated with Visceral Fat Accumulation in Adults 20–76 Years of Age. *NPJ Biofilms Microbiomes* 5, 28. doi:10.1038/s41522-019-0101-x
- Park, J. H., Seo, I., Shim, H. m., and Cho, H. (2020). Melatonin Ameliorates SGLT2 Inhibitor-induced Diabetic Ketoacidosis by Inhibiting Lipolysis and Hepatic Ketogenesis in Type 2 Diabetic Mice. *J. Pineal Res.* 68 (2), e12623. doi:10.1111/jpi.12623
- Pedersen, H. K., Gudmundsdottir, V., Nielsen, H. B., Hyötyläinen, T., Nielsen, T., Jensen, B. A. H., et al. (2016). Human Gut Microbes Impact Host Serum Metabolome and Insulin Sensitivity. *Nature* 535 (7612), 376–381. doi:10.1038/nature18646
- Petersen, L. M., Bautista, E. J., Nguyen, H., Hanson, B. M., Chen, L., Lek, S. H., et al. (2017). Community Characteristics of the Gut Microbiomes of Competitive Cyclists. *Microbiome* 5 (1), 98. doi:10.1186/s40168-017-0320-4
- Plovier, H., Everard, A., Druart, C., Depommier, C., Van Hul, M., Geurts, L., et al. (2017). A Purified Membrane Protein from *Akkermansia muciniphila* or the Pasteurized Bacterium Improves Metabolism in Obese and Diabetic Mice. *Nat. Med.* 23 (1), 107–113. doi:10.1038/nm.4236
- Quan, L.-H., Zhang, C., Dong, M., Jiang, J., Xu, H., Yan, C., et al. (2020). Myristoleic Acid Produced by Enterococci Reduces Obesity through Brown Adipose Tissue Activation. *Gut* 69 (7), 1239–1247. doi:10.1136/gutjnl-2019-319114
- Rajilić-Stojanović, M., Jonkers, D. M., Salonen, A., Hanevik, K., Raes, J., Jalanka, J., et al. (2015). Intestinal Microbiota and Diet in IBS: Causes, Consequences, or Epiphenomena? *Am. J. Gastroenterol.* 110 (2), 278–287. doi:10.1038/ajg.2014.427
- Ramette, A. (2007). Multivariate Analyses in Microbial Ecology. *FEMS Microbiol. Ecol.* 62 (2), 142–160. doi:10.1111/j.1574-6941.2007.00375.x
- Reichardt, N., Duncan, S. H., Young, P., Belenguer, A., McWilliam Leitch, C., Scott, K. P., et al. (2014). Phylogenetic Distribution of Three Pathways for Propionate Production within the Human Gut Microbiota. *ISME J.* 8 (6), 1323–1335. doi:10.1038/ismej.2014.14
- Roden, M., and Shulman, G. I. (2019). The Integrative Biology of Type 2 Diabetes. *Nature* 576 (7785), 51–60. doi:10.1038/s41586-019-1797-8
- Rodriguez, J., Hiel, S., Neyrinck, A. M., Le Roy, T., Pötgens, S. A., Leyrolle, Q., et al. (2020). Discovery of the Gut Microbial Signature Driving the Efficacy of Prebiotic Intervention in Obese Patients. *Gut* 69 (11), 1975–1987. doi:10.1136/gutjnl-2019-319726
- Rothschild, D., Weissbrod, O., Barkan, E., Kurilshikov, A., Korem, T., Zeevi, D., et al. (2018). Environment Dominates over Host Genetics in Shaping Human Gut Microbiota. *Nature* 555 (7695), 210–215. doi:10.1038/nature25973
- Rumberger, J. M., Arch, J. R. S., and Green, A. (2014). Butyrate and Other Short-Chain Fatty Acids Increase the Rate of Lipolysis in 3T3-L1 Adipocytes. *PeerJ* 2, e611. doi:10.7717/peerj.611
- Saltiel, A. R., and Olefsky, J. M. (2017). Inflammatory Mechanisms Linking Obesity and Metabolic Disease. *J. Clin. Invest.* 127 (1), 1–4. doi:10.1172/JCI92035
- Sanna, S., van Zuydam, N. R., Mahajan, A., Kurilshikov, A., Vich Vila, A., Vösa, U., et al. (2019). Causal Relationships Among the Gut Microbiome, Short-Chain Fatty Acids and Metabolic Diseases. *Nat. Genet.* 51 (4), 600–605. doi:10.1038/s41588-019-0350-x
- Scherer, T., O'Hare, J., Diggs-Andrews, K., Schweiger, M., Cheng, B., Lindtner, C., et al. (2011). Brain Insulin Controls Adipose Tissue Lipolysis and Lipogenesis. *Cel. Metab.* 13 (2), 183–194. doi:10.1016/j.cmet.2011.01.008
- Schwartz, A., Taras, D., Schäfer, K., Beijer, S., Bos, N. A., Donus, C., et al. (2010). Microbiota and SCFA in Lean and Overweight Healthy Subjects. *Obesity (Silver Spring)* 18 (1), 190–195. doi:10.1038/oby.2009.167
- Schwimmer, J. B., Johnson, J. S., Angeles, J. E., Behling, C., Belt, P. H., Borecki, I., et al. (2019). Microbiome Signatures Associated with Steatohepatitis and Moderate to Severe Fibrosis in Children with Nonalcoholic Fatty Liver Disease. *Gastroenterology* 157 (4), 1109–1122. doi:10.1053/j.gastro.2019.06.028
- Segata, N., Izard, J., Waldron, L., Gevers, D., Miropolsky, L., Garrett, W. S., et al. (2011). Metagenomic Biomarker Discovery and Explanation. *Genome Biol.* 12 (6), R60. doi:10.1186/gb-2011-12-6-r60
- Seo, S.-H., Unno, T., Park, S.-E., Kim, E.-J., Lee, Y.-M., Na, C.-S., et al. (2019). Korean Traditional Medicine (Jakyakgamcho-Tang) Ameliorates Colitis by Regulating Gut Microbiota. *Metabolites* 9 (10), 226. doi:10.3390/metabo9100226
- Shi, Y., Kellingray, L., Zhai, Q., Gall, G. L., Narbad, A., Zhao, J., et al. (2018). Structural and Functional Alterations in the Microbial Community and Immunological Consequences in a Mouse Model of Antibiotic-Induced Dysbiosis. *Front. Microbiol.* 9, 1948. doi:10.3389/fmicb.2018.01948
- Shiau, M.-Y., Chuang, P.-H., Yang, C.-P., Hsiao, C.-W., Chang, S.-W., Chang, K.-Y., et al. (2019). Mechanism of Interleukin-4 Reducing Lipid Deposit by Regulating Hormone-Sensitive Lipase. *Sci. Rep.* 9 (1), 11974. doi:10.1038/s41598-019-47908-9
- Si, J., You, H. J., Yu, J., Sung, J., and Ko, G. (2017). *Prevotella* as a Hub for Vaginal Microbiota under the Influence of Host Genetics and Their Association with Obesity. *Cell Host & Microbe* 21 (1), 97–105. doi:10.1016/j.chom.2016.11.010
- Stanislowski, M. A., Dabelea, D., Wagner, B. D., Sontag, M. K., Lozupone, C. A., and Eggesbø, M. (2017). Pre-pregnancy Weight, Gestational Weight Gain, and the Gut Microbiota of Mothers and Their Infants. *Microbiome* 5 (1), 113. doi:10.1186/s40168-017-0332-0
- Terzo, S., Mulè, F., Caldara, G. F., Baldassano, S., Puleio, R., Vitale, M., et al. (2020). Pistachio Consumption Alleviates Inflammation and Improves Gut Microbiota Composition in Mice Fed a High-Fat Diet. *Ijms* 21 (1), 365. doi:10.3390/ijms21010365
- Tirosch, A., Calay, E. S., Tuncman, G., Claiborn, K. C., Inouye, K. E., Eguchi, K., et al. (2019). The Short-Chain Fatty Acid Propionate Increases Glucagon and FABP4 Production, Impairing Insulin Action in Mice and Humans. *Sci. Transl. Med.* 11 (489), eaav0120. doi:10.1126/scitranslmed.aav0120

- Tremaroli, V., and Bäckhed, F. (2012). Functional Interactions between the Gut Microbiota and Host Metabolism. *Nature* 489 (7415), 242–249. doi:10.1038/nature11552
- Truong, D. T., Tett, A., Pasolli, E., Huttenhower, C., and Segata, N. (2017). Microbial Strain-Level Population Structure and Genetic Diversity from Metagenomes. *Genome Res.* 27 (4), 626–638. doi:10.1101/gr.216242.116
- Tuovinen, E., Keto, J., Nikkilä, J., Mättö, J., and Lähteenmäki, K. (2013). Cytokine Response of Human Mononuclear Cells Induced by Intestinal Clostridium Species. *Anaerobe* 19, 70–76. doi:10.1016/j.anaerobe.2012.11.002
- Turnbaugh, P. J., Ley, R. E., Mahowald, M. A., Magrini, V., Mardis, E. R., and Gordon, J. I. (2006). An Obesity-Associated Gut Microbiome with Increased Capacity for Energy Harvest. *Nature* 444 (7122), 1027–1031. doi:10.1038/nature05414
- Udayappan, S., Manneras-Holm, L., Chaplin-Scott, A., Belzer, C., Herrema, H., Dallinga-Thie, G. M., et al. (2016). Oral Treatment with *Eubacterium Hallii* Improves Insulin Sensitivity in Db/db Mice. *NPJ Biofilms Microbiomes* 2, 16009. doi:10.1038/npjbiofilms.2016.9
- van den Munckhof, I. C. L., Kurilshikov, A., Ter Horst, R., Riksen, N. P., Joosten, L. A. B., Zhernakova, A., et al. (2018). Role of Gut Microbiota in Chronic Low-Grade Inflammation as Potential Driver for Atherosclerotic Cardiovascular Disease: a Systematic Review of Human Studies. *Obes. Rev.* 19 (12), 1719–1734. doi:10.1111/obr.12750
- Virtue, A. T., McCright, S. J., Wright, J. M., Jimenez, M. T., Mowel, W. K., Kotzin, J. J., et al. (2019). The Gut Microbiota Regulates white Adipose Tissue Inflammation and Obesity via a Family of microRNAs. *Sci. Transl. Med.* 11 (496), eaav1892. doi:10.1126/scitranslmed.aav1892
- Wang, J., Wang, P., Li, D., Hu, X., and Chen, F. (2020). Beneficial Effects of Ginger on Prevention of Obesity through Modulation of Gut Microbiota in Mice. *Eur. J. Nutr.* 59 (2), 699–718. doi:10.1007/s00394-019-01938-1
- Wang, Y., Fei, Y., Liu, L., Xiao, Y., Pang, Y., Kang, J., et al. (2018). Polygonatum Odorum Polysaccharides Modulate Gut Microbiota and Mitigate Experimentally Induced Obesity in Rats. *Ijms* 19 (11), 3587. doi:10.3390/ijms19113587
- Wei, X., Tao, J., Xiao, S., Jiang, S., Shang, E., Zhu, Z., et al. (2018). Xiexin Tang Improves the Symptom of Type 2 Diabetic Rats by Modulation of the Gut Microbiota. *Sci. Rep.* 8 (1), 3685. doi:10.1038/s41598-018-22094-2
- Yin, C., Liu, W. h., Liu, Y., Wang, L., and Xiao, Y. (2019). PID1 Alters the Antilipolytic Action of Insulin and Increases Lipolysis via Inhibition of AKT/PKA Pathway Activation. *PLoS One* 14 (4), e0214606. doi:10.1371/journal.pone.0214606
- Ze, X., Duncan, S. H., Louis, P., and Flint, H. J. (2012). Ruminococcus Bromii Is a keystone Species for the Degradation of Resistant Starch in the Human colon. *ISME J.* 6 (8), 1535–1543. doi:10.1038/ismej.2012.4
- Zhang, H., Ta, N., Chen, P., and Wang, H. (2017). Erchen Decoction and Linguizhugan Decoction Ameliorate Hepatic Insulin Resistance by Inhibiting IRS-1Ser307 Phosphorylation *In Vivo* and *In Vitro*. *Evidence-Based Complement. Altern. Med.* 2017, 1–11. doi:10.1155/2017/1589871
- Zhang, L., Zhou, W., Zhan, L., Hou, S., Zhao, C., Bi, T., et al. (2020a). Fecal Microbiota Transplantation Alters the Susceptibility of Obese Rats to Type 2 Diabetes Mellitus. *Aging* 12 (17), 17480–17502. doi:10.18632/aging.103756
- Zhang, M., Shao, Y., Gao, B., Chen, J., Zhang, P., Hu, Y., et al. (2020b). Erchen Decoction Mitigates Lipid Metabolism Disorder by the Regulation of PPAR γ and LPL Gene in a High-Fat Diet C57BL/6 Mice Model. *Evidence-Based Complement. Altern. Med.* 2020, 1–8. doi:10.1155/2020/9102475
- Zhang, M., Zhu, J., Zhang, X., Zhao, D.-g., Ma, Y.-y., Li, D., et al. (2020c). Aged Citrus Peel (Chenpi) Extract Causes Dynamic Alteration of Colonic Microbiota in High-Fat Diet Induced Obese Mice. *Food Funct.* 11 (3), 2667–2678. doi:10.1039/c9fo02907a
- Zhang, X., Zhao, S., Song, X., Jia, J., Zhang, Z., Zhou, H., et al. (2018). Inhibition Effect of glycyrrhiza Polysaccharide (GCP) on Tumor Growth through Regulation of the Gut Microbiota Composition. *J. Pharmacol. Sci.* 137 (4), 324–332. doi:10.1016/j.jphs.2018.03.006
- Zhou, D., Pan, Q., Xin, F.-Z., Zhang, R.-N., He, C.-X., Chen, G.-Y., et al. (2017). Sodium Butyrate Attenuates High-Fat Diet-Induced Steatohepatitis in Mice by Improving Gut Microbiota and Gastrointestinal Barrier. *Wjg* 23 (1), 60–75. doi:10.3748/wjg.v23.i1.60
- Zhou, W., Xu, H., Zhan, L., Lu, X., and Zhang, L. (2019). Dynamic Development of Fecal Microbiome during the Progression of Diabetes Mellitus in Zucker Diabetic Fatty Rats. *Front. Microbiol.* 10, 232. doi:10.3389/fmicb.2019.00232
- Zhu, L., Baker, S. S., Gill, C., Liu, W., Alkhoury, R., Baker, R. D., et al. (2013). Characterization of Gut Microbiomes in Nonalcoholic Steatohepatitis (NASH) Patients: a Connection between Endogenous Alcohol and NASH. *Hepatology* 57 (2), 601–609. doi:10.1002/hep.26093
- Zimmermann, R., Strauss, J. G., Haemmerle, G., Schoiswohl, G., Birner-Gruenberger, R., Riederer, M., et al. (2004). Fat Mobilization in Adipose Tissue Is Promoted by Adipose Triglyceride Lipase. *Science* 306 (5700), 1383–1386. doi:10.1126/science.1100747

Conflict of Interest: The authors declare that the research was conducted in the absence of any commercial or financial relationships that could be construed as a potential conflict of interest.

The handling editor declared a past co-authorship with several of the authors ZW, LZ.

Copyright © 2021 Zhao, Zhan, Zhou, Chen, Luo, Zhang, Weng, Zhao and Liu. This is an open-access article distributed under the terms of the Creative Commons Attribution License (CC BY). The use, distribution or reproduction in other forums is permitted, provided the original author(s) and the copyright owner(s) are credited and that the original publication in this journal is cited, in accordance with accepted academic practice. No use, distribution or reproduction is permitted which does not comply with these terms.

GLOSSARY

AKT	protein kinase B	IRS1	insulin receptor substrate 1
ALT	alanine aminotransferase	ITT	insulin tolerance test
ANOVA	analysis of variance	LDA	linear discriminant analysis
AST	aspartate aminotransferase	LDL-C	low-density lipoprotein cholesterol
ASVs	amplitude sequence variables	LEfSe	LDA effect size
ATGL	adipose triglyceride lipase	PCoA	principal coordinates analysis
AUC	area under the curve	PKA	protein kinase A
BUN	blood urea nitrogen	PLS-DA	partial least squares discrimination analysis
Cr	creatinine	SCFAs	short-chain fatty acids
ECD	Erchen Decoction	SEM	standard error of the mean
FFA	free fatty acids	TC	total cholesterol
HDL-C	high-density lipoprotein cholesterol	TG	triglycerides
HE	hematoxylin-eosin	UHPLC-ESI-Q-TOF-MS	ultraperformance liquid chromatography-electrospray ionization-quadrupole-time of flight-mass spectrometry
HOMA-IR	homeostasis model assessment-insulin resistance	UPLC-MS/MS	ultraperformance liquid chromatography-tandem mass spectrometry
HPLC	high performance liquid chromatography	WAT	white adipose tissue
HSL	hormone-sensitive triglyceride lipase	ZDF rats	Zucker diabetic fatty rats
IR	insulin resistance	ZL rats	Zucker lean rats



Metabolomics Reveals the Mechanisms for the Pulmonary Toxicity of *Siegesbeckia orientalis* L. and the Toxicity-Reducing Effect of Processing

OPEN ACCESS

Edited by:

Sayeed Ahmad,
Jamia Hamdard University, India

Reviewed by:

Vivekananda Mandal,
Guru Ghasidas Vishwavidyalaya, India
Hua Yu,
University of Macau, China
Xiuqiong Fu,
Hong Kong Baptist Hospital,
Hong Kong

*Correspondence:

Gang Cao
caogang33@163.com
Tao Su
sutao@gzucm.edu.cn

[†]These authors have contributed
equally to this work

Specialty section:

This article was submitted to
Ethnopharmacology,
a section of the journal
Frontiers in Pharmacology

Received: 17 November 2020

Accepted: 06 April 2021

Published: 09 August 2021

Citation:

Jiang T, Liu L, Zhang M, Qiao Z,
Zhao T, Su J, Cao G and Su T (2021)
Metabolomics Reveals the
Mechanisms for the Pulmonary
Toxicity of *Siegesbeckia orientalis*
L. and the Toxicity-Reducing Effect
of Processing.
Front. Pharmacol. 12:630319.
doi: 10.3389/fphar.2021.630319

Ting Jiang^{1†}, Linsheng Liu^{2†}, Mi Zhang¹, Zhiping Qiao¹, Tingxiu Zhao³, Junfang Su³,
Gang Cao^{4*} and Tao Su^{1,4*}

¹International Institute for Translational Chinese Medicine, School of Pharmaceutical Sciences, Guangzhou University of Chinese Medicine, Guangzhou, China, ²Department of Clinical Pharmacology, The First Affiliated Hospital of Soochow University, Suzhou, China, ³School of Basic Medical Sciences, Guangzhou University of Chinese Medicine, Guangzhou, China, ⁴School of Pharmacy, Zhejiang Chinese Medical University, Hangzhou, China

Siegesbeckia orientalis L. (SO) is a commonly used Chinese medicinal herb. It has long been used as a remedy in traditional Chinese medicine (TCM) for symptoms that resemble inflammatory joint disorders. However, it is slightly toxic. According to the TCM theory, processing can reduce the toxicity of the herbs. Here, we performed metabolomics to determine whether processing with rice wine reduces the toxicity of raw SO, and to explore the mechanisms underlying the raw SO-induced toxicity and the toxicity-reducing effect of processing. Our results showed that raw SO has long-term toxicity in rats. It significantly elevated the serum level of LDH and caused histopathological damages in the lung tissues. It is worth noting that the LDH level in the PSO group was lower than that in the raw SO group, and the damages in lung tissues were relatively mild in PSO-treated rats, suggesting that processing reduces the pulmonary toxicity of the raw. Moreover, a total of 32 significantly changed metabolites were identified. Based on the MetaboAnalyst pathway analysis, we found that two characteristic metabolic pathways including alanine, aspartate and glutamate metabolism and glycerophospholipid metabolism were only changed in the raw SO group, while histidine metabolism was only changed in the PSO group, which suggests that induction of oxidative stress contributes to raw SO-induced pulmonary toxicity, and free radical scavenging might be responsible for the toxicity-reducing effect of processing. Our data shed new light on how raw SO induces pulmonary toxicity and how the toxicity can be reduced by processing. This study not only provides scientific justifications for the traditional processing theory of SO, but also helps to optimize the processing protocol and the clinical drug combination of SO.

Keywords: *Siegesbeckia orientalis* L., processing with rice wine, pulmonary toxicity, metabolomics, oxidative stress

INTRODUCTION

Siegesbeckia orientalis L. (SO), a traditional Chinese medicinal herb, was recorded to be able to eliminate the wind-dampness and soothe the painful joints (the State Commission of Chinese Pharmacopoeia, 2020), and to be slightly toxic in *Xinxu Bencao* (657–659 A.D., Tang Dynasty in China). SO is commonly used in managing traditional Chinese medicine (TCM) symptoms that resemble joint inflammatory disorders such as rheumatoid arthritis (RA). Chemical studies have revealed that SO contains terpenoids, glycosides, etc. Toxicological studies have demonstrated that the water extract of SO has acute toxicity in animals (Guan et al., 2007). In addition, reversible pulmonary toxicity of SO is observed in a subacute toxicity study in mice (Guan et al., 2008). SO is used as a long-term drug for treating chronic diseases such as RA and hypertension in clinical practice. However, up to now, the long-term toxicity of SO remains unknown, and the mechanisms underlying the raw SO-induced toxicity is still not fully understood.

Raw Chinese medicinal herbs are subjected to processing before they are used for clinical prescriptions or for preparing proprietary Chinese medicines. According to the TCM theory, processing can reduce the toxicity of the herbs. As recorded in Chinese Pharmacopoeia, SO is usually processed with rice wine. In our previous study, we have demonstrated that PSO is less toxic than raw SO as demonstrated in our tested human embryonic lung cells (MRC-9) (Su et al., 2014). However, up to now, the underlying toxicity-reducing mechanisms of processing are not known.

Chinese medical herbs have multiple chemical components and the multi-target nature (Yu et al., 2012), hence, using conventional research approaches such as biochemical and histological analyses to elucidate the mechanisms for herbal toxicities and the toxicity-reducing effect of processing have limitations. Metabolomics is a systematic approach for analyzing the small-molecule metabolites using various analytical methods, it can figure out the biological implications of the metabolites using bioinformatics means, and it has emerged as a powerful approach for this kind of studies (Tan et al., 2014). Here, for the first time, we explored the mechanisms underlying the raw SO-induced pulmonary toxicities and the toxicity-reducing effect of processing using metabolomics.

MATERIALS AND METHODS

Chemicals and Reagents

Raw SO (the dried aerial part of *Siegesbeckia orientalis* L.) was collected from Ganzhou (Jiangxi province, China). Rice wine was purchased from Zhejiang Tapai Shaoxing Wine Co., Ltd. (Zhejiang province, China). LC–MS grade acetonitrile, methanol, and formic acid (FA) were purchased from CNW Technologies (Germany). Kirenol was purchased from Shanghai Yuanye Bio-Technology Co., Ltd. (Shanghai,

China). Adonitol was purchased from Sigma-Aldrich (MO, United States). Milli-Q water was prepared using a Milli-Q system (Millipore, MA, United States). The commercial kits including creatine kinase (CK), lactate dehydrogenase (LDH), urea, aspartate aminotransferase (AST), and alanine aminotransferase (ALT) were purchased from Shenzhen Mindray Bio-Medical Electronics Co., Ltd. (Guangdong province, China). Malondialdehyde (MDA) was purchased from Nanjing Jiancheng Bioengineering Institute (Jiangsu province, China).

Preparation of Raw SO and PSO Extracts

The authentication of SO was confirmed in accordance with the corresponding monograph in CP 2020 (2020 edition of CP) by the corresponding author. Voucher specimens of raw SO (No. 20180510) and rice wine were deposited at the International Institute for Translational Chinese Medicine, Guangzhou University of Chinese Medicine.

PSO preparation: As shown in our previous study, 100 ml of rice wine (containing 15% ethanol): water/20:80 (v/v) was sprayed onto 100 g SO and allowed to be completely absorbed in a covered container for 1.5 h. Subsequently, the mixture was steamed for 5 h, cooled, and then dried at 40°C in a Memmert UFE500 oven (Su et al., 2014).

Raw SO and PSO extracts preparation: Raw SO or PSO (500 g) was reflux-extracted twice with water (1:10, w/v) for 2 h each. The combined extracts were filtered after cooling and then concentrated under reduced pressure to remove the water. The powdered SO (yield: 18.5%) and PSO (yield: 14.9%) extracts were obtained by lyophilizing of the concentrated samples with a VirTis Freeze Dryer (The VirTis Company, New York, United States). Powdered SO or PSO was dissolved in water to prepare raw SO and PSO solution. Detailed information of the high performance liquid chromatography (HPLC) analysis was shown in Supplementary Materials. Results showed that the contents of kirenol in raw SO and PSO were 0.13 and 0.07%, respectively (Supplementary Figure S1).

Animals and Treatments

A total of 24 male SD rats (200 ± 20 g, 6–8 weeks) were obtained from the Laboratory Animal Center of Southern Medical University [License number: SCXK (GZ)2016-0041; Guangzhou, China] and kept in the animal laboratory [License number: SYXK (GZ) 2019-0144] at the International Institute for Translational Chinese Medicine, Guangzhou University of Chinese Medicine (Guangzhou, China). Animal experiments were approved by the Guangzhou University of Chinese Medicine Animal Care and Use Committee (Guangzhou, China) and conducted according to the ethical standards and national guidelines. Every effort was made to reduce the number of animals used and minimize their pain and distress. After one week of acclimatization, rats were randomly divided into three groups ($n = 8$), and daily intragastrically administered an equal volume of the vehicle, raw SO or PSO extract at a dosage of 5 g/kg/day for 6 months. The experimental design was shown in Supplementary Figure S2.

Animal Sample Preparation

Blood samples were collected from the retro-orbital venous plexus each month. The blood samples were centrifuged at 3500 rpm for 10 min after standing for 2 h at 4°C. The serum was then transferred into new tubes and stored at -80°C for further analysis. A portion of the collected serum was used for routine biochemical analyses of the creatine kinase (CK), lactate dehydrogenase (LDH), urea, aspartate transaminase (AST), alanine transaminase (ALT), and plasma malondialdehyde (MDA) levels according to the manufacturer's instructions of the respective commercial assay kits. At the end of the experiment, all rats were sacrificed followed by blood collection. Fresh cardiac, hepatic, lung, and renal tissues were dissected and fixed in 10% neutral buffered formaldehyde at 4°C for paraffin embedment. Organ samples (4 µm) were sectioned and stained with H&E, and finally examined under light microscopy.

100 µL of serum was transferred and 400 µL extract solution (acetonitrile: methanol = 1:1) containing internal standard (adonitol, 1 µg/ml) was added. After 30 s vortex, samples were sonicated for 5 min in an ice-water bath. Then the samples were incubated at -40°C for 1 h and centrifuged at 10,000 rpm for 15 min at 4°C. 400 µL of supernatant was transferred to a fresh tube and dried in a vacuum concentrator at 37°C. Then, the dried samples were reconstituted in 100 µL of 50% acetonitrile by sonication on ice for 10 min. The constitution was then centrifuged at 13000 rpm for 15 min at 4°C, and 60 µL of supernatant was transferred to a fresh glass vial for LC/MS analysis. The quality control (QC) sample was prepared by mixing an equal aliquot of the supernatants from all the samples.

LC-TOF-MS/MS Analyses

The UHPLC separation was carried out using an ExionLC Infinity series UHPLC System (AB Sciex), equipped with a UPLC BEH Amide column (2.1 × 100 mm, 1.7 µm, Waters). The mobile phase consisted of 25 mmol/L ammonium acetate and 25 mmol/L ammonia hydroxide in water A) and acetonitrile B). The analysis was carried with an elution gradient as follows: 0–0.5 min, 95%B; 0.5–7.0 min, 95%–65% B; 7.0–8.0 min, 65%–40% B; 8.0–9.0 min, 40% B; 9.0–9.1 min, 40–95% B; 9.1–12.0 min, 95% B. The column temperature was 25°C. The auto-sampler temperature was 4°C, and the injection volume was 2 µL (pos) or 3 µL (neg), respectively.

The TripleTOF 5600 mass spectrometry (AB Sciex) was used for its ability to acquire MS/MS spectra on an information-dependent basis (IDA) during an LC/MS experiment. In this mode, the acquisition software (Analyst TF 1.7, AB Sciex) continuously evaluates the full scan survey MS data as it collects and triggers the acquisition of MS/MS spectra depending on preselected criteria. In each cycle, the most intensive 12 precursor ions with intensity above 100 were chosen for MS/MS at collision energy (CE) of 30 eV. The cycle time was 0.56 s. ESI source conditions were set as following: gas 1 as 60 psi, gas 2 as 60 psi, curtain gas as 35 psi, source temperature as 600°C, declustering potential as 60 V, and ion spray voltage floating (ISVF) as 5,000 V or -4,000 V in positive or negative modes, respectively.

Sequence Analysis

The pooled quality control (QC) sample was analyzed at the beginning, the end, and randomly through the analytical run to monitor the stability of sequence analysis. The typical batch sequence of serum samples consisting of consecutive analysis cycles of 1 QC serum sample (at the beginning of the study) follow by 8 unknown serum samples. Meanwhile, samples were analyzed in a random order for a normal good practice. An identical sequence was repeated to complete the total set of injections ($n = 28$, including QCs) analyzed in less than one day per mode.

LC-MS Data Processing

Rat serum samples were analyzed by an untargeted metabolomics approach based on UPLC-Q-TOF/MS. The MS raw data (.wiff) files were converted to the mzXML format by ProteoWizard, and processed by R package XCMS (version 3.2). Principle component analysis (PCA) and orthogonal projection to latent structures discriminant analysis (OPLS-DA) were used to assess the data. Major metabolites were screened and identified using in-house libraries and the METLIN (<http://metlin.scripps.edu>) database, the MassBank database (<http://www.massbank.jp/>), the Human Metabolome Database (HMDB) (<http://www.hmdb.ca/>), or the LipidMaps database (<http://www.lipidmaps.org>) based on accurate mass measurements (mass errors <5 ppm) and MS/MS fragment information.

Statistical Analysis

Results of the biochemical assays were presented as Mean ± SEM. These data were analyzed by one-way ANOVA followed by the Dunnett's multiple comparisons using GraphPad Prism version 7.0 (GraphPad Software, San Diego, CA, United States). $p < 0.05$ was considered statistically significant.

RESULTS

Biochemical Changes

The serum levels of AST, ALT, Urea, CK, and LDH were measured in each rat every month. ALT and AST are the markers of hepatic damage; Urea is a marker of renal damage; CK is a marker of cardiac damage. However, currently, no specific markers were used for evaluating the lung damage. It is known when an organ is damaged, LDH will be released into the circulation, which is known as a biomarker for tissue damage. Moreover, it has also been reported that the measurement of LDH activity in lung lavage fluid can assess the extent of cell damage (Gao et al., 2013). Here, we found that the serum level of LDH in raw SO group was significantly higher than that in the control group after 6-months treatment ($p < 0.01$). It is worth noting that, the LDH level in the PSO group was lower than that in the raw SO group ($p < 0.05$) (**Figure 1**), suggesting that processing significantly reduced the LDH level in the serum. Although raw SO increased the levels of CK and AST in the serum when compared to the control groups, they did not reach statistical significance. In addition, we also found that both

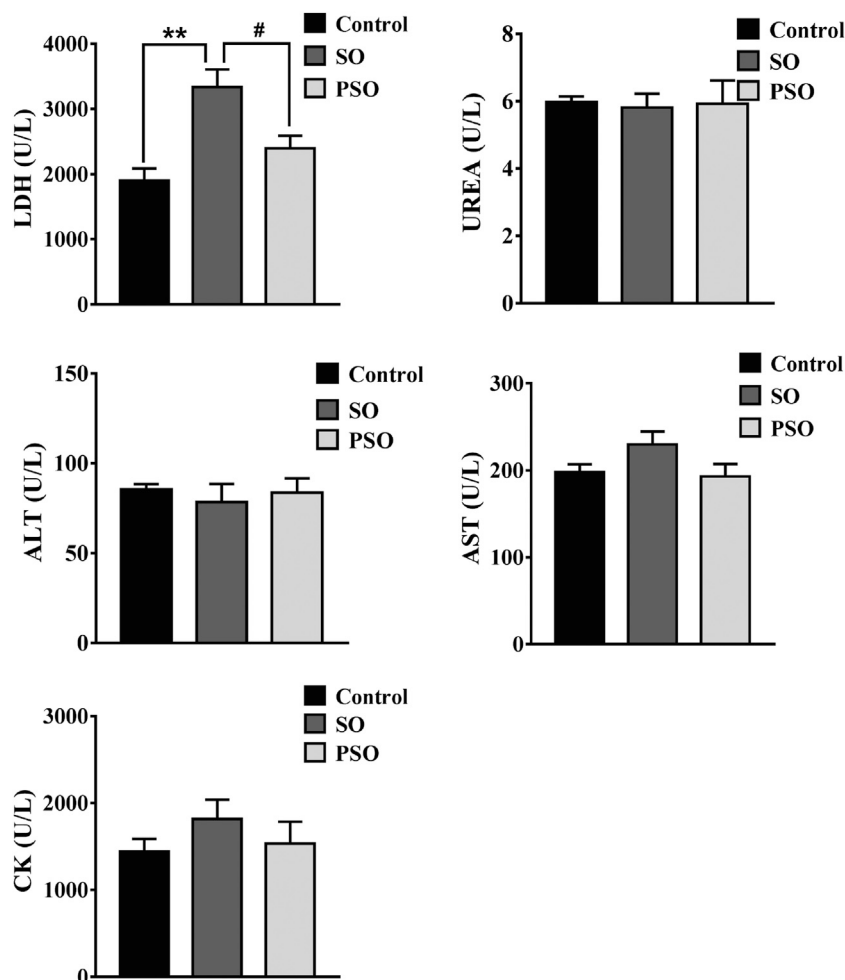


FIGURE 1 | Biochemical parameters in the serum of vehicle-, raw SO- and PSO-treated rats at month 6. ** $p < 0.01$ vs. control; # $p < 0.05$ vs. raw SO.

raw SO and PSO did not significantly affect the serum levels of ALT, AST, Urea, and CK in the earlier stage of the treatment, suggesting that the treatments at the early stage have no obvious liver, kidney and heart toxicities were observed in these rats (Supplementary Figure S3).

Histopathological Changes

H&E staining was used to further examine the treatment-induced toxicities in heart, liver, lung, and kidney tissues. We found that histopathological damages were observed in the lung tissues of the raw SO-treated rats as indicated by a lot of inflammatory cells infiltration, and along with the cells edema; while, the damages were relatively mild in PSO-treated rats. Liver and heart sections showed little pathological damages in the raw SO group (Figure 2), suggesting that long-term administration of raw SO may not cause obvious damages in the liver and heart when compared to the lung. Combining the pathological examination and the biochemical results, we strongly suggest that raw SO mainly causes pulmonary toxicity, which can be significantly reduced by processing.

Identification of Differential Metabolites

Total ion chromatogram (TIC) chromatograms of the serum samples were obtained from vehicle-, raw SO-, and PSO-treated rats (Supplementary Figure S4). Metabolomics chromatograms obtained through LC-Q-TOF/MS using the ESI⁺ and ESI⁻ modes revealed distinct differences. In total, 32 altered metabolites were authentically identified, including amino acids, lipids, hydrocarbons, and nucleotides. The heatmap figure showed the detailed information (Supplementary Figure S5). Based on the information obtained from LC-Q-TOF/MS, general OPLS-DA and PCA models were calculated to detect the significantly changed metabolites ($VIP > 1$ or $p < 0.05$) among the control, raw SO and PSO groups. PCA scores (PC1: 14.4%, PC2: 12.4%, PC3: 9.32%) showed that the three groups were clustered (Figure 3A). The multiple pattern recognition method of partial least squares discriminant analysis was adopted based on the basis of the metabolic changes in the three groups as revealed by TIC chromatograms. As shown in the PLS-DA scores plot (Figure 3B, $R_2X = 0.41$, $R_2Y = 0.841$, $Q_2 = 0.388$), we found that the distribution of each group was concentrated, and the

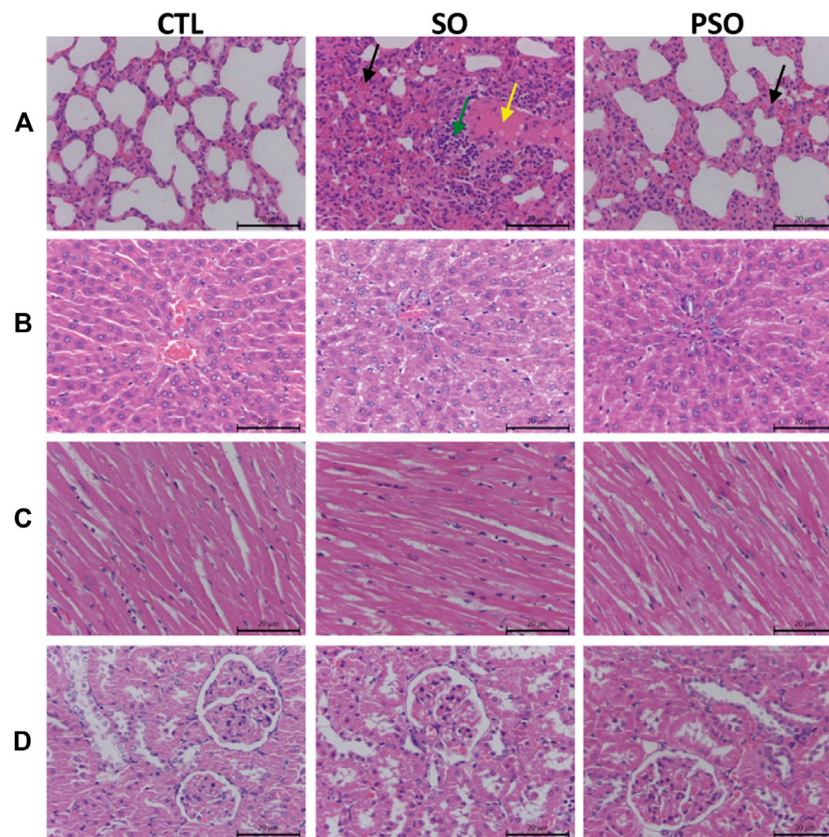


FIGURE 2 | Histopathological examinations of the lung, liver, heart, and kidney tissues in vehicle-, raw SO- and PSO-treated rats. H&E staining, 200x. **(A)** Lung tissue of each group: yellow arrow represents serous exudation in the alveolar cavities, green arrow represents inflammatory cell infiltration, black arrow represents the thickened alveolar septum, and the capillaries are dilated and congested; **(B)** liver tissue of each group; **(C)** heart tissue of each group; and **(D)** kidney tissue of each group.

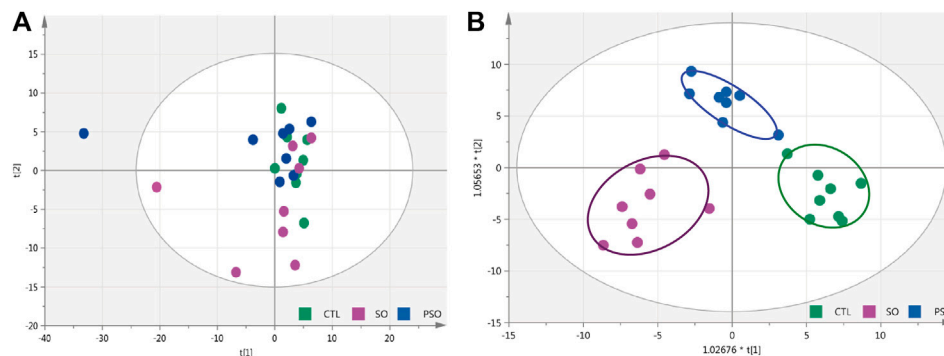


FIGURE 3 | PCA and OPLS-DA modeling were used to differentiate the rat serum metabolomic patterns after raw SO and PSO treatment. **(A)** PCA modeling; **(B)** OPLS-DA modeling. Control group (green), raw SO group (violet), and PSO group (blue).

distance between the raw SO group and control group was far, while that between the PSO group and the control group was comparatively shorter, suggesting that significant changes of the metabolites in the serum levels are shown after the administration of raw SO in rats.

As shown in **Table 1**, a total of 32 metabolites were significantly changed when compared to the control group, among them, 10 metabolites were significantly downregulated including LysoPC(20:4), LysoPC(22:6), and glucosylsphingosine, while 22 metabolites were significantly upregulated including

TABLE 1 | Significantly altered metabolites in the serum samples of vehicle-, raw SO- and PSO-treated rats. ↑: upregulation; ↓: downregulation; —: no significant change.

Super-pathway	Sub-pathway	No.	Metabolites	SO vs. CTL	PSO vs. CTL
Amino acid	Cysteine metabolism	1	Acetylcysteine	↓	↓
	Tryptophan	2	D-Tryptophan	↓	↓
	Metabolism	3	L-Glutamine	↑	—
	Arginine biosynthesis	4	L-Aspartic	↑	—
Lipid	Glycerophospholipid metabolism	5	Phosphorylcholine	↑	—
		6	PC (16:0/16:0)	↑	↑
		7	PE (16:0/20:1)	↑	↑
		8	PE (22:5/22:6)	↑	↑
		9	PE (22:6/P-18:0)	↑	↑
		10	PE-NMe (16:0/16:0)	↑	↑
		11	PC (16:0/16:0)	↑	↑
		12	PC (P-18:1/18:4)	↑	↑
	Lysophospholipid metabolism	13	LysoPA (18:1)	↑	—
		14	LysoPC (20:4)	↓	—
		15	LysoPC (22:2)	↑	↑
		16	LysoPC (22:6)	↓	—
		17	LysoPC (24:1)	↑	↑
		18	LysoPC (26:1)	↑	—
		19	LysoPE (18:1)	↑	—
		20	DG (20:4/18:2/0:0)	↓	↓
	Diglyceride metabolism	20	DG (20:4/18:2/0:0)	↓	↓
	Glycosphingolipids	21	Glucosylsphingosine	↓	—
	Sphingomyelin metabolism	22	SM (d18:1/16:0)	↑	↑
		23	SM (d18:1/24:1)	↑	↑
	Fatty acid metabolism	24	Docosahexaenoic acid	↑	—
		25	Hexadecanedioic acid	↑	—
		26	Hexadecanoic acid	↑	↓
		27	Oleamide	↓	↑
		28	Gamma-Linolenic acid	↓	↓
		29	Myristic acid	↓	—
		30	Vaccenyl carnitine	↑	↑
Hydrocarbon	Oxidation of fatty acids	31	Dodecanoylcarnitine	↑	—
Nucleotide	Purine metabolism	32	Guanine	↓	—

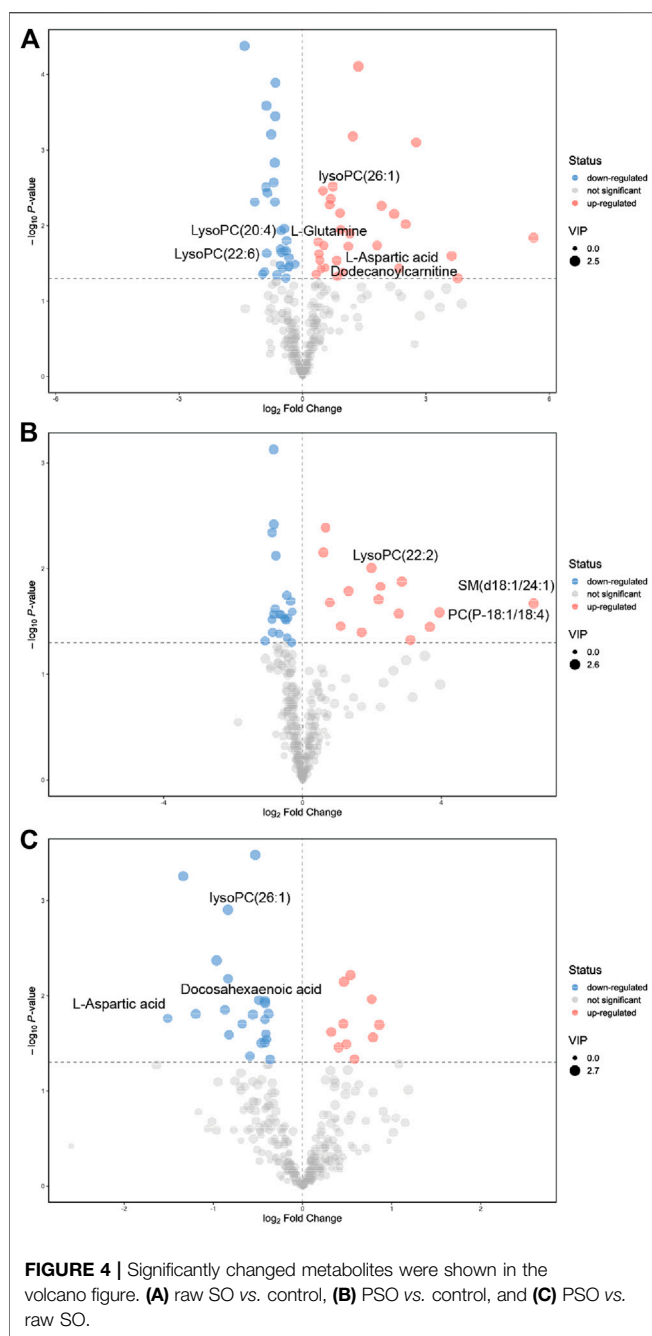
L-glutamine, L-aspartic acid, and phosphorylcholine. For the PSO group, we found that 5 metabolites were significantly downregulated including acetylcysteine, D-tryptophan, and gamma-linolenic acid, while 14 metabolites were significantly upregulated including PC (16:0/16:0), PE(16:0/20:1), and PE (22:5/22:6). Interestingly, 14 metabolites which obviously altered in the raw SO group, showed no significant differences in the PSO group, which is similar to the control group. The volcano figure can also show the metabolites fluctuation of various compounds (**Figure 4**). These altered metabolites may partly explain the toxicity that is caused by raw SO and the toxicity-reducing effect of processing.

Metabolic Pathway and Network Function Analyses

To further understand the correlation between the candidate metabolites and the biological association networks, we performed pathway analysis using MetaboAnalyst (<https://www.metaboanalyst.ca/>) pathway analysis. As shown in **Figure 5**, four significant metabolic pathways including arginine biosynthesis,

glycerophospholipid metabolism, D-glutamine, and D-glutamate metabolism, and alanine, aspartate, and glutamate metabolism were identified in the serum samples of raw SO-treated rats; while, histidine metabolism, arginine biosynthesis, and D-glutamine and D-glutamate metabolism were identified in the serum samples of PSO-treated rats.

Among them, two characteristic metabolic pathways alanine, aspartate and glutamate metabolism and glycerophospholipid metabolism were only changed in the raw SO group. It was reported that both glycerophospholipid metabolism (Wang et al., 2019) and arginine biosynthesis (Mizrahi and Warner, 2018) are closely related to oxidative stress. Therefore, we speculated that the raw SO-induced oxidative stress response may underlie the pulmonary toxicity. In addition, histidine metabolism was only changed in the PSO group. Studies suggested that histidine, an amino acid that is essential to humans, exerts favorable cytoprotective effects against oxidative stress as have been demonstrated both *in vivo* and *in vitro*, which has been shown to scavenging free radicals (Vera-Aviles et al., 2018). Hence, we speculated that free radical scavenging may be responsible for the toxicity-reducing effect of processing.



Verification of the Mechanisms Underlying the Raw SO-Induced Pulmonary Toxicity and the Toxicity-Reducing Effect of Processing

In an attempt to verify the highlighted biological functions, we examined the MDA contents in the serum samples of vehicle-, raw SO-, and PSO-treated rats. MDA, a classic biomarker of oxidative stress, is produced by free radicals in the body (Lykkesfeldt, 2007). It is also widely used as an indicator of the free radical level. As shown in **Figure 6**, we found that raw SO

treatment significantly increased the serum MDA content when compared to the vehicle control group ($p < 0.05$), suggesting that raw SO causes oxidative stress in the rats. While the MDA content in the PSO group was lower than that in the raw SO group ($p < 0.05$), and no significant difference was observed between the control and PSO groups, suggesting that processing reduces the oxidative stress-causing effects of raw SO or processing enabled the herb to possess a free radical scavenging property. These findings also suggest that free radical scavenging may be responsible for the pulmonary toxicity-reducing effect of processing.

DISCUSSION

Raw SO is toxic, studies have demonstrated that the water extract of SO has acute and subacute toxicities (Guan et al., 2007; Guan et al., 2008). However, the long-term toxicity of SO is unknown. It is worth noting that in clinical practice SO is commonly used for treating chronic diseases, such as RA and hypertension, which require long-term treatment. Therefore, it is necessary to explore the long-term toxicity of this herb. In this study, we explored the long-term toxicity of SO, and revealed the molecular mechanisms underlying the raw SO-induced toxicity. In the future, toxicity studies in the disease models will be conducted.

According to the TCM theory, processing can reduce the toxicity of the herbs. The theory has been supported by modern toxicology studies. In our previous study, PSO was demonstrated less toxic than raw SO in our tested MRC-9 cells (Su et al., 2014). However, the mechanisms of raw SO-induced toxicities and the toxicity-reducing effect of processing are still not fully understood. Here, we conducted the metabolomics study to explore the mechanisms that underlie the raw SO-induced pulmonary toxicity and the toxicity-reducing effect of processing.

In this study, a total of 32 metabolites are significantly altered including amino acids, lipids, hydrocarbons and nucleotides, they were authentically identified in the serum samples of vehicle-, raw SO-, and PSO-treated rats (**Table 1**). In the raw SO group, 22 metabolites were upregulated, while 10 metabolites were downregulated. In the PSO group, 13 metabolites were upregulated, 5 metabolites were downregulated, and the other 14 metabolites are not significantly different when compared to the healthy rats.

Among all the metabolites, 8 characteristic metabolites including L-glutamine, L-aspartic acid, phosphorylcholine, lysoPA (18:1), lysoPC (26:1), lysoPE (18:1), docosahexaenoic acid, and dodecanoylcarnitine were only upregulated in the raw SO group, and they do not show changes in the PSO group. Among them, two were amino acids. The observed changes in amino acid contents should be due to the modulation of the endogenous amino acid metabolism system, but not the loading of the exogenous amino acid. In our experiments, we had fasted the rats for 12 h before blood sample collection. The half-lives of exogenous amino acids in rats are very short (Su et al., 2016). Hence, the exogenous amino acids should have been eliminated within 12 h and cannot be detected in the serum. Glutamine is metabolized by glutaminase-1 (GLS1) to form the gas NH_3 . NH_3

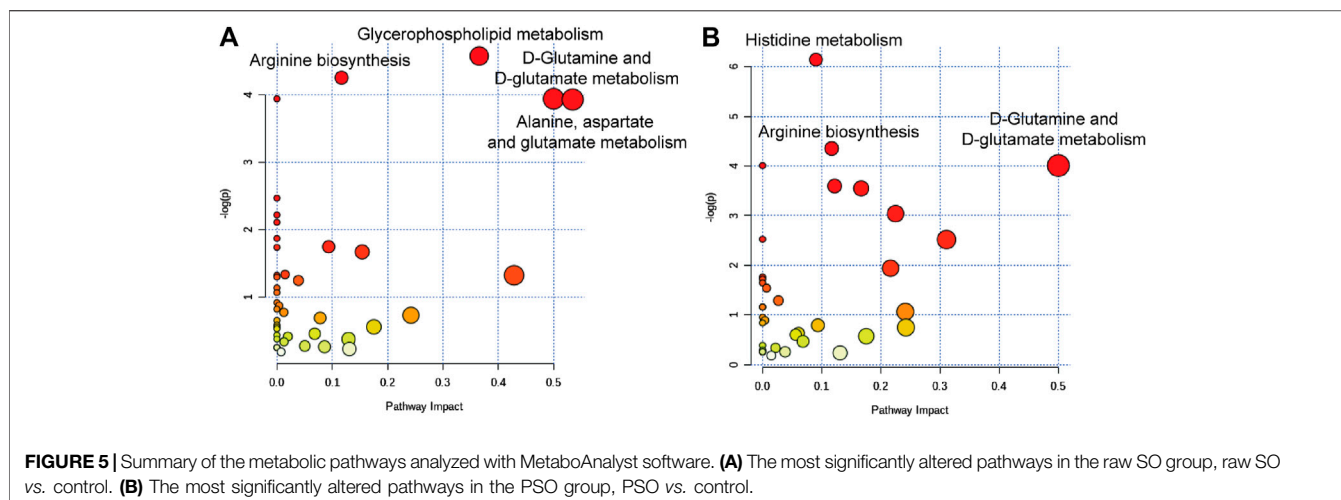


FIGURE 5 | Summary of the metabolic pathways analyzed with MetaboAnalyst software. **(A)** The most significantly altered pathways in the raw SO group, raw SO vs. control. **(B)** The most significantly altered pathways in the PSO group, PSO vs. control.

stimulated the production of mitochondrial reactive oxygen species (ROS) which causes the activation and translocation of the NF-E2-related factor-2 transcription factor (Nrf2) into the nucleus, where it binds to the antioxidant responsive element (ARE) in the promoter region of the gene to trigger HO-1 transcription (Durante, 2019). It is reported that glutamine metabolism is required for collagen protein synthesis in lung fibroblasts (Hamanaka et al., 2019), and excessive proliferation of lung fibroblasts could cause lung toxicity (Huang et al., 2012). Here, in this study, we found that glutamine was only upregulated in the raw SO group, suggesting that raw SO was more toxic than PSO. Aspartic acid is an α -amino acid. The study reports that aspartic acid at high dose levels has toxicity in kidneys and salivary glands in Fischer rats (Tada et al., 2008). Docosahexaenoic acid (DHA) is a polyunsaturated ω -3 fatty acid. Some studies suggest that the elevated levels of DHA are associated with decreased risk of dementia, while, other studies reported that DHA micelles stabilized protofibrillar A β 42 to prevent further fibrillization

(Hashimoto et al., 2008). Unfortunately, these protofibrils induced toxicity in PC-12 cells, suggesting that DHA may act as a double-edged sword. Depending on the context, DHA may actually exacerbate the pathology of Alzheimer's disease (Cole and Frautschy, 2006). Thus, too high or too low concentration of DHA in raw SO-treated rats may cause physiological changes. In addition, by comparing the concentration of dodecanoylcarnitine in the tissues and the urine of healthy and cancer patients, the dodecanoylcarnitine concentrations are higher in both cancer tissues (compared with the paired normal tissue) and in urine of cancer patients (compared with control urine), suggesting that dodecanoylcarnitine is highly expressed in an abnormal physiological state (Niziol et al., 2018), which also implies that raw SO treatment changes the physiological state and finally upregulated the content of dodecanoylcarnitine in the rats. Phosphorylcholine (PC), the polar headgroup of the membrane phospholipid phosphatidylcholine, which is a pro-inflammatory epitope in OxPLs and is recognized as a danger-associated molecular pattern by the innate immune system (Miller et al., 2011). Thus, elevation of this pro-inflammatory molecule in raw SO indicates that it has a strong pro-inflammatory effect, which may partly explain the toxicity that is caused by raw SO, and the reason for our observed inflammatory-cell infiltration in the lung tissues of raw SO-treated rats.

Besides the above eight metabolites that were only upregulated in the raw SO-treated group, another four metabolites were only downregulated in the raw SO group but not in the PSO group. Take glucosylsphingosine as an example, glucosylsphingosine is a key biomarker of Gaucher disease (Murugesan et al., 2016). It is believed to be responsible for macrophagic organ infiltration and the subsequent development of organomegaly, which could cause hematological and visceral changes in animals (Lukas et al., 2017). Myristic acid, is also known as tetradecanoic acid, which is a side chain of phorbol myristate acetate (PMA). It activates human polymorphonuclear leukocytes to produce oxygen radicals more potently than PMA does (Tada et al., 2009). Although the levels of these two metabolites were downregulated in the raw SO group, we know that the organism is a balanced environment, and either too high or

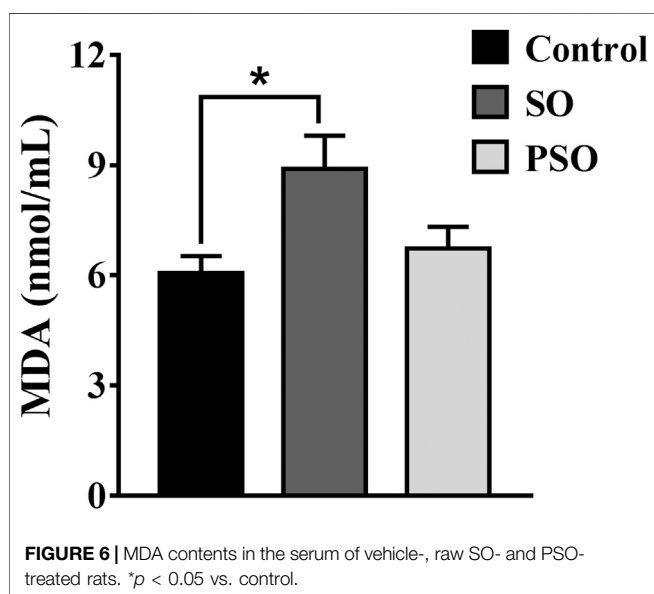


FIGURE 6 | MDA contents in the serum of vehicle-, raw SO- and PSO-treated rats. * $p < 0.05$ vs. control.

too low will have some effects. Whether these changes underlie the toxicity caused by raw SO deserves further investigation.

In addition, 12 metabolites including PE (16:0/20:1), PE (22:5/22:6), and PC (P-18:1/18:4) were upregulated; while, 4 metabolites including acetylcysteine, tryptophan and DG (20:4/18:2/0:0) were downregulated in both raw SO and PSO groups, which may explain the common efficacies of both raw SO and PSO.

CONCLUSION

In summary, we for the first time demonstrated that processing with rice wine significantly reduced the long-term toxicity of raw SO, which supports the TCM theory that “processing can reduce the toxicity of raw SO.” Induction of oxidative stress underlies the raw SO-induced pulmonary toxicity, and free radical scavenging was, at least in part, responsible for the toxicity-reducing effect of processing. Our study sheds new light on the mechanisms underlying the raw SO-induced pulmonary toxicity and the toxicity-reducing effect of processing with rice wine. This study not only provides a scientific justification for the traditional processing theory but also should guide rational and safe clinical applications of SO by helping in optimizing its processing procedure and clinical compatibility.

DATA AVAILABILITY STATEMENT

The original contributions presented in the study are included in the article/**Supplementary Material**; further inquiries can be directed to the corresponding authors.

REFERENCES

- Cole, G. M., and Frautschy, S. A. (2006). Docosahexaenoic Acid Protects from Amyloid and Dendritic Pathology in an Alzheimer's Disease Mouse Model. *Nutr. Health* 18, 249–259. doi:10.1177/026010600601800307
- Durante, W. (2019). The Emerging Role of L-Glutamine in Cardiovascular Health and Disease. *Nutrients* 11, 2092. doi:10.3390/nu11092092
- Gao, T. T., Kong, M., Dai, Q., and Shun, Q. (2013). Advances in Biomarkers of Lung Injury. *Chin. J. New Drugs* 22, 429–432. doi:10.5246/jcps.2013.05.064
- Guan, J. H., Xue, Z., Liu, B. C., and Ren, J. B. (2008). An Experimental Study on Pulmonary Toxicity of Siegesbeckia Orientalis L. Water Extracts in Mice. *China J. Chin. Materia Med.* 33, 2820–2822.
- Guan, J. H., Xue, Z., and Ren, J. B. (2007). Experimental Study on Acute and Subacute Toxicities of Water Decoction of Herba Siegesbeckiae in Mice. *Chin. J. Exp. Traditional Med. Formulae* 13, 49–51.
- Hamanaka, R. B., O'Leary, E. M., Witt, L. J., Tian, Y., Gökalp, G. A., Meliton, A. Y., et al. (2019). Glutamine Metabolism Is Required for Collagen Protein Synthesis in Lung Fibroblasts. *Am. J. Respir. Cell Mol. Biol.* 61, 597–606. doi:10.1165/rcmb.2019-0008oc
- Hashimoto, M., Shahdat, H. M., Yamashita, S., Katakura, M., Tanabe, Y., Fujiwara, H., et al. (2008). Docosahexaenoic Acid Disrupts in Vitro amyloid β 1-40 fibrillation and Concomitantly Inhibits Amyloid Levels in Cerebral Cortex of Alzheimer's Disease Model Rats. *J. Neurochem.* 107, 1634–1646. doi:10.1111/j.1471-4159.2008.05731.x
- Huang, S. M., Zuo, X., Li, J. J. E., Li, S. F. Y., Bay, B. H., and Ong, C. N. (2012). Metabolomics Studies Show Dose-dependent Toxicity Induced by

ETHICS STATEMENT

The animal study was reviewed and approved by the Guangzhou University of Chinese Medicine Animal Care and Use Committee.

AUTHOR CONTRIBUTIONS

TJ, LL, MZ, and ZQ performed the majority experiments and analyzed the data. JS and TZ helped for the H&E examination. TS, TJ, and LL interpreted the data. GC participated in the experimental plan. TS supervised the study, drafted and finalized the manuscript. All authors have read and approved the final manuscript.

FUNDING

This work was supported by the National Natural Science Foundation of China (81703705 and 82074019), the Opening Project of Zhejiang Provincial Preponderant and Characteristic Subject of Key University (Traditional Chinese Pharmacology), Zhejiang Chinese Medical University (ZYAOX2018010), and the Guangdong Key Laboratory for Translational Cancer Research of Chinese Medicine (2018B030322011).

SUPPLEMENTARY MATERIAL

The Supplementary Material for this article can be found online at: <https://www.frontiersin.org/articles/10.3389/fphar.2021.630319/full#supplementary-material>.

- SiO₂Nanoparticles in MRC-5 Human Fetal Lung Fibroblasts. *Adv. Healthc. Mater.* 1, 779–784. doi:10.1002/adhm.201200114
- Lukas, J., Cozma, C., Yang, F., Kramp, G., Meyer, A., Nessler, A. M., et al. (2017). Glucosylsphingosine Causes Hematological and Visceral Changes in Mice—Evidence for a Pathophysiological Role in Gaucher Disease. *Int. J. Mol. Sci.* 18, 2192. doi:10.3390/ijms18102192
- Lykkesfeldt, J. (2007). Malondialdehyde as Biomarker of Oxidative Damage to Lipids Caused by Smoking. *Clinica. Chim. Acta* 380, 50–58. doi:10.1016/j.cca.2007.01.028
- Miller, Y. I., Choi, S. H., Wiesner, P., Fang, L., Harkewicz, R., Hartvigsen, K., et al. (2011). Oxidation-specific Epitopes Are Danger-Associated Molecular Patterns Recognized by Pattern Recognition Receptors of Innate Immunity. *Circ. Res.* 108, 235–248. doi:10.1161/circresaha.110.223875
- Mizrahi, V., and Warner, D. F. (2018). Death of *Mycobacterium tuberculosis* by L-Arginine Starvation. *Proc. Natl. Acad. Sci. U. S. A.* 115, 9658–9660. doi:10.1073/pnas.1813587115
- Murugesan, V., Chuang, W. L., Liu, J., Lischuk, A., Kacena, K., Lin, H., et al. (2016). Glucosylsphingosine Is a Key Biomarker of Gaucher Disease. *Am. J. Hematol.* 91, 1082–1089. doi:10.1002/ajh.24491
- Niziol, J., Bonifay, V., Ossolinski, K., Ossolinski, T., Ossolinska, A., Sunner, J., et al. (2018). Metabolomic Study of Human Tissue and Urine in Clear Cell Renal Carcinoma by LC-HRMS and PLS-DA. *Anal. Bioanal. Chem.* 410, 3859–3869. doi:10.1007/s00216-018-1059-x
- Su, T., Tan, Y., Tsui, M. S., Yi, H., Fu, X. Q., Li, T., et al. (2016). Metabolomics Reveals the Mechanisms for the Cardiotoxicity of Pinelliae Rhizoma and the Toxicity-Reducing Effect of Processing. *Sci. Rep.* 6, 34692. doi:10.1038/srep34692

- Su, T., Yu, H., Kwan, H. Y., Ma, X. Q., Cao, H. H., Cheng, C. Y., et al. (2014). Comparisons of the Chemical Profiles, Cytotoxicities and Anti-inflammatory Effects of Raw and Rice Wine-processed Herba Siegesbeckiae. *J. Ethnopharmacol.* 156, 365–369. doi:10.1016/j.jep.2014.09.038
- Tada, M., Ichiishi, E., Saito, R., Emoto, N., Niwano, Y., and Kohno, M. (2009). Myristic Acid, a Side Chain of Phorbol Myristate Acetate (PMA), Can Activate Human Polymorphonuclear Leukocytes to Produce Oxygen Radicals More Potently Than PMA. *J. Clin. Biochem. Nutr.* 45, 309–314. doi:10.3164/jcbs.09-30
- Tada, Y., Yano, N., Takahashi, H., Yuzawa, K., Ando, H., Kubo, Y., et al. (2008). Toxic Effects of L-Aspartic Acid at High Dose Levels on Kidneys and Salivary Glands in Fischer 344 Rats Detected in a 90-day Feeding Study. *Food Chem. Toxicol.* 46, 2789–2795. doi:10.1016/j.fct.2008.05.013
- Tan, Y., Ko, J., Liu, X., Lu, C., Li, J., Xiao, C., et al. (2014). Serum Metabolomics Reveals Betaine and Phosphatidylcholine as Potential Biomarkers for the Toxic Responses of Processed Aconitum Carmichaelii Debx. *Mol. Biosyst.* 10, 2305–2316. doi:10.1039/c4mb00072b
- Vera-Aviles, M., Vantana, E., Kardinasari, E., Koh, N., and Latunde-Dada, G. (2018). Protective Role of Histidine Supplementation against Oxidative Stress Damage in the Management of Anemia of Chronic Kidney Disease. *Pharmaceuticals* 11, 111. doi:10.3390/ph11040111
- Wang, X., Xu, Y., Song, X., Jia, Q., Zhang, X., Qian, Y., et al. (2019). Analysis of Glycerophospholipid Metabolism after Exposure to PCB153 in PC12 Cells through Targeted Lipidomics by UHPLC-MS/MS. *Ecotoxicol. Environ. Saf.* 169, 120–127. doi:10.1016/j.ecoenv.2018.11.006
- Yu, S., Guo, Z., Guan, Y., Lu, Y. Y., Hao, P., Li, Y., et al. (2012). Combining ZHENG Theory and High-Throughput Expression Data to Predict New Effects of Chinese Herbal Formulae. *Evid. Based Complement. Alternat. Med.* 2012, 986427. doi:10.1155/2012/986427

Conflict of Interest: The authors declare that the research was conducted in the absence of any commercial or financial relationships that could be construed as a potential conflict of interest.

Publisher's Note: All claims expressed in this article are solely those of the authors and do not necessarily represent those of their affiliated organizations, or those of the publisher, the editors and the reviewers. Any product that may be evaluated in this article, or claim that may be made by its manufacturer, is not guaranteed or endorsed by the publisher.

Copyright © 2021 Jiang, Liu, Zhang, Qiao, Zhao, Su, Cao and Su. This is an open-access article distributed under the terms of the Creative Commons Attribution License (CC BY). The use, distribution or reproduction in other forums is permitted, provided the original author(s) and the copyright owner(s) are credited and that the original publication in this journal is cited, in accordance with accepted academic practice. No use, distribution or reproduction is permitted which does not comply with these terms.



Ethnopharmacological, Phytochemical, Pharmacological, and Toxicological Review on *Senna auriculata* (L.) Roxb.: A Special Insight to Antidiabetic Property

Guruprasad C. Nille^{1*†}, Shardendu Kumar Mishra^{2†}, Anand Kumar Chaudhary¹ and K. R. C. Reddy¹

¹Department of Rasa Shastra and Bhaishajya Kalpana, Faculty of Ayurveda, Institute of Medical Sciences, Varanasi, India,

²Department of Pharmacology, Institute of Pharmacy, Ram-Eesh Institute of Vocational & Technical Education, Greater Noida, India

OPEN ACCESS

Edited by:

Sayed Ahmad,
Jamia Hamdard University, India

Reviewed by:

Sefirin Djiogue,
University of Yaounde I, Cameroon
Mahmoud Fahmi Elsebai,
Mansoura University, Egypt

*Correspondence:

Guruprasad C. Nille
drguruprasadnille0412@gmail.com

[†]These authors have contributed
equally to this work and share first
authorship

Specialty section:

This article was submitted to
Ethnopharmacology,
a section of the journal
Frontiers in Pharmacology

Received: 30 December 2020

Accepted: 09 August 2021

Published: 24 August 2021

Citation:

Nille GC, Mishra SK, Chaudhary AK
and Reddy KRC (2021)
Ethnopharmacological,
Phytochemical, Pharmacological, and
Toxicological Review on *Senna*
auriculata (L.) Roxb.: A Special Insight
to Antidiabetic Property.
Front. Pharmacol. 12:647887.
doi: 10.3389/fphar.2021.647887

Avartaki (*Senna auriculata* (L.) Roxb. syn. *Cassia auriculata* L.; Family- Fabaceae) is a traditional medicinal plant, widely used for the treatment of various ailments in Ayurveda and Siddha system of medicine in India. Almost all the parts of the plant, such as flowers, leaves, seeds, barks, and roots have been reported for their medicinal uses. Traditionally, it has been used in the treatment of diabetes, asthma, rheumatism, dysentery, skin disease, and metabolic disorders. The principle phytochemicals in *Senna auriculata* (L.) Roxb. are alkaloids, anthraquinone, flavone glycosides, sugar, saponins, phenols, terpenoids, flavonoids, tannins, steroids, palmitic acid, linoleic acid, benzoic acid 2-hydroxyl methyl ester, 1-methyl butyl ester, resorcinol, α -tocopherol- β -D-mannosidase, epicatechin, ferulic acid, quercetin-3-O-rutinoside, quercetin, proanthocyanidin B1. The extracts from its different parts and their isolated compounds possess a wide range of pharmacological activities such as antidiabetic, antioxidant, anti-inflammatory, antihyperlipidemic, hepatoprotective, nephroprotective, cardioprotective, anti-atherosclerotic, anticancer, antimutagenic, antimicrobial, antiulcer, antipyretic, anthelmintic, immunomodulatory, antifertility, anti-venom, and anti-melanogenesis. The toxicological findings from preclinical studies ensured the safety of the plant, but comprehensive clinical studies are required for the safety and efficacy of the plant in humans. The current review article aimed to provide up-to-date information about *Senna auriculata* (L.) Roxb. covering its ethnomedicinal, phytochemical, pharmacological, and toxicological aspects with special emphasis on its clinical implications in diabetes.

Keywords: *Cassia auriculata* L., ayurveda, antidiabetic, ethnomedicine, insulinogenic, Siddha, quercetin

INTRODUCTION

The extensive use of medicinal plants to discover new therapeutics or active pharmacological compounds is the urgent need to tackle challenging non-communicable diseases (NCDs). Around 71% of the mortality worldwide has resulted due to NCDs, including the deaths of 40 million populations worldwide per year (Naghavi et al., 2017). In India alone, 60% of the

deaths occur due to NCDs (Nethan et al., 2017). Diabetes and hypertension are the major contributory illnesses amidst the deaths caused by NCDs (Madavanakadu Devassy et al., 2020).

India has a great heritage of traditional system of medicines like Ayurveda, Siddha, and Unani, where hundreds of medicinal plants are being used to treat various diseases with their known ethnopharmacological evidence. *Senna auriculata* (L.) Roxb. syn. *Cassia auriculata* L., family Fabaceae (former Caesalpiniaceae) is one of the medicinal plants that has been used traditionally in Ayurveda, Siddha, and Unani since the 15th century. It is commonly known as Tanner's Senna/Cassia and Mature Tea Tree in English; *Avartaki*, *Pitapuspa*, *Pitkalika*, *Manojyna*, *Pitkala*, *Charmaranga* in Sanskrit; *Tarwar*, *Awai*, *Tarval* in Hindi; *Tangedu*, *Merakatangeedu* in Telugu, and *Arsual*, *Taravada*, *Tarwad* in Marathi. This shrub is widely spread in India, covering its southern, westerns, and central dry zones and also in Sri Lanka (Gupta and Sharma, 2007; Nille and Reddy, 2017; Win and Min, 2018).

The current review aimed to investigate the ethnomedicinal uses, phytochemical, pharmacological, and toxicological studies of the *Senna auriculata* (L.) Roxb., and endeavored to validate the experimental studies in terms of scientific data concerning the therapeutic implications of active metabolites of the plant.

METHODOLOGY

In the present review, the available literature has been explored from Ayurvedic classical texts, various published technical reports, online scientific data by accessing Scopus directory, Google Scholar, PubMed, Science Direct, EMBASE, SciFinder, Web of Science for its ethnomedicinal uses, phytochemistry, pharmacology, and biomedical applications. The following keywords were used: "*Senna auriculata* (L.) Roxb.," "*Cassia auriculata* L.," "Avartaki," "Avarai," "Tanner's cassia," "phytochemistry," "antihyperglycemic," "oxidative stress," "antidiabetic," "hepatoprotective," "insulinogenic," "anti-inflammatory," "immunomodulator," "antioxidant," "antihyperlipidemic," "mechanism of action" with their corresponding Medical Subject Headings (MeSH) terms using conjunctions OR/AND. The search was centered on identifying Ayurvedic claims in the available ethnomedicinal, phytochemical, pharmacological, clinical, and safety reports to understand the role of *Senna auriculata* (L.) Roxb. syn. *Cassia auriculata* L. in diabetes and other NCDs. The literature search was commenced before April 2021 and searches were limited to the English language.

BOTANICAL ASPECTS OF SENNA AURICULATA (L.) ROXB

Senna auriculata (L.) Roxb. is found in wooden grasslands up to a height of 500 m. It breeds wild in dry regions with annual precipitation of 300 mm. It grows well in areas with an annual temperature range of 15–28°C and needs full sun for its growth. It



FIGURE 1 | Flower & Leaves of *Senna auriculata* (L.) Roxb.

is a branched shrub with height of 1.5–5 m, trunk diameter of 20 cm and brown lenticellate bark (Kirtikar and Basu, 1918).

Leaves: Leaves are dull green in color, alternate, stipulate, paripinnate arrangement with 16–24 pairs of leaflets. Leaves are narrowly rough, pubescent and thin, with vertical and linear gland between the leaflets (**Figure 1**). It is short-stalked, 20–25 mm long, 10–13 mm wide; marginally overlapping, rectangular, dull-witted at both ends, and glabrous (Kirtikar and Basu, 1918; Evans, 1996).

Flowers: Flowers are bright yellow and irregular and large (50 mm) and have axillary raceme inflorescence, 2–8 flowered (**Figure 1**). Flowers are bisexual, zygomorphic, pentamerous, 4–5 cm; sepals are rounded at apex, imbricate; petals free, imbricate, unequal, 1.5–3 cm long; stamens 10, the 3 lower ones large stand fertile, others usually sterile; ovary superior, falcate, with 1.5 cm long, stalked, style (fruit a flattened) cylindrical pod 5–18 × 1–2 cm, transversely undulate between the 10–20 seeds, indehiscent, green turning to brown when mature (Kirtikar and Basu, 1918; Evans, 1996).

Fruits: Fruits are green or light brown, and have legume which is 7–11 cm long, 1.5 cm wide, rectangular, long style base, flat, thin, undulate crimped (**Figure 2**). It has about 12–20 seeds per



FIGURE 2 | Fruits & Leaves of *Senna auriculata* (L.) Roxb.

fruit, each in its distinct cavity (Kirtikar and Basu, 1918; Evans, 1996).

TRADITIONAL AND ETHNOPHARMACOLOGICAL USES OF *SENNA AURICULATA* (L.) ROXB

The foremost description of the *Senna auriculata* (L.) Roxb. is available in *Kaiyadeva Nighantu*, a classical Ayurveda text (15th century), where its *Pramehahara* property (antidiabetic action) through different botanical parts of the plant has been mentioned. Flowers have *Pramehashamana* property (antidiabetic action). Tender fruits have mentioned for their *Vamihara* (antiemetic), *Krimihara* (anthelmintic), *Sarvapramehahara* (antidiabetic), *Trishnaghna* (thirst alleviating), *Akshihita* (eye tonic), *Ruchya* (appetizing) properties. Seeds are useful as *Madhumehaghna* (antidiabetic), *Vishahara* (antidote), *Raktaatisaraghna* (anti-diarrheal). Roots are mentioned for *Trishnahara* (thirst alleviating), *Pramehaghna* (antidiabetic), *Shwasaghna* (antiasthmatic), *Raktapittashaman* (antihemorrhagic), *Shukrakshayahara* (sperm enhancing) properties (Sharma and Sharma, 1979). The leaf macerate of *Senna auriculata* (L.) Roxb. was used traditionally to treat inflammation specifically in Maharashtra, Andhra Pradesh, and Gujarat. It also effectively reduces pain and inflammation in joint disorders. The leaves of *Senna auriculata* (L.) Roxb. are also effective in muscle pain, irregular muscle contraction, body pain, gastritis, skin sores and ulcers. The flowers are effectively used as health beneficial agents. The crushed flowers are mixed with goat milk to cure sexually transmitted diseases. The dried powder of flowers of *Senna auriculata* (L.) Roxb. is used to clean the hair, and taken by diabetic patients and in fever. The root is used by chewing, and the juice is swallowed to cure abdominal complaints, vomiting, urinary discharges, tumors and diarrhea. Powder of bark is used to treat toothache by applying it to the gums. The fruits are used in helminthic infections (Punjani, 2002; Punjani and Kumar, 2002;

Duraipandiyan et al., 2006; Pawar and Patil, 2007; Ignacimuthu et al., 2008; Kosalge and Fursule, 2009; Thirumalai et al., 2009; Patel et al., 2010; Jagatheeswari, 2012).

METABOLITES OF *SENNA AURICULATA* (L.) ROXB

The flower, leaves, roots and seed were investigated with advanced spectroscopic and chromatographic techniques and found various active metabolites with therapeutic implications against different diseases. The flowers of *Senna auriculata* (L.) Roxb. reported a significant amount of alkaloids, glycosides, saponins, polyphenols, tannins, phloro-tannins, terpenoids, triterpenes, carbohydrates, proteins, amino acids, anthraquinone, aloe-emodin, and sitosterols. These metabolites attributed towards the pharmacological action in diabetes mellitus and other ailments.

Leaves of *Senna auriculata* (L.) Roxb. shows the presence of 3-o-methy-d glucose, alpha-tocopherol-beta-D-mannosidase, n-hexadecanoic acid, resorcinol, octadecenal and carboxylic acid. The seeds of *Senna auriculata* (L.) Roxb. reported with presence of fatty acids content are palmitic, oleic, and linoleic acids. The ethanolic seed extract showed the presence of benzoic acid, 2-hydroxyl methyl ester, glycine, n-(trifluoroacetyl), 1-methylbutyl ester, cupric acid ethyl ester, resorcinol, water-soluble galactomannan like beta-D-manopyranosyl-1(1-4)-o-beta-D-manopyranosyl (1-4)-o-beta-D-monopyranose. The reported metabolites have potential role in oxidative stress, microbial infections and inflammation related diseases.

Roots of *Senna auriculata* (L.) Roxb. shows the presence of anthraquinone glycosides such as 1,3-dihydroxy-2-methylanthraquinone, 1,8-dihydroxy-6-methoxy-2-methylanthraquinone-3-o-rutinoside, 1,8-dihydroxy-2-methylanthraquinone-3-o-rutinoside, flavone glycoside, and two leucoanthocyanins like leucocyanidin-3-o-

TABLE 1 | Metabolites of *Senna auriculata* (L.) Roxb.

S No.	Name of metabolites	Isolated from a plant part	References
1.	Emodin (1)	Leaves	Nageswara Rao et al. (2000)
2.	Di-(2-ethyl)-hexylphthalate (2)	Leaves	Nageswara Rao et al. (2000)
3.	Phytol (3)	Leaves	Senthilkumar and Vijayakumari (2012)
4.	<i>E</i> -10- pentadecenol (4)	Leaves	Senthilkumar and Vijayakumari (2012)
5.	Resorcinol (5)	Leaves	Senthilkumar and Vijayakumari (2012)
6.	3- <i>O</i> -methyl- <i>D</i> -glucose (6)	Leaves	Senthilkumar and Vijayakumari (2012), Anandan et al. (2011)
7.	1,14-tetradecanediol (7)	Leaves	Senthilkumar and Vijayakumari (2012)
8.	3,7,11,15- tetramethyl-2-hexadecen-1-ol (8)	Leaves	Senthilkumar and Vijayakumari (2012)
9.	Azulene (9)	Leaves	Senthilkumar and Vijayakumari (2012)
10.	1,2,3,5,6,7,8,8a-octahydro-1,4-dimethyl-7-(1-methylethenyl)	Leaves	Senthilkumar and Vijayakumari (2012)
11.	1,2- benzene dicarboxylic acid (10)	Leaves	Senthilkumar and Vijayakumari (2012)
12.	Diisooctyl ester	Leaves	Senthilkumar and Vijayakumari (2012)
13.	Squalene (11)	Leaves	Senthilkumar and Vijayakumari (2012)
14.	1-cyclohexylnonene (12)	Leaves	Senthilkumar and Vijayakumari (2012)
15.	1-4 - [(2- diethylamino) ethylamino[6-methyl-2-pyrimidinyl]-3-[3,4,5- trimethoxyphenyl] guanidine (13)	Leaves	Senthilkumar and Vijayakumari (2012)
16.	α -tocopherol- β - d -mannoside (14)	Leaves	Anandan et al. (2011)
17.	<i>n</i> -hexadecanoic acid (15)	Leaves	Anandan et al. (2011)
18.	13-octadecenal (16)	Leaves	Anandan et al. (2011)
19.	1,2,3,4-tetrahydroisoquinolin-6-ol-1-carboxylic acid (17)	Leaves	Anandan et al. (2011)
20.	Benzaldehyde (18)	Leaves	Anandan et al. (2011)
21.	1,6-anhydro- β - <i>D</i> -glucopyranose (19)	Leaves	Anandan et al. (2011)
22.	1,2-benzenedicarboxylic acid (20)	Leaves	Anandan et al. (2011)
23.	Bis (2-methylpropyl) ester	Leaves	Anandan et al. (2011)
24.	Benzenamine,2,3,4,5,6- pentamethyl (21)	Leaves	Anandan et al. (2011)
25.	13-oxabicyclo [10.1.0] tridecane (22)	Leaves	Anandan et al. (2011)
26.	1-tridecyne (23)	Leaves	Anandan et al. (2011)
27.	1- <i>E</i> ,11, <i>Z</i> -13-octadecatriene (24)	Leaves	Anandan et al. (2011)
28.	<i>a</i> -tocophero (25)	Leaves	Anandan et al. (2011)
29.	<i>N</i> -acetyl tyramine (26)	Leaves	Anandan et al. (2011)
30.	<i>n</i> -hexadecanoic acid (15)	Seed/Pod	Suresh et al. (2007), Raj et al. (2012), Puranik et al. (2011)
31.	Linoleic acid (27)	Seed/Pod	Suresh et al. (2007), Raj et al. (2012), Puranik et al. (2011)
32.	Oleic acid (28)	Seed/Pod	Suresh et al. (2007), Raj et al. (2012), Puranik et al. (2011)
32.	<i>E</i> , <i>Z</i> -1,3,12-nonadecatriene (29)	Seed/Pod	Suresh et al. (2007), Raj et al. (2012), Puranik et al. (2011)
34.	Stearic acid (30)	Seed/Pod	Suresh et al. (2007), Raj et al. (2012), Puranik et al. (2011)
35.	Benzoic acid (31)	Seed/Pod	Suresh et al. (2007), Raj et al. (2012), Puranik et al. (2011)
36.	2-hydroxyl-methyl ester (32)	Seed/Pod	Suresh et al. (2007), Raj et al. (2012), Puranik et al. (2011)
37.	β -ethoxypropionaldehyde diethyl acetal (33)	Seed/Pod	Suresh et al. (2007), Raj et al. (2012), Puranik et al. (2011)
38.	Ethyl caprylate (34)	Seed/Pod	Suresh et al. (2007), Raj et al. (2012), Puranik et al. (2011)
39.	2-methoxy-4-vinylphenol (35)	Seed/Pod	Suresh et al. (2007), Raj et al. (2012), Puranik et al. (2011)
40.	<i>N</i> -(trifluoroacetyl)-,1-methylbutyl ester	Seed/Pod	Suresh et al. (2007), Raj et al. (2012), Puranik et al. (2011)
41.	2,3-dihydro-3,5-dihydroxy-6-methyl- 4 <i>H</i> - pyran-4-one	Seed/Pod	Suresh et al. (2007), Raj et al. (2012), Puranik et al. (2011)
42.	Dodecanoic acid (36)	Seed/Pod	Suresh et al. (2007), Raj et al. (2012), Puranik et al. (2011)
43.	3'5'-dimethoxyacetophenone (37)	Seed/Pod	Suresh et al. (2007), Raj et al. (2012), Puranik et al. (2011)
44.	Palmitic acid (38)	Seed/Pod	Suresh et al. (2007), Raj et al. (2012), Puranik et al. (2011)
45.	β -monoglyceride (39)	Seed/Pod	Suresh et al. (2007), Raj et al. (2012), Puranik et al. (2011)
46.	α -tocopherol (25)	Seed/Pod	Suresh et al. (2007), Raj et al. (2012), Puranik et al. (2011)
47.	Stigmasta-5,23-dien-3-ol (40)	Seed/Pod	Suresh et al. (2007), Raj et al. (2012), Puranik et al. (2011)
48.	Epicatechin (41)	Seed/Pod	Suresh et al. (2007), Raj et al. (2012), Puranik et al. (2011)
49.	Procyanidin B1 (42)	Seed/Pod	Suresh et al. (2007), Raj et al. (2012), Puranik et al. (2011)
50.	Auriculataosides-A (43)	Seed/Pod	Wang et al. (2019)
51.	Auriculataosides- B (44)	Seed/Pod	Wang et al. (2019)
52.	Rumejaposides-E (45)	Seed/Pod	Wang et al. (2019)
53.	Rumejaposides-F (46)	Seed/Pod	Wang et al. (2019)
54.	5- <i>O</i> -methylquercetin-7- <i>O</i> -glucoside (47)	Flower	Manogaran and Sulochana (2004)
55.	Propanoic acid	Flower	Venkatachalam et al. (2013)
56.	Kaempferol-3- <i>O</i> -rutinoside (48)	Stem	Juan-Badaturuge et al. (2011), Habtemariam (2013)
57.	Rutin (49)	Stem	Juan-Badaturuge et al. (2011), Habtemariam, (2013)
58.	Kaempferol (50)	Stem	Juan-Badaturuge et al. (2011), Habtemariam (2013)
59.	Quercetin (51)	Stem	Juan-Badaturuge et al. (2011), Habtemariam (2013)
60.	Luteolin (52)	Stem	Juan-Badaturuge et al. (2011), Habtemariam (2013)
61.	Glycine, <i>N</i> -(trifluoroacetyl)-, 1-methylbutyl ester (53)	Stem	Juan-Badaturuge et al. (2011), Habtemariam (2013), Suresh et al. (2007), Raj et al. (2012), Puranik et al. (2011)

(Continued on following page)

TABLE 1 | (Continued) Metabolites of *Senna auriculata* (L.) Roxb.

S No.	Name of metabolites	Isolated from a plant part	References
62.	Leucopelargonidins (54)	Aerial Part	Juan-Badaturuge et al. (2011), Habtemariam (2013), Suresh et al. (2007), Raj et al. (2012), Puranik et al. (2011), Manogaran and Sulochana, (2004)
63.	Oleanolic acid (55)	Aerial Part	Juan-Badaturuge et al. (2011), Habtemariam (2013), Suresh et al. (2007), Raj et al. (2012), Puranik et al. (2011), Manogaran and Sulochana, (2004)
64.	Chrysophanol (56)	Aerial Part	Juan-Badaturuge et al. (2011), Habtemariam (2013), Suresh et al. (2007), Raj et al. (2012), Puranik et al. (2011), Manogaran and Sulochana, (2004)
65.	1,3-dihydroxy-2-methylanthraquinone (57)	Aerial Part	Juan-Badaturuge et al. (2011), Habtemariam (2013), Suresh et al. (2007), Raj et al. (2012), Puranik et al. (2011), Manogaran and Sulochana, (2004)
66.	1,2,3,4-Tetrahydroisoquinolin-6-ol-1-carboxylic acid (58)	Aerial Part	Juan-Badaturuge et al. (2011), Habtemariam (2013), Suresh et al. (2007), Raj et al. (2012), Puranik et al. (2011), Manogaran and Sulochana, (2004)
67.	d – glucopyranoside (59)	Aerial Part	Juan-Badaturuge et al. (2011), Habtemariam, (2013), Suresh et al. (2007), Raj et al. (2012), Puranik et al. (2011), Manogaran and Sulochana (2004)
68.	1,6,8-trihydroxy-3-methylanthraquinone (60)	Aerial Part	Juan-Badaturuge et al. (2011), Habtemariam (2013), Suresh et al. (2007), Raj et al. (2012), Puranik et al. (2011), Manogaran and Sulochana, (2004)
69.	1-cyclohexylnonene (61)	Aerial Part	Juan-Badaturuge et al. (2011), Habtemariam, (2013), Suresh et al. (2007), Raj et al. (2012), Puranik et al. (2011), Manogaran and Sulochana (2004)
70.	1,8-dihydroxy-3-methoxy-6-methylanthracene-9,10-dione (62)	Aerial Part	Juan-Badaturuge et al. (2011), Habtemariam, (2013), Suresh et al. (2007), Raj et al. (2012), Puranik et al. (2011), Manogaran and Sulochana (2004)
71.	1,14-tetradecanediol (63)	Aerial Part	Juan-Badaturuge et al. (2011), Habtemariam, (2013), Suresh et al. (2007), Raj et al. (2012), Puranik et al. (2011), Manogaran and Sulochana (2004)
72.	E -10-pentadecenol (64)	Aerial Part	Juan-Badaturuge et al. (2011), Habtemariam (2013), Suresh et al. (2007), Raj et al. (2012), Puranik et al. (2011), Manogaran and Sulochana (2004)
73.	3,7,11,15-tetramethyl-2-hexadecen-1-ol (65)	Aerial Part	Juan-Badaturuge et al. (2011), Habtemariam (2013), Suresh et al. (2007), Raj et al. (2012), Puranik et al. (2011), Manogaran and Sulochana (2004)
74.	Sitosterol (66)	Aerial Part	Juan-Badaturuge et al. (2011), Habtemariam (2013), Suresh et al. (2007), Raj et al. (2012), Puranik et al. (2011), Manogaran and Sulochana (2004)
75.	Di-(2-ethyl) hexylphthalate (67)	Aerial Part	Juan-Badaturuge et al. (2011), Habtemariam (2013), Suresh et al. (2007), Raj et al. (2012), Puranik et al. (2011), Manogaran and Sulochana (2004)

rhamnopyroside and leucopelonidin-3-o-1-rhamanopyroside. The list of reported metabolites is enlisted in **Table 1** and **Figures 3A,B**.

PHARMACOLOGICAL ACTIONS OF *SENNA AURICULATA* (L.) ROXB

Antidiabetic Activity

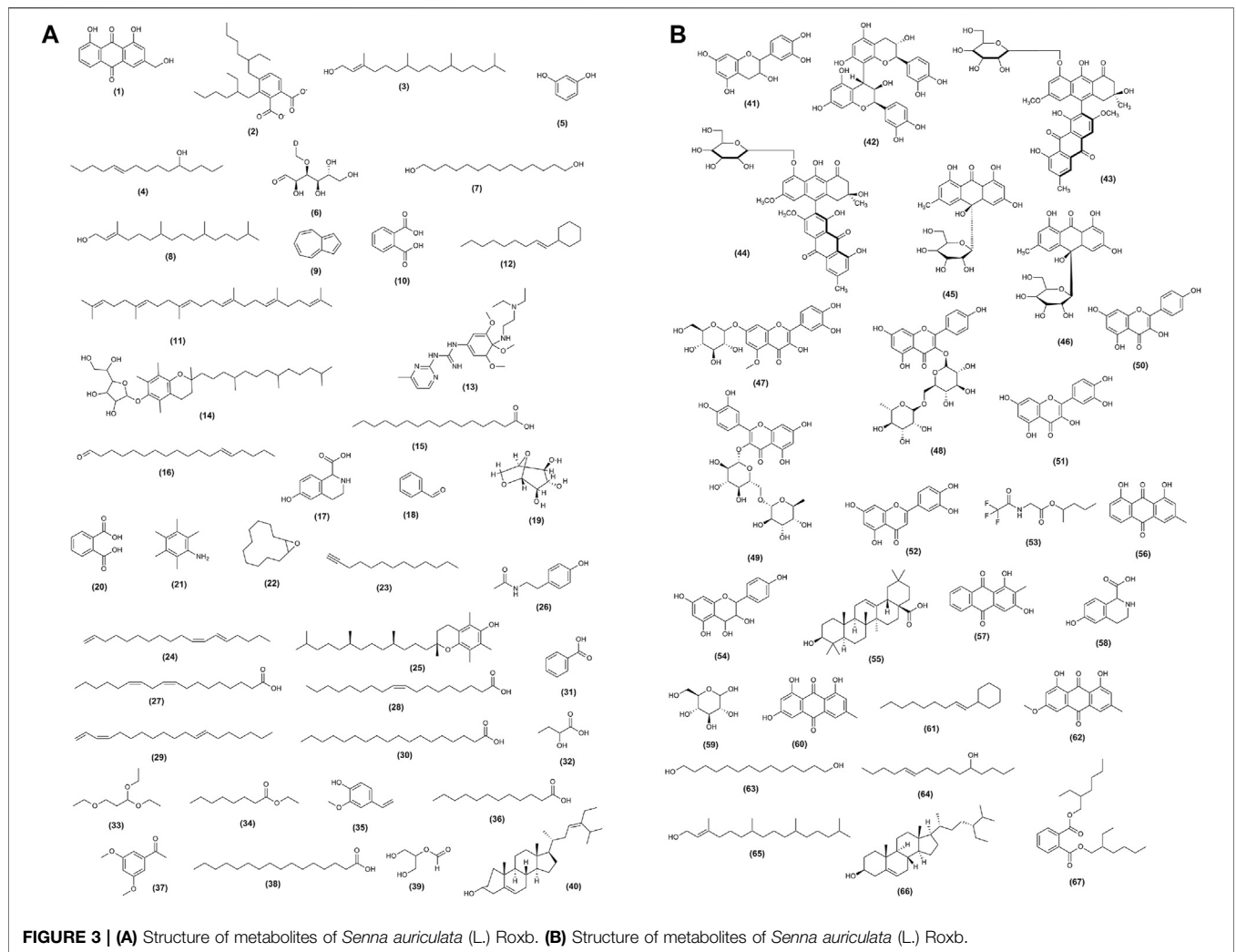
Antihyperglycemic Activity of Plant Parts of *Senna auriculata* (L.) Roxb

Leaves

Antihyperglycemic activity of *Senna auriculata* (L.) Roxb. leaves extract has experimentally been proven in different diabetic animal models (Rajagopal et al., 2003; Gupta et al., 2009a; Gupta et al., 2009b; Gupta et al., 2010). The aqueous extract

of leaves of *Senna auriculata* (L.) Roxb. is reported to reduce the blood glucose levels in STZ induced diabetic rats (Gupta et al., 2011). Further, Gupta et al. (2009c) reported the potential antihyperglycemic effects of STZ induced mild and severely diabetic rats on the administration of the aqueous extract of leaves in 400 mg/kg body weight dose for 3 weeks. The 13.9% and 17.4% reduction in fasting blood glucose was observed after 5 h of dose administration in mild and severely diabetic rats respectively. The ethanolic extract of *Senna auriculata* (L.) Roxb. leaf showed significant reduction of blood glucose ($p < 0.05$) at a dose of 150 mg/kg of body weight for 2 weeks in alloxan induced diabetic rats. The results were compared with a standard drug, glibenclamide (Mohan et al., 2011).

The leaves of *Senna auriculata* (L.) Roxb has various antidiabetic metabolites which are enlisted in **Table 1**. n-hexadecanoic acid, emodin (1,3,8-trihydroxy-6-methylanthracene-9,10-dione), and



squalene are evaluated for their antidiabetic potential and reported with their mechanistic pathways involved in the amelioration of diabetes (Wang et al., 2006; Wang et al., 2012; Liu et al., 2018; Tan et al., 2019). These metabolites might be responsible for the antihyperglycemic effects of leaves of *Senna auriculata* (L.) Roxb.

Flower

Aqueous extract of *Senna auriculata* (L.) Roxb. flower has shown promising antihyperglycemic activity in a dose 450 mg/kg body weight which found more significant than the doses of 150 and 300 mg/kg body weight. Similarly, the significant reduction in the urine sugar was found with aqueous extract of *Senna auriculata* (L.) Roxb. at doses of 150 and 300 mg/kg body weight whereas, at 450 mg/kg dose, sugar was absent in the urine of experimental diabetic rats. The result was more promising than glibenclamide-treated rats (Latha and Pari, 2003a; Latha and Pari, 2003b). Also, Jain and Sharma, (1997) reported the anti-diabetic potential of the aqueous flower extract of *Senna auriculata* (L.) Roxb.

The ethanol extract of *Senna auriculata* (L.) Roxb. flower possesses antidiabetic agents such as flavonoids and phenolic acids. The anti-diabetic activity of water-soluble fraction of

the ethanol extract was compared with aqueous extract of the flower where it was found that ethanol extract exhibited a more significant reduction in blood glucose level at a dose of 250 and 500 mg/kg of the body weight in alloxan-induced diabetic rats. The highly significant ($p < 0.001$) results of ethanol extract of the flower might be due to the metabolites present in the water-soluble fraction of the ethanolic extract (Hakkim et al., 2007). Similarly, it is observed that the ethanolic extract exhibits anti-diabetic activity and provides significant protection in streptozotocin-nicotinamide induced diabetic rats ($p < 0.05$) and the results were statistically significant in comparison to the standard glibenclamide (Nalla et al., 2012).

Jarald et al. (2010) performed an experimental study with various extracts of flowers of *Senna auriculata* (L.) Roxb. in alloxan-induced diabetic rats to check their anti-hyperglycemic activities. Amongst different extracts, the chloroform extract was reported to have more hypoglycemic effects followed by the water-soluble fraction of ethanolic extract and ethanolic extract. The results found comparable with the standard drug, glibenclamide.

Various active compounds from the flowers of *Senna auriculata* (L.) Roxb. have been isolated and their potential antidiabetic activity has been reported with experimental evidence. Venkatachalam et al. (2013) reported the presence of propanoic acid, 2-(3-acetoxy-4,4,14-trimethylandro-8-en-17-yl) as an active principle of the n-butanol fraction of hydromethanolic flower extract of *Senna auriculata* (L.) Roxb. Propanoic acid showed potential hypoglycemic effects both in the bioassay-guided study as well as *in vivo* study, due to its protein tyrosine phosphatase 1B (PTP 1B) inhibitory action. The isolated phytochemical compound exerted comparable result as that of standard drug, glibenclamide. Mishra et al. (2010) and Jyothi et al. (2012) have also demonstrated the anti-diabetic potential of flowers of *Senna auriculata* (L.) Roxb. Oleanolic acid, a natural triterpenoid present in the aerial part of *Senna auriculata* (L.) Roxb. (Manogaran and Sulochana, 2004; Suresh et al., 2007; Juan-Badaturuge et al., 2011; Puranik et al., 2011; Raj et al., 2012; Habtemariam, 2013) exhibited a significant blood-glucose-lowering and weight-losing activity in STZ-induced diabetic rats (Wang et al., 2011). Further, Gao et al. (2007) reported that oleanolic acid, when administered in a dosage of 100 and 200 mg/kg body weight/day, for 40 days, showed a significant hypoglycemic effect in STZ-induced diabetic rats.

Bark

The methanolic extract of *Senna auriculata* (L.) Roxb. bark found effective in lowering the blood glucose level. After the administration of the bark extract to diabetic rats, it was observed that the blood glucose level reduced with a deviation of 80.9% when compared that on first day (Shiradkar et al., 2011). Moreover, Daisy and Jeeva Kani (2012) demonstrated the potent anti-diabetic effect of the methanolic extract of *Senna auriculata* (L.) Roxb. bark. The result was compared with hexane, ethyl acetate, and aqueous extracts where methanolic bark extract was found to be more effective in diabetic rats. Juan-Badaturuge et al. (2011) and Habtemariam (2013) reported the presence of rutin, quercetin, and kaempferol in the extracts of bark of *Senna auriculata* (L.) Roxb. Rutin and kaempferol have been reported to exhibit antihyperglycaemic and antioxidant activity in STZ-induced diabetic rats (Kamalakkannan and Prince, 2006; Govindasamy, 2020). Besides, quercetin has also been reported for antihyperglycemic potential due to its pleiotropic mechanisms. It showed the enhancement of insulin sensitivity, promotion of glycogen synthesis, improvement in insulin resistance by promoting its sensitization, and stimulation of pancreatic β -cell proliferation (Salehi et al., 2020). Therefore, the metabolites present in the bark may contribute to the antihyperglycemic action of the bark of *Senna auriculata* (L.) Roxb.

Seed

Jain and Sharma (1967) reported the antidiabetic activity of the aqueous extract of seed of *Senna auriculata* (L.) Roxb. The hypoglycemic role of the ethanolic seed extract in alloxan-induced diabetic rats has been demonstrated at a dose of 400 mg/kg body weight where the result was comparable with that of the standard drug, gliclazide. Also, the urine sugar was

found absent in seed extract and gliclazide treated diabetic rats (Subramanian et al., 2011). Moreover, the ethanolic extract, aqueous extract, and petroleum ether fraction at a dose of 300 mg/kg body weight has reported for their significant ($p < 0.001$) blood-glucose-lowering activity in STZ-induced diabetic rats. The result was compared with the standard drug, metformin (250 mg/kg body weight) (Dama and Bhanoji Rao, 2011). Aruna and Roopa (2011) demonstrated the anti-diabetic potential of petroleum ether and ethyl acetate extract of *Senna auriculata* (L.) Roxb. seeds in alloxan-induced diabetic rats. It was found that both the extracts possess significant ($p < 0.05$) anti-diabetic activity when compared with the standard drug, tolbutamide (250 mg/kg body weight).

Seeds of *Senna auriculata* (L.) Roxb. is a rich source of antidiabetic metabolites like Linoleic acid, *n*-hexadecanoic acid, Oleic acid, Epicatechin, Procyanidin B1, Dodecanoic acid, Stearic acid, etc. (Suresh et al., 2007; Puranik et al., 2011; Raj et al., 2012). George et al. (2018) discussed the findings of Wu and colleagues' pooled analysis (Wu et al., 2017), where it is recommended to take increased dietary intake of linoleic acid-rich vegetable foods for the prevention of diabetes. Similarly, a higher intake of linoleic acid resulted in better glycemic control and improved insulin sensitivity (Belury et al., 2018). Further, oleic acid also accounted for the prevention of Type 2 Diabetes Mellitus, where it was observed that oleic acid might have some metformin-like effects (Palomer et al., 2018). The consumption of epicatechin, a natural flavonoid found in the seeds of *Senna auriculata* (L.) Roxb. has been reported to reduce blood glucose levels in diabetic patients (Abdulkhaleq et al., 2017). Furthermore, procyanidin B1 (PB1) has a significant hypoglycemic action. Li et al. (2021) investigated the interaction mechanisms of PB1 with protein tyrosine phosphatase-1B (PTP1B), where a binding affinity of PTP1B to PB1 resulted in down-regulation of the expression level of PTP1B in insulin-resistant HepG2 cells. Similarly, the oral administration of graded doses of dodecanoic acid (125, 250, and 500 mg/kg) significantly reduced the fasting blood glucose level in a dose-dependent manner in hyperglycemic rats (Alex et al., 2020). Tsuchiya et al. (2013) demonstrated the role of stearic acid as a potent PTP1B inhibitor *in vitro*. It is suggested that stearic acid may enhance insulin receptor signaling by inhibiting the PTP1B activity and promotes glucose uptake into adipocytes.

Although the preclinical data and pharmacological actions of various antidiabetic metabolites support each other, no clinical data is available so far. Further *in vivo* studies are expected to calibrate the antihyperglycemic role of several metabolites present in the seeds of *Senna auriculata* (L.) Roxb.

Root

Salma et al. (2021) demonstrated antihyperglycemic activity of methanolic extract of the root of *Senna auriculata* (L.) Roxb. in a high-fat diet-induced type 2 diabetes mellitus C57BL/6 mouse model. The methanolic extract (150 mg/kg body weight) could reduce the blood glucose level gradually in 8 weeks of the experiment. The results were similar when compared to a metformin-treated group of diabetic mice. The highest amount



FIGURE 4 | Pictorial presentation of different plant parts of *Senna auriculata* (L.) Roxb. and their anti-diabetic mode of actions.

of total polyphenols was present in the methanolic extract of root than its aqueous, ethanolic, and chloroform extracts. Further, the HPLC profile of polyphenols showed that coumaric acid is present in the methanolic extract of the root, which attributed to the antihyperglycemic activity of *Senna auriculata* (L.) Roxb. (Salma et al., 2021). The p-Coumaric acid, the most abundant isomer of Coumaric acid, displayed a substantial increase in the enzyme activity and improved the glucose consumption by the hepatic tissues when administered orally in STZ-induced diabetic rats. It normalizes disturbed glucose metabolism by decreasing hepatic glucose production through insulin release. Besides, it exhibited antihyperglycemic activity by protecting β -cells of the pancreas (Amalan et al., 2016). Thus, the methanolic extract of the root of *Senna auriculata* (L.) Roxb. may have strong antihyperglycemic effects due to the presence of coumaric acid.

Various antidiabetic metabolites present in the plant parts and their different extracts are responsible for the antihyperglycemic action. These metabolites may correct pathological changes, and further studies are needed to review their mode of action. The results were compared with available standard oral hypoglycemic agents and found significant at different levels. Altogether, all the botanical parts of *Senna auriculata* (L.) Roxb. exhibit antidiabetic activities and play a pivotal role in the correction of the

pathological mechanism by regulating the metabolic pathways, enzymatic activities, and gene expressions (Figure 4).

Insulinogenic Action

Various plant parts of *Senna auriculata* (L.) Roxb. have been reported to possess an insulinogenic action. The different extracts stimulate the insulin secretion by increasing the number of islets and β -cells and it is evidenced with the increased amount of C-peptide and histological pancreatic sections. The administration of the aqueous leaf extract of *Senna auriculata* (L.) Roxb. demonstrated the insulinogenic action in mildly and severely diabetic rats. The C-peptide level was also found increased. Pancreatic sections have confirmed the increased number of islets and β -cells. The result was similar to that of the standard drug, glibenclamide (Gupta et al., 2010).

The aqueous flower extract of *Senna auriculata* (L.) Roxb. exhibited the antihyperglycemic action by increasing the level of insulin in diabetic rats which resulted into the increased uptake of blood glucose by peripheral tissue (Pari et al., 2001). Furthermore, the water-soluble fraction of ethanolic extract of *Senna auriculata* (L.) Roxb. flower was found significantly effective ($p < 0.001$) than its aqueous extract ($p < 0.05$) in reducing the blood glucose due to its insulinogenic action in alloxan-induced diabetic rats (Hakkim et al., 2007). Kalaivani et al. (2008) reported the possibility of regeneration of β -cells in *Senna auriculata* (L.) Roxb. leaves and

flowers extracts administered diabetic rats. Moreover, oleanolic acid, an antidiabetic metabolite present in the aerial part of *Senna auriculata* (L.) Roxb. may directly improve insulin biosynthesis, secretion, and signaling by modulating the enzymes connected to insulin activities. It also protects the β -cells and preserves their functionality (Castellano et al., 2013). Similarly, Jyothi et al. (2012) reported the insulinogenic action of *Senna auriculata* (L.) Roxb. flowers.

To study insulin interaction in humans, erythrocytes have been used as a cellular model (Gambhir et al., 1978; DePirro et al., 1980; McElduff and Eastman, 1981; Ward and Harrison, 1986). Insulin binding is found to be decreased in diabetes mellitus (Kolterman et al., 1981; Olefsky and Kolterman, 1981). Pari et al. (2007) used the circulating erythrocytes to find out the insulin-receptor-binding effect of flower extract of *Senna auriculata* (L.) Roxb. in STZ-induced diabetic rats. It was found that the number of insulin receptors was increased on erythrocyte receptors membranes in STZ-induced diabetic control rats. The administration of flower extract resulted in increased total erythrocyte receptors membrane insulin binding sites as well as plasma insulin. *Senna auriculata* (L.) Roxb. flower extract stimulates insulin secretion and increases the number of insulin binding sites.

Senna auriculata (L.) Roxb. seed extract has also been reported to possess an insulinogenic action in alloxan-induced diabetic rats. The administration of seed extract resulted in increased insulin levels due to the activation of β -cells (Subramanian et al., 2011). Dodecanoic acid, also known as lauric acid, an antidiabetic metabolite, is present in the seed part of the *S. auriculata* (L.) Roxb. (Suresh et al., 2007; Puranik et al., 2011; Raj et al., 2012). Alex et al. (2020) reported that dodecanoic acid (250 and 500 mg/kg body weight) stimulated the pancreatic β -cells to synthesize and secrete the insulin to maintain glucose homeostasis in a high-fat diet/STZ-induced type 2 diabetic rat models. The methanolic extract of *Senna auriculata* (L.) Roxb. bark potentiated the levels of insulin and C-peptide in diabetic rats. The activated remnant β -cells found in histological sections of the pancreas (Daisy and Jeeva Kani, 2012). Mohan et al. (2011) also reported the insulinogenic action of ethanolic extract of *S. auriculata* (L.) Roxb. leaf by its insulin release stimulatory effect in alloxan-induced diabetic rats.

The various extracts of botanical parts of *Senna auriculata* (L.) Roxb. demonstrated insulinogenic action. It is due to an increased number of β -cells and regeneration and activation of remnant β -cells. Moreover, the increased level of plasma insulin is evidenced with raised C-peptide level, a part of proinsulin, and a measure of insulin secretion. The metabolites and their pleiotropic mechanisms should also be studied extensively through *in vitro* and *in vivo* studies to know the insulinogenic action of *Senna auriculata* (L.) Roxb.

Role in Carbohydrate Metabolism and Regulation of Enzymatic Activities

Liver and pancreas ailments hamper the biochemical pathways in the human body and cause deranged glucose metabolism. The liver and pancreas play a vital role in governing carbohydrate

metabolism. They maintain blood glucose and also regulate blood glucose supply to other organs.

Inhibition of Alpha-Amylase and Alpha-Glucosidase Enzymes

Starch and sucrose are the main components of carbohydrates. The enzyme alpha-amylase of saliva and pancreatic juice decomposes starch into oligosaccharides. The alpha-glucosidase enzyme catalyses the cleavage of glucose from disaccharides and oligosaccharides. Hence, the use of Alpha-glucosidase inhibitors is considered one of the effective treatments of diabetes mellitus as they retard digestion of both sucrose and starch.

The alpha-amylase inhibition activity of extract of bud and flowers of *Senna auriculata* (L.) Roxb. have been revealed where the bud extract showed higher inhibition activity compared to flower extract (Nambirajan et al., 2018). Also, the hydroalcoholic extract of aerial parts of *Senna auriculata* (L.) Roxb. showed the concentration-dependent alpha-amylase inhibition activity which found better than standard drug, acarbose (Mhetre et al., 2014).

The alpha-glucosidase enzyme plays a dominant role in the digestion of the sucrose and starch and its inhibition slows down the process of carbohydrate digestion. It is reported that *Senna auriculata* (L.) Roxb. bud extract and *Senna auriculata* (L.) Roxb. flower extract possess glucosidase inhibitory activity. The concentration of the bud and flower extracts shows a direct proportion to the inhibition of α glucosidase enzyme (Nambirajan et al., 2018). Alpha-glucosidase inhibitory activity of the hydroalcoholic extract of aerial parts of *Senna auriculata* (L.) Roxb. was found higher than the standard acarbose (Mhetre et al., 2014). Methanol extracts of dried flowers of *Senna auriculata* (L.) Roxb. were found to have a potential alpha-glucosidase inhibitory activity as compared to acarbose in rats. The ED₅₀ of the methanol extracts of dried flowers (4.9 mg/kg) exhibited the antihyperglycemic effect as potent as that of standard drug, acarbose (ED₅₀ 3.1 mg/kg) in maltose loaded Sprague Dawley Rats (Abesundara et al., 2004).

The metabolites present in the *Senna auriculata* (L.) Roxb. extracts of acetone, ethanol, and water indicated the presence of flavonoids, tannins, reducing sugar, and saponins. The active components of the extracts compete with the substrate for binding to the active site of the enzyme and prevent the breaking down of oligosaccharides to disaccharides. Kwon et al. (2007a) reported that natural alpha-glucosidase inhibitors from plants inhibit alpha-glucosidase activity and can be potentially used as a safe and effective therapy for postprandial hyperglycemia. Previous studies on alpha-amylase and alpha-glucosidase inhibitors isolated from medicinal plants suggest that several potential inhibitors belong to the flavonoid class, which has features of inhibiting alpha-amylase and alpha-glucosidase activities (Kwon et al., 2007b). *Senna auriculata* (L.) Roxb. is a rich source of flavonoids such as kaempferol-3-O-rutinoside, kaempferol and quercetin (Juan-Badaturge et al., 2011; Habtemariam, 2013). It was evident that kaempferol-3-O-rutinoside is a potent inhibitor of alpha-glucosidase *in vitro* and showed 8-fold activity than the standard drug, acarbose (Habtemariam, 2011).

Altogether, the effective inhibition of alpha-amylase and alpha-glucosidase might be due to the presence of enzyme inhibiting metabolites present in *Senna auriculata* (L.) Roxb. However, more *in vitro* and *in vivo* studies would be helpful to find out the pathways involved in the regulation of enzymatic activities.

Activation of Hexokinase

Enzymatic activity of hexokinase solely depends on insulin response and it is found affected in insulin-deficient diabetic rat liver (Gupta et al., 1997). *Senna auriculata* (L.) Roxb. is reported to play an important role in the activation of hexokinase in alloxan-induced diabetic rats which found resulted in increased glycolysis and glucose consumption for energy production (Krentz, 2003). The insulinogenic action of *Senna auriculata* (L.) Roxb. stimulates hexokinase activity which aids its role in glycolysis in all body tissues.

Inhibition of Glucose-6-Phosphatase and Fructose-1,6-Biphosphatase Enzymes

The role of Glucose-6-phosphatase and fructose-1,6-biphosphatase is also important in glucose homeostasis (Berg et al., 2001). These enzymes are known as gluconeogenic enzymes and insulin deficiency results in their activation in diabetes. It was found that the administration of *Senna auriculata* (L.) Roxb. effectively reduced the gluconeogenesis and resulted in decreased blood glucose level in diabetic rats. The augmented plasma insulin level by *Senna auriculata* (L.) Roxb. resulted in the reduced levels of glucose-6-phosphatase and fructose-1,6-biphosphatase enzymes in diabetic rats (Khader et al., 2017). Daisy and Jeeva Kani (2012) also reported the gluconeogenesis inhibitory action of *Senna auriculata* (L.) Roxb. bark extract.

Glycogen Synthesis

The healthy liver plays an important role in glycogen synthesis. It is the primary intracellular storage form of glucose and monitored by plasma insulin level and glycogen synthetase system (Garvey, 1992). The impaired capacity of the liver to synthesize glycogen was observed in diabetes due to lack of insulin. The dianthrone rich alcoholic flower extract of *Senna auriculata* (L.) Roxb. has demonstrated the increase in insulin secretion and activation of glycogen synthetase system which resulted in improved liver glycogen content (Khader et al., 2017).

Insulin deficiency in diabetes severely hampers the activities of glycolytic and gluconeogenic enzymes (Anderson and Stowring, 1973). Insulin is important for glucose uptake, phosphorylation of glucose and the glucose-6-phosphate entry into the pentose phosphate pathway in the liver (Ramachandran et al., 2003). The insulinogenic action of different extract of *Senna auriculata* (L.) Roxb. might be responsible for the modifications in enzymatic activities and reducing the blood glucose level (Kalaivani et al., 2008).

The flower extract of *Senna auriculata* (L.) Roxb. has also been reported for its salutary effect on hepatic enzymes involved in the carbohydrate mechanism. The flower extract (450 mg/kg body

weight) was found significant when compared with the standard drug, glibenclamide (600 µg/kg body weight) in increasing the hexokinase activity and decreasing the gluconeogenic enzyme activity in STZ-induced diabetic rats. The increased plasma insulin level in flower extract-fed diabetic rats was responsible for the modulation of hepatic carbohydrate metabolic enzymes (Latha and Pari, 2003a; Latha and Pari, 2003b).

The liver glycogen level and glycogen synthetase system depend on adequate plasma insulin level. The water-soluble fraction of ethanol extract of flower of *Senna auriculata* (L.) Roxb. significantly ($p < 0.001$) elevated the levels of hepatic glycogen and glycogen synthase due to its insulinogenic effects (Hakim et al., 2007). Similarly, glucokinase, one of the key enzymes in the liver, regulate the storage and disposal of glucose. The decreased enzymatic activity of glucokinase in STZ-induced diabetic rats was found elevated with *Senna auriculata* (L.) Roxb. bark extract treatment (Daisy and Jeeva Kani, 2012). Altogether, *Senna auriculata* (L.) Roxb. reveals its active role in the correction of the deranged carbohydrate metabolism by regulating the various enzymatic activities in the liver (Figure 5).

Regulation of Gene Expression in Liver

IRS-2 gene arbitrates insulin activity through the PI3K-Akt pathway in the liver (Eckstein et al., 2017). Also, IRS-2 plays a major role in suppressing gluconeogenesis and apoptosis (Valverde et al., 2004). It is found that mice lacking IRS-2 have a better chance to develop diabetes (Kubota et al., 2000). The failure in the expression of IRS-2 has observed in diabetic individuals (Gunton et al., 2005). Besides, IRS-2 gene inactivation in the human will result in peripheral insulin resistance and absence of β cell expansion which may cause hyperglycaemia, diabetes and death. Treatment with *Senna auriculata* (L.) Roxb. bud extract showed the upregulation of the IRS-2 gene expression in the liver (Nambirajan et al., 2018). Also, polyphenols from *Senna auriculata* (L.) Roxb. flowers were found able to enhance IRS-2, glucose transporters, and Akt gene expression in livers of T2DM rats (Mohd Fauzi et al., 2017) (Figure 6).

Hepatoprotective Action

The liver is a vital organ involved in the metabolism of food and drugs in the human body. The various toxicants and chemicals in the form of drugs and food result in different liver ailments. *Senna auriculata* (L.) Roxb. is used in liver diseases, in the traditional systems of Indian medicine. The folk claims have been validated with different experimental works. The various extracts from the leaves and root of *Senna auriculata* (L.) Roxb. are reported to exert a hepatoprotective role in oxidative stress-induced, ethanol and anti-tubercular-drug induced, hepatotoxicity in rats (Rajagopal et al., 2003; Jaydeokar et al., 2014), and D-galactosamine (D-GalN)-induced cytotoxicity in mouse hepatocytes (Nakamura et al., 2014). The hepatoprotective effects of methanolic extract of leaf and revertible histopathological changes in the carbon tetrachloride-induced liver damage in Wistar albino rats (Dhanasekaran and Ganapathy, 2011) have been documented. The drug

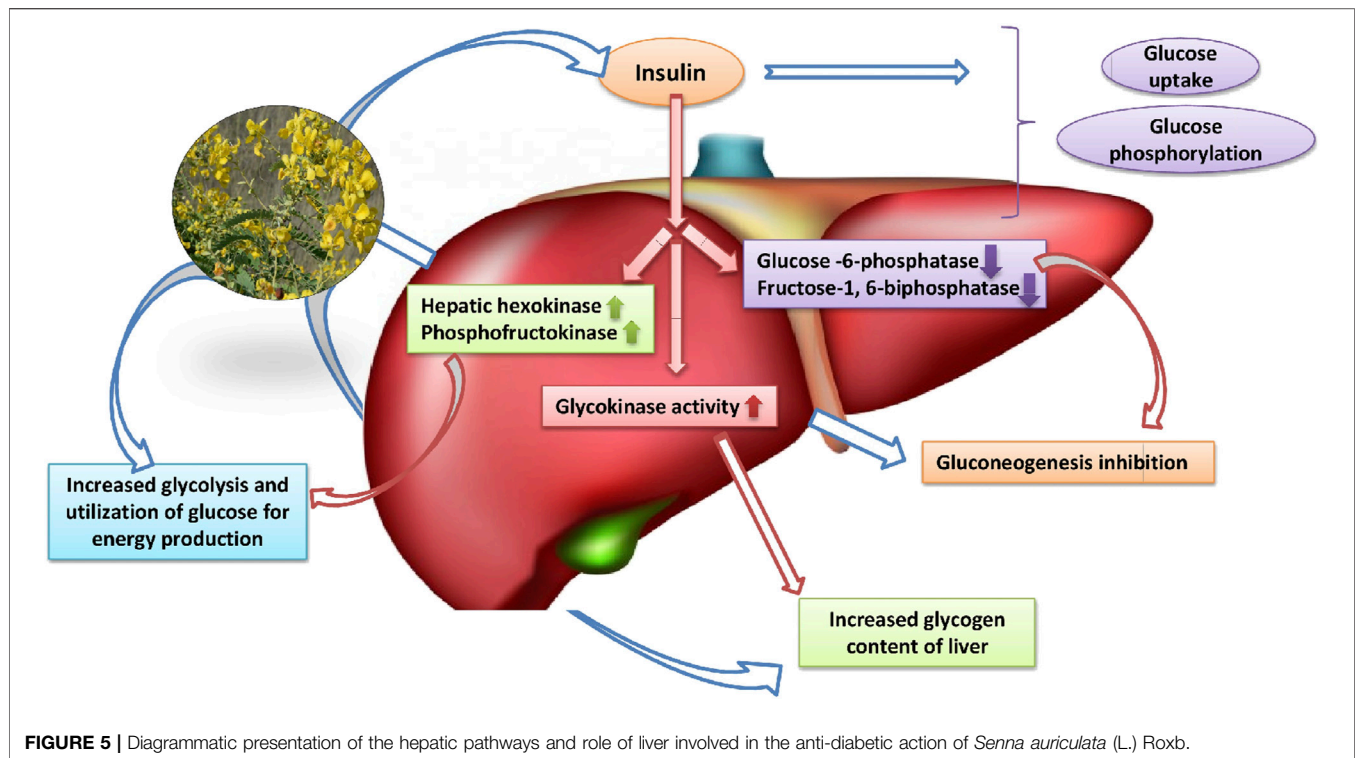


FIGURE 5 | Diagrammatic presentation of the hepatic pathways and role of liver involved in the anti-diabetic action of *Senna auriculata* (L.) Roxb.

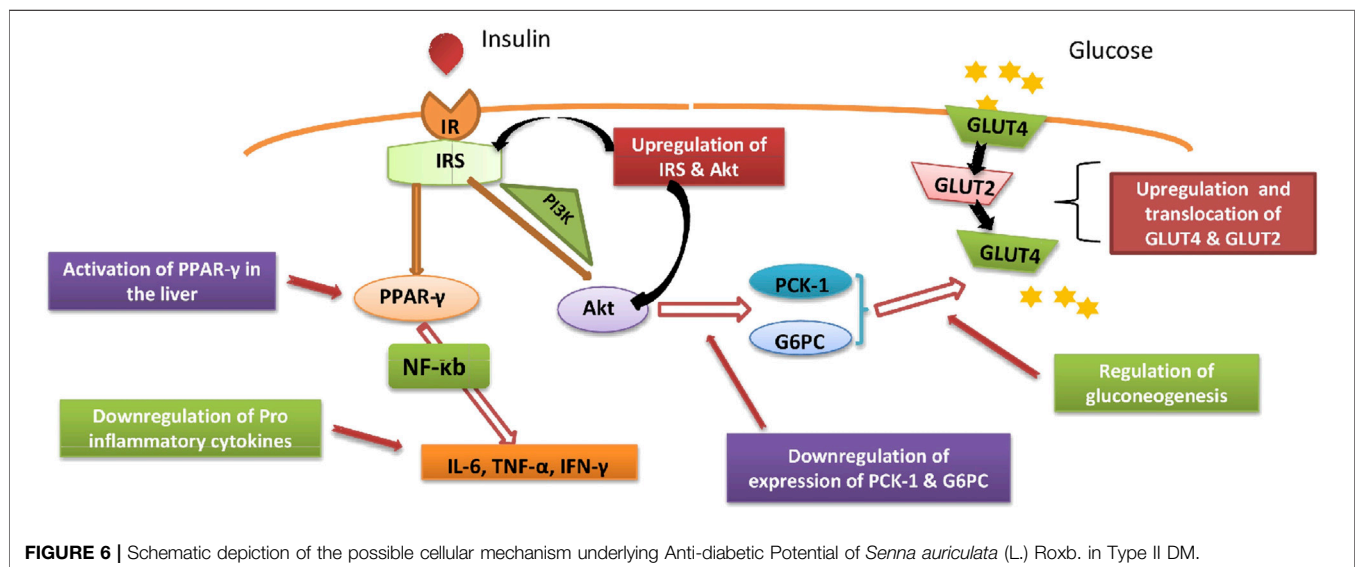


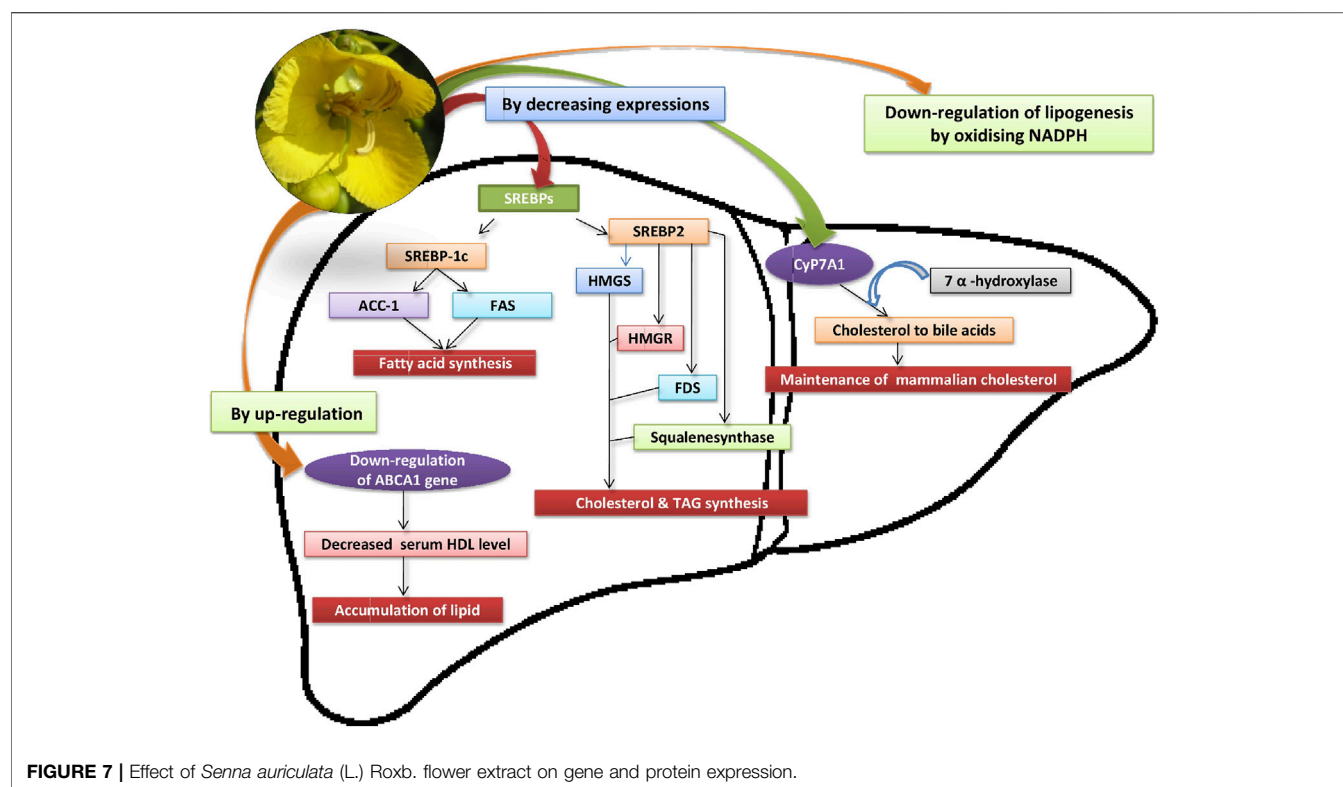
FIGURE 6 | Schematic depiction of the possible cellular mechanism underlying Anti-diabetic Potential of *Senna auriculata* (L.) Roxb. in Type II DM.

paracetamol-induced liver toxicity has also been found protected with the aqueous and methanolic extracts of the flowers of the *Senna auriculata* (L.) Roxb. (Chauhan et al., 2009).

The levels of AST and ALT were found raised in alloxan-induced diabetic rats. The oral administration of water-soluble fraction of ethanol extract of flower of *Senna auriculata* (L.) Roxb. could efficiently ($p < 0.001$) reduce the AST and ALT levels.

Further, the increased values of acid phosphatase (ACP) and alkaline phosphatase (ALP) in alloxan-induced diabetic rats were also declined with the administration of water-soluble fraction of ethanol extract (Hakim et al., 2007).

Taken together, these outcomes supports the traditional use of *Senna auriculata* (L.) Roxb. as a hepatoprotective agent. However, there is a need for clinical evidence to confirm and



validate the folklore claims, as human studies have not been performed so far.

Prophylactic Action on Pancreatitis

The aqueous leaf extract of *Senna auriculata* (L.) Roxb. demonstrated the prophylactic effect on ethanol-induced pancreatitis in a rat model. A significant reduction in the increased pancreatic enzymes such as serum α -amylase and lipase was observed at a dose of 400 mg/kg body weight. Histopathological studies also revealed normal findings in extract-treated rats (Gupta et al., 2016).

Antihyperlipidemic Action

Several phytochemical compounds have been isolated from different plant parts of *Senna auriculata* (L.) Roxb. The isolated compounds such as kaempferol-3-O-rutinoside, quercetin, rutin, and luteolin exhibit different pharmacological actions (Juan-Badaturuge et al., 2011). The antihyperlipidemic potential of crude extract and isolated compounds could be demonstrated by observing their pancreatic lipase inhibitory action. Among the isolated compounds from the aerial parts of *Senna auriculata* (L.) Roxb., kaempferol-3-O-rutinoside possesses most potential pancreatic lipase inhibitory action ($IC_{50} = 2.9 \pm 0.50$ mM) than that of rutin, luteolin and quercetin. Moreover, the crude extract of *Senna auriculata* (L.) Roxb. demonstrated inhibition of pancreatic lipase at IC_{50} of 6.0 ± 1.0 mg/ml (Juan-Badaturuge et al., 2011; Habtemariam, 2013). Oleanolic acid, a metabolite present in the aerial part of *Senna auriculata* (L.)

Roxb. (Juan-Badaturuge et al., 2011), when administered in the dosage of 100 and 200 mg/kg body weight/day for 40 days, showed improved lipid profile in STZ-induced diabetic rats (Gao et al., 2007). Similarly, Vijayaraj et al. (2013) also reported the antihyperlipidemic effects of different extracts of *Senna auriculata* (L.) Roxb.

The *Senna auriculata* (L.) Roxb. leaves extract exhibited hypolipidemic effects by reducing cholesterol, triglycerides and LDL levels and increasing the levels of HDL in diabetic rats. The atherogenic index was also found raised indicating the cardiovascular risk preventive role of *Senna auriculata* (L.) Roxb. (Gupta et al., 2009c). In another study, leaves extract of *Senna auriculata* (L.) Roxb. has shown its reversal effects on dyslipidemia and apolipoprotein B (Gupta et al., 2011).

Furthermore, the ethanolic extract of flowers of *Senna auriculata* (L.) Roxb. demonstrated antihyperlipidemic effects in Triton WR 1339 (300 mg/kg body weight) induced hyperlipidemia in male albino Wistar rats. The flower extract at dose 450 mg/kg body weight/day found more significant ($p < 0.001$) in reducing the total cholesterol, triglyceride, low-density lipoprotein (LDL) and very-low-density lipoprotein (VLDL) levels and increasing the levels of HDL than the standard drug, lovastatin. The antihyperlipidemic effects of ethanolic extract of *Senna auriculata* (L.) Roxb. flowers might be exhibited due to reduced cholesterol biosynthesis by HMG-CoA reductase inhibition in the liver or by up-regulation of LDL receptors in the liver which involve in hepatic cholesterol clearance (Oh et al., 2006; Vijayaraj et al., 2013).

Similarly, in another study, the expression levels of the key genes involved in the cholesterol metabolism were examined in Triton

WR-1339 induced hyperlipidemia in the male albino Wistar rats. It was found that the treatment with ethanol extract of *Senna auriculata* (L.) Roxb. flowers (300 mg/kg body weight) resulted in the reversal of altered protein and genes expression levels of HMGR, HMGs, SREBP-1c, ACC1, SREBP-2, CYP7A1, and ABCA1 to near-normal levels (Figure 7). The results were comparable with the standard drug, atorvastatin (Vijayakumar and Nachiappan, 2017).

Moreover, an aqueous extract of *Senna auriculata* (L.) Roxb. flower may also capable to oxidize the NADPH, a co-factor in the lipid metabolism. The increased activity of glucose-6-phosphatase reduces NADP⁺ to NADPH by providing H⁺ which is helpful in the fat synthesis from carbohydrates. The administration of flower extract reduced glucose-6-phosphatase activity and produced high NADP⁺ from NADPH which ultimately resulted in down-regulation of lipogenesis (Pari and Latha, 2002).

Hakkim et al. (2007) compared the antihyperlipidemic potential of both aqueous extract and a water-soluble fraction of ethanol extract of *Senna auriculata* (L.) Roxb. flowers in alloxan-induced diabetic rats. It was found that the ethanol extract was exhibited significant ($p < 0.001$) reduction in the increased levels of triglycerides and total cholesterol than aqueous extract ($p < 0.05$) in diabetic rats. The restricted cholesterologenesis and reduced fatty acid synthesis were possible involved mechanism with the extracts of *Senna auriculata* (L.) Roxb. flowers in lowering of total cholesterol and triglycerides level in diabetic rats.

The seed extract of *Senna auriculata* (L.) Roxb. was also demonstrated antilipidemic activity where the significant reduction in cholesterol, triglycerides, LDL and increase in the HDL levels were observed in alloxan-induced diabetic rats (Subramanian et al., 2011). Furthermore, different extracts of seed such as aqueous, ethanolic, and pet ether and chloroform fractions were also ameliorated the altered levels of cholesterol and triglycerides in STZ-induced diabetic rats (Dama and Bhanoji Rao, 2011). Although it possesses antihyperlipidemic action, the effect in humans should be studied extensively.

Antiatherosclerotic and Cardioprotective Action

The chronic diabetic state is often associated with cardiovascular risk development by atherosclerosis due to hypercholesterolemia, oxidative damage, activation of the inflammatory cascade and associated endothelial dysfunction and defective coagulation (Esterbauer et al., 1993; Dominiczak, 1998; Rask-Madsen and King, 2005). The oral administration of aqueous extract of *Senna auriculata* (L.) Roxb. leaves (400 mg/kg body weight) demonstrated potential anti-atherosclerotic action in STZ-induced diabetic rats. The extract suppressed lipid peroxidation and reduced the levels of oxidized LDL, soluble vascular cell adhesion molecule-1 and plasma fibrinogen. The increased serum nitric oxide level was also observed in extract-fed diabetic rats. It was also confirmed in histomorphological studies that the heart myocardium of extract-fed diabetic animals was showing normal morphology, whereas vacuolation was observed in the myocytes of the control diabetic rats (Gupta et al., 2011).

Lipid peroxidation inhibiting action, free radical scavenging activity, and anti-inflammatory action of different phytochemicals such as flavonoids, saponins, alkaloids and tannins etc. present in the aqueous extract of *Senna auriculata* (L.) Roxb. leaves may exhibit the significant anti-atherosclerotic and cardioprotective role in diabetic complications. For example, the leaves of *Senna auriculata* (L.) Roxb. is a rich source of squalene, a naturally occurring triterpenic hydrocarbon (Senthilkumar and Vijayakumari, 2012). Liu et al. (2018) demonstrated the effect of squalene on plasma and hepatic lipid levels of obese/diabetic KK-A^y mice and wild-type C57BL/6J mice. The administration of squalene was resulted in an increased HDL cholesterol level, an essential anti-atherosclerotic factor, while no significant difference was found in other lipid levels. Besides, the HDL level was found raised, especially in an obese/diabetes mouse model compared with normal mice. Hence, squalene may play a crucial role behind the anti-atherosclerotic and cardioprotective action of *Senna auriculata* (L.) Roxb. However, more research is needed to clarify the effect of extracts of leaves of *S. auriculata* (L.) Roxb. on the lipid metabolism and dynamics related to atherosclerosis. Overall, the different extracts of *Senna auriculata* (L.) Roxb. play an important role in the prevention of atherosclerosis due to their anti-hyperlipidemic effect (Pari et al., 2001). Only a few *in vivo* studies are available for the antiatherosclerotic effect of *Senna auriculata* (L.) Roxb. Besides, more preclinical and clinical studies should be conducted to validate its promising protective effect against atherosclerosis associated with metabolic diseases.

Antifertility Action

In the early stages of pregnancy, the embryo nutrition and prevention of early abortion depend on the proper secretion of estrogen from corpus lutea. The methanolic extract of *Senna auriculata* (L.) Roxb. bark has demonstrated significant antifertility activity in experimental rats at doses of 100 and 200 mg/kg body weight. The oral administration of methanolic bark extract was continued for 7 days during the estrous stage of experimental rats. After dissecting the pregnant rats on day 10, it was observed that the number of corpus lutea reduced significantly, and there was an increased number of resorptions in the extract-fed rats. The effects were dose-dependent, where the extract at a dose of 200 mg/kg showed 100% antifertility activity. *Senna auriculata* (L.) Roxb. possesses potential antifertility activity, which may exhibit due to its antiestrogenic action (Shiradkar et al., 2011). The extract of the bark of *Senna auriculata* (L.) Roxb. is reported to have flavonoids such as luteolin, kaempferol, and quercetin (Juan-Badaturge et al., 2011; Habtemariam, 2013). Lu et al. (2012) reported luteolin, kaempferol, and quercetin as inhibitors of estrogen biosynthesis *in vivo*. Further studies are required to investigate the role of metabolites present in different extracts of *Senna auriculata* (L.) Roxb. for its antiestrogenic and antifertility activity.

Cytotoxic Activity

The various isolated compounds and extracts of medicinal plants have been reported for their anticancer effects and may act as novel chemopreventive agents in the management of various

types of cancer (Aruna and Sivaramakrishnan, 1990; Graham et al., 2000; Moongkarndi et al., 2004). Many phytochemical compounds having anti-cancer effects such as flavonoids, procyanidins and triterpene glycosides have reported to be present in different parts of the *Senna auriculata* (L.) Roxb. plant and been isolated and evaluated for their cytotoxic actions (Ye et al., 1999; Sanghi et al., 2000; Nakamura et al., 2003; Kumaran and Karunakaran, 2007). An isolated compound, 4-(4-chlorobenzyl)-2,3,4,5,6,7-hexahydro-7-(2ethoxyphenyl)benzo[h][1,4,7]triazecin-8(1H)-one, from *Senna auriculata* (L.) Roxb. leaves has demonstrated cytotoxic effects on human colon cancer cell line HCT 15 and induced apoptosis mediated cell death. The cytotoxicity of the isolated compound was due to its high lipophilicity resulted in the loss of membrane integrity of the cancer cells. The compound was also found to cause membrane disintegration and it was confirmed with the significant release of lactate dehydrogenase (LDH) from damaged cell membrane as a result of its apoptosis (Esakkirajan et al., 2014). Similarly, Prasanna et al. (2009) reported the anti-cancer activity of ethanolic extract of *Senna auriculata* (L.) Roxb. leaves in human breast adenocarcinoma MCF-7 and human larynx carcinoma Hep-2 cell lines. The extract exhibited a dose-dependent anti-cancer activity with IC₅₀ values of 400 µg in MCF-7 cells and 500 µg in Hep-2 cells. The inhibition of the growth of extract-treated MCF-7 and Hep-2 cell lines was observed due to nuclear fragmentation and condensation followed by apoptosis mediated inhibition of the proliferation of both the cells. In the same way, another isolated compound, 3-O-beta-D-xylopyranosides (triterpene glycosides), form *C. dahirica* (Tian et al., 2006), which also found present in *Senna auriculata* (L.) Roxb. (Sanghi et al., 2000) and *Actaea asiatica* (Gao et al., 2006), showed anti-cancer activity against HepG2 cell, and hepatoma cells (Tian et al., 2006), and MCF-7 cell line (Gao et al., 2006).

However, very few studies were undertaken to establish the cytotoxic effect of *Senna auriculata* (L.) Roxb., due to which it is pretty early to come to any conclusion for its therapeutic implications in cancer patients.

Immunomodulatory Effect

The flower extract from *Senna auriculata* (L.) Roxb. showed significant immunomodulatory effect in aged rats. The administration of extract in aged rats at different doses was found to activate T cell immunity with increased T and B cell percentage accompanied by an enhanced proliferation of splenocytes in both resting and LPS-stimulated cells. The increased number of T cells was further supported by observing the elevated counts of CD4⁺, CD8⁺, and CD25⁺ regulatory cells. Furthermore, the supplementation of polyphenols decreased ROS production by neutrophils in response to phorbol myristate acetate (PMA) and *Escherichia coli* activation that could conceivably harm multiple biological systems in aged individuals (John et al., 2011).

Rutin, the major metabolite present in flower extract of *Senna auriculata* (L.) Roxb. possesses therapeutic activity and shows potential as analgesic, anti-inflammatory, organ-

transplantation, and anticancer effects. A report indicated the protective effect of rutin on humoral and cellular immunity in rat model and caused a significant elevation in antibody titer and total antibody levels (Ganeshpurkar et al., 2017). Thus, we can propose the possible role of rutin and other polyphenols present in *Senna auriculata* (L.) Roxb. as immunomodulatory agent.

Nephroprotective Activity

The nephroprotective activity of ethanolic extract of *Senna auriculata* (L.) Roxb. root was evaluated in cisplatin- and gentamicin-induced renal injury in experimental rats. It was observed that the root extract reduced elevated levels of blood urea and serum creatinine effectively at a dosage of 300 and 600 mg/kg body weight in the cisplatin model and a dose of 600 mg/kg body weight in the gentamicin model (Annie et al., 2005). The ethanolic root extract could demonstrate the nephroprotective activity in cisplatin- and gentamicin-induced renal injury in male albino rats due to its antioxidant and nitric oxide free-radical-scavenging effects.

Antipyretic Activity

The fraction of ethanolic extract of *Senna auriculata* (L.) Roxb. leaves and flowers, at doses ranging from 250 to 600 mg/kg body weight, showed significant antipyretic activity in yeast-induced pyrexia in experimental rats. The effects were comparable to that of a standard drug, aspirin (Vedavathy and Rao, 1991).

Antiviral Activity

The antiviral activity of methanolic extract of flowers of *Senna auriculata* (L.) Roxb. was investigated in different cell lines, such as HeLa, Vero, Crandell Reus feline kidney (CRFK), and HEL cell cultures. The methanolic flower extract showed the strongest antiviral activity against herpes simplex-1 and 2, and moderate activity against vaccinia, vesicular stomatitis, coxsackie, respiratory syncytial, feline corona, feline herpes, parainfluenza, reo-1, sindbis, and puntatoro viruses (Arthanari et al., 2013). The methanolic extract of *Senna auriculata* (L.) Roxb. flowers could be a vital source of anti-herpetic compounds possessing antiviral activity against the double-stranded DNA enveloped Herpes simplex virus (HSV -1 and 2).

Anthelmintic Activity

The anthelmintic activity of methanolic and ethanolic extract of *Senna auriculata* (L.) Roxb. leaves against earthworm was investigated at the dose level of 20, 40, 60 mg/ml. The standard anthelmintic albendazole was used to compare the results. All the extracts showed the concentration-dependent anthelmintic property. *Senna auriculata* (L.) Roxb. leaves exhibited significant effects ($p < 0.05$) at the tested concentrations (20, 40, and 60 mg/ml) as determined by the paralysis and death time. Among all extracts, methanolic extract (40 and 60 mg/ml) was reported its efficacy at par in causing paralysis and death of earthworm at all concentrations (Chaudhary and Kumar, 2014). The anthelmintic property of *Senna auriculata* (L.) Roxb. may be attributed to the metabolites

especially tannins and phenolic compounds. Tannins act by binding to free protein in the gastrointestinal tract of the host or glycoprotein on the cuticle of the parasite and phenolic compounds by uncoupling oxidative phosphorylation hinder the energy production in helminth parasites (Sreejith, et al., 2013; Athnasiadou, et al., 2001). Further, *in vivo* and *in vitro* studies are needed to determine the role of metabolites present in different extracts of *Senna auriculata* (L.) Roxb. and to verify the anthelmintic activity.

Anti-Melanogenesis Activity

Wang et al. (2019) studied the effect of *Senna auriculata* (L.) Roxb. in the inhibition of melanogenesis in B16 melanoma 4A5 cells. The presence of auriculataosides A and B (phlegmacin-type anthracenone dimer glycosides) in *Senna auriculata* (L.) Roxb. indicated in inhibition of microphthalmia-associated transcription factor, tyrosinase, tyrosinase-related protein (TRP)-1, and TRP-2 protein expression. The methanolic extract in the concentration range of 1–100 µg/ml exhibited significant inhibition of melanogenesis. These dimer glycosides were isolated from the methanolic fraction, and their inhibitory activity were detected in the dose range of 0.03–0.3 µM.

Antioxidant Activity

The various studies suggested the potency of *Senna auriculata* (L.) Roxb. as antioxidant agents in several assays such as ferric reducing antioxidant power (FRAP), 1,1-diphenyl-2-picrylhydrazyl (DPPH) free radical scavenging, hydroxyl radical scavenging, phosphomolybdenum reducing power, β-carotene bleaching assay, hydrogen peroxide radical scavenging, metal chelating activity, and deoxyribose degradation (Kolar et al., 2018). The antioxidant property of the *Senna auriculata* (L.) Roxb. measured by FRAP and DPPH assay was highest in flower extracts i.e. 161.5 mg AAE/g.

The methanolic and ethanolic extract of *Senna auriculata* (L.) Roxb. has potential free radical scavenging action in both 2,2'-azinobis-(3-ethylbenzothiazoline-6-sulfonic acid) (ABTS) and 1,1-diphenyl-2-picrylhydrazyl (DPPH) assays (Kumaran and Karunakaran, 2007). Jeyashanthi and Ashok (2010) studied that flower extract of *Senna auriculata* (L.) Roxb. significantly lowers the TBARS (thiobarbituric acid reactive substances), hydrogen peroxide, and conjugated dienes and exert a potential antioxidant activity. The extracts also increase the important antioxidant enzymes like glutathione, catalase, superoxide dismutase, ascorbic acid, and vitamin E level in rats (Jeyashanthi and Ashok, 2010). The treatment with the leaf extract of *Senna auriculata* (L.) Roxb. at 400 mg/kg exhibited significant decrease in serum levels of oxidized low-density lipoprotein (Ox LDL) and TBARS (Gupta et al., 2009c). The alcoholic extract of the aerial part of *Senna auriculata* (L.) Roxb. exhibited potent antioxidant activity when assessed by DPPH radical scavenging, lipid peroxidation, and reducing power analysis (Juan-Badaturge et al., 2011).

The phosphomolybdenum assay involves the reduction of Mo (VI) to Mo (V) in the presence of antioxidant compound and subsequent formation of a green phosphate Mo (V) complex at acidic pH. The flower extracts (63.8 mg AAE/g)

showed higher antioxidant activity of *Senna auriculata* (L.) Roxb. The highest ferrous ion chelating activity (90.05%) is reported in the extracts of flowers of *Senna auriculata* (L.) Roxb. (Kolar et al., 2018).

Oxidative stress is the main etiology behind many diseases and the antioxidant potential of *Senna auriculata* (L.) Roxb. along with above reported studies, supports its medicinal use in diabetes like metabolic diseases. The presence of polyphenols like rutin and kaempferol might be responsible for its free radical scavenging activity. Hence, these scientific evidence propose the possible therapeutic benefits of *Senna auriculata* (L.) Roxb. in various diseases.

Antimutagenic Activity

The antimutagenic activity of ethyl acetate extract of *Senna auriculata* (L.) Roxb. in cyclophosphamide induced chromosomal damage in bone marrow cells of albino mice was studied by Panigrahy et al. (2011). At dose level of 100 and 200 mg/kg, it provides a significant protection ($p < 0.05$) against chromosomal aberration due to presence of flavonoids in ethyl acetate extract.

The concentration-dependent inhibitory effect of the methanolic extract of *Senna auriculata* (L.) Roxb. bark on the mutagenicity of Acridine orange (AO) was studied at the concentration of 2.3, 11.4 and 22.8 µM. The probable mechanism of antimutagenic activity of methanolic extract of *Senna auriculata* (L.) Roxb. bark, could be due to presence of excellent scavengers of reactive oxygen species (ROS) like singlet oxygen and/or superoxide anion radical which play a central role in multistage mutagenesis and carcinogenesis (EFSA Scientific Committee, 2011; Deshpande et al., 2013a; Deshpande et al., 2013b).

Antimicrobial Activity

Senna auriculata (L.) Roxb. exhibited the antimicrobial activity against *Escherichia coli*, *Salmonella typhi*, *Proteus mirabilis*, and *Klebsiella pneumoniae*. The studies on the antibacterial activity of alcoholic and aqueous extracts of flower of *Senna auriculata* (L.) Roxb. were demonstrated by using *Staphylococcus aureus*, *Enterococcus faecalis*, *Bacillus subtilis*, *Salmonella typhi*, *Salmonella paratyphi A*, *Escherichia coli*, *Proteus mirabilis*, *Pseudomonas aeruginosa*, *Klebsiella pneumoniae*, *Vibrio cholerae*, and *Shigella dysenteriae*. The maximum activity was observed against all organisms except *Pseudomonas aeruginosa* and *Klebsiella pneumoniae*. The minimum inhibitory concentration ranged between 12.5 and 75 mg/ml depending on micro-organism and various extract. This study confirmed the antimicrobial activity of flower extract of *Senna auriculata* (L.) Roxb. and reported that it exhibits significant broad-spectrum activity against *Bacillus subtilis* and *Staphylococcus aureus* (Perumalsamy and Ignacimuthu, 2000).

Another study was performed to evaluate the antimicrobial activity of aerial parts of *Senna auriculata* (L.) Roxb. The chloroform extract of *Senna auriculata* (L.) Roxb. were shown to possess an antimicrobial activity against 2 g positive and 2 g-negative human pathogenic bacteria, viz. *Bacillus subtilis*,

Staphylococcus aureus, *Pseudomonas aeruginosa*, *Escherichia coli* and fungus cultures such as *Candida albicans* and *Aspergillus niger*. The extract showed antibacterial activity at all concentrations selected, but only the extract with the concentration of 300 µg/ml showed maximum antibacterial activity against all the organisms except *Pseudomonas aeruginosa* which were comparable with the standard control, amikacin. The antifungal activity of chloroform extract of *Senna auriculata* (L.) Roxb. revealed significant effect against *Candida albicans* and *Aspergillus niger* with the net inhibition zone of 14 and 14 mm, respectively, at 300 µg/ml concentration, which is almost comparable with standard control, ketoconazole used as an antifungal agent (Raja et al., 2013; Gharge et al., 2017).

The saponins rich fraction of roots of *Senna auriculata* (L.) Roxb. was evaluated for antimicrobial activity against *P. vesicularis*, *Streptococcus faecalis*, *Aeromonas hydrophilia*, *Salmonella typhae*, *Staphylococcus cohnii*, *Serratia ficaria*, and *E. coli* at concentration of 12.5, 25, 37.5 and 50 mg/ml. Antimicrobial activity of *Senna auriculata* (L.) Roxb. was carried out by well diffusion method. The result indicates the saponins rich fraction of roots of *Senna auriculata* (L.) Roxb. might be exploited as natural drug for the treatment of several infectious diseases caused by these organisms (Deshpande et al., 2013a; Deshpande et al., 2013b).

Further, Win and Min (2018) evaluated the antimicrobial activities of chloroform, acetone, methanol, ethyl acetate, and ethanol extracts of leaves of *Senna auriculata* (L.) Roxb. by using the agar-well diffusion method. The acetone extract exhibited maximum antimicrobial activity against *Pseudomonas aeruginosa*, *Bacillus pumalis*, and *Escherichia coli*, whereas the ethanol extract showed more antimicrobial activities against *Bacillus subtilis* and *Candida albicans*.

Thus, above data suggested that plant possess a good antimicrobial activity against various strains of pathogenic bacteria and fungus. The ethno-pharmacological utility of *Senna auriculata* (L.) Roxb. has been proven by cited studies but future prospects about the identification of active metabolites for the same is highly suggested, as their mechanism of action will determine its further therapeutic implications.

Anti-Ulcer Activity

The anti-ulcer activity of methanolic extract of *Senna auriculata* (L.) Roxb. leaves (300 mg/kg body weight) was evaluated against pylorus ligation induced gastric ulcers, and the results were compared with the standard drug famotidine (10 mg/kg body weight) (Ahmed et al., 2010). It was observed that the *Senna auriculata* (L.) Roxb. leaf extract decreased the number of ulcers in pyloric ligated rats with a significant reduction in the gastric volume, free and total acidity, and ulcerative index.

Anti-Inflammatory Activity

Mali et al. (2012) reported the role of *Senna auriculata* (L.) Roxb. leaf extracts viz. methanolic, ethyl acetate aqueous, and hydroalcoholic extracts in inflammation by using carrageenan

induced paw edema. The highest inhibitory action in inflammation was exerted by methanolic extract. The methanolic extract showed significant anti-inflammatory potential at 6 h with percentage inhibition of 37% at 250 mg/kg and 31.63% at 500 mg/kg. This effect was attributed due to presence of alkaloids, flavonoids, tannins, and steroids. The ethyl acetate extract of *Senna auriculata* (L.) Roxb. at 250 & 500 mg/kg showed significant activity in second phase of inflammation induced by carrageenan with percentage inhibition of 34.16 and 30.79% respectively. The aqueous extract of *Senna auriculata* (L.) Roxb. (250 & 500 mg/kg) showed significant activity at 6 h with percentage inhibition of 31.06 and 30.62% respectively. The hydroalcoholic extract of *Senna auriculata* (L.) Roxb. in 250 & 500 mg/kg exerted significant activity at 6 h with percentage inhibition of 23.73 and 30.95% respectively. The standard indomethacin showed significant activity maximum at 6 h with percentage inhibition of 42.56%.

The presence of polyphenols in flower viz. rutin is responsible for the suppression of pro-inflammatory mediator's release and expression of the inflammatory proteins such as adhesion molecules, COX, and NOS (Lilian et al., 1998; Habtemariam and Belai, 2018). Hence, the anti-inflammatory potential of *Senna auriculata* (L.) Roxb. has been proven its traditional uses in inflammation and needs further studies involving clinical subjects for its scientific and regulatory approval.

HERBAL DRUG-DRUG INTERACTIONS

The concurrent use of an herbal tea prepared from the flowers of the *Senna auriculata* (L.) Roxb. and theophylline performed a significant drug interaction. Their concurrent administration resulted in an increased steady-state level (32.5%) of drug theophylline (Thabrew et al., 2004). Similarly, they have also reported the potential drug interaction between *Senna auriculata* (L.) Roxb. tea and antiepileptic drug carbamazepine in experimental rats. The concurrent administration of herbal tea and carbamazepine in rats elevated (47.1%) the blood levels of the carbamazepine significantly than the levels in animals treated with carbamazepine alone. Therefore, the patients who have advised theophylline or carbamazepine should avoid the concurrent use of herbal tea prepared from *Senna auriculata* (L.) Roxb. flowers to influence the bioavailability of theophylline.

Puranik et al. (2011) reported safety pharmacology and pharmacokinetic herb-drug interaction studies of a hydro-alcoholic and supercritical extract of *Senna auriculata* (L.) Roxb. with metformin. Both these extracts were found safe at tested doses. However, the co-administration of technology-based supercritical extract (1,000 mg/kg) and metformin showed a significant decline (60%) in the absorption of metformin. The traditionally prepared hydro-alcoholic extract did not show any change in the pharmacokinetics of metformin. Furthermore, Elango et al. (2015) demonstrated the pharmacodynamic and pharmacokinetic interactions on

TABLE 2 | List of formulations in which *Senna auriculata* (L.) Roxb. is used as principal ingredient.

Sr. No.	Name of formulation	Ingredients	Indications	References
	Diasulin	<i>Senna auriculata</i> (L.) Roxb., <i>Curcuma longa</i> Linn., <i>Gymnema sylvestre</i> R. Br., <i>Coccinia indica</i> W. & A., <i>Momordica charantia</i> Linn., <i>Scoparia dulcis</i> Linn., <i>Syzygium cumini</i> Linn., <i>Trigonella foenumgraecum</i> Linn., <i>Tinospora cordifolia</i> Willd Miers.	Diabetes mellitus	Srivastava et al. (2012), Saravanan and Pari (2005)
2.	Sugnil	<i>Aristolochia bracteata</i> Retz., <i>Shorea roxburghii</i> G. Don, <i>Senna auriculata</i> (L.) Roxb., <i>Casearia esculanta</i> Roxb., <i>Coscinium fenestratum</i> (Gaertn) Colebr, <i>Curcuma longa</i> Linn., <i>Eugenia jambolana</i> Lam., <i>Gymnema sylvestre</i> R. Br., Triphala (three myrobalans)	Microvascular complications in Diabetes mellitus	Karthikeyan et al. (2011a), Karthikeyan et al. (2011b).
3.	Kalpa herbal tea	<i>Senna auriculata</i> (L.) Roxb.	Diabetes mellitus	Nille et al. (2016a)
4.	Avarai panchanga choornam	Equal quantities of fruits, leaves, roots, flowers, and bark of <i>Senna auriculata</i> (L.) Roxb.	Diabetes mellitus, Obesity	Latha and Pari, (2003a), Latha and Pari (2003b)
5.	Avarai kudineer	<i>Senna auriculata</i> (L.) Roxb., <i>C. fistula</i> Linn., <i>Syzygium cumini</i> Linn., <i>Olax scandens</i> Roxb., <i>Saussurea lappa</i> C.B. Clarke, <i>Terminalia arjuna</i> Roxb., <i>Cyperus rotundus</i> Linn.	Diabetes mellitus, Microbial and fungal infection	Rajalakshmi et al. (2018), Kumar et al. (2019), Prakash et al. (2014)
6.	Talapotaka churna	<i>Senna auriculata</i> (L.) Roxb., <i>Emblica officinalis</i> Gaertn, <i>Berberis aristata</i> DC., <i>Curcuma longa</i> Linn.	Diabetes mellitus, Obesity	Nille et al. (2016b)
7.	Avaram Poo	<i>Senna auriculata</i> (L.) Roxb. flower water extract	Diabetes mellitus	Sankhari (2019)
8.	Diazen	<i>Gymnema sylvestre</i> R. Br., <i>Momordica charantia</i> Linn, <i>Eugenia jambolana</i> Lam., <i>Tinospora cordifolia</i> Willd Miers, <i>Trigonella foenumgraecum</i> Linn., <i>Withania somnifera</i> Linn., <i>Senna auriculata</i> (L.) Roxb., <i>Aegle marmelos</i> Corr., <i>Azadirachta indica</i> A. Juss, <i>Curcuma longa</i> Linn.	Diabetes mellitus	Mishra and Mishra (2012)
9.	Hyponidd	<i>Pterocarpus marsupium</i> Roxb., <i>Gymnema sylvestre</i> R. Br., <i>Syzygium cumini</i> Linn., <i>Momordica charantia</i> Linn., <i>Enicostemma littorale</i> Blume, <i>Emblica officinale</i> Gaertn, <i>Curcuma longa</i> Linn., <i>Melia azadirachta</i> Linn., <i>Tinospora cordifolia</i> Willd Miers, <i>Senna auriculata</i> (L.) Roxb., Trivang Bhasma and Shilajit.	Diabetes mellitus, Polycystic ovarian syndrome	Poongothai et al. (2002), Babu and Stanely Mainzen Prince (2004)
10.	Dia Sakthi	<i>Centella asiatica</i> Linn., <i>Curcuma longa</i> Linn., <i>Senna auriculata</i> (L.) Roxb., <i>Phyllanthus amarus</i> Schumacher & Thonn., <i>Tinospora cordifolia</i> Willd Miers, <i>Syzygium cumini</i> Linn., Abrega Chendooram, Linga Chendooram, Triphala Chooma	Diabetes mellitus	Nille and Reddy (2015)
11.	Dianex	<i>Aegle marmelos</i> Corr., <i>Gymnema sylvestre</i> R. Br., <i>Eugenia jambolana</i> Lam., <i>Momordica charantia</i> Linn., <i>Azadirachta indica</i> A. Juss, <i>Senna auriculata</i> (L.) Roxb., <i>Withania somnifera</i> Linn., <i>Curcuma longa</i> Linn.	Diabetes mellitus	Mutalik et al. (2003), Mutalik et al. (2005), Sudha et al. (2005)
12.	Diakyur	<i>Senna auriculata</i> (L.) Roxb., <i>Cassia javanica</i> Linn., <i>Gymnema sylvestre</i> R. Br., <i>Mucuna pruriens</i> Linn., <i>Salacia reticulata</i> Linn., <i>Syzygium cumini</i> Linn., <i>Terminalia arjuna</i> Roxb.	Diabetes mellitus	Joshi et al. (2007)
13.	Diamed	<i>Azadirachta indica</i> A. Juss, <i>Senna auriculata</i> (L.) Roxb., <i>Momordica charantia</i> Linn.	Diabetes mellitus	Pari et al. (2001)
14.	Mersina	<i>Gymnema sylvestre</i> R. Br., <i>Momordica charantia</i> Linn., <i>Syzygium cumini</i> Linn., <i>Phyllanthus emblica</i> Linn., <i>Trigonella foenumgraecum</i> Linn., <i>Coccinia indica</i> W. & A., <i>Tinospora cordifolia</i> Willd Miers, <i>Melia azadirachta</i> , Javakhar, <i>Senna auriculata</i> (L.) Roxb.	Diabetes mellitus	Belemkar and Veeranjanyulu (2009)
15.	Byesukar	<i>Senna auriculata</i> (L.) Roxb., <i>Eugenia jambolana</i> Lam., <i>Thespesia populnea</i> Soland ex Correa	Diabetes mellitus	Guruvayoorappan and Sudha (2008)
16.	Diabkil	<i>Azadirachta indica</i> A. Juss, <i>Momordica charantia</i> Linn., <i>Tinospora cordifolia</i> Willd Miers, <i>Senna auriculata</i> (L.) Roxb., <i>Curcuma longa</i> Linn., <i>Terminalia arjuna</i> Roxb., <i>Piper nigrum</i> Linn., Shilajit, <i>Chlorophytum borivilianum</i> Sant., <i>Trigonella foenumgraecum</i> Linn., <i>Gymnema sylvestre</i> R. Br.	Diabetes mellitus	Grover and Bafna (2013)

co-administration of metformin and aqueous extract of *Senna auriculata* (L.) Roxb. leaves. The reduced dose of metformin (45 mg/kg) when combined with *Senna auriculata* (L.) Roxb. leaf extract (500 mg/kg) exhibited a similar blood-glucose-lowering effect of metformin (90 mg/kg) alone.

Further studies are needed to discover the possible pharmacodynamic and pharmacokinetic interactions between *Senna auriculata* (L.) Roxb. and various oral hypoglycemic agents to avoid serious adverse events in diabetic patients upon their concurrent use.

FORMULATIONS OF *SENNA AURICULATA* (L.) ROXB

Senna auriculata (L.) Roxb. is one of the main ingredients of many Ayurvedic and Siddha formulations available in the market. These formulations are commonly being used in diabetes, hyperlipidemia, obesity, and diabetic-associated co-morbidities. The formulations available in the market are enlisted in **Table 2**.

Toxicity Profile of *Senna auriculata* (L.) Roxb

Sabu and Subburaju (2002) carried out an acute toxicity study on aqueous extract of *Senna auriculata* (L.) Roxb. (leaf) on normal healthy albino Wistar rats at different doses (500, 1,000, 2,000, 5,000 mg/kg body weight). They showed that the extract did not produce any mortality up to the highest dose tested i.e. 5,000 mg/kg body weight. Also, animals did not exhibit any toxic signs like restlessness, respiratory depression, convulsion or coma.

In an acute toxicity study on albino Wistar male rats using ethanol extract of *Senna auriculata* (L.) Roxb. root suspended in acacia up to a dose 3,000 mg/kg body weight per oral observed that the alcoholic extract of *Senna auriculata* (L.) Roxb. did not produce any significant changes in the autonomic or behavioral changes including death during the observation period (Annie et al., 2005). Deshpande et al. (2013a) also carried out an acute toxicity study (OECD 423 guideline) at different dose levels of 5, 50, 300, and 2,000 mg/kg of ethyl acetate extract of roots of *Senna auriculata* (L.) Roxb. The rats did not show any toxic effects as well as any significant variation in their behavior. Acute toxicity studies of ethanol and aqueous extract of *Senna auriculata* (L.) Roxb. flowers on healthy adult male albino rats at a dose of 100, 500, 1,000, and 3,000 mg/kg body weight indicated the non-toxic nature of extracts in terms of mortality (Hakim et al., 2007).

Gupta et al. (2009a) studied the toxicity of aqueous extract of *Senna auriculata* (L.) Roxb. leaves at a dose of 1,000 and 2,000 mg/kg body weight per oral once a daily for 3 weeks. The rats treated with 1,000 and 2,000 mg/kg doses of extract did not show any drug-induced physical signs of toxicity during the complete experimental period and no mortality was noted.

CLINICAL STUDIES

Nille et al. (2018) evaluated the antidiabetic potential of *Talapotaka churna* (4g TID), a polyherbal formulation containing *Senna auriculata* (L.) Roxb. as a major ingredient, in Type II Diabetes Mellitus patients. The results were compared with the standard drug, glimepiride (1 mg BD). In the 2 months of the clinical trial, *Talapotaka churna* improved the symptoms of diabetes such as polyurea, polyphagia, and polydipsia with effective reduction ($p < 0.05$) in fasting and postprandial blood glucose levels. Further, a significant ($p < 0.01$) improvement was reported in disturbed biochemical parameters such as serum creatinine, SGOT, SGPT, and lipid profile.

Similarly, the aqueous extract of *Senna auriculata* (L.) Roxb. flowers demonstrated a potential anti-hyperglycemic effect in

pre-diagnosed type-2 diabetes mellitus subjects. A significant result ($p < 0.001$) was observed in 30 days of oral administration of flower extract with the effective reduction in fasting as well as postprandial blood glucose level (Sankhari, 2019).

Very little clinical data is available, and further extensive clinical studies are needed to support the experimental outcomes of *in vivo* studies and propose the antidiabetic potential of *Senna auriculata* (L.) Roxb. in human participants.

PERSPECTIVES AND FUTURE DIRECTIONS

The present review provides comprehensive data, relevant ethnomedicinal uses, details of metabolites, pharmacological activities of crude and various extracts along with pure compounds, marketed formulations, and its safety profile. Investigations on extracts and metabolites of *Senna auriculata* (L.) Roxb. provides a scientific evidences to explore the clinical implications as antidiabetic, antioxidant, anti-inflammatory, antihyperlipidemic, hepatoprotective, nephroprotective, cardioprotective, anti-atherosclerotic, anticancer, antimutagenic, antimicrobial, antiulcer, antipyretic, anthelmintic, immunomodulatory, antifertility, and anti-melanogenesis potentials with different underlying signaling pathways. The biological potential and mechanisms of action of many metabolites are need to be scientifically investigated for their molecular modes of action and bioactivities. It could provide a lead for further advancement into therapeutics. Well-organized, well-designed, and multicentric clinical studies should be warranted to evaluate the clinical efficacy and safety of the standardized extracts of *Senna auriculata* (L.) Roxb. carrying pharmacologically active metabolites. There are limited data from clinical reports on diabetes and associated complications. Based on available evidence data, it is advised that *Senna auriculata* (L.) Roxb. could be used as an adjunct to the current therapy for diabetes and other metabolic disorders.

CONCLUSION

Though the available experimental evidence insinuates the therapeutic potential of *Senna auriculata* (L.) Roxb., to date, it's an unexploited plant species in clinical practice. The reason is the scattered experimental data and scarcity of clinical evidence. The present review focuses on addressing the safe pharmacological actions of *Senna auriculata* (L.) Roxb. on multiple pathways involved in the pathogenesis of diabetes and various other diseases, which also indulges its ethnomedicinal uses in diabetes mellitus. Also, the extensive animal studies involved different extracts of all the botanical parts of *Senna auriculata* (L.) Roxb., which provides the limelight for the traditional claims and its medicinal uses in various ailments in folkloric practices. The metabolites present in the *Senna auriculata* (L.) Roxb. provide an ultimate scope for its wide acceptance in the scientific community to discover and

produce synthetic molecules as an adjunct to the current therapy in NCDs. Its commercial cultivation and safety pharmacology aspects will contribute to the national economy and would be helpful to reduce the burden of NCDs with its medicinal uses.

REFERENCES

- Abdulkhaleq, L. A., Assi, M. A., Noor, M. H. M., Abdullah, R., Saad, M. Z., and Taufiq-Yap, Y. H. (2017). Therapeutic Uses of Epicatechin in Diabetes and Cancer. *Vet. World*. 10 (8), 869–872. doi:10.14202/vetworld.2017.869-872
- Abesundara, K. J., Matsui, T., and Matsumoto, K. (2004). Alpha-Glucosidase Inhibitory Activity of Some Sri Lanka Plant Extracts, One of Which, *Cassia auriculata*, Exerts a Strong Antihyperglycemic Effect in Rats Comparable to the Therapeutic Drug Acarbose. *J. Agric. Food Chem.* 52 (9), 2541–2545. doi:10.1021/jf035330s
- Ahmed, M. F., Thayyil, H., Rasheed, A. S., and Ibrahim, M. (2010). Anti-Ulcer Activity of *Cassia auriculata* Leaf Extract. *Pharmacognosy J.* 2 (16), 53–57. doi:10.1016/S0975-3575(10)80050-1
- Alex, E. A., Dubo, A. B., Ejiogu, D. C., Iyomo, K. W., Jerome, K. V., Aisha, N. D., et al. (2020). Evaluation of Oral Administration of Lauric Acid Supplement on Fasting Blood Glucose Level and Pancreatic Histomorphological Studies in High Fat Diet/Streptozotocin-Induced Type 2 Diabetic Male Wistar Rats. *J. Diab Metab.* 1 (11), 849–857. doi:10.35248/2155-6156.20.11.84
- Amalan, V., Vijayakumar, N., Indumathi, D., and Ramakrishnan, A. (2016). Antidiabetic and Antihyperlipidemic Activity of p-Coumaric Acid in Diabetic Rats, Role of Pancreatic GLUT 2: *In Vivo* Approach. *Biomed. Pharmacother.* 84 (84), 230–236. doi:10.1016/j.biopha.2016.09.039
- Anandan, A., Eswaran, R., Doss, A., Sangeetha, G., and Anand, S. P. (2011). Chemical Compounds Investigation of *Cassia auriculata* Leaves- A Potential Folklore Medicinal Plant. *Bull. Environ. Pharmacol. Life Sci.* 1 (1), 20–23.
- Anderson, J. W., and Stowring, L. (1973). Glycolytic and Gluconeogenic Enzyme Activities in Renal Cortex of Diabetic Rats. *Am. J. Physiol.* 224 (4), 930–936. doi:10.1152/ajplegacy.1973.224.4.930
- Annie, S., Rajagopal, P. L., and Malini, S. (2005). Effect of *Cassia auriculata* Linn. Root Extract on Cisplatin and Gentamicin-Induced Renal Injury. *Phytomedicine* 12 (8), 555–560. doi:10.1016/j.phymed.2003.11.010
- Artharani, S., Vanitha, J., Krishnaswami, V., Renukadevi, P., Deivasigamani, K., and De Clercq, E. (2013). *In Vitro* Antiviral and Cytotoxic Screening of Methanolic Extract of *Cassia auriculata* Flowers in HeLa, Vero, CRFK and HEL Cell Lines. *Drug Invention Today* 5 (1), 28–31. doi:10.1016/j.dit.2013.03.001
- Aruna, K., and Sivaramakrishnan, V. M. (1990). Plant Products as Protective Agents against Cancer. *Indian J. Exp. Biol.* 28 (11), 1008–1011.
- Aruna, P., and Roopa, K. (2011). Evaluation of Antidiabetic Activity of *Cassia auriculata* Linn Seeds for Alloxan Induced Diabetes in Rats. *J. Pharm. Res.* 1 (1), 30–33.
- Athnasiadou, S., Kyriazakis, I., Jackson, F., and Coop, R. L. (2001). Direct Anthelmintic Effects of Condensed Tannins Towards Different Gastrointestinal Nematodes of Sheep: *In Vitro* and *In Vivo* Studies. *Vet. Parasitol.* 99 (3), 205–219. doi:10.1016/S0304-4017(01)00467-8
- Babu, P. S., and Stanely Mainzen Prince, P. (2004). Antihyperglycaemic and Antioxidant Effect of Hyponid, an Ayurvedic Herbomineral Formulation in Streptozotocin-Induced Diabetic Rats. *J. Pharm. Pharmacol.* 56 (11), 1435–1442. doi:10.1211/0022357044607
- Belemkar, S., and Veeranjanyulu, A. (2009). Toxicological Studies on Ayurvedic Formulation Mersina in Albino Rats. *Arch. Pharm. Sci. Res.* 1 (2), 130–137.
- Belury, M. A., Cole, R. M., Snoko, D. B., Banh, T., and Angelotti, A. (2018). Linoleic Acid, Glycemic Control and Type 2 Diabetes. *Prostaglandins Leukot. Essent. Fatty Acids*. 132, 30–33. doi:10.1016/j.plefa.2018.03.001
- Berg, J. M., Tymoczko, J. L., and Stryer, L. (2001). “Glycolysis and Gluconeogenesis,” in *Biochemistry*, Editors J. M. Berg, J. L. Tymoczko, and L. Stryer (New York: WH Freeman and Company), 425–464.
- Castellano, J. M., Guinda, A., Delgado, T., Rada, M., and Cayuela, J. A. (2013). Biochemical Basis of the Antidiabetic Activity of Oleoanolic Acid and Related Pentacyclic Triterpenes. *Diabetes* 62 (6), 1791–1799. doi:10.2337/db12-1215
- Chaudhary, S., and Kumar, A. (2014). Phytochemical Analysis and Assessment of *In-Vitro* Anthelmintic Activity of *Cassia auriculata* Linn. *Am. J. Phytomedicine Clin. Therap.* 2, 161–167.
- Chauhan, K. N., Patel, M. B., Valera, H. R., Patil, S. D., and Surana, S. J. (2009). Hepatoprotective Activity of Flowers of *Cassia Auriculata* R. Br. Against Paracetamol Induced Liver Injury. *J. Nat. Remedies* 9 (1), 85–90. doi:10.18311/jnr/2009/226
- Daisy, P., and Jeeva Kani, F. G. (2012). Evaluation of Antidiabetic Activity of Various Extracts of *Cassia Auriculata* linn. Bark on Streptozotocin- Induced Diabetic Wistar Rats. *Int. J. Pharm. Pharm. Sci.* 4 (4), 312–318.
- Dama, G. Y., and Bhanoji Rao, M. E. (2011). Anti-Diabetic Activity of *Cassia auriculata* (Linn) wall, Seeds on Streptozotocin Induced Diabetic Rats. *Deccan J. Nat. Prod.* 2 (3), 36–51.
- DePirro, R., Fusco, A., Lauro, R., Testa, I., Ferreti, F., and DeMartini, C. (1980). Erythrocyte Insulin Receptors in Non-Insulin-Dependent Diabetes Mellitus. *Diabetes* 29, 96–99. doi:10.1007/s12038-008-0022-y
- Deshpande, S., Kewatkar, S., and Paithankar, V. (2013a). Antimicrobial Activity of Saponins Rich Fraction of *Cassia auriculata* Linn against Various Microbial Strains. *Int. Curr. Pharm. J.* 2 (4), 85–87. doi:10.3329/icpj.v2i4.14056
- Deshpande, S. S., Kewatkar, S. M., and Paithankar, V. V. (2013b). Anticlastogenic Activity of Flavonoid Rich Extract of *Cassia auriculata* Linn. On Experimental Animal [Corrected]. *Indian J. Pharmacol.* 45 (2), 184–186. doi:10.4103/0253-7613.108314
- Dhanasekar, J. J., and Ganapathy, M. (2010). Hepatoprotective Effect of *Cassia auriculata* L. Leaf Extract on Carbon Tetrachloride Intoxicated Liver Damage in Wistar Albino Rats. *Asian J. Biochem.* 6 (1), 104–112. doi:10.3923/ajb.2011.104.112
- Dominiczak, M. H. (1998). Hyperlipidaemia and Cardiovascular Disease. *Curr. Opin. Lipidol.* 9, 609–611. doi:10.1097/00041433-199812000-00015
- Duraipandiyar, V., Ayyanar, M., and Ignacimuthu, S. (2006). Antimicrobial Activity of Some Ethnomedicinal Plants Used by Paliyar Tribe from Tamil Nadu, India. *BMC Complement. Altern. Med.* 6, 35. doi:10.1186/1472-6882-6-35
- Eckstein, S. S., Weigert, C., and Lehmann, R. (2017). Divergent Roles of IRS (Insulin Receptor Substrate) 1 and 2 in Liver and Skeletal Muscle. *Curr. Med. Chem.* 24 (17), 1827–1852. doi:10.2174/0929867324666170426142826
- EFSA Scientific Committee (2011). Draft Scientific Opinion on Genotoxicity Testing Strategies Applicable in Food and Feed Safety Assessment. Available at: <http://www.efsa.europa.eu>
- Elango, H., Ponnusankar, S., and Sundaram, S. (2015). Assessment of Pharmacodynamic and Pharmacokinetic Interaction of Aqueous Extract of *Cassia auriculata* L. and Metformin in Rats. *Pharmacogn Mag.* 11 (3), S423–S426. doi:10.4103/0973-1296.168986
- Esakkirajan, M., Prabhu, N. M., Arulvasu, C., Beulaja, M., Manikandan, R., Thiagarajan, R., et al. (2014). Anti-Proliferative Effect of a Compound Isolated From *Cassia auriculata* against Human Colon Cancer Cell Line HCT 15. *Spectrochim Acta A. Mol. Biomol. Spectrosc.* 120, 462–466. doi:10.1016/j.saa.2013.09.102
- Esterbauer, H., Wäg, G., and Puhl, H. (1993). Lipid Peroxidation and its Role in Atherosclerosis. *Br. Med. Bull.* 49, 566–576. doi:10.1093/oxfordjournals.bmb.a072631
- Evans, W. C. (1996). *Trease and Evans' Pharmacognosy*. 14th Edn. Orlando, FL: Harcourt Brace and Company Asia Pvt. Ltd, 235.
- Gambhir, K. K., Archer, J. A., and Bradley, C. J. (1978). Characteristics of Human Erythrocyte Insulin Receptors. *Diabetes* 27, 701–708. doi:10.2337/diab.27.7.701
- Ganeshpurkar, A., Saluja, A., and Saluja, A. K. (2017). The Pharmacological Potential of Rutin. *Saudi Pharm. J.* 25, 149–164. doi:10.1016/j.jsps.2016.04.025
- Gao, D., Li, Q., Li, Y., Liu, Z., Liu, Z., Fan, Y., et al. (2007). Antidiabetic Potential of Oleoanolic Acid From *Ligustrum Lucidum* Ait. *Can. J. Physiol. Pharmacol.* 85 (11), 1076–1083. doi:10.1139/Y07-098

AUTHOR CONTRIBUTIONS

SM and GN worked on literature search, wrote and edited the manuscript while AC and KR gave ideas and proof-read the manuscript.

- Gao, J., Huang, F., Zhang, J., Zhu, G., Yang, M., and Xiao, P. (2006). Cytotoxic Cycloartane Triterpene Saponins From *Actaea asiatica*. *J. Nat. Prod.* 69 (10), 1500–1502. doi:10.1021/np060113h
- Garvey, W. T. (1992). Glucose Transport and NIDDM. *Diabetes Care* 15 (3), 396–417. doi:10.2337/diacare.15.3.396
- George, H., Catherine, C., and Grant, S. (2018). Linoleic Acid and Diabetes Prevention. *Lancet Diabetes Endocrinol.* 6 (1), 12–13. doi:10.1016/s2213-8587(17)30404-7
- Gharge, V. G., Shelar, P. A., Ghadge, D. M., Patil, A. A., Bhandwalkar, O. S., and Yadav, A. V. (2017). Pharmacognostical, Phytochemical and Antimicrobial Studies of Leaves. *Rese. Jour. Pharmac. Phytoch.* 9 (2), 87–94. doi:10.5958/0975-4385.2017.00016.4
- Govindasamy, C. (2020). Kaempferol, a Flavonoid, Ameliorates Hyperglycemia by Attenuating the Key Enzymes of Carbohydrate Metabolism in Streptozotocin-Induced Experimental Diabetic Rats. *Progr Nutr.* 21 (2-S), 65–72. doi:10.23751/pn.v21i2-S.6329
- Graham, J. G., Quinn, M. L., Fabricant, D. S., and Farnsworth, N. R. (2000). Plants Used against Cancer - An Extension of the Work of Jonathan Hartwell. *J. Ethnopharmacol.* 73, 347–377. doi:10.1016/s0378-8741(00)00341-x
- Grover, N., and Bafna, P. (2013). Protective Effect of Co-administration of *Cassia Auriculata* and Pioglitazone in Diabetic Rats. *Eur. J. Exp. Biol.* 3 (2), 231–241.
- Gunton, J. E., Kulkarni, R. N., Yim, S., Okada, T., Hawthorne, W. J., Tseng, Y. H., et al. (2005). Loss of ARNT/HIF1 β Mediates Altered Gene Expression and Pancreatic-Islet Dysfunction in Human Type 2 Diabetes. *Cell* 122 (3), 337–349. doi:10.1016/j.cell.2005.05.027
- Gupta, A. K., and Sharma, M. (2007). *Reviews on Indian Medicinal Plants*. 2nd Edn. New Delhi, India: Medicinal Plants Unit ICMR, 620.
- Gupta, B. L., Nehal, M., and Baquer, N. Z. (1997). Effect of Experimental Diabetes on the Activities of Hexokinase, Glucose-6-Phosphate Dehydrogenase and Catecholamines in Rat Erythrocytes of Different Ages. *Indian J. Exp. Biol.* 35 (7), 792–795.
- Gupta, G., Sharma, S. B., Gupta, R., Gupta, S., and Singh, U. R. (2016). Assessment of Prophylactic Effect of *Senna auriculata* (L.) Roxb. Leaves on Alcohol-Induced Pancreatitis in Rat Model. *Indian J. Exp. Biol.* 54, 612–614.
- Gupta, S., Sharma, S. B., Prabhu, K. M., and Bansal, S. K. (2009a). Protective Role of *Cassia Auriculata* Leaf Extract on Hyperglycemia-Induced Oxidative Stress and its Safety Evaluation. *Indian J. Biochem. Biophys.* 46, 371–377.
- Gupta, S., Sharma, S. B., and Prabhu, K. M. (2009b). Ameliorative Effect of *Cassia auriculata* L. Leaf Extract on Glycemic Control and Atherogenic Lipid Status in Alloxan-Induced Diabetic Rabbits. *Indian J. Exp. Biol.* 47, 974–980.
- Gupta, S., Sharma, S. B., Bansal, S. K., and Prabhu, K. M. (2009c). Antihyperglycemic and Hypolipidemic Activity of Aqueous Extract of *Cassia auriculata* L. Leaves in Experimental Diabetes. *J. Ethnopharmacol.* 123, 499–503. doi:10.1016/j.jep.2009.02.019
- Gupta, S., Sharma, S. B., Singh, U. R., Bansal, S. K., and Prabhu, K. M. (2010). Elucidation of Mechanism of Action of *Cassia auriculata* Leaf Extract for its Antidiabetic Activity in Streptozotocin-Induced Diabetic Rats. *J. Med. Food.* 13, 528–534. doi:10.1089/jmf.2009.1253
- Gupta, S., Sharma, S. B., Singh, U. R., and Bansal, S. K. (2011). Salutary Effect of *Cassia auriculata* L. Leaves on Hyperglycemia-Induced Atherosclerotic Environment in Streptozotocin Rats. *Cardiovasc. Toxicol.* 11, 308–315. doi:10.1007/s12012-011-9120-4
- Guruvayoorappan, C., and Sudha, G. (2008). Phytopharmacological Evaluation of Byesukar for Hypoglycaemic Activity and its Effect on Lipid Profile and Hepatic Enzymes of Glucose Metabolism in Diabetic Rats. *Ann. Hepatol.* 7 (4), 358–363. doi:10.1016/s1665-2681(19)31837-x
- Habtemariam, S. (2011). A-Glucosidase Inhibitory Activity of Kaempferol-3-O-Rutinoside. *Nat. Prod. Commun.* 6 (2), 201–203. doi:10.1177/1934578x1100600211
- Habtemariam, S. (2013). Antihyperlipidemic Components of *Cassia auriculata* Aerial Parts: Identification Through *In Vitro* Studies. *Phytother Res.* 27 (1), 152–155. doi:10.1002/ptr.4711
- Habtemariam, S., and Belai, A. (2018). Natural Therapies of the Inflammatory Bowel Disease: The Case of Rutin and its Aglycone, Quercetin. *Mini Rev. Med. Chem.* 18 (3), 234–243. doi:10.2174/1389557517666170120152417
- Hakim, F. L., Girija, S., Kumar, R. S., and Jalaludeen, M. D. (2007). Effect of Aqueous and Ethanol Extracts of *Cassia auriculata* L. Flowers on Diabetes Using Alloxan Induced Diabetic Rats. *Int. J. Diabetes Metab.* 15, 100–106.
- Ignacimuthu, S., Ayyanar, M., and Sankarasivaraman, K. (2008). Ethnobotanical Study of Medicinal Plants Used by Paliyar Tribals in Theni District of Tamil Nadu, India. *Fitoterapia.* 79 (7–8), 562–568. doi:10.1016/j.fitote.2008.06.003
- Jagatheeswari, D. (2012). A Survey of Some Medicinally Essential Plants in Villupuram District of Tamil Nadu, India. *Int. J. Pharm. Biol. Arch.* 3 (4), 905–909.
- Jain, S. R., and Sharma, S. N. (1997). Hypoglycaemic Drugs of Indian Indigenous Origin. *Planta Med.* 15 (4), 439–442. doi:10.1055/s-0028-1100005
- Jarald, E. E., Joshi, S. B., and Jain, D. C. (2010). Antidiabetic Activity of Extracts and Fraction of *Cassia auriculata* Linn. *J. Nat. Remedie* 10 (1), 17–26. doi:10.18311/jnr/2010/421
- Jaydeokar, A. V., Bandawane, D. D., Bibave, K. H., and Patil, T. V. (2014). Hepatoprotective Potential of *Cassia auriculata* Roots on Ethanol and Antitubercular Drug-Induced Hepatotoxicity in Experimental Models. *Pharm. Biol.* 52 (3), 344–355. doi:10.3109/13880209.2013.837075
- Jeyashanthi, N., and Ashok, V. (2010). Anti-oxidative Effect of *Cassia auriculata* on Streptozotocin Induced Diabetic Rats. *Indian J. Clin. Biochem.* 25 (4), 429–434. doi:10.1007/s12291-010-0040-z
- John, C. M., Sandrasaigaran, P., Tong, C. K., Adam, A., and Ramasamy, R. (2011). Immunomodulatory Activity of Polyphenols Derived From *Cassia auriculata* Flowers in Aged Rats. *Cell Immunol.* 271 (2), 474–479. doi:10.1016/j.cellimm.2011.08.017
- Joshi, C. S., Priya, E. S., and Venkataraman, S. (2007). Hypoglycemic and Antilipidperoxidative Effects of a Polyherbal Formulation, Diakur, in Experimental Animal Models. *J. Health Sci.* 53 (6), 734–739. doi:10.1248/jhs.53.734
- Juan-Badaturge, M., Habtemariam, S., and Thomas, M. J. K. (2011). Antioxidant Compounds From a South Asian Beverage and Medicinal Plant, *Cassia Auriculata*. *Food Chem.* 125 (1), 221–225. doi:10.1016/j.foodchem.2010.08.065
- Jyothi, S. G., Chavan, S. C. S., and Somashekaraiah, B. V. (2012). *In Vitro* and *In Vivo* Antioxidant and Antidiabetic Efficacy of *Cassia auriculata* L. Flowers. *Glob. J. Pharmacol.* 6 (1), 33–40.
- Kalaivani, A., Umamaheswari, A., Vinayagam, A., and Kalaivani, K. (2008). Anti-Hyperglycemic and Antioxidant Properties of *Cassia Auriculata* Leaves and Flowers on Alloxan Induced Diabetic Rats. *Pharmacologyonline* 1, 204–217.
- Kamalakkannan, N., and Prince, P. S. (2006). Antihyperglycaemic and Antioxidant Effect of Rutin, a Polyphenolic Flavonoid, in Streptozotocin-Induced Diabetic Wistar Rats. *Basic Clin. Pharmacol. Toxicol.* 98, 97–103. doi:10.1111/j.1742-7843.2006.pto_241.x
- Karthikeyan, P., Sridhar, S., and Anuradha, C. V. (2011a). Antihyperlipidemic Potential of a Traditional Siddha Polyherbal Formulation Sugnil in Streptozotocin-Induced Diabetic Rats. *Int. J. Curr. Res.* 3 (11), 331–335.
- Karthikeyan, P., Sridhar, S., and Anuradha, C. V. (2011b). Evaluation of Antidiabetic Efficacy of A Siddha Polyherbal Formulation (Sugnil) in Streptozotocin Induced Diabetic Rats. *Int. J. Pharm. Technol.* 3 (3), 3001–3014.
- Khader, S. A., Syed Zameer Ahmed, S., Balasubramanian, S. K., Arunachalam, T. K., Kannappan, G., Mahboob, M. R., et al. (2017). Modulatory Effect of Dianthrone Rich Alcoholic Flower Extract of *Cassia auriculata* L. On Experimental Diabetes. *Integr. Med. Res.* 6 (2), 131–140. doi:10.1016/j.imr.2017.01.007
- Kirtikar, K. R., and Basu, B. D. (1918). *Indian Medicinal Plants*. 2nd Edn. Allahabad, India: Lalit Mohan Basu, 864–870.
- Kolar, F. R., Gogi, C. L., Khudavand, M. M., Choudhari, M. S., and Patil, S. B. (2018). Phytochemical and Antioxidant Properties of Some *Cassia* Species. *Nat. Prod. Res.* 32 (11), 1324–1328. doi:10.1080/14786419.2017.1342085
- Kolterman, O. G., Gray, R. S., Griffin, J., Burstein, P., Insel, J., Scarlett, J. A., et al. (1981). Receptor and Postreceptor Defects Contribute to the Insulin Resistance in Noninsulin-Dependent Diabetes Mellitus. *J. Clin. Invest.* 68, 957–969. doi:10.1172/JCI110350
- Kosalge, S. B., and Fursule, R. A. (2009). Investigation of Ethnomedicinal Claims of Some Plants Used by Tribals of Satpuda Hills in India. *J. Ethnopharmacol.* 121 (3), 456–461. doi:10.1016/j.jep.2008.11.017
- Krentz, A. J. (2003). Lipoprotein Abnormalities and Their Consequences for Patients with Type 2 Diabetes. *Diabetes Obes. Metab.* 5 (Suppl. 1), S19–S27. doi:10.1046/j.1462-8902.2003.0310.x
- Kubota, N., Tobe, K., Terauchi, Y., Eto, K., Yamauchi, T., Suzuki, R., et al. (2000). Disruption of Insulin Receptor Substrate 2 Causes Type 2 Diabetes Because of

- Liver Insulin Resistance and Lack of Compensatory Beta-Cell Hyperplasia. *Diabetes* 49 (11), 1880–1889. doi:10.2337/diabetes.49.11.1880
- Kumar, V. P., Sakthi, G., and Bimini, M. (2019). A Case Series on Management of Type II Diabetes Mellitus Through Siddha Medicine. *J. Res. Biomed. Sci.* 2 (4), 112–117.
- Kumaran, A., and Karunakaran, R. J. (2007). Antioxidant Activity of *Cassia auriculata* Flowers. *Fitoterapia* 78 (1), 46–47. doi:10.1016/j.fitote.2006.09.022
- Kwon, O., Eck, P., Chen, S., Corpe, C. P., Lee, J. H., Kruhlak, M., et al. (2007a). Inhibition of the Intestinal Glucose Transporter GLUT2 by Flavonoids. *FASEB J.* 21 (2), 366–377. doi:10.1096/fj.06-6620com
- Kwon, Y.-I., Apostolidis, E., and Shetty, K. (2007b). Evaluation of Pepper (*Capsicum Annuum*) for Management of Diabetes and Hypertension. *J. Food Biochem.* 31 (3), 370–385. doi:10.1111/j.1745-4514.2007.00120.x
- Latha, M., and Pari, L. (2003a). Antihyperglycaemic Effect of *Cassia auriculata* in Experimental Diabetes and its Effects on Key Metabolic Enzymes Involved in Carbohydrate Metabolism. *Clin. Exp. Pharmacol. Physiol.* 30, 38–43. doi:10.1046/j.1440-1681.2003.03785.x
- Latha, M., and Pari, L. (2003b). Preventive Effects of *Cassia auriculata* L. Flowers on Brain Lipid Peroxidation in Rats Treated with Streptozotocin. *Mol. Cell Biochem.* 243 (1–2), 23–28. doi:10.1023/a:1021697311150
- Li, B., Fu, R., Tan, H., Zhang, Y., Teng, W., Li, Z., et al. (2021). Characteristics of the Interaction Mechanisms of Procyanidin B1 and Procyanidin B2 With Protein Tyrosine phosphatase-1B: Analysis by Kinetics, Spectroscopy Methods and Molecular Docking. *Spectrochim. Acta A: Mol. Biomol. Spectrosc.* 259 (259), 119910. doi:10.1016/j.saa.2021.119910
- Lilian, E. P., Teresita, G., Americo, O. J., and Eduardo, G. (1998). Acute and Chronic Anti-Inflammatory Effects of Plant Flavonoids. *Il Farmaco.* 53, 421–424. doi:10.1016/s0014-827x(99)00014-2
- Liu, S., Hosokawa, M., and Miyashita, K. (2018). Dietary Effect of Squalene on Lipid Metabolism of Obese/Diabetes KK-Ay Mice and Wild-Type C57BL/6J Mice. *Food Nutr. Sci.* 09, 1498–1513. doi:10.4236/fns.2018.912108
- Lu, D. F., Yang, L. J., Wang, F., and Zhang, G. L. (2012). Inhibitory Effect of Luteolin on Estrogen Biosynthesis in Human Ovarian Granulosa Cells by Suppression of Aromatase (CYP19). *J. Agric. Food Chem.* 60 (34), 8411–8418. doi:10.1021/jf3022817
- Madavanakadu Devassy, S., Benny, A. M., Scaria, L., Nannatt, A., Fendt-Newlin, M., Joubert, J., et al. (2020). Social Factors Associated with Chronic Non-Communicable Disease and Comorbidity With Mental Health Problems in India: A Scoping Review. *BMJ Open* 10, e035590. doi:10.1136/bmjopen-2019-035590
- Mali, A. A., Hivrale, M. G., Bandawane, D. D., and Chaudhari, P. D. (2012). Study of Anti-Inflammatory Activity of *Cassia auriculata* Linn. Leaves in Wistar Rats. *Indian Drugs* 49 (11), 44–47.
- Manogaran, S., and Sulochana, N. (2004). Anti-inflammatory Activity of cassia Auriculata. *Anc Sci. Life.* 24 (2), 65–67.
- McEllduff, A., and Eastman, C. J. (1981). The Effect of Sulfhydryl Active Agents on Insulin Binding to the Erythrocyte Insulin Receptor. *J. Recept Res.* 2, 87–95. doi:10.1038/icb.1981.37
- Mhetre, N. K., Bandawane, D. D., and Patel, A. N. (2014). Antihyperglycemic Activity of Hydroalcoholic Extract of *Cassia auriculata* Linn. (Caesalpinaceae) Aerial Parts in Streptozotocin Induced Diabetic Rats. *Pharmacologia* 5 (5), 155–171. doi:10.5567/pharmacologia.2014.155.171
- Mishra, S. B., Rao, C. H. V., Ojha, S. K., Vijayakumar, M., Verma, A., and Alok, S. (2010). An Analytical Review of Plants for Anti-Diabetic Activity with Their Phytoconstituent & Mechanism of Action. *Int. J. Pharm. Sci. Res.* 1 (1), 29–46. doi:10.13040/IJPSR.0975-8232.1(1).29-46
- Mishra, S. S., and Mishra, A. N. (2012). Efficacy of Ayurvedic/Herbal Patent Medicines in Type 2 Diabetes Mellitus as Per the Claim. *Glob. J. Res. Med. Plants Indigen. Med.* 1 (9), 427–439.
- Mohan, V. R., Shanmugasundaram, R., Kalpana, D. V., Tresina, S. P., and Maruthupandian, A. (2011). Antidiabetic, Antihyperlipidaemic and Antioxidant Activity of *Senna auriculata* (L.) Roxb. Leaves in Alloxan Induced Diabetic Rats. *Int. J. PharmTech Res.* 3 (2), 747–756.
- Mohd Fauzi, F., John, C. M., Karunanidhi, A., Mussa, H. Y., Ramasamy, R., Adam, A., et al. (2017). Understanding the Mode-of-Action of *Cassia Auriculata* via *In Silico* and *In Vivo* Studies Towards Validating it as a Long Term Therapy for Type II Diabetes. *J. Ethnopharmacol.* 197, 61–72. doi:10.1016/j.jep.2016.07.058
- Moongkarndi, P., Kosem, N., Luanratana, O., Jongsomboonkusol, S., and Pongpan, N. (2004). Antiproliferative Activity of Thai Medicinal Plant Extracts on Human Breast Adenocarcinoma Cell Line. *Fitoterapia* 75, 375–377. doi:10.1016/j.fitote.2004.01.010
- Mutalik, S., Chetana, M., Sulochana, B., Devi, P. U., and Udupa, N. (2005). Effect of Dianex, a Herbal Formulation on Experimentally Induced Diabetes Mellitus. *Phytother. Res.* 19, 409–415. doi:10.1002/ptr.1570
- Mutalik, S., Sulochana, B., Chetana, M., Udupa, N., and Uma Devi, P. (2003). Preliminary Studies on Acute and Subacute Toxicity of an Antidiabetic Herbal Preparation, Dianex. *Indian J. Exp. Biol.* 41, 316–320.
- Nageswara Rao, G., Mahesh Kumar, P., Dhandapani, V. S., Rama Krishna, T., and Hayashi, T. (2000). Constituents of *Cassia auriculata*. *Fitoterapia* 71 (1), 82–83. doi:10.1016/s0367-326x(99)00108-2
- Naghavi, M., Abajobir, A. A., and Abbafati, C. (2017). Global, Regional, and National Age-Sex Specific Mortality for 264 Causes of Death, 1980–2016: A Systematic Analysis for the Global Burden of Disease Study 2016. *Lancet* 390, 1151–1210. doi:10.1016/S0140-6736(17)32152-9
- Nakamura, C., Yasumoto, E., Nakano, K., Nakayachi, T., Hashimoto, K., Kusama, K., et al. (2003). Changes in Intracellular Concentrations of Polyamines During Apoptosis of HL-60 Cells. *Anticancer Res.* 23 (6C), 4797–4803.
- Nakamura, S., Xu, F., Ninomiya, K., Nakashima, S., Oda, Y., Morikawa, T., et al. (2014). Chemical Structures and Hepatoprotective Effects of Constituents From *Cassia auriculata* Leaves. *Chem. Pharm. Bull.* 62 (10), 1026–1031. doi:10.1248/cpb.c14-00420
- Nalla, S., Goli, V., Sabat, M., Komati, S., Begam, N., and Rao Kokkiral, V. (2012). Salubrious Effect of Ethanolic Extract of *Cassia auriculata* Linn., in Streptozotocin-Nicotinamide Induced Diabetes in Rat Model. *Asian J. Pharm. Tech.* 2 (3), 104–106.
- Nambirajan, G., Karunanidhi, K., Ganesan, A., Rajendran, R., Kandasamy, R., Elangovan, A., et al. (2018). Evaluation of Antidiabetic Activity of Bud and Flower of Avaram Senna (*Cassia auriculata* L.) in High Fat Diet and Streptozotocin Induced Diabetic Rats. *Biomed. Pharmacother.* 108, 1495–1506. doi:10.1016/j.biopha.2018.10.007
- Nethan, S., Sinha, D., and Mehrotra, R. (2017). Non Communicable Disease Risk Factors and Their Trends in India. *Asian Pac. J. Cancer Prev.* 18 (7), 2005–2010. doi:10.22034/APJCP.2017.18.7.2005
- Nille, G. C., Mishra, S., Trigunayat, A., and Reddy, K. R. C. (2016a). Comparative Antidiabetic Investigation of Talapataka Churna and Avaraki Churna in STZ-Induced Diabetic Rats. *Asian J. Pharmaceut.* 10 (3), S243–S249. doi:10.22377/ajp.v10i03.761
- Nille, G. C., Reddy, K. R. C., Mishra, S., and Trigunayat, A. (2016b). Hypoglycemic Effect of Talapataka Churna in Streptozotocin Induced Hyperglycemia in Rats. *Int. J. Green. Pharm.* 10 (3), 178–182.
- Nille, G. C., and Reddy, K. R. C. (2015). A Phytopharmacological Review of Plant – *Cassia auriculata*. *Int. J. Pharm. Bio Arch.* 6 (6), 1–9. doi:10.22377/IJPBA.V6I6.1447
- Nille, G. C., and Reddy, K. R. C. (2017). Talapataka Pushpa: A Promising Herbal Remedy for Diabetes Mellitus. *Asian J. Pharmaceutics.* 11 (4), S690–S695.
- Nille, G. C., Reddy, K. R. C., and Tripathi, J. S. (2018). Clinical Evaluation of Talapataka Churna – A Polyherbal Ayurvedic Formulation in Type 2 Diabetes Mellitus. *Indian J. Tradit. Knowl.* 17 (1), 168–175.
- Oh, P. S., Lee, S. J., and Lim, K. T. (2006). Hypolipidemic and Antioxidative Effects of the Plant Glycoprotein (36 kDa) from *Rhus verniciflua* Stokes Fruit in Triton WR-1339-Induced Hyperlipidemic Mice. *Biosci. Biotechnol. Biochem.* 70, 447–456. doi:10.1271/bbb.70.447
- Olefsky, J. M., and Kolterman, O. G. (1981). Mechanisms of Insulin Resistance in Obesity and Noninsulin-Dependent (Type II) Diabetes. *Am. J. Med.* 70 (1), 151–168. doi:10.1016/0002-9343(81)90422-8
- Palomer, X., Pizarro-Delgado, J., Barroso, E., and Vázquez-Carrera, M. (2018). Palmitic and Oleic Acid: The Yin and Yang of Fatty Acids in Type 2 Diabetes Mellitus. *Trends Endocrinol. Metab.* 29 (3), 178–190. doi:10.1016/j.tem.2017.11.009
- Panigrahy, S., Jatawa, S., and Tiwari, A. (2011). Therapeutic Use of Cyclophosphamide and its Cytotoxic Action: A Challenge for Researchers. *J. Pharm. Res.* 4 (8), 2755–2757.

- Pari, L., and Latha, M. (2002). Effect of *Cassia auriculata* Flowers on Blood Sugar Levels, Serum and Tissue Lipids in Streptozotocin Diabetic Rats. *Singapore Med. J.* 43 (12), 617–621.
- Pari, L., Ramakrishnan, R., and Venkateswaran, S. (2001). Antihyperglycaemic Effect of Diamed, a Herbal Formulation, in Experimental Diabetes in Rats. *J. Pharm. Pharmacol.* 53 (8), 1139–1143. doi:10.1211/0022357011776397
- Pari, L., Murugan, P., and Appa Rao, C. (2007). Influence of *Cassia auriculata* Flowers on Insulin Receptors in Streptozotocin Induced Diabetic Rats: Studies on Insulin Binding to Erythrocytes. *Afr. J. Biochem. Res.* 1 (7), 148–155. doi:10.5897/AJBR.9000141
- Patel, Y. S., Joshi, E. P., and Joshi, P. N. (2010). Ethnobotanical Study of Tapkeshwari Hill, Bhuj, Kachchh, India. *Life Sci. Leaflets.* 2, 22–31.
- Pawar, S., and Patil, D. A. (2007). Ethnomedicinal Uses of Barks in Jalgaon District. *Nat. Prod. Radiance.* 6 (4), 341–346.
- Poongothai, S., Karkuzhali, K., Sharadha, J., Deepa, R., and Mohan, V. (2002). Evaluation of Safety and Efficacy of Hyponidd, an Ayurvedic Compound: A Double Blind, Placebo-Controlled Study in Type 2 Diabetic Patients with Secondary Failure to Oral Drugs. *Int. J. Diabetes Developing Countries* 22, 19–24.
- Prakash, Y. G., Gopal, V., and Thanka, J. (2014). “Aavarai Kudineer”- A Potent Polyherbal Siddha Formulation for Management of Diabetes Mellitus. *Int. J. Pharm. Dev. Technol.* 4 (2), 98–103.
- Prasanna, R., Harish, C. C., Pichai, R., Sakthisekaran, D., and Gunasekaran, P. (2009). Anti-Cancer Effect of *Cassia auriculata* Leaf Extract *In Vitro* through Cell Cycle Arrest and Induction of Apoptosis in Human Breast and Larynx Cancer Cell Lines. *Cell Biol Int.* 33, 127–134. doi:10.1016/j.cellbi.2008.10.006
- Punjani, B. L. (2002). Ethnobotanical Aspects of Some Plants of Aravalli Hills in North Gujarat. *Anc Sci. Life.* 21 (4), 268–280.
- Punjani, B. L., and Kumar, V. (2002). Folk Medicinal Plants Used for Skin Disorders in the Tribal Pockets of Sabarkantha District, Gujarat. *J. Nat. Remedies.* 2 (1), 84–87. doi:10.18311/jnr/2002/351
- Puranik, A. S., Halade, G., Kumar, S., Mogre, R., Apte, K., Vaidya, A. D., et al. (2011). *Cassia auriculata*: Aspects of Safety Pharmacology and Drug Interaction. *Evid. Based Complement. Alternat Med.* 2011, 915240. doi:10.1093/ecam/nep237
- Raj, J. Y., Peter, M. P. J., and Joy, V. (2012). Chemical Compounds Investigation of *Cassia auriculata* Seeds: a Potential Folklore Medicinal Plant. *Asian J. Plant Sci. Res.* 2 (2), 187–192. doi:10.5923/j.plant.20120201.02
- Raja, D. K., Jeganathan, N. S., and Manavalan, R. (2013). *In Vitro* antimicrobial Activity and Phytochemical Analysis of *Cassia auriculata* Linn. *Int. Curr. Pharm. J.* 2 (6), 105–108. doi:10.3329/icpj.v2i6.14869
- Rajagopal, S. K., Manickam, P., Periyasamy, V., and Namasivayam, N. (2003). Activity of *Cassia auriculata* Leaf Extract in Rats With Alcoholic Liver Injury. *J. Nutr. Biochem.* 14 (8), 452–458. doi:10.1016/S0955-2863(03)00053-6
- Rajalakshmi, K., Shanmugapriya, P., Christian, G., Gladys, J., Banumathi, V., and Geethalakshmi, S. (2018). Antimicrobial Potential of Siddha Polyherbal Formulation Aavarai Kudineer. *J. Pure Appl. Microbio.* 12 (2), 1019–1025. doi:10.22207/jpam.12.2.66
- Ramachandran, B., Kandaswamy, M., Narayanan, V., and Subramanian, S. (2003). Insulin Mimetic Effects of Macrocyclic Binuclear Oxovanadium Complexes on Streptozotocin-Induced Experimental Diabetes in Rats. *Diabetes Obes. Metab.* 5 (6), 455–461. doi:10.1046/j.1463-1326.2003.00302.x
- Rask-Madsen, C., and King, G. L. (2005). Proatherosclerotic Mechanisms Involving Protein Kinase C in Diabetes and Insulin Resistance. *Arterioscler Thromb. Vasc. Biol.* 25, 487–496. doi:10.1161/01.ATV.0000155325.41507.e0
- Sabu, M. C., and Subburaju, T. (2002). Effect of *Cassia auriculata* Linn. On Serum Glucose Level, Glucose Utilization by Isolated Rat Hemidiaphragm. *J. Ethnopharmacol.* 80 (2-3), 203–206. doi:10.1016/S0378-8741(02)00026-0
- Salehi, B., Machin, L., Monzote, L., Sharifi-Rad, J., Ezzat, S. M., Salem, M. A., et al. (2020). Therapeutic Potential of Quercetin: New Insights and Perspectives for Human Health. *ACS Omega* 5 (20), 11849–11872. doi:10.1021/acsomega.0c01818
- Salma, B., Janhavi, P., Muthaiah, S., Veeresh, P., Santhepete Nanjundaiah, M., Divyashree, S., et al. (2021). Ameliorative Efficacy of the *Cassia auriculata* Root against High-Fat-Diet + STZ-Induced Type-2 Diabetes in C57BL/6 Mice. *ACS Omega* 6 (1), 492–504. doi:10.1021/acsomega.0c04940
- Samy, R. P., and Ignacimuthu, S. (2000). Antibacterial Activity of Some Folklore Medicinal Plants Used by Tribals in Western Ghats of India. *J. Ethnopharmacol.* 69 (1), 63–71. doi:10.1016/S0378-8741(98)00156-1
- Sanghi, R., Tripathi, K., and Sharma, J. P. (2000). New Triterpenoid, O-Beta-D-Xylopyranosides From *Cassia Auriculata*. *Ind. J. Chem. Section B, Org. Including Med.* 39 (6), 477–479.
- Sankhari, J. (2019). Effectiveness of *Cassia auriculata* Flower (Avaram Poo) Extract in Reducing Blood Glucose Among Pre-Diagnosed Type 2 Diabetes Mellitus Clients in Selected Area of Puducherry, India. *Life: Int. J. Health Life-sciences.* 5 (1), 126–136.
- Saravanan, R., and Pari, L. (2005). Antihyperlipidemic and Antiperoxidative Effect of Diasulin, a Polyherbal Formulation in Alloxan Induced Hyperglycemic Rats. *BMC Complement. Altern. Med.* 5 (14), 14–18. doi:10.1186/1472-6882-5-14
- Senthilkumar, S., and Vijayakumari, K. (2012). GC-MS Analysis of *Cassia auriculata* Linn Leaf Extract-Traditional Valuable Plant. *Int. J. Deccan Pharm. Life Sci.* 3 (2), 104–109.
- Sharma, P. V., and Sharma, G. P. (1979). *Kaiyadeva Nighantu*. 1st Edn. Varanasi, India: Chaukhambha Orientalia, 184.
- Shiradkar, M., Pawankumar, G., and Shah, K. (2011). Pharmacological Evaluation of *Cassia auriculata* Bark Extract. *Int. J. Pharma Bio Sci.* 2 (1), 758–766.
- Sreejith, M., Kannappan, N., Santhiagu, A., and Mathew, A. P. (2013). Phytochemical, Anti-Oxidant and Anthelmintic Activities of Various Leaf Extracts of *Flacourtia sepiaria* Roxb. *Asian Pac. J. Trop. Biomed.* 3 (3), 947–953. doi:10.1016/S2221-1691(13)60184-7
- Srivastava, S., Lal, V. K., and Pant, K. K. (2012). Polyherbal Formulations Based on Indian Medicinal Plants as Antidiabetic Phytotherapeutics. *Phytopharmacology.* 2 (1), 1–15.
- Subramanian, S., Uma, S. K., and Sriram Prasath, G. (2011). Biochemical Evaluation of Antidiabetic, Antilipidemic and Antioxidant Nature of *Cassia auriculata* Seeds Studied in Alloxan-Induced Experimental Diabetes in Rats. *Int. J. Pharm. Sci. Rev. Res.* 11 (2), 137–144.
- Sudha, V., Bairy, K. L., Shashikiran, U., Sachidananda, A., Jayaprakash, B., and Shalini, S. (2005). Efficacy and Tolerability of Dianex in Type 2 Diabetes Mellitus: a Non Randomized, Open Label Non-comparative Study. *Med. J. Malaysia.* 60 (2), 204–211.
- Suresh, H. M., Hatapakki, B. C., Shivakumar, S. I., Hallikeri, C. S., Swamy, B. M., and Chandur, V. K. (2007). Laxative Activity of *Cassia auriculata* Pods in Rats. *J. Nat. Rem.* 7 (1), 150–154.
- Tan, D. C., Kassim, N. K., Ismail, I. S., Hamid, M., and Ahamad Bustamam, M. S. (2019). Identification of Antidiabetic Metabolites from *Paederia Foetida* L. Twigs by Gas Chromatography-Mass Spectrometry-Based Metabolomics and Molecular Docking Study. *Biomed. Res. Int.* 2019, 7603125. doi:10.1155/2019/7603125
- Thabrew, M. I., Munasinghe, T. M., Senarath, S., and Yapa, R. M. (2004). Effects of *Cassia Auriculata* and *Cardospermum Halicacabum* Teas on the Steady State Blood Levels of Theophylline in Rats. *Drug Metabol Drug Interact.* 20 (4), 263–272. doi:10.1515/dmd.2004.20.4.263
- Thirumalai, T., Kelumalai, E., and Senthilkumar, B. (2009). Ethnobotanical Study of Medicinal Plants Used by the Local People in Vellore District, Tamilnadu, India. *Ethnobotanical Leaflets.* 2009 (10), 10.
- Tian, Z., Si, J. Y., Chen, S. B., Yang, M. S., Xiao, P. G., and Wu, E. X. (2006). [Cytotoxicity and Mechanism of 23-O-Acetylcimigenol-3-O-Beta-D-Xylopyranoside on HepG2 Cells]. *Zhongguo Zhong Yao Za Zhi.* 31 (21), 1818–1821.
- Tsuchiya, A., Kanno, T., and Nishizaki, T. (2013). Stearic Acid Serves as a Potent Inhibitor of Protein Tyrosine Phosphatase 1B. *Cell Physiol Biochem.* 32, 1451–1459. doi:10.1159/000356582
- Valverde, A. M., Fabregat, I., Burks, D. J., White, M. F., and Benito, M. (2004). IRS-2 Mediates the Antiapoptotic Effect of Insulin in Neonatal Hepatocytes. *Hepatology* 40 (6), 1285–1294. doi:10.1002/hep.20485
- Vedavathy, S., and Rao, K. N. (1991). Antipyretic Activity of Six Indigenous Medicinal Plants of Tirumala Hills, Andhra Pradesh, India. *J. Ethnopharmacol.* 33, 193–196. doi:10.1016/0378-8741(91)90178-g
- Venkatachalam, M., Singaravelu, G., Govindaraju, K., and Ahn, J. S. (2013). PTP 1B Inhibitory Action of a Phytochemical Propionic Acid, 2-(3-Acetoxy-4,4,14-Trimethylandro-8-En-17-Yl). *Curr. Sci.* 105 (6), 827–832.
- Vijayakumar, R., and Nachiappan, V. (2017). *Cassia auriculata* Flower Extract Attenuates Hyperlipidemia in Male Wistar Rats by Regulating the Hepatic

- Cholesterol Metabolism. *Biomed. Pharmacother.* 95, 394–401. doi:10.1016/j.biopha.2017.08.075
- Vijayaraj, P., Muthukumar, K., Sabarirajan, J., and Nachiappan, V. (2013). Antihyperlipidemic Activity of *Cassia auriculata* Flowers in Triton WR 1339 Induced Hyperlipidemic Rats. *Exp. Toxicol. Pathol.* 65 (1–2), 135–141. doi:10.1016/j.etp.2011.07.001
- Wang, J., Huang, H., Liu, P., Tang, F., Qin, J., Huang, W., et al. (2006). Inhibition of Phosphorylation of P38 MAPK Involved in the protection of Nephropathy by Emodin in Diabetic Rats. *Eur. J. Pharmacol.* 553 (1–3), 297. doi:10.1016/j.ejphar.2006.08.087
- Wang, W., Zhang, Y., Nakashima, S., Nakamura, S., Wang, T., Yoshikawa, M., et al. (2019). Inhibition of Melanin Production by Anthracenone Dimer Glycosides Isolated From *Cassia auriculata* Seeds. *J. Nat. Med.* 73 (3), 439–449. doi:10.1007/s11418-018-01276-2
- Wang, X., Li, Y. L., Wu, H., Liu, J. Z., Hu, J. X., Liao, N., et al. (2011). Antidiabetic Effect of Oleanolic Acid: a Promising Use of a Traditional Pharmacological Agent. *Phytother. Res.* 25 (7), 1031–1040. doi:10.1002/ptr.3385
- Wang, Y. J., Huang, S. L., Feng, Y., Ning, M. M., and Leng, Y. (2012). Emodin, an 11 β -Hydroxysteroid Dehydrogenase Type 1 Inhibitor, Regulates Adipocyte Function *In Vitro* and Exerts Anti-diabetic Effect in Ob/ob Mice. *Acta Pharmacol. Sin.* 33 (9), 1195–1203. doi:10.1038/aps.2012.87
- Ward, G. M., and Harrison, L. C. (1986). Structure of the Human Erythrocyte Insulin Receptor. *Diabetes* 35, 101–105. doi:10.2337/diab.35.1.101
- Win, E. T., and Min, A. K. (2018). Investigation of Phytochemical Constituents, Physicochemical Properties and Antimicrobial Activities from the Leaves of *Senna auriculata* (L.) Roxb. *J. Myanmar Acad. Arts Sci.* 16 (4), 295–314.
- Wu, J. H. Y., Marklund, M., Imamura, F., Tintle, N., Ardisson Korat, A. V., de Goede, J., et al. (2017). Omega-6 Fatty Acid Biomarkers and Incident Type 2 Diabetes: Pooled Analysis of Individual-Level Data for 39 740 Adults From 20 Prospective Cohort Studies. *Lancet Diabetes Endocrinol.* 5, 965–974. doi:10.1016/S2213-8587(17)30307-8
- Ye, X., Krohn, R. L., Liu, W., Joshi, S. S., Kuszynski, C. A., McGinn, T. R., et al. (1999). The Cytotoxic Effects of a Novel IH636 Grape Seed Proanthocyanidin Extract on Cultured Human Cancer Cells. *Mol. Cell Biochem.* 196 (1–2), 99–108. doi:10.1007/978-1-4615-5097-6_12
- Conflict of Interest:** The authors declare that the research was conducted in the absence of any commercial or financial relationships that could be construed as a potential conflict of interest.
- Publisher's Note:** All claims expressed in this article are solely those of the authors and do not necessarily represent those of their affiliated organizations, or those of the publisher, the editors and the reviewers. Any product that may be evaluated in this article, or claim that may be made by its manufacturer, is not guaranteed or endorsed by the publisher.
- Copyright © 2021 Nille, Mishra, Chaudhary and Reddy. This is an open-access article distributed under the terms of the Creative Commons Attribution License (CC BY). The use, distribution or reproduction in other forums is permitted, provided the original author(s) and the copyright owner(s) are credited and that the original publication in this journal is cited, in accordance with accepted academic practice. No use, distribution or reproduction is permitted which does not comply with these terms.



Supercritical Carbon Dioxide Extracts of *Cordyceps sinensis*: Chromatography-based Metabolite Profiling and Protective Efficacy Against Hypobaric Hypoxia

Jigni Mishra¹, Washim Khan^{2,3}, Sayeed Ahmad² and Kshipra Misra^{1*}

¹Save The Environment, Gurugram, India, ²Bioactive Natural Products Laboratory, Department of Pharmacognosy and Phytochemistry, School of Pharmaceutical Education and Research, Jamia Hamdard, New Delhi, India, ³National Center for Natural Products Research, The University of Mississippi, Oxford, MS, United States

OPEN ACCESS

Edited by:

Chandra Kant Katiyar,
Emami, India

Reviewed by:

Anthony Booker,
University of Westminster,
United Kingdom
Zoran Petar Zekovic,
University of Novi Sad, Serbia

*Correspondence:

Kshipra Misra
kmisra99@yahoo.com

Specialty section:

This article was submitted to
Ethnopharmacology,
a section of the journal
Frontiers in Pharmacology

Received: 13 November 2020

Accepted: 10 August 2021

Published: 26 August 2021

Citation:

Mishra J, Khan W, Ahmad S and
Misra K (2021) Supercritical Carbon
Dioxide Extracts of *Cordyceps*
sinensis: Chromatography-based
Metabolite Profiling and Protective
Efficacy Against Hypobaric Hypoxia.
Front. Pharmacol. 12:628924.
doi: 10.3389/fphar.2021.628924

The toxicity and disposal concerns of organic solvents used in conventional extraction purposes has entailed the need for greener alternatives. Among such techniques, supercritical fluid extraction (SFE) has gained popularity by yielding extracts of high purity in a much faster manner. Carbon dioxide (CO₂) is generally preferred as a supercritical solvent because of its lower temperature requirements, better diffusivity and easy removal. The present study describes the characterization of supercritical CO₂ extracts of Indian variety of *Cordyceps sinensis* (CS)- a high-altitude medicinal mushroom widely revered in traditional medicine for its extensive anti-hypercholesterolemic, anti-inflammatory, anti-proliferative and energy-enhancing properties. Experimental parameters viz. 300 and 350 bar of extraction pressure, 60°C of temperature, 0.4 L/h CO₂ of flow rate and use of 1% (v/v) of ethanol as entrainer were optimized to prepare three different extracts namely, CSF1, CSF2 and CSF3. High-performance thin-layer chromatography (HPTLC) was used for assessing the quality of all the extracts in terms of cordycepin, the pivot biomarker compound in CS. Characterization by HPTLC and GC-MS confirmed the presence of flavonoids and nucleobases and, volatile organic compounds (VOCs), respectively. The chromatographic data acquired from metabolite profiling were subjected to chemometric analysis in an open source R studio which illustrated interrelatedness between CSF1 and CSF2 in terms of two major principal components. i.e. Dim 1 and Dim 2 whose values were 40.33 and 30.52% in variables factor map plotted using the HPTLC-generated retardation factor values. The factor maps based on retention times of the VOCs exhibited a variance of Dim 1 = 43.95% and Dim 2 = 24.85%. Furthermore, the extracts demonstrated appreciable antibacterial activity against *Escherichia coli* and *Salmonella typhi* by generation of reactive oxygen species (ROS), protein leakage and efflux pump inhibition within bacterial pathogens. CSFs were elucidated to be significantly cytoprotective ($p < 0.05$) in a simulated hypobaric hypoxia milieu (0.5% oxygen). CSF2 showed the best results by effectively improving the viability of human embryonic kidney (HEK 293) cells to $82.36 \pm 1.76\%$ at an optimum dose of 100 µg/ml. Levels of hypoxia inducible factor-1 alpha (HIF-1α) were modulated four-fold

upon supplementation with CSF2. The results collectively evinced that the CSF extracts are substantially bioactive and could be effectively utilized as mycotherapeutics for multiple bioeffects.

Keywords: *Cordyceps sinensis* (Berk) Sacc., GC-MS, HPTLC, metabolomics, supercritical fluid extract, hypobaric hypoxia (HH)

INTRODUCTION

The increasing popularity of alternative healthcare has opened new dimensions for extraction of high value-added products from natural sources like medicinal plants and mushrooms. Though conventional extraction techniques like maceration, Soxhlet extraction, hydro-distillation, pressurised liquid extraction, etc. have been adopted for product development, however, certain disadvantages such as high operational energy requirements, use of expensive and toxic organic solvents, disposal concerns of the solvents, lesser selectivity in extraction and loss of volatile compounds have entailed the search for an efficient, environment friendly extraction approach (Malaman et al., 2011). One such approach is “supercritical fluid extraction” that utilizes supercritical fluids that above their critical points exhibit dual liquid-like and gas-like nature. In this manner, supercritical fluids are capable of solvent power with negligible surface tension as well as excellent mass transfer properties (Pronyk and Mazza, 2009). Although supercritical water and carbon dioxide (CO₂) have garnered major attention amongst researchers for extracting superior quality cosmeceuticals, essences, fragrances, pharmaceuticals from medicinal herbs, CO₂ happens to be advantageous in industrial bioprocessing owing to its comparatively moderate supercritical temperature, better diffusivity, low viscosity and easy recovery in addition to being an economical solvent, nonflammable and recyclable gas (Montesantos and Maschietti, 2020). Previous literature evidence that CO₂ is contemplated to be a better supercritical fluid than other solvents like water (Kumoro et al., 2010). In case of water, the temperature requirement is relatively much higher than that for CO₂. For instance, in a study describing the preparation of tumuji oil, a temperature of 500°C was used (Meng et al., 2006). Similarly, for extracting Huadian oil shale using water in supercritical state, the temperature required was 373°C (Hu et al., 1999). Such higher temperatures are not suitable for extraction of bioactive compounds from natural sources because of their thermolabile properties. In this perspective, CO₂ is preferred as a solvent especially in the areas of functional food and pharmacological products because of its moderate supercritical points (Norodin et al., 2016; Bittencourt et al., 2021). Therefore, in the present study, supercritical CO₂ extraction was employed to prepare bioactive extracts from Indian high-altitude variety of medicinal mushroom, *Cordyceps sinensis*, popularly known as “keera jhari” in the Kumaon region of Indian Himalayas, from where the particular variety used in current study is sourced (Pal and Misra, 2018).

C. sinensis has been extensively revered as “ethnomedicine” in ancient medicinal systems like Ayurveda and traditional Chinese

medicine, due to its multitude of health benefits like anti-inflammatory, antioxidant, cardioprotective, endurance enhancing, hepatoprotective, etc. effects. Recent research has established evidence-based pharmacological effects by demonstrating the potential of *C. sinensis* as anti-proliferative, immunomodulatory, cardiostimulant and the like (Holliday and Cleaver, 2008). It has been widely acclaimed in previous literature for its efficacy in modulating physiological systems including the circulatory, immune, hematogenic, cardiovascular, respiratory and glandular systems of the human body under various stressful conditions (Koh et al., 2003; Yi et al., 2004; Jordan et al., 2008; Ahmed et al., 2012; Nie et al., 2013; Yan et al., 2013; Rajput et al., 2021). The substantial therapeutic value of *C. sinensis* can be attributed to its rich chemical composition encompassing glycosides, lipids, phenolics, proteins and peptides, sterols and so forth (Rajput et al., 2020).

Although the restorative potential of *C. sinensis* has been harnessed for formulation of numerous medicinal products and supplements, however its role in the management of high-altitude-induced maladies namely, acute mountain sickness (AMS), chill blains, high-altitude cerebral edema (HACE), high-altitude pulmonary edema (HAPE) and hypothermia are relatively untapped. Only few researchers have reported the considerable potential of *C. sinensis* in amelioration of adverse effects brought about by high-altitude hypoxia. For instance, aqueous alcoholic extracts of *C. sinensis* have restorative effects to treat hypoxic pulmonary hypertension by downregulating the expression of PCNA, c-fos and c-jun (Gao et al., 2010). Chen et al. (2014) have shed light on the vital role of a supplement composed of *Rhodiola crenulata* and *C. sinensis* in augmenting aerobic performance of healthy male subjects during a 2-wk high-altitude training regime where significant normalization of parasympathetic nervous system action and a prolonged exhaustive run time was observed. In studies carried out by our group, it has been observed that aqueous extracts and phenolic rich fractions of Indian Himalayan variety of *C. sinensis* have substantially averted the debilitating impact of hypobaric hypoxia *in vitro* in various mammalian cell lines namely, A549, HT22, HEK 293 cell lines and, *in vivo* in male Sprague Dawley rat models (Singh et al., 2013; Pal et al., 2015; Rajput et al., 2020). To further establish the promising adaptogenic potential of *C. sinensis* in a hypobaric hypoxia milieu, supercritical fluid extracts were prepared from *C. sinensis* (“CSF extracts”) using supercritical CO₂ as main solvent and ethanol as entrainer. The extracts were well characterized by high-performance thin layer chromatography (HPTLC) in terms of cordycepin, flavonoids and nucleobases and in terms of volatile organic compounds (VOCs) by gas chromatography-mass spectrometry (GC-MS).

Chromatography-based metabolomics using principal component analysis was carried out to group the extracts based on their metabolite content. Cognate bioactivities viz., free radical scavenging, ferric ion reduction and bactericidal action against *Escherichia coli* (*E. coli*) and *Salmonella typhi* (*S. typhi*) were revealed. These are common pathogenic bacteria whose invasion in human host cells is reportedly aggravated under hypoxia conditions (Ding et al., 2001; Jennewein et al., 2015). Since the main objective of the present study was to establish the efficacy of supercritical CO₂ extracts of *C. sinensis* for recuperation in low oxygen tension, hence the selection of the abovementioned bacterial strains was considered relevant. Furthermore, the protective role of the fractions in resolving hypoxia-instigated concerns were thoroughly studied *in vitro* in HEK 293 cell lines where CSF extract significantly recuperated cellular viability under oxygen deficient conditions and also modulated levels of major hypoxia transcription factor, i.e., hypoxia inducible factor-1 alpha or, “HIF-1 α .”

The novelty of the present manuscript resides in the fact that the protective action of supercritical CO₂ extracts of *C. sinensis* against hypobaric hypoxia has been addressed for the very first time. Reports pertaining to hypoxia protective action are not available for supercritical extracts of any species of *Cordyceps* genus. In our earlier studies, anti-hypoxia effects of phenolic fractions and aqueous extracts (prepared by accelerated solvent extraction) of Indian Himalayan variety of *C. sinensis* were confirmed (Singh et al., 2013; Rajput et al., 2020). However, this is the very first time that supercritical carbon dioxide extracts of this variety have been researched. This is the first study of its kind that provides a detailed insight into the protective role of *C. sinensis* supercritical CO₂ extracts against a hypobaric hypoxia milieu. These observations, along with metabolomics performed on chromatography profiling can further be taken up as a lead for value-added product development, especially against high-altitude malaises.

MATERIALS AND METHODS

Chemicals and Reagents

Ultra-pure, molecular grade chemicals from Sigma-Aldrich (St. Louis, MO, United States) were used in the entire study. Solvents were purchased from Merck (Rahway, NJ, United States). Water used throughout was of Millipore grade (Merck, United States). Powder of *C. sinensis* was commercially procured from Aryan Mushroom (Batch No. CO-1601; Delhi, India). The average particle size of *C. sinensis* powder was 300 μ m, as determined using Supra scanning electron microscope (Carl Zeiss, Germany). Bacterial strains used were *E. coli* (ATCC 9837) and *S. typhi* (clinical isolate from All India Institute of Medical Sciences, Delhi, India). HEK 293 cell line was procured from National Centre for Cell Science (Pune, India). Nutrient agar, nutrient broth and antibiotic solutions used were from HiMedia® (Mumbai, India). Dulbecco's minimal essential medium (DMEM) used in cell culture studies was procured from HiMedia® (Mumbai, India).

Preparation of *C. sinensis* Supercritical Extracts

The supercritical fluid extracts of *C. sinensis* collectively referred to as “CSF extracts” were prepared in SFE-500R system (Thar, Pittsburgh, United States), by modifying a methodology reported earlier (Miao et al., 2010). The instrument had two separate feed lines for CO₂ and the entrainer (here, ethanol). The optimum pressure and temperature for preparing CSF extracts in the current study were finalized after evaluating the yields (% w/w) obtained from a combination of four extraction pressures viz., 200, 250, 300 and 350 bar and three temperatures of 40, 50 and 60°C. The afore stated pressures and temperatures were selected by keeping in consideration the type of bioactive molecules (flavonoids, nucleobases and VOCs) being targeted putatively in the extracts (He et al., 2005; Liza et al., 2010; Shan et al., 2012). CO₂ flow rate was maintained at 0.4 L/h. Ethanol 1% (v/v) was used as an entrainer/co-solvent. Amongst all the combinations of extraction pressures and temperatures tested, the ones giving extracts of highest yields (“CSF1” followed by “CSF2”) were selected as the optimum extraction conditions. Maintaining the same extraction parameters as “CSF1,” but without the use of entrainer, resulted in extraction of “CSF3.” In the experimental procedure, CO₂ from the cylinder was released *via* a cooling bath in order to hold a constant temperature for ensuring a constant feeding rate of the pump. Subsequently, the mixture of *C. sinensis* powder, supercritical CO₂ and ethanol for CSF1 and CSF2 and *C. sinensis* powder and only supercritical CO₂ in case of CSF3 were contacted in a mixer. The temperature of the reaction mixture was controlled by a heating jacket. At extraction pressure of 300 bar, an extraction time of 2 h was maintained for acquiring CSF1 and CSF3. For CSF2, the extraction pressure was higher i.e., 350 bar, hence the time was reduced to 1.5 h. After an extraction time period of 2, 1.5 and 2 h for CSF1, CSF2 and CSF3 separately, the ensuing extracts were collected in the separation vessel. All the procedural parameters were regulated by the instrument console.

Characterization of the CSF Extracts by HPTLC

Chemical characterization of the CSF extracts in terms of cordycepin, nucleobases and flavonoids was accomplished by HPTLC. The entire HPTLC analysis was accomplished on a CAMAG system (Muttentz, Switzerland) consisting of a Linomat 5 sample applicator, TLC Scanner 3 and Reprostar 3 documentation system. The samples were applied by means of a Hamilton microsyringe (100 μ L) on 20 \times 10 cm glass backed silica gel 60 F₂₅₄ HPTLC plates (Merck, Billerica, MA, United States). Spectral scanning was done using winCats software (version 1.4.4.6337).

HPTLC Analysis of Cordycepin

Quality assessment of the supercritical CO₂ extracts was performed by characterizing them in terms of the major biomarker metabolite of *C. sinensis*, i.e. “cordycepin” or 3'-

deoxyadenosine. Here, 0.5 mg of cordycepin was dissolved in 1 ml of methanol to form the cordycepin standard solution. For sample preparation, 20 mg of each CSF extract was dissolved in 10 ml of methanol thus, forming final sample concentration of 2 mg/ml. Three different application volumes (0.5, 1 and 2 μ l) of cordycepin standard solution and 20 μ l of each sample was applied onto separate lanes of uniform band thickness of 6 mm on a silica gel plate. The plate was developed using a mobile phase comprising chloroform, methanol and water in a ratio of 52: 7: 0.5 (v/v/v) (Sari et al., 2016). The plate was developed in a CAMAG twin-trough vertical development chamber, pre saturated with mobile phase. The solvent front was maintained till 85 mm. Thereafter, the plate was subjected to densitometric scanning at 254 nm in absorption mode, with deuterium as the light source. Slit width was $6 \times 0.3 \mu\text{m}$. Quantities of cordycepin in the three CSF extracts were computed from the corresponding peak areas generated by winCats software.

HPTLC Analysis of Nucleobases

For quantification of nucleobases, specifically, thymine, uracil, adenine, cytosine, guanine and guanosine present in CSFs by HPTLC, stock solutions of the standard nucleobases were prepared by dissolving 0.5 mg of each standard in 1 ml of methanol and vortexing the same for 10 min. A standard mixture comprising equal volume from each of these six standard nucleobase solutions was prepared. CSF samples were prepared as mentioned in previous paragraph. Then, 6, 7 and 8 μ l of the standard mixture and 20 μ l of individual CSF extract were applied on silica gel plates as mentioned above. The constituent nucleobases were identified by developing the plate in a solvent system composed of dichloromethane, methanol and formic acid in a ratio of 8: 2.25: 0.8 (v/v/v) (Mishra et al., 2018b). All the analytical parameters for separation and quantification of nucleobases were retained as described in the previous section for cordycepin.

HPTLC Analysis of Flavonoids

A standard mixture of flavonoids containing equal volume of quercetin, gallic acid, ascorbic acid and rutin was made up in a similar manner as that for nucleobases. Flavonoids present in the CSF samples were separated and quantitated using a mobile phase constituted of ethyl acetate: dichloromethane: formic acid: glacial acetic acid: methanol in a ratio of 10:10:1:1:2 (v/v/v/v/v) (Bhardwaj et al., 2015). Rest analytical and detection parameters were maintained as described in the previous sections.

Characterization of the CSF Extracts by GC-MS

Detection of VOCs present in CSFs was carried out upon a fused silica stationary phase Rtx-5MS, having dimensions 30 m \times 0.25 mm, 2 μm . GC-MS analysis was conducted using a Shimadzu QP2010 system (Kyoto, Japan), equipped with an AOC-20i autosampler. The following analytical parameters were set: sample injection volume: 1 μ l; injection temperature: 260°C; purge rate: 3 ml/min; gas flow rate: 1.21 ml/min; column

temperature: initial at 60°C for 2 min, then ramped at a rate of 10°C/min till 280°C; total run time: 27 min. An electron beam of 70 eV was used for ionization of samples. VOCs detected in the supercritical extracts were confirmed by matching their respective mass spectra and retention times with existing entries in NIST library (Cui et al., 2017).

Metabolomics Studies by Principal Component Analysis

The metabolite profiling acquired from HPTLC and GC-MS analyses were utilized as input data to derive reliability patterns among the CSF extracts by means of chemometrics. Here, principal component analysis (PCA) for data reduction was realized in an open source R studio: A Language and Environment for Statistical Computing (R Foundation for Statistical Computing, Vienna, Austria (<http://cran.r-project.org/>). The entire datasets comprising retardation factors and peak areas of various nucleobases and flavonoids in CSF extracts in case of HPTLC, and the retention times and area percentages of constituent VOCs from GC-MS output were represented in terms of two principal components denoted as “Dim1” and “Dim2” in separate variables factor maps generated from PCA. This facilitated drawing interrelatedness patterns among the CSF extracts while ensuring data compression (Bhardwaj et al., 2017).

Antioxidant Potential of the CSF Extracts

The antioxidant potency of *C. sinensis* supercritical CO₂ extracts was adjudged by evaluating their free radical scavenging potential for 2,2'-azino-bis(3-ethylbenzothiazoline-6-sulphonic acid (ABTS) and 2,2-diphenyl-1-picryl-hydrazyl-hydrate (DPPH) radicals as well as by determining the ferric ion reducing antioxidant power (FRAP), as detailed below.

DPPH Assay

Various concentrations viz., 10, 5, 2.5, 1.25 and 1 mg/ml of the supercritical fluid extracts were prepared. 24 mg of DPPH powder was dissolved in 100 ml of ethanol. 10 ml of this solution was mixed well with 45 ml of methanol. Absorbance was adjusted to 1.1 ± 0.02 units at 515 nm to form the working solution. Then, 10 μ l of sample was added to 190 μ l of this working solution and left undisturbed for 2 h to allow proper reaction with the stable DPPH radical. A change in colour from deep violet to light yellow was measured at 515 nm. Results were represented in terms of micromole Trolox equivalent per gram of extract ($\mu\text{M TE/g}$ of extract) (Mishra et al., 2018a).

ABTS Assay

ABTS free radical scavenging assay was determined as reported elsewhere (Sharma et al., 2015). Trolox ranging from 800 to 50 μM were taken as standards to plot the standard curve. Different concentrations viz., 10, 5, 2.5, 1.25 and 1 mg/ml of all the CSF extracts were prepared. ABTS free radical scavenging values of CSF extracts were expressed as $\mu\text{M TE/g}$ of extract. Absorbances were recorded at 734 nm.

FRAP Assay

FRAP values of CSF extracts were determined using a method described previously (Mishra et al., 2018b). Various concentrations of Trolox over a range of 400–12.5 μM were taken as standards. Different concentrations (10, 5, 2.5, 1.25 and 1 mg/ml) of all the CSF extracts were prepared. Results were expressed as $\mu\text{M TE/g}$ of extract. Final absorbances were recorded at 593 nm.

Antibacterial Efficacy of the CSFs

Screening of CSF Extracts for Antibacterial Activity

Glycerol stocks of two bacterial strains: *E. coli* and *S. typhi* were revived in nutrient broth for 16–18 h at 37°C, in an incubator-cum-shaker (Orbitek, Chennai, India), at 90 rpm. The pure cultures obtained were streaked on nutrient agar medium. Antibacterial action of CSF1, CSF2 and CSF3 against *E. coli* and *S. typhi* was determined by Kirby Bauer disk diffusion technique (Mishra et al., 2018a). Briefly, 100 $\mu\text{g/ml}$ of each CSF extract dissolved in nutrient broth was applied onto spherical disks made out of Whatman No.1 filter paper. The dried disks were placed on nutrient agar medium plates swabbed with bacterial pathogens under study. Thereafter, these plates were incubated at 37°C for 16–18 h at a shaking speed of 90 rpm. Prominent zones of inhibition formed around the disks were indicative of antibacterial activity. Kanamycin and nutrient broth were taken as the positive and negative controls, respectively.

Determination of Minimal Inhibitory Concentration

Bacterial colonies approximately, 16–18 h old, cultured on nutrient agar medium were diluted in 0.8% physiological saline to prepare a 0.1 McFarland suspension. The bacterial cultures were inoculated in test tubes containing 5 ml nutrient broth. To these tubes, the specific CSF extracts were added in concentrations over a range of 10–100 $\mu\text{g/ml}$ and incubated at 37°C for 16–18 h at 90 rpm. The lowest concentration of an extract demonstrating inhibition of bacterial growth was determined to be its minimal inhibitory concentration (MIC) for a given bacterial pathogen (Zhang et al., 2015). Kanamycin and pure nutrient broth medium were used as the positive and negative controls, respectively.

Generation of Reactive Oxygen Species Within Bacterial Cells

Reactive oxygen species (ROS) generation in a bacterial cell upon treatment with a specific CSF extract as a potential antibacterial mechanism was investigated by a method described previously (Zhang et al., 2015). Various concentrations of the CSF samples were added to nutrient broth tubes containing bacterial cells at density of 10^5 CFU/ml and incubated at 37°C for 3 h. The cultures were then centrifuged at 4°C for 15 min at a speed of $500 \times g$, and the resultant supernatant was treated with 50 μM of 2',7'-dichlorofluorescein diacetate (DCFDA), for 1 h at 37°C, in dark. A control group untreated with DCFDA was taken as control. The level of ROS generated in the bacterial cultures was recorded in triplicates using a fluorescence

spectrophotometer (Cary Eclipse, Santa Clara, CA, United States) at an excitation wavelength of 485 nm and emission wavelength of 528 nm.

Protein Leakage in Bacterial Cells

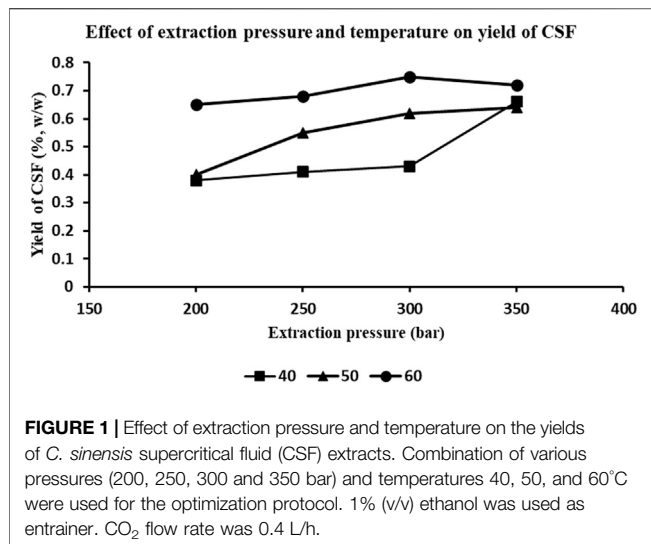
Protein leakage instigated within the bacterial pathogen's cellular environment triggered by particular CSF extracts as yet another antibacterial mechanism was examined (Zhang et al., 2015). Here, 16–18 h old cultures of bacteria in nutrient broth were centrifuged at 10,000 rpm for 20 min, followed by re-suspension in 0.8% physiological saline. After this, the bacterial cells were treated with CSF extracts of varied concentrations. Following an incubation period of 3 h, each bacterial suspension was centrifuged at 12,000 rpm for 15 min and the supernatant was analysed for protein content by Bradford method. Protein concentration at 595 nm was determined using bovine serum albumin (BSA) as standard.

Inhibition of Efflux Pumps in Bacterial Cells

Bacterial cultures inoculated in nutrient broth were incubated overnight for 24 h at 37°C at 95 rpm. The culture was then centrifuged for 5 min at 4000 rpm. Discarding the supernatant, the pellet collected was suspended in nutrient broth. A 500 $\mu\text{g/ml}$ sample of each CSF extract was prepared in nutrient broth. To individual wells of a 96 well microtiter plate, 150 μl nutrient broth containing bacterial inoculum, 20 μl ethidium bromide (EtBr) and 50 μl of the respective CSF sample was added and incubated for 10 min at room temperature. Thereafter, fluorescence was recorded using a fluorescence spectrophotometer over 30 min with interims of 5 min, at an excitation wavelength of 530 nm and emission wavelength of 600 nm. In this study, 5 μl of carbonyl cyanide 3-chlorophenylhydrazone or, "CCCP" known to be an effective efflux pump inhibitor was taken as the positive control and water served as negative control (Kumar et al., 2016).

Protective Action of CSF Extracts Against Hypobaric Hypoxia in Human Embryonic Kidney Cell Line

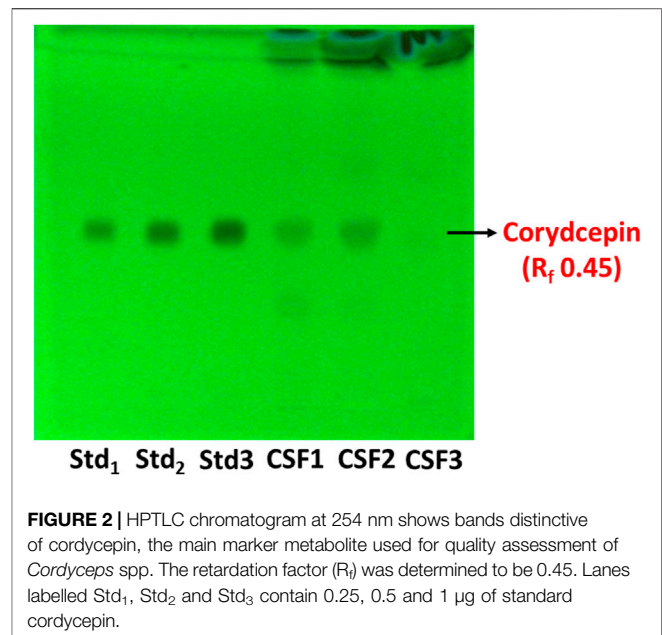
The protective effects of the *C. sinensis* supercritical fluid extract in recuperating human embryonic kidney cells (HEK 293) from hypoxic stress was evaluated by segregating the experimental cells into four groups for every dose (50/75/100/125 $\mu\text{g/ml}$) of each CSF extract. The groups were: normoxia control (N), normoxia supplemented with CSF extract (N+sample), hypoxia control (H) and, hypoxia supplemented with CSF extract (H+sample). Initially, the cells were cultured in high glucose DMEM (Dulbecco Minimal Essential Medium), (pH 7.2, 37°C, 5% CO_2) supplemented with antibiotics gentamycin sulphate (100 mg/L) and penicillin (100 mg/L) and enriched with foetal bovine serum (FBS) (10%, v/v) as described in a previous study (Kirar et al., 2017). Cells were grown in 96-well microtitre plates (Nunc, Roskilde, Denmark), maintaining a cell density of 10^5 cells/ cm^2 , and placed in incubator (New Brunswick, Galaxy 170R, Hamburg, Germany) with 21% O_2 i.e., normoxic condition. Experiments were conducted only on cells that were at least 80% confluent.



For hypoxia stress, cells were cultured for 24 h in a low oxygen environment (0.5% O₂, 5% CO₂ and 94.5% N₂) in New Brunswick Galaxy 48R hypoxia incubator (Hamburg, Germany). Cellular viability of the cells was determined using MTT assay (Mosmann, 1983). Different concentrations (50, 75, 100 and 125 µg/ml) of CSF extracts were supplemented to the growth medium, according to the aforementioned grouping. Dose of each CSF extract demonstrating maximum restoration of cellular viability under hypoxic conditions was inferred as its corresponding optimum dose.

Western Blotting for Assessing Effect of CSF Extract on HIF-1α Levels

Post hypoxia exposure, cells were de-adhered from the T25 flask by trypsinization (0.1%, v/v in PBS) for about 5 min. Cells were homogenized in radioimmunoprecipitation assay buffer (50 mM/L Tris-HCl, 150 mM/L NaCl, 0.1% sodium dodecyl sulfate, 1% NP-40, 0.5% deoxycholate, and protease inhibitor cocktail 5 µl/ml (MP Biomedicals, Ilkirch, France) and centrifuged at 12,000 × g at 4°C for 30 min. The supernatant collected contained cytosolic fractions. Total protein was estimated by Lowry's method (Nehra et al., 2015). For Western blotting, 25 µg of cytosolic protein was resolved in 10% SDS-PAGE (sodium dodecyl sulphate-polyacrylamide gel electrophoresis) and transferred onto nitrocellulose membrane (Millipore, Bedford, MA, United States) via semi-dry trans-blot system (BioRad, Hercules, CA, United States) at 15–20 V for 60 min. Membranes were blocked in blocking buffer composed of 3–5% bovine serum albumin in 0.5% Tris-buffered saline-Tween® (TBST), for 2 h and incubated with primary antibody i.e., polyclonal HIF-1α antibody (1:1000 dilution, E-AB-31662; Elabscience Biotechnology Inc., Houston, TX, United States) for 2 h. After washing in TBST, the membranes were incubated with appropriate secondary antibodies (1:20,000–30,000) (Santa Cruz Biotechnology, Dallas, TX, United States) at room temperature for 1 h, on dancing shaker. HIF-1α being probed was visualized



using H₂O₂/3,3',5,5'-tetramethylbenzidine (TMB) (Sigma-Aldrich, St. Louis, MO, United States). Quantitation was done by densitometric analysis using ImageJ software (Kirar et al., 2017).

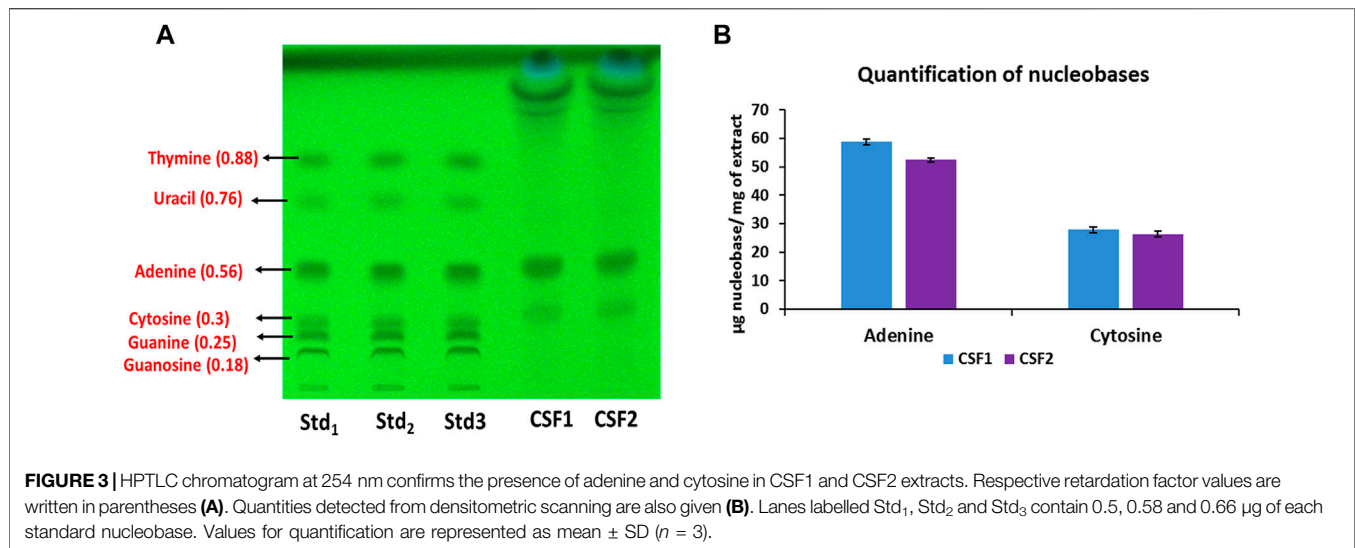
Statistical Analysis

Quantitation in all the HPTLC experiments were performed in triplicates. Data from antioxidant, antibacterial and *in vitro* cell culture assays were acquired in triplicate manner for all the CSF extracts in order to determine reproducibility. Results have been expressed as mean ± SD. All the statistical analyses viz., computation of mean and standard deviations were performed using Statistical Package for the Social Sciences (SPSS) software version V 2.21 (IBM, Chicago, IL, United States). One way analysis of variance (ANOVA) was applied to check the level of significance by Bonferroni *post hoc* tests. In all the tests, *p* < 0.05 was taken as a criterion for statistical significance.

For construction of variables factor maps by PCA, data acquisition and processing including generation of covariance matrices and proportion of variances were generated by R, version 4.0.3 (<http://cran.r-project.org/>).

RESULTS

The different combinations of four extraction pressures and three extraction temperatures resulted in acquisition of 12 supercritical CO₂ extracts, of varying yields. The effect of extraction pressures and temperatures on the yields of extracts is depicted in **Figure 1**. It is observed that the yields incremented with a combination of rising pressure and temperature, except for 350 bar and 60°C, which displayed lesser yield than that at 300 bar and 60°C. The maximal yields were achieved with combination of 1) extraction pressure of 300 bar and temperature of 60°C (extract labelled



“CSF1”) and, 2) extraction pressure of 350 bar and temperature of 60°C (extract labelled “CSF2”). Keeping the former condition intact but without the use of entrainer yielded the third extract “CSF3.” These three *C. sinensis* supercritical CO₂ extracts, were collectively referred to as “CSF extracts.” The yields were 0.75, 0.72 and 0.53% (w/w), for CSF1, CSF2 and CSF3, correspondingly. The physical properties of all the *C. sinensis* supercritical extracts were viewed to be sticky in nature and dark brownish in colour.

HPTLC Characterization Confirmed the Presence of Cordycepin, Flavonoids and Nucleobases in the CSF Extracts

HPTLC fingerprinting given in Figure 2 illustrated distinct bands indicative of cordycepin, the main marker metabolite of *C. sinensis* in CSF1 and CSF2, but not in CSF3. Cordycepin was quantitated to be fairly more in CSF1 with 296.6 ± 15.3 µg/mg of extract than CSF2 (267.1 ± 9.2 µg/mg of extract).

Figure 3A represents the HPTLC chromatogram for identification of nucleobases in *C. sinensis* supercritical extracts. Among the nucleobases under consideration, adenine and cytosine were detected in CSF1 and CSF2. Figure 3B denotes the quantities of these nucleobases as calculated from densitometric scanning. It was perceived that CSF1 consisted of a marginally higher content of adenine (58.85 ± 0.24 µg/mg of extract) and cytosine (27.94 ± 1.81 µg/mg of extract) than that in CSF2, where adenine content was 52.43 ± 0.68 µg/mg of extract and cytosine was 26.35 ± 1.07 µg/mg of extract.

Figure 4A represents the HPTLC profiling for flavonoids detected in *C. sinensis* supercritical extracts. Here, presence of ascorbic acid, gallic acid and quercetin was confirmed in CSF1 and CSF2. Figure 4B denotes the quantities of these flavonoids as measured using densitometric scanning. It was clearly seen that CSF1 possessed the highest quantity of all three aforesaid flavonoids having ascorbic acid, gallic acid and quercetin in amounts of 15.2 ± 0.6 , 3.8 ± 0.48 and 10.63 ± 0.26 µg/mg of

extract. Corresponding values of CSF2 were 14.48 ± 0.5 , 3.18 ± 0.19 and 8.55 ± 0.28 µg/mg of extract. CSF3 was found to have only quercetin (2.31 ± 0.27 µg/mg of extract). The identification and quantification of bands corresponding to standard nucleobases or flavonoids has been performed within the permissible evaluation window of winCATS software.

Presence of Putative Bioactive VOCs Verified by GC-MS Analysis

The CSF extracts were observed to comprise various VOCs inclusive of alcohols, esters, stearates, terpenes, etc. The major VOCs detected in the supercritical CO₂ extracts with their respective retention times, peak areas and area percentages are depicted in Tables 1–3 for CSF1, CSF2 and CSF3, respectively. Results based on the area percentages of individual VOCs established that 9,12-octadecadienoic acid (Z,Z)- or, α-linoleic acid was the most abundant VOC in CSF1; 9,12-octadecadienoic acid (Z,Z)-, trimethylsilyl ester i.e., linoleic acid trimethylsilyl ester was the most abundant VOC in CSF2 whereas hexadecanoic acid, trimethylsilyl ester (palmitic acid TMS) was the most abundant VOC in CSF3. Total ion chromatograms of the aforesaid most abundant VOCs are represented in Figure 5. All the three supercritical extracts individually had certain VOCs which are unique to each of them, thus proving that every individual sample had its own distinct characteristics in terms of bioactivity, as discoursed later.

Metabolomics by PCA Based on Chromatographic Data Verified Inter-relatedness Between CSF1 and CSF2

The chromatographic data acquired from metabolite profiling were subjected to chemometric analysis in an open source R studio, to carry out data reduction and pattern recognition. In case of both HPTLC and GC-MS data, two major principal components, represented as Dim1 and Dim2 depicted the overall variance over

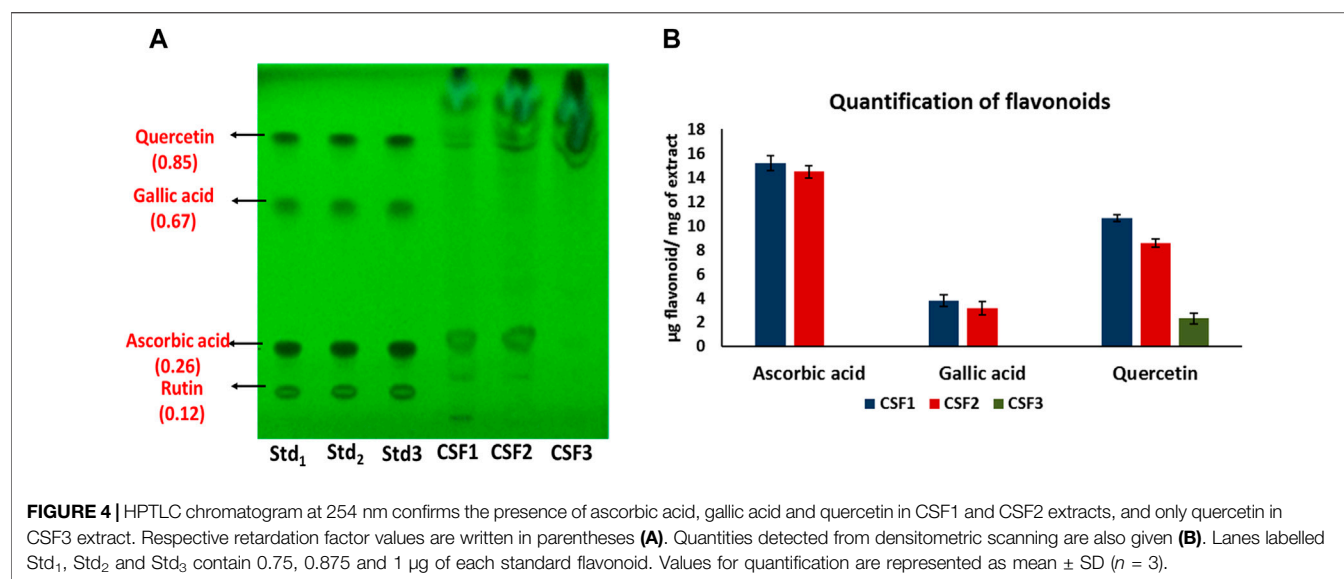


TABLE 1 | List of major volatile organic compounds detected in CSF1 extract by GC-MS.

Peak	Retention time (R_t), min	Area	Area%	Name
1	26.121	419,928	0.29	1-TETRADECANOL, ACRYLATE
2	29.466	444,072	0.30	TETRADECANOIC ACID, TRIMETHYLSILYL ESTER
3	29.803	1,550,751	1.07	PENTADECANOIC ACID
4	31.056	858,623	0.59	HEXADECANOIC ACID, METHYL ESTER
5	31.596	2,185,882	1.50	<i>n</i> -PENTADECANOIC ACID, TRIMETHYLSILYL ESTER
6	32.152	20,965,594	14.40	PENTADECANOIC ACID
7	32.673	1,888,914	1.30	HEXADECANOIC ACID, ETHYL ESTER
8	33.776	2,952,332	2.03	HEXADECANOIC ACID, TRIMETHYLSILYL ESTER
9	34.165	1,824,254	1.25	9-OCTADECENOIC ACID (Z-)
10	34.609	6,324,673	4.34	9,12-OCTADECADIENOIC ACID (Z,Z)-, METHYL ESTER
11	35.484	56,200,296	38.60	9,12-OCTADECADIENOIC ACID (Z,Z)-
12	35.650	10,256,586	7.04	ETHYL (9Z,12Z)-9,12-OCTADECADIENOATE #
13	36.364	2,484,453	1.71	LINOSAEURE, TRIMETHYLSILYL ESTER
14	37.597	1,243,151	0.85	OCTANAMIDE, N-(2-HYDROXYETHYL)-
15	38.138	1,785,300	1.23	METHYL OCTADEC-9,12-DIENOATE
16	39.930	759,375	0.52	1,2-BENZENEDICARBOXYLIC ACID
17	42.270	679,937	0.47	13-DOCOSENAMIDE, (Z)-
18	42.475	592,267	0.41	DECANEDIOIC ACID, BIS (2-ETHYLHEXYL) ESTER
19	43.567	790,657	0.54	TETRACONTANE
20	45.138	9,853,510	6.77	9(11)-DEHYDROERGOSTERYL BENZOATE
21	45.618	1,157,108	0.79	9(11)-DEHYDROERGOSTERYL BENZOATE
22	45.936	1,053,723	0.72	HEXADECANOIC ACID, METHYL ESTER
23	46.907	537,691	0.37	TETRACONTANE
24	47.115	717,398	0.49	PYRAZINE, TETRAKIS (1-METHYLETHYL)-
25	49.081	1,162,320	0.80	ERGOSTA-5,7,9(11),22-TETRAEN-3-OL, (3 β ,22 E)
26	50.015	6,610,013	4.54	ERGOSTEROL
27	51.612	3,491,024	2.40	16-HENTRIACONTANONE
28	55.315	6813,607	4.68	10,13-DIMETHYL-17-(1,4,5-TRIMETHYL-HEX-2-ENYL)
		145,603,439	100	

The retention times, peak areas and area percentages are indicated.

the entire dataset. The primary axis, i.e., the first principal component describes majority of the variance in a factor map.

For HPTLC data, all the retardation factors from analysis of both nucleobases as well as flavonoids were taken into account to form data matrix. Information pertaining to retardation factor

values and peak areas of 98 metabolites were compressed to manifest the entire data in form of Dim 1 and Dim 2, whose values were 40.33 and 27.91% in variables factor map (Figure 6A). Data compression in PCA ensures that there is no loss in variances while describing the dataset.

TABLE 2 | List of major volatile organic compounds detected in CSF2 extract by GC-MS.

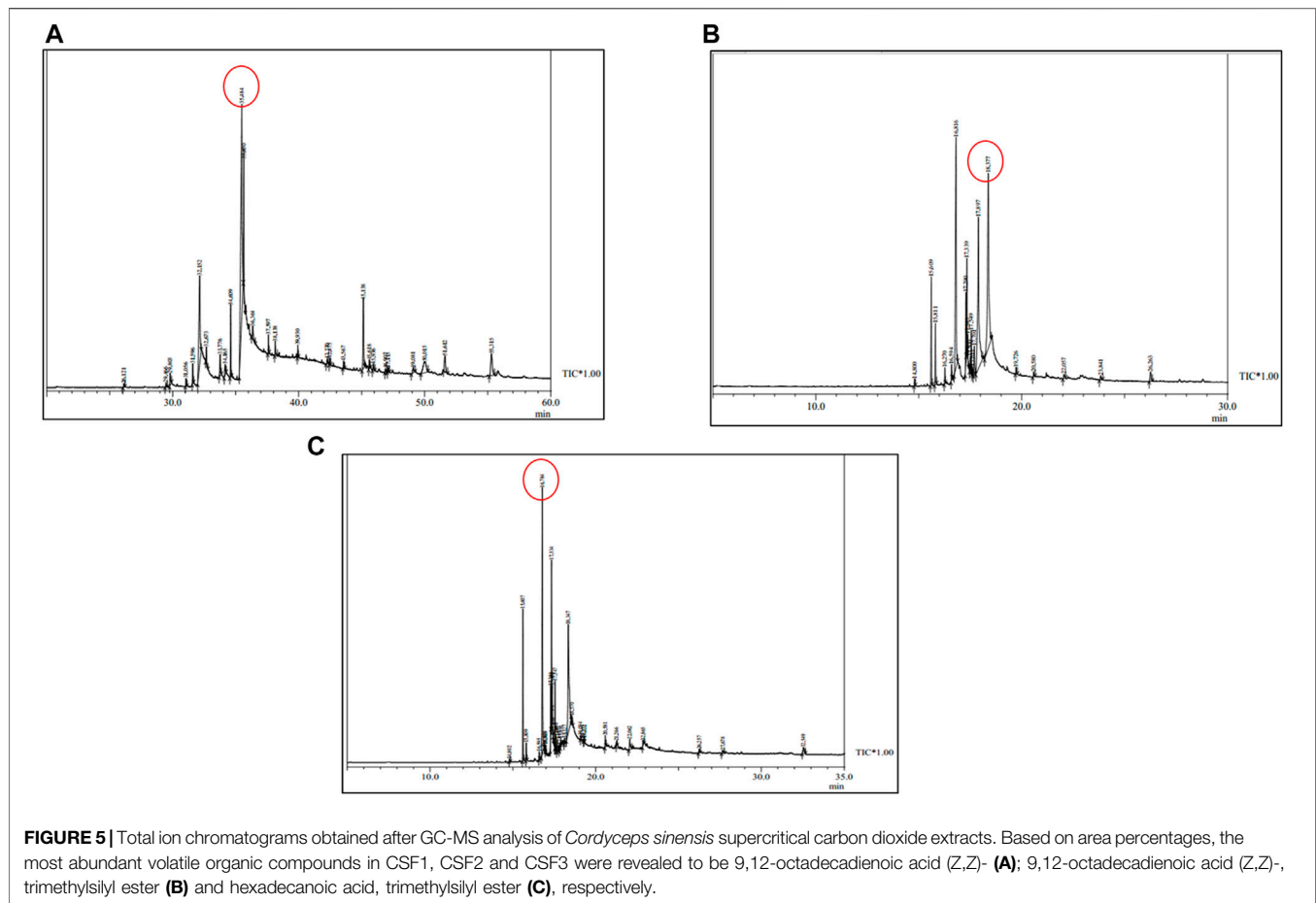
Peak	Retention time (R _t), min	Area	Area%	Name
1	14.800	145,752	0.36	TETRADECANOIC ACID, TRIMETHYLSILYL ESTER
2	15.609	2,388,227	5.84	HEXADECANOIC ACID, METHYL ESTER
3	15.811	1,402,036	3.43	<i>n</i> -PENTADECANOIC ACID, TRIMETHYLSILYL ESTER
4	16.270	322,754	0.79	HEXADECANOIC ACID, ETHYL ESTER
5	16.594	312,992	0.76	<i>cis</i> -9-HEXADECENOIC ACID, TRIMETHYLSILYL ESTER
6	16.816	9,859,447	24.09	HEXADECANOIC ACID, TRIMETHYLSILYL ESTER
7	17.290	1,431,582	3.50	9,12-OCTADECADIENOIC ACID (Z,Z)-, METHYL ESTER
8	17.339	1,803,748	4.41	9-OCTADECENOIC ACID, METHYL ESTER
9	17.383	353,836	0.86	9-OCTADECENOIC ACID (Z-), METHYL ESTER
10	17.500	253,523	0.62	9,12-OCTADECADIENOIC ACID (Z,Z)-, TRIMETHYLSILYL ESTER
11	17.549	765,219	1.87	METHYL STEARATE
12	17.611	176,041	0.43	METHYL 15-HYDROXY-9,12-OCTADECADIENOATE
13	17.701	933,283	2.28	HEPTADECANOIC ACID, TRIMETHYLSILYLESTER
14	17.897	9,004,280	22.00	9,12-OCTADECADIENOIC ACID (Z,Z)-
15	18.377	10,633,336	25.99	9,12-OCTADECADIENOIC ACID (Z,Z)-, TRIMETHYLSILYL ESTER
16	19.726	192,583	0.47	CYCLOPROPANEOCTANOIC ACID,2-[(2-ETHYLCYCLOPROPYL)METHYL ESTER]
17	20.580	134,002	0.33	1,3,5-TRISILACYCLOHEXANE
18	22.057	194,423	0.48	1,3-DIOXOLANE, 2-METHOXY-4-HEXADECENYL ESTER
19	23.841	150,386	0.37	SQUALENE
20	26.263	462,562	1.13	9(11)-DEHYDROERGOSTERYL BENZOATE
		409,200,002	100	

The retention times, peak areas and area percentages are indicated.

TABLE 3 | List of major volatile organic compounds detected in CSF3 extract by GC-MS.

Peak	Retention time (R _t), min	Area	Area%	Name
1	14.802	28,836	0.21	TETRADECANOIC ACID, TRIMETHYLSILYL ESTER
2	15.607	1,519,042	11.10	HEXADECANOIC ACID, METHYL ESTER
3	15.809	192,622	1.41	<i>n</i> -PENTADECANOIC ACID, TRIMETHYLSILYL ESTER
4	16.595	75,701	0.55	OCTADECANOIC ACID, METHYL ESTER
5	16.784	3,575,513	26.14	HEXADECANOIC ACID, TRIMETHYLSILYL ESTER
6	16.924	45,600	0.33	ANDROST-1-EN-3-ONE, 17-HYDROXY (5.α., 17.β.)-
7	16.980	157,023	1.15	17-OCTADECEN-14-YNOIC ACID, METHYL ESTER
8	17.284	463,156	3.39	9,12-OCTADECADIENOIC ACID (Z,Z)-, METHYL ESTER
9	17.334	1,503,058	10.99	9-OCTADECENOIC ACID, METHYL ESTER
10	17.380	240,987	1.76	9-OCTADECENOIC ACID (Z-), METHYL ESTER
11	17.436	51,640	0.38	METHYL OCTADEC-9,12-DIENOATE
12	17.547	647,472	4.73	METHYL STEARATE
13	17.608	142,648	1.04	METHYL 15-HYDROXY-9,12-OCTADECADIENOATE
14	17.697	210,047	1.54	HEPTADECANOIC ACID, TRIMETHYLSILYL ESTER
15	17.813	60,642	0.44	4-BROMOBUTANOIC ACID, DODEC-3-YNYL ESTER
16	17.891	78,198	0.57	OXACYCLOHEPTADEC-8-EN-2-ONE, (8Z)
17	18.127	65,294	0.48	9,12-OCTADECADIENOIC ACID, METHYL ESTER
18	18.347	3,477,306	25.42	9,12-OCTADECADIENOIC ACID (Z,Z)-, TRIMETHYLSILYL ESTER
19	18.570	102,810	0.75	OCTADECANOIC ACID, TRIMETHYLSILYL ESTER
20	19.094	30,316	0.22	DOCOSANOIC ANHYDRIDE
21	19.272	28,802	0.21	2, PYRROLIDINONE, 1-[2-(4-PIPERIDINYL)ETHYL]-
22	19.322	24,106	0.18	EICOSANOIC ACID, METHYL ESTER
23	20.582	149,004	1.09	1,3,5-TRISILACYCLOHEXANE
24	21.266	59,380	0.43	HEXADECANOIC ACID, 4-TRIMETHYLSILYL ESTER
25	22.062	249,823	1.83	5,5-DIMETHYL-1,3-DIOXANE-2-ETHANOL, TERT-BUTYLDIMETHYLILYL ESTER
26	22.865	95,494	0.70	9-OCTADECENOIC ACID (Z)-,2-TRIMETHYLSILYL ESTER
27	26.257	851,928	0.62	9(11)-DEHYDROERGOSTERYL BENZOATE
28	27.678	91,601	0.67	STIGMASTA-4,7,22-TRIEN-3.BETA.-OL
29	32.549	229,002	1.67	16-HENTRIACONTANONE
		13,680,321	100	

The retention times, peak areas and area percentages are indicated.



Similarly, the factor map constructed on basis of retention times of 67 constituent VOCs exhibited a variance of Dim 1 = 43.95% and Dim 2 = 24.85% (Figure 6B).

It can be clearly seen that CSF3 was present in separate quadrants, distinctive from CSF1 and CSF2, in case of both HPTLC as well as GC-MS profiling. This can be linked to the difference in metabolome owing to variation in extract preparation protocol. Moreover, the presence of CSF1 and CSF2 in the same quadrant and their proximity to each other illustrated their obvious interrelatedness (Figure 6).

CSF Extracts Exhibited Substantial Free Radical Scavenging and FRAP Activities

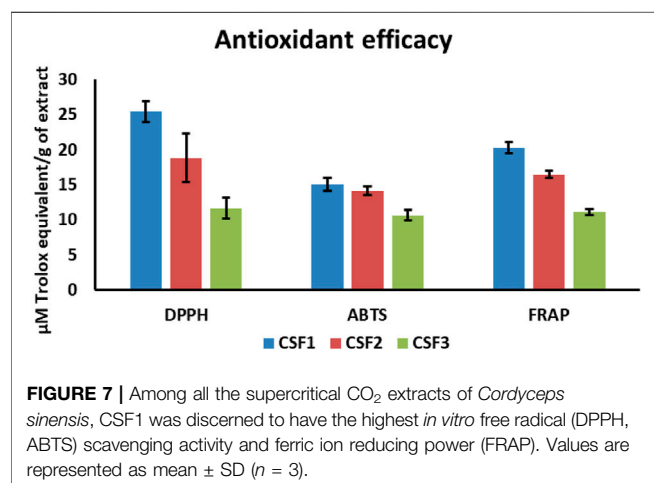
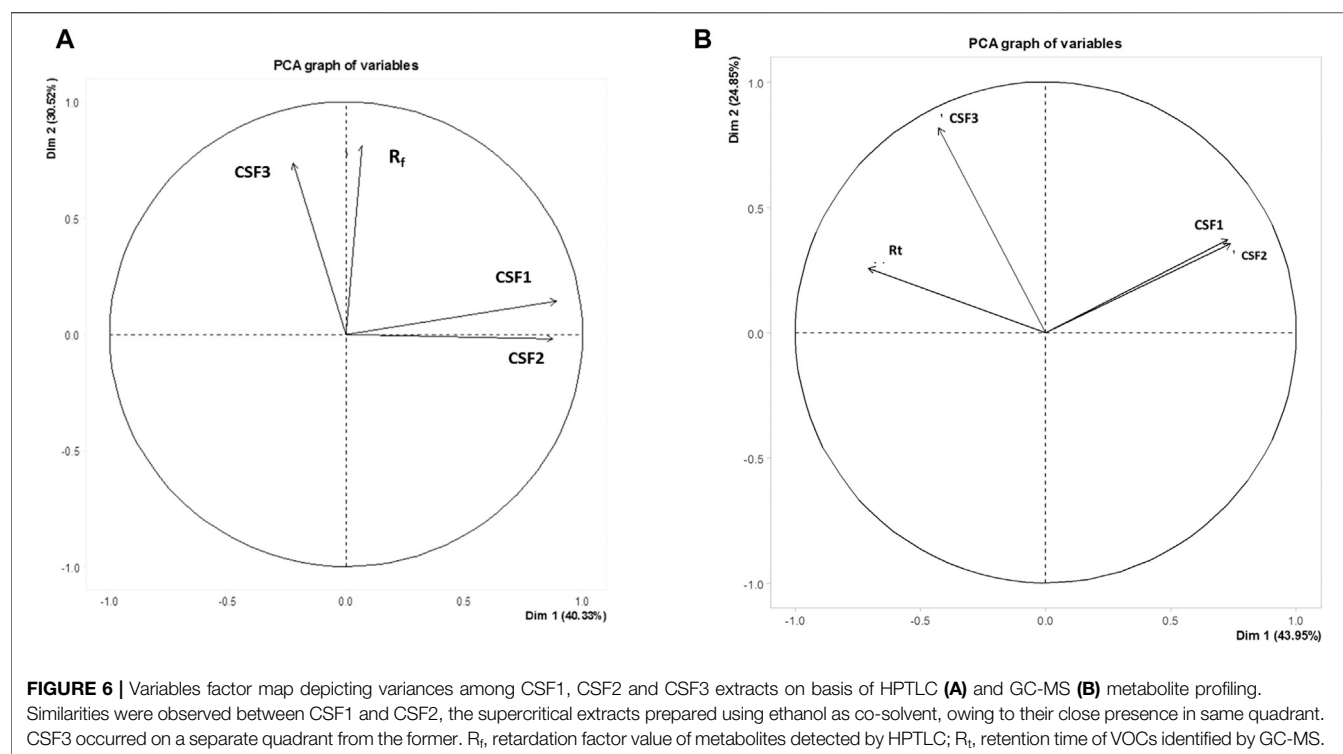
All the CSF extracts were capable of antioxidant power by virtue of free radical scavenging as well as ferric ion reduction. DPPH radical scavenging activities were 25.39 ± 1.48 , 18.82 ± 3.42 , and 11.65 ± 1.44 $\mu\text{M TE/g}$ of extract, in that order for CSF1, CSF2 and CSF3. Similarly, ABTS assays brought out an activity of 15.05 ± 0.91 , 14.12 ± 0.65 , and 10.64 ± 0.72 $\mu\text{M TE/g}$ of extract, correspondingly for CSF1, CSF2 and CSF3. FRAP results of the three supercritical CO_2 extracts explicated the antioxidant potential as 20.22 ± 0.82 , 16.47 ± 0.44 and 11.14 ± 0.43 $\mu\text{M TE/g}$ of extract. Overall, it can be verified from

above results that CSF1 had the highest antioxidant potency over the rest supercritical fluid extracts (Figure 7).

CSF Extracts Were Observed to Be Potent Antibacterial Leads Against *E. coli* and *S. typhi*

The significant presence of bioactive metabolites in the CSF extracts and their effective antioxidant abilities stimulated exploration of further bioeffects. In this context, evaluation of antibacterial activities clearly exhibited the efficacy of all three CSF extracts as potential antibacterial agents against pathogenic strains of *E. coli* and *S. typhi*.

For CSF1, agar disc diffusion studies brought out distinct zones of inhibition of diameters 7.0 ± 0.5 mm and 8.5 ± 0.7 mm against *E. coli* and *S. typhi*. Likewise, CSF2 wielded zones of inhibition of 7.5 ± 0.7 mm and 8.2 ± 1.0 mm averting *E. coli* and *S. typhi*. For these two pathogens, CSF3 exerted comparatively lesser antibacterial action wherein the zones of inhibition were 6.5 ± 0.5 mm and 6.5 ± 1.5 mm. The positive control, kanamycin gave distinct zones of inhibition of 30 ± 2 mm against *E. coli* and 35 ± 1.5 mm against *S. typhi*. The zones of inhibition and MIC values of all CSF extracts are noted in Table 4. Representative figure illustrating discrete zones of inhibition of CSF1 and CSF2 against *S. typhi* is given in Figure 8A.



Owing to promising insights of CSF extracts being prospective antibacterials, certain typical mechanisms of inhibitory action were examined. Generation of ROS, induction of protein leakage and inhibition of efflux pumps were confirmed to be the modes of antibacterial action.

ROS generated in bacterial microenvironment after exposure to CSF extracts were measured using DCFDA. A linearly upward trend was indicated in levels of ROS formed with increasing doses of CSF1, CSF2 and CSF3 over 50–125 $\mu\text{g/ml}$, against both *E. coli* (Figure 8B) and *S. typhi* (Figure 8C). The bactericidal action was also analysed by probing concomitant leakage of intracellular proteins upon treatment with the CSF extracts. Results portrayed

TABLE 4 | Inhibitory action of *Cordyceps sinensis* supercritical carbon dioxide extracts on bacterial pathogens, *Escherichia coli* and *Salmonella typhi*.

Extract	Zone of inhibition (mm)	MIC ($\mu\text{g/ml}$)
CSF1:		
<i>E. coli</i>	7.0 ± 0.5	50
<i>S. typhi</i>	8.5 ± 0.7	35
CSF2:		
<i>E. coli</i>	7.5 ± 0.7	40
<i>S. typhi</i>	8.2 ± 1.0	45
CSF3:		
<i>E. coli</i>	6.5 ± 0.5	60
<i>S. typhi</i>	6.5 ± 1.5	65
Kanamycin:		
<i>E. coli</i>	30 ± 2	5
<i>S. typhi</i>	35 ± 1.5	5

Values for diameters of zones of inhibition (in mm) are given as mean \pm SD ($n = 3$). Values in $\mu\text{g/ml}$ indicate the specific minimal inhibitory concentrations (MIC). Kanamycin antibiotic was taken as the positive control against both pathogenic strains.

that incremented doses of these extracts resulted in higher amount of protein leakage from the bacterial pathogens—*E. coli* as seen from Figure 8D and *S. typhi* (Figure 8E). This observation was consonant with those obtained for ROS generation that the extent of bactericidal action was proportionate to CSF extract doses. Figures 8B–E also depict that CSF2 showed the most potent abilities in generation of ROS and eliciting protein leakage in the bacterial pathogens.

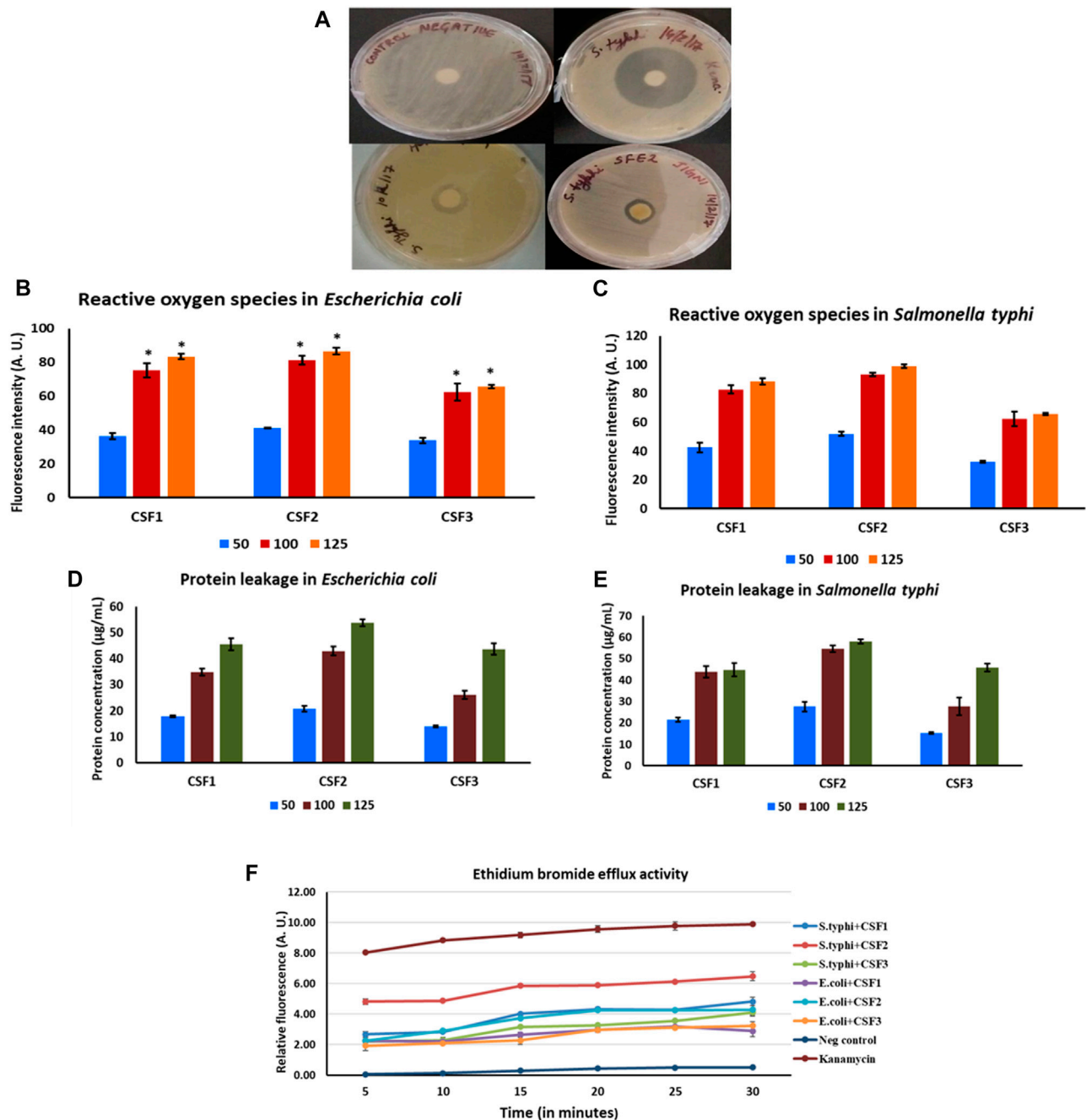
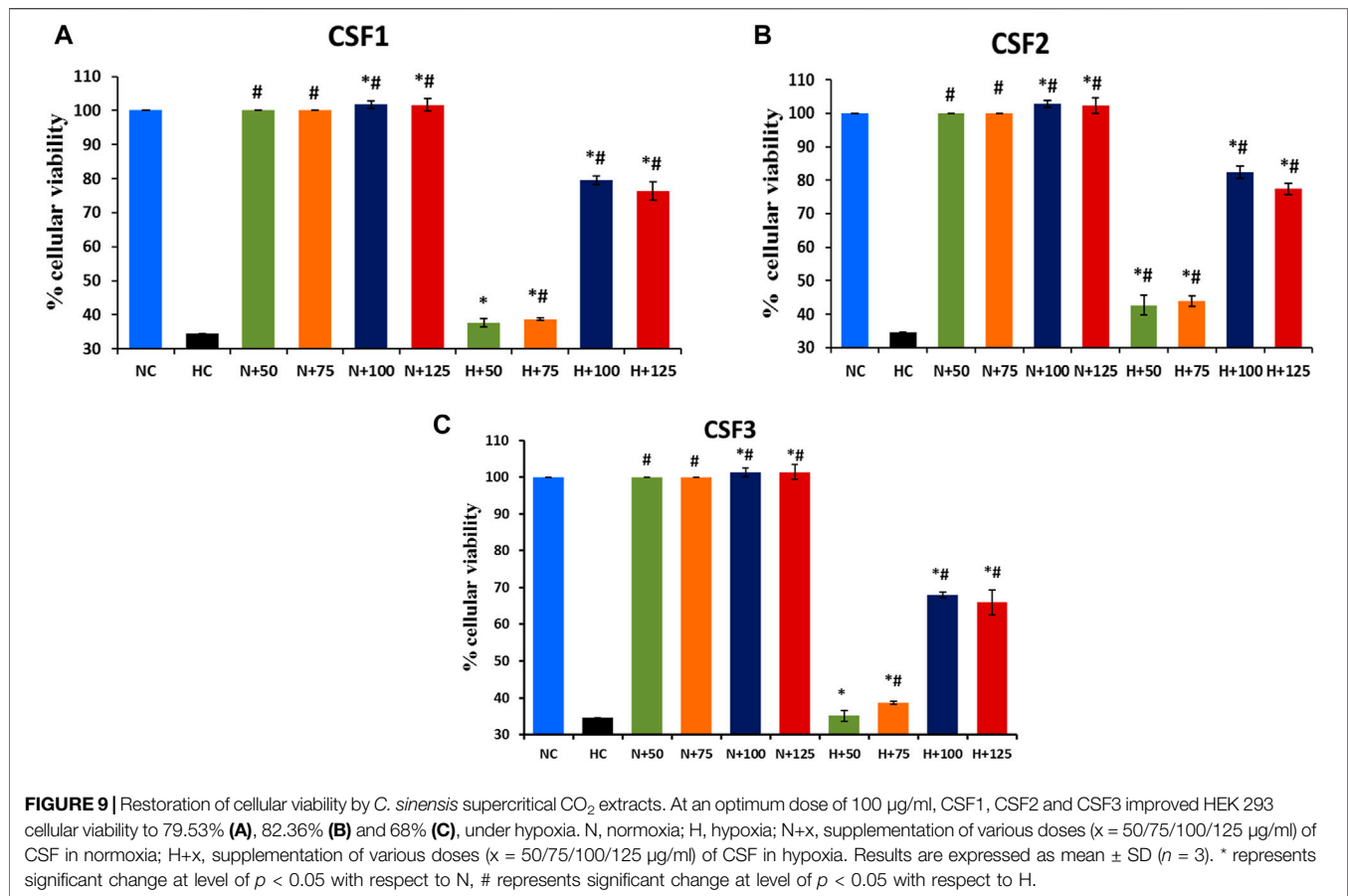


FIGURE 8 | Distinct zones of inhibition after treatment with CSF1 and CSF2 extracts, against pathogenic *Salmonella typhi* can be clearly seen (A). Generation of reactive oxygen species after treatment with different doses (50, 100, 125 µg/ml) of *Cordyceps sinensis* supercritical fluid extracts within *E. coli* (B) and *S. typhi* (C) was deduced as a potential antibacterial mode of action. Induction of protein leakage of aforesaid extracts against *E. coli* (D) and *S. typhi* (E) was confirmed to be yet another inhibitory mechanism. The supercritical fluid extracts also led to inhibition of efflux pump activities in the bacterial cells (F). Nutrient broth and kanamycin acted as negative and positive controls, respectively. Data are expressed as mean ± SD ($n = 3$). * represents significant change at level of $p < 0.05$.

Besides, it was also proven that CSF2 followed by CSF1 and finally, CSF3 effectually displayed EtBr efflux pump inhibitory activity against *E. coli* and *S. typhi*, thus revealing yet another essential mode of bactericidal action. The results are indicated in Figure 8F.

CSF Extracts Conferred Protective Action in HEK 293 Cells Against Hypobaric Hypoxia

Previous literature has sufficient evidence to testimony that hypoxic stress noticeably damages the normal functioning of kidney, thus leading to renal failure (Fu et al., 2016). Thus, it is



imperative to develop therapeutics for recuperating the detrimental effects of hypobaric hypoxia. With this perspective, the proficiency of *C. sinensis* supercritical CO₂ extracts as protective leads against hypoxia in human embryonic kidney, HEK 293 cells was probed.

Exposure to hypoxia in culture conditions significantly reduced the viability of HEK 293 cells to 37.5%, in contrast to 100% cell viability under normoxia. Significant restoration (*p* < 0.05) of cell viability under hypoxic milieu was brought about by the addition of CSF extracts. The effect of *C. sinensis* supercritical extracts in efficaciously countering the debilitating impact of hypoxia milieu is shown in **Figure 9**. Out of all the different doses that is, 50/75/100/125 µg/ml of the subject extracts being studied, 100 µg/ml was ascertained to be the optimal dose. The best cytoprotective action against hypoxia was conferred by CSF2 whose optimum dose of 100 µg/ml revived cell viability to $82.36 \pm 1.76\%$ (**Figure 9B**). This was followed by CSF1 and then CSF3 that improved cellular viability to $79.53 \pm 1.33\%$ (**Figure 9A**) and $68 \pm 0.75\%$ (**Figure 9C**), in that order.

CSF2 Efficiently Modulated HIF-1α in HEK-293 Cells, as a Predominant Protective Mechanism Against Hypobaric Hypoxia

The effect of the CSF extract showing highest protective potential, i.e., CSF2 was studied on modulation of HIF-1α, the main marker

of cell survivability under low oxygen tension. Western blotting experiments brought out that level of HIF-1α, which was otherwise heightened in hypoxia conditions, was visibly diminished after supplementation with CSF2. β-Actin served as the loading control (**Figure 10A**). Densitometry by ImageJ revealed that CSF2 influenced a four-fold downregulation in the levels of HIF-1α, as verified from **Figure 10B**.

DISCUSSION

The use of supercritical fluids is gaining ground as a “green technology” for faster production of bioactive extracts of higher purity, with the use of non-toxic solvents like water or CO₂. It is worth mentioning here that water has a critical temperature of 374°C and critical pressure of 22.1 MPa whereas CO₂ has parallel values of 31.2°C and 7.3 MPa. These moderate operational requirements of CO₂ make it a preferred choice over water in supercritical fluid extraction. The major advantages of using supercritical CO₂ from a pharmacological viewpoint is that, since the process parameters i.e., supercritical conditions are moderate, there is no risk of extract degradation. In addition, by bringing about slight variations in temperature or pressure, the selectivity of target compound can be varied. Moreover, CO₂ as a solvent is categorized as GRAS (“generally regarded as safe”), hence end products are not harmful or toxic. Also, the products

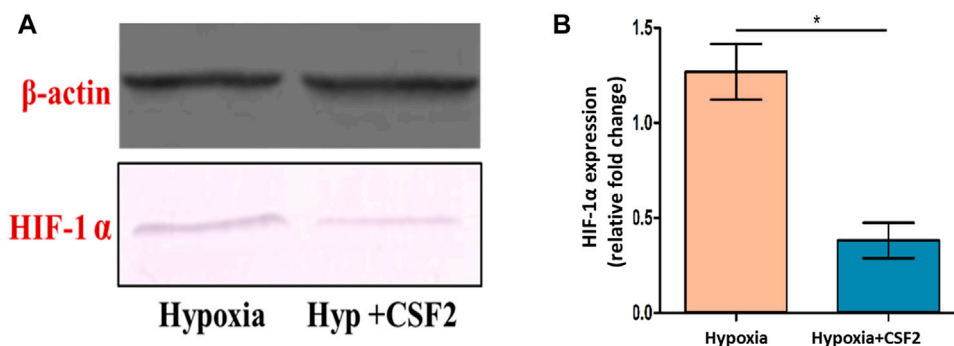


FIGURE 10 | Western blot showing level of hypoxia inducible factor-1 alpha (HIF-1 α) (A), which otherwise elevated under hypoxia stress, was decreased after supplementation with CSF2 (B). Hypoxia+CSF2 indicates supplementation of 100 μ g/ml of CSF2 extract in HEK 293 cells being cultured in low oxygen tension (0.5% O₂). Results are expressed as mean \pm SD ($n = 3$). * represents significant change at level $p < 0.05$.

are almost residue free; even if co-solvents like ethanol are added, they are easily removed (Bhusnure et al., 2015). Also, carbon dioxide has low viscosity and better diffusivity capacity in solid matrices owing to its dual gaseous and liquid-like properties, thus efficiently solubilizing the desired bioactive compounds (Capuzzo et al., 2013). Supercritical CO₂ has been reportedly used for separation of alkaloids, carotenoids, essential oils, flavones, preparation of several value-added pharmaceuticals, cosmetics, nutraceuticals, food additives, etc. (Machmudah et al., 2006; Takeuchi et al., 2010; Rahimi et al., 2011; Kagliwal et al., 2012).

The only shortcoming linked to the usage of supercritical CO₂ is its low polarity index that obstructs efficient extraction of polar compounds. This limitation is overcome with the addition of entrainers or co-solvents like methanol, ethanol, or water. Use of co-solvents indirectly enhances the solute contact with solvent, thus, offering an augmented overall solubility and optimum mass transfer, especially of bioactive polar compounds in the extract (Walsh et al., 1987; Pronyk and Mazza, 2009). Previous reports cite that the usage of co-solvents result in efficient extraction of polar compounds (Antunes-Ricardo et al., 2017; Wrona et al., 2017). It is always ensured that the co-solvent is added temperately, mostly ranging from 1 to 5% (w/w) so as to minimize time taken for its removal or recovery, *per se*. Ethanol being a food grade modifier is often used as the co-solvent for choice while preparing supercritical extracts for pharmacological or nutraceutical purposes (Sovová et al., 2001; Macías-Sánchez et al., 2009; Capuzzo et al., 2013; Nagavekar and Singhal, 2018) including separation of bioactive compounds from various traditional Chinese medicinal sources (Li, 2007). In this outlook, supercritical CO₂ along with ethanol as an entrainer was used for preparing supercritical extracts from the Indian high-altitude variety of “keera jhari” or *C. sinensis*.

Previous studies have established that an increase in extraction pressure enhances the fluid density, thus, increasing the solvating power, hence resulting in higher extraction yield. However, the effect of temperature in supercritical fluid extraction is not always linear. The influence of temperature on extraction is a lot more difficult to predict than that of pressure due to the above stated counter effects. An increase in temperature might lead to increase or decrease in yield, or even not affect the yield at all, depending

on the competing effect between fluid density and solute vapor pressure (Shao et al., 2014; Danlami et al., 2015; Hamid et al., 2018).

The results in our study were in agreement with the aforesaid observations where the higher yields were obtained with the highest extraction pressures, i.e., 300 and 350 bar. Also, the yields incremented with a combination of rising pressure and temperature, except for 350 bar and 60°C, which displayed lesser yield than that at 300 bar and 60°C (Figure 1). Since the major objective of our study was to establish the bioefficacy of the *C. sinensis* supercritical CO₂ extracts rather than an elaborate response-based analysis, we selected only those extracts of maximal yields, i.e., CSF1 (300 bar, 60°C) and CSF2 (350 bar, 60°C) for further analyses. For preparation of CSF3, i.e., without entrainer, the best yielding combination of pressure of 300 bar and temperature of 60°C was maintained.

With respect to the flow rate, certain studies have reported that higher solvent flow rate raises the operational and capital costs. Moreover, efficiency of the column is compromised with increased CO₂ flow rate, since the HTU (height of a transfer unit) increases with increasing CO₂ loading. Also, a high flow rate may cause decrease in the yield either by increasing analyte loss during fluid decompression or by increasing the pressure drop across the extraction cell. On the other hand, a very low flow rate might not facilitate ideal extraction at all (Mendiola et al., 2013; Shao et al., 2014). Keeping these factors in consideration, a moderate flow rate of 0.4 L/h was maintained in this study.

The three final extracts - CSF1, CSF2 and CSF3 had yields 0.75, 0.72 and 0.53% (w/w), respectively. Akanda et al. (2012) have cited that pressure, temperature and time can influence the supercritical extraction procedure, in turn, affecting the yields. The manner in which the above parameters affect the actual extraction depends on the type of the raw material and also on the target metabolite. In the present study, the extraction temperature was kept constant at 60°C. A pressure of 300 bar was applied over 2 h for CSF1. A higher pressure i.e., 350 bar was applied for a shorter time to obtain CSF2. The better yield of CSF1 than CSF2, despite a marginally higher extraction pressure, can be ascribed to the longer extraction time in the former. The noticeably lower yield of CSF3 highlighted the significant procedural impact of

ethanol as a co-solvent, which at a volume as low as 1%, enhanced the overall yield, and also the content of metabolites in CSF1 and CSF2, as discussed in subsequent paragraphs. The yields in current study were lower than conventional extraction methods wherein the yield of aqueous extract obtained by hot water extraction was reportedly 25.4% (Zheng et al., 2008). The yield as observed in case of accelerated solvent extraction was 33.3% (Rakhee et al., 2016). Despite lower yields, the supercritical CO₂ extracts prepared here were rich in bioactive metabolites as discussed in following paragraphs.

The supercritical extracts were quantitatively characterized by HPTLC in terms of cordycepin, nucleobases and flavonoids. High throughput, ease of workflow and efficient automation in HPTLC procedure makes it an ideal tool for identification and quantification of bioactive molecules in natural extracts (El-Gindy et al., 2001). Cordycepin or 3'-deoxyadenosine, the predominant functional marker of *Cordyceps* spp. was quantified by HPTLC for quality assessment of the CSFs. It was found that CSF1 and CSF2 exhibited distinct bands suggestive of cordycepin, at quantities $296.6 \pm 15.3 \mu\text{g/g}$ extract and $267.1 \pm 9.2 \mu\text{g/g}$ extract, respectively. As depicted in **Figure 1**, there was a directly proportionate effect of extraction pressure on the extract yield, except the decrease at 350 bar, 60°C. Thus, CSF1 had better yield than CSF2. This lesser overall yield of CSF2 than CSF1 possibly influenced the lesser amount of cordycepin in CSF2, in comparison to CSF1. In addition, the longer extraction time period also contributed to the higher quantity of cordycepin detected in CSF1. CSF3, whose preparation was bereft of ethanol as co-solvent did not display any band specific to cordycepin, thus, indicating that ethanol was essential to extract out polar compounds. Cordycepin has been noted to exert anti-proliferative activity on cancerous cell lines like human colorectal adenocarcinoma, HT-29 and human colorectal carcinoma, HCT 116 (Lee et al., 2013; Jeong and Choi, 2014). Cordycepin has also been seen to elicit apoptosis in human leukemia cells *via* ROS-mediated caspase pathway. In line of this, presence of cordycepin in CSF1 and CSF2 indicated their potential bioactive properties.

Nucleobases identified in CSF1 and CSF2 extracts were adenine and cytosine, as seen in **Figure 3**. The markedly better content of these two nucleobases typically coincided with the higher yield and longer extraction time for procuring CSF1, in comparison to CSF2. Adenine plays key role in cellular respiration in higher organisms and cytosine is essential for energy transport (Hasan et al., 2019). Hence, availability of these nucleobases suggested their prospective bioeffects, especially from a hypoxia-protective standpoint.

Flavonoids encompass a class of bioactive compounds occurring in medicinal plants and mushrooms that have established benefits towards improvement of human health (Nijveldt et al., 2001). Specifically, quercetin, gallic acid, ascorbic acid and rutin were selected as the standard flavonoids for identification in *C. sinensis* supercritical extracts due to their reported anti-carcinogenic, anti-mutagenic and anti-oxidative modes of actions. In addition, supplementation of flavonoids in diet of human volunteers has been cited to induce free radical scavenging, blood viscosity lowering and

enhancement of function of vital organs (Hoensch and Kirch, 2005). Similar to cordycepin and nucleobases, even flavonoids namely, quercetin, gallic acid and ascorbic acid were quantitated to be more in CSF1 than CSF2 (**Figure 4**). These being polar compounds were not extracted efficiently in CSF3, which contained only quercetin.

HPTLC analysis clearly revealed that CSF1 had an overall higher content of all the aforementioned bioactive compounds than CSF2. This was possibly due to the fact that at a constant temperature, a rise in pressure increased the density of solvent, thus, solubilizing more quantities of flavonoids and nucleobases (Miao et al., 2010). A further increase in extraction pressure resulted in decreased vapour pressure which restricted solubility, hence the marginally lower quantities of compounds in CSF2. Nonetheless, presence of bioactive metabolites was confirmed in CSF1 and CSF2 which prompted investigation of their multifarious bioactivities as elaborated later.

VOCs have been extensively studied for diverse bioeffects. The types of VOCs expected in the supercritical CO₂ extracts in this study were fatty acids, fatty acid methyl esters and trimethylsilyl esters. Similar compounds have been reported in many medicinal plants and fungi (Dey and Chaudhuri, 2016; Adeoye-Isijola et al., 2018). As instance, hexadecanoic acid methyl ester, 9,12-octadecadienoic acid and 11-octadecenoic acid, methyl ester are known to impart anti-inflammatory, hypocholesterolemic and antimicrobial effects (Kalpana et al., 2012). Methyl stearate influences intestinal lipid metabolism regulation and also leads to antinociceptive, antioxidant, antifungal effects and so forth (Adnan et al., 2019). GC-MS analysis of supercritical extracts from *C. sinensis* have unveiled the presence of 9-octadecenoic acid, 9,12-octadecadienoic acid and hexadecanoic acid as the chief VOCs (Jianya et al., 2006).

In the current study, similar VOCs were perceived in CSF extracts (**Tables 1–3** and **Figure 5**). 9,12-octadecadienoic acid (Z,Z)- was the most abundant VOC in CSF1 which is known to possess substantial antimicrobial, antioxidant, diuretic and hepatoprotective properties (Adeoye-Isijola et al., 2018). Also, it is capable of anti-arthritis, anti-histaminic and hypocholesterolemic activities (Kalaivani et al., 2012). In CSF2, 9,12-octadecadienoic acid (Z,Z)-, trimethylsilyl ester was major VOC which presumably has diuretic, hypocholesterolemic and skin protectant properties in addition to anti-androgenic and anti-histaminic abilities (Sudha et al., 2013; Abubakar and Majinda, 2016). Finally, CSF3's most abundant VOC was seen to be hexadecanoic acid, trimethylsilyl ester which has antioxidant and contraceptive-like effects along with antimicrobial and free scavenging activities (Jain et al., 2012; Patil et al., 2013). These well recognized curative properties of constituent VOCs in all three CSF extracts motivated exploration of varied bioactivities of these extracts.

Metabolomics has emerged as an effective approach, especially while standardizing the pharmacological implications of the vast metabolome of natural extracts (Khan et al., 2017). Application of metabolomics by principal component analysis to the chromatographic profiling obtained from HPTLC and GC-MS, deliberated relatedness between the various supercritical extracts. Peak areas and retardation factor values in HPTLC, and area

percentages and retention times from GC-MS acted as input data for plotting the variables factor map. PCA works by decomposition of the eigenvector. Mean centring of data and data normalization are integral in this analysis. The primary axis representing the first principal component ("PC") or Dim 1 is responsible for describing maximum variance in the dataset. The next PC defines rest of the major variance as Dim 2. In present context, an overall variance of 70.85% in terms of metabolites detected by HPTLC was established. For GC-MS, summative variance with respect to metabolites detected, identified or otherwise, was 68.8%. Similarities in metabolite profiling between CSF1 and CSF2, as discussed in "Results" section, was corroborated by the proximal presence of these two extracts in same quadrant of variables factor map (Figure 6).

Extracts from medicinal mushrooms like *Coprinopsis atramentaria*, *Xerocomus chrysenteron*, *Ganoderma lucidum* and *Cordyceps sinensis* possess remarkable antioxidant abilities which is often accredited to their noteworthy content of flavonoids, phenolics, nucleobases and also VOCs (Pal et al., 2015; Bhardwaj et al., 2017). Supercritical CO₂ fractions from *C. sinensis* have been proven to possess excellent antioxidant effects (Wang et al., 2005). In line of this, the current study brought out efficient free radical (ABTS and DPPH) scavenging and FRAP of all three CSF samples. As reported earlier, flavonoids and VOCs are powerful antioxidant agents and often play key roles in antiviral and anti-proliferative features of natural extracts (Agati et al., 2012; Abubakar and Majinda, 2016). This validated the distinctive antioxidant efficacy of CSF1 followed by CSF2, which was much higher than that in CSF3 (Figure 7). This was plausibly because of higher amount of component polar compounds like flavonoids and nucleobases in the former two extracts due to use of co-solvents (Oman et al., 2013).

Incidence of increased bacterial resistance to synthetic antibiotics and related drugs has set the foreground to survey antibacterial candidates from natural sources (Alves et al., 2012). Supercritical fluid extracts from medicinal sources like *Ginkgo biloba* and palm are already known to have effective antibacterial and antifungal properties (Akanda et al., 2012; Oman et al., 2013). Concomitant to this, CSF1, CSF2 and CSF3 exerted bactericidal action against *S. typhi* and *E. coli*.

In addition to this, the prevalence of *E. coli* infection has been deemed to be more severe in uropathogenic infections. A study by Lin et al. (2015) had pointed out the importance of transcriptional regulator HIF-1 α in innate defense against uropathogenic *E. coli* urinary tract infection. This was relevant to our study since we have used HEK 293 as cell culture model and have elaborated the modulation brought about by CSF extract on HIF-1 α . Thus, the concerted effect of *C. sinensis* supercritical CO₂ extracts in hindering the growth of *E. coli* while normalizing the adverse effects of hypoxia conditions in kidney cell line could be correlated here. As seen in Table 4, CSF1 and CSF2 displayed much better deterrent action with lower MIC values. The antimicrobial property of the *C. sinensis* supercritical extracts can be attributed to the presence of flavonoids like ascorbic acid and gallic acid (Pal et al., 2015). Besides, the constituent VOCs certainly contributed to the noticeable antibacterial activity. In the endeavour to deduce probable modes of antibacterial action,

ROS generation within the bacterial cells was observed as a primary mechanism. Amount of ROS generated and hence the degree of bactericidal action, incremented in a dose dependent manner for all the extracts (Figure 8). Recent literature has evidenced the effect of herbal extracts on cellular membrane damage by generating ROS formation in multidrug-resistant *Acinetobacter baumannii* (Zhang et al., 2015; Tang et al., 2016). The dose dependent increase in ROS generation is in accord with previous papers stating that natural compounds act as ROS producers to evoke antimicrobial response (Jiang et al., 2007).

As yet another inhibitory mode, protein leakage in pathogenic bacterial cells was confirmed. The effectiveness of *C. sinensis* supercritical extracts in inducing dose dependent protein leakage is probably indorsed to the richness of these samples in constituent mycoconstituents like flavonoids, nucleobases and bioactive VOCs, as proven from HPTLC and GC-MS experiments. These results are in concurrence to previous reports that flavonoids and VOCs are capable of conferring antimicrobial resistance against pathogenic microorganisms (Abubakar and Majinda, 2016; Singh et al., 2016).

Efflux pumps have been manifested to be major defensive components in Gram negative bacteria by causing active extrusion of antibiotic or related interventions from the periplasm and/or cytoplasm. In this manner, efflux pumps are discerned to render such bacterial pathogens resistant against antibacterial drugs. This type of resistance is often fathomed by the degree of EtBr efflux since viable bacterial cells curb uptake of EtBr via active efflux pump inhibitors. As a result, EtBr accumulates in bacterial cells with compromised membranes only, consequently emitting a strong fluorescence. In current study it was seen that CSF2, followed by CSF1 and finally CSF3 revealed efflux pump inhibitory activity against *S. typhi* and *E. coli*, designating their potency against these strains. Relative fluorescence suggesting EtBr accumulation is given in Figure 8F. A study by Lechner et al. (2008) portrays that plant phenolic compounds and flavonoids act as efflux pump inhibitors in *Mycobacterium smegmatis*. Also, secondary metabolites in herbal sources exhibit similar effect (Kumar et al., 2016). Hence, in concurrence to above observations and similar to ROS generation and protein leakage, the bioactive constituents detected in CSF1, CSF2 and CSF3 contributed to the efflux pump inhibition. Afore stated results attest the overall better antibacterial properties of CSF2, trailed closely by CSF1, corroborating the importance of ethanol as a co-solvent while preparing bioactive supercritical extracts.

Various restorative abilities of the medicinal mushroom under consideration have been well elaborated in evidence based medicinal systems. However, there are only few reports that describe the efficacy of *C. sinensis* in countering hypoxia-induced maladies. For instance, treatment with *C. sinensis* aqueous extracts imparted tolerance in adenocarcinoma human alveolar basal epithelial, A549 cell lines against hypoxia by declining ROS generation and lipid peroxidation. Cellular viability was restored up to 52% in the A549 cells. Expression of HIF-1 α , NRF-2 and NF- κ B were duly tempered, thus, proving the effectiveness of *C. sinensis* in hypoxia tolerance (Singh et al., 2013). Similarly, hydroethanolic extracts of *C. sinensis* endorsed

defence against hypoxia in neuronal hippocampal cells HT22, by accentuating cell viability to about 72% and also by enhancing anti-inflammatory cytokines and deterring pro-inflammatory cytokines (Pal et al., 2015). Phenolic fractions from *C. sinensis* conferred appreciable protective action against hypobaric hypoxia milieu in HEK 293 cell lines by recuperating cellular viability up to 79.5%. Additionally, these phenolic fractions catalysed a reduction in levels of superoxide dismutase and oxidized glutathione in experimental male Sprague Dawley rats, within a simulated hypobaric hypoxic setting (Rajput et al., 2020). Owing to above promising results, the *C. sinensis* supercritical CO₂ extracts were explored for hypoxia protective action in HEK 293 cell line. It was established that CSF2 proved to be a more prospective lead than the other supercritical CO₂ extracts as well as the aforesaid extracts (aqueous, hydroethanolic and phenolic) to overcome the loss in cellular viability in mammalian cells *in vitro* under low oxygen tension by reviving cellular viability to 82.36% (Figure 9). Bioactive constituents namely, ascorbic acid, rutin as well as adenine atone reduction of cell death *in vitro* under low oxygen stress conditions and therefore, possibly aided the role of CSF2 as therapeutic lead against hypobaric hypoxia (Winter et al., 2016; Patil et al., 2017).

Furthermore, in order to elucidate the mechanism by which CSF2 extract confers protection against hypoxia *in vitro*, its effect in modulating HIF-1 α was investigated. HIF-1 α , the subunit of HIF-1 transcription factor, is the most important functional component of cellular homeostasis under low oxygen stress that regulates cellular redox status (Nehra et al., 2015). In stark contrast to normoxia conditions, the level of HIF-1 α gets overexpressed manifold in oxygen deficient milieu. However, treatment with appropriate therapeutic candidates leads to downregulation of this transcription factor. Congruent results were obtained in current study, where Western blotting analyses explicated that supplementation with optimal dose of CSF2 extensively downregulated the levels of HIF-1 α by four-fold thus, establishing its prominent protective role against hypoxic insult in HEK 293 cells (Figure 10).

The major objective of the present study was to establish *C. sinensis* supercritical CO₂ extracts as prospective therapeutic in a holistic manner. Extracts prepared from medicinal plants and mushrooms consist of a plethora of bioactive compounds. Bio-effects imparted from such extracts are a result of synergistic and/or additive action of various molecules (Zhao et al., 2015; Segneanu et al., 2017; Gupta et al., 2018; Das et al., 2020). This study has confirmed varied activities viz., antioxidant, antibacterial and

hypoxia protective action of the supercritical extracts in consideration which largely is because of their richness in terms of different metabolites e.g. flavonoids, nucleobases and VOCs.

CONCLUSION

The present research highlighted multifarious pharmacological properties of the well revered medicinal mushroom, *Cordyceps sinensis*. Supercritical fluid extraction using CO₂ yielded three distinct extracts of superior quality. Elaborate chromatography-based metabolite profiling by HPTLC and GC-MS signposted the rich chemical composition of *C. sinensis*. Application of metabolomics on the chromatographic data by principal component analysis helped in confirming similarities between CSF1 and CSF2. Overall, the results strongly indicate that *C. sinensis* supercritical fluid extracts can be projected as candidates for mycotherapeutics development, especially for recuperation against hypobaric hypoxia. Furthermore, determination of bioprocess efficiency in terms of product quality and yield needs to be addressed to materialize the use of above extracts on an industrial scale.

DATA AVAILABILITY STATEMENT

The raw data supporting the conclusions of this article will be made available by the authors, without undue reservation.

AUTHOR CONTRIBUTIONS

JM performed the chromatographic, metabolomics, microbiological and cell culture procedures and also, wrote the manuscript. WK conducted the extraction experimentation and its data interpretation. SA contributed to conceptualization and data investigation. KM planned the overall work and critically evaluated all the data and manuscript.

FUNDING

The authors are thankful to Bioactive Natural Product Laboratory, Department of Pharmacognosy and Phytochemistry, Jamia Hamdard University, New Delhi for their constant support throughout this study.

REFERENCES

- Abubakar, M. N., and Majinda, R. R. T. (2016). GC-MS Analysis and Preliminary Antimicrobial Activity of *Albizia Adianthifolia* (Schumacher) and *Pterocarpus Angolensis* (DC). *Medicines (Basel)* 3, 3. doi:10.3390/medicines3010003
- Adeoye-Isijola, M. O., Olusola Olajuyigbe, O., Jonathan, S. G., and Coopoomsamy, R. M. (2018). Bioactive Compounds in Ethanol Extract of *Lentinus Squarrosulus* Mont - A Nigerian Medicinal Macrofungus. *AJTAM* 15, 42–50. doi:10.21010/ajtam.v15i2.6
- Adnan, M., Nazim Uddin Chy, M., Mostafa Kamal, A. T. M., Azad, M. O. K., Paul, A., Uddin, S. B., et al. (2019). Investigation of the Biological Activities and Characterization of Bioactive Constituents of *Ophiorrhiza Rugosa* Var. *Prostrata* (D. Don) & *Mondal* Leaves through In Vivo, In Vitro, and In Silico Approaches. *Molecules* 24, 1367. doi:10.3390/molecules24071367
- Agati, G., Azzarello, E., Pollastri, S., and Tattini, M. (2012). Flavonoids as Antioxidants in Plants: Location and Functional Significance. *Plant Sci.* 196, 67–76. doi:10.1016/j.plantsci.2012.07.014
- Ahmed, A. F., El-Maraghy, N. N., Abdel Ghaney, R. H., and Elshazly, S. M. (2012). Therapeutic Effect of Captopril, Pentoxifylline, and *Cordyceps Sinensis* in Pre-

- hepatic portal Hypertensive Rats. *Saudi J. Gastroenterol.* 18, 182–187. doi:10.4103/1319-3767.96451
- Akanda, M. J., Sarker, M. Z., Ferdosh, S., Manap, M. Y., Ab Rahman, N. N., and Ab Kadir, M. O. (2012). Applications of Supercritical Fluid Extraction (SFE) of Palm Oil and Oil from Natural Sources. *Molecules* 17, 1764–1794. doi:10.3390/molecules17021764
- Alves, M. J., Ferreira, I. C., Dias, J., Teixeira, V., Martins, A., and Pintado, M. (2012). A Review on Antimicrobial Activity of Mushroom (Basidiomycetes) Extracts and Isolated Compounds. *Planta Med.* 78, 1707–1718. doi:10.1055/s-0032-1315370
- Antunes-Ricardo, M., Gutiérrez-Urbe, J. A., and Guajardo-Flores, D. (2017). Extraction of Isorhamnetin Conjugates from *Opuntia Ficus-indica* (L.) Mill Using Supercritical Fluids. *J. Supercrit. Fluids* 119, 58–63. doi:10.1016/j.supflu.2016.09.003
- Bhardwaj, A., Gupta, P., Kumar, N., Mishra, J., Kumar, A., Rakhee, R., et al. (2017). Lingzhi or Reishi Medicinal Mushroom, *Ganoderma Lucidum* (Agaricomycetes), Inhibits *Candida* Biofilms: A Metabolomic Approach. *Int. J. Med. Mushrooms* 19, 685–696. doi:10.1615/IntJMedMushrooms.2017021225
- Bhardwaj, A., Pal, M., Srivastava, M., Tulsawani, R., Sugadev, R., and Misra, K. (2015). HPTLC Based Chemometrics of Medicinal Mushrooms. *J. Liquid Chromatogr. Relat. Tech.* 38, 1392–1406. doi:10.1080/10826076.2015.1050501
- Bhusnure, O. G., Gholve, S. B., Giram, P. S., Borsure, V. S., Jadhav, P. P., Satpute, V. V., et al. (2015). Importance of Supercritical Fluid Extraction Techniques in Pharmaceutical Industry: A Review. *Indo Am. J. Pharm. Res.* 5, 3785–3801.
- Bittencourt, G., Aredo, V., and Oliveira, A. L. d. (2021). Behavior of Beeswax and Edible Oils Mixtures in Supercritical Carbon Dioxide at Moderate Temperature. Authorea [Preprint]. Available at: <https://www.authorea.com/users/405154/articles/516174> (Accessed May 20, 2021). doi:10.22541/au.161720394.43072696/v1
- Capuzzo, A., Maffei, M. E., and Occhipinti, A. (2013). Supercritical Fluid Extraction of Plant Flavors and Fragrances. *Molecules* 18, 7194–7238. doi:10.3390/molecules18067194
- Chen, C. Y., Hou, C. W., Bernard, J. R., Chen, C. C., Hung, T. C., Cheng, L. L., et al. (2014). Rhodiola Crenulata- and Cordyceps Sinensis-Based Supplement Boosts Aerobic Exercise Performance After Short-Term High Altitude Training. *High Alt. Med. Biol.* 15, 371–379. doi:10.1089/ham.2013.1114
- Cui, D. N., Wang, X., Chen, J. Q., Lv, B., Zhang, P., Zhang, W., et al. (2017). Quantitative Evaluation of the Compatibility Effects of Huangqin Decoction on the Treatment of Irinotecan-Induced Gastrointestinal Toxicity Using Untargeted Metabolomics. *Front. Pharmacol.* 8, 211. doi:10.3389/fphar.2017.00211
- Danlami, J. M., Zaini, M. A. A., Arsad, A., and Yunus, M. A. C. (2015). A Parametric Investigation of Castor Oil (Ricinus Communis L) Extraction Using Supercritical Carbon Dioxide Via Response Surface Optimization. *J. Taiwan Inst. Chem. Eng.* 53, 32–39. doi:10.1016/j.jtice.2015.02.033
- Das, G., Shin, H. S., Leyva-Gómez, P., Prado-Audelo, M. L. D., Cortes, H., Singh, Y. D., et al. (2020). *Cordyceps* spp.: A Review on its Immune-Stimulatory and Other Biological Potentials. *Front. Pharmacol.* 11, 602364. doi:10.3389/fphar.2020.602364
- Dey, P., and Chaudhuri, T. K. (2016). Phytochemical Characterization of Dioscorea Alata Leaf and Stem by Silylation Followed by GC-MS Analysis. *J. Food Biochem.* 40, 630–635. doi:10.1111/jfbc.12235
- Ding, J., Magnotti, L. J., Huang, Q., Xu, D. Z., Condon, M. R., and Deitch, E. A. (2001). Hypoxia Combined with *Escherichia coli* Produces Irreversible Gut Mucosal Injury Characterized by Increased Intestinal Cytokine Production and DNA Degradation. *Shock* 16, 189–195. doi:10.1097/00024382-200116030-00004
- El-Gindy, A., Ashour, A., Abdel-Fattah, L., and Shabana, M. M. (2001). Spectrophotometric and HPTLC-Densitometric Determination of Lisinopril and Hydrochlorothiazide in Binary Mixtures. *J. Pharm. Biomed. Anal.* 25, 923–931. doi:10.1016/S0731-7085(01)00382-X
- Fu, Q., Colgan, S. P., and Shelley, C. S. (2016). Hypoxia: The Force that Drives Chronic Kidney Disease. *Clin. Med. Res.* 14, 15–39. doi:10.3121/cmr.2015.1282
- Gao, B. A., Yang, J., Huang, J., Cui, X. J., Chen, S. X., Den, H. Y., et al. (2010). *Cordyceps Sinensis* Extract Suppresses Hypoxia-Induced Proliferation of Rat Pulmonary Artery Smooth Muscle Cells. *Saudi Med. J.* 31, 974–979.
- Gupta, S., Summuna, B., Gupta, M., and Annepu, S. K. (2018). “Edible Mushrooms: Cultivation, Bioactive Molecules, and Health Benefits,” in *Bioactive Molecules in Food*. Editors J. M. Mérillon and K. Ramawat (Berlin: Springer), 1–33. doi:10.1007/978-3-319-54528-8_86-1
- Hamid, M. A., Bakar, N. A., Park, C. S., Ramli, F., and Wan, W. R. (2018). Optimisation of Alpha Mangostin Extraction Using Supercritical CO₂ from *Garcinia mangostana*. *Chem. Eng. Trans.* 63, 577–582. doi:10.3303/CET1863097
- Hasan, H. M. I., Yahya, A. I., Hassan, S. S., and Salama, M. M. (2019). Biological Study of Transition Metal Complexes with Adenine Ligand. *Proceedings* 41, 77. doi:10.3390/ecsoc-23-06601
- He, G. Q., Xiong, H. P., Chen, Q. H., Ruan, H., Wang, Z. Y., and Traoré, L. (2005). Optimization of Conditions for Supercritical Fluid Extraction of Flavonoids from Hops (*Humulus Lupulus* L.). *J. Zhejiang Univ. Sci. B.* 6, 999–1004. doi:10.1631/jzus.2005.B0999
- Hoensch, H. P., and Kirch, W. (2005). Potential Role of Flavonoids in the Prevention of Intestinal Neoplasia: A Review of Their Mode of Action and Their Clinical Perspectives. *Int. J. Gastrointest. Cancer* 35, 187–195. doi:10.1385/IJGC:35:3:187
- Holliday, J. C., and Cleaver, M. P. (2008). Medicinal Value of the Caterpillar Fungi Species of the Genus *Cordyceps* (Fr.) Link (Ascomycetes). A Review. *Int. J. Med. Mushr* 10, 219–234. doi:10.1615/IntJMedMushr.v10.i3.30
- Hu, H., Zhang, J., Guo, S., and Chen, G. (1999). Extraction of Huadian Oil Shale with Water in Sub- and Supercritical States. *Fuel* 78, 645–651. doi:10.1016/S0016-2361(98)00199-9
- Jain, S. C., Pancholi, B., and Jain, R. (2012). Antimicrobial, Free Scavenging Activities and Chemical Composition of *Peltophorum pterocarpum* Baker Ex K. Heyne Stem Extract. *Der. Pharma. Chemica.* 4, 2073–2079.
- Jenneweine, J., Matuszak, J., Walter, S., Felmy, B., Gendera, K., Schatz, V., et al. (2015). Low-oxygen Tensions Found in Salmonella-infected Gut Tissue Boost Salmonella Replication in Macrophages by Impairing Antimicrobial Activity and Augmenting Salmonella Virulence. *Cell. Microbiol.* 17, 1833–1847. doi:10.1111/cmi.12476
- Jeong, J. W., and Choi, Y. H. (2014). Cordycepin Inhibits Migration and Invasion of HCT116 Human Colorectal Carcinoma Cells by Tightening of Tight Junctions and Inhibition of Matrix Metalloproteinase Activity. *J. Korean Soc. Food Sci. Nutr.* 43, 86–92. doi:10.3746/jkfn.2014.43.1.086
- Jiang, N., Tan, N. S., Ho, B., and Ding, J. L. (2007). Respiratory Protein-Generated Reactive Oxygen Species as an Antimicrobial Strategy. *Nat. Immunol.* 8, 1114–1122. doi:10.1038/ni1501
- Jianya, L., Lanting, D., Xiaoli, D., and Yong, D. (2006). GC-MS Analysis of Supercritical Carbon Dioxide Extraction from the Stroma of *Cordyceps Sinensis*. *Mycosystema* 25, 138–141.
- Jordan, J. L., Sullivan, A. M., and Lee, T. D. (2008). Immune Activation by a Sterile Aqueous Extract of *Cordyceps Sinensis*: Mechanism of Action. *Immunopharmacol. Immunotoxicol.* 30, 53–70. doi:10.1080/08923970701812332
- Kagilwal, L. D., Pol, A. S., Patil, S. C., Singhal, R. S., and Patravale, V. B. (2012). Antioxidant-rich Extract from Dehydrated Seabuckthorn Berries by Supercritical Carbon Dioxide Extraction. *Food Bioproc. Technol.* 5, 2768–2776. doi:10.1007/s11947-011-0613-8
- Kalaivani, C. S., Sathish, S. S., Janakiraman, N., and Johnson, M. (2012). GC-MS Studies on *Andrographis Paniculata* (Burm. f.) Wall. Ex Nees a Medicinally Important Plant. *Int. J. Med. Arom. Plants* 2, 69–74.
- Kalpana, D. V., Shanmugasundaram, R., and Mohan, V. R. (2012). GC-MS Analysis of Ethanol Extract of *Entada Purusaetha* DC Seed. *Biosci. Discover.* 3, 30–33.
- Khan, W., Parveen, R., Chester, K., Parveen, S., and Ahmad, S. (2017). Hypoglycemic Potential of Aqueous Extract of *Moringa Oleifera* Leaf and In Vivo GC-MS Metabolomics. *Front. Pharmacol.* 8, 577. doi:10.3389/fphar.2017.00577
- Kirar, V., Nehra, S., Mishra, J., Rakhee, R., Saraswat, D., and Misra, K. (2017). Lingzhi or Reishi Medicinal Mushroom, *Ganoderma Lucidum* (Agaricomycetes), as a Cardioprotectant in an Oxygen-Deficient Environment. *Int. J. Med. Mushrooms* 19, 1009–1021. doi:10.1615/IntJMedMushrooms.2017024584
- Koh, J. H., Kim, K. M., Kim, J. M., Song, J. C., and Suh, H. J. (2003). Antifatigue and Antistress Effect of the Hot-Water Fraction from Mycelia of *Cordyceps Sinensis*. *Biol. Pharm. Bull.* 26, 691–694. doi:10.1248/bpb.26.691
- Kumar, S., He, G., Kakarla, P., Shrestha, U., Ranjana, K. C., Ranaweera, I., et al. (2016). Bacterial Multidrug Efflux Pumps of the Major Facilitator Superfamily

- as Targets for Modulation. *Infect. Disord. Drug Targets* 16, 28–43. doi:10.2174/1871526516666160407113848
- Kumoro, A. C., Hasan, M., and Singh, H. (2010). Extraction of Sarawak Black Pepper Essential Oil Using Supercritical Carbon Dioxide. *Arab J. Sci. Eng.* 35, 7–16.
- Lechner, D., Gibbons, S., and Bucar, F. (2008). Plant Phenolic Compounds as Ethidium Bromide Efflux Inhibitors in *Mycobacterium Smegmatis*. *J. Antimicrob. Chemother.* 62, 345–348. doi:10.1093/jac/dkn178
- Lee, S. Y., Debnath, T., Kim, S. K., and Lim, B. O. (2013). Anti-cancer Effect and Apoptosis Induction of Cordycepin through DR3 Pathway in the Human Colonic Cancer Cell HT-29. *Food Chem. Toxicol.* 60, 439–447. doi:10.1016/j.fct.2013.07.068
- Li, S. (2007). “Application of Supercritical Fluids in Traditional Chinese Medicines and Natural Products,” in *Supercritical Fluid Extraction of Nutraceuticals and Bioactive Compounds*. Editor J. L. Martinez (Boca Raton, FL: CRC Press), 215–242. doi:10.1201/9781420006513.ch7
- Lin, A. E., Beasley, F. C., Olson, J., Keller, N., Shalwitz, R. A., Hannan, T. J., et al. (2015). Role of Hypoxia Inducible Factor-1 α (HIF-1 α) in Innate Defense against Uropathogenic *Escherichia coli* Infection. *Plos Pathog.* 11, e1004818. doi:10.1371/journal.ppat.1004818
- Liza, M. S., Abdul Rahman, R., Mandana, B., Jinap, S., Rahmat, A., Zaidul, I. S. M., et al. (2010). Supercritical Carbon Dioxide Extraction of Bioactive Flavonoid from *Strobilanthes crispus* (Pecah Kaca). *Food Bioprod. Process.* 88, 319–326. doi:10.1016/j.fbp.2009.02.001
- Machmudah, S., Shotipruk, A., Goto, M., Sasaki, M., and Hirose, T. (2006). Extraction of Astaxanthin from *Haematococcus pluvialis* Using Supercritical CO₂ and Ethanol as Entrainer. *Ind. Eng. Chem. Res.* 45, 3652–3657. doi:10.1021/ie051357k
- Macías-Sánchez, M. D., Serrano, C. M., Rodríguez, M. R., and Martínez de la Ossa, E. (2009). Kinetics of the Supercritical Fluid Extraction of Carotenoids from Microalgae with CO₂ and Ethanol as Cosolvent. *Chem. Eng. J.* 150, 104–113. doi:10.1016/j.cej.2008.12.006
- Malaman, F. S., Moraes, L. A. B., West, C., Ferreira, N. J., and Oliveira, A. L. (2011). Supercritical Fluid Extracts from the Brazilian Cherry (*Eugenia Uniflora* L.): Relationship Between the Extracted Compounds and the Characteristic Flavour Intensity of the Fruit. *Food Chem.* 124, 85–92. doi:10.1016/j.foodchem.2010.05.109
- Mendiola, J. A., Herrero, M., Castro-Puyana, M., and Ibáñez, E. (2013). “CHAPTER 6. Supercritical Fluid Extraction,” in *Natural Product Extraction: Principles and Applications*. Editors M. A. Rostagno and J. M. Prado (Cambridge, UK: The Royal Society of Chemistry), 196–230. doi:10.1039/9781849737579-00196
- Meng, M., Hu, H., Zhang, Q., and Ding, M. (2006). Extraction of Tumuji Oil Sand with Sub- and Supercritical Water. *Energy Fuels* 20, 1157–1160. doi:10.1021/ef050418o
- Miao, S.-F., Yu, J.-P., Du, Z., Guan, Y.-X., Yao, S.-J., and Zhu, Z.-Q. (2010). Supercritical Fluid Extraction and Micronization of Ginkgo Flavonoids from *Ginkgo Biloba* Leaves. *Ind. Eng. Chem. Res.* 49, 5461–5466. doi:10.1021/ie902001x
- Mishra, J., Joshi, A., Rajput, R., Singh, K., Bansal, A., and Misra, K. (2018b). Phenolic Rich Fractions from Mycelium and Fruiting Body of *Ganoderma Lucidum* Inhibit Bacterial Pathogens Mediated by Generation of Reactive Oxygen Species and Protein Leakage and Modulate Hypoxic Stress in HEK 293 Cell Line. *Adv. Pharmacol. Sci.* 2018, 6285615. doi:10.1155/2018/6285615
- Mishra, J., Rajput, R., Singh, K., Puri, S., Goyal, M., Bansal, A., et al. (2018a). Antibacterial Natural Peptide Fractions from Indian *Ganoderma Lucidum*. *Int. J. Pept. Res. Ther.* 24, 543–554. doi:10.1007/s10989-017-9643-z
- Montesantos, N., and Maschietti, M. (2020). Supercritical Carbon Dioxide Extraction of Lignocellulosic Bio-Oils: The Potential of Fuel Upgrading and Chemical Recovery. *Energies* 13, 1600. doi:10.3390/en13071600
- Mosmann, T. (1983). Rapid Colorimetric Assay For Cellular Growth and Survival: Application To Proliferation and Cytotoxicity Assays. *J. Immunol. Methods* 65, 55–63. doi:10.1016/0022-1759(83)90303-4
- Nagavekar, N., and Singhal, R. S. (2018). Enhanced Extraction of Oleoresin from Piper Nigrum by Supercritical Carbon Dioxide Using Ethanol as a Co-solvent and its Bioactivity Profile. *J. Food Process. Eng.* 41, e12670. doi:10.1111/jfpe.12670
- Nehra, S., Bhardwaj, V., Kalra, N., Ganju, L., Bansal, A., Saxena, S., et al. (2015). Nanocurcumin Protects Cardiomyoblasts H9c2 from Hypoxia-Induced Hypertrophy and Apoptosis by Improving Oxidative Balance. *J. Physiol. Biochem.* 71, 239–251. doi:10.1007/s13105-015-0405-0
- Nie, S., Cui, S. W., Xie, M., Phillips, A. O., and Phillips, G. O. (2013). Bioactive Polysaccharides from *Cordyceps Sinensis*: Isolation, Structure Features and Bioactivities. *Bioactive Carbohydr. Diet. Fibre* 1, 38–52. doi:10.1016/j.bcdf.2012.12.002
- Nijveldt, R. J., Van Nood, E., Van Hoorn, D. E., Boelens, P. G., Van Norren, K., and Van Leeuwen, P. A. (2001). Flavonoids: A Review of Probable Mechanisms of Action and Potential Applications. *Am. J. Clin. Nutr.* 74, 418–425. doi:10.1093/ajcn/74.4.418
- Norodin, N. S. M., Salleh, L. M., Hartati, N. M., and Mustafa, N. M. (2016). Supercritical Carbon Dioxide (SC-CO₂) Extraction of Essential Oil from *Swietenia Mahagoniseeds*. *IOP Conf. Ser. Mater. Sci. Eng.* 162, 012030–012037. doi:10.1088/1757-899X/162/1/012030
- Oman, M., Škerget, M., and Knez, Z. (2013). Application of Supercritical Fluid Extraction for Separation of Nutraceuticals and Other Phytochemicals from Plant Material. *Maced. J. Chem. Chem. Eng.* 32, 183–226. doi:10.20450/mjce.2013.443
- Pal, M., Bhardwaj, A., Manickam, M., Tulsawani, R., Srivastava, M., Sugadev, R., et al. (2015). Protective Efficacy of the Caterpillar Mushroom, *Ophiocordyceps Sinensis* (Ascomycetes), from India in Neuronal Hippocampal Cells against Hypoxia. *Int. J. Med. Mushrooms* 17, 829–840. doi:10.1615/IntJMedMushrooms.v17.i9.30
- Pal, M., and Misra, K. (2018). “Cordyceps sp.: The Precious Mushroom for High-Altitude Maladies,” in *Management of High-Altitude Pathophysiology*. Editors K. Misra, P. Sharma, and A. Bhardwaj (Cambridge, MA: Academic Press), 93–114. doi:10.1016/B978-0-12-813999-8.00006-9
- Patil, S. J., Venkatesh, S., Vishwanatha, T., Banagar, S. R., Banagar, R. J., and Patil, S. B. (2013). GC-MS Analysis of Bioactive Constituents from the Petroleum Ether Extract of *Citrus Medica* Seeds. *World J. Pharm. Pharm. Sci.* 3, 1239–1249. doi:10.5455/wjpp.2013.3.134-138
- Patil, S. L., Swaroop, K., Kakde, N., and Somashekarappa, H. M. (2017). In Vitro Protective Effect of Rutin and Quercetin Against Radiation-Induced Genetic Damage in Human Lymphocytes. *Indian J. Nucl. Med.* 32, 289–295. doi:10.4103/ijnm.IJNM_30_17
- Pronyk, C., and Mazza, G. (2009). Design and Scale-Up of Pressurized Fluid Extractors for Food and Bioproducts. *J. Food Eng.* 95, 215–226. doi:10.1016/j.jfoodeng.2009.06.002
- Rahimi, E., Prado, J. M., Zahedi, G., and Meireles, M. A. A. (2011). Chamomile Extraction with Supercritical Carbon Dioxide: Mathematical Modeling and Optimization. *J. Supercrit. Fluids* 56, 80–88. doi:10.1016/j.supflu.2010.11.008
- Rajput, R., Sharma, P., Mishra, J., Bhardwaj, A., Sharma, R. K., Singh, K., et al. (2020). Bioactive Fractions from the Chinese Caterpillar Mushroom, *Ophiocordyceps Sinensis* (Ascomycetes), Elucidate Adaptogenic Role against Hypoxia Stress. *Int. J. Med. Mushrooms* 22, 1121–1133. doi:10.1615/IntJMedMushrooms.2020036713
- Rajput, R., Sethy, N. K., Bhargava, K., Misra, K., and Singh, V. K. (2016). Phytochemical and Proteomic Analysis of a High-Altitude Medicinal Mushroom *Cordyceps Sinensis*. *J. Proteins Proteom.* 7, 187–197.
- RakheeSethy, N. K., Bhargava, K., Misra, K., and Singh, V. K. (2016). Phytochemical and Proteomic Analysis of a High Altitude Medicinal Mushroom *Cordyceps Sinensis*. *J. Proteins Proteomics* 7, 187–197.
- Rakhee, R., Mishra, J., Yadav, R. B., Meena, D. K., Arora, R., Sharma, R. K., et al. (2021). Novel Formulation Development from *Ophiocordyceps Sinensis* (Berk.) for Management of High-Altitude Maladies. *3 Biotech.* 11, 1–11. doi:10.1007/s13205-020-02536-311
- Sari, N., Suparmin, A., Kato, T., and Park, E. Y. (2016). Improved Cordycepin Production in a Liquid Surface Culture of *Cordyceps Militaris* Isolated from Wild Strain. *Biotechnol. Bioproc. E* 21, 595–600. doi:10.1007/s12257-016-0405-0
- Segneanu, A. E., Velciov, S. M., Olariu, S., Cziple, F., Damian, D., and Grozescu, I. (2017). “Bioactive Molecules Profile from Natural Compounds,” in *Amino Acid-New Insights and Roles in Plant and Animal*. Editors T. Asao and M. Asaduzzaman (London, UK: IntechOpen), 209–228. doi:10.5772/intechopen.68643

- Shan, B., Xie, J.-H., Zhu, J.-H., and Peng, Y. (2012). Ethanol Modified Supercritical Carbon Dioxide Extraction of Flavonoids from *Momordica Charantia* L. And its Antioxidant Activity. *Food Bioprod. Process.* 90, 579–587. doi:10.1016/j.fbp.2011.09.004
- Shao, Q., Deng, Y., Liu, H., Zhang, A., Huang, Y., Xu, G., et al. (2014). Essential Oils Extraction from *Anoetochilus Roxburghii* Using Supercritical Carbon Dioxide and Their Antioxidant Activity. *Ind. Crops Prod.* 60, 104–112. doi:10.1016/j.indcrop.2014.06.009
- Sharma, P., Suryakumar, G., Singh, V., Misra, K., and Singh, S. B. (2015). In Vitro Antioxidant Profiling of Seabuckthorn Varieties and Their Adaptogenic Response to High Altitude-Induced Stress. *Int. J. Biometeorol.* 59, 1115–1126. doi:10.1007/s00484-014-0925-2
- Singh, J. P., Kaur, A., Singh, N., Nim, L., Shevkani, K., Kaur, H., et al. (2016). In Vitro Antioxidant and Antimicrobial Properties of Jambolan (*Syzygium Cumini*) Fruit Polyphenols. *LWT Food Sci. Techn.* 65, 1025–1030. doi:10.1016/j.lwt.2015.09.038
- Singh, M., Tulsawani, R., Koganti, P., Chauhan, A., Manickam, M., and Misra, K. (2013). *Cordyceps Sinensis* Increases Hypoxia Tolerance by Inducing Heme Oxygenase-1 and Metallothionein Via Nrf2 Activation in Human Lung Epithelial Cells. *Biomed. Res. Int.* 2013, 569206. doi:10.1155/2013/569206
- Sovová, H., Stateva, R. P., and Galushko, A. A. (2001). Solubility of β -carotene in Supercritical CO₂ and the Effect of Entrainers. *J. Supercrit. Fluids* 21, 195–203. doi:10.1016/S0896-8446(01)00101-2
- Sudha, T., Chidambarampillai, S., and Mohan, V. R. (2013). GC-MS Analysis of Bioactive Components of Aerial Parts of *Fluggea Leucopyrus* Willd. (Euphorbiaceae). *J. Appl. Pharmaceut. Sci.* 3, 126–130. doi:10.7324/JAPS.2013.3524
- Takeuchi, T. M., Rubano, M. L., and Meireles, M. A. A. (2010). Characterization and Functional Properties of Macela (*Achyrocline Satureioides*) Extracts Obtained by Supercritical Fluid Extraction Using Mixtures of CO₂ Plus Ethanol. *Food Bioproc. Technol.* 3, 804–812. doi:10.1007/s11947-009-0309-5
- Tang, B., Zhang, D., Li, S., Xu, Z., Feng, X., and Xu, H. (2016). Enhanced Poly (γ -Glutamic Acid) Production By H₂O₂-Induced Reactive Oxygen Species in The Fermentation of *Bacillus Subtilis* NX-2. *Biotechnol. Appl. Biochem.* 63, 625–632. doi:10.1002/bab.1416
- Walsh, J. M., Ikononou, G. D., and Donohue, M. D. (1987). Supercritical Phase Behavior: The Entrainer Effect. *Fluid Phase Equilibria* 33, 295–314. doi:10.1016/0378-3812(87)85042-2
- Wang, B. J., Won, S. J., Yu, Z. R., and Su, C. L. (2005). Free Radical Scavenging and Apoptotic Effects of *Cordyceps Sinensis* Fractionated by Supercritical Carbon Dioxide. *Food. Chem. Toxicol.* 43, 543–552. doi:10.1016/j.fct.2004.12.008
- Winter, J., Klumpe, I., Heger, J., Rauch, U., Schultheiss, H. P., Landmesser, U., et al. (2016). Adenine Nucleotide Translocase 1 Overexpression Protects Cardiomyocytes Against Hypoxia Via Increased ERK1/2 and AKT Activation. *Cell. Signal.* 28, 152–159. doi:10.1016/j.cellsig.2015.11.002
- Wrona, O., Rafińska, K., Możński, C., and Buszewski, B. (2017). Supercritical Fluid Extraction of Bioactive Compounds from Plant Materials. *J. AOAC Int.* 100, 1624–1635. doi:10.5740/jaoacint.17-0232
- Yan, X. F., Zhang, Z. M., Yao, H. Y., Guan, Y., Zhu, J. P., Zhang, L. H., et al. (2013). Cardiovascular Protection and Antioxidant Activity of the Extracts from the Mycelia of *Cordyceps Sinensis* Act Partially Via Adenosine Receptors. *Phytother. Res.* 27, 1597–1604. doi:10.1002/ptr.4899
- Yi, X., Xi-zhen, H., and Jia-shi, Z. (2004). Randomized Double-Blind Placebo-Controlled Clinical Trial and Assessment of Fermentation Product of *Cordyceps Sinensis* (Cs-4) in Enhancing Aerobic Capacity and Respiratory Function of the Healthy Elderly Volunteers. *Chin. J. Integr. Med.* 10, 187–192. doi:10.1007/BF02836405
- Zhang, L., Xu, S.-g., Liang, W., Mei, J., Di, Y.-y., Lan, H.-h., et al. (2015). Antibacterial Activity and Mode of Action of *Mentha Arvensis* Ethanol Extract Against Multidrug-Resistant *Acinetobacter Baumannii*. *Trop. J. Pharm. Res.* 14, 2099–2106. doi:10.4314/tjpr.v14i11.21
- Zhao, Y., Wu, Y., and Wang, M. (2014). “Bioactive Substances of Plant Origin,” in *Handbook of Food Chemistry*. Editors P. Cheung and B. Mehta (Berlin, Heidelberg: Springer), 1–35. doi:10.1007/978-3-642-41609-5_13-1
- Zheng, L. P., Gao, L. W., Zhou, J. Q., Sima, Y. H., and Wang, J. W. (2008). Antioxidant Activity of Aqueous Extract of a *Tolypocladium* Sp. Fungus Isolated from Wild *Cordyceps Sinensis*. *Afr. J. Biotechnol.* 7, 3004–3010.

Conflict of Interest: The authors declare that the research was conducted in the absence of any commercial or financial relationships that could be construed as a potential conflict of interest.

Publisher's Note: All claims expressed in this article are solely those of the authors and do not necessarily represent those of their affiliated organizations, or those of the publisher, the editors and the reviewers. Any product that may be evaluated in this article, or claim that may be made by its manufacturer, is not guaranteed or endorsed by the publisher.

Copyright © 2021 Mishra, Khan, Ahmad and Misra. This is an open-access article distributed under the terms of the Creative Commons Attribution License (CC BY). The use, distribution or reproduction in other forums is permitted, provided the original author(s) and the copyright owner(s) are credited and that the original publication in this journal is cited, in accordance with accepted academic practice. No use, distribution or reproduction is permitted which does not comply with these terms.



Dose-Effect/Toxicity of Bupleuri Radix on Chronic Unpredictable Mild Stress and Normal Rats Based on Liver Metabolomics

Peng Wang^{1†}, Xiaoxia Gao^{1,2*†}, Meili Liang¹, Yuan Fang¹, Jinping Jia³, Junsheng Tian^{1,2}, Zhenyu Li^{1,2} and Xuemei Qin^{1,2*}

¹Modern Research Center for Traditional Chinese Medicine, Shanxi University, Taiyuan, China, ²Key Laboratory of Chemical Biology and Molecular Engineering of Ministry Education of Shanxi University, Taiyuan, China, ³Scientific Instrument Center, Shanxi University, Taiyuan, China

OPEN ACCESS

Edited by:

Sayed Ahmad,
Jamia Hamdard University, India

Reviewed by:

Mi Mi Tang,
Central South University, China
Yubo Li,
Tianjin University of Traditional
Chinese Medicine, China

*Correspondence:

Xiaoxia Gao
gaoxiaoxia@sxu.edu.cn
Xuemei Qin
qinxm@sxu.edu.cn

[†]These authors have contributed
equally to this work

Specialty section:

This article was submitted to
Ethnopharmacology,
a section of the journal
Frontiers in Pharmacology

Received: 09 November 2020

Accepted: 24 August 2021

Published: 07 September 2021

Citation:

Wang P, Gao X, Liang M, Fang Y, Jia J,
Tian J, Li Z and Qin X (2021) Dose-
Effect/Toxicity of Bupleuri Radix on
Chronic Unpredictable Mild Stress and
Normal Rats Based on
Liver Metabolomics.
Front. Pharmacol. 12:627451.
doi: 10.3389/fphar.2021.627451

Depression, one of the most prevalent psychiatric diseases, affects the quality of life of millions of people. Studies have shown that the lower polar fraction of Bupleuri Radix (PBR) elicited therapeutic effects in chronic unpredictable mild stress (CUMS) rats. In contrast, comparatively mild liver injury was observed in normal rats administered a high PBR dose. It is essential to clarify the effective and safe dose of PBR and its dose-effect/toxicity relationship. In this study, we used the CUMS model to evaluate the effects and toxicities of PBR and to decipher the dose-effect/toxicity relationship and mechanism using the liver metabolomics combined with multivariate statistical analysis. In CUMS rats, PBR improved the depression-like behaviors including reduced body growth rate, anhedonia, and locomotor activities, and markedly reduced the contents of alanine aminotransferase (ALT) and aspartate aminotransferase (AST). In control rats, PBR treatment altered ALT and AST from typical levels. Moreover, the effective dose range for CUMS rats was 12.6–163 g (herb)/kg, the median toxicity dose for CUMS and normal rats were 388 and 207 g (herb)/kg. The toxicological results showed that the cytokeratin-18 fragment level was increased significantly in CUMS rats given with 100 g (herb)/kg PBR. After a comprehensive analysis, the use of PBR dose was determined to be 12.6–50 g (herb)/kg. In CUMS rats, PBR could reverse amino acid metabolism, energy metabolism, sphingolipid metabolism, and β -oxidation of fatty acids to produce an anti-depressant effect in a dose-dependent manner. In control rats, two additional metabolic pathways were significantly perturbed by PBR, including glycerophospholipid metabolism and bile acid metabolism. Moreover, the comprehensive metabolic index including dose-effect index (DEI) and dose toxicity index (DTI) had a remarkable ability (ROC = 0.912, ROC = 0.878) to predict effect and toxicity. The DEI and DTI were used to determine the dose range of effect and toxicity which was shown high concordance with previous results. Furthermore, the CUMS rats possessed a higher toxicity tolerance dose of PBR which was consistent with the theory of “You Gu Wu Yun” in traditional Chinese medicine. The metabolomics techniques combined with correlation analysis could be used to discover indicators for comprehensive evaluations of efficacy and toxicity.

Keywords: bupleuri radix, anti-depression, dose- effect/toxicity, UHPLC-MS, CUMS, liver metabolomics

INTRODUCTION

Depression, a complicated psychiatric disorder, leads to low morale, weight loss, and anhedonia (Fabricatore and Wadden, 2006; Paykel, 2006). It is considered the fourth leading cause of disability worldwide and the third leading cause of global disease burden (Sayers, 2001; Mathers and Loncar, 2006). The current clinical anti-depressant drugs are ineffective on at least a quarter of patients and produce side effects such as psychomotor impairment, dependence and hepatotoxic reactions (Sarko, 2000; Ishino and Park, 2013; Voican et al., 2013). Traditional Chinese medicines (TCMs) might offer here new options for depression therapy (Liu et al., 2021). Therefore, research studies have paid increasing attention to the TCMs in treating depression.

Bupleuri Radix, the root of *Bupleurum chinense* DC. or *Bupleurum scorzonrifolium* Wild., and is one of the most popular traditional Chinese medicines (TCMs) over the past 2,000 years. The main pharmacological effects of Bupleuri Radix are soothing the liver and relieving depression, evacuating fever, and elevating “Yang Qi” (The Pharmacopoeia Commission of the PRC, 2020). Clinical studies have shown that Bupleuri Radix has also been used for anti-virus infection, anti-acute radiation injury, anti-ulcer effect, reducing blood lipid, inducing serum interferon, enhancing immune function, etc. (Xing, et al., 2017; Jiang et al., 2020). Along with the steadily increasing use of Bupleuri Radix, safety has been highlighted. The effect of “robbing liver yin” of Bupleuri Radix had been widely reported since the Ming and Qing Dynasties (Teo et al., 2016). Modern studies have shown that Bupleuri Radix caused acute liver injury, hepatocyte apoptosis, and acute hepatitis following overdose or long-term, unrestricted and unjustified use (Wang and Song, 2014). Some components in the sibling species of Bupleuri Radix including bupleurotoxin, acetyl bupleurotoxin, and saikosaponin D have been reported neurotoxic effect and hepatotoxicity, respectively (Zhang et al., 2014; Zhang F. et al., 2015). In our previous study, the Bupleuri Radix improved depression-like behaviors in chronic unpredictable mild stress rats (CUMS, a depression model of depression, Zhou et al., 2011; Liu et al., 2013). The lower polar fraction of Bupleuri Radix (PBR) had the strongest antidepressant activity than other parts of Bupleuri Radix (Meng et al., 2020). However, comparatively mild liver injury was observed in normal rats administered high doses (Gao et al., 2017).

The liver is the center of material metabolism and energy metabolism. It plays diverse biological roles in oxidative stress and glycogen storage. In traditional Chinese medicine (TCM), the liver has become the main target organ of depression treatment (Jia et al., 2016; Jia et al., 2017). Depression is considered to be “liver qi stagnation”, and relieving “liver qi stagnation” is regarded as an effective method for treating depression in TCM theory (Li, et al., 2020; Chen, et al., 2020a). Xiaoyao San and Radix Bupleuri were the well-known TCM formula for the treatment of depression by relieving “liver qi stagnation” (Liu, et al., 2021; Zhang, et al., 2020). In addition, modern pharmacological studies have shown that chronic stress might cause liver injury by disturbing hepatic function indices (Chen, et al., 2020b), hepatic metabolic profile (Gao, et al., 2017), and the

genes expression in phospholipid and primary bile acid biosynthesis pathways (Jia, et al., 2016; Tian, et al., 2017). Furthermore, clinical studies have shown that chronic and acute liver disease patients exhibited different degrees of depression reversely (Nardelli et al., 2013; Suh, et al., 2013; Youssef et al., 2013). Therefore, the liver was selected as a primary target organ of efficacy and toxicity for PBR. Metabonomics is widely used to discover biomarkers and recognize key pathways involved in biological processes (Medina et al., 2014). Currently, Liquid chromatography with mass spectrometry (LC-MS) is becoming the mainstream platform for metabonomics research because of its rapid analysis, high resolution, and high sensitivity (Theodoridis et al., 2012). Advanced analytical techniques of LC-MS and computational methods of metabonomics technologies can provide unique and fundamental insights into disease and therapeutic progression.

In this study, liver metabonomics combined with correlation analysis was applied to characterize the metabolic profile of CUMS rats and the dose-effect/toxicity relationship of PBR in the physiological and pathological conditions of rats (Figure 1). This study provides an objective reference for the evaluation of the safety and effectiveness of PBR.

MATERIALS AND METHODS

Instruments, Chemicals and Reagents

An UltiMate 3,000 ultrahigh performance liquid chromatography (UHPLC, Thermo-Fisher, United States) in tandem with a Q Exactive Orbitrap-MS (Thermo-Fisher Scientific, United States) was used. Xcalibur workstation (Thermo Fisher Scientific, United States), IKA T10 tissue homogenizer (Ningbo Xinzhi Biotechnology Co., Ltd, China), Neofuge13R high-speed freezing centrifuge (Likang Biotechnology Company, China), and MX-S Adjustable mixer (Scilogex, United States) were used. LC-MS grade acetonitrile and HPLC grade formic acid were obtained from Thermo-Fisher (United States).

Preparation of PBR

The preparation of PBR was briefly described in our previous study (Gao et al., 2017). Five kilograms of Bupleuri Radix (Shanxi Huayang Pharmaceutical Co., Ltd., China) were extracted three times with 95% fresh ethanol, each extraction was performed for 2 h. The mixture was filtered, and the filtrate was concentrated under reduced pressure to obtain an aqueous solution. For further extraction, the aqueous solution was extracted three times with an equal volume of petroleum ether by using 30 min ultrasonication. The petroleum ether fraction (approximately 128.5 g, with an extract yield of 2.57%) was obtained after concentration and drying (60°C).

To assure the quality of PBR, eight polyacetylene compounds from PBR were detected by UPLC Photodiode Array (PDA) analysis in our previous study (Zhang et al., 2017). In this study, the contents of the main active compounds of (2Z, 8E, 10E)-pentadecatriene-4,6-diyn-1-ol and bupleurnol in PBR were 3.62 mg/g and 1.88 mg/g detected by UPLC-PDA. Polyacetylenes accounted for approximately 30% of the total components in PBR, using a quantitative analysis of multiple

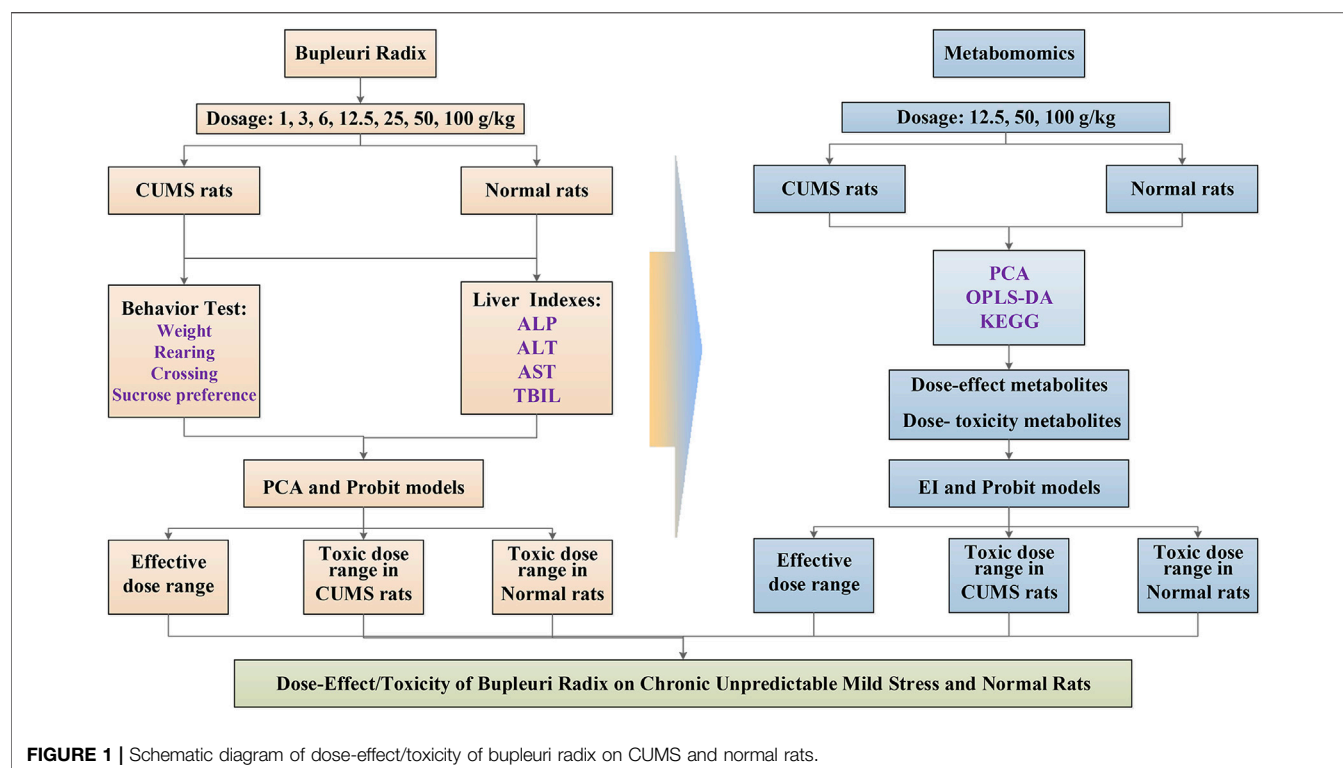


FIGURE 1 | Schematic diagram of dose-effect/toxicity of bupleuri radix on CUMS and normal rats.

components by a single marker (QAMS, Xie et al., 2010; **Supplementary Figure S1, 2**).

PBR extract and venlafaxine was dissolved in distilled water containing 0.5% CMC-Na and 0.5% Tween-80 at seven concentrations of 0.1, 0.3, 0.6, 1.25, 2.5, 5.0, and 10.0 g (herb)/mL for PBR and 3.5 mg/ml for venlafaxine for administration of animal experiments. Among them, the 12.5 g (herb)/kg PBR was regarded as the medium dose, which was based on the effective dose reported in previous research (Gao et al., 2013).

Animals

136 healthy, adult, 6 weeks old male Sprague-Dawley (SD) rats, 200 ± 20 g weight, license NO. SCXK (JING 2012-0001) were purchased from the Experimental Animal Center of Beijing Weitong Lihua Technology Co. Ltd. (China). The rats were acclimatized for 1 week and maintained on a 12 h light/dark cycle (lights on from 6:00 a.m. to 6:00 p.m.), 30–70% relative humidity and temperature (23–27°C) with a commercial diet and water available. All animal experiments were performed under the NIH Guidelines for Care and Use of Laboratory Animals (United States) and the Prevention of Cruelty to Animals Act (1986) of China, and the experiments were approved by the Animal Ethics Committee of Shanxi University (ethical batch number: SXULL2019004).

Drug Administration and Experimental Design

After 1 week of adaptation, the animals were randomly divided into 17 groups ($n = 8$): [CM] CUMS rats, [K] control rats,

[C1] ~ [C7] CUMS rats given PBR (7 different dosages), [Z1] ~ [Z7] control rats administered PBR, and [CY] CUMS rats administered venlafaxine hydrochloride as a positive control (**Table 1**). The different oral doses of PBR were 1, 3, 6, 12.5, 25, 50, and 100 g (herb)/kg, and the oral dose of venlafaxine was 35 mg/kg. All rats were administered agents by gavage at a dose of 10 ml/kg body weight once daily for 21 days, 1 h before modeling.

The control rats were housed together, while the CUMS rats were housed alone and exposed to nine mild stressors randomly every day including swimming in 4°C cold water for 5 min, foot shocking for 2 min (36 V, one shock/2 s, 10 s duration), tail clamping for 2 min, noise for 3 h (60 dB), day-night reversal (12 h/12 h), exposure to an experimental room at 45°C for 10 min, constraint for 3 h, food deprivation for 24 h, and water deprivation for 24 h (**Supplementary Table S1**; Gao et al., 2017).

Behavioral Tests and Measurement of Liver Function

During the experiment, all the behavioral tests were measured in day 0 (served as the baseline) and day 21. The rats were weighed and this index reflected the basic survival state of the rats. The open-field test was conducted to measure the number of rearings (defined as standing upright on the hind legs) and the number of crossings (grid lines crossed by the rat with at least three paws). The different forms of activity were used to assess the rats' mobility. Sucrose preference values were calculated as the percentage of 1% sucrose solution consumed relative to the total liquid intake within 4 h. This test was used to assess

TABLE 1 | Animal grouping and processing.

Group	Animal model	Drug	Dosage (g/kg)	Administration
K	—	Solvent	—	Intragastrical
CM	CUMS	Solvent	—	Intragastrical
CY	CUMS	Venlafaxine hydrochloride	0.035	Intragastrical
C1	CUMS	PBR	1	Intragastrical
C2	CUMS	PBR	3	Intragastrical
C3	CUMS	PBR	6	Intragastrical
C4	CUMS	PBR	12.5	Intragastrical
C5	CUMS	PBR	25	Intragastrical
C6	CUMS	PBR	50	Intragastrical
C7	CUMS	PBR	100	Intragastrical
Z1	—	PBR	1	Intragastrical
Z2	—	PBR	3	Intragastrical
Z3	—	PBR	6	Intragastrical
Z4	—	PBR	12.5	Intragastrical
Z5	—	PBR	25	Intragastrical
Z6	—	PBR	50	Intragastrical
Z7	—	PBR	100	Intragastrical

Note: [CM] CUMS rats, [K] control rats, [C1] ~ [C7] CUMS rats given PBR (7 different dosages), [Z1] ~ [Z7] control rats administered PBR, and [CY] CUMS rats administered venlafaxine hydrochloride. The solvent was water containing 0.5% CMC-Na and 0.5% Tween-80. All the rats were given agents at a dose of 10 ml/kg body weight.

anhedonia-like behavior. The growth rate ($\Delta\%$) of body weight, rearings, crossings, and sucrose preference values were calculated using the formula $(F_{21}-F_0)/F_0$, where F_{21} were the body weight, rearings, crossings, and sucrose preference values on the day 21, and F_0 were the body weight, rearings, crossings, and sucrose preference values on the day 0. The growth rate was used to reflect the behavioral changes in CUMS and control rats between day 0 and 21.

The rats were anesthetized with 10% chloral hydrate at 8:00 a.m. on day 21. Blood was collected from rats 1 h after administration from the abdominal aorta. After 30 min incubation, the serum was separated by centrifugation at 3,500 rpm for 15 min, and then stored at -80°C . Then, the rats were sacrificed by cervical dislocation, and the liver was quickly removed, frozen in liquid nitrogen, and stored at -80°C .

A portion of the serum was used for quantification of alanine aminotransferase (ALT), aspartate aminotransferase (AST), alkaline phosphatase (ALP), and total bilirubin (TBIL) using an automated biochemical analyzer (Konelab PRIME 7.2.1, Finland). Cytokeratin-18 fragment (CK-18F) was quantitatively measured in the serum and liver using the M30 Apoptosense ELISA kit (Shanghai Enzyme-linked Biotechnology Co., Ltd., China). These biochemical indices were examined to assess hepatic function.

Sample Preparation

To extract metabolites, each liver tissue sample (250 mg) was thawed, and 1,500 μL of chilled acetonitrile containing 0.2% formic acid was added. The sample was homogenized in an ice bath and centrifuged at 13,000 rpm for 15 min at 4°C . The supernatant was transferred to a fresh tube and dried in a refrigerated vacuum centrifugal dryer. The dried residue was dissolved in 500 μL of the solvent containing 0.1% formic acid water-acetonitrile (9:1, v/v) and centrifuged at 13,000 rpm for 15 min at 4°C . A 5 μL supernatant was injected for UHPLC-MS analysis.

LC-MS Analysis

UHPLC Q Exactive Orbitrap-MS conditions for liver analysis were the same as those described in our previous study (Gao et al., 2017). UHPLC was performed using a Thermo-Fisher UHPLC coupled to a Q Exactive Orbitrap-MS (Thermo-Fisher, United States). Chromatographic separation was achieved on a Waters ACQUITY UPLC HSS T3 column (2.1×100 mm, $1.8 \mu\text{m}$) maintained at 40°C . The mobile phase consisted of 0.1% formic acid in water (A) and 0.1% formic acid in acetonitrile (B), respectively, and operated under the following program with a flow rate of 0.2 ml/min: 0–2 min, 2% B; 2–3 min, 2–35% B; 3–17 min, 35–70% B; 17–18 min, 70% B; 18–29 min, 70–98% B; 29–31 min, 98% B; 31–33 min, 98–2% B; 33–35 min, 2% B. The sample injection volume was 5 μL . The mass spectrometer was fitted with an electrospray ionization source, and the ESI source was used in both positive and negative ion modes at a temperature of 320°C . Nitrogen was used as the sheath and auxiliary gas at flow rates of 35 and 10 arb. The heater gas temperature was 300°C , and MS data were collected in the full-scan mode in the m/z range of 100–1,500.

Quality control (QC) samples were processed in the same way as the analytical samples and injected throughout the run to monitor the LC/MS platform's stability.

Behavioral Regulation Index (BRI) and Liver Composite Index (LCI)

The behavioral findings and liver biochemical indexes were regarded as the primary evaluation metrics to determine the effect and toxicity dose range of PBR. The behavioral regulation index (BRI) and liver composite index (LCI) were presented as composite scores by combining behavioral indexes and liver biochemical indexes. In this study, principal component analysis (PCA) was used to calculate BRI and LCI, with the formula:

$$f_1 = k_1zx_1 + k_2zx_2 + k_3zx_3 + k_4zx_4 \quad (1)$$

$$f_2 = k_5zx_1 + k_6zx_2 + k_7zx_3 + k_8zx_4 \quad (2)$$

$$f = \frac{\lambda_1}{\lambda_1 + \lambda_2}f_1 + \frac{\lambda_2}{\lambda_1 + \lambda_2}f_2 \quad (3)$$

Where f was the composite score of BRI or LCI, f_1 and f_2 were the first principal component PC1 and the second principal component PC2 of BRI or LCI. x_1 , x_2 , x_3 , and x_4 represented body weight, sucrose preference, ambulation number, and rearing number for BRI or the levels of ALT, AST, ALP, and TBIL for LCI, zx was the standardized raw variable of x_i , λ was the rate of variance contribution, and k was the score of each group for every principal component.

The determination of the effective dose range for CUMS rats and the TD50 (median toxicity dose) for CUMS and control rats was as follows. Firstly, the effective and safe range was determined respectively based on the behavior and liver function of control rats (Mean \pm 1.96SD, Xie et al., 2010). Secondly, after administration with PBR, the CUMS rats adjusted to the effective range were defined as positive samples for effect, and the CUMS and control rats deviated from the safe range were defined as positive samples for toxicity. Finally, the numbers of positive samples were counted in different groups, and probit regression was used to determine the dose range of effect and toxicity.

Data Processing and Statistical Analysis

Raw data were processed using Compound Discoverer 2.0 (Thermo Fisher, United States) to obtain the matched and aligned peak data. The processing parameters were as follows: m/z 100–1,500 Da; mass tolerance 5 ppm, RT tolerance 0.05 min, and S/N threshold 3.

The data matrix was established by aligning peaks with the exact retention time and normalizing the peak value. The (Rt)-m/z pair from each file was subjected to multivariate analysis using SIMCA-P software (version 13.0, Umetrics, Sweden), including PCA, partial least-squares discriminant analysis (PLS-DA), and orthogonal partial least squares (OPLS) discriminant analysis of the data from both positive and negative modes. PCA was performed to discern the natural separation between different stages of the samples by visual inspection of the score plots. The PLS-DA model was acquired by projecting the predicted variables and observable variables into a new space. In the OPLS-DA model, samples from different groups were classified, and the results were visualized as score plots to show the group clusters, and S-plots to show the variables contributing to classification. The variable importance in the projection (VIP) value reflects the influence of every variable on the classification, and the independent sample t -test was also included in the analysis of the discriminating variables. $p < 0.05$, and $VIP > 1$ were considered statistically significant.

The Human Metabolome Database (HMDB), KEGG, and the LIPIDMAPS-Nature Lipidomics Gateway (<http://www.lipidmaps.org/>) and related literature were queried with the exact masses of the metabolites to identify the differential

metabolites and to understand better the metabolic pathways affected by CUMS stress or PBR. The metabolite correlation network and metabolic networks were constructed using Cytoscape software (v.3.5.0).

Dose-Effect and Dose-Toxicity Metabolic Screening

For further screening of the dose-effect and dose-toxicity metabolites, the related metabolites were analyzed by correlation analysis (SPSS 21, Pearson correlation analysis) between the different metabolites and the different dosages with $p > 0.05$. The dose-effect and dose-toxicity metabolites were obtained based on regression analysis (Prism 8.0, linear regression analysis) between the related metabolites and dosages with $R > 0.6$.

Construction and Evaluation of Dose-effect and Dose-toxicity Models

In this study, four models were used to integrate dose-response and dose-toxicity metabolites, including PCA, effect index (EI), SUM, and (R) SUM (additivity related to metabolites' R-values), and then the ROC curve was used to evaluate the performance of the four models and metabolites.

Dose-Effect and Dose-toxicity Index Calculations and Evaluations

In this study, the dose-effect index (DEI) and dose toxicity index (DTI) of each sample was used as the composite indicator. The formula for calculating DEI and DTI was as follows (Zhang ZZ, et al., 2015).

$$DEI = \sum_{i=1}^n \left| \frac{Ci - \bar{C}Mi}{\bar{C}Mi - \bar{K}i} \right| \times 100\% \quad (5)$$

$$DTI = \sum_{i=1}^n \left| \frac{Zi - \bar{K}i}{\bar{K}i} \right| \times 100\% \quad (6)$$

Ci was the relative level of one of the metabolites in every rat in the C4, C6, and C7 groups, Zi was the relative level of one of the metabolites in each rat in the Z4, Z6, and Z7 groups, Ki was the average relative level of one of the metabolites in the K group, and $\bar{C}Mi$ was the average relative level of one metabolite in the CM group.

The dose-effect and dose-toxicity relationships were evaluated using regression analysis (Prism 8.0, linear regression analysis).

Statistical Analysis

Quantitative data were presented as the mean \pm SD. The significance of differences between groups in terms of behavioral changes was determined using one-way ANOVA with SPSS software (version 21.0). Student's t -test was used to compare two groups, and statistical significance was set at $p < 0.05$.

TABLE 2 | Behavior on CUMS and healthy rats administration with PBR (Mean \pm SD, $n = 8$).

Group	Weight ($\Delta\%$)	Rearings ($\Delta\%$)	Crossings ($\Delta\%$)	Sucrose preference value ($\Delta\%$)
C1	0.351 \pm 0.011**	-0.394 \pm 0.181 ^{##}	-0.261 \pm 0.037**	-0.37 \pm 0.053 ^{###}
C2	0.311 \pm 0.006*	-0.486 \pm 0.259 ^{##}	-0.303 \pm 0.075*	-0.18 \pm 0.045 [#]
C3	0.339 \pm 0.007**	-0.532 \pm 0.106 ^{##}	-0.342 \pm 0.187 [#]	-0.22 \pm 0.064 ^{##}
C4	0.342 \pm 0.008**	0.294 \pm 0.112 ^{###}	-0.253 \pm 0.102**	-0.293 \pm 0.076 ^{###}
C5	0.308 \pm 0.001*	0.283 \pm 0.201 ^{###}	-0.186 \pm 0.070**	-0.24 \pm 0.034 ^{##}
C6	0.312 \pm 0.004*	0.126 \pm 0.042**	0.134 \pm 0.044 ^{###}	0.188 \pm 0.051*
C7	0.181 \pm 0.009 ^{###}	0.052 \pm 0.022**	-0.032 \pm 0.008 ^{###}	-0.29 \pm 0.083 [#]
Z1	0.312 \pm 0.007**	0.094 \pm 0.081**	-0.277 \pm 0.048*	0.136 \pm 0.025*
Z2	0.316 \pm 0.005**	0.104 \pm 0.059**	-0.268 \pm 0.059*	0.166 \pm 0.048*
Z3	0.318 \pm 0.017**	0.148 \pm 0.086**	-0.312 \pm 0.086*	0.103 \pm 0.053*
Z4	0.314 \pm 0.002**	0.078 \pm 0.051**	-0.329 \pm 0.102*	0.149 \pm 0.063*
Z5	0.308 \pm 0.007**	0.114 \pm 0.014**	-0.316 \pm 0.081*	0.114 \pm 0.074*
Z6	0.315 \pm 0.004**	0.126 \pm 0.053**	-0.283 \pm 0.039*	0.124 \pm 0.048*
Z7	0.309 \pm 0.011**	0.058 \pm 0.036**	-0.296 \pm 0.019*	0.096 \pm 0.043*
CM	0.243 \pm 0.008 ^{##}	-0.381 \pm 0.235 ^{##}	-0.3932 \pm 0.193 ^{##}	-0.2 \pm 0.028 [#]
CY	0.294 \pm 0.014*	-0.398 \pm 0.179 ^{##}	-0.292 \pm 0.075*	0.118 \pm 0.022*
K	0.313 \pm 0.009**	0.121 \pm 0.083**	-0.307 \pm 0.096*	0.037 \pm 0.009*

Note: [CM] CUMS rats, [K] control rats, [C1] ~ [C7] CUMS rats given PBR (7 different dosages), [Z1] ~ [Z7] control rats administered PBR, and [CY] CUMS rats administered venlafaxine hydrochloride. #, compared with the K group ($\#p < 0.05$, $\#\#p < 0.01$); *, compared with the CM group ($*p < 0.05$, $**p < 0.01$).

RESULTS

The Dose Range of the Effects and Toxicity in CUMS and Control Rats Administered PBR

Behavioral and Liver Function Indexes on CUMS and Control Rats Administration With PBR

The results of the behavioral tests, including body weight, sucrose preference test, and open-field test during the stress period of 21 days in CUMS and control rats are shown in **Table 2** and **Supplementary Table S2**. PCA was applied to the behavior indexes, and the PCA scores were expressed in two-dimensional scatter plots (PC1 and PC2 plotted on the x and y axes, respectively). The PCA score plot revealed the separation of CUMS rats from normal rats, suggesting that depressive-like behaviors developed in CUMS rats (**Supplementary Figure S3A**). The PCA score plot of C1-C7 groups was observed in the K and CM groups, indicating that the depressive-like behavior of CUMS rats was altered by PBR administration but existed in an effective dose range. As shown in **Table 2**, the growth rate ($\Delta\%$) of body weight, rearings, crossings and sucrose preference values slower significantly ($p < 0.05$) in CUMS rats compared with the control group, and the concentration range of 12.5–100 g/kg (C4–C7) of the PBR significantly reversed the decrease of the growth rate, especially in the C6 group (50 g/kg), suggesting that PBR played an anti-depression role in improving the slow body weight gain, anhedonia, and locomotor activities in CUMS rats. However, there was no distinct impact of PBR on control rats (**Table 2** and **Supplementary Table S2**).

Similarly, PCA was applied for liver function indices, and no obvious distinction was observed in the PCA score plot of each group (**Supplementary Figure S3B**), suggesting that there were no significant differences in liver function between the groups.

TABLE 3 | Liver function indexes in CUMS and healthy rats administration with PBR (Mean \pm SD, $n = 8$).

Group	ALP	ALT	AST	TBIL
C1	226.5 \pm 36.7 ^{###}	51.8 \pm 6.3 ^{**}	129.3 \pm 8.6 ^{**}	11.1 \pm 2.6
C2	196.6 \pm 39.7	59.1 \pm 21.6*	121.5 \pm 21.1 ^{###}	7.3 \pm 1.0 [#]
C3	193.9 \pm 28.4	64.1 \pm 37.9	120.6 \pm 10.2 ^{**}	5.5 \pm 2.7 [#]
C4	176.8 \pm 38.6	62.0 \pm 9.3	118.3 \pm 26.8 ^{###}	6.7 \pm 2.9 [#]
C5	229.5 \pm 45.1	59.5 \pm 13.4	137.2 \pm 30.5*	7.7 \pm 1.5 [#]
C6	267.8 \pm 46.36 ^{###}	67.1 \pm 11.4	154.3 \pm 18.6	9.2 \pm 3.3
C7	251.6 \pm 50.3 ^{###}	72.8 \pm 14.9	141.1 \pm 32.7*	7.7 \pm 1.5 [#]
Z1	189.9 \pm 28.6	64.2 \pm 8.5	141.7 \pm 17.6	9.6 \pm 1.9
Z2	196.2 \pm 28.6	66.9 \pm 11.7	149.6 \pm 15.5	10.7 \pm 2.1*
Z3	235.3 \pm 65.2 ^{##}	69.5 \pm 11.4	161.7 \pm 29.3	13.3 \pm 5.2*
Z4	186.9 \pm 22.7	84.7 \pm 20.6	152.6 \pm 22.0	10.3 \pm 4.3*
Z5	200.7 \pm 37.0 ^{##}	87.6 \pm 14.1	179.6 \pm 25.2	10.0 \pm 3.3*
Z6	240.2 \pm 55.1 ^{##}	69.3 \pm 12.1	123.5 \pm 28.3 ^{##}	9.0 \pm 4.0*
Z7	251.6 \pm 50.3 ^{###}	68.6 \pm 19.4	148.9 \pm 35.6	6.8 \pm 1.2 [#]
CM	169.9 \pm 24.4	78.8 \pm 26.2	172.8 \pm 44.6	8.7 \pm 3.5 [#]
K	173.4 \pm 19.4	64.0 \pm 17.0	156.8 \pm 44.5	10.8 \pm 2.3*

Note: [CM] CUMS rats, [K] control rats, [C1] ~ [C7] CUMS rats given PBR (7 different dosages), [Z1] ~ [Z7] control rats administered PBR, and [CY] CUMS rats administered venlafaxine hydrochloride. #, compared with the K group ($\#p < 0.05$, $\#\#p < 0.01$, $\#\#\#p < 0.001$); *, compared with the CM group ($*p < 0.05$, $**p < 0.01$, $***p < 0.001$).

However, deviations were observed in the C1–C7, Z1–Z7, and CM groups compared with the normal group, occurring at various levels, suggesting that the modeling and administration caused changes in body liver function. As shown in **Table 3**, the levels of ALT and AST were markedly reduced in CUMS rats administered with low-dose and medium-dose treatment with PBR (C1–C5, 1–25 g/kg), suggesting that the lower doses of PBR showed obvious protective effects on liver function. While in control rats (**Table 3**), high-dose and medium-dose-treatment of PBR (Z4–Z7, 12.5–100 g/kg) deviated ALT and AST from the normal range, suggested that PBR in the concentration of D4 ~

TABLE 4 | The rates of effect and toxicity on CUMS and normal rats administration with PBR.

Dose (g/kg)	Total samples	Effect [BRI, efficiency rate (%)]		Toxicity [LCI, toxicity rate (%)]	
		CUMS rats	Control rats	CUMS rats	Control rats
0	8	0	100	25	0
1	8	50	100	0	0
3	8	25	100	12.5	12.5
6	8	75	100	12.5	0
12.5	8	62.5	100	12.5	12.5
25	8	62.5	100	25	0
50	8	75	100	0	25
100	8	75	100	25	12.5

D7 could cause liver injury in control rats. Thus, further research could be carried out to explore whether the administration of PBR caused liver damage and the toxicity dose range of PBR in CUMS and normal rats.

PCA Analysis of BRI and LCI

For BRI, the variance contribution rate of the first principal component PC1 was 53%, and PC2 was 28%, accounting for 81% of the information of the original data set cumulatively (>80%). For LCI, the variance contribution rates of PC1 and PC2 were 52.9 and 35.5%, respectively, and the total variance contribution rate was 89% (>80%). The BRI and LCI can be expressed as Eqs 6–8 and Eqs 9–11.

For BRI,

$$f_1 = 0.517zx_1 - 0.131zx_2 + 0.52zx_3 + 0.165zx_4 \quad (6)$$

$$f_2 = 0.196zx_1 + 0.66zx_2 + 0.169zx_3 - 0.623zx_4 \quad (7)$$

$$f_{(BRI)} = 0.65f_1 + 0.35f_2 \quad (8)$$

For LCI,

$$f_1 = 0.115zx_1 + 0.758zx_2 + 0.803zx_3 + 0.721zx_4 \quad (9)$$

$$f_2 = 0.977zx_1 + 0.134zx_2 - 0.212zx_3 - 0.061zx_4 \quad (10)$$

$$f_{(LCI)} = 0.6f_1 + 0.4f_2 \quad (11)$$

The Dose Range of Effect and Toxicity Based on Behavior and Liver Indexes

From these two standard accuracy indices of the K group, the threshold values of efficacy and toxicity were determined (mean \pm 1.96 SD) and used to screen for the effects and toxicity responses (Table 4). Ultimately, the probit function was used to calculate the dose range. The obtained effective dose range for the CUMS rats was from 12.6 g/kg to 163 g/kg (EC_{50} – EC_{95}) with the regression function $PROBIT(P) = -0.139 + 0.11x$, and the TC_{50} for CUMS and normal rats was 388 g/kg and 207 g/kg with the regression function $PROBIT(P) = -1.156 + 0.03x$ and $PROBIT(P) = -1.669 + 0.081x$. The results suggested that a broad effective dose range of PBR was observed in CUMS rats, and the lowest dose (12.6 g/kg) was consistent with these results in the behavioral test. The subthreshold toxicity doses of the CM group were higher than those of normal rats administered PBR, which revealed that the liver function of normal rats was more susceptible to PBR.

However, the specific mechanism of effect and toxicity of PBR in CUMS and normal rats remained to be determined.

Comprehensive indicators, including BRI and LCI, showed a dose-dependent effect, and the regression models were used for dose-effect/toxicity relationship assessment (Supplementary Figure S4). The results showed that BRI and LCI exhibited a strong dose-effect/toxicity relationship evaluation ($R > 0.8$).

CK-18F Levels in Serum and Liver Samples of CUMS and Control Rats Administered PBR

As shown in Figure 2, there was no significant difference in the CK-18F level in serum and liver between the CM and K groups. In CUMS rats, the content of CK-18F did not significantly change in the serum of C1–C7 groups (Figure 2A) but increased significantly in the liver of the C7 group compared with the K group ($p < 0.001$, Figure 2B), suggesting that rats administrated with 100 g/kg PBR exhibited severe liver damage. After a comprehensive analysis, the effective dose range of PBR was 12.6–50 g/kg. In normal rats, CK-18F levels in the serum of the Z6–Z7 group were significantly increased ($p < 0.05$) (Figure 2C). In the liver, the CK-18F level in the Z5–Z6 groups was increased ($p < 0.05$) and significantly increased in the Z7 group compared with the K group ($p < 0.001$, Figure 2D).

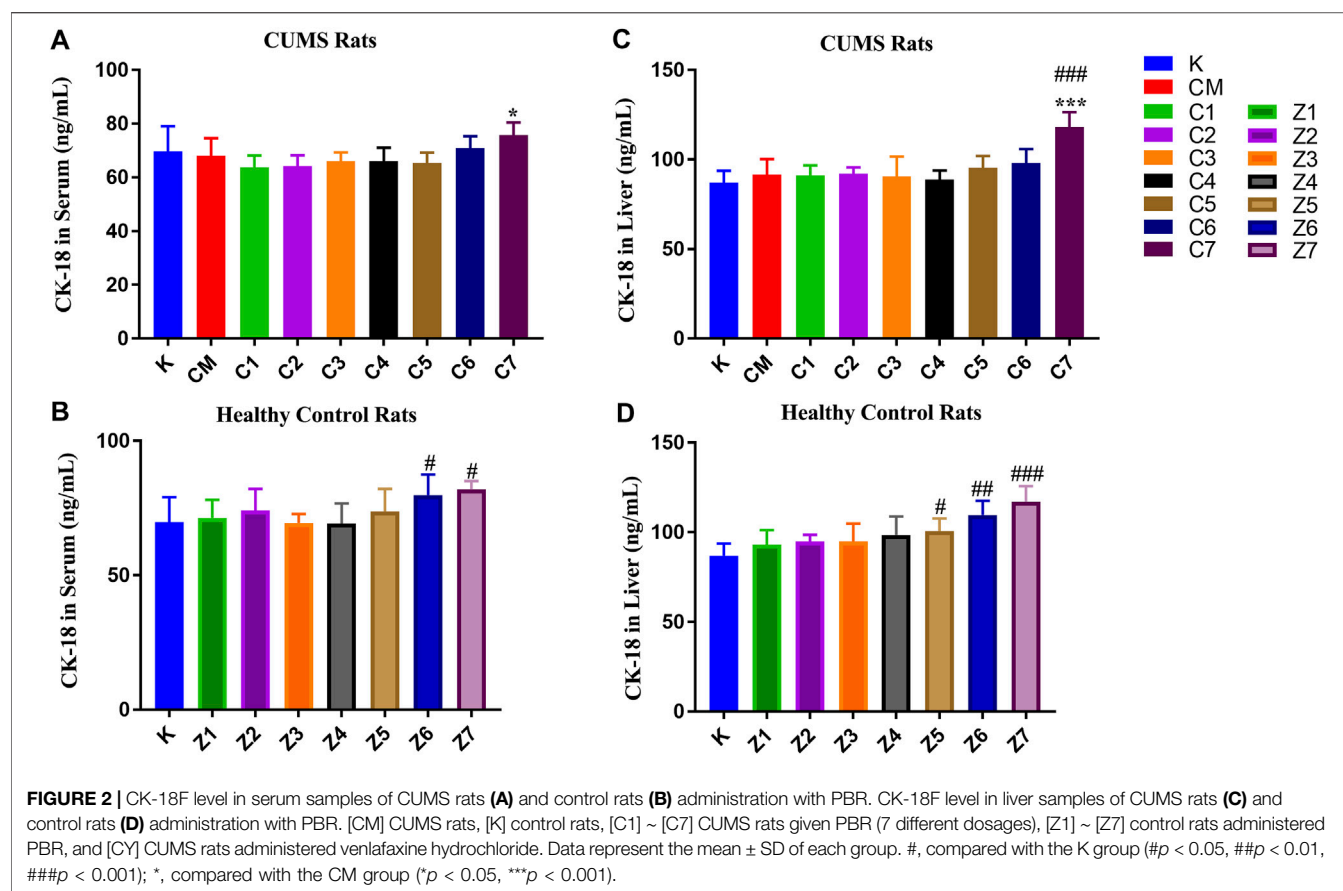
To determine the specific mechanism of effect and toxicity of PBR in CUMS and normal rats, the lowest effective dose [C4] group, the most effective dose [C6] group, and the toxic dose [C7] group, and three corresponding groups [Z4], [Z6], and [Z7] were chosen for metabolomics analysis.

PBR Adjusted Differentially on Metabolites of Rat Liver by UHPLC-MS

Assessment of Stability in UPLC-MS System

The metabolic profiles of the liver samples were characterized using UHPLC-Q Exactive Orbitrap-MS. Typical total ions chromatograph (TIC) of [CM], [C4], [C6], [C7], [K], [Z4], [Z6], and [Z7] showed approximately 8,671 ions, and 409 metabolites were identified in the sample (Figure 3). The metabolites were mainly high polarity compounds including amino acids, sphingolipids, bile acids, etc.

The stability of the LC-MS system was assessed using QC samples. The PCA score plot indicated that the QC samples were tightly clustered (Supplementary Figure S5). Moreover, the peak areas and retention times of the ten extracted ions in the QC samples



also showed good stability (Supplementary Table S3). The RSDs of the ten peaks were 0.22–3.85% for retention times, $3.76\text{--}9.66 \times 10^{-5}\%$ for the m/z value, respectively. These results indicate that the UPLC-MS system is robust for metabolomic analysis.

Multivariate Statistical Analysis

A snapshot of the systematic metabolism in the [CM], [K], [C4], [C6], and [C7] groups was obtained using PLS-DA pattern recognition analysis. An obvious separation was observed between [CM] and [K], indicating that the alterations in metabolic profiles were related to CUMS stress. In addition, [C4], [C6], and [C7] moved away from [CM] in a dose-dependent manner in PLS-DA (Figure 4A), suggesting that the differences in metabolic profiles were related to the effects of PBR on CUMS-induced rats. The reliability of the multiple pattern recognition methods was evaluated by the R^2Y and Q^2 values (R^2Y represents goodness of fit, and Q^2 indicates goodness of prediction). The R^2Y and Q^2 were 0.901 and 0.651, indicating that the PLS-DA model could accurately describe the data. These results of the permutation tests showed that the two models were credible without overfitting (Figure 4A).

CUMS Induced Deviation of Liver Metabolic Profile in Rats

To discover the liver metabolites between the [CM] and [K] groups, OPLS-DA analysis was applied to eliminate unrelated

variations in the spectra. The OPLS-DA score plot showed a statistically significant difference between the [CM] and [K] groups (Figure 4C), indicating a similar result that metabolic profiles were significantly altered in rat liver with CUMS stress. The corresponding OPLS S-plot (Figure 4E) in turn showed the contribution of different variables and ions far away from the origin were deemed as potential biomarkers. As a result, 21 candidates were screened from the corresponding S-plot between the [CM] and [K] groups with $VIP > 1.0$. The changes in these potential biomarkers are listed in Table 5 and Figures 5A,B,D. Compared with the [K] group, the levels of 15 metabolites, including leucine, betaine, isoleucine, valine, phenylpyruvic acid, L-tyrosine, nicotinamide, adenine, adenosine, xanthine, sphinganine, lysoPC (16:1 (9Z)), phytosphingosine, taurodeoxycholic acid, and taurochenodeoxycholic acid, decreased significantly in the [CM] group. In contrast, six metabolites, including 2-phenylacetamide, N6-acetyl-L-lysine, L-carnitine, L-acetylcarnitine, propionylcarnitine, and succinic acid, increased significantly in the [CM] group.

PBR Reversed Metabolic Profile in CUMS-induced Rats

After the administration of PBR, 17 differential metabolites were call-backed close to the [K] group after PBR treatment in the [C4], [C6], and [C7] groups, except L-carnitine, L-acetylcarnitine, and propionylcarnitine with an over-reversed regulation at the

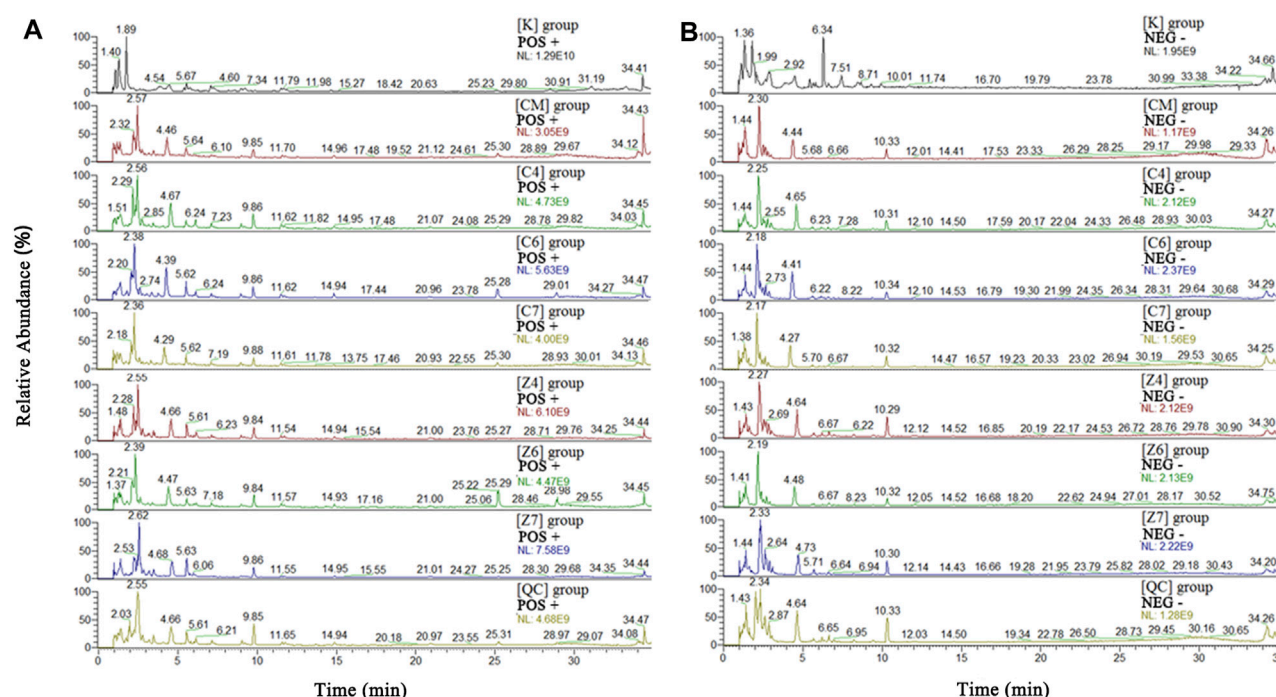


FIGURE 3 | Total ions chromatograph (TIC) in positive (A) and negative (B) ion of [K], [CM], [C1]–[C7], [Z1]–[Z7] and [QC] group. [CM] CUMS rats, [K] control rats, [C1] ~ [C7] CUMS rats given PBR (7 different dosages), [Z1] ~ [Z7] control rats administered PBR, and [CY] CUMS rats administered venlafaxine hydrochloride.

D7 dose. LysoPC (16:1 (9Z)), taurodeoxycholic acid, taurochenodesoxycholic acid, and succinic acid were not reversed at D6 and D7 of PBR.

The metabolic pathway was established based on related literature and the KEGG database to understand the correlation between these potential biomarkers. These metabolites were linked to amino acid metabolism, energy metabolism, β -oxidation of fatty acids, sphingolipid metabolism, glycerophospholipid metabolism, and bile acid metabolism (Figure 6). Next, differential metabolite pathway enrichment was performed using MetaboAnalyst software. Seven amino acid metabolism and sphingolipid metabolism pathways were obtained by impact value > 0.1 and $-\log P > 4$ (Figure 7A), such as valine, leucine, and isoleucine biosynthesis, valine, leucine, and isoleucine degradation, aminoacyl-tRNA biosynthesis, phenylalanine metabolism, among others.

Differential Metabolic Profile in Control Rats

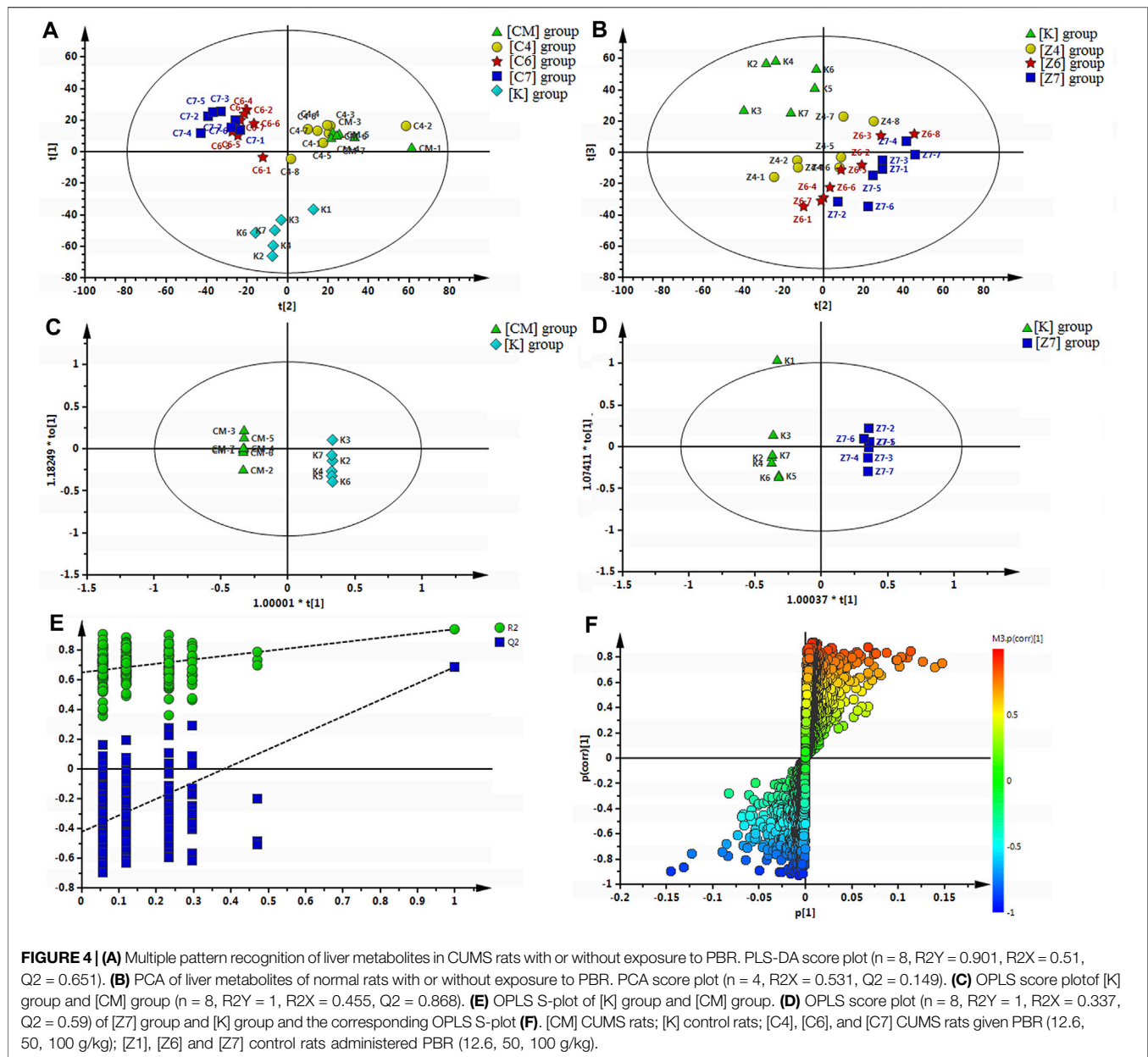
A significant separation was observed in the PCA score plots of the [K], [Z4], [Z6], and [Z7] groups (Figure 4B), suggesting that PBR could affect the metabolic profile of control rats. The goodness values of $R^2 Y = 0.929$ and $Q^2 = 0.516$ in the OPLS models in [Z7] versus [K] were computed, demonstrating that the models were reliable (Figure 4D). The contributions of different variables in [Z7] and [K] were extracted from the corresponding OPLS S-plots (Figure 4F).

As a result, 20 metabolites were significantly perturbed by PBR in normal rats (Table 6). Compared with the [K] group, leucine,

isoleucine, valine, hypoxanthine, adenine, adenosine, malic acid, sphinganine, phytosphingosine, lysoPE [0:0/20:4 (8Z, 11Z, 14Z, 17Z)], L-carnitine, L-acetylcarnitine, propionylcarnitine, taurodeoxycholic acid, taurochenodesoxycholic acid, and ascorbic acid-2-sulfate decreased significantly in the [Z4], [Z6], and [Z7] groups (Figures 5B,C,E). In contrast, the levels of other metabolites, including N6-acetyl-L-lysine, succinic acid, adenosine 2'-phosphate, and glycocholic acid, increased significantly in the [Z4], [Z6], and [Z7] groups. The changes in metabolites were associated with amino acid metabolism, energy metabolism, sphingolipid metabolism, glycerophospholipid metabolism, fatty acid β -oxidation, and bile acid metabolism (Figure 6). Similarly, five pathways in amino acid metabolism, energy metabolism, sphingolipid metabolism, and bile acid metabolism were considered to be the most pertinent in control rats given PBR, such as valine, leucine, and isoleucine biosynthesis; valine, leucine, and isoleucine degradation; and sphingolipid metabolism (Figure 7B).

Metabolic Network Analysis of Metabolites in Both CUMS and Control Rats

Metabolites in both CUMS and control rats, six of them were returned to a healthy level after PBR treatment of CUMS-induced depression, including betaine, tyrosine, 2-phenylacetamide, phenylpyruvic acid, nicotinamide, and xanthine, while they were not significantly affected in control rats. This result



indicated that these six metabolites were highly correlated with the pharmacological effects of PBR and were associated with amino acid metabolism, sphingolipid metabolism, and energy metabolism (Figure 7C).

In addition, another 11 metabolites showed the same regulative differential metabolites in both CUMS and control rats administered with PBR ($p < 0.05$, Figure 7C), including valine, isoleucine, leucine, N6-acetyl-L-lysine, phytosphingosine, sphinganine, adenine, adenosine, L-carnitine, L-acetylcarnitine, and propionylcarnitine, which were associated with amino acid metabolism, fatty acid β oxidation, sphingolipid metabolism, and energy metabolism (Figure 7C). Among these, 3-acyl carnitines (L-carnitine, L-acetylcarnitine, and propionyl carnitine) were decreased

after PBR administration in both control and CUMS rats and could be significantly reversed to the level of the [K] group in the [C4] and [C6] groups. The other eight differential metabolites were reversed in both CUMS and control rats, indicating that the PBR might regulate the same sites under different body conditions, which caused it to present an opposite change tendency.

The rest of eight metabolites were significantly altered in control rats after PBR treatment, including glycocholic acid, taurodeoxycholic acid, taurochenodesoxycholic acid, hypoxanthine, adenosine 2'-phosphate, malic acid, succinic acid, and lysoPE (0:0/20:4 (8Z, 11Z, 14Z, 17Z)), which were associated with energy metabolism, glycerophospholipid metabolism, and bile acid metabolism (Figure 7C).

TABLE 5 | Identified differential metabolites in the liver of CUMS rats.

No	Metabolites	TR (min)	m/z	Ion	CM/K	C7/CM	C6/CM	C4/CM	Metabolic pathway
1	Betaine	1.82	118.0864	M + H	↓ ^a	↑ ^a	↑	↑ ^a	Glycine, serine and threonine metabolism
2	Leucine ^b	3.16	132.1025	M + H	↓ ^a	↑ ^a	↑ ^a	↑ ^a	Amino acid metabolism
3	Isoleucine ^b	3.42	132.1025	M + H	↓ ^a	↑ ^a	↑ ^a	↑ ^a	Amino acid metabolism
4	Valine ^b	1.40	118.0864	M + H	↓ ^a	↑ ^a	↑	↑ ^a	Amino acid metabolism
5	2-Phenylacetamide	3.43	136.0756	M + H	↑ ^a	↓ ^a			Phenylalanine metabolism
6	Phenylpyruvic acid	3.13	165.0533	M-H	↓ ^a	↑ ^a	↑	↑	Phenylalanine metabolism
7	L-Tyrosine	2.78	182.0811	M + H	↓ ^a	↑ ^a	↑	↑	Phenylalanine metabolism
8	N6-Acetyl-L-lysine	3.31	189.1232	M + H	↑ ^a	↓	↓ ^a	↓ ^a	Lysine degradation
9	Nicotinamide	1.85	123.0554	M + H	↓ ^a	↑ ^a	↑	↑	Nicotinate and nicotinamide metabolism
10	Adenine	3.79	136.062	M + H	↓ ^a	↑ ^a	↑ ^a		Purine metabolism
11	Adenosine	3.46	268.1036	M + H	↓ ^a	↑ ^a	↑ ^a	↑	Purine metabolism
12	Xanthine	2.80	153.0406	M + H	↓ ^a	↑ ^a	↑	↑	Purine metabolism
13	L-Carnitine	1.39	162.1126	M + H	↑ ^a	↓ ^a	↓ ^a	↓ ^a	β-oxidation of fatty acid
14	L-Acetylcarnitine	2.36	204.1229	M + H	↑ ^a	↓ ^a	↓ ^a	↓	β-oxidation of fatty acid
15	Propionylcarnitine	4.45	218.1386	M + H	↑ ^a	↓ ^a	↓ ^a	↓ ^a	β-oxidation of fatty acid
16	Sphinganine	14.41	302.3058	M + H	↓ ^a	↑	↑ ^a	↑	sphingolipid metabolism
17	Phytosphingosine	11.73	318.3004	M + H	↓ ^a	↑ ^a	↑	↑	sphingolipid metabolism
18	Succinic acid	2.99	117.0185	M-H	↑ ^a		↓	↓	Citrate cycle
19	LysoPC [16:1 (9Z)]	15.94	494.3237	M + H	↓ ^a		↑		Glycerophospholipid metabolism
20	Taurodeoxycholic acid ^b	8.34	500.3014	M + H	↑ ^a	↑			Bile acid metabolism
21	Taurochenodeoxycholic acid	10.27	500.3014	M + H	↓ ^a	↑			Bile acid metabolism

Note: [CM] CUMS rats, [K] control rats, [C1] ~ [C7] CUMS rats given PBR (7 different dosages). ↑ shows up-regulated metabolite; ↓ shows down-regulated metabolite.

^aMeans a statistically significant difference at $p < 0.05$.

^bValidated with standard. [CM] group compared with [K] group, CM/K; [C4] group compared with [CM] group, C4/CM; [C6] group compared with [CM] group, C6/CM; [C7] group compared with [CM] group, C7/CM.

The metabolic networks involved in some enzymes and genes were constructed using Cytoscape to understand better the potential biomarkers' internal correlation in terms of enzyme or gene levels. The metabolic networks that were established based on the markedly differential metabolites are shown in **Figure 8**. Valine, leucine, isoleucine, and others involved in amino acid metabolism are shown in **Figure 8A**. Adenine, xanthine, malic acid, and others were also involved in energy metabolism (**Figure 8B**). As shown in **Figures 8C–E**, phytosphingosine, and sphinganine were involved in sphingolipid metabolism, L-carnitine and O-acetylcarnitine were involved in the β-oxidation of fatty acids, and glycocholate and taurodeoxycholate were involved in bile acid metabolism.

Dose-Effect/Toxicity Relationship Analysis

Dose-Effect and Dose-Toxicity Metabolites Screening

The relationship of dose-effect/toxicity was mainly to show the dose-dependence of metabolites by calculating the correlation between metabolite concentrations and dose. The correlations of dose-effect and dose-toxicity are shown in **Figure 9A**. Nine of the metabolites were significantly related to the drug effect ($p < 0.05$), including adenine, isoleucine/leucine, betaine, L-valine, nicotinamide, propionylcarnitine, 2-phenylacetamide, L-acetylcarnitine, and L-carnitine. Sixteen metabolites were significantly related to drug toxicity ($p < 0.05$), including adenine, adenosine-2'-phosphate, L-valine, N6-Acetyl-L-lysine, adenosine, phytosphingosine, taurodeoxycholic acid, lysoPE [0:0/20:4 (8Z, 11Z, 14Z, 17Z)], hypoxanthine, L-acetylcarnitine, malic acid, and ascorbic acid-2-sulfate. In **Figure 9B**, the regression curve of dose-effect and dose-toxicity showed the capability of evaluating the

intensities of the relationship. Five pharmacodynamic metabolites, including isoleucine/leucine, L-valine, 2-phenylacetamide, L-acetylcarnitine, and L-carnitine, or five toxic metabolites including adenosine-2'-phosphate, L-valine, L-acetylcarnitine, malic acid, and ascorbic acid-2-sulfate were screened with $R > 0.6$.

Model Comparison

To better evaluate the dose-effect/toxicity relationship of PBR, four computational methods including PCA analysis, EI analysis, the sum of metabolites (SUM), and (R)SUM were used to integrate the pharmacodynamic and toxic metabolites. The receiver operating characteristic curves (ROC) was applied to evaluate the computational methods. The evaluation results of the five pharmacodynamic metabolites and five toxic metabolites are shown in **Figure 10** (ROC, 0.7222–0.7632 and 0.506–0.718), indicating that the metabolites have some ability to evaluate effect and toxicity. Furthermore, the four computational methods' ROC was 0.7398–0.9123 and 0.658–0.878, suggesting that all computational methods could improve the evaluation ability of metabolites to different degrees. The improvement in EI analysis was the most significant, indicating that the EI analysis was suitable for integrating metabolites. Therefore, EI analysis was used to calculate the dose-effect/toxicity indices (DEI/DTI) and estimate the dose-effect/toxicity relationship.

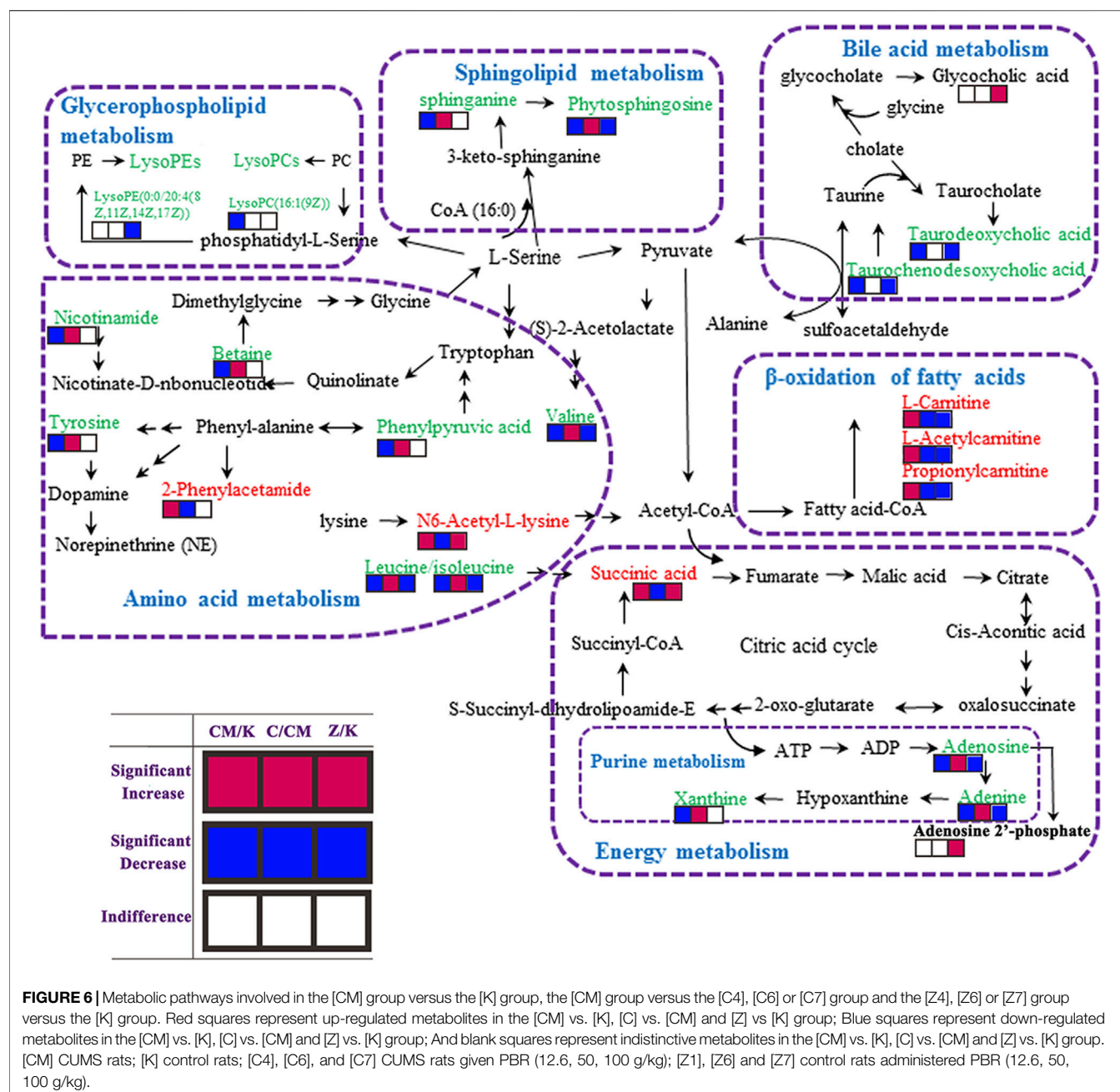
Dose-Effect/Toxicity Indices

The values of DEI and DTI in both CUMS and control rats following PBR treatment with C4, C6, and C7 dosage are shown in **Figure 11**. The DEI and DTI significantly increased with dosage augment. Regression models were used for the dose-effect/toxicity

difference might be resulting from the inconformity of dosage groups in the metabonomics analysis.

DISCUSSION

Bupleuri Radix, a top grade herbal drug in Shennong's Materia Medica, soothes the liver and relieves stagnation. This study focused on the effective and safe dose of PBR and its dose-effect/toxicity relationship. First, the BRI and LCI were obtained by integrated behavioral and liver indices and used



to determine the dose range of effect and toxicity. The results showed that the effective dose range for CUMS rats was 12.6–163g (herb)/kg, the TD50 (median toxicity dose) for CUMS and normal rats were 388 and 207 g (herb)/kg, and the toxicological results showed that rats administrated with 100 g/kg PBR exhibited severe liver damage. After a comprehensive analysis, the use of PBR dose was determined to be 12.6–50 g (herb)/kg. Second, liver metabolomics was applied to gain insight into the related mechanisms, and the results showed that PBR could reverse amino acid metabolism, energy metabolism, sphingolipid metabolism, and β -oxidation of fatty acids based on liver metabolic profiles to produce an

anti-depressant effect in a dose-dependent manner in CUMS rats. Extra two metabolic pathways, including glycerophospholipid metabolism and bile acid metabolism, were significantly perturbed in normal rats administered PBR. Finally, the dose-effect index (DEI) and dose toxicity index (DTI) were obtained by integrating the effects and toxic metabolites and were applied to precisely evaluate the dose-effect/toxicity relationship of PBR. The results showed that DEI and DTI had a remarkable ability to estimate the effect and toxicity. In addition, the DEI and DTI was used to determine the dose range of effect and toxicity, and it demonstrated high concordance with pre-experiment results. The CUMS

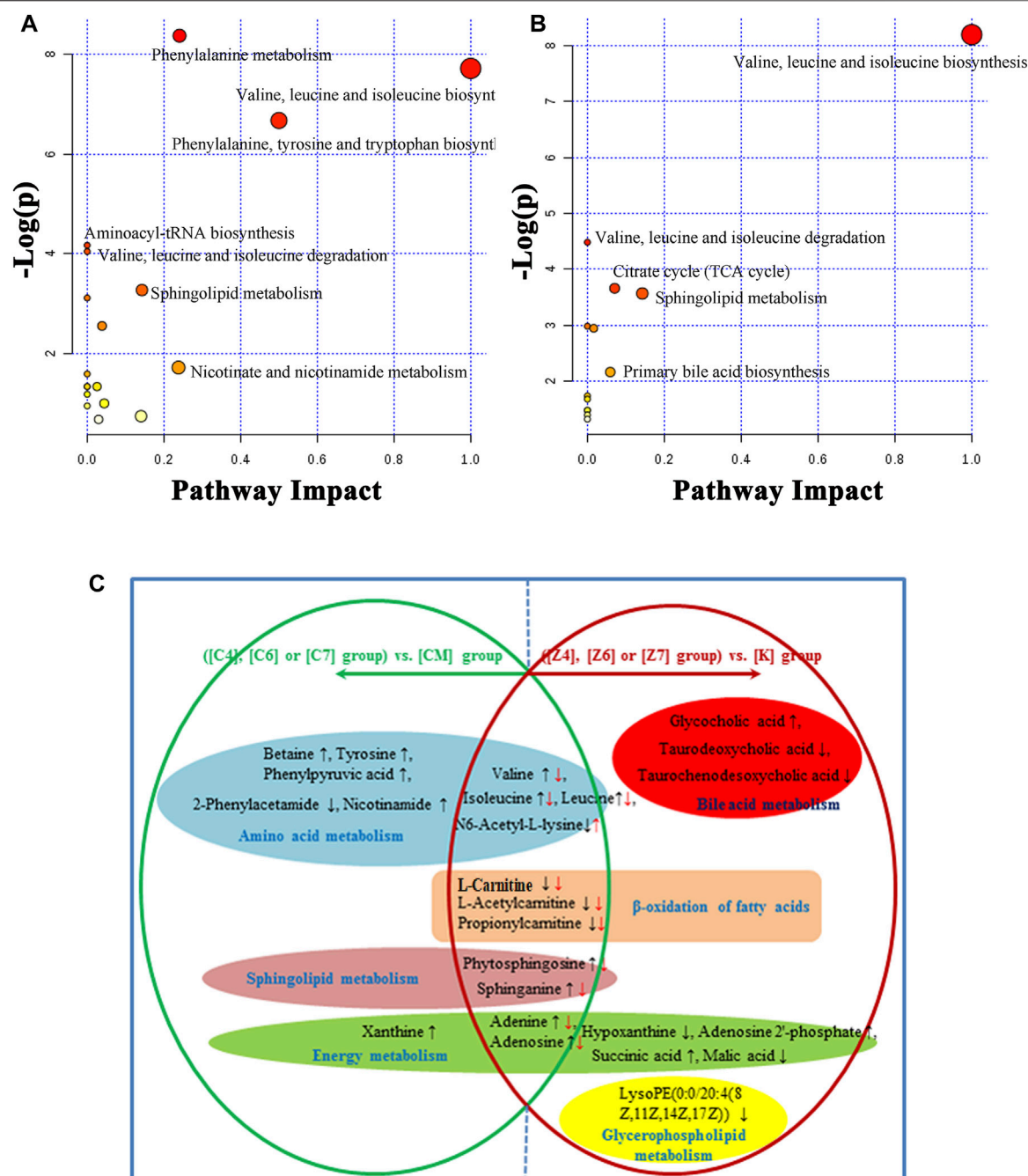


FIGURE 7 | (A) Summary of pathways analysis of CUMS rats with PBR treatment with MetaboAnalyst. **(B)** Summary of pathways analysis of healthy rats with PBR administration with MetaboAnalyst. Each point represents one metabolic pathway; the size of dot and shades of color are positively correlated with the impact of the metabolic pathway. **(C)** Different metabolites and corresponding pathways in CUMS rats or healthy rats following PBR administration. “↑” and “↓” represent that the metabolite is up- or down-regulated in CUMS rats or healthy rats following PBR administration. [CM] CUMS rats; [K] control rats; [C4], [C6], and [C7] CUMS rats given PBR (12.6, 50, 100 g/kg); [Z1], [Z6] and [Z7] control rats administered PBR (12.6, 50, 100 g/kg).

possessed a higher toxicity tolerance dose of PBR, which was consistent with the theory of “You Gu Wu Yun” in TCM. “You Gu Wu Yun” theory suggested that the toxic herb would not produce toxicity in a corresponding pathological state; on the contrary, it would have a therapeutic effect (Tan et al., 2013).

In this study, behavioral research suggested that PBR had a positive anti-depressant effect on CUMS rats but no distinct impact on control rats. However, there were larger intra-group errors in behavioral tests, and liver function, especially in the sucrose preference test. This may be due to the individual

TABLE 6 | Identified differential metabolites in the liver of healthy rats.

No	Metabolites	T _R (min)	m/z	Ion	Z4/K	Z6/K	Z7/K	Metabolic pathway
1	Leucine ^b	3.16	132.1025	M + H	↓ ^a	↓ ^a	↓ ^a	Amino acid metabolism
2	Isoleucine ^b	3.42	132.1025	M + H	↓ ^a	↓ ^a	↓ ^a	Amino acid metabolism
3	Valine ^b	1.40	118.0864	M + H	↓ ^a	↓ ^a	↓ ^a	Amino acid metabolism
4	N6-Acetyl-L-lysine	3.31	189.1232	M + H	↑	↑ ^a	↑ ^a	Lysine degradation
5	Hypoxanthine	4.39	137.0458	M + H	↓	↓ ^a	↓ ^a	Purine metabolism
6	Adenine	3.79	136.062	M + H	↓ ^a	↓ ^a	↓ ^a	Purine metabolism
7	Adenosine	3.46	268.1036	M + H	↓ ^a	↓ ^a	↓ ^a	Purine metabolism
8	Adenosine 2'-phosphate	1.78	348.0701	M + H		↑ ^a	↑ ^a	Purine metabolism
9	Succinic acid	2.99	117.0185	M-H		↑ ^a	↑ ^a	Citrate cycle
10	Malic acid	1.69	133.0135	M-H		↓ ^a	↓ ^a	Citrate cycle
11	Sphinganine	14.41	302.3058	M + H	↓ ^a	↓ ^a	↓ ^a	sphingolipid metabolism
12	Phytosphingosine	11.73	318.3004	M + H	↓ ^a	↓ ^a	↓ ^a	sphingolipid metabolism
13	LysoPE [0:0/20:4 (8Z,11Z,14Z,17Z)]	16.59	502.2918	M + H	↓	↓	↓ ^a	Glycerophospholipid metabolism
14	L-Carnitine	1.39	162.1126	M + H		↓ ^a	↓ ^a	β-oxidation of fatty acid
15	L-Acetylcarnitine	2.36	204.1229	M + H		↓ ^a	↓ ^a	β-oxidation of fatty acid
16	Propionylcarnitine	4.45	218.1386	M + H	↓ ^a	↓ ^a	↓ ^a	β-oxidation of fatty acid
17	Glycocholic acid	9.98	464.3021	M-H	↑	↑ ^a	↑ ^a	Bile acid metabolism
18	Taurodeoxycholic acid ^b	8.34	498.2897	M-H	↓	↓ ^a	↓ ^a	Bile acid metabolism
19	Taurochenodesoxycholic acid	10.27	498.2897	M-H	↓	↓ ^a	↓ ^a	Bile acid metabolism
20	Ascorbic acid-2-sulfate	1.82	254.9817	M + H			↓ ^a	oxidative stress

Note: [K] control rats, [Z1] ~ [Z7] control rats administered PBR (7 different dosages). ↑ shows up-regulated metabolite; ↓ shows down-regulated metabolite.

^aMeans a statistically significant difference at $p < 0.05$.

^bValidated with standard. [Z4] group compared with [K] group, Z4/K; [Z6] group compared with [K] group, Z6/K; [Z7] group compared with [K] group, Z7/K.

differences in animals. Consequently, larger sample size is needed to obtain a meaningful statistical difference in the future. In addition, to comprehensively evaluate the efficacy and toxicity, the overall pharmacological potency was applied to evaluate the activity and toxicity of PBR, and the BRI and LCI, which were obtained by integrated behavioral tests and liver indices, were used to determine the dose range of effect and toxicity. The results showed that BRI and LCI could better evaluate the efficacy and toxicity and showed a dose-dependent effect.

CK-18F is considered a biomarker of cell death and has been used as a predictive indicator of drug-induced liver injury (DILI, Kakisaka et al., 2017). In this study, the content of CK-18F changed more in the liver than in the serum of CUMS and normal rats administered PBR. In control rats, the CK-18F level was increased in the Z5-Z7 group (25–100 g/kg) compared with the K group, indicating that the control rats showed a risk of DILI at 25–100 g/kg. However, in the CUMS rats, there was no significant change in CK-18F level at the dose of C5-C6 (25–50 g/kg), but a significant increase at the dose of C7 (100 g/kg), indicating that CUMS stress attenuated the risk of DILI at the medium dose of PBR (25–50 g/kg), which was consistent with the theory of “You Gu Wu Yun” in TCM. However, this study does not verify the toxic dose of PBR. The *in vivo* and *in vitro* experiments will be used to verify the findings of the study in the next step.

The metabolomic changes were performed using the metabolomics method in this study. In the protein precipitation method, the effects of precipitators (methanol, acetonitrile, acetonitrile-0.1% formic acid, methanol-0.1% formic acid) were compared. In the liquid chromatography conditions, the effects of different acids including formic acid, trifluoroacetic acid, and phosphoric acid, as well as the amount of

acid (0.1, 0.2, and 0.3%) added into the mobile phase was compared and the chromatographic conditions of the mobile phase and gradient elution system were optimized to gain more information of metabolites. In addition, The QC samples were added in the process and observed tightly clustered in the result of PCA, suggesting that UHPLC-MS was a stable and reliable instrument in this population. The standards of metabolites were used to perform and ensure the accuracy of identification.

The perturbation of the amino acid neurotransmitter system plays an important role in the pathogenesis of depression (Ni et al., 2008). Amino acid metabolism is shown in **Figure 8A**. PBR mainly regulated branched-chain amino acids and affects synthetic norepinephrine (NE) in the treatment of depression. The delivery of branched-chain amino acids through the blood-brain-carrier system is closely related to the rate of 5-HT synthesis. In addition, branched-chain amino acids, especially leucine, play a major role in the differentiation of glutamate and glutamine in astrocytes, thereby maintaining the steady-state balance of brain nitrogen. It also affects the function of the central nervous system (Shimomura and Harris, 2006). More importantly, leucine and isoleucine can increase the expression of BDNF in hippocampal neurons, and BDNF dominates the signal transduction pathways associated with depression (Furukawa-Hibi et al., 2011). In this study, the changes in leucine, isoleucine, and valine were consistent with the results of serum metabolomics (Gao et al., 2017), suggesting that branched-chain amino acids, including leucine, isoleucine, and valine, were potential markers for PBR in the treatment of depression. Both L-tyrosine and phenylalanine are synthetic precursors of NE (Meyers, 2000), while phenylalanine metabolism produces phenylpyruvic acid and 2-phenylacetamide. A study (Wang, 2001) reported that elevated phenylalanine/tyrosine ratios could cause damage to

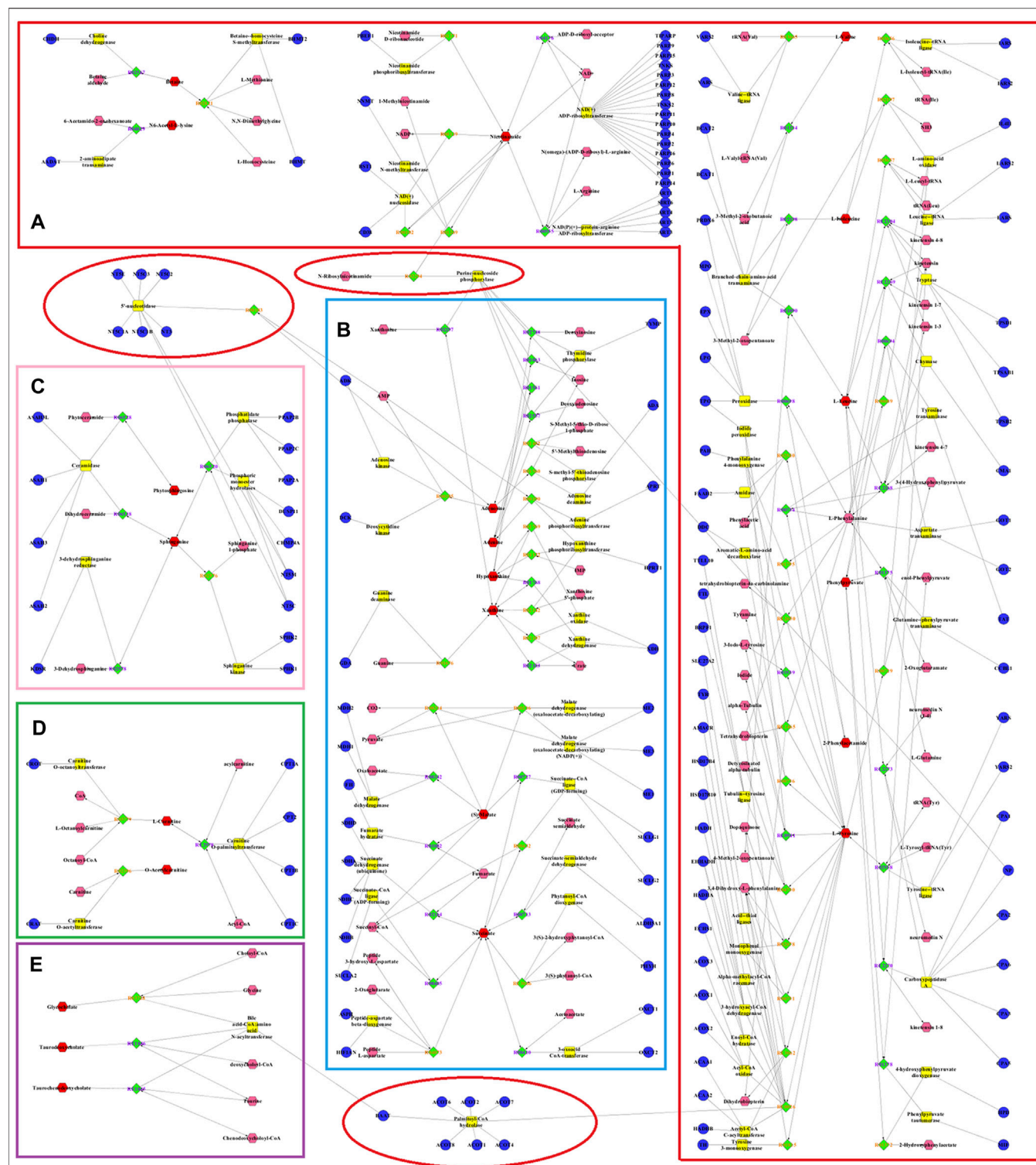


FIGURE 8 | Metabolic networks involved in enzymes and genes were established based on the differential metabolites in both CUMS and healthy rats following PBR treatment. The metabolic networks of amino acid metabolism (A), energy metabolism (B), sphingolipid metabolism (C), β -oxidation of fatty acid (D) and bile acid metabolism (E).

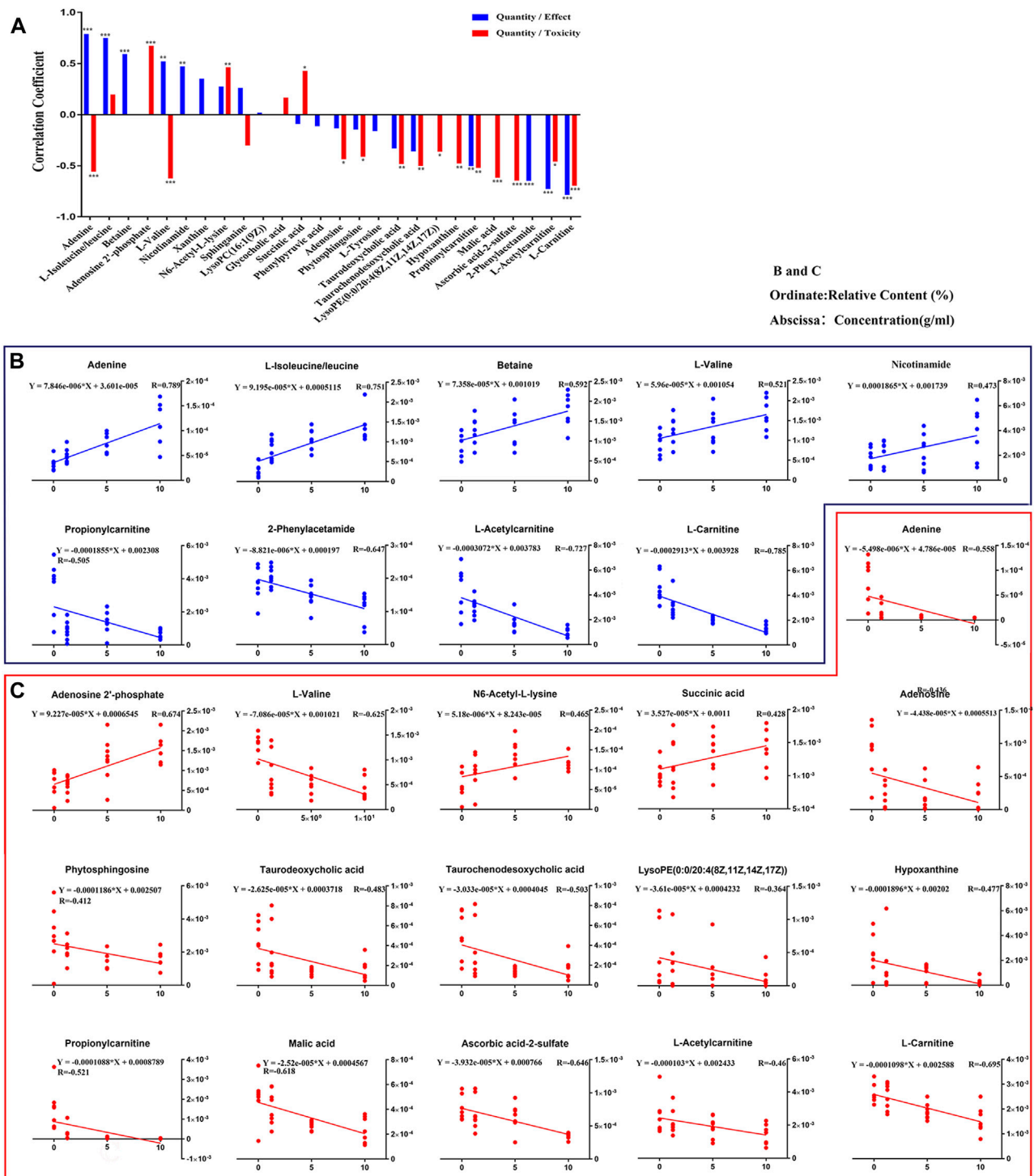


FIGURE 9 | Relationships involved in Dose-Effect and Dose-Toxicity were established based on the differential metabolites in both CUMS and healthy rats following PBR treatment. Correlation of Quantity/Effect and Quantity/Toxicity (A). Regression curve of Dose-Effect (B) and Dose-Toxicity (C).

the nervous system, leading to depression, mental development defects, and mental disorders. In this study, tyrosine and phenylpyruvic acid were significantly decreased, and 2-phenylacetamide was significantly

increased in the liver of CUMS rats, suggesting that the perturbation of phenylalanine metabolism might cause NE synthesis deficiency, leading to the occurrence of depression.

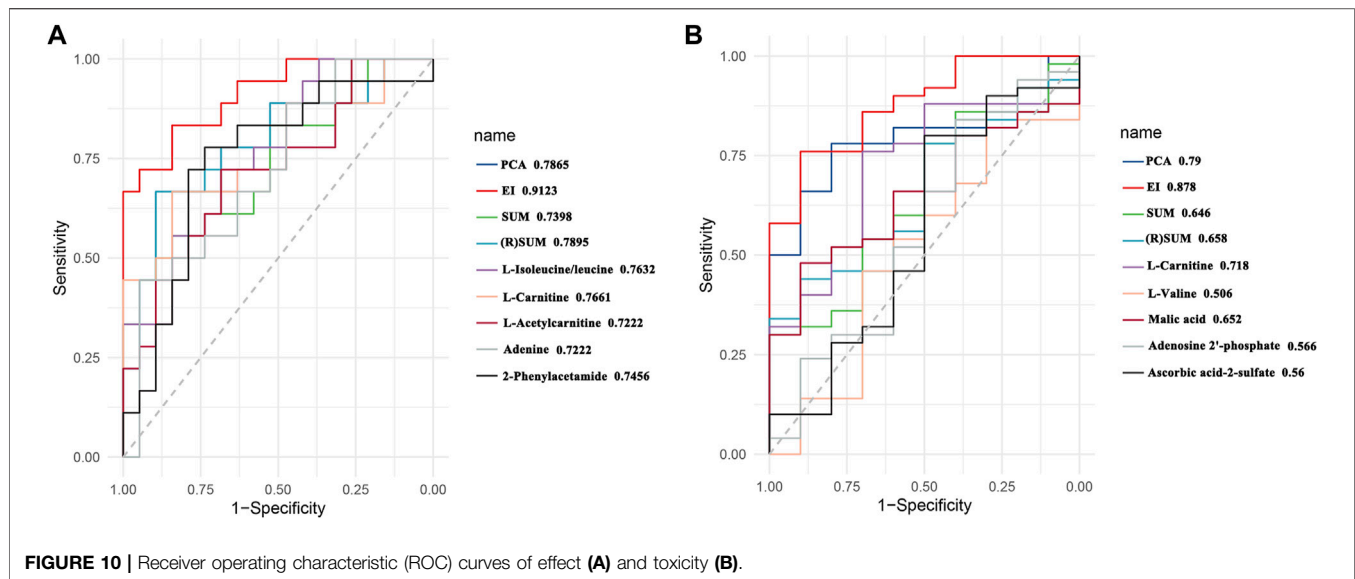


FIGURE 10 | Receiver operating characteristic (ROC) curves of effect (A) and toxicity (B).

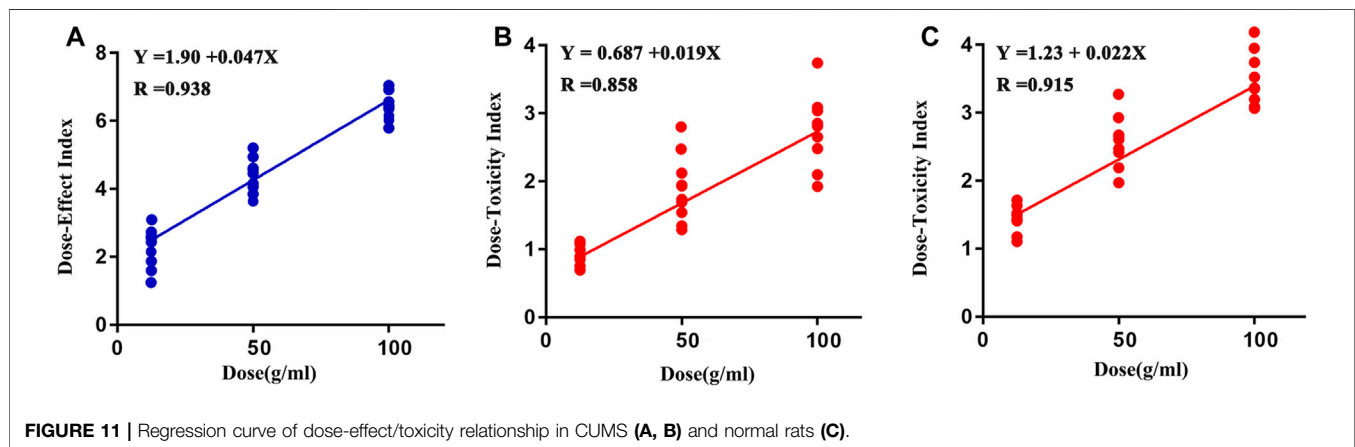


FIGURE 11 | Regression curve of dose-effect/toxicity relationship in CUMS (A, B) and normal rats (C).

N6-acetyl-L-lysine is an acetylated lysine. Acetylation of lysine is a reversible modification of the protein residue after translation, which has been considered as a novel regulatory factor of mitochondrial bioenergy in recent years, and the regulatory factor controls massive cellular life processes (Anderson and Hirsche, 2012; Thapa et al., 2017). The increase of N6-acetyl-L-lysine in the liver of CUMS rats indicated that stress might disturb healthy mitochondrial biological function. Betaine is an osmotic pressure molecule that accumulates in tissues, regulating cell volume (Schliess and Haussinger, 2002; Lang, 2007). It is also an important methyl donor so that homocysteine can methylate to methionine and plays a vital role in biological functions (Lever and Slow, 2010). Nicotinamide is involved in the tryptophan/kynurenine metabolic pathway. Additionally, both betaine and nicotinamide have a synergistic effect on synthetic anti-depressant drugs. The combination of betaine and s-adenosylmethionine in treating patients with mild to moderate depression is superior to s-adenosylmethionine alone. The combination of nicotinamide

and tryptophan can significantly enhance the therapeutic effects by reducing the peripheral catabolism of tryptophan (Chouinard et al., 1977). In this study, the levels of amino acids and their metabolites were significantly decreased in CUMS rats. After the administration of PBR, these metabolites were significantly reversed to healthy, indicating that PBR produced anti-depressant effects by regulating amino acid neurotransmitter system metabolism. However, the branched-chain amino acids (leucine, isoleucine, and valine) were significantly reduced in the liver of control rats with PBR treatment, indicating that the amino acid transport was obstructed so that hepatic cells could not effectively absorb amino acids and ultimately cause liver injury. In this study, the levels of N6-acetyl-L-lysine were significantly increased in the liver of control rats with PBR treatment, indicating that the enhancement of lysine acetylation may disturb mitochondrial and cell functions and lead to liver cell damage.

The metabolic networks of energy metabolism involved in potential enzymes and genes are shown in Figure 8B. Energy is

an indispensable factor in the survival of an organism. It has been reported that insufficient energy is closely related to depression. The conversion of adenine produces xanthine. Both xanthine and adenine are intermediate metabolites of adenosine, which play an important role in converting ATP and ADP (Su et al., 2014). In this study, the levels of xanthine, adenine, and adenosine were significantly decreased in the liver of CUMS rats, indicating that depression could weaken adenosine metabolism and reduce the function of energy conversion pathways in depressed patients. Similarly, malic acid and succinic acid are intermediates of the tricarboxylic acid (TCA) cycle. Their presence in the [CM] group indicated that the TCA cycle and energy metabolism in patients with depression was disturbed. After the administration of PBR, the reduced concentrations of xanthine, adenine, and adenosine in the liver were significantly reversed to healthy, indicating that PBR produced anti-depressant effects by regulating energy metabolism. However, the levels of hypoxanthine, adenine, and adenosine were significantly reduced, and adenosine 2'-phosphate was increased in the liver of control rats with PBR treatment, indicating that high doses of PBR may cause the adenosine metabolism to weaken and abnormal, and then cause the function of energy conversion pathways to attenuate, ultimately leading to hepatic cell damage due to insufficient energy supply for the survival of hepatic cells. Similarly, malic acid and succinic acid are intermediates in the TCA cycle, and their levels are abnormal in the liver of control rats with PBR treatment, indicating that high doses of PBR may lead to TCA weakening and abnormalities, leading to hepatic cell damage due to insufficient supply for normal survival processes of the hepatic cell.

Sphingolipid metabolism is shown in **Figure 8C**. Sphingolipids are an important component of meningeal lipids. An increased concentration of sphingolipids is closely related to depression (Dinoff et al., 2017). A study reported that sphingolipid levels in serum samples were significantly higher in depressed patients than in healthy individuals (Gracia-Garcia et al., 2011). In this study, the levels of phytosphingosine and sphinganine were significantly decreased in the livers of CUMS rats. After the administration of PBR, their levels in the liver of CUMS rats were significantly reversed to healthy, indicating that PBR produced anti-depressant effects by regulating sphingolipid metabolism. It has been reported that sphingomyelinase activation is a response to tumor necrosis factor- α (TNF- α) and other cytokines. Sphingomyelinase activation and C16-ceramide production are involved in TNF- α -induced hepatocyte apoptosis (Kolesnick et al., 1998). In addition, the dynamic balance of intracellular ceramide and sphingosine 1-phosphate (ceramide/S1P) may determine cell survival (Osawa et al., 2005), suggesting that sphingolipids are closely linked to the activity and survival of cells. In this study, the PBR produced disturbances to endogenous metabolites of hepatic sphingolipids in control rats administered with PBR, including sphinganine and phytosphingosine, suggesting that high-dose PBR might cause liver damage by altering hepatocyte survival and membrane structure.

The metabolic networks of β -oxidation of fatty acids are shown in **Figure 8D**. β -oxidation of fatty acids is an important pathway for fatty acid decomposition and energy production, and

its abnormality can lead to dysfunction of the nervous system. Acyl carnitines are long-chain acyl fatty acid esters of carnitine. They can carry long-chain fatty acids from the cytoplasm into the mitochondria, allowing long-chain fatty acids to oxidize in the mitochondria to produce energy. However, this transportation is dependent on carnitine (Malaguarnera et al., 2011; Ren et al., 2013). In this study, the levels of L-carnitine, L-acetylcarnitine, and propionylcarnitine were significantly increased in the liver of CUMS rats, indicating that the transportation of long-chain fatty acids into the mitochondria was disturbed, thereby interfering with the energy production of the long-chain fatty acid oxidation process. After the administration of PBR, the concentrations of L-carnitine, L-acetylcarnitine, and propionylcarnitine in D4 and D6 were significantly reversed to healthy, indicating that PBR produced an anti-depressant effect by regulating β -oxidation of fatty acids. Another study (Devaux, 1991) reported that acetyl-L-carnitine treatment improved liver function and quality of life in patients with mild hepatic encephalopathy. Therefore, in normal rats, the levels of acyl-carnitine were significantly decreased in the liver of control rats administered with PBR, indicating that PBR may alter acyl-carnitine to cause mitochondrial β -oxidation of fatty acid dysfunction, resulting in energy deficiency and eventually leading to liver damage.

The glycerophospholipid metabolism was only significantly changed in the livers of control rats administered with PBR. Lysophosphatidylethanolamine (LysoPEs) is produced by the metabolism of phosphatidylethanolamine (PE). Both PE and sphingolipids are the main components of cell membrane phospholipids and are distributed asymmetrically in the plasma membrane. Most PEs are embedded in the inner membrane of the cell membrane and constitute the membrane phospholipid bilayer (Jaeschke et al., 2002). The abnormality of LysoPEs in control rats administered with PBR suggested that PEs were perturbed, further affecting the plasma membrane structure and permeability. In this study, LysoPE [0:0/20:4 (8Z, 11Z, 14Z, 17Z)] was significantly decreased in the livers of control rats administered with PBR, indicating that PBR might cause liver damage by changing the structural integrity and permeability of the plasma membrane in normal rats. Bile acid metabolism is shown in **Figure 8E**. Bile acid metabolism was also significantly changed in control rats administered with PBR. Bile acids are sensitive indicators of liver and liver damage. Abnormally elevated bile acids, such as cholestasis, can cause the accumulation of toxic bile acids in the liver, leading to pathophysiological effects, including mitochondrial dysfunction and overproduction of reactive oxygen and nitrogen (Palmeira and Rolo, 2004; Tan et al., 2007). More importantly, slight liver damage can cause bile acid perturbation in the serum and liver (Yamazaki et al., 2013). Various liver diseases, such as non-alcoholic fatty liver disease and drug-induced liver injury, can increase intrahepatic bile acid levels (Lake et al., 2013). In this study, glycocholic acid was significantly elevated in the liver, which was consistent with the results of serum metabolomics of control rats administered with PBR, indicating that high-dose PBR might accumulate intrahepatic bile acid and cause liver injury.

In this study, 8,671 metabolites were measured, and 409 metabolites were identified in the sample. The metabolites were

mainly high polarity compounds including amino acids, sphingolipids, bile acids, etc. While the less polarity compounds such as fatty acids and lipid metabolites were difficult to be detected. The GC-MS serum metabolomics was performed and the fatty acids were detected in our previous study (Gao, et al., 2014). The results showed that depression was associated with amino acid metabolism and energy metabolism, which were consistent with the results of this study. Therefore, the targeted metabolomics was applied to quantify the metabolites of amino acid metabolism and energy metabolism in follow-up studies.

The dose-effect/toxicity relationship is the essence of the clinical use of TCM. Because of the multi-component and multi-target characteristics of TCM (Wang et al., 2010), a comprehensive evaluation of the dose-effect/toxicity relationship is important to allow its application in modern medical practice. Although some convenient and effective evaluation indices have been used in previous dose-effect/toxicity studies, including body weight, blood pressure, blood glucose, transaminase, platelets, and cell number, there are still many disease effect indices that lack quantification, and depression is a major disease. With the development of studies regarding the essence of TCM syndrome based on metabonomics, the importance of metabonomics for evaluating overall effects was gradually being recognized (Wang et al., 2010). After administration, the endogenous small molecules shifted in the same direction as the dose increased. Metabolites representing the organic state were screened and integrated into a dose-effect/toxicity relationship analysis. A significant dose-effect/toxicity relationship was observed with a high dose-dependence. The results showed that the comprehensive index was better for evaluating the dose-effect/toxicity relationship, which is consistent with the fact that it may be caused by the multi-component and multi-target characteristics of the TCM. In this study, four-function models were compared for metabolite integration, and the results showed that the different models might influence the evaluation characteristics of the metabolites. Therefore, exploring a more suitable functional model would help construct a metabolic evaluation system for depression. However, it is necessary to verify effect/toxicity biomarkers of PBR. The *vitro* cell experiments would be used to verify the specificity and accuracy of toxicity biomarkers in follow-up studies.

CONCLUSIONS

The current study demonstrates that the effective dose range and median toxicity dose of PBR for CUMS rats are 12.6–50 g (herb)/kg and 388 g (herb)/kg, and PBR produces anti-depressant effects by reversing amino acid metabolism, energy metabolism, sphingolipid metabolism, and β -oxidation of fatty acids in CUMS rats. In control rats, the median toxicity dose of PBR is 207 g (herb)/kg, and extra two metabolic pathways including glycerophospholipid metabolism and bile acid metabolism are significantly perturbed after administration with PBR. Moreover, the comprehensive metabolic indexes including DEI and DTI have a remarkable ability to predict effect and toxicity which needs further follow-up validation. Furthermore, the CUMS rats possessed a higher

toxicity tolerance dose of PBR, which was consistent with the theory of “You Gu Wu Yun”. These results indicate that the metabonomics techniques combined with correlation analysis could be used to discover indicators for comprehensive evaluations of efficacy and toxicity.

DATA AVAILABILITY STATEMENT

The original contributions presented in the study are included in the article/**Supplementary Material**, further inquiries can be directed to the corresponding authors.

ETHICS STATEMENT

This animal study were performed under the NIH Guidelines for Care and Use of Laboratory Animals (United States) and the Prevention of Cruelty to Animals Act (1986) of China, and approved by the Animal Ethics Committee of Shanxi University (ethical batch number: SXULL2019004).

AUTHOR CONTRIBUTIONS

PW and XG conceived and designed the experiments; PW and XG wrote the paper; ML and YF performed the experiments; PW and YF analyzed the data; JJ detected samples with UHPLC-MS; JT, ZL, and XQ design of the study and writing the protocol. All authors have approved the final version of the manuscript.

FUNDING

This study was supported by the National Natural Science Foundation of China (Grant No. 81473415), the National Natural Science Foundation of China (Grant No. 8217142774), the Outstanding Youth Foundation project of Applied Basic Research Project of Shanxi Province (Grant No. 201701D211009), Social Development Projects of Key R&D Programs in Shanxi Province Key Research and Development (R&D) Projects of Shanxi Province (Grant No. 201803D31019), Shanxi Key Laboratory of Active constituents Research and Utilization of TCM (Grant No. 201605D111004), Special Scientific Research on Major New Drug Creation by the Ministry of Science and Technology (Grant No. 2017ZX09301-047), National Key R&D Program of China (Grant No. 2019YFC1710800), Science and technology innovation team of Shanxi Province (Grant No. 201605D131045-18) and “1,331 Engineering Project” of Shanxi Province.

SUPPLEMENTARY MATERIAL

The Supplementary Material for this article can be found online at: <https://www.frontiersin.org/articles/10.3389/fphar.2021.627451/full#supplementary-material>

REFERENCES

- Anderson, K. A., and Hirschey, M. D. (2012). Mitochondrial Protein Acetylation Regulates Metabolism. *Essays. Biochem.* 52 (1), 23–35. doi:10.1042/bse0520023
- Chen, C., Yin, Q., Tian, J., Gao, X., Qin, X., Du, G., et al. (2020a). Studies on the Potential Link between Antidepressant Effect of Xiaoyao San and its Pharmacological Activity of Hepatoprotection Based on Multi-Platform Metabolomics. *J. Ethnopharmacol.* 249 (249), 112432. doi:10.1016/j.jep.2019.112432
- Chen, J. Q., Chen, Y. Y., Tao, H. J., Pu, Z. J., Shi, X. Q., Zhang, J., et al. (2020b). An Integrated Metabolomics Strategy to Reveal Dose-Effect Relationship and Therapeutic Mechanisms of Different Efficacy of Rhubarb in Constipation Rats. *J. Pharm. Biomed. Anal.* 177 (177), 112837. doi:10.1016/j.jpba.2019.112837
- Chouinard, G., Young, S. N., Annable, L., and Sourkes, T. L. (1977). Tryptophan-nicotinamide Combination in Depression. *Lancet* 1 (8005), 249. doi:10.1016/S0140-6736(77)91036-4
- Devaux, P. F. (1991). Static and Dynamic Lipid Asymmetry in Cell Membranes. *Biochemistry* 30 (5), 1163–1173. doi:10.1021/bi00219a001
- Dinoff, A., Herrmann, N., and Lanctôt, K. L. (2017). Ceramides and Depression: A Systematic Review. *J. Affect. Disord.* 213 (15), 35–43. doi:10.1016/j.jad.2017.02.008
- Fabricatore, A. N., and Wadden, T. A. (2006). Obesity. *Annu. Rev. Clin. Psychol.* 2 (2), 357–377. doi:10.1146/annurev.clinpsy.2.022305.095249
- Furukawa-Hibi, Y., Nitta, A., Ikeda, T., Morishita, K., Liu, W., Ibi, D., et al. (2011). The Hydrophobic Dipeptide Leu-Ile Inhibits Immobility Induced by Repeated Forced Swimming via the Induction of BDNF. *Behav. Brain Res.* 220 (2), 271–280. doi:10.1016/j.bbr.2011.02.003
- Gao, X., Guo, B., Yang, L., Liu, J., Zhang, X., Qin, X., et al. (2014). Selection and Dynamic Metabolic Response of Rat Biomarkers by Metabonomics and Multivariate Statistical Analysis Combined with GC-MS. *Pharmacol. Biochem. Behav.* 117, 85–91. doi:10.1016/j.pbb.2013.12.013
- Gao, X., Liang, M., Fang, Y., Zhao, F., Tian, J., Zhang, X., et al. (2017). Deciphering the Differential Effective and Toxic Responses of Bupleuri Radix Following the Induction of Chronic Unpredictable Mild Stress and in Healthy Rats Based on Serum Metabolic Profiles. *Front. Pharmacol.* 8 (3), 995. doi:10.3389/fphar.2017.00995
- Gao, X. X., Cui, J., Zheng, X. Y., Li, Z. Y., Choi, Y. H., Zhou, Y. Z., et al. (2013). An Investigation of the Antidepressant Action of Xiaoyaosan in Rats Using Ultra Performance Liquid Chromatography-Mass Spectrometry Combined with Metabonomics. *Phytother. Res.* 27 (7), 1074–1085. doi:10.1002/ptr.4805
- Gracia-Garcia, P., Rao, V., Haughey, N. J., Bandaru, V. V., Banduru, V. V., Smith, G., et al. (2011). Elevated Plasma Ceramides in Depression. *J. Neuropsychiatry Clin. Neurosci.* 23 (2), 215–218. doi:10.1176/appi.neuropsych.274correction10.1176/jnp.23.2.jnp215
- Jaeschke, H., Gores, G. J., Cederbaum, A. I., Hinson, J. A., Pessayre, D., and Lemaster, J. J. (2002). Mechanisms of Hepatotoxicity. *Toxicol. Sci.* 65 (2), 166–176. doi:10.1002/(SICI)1097-4652(199809)176:33.0.CO;2-Z
- Jia, H. M., Li, Q., Zhou, C., Yu, M., Yang, Y., Zhang, H. W., et al. (2016). Chronic Unpredictable Mild Stress Leads to Altered Hepatic Metabolic Profile and Gene Expression. *Sci. Rep.* 6 (6), 23441. doi:10.1038/srep23441
- Jia, H. M., Yu, M., Ma, L. Y., Zhang, H. W., and Zou, Z. M. (2017). Chaihu-shu-gan-san Regulates Phospholipids and Bile Acid Metabolism against Hepatic Injury Induced by Chronic Unpredictable Stress in Rat. *J. Chromatogr. B Analyt. Technol. Biomed. Life Sci.* 1064 (1064), 14–21. doi:10.1016/j.jchromb.2017.08.003
- Jiang, H., Yang, L., Hou, A., Zhang, J., Wang, S., Man, W., et al. (2020). Botany, Traditional Uses, Phytochemistry, Analytical Methods, Processing, Pharmacology and Pharmacokinetics of Bupleuri Radix: A Systematic Review. *Biomed. Pharmacother.* 131 (2), 110679. doi:10.1016/j.biopha.2020.110679
- Kakisaka, K., Yoshida, Y., Suzuki, Y., Sato, T., Kuroda, H., Miyasaka, A., et al. (2017). Serum Markers for Mitochondrial Dysfunction and Cell Death Are Possible Predictive Indicators for Drug-Induced Liver Injury by Direct Acting Antivirals. *Hepatol. Res.* 48 (1), 78–86. doi:10.1111/hepr.12893
- Kolesnick, R. N., and Krönke, M. (1998). Regulation of Ceramide Production and Apoptosis. *Annu. Rev. Physiol.* 60 (1), 643–665. doi:10.1146/annurev.physiol.60.1.643
- Lake, A. D., Novak, P., Shipkova, P., Aranibar, N., Robertson, D., Reilly, M. D., et al. (2013). Decreased Hepatotoxic Bile Acid Composition and Altered Synthesis in Progressive Human Nonalcoholic Fatty Liver Disease. *Toxicol. Appl. Pharmacol.* 268 (2), 132–140. doi:10.1016/j.taap.2013.01.022
- Lang, F. (2007). Mechanisms and Significance of Cell Volume Regulation. *J. Am. Coll. Nutr.* 26, 613s–623s. doi:10.1080/07315724.2007.10719667
- Lever, M., and Slow, S. (2010). The Clinical Significance of Betaine, an Osmolyte with a Key Role in Methyl Group Metabolism. *Clin. Biochem.* 43 (9), 732–744. doi:10.1016/j.clinbiochem.2010.03.009
- Li, X. J., Qiu, W. Q., Da, X. L., Hou, Y. J., Ma, Q. Y., Wang, T. Y., et al. (2020). A Combination of Depression and Liver Qi Stagnation and Spleen Deficiency Syndrome Using a Rat Model. *Anat. Rec. (Hoboken)* 303 (8), 2154–2167. doi:10.1002/ar.24388
- Liu, J. L., Lan, Y., Jie, C., Guo, B. R., Qin, X. M., and Gao, X. X. (2013). Preliminary Study on Serum Pharmacokinetics of Petroleum Ether Fraction in Ethanol Extract from Xiaoyao Powder Based on UPLC-PDA. *Chin. Tradit. Herbal Drugs* 44 (20), 2816–2822. doi:10.7501/j.issn.0253-2670.2013.20.006
- Liu, X.-j., Liu, H.-l., Zhao, D., Wei, F.-x., Wang, Y.-z., Lv, M., et al. (2021). Hepatic Metabolomics of the Compatibility Effect of Xiaoyaosan on CUMS-Induced Depression Based on the TCM Theory of "Treating Diseases via Regulating the Liver's Function". *J. Pharm. Biomed. Anal.* 201 (201), 114123. doi:10.1016/j.jpba.2021.114123
- Malaguarnera, M., Bella, R., Vacante, M., Giordano, M., Malaguarnera, G., Gargante, M. P., et al. (2011). Acetyl-L-carnitine Reduces Depression and Improves Quality of Life in Patients with Minimal Hepatic Encephalopathy. *Scand. J. Gastroenterol.* 46 (6), 750–759. doi:10.3109/00365521.2011.565067
- Mathers, C. D., and Loncar, D. (2006). Projections of Global Mortality and burden of Disease from 2002 to 2030. *Plos Med.* 3 (11), e442. doi:10.1371/journal.pmed.0030442
- Medina, S., Dominguez-Perles, R., Gil, J. I., Ferreres, F., and Gil-Izquierdo, A. (2014). Metabolomics and the Diagnosis of Human Diseases-Aa Guide to the Markers and Pathophysiological Pathways Affected. *Curr. Med. Chem.* 21 (7), 823–848. doi:10.2174/0929867320666131119124056
- Meng, M., Feng, Y., Wang, P., Feng, J., Qin, X., and Gao, X. (2020). Regulatory Effect of Polar Extract of Poria Cocos on Neurotransmitter and Circadian Rhythm Disorder in CUMS Rats. *Chin. Tradit. Herbal Drugs* 51 (1), 118–126. doi:10.7501/j.issn.0253-2670.2020.01.017
- Meyers, S. (2000). Use of Neurotransmitter Precursors for Treatment of Depression. *Altern. Med. Rev.* 5 (1), 64–71. doi:10.5465/AMBPP.2011.65869681
- Nardelli, S., Pentassuglio, I., Pasquale, C., Ridola, L., Moscucci, F., Merli, M., et al. (2013). Depression, Anxiety and Alexithymia Symptoms Are Major Determinants of Health Related Quality of Life (HRQoL) in Cirrhotic Patients. *Metab. Brain Dis.* 28 (2), 239–243. doi:10.1007/s10111-012-9364-0
- Ni, Y., Su, M., Lin, J., Wang, X., Qiu, Y., Zhao, A., et al. (2008). Metabolic Profiling Reveals Disorder of Amino Acid Metabolism in Four Brain Regions from a Rat Model of Chronic Unpredictable Mild Stress. *FEBS Lett.* 582 (17), 2627–2636. doi:10.1016/j.febslet.2008.06.040
- Osawa, Y., Uchinami, H., Bielawski, J., Schwabe, R. F., Hannun, Y. A., and Brenner, D. A. (2005). Roles for C16-Ceramide and Sphingosine 1-phosphate in Regulating Hepatocyte Apoptosis in Response to Tumor Necrosis Factor-Alpha. *J. Biol. Chem.* 280 (30), 27879–27887. doi:10.1074/jbc.M503002200
- Palmeira, C. M., and Rolo, A. P. (2004). Mitochondrially-mediated Toxicity of Bile Acids. *Toxicology* 203, 1–15. doi:10.1016/j.tox.2004.06.001
- Park, S. H., and Ishino, R. (2013). Liver Injury Associated with Antidepressants. *Curr. Drug Saf.* 8 (3), 207–223. doi:10.2174/1574886311308030011
- Paykel, E. S. (2006). Depression: Major Problem for Public Health. *Epidemiol. Psychiatr. Soc.* 15 (1), 4–10. doi:10.1017/S1121189X00001974
- Ren, J., Lakoski, S., Haller, R. G., Sherry, A. D., and Malloy, C. R. (2013). Dynamic Monitoring of Carnitine and Acetylcarnitine in the Trimethylamine Signal after Exercise in Human Skeletal Muscle by 7T 1H-MRS. *Magn. Reson. Med.* 69 (1), 7–17. doi:10.1002/mrm.24249
- Sarko, J. (2000). Antidepressants, Old and New. A Review of Their Adverse Effects and Toxicity in Overdose. *Emerg. Med. Clin. North. Am.* 18 (4), 637–654. doi:10.1016/S0733-8627(05)70151-6

- Sayers, J. (2001). World Health Organization. The World Health Report 2001-Mental Health: New Understanding, New Hope. *B. World Health. Organ* 79 (11), 1085. doi:10.1590/S0042-96862001001100014
- Schliess, F., and Häussinger, D. (2002). The Cellular Hydration State: a Critical Determinant for Cell Death and Survival. *Biol. Chem.* 383 (3-4), 577-583. doi:10.1515/BC.2002.059
- Shimomura, Y., and Harris, R. A. (2006). Metabolism and Physiological Function of Branched-Chain Amino Acids: Discussion of Session 1. *J. Nutr.* 136 (1), 232s-3S. doi:10.1093/jn/136.1.232S
- Su, Z. H., Jia, H. M., Zhang, H. W., Feng, Y. F., An, L., and Zou, Z. M. (2014). Hippocampus and Serum Metabolomic Studies to Explore the Regulation of Chaihu-Shu-Gan-San on Metabolic Network Disturbances of Rats Exposed to Chronic Variable Stress. *Mol. Biosyst.* 10 (3), 549-561. doi:10.1039/c3mb70377k
- Suh, J. I., Sakong, J. K., Lee, K., Lee, Y. K., Park, J. B., Kim, D. J., et al. (2013). Anxiety and Depression Propensities in Patients with Acute Toxic Liver Injury. *World J. Gastroenterol.* 19 (47), 9069-9076. doi:10.3748/wjg.v19.i47.9069
- Tan, K. P., Yang, M., and Ito, S. (2007). Activation of Nuclear Factor (Erythroid-2 like) Factor 2 by Toxic Bile Acids Provokes Adaptive Defense Responses to Enhance Cell Survival at the Emergence of Oxidative Stress. *Mol. Pharmacol.* 72 (5), 1380-1390. doi:10.1124/mol.107.039370
- Tan, Y., Li, J., Liu, X., Ko, J., He, X., Lu, C., et al. (2013). Deciphering the Differential Toxic Responses of Radix Aconiti Lateralis Praeparata in Healthy and Hydrocortisone-Pretreated Rats Based on Serum Metabolic Profiles. *J. Proteome Res.* 12 (5), 513-524. doi:10.1021/pr300965d
- Teo, D. C., Ng, P. S., Tan, S. H., Lim, A. T., Toh, D. S., Chan, S. Y., et al. (2016). Drug-induced Liver Injury Associated with Complementary and Alternative Medicine: A Review of Adverse Event Reports in an Asian Community from 2009 to 2014. *BMC Complement. Altern. Med.* 16, 192. doi:10.1186/s12906-016-1168-z
- Thapa, D., Zhang, M., Manning, J. R., Guimarães, D. A., Stoner, M. W., O'Doherty, R. M., et al. (2017). Acetylation of Mitochondrial Proteins by GCN5L1 Promotes Enhanced Fatty Acid Oxidation in the Heart. *Am. J. Physiol. Heart Circ. Physiol.* 313 (2), H265. doi:10.1152/ajpheart.00752.2016
- The Pharmacopoeia Commission of the PRC (2015). *Pharmacopoeia of People's republic of China*. Beijing: Chem. Indust. Press, 263-264.
- Theodoridis, G. A., Gika, H. G., Want, E. J., and Wilson, I. D. (2012). Liquid Chromatography-Mass Spectrometry Based Global Metabolite Profiling: a Review. *Anal. Chim. Acta* 711, 7-16. doi:10.1016/j.aca.2011.09.042
- Tian, J., Zhu, J., Yi, Y., Li, C., Zhang, Y., Zhao, Y., et al. (2017). Dose-related Liver Injury of Geniposide Associated with the Alteration in Bile Acid Synthesis and Transportation. *Sci. Rep.* 7, 8938. doi:10.1038/s41598-017-09131-2
- Voican, C. S., Corruble, E., Naveau, S., and Perlemuter, G. (2013). Antidepressant-Induced Liver Injury: A Review for Clinicians. *Am. J. Psychiatry* 171 (4), 404-415. doi:10.1176/appi.ajp.2013.13050709
- Wang, G. G. A., J. Y., Liu, L. S., Cao, B., Zheng, T., Shi, J., and Li, M. J. (2010). *A Method for Quantitative Evaluation of Pharmacodynamics by Metabonomics*. Patent Application Number: 201010141863.2.
- Wang, Q. P. (2001). Epilogue. *J. Clin. Pathol.* 587 (21), 451-453. doi:10.3969/j.issn.1673-2588.2001.06.01210.1016/b978-075065382-4.50016-9
- Wang, Q. Q., and Song, J. P. (2014). On "Rob 'yin' of Liver by Bupleurum. *Clin. J. Tradit. Chin. Med.* 1, 55-56. doi:10.16448/j.cjctm.2014.01.039
- Xie, T., Zhao, C. X., and Fan, W. L. (2010). Study of normal Value Ranges for Key Indexes of SD Rat in 30 Days Feeding Test. *Chin. J. Health Lab. Technol.* 20 (12), 1927-1931.
- Xing, J., Sun, H. M., Jia, J. P., Qin, X. M., and Li, Z. Y. (2017). Integrative Hepatoprotective Efficacy Comparison of Raw and Vinegar-Baked Radix Bupleuri Using Nuclear Magnetic Resonance-Based Metabolomics. *J. Pharm. Biomed. Anal.* 138 (18), 215-222. doi:10.1016/j.jpba.2017.02.015
- Yamazaki, M., Miyake, M., Sato, H., Masutomi, N., Tsutsui, N., Adam, K. P., et al. (2013). Perturbation of Bile Acid Homeostasis Is an Early Pathogenesis Event of Drug Induced Liver Injury in Rats. *Toxicol. Appl. Pharmacol.* 268 (1), 79-89. doi:10.1016/j.taap.2013.01.018
- Youssef, N. A., Abdelmalek, M. F., Binks, M., Guy, C. D., Omenetti, A., Smith, A. D., et al. (2013). Associations of Depression, Anxiety and Antidepressants with Histological Severity of Nonalcoholic Fatty Liver Disease. *Liver Int.* 33, 1062-1070. doi:10.1111/liv.12165
- Zhang, F., Chen, L., Jin, H., Shao, J., Wu, L., Lu, Y., et al. (2015a). Activation of Fas Death Receptor Pathway and Bid in Hepatocytes Is Involved in Saikosaponin D Induction of Hepatotoxicity. *Environ. Toxicol. Pharmacol.* 41 (2), 8-13. doi:10.1016/j.etap.2015.11.005
- Zhang, F., Fang, Y., Zhou, Y. Z., Tian, J. S., Qin, X. M., and Gao, X. X. (2017). Quantitative Analysis of Eight Polyacetylenes Derived from Bupleuri Radix by Ultra-performance Liquid Chromatography Coupled with Photodiode Array Detector. *Zhongguo Zhong Yao Za Zhi* 42 (9), 1704-1710. doi:10.19540/j.cnki.cjcm.20170308.001
- Zhang, H., Zhang, S., Hu, M., Chen, Y., Wang, W., Zhang, K., et al. (2020). An Integrative Metabolomics and Network Pharmacology Method for Exploring the Effect and Mechanism of Radix Bupleuri and Radix Paeoniae Alba on Anti-depression. *J. Pharm. Biomed. Anal.* 189 (189), 113435. doi:10.1016/j.jpba.2020.113435
- Zhang, Z., Lu, C., Liu, X., Su, J., Dai, W., Yan, S., et al. (2014). Global and Targeted Metabolomics Reveal that Bupleurotoxin, a Toxic Type of Polyacetylene, Induces Cerebral Lesion by Inhibiting GABA Receptor in Mice. *J. Proteome Res.* 13 (2), 925-933. doi:10.1021/pr400968c
- Zhang, Z. Z., Fan, M. L., Hao, X., Qin, X. M., and Li, Z. Y. (2015b). Integrative Drug Efficacy Assessment of Danggui and European Danggui Using NMR-Based Metabolomics. *J. Pharm. Biomed. Anal.* 120 (15), 1-9. doi:10.1016/j.jpba.2015.12.001
- Zhou, Y., Lu, L., Li, Z., Gao, X., Tian, J., Zhang, L., et al. (2011). Antidepressant-like Effects of the Fractions of Xiaoyaosan on Rat Model of Chronic Unpredictable Mild Stress. *J. Ethnopharmacol.* 137 (1), 236-244. doi:10.1016/j.jep.2011.05.016

Conflict of Interest: The authors declare that the research was conducted in the absence of any commercial or financial relationships that could be construed as a potential conflict of interest.

Publisher's Note: All claims expressed in this article are solely those of the authors and do not necessarily represent those of their affiliated organizations, or those of the publisher, the editors and the reviewers. Any product that may be evaluated in this article, or claim that may be made by its manufacturer, is not guaranteed or endorsed by the publisher.

Copyright © 2021 Wang, Gao, Liang, Fang, Jia, Tian, Li and Qin. This is an open-access article distributed under the terms of the Creative Commons Attribution License (CC BY). The use, distribution or reproduction in other forums is permitted, provided the original author(s) and the copyright owner(s) are credited and that the original publication in this journal is cited, in accordance with accepted academic practice. No use, distribution or reproduction is permitted which does not comply with these terms.

GLOSSARY

ALP alkaline phosphatase

ALT alanine aminotransferase

AST aspartate aminotransferase

BRI Behavioral Regulation Index

ceramide/S1P ceramide and sphingosine 1-phosphate

CK-18F cytokeratin-18 fragment

CUMS chronic unpredictable mild stress

DEI dose-effect index

DILI drug-induced liver injury

DTI dose toxicity index

EI effect index

LCI Liver Composite Index

LC-MS the liquid chromatography with mass spectrometry

LysoPEs Lysophosphatidylethanolamine

NE norepinephrine

OPLS orthogonal partial least squares

PBR lower polar fraction of Bupleuri Radix

PCA principal component analysis

PDA Photodiode Array

PE phosphatidylethanolamine

PLS-DA partial least-squares discriminant analysis

QAMS quantitative analysis of multiple components by a single marker

QC Quality control

ROC receiver operating characteristic

TBIL total bilirubin

TCA tricarboxylic acid

TCM traditional Chinese medicine

TD50 median toxicity dose

TNF- α tumor necrosis factor-alpha

TIC total ions chromatograph

UHPLC ultra-performance liquid chromatography system



The Novel Chinese Medicine JY5 Formula Alleviates Hepatic Fibrosis by Inhibiting the Notch Signaling Pathway

Yadong Fu^{1,2,3†}, Zhun Xiao^{1,2,3†}, Xiaoting Tian^{4†}, Wei Liu^{1,3}, Zhou Xu⁴, Tao Yang⁵, Yonghong Hu^{1,3}, Xiaoxi Zhou^{1,3}, Jing Fang^{1,3}, Siqi Gao^{1,2,3}, Dingqi Zhang^{1,3}, Yongping Mu^{1,3}, Hua Zhang^{1,3}, Yiyang Hu^{1,3}, Chenggang Huang^{4*}, Jiamei Chen^{1,3*} and Ping Liu^{1,2,3*}

¹Key Laboratory of Liver and Kidney Diseases (Ministry of Education), Institute of Liver Diseases, Shuguang Hospital Affiliated to Shanghai University of Traditional Chinese Medicine, Shanghai, China, ²Institute of Interdisciplinary Integrative Medicine Research, Shanghai University of Traditional Chinese Medicine, Shanghai, China, ³Shanghai Key Laboratory of Traditional Chinese Clinical Medicine, Shanghai, China, ⁴Shanghai Institute of Materia Medica, Chinese Academy of Sciences, Shanghai, China, ⁵Department of Cardiology, Cardiovascular Research Institute, Shuguang Hospital Affiliated to Shanghai University of Traditional Chinese Medicine, Shanghai, China

OPEN ACCESS

Edited by:

Pulok Kumar Mukherjee,
Institute of Bio-Resources and
Sustainable Development (IBSD), India

Reviewed by:

Lei Gao,
Southern Medical University, China
Jian-Ming Zheng,
Huashan Hospital, China

*Correspondence:

Ping Liu
liuliver@vip.sina.com
Jiamei Chen
cjm0102@126.com
Chenggang Huang
cghuang3208@126.com

[†]These authors have contributed
equally to this work and share first
authorship

Specialty section:

This article was submitted to
Ethnopharmacology,
a section of the journal
Frontiers in Pharmacology

Received: 23 February 2021

Accepted: 06 September 2021

Published: 22 September 2021

Citation:

Fu Y, Xiao Z, Tian X, Liu W, Xu Z,
Yang T, Hu Y, Zhou X, Fang J, Gao S,
Zhang D, Mu Y, Zhang H, Hu Y,
Huang C, Chen J and Liu P (2021) The
Novel Chinese Medicine JY5 Formula
Alleviates Hepatic Fibrosis by Inhibiting
the Notch Signaling Pathway.
Front. Pharmacol. 12:671152.
doi: 10.3389/fphar.2021.671152

Advanced liver fibrosis can lead to cirrhosis, resulting in an accelerated risk of hepatocellular carcinoma and liver failure. Fuzheng Huayu formula (FZHY) is a traditional Chinese medicine formula treated liver fibrosis in China approved by a Chinese State Food and Drug Administration (NO: Z20050546), composed of *Salvia Miltiorrhiza* bge., *Prunus davidiana* (Carr.) Franch., cultured *Cordyceps sinensis* (BerK.) Sacc. Mycelia, *Schisandra chinensis* (Turcz.) Baill., *Pinus massoniana* Lamb., and *Gynostemma pentaphyllum* (Thunb.) Makino. However, the main active substances and mechanism of FZHY are unclear. The aim of this study is to identify a novel anti-fibrotic compound, which consists of the main active ingredients of FZHY, and investigate its mechanism of pharmacological action. The main active ingredients of FZHY were investigated by quantitative analysis of FZHY extracts and FZHY-treated plasma and liver in rats. The anti-fibrotic composition of the main active ingredients was studied through uniform design *in vivo*, and its mechanism was evaluated in carbon tetrachloride (CCl₄)- and bile duct ligation (BDL)-induced liver fibrosis models in rats and mice, and transforming growth factor beta 1-induced LX-2 cell activation model *in vitro*. A novel Chinese medicine, namely JY5 formula, consisting of salvianolic acid B, schisantherin A, and amygdalin, the main active ingredients of FZHY, significantly alleviated hepatic hydroxyproline content and collagen deposition in CCl₄- and BDL-induced fibrotic liver in rats and mice. In addition, JY5 inhibited the activation of hepatic stellate cells (HSCs) by inactivating Notch signaling *in vitro* and *in vivo*. In this study, we found a novel JY5 formula, which exerted anti-hepatic fibrotic effects by inhibiting the Notch signaling pathway, consequently suppressing HSCs activation. These results provide an adequate scientific basis for clinical research and

Abbreviations: FZHY, fuzheng huayu formula; SORA, sorafenib; HSCs, hepatic stellate cells; ECM, extracellular matrix; TCM, traditional Chinese medicine; KCs, kupffer cells; LSECs, liver sinusoidal endothelial cells; CCl₄, carbon tetrachloride; BDL, bile duct of ligation; ALT, alanine aminotransferase; AST, aspartate aminotransferase; ALP, alkaline phosphatase; TBil, total bilirubin; DBil, direct bilirubin; TBA, total bile acids; Hyp, hydroxyproline; IHC, immunohistochemical; H&E, hematoxylin & eosin; SR, sirius red; α -SMA, α -smooth muscle actin; RBP- κ B, recombination signal binding protein- κ B; HCC, hepatocellular carcinoma; NICD, notch intracellular domain.

application of the JY5 formula, which may be a potential novel therapeutic candidate for liver fibrosis.

Keywords: traditional Chinese medicine, JY5 formula, fuzheng huayu, hepatic fibrosis, notch signaling pathway

INTRODUCTION

Liver fibrosis is a common pathological feature of chronic liver diseases including chronic viral hepatitis, metabolic-associated fatty liver disease, and cholestatic liver diseases. It is a consequence of an abnormal wound healing response, characterized by excessive deposition of extracellular matrix (ECM). If the injury persists, liver fibrosis can progress to cirrhosis and hepatocellular carcinoma, ultimately leading to liver failure (Friedman, 2015). The effective treatment for liver fibrosis is to address the root cause and prevent progression. Some clinical studies (Lee et al., 2015) have shown that liver fibrosis, even early cirrhosis, is reversible, providing reliable evidence for conducting clinical studies on anti-hepatic fibrosis drugs. With several types of animal models of liver fibrosis becoming increasingly mature, there has been a greater understanding of the pathogenesis of liver fibrosis in the last few decades (Cordero-Espinoza and Huch, 2018). A number of anti-hepatic fibrosis drug studies have been conducted in recent years, some of which have been researched in clinical trials (Lemoinne and Friedman, 2019). However, to date, there are no clinically approved by FDA or effective medical therapies aimed specifically towards hepatic fibrosis.

Traditional Chinese medicine (TCM) has marked clinical effects on the treatment of liver fibrosis. Among these, Fuzheng Huayu (FZHY) formula which composed of *Salvia miltiorrhiza* Bunge (Danshen), *Prunus davidiana* (Carrišre) Franch (Taoren), cultured *Cordyceps sinensis* (BerK.) Sacc. Mycelia (Chongcao), *Schisandra chinensis* (Turcz.) Baill (Wuweizi), *Pinus massoniana* Lamb. (Songhuafen), and *Gynostemma pentaphyllum* (Thunb.) Makino (Jiaogulan), is a complex preparation to treat liver fibrosis in China approved by a Chinese State Food and Drug Administration (NO: Z20050546). The anti-fibrotic effect has been confirmed in a phase II clinical trial of hepatic fibrosis post-hepatitis C in the United States (Zhang and Schuppan, 2014). However, there are some challenges with TCM, such as its multi-component, multi-target, ill-defined active ingredients and mechanisms, which limit their clinical application. In recent years, our team has conducted a large amount of research to elucidate the mechanisms underlying the role of FZHY in the prevention and treatment of chronic liver diseases, including inhibiting the inflammatory response, protecting hepatocytes (to relieve hepatocyte damage and inhibit hepatocyte apoptosis), inhibiting hepatic stellate cell (HSC) activation, reducing collagen deposition, inhibiting Kupffer cell (KC) activation, inhibiting liver sinusoidal endothelial cell (LSEC) capillarization and angiogenesis, and promoting liver regeneration (Liu et al., 2009; Chen et al., 2019). We further studied the anti-fibrosis effects of different compounds of FZHY. Phenolic acids in *Salvia miltiorrhiza* play a prominent role in inhibiting the inflammatory

response, protecting hepatocytes, and inhibiting HSC activation (Wang et al., 2012; Tao et al., 2013; Kan et al., 2014; Yan et al., 2017; Wang et al., 2019). Amygdalin, as one of the major active compounds of *Peach kernel*, has the main role in inhibiting the inflammatory response, reducing collagen deposition, and inhibiting HSC activation (Luo et al., 2016; Luo et al., 2018). The lignan compounds from *Schisandrae* play an important role in protecting hepatocytes and inhibiting HSC activation (Kang et al., 2019; He et al., 2020). These findings suggest that the related bioactive ingredients in FZHY may have anti-fibrotic effects.

Notch signaling is a highly conservative pathway during evolution. Notch receptors interact with ligands on the surface of adjacent cells, then cleave inside the cell membrane, translocate into the nucleus, and regulate the transcription of multiple target genes. Previous studies (Adams and Jafar-Nejad, 2019) have shown that as an important intercellular or intracellular signaling pathway, Notch plays an important role in liver development and pathophysiology. Notch has a great impact on the occurrence and development of hepatic fibrosis and can interact with transforming growth factor beta (TGF- β), Hedgehog, and Hippo signaling pathways to mediate cell-cell interactions. Activation of HSCs is a critical cellular event in liver fibrosis. HSCs transdifferentiate into myofibroblasts, accompanied by activation of Notch signaling pathway (Zhang et al., 2015). After Notch activity levels are suppressed, this process can be reversed. In addition, with the progression of liver fibrosis induced by carbon tetrachloride (CCl₄) and bile duct ligation (BDL), the Notch signaling pathway is significantly activated. Efficient inhibition of the Notch pathway can significantly mitigate liver fibrosis and reduce hepatocyte apoptosis (Chen et al., 2012). Thus, targeting the Notch signaling pathway can regulate the activation of HSCs, thereby suppressing the occurrence and progression of hepatic fibrosis.

In this study, we found that salvianolic acid B, schisantherin A, and amygdalin were the main active ingredients of FZHY formula by quantitative analysis of FZHY extracts and FZHY-treated plasma and liver in rats. A novel TCM formula, namely JY5, was obtained through uniform design. The anti-hepatic fibrosis efficacy of JY5 was comparable to that of FZHY in CCl₄-induced hepatic fibrosis in rats (**Supplementary Figures S3 and S4**). Further studies demonstrated that JY5 alleviated liver fibrosis by inhibiting the activation of HSCs via inhibition of the Notch signaling pathway.

MATERIALS AND METHODS

Animals

Adult Wistar or Sprague-Dawley male rats (160–180 g, specific pathogen-free [SPF] grade) were purchased from Shanghai Xipuer-Bikai Experimental Animal Co., Ltd (Shanghai, China)

and fed in the Laboratory Animal Center at School of Pharmacy, Fudan University (Shanghai, China). Adult male C57/BL6 mice (aged 6–8 weeks, 18–20 g, SPF grade) were purchased from Shanghai Southern Model Biotechnology Co., Ltd (Shanghai, China) and maintained in the Shanghai Research Center of the Southern Model Organisms (Shanghai, China). Rats and mice were housed under constant conditions (ambient temperature $25 \pm 2^\circ\text{C}$, relative humidity 40–60%, and 12/12 h light-dark cycle) with free access to standard diet and water. All rat experiments were reviewed and approved by the Experimental Animal Ethics Committee of School of Pharmacy, Fudan University (Approval No. 2018–07-SZYD-LP-01). All mice experiments were approved by the Institutional Animal Care and Use Committee (IACUC) at Shanghai Research Center of the Southern Model Organisms (Approval No. 2019–0031).

Drugs

Reference standards: salvianolic acid B, salvianic acid, salvanic acid A, rosmarinic acid, gypenoside XLIX, ginsenoside Rb3, amygdalin, schisantherin A, schisandrol A, schisandrol B, deoxyschizandrin, schisandrin B, tanshinone, cryptotanshinone, adenosine, and cordycepin were purchased from Shanghai Standard Technology Co., Ltd (Shanghai, China). The purity of all standards was more than 98%. FZHY decoction: mixture of *Salvia miltiorrhiza* Bunge at 533 g, *Prunus davidiana* (CarriŠre) Franch. at 133 g, and *Gynostemma pentaphyllum* (Thunb.) Makino at 400 g, was heated to boiling with water for 2 h for the first time and for 1.5 h for the second time. The combined decoction was filtered, and concentrated to a relative density at 1.20 g/ml ($50\text{--}55^\circ\text{C}$). After cooling down, the decoction was precipitated by adding 70% alcohol, and then filtrate 1 was generated after filtration and concentration. A combination of cultured *Cordyceps sinensis* (BerK.) Sacc. Mycelia at 267 g and *Schisandra chinensis* (Turcz.) Baill. at 133 g was heated with 70% alcohol for 2 h for the first time and 1.5 h for the second time, and the combined decoction was filtered and concentrated as filtrate 2. *Pinus massoniana* Lamb. at 133 g was infiltrated with 50% alcohol for 4 h for the first time and 2 h for the second time, and the combined decoction was filtered and concentrated as filtrate 3. Filtrates 1–3 were combined and concentrated to 800 ml at 2 g raw drug/mL. The voucher specimens, *Salvia miltiorrhiza* Bunge (No. 1600001), *Prunus davidiana* (CarriŠre) Franch. (No. 1600002), *Gynostemma pentaphyllum* (Thunb.) Makino (No. 1600003), cultured *Cordyceps sinensis* (BerK.) Sacc. Mycelia (No. 1600004), *Schisandra chinensis* (Turcz.) Baill. (No. 1600005), and *Pinus massoniana* Lamb. (No. 1600006) were deposited in the Shanghai Institute of Materia Medica.

Pharmacokinetic Study of Fuzheng Huayu Decoction in Rats

This study was conducted according to the guidelines of the IACUC of the Shanghai Institute of Materia Medica, Chinese Academy of Sciences (Shanghai, China). The experimental protocol is shown in **Supplementary Material: Materials and Methods 1.1**.

Instrumentation

There were 16 compounds determined in various biosamples by the UltiMate 3000 ultra-high-performance liquid chromatograph linked to the active quadrupole electrostatic field orbital trap high-resolution mass spectrometer, connected to an electrospray ionization source (Thermo Fisher Scientific, Waltham, MA, United States). The operating parameters were set as shown in **Supplementary Material: Materials and Methods 1.2**.

Experimental Liver Fibrosis Models

CCl_4 -induced liver fibrosis rat model, BDL-induced liver fibrosis rat model, and CCl_4 -induced liver fibrosis mouse model were used in this study. The experimental protocols are shown in **Supplementary Material: Materials and Methods 1.3**.

Cell Culture

The immortalized human hepatic stellate cell line (LX-2) was provided by the Institute of Liver diseases, Shanghai University of Traditional Chinese Medicine (Shanghai, China). LX-2 cells (1.25×10^5) were seeded in 6 cm dishes or 6-well plates and maintained in Dulbecco's Modified Eagle Medium containing 1% penicillin/streptomycin and 10% fetal bovine serum at 37°C and 5% CO_2 . After post-inoculation for 24 h, all LX-2 cells except the control group were treated with TGF- β 1 (5 ng/ml), and simultaneously treated with different concentrations of JY5 as follows: low-dose group (6.587 $\mu\text{g/ml}$) (salvianolic acid B 8 μM , amygdalin 0.25 μM , schisantherin A 1 μM), medium-dose group (13.174 $\mu\text{g/ml}$) (salvianolic acid B 16 μM , amygdalin 0.5 μM , schisantherin A 2 μM), and high-dose group (26.348 $\mu\text{g/ml}$) (salvianolic acid B 32 μM , amygdalin 1 μM , schisantherin A 4 μM). SB431542 (10 μM), a TGF- β receptor inhibitor, was used as a positive control. After incubation for 24 h, LX-2 cells were lysed and collected for Western blotting and quantitative PCR (qPCR) analysis.

Serum Biochemistry Analysis

Serum alanine aminotransferase (ALT), aspartate aminotransferase (AST), alkaline phosphatase (ALP), total bilirubin (TBil), direct bilirubin (DBil), and total bile acid (TBA) levels were measured using the TBA-40FR automatic biochemistry analyzer (Toshiba Medical, Tokyo, Japan) at the Science and Technology Experiment Center, Shanghai University of TCM.

Histopathological and Immunohistochemical Analysis

Liver injury and fibrosis were assessed with hematoxylin and eosin (H&E) and Sirius Red (SR) staining using 4 μm thick paraffin-embedded liver sections. Immunohistochemistry (IHC) staining of collagen type I (Col-I), Col-IV, α -smooth muscle actin (α -SMA), and desmin was performed. The detailed protocols are shown in **Supplementary Material: Materials and Methods 1.4**.

Hepatic Hydroxyproline Content Assay

According to the kit instructions, hydroxyproline (Hyp) content in liver tissue was detected using the Hydroxyproline Testing Kit-

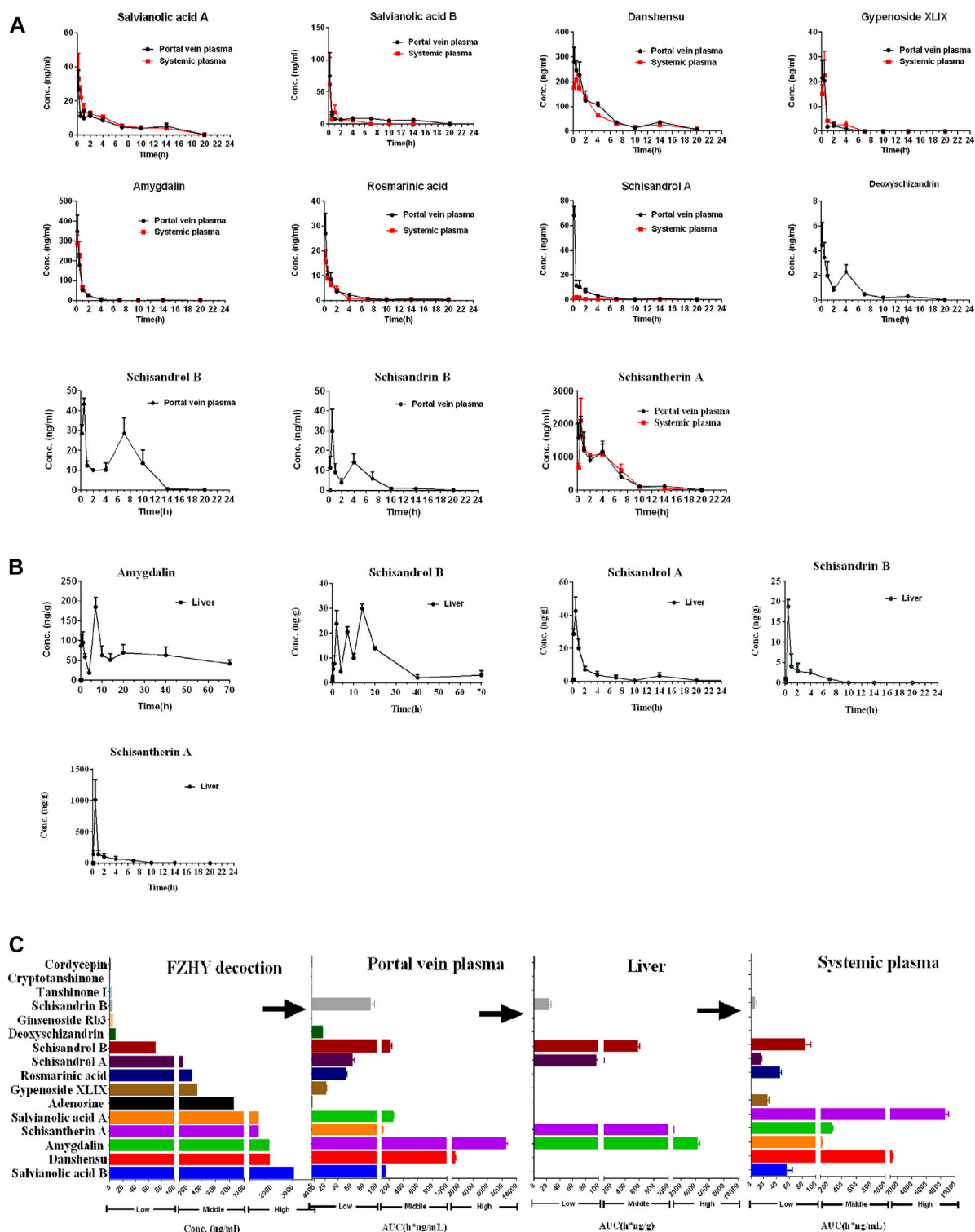


FIGURE 1 | Quantitative analysis of FZHY decoction and FZHY biological samples. Concentration–time curves of compounds in the plasma (A) and liver (B) after oral administration of FZHY decoction (20 g/kg) in rats ($n = 5$). (C) Summary of the contents and AUC of compounds in the FZHY decoction or FZHY biological samples.

TABLE 1 | The PK parameters of 11 compounds in the portal vein plasma, systemic plasma and liver, following oral administration of FZHY decoction in rats.

Compounds	Portal vein plasma			Systemic plasma		
	T _{max} (h)	C _{max} (ng/ml)	AUC(h*ng/ml)	T _{max} (h)	C _{max} (ng/ml)	AUC(h*ng/ml)
Salvianolic acid A	0.167	26.7 ± 11.2	108.7 ± 9.1	0.167	33.1 ± 14.9	122.3 ± 5.7
Salvianolic acid B	0.167	74.8 ± 36.4	144.4 ± 7.3	0.167	61.5 ± 42.1	55.9 ± 18.6
Danshensu	0.167	279.8 ± 58.8	1515.9 ± 64.6	0.5	206.6 ± 41.6	1362 ± 95
Gypenoside XLIX	0.5	21.5 ± 7.3	21.3 ± 3.5	0.5	22.4 ± 9.8	26.4 ± 3.8
Amygdain	0.167	347.7 ± 82.5	254.7 ± 23.2	0.167	286.2 ± 44.2	262.8 ± 23.9
Rosmarinic acid	0.167	27.1 ± 8.1	51.9 ± 4	0.167	15.4 ± 4.9	45.5 ± 4.7
Schisandrol A	0.167	68.2 ± 7.2	62 ± 8.6			
Schisandrol B	0.5	43.4 ± 3	215.1 ± 49.3	0.5	35.9 ± 0.6	84.3 ± 19.8
Deoxyschizandrin	0.167	4.4 ± 1.8	15.6 ± 1.1			
Schisandrin B	0.5	29.9 ± 11	89.4 ± 15.7			
Schisantherin A	0.5	1657.7 ± 584.3	8542.1 ± 566.2	0.5	2094.4 ± 681	8672.6 ± 1093.6

Compounds	Liver		
	T _{max} (h)	C _{max} (ng/g)	AUC(h*ng/g)
Amygdain	7	185 ± 24.1	4423.2 ± 599.8
Schisandrol A	0.5	42.5 ± 8.4	96.4 ± 13.7
Schisandrol B	14	29.9 ± 1.8	578.7 ± 50.3
Schisandrin B	0.5	18.7 ± 1.7	24.1 ± 4.6
Schisantherin A	0.5	1011.1 ± 322.6	1070.3 ± 103.4

Alkaline Hydrolysis Method (Cat No. A030-2; Nanjing Jiancheng Bioengineering Institute, Nanjing, China).

Western Blot Analysis

Total protein in liver tissues or cells was extracted using RIPA lysis buffer containing proteinase and phosphatase inhibitor (Cat No. P0013B; Biyuntian Biotechnology Co., Ltd., Shanghai, China). Total protein concentration was determined using a BCA protein assay kit (Lot TD265229; Thermo Fisher Scientific). Proteins (30–50 µg) were denatured at 100°C for 5 min, and then separated by 8% or 10% sodium dodecyl sulfate–polyacrylamide gel electrophoresis. The proteins were electrotransferred onto polyvinylidene fluoride (PVDF) membranes. The membranes were blocked in 5% BSA at room temperature for 60 min, and then incubated with primary antibody (**Supplementary Table S1**) overnight at 4°C. The following day, the membranes were incubated in the dark for 1 h at room temperature with fluorescence-labeled secondary antibody (**Supplementary Table S1**). The PVDF membranes were scanned using the Odyssey 2.1 software of Odyssey infrared scanner (LI-COR Biosciences, Lincoln, NE, United States). After scanning, target protein bands were cut out according to the molecular weight of target protein without any edit. The greyscale values relative to GAPDH of the target proteins were analyzed using ImageJ software.

Quantitative PCR Analysis

Total RNA in liver tissues or cells was extracted and reverse transcribed using a nucleic acid purification kit (Code: NPK-201F, Lot. 742,100; Toyobo Co., Ltd., Osaka, Japan) and the ReverTra Ace qPCR RT Kit (Code: FSQ-301, Lot. 616,800; Toyobo Co., Ltd., Osaka, Japan). The qPCR primer sequence information is listed in **Supplementary Table S2**. The PCR cycling program was 95°C for 60 s, 40 cycles of 95°C for 15 s, and 60°C for 60 s, followed by melting curve analysis. The GAPDH gene was used as the internal reference

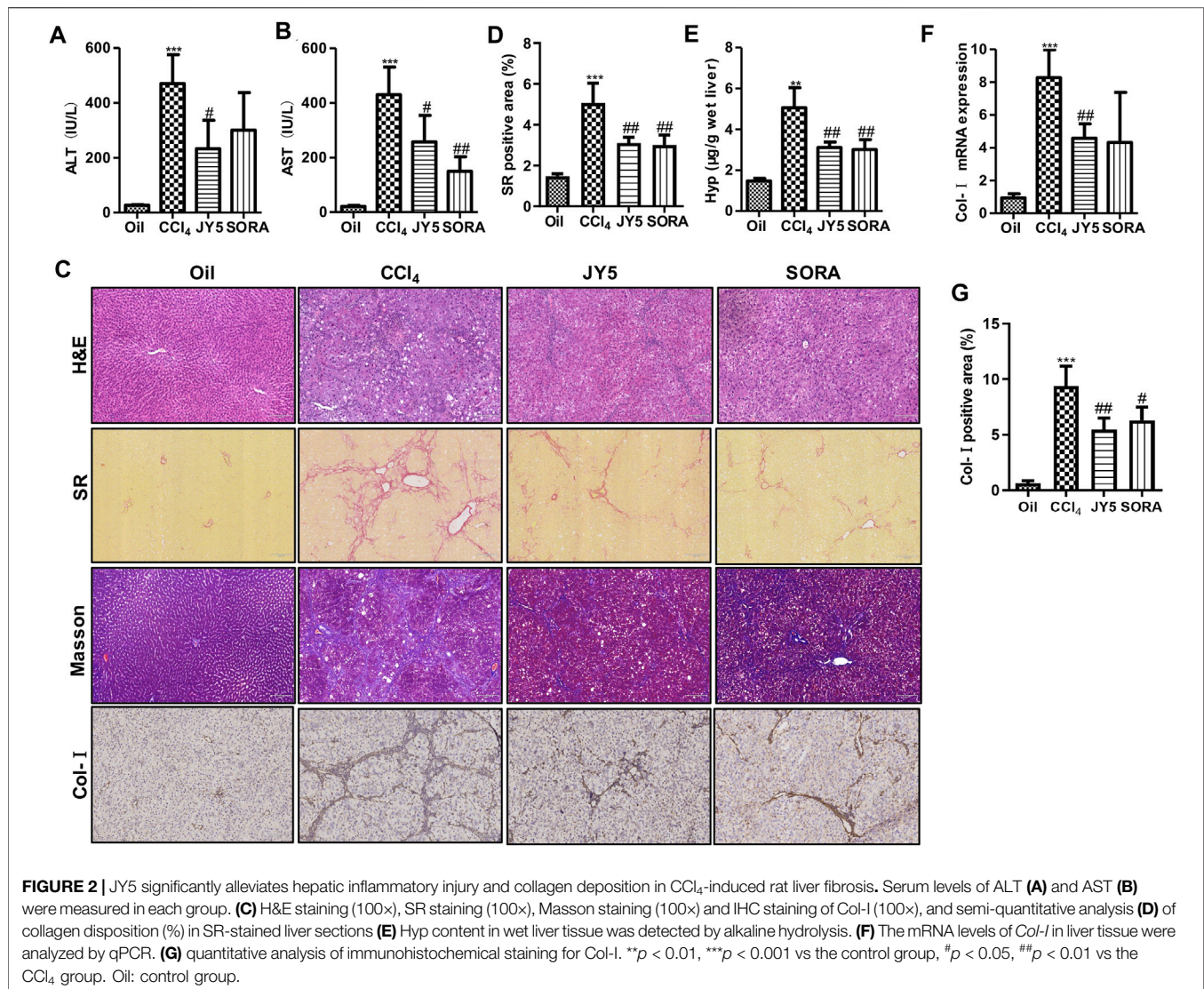
for normalization of the target genes. The relative mRNA expression of each group was calculated using the $2^{-\Delta\Delta Ct}$ method.

Dual-Luciferase Reporter Assay

The transcriptional activity of Notch was measured using RBP-κβ luciferase reporter plasmid constructed by Shanghai Jikai Gene Chemical Technology Co. Ltd. following the supplier's instructions. The RBP-κB-Luc vector were engineered in GV238 backbone vector. The target gene sequence of RBP-κB (NM_005,349-promoter-1) was amplified by PCR using the primers as follows: forward: 5'-CTAGCCTAGGCGACAGAGCAAG-3'; reverse: 5'-CTTTATGTTTTTGGCGTCTTCCA-3'. The amplicons were inserted into the cloning sites of KpnI and XhoI located upstream of the firefly luciferase gene, and then a dual-luciferase reporter assay was performed using Dual-Lumi™ luciferase reporter gene assay kit (RG088S, Beyotime Biotechnology, China). The transiently co-transfected LX-2 cells with the corresponding transfection mix containing 200 ng RBP-κB-Luc plasmid (firefly) and 20 ng pRL-TK control vector (renilla) using Lip8000™ (C0533, Beyotime Biotechnology, China) were treated with TGF-β1 (5 ng/ml), and simultaneously treated with salvianolic acid B (32 µM), amygdalin (1 µM), schisantherin A (4 µM) or JY5 (26.348 µg/ml) for 24 h, respectively. RBP-κB luciferase activity was detected by Dual-Lumi™ luciferase reporter gene assay kit following the manufacturer's instructions. With renilla luciferase as the internal control in each transfection, the relative luciferase activity was calculated as the ratio of firefly-to-renilla luciferase activity.

Statistical Analysis

All data were analyzed using the SPSS 21.0 software package. All data are expressed as the mean ± standard deviation (SD).



Comparisons between multiple groups were analyzed by the one-way analysis of variance, followed by the least significant difference test. *p* < 0.05 was considered statistically significant. In addition, the pharmacokinetic (PK) parameters were calculated by noncompartmental analysis in WinNonlin software with a sparse sampling algorithm (Pharsight 6.2, Cary, NC, United States).

RESULT

Quantitative Analysis of Fuzheng Huayu Decoction and Fuzheng Huayu Biological Samples

The chemical structure and concentration of 16 compounds in the FZHY decoction (2 g/ml) are shown in **Supplementary**

Figures S1, S2 and Supplementary Table S3 respectively. The concentration–time curves of compounds in the plasma and liver after oral administration of FZHY decoction (20 g/kg) in rats are shown in **Figures 1A,B**, and the corresponding PK parameters are shown in **Table 1**. The summary of the contents and area under the curve (AUC) of compounds in the FZHY decoction or FZHY biological samples are shown in **Figure 1C**. There were 16 compounds determined in the FZHY decoction, including six derived from *Salvia miltiorrhiza*, five derived from *Schisandra chinensis*, two derived from *Gynostemma pentaphyllum*, two from *Cordyceps mycelium*, and one compound from *Gynostemma pentaphyllum*. Among the compounds, salvianolic acid B had the highest content in the FZHY decoction, followed by danshensu, amygdalin, schisantherin A, and salvianolic acid A (concentration ≥ 1000 μg/ml). Adenosine, gypenoside XLIX, rosmarinic acid, and schisandrol A were in the middle

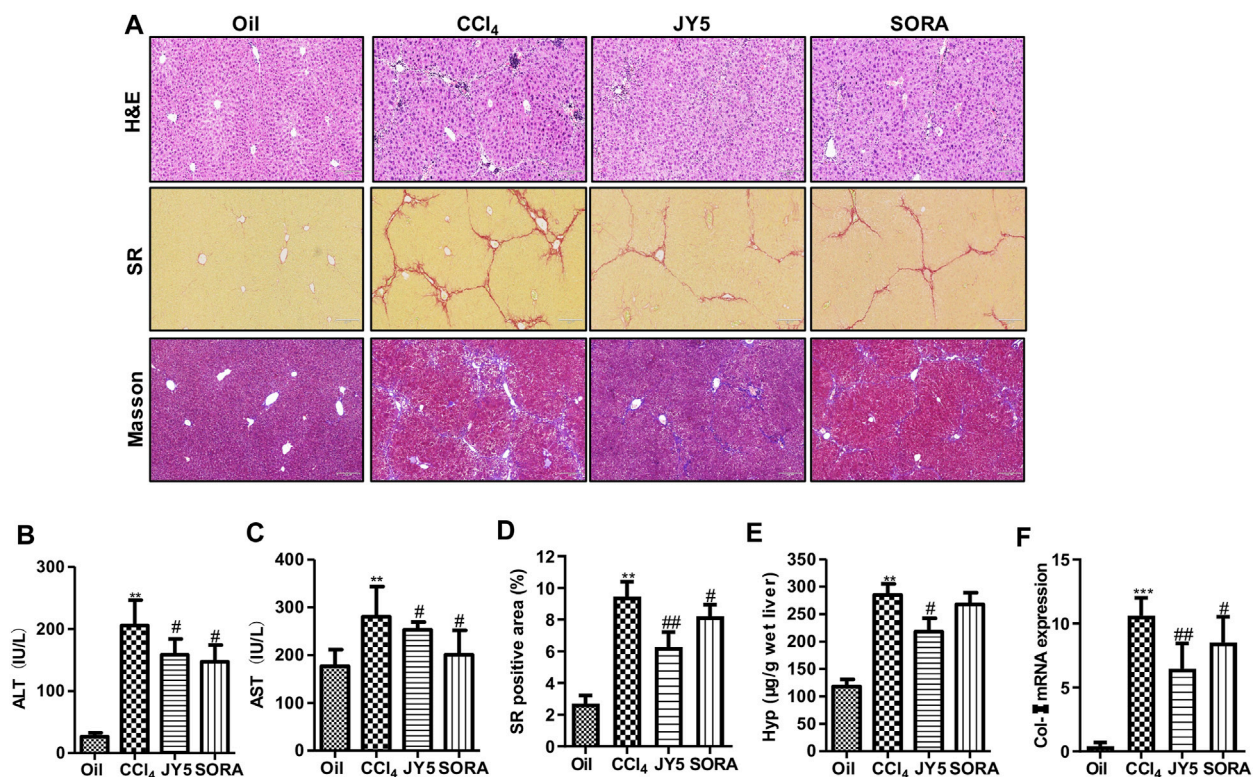


FIGURE 3 | JY5 significantly alleviates hepatic inflammatory injury and collagen deposition in CCl₄-induced mouse liver fibrosis. **(A)** H&E staining (100×), SR staining (100×) and Masson staining (100×) in liver tissue. Serum levels of ALT **(B)** and AST **(C)** were measured in each group. **(D)** Semi-quantitative analysis of collagen disposition (%) in SR-stained liver sections. **(E)** Hyp content in wet liver tissue was detected by alkaline hydrolysis. **(F)** The mRNA expression of *Col-1* in mice liver tissue was analyzed by qPCR. ** $p < 0.01$, *** $p < 0.001$ vs the control group, # $p < 0.05$, ## $p < 0.01$ vs the CCl₄ group. Oil: control group.

content group (100 μg/ml < concentration < 1000 μg/ml), and the concentrations of the remaining compounds, including schisandrol B, deoxyschizandrin, ginsenoside Rb3, schisandrin B, tanshinone I, cryptotanshinone, and cordycepin, were very low (concentration ≤ 100 μg/ml). The portal vein blood is the first site after gut absorption but before hepatic disposition, which is responsible for transferring the substances to the liver post-dose. Following oral administration of FZHY in rats, there were 11 compounds accurately detected in the portal vein plasma, of which tanshinone I, cryptotanshinone, cordycepin, ginsenoside Rb3, and adenosine were undetected, probably due to the low content in the formula or poor physicochemical property. T_{max} s of all compounds were within 0.5 h in portal vein plasma, indicating fast absorption. Schisantherin A exhibited maximum exposure in the portal vein plasma, followed by danshensu ($AUC \geq 1000$ h*ng/mL). Four compounds, including amygdalin, schisandrol B, salvianolic acid B, and salvianolic acid A, belonged to the middle exposure group (100 h*ng/mL < concentration < 1000 h*ng/mL). The remaining five compounds were in the low exposure group ($AUC \leq 100$ h*ng/mL). After hepatic disposition, the compounds were transported to the systemic plasma, which is responsible for delivering substances

to the other organs, except the liver. Compared to those in the portal vein plasma, there were eight compounds determined in the systemic plasma, of which schisandrol A, schisandrin B, and deoxyschizandrin were undetected. Similar to those in the portal vein plasma, the absorption of those compounds was quick; schisantherin A and danshensu were in the high exposure group ($AUC \geq 1000$ h*ng/mL), and schisantherin A had the highest exposure in the systemic plasma. The middle exposure group (100 h*ng/mL < $AUC < 1000$ h*ng/mL) included amygdalin and salvianolic acid A; the remaining compounds belonged to the low exposure group ($AUC \leq 100$ h*ng/mL). Following oral administration of FZHY decoction, only five compounds were detected in the liver. T_{max} s of schisandrol A, schisandrin B, and schisantherin A was 0.5 h, similar to that in the plasma. By contrast, T_{max} s of schisandrol B and amygdalin was 14 and 7 h, respectively, consistent with their multi-peak phenomenon in the concentration-time curves. By contrast to levels in the plasma, amygdalin had the highest hepatic exposure, followed by schisantherin A, whose exposure was >1000 h*ng/g. Schisantherin A was in the middle exposure group (100 h*ng/g < $AUC < 1000$ h*ng/g), and the hepatic exposure of schisandrol A and schisandrin B was very low ($AUC \leq 100$ h*ng/g). Finally, salvianolic acid B, schisantherin

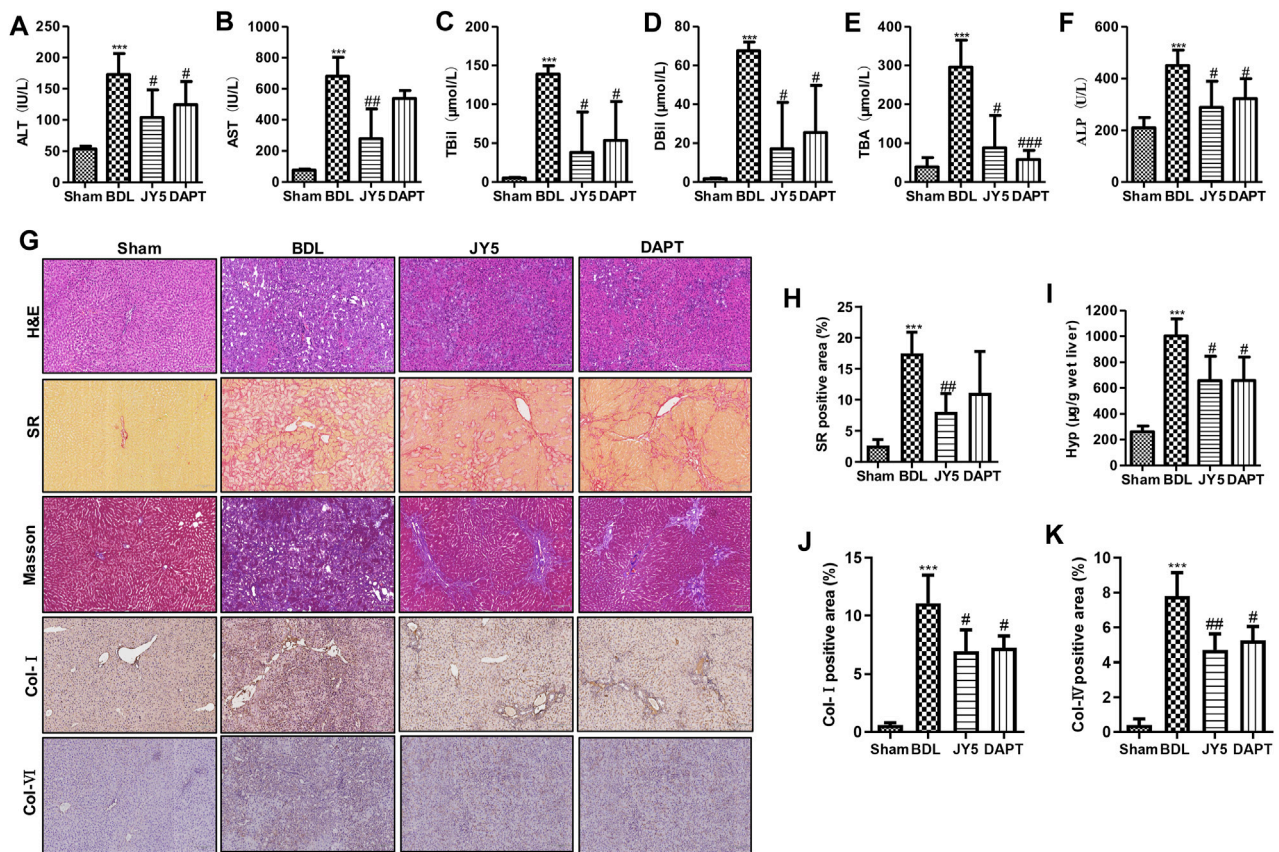


FIGURE 4 | JY5 significantly alleviates hepatic inflammatory injury and collagen deposition in BDL-induced rat liver fibrosis. The levels of serum ALT (A), AST (B), TBil (C), DBil (D), TBA (E), and ALP (F) were measured in each group. (G) H&E staining (100 \times), SR staining (100 \times), Masson staining (100 \times) and IHC for Col-I and Col-IV (100 \times) staining, and semi-quantitative analysis (H) of collagen disposition (%) in SR-stained liver sections. (I) Hyp content in wet liver tissue was detected by alkaline hydrolysis. Quantitative analysis of immunohistochemical staining for Col-I (J) and Col-IV (K). *** p < 0.001 vs the sham group, # p < 0.05, ## p < 0.01 vs the BDL group.

A, and amygdalin, which had the highest content in the FZHY decoction, plasma, and liver, respectively, were selected to evaluate the anti-hepatic fibrosis effects *in vivo*.

JY5 Significantly Alleviates Hepatic Injury and Collagen Deposition in CCl₄-Induced Rat and Mouse Liver Fibrosis

Compared with the control group (Oil), the levels of serum ALT and AST were significantly increased in the CCl₄ group. After treatment with JY5 (salvianolic acid: B 16 mg/kg, amygdalin: 0.5 mg/kg, schisantherin A: 2 mg/kg) or FZHY (2 g/kg), the levels of ALT and AST were significantly decreased (Figures 2A,B and Supplementary Figures S3D,E). The serum AST level was decreased in the sorafenib group (SORA, 5 mg/kg) compared with the CCl₄ group (Figure 2B). H&E staining showed that the hepatic lobular structure was severely collapsed with formation of more complete pseudo-lobules in the CCl₄ group. As the fibrous tissue became denser, the hepatocytes were disordered and ballooning degeneration

occurred. There was a large number of inflammatory cells infiltration surrounding the hepatic sinusoid, central vein, and portal tract. The above lesions were obviously attenuated with less pseudo-lobules and inflammatory cells infiltration, after treatment with JY5 or FZHY or SORA (Supplementary Figure S3A and Figure 2C, upper panel). SR and Masson staining showed that compared to the control group, collagen deposition was obviously increased in the CCl₄ group. The fibrotic septum became significantly widened and distributed from the portal tract to the periphery in a reticular manner, forming pseudo-lobules with varying sizes. By contrast, collagen deposition was obviously decreased, the fibrotic septum became narrower, and pseudo-lobules structures were observed less in the JY5-, FZHY-, or SORA-treated groups (Supplementary Figure S3A, lower panel and Figure 2C, middle panel). Both the hepatic Hyp content and collagen deposition were significantly increased in the CCl₄ group compared to the control group. The above indicators were significantly reduced after intervention with JY5, FZHY, or SORA (Supplementary Figures S3B,C and Figures 2D,E). These

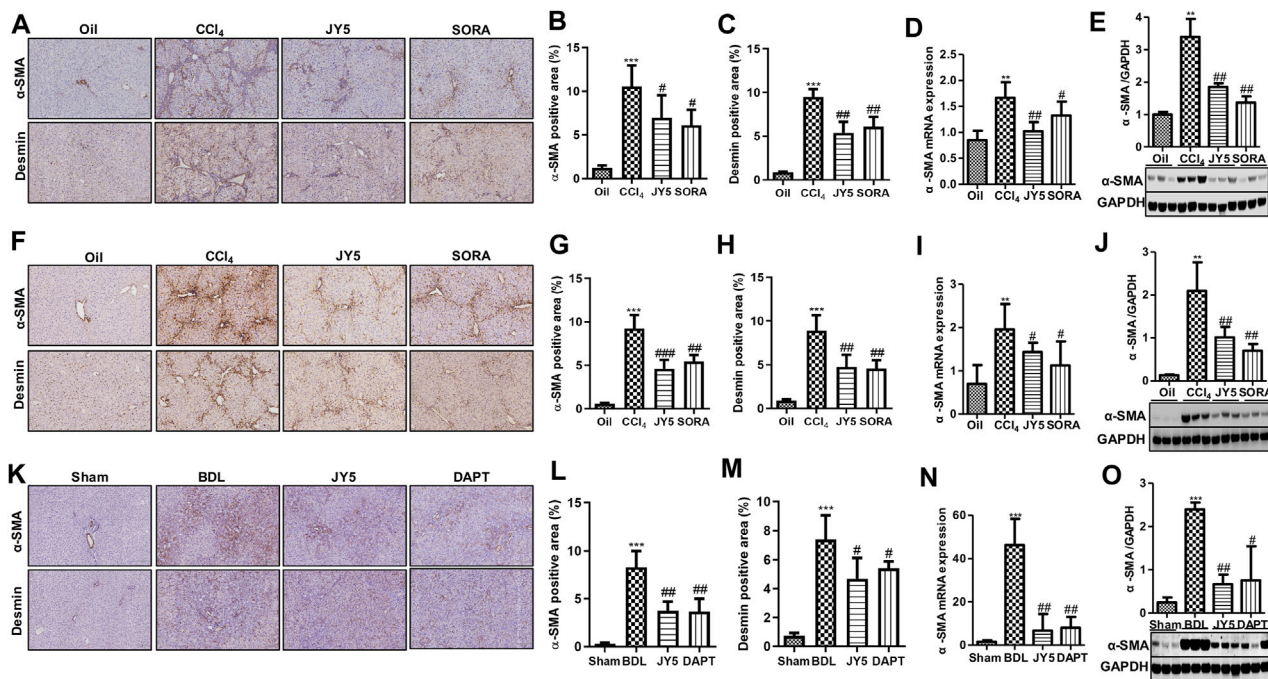


FIGURE 5 | JY5 inhibits the activation of HSCs *in vivo*. **(A)** In the CCl₄-induced rat liver fibrosis experiment, representative images of IHC (100×) staining for α -SMA and desmin. Quantitative analysis of immunohistochemical staining for α -SMA **(B)** and desmin. **(C)** The protein and mRNA levels of α -SMA were, respectively, analyzed by qPCR **(D)** and Western blotting **(E)**. **(F)** In the CCl₄-induced liver fibrosis mice experiment, representative images of IHC (100×) staining for α -SMA and desmin in liver tissue from mice treated with the various treatments. Quantitative analysis of immunohistochemical staining for α -SMA **(G)** and desmin. **(H)** The protein and mRNA levels of α -SMA in mice liver tissue were, respectively, analyzed by qPCR **(I)** and Western blotting **(J)**. **(K)** In the BDL-induced rat liver fibrosis experiment, representative images of IHC (100×) staining for α -SMA and desmin in liver tissue. Quantitative analysis of immunohistochemical staining for α -SMA **(L)** and desmin **(M)**. The protein and mRNA expression of α -SMA was, respectively, analyzed by qPCR **(N)** and Western blotting **(O)**. ** p < 0.01, *** p < 0.001 vs the control group or sham group, # p < 0.05, ## p < 0.01 vs the CCl₄ group or BDL group. Oil: control group.

results demonstrated that JY5 formula had significant anti-hepatic fibrosis effects. IHC staining showed that compared with the control group, Col-I expression was visible in the fibrotic septum in the CCl₄ group. By contrast, JY5 and SORA significantly reduced Col-I expression in the liver tissue (**Figure 2C**, lower panel and **Figure 2G**). In addition, qPCR results showed that *Col-I* mRNA expression was significantly more elevated in the CCl₄ group than in the control group. However, compared to the CCl₄ group, *Col-I* mRNA expression was significantly reduced in the JY5-treated group (**Figure 2F**). Consistent with the CCl₄-induced rat liver fibrosis model, JY5 (salvianolic acid B, 22.4 mg/kg amygdalin, 0.7 mg/kg schisantherin A, 2.8 mg/kg) significantly alleviated hepatic injury and collagen deposition in CCl₄-induced liver fibrosis in mice (**Figure 3**).

JY5 Significantly Alleviates Hepatic Injury and Collagen Deposition in Bile Duct Ligation-Induced Rat Liver Fibrosis

Compared with the sham group, the levels of ALT, AST, TBil, DBil, TBA, and ALP were significantly increased in the BDL group. After JY5 (salvianolic acid B, 16 mg/kg amygdalin,

0.5 mg/kg schisantherin A, 2 mg/kg) or DAPT (30 mg/kg) treatment, the levels of ALT, AST, TBil, DBil, TBA, and ALP were significantly decreased (**Figures 4A–F**). Consistent with CCl₄-induced liver fibrosis, JY5 reduced hepatic Hyp content and collagen deposition, and downregulated the expression of Col-I and Col-IV in BDL-induced rat liver fibrosis (**Figures 4G–K**). These results suggest that JY5 significantly alleviates hepatic injury and collagen deposition in BDL-induced liver fibrosis.

JY5 Significantly Represses the Activation of Hepatic Stellate Cells *In Vivo*

In both the CCl₄-induced rat and mouse liver fibrosis experiments, IHC staining showed that high α -SMA and desmin was expressed in the fibrotic septum in the CCl₄ group. By contrast, both α -SMA⁽⁺⁾ cells and desmin⁽⁺⁾ cells were decreased in the JY5- and SORA-treated group (**Figures 5A–C, F–H**). Western blot analysis and qPCR showed that α -SMA expression was significantly elevated compared to the control group. However, compared to the CCl₄ group, both α -SMA mRNA and protein expression was significantly reduced in the JY5- and SORA-treated groups (**Figures**

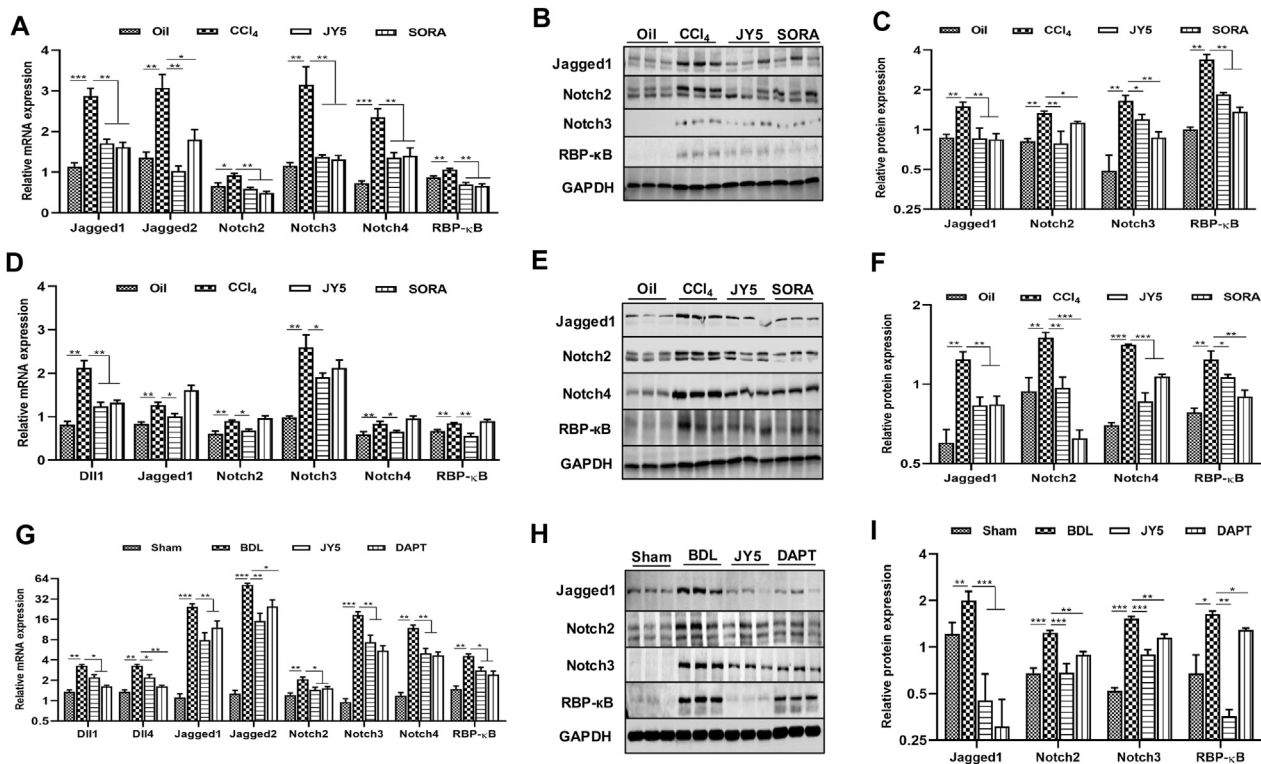


FIGURE 6 | JY5 may ameliorate liver fibrosis by inhibiting the Notch signaling pathway *in vivo*. (A) In the CCl₄-induced rat liver fibrosis experiment, the mRNA levels of *Jagged1*, *Jagged2*, *Notch2*, *Notch3*, *Notch4* and *RBP-κB* were measured by qPCR. Western blotting (B) and quantitative analysis (C) of Jagged1, Notch2, Notch3 and RBP-κB protein. (D) In the CCl₄-induced liver fibrosis mice experiment, the mRNA levels of *Dll1*, *Jagged1*, *Notch2*, *Notch3*, *Notch4* and *RBP-κB* were measured by qPCR. Western blotting (E) and quantitative analysis (F) of Jagged1, Notch2, Notch4 and RBP-κB protein. (G) In the BDL-induced rat liver fibrosis experiment, the mRNA levels of *Dll1*, *Dll4*, *Jagged1*, *Jagged2*, *Notch2*, *Notch3*, *Notch4* and *RBP-κB* were measured by qPCR. Western blotting (H) and quantitative analysis (I) of Jagged1, Notch2, Notch3 and RBP-κB protein. **p* < 0.05, ***p* < 0.01, ****p* < 0.001 vs the control group or sham group, #*p* < 0.05, ##*p* < 0.01, ###*p* < 0.001 vs the CCl₄ group or BDL group. Oil: control group.

5D,E,I,J). Similarly, in the BDL-induced liver fibrosis experiment, the treatment effect of JY5 was consistent with the results in the CCl₄-induced liver fibrosis experiments (Figures 5K–O). These results demonstrate that JY5 significantly represses the activation of HSCs in CCl₄- and BDL-induced liver fibrosis.

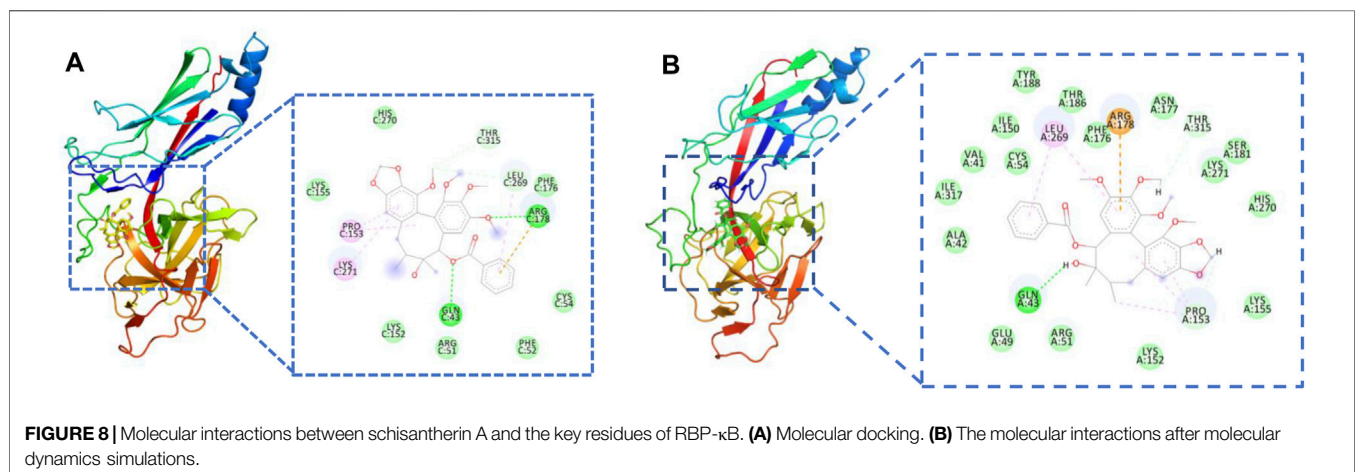
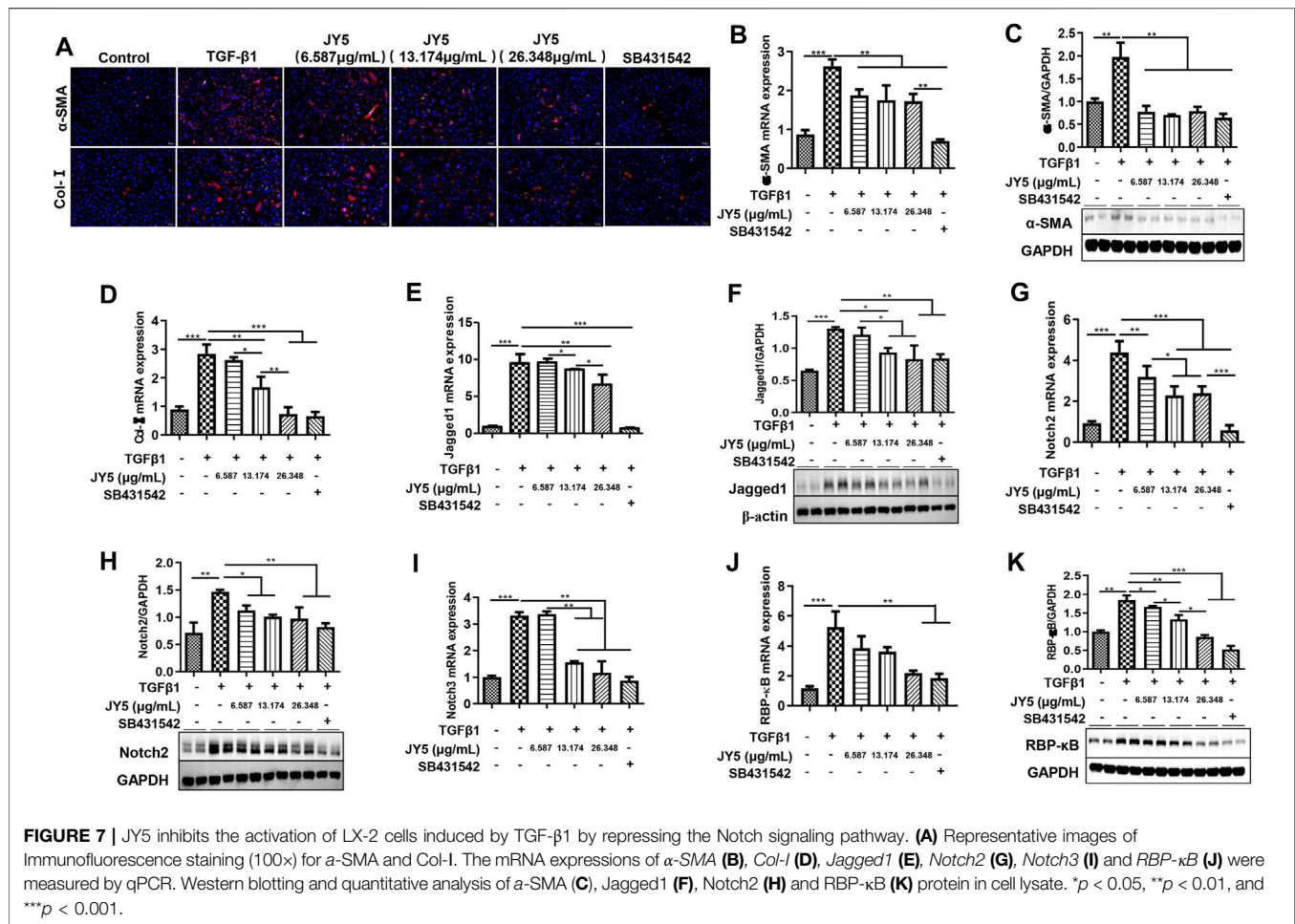
JY5 Significantly Inhibits Activation of the Notch Signaling Pathway *In Vivo*

In the CCl₄-induced liver fibrosis rat experiment, qPCR showed that the mRNA expressions of *Jagged1*, *Jagged2*, *Notch2*, *Notch3*, *Notch4* and *recombination signal binding protein-κB* (*RBP-κB*) were significantly more upregulated in the CCl₄ group than those in the control group. However, compared to the CCl₄ group, the mRNA expressions of *Jagged1*, *Jagged2*, *Notch2*, *Notch3*, *Notch4*, and *RBP-κB* were significantly reduced in the JY5- and SORA-treated groups (Figure 6A). Western blotting showed that the protein expression of Jagged1, Notch2, Notch3 and RBP-κB was significantly increased in the CCl₄ group, compared to the control group. Above these proteins expression was significantly more reduced in the JY5- and SORA-treated groups than in the CCl₄

group (Figures 6B,C). While in CCl₄-induced liver fibrosis mice experiment, JY5 not only decreased the mRNA expressions of *Jagged1*, *Notch2*, *Notch3*, *Notch4* and *RBP-κB*, but also downregulated the expression of *Dll1* (Figure 6D). Western blotting showed that the proteins expression of Jagged1, Notch2, Notch4 and RBP-κB was significantly more reduced in the JY5- and SORA-treated groups than in the CCl₄ group (Figures 6E,F). Consistent with the CCl₄-induced rat liver fibrosis model, JY5 decreased the expressions of *Jagged1*, *Notch2*, *Notch3*, *Notch4* and *RBP-κB* in the BDL-induced liver fibrosis model. In addition, the mRNA expressions of *Dll1*, *Dll4* and *Jagged two* were significantly decreased after treatment with JY5 (Figures 6G–I). These results suggest that JY5 can significantly inhibit the activation of Notch signaling pathway in CCl₄- and BDL-induced liver fibrosis.

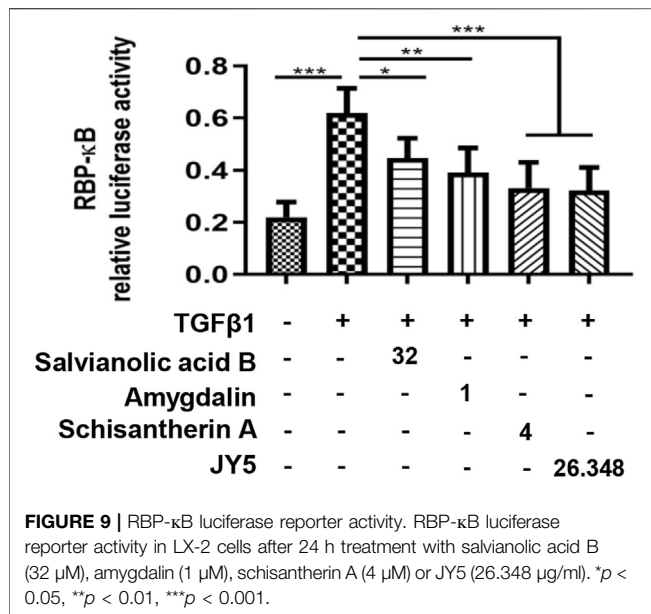
JY5 may Inhibit the Activation of LX-2 Cells Induced by TGF-β1 by Regulating the Notch Signaling Pathway

LX-2 cells were activated by TGF-β1 to observe the effect of JY5 at various concentrations *in vitro*. Immunofluorescence showed



that both α -SMA⁽⁺⁾ cells and Col-I⁽⁺⁾ cells were significantly elevated in TGF- β 1-treated cells compared to the control cells. However, these positive cells were significantly reduced after treatment with various concentrations of JY5 and SB431542 (**Figure 7A**). qPCR showed that the mRNA levels of α -SMA, Col-I, Jagged1, Notch2, Notch3 and RBP- κ B were significantly

elevated in TGF- β 1-treated cells compared to the control cells. However, above these genes mRNA expression were significantly reduced after treatment with various concentrations of JY5. Col-I, Jagged1, Notch2 and Notch3 mRNA expressions were significantly decreased in the high-dose JY5 group, compared to the low-dose JY5 group (**Figures 7B,D,E,G,I,J**). Western blot



analysis showed that the protein expressions of α-SMA, Jagged1, Notch2 and RBP-κB were significantly increased after treatment with TGF-β1. Compared with the TGF-β1 group, above these proteins expression were significantly reduced in the JY5-treated groups. Of these, the protein expression of Jagged1 and RBP-κB was significantly reduced in the high-dose JY5 group, compared to the low-dose JY5 groups (Figures 7C,F,H,K). These results suggest that JY5 may inhibit the activation of LX-2 cells induced by TGF-β1 by regulating the Notch signaling pathway.

Molecular Docking and molecular Dynamics Simulations

To investigate the binding mechanism of JY5 towards Jagged1, Notch2 and RBP-κB, molecular docking and molecular dynamics simulations were conducted. The lowest binding energy docking module was schisantherin A interacted with RBP-κB (Supplementary Table S4), and the intermolecular interactions have shown that schisantherin A has formed hydrogen bond with residues Gln43 and Arg178 of RBP-κB respectively (Figure 8A), and the results of molecular dynamics simulations also shown that schisantherin A has formed hydrogen bond with residues Gln43 (Supplementary Figure S5, Figure 8B), which suggested that RBP-κB may be the specific target by which JY5 regulated the Notch pathway.

We proceeded to test whether JY5-mediated RBP-κB was accompanied by transcriptional activation of RBP-κB using luciferase reporter assay. Exposure of LX-2 cells to TGF-β1 for 24 h resulted in a statistically significant increase in RBP-κB luciferase reporter activity (Figure 9), however, after simultaneously treated with salvianolic acid B, amygdalin, schisantherin A or JY5 for 24 h (Figure 9), the RBP-κB luciferase reporter activity was reduced, which further suggested that RBP-κB may be the target by which JY5 regulated the Notch pathway.

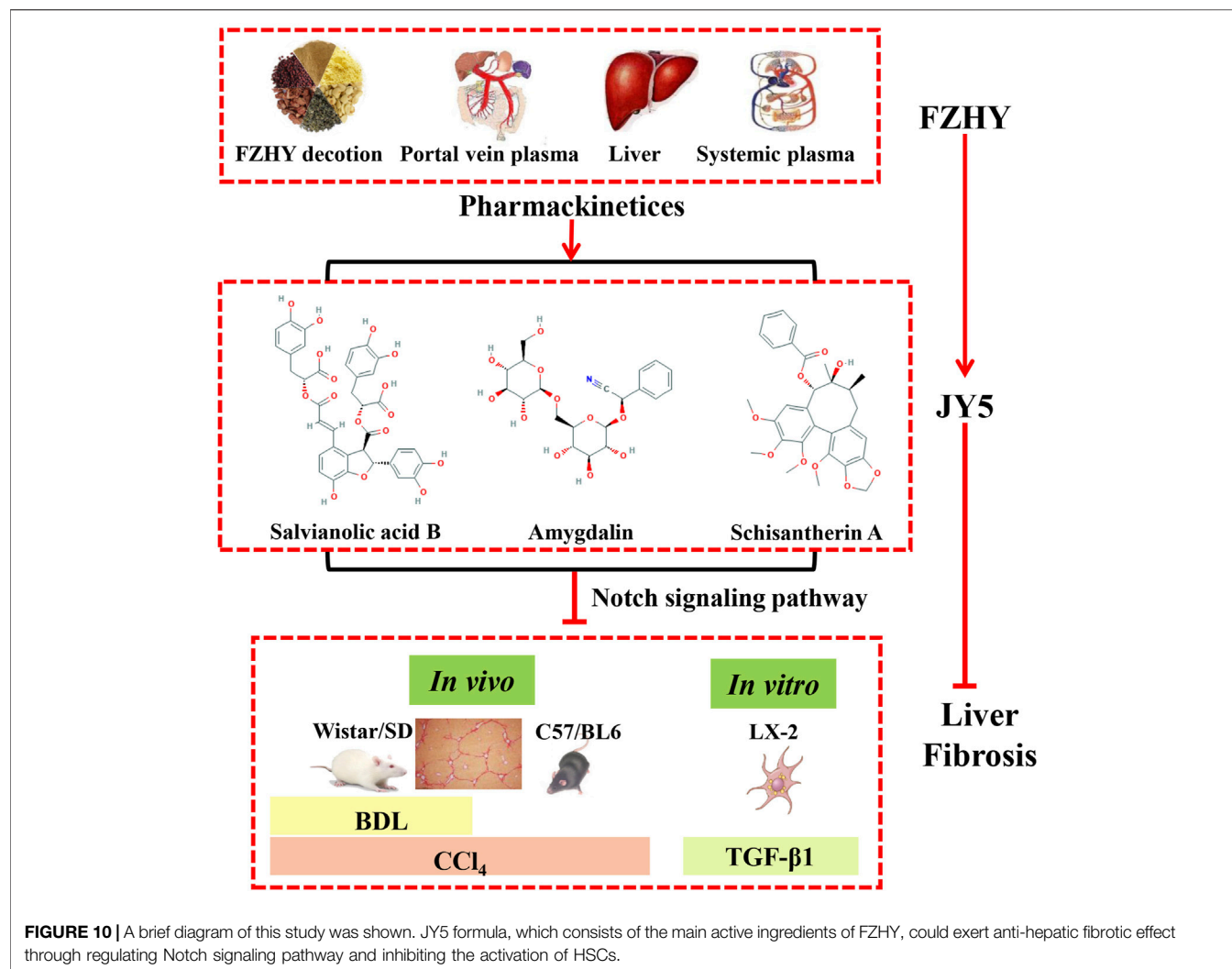
DISCUSSION

Liver fibrosis is an abnormal repair response to tissue damage, characterized by excessive deposition of ECM, leading to the persistence and development of pathological scar. Hepatic fibrosis is common in most chronic liver diseases process, which is a clinically important problem. To develop effective anti-hepatic fibrotic drugs, researchers have conducted a large number of basic and clinical studies. Despite achieving certain results in recent years, most of these drugs are in the preclinical or clinical trials stage, and some have failed clinical trials due to severe toxic side effects (Yoon et al., 2016). TCM has marked clinical effects on the treatment of liver fibrosis, which are closely correlated with its characteristics of multi-ingredients compatibility and multi-targets. However, the components of TCM are complex, and their mechanisms are not very clear, which somewhat increases the complexity of TCM studies. Regarding the intensive development of multidisciplinary crossover study, active ingredients screening, extraction, and purification from Chinese herbs provide a new approach for TCM formula research.

Salvianolic acid B is the main water-soluble phenolic acid compound. Numerous studies (Yan et al., 2010; Wang et al., 2012; Tao et al., 2013; Yan et al., 2017) have indicated that salvianolic acid B exerts significant anti-hepatic fibrosis effects through the following mechanisms: inhibiting the activation of HSCs by downregulating the TGF-β1/SMAD signaling pathway, protecting hepatocytes from apoptosis via inhibiting death receptor pathway, and stabilizing the mitochondrial membrane and regulating NF-κB/IκBα signaling pathway. Amygdalin is the major ingredient of peach kernel. Amygdalin can inhibit the activation of HSCs by downregulating the TGF-β/CTGF signaling pathway and induce activated HSC apoptosis by upregulating Bax gene expression, subsequently exerting anti-hepatic fibrotic effects (Luo et al., 2016; Luo et al., 2018). Lignans are the main bioactive components of Schisandrae. Studies have shown that these lignans can suppress inflammation, protect hepatocytes, and inhibit the activation of HSCs by downregulating the TGFβ/SMAD and MAPK signaling pathways (He et al., 2020).

In this study, we measured the content of various compounds in FZHY extract, plasma, and liver in rats after intragastric administration of FZHY. We obtained the three main bioactive ingredients of FZHY: salvianolic acid B, which had the highest content in FZHY extract; schisantherin A, which had maximum exposure in plasma; and amygdalin, which had highest hepatic exposure in the liver. Then we conducted uniform design and validation experiments to explore their composition and determine the best ratio for treating the rat hepatic fibrosis model. We obtained a new formula, namely JY5, which had anti-fibrotic effects comparable to that of FZHY. Further studies have shown that JY5 can significantly decrease serum ALT and AST levels and inhibit inflammation reaction while reducing collagen deposition in CCl₄-or BDL-induced liver fibrosis models.

The activation of HSCs is a pivotal event in liver fibrosis. Under persistent stimulation from CCl₄ and BDL, HSCs are



largely activated and transformed into myofibroblasts, which cause excessive ECM accumulated in the liver, eventually leading to hepatic fibrosis formation. Activated HSCs, as one of the main sources of hepatic ECM, can secrete Col-I and Col-III proteins. α -SMA is a specific marker of activated HSCs. This study found that JY5 significantly reduced the mRNA and protein expression of α -SMA, and decreased *Col-I* mRNA expression in CCl₄- and BDL-induced liver fibrosis in rats and mice. The results were further confirmed in TGF- β 1-induced LX-2 cell activation. JY5 significantly downregulated the expressions of α -SMA and *Col-I* in activated LX-2 cells induced by TGF- β 1. These results suggest that JY5 significantly inhibits the activation of HSCs.

Notch signaling is a highly conserved pathway evolutionarily, which influences intercellular signal transduction and cell fate decisions, and regulates the growth and development homeostasis of multiple tissues and organs, and in particular, the progression and development of diseases (Siebel and Lendahl, 2017). The Notch signaling pathway mainly consists of four Notch receptors (Notch1, Notch2,

Notch3, Notch4), five Notch ligands (Jagged1, Jagged2, Dll1, Dll3, Dll4), and the transcriptional regulatory elements of downstream signals (D'Souza et al., 2010). Previous studies (Ni et al., 2018) have shown that Notch plays an important role in the progress and development of hepatic fibrosis, which can interact with other signaling pathways such as TGF- β , Hedgehog, and Hippo. TGF- β 1 can promote the proliferation and activation of HSC-T25 cells by regulating the Notch signaling pathway (Aimaiti et al., 2019). The Jagged1 gene was successfully knocked down by using rAAV1-Jagged1-shRNA in CCl₄-induced liver fibrosis, resulting in alleviation of liver fibrosis (Tang et al., 2017). In addition, knockout of the RBP- κ B gene, which is considered a key transcription factor in the Notch pathway, can inhibit the proliferation and activation of HSCs to alleviate CCl₄-induced liver fibrosis in mice (He et al., 2015). Blockade of the Notch pathway can effectively inhibit the activation of HSCs, which in turn attenuates liver fibrosis. In this study, the expressions of Jagged1, Jagged2, Notch2, Notch3, Notch4, and RBP- κ B were significantly increased in CCl₄- and BDL-induced liver fibrosis in rats and

mice. While after intervention with JY5, the expressions of these Notch-related genes and proteins were significantly decreased. This was further confirmed by LX-2 cell activation induced by TGF- β 1 experiments *in vitro*. These results suggest that JY5 might exert anti-fibrotic effects by regulating the Notch signaling pathway to inhibit the activation of HSCs.

In this study, we used SORA and DAPT as positive controls. SORA, as a multi-receptor tyrosine kinase inhibitor that can inhibit the proliferation of multiple tumor cells and promote cell apoptosis, is commonly used for the treatment of hepatocellular carcinoma clinically (Keating, 2017). DAPT, as a γ -secretase inhibitor, can block the release of the Notch intracellular domain, thereby inhibiting activation of the Notch signaling pathway (Ni et al., 2018). In accordance with previous studies (Deng et al., 2013; Zhang et al., 2016), our results show that both SORA and DAPT have significant anti-hepatic fibrosis effects. Interestingly, SORA also can significantly downregulate the mRNA expressions of *Jagged1*, *Jagged2*, *Notch2*, *Notch3*, *Notch4* and *RBP- κ B*, and the protein expression of RBP- κ B. We speculate that SORA exerts anti-hepatic fibrosis effects, which might be related to the regulation of the Notch pathway; however, the precise mechanism needs to be further investigated. In addition, DAPT inhibits liver fibrosis by blocking the Notch pathway (Chen et al., 2012). This conclusion was further confirmed in our study. However, it is important to note that γ -secretase inhibitors, as a nonspecific Notch blocker, have shown severe side effects in clinical trials (Ni et al., 2018). So the clinical application of DAPT may be limited. Compared with SORA and DAPT, JY5 may have synergistic anti-fibrosis effects via multiple pathways, not specifically blocking a particular target or pathway, which confers relatively higher safety and more effectiveness.

The results of molecular docking, molecular dynamics simulations and RBP- κ B luciferase reporter assay suggested that RBP- κ B may be the specific target by which JY5 regulated the Notch pathway. In addition, given that JY5, as a component of TCM compounds, has shown good efficacy in two different liver fibrosis models, we speculate that JY5 might alleviate hepatic fibrosis through other mechanisms. In response to these issues, a series of related studies to elaborate upon the compatibility mechanisms of anti-liver fibrosis effect of JY5 will be conducted. These studies will provide an adequate scientific basis for clinical research and application of JY5 formula.

CONCLUSION

In summary, we obtained a novel anti-hepatic fibrosis component of TCM compounds, namely, JY5, through uniform design and validation experiments *in vivo*, and explored its part of

mechanisms for the first time. Our study showed that JY5 may exert anti-hepatic fibrotic effects by regulating the Notch signaling pathway to inhibit the activation of HSCs (Figure 10). Thus, the JY5 formula may be a potential novel therapeutic candidate for liver fibrosis.

DATA AVAILABILITY STATEMENT

The raw data supporting the conclusion of this article will be made available by the authors, without undue reservation.

ETHICS STATEMENT

The animal study was reviewed and approved by The Experimental Animal Ethics Committee of School of Pharmacy, Fudan University, and the Institutional Animal Care and Use Committee (IACUC) at Shanghai Research Center of the Southern Model Organisms.

AUTHOR CONTRIBUTIONS

YF, ZX, XT, CH, JC and PL wrote the manuscript and were involved with project concept and submission; YF, ZX and XT completed the main part of the experiment; WL, XZ, YH, TY and JF participated in the pharmacokinetic experiment; XZ, SG and YM participated in the *in vivo* experiment; DZ, HZ and YH participated in the *in vitro* experiment; CH, JC and PL revised the manuscript and were responsible for final approval. All authors read and approved the final manuscript.

FUNDING

This work is supported by National Natural Science Foundation of China (grant numbers 81530101, 81973613); Shanghai Rising-Star Program (grant number 19QA1408900); National Science and Technology Major Project of the Ministry of Science and Technology of China (grant number 2019ZX09201001-001-008); and Youth Innovation Promotion Association of Chinese Academy of Sciences (grant number 2019280).

SUPPLEMENTARY MATERIAL

The Supplementary Material for this article can be found online at: <https://www.frontiersin.org/articles/10.3389/fphar.2021.671152/full#supplementary-material>

REFERENCES

- Adams, J. M., and Jafar-Nejad, H. (2019). The Roles of Notch Signaling in Liver Development and Disease. *Biomolecules* 9 (10), 1–20. doi:10.3390/biom9100608
- Aimaiti, Y., Yusufkadi, M., Li, W., Tuerhongjiang, T., Shadike, A., Meieriyai, A., et al. (2019). TGF- β 1 Signaling Activates Hepatic Stellate Cells through Notch Pathway. *Cytotechnology* 71 (5), 881–891. doi:10.1007/s10616-019-00329-y
- Chen, J., Hu, Y., Chen, L., Liu, W., Mu, Y., and Liu, P. (2019). The Effect and Mechanisms of Fuzheng Huayu Formula against Chronic Liver Diseases. *Biomed. Pharmacother.* 114, 108846. doi:10.1016/j.biopha.2019.108846
- Chen, X., Zheng, S., Qi, D., Zheng, S., Guo, J., Zhang, S., et al. (2012). Inhibition of Notch Signaling by a γ -secretase Inhibitor Attenuates Hepatic Fibrosis in Rats. *PLoS One* 7 (10), e46512. doi:10.1371/journal.pone.0046512
- Cordero-Espinoza, L., and Huch, M. (2018). The Balancing Act of the Liver: Tissue Regeneration versus Fibrosis. *J. Clin. Invest.* 128 (1), 85–96. doi:10.1172/JCI93562
- Deng, Y. R., Ma, H. D., Tsuneyama, K., Yang, W., Wang, Y. H., Lu, F. T., et al. (2013). STAT3-mediated Attenuation of CCl₄-Induced Mouse Liver Fibrosis by the Protein Kinase Inhibitor Sorafenib. *J. Autoimmun.* 46, 25–34. doi:10.1016/j.jaut.2013.07.008
- D'Souza, B., Meloty-Kapella, L., and Weinmaster, G. (2010). Canonical and Non-canonical Notch Ligands. *Curr. Top. Dev. Biol.* 92, 73–129. doi:10.1016/S0070-2153(10)92003-6
- Friedman, S. L. (2015). Hepatic Fibrosis: Emerging Therapies. *Dig. Dis.* 33 (4), 504–507. doi:10.1159/000374098
- He, F., Guo, F. C., Li, Z., Yu, H. C., Ma, P. F., Zhao, J. L., et al. (2015). Myeloid-specific Disruption of Recombination Signal Binding Protein J κ Ameliorates Hepatic Fibrosis by Attenuating Inflammation through Cylindromatosis in Mice. *Hepatology* 61 (1), 303–314. doi:10.1002/hep.27394
- He, X., Chen, J., Mu, Y., Zhang, H., Chen, G., Liu, P., et al. (2020). The Effects of Inhibiting the Activation of Hepatic Stellate Cells by Lignan Components from the Fruits of Schisandra Chinensis and the Mechanism of Schisanhenol. *J. Nat. Med.* 74 (3), 513–524. doi:10.1007/s11418-020-01394-w
- Kan, S., Chen, Z., Shao, L., and Li, J. (2014). Transformation of Salvianolic Acid B to Salvianolic Acid a in Aqueous Solution and the *In Vitro* Liver Protective Effect of the Main Products. *J. Food Sci.* 79 (4), C499–C504. doi:10.1111/1750-3841.12415
- Kang, D., Shao, Y., Zhu, Z., Yin, X., Shen, B., Chen, C., et al. (2019). Systematically Identifying the Hepatoprotective Ingredients of Schisandra Lignan Extract from Pharmacokinetic and Pharmacodynamic Perspectives. *Phytomedicine* 53, 182–192. doi:10.1016/j.phymed.2018.09.010
- Keating, G. M. (2017). Sorafenib: A Review in Hepatocellular Carcinoma. *Target. Oncol.* 12 (2), 243–253. doi:10.1007/s11523-017-0484-7
- Lee, Y. A., Wallace, M. C., and Friedman, S. L. (2015). Pathobiology of Liver Fibrosis: a Translational success story. *Gut* 64 (5), 830–841. doi:10.1136/gutjnl-2014-306842
- Lemoine, S., and Friedman, S. L. (2019). New and Emerging Anti-fibrotic Therapeutics Entering or Already in Clinical Trials in Chronic Liver Diseases. *Curr. Opin. Pharmacol.* 49, 60–70. doi:10.1016/j.coph.2019.09.006
- Liu, C., Hu, Y., Xu, L., Liu, C., and Liu, P. (2009). Effect of Fuzheng Huayu Formula and its Actions against Liver Fibrosis. *Chin. Med.* 4, 12. doi:10.1186/1749-8546-4-12
- Luo, H., Zhao, F., Zhang, F., and Liu, N. (2018). Influence of Amygdalin on PDG, IGF and PDGFR Expression in HSC-T6 Cells. *Exp. Ther. Med.* 15, 3693–3698. doi:10.3892/etm.2018.5886
- Luo, H., Li, L., Tang, J., Zhang, F., Zhao, F., Sun, D., et al. (2016). Amygdalin Inhibits HSC-T6 Cell Proliferation and Fibrosis through the Regulation of TGF- β /CTGF. *Mol. Cell. Toxicol.* 12 (3), 265–271. doi:10.1007/s13273-016-0031-0
- Ni, M. M., Wang, Y. R., Wu, W. W., Xia, C. C., Zhang, Y. H., Xu, J., et al. (2018). Novel Insights on Notch Signaling Pathways in Liver Fibrosis. *Eur. J. Pharmacol.* 826, 66–74. doi:10.1016/j.ejphar.2018.02.051
- Siebel, C., and Lendahl, U. (2017). Notch Signaling in Development, Tissue Homeostasis, and Disease. *Physiol. Rev.* 97 (4), 1235–1294. doi:10.1152/physrev.00005.2017
- Tang, G., Weng, Z., Song, J., and Chen, Y. (2017). Reversal Effect of Jagged1 Signaling Inhibition on CCl₄-Induced Hepatic Fibrosis in Rats. *Oncotarget* 8 (37), 60778–60788. doi:10.18632/oncotarget.18484
- Tao, Y. Y., Wang, Q. L., Shen, L., Fu, W. W., and Liu, C. H. (2013). Salvianolic Acid B Inhibits Hepatic Stellate Cell Activation through Transforming Growth Factor Beta-1 Signal Transduction Pathway *In Vivo* and *In Vitro*. *Exp. Biol. Med. (Maywood)* 238 (11), 1284–1296. doi:10.1177/1535370213498979
- Wang, R., Song, F., Li, S., Wu, B., Gu, Y., and Yuan, Y. (2019). Salvianolic Acid A Attenuates CCl₄-Induced Liver Fibrosis by Regulating the PI3K/AKT/mTOR, Bcl-2/Bax and Caspase-3/cleaved Caspase-3 Signaling Pathways. *Drug Des. Devel. Ther.* 13, 1889–1900. doi:10.2147/DDDT.S194787
- Wang, R., Yu, X.-Y., Guo, Z.-Y., Wang, Y.-J., Wu, Y., and Yuan, Y.-F. (2012). Inhibitory Effects of Salvianolic Acid B on CCl₄-Induced Hepatic Fibrosis through Regulating NF-Kb/ikba Signaling. *J. Ethnopharmacology* 144 (3), 592–598. doi:10.1016/j.jep.2012.09.048
- Yan, X., Zhou, T., Tao, Y., Wang, Q., Liu, P., and Liu, C. (2010). Salvianolic Acid B Attenuates Hepatocyte Apoptosis by Regulating Mediators in Death Receptor and Mitochondrial Pathways. *Exp. Biol. Med. (Maywood)* 235 (5), 623–632. doi:10.1258/ebm.2009.009293
- Yan, X. F., Zhao, P., Ma, D. Y., Jiang, Y. L., Luo, J. J., Liu, L., et al. (2017). Salvianolic Acid B Protects Hepatocytes from H₂O₂ Injury by Stabilizing the Lysosomal Membrane. *World J. Gastroenterol.* 23 (29), 5333–5344. doi:10.3748/wjg.v23.i29.5333
- Yoon, Y. J., Friedman, S. L., and Lee, Y. A. (2016). Antifibrotic Therapies: Where Are We Now?. *Semin. Liver Dis.* 36 (1), 87–98. doi:10.1055/s-0036-1571295
- Zhang, L., and Schuppan, D. (2014). Traditional Chinese Medicine (TCM) for Fibrotic Liver Disease: hope and Hype. *J. Hepatol.* 61 (1), 166–168. doi:10.1016/j.jhep.2014.03.009
- Zhang, Q. D., Xu, M. Y., Cai, X. B., Qu, Y., Li, Z. H., and Lu, L. G. (2015). Myofibroblastic Transformation of Rat Hepatic Stellate Cells: the Role of Notch Signaling and Epithelial-Mesenchymal Transition Regulation. *Eur. Rev. Med. Pharmacol. Sci.* 19 (21), 4130–4138.
- Zhang, X., Du, G., Xu, Y., Li, X., Fan, W., Chen, J., et al. (2016). Inhibition of Notch Signaling Pathway Prevents Cholestatic Liver Fibrosis by Decreasing the Differentiation of Hepatic Progenitor Cells into Cholangiocytes. *Lab. Invest.* 96 (3), 350–360. doi:10.1038/labinvest.2015.149

Conflict of Interest: The authors declare that the research was conducted in the absence of any commercial or financial relationships that could be construed as a potential conflict of interest.

Publisher's Note: All claims expressed in this article are solely those of the authors and do not necessarily represent those of their affiliated organizations, or those of the publisher, the editors and the reviewers. Any product that may be evaluated in this article, or claim that may be made by its manufacturer, is not guaranteed or endorsed by the publisher.

Copyright © 2021 Fu, Xiao, Tian, Liu, Xu, Yang, Hu, Zhou, Fang, Gao, Zhang, Mu, Zhang, Hu, Huang, Chen and Liu. This is an open-access article distributed under the terms of the Creative Commons Attribution License (CC BY). The use, distribution or reproduction in other forums is permitted, provided the original author(s) and the copyright owner(s) are credited and that the original publication in this journal is cited, in accordance with accepted academic practice. No use, distribution or reproduction is permitted which does not comply with these terms.



Standardization of *Berberis aristata* DC and *Nigella sativa* L. Using HPTLC and GCMS and Their Antineoplasia Activity in 7,12-Dimethylbenz[a]anthracene-Induced Mouse Models

Mohd Mazhar* and S S Agrawal

Department of Pharmacology, School of Pharmaceutical Sciences, Delhi Pharmaceutical Sciences & Research University, New Delhi, India

OPEN ACCESS

Edited by:

Sayeed Ahmad,
Jamia Hamdard University, India

Reviewed by:

Amit Kar,
Institute of Bio-Resources and
Sustainable Development (IBSD), India
Anju Dhiman,
Maharshi Dayanand University, India

*Correspondence:

Mohd Mazhar
mohdmazhar32@gmail.com

Specialty section:

This article was submitted to
Ethnopharmacology,
a section of the journal
Frontiers in Pharmacology

Received: 15 December 2020

Accepted: 02 August 2021

Published: 30 November 2021

Citation:

Mazhar M and Agrawal SS (2021)
Standardization of *Berberis aristata* DC
and *Nigella sativa* L. Using HPTLC and
GCMS and Their Antineoplasia Activity
in 7,12-Dimethylbenz[a]anthracene-
Induced Mouse Models.
Front. Pharmacol. 12:642067.
doi: 10.3389/fphar.2021.642067

Berberis aristata DC and *Nigella sativa* L. are officially listed in various Indian Pharmacopoeia and AYUSH official documents. Prescribed for different ailments for proven medicinal activities, they thus became part of polyherbal medications. With reverse pharmacology and scientific validation, more than 30 patents are filed on different formulations of *B. aristata* and granted. *Nigella sativa* L. has been broadly studied for its therapeutic potential and wide range of activities against cardiovascular, diabetic, cancer, and life style disorders. Thus, this study is aimed at standardizing *B. aristata* and *N. sativa* and their antineoplasia activity in 7, 12-dimethylbenz[a]anthracene (DMBA)-induced mouse models. Molecular docking was done using the Schrodinger program Maestro 9.0. Herbal extracts and essential oil (*B. aristata* and *N. sativa*) were standardized and quantified using high-performance thin-layer chromatography (HPTLC) (CAMAG) and gas chromatography-mass spectrometry (GCMS) (Agilent 2010GC System) with validated methods. DMBA was administered orally once a week (1mg/200 μ L) to each animal except the normal control. Hematology, histopathology, and immunoassays were performed, and data were analyzed and depicted with GraphPad and SPSS. In molecular docking, thymoquinone showed the highest docking score (9.519, 9.211, and 9.042, respectively) in the active site pockets of IL6 (PDB ID: 4CNI and 5FCU), TNF (PDB ID: 2A25), and VEGF (PDB ID: 4KZN). Out of all four target sites, thymoquinone and berberine showed good binding affinity with IL6 (PDB ID: 4CNI) compared to α - and β -pinenes. HPTLC analysis of the hydroalcoholic extract showed the presence of berberine both qualitatively and quantitatively (5.4% berberine), and thymoquinone detected 0.17% in the *N. sativa* extract. GCMS for essential oil showed 26 compounds including \pm pinene. Leukocytes and erythrocytes of *N. sativa* and *B. aristata* were analyzed, and significant improvements were recorded ($P < 0.05$) and graphically presented. Mean survival time was calculated by the Kaplan Meier method (119 days). Immunoassay analyses were conducted, namely, TNF- α and VEGF, and interpreted and marked.

Keywords: antineoplasia, GCMS, HPTLC, molecular docking, phytopharmaceuticals

INTRODUCTION

Certain chemotherapeutic agents have been aborted for use in the treatment of malignancy because of their toxicity. Over these years, there has been an increase in medical research in a broad range of therapeutics, many of which use plant-derived lead compounds (Vincristine and Paclitaxel) and are under extensive research for cancer cure. When the world is moving toward organic products, certain plants are thought to have enormous potential of cure against incurable diseases like cancer and COVID 19, and thereby, these create a pool of natural chemicals that may provide a therapeutic effect against cancer and other malignancies. Herbal medicines are in practice and considered the second method to treat cancer in developing nations (Kennedy, 2005; Ezeome and Anarado, 2007). *B. aristata* DC (family: Berberidaceae) is the main constituent of rasaut, darvyadi (kvatha, leha, taila), rasanjana, and Dashanga lepa. Aromoline, oxyberberine, oxyacanthine, berbamine, berberine chloride, 1-O-methylpakistanine, and pseudopalmatine chloride are the main chemical constituents of *B. aristata* (Pasrija et al., 2010). Antidiarrheal activity, cardioprotective hepatoprotective activity, antidiabetic activity, and anticancer activity are reported. Being potential therapeutic agents, more than 30 patents are filed on the different formulations granted and marketed (4, 5). *Nigella sativa* L. (Ranunculaceae) has been researched for its pharmacological potential and shown to possess a wide spectrum of activities, namely, diuretic, cardioprotective, antihyperglycemic, antineoplastic, analgesic, antimicrobial, anti-inflammatory, spasmolytic, hepatoprotective, nephroprotective, and antioxidant properties (6). Most of the therapeutic properties of this plant are due to the presence of thymoquinone (TQ), which is a major active chemical component of the essential oil. α -Pinene and β -pinene are other biomarkers that possess biological activity (6). In silico methods have been designed, developed, and applied to pharmacology hypothesis development and testing using software, for example, FoldX. In silico methods are primarily used alongside the generation of *in vitro* data and their correlation, with both to create the model and to test it. Such models have seen frequent use in the drug discovery and optimization of novel molecules with affinity to a target, the clarification of pharmacokinetics and pharmacodynamics, and physicochemical characterization. With this background, we aimed at standardizing *B. aristata* (bark) and *N. sativa* L. (black seed) using high-performance thin-layer chromatography (HPTLC) and gas chromatography–mass spectrometry (GCMS) and their antineoplasia activity in 7,12-dimethylbenz[a]anthracene (DMBA)-induced mouse models.

MATERIALS AND METHODOLOGY

Molecular Docking

Docking studies were performed to study the molecular binding energy and patterns of some natural derivatives with the active site pockets of crystal structures of IL6 (PDB ID: 4CNI and 5FCU), IL10 (PDB ID: 1WQ8), TNF (PDB ID: 2AZ5), and VEGF (PDB ID: 4KZN) using the Schrodinger program Maestro 9.0.

TABLE 1 | Docking and gliding with their respective PDB codes.

PDB	Compound	Docking score	Glide score
TNF-2AZ5	Thymoquinone	4.468	4.468
	Berberine	4.426	4.426
	α -Pinene	4.150	4.150
	β -Pinene	4.173	4.173
VEGF-4KZN	Thymoquinone	4.525	4.525
	Berberine	2.948	2.948
	α -Pinene	2.963	2.963
	β -Pinene	3.978	3.978

The binding energies and their respective docking scores of all synthesized molecules are summarized in a tabular form and represented in **Table 1**.

Collection and Authentication

B. aristata (bark) and *N. sativa* (seeds) were collected from Delhi, and both were authenticated by NISCAIR (Reference No. NISCAIR/RHMD/Consult/2018/3136-85-1/2).

Chemicals and Materials

Berberine chloride was procured from Prolab Marketing Pvt. Ltd. (India), and thymoquinone and α - and β -pinene were procured from TCI Chemicals (India).

All the described chemicals and reagents used in the present study were HPLC-grade-certified.

Extraction

1) *B. aristata* Bark: The bark (2 kg) was air-dried, crushed to smaller pieces, re-dried, and coarsely powdered and was then exhaustively extracted with water:alcohol (95%, methanol) (1:1) in Soxhlet's apparatus for 72 h. The extract was dried using an Allied lyophilizer with a co-solvent system (the temperature at -80°C and the pressure at 760 Pa), and a dark-brown mass (2.5%) was obtained. 2) *Nigella sativa* L.: Continuous hot solvent extraction was performed with Soxhlet's apparatus for 6 h at 40°C using a coarse powdered crude drug to hydroalcoholic methanol ratio of 1:10 gmL^{-1} (Alhaj et al., 2008), and the percentage yield obtained was 5.16%. 3) Essential oil extraction: In a Clevenger apparatus, each plant material was separately soaked in distilled water (1 L) at 90°C for 6 h (Nair et al., 2018). Using hydrodistillation, the volatile components were collected by the addition of equal volumes of n-hexane, dried over anhydrous sodium sulfate, stored in an amber-colored bottle (-20°C) with a label. The extract yield was calculated as 0.50 to 0.60% with repetitions.

Preparation of Standard Solutions

The berberine Cl working standard was accurately weighed and transferred to 10 mg/10 ml and dissolved in methanol to obtain a solution concentration of 1 mcg/ μL (for HPTLC), and in the same way, three sets of controls for berberine were prepared from a separate stock so as to lie in the lowest, middle, and highest regions of the calibration curves. Similarly, 1 ppm thymoquinone standard solution was prepared for the calibration curve.

TABLE 2 | Absorbance versus concentrations of α -tocopherol, *B. aristata*, and *N. sativa*.

Conc. ($\mu\text{g/ml}$)	% Inhibition of tocopherol	% Inhibition of <i>B. aristata</i>	% Inhibition of <i>N. sativa</i>
100	38	29	34
80	32	21	30
60	28	17	25
40	21	13	21.9
20	18.8	4	17.7
Mean	22.6	11.33333	25.72
SD	± 7.13	± 8.84	± 6.44
Pearson correlation	0.991*	0.988*	0.988*
Sig. (two-tailed)	0.0001	0.002	0.000
N	5	5	5

*Correlation is significant at the 0.01 level (two-tailed).

DPPH Assay

The 2,2-diphenyl-1-picryl-hydrazyl-hydrate (DPPH) assay was performed as per Brand-Williams et al. (1995). The reagent is prepared by dissolving DPPH (11.82 mg) in 500 ml of ethanol to meet 6×10^{-5} mol/L solution. α -Tocopherol acetate is treated as a standard antioxidant (1000 $\mu\text{g/ml}$ with ethanol). The stock solution is further diluted to make concentrations of 20, 40, 60, 80, and 100 $\mu\text{g/ml}$ with methanol. Each herbal extract test solution is prepared by dissolving 1000 $\mu\text{g/ml}$ with ethanol. Methanol was used as a blank solution and control. 0.2 ml of methanol is mixed with 7.8 ml of DPPH, as shown in Table 2.

In vitro Activity (MTT Assay)

1 mg/10 ml of anastrozole used as a positive control and different concentrations of anastrozole (1, 10, 100, 200, and 500 μM) were used. DMSO at 0.04% was used as a solvent control, whereas a negative control (medium) and positive control (anastrozole) were used as treatments. The cell line was purchased from the National Center for Cell Sciences, Pune, with a seeding density of 2.0×10^4 cells/well stored in liquid nitrogen for further testing purposes. Before the 3-(4,5-dimethylthiazol-2-yl)-2,5-diphenyltetrazolium bromide (MTT) assay, MCF-7 cells were thawed at $37 \pm 1^\circ\text{C}$ in a gaseous environment of $5 \pm 1\%$ carbon dioxide in a humid environment in tissue culture flasks containing the medium, Dulbecco's modified Eagle's medium (DMEM) (Genetix Biotech Asia) supplemented with 10% fetal bovine serum (Genetix Biotech Asia) and penicillin (100 units) and streptomycin (100 μg) antibiotics (Genetix Biotech Asia) to obtain the subconfluence of cells (70–90% confluent). Test solution concentrations are presented in Table 3.

Instrumentation: (I) High-Performance Thin-Layer Chromatography

CAMAG Automatic TLC Sampler 4 (New ATS4) is used for the identification using a D_2 lamp at a wavelength of 254 nm, with a PM high voltage (286 V). Methanol is used as the sample solvent type having a dosage speed of 150 nL/, an inert gas (N_2) is used as the spray gas, and Merck silica gel 60F 254 is used as the stationary phase. The bond length is kept at 8.0 mm with a syringe size of 25 μL in all tracks. n-Butanol:acetic acid:water

(3:1:1) (v/v/v) and C_6H_{14} : $\text{CH}_3\text{COOC}_2\text{H}_5$ (8:2) v/v are used as mobile phases in a twin trough chamber (20×10 cm) for *B. aristata* and *N. sativa* L., respectively, and drying is done at room temperature. Scanning is performed at a speed of 20 mm/s with slit dimensions of 6.00×0.45 mm.

2) GCMS analysis: Filtered through 0.25 μM PTFE; then, a volume of 2 μL was injected at a split ratio of 1:40 into an Agilent 2010 Gas Chromat System and a CTPAL autosampler with a silica column ($30 \text{ m} \times 0.25 \text{ mm}$, film thickness 0.25 μm) and interfaced with an electron ion spray mass detector (m/z 40–650 at 1250 s/scan). The interface was set up at 290°C , and the ion source was adjusted to 220°C with the carrier gas (helium at 2 mLmin^{-1}). After a 2 min solvent setback time at 70°C , the oven temperature was increased to 5°C/min – 280°C with a solvent cut time of 4.50 min. The pressure was kept at 69.0 kPa, and a total flow of 52.6 mLmin^{-1} , a column flow of 1.21 mLmin^{-1} , and a linear velocity of 39.9 cm s^{-1} were maintained. The volatile constituents were identified by matching the retention index and fragmentation pattern data with those of the standards using WILEY and NIST(12).

Animal Study

Female Swiss albino mice from the institute animal house, 14–15 weeks old, weighing 24–28 g, were arranged into 10 groups ($n = 6$ animals per group), and DMBA was administered orally once a week (1 mg/200 μL olive oil) to each animal except the normal control, Group II: disease control, vehicle-treated Group III: marketed standard Anastrozole, 1 mg/kg, Group IV: thymoquinone, 10 mg/kg, Group V: α -pinene, 0.50 ml/kg, Group VI: β -pinene, 200 mg/kg, Group VII: *Nigella sativa* L. extract, 200 mg, Group VIII: *N. sativa* oil, 50 μL , Group IX: berberine Cl, 30 mg, Group X *B. aristata* extract, 400 mg). The standard and validated conditions maintained were a temperature of $20 \pm 1^\circ\text{C}$ and a relative humidity (RH) of $50 \pm 5\%$, and mice were fed a standard rodent diet and water ad libitum and sustained at a 12 h light/dark cycle. All experimental procedures were carried out in compliance with the Declaration of Helsinki and the protocol approved by the Ethical Committee of DIPSA (IAEC/2016-I-Prot.No-17), India. The blood samples were collected using a Retro-orbital, stored in a preheparinized vacutainer, stored under standard conditions, and sent to the lab, and doses are calculated as per OECD guidelines, 2014.

TABLE 3 | Final stock concentration in the study for MTT Assay.

S. No.	Test name	Final stock in DMEM	Concentration in RPMI
1	Thymoquinone	12.5 µg/ml	(2.5 ,5 ,7.5 ,10 ,12.5) µg/ml
2	Berberine chloride	1 µM	1 µM(10 ,100 ,200 ,500) nm
3	α-Pinene	100 µg/ml	(5, 10 ,20 ,30 ,40) µg/ml
4	β-Pinene	25 µg/ml	Aruna and Sivaramakrishnan (1990); Banchrof et al. (1996); Bower et al. (2002); Organization (2007); Saied et al. (2007)
5	<i>Berberis aristata</i> extract	500 µg/ml	(1, 10, 50, 300, 500) µg/ml
3	<i>Nigella sativa</i> extract	250 µg/ml	(250, 200, 170, 110, 45) µg/ml
4	<i>Nigella sativa</i> oil	1%	(0.60, 0.50, 0.40, 0.30, 0.20)%

Tissue specimens from the mammary gland of female mice of each experimental groups were fixed in neutral buffered formalin 10% and processed by a conventional verified method, embedded in paraffin, sectioned at 4–5 µm, and stained with dyes, namely, hematoxylin and eosin (10).

Immunohistochemistry: The procedure for immunohistochemical analysis was performed as described previously (Liu et al., 2009). Tumor tissues were sectioned at a thickness of 4 µm and incubated in methanol (0.3% H₂O₂) for 30 min and treated with 0.1% Triton X-100 for 10 min. The sections were washed with PBS three times and blocked with 1% bovine serum albumin and 0.01% Triton X-100 for 1 h at room temperature. The sections were incubated with the VEGF antibody (1:100) or TNF α (1:50) or the TGF β antibody overnight at 4°C. Negative controls were analyzed by staining with isotype-matched IgG or PBS. Following rinsing in PBS, the sections were incubated with anti-mouse biotinylated monoclonal secondary antibodies for 1 h at room temperature. The sections were washed three times with PBS and then incubated in avidin–biotin, and IHC slides were examined under a microscope (Olympus CX31; Olympus Corporation, Tokyo, Japan) and analyzed by Advance Histo lab.

RESULTS AND DISCUSSION

Molecular Docking

Docking studies were carried out to study the molecular binding pattern of natural derivatives with the active site pockets of crystal structures of IL6 (PDB ID: 4CNI and 5FCU), IL10 (PDB ID:

1WQ8), TNF (PDB ID: 2AZ5), and VEGF (PDB ID: 4KZN), and adaptable resolution (<2 Å) and the docking score are the criteria. The binding energies and docking scores of all synthesized molecules are represented in **Table 1**. Docking of the compounds thymoquinone, berberine, α-pinene, and β-pinene into the active sites of enzymes revealed that several molecular interactions (hydrogen bonds, π-interactions, and hydrophobic interactions) were considered to be responsible for the observed affinity of the compound. Thymoquinone formed only one hydrogen bond between oxygen of the –C=O group of thymoquinone and amino acid PHE 33. Berberine formed one hydrogen bond between hydrogen of the dioxane ring of berberine and amino acid ASP 31, and another hydrogen bond is formed between hydrogen of the phenyl ring of berberine with SER 102 amino acid. α-Pinene and β-pinene showed no hydrogen bond; they only show bad contact with amino acids (**Figures 1A,B,C,D**) and showed the details of binding modes of the docked compounds thymoquinone, berberine, α-pinene, and β-pinene, thus exhibiting the antitumor properties in the targeted herbal drug extract.

Anti-oxidant Activity (DPPH Assay)

The antiradical activities of *B. aristata* and *N. sativa* and their radical forms are studied and results are presented in **Table 2**. DPPH has an absorption band at 515 nm which disappears upon reduction by an antiradical compound (Brand-Williams et al., 1995). Phytochemistry explained (Bors, 1996) that more phenolic groups were believed to produce more antioxidant activity. Many plant constituents scavenge free radicals. **Figure 2** explains the potential of the extract in determining the significant antioxidant activity from

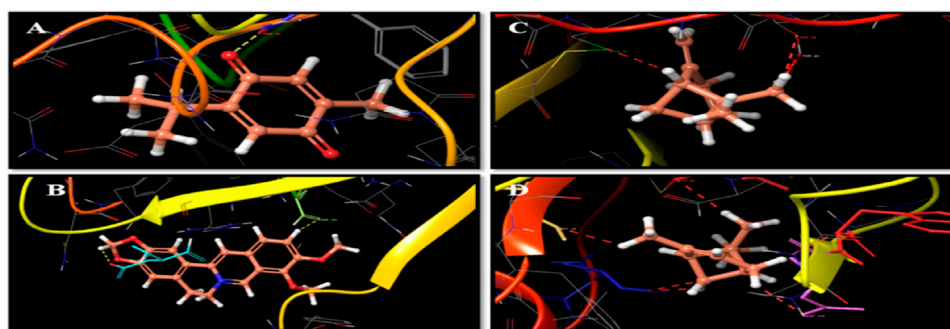
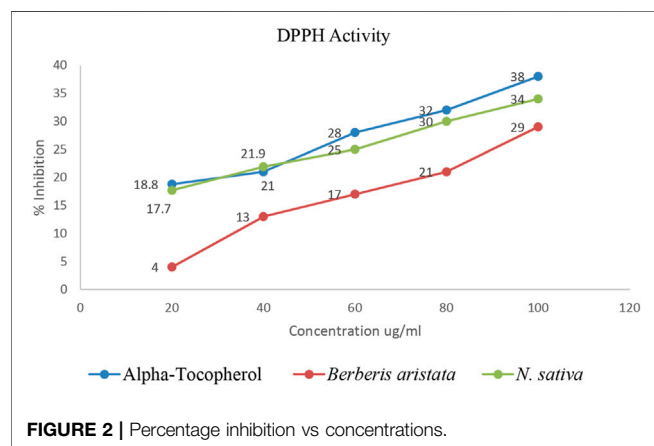


FIGURE 1 | (A) Thymoquinone and amino acid PHE 33 interactions. (B) Berberine, amino acid ASP 31, and hydrogen bond interactions. (C) β-Pinene interaction with amino acid cysteine. (D) α-Pinene interaction with amino aspartate.

TABLE 4 | Inhibitory concentration (IC₅₀) values of standards and test compounds.

S. No.	Name	IC ₅₀
1	Anastrozole	412.28 nM (±47.74)
2	Berberine Cl	686.49 nM (±161.46)
3	Thymoquinone	7.5 µg/ml (±0.202)
4	α-Pinene	6.72 µg/ml (±1.34)
5	β-Pinene	11.08 µg/ml (±0.63)
6	<i>B. aristata</i> extract	103.72 µg/ml (±54.17)
7	<i>Nigella sativa</i> extract	107.89 mg/ml (±12.05)
8	<i>Nigella sativa</i> oil	0.33% (±0.026)

Values are expressed in mean n = 3, SD (±).

**FIGURE 2 |** Percentage inhibition vs concentrations.

natural sources. Demand for the natural antioxidants is shooting up nowadays as nutraceuticals, biopharmaceuticals, and food additives due to consumer preference. Dietary intake of antioxidant foods decreases the incidence of human diseases. Also, plant-based antioxidants are preferred against the synthetic ones because of their multiple mechanisms of actions and non-toxic nature. Our study used the bark of *B. aristata* and *N. sativa* that contains the berberine and thymoquinone active constituents, respectively, and other phytoconstituents including phenolic compounds.

MTT Assay

As per the objective of the study, MTT assay were performed to find out the inhibitory concentration of various standards and test samples (*B. aristata* and *N. sativa* Extracts). The results are presented into graphical data **Figure 3** and respective IC₅₀ values expressed in **Table 4** (sample *n* = 3 and standard deviation).

CHROMATOGRAPHY

B. aristata Characterization

Optimization of the HPTLC solvent system for quantitative analysis was done using a combination of solvent systems of varying polarity, and the most suitable solvent system was found to be *n* butanol:acetic acid:water (3:1:1) v/v/v. Quantitative analysis for berberine was performed through HPTLC techniques, and the result showed that the content of berberine in *B. aristata* was found to be 53.5 µg in 1 mg through HPTLC techniques compared to standard

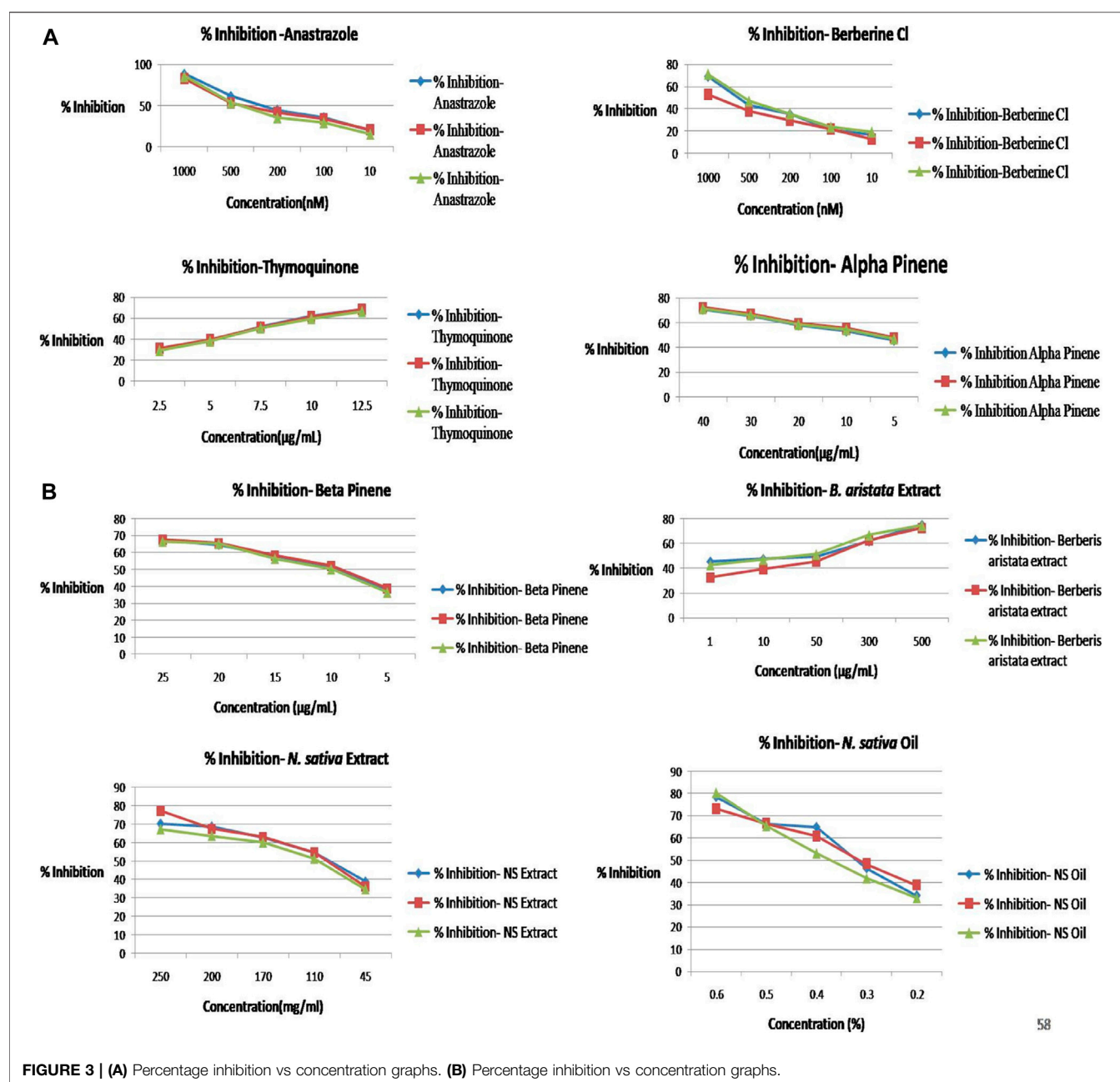
berberine Cl. The respective HPTLC chromatograms of bark extracts are presented in **Figures 4A,B**. In the present analysis, the calibration curve of standard berberine was found to be linear ($y = -4.097 \times 10^{-13} x^2 + 7.5666 \times 10^{-7} x + 5.943 \times 10^{-2}$, *R* = 99.99), which is presented in **Figure 4C**. The interpretation of results suggests that the sample contained a considerable amount of berberine of 53.5 µg in 1 mg of the solution, which is approximately 5.4%.

Nigella sativa L. Characterization

C₆H₁₄: CH₃COOC₂H₅ (8:2) v/v used as a mobile phase for quantitative and qualitative analysis of thymoquinone in the *Nigella sativa* L. extract done using HPTLC methods, and the result showed that the presence of thymoquinone in *Nigella sativa* was found to be 17.3 mg per 10 g compared to the pure compound thymoquinone. The respective HPTLC chromatograms of thymoquinone and the herbal extract are shown in **Figures 4E–F**. During the present study, the calibration curve of standard thymoquinone was found to be linear ($y = -3.761 \times 10^{-16} x^2 + 6.272 \times 10^{-9} x + 8.375 \times 10^{-3}$, *R* = 99.98%), which is presented in **Figure 4G**. Graphical data of standard thymoquinone and the *N. sativa* extract are presented in **Figure 4H**. The percentage of thymoquinone detected was 0.17% w/w.

Results revealed the presence of several constituents in the extracts as evidenced with the chromatogram of the methanolic extract of *B. aristata* and *Nigella sativa*, which showed 10 peaks at different R_f values and the peak area at 366 nm in *n* butanol:acetic acid:water (3:1:1) v/v/v and *n* hexane: ethyl acetate (Ezeome and Anarado, 2007; Alhaj et al., 2008) v/v solvent systems, whereas peaks were present in the HPTLC fingerprinting chromatogram at 254 nm of both extracts. The number of constituents (No. of peaks-11) in the extract and their retention factors (R_f) and chromatographic profiles are shown in **Figures 4A–D**. The chromatogram of 26 compounds was obtained by GCMS analysis of NS (**Table 5**).

The major compounds that could be identified were linoleic acid (66.2%), β-pinene (13.66%), hexadecanoic acid (5.69%), thymoquinone (0.76%), and α-pinene (0.25%). Until 2018, 39 clinical trials are recorded to berberine, and some of them are in phases II and III. The thymoquinone molecule has registered with 17 clinical trials, and nine have been completed with promising results; however, two new clinical trials were recruited until 2019. Toxicological and reference standards both together may evolve the new paradigm in treating the illness with herbal drugs. With the advancement of technology, it is evident that the herbal industry needs to follow strict guidelines, and such regulations are necessary for quality control and assurance to bring potential evidenced research on phytopharmaceuticals. Herbal drug regulations and their harmonization in Asia, Europe, and the United States may stimulate and strengthen phytopharmaceuticals by using the modern analytical techniques for standardization of marker compounds (Choudhary and Sekhon, 2011). As per WHO guidelines, 2007, quality of the herbal product needs to be standardized with respect to safety before releasing it into the market (15).



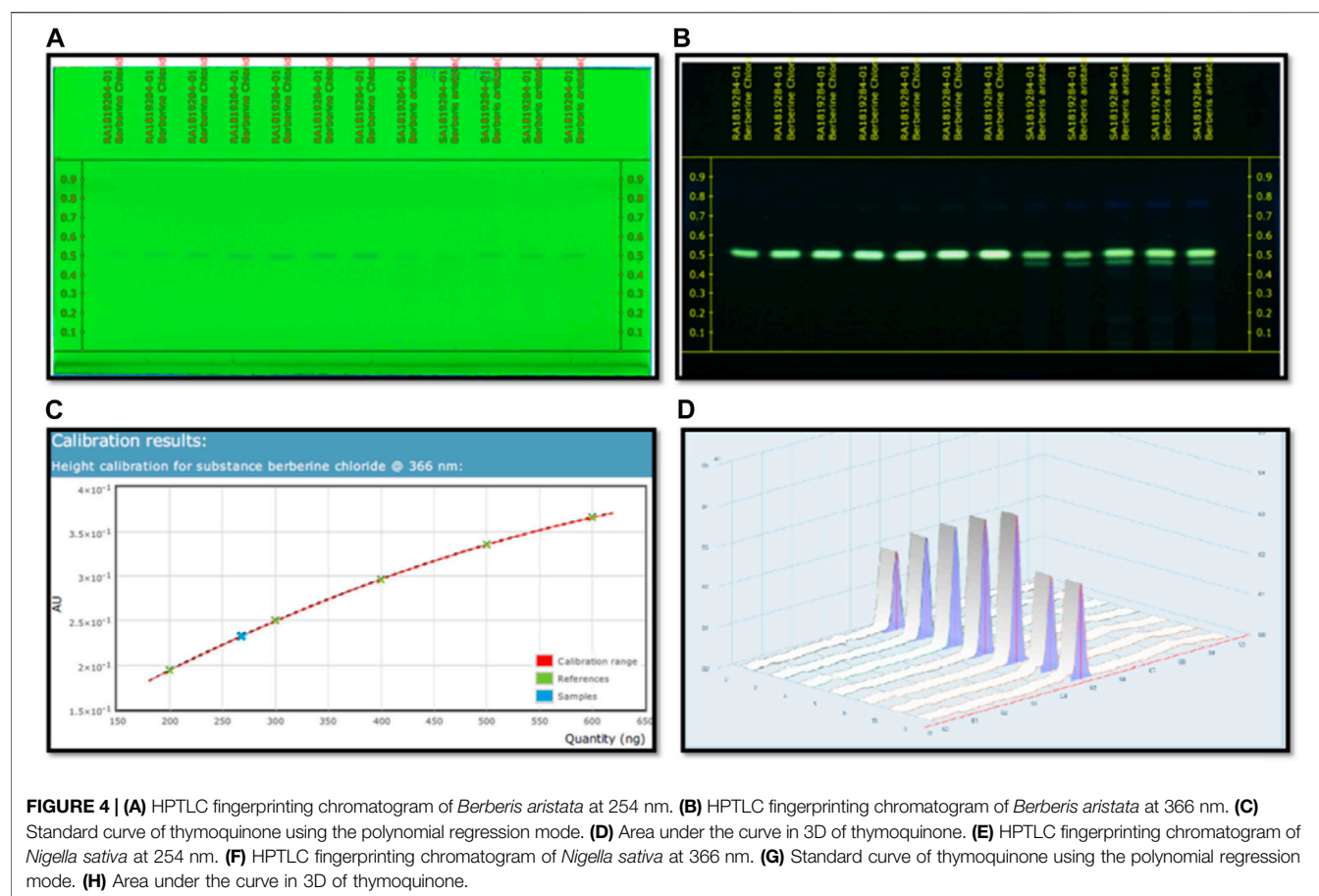
Mean Survival Time

A reliable criterion for judging the value of any anticancer drug is prolongation of the life span. Anastrazole showed the highest increase in life span of tumor-bearing animals and significantly increased the mean survival time (MST) to 112 days. Neither the BA extract nor the NS extract was not as effective as anastrazole and increased the MST to only 107 and 108 days; however, their marker compounds thymoquinone and berberine showed potential increment in MST. The higher rate of reduction in tumor volume indicated that *B. aristata* and *N. sativa* played a direct role in killing tumor cells and enhanced the curative effect of tumor chemotherapy. A decrease in tumor volume mentioned

above reduced the tumor burden and might have enhanced the life span of the tumor-bearing mice (Figure 5) and increased the MST (16).

Hematology

The elevated white blood cell (WBC) count in tumor-bearing mice was significantly reduced by anastrazole, thymoquinone, and berberine and relatively less reduced by the *B. aristata* and *N. sativa* extract treatments, which were significant ($p < 0.05$) and potentially reversed the tumor-induced rise in total counts of WBC (Figure 6B). However, the extracts were not as efficacious as anastrazole in reversing the tumor-induced total counts.



The anastrozole, thymoquinone, and berberine treatments inhibit tumor cell growth, enhance the survival of treated mice, and restore the hematological parameters. Thus, the present study suggested that *B. aristata* and *N. sativa* possess potent antitumor activity and increase the life span of the treated animal. However *B. aristata* (400 mg/kg) shows more significant antitumor activity among all test extract groups in the animal study. Usually, in cancer chemotherapy, the major problems that are being encountered are myelosuppression and anemia, but the results have clearly shown that BS and NS treatments have brought back not only the hemoglobin content to normal but also the red blood cell (RBC) count to normal (Figure 6C). Anastrozole as well as the extracts reversed these changes significantly ($p < 0.05$). However, the extracts were less efficacious than anastrozole in their effects, but their respective marker compounds showed relatively good effects on the RBC count ($p < 0.05$). Tumor development in the animals caused significant anemia (a decrease in hemoglobin content), while anastrozole treatment reversed this significantly ($p < 0.05$). The treatments with α -pinene, β -pinene, and the *N. sativa* extract failed to correct the anemia (Figures 6A,C), but thymoquinone, berberine, and the *B. aristata* extract were found to be significant ($p < 0.05$). Analysis of the hematological parameters showed a minimum toxic effect

in the mice, which were treated with both extracts (Figures 6A–C).

HISTOLOGY AND IMMUNOHISTOCHEMISTRY

A variety of herbal extracts were practiced for treating a number of diseases affecting the human body. Therefore, the objective of the current study was to evaluate the efficacy of *N. sativa* and *B. aristata* extracts on suppressing the several underlying tumor pathologies. For *in vivo* experiments, the DMBA mouse model was used to evaluate the protective effects of the lead herbal extracts (Russo et al., 2000). Active proliferation of the terminal ducts in the breast tissue for the mouse becomes very susceptible to carcinogens and tumor development (Ariazi et al., 2005). The histopathological examination of the current study revealed that DMBA-treated mice supplemented with TQ, the berberine NS extract, NS oil, and BA extracts showed suppression in the progress of the tumor cell proliferation (Figures 7D,G,H,J). In agreement with our findings (19), there was a limitation in the neoplastic changes during the sequential steps of carcinogenesis in DMBA-treated male Syrian hamsters supplemented with *N. sativa*. Another study found that the anticarcinogenic efficiency of *N. sativa*

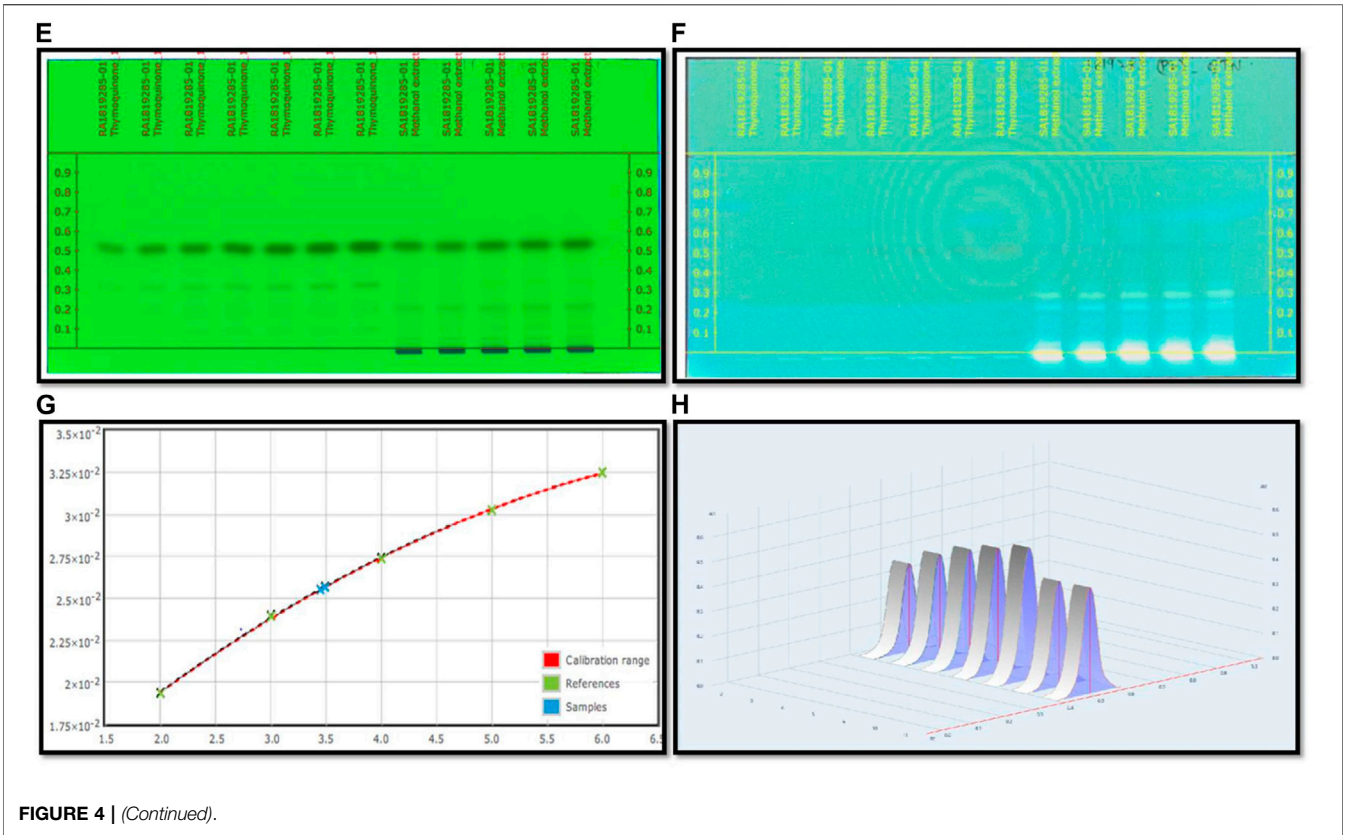
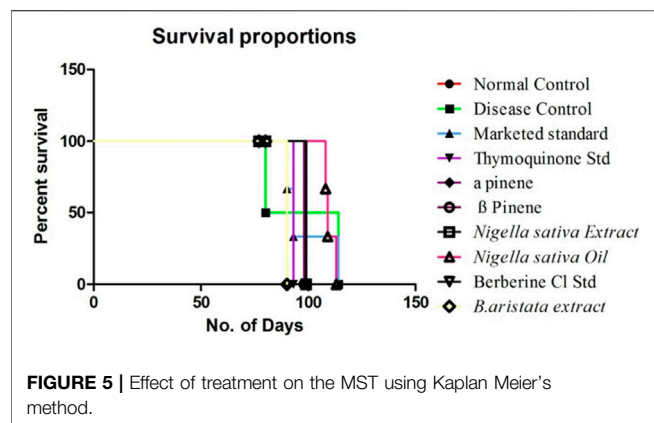


TABLE 5 Composition of <i>N. sativa</i> oil: integration peak, R time, area, and % area.						
Peak	R. Time	Area	Area%	Name	CAS No. (FFNSC 2 Lib)	
1	6.532	3,008,277	0.36	Thujene α	2867-05-2 (FFNSC 2 Lib)	
2	6.813	75,532,375	8.93	Bicyclo[3.1.1]hept-2-ene, 2,6,6-trimethyl-80-56-8 (FFNSC 2 Lib)		
3	7.308	1,063,045	0.13	Camphene α	79-92-5 (FFNSC 2 Lib)	
4	8.414	115,567,825	13.66	Pinene oxide β	6931-54-0 (FFNSC 2 Lib)	
5	10.244	9,042,970	1.07	Cymene <para>	99-87-6 (FFNSC 2 Lib)	
6	10.408	342,467	0.04	Cyclohexene, 1-methyl-4-(1-methylethenyl)-,(S)-	5989-54-8 (FFNSC 2 Lib)	
7	13.368	4,033,463	0.48	3-Oxatricyclo[4.1.1.0(2,4)]octane, 2,7,7-trimethyl-	1686-14-2 (FFNSC 2 Lib)	
8	13.904	2,122,686	0.25	Pinene oxide α	1686-14-2 (FFNSC 2 Lib)	
9	14.261	1,263,376	0.15	(1R,4R,5S)-1-Isopropyl-4-methoxy-4-methylbicyclo[3.1.0]hexane	11001111-06-5(FFNSC 2 Lib) 11	
10	15.158	365,669	0.04	Nopinone	24,903-95-5 (FFNSC 2 Lib)	
11	15.330	2,293,068	0.27	Pinocarveol	5947-36-4 (FFNSC 2 Lib)	
12	16.227	1,444,460	0.17	Pinocarvone	30,460-92-5 (FFNSC 2 Lib)	
13	17.736	2,646,046	0.31	Myrtenal	564-94-3 (FFNSC 2 Lib)	
14	18.319	835,255	0.10	Verbenone	80-57-9 (FFNSC 2 Lib)	
15	20.305	6,423,268	0.76	Thymoquinone	6617-34-1 (NIST14 Lib)	
16	22.575	568,936	0.07	Thujyl acetate <neoiso-3-> DB5-1081 (Classical name = neo-3-)	0-00-0(SZTERP Lib)	
17	22.869	876,235	0.10	Pinocarveol <trans-> DB5-724	0-00-0(SZTERP Lib)	
18	26.892	1,176,740	0.14	(+)-Longifolene	475-20-70(NIST14s Lib)	
19	34.853	462,953	0.05	Dodecane	112-40-3 (FFNSC 2 Lib)	
20	41.091	397,933	0.05	Tetradecanoic acid	544-63-8 (FFNSC 2 Lib)	
21	48.341	48,096,480	5.69	Hexadecanoic acid	57-10-3 (FFNSC 2 Lib)	
22	51.439	2,139,770	0.25	9,12-Octadecadienoic acid (Z,Z)-, methyl ester	56,599-58-7 (NIST14 Lib)	
23	51.653	5,090,837	0.60	9-Undecenal, 2,10-dimethyl-	0—00-0 (NIST14 Lib)	
24	54.211	560,235,582	66.24	Linoleic acid	506—21-8 (NIST14 Lib)	
25	61.160	478,053	0.06	3-Cyclopentylpropionic acid, 2-dimethylaminoethyl ester	0-00-0 (NIST14 Lib)	
26	65.858	278,309	0.03	Squalene	1111-02-4 (NIST14 Lib)	
	Total	845,786,078	100.00			



was found with the increase of glutathione-S-transferase activity (Aruna and Sivaramakrishnan, 1990). In line with these findings, the results of the current study found that NS oil and TQ were able to decrease the progress of tumors as well as decrease the values of TNF- α . Treatment with pure anastrozole caused partial necrosis of tumor tissues remaining in the form of “islands” (Figure 7C) and no effect observed with the vehicle-treated group, and a significant therapeutic effect was observed in tumor tissues after treatment with anastrozole, thymoquinone, and berberine (Figures 7C, D, I). We observed tumor cells with cytoplasm vacuolization and signs of karyolysis and inflammatory lymphocytic infiltration expressed weakly around the tumor (Figure 7B).

In our experiments, treatments with α - and β -pinene administered to mice did not induce changes in histology compared to the normal control group treated with the vehicle (Figures 7E–F). Protective effects could be explained by the ability of phytoconstituents (berberine) to inhibit the tumor cell target, which could account for the observed cancer protective potential of *B. aristata* that is pro-apoptotic and endowed with cell cycle arrest properties. However, anastrozole (1 mg/kg), berberine (30 mg/kg), and the *B. aristata* extract (400 mg/kg) against DMBA induced significantly improved tumor pathology. The ductal epithelial cells were bigger than normal cells and had an increased cytoplasm nucleus, which was observed in the group treated with the *B. aristata* extract.

Immunohistochemistry

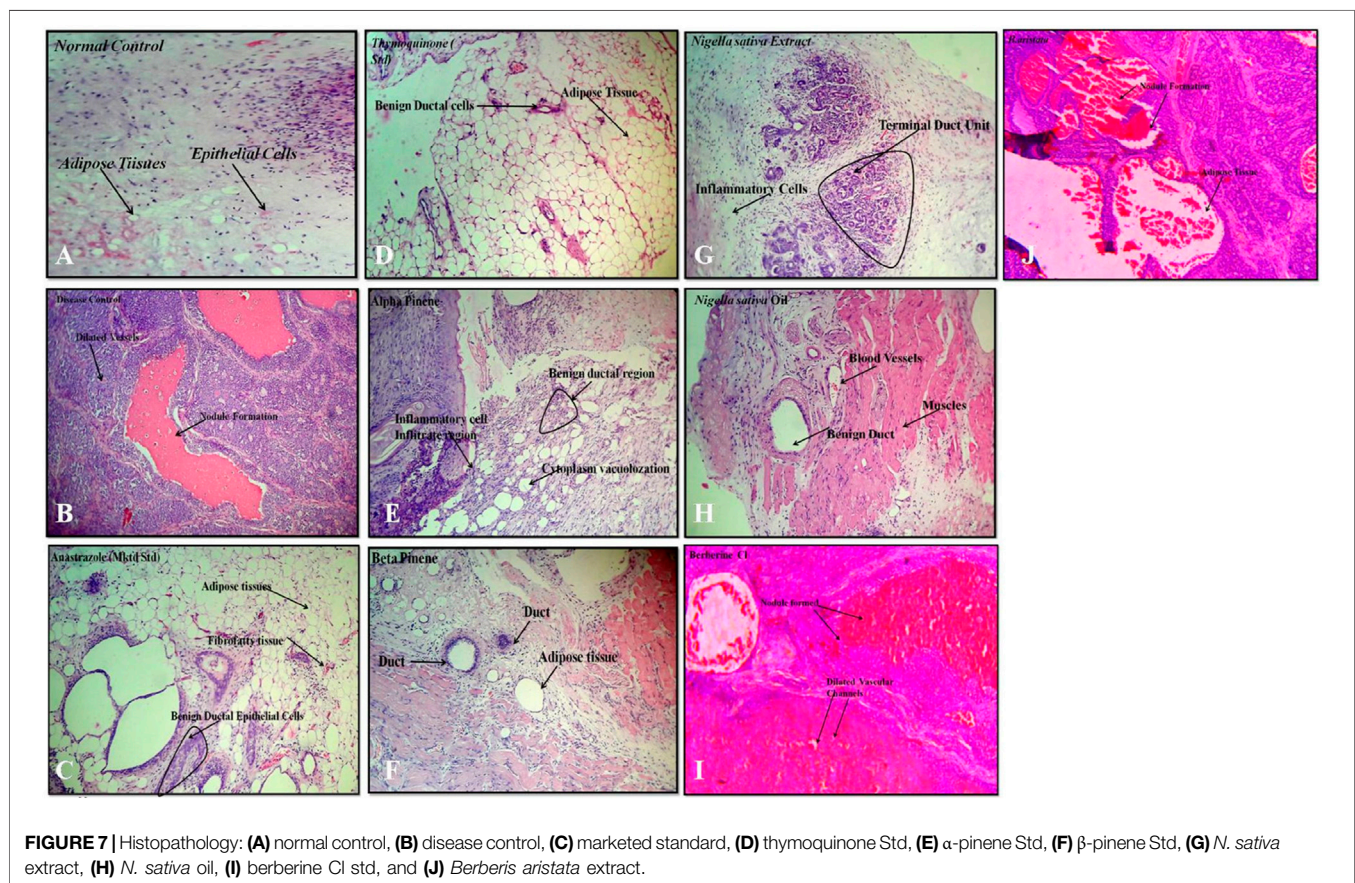
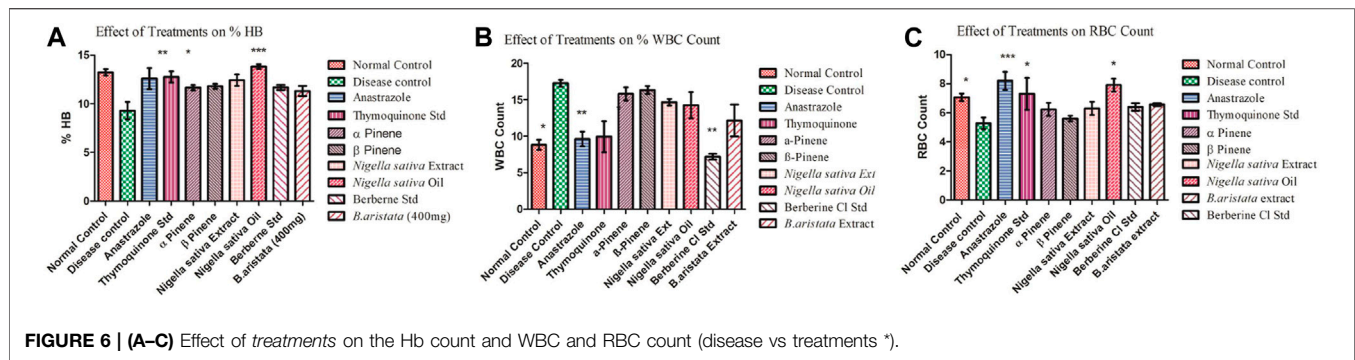
Tumor necrosis factor alpha (TNF- α) is a master pro-inflammatory cytokine and multifunctional cytokine involved in apoptosis, inflammation, and immunity (21). TNF- α has been reported to be elevated in the serum of patients diagnosed with advanced stages and correlate with an increased number and size of metastatic sites (Berberoglu et al., 2004). Therefore, the TNF-TNFR2 axis was implicated in the suppression of immune response and affects tumor progression and metastasis (Mantovani et al., 2008). In the following sections, we will interpret a possible role of targeting TNF- α interactions with the herbal extract

platform in the tumor. Positive staining for TNF- α was observed in all the groups (Figures 8B–J), except that the normal control group showed the negative expressions (Figure 8A). In the disease control group treated with the vehicle, the strong positive expressions of TNF- α were shown (Figure 8B); however, the group treated with anastrozole showed the least expression for TNF- α (Figure 8C) and thus an increase in MST. On comparing the group treated with the thymoquinone standard, α - and β -pinene with the *N. sativa* extract and NS oil were more promising and showed potency in reducing TNF- α , but NS oil has relatively less expression than the *N. sativa* extract. α - and β -pinene showed moderate TNF- α on comparing with the anastrozole-treated group.

Results depict that NS oil showed less TNF- α expression, that is, its phytoconstituent contained thymoquinone, and thus enabled an increase in the MST. The pure compound has better efficacy and potency among all the other standard compounds, and NS oil showed more efficacy due to the presence of thymoquinone. Now, comparing the standard treated group (Figure 8C) with pure berberine (30 mg/kg) and *B. aristata* (400 mg/kg) among test compounds, pure berberine showed (Figure 8I) moderately strong cytoplasmic positivity for TNF- α in the ductal epithelial cells; however, treatment with the *B. aristata* extract showed (Figure 8J) less strong cytoplasmic positivity for TNF- α . On the basis of TNF- α expression, pure compounds have more antitumor potency against the extracts. The increased levels of TNF- α in the DMBA group, as compared to the control group, agree with the findings of other studies (Ardizzoia et al., 1992; Bower et al., 2002). This high level may be due to increased production by the tumor-infiltrating lymphocytes and/or by the tumor cells (Lind et al., 1993; Kopreski et al., 1996).

Vascular Endothelial Growth Factor

VEGF is a potent angiogenic factor and upregulated in many tumors, and its contribution to tumor angiogenesis is well defined. It is the key mediator of angiogenesis and binds two VEGF receptors (VEGF receptor-1 and VEGF receptor-2), which are expressed on vascular endothelial cells. Different agents including antibodies, aptamers, peptides, and small molecules have been extensively investigated to block VEGF and its pro-angiogenic functions. For multicellular tumor clones to grow beyond this size, they must recruit new blood vessels by angiogenesis and vasculogenesis. In the present study, all tumor disease controls (Figures 9B) to treatments (Figures 9C–J) were found to be VEGF-positive, which is in agreement with previous reports. Not only does VEGF have a direct influence on breast cancer invasion and migration but also it has been shown to act as a survival factor for metastatic breast carcinoma cells (Pidgeon et al., 2001). Studies in the laboratory have shown that VEGF protects both human and murine breast carcinoma cells from apoptosis (Chung et al., 2002). The standard group showed (Figure 9C) very weak cytoplasmic positivity for VEGF in the ductal epithelial cells on comparing with the disease control group (Figure 9B). This indistinct feature elaborates the



potential role of VEGF in tumor pathogenesis with the past studies (Torres et al., 2016). Thymoquinone showed (Figure 9D) poor positive expression of VEGF in the ductal epithelial cells, which is similar to other studies that proved that thymoquinone attenuated tumorigenic signaling, including those controlled by EGF, FGF, VEGF, TGF, and various metastatic, angiogenic, and pro-mitogenic factors (Rashid et al., 2019). α-pinene (Figure 9E) showed moderately strong cytoplasmic positivity for VEGF in the ductal epithelial cells and β-pinene (Figure 9F) depicted moderately strong cytoplasmic positivity for VEGF in the ductal epithelial cells, which mean that these isomers have

less affinity toward the VEGF receptors and thus are unable to cause the apoptotic action in tumor tissues. The *N. sativa* extract (Figure 9G) and NS oil (Figure 9H) show moderate cytoplasmic positivity for VEGF in the ductal epithelial cells; thus, the NS extract and NS oil have anti-VEGF potential in this regime (Zhang et al., 2014) and demonstrated that berberine inhibits the expression of hypoxia-inducible factor 1α and increases the expression level of VEGF in prostate cancer. Therefore, the anticancer effect of berberine hydrochloride on tumor cells may occur via the activation of the VEGF signaling pathway. The berberine Cl Std (Figure 9I) tissue shows moderately strong cytoplasmic positivity for VEGF in

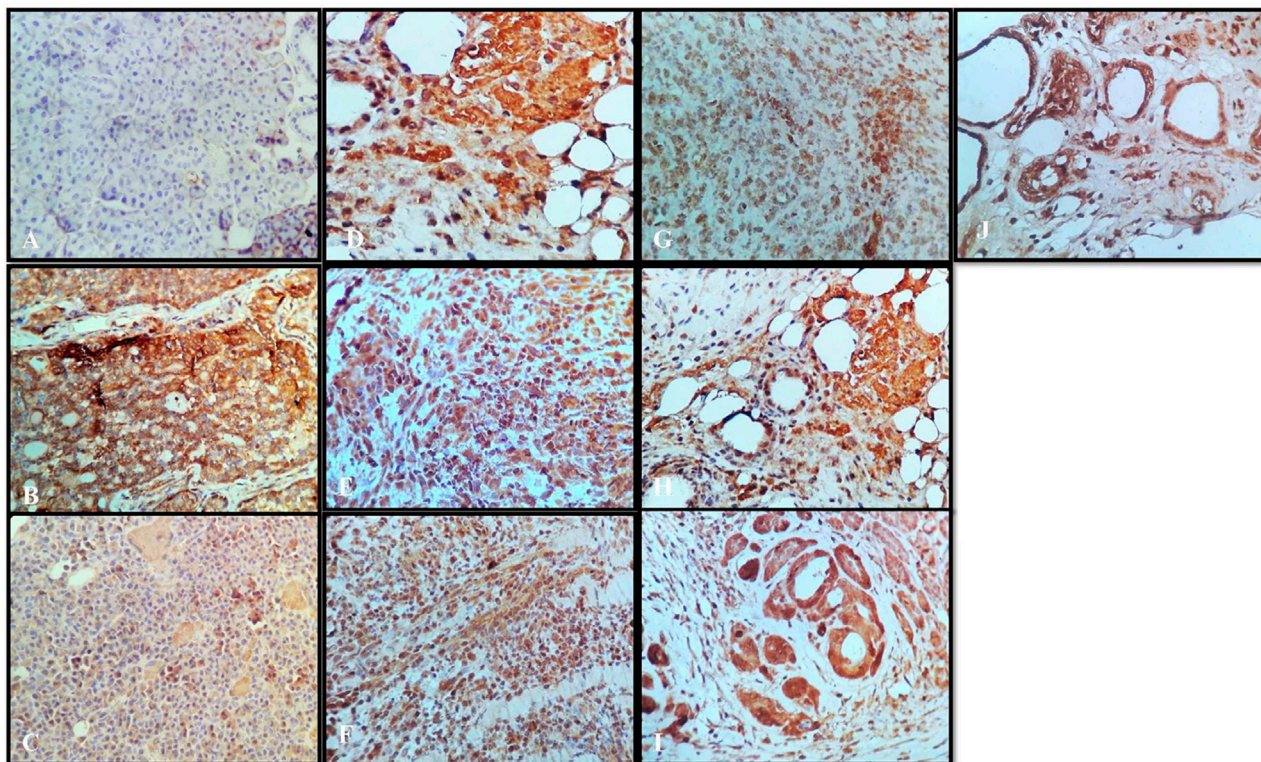


FIGURE 8 | Immunohistochemistry TNF- α : (A) normal control, (B) disease control, (C) marketed standard, (D) thymoquinone Std, (E) α -pinene Std, (F) β -pinene Std, (G) *N. sativa* extract, (H) *N. sativa* oil, (I) berberine Cl Std, and (J) *Berberis aristata* extract.

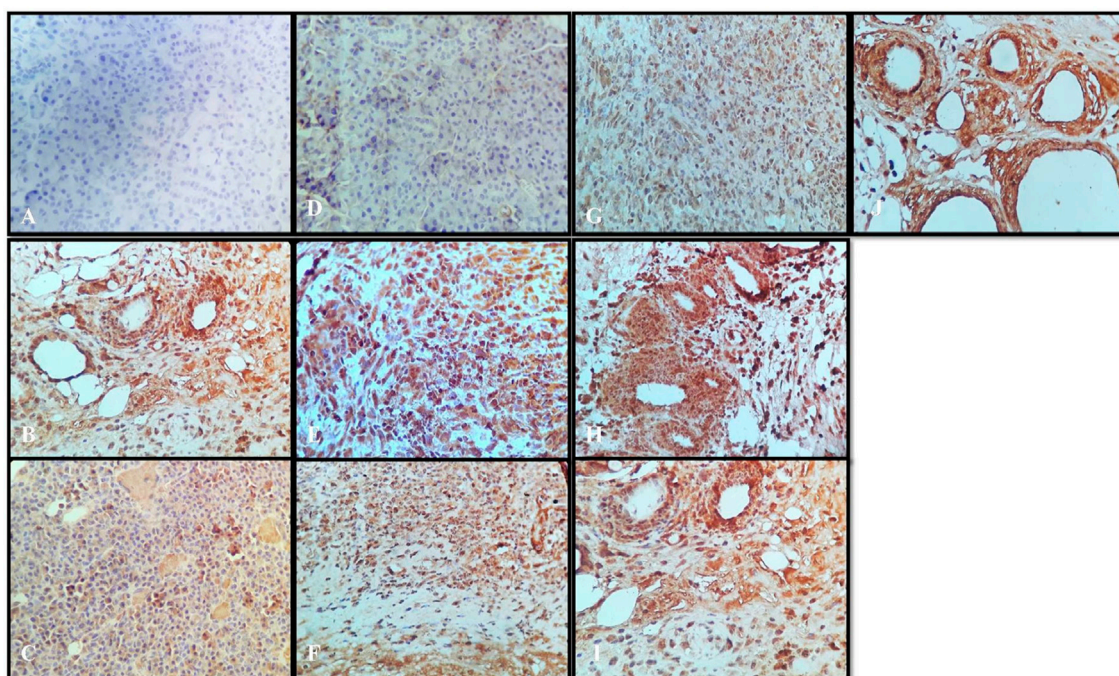


FIGURE 9 | Immunohistochemistry VEGF: (A) normal control, (B) disease control, (C) marketed standard, (D) Thymoquinone Std, (E) α -pinene Std, (F) β -pinene Std, (G) *N. sativa* extract, (H) *N. sativa* oil, (I) berberine Cl Std, (J) *Berberis aristata* extract.

the ductal epithelial cells; however, the *B. aristata* extract (**Figure 9J**) depicted weak cytoplasmic positivity for VEGF.

CONCLUSION

In conclusion, the results of the present study give clear evidence that the *N. sativa* extract and *B. aristata* extract and their marker compounds thymoquinone, \pm pinene, and berberine Cl induce no harmful effects on female mice. Moreover, they exert a protective effect against the DMBA-induced tumor model. The antioxidant property is mediated by their actions and investigating other underlying mechanisms, merits, and further studies. The present study thus demonstrated the chemopreventive potential of thymoquinone, \pm pinene and berberine Cl in the DMBA-induced tumor model. Despite the exact mechanism of action of chemopreventive potential of marker compounds, the antilipidperoxidative, antioxidant, and modulating effects on the detoxification cascade could play a possible role.

DATA AVAILABILITY STATEMENT

The raw data supporting the conclusions of this article will be made available by the authors, without undue reservation.

REFERENCES

- Ahmad, A., Husain, A., Mujeeb, M., Khan, S. A., Najmi, A. K., Siddique, N. A., et al. (2013). A Review on Therapeutic Potential of Nigella Sativa: A Miracle Herb. *Asian Pac. J. Trop. Biomed.* 3 (5), 337–352. doi:10.1016/s2221-1691(13)60075-1
- Alhaj, N. A., Shamsudin, M. N., Zamri, H. F., and Abdullah, R. (2008). Extraction of Essential Oil from Nigella Sativa Using Supercritical Carbon Dioxide: Study of Antibacterial Activity. *Am. J. Pharmacol. Toxicol.* 3, 225–228. doi:10.3844/ajptsp.2008.225.228
- Ardizzoia, A., Lissoni, P., Brivio, F., Tisi, E., Perego, M. S., Grassi, M. G., et al. (1992). Tumor Necrosis Factor in Solid Tumors: Increased Blood Levels in the Metastatic Disease. *J. Biol. Regul. Homeost. Agents* 6 (3), 103–107.
- Ariazi, J. L., Haag, J. D., Lindstrom, M. J., and Gould, M. N. (2005). Mammary Glands of Sexually Immature Rats Are More Susceptible Than Those of Mature Rats to the Carcinogenic, Lethal, and Mutagenic Effects of N-Nitroso-N-Methylurea. *Mol. Carcinog.* 43 (3), 155–164. doi:10.1002/mc.20104
- Aruna, K., and Sivaramakrishnan, V. M. (1990). Plant Products as Protective Agents against Cancer. *Indian J. Exp. Biol.* 28 (11), 1008–1011.
- Banchroff, J., Steven, A., and Turner, D. (1996). *Theory and Practice of Histopathological Techniques*. New York, London, San Francisco, Tokyo: Churchill Livingstone.
- Berberoglu, U., Yildirim, E., and Celen, O. (2004). Serum Levels of Tumor Necrosis Factor Alpha Correlate with Response to Neoadjuvant Chemotherapy in Locally Advanced Breast Cancer. *Int. J. Biol. Markers* 19 (2), 130–134. doi:10.1177/172460080401900207
- Bors, W. (1996). *Flavonoids and Polyphenols: Chemistry and Biology*. Japan: Handbook of antioxidants, 409–411. doi:10.1016/s1074-5521(96)90124-6
- Bower, J. E., Ganz, P. A., Aziz, N., and Fahey, J. L. (2002). Fatigue and Proinflammatory Cytokine Activity in Breast Cancer Survivors. *Psychosomatic Med.* 64 (4), 604–611. doi:10.1097/00006842-200207000-00010
- Brand-Williams, W., Cuvelier, M. E., and Berset, C. (1995). Use of a Free Radical Method to Evaluate Antioxidant Activity. *LWT - Food Sci. Tech.* 28 (1), 25–30. doi:10.1016/s0023-6438(95)80008-5

ETHICS STATEMENT

The animal study was reviewed and approved by the Delhi Institute of Pharmaceutical research.

AUTHOR CONTRIBUTIONS

MM, research planning and conduction, data collection, data analysis and interpretation, drafting the article, critical revision of the article, and final approval of the version to be published; SA, conception or design of the work.

ACKNOWLEDGMENTS

We are thankful to India Pharmacopeia Commission and Anchrom Laboratory Mumbai for helping in the HPTLC analysis.

SUPPLEMENTARY MATERIAL

The Supplementary Material for this article can be found online at: <https://www.frontiersin.org/articles/10.3389/fphar.2021.642067/full#supplementary-material>

- Choudhary, N., and Sekhon, B. S. (2011). An Overview of Advances in the Standardization of Herbal Drugs. *J. Pharm. Edu. Res.* 2 (2), 55.
- Chung, T. K. H., Cheung, T. H., Lo, W. K., Yim, S. F., Yu, M. Y., Krajewski, S., et al. (2002). Expression of Apoptotic Regulators and Their Significance in Cervical Cancer. *Cancer Lett.* 180 (1), 63–68. doi:10.1016/s0304-3835(01)00842-4
- Clarke, R. B., Howell, A., Potten, C. S., and Anderson, E. (1997). Dissociation between Steroid Receptor Expression and Cell Proliferation in the Human Breast. *Cancer Res.* 57 (22), 4987–4991.
- Ezeome, E. R., and Anarado, A. N. (2007). Use of Complementary and Alternative Medicine by Cancer Patients at the University of Nigeria Teaching Hospital, Enugu, Nigeria. *BMC Complement. Altern. Med.* 7, 28. doi:10.1186/1472-6882-7-28
- Kennedy, J. (2005). Herb and Supplement Use in the US Adult Population. *Clin. Ther.* 27 (11), 1847–1858. doi:10.1016/j.clinthera.2005.11.004
- Khan, W., Chester, K., Anjum, V., Ahmad, W., Ahmad, S., Narwaria, A., et al. (2017). Chromatographic Profiling of Pancharishta at Different Stages of its Development Using HPTLC, HPLC, GC-MS and UPLC-MS. *Phytochemistry Lett.* 20, 391–400. doi:10.1016/j.phytol.2017.04.034
- Khurm, M., Chaudhry, B., Uzair, M., and Janbaz, K. (2016). Antimicrobial, Cytotoxic, Phytotoxic and Antioxidant Potential of Heliotropium Strigosum Willd. *Medicines* 3 (3), 20. doi:10.3390/medicines3030020
- Kopreski, M. S., Lipton, A., Harvey, H. A., and Kumar, R. (1996). Growth Inhibition of Breast Cancer Cell Lines by Combinations of Anti-p185her2 Monoclonal Antibody and Cytokines. *Anticancer Res.* 16 (1), 433–436.
- Lind, D. S., Tuttle, T. M., Bethke, K. P., Frank, J. L., McCrady, C. W., and Bear, H. D. (1993). Expansion and Tumour Specific Cytokine Secretion of Bryostatin-Activated T-Cells from Cryopreserved Axillary Lymph Nodes of Breast Cancer Patients. *Surg. Oncol.* 2 (5), 273–282. doi:10.1016/s0960-7404(06)80002-2
- Liu, Y., Chen, G., Ma, C., Bower, K. A., Xu, M., Fan, Z., et al. (2009). Overexpression of Glycogen Synthase Kinase 3 β Sensitizes Neuronal Cells to Ethanol Toxicity. *J. Neurosci. Res.* 87 (12), 2793–2802. doi:10.1002/jnr.22098
- Mantovani, A., Allavena, P., Sica, A., and Balkwill, F. (2008). Cancer-related Inflammation. *nature* 454 (7203), 436–444. doi:10.1038/nature07205
- Nair, C. J., Ahamad, S., Khan, W., Anjum, V., and Mathur, R. (2018). Gas Chromatography-Mass Spectrometric Determination of Components of Leaves of Aegle Marmelos and Psidium Guajava and Seeds of Nigella Sativa and Correlation with In Vitro Antioxidant Activity. *Pharmacognosy Res.* 10 (2), 230.

- Organization, W. H. (2007). *WHO Guidelines on Good Manufacturing Practices (GMP) for Herbal Medicines*. Geneva: World Health Organization.
- Pasrija, A., Singh, R., and Katiyar, C. K. (2010). Validated HPLC-UV Method for the Determination of Berberine in Raw Herb Daruharidra (Berberis Aristata DC), its Extract, and in Commercially Marketed Ayurvedic Dosage Forms. *Int. J. Ayurveda Res.* 1 (4), 243–246. doi:10.4103/0974-7788.76789
- Pidgeon, G. P., Barr, M. P., Harmey, J. H., Foley, D. A., and Bouchier-Hayes, D. J. (2001). Vascular Endothelial Growth Factor (VEGF) Upregulates BCL-2 and Inhibits Apoptosis in Human and Murine Mammary Adenocarcinoma Cells. *Br. J. Cancer* 85 (2), 273–278. doi:10.1054/bjoc.2001.1876
- Rashid, M., Sanjarin, F., and Sabouni, F. (2019). Thymoquinone Effects on Cell Viability, Apoptosis and VEGF-A Gene Expression Level in AGS(CRL-1739) Cell Line. *Acamc* 19 (6), 820–826. doi:10.2174/1871520619666190206163504
- Russo, J., Hu, Y.-F., Yang, X., and Russo, I. H. (2000). Chapter 1: Developmental, Cellular, and Molecular Basis of Human Breast Cancer. *JNCI Monogr.* 2000 (27), 17–37. doi:10.1093/oxfordjournals.jncimonographs.a024241
- Saied, S., Batool, S., and Naz, S. (2007). Phytochemical Studies of Berberis Aristata. *J. Basic Appl. Sci.*, 1–3.
- Salem, M. L., Alenzi, F. Q., and Attia, W. Y. (2011). Thymoquinone, the Active Ingredient of Nigella Sativaseeds, Enhances Survival and Activity of Antigen-specific CD8-Positive T Cells in Vitro. *Br. J. Biomed. Sci.* 68 (3), 131–137. doi:10.1080/09674845.2011.11730340
- Torres, A., Vargas, Y., Uribe, D., Carrasco, C., Torres, C., Rocha, R., et al. (2016). Pro-apoptotic and Anti-angiogenic Properties of the α/β -Thujone Fraction from Thuja Occidentalis on Glioblastoma Cells. *J. Neurooncol.* 128 (1), 9–19. doi:10.1007/s11060-016-2076-2
- Wanebo, H. J., and Clarkson, B. D. (1965). Essential Macroglobulinemia. *Ann. Intern. Med.* 62 (5), 1025–1045. doi:10.7326/0003-4819-62-5-1025
- Zhang, Q., Zhang, C., Yang, X., Yang, B., Wang, J., Kang, Y., et al. (2014). Berberine Inhibits the Expression of Hypoxia Induction Factor-1alpha and Increases the Radiosensitivity of Prostate Cancer. *Diagn. Pathol.* 9 (1), 98. doi:10.1186/1746-1596-9-98

Conflict of Interest: The authors declare that the research was conducted in the absence of any commercial or financial relationships that could be construed as a potential conflict of interest.

Publisher's Note: All claims expressed in this article are solely those of the authors and do not necessarily represent those of their affiliated organizations or those of the publisher, the editors, and the reviewers. Any product that may be evaluated in this article or claim that may be made by its manufacturer is not guaranteed or endorsed by the publisher.

Copyright © 2021 Mazhar and Agrawal. This is an open-access article distributed under the terms of the Creative Commons Attribution License (CC BY). The use, distribution or reproduction in other forums is permitted, provided the original author(s) and the copyright owner(s) are credited and that the original publication in this journal is cited, in accordance with accepted academic practice. No use, distribution or reproduction is permitted which does not comply with these terms.



Metabolomic Profiling and Immunomodulatory Activity of a Polyherbal Combination in Cyclophosphamide-Induced Immunosuppressed Mice

Sultan Zahiruddin¹, Abida Parveen^{1,2}, Washim Khan^{1,3†}, Mohammad Ibrahim¹, Muzamil Y. Want⁴, Rabea Parveen^{1,5} and Sayeed Ahmad^{1*}

¹Bioactive Natural Product Laboratory, Department of Pharmacognosy and Phytochemistry, School of Pharmaceutical Education and Research, Jamia Hamdard, New Delhi, India, ²Department of Clinical Research, School of Interdisciplinary Sciences and Technology, Jamia Hamdard, New Delhi, India, ³National Center for Natural Products Research, School of Pharmacy, University of Mississippi, Oxford, MS, United States, ⁴Roswell Park Comprehensive Cancer Center, Buffalo, NY, United States, ⁵Department of Biosciences, Jamia Millia Islamia, New Delhi, India

OPEN ACCESS

Edited by:

Michael Heinrich,
UCL School of Pharmacy,
United Kingdom

Reviewed by:

Amit Krishna De,
Indian Science Congress Association,
India
Amitabha Dey,
Pfizer, India
Sharad Srivastava,
Council of Scientific and Industrial
Research (CSIR), India

*Correspondence:

Sayeed Ahmad
sahmad_jh@yahoo.co.in

†Present address:

Washim Khan

Specialty section:

This article was submitted to
Ethnopharmacology,
a section of the journal
Frontiers in Pharmacology

Received: 29 December 2020

Accepted: 18 November 2021

Published: 03 January 2022

Citation:

Zahiruddin S, Parveen A, Khan W,
Ibrahim M, Want MY, Parveen R and
Ahmad S (2022) Metabolomic Profiling
and Immunomodulatory Activity of a
Polyherbal Combination in
Cyclophosphamide-Induced
Immunosuppressed Mice.
Front. Pharmacol. 12:647244.
doi: 10.3389/fphar.2021.647244

The study was aimed to develop a characterized polyherbal combination as an immunomodulator containing *Phyllanthus emblica* L., *Piper nigrum* L., *Withania somnifera* (L.) Dunal, and *Tinospora cordifolia* (Willd.) Miers. Through response surface methodology (RSM), the ratio of aqueous extracts of four plant materials was optimized and comprised 49.76% of *P. emblica*, 1.35% of *P. nigrum*, 5.41% of *W. somnifera*, and 43.43% of *T. cordifolia* for optimum immunomodulatory activity. The optimized combination showed antioxidant potential and contains more than 180 metabolites, out of which gallic acid, quercetin, ellagic acid, caffeic acid, kaempferitrin, and *p*-coumaric acid are some common and significant metabolites found in plant extracts and in polyherbal combination. Treatment with the polyherbal combination of different doses in cyclophosphamide-induced immunosuppressed mice significantly ($p < 0.01$) enhanced the subsets of immune cells such as natural killer (NK) cells (60%), B cells (18%), CD4 cells (14%), and CD8 cells (7%). The characterized polyherbal combination exhibited potent immunomodulatory activity, which can be further explored clinically for its therapeutic applicability.

Keywords: metabolomics, immunomodulatory activity, splenocyte, *Phyllanthus emblica*, *Withania somnifera*, *Tinospora cordifolia*

INTRODUCTION

Herbs are in increasing demand in developed and developing countries for primary health care. Plant-based products have been extensively exploited as an essential source for drugs because of their biological activities and higher safety margins. Immunomodulation using medicinal plants can provide a substitute for conventional therapy for a variety of diseases, especially when the host's defense mechanism has to be generated under the conditions of an impaired immune response (Ganju et al., 2003). People, every year, turn to herbal medicine because they believe that plant remedies are free from undesirable side effects. It is also known that herbs have been used in

traditional systems of medicine as an immunomodulator for a decade (Kumar et al., 2012; Nagoba and Davane, 2018). Plant extracts have been proven for their activity in boosting the humoral (Rehman et al., 1999) as well as cell-mediated immunity against viruses, bacteria, fungi, and cancer (Sarvanandaa et al., 2018). In the Indian traditional system of medicine, several food-grade plants have been used as immunomodulators, and most of them were proven individually for their immune-enhancing effect. The bioactive constituents of these plants that are responsible for the activity were also determined. In recent years, many herbs from the Indian system of medicine that modulate the immune system of the body were scientifically validated. Some herbs such as *Phyllanthus emblica* L. (family: Phyllanthaceae) (Liu et al., 2012), *Piper nigrum* L. (family: Piperaceae) (Majdalawieh and Carr, 2010), *Tinospora cordifolia* (Willd.) Miers (family: Menispermaceae) (Mathew and Kuttan, 1999), *Withania somnifera* (L.) Dunal (family: Solanaceae) (Davis and Kuttan, 2000), *Curcuma longa* L. (family: Zingiberaceae) (Kim et al., 2014), *Ocimum sanctum* L. (family: Lamiaceae) (Mondal et al., 2011), *Azadirachta indica* A. Juss. (family: Meliaceae) (van der Nat et al., 1987), *Achilla millefolium* L. (family: Asteraceae) (Mohammed Al-Ezzy et al., 2018), and many more are the reported herbs exhibiting excellent immunomodulatory activity. Based on our preliminary study, we focused only on the first four plants, namely, *P. emblica*, *P. nigrum*, *T. cordifolia*, and *W. somnifera*.

P. emblica, Indian gooseberry, is an essential medicinal plant in the Indian traditional system of medicine and is used as a dietary combination. It has various properties that can combat age-related illnesses such as cancer, cardiac diseases, renal failure, immune deficiency, arthritis, cataracts, and wrinkling of the skin (Mathai et al., 2015). *T. cordifolia* is of great interest to scientists around the world due to its anti-inflammatory, antiarthritic, antioxidant, antiallergic, antistress, antileprotic, antimalarial, hepatoprotective, immunomodulatory activities (More and Pai, 2011; Alsuhaibani and Khan, 2017). The modern medical literature, as well as traditional medical literature, reports many potential health benefits of *W. somnifera* in stress, neurotoxicity, and immune disorders (Singh et al., 2011; Zahiruddin et al., 2020). *P. nigrum* is used extensively as a spice around the world and in traditional medicine as an antioxidant, antimicrobial, anticarcinogenic, anti-inflammatory, and gastroprotective drug (Parveen et al., 2015; Bui et al., 2019). These four selected plant extracts were further subjected to optimization of the ratio by response surface methodology (RSM) to develop a polyherbal combination.

Across the globe, several herbal formulations are being sold claiming to be immunomodulators. Vivartana, Chyawanprash, Brahma Rasayana, IM-133, and Septilin are the few formulations used in the Indian traditional system of medicine, which have been experimentally proven as immunomodulators (Gnanasekaran et al., 2015). But these formulations have not been fully explored scientifically, and the dose and frequency of these formulations are much higher than those of modern medicines. In the present study, we selected eight traditionally used plants according to the literature reported for

immunomodulatory activity, and out of eight, only four named *P. emblica*, *P. nigrum*, *T. cordifolia*, and *W. somnifera* were found to be the best immunomodulators in our preliminary studies. These four selected plants were used to develop a polyherbal combination. The proposed study aims to develop a polyherbal combination as an immunomodulator, which can be used for the management of immunity for the prevention of various bacterial and viral infections. This herbal combination has been chromatographically characterized and scientifically validated through *in vitro* and *in vivo* experiments.

METHODOLOGY

Collection of Plant Materials

The fruits of *P. emblica*, *P. nigrum*, stem of *T. cordifolia*, and roots of *W. somnifera* were purchased from Universal Biotech, Farash Khana, Delhi, India. The voucher specimens (*P. emblica*-BNPL/JH/Ph.D/12/17/01, *T. cordifolia*-BNPL/JH/Ph.D/12/17/02, *W. somnifera*-BNPL/JH/Ph.D/12/17/03, and *P. nigrum*-BNPL/JH/Ph.D/12/17/04) of each plant material have been deposited in the Bioactive Natural Product Laboratory (BNPL), Jamia Hamdard, New Delhi, India, for future reference.

Preparation of the Extract

Accurately weighed 150 g of powder of each plant material were divided into three equal parts. These were macerated overnight using water, ethanol, and 50% ethanol to form aqueous extract (AE), ethanolic extract (EE), and hydroethanolic extract (HEE), respectively. The EE and HEE were further refluxed for 3 h after maceration. All three extracts were filtered, and the filtrate was evaporated to dryness under reduced pressure. The extractive values and percentage yields of different extracts were calculated and stored at 4°C for further analysis.

Quantitative Analysis of Specific Marker Compounds From Raw Extracts

Gallic acid, piperine, berberine, and withaferin-A were selected as specific marker compounds for fruits of *P. emblica*, *P. nigrum*, stem of *T. cordifolia*, and roots of *W. somnifera*, respectively (Chatterjee et al., 2012; Gorgani et al., 2017; Neag et al., 2018; Tiwari et al., 2018). These markers were quantified using high-performance thin-layer chromatography (HPTLC). Ten milligrams of each extract were dissolved separately in high-performance liquid chromatography (HPLC)-grade methanol to get 10-mg/ml solutions. The stock solutions of standard gallic acid, berberine, piperine, and withaferin-A (Sigma Aldrich, India) were prepared in HPLC-grade methanol to get a concentration of 500 µg/ml. The prepared samples were filtered using a 0.2-µm polytetrafluoroethylene (PTFE) membrane filter before HPTLC analysis. The prepared extracts and standards were applied separately on Silica gel 60 F254 precoated TLC plates, 10 cm × 10 cm (Merck, Germany), with the help of a Camag Linomat (CAMAG, Switzerland) applicator with nitrogen flow providing a delivery speed of 120 nl/s from the syringe. Toluene:ethyl acetate:formic acid (5:4:1; v/v/v) were used as developing solvents for

TABLE 1 | Four-variable Box–Behnken design with experimental and predicted values of pinocytic and splenocyte proliferation of different combinations of aqueous extracts.

Run no.	Concentration of aqueous extract (mg)				Pinocytic activity		Splenocyte proliferation	
	A	B	C	D	Predicted	Actual	Predicted	Actual
1	100	6	455	333	0.028	0.058	0.027	0.012
2	1,000	6	455	333	0.027	0.019	0.180	0.220
3	100	60	455	333	0.017	0.004	0.055	0.110
4	1,000	60	455	333	0.180	0.150	0.031	0.081
5	550	33	10	6	0.004	0.033	0.260	0.240
6	550	33	900	6	0.059	0.051	0.240	0.270
7	550	33	10	660	0.078	0.076	0.240	0.320
8	550	33	900	660	0.110	0.067	0.047	0.160
9	100	33	455	6	0.022	0.001	0.140	0.077
10	1,000	33	455	6	0.067	0.083	0.240	0.260
11	100	33	455	660	0.055	0.053	0.240	0.160
12	1,000	33	455	660	0.055	0.091	0.140	0.150
13	550	6	10	333	0.059	0.070	0.280	0.270
14	550	60	10	333	0.029	0.040	0.220	0.180
15	550	6	900	333	0.005	0.007	0.140	0.130
16	550	60	900	333	0.110	0.110	0.240	0.190
17	100	33	10	333	0.028	0.017	0.052	0.120
18	1,000	33	10	333	0.170	0.130	0.320	0.250
19	100	33	900	333	0.062	0.071	0.074	0.100
20	1,000	33	900	333	0.039	0.048	0.260	0.150
21	550	6	455	6	0.020	0.008	0.160	0.190
22	550	60	455	6	0.070	0.077	0.230	0.220
23	550	6	455	660	0.063	0.070	0.270	0.230
24	550	60	455	660	0.048	0.074	0.230	0.160
25	550	33	455	333	0.120	0.057	0.260	0.230
26	550	33	455	333	0.071	0.057	0.230	0.230
27	550	33	455	333	0.012	0.057	0.240	0.230
28	550	33	455	333	0.100	0.057	0.290	0.230
29	550	33	455	333	0.005	0.057	0.120	0.230

A: *P. emblica*; B: *P. nigrum*; C: *W. somnifera*; D: *T. cordifolia*. Levels for *P. emblica* concentration are 100 mg (–1), 550 mg (0), and 1,000 mg (+1); for *P. nigrum* are 6 mg (–1), 33 mg (0), and 60 mg (+1); for *W. somnifera* are 10 mg (–1), 455 mg (0), and 900 mg (+1); and for *T. cordifolia* are 6 mg (–1), 333 mg (0), and 660 mg (+1).

gallic acid, piperine, and withaferin-A. For berberine, *n*-butanol:water:acetic acid (4:5:1; v/v/v) was used as a developing solvent. Plates were developed horizontally in a CAMAG twin trough glass chamber (10 cm × 10 cm), which was presaturated with the mobile phase for 30 min. The developed plates were air-dried and scanned by CAMAG TLC densitometric scanner III operated by WinCATs software. Gallic acid and piperine were scanned at 254 nm, while berberine was scanned at 366 nm. For quantitative analysis of withaferin-A, the air-dried plate was derivatized by dipping in 5% anisaldehyde sulfuric acid solution and scanned at 540 nm.

Response Surface Methodology for Optimization of Extract Ratio

RSM was used to optimize the ratio of four extracts, which is a collection of statistical techniques to design experiments, build models, evaluate the effect of factors, and find the optimum conditions. Four extracts at three different concentration levels were combined by Box–Behnken response surface design (BBD), where pinocytic activity in macrophages and splenocyte proliferation assay were taken as the response of different combinations. Different concentrations of the aqueous extract of *P. emblica*, *P. nigrum*, *W. somnifera*, and *T. cordifolia* were

selected to optimize the effective concentration. The dose of each selected plant extract was calculated from its extractive values, which is equivalent to the dose mentioned in Ayurveda Pharmacopoeia of the respective plant materials. The selected concentrations for *P. emblica* were 100 mg (–1), 550 mg (0), and 1,000 mg (+1); concentrations of *P. nigrum* were 6 mg (–1), 33 mg (0), and 60 mg (+1); concentrations of *W. somnifera* were 10 mg (–1), 455 mg (0), and 900 mg (+1); and the concentration levels for *T. cordifolia* were 6 mg (–1), 333 mg (0), and 660 mg (+1). A total of 29 experimental combinations with three central points were generated through BBD using Design Expert 8.0.1.7 software (Stat-Ease Inc., USA), and all these combinations were tested for their pinocytic activity in macrophages and splenocyte proliferation assay (Table 1). The point prediction tool of the software determined an optimum value of the factors for the maximum *in vitro* immunomodulatory activity.

Metabolomic Profiling of Extracts and the Developed Polyherbal Combination by Ultra-Performance Liquid Chromatography-Mass Spectrometry

The optimized polyherbal combination and four aqueous extracts used to make the polyherbal combination were dissolved

separately in LC-MS-grade methanol and filtered through a 0.2- μ m membrane filter. The filtered solutions were diluted in a ratio of 1:5 (v/v) using methanol. High-throughput profiling of metabolites was carried out by ultra-performance liquid chromatography-mass spectrometry (UPLC-MS) (Zahiruddin et al., 2017). The UPLC was performed on a Water's ACQUITY UPLCTM system (Serial No. F09 UPB 920M; Model code # UPB, Waters Corp., MA, USA) equipped with a binary solvent delivery system, an auto-sampler, column manager, and a tunable MS detector (Serial No. JAA 272; Synapt; Waters, Manchester, UK) installed and controlled by Mass Lynx V 4.1 (Waters, USA). Data acquisition has been carried out in positive modes. Chromatography was performed using acetonitrile (A) and water (B) as the mobile phase on a monolithic capillary silica-based C18 column [ACQUITY UPLC(R) BEH C18, 1.7 μ m, 2.1 \times 100 mm], with the pre-column split ratio of 1:5 min at ambient temperature. Chromatographic separation was achieved by gradient elution mode (initially, 10% A; 0–5 min 40% A; 5–10 min 60% A; 10–13 min, 90% A; 13–15 min, 100% A; 15–16 min 10% A), and the total run time was 16 min. The flow rate of the nebulizer gas was set at 10 μ l/min; for the cone gas, set to 50 L/h, and the source temperature was set at 100°C. The cone and capillary voltages were set to 40.0 and 3.0 kV, respectively. For collision, argon was employed at a pressure of 5.3×10^{-5} Torr. The accurate mass and composition for the precursor ions and the fragment ions were calculated using the Mass Lynx V 4.1 software incorporated in the instrument.

Raw data obtained from UPLC-MS analysis were processed in Progenesis Software (Waters, USA). By using this software, the maximum number of mass peaks was detected, which were further identified through the library based on their molecular weight. Chromatographically separated and identified metabolites were matched with the plant's native metabolites. All detected metabolites were processed in XLStat software for statistical differentiation between the plants used for the development of polyherbal combination. A metabolite-based comparison was performed in different extracts to identify the major metabolites present in the specific plant extract.

Characterization of Polyherbal Combination Determination of Total Phenol and Flavonoid Contents

The total phenol content (TPC) and the total flavonoid content (TFC) of the polyherbal combination were determined using the Folin–Ciocalteu (FC) and aluminum chloride methods, respectively (Khan et al., 2017). The optimized combination was dissolved in methanol to prepare 5 mg/ml. For the determination of the total phenolic content (TPC), 500 μ l of methanolic solution (5 mg/ml) was thoroughly mixed with 2.5 ml FC and 2.5 ml of sodium carbonate (7.5% w/v). The mixture was incubated for 30 min at room temperature, and after incubation, absorbance was measured at 765 nm. For the determination of the TFC, 0.1 ml of aluminum chloride (10% w/v) and 0.1 ml of potassium acetate (0.1 mM) were added in 500 μ l of sample solution (5 mg/ml). The resulting mixture solution was kept at room temperature for 30 min, and absorbance was measured at 415 nm. TPC and TFC were calculated from the calibration curve

of gallic acid and rutin (Sigma Aldrich, India), respectively, and the results were expressed as milligrams gallic acid and rutin, respectively, equivalent per gram weight of the polyherbal combination.

Antioxidant Activity of the Optimized Combination

The antioxidant potential of the developed polyherbal combination was determined by measuring the scavenging potential of 2,2-diphenyl-1-picrylhydrazyl (DPPH; SRL, India). One milliliter of freshly prepared DPPH solution (0.3 mM in methanol) was mixed with 1.0 ml of optimized combination dissolved in water. The resulting mixture was kept at room temperature in the dark for 25 min, and after incubation, absorbance was recorded at 515 nm. Different concentrations of optimized combinations were used to determine DPPH radical scavenging activity (Liu et al., 2009). The ability of the sample to scavenge the DPPH radicals was calculated using the following formula:

$$\text{DPPH radical scavenging effect} = (A_{\text{control}} - A_{\text{sample}}) \times 100 / A_{\text{control}}$$

where A_{control} is the absorbance of the DPPH solution without polyherbal combination; A_{sample} is the absorbance of the sample with DPPH solution.

To determine the reducing power, 500 μ l of an aqueous solution of the optimized combination was thoroughly mixed with 2.5 ml of potassium ferricyanide (1% w/w) and 2.5 ml of phosphate buffer (pH 6.6), and the mixture was incubated for 30 min in a water bath at 50°C. After incubation, the mixture was cooled, and 2.5 ml of trichloroacetic acid (10% w/v in water) was added. Furthermore, it was centrifuged and the supernatant was diluted with an equal amount of deionized water, and freshly prepared 0.5 ml of ferric chloride (0.1% w/w) was added. The mixture was thoroughly mixed, and its absorbance was measured at 700 nm (Bhalodia et al., 2013). For control, water was used in place of an optimized combination, and the reducing power was compared with the control. For both assays, ascorbic acid was used as a positive control.

In Vitro Immunomodulatory Activity of the Developed Polyherbal Combination Animals

BALB/c mice (6 weeks old, 25 ± 5 g) were provided by Central Animal House Facility, Jamia Hamdard (Registration No. 173/GO/RE/S/2000/CPCSEA). Before initiation of the experiment, all experimental protocols were approved by the Institutional Animal Ethics Committee, and the experiments were strictly carried out according to the guidelines of the committee (Animal Approval Number 1551). The animals were housed in a polypropylene cage and placed in the experimental room, where they were allowed to acclimatize for a week before the experiment. An air conditioning unit (with 10% air exchange per hour) was maintained along with a relative humidity of 50 ± 10 RH, 12/12 h light–dark cycle, and a temperature of $25^\circ\text{C} \pm 2^\circ\text{C}$ was kept in the animal house facility throughout the experimental period.

Splenocyte Proliferation Assay

BALB/c mice were euthanized, and the spleen was removed aseptically for isolation of splenocytes. The spleen was further homogenized using sterile phosphate-buffered saline (PBS) by passing it through a mesh (0.4 microns) and centrifuged at $300 \times g$ for 5 min. Red blood cells (RBCs) were lysed from the cell pellet by adding 500 μ l of lysis buffer (Tris-HCl-NH₄Cl, pH 7.2). The reaction was stopped by adding Roswell Park Memorial Institute (RPMI) medium (RPMI-1640, Millipore Sigma Aldrich, India) and washed two times to remove any debris. The cell pellet was resuspended in RPMI medium to get 3.0×10^6 cells/ml, and 100 μ l of cell suspension was seeded per well in a 96-well plate. Here, 25 μ l of mitogen concanavalin A (Con A; 2.0 μ g/ml) was added, and 25 μ l of the polyherbal combination was added to the cells per well containing splenocytes and incubated at 37°C in a CO₂ incubator for 72 h. After incubation, 20 μ l of tetrazolium dye 3-(4,5-dimethylthiazol-2-yl)-2,5-diphenyltetrazolium bromide (MTT) were added and incubated at 37°C, 5% CO₂ for another 6 h. Furthermore, the tetrazolium crystals formed in live cells were dissolved after 6 h of incubation, and cell proliferation was measured at 490 nm using a microplate reader (Shi and Fu, 2011). The media treated with polyherbal combination was used as a negative control, and spleen cell treated with levamisole was used as the positive control.

Pinocytic Activity Assay

One milliliter of thioglycolate (1.0 mg/ml in PBS) was injected intraperitoneally (i.p.) in 2 mice, and peritoneal macrophages were isolated after 48 h by injecting PBS into the peritoneal cavity. Isolated macrophages were washed twice with media and resuspended at 1.0×10^6 cells/ml in RPMI medium containing 10% fetal bovine serum (FBS). Here, 200 μ l of cells were transferred to 96-well plates and incubated overnight at 37°C, 5% CO₂ to allow macrophages to adhere to the plate. Non-adherent cells were gently washed with RPMI medium, and 100 μ l of fresh RPMI medium was added to each well. Furthermore, 25 μ l of the polyherbal combination was added to the cells in each well and incubated for 48 h at 5% CO₂ and 37°C. After incubation, 100 μ l of neutral red solution (0.1% in 10 mM PBS) was added, and after 2 h of incubation, a free neutral red solution was removed by gently washing the cells with PBS. The macrophages were further lysed by adding 100 μ l of neutral red detainer (ethanol and 0.1% acetic acid in a ratio of 1:1, v/v) and incubated at room temperature overnight, and optical density was recorded the next day at 540 nm (Shi and Fu, 2011). For negative control, RPMI medium was used in place of the combination, and the results were expressed as compared to the negative control.

Immunoprotective Effect of the Polyherbal Combination

To determine the effect of the developed polyherbal combination on the immune system, BALB/c mice (25 ± 5 g) were used for the study. Animals were randomly divided into seven groups consisting of six animals per group. Groups I–III received normal saline for 14 days, and group I served as normal control. In addition to normal saline, Groups II and III received polyherbal combination at an oral dose of

260 and 520 mg/kg, respectively, for 14 days. Groups II and III served as a sham control of the polyherbal combination. Groups IV–VII received cyclophosphamide (80 mg/kg, i.p.) for 4 days of the experimental period (from days 8 to 11), followed by a washout and normalization period of cyclophosphamide for 3 days. In addition to cyclophosphamide, Group IV received normal saline throughout the experimental period and served as a toxic control; Group V and Group VI received polyherbal combination orally at a dose of 260 and 520 mg/kg, respectively; Group VII received levamisole hydrochloride at a dose of 10 mg/kg orally for 14 days and served as a positive control. The oral dose of the polyherbal combination was decided on the basis of the RSM result and administered as a suspension in 0.1% carboxymethylcellulose. At the end of the experiment, blood samples were collected from each animal from the retro-orbital vein and used for further analysis.

Determination of Fluorocytometry-Based Immunological Parameters

Blood samples were collected at the end of the 14-day study period in anticoagulant-containing collection tubes. The RBCs were lysed using ammonium-chloride-potassium (ACK) lysis buffer for 10 min at room temperature, and the reaction was stopped by adding RPMI medium. For flow cytometry analysis, cells were washed twice with cold FACS buffer and pelleted by centrifugation at 400 g for 5 min. Cells were resuspended in FACS buffer containing antibodies at 1:100 dilution (CD3e-FITC, CD4-PE-Cy7, CD8-APC-Cy7, CD19-APC, and CD335-PE) and incubated for 25 min at 4°C in the dark. After the incubation period, cells were washed twice with FACS buffer and resuspended in 200 μ l of FACS buffer before being acquired on a BD LSR II flow cytometer (BD Bioscience, USA). Data were analyzed using FCS Express 7 Research Edition, and results were expressed in terms of percentage of CD4 cells, CD8 cells, natural killer (NK) cells, and B cells. The gating strategy for selected populations of T cells, B cells, and NK cells is shown in **Figure 1**.

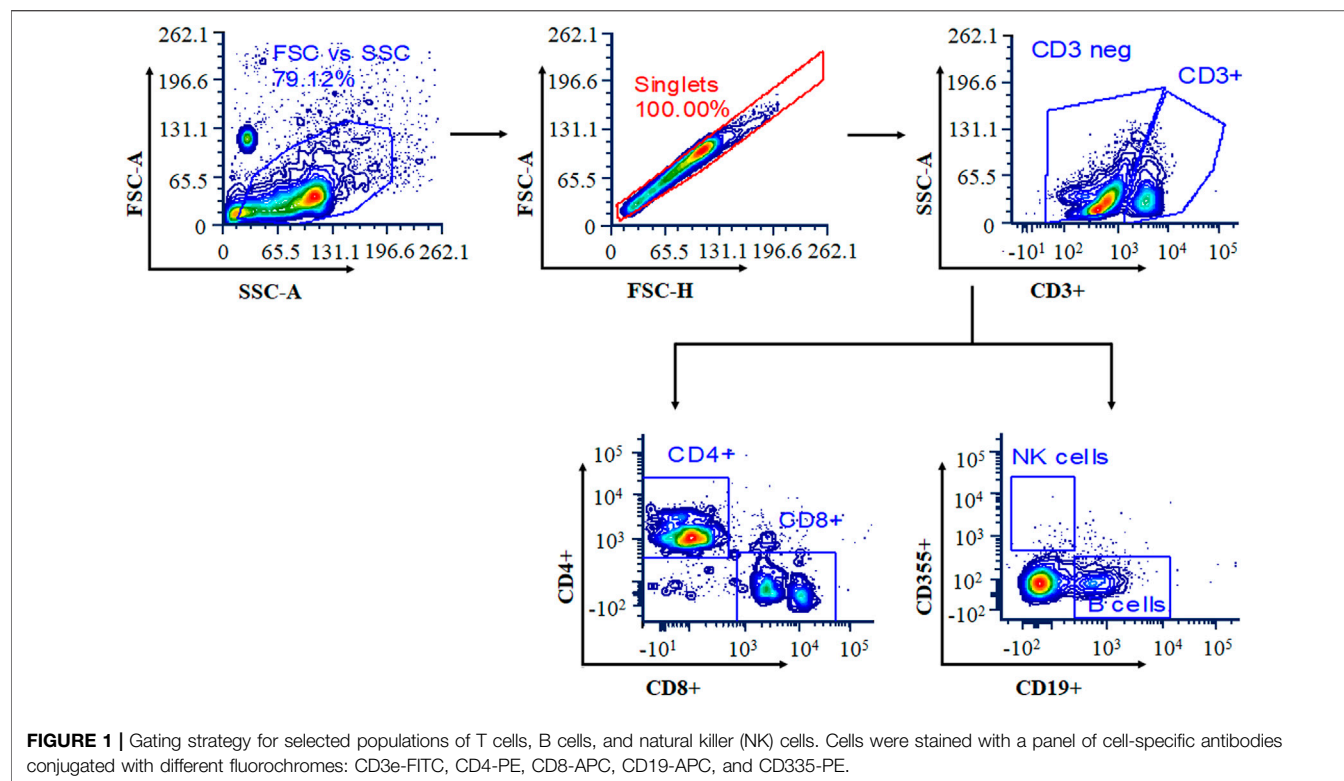
Determination of Hematological Parameters

Blood samples from mice were collected in a tube containing ethylenediaminetetraacetic acid (EDTA), and white blood cell (WBC), RBC, hemoglobin (HGB), and platelet (PLT) counts were determined using a fully automated hematology analyzer (XP 100, Sysmex, Japan) (Anjum et al., 2017).

Statistical Analysis

Data are shown as mean \pm SEM, and the difference between groups was analyzed by two-way ANOVA followed by Bonferroni posttest using GraphPad Prism 5.00. A p-value < 0.05 was considered statistically significant.

The ANOVA provision of Design Expert was used to establish statistical validation of the equation supplied by the software. Using BBD and the Design Expert 8.0.1.7 program (Stat-Ease Inc., USA), a total of 29 experimental combinations with three central points were created, and all of these combinations were evaluated for pinocytic activity and splenocyte proliferation assay. The models were assessed using R^2 values and statistically significant coefficients. The validation of the RSM results was carried out to determine the optimal combination compositions across the entire experimental



region. ANOVA was used to justify the inadequacies of the models. After fitting the data to multiple models (linear, 2FI, quadratic, and cubic) and performing an ANOVA, it was found that the quadratic polynomial and 2FI models were the best fit for the splenocyte proliferation assay and pinocytic activity, respectively. The experimental values of the reactions were compared to the expected values quantitatively. MS-Excel was also used to create linear regression charts between the actual and predicted response values. The Box-Cox plot was used to describe the appropriate power transformation of the response data.

Principal component analysis (PCA) is a powerful statistical tool for data analysis and expression that can highlight the similarities and differences of sets. Raw data obtained from the UPLC-MS analysis were processed in the Progenesis software (Waters, USA). Using this software, the maximum number of mass peaks can be captured and further identified by the library on the basis of their molecular weight. All detected metabolites are processed in the XLStat software to make a statistical difference between plants used to develop a polyherbal combination.

RESULTS

The plant materials used in the present study were authenticated according to the protocol of Indian Pharmacopoeia (Anonymous, 2010). The authenticated plant materials were extracted in three different solvents (aqueous, ethanol, and hydroethanol) by overnight maceration followed by reflux. We have evaluated aqueous, ethanolic, and hydroethanolic extracts from eight plants for their *in vitro* immunomodulatory activity. From eight plants, only

aqueous extracts of *P. emblica*, *T. cordifolia*, *W. somnifera*, and *P. nigrum* were found to be the best immunomodulators on the basis of their *in vitro* immunomodulatory activity and extractive yield.

Quantitative Estimation of Specific Markers

The aqueous extracts of four selected plants were chemically characterized by quantifying specific markers present in them. The linear regression calibration curves plotted between the peak area vs. concentration were linear for all standards, namely, gallic acid, berberine, piperine, and withaferin-A, with good linear relationships ($r^2 = 0.99$). Well-separated bands of gallic acid, berberine, piperine, and withaferin-A were visualized at R_f 0.44, 0.46, 0.69, and 0.35, respectively. HPTLC chromatograms of gallic acid, piperine, berberine, and withaferin-A in the optimized extract are shown in **Supplementary Figures S1–S4**. The percentages of gallic acid in *P. emblica*, piperine in *P. nigrum*, berberine in *T. cordifolia*, and withaferin-A in *W. somnifera* were found to be $5.01\% \pm 0.07\%$, $1.62\% \pm 0.01\%$, $1.04\% \pm 0.02\%$, and $2.35\% \pm 0.04\%$, respectively, of total weight (w/w).

Response Surface Methodology-Based Optimization of Extract Ratio for the Development of the Polyherbal Combination

The aqueous extracts of these four plants were optimized in ratios by RSM to develop a polyherbal combination. A BBD with three levels was used for all four extracts of *P. emblica* (A), *P. nigrum* (B), *W. somnifera* (C), and *T. cordifolia* (D) to finalize their ratio for the development of a polyherbal combination. The range of

TABLE 2 | ANOVA of the quadratic response surface model for splenocyte proliferation and response surface 2FI model for pinocytic activity in Box–Bhenken design experiments.

Parameters	For splenocyte proliferation	For pinocytic activity
Regression		
Sum of square	0.136	0.0402
Df	14	10
Mean squares	0.0097	0.004
F value	1.337	2.7203
P	0.297	0.0311
Residual		
Sum of square	0.102	0.0266
Df	14	18
Mean square	0.0073	0.00147
Lack of fit test		
Sum of square	0.0845	0.0126
Df	10	14
Mean squares	0.0084	0.0009
F value	1.901	0.2601
p-value	0.2805	0.973
Coefficient correlation (r^2)	0.572	0.6017
Coefficient of variation (CV %)	45.936	67.52
Adequate precision value	4.965 (>4)	7.221(>4)

variables, designs, and results obtained for splenocyte proliferation and pinocytic activity is presented in **Table 1**. The results were the average of three independent assays. The experimental results were modeled with a second-order quadratic and two-factor interaction (2FI) model to explain the dependence of *in vitro* immunomodulatory activity on different factors. The experimental data obtained from BBD to predict splenocyte proliferation and pinocytic activity are expressed by the following equation.

Splenocyte proliferation assay: $0.2292 + 0.04425 A - 0.009666667 B - 0.031833333 C - 0.0075 D - 0.05987 AB - 0.021125 AC - 0.0485 AD + 0.0395 BC - 0.024625 BD - 0.045375 CD - 0.080183333 A^2 - 0.042433333 B^2 + 0.005566667 C^2 + 0.013066667 D^2$.

Pinocytic activity: $0.056965517 + 0.029958333 A + 0.018291667 B + 0.002208333 C + 0.014791667 D + 0.04925 AB - 0.041375 AC - 0.011 AD + 0.0335 BC - 0.016375 BD - 0.00675 CD$.

ANOVA for optimizing the ratio of four extracts to develop a polyherbal combination showed that the regression model was significant and the lack of fit was insignificant for both the splenocyte proliferation assay and pinocytic activity (**Table 2**).

The Model F-value of 2.72 of pinocytic activity implies that the model is significant. There is only a 3.11% chance that a “Model F-value” this large could occur due to noise. The “Lack of Fit F-value” of 0.26 implies that the lack of fit is not significant relative to the pure error. A nonsignificant lack of fit is good for the model. The “Adeq Precision 7.22” indicating the excellent signal-to-noise ratio and >4 is desirable. This model is used to navigate the design space. However, for the splenocyte proliferation assay, the “Predicted R^2 ” of (−1.1524982) negative implies that the overall mean is a better predictor of the response than the current model. It showed Adeq precision of

4.96, indicating a good signal-to-noise ratio. **Figures 2, 3** are the three-dimensional (3D) representation of the interacting effect of different plant extracts on the proliferation of splenocytes and pinocytic activity, respectively. A contour plot is a two-dimensional (2D) representation of the responses plotted against a combination of numerical factors and/or mixture components. It shows the relationship between the responses, the mixture components, and/or the statistical elements. **Supplementary Figures S5–S6** represent the interactions among the various factors on splenocyte proliferation and pinocytic activity, respectively.

The optimal ratio of four different extracts for the maximum pinocytic activity and splenocyte proliferation assay was 49.76%, 1.35%, 5.41%, and 43.33% for *P. emblica*, *P. nigrum*, *W. somnifera*, and *T. cordifolia*, respectively. The defined polyherbal combination predicted an improvement in splenocyte proliferation up to 32.7% and pinocytic activity by 11.8%. These optimized values of the ratio of four extracts were validated by *in vitro* immunomodulatory activity. The statistically developed polyherbal combination exhibited a 34% increase in splenocyte cell proliferation and 10.7% pinocytic activity, indicating a 90%–115% validation of the predicted model.

Metabolomic Profiling of the Extract and the Developed Combination by Ultra-Performance Liquid Chromatography-Mass Spectrometry

UPLC-MS analysis files were processed through progenesis software to detect the maximum possible ions. Metlin, Massbank, and the chemical library were used to identify the ions and set tolerance levels below 10 ppm. In these four extracts and in combination, more than 5,000 ions were detected. These

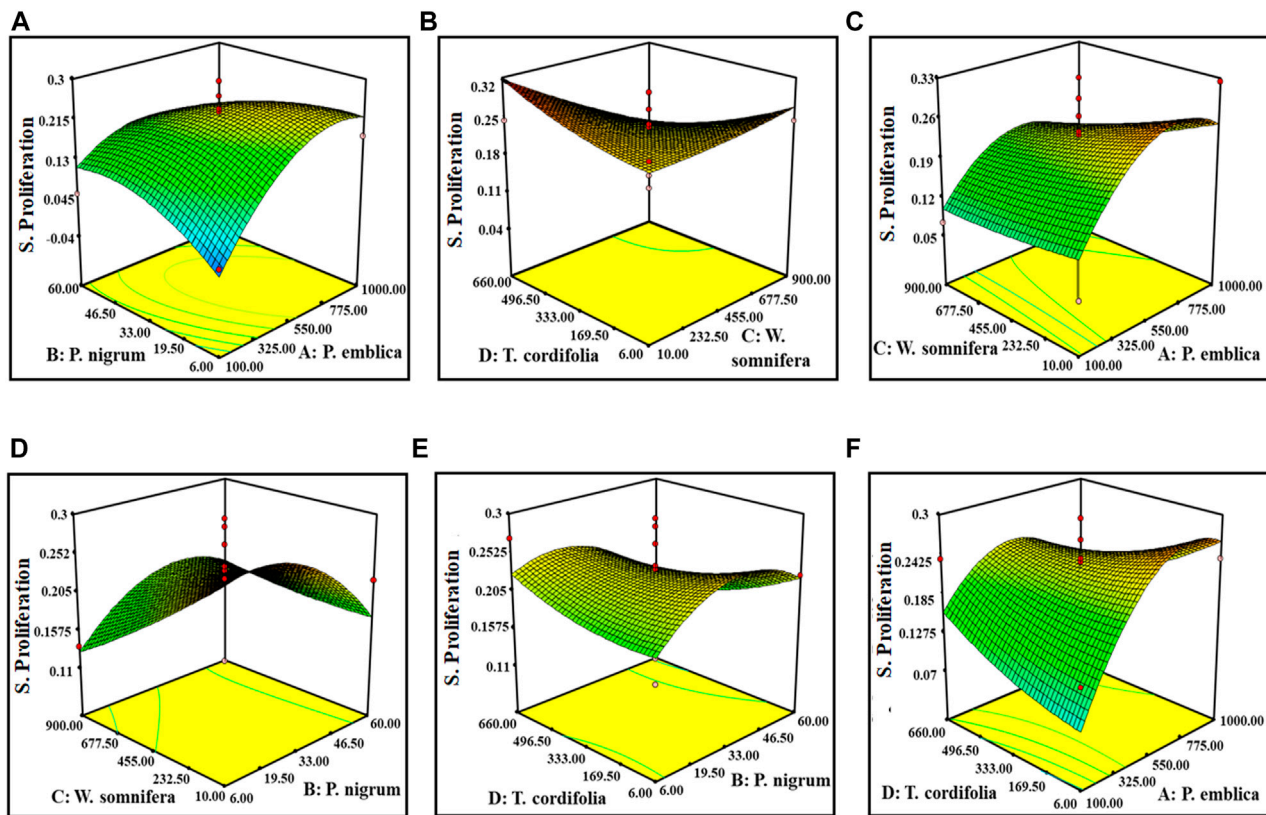


FIGURE 2 | Response surface graph showing the interaction among four extract concentrations and splenocyte proliferation activity. Interaction between (A) *P. emblica* and *P. nigrum*, (B) *P. emblica* and *W. somnifera*, (C) *P. emblica* and *T. cordifolia*, (D) *P. nigrum* and *W. somnifera*, (E) *P. nigrum* and *T. cordifolia*, and (F) *W. somnifera* and *T. cordifolia*.

ions were from molecular ion peaks and/or may be from the fragmentation of molecular ion peaks. All of these ions were detected and processed through progenesis software and identified by a database based on their m/z values. From the whole mass range, the detected ions were statistically differentiated through the S-plot, and the major metabolites causing differentiation between one extract and another were screened. The main abundant metabolites of the extracts and the combination are summarized in **Supplementary Table S1**. Most of the metabolites found are also reported in these plant extracts. Some common and major metabolites of *P. emblica* are phyllanemblin (R_t 1.25), gallic acid (R_t 2.08), quercetin (R_t 6.02), caffeic acid (R_t 4.59), ellagic acid (R_t 4.13), and punigluconin (R_t 8.05). Similarly, digallic acid (R_t 2.92), 7-hydroxyflavanone (R_t 2.92), caffeic acid (R_t 4.59), schaftoside (R_t 4.56), syringin (R_t 4.59), jatrorrhizine (R_t 4.40), and sinapic acid (R_t 1.65) are found in *T. cordifolia*. Withaferin (R_t 5.25), withanolide (R_t 7.35), chlorogenic acid (R_t 4.16), and anaferrine (R_t 6.30) were found in *W. somnifera*. Justicidin B (R_t 1.15), apiin (R_t 4.56), papaverine (R_t 4.78), piperazinamine (R_t 5.37), piperine (R_t 7.54), piperanine (R_t 9.78), and cubebin (R_t 7.69) are some metabolites found in *P. nigrum*. Some specific metabolites are found only in a single plant extract and a combination. The structure of major metabolites is summarized in **Supplementary**

Figure S7. However, the results of UPLC-MS analysis were processed through PCA. As per the PCA plots (**Supplementary Figure S8**), all the aqueous extracts show different types of metabolites, and it can be seen in the distribution of the aqueous extract in a different quadrant. All of these compounds are not being detected in combination due to their abundance in the extract. Several metabolites are also found in all extracts and in combination. Gallic acid (R_t 2.08), quercetin (R_t 6.02), ellagic acid (R_t 4.13), caffeic acid (R_t 4.59), kaempferitrin (R_t 5.02), and *p*-coumaric acid (R_t 1.25) are some common and significant metabolites also found in all the extracts and in combination.

Characterization of the Developed Polyherbal Combination

The optimized combination was characterized by determining their phenolic and flavonoid contents. Phenolic and flavonoid contents were expressed as gallic acid and rutin equivalent, respectively. The phenolic and flavonoid contents of the optimized combination were found to be 29.32% and 17.65% w/w of the polyherbal combination, respectively. The plants present in the polyherbal combination are the most abundant sources of phenolic and flavonoid metabolites, which may be

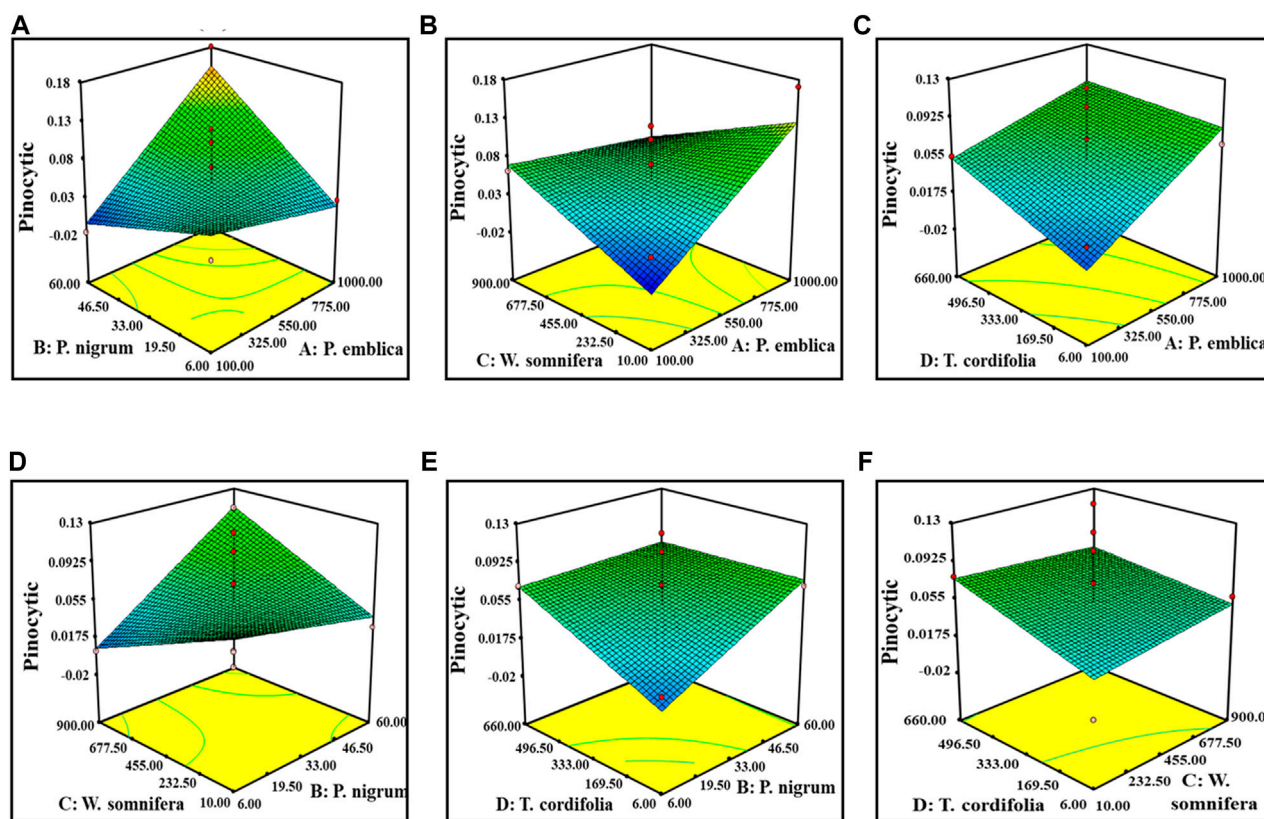


FIGURE 3 | Response surface graph showing the interaction among four extract concentrations and pinocytic activity. Interaction between (A) *P. emblica* and *P. nigrum*, (B) *P. emblica* and *W. somnifera*, (C) *P. emblica* and *T. cordifolia*, (D) *P. nigrum* and *W. somnifera*, (E) *P. nigrum* and *T. cordifolia*, and (F) *W. somnifera* and *T. cordifolia*.

responsible for their bioactivity (Mishra et al., 2013; Zhang et al., 2017; Tungmunthum et al., 2018).

The developed polyherbal combination showed a potent DPPH radical scavenging potential, and IC_{50} was recorded as 82.54 ± 2.54 $\mu\text{g/ml}$ and was comparable to a standard antioxidant compound, ascorbic acid (IC_{50} 55.37 ± 1.25). The IC_{50} of a compound is inversely proportional to its antioxidant activity, as it expresses the concentration of antioxidants required to decrease the concentration of DPPH by 50%. The presence of antioxidants in the herbal combination causes a reduction of Fe^{3+} to Fe^{2+} form. At 120 $\mu\text{g/ml}$, the polyherbal combination showed the maximum reducing power, which is equivalent to 80 $\mu\text{g/ml}$ of ascorbic acid.

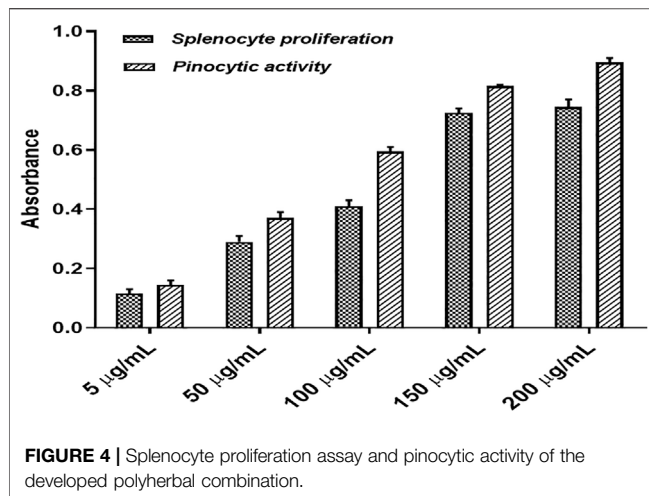
In Vitro Immunomodulatory Activity of the Developed Polyherbal Combination

The splenocytes isolated from the culture in RPMI medium for 72 h with or without polyherbal combination were counted for viability using the MTT assay. It was observed that splenocytes proliferate more when treated with the polyherbal combination compared to untreated cells. Here, five different concentrations (5–200 $\mu\text{g/ml}$) of the polyherbal combination were tested for the splenocyte proliferation assay, and it was found that there was a dose-dependent increase in cell proliferation up to the

concentration of 150 $\mu\text{g/ml}$. In contrast, the concentration above 150 $\mu\text{g/ml}$ showed no significant increment in the number of cells (Figure 4). However, all five concentrations of the combination showed dose-dependent pinocytic activity. Macrophages are the first-line defense against the antigen, and pinocytic activity is one of the distinguished methods to determine macrophage activation. We cultured mouse peritoneal macrophages in RPMI medium with or without supplementation of external stimuli and, after 48 h of incubation, used neutral red, which is readily taken up by macrophages to measure pinocytic activity. After the incubation with neutral red, the macrophages were lysed to measure the concentration of neutral red and determine the extent of pinocytic activity by macrophages. The enhancement of pinocytic activity by macrophages was expressed as the increase in neutral red concentration in cells treated with external stimuli as compared to untreated cells (Figure 4).

Effect of the Polyherbal Combination on Immunological Parameters Hematological Parameters

Without affecting HGB content and RBC count, a significant reduction in lymphocyte, WBC, and platelet counts was observed



in cyclophosphamide-induced immunosuppressed mice. This change has been reversed and almost normalized upon administration of both doses of the polyherbal combination. **Table 3** shows the hematological parameters in mice from all groups. Healthy mice treated with the polyherbal combination showed a slight increase in favorable immune cells such as platelets, lymphocytes, and WBCs.

Immunomodulatory Parameters

The effect of the developed polyherbal combination on the immune system was measured by analyzing the percentage of increase or decrease in T cells, B cells, and NK cells. An increase in T-cell proliferation was observed in the cyclophosphamide-induced immunosuppressed mouse model when treated with the polyherbal combination (**Figure 5**). Cyclophosphamide treatment resulted in a significant reduction in CD4⁺ and CD8⁺ T cells, NK cells, and B cells. Two doses of the polyherbal combination (260 and 520 mg/kg) were administered orally to normal and immunosuppressed mice. Treatment with the developed polyherbal combination in cyclophosphamide-induced immunosuppressed mice resulted in a significant increase in the number of CD4⁺ and CD8⁺ T cells. Both doses, 260 and 520 mg/kg, increased CD4 cells by 18.25% and 22.56%, respectively, compared to 8.50% in the toxic control. A significant increase in the population of B cells

was observed; similarly, a significant increase in NK cells was recorded in immunosuppressed mice treated with the polyherbal combination. The polyherbal combination elicited a proportional enhancement of the immune cell population, with the maximum response being at 520 mg/kg dose (**Figure 5**). In normal mice administered the polyherbal combination, a slight but not significant increase in the number of the immune cell population was observed, such as CD4⁺ T cells (2%), CD8⁺ T cells (3%), NK cells (9%), and B cells (3%).

DISCUSSION

In the Indian traditional system of medicine, more than 30 plants have been used, individually or in polyherbal combinations, for immune disorders. On the basis of the reported literature, we have chosen eight plant materials and screened them for immunomodulatory activity. The aqueous, ethanolic, and hydroethanolic extracts of these plants were screened for their splenocyte proliferation assay and pinocytic activity. Based on their extractive values and *in vitro* immunomodulatory activities, the aqueous extracts of four plants were selected for the development of a polyherbal immunomodulator, although hydroethanolic extractive values of some plants were found to be higher compared to aqueous and ethanolic extracts. In the present investigation, we considered only aqueous extracts because they are preferred over other preparations of traditional formulations and are considered much safer as compared to other extracts (Mensah et al., 2019). The aqueous extracts of these four plants underwent ratio optimization for the development of the polyherbal combination.

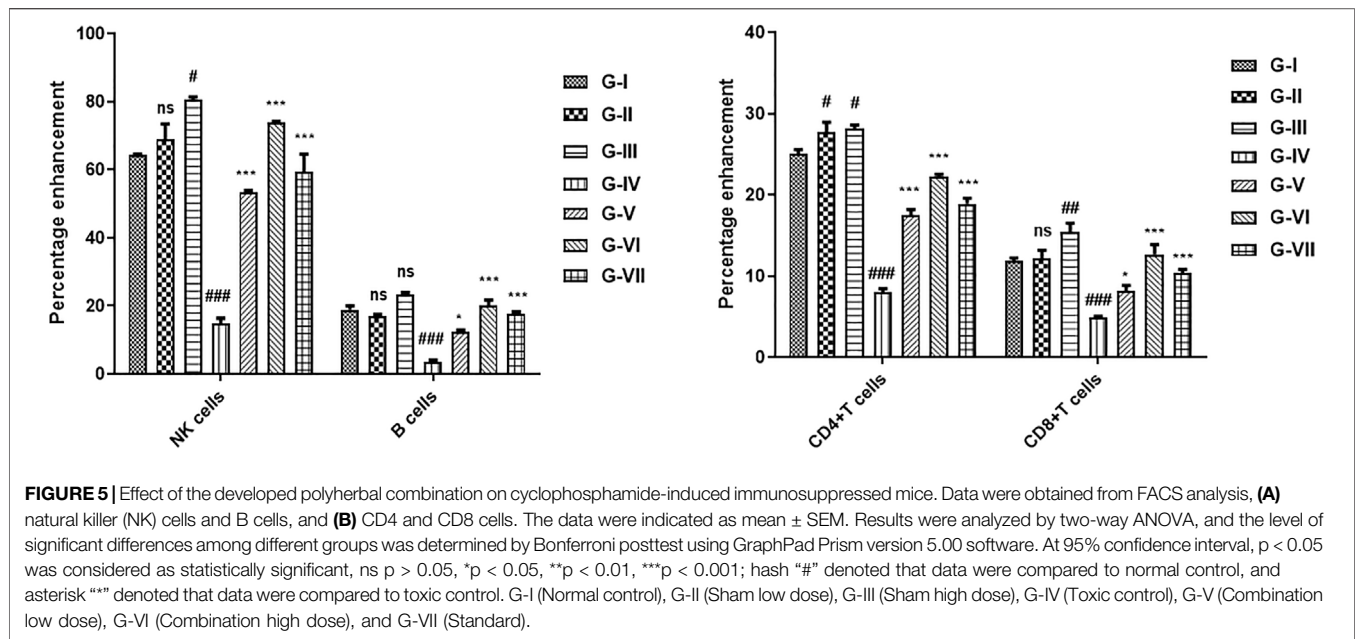
The application of RSM allowed the simultaneous determination of the main and interaction effects of different concentrations of all the extracts on *in vitro* pinocytic and splenocyte proliferation assay (Shahab et al., 2020). The data pertaining to various models (linear, 2FI, quadratic, and cubic) and their subsequent ANOVA revealed that splenocyte proliferation assay and pinocytic activity were the most suitably defined with the quadratic polynomial and 2FI models, respectively.

The plot indicated that the residuals follow a normal distribution and approximately form a straight line (**Figure 6**). “Adequate Precision” is an index that measures the signal-to-

TABLE 3 | Effect of polyherbal combination on hematological parameters of mice after the end of treatment.

Hematological parameter	G-I	G-II	G-III	G-IV	G-V	G-VI	G-VII
HGB (g/dl)	11.22 ± 0.47	13.61 ± 0.77 ^{###}	10.92 ± 0.64 ^{ns}	11.82 ± 0.45 ^{ns}	11.63 ± 0.98 ^{ns}	12.21 ± 1.11 ^{ns}	12.44 ± 0.54 ^{ns}
Neutrophil (×10 ³ /µl)	4.12 ± 0.08	5.87 ± 0.44 [#]	4.14 ± 0.01 ^{ns}	5.74 ± 0.22 [#]	4.27 ± 0.05 ^{ns}	4.88 ± 0.08 ^{ns}	4.34 ± 0.07 ^{ns}
Lymphocyte (×10 ³ /µl)	7.23 ± 0.07	8.11 ± 0.14 ^{ns}	9.33 ± 0.08 ^{##}	4.25 ± 0.21 ^{###}	5.45 ± 0.04 ^{ns}	6.99 ± 0.05 ^{***}	6.11 ± 0.14 [*]
WBC (×10 ³ /µl)	6.24 ± 0.09	6.91 ± 0.09 ^{ns}	7.88 ± 0.07 [#]	3.33 ± 0.14 ^{###}	5.33 ± 0.11 ^{**}	6.74 ± 0.45 ^{***}	6.14 ± 0.11 ^{***}
RBC (×10 ⁶ /µl)	6.02 ± 0.12	6.47 ± 0.47 ^{ns}	6.98 ± 0.45 ^{ns}	6.06 ± 0.13 ^{ns}	5.84 ± 0.02 ^{ns}	6.94 ± 0.31 ^{ns}	7.09 ± 0.23 ^{ns}
PLT (×10 ⁵ /µl)	7.45 ± 0.12	8.44 ± 1.11 ^{ns}	12.36 ± 0.11 ^{###}	5.93 ± 0.54 ^{ns}	10.70 ± 0.45 ^{**}	10.24 ± 0.47 ^{***}	11.32 ± 0.45 ^{***}

HGB, hemoglobin; PLT, platelet; RBC, red blood cell; WBC, white blood cell; G-I, Normal control; G-II, Combination low dose sham; G-III, Combination high dose sham; G-IV, Toxic control; G-V, Combination low dose; G-VI, Combination high dose; G-VII, Standard treated group. The data were indicated as mean ± SEM. Results were analyzed by two-way ANOVA, and the level of significant differences among different groups was determined by Bonferroni posttest using GraphPad Prism version 5.00 software. At 95% confidence interval, $p < 0.05$ was considered as statistically significant, ns $p > 0.05$, * $p < 0.05$, ** $p < 0.01$, *** $p < 0.001$; hash “#” denoted that data were compared to normal control, and asterisk “***” denoted that data were compared to toxic control.



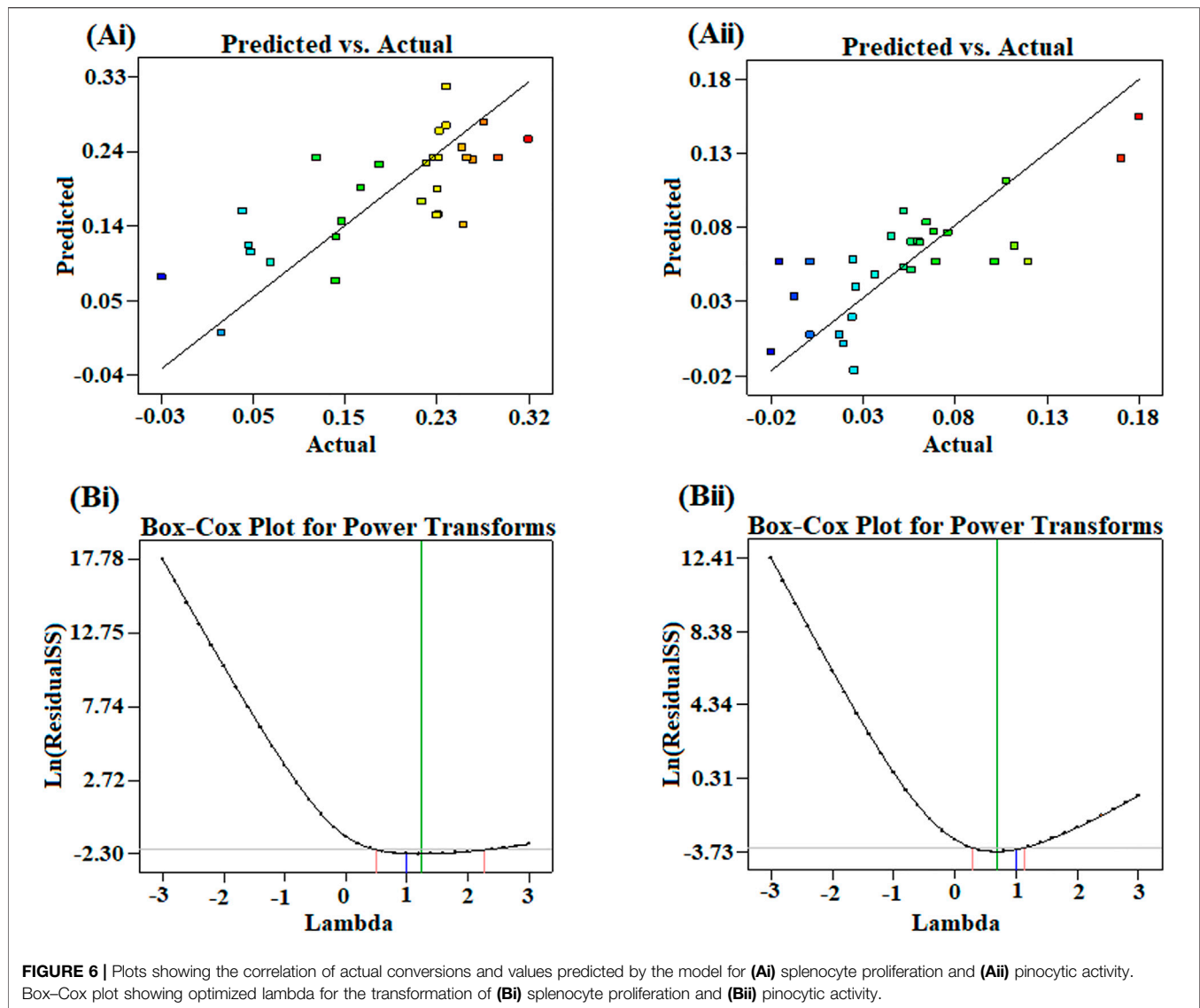
noise ratio. A ratio of greater than 4 is desirable. In this study, the computed ratio of 4.96 and 7.21 for splenocyte proliferation assay and pinocytic activity, respectively, indicated an adequate signal. These results are indicative of maximum predictive responses with constant variance and quadratic model accuracy demonstrating a good reproducibility of the data. The optimum conditions were determined using RSM with a four-factor, two-level BBD. It was also estimated using regression equation for finding the best range of parameters achieving maximum splenocyte proliferation and pinocytic activity. To describe the suitable power transformation of response data, the Box–Cox plot was used (Vélez et al., 2015), since lambda (λ) is the most appropriate power transformation to apply the response data (Figure 6B).

From the point prediction tools, we have checked the effect of different doses of the extract. Upon increasing the dose of *P. emblica* up to 730 mg (100–730 mg), it increased the proliferation of the splenocytes and the pinocytic activity of macrophages, but after that point, the proliferation of splenocytes decreased but no significant change in the pinocytic activity. At an optimal level of *P. emblica* (750 mg), the increased dose of *P. nigrum* up to 22.2 mg was directly proportional to the *in vitro* immunomodulatory activity in both the assays. Furthermore, inverse proliferation was observed. At an optimal level of *P. emblica* (750 mg) and *P. nigrum* (20.59 mg), the concentration of *W. somnifera* was found inversely proportional to the *in vitro* immunomodulatory activity. At a low concentration of *T. cordifolia*, increased splenocyte proliferation and lower pinocytic activity were predicted when the levels of *P. emblica*, *P. nigrum*, and *W. somnifera* was at the optimal level. Individually, a dose of *P. nigrum* up to 41 mg increased splenocyte proliferation and decreased pinocytic activity, while, after this level, splenocyte proliferation was decreased, but no changes in pinocytic activity were measured. *W. somnifera*

individually did not cause any change in pinocytic activity but was directly proportional to the proliferation of splenocytes. Similarly, *T. cordifolia* on a lower dose caused an increase in the proliferation of splenocytes and *vice versa* for pinocytic activity.

The combination has shown a better antioxidant potential compared to individual extracts. A lower value of IC_{50} ($82.54 \pm 2.54 \mu\text{g/ml}$) indicates a higher antioxidant activity of the combination. The plant extracts used in the polyherbal combination contained a higher amount of phenolics and flavonoids and may be responsible for antioxidant activity (Liu et al., 2009). The antioxidant potential exhibited by the developed combination might be due to the presence of secondary metabolites from selected plants. In particular, *P. emblica* contains hydrolyzable tannins with low molecular weight having a very strong antioxidant action (Ghosal et al., 1996; Singh et al., 2015), whereas *W. somnifera* contains withanolides, naturally occurring steroidal lactones having strong antioxidant properties (Devkar et al., 2014; Zahiruddin et al., 2020). Similarly, a strong antioxidant potential was also reported for the aqueous extract of *T. cordifolia* (Premanath and Lakshmidhevi, 2010) and *P. nigrum* (Gülçin, 2005). Our findings strongly suggest that these plant materials are promising sources of natural antioxidants.

The developed polyherbal combination showed not only immunomodulatory activity *in vitro* but also potential immunomodulatory activity against cyclophosphamide-induced immunosuppressed mice. Cyclophosphamide is known to cause a significant reduction in WBC and lymphocyte count (Huyan et al., 2011), and in this study, the effects of the polyherbal combination was tested on cyclophosphamide-induced immunosuppressed mice. The impact of the developed polyherbal combination was evaluated on HGB, neutrophils, lymphocytes, WBC, RBC, and platelet counts in cyclophosphamide-induced immunosuppressed mice.



Lymphocyte, WBC, and platelet counts were significantly decreased upon cyclophosphamide treatment but reversed upon the treatment with the polyherbal combination. Even in healthy mice treated with the polyherbal combination, a slight increase in these cells was recorded.

WBCs are produced from the bone marrow, which is the most affected organ during immunosuppression therapy, as indicated by WBC and platelet counts (Vigila and Baskaran, 2008). Mice treated with cyclophosphamide showed a significant reduction in total platelet and WBC counts and recovered on treatment with both doses of combination. These results indicate that the herbal combination can modulate bone marrow activity, mainly suppression and stimulation, to counteract cyclophosphamide-induced myelosuppression. On the other hand, lymphocytes are a type of WBCs that are of fundamental significance. They regulate the specificity of the immune response to infectious microorganisms and other foreign bodies. Total lymphocyte counts were increased

significantly in mice of all groups treated with the developed polyherbal combination compared to negative control mice. Our results also showed that there was no significant change in the RBC count in any group of mice. For a proper immune system, there should be harmony in RBC and WBC counts (El Bishlawy, 1999), and the developed polyherbal combination maintained the harmony. The results indicated that the developed polyherbal combination is highly efficient in augmenting the immune responses by enhancing the population of T cells and B cells but not NK cells. Since T cells play an important role in regulating the immune response, being responsible for cell-mediated immunity, in a balanced immune system, rapid T-cell proliferation following antigen stimulus is governed by subsequent differentiation of T cells into effectors cells (Luckheeram et al., 2012). Modifications of WBCs and differential counts are important signs of immune response and were supported by enhanced CD4 and CD8 cell counts.

The results of the developed polyherbal combination supported the traditional claims of plants used for an immunomodulatory activity. Previously, aqueous extracts of these four plant materials were tested for their immune enhancing potential. For example, the aqueous extract of *T. cordifolia* can modulate the immune system by increasing the count of WBC, and the aqueous extract is superior to the alcoholic extract (Manjrekar et al., 2000). Similarly, the root extract of *W. somnifera* also proved its T-cell enhancement, splenocyte cell proliferation, and stimulation of phagocytosis of macrophages (Davis and Kuttan, 2000). It has been also proven that the aqueous extract of *P. nigrum* causes splenocyte proliferation in a dose-dependent manner (Majdalawieh and Carr, 2010), and this report agrees with our *in vitro* results. The aqueous extract of these plant materials contains phenolic and flavonoids as the major group of constituents. These phenolic metabolites can promote nonspecific immune function, proliferate splenocytes, and enhance humoral immune responses and NK cell activity (Liu et al., 2012).

We have screened this developed polyherbal combination and the individual extracts for the identification of major metabolites. Of the identified metabolites, several metabolites were previously tested for immunomodulatory activity. Among different metabolites, cordifolioside A and tinocordiside present in the extract of *T. cordifolia* showed immunomodulatory activity (Sharma et al., 2012), and these compounds are also found in our developed polyherbal combination.

Gallic acid (R_t 2.08) and ellagic acid (R_t 4.13) have been reported to stimulate immune cells and can improve the immune cell population damaged by cyclophosphamide. Moreover, these compounds were both found in the extracts and also in the developed combination. Withaferin A (R_t 5.25) and withanolide (R_t 9.09) are the major metabolites found in the aqueous extract of *W. somnifera* and in the developed combination (Furmanowa et al., 2001). These two compounds activated phagocytosis and peritoneal macrophages, increased the secretion of lysosomal enzymes, and selectively enhanced the CD4 and CD8 counts (Bani et al., 2006). Asperuloside (R_t 9.47) increased the T-cell count, followed by increased secretion of interferon (IFN)- γ and tumor necrosis factor (TNF)- α , thereby enhancing the function of immune effector cells *via* induction of inflammatory cytokines (Chan et al., 2020). Asperuloside was found in *P. emblica* and *W. somnifera* extracts as well as in the developed polyherbal combination. Caffeic acid phenethyl ester (R_t 2.92) was found in all the extracts except *P. nigrum*. It increased T-lymphocyte production and enhanced the T cell-mediated immune response (Park et al., 2004). While caffeic acid (R_t 4.59) was present in all the extracts and also in the developed combination, it can increase NK cell activation and proliferate splenic T cells (Kilani-Jaziri et al., 2017).

Several formulations composed of these plant materials are available in the market claiming immunomodulatory activity. We have compared their activity with the results of the

proposed combination on the basis of the reported literature. Gnanasekaran et al. (2015) reported that Chyawanprash could increase the total leukocyte in cyclophosphamide-induced immunosuppressed mice but not up to the normal level. Treatment with the developed combination of cyclophosphamide-induced immunosuppressed mice resulted in complete normalization of the total leukocyte count. Septilin, a well-known and widely used compound formulation in India, is composed of two powders and six plant extracts, in which *T. cordifolia* and *P. emblica* are the major ones. This formulation does cause the proliferation of splenocytes and increase in the lymphocyte count (Daswani and Yegnanarayan, 2002). But the level of significance is lower than the results obtained using our polyherbal combination. However, a real comparative analysis is ongoing in our laboratory. From these preliminary results, we can say that the developed polyherbal combination is better in terms of both *in vitro* and *in vivo* immune stimulating activity. The developed combination has been characterized by measuring the metabolomic content, thereby identifying the active constituents.

CONCLUSIONS AND PERSPECTIVES

The developed polyherbal combination containing *P. emblica*, *P. nigrum*, *W. somnifera*, and *T. cordifolia* exhibited potent immunomodulatory activity through stimulating pinocytosis and splenocyte proliferation. It also enhanced the subsets of various immune cells, mainly NK cells, B cells, CD4, and CD8 T cells, in cyclophosphamide-induced immunosuppressed mice. This immunomodulatory potential may be attributed to the presence of a group of metabolites in the polyherbal combination such as phenols, flavonoids, tannins, alkaloids, and glycosides exhibiting multiple mechanisms. The metabolomic profiling of the extracts and polyherbal combination through UPLC-MS revealed the presence of more than 180 metabolites, and PCA showed a wide array of metabolites, which are distributed in different quadrants. The polyherbal combination studied can be explored for its protective potential against various immunosuppressing clinical conditions and microbial attacks. Further research for its complete efficacy evaluation, development of its dosage form for its utilization in health care, and its in-depth metabolic characterization are in progress. It would be also interesting to check the pharmacokinetic profiling of the developed polyherbal combination with respect to specific marker constituents present in it.

DATA AVAILABILITY STATEMENT

The raw data supporting the conclusions of this article will be made available by the authors, without undue reservation, to any qualified researcher.

ETHICS STATEMENT

The animal study was reviewed and approved by IAEC, Jamia Hamdard, New Delhi, India (Registration No. 173/GO/RE/S/2000/CPCSEA).

AUTHOR CONTRIBUTIONS

SZ contributed to conceptualization, literature review, experimental studies, data curation, data interpretation, and writing the original drafts. AP and MI contributed to experimental studies and data curation. WK contributed to the interpretation of data and article preparation. MW contributed to statistical analysis. RP contributed to the investigation and article

preparation. SA contributed to conceptualization, investigation, data interpretation, and article critical evaluation.

ACKNOWLEDGMENTS

The authors are thankful to Bioactive Natural Product Laboratory, Jamia Hamdard, for providing the necessary chemicals and facilities required for the present work.

SUPPLEMENTARY MATERIAL

The supplementary material for this article can be found online at: <https://www.frontiersin.org/articles/10.3389/fphar.2021.647244/full#supplementary-material>

REFERENCES

- Alsuhailani, S., and Khan, M. A. (2017). Immune-Stimulatory and Therapeutic Activity of *Tinospora Cordifolia*: Double-Edged Sword against Salmonellosis. *J. Immunol. Res.* 2017, 1–9. doi:10.1155/2017/1787803
- Anjum, V., Arora, P., Ansari, S. H., Najmi, A. K., and Ahmad, S. (2017). Antithrombocytopenic and Immunomodulatory Potential of Metabolically Characterized Aqueous Extract of *Carica Papaya* Leaves. *Pharm. Biol.* 55, 2043–2056. doi:10.1080/13880209.2017.1346690
- Anonymous (2010). *Indian Pharmacopoeia Commission, Ministry of Health and Family Welfare*, 3. Ghaziabad: Government of India.
- Bani, S., Gautam, M., Sheikh, F. A., Khan, B., Satti, N. K., Suri, K. A., et al. (2006). Selective Th1 Up-Regulating Activity of *Withania Somnifera* Aqueous Extract in an Experimental System Using Flow Cytometry. *J. Ethnopharmacol.* 107, 107–115. doi:10.1016/j.jep.2006.02.016
- Bhalodia, N., Nariya, P., Shukla, V., and Acharya, R. (2013). *In Vitro* antioxidant Activity of Hydro Alcoholic Extract from the Fruit Pulp of *Cassia Fistula* Linn. *AYU* 34, 209. doi:10.4103/0974-8520.119684
- Bui, T. T., Piao, C. H., Hyeon, E., Fan, Y., Van Nguyen, T., Jung, S. Y., et al. (2019). The Protective Role of Piper Nigrum Fruit Extract in an Ovalbumin-Induced Allergic Rhinitis by Targeting of NF- κ Bp65 and STAT3 Signalings. *Biomed. Pharmacother.* 109, 1915–1923. doi:10.1016/j.biopha.2018.11.073
- Chan, Y., Ng, S. W., Xin Tan, J. Z., Gupta, G., Tambuwala, M. M., Bakshi, H. A., et al. (2020). Emerging Therapeutic Potential of the Iridoid Molecule, Asperuloside: A Snapshot of its Underlying Molecular Mechanisms. *Chemico-Biological Interactions* 315, 108911. doi:10.1016/j.cbi.2019.108911
- Chatterjee, A., Chatterjee, S., Biswas, A., Bhattacharya, S., Chattopadhyay, S., and Bandyopadhyay, S. K. (2012). Gallic Acid Enriched Fraction of *Phyllanthus emblica* Potentiates Indomethacin-Induced Gastric Ulcer Healing via E-NOS-Dependent Pathway. *Evid Based. Complement. Altern. Med.* 2012, 1–13. doi:10.1155/2012/487380
- Daswani, B. R., and Yegnanarayan, R. (2002). Immunomodulatory Activity of Septilin, a Polyherbal Preparation. *Phytother. Res.* 16, 162–165. doi:10.1002/ptr.996
- Davis, L., and Kuttan, G. (2000). Immunomodulatory Activity of *Withania Somnifera*. *J. Ethnopharmacology* 71 (1–2), 193–200. doi:10.1016/S0378-8741(99)00206-8
- Devkar, S., Jagtap, S., Katyare, S., and Hegde, M. (2014). Estimation of Antioxidant Potential of Individual Components Present in Complex Mixture of *Withania somnifera* (Ashwagandha) Root Fraction by Thin-Layer Chromatography-2,2-Diphenyl-1-Picrylhydrazyl Method. *J. Planar Chromatogr. - Mod. TLC* 27, 157–161. doi:10.1556/JPC.27.2014.3.2
- El Bishlawy, I. M. (1999). Red Blood Cells, Hemoglobin and the Immune System. *Med. Hypotheses* 53, 345–346. doi:10.1054/mehy.1997.0778
- Furmanowa, M., Gajdzis-Kuls, D., Ruszkowska, J., Czarnocki, Z., Obidoska, G., Sadowska, A., et al. (2001). *In Vitro* Propagation of *Withania Somnifera* and Isolation of Withanolides with Immunosuppressive Activity. *Planta Med.* 67, 146–149. doi:10.1055/s-2001-11494
- Ganju, L., Karan, D., Chanda, S., Srivastava, K. K., Sawhney, R. C., and Selvamurthy, W. (2003). Immunomodulatory Effects of Agents of Plant Origin. *Biomed. Pharmacother.* 57 (7), 296–300. doi:10.1016/S0753-3322(03)00095-7
- Ghosal, S., Tripathi, V. K., and Chauhan, S. (1996). ChemInform Abstract: Active Constituents of *Emblica Officinalis*. Part 1. The Chemistry and Antioxidative Effects of Two New Hydrolysable Tannins, Emblicanin A (Ia) and B (Ib). *ChemInform* 27. doi:10.1002/chin.199647279
- Gnanasekaran, S., Sakthivel, K. M., and Chandrasekaran, G. (2015). Immunostimulant and Chemoprotective Effect of Vivartana, a Polyherbal Formulation against Cyclophosphamide Induced Toxicity in Swiss Albino Mice. *J. Exp. Ther. Oncol.* 11, 51–61.
- Gorgani, L., Mohammadi, M., Najafpour, G. D., and Nikzad, M. (2017). Piperine-The Bioactive Compound of Black Pepper: From Isolation to Medicinal Formulations. *Compr. Rev. Food Sci. Food Saf.* 16, 124–140. doi:10.1111/1541-4337.12246
- Gülçin, İ. (2005). The Antioxidant and Radical Scavenging Activities of Black Pepper (*Piper Nigrum*) Seeds. *Int. J. Food Sci. Nutr.* 56, 491–499. doi:10.1080/09637480500450248
- Huyan, X. H., Lin, Y. P., Gao, T., Chen, R. Y., and Fan, Y. M. (2011). Immunosuppressive Effect of Cyclophosphamide on white Blood Cells and Lymphocyte Subpopulations from Peripheral Blood of Balb/c Mice. *Int. Immunopharmacol.* 11, 1293–1297. doi:10.1016/j.intimp.2011.04.011
- Khan, W., Parveen, R., Chester, K., Parveen, S., and Ahmad, S. (2017). Hypoglycemic Potential of Aqueous Extract of *Moringa Oleifera* Leaf and *In Vivo* GC-MS Metabolomics. *Front. Pharmacol.* 8, 577. doi:10.3389/fphar.2017.00577
- Kilani-Jaziri, S., Mokdad-Bzeouich, I., Krifa, M., Nasr, N., Ghedira, K., and Chekir-Ghedira, L. (2017). Immunomodulatory and Cellular Anti-Oxidant Activities of Caffeic, Ferulic, and p-Coumaric Phenolic Acids: A Structure-Activity Relationship Study. *Drug Chem. Toxicol.* 40, 416–424. doi:10.1080/01480545.2016.1252919
- Kim, O. K., Yoo, S. A., Nam, D.-E., Kim, Y., Kim, E., Jun, W., et al. (2014). Immunomodulatory Effects of Curcuma Longa L. Extract in LP-BM5 Murine Leukemia Viruses-Induced Murine Acquired Immune Deficiency Syndrome. *J. Korean Soc. Food Sci. Nutr.* 43, 1317–1324. doi:10.3746/jkfn.2014.43.9.1317
- Kumar, D., Arya, V., Kaur, R., Bhat, Z. A., Gupta, V. K., and Kumar, V. (2012). A Review of Immunomodulators in the Indian Traditional Health Care System. *J. Microbiol. Immunol. Infect.* 45, 165–184. doi:10.1016/j.jmii.2011.09.030
- Liu, S., Lin, J., Wang, C., Chen, H., and Yang, D. (2009). Antioxidant Properties of Various Solvent Extracts from Lychee (Litchi Chinensis Sonn.) Flowers. *Food Chem.* 114, 577–581. doi:10.1016/j.foodchem.2008.09.088
- Liu, X., Zhao, M., Wu, K., Chai, X., Yu, H., Tao, Z., et al. (2012). Immunomodulatory and Anticancer Activities of Phenolics from *Emblica* Fruit (*Phyllanthus Emblica* L.). *Food Chem.* 131, 685–690. doi:10.1016/j.foodchem.2011.09.063

- Luckheeram, R. V., Zhou, R., Verma, A. D., and Xia, B. (2012). CD4+T Cells: Differentiation and Functions. *Clin. Develop. Immunol.* 2012, 1–12. doi:10.1155/2012/925135
- Majdalawieh, A. F., and Carr, R. I. (2010). *In Vitro* investigation of the Potential Immunomodulatory and Anti-cancer Activities of Black Pepper (*Piper Nigrum*) and Cardamom (*Elettaria Cardamomum*). *J. Med. Food* 13, 371–381. doi:10.1089/jmf.2009.1131
- Manjrekar, P. N., Jolly, C. I., and Narayanan, S. (2000). Comparative Studies of the Immunomodulatory Activity of *Tinospora Cordifolia* and *Tinospora Sinensis*. *Fitoterapia* 71, 254–257. doi:10.1016/S0367-326X(99)00167-7
- Mathai, R. T., Tonse, R., Kalekhan, F., Colin, M. D., Prabhu, H. S., Rao, S., et al. (2015). “Amla in the Prevention of Aging,” in *Foods and Dietary Supplements in the Prevention and Treatment of Disease in Older Adults*. Waltham, MA: Academic Press, 29–35. doi:10.1016/B978-0-12-418680-4.00003-8
- Mathew, S., and Kuttan, G. (1999). Immunomodulatory and Antitumour Activities of *Tinospora Cordifolia*. *Fitoterapia* 70, 35–43. doi:10.1016/S0367-326X(98)00017-3
- Mensah, M. L. K., Komlaga, G., Forkuo, A. D., Firempong, C., Anning, A. K., and Dickson, R. A. (2019). “Toxicity and Safety Implications of Herbal Medicines Used in Africa,” in *Herbal Medicine*. doi:10.5772/intechopen.72437
- Mishra, A., Kumar, S., and Pandey, A. K. (2013). Scientific Validation of the Medicinal Efficacy of *Tinospora Cordifolia*. *Scientific World J.* 2013, 1–8. doi:10.1155/2013/292934
- Mohammed Al-Ezzy, R., Anee, R. S. A. A., and Ibrahim, N. A. (2018). Assessments of Immunological Activity of *Achillea Millefolium* Methanolic Extract on Albino Male Mice. *J. Pharm. Pharmacol.* 6, 563–569. doi:10.17265/2328-2150/2018.06.002
- Mondal, S., Varma, S., Bamola, V. D., Naik, S. N., Mirdha, B. R., Padhi, M. M., et al. (2011). Double-Blinded Randomized Controlled Trial for Immunomodulatory Effects of Tulsi (*Ocimum Sanctum* Linn.) Leaf Extract on Healthy Volunteers. *J. Ethnopharmacology* 136, 452–456. doi:10.1016/j.jep.2011.05.012
- More, P., and Pai, K. (2011). Immunomodulatory Effects of *Tinospora Cordifolia* (Guduchi) on Macrophage Activation. *Biol. Med.* 3 (2), 134–140.
- Nagoba, B., and Davane, M. (2018). Natural Immunomodulators. *J. Immunol. Microbiol.* 2 (1), 2.
- Neag, M. A., Mocan, A., Echeverria, J., Pop, R. M., Bocsan, C. I., Crișan, G., et al. (2018). Berberine: Botanical Occurrence, Traditional Uses, Extraction Methods, and Relevance in Cardiovascular, Metabolic, Hepatic, and Renal Disorders. *Front. Pharmacol.* 9, 557. doi:10.3389/fphar.2018.00557
- Park, J. H., Lee, J. K., Kim, H. S., Chung, S. T., Eom, J. H., Kim, K. A., et al. (2004). Immunomodulatory Effect of Caffeic Acid Phenethyl Ester in Balb/c Mice. *Int. Immunopharmacology* 4, 429–436. doi:10.1016/j.intimp.2004.01.013
- Parveen, B., Pillai, K. K., Tamboli, E. T., and Ahmad, S. (2015). Effect of Piperine on Pharmacokinetics of Sodium Valproate in Plasma Samples of Rats Using Gas Chromatography-Mass Spectrometry Method. *J. Pharm. Bioall Sci.* 7, 317. doi:10.4103/0975-7406.168036
- Premanath, R., and Lakshmidhevi, N. (2010). Studies on Anti-oxidant Activity of *Tinospora Cordifolia* (Miers.) Leaves Using *In Vitro* Models. *J. Am. Sci.* 6, 736–743.
- Rehman, J., Dillow, J. M., Carter, S. M., Chou, J., Le, B., and Maisel, A. S. (1999). Increased Production of Antigen-specific Immunoglobulins G and M Following *In Vivo* Treatment with the Medicinal Plants *Echinacea Angustifolia* and *Hydrastis Canadensis*. *Immunol. Lett.* 68, 391–395. doi:10.1016/S0165-2478(99)00085-1
- Sarvanandaa, L., Premarathna, A. D., and Karunarathnad, S. C. (2018). Immunomodulatory Effect of *Cardiospermum Halicacabum* against Cancer. *Biomed. J. Scientific Tech. Res.* 10 (4), 7916–7919. doi:10.26717/bjstr.2018.10.001976
- Shahab, M. S., Rizwanullah, M., Alshehri, S., and Imam, S. S. (2020). Optimization to Development of Chitosan Decorated Polycaprolactone Nanoparticles for Improved Ocular Delivery of Dorzolamide: *In Vitro*, *Ex Vivo* and Toxicity Assessments. *Int. J. Biol. Macromolecules* 163, 2392–2404. doi:10.1016/j.jbiomac.2020.09.185
- Sharma, U., Bala, M., Kumar, N., Singh, B., Munshi, R. K., and Bhalerao, S. (2012). Immunomodulatory Active Compounds from *Tinospora Cordifolia*. *J. Ethnopharmacology* 141, 918–926. doi:10.1016/j.jep.2012.03.027
- Shi, L., and Fu, Y. (2011). Isolation, Purification, and Immunomodulatory Activity *In Vitro* of Three Polysaccharides from Roots of *Cudrania Tricuspidata*. *Acta Biochim. Biophys. Sinica* 43, 418–424. doi:10.1093/abbs/gmr024
- Singh, M., Khan, M. A., Khan, M. S., Ansari, S. H., and Ahmad, S. (2015). Quality Assessment and Evaluation of *In-Vitro* Antioxidant Potential of *Phyllanthus Emblica* L. *Indian J. Traditional Knowledge* 14 (2), 265–272.
- Singh, N., Bhalla, M., de Jager, P., and Gilca, M. (2011). An Overview on Ashwagandha: A Rasayana (Rejuvenator) of Ayurveda. *Afr. J. Trad. Compl. Alt. Med.* 8, 208–213. doi:10.4314/ajtcam.v8i5S.9
- Tiwari, S., Atluri, V. S. R., Yndart Arias, A., Jayant, R. D., Kaushik, A., Geiger, J., et al. (2018). Withaferin A Suppresses Beta Amyloid in APP Expressing Cells: Studies for Tat and Cocaine Associated Neurological Dysfunctions. *Front. Aging Neurosci.* 10, 291. doi:10.3389/fnagi.2018.00291
- Tungmunthum, D., Thongboonyou, A., Pholboon, A., and Yangsabai, A. (2018). Flavonoids and Other Phenolic Compounds from Medicinal Plants for Pharmaceutical and Medical Aspects: An Overview. *Medicines (Basel)* 5, 93. doi:10.3390/medicines5030093
- van der Nat, J. M., Klerx, J. P., van Dijk, H., De Silva, K. T., and Labadie, R. P. (1987). Immunomodulatory Activity of an Aqueous Extract of *Azadirachta indica* Stem Bark. *J. Ethnopharmacol.* 19, 125–131. doi:10.1016/0378-8741(87)90036-5
- Vélez, J. I., Correa, J. C., and Marmolejo-Ramos, F. (2015). A New Approach to the Box-Cox Transformation. *Front. Appl. Math. Stat.* 1, 12. doi:10.3389/fams.2015.00012
- Vigila, A. G., and Baskaran, X. (2008). Immunomodulatory Effect of Coconut Protein on Cyclophosphamide Induced Immune Suppressed Swiss Albino Mice. *Ethnobotanical Leaflets*.
- Zahiruddin, S., Basist, P., Parveen, A., Parveen, R., Khan, W., Gaurav, et al. (2020). Ashwagandha in Brain Disorders: A Review of Recent Developments. *J. Ethnopharmacology* 257, 112876. doi:10.1016/j.jep.2020.112876
- Zahiruddin, S., Khan, W., Nehra, R., Alam, M. J., Mallick, M. N., Parveen, R., et al. (2017). Pharmacokinetics and Comparative Metabolic Profiling of Iridoid Enriched Fraction of *Picrorhiza Kurroa* - an Ayurvedic Herb. *J. Ethnopharmacology* 197, 157–164. doi:10.1016/j.jep.2016.07.072
- Zhang, J., Miao, D., Zhu, W. F., Xu, J., Liu, W. Y., Kitdamrongtham, W., et al. (2017). Biological Activities of Phenolics from the Fruits of *Phyllanthus Emblica* L. (Euphorbiaceae). *Chem. Biodivers* 14, e1700404. doi:10.1002/cbdv.201700404

Conflict of Interest: The authors declare that the research was conducted in the absence of any commercial or financial relationships that could be construed as a potential conflict of interest.

Publisher's Note: All claims expressed in this article are solely those of the authors and do not necessarily represent those of their affiliated organizations or those of the publisher, the editors, and the reviewers. Any product that may be evaluated in this article, or claim that may be made by its manufacturer, is not guaranteed or endorsed by the publisher.

Copyright © 2022 Zahiruddin, Parveen, Khan, Ibrahim, Want, Parveen and Ahmad. This is an open-access article distributed under the terms of the Creative Commons Attribution License (CC BY). The use, distribution or reproduction in other forums is permitted, provided the original author(s) and the copyright owner(s) are credited and that the original publication in this journal is cited, in accordance with accepted academic practice. No use, distribution or reproduction is permitted which does not comply with these terms.

Advantages of publishing in Frontiers



OPEN ACCESS

Articles are free to read
for greatest visibility
and readership



FAST PUBLICATION

Around 90 days
from submission
to decision



HIGH QUALITY PEER-REVIEW

Rigorous, collaborative,
and constructive
peer-review



TRANSPARENT PEER-REVIEW

Editors and reviewers
acknowledged by name
on published articles

Frontiers

Avenue du Tribunal-Fédéral 34
1005 Lausanne | Switzerland

Visit us: www.frontiersin.org

Contact us: frontiersin.org/about/contact



REPRODUCIBILITY OF RESEARCH

Support open data
and methods to enhance
research reproducibility



DIGITAL PUBLISHING

Articles designed
for optimal readership
across devices



FOLLOW US

@frontiersin



IMPACT METRICS

Advanced article metrics
track visibility across
digital media



EXTENSIVE PROMOTION

Marketing
and promotion
of impactful research



LOOP RESEARCH NETWORK

Our network
increases your
article's readership